Vol. 23, No. 1, March, 2024
ISSN (Print): 0972-6268; ISSN (Online) : 2395-3454

NATURE ENVIRONMENT & POLLUTION TECHNOLOGY

A Multidisciplinary, International Journal on Diverse Aspects of Environment

Technoscience Publications
website: www.neptjournal.com

Technoscience Publications
A-504, Bliss Avenue, Balewadi,
Opp. SKP Campus, Pune-411 045
Maharashtra, India

www.neptjournal.com

Nature Environment and Pollution Technology

(An International Quarterly Scientific Research Journal)

Published by : Mrs. T. P. Goel, Technoscience Publications, A-504, Bliss Avenue, Balewadi, Pune-411 045, Maharashtra, India

E-mail : contact@neptjournal.com; operations@neptjournal.com

INSTRUCTIONS TO AUTHORS

Scope of the Journal

The Journal publishes original research/review papers covering almost all aspects of environment like monitoring, control and management of air, water, soil and noise pollution; solid waste management; industrial hygiene and occupational health hazards; biomedical aspects of pollution; conservation and management of resources; environmental laws and legal aspects of pollution; toxicology; radiation and recycling etc. Reports of important events, environmental news, environmental highlights and book reviews are also published in the journal.

Format of Manuscript

- The manuscript (mss) should be typed in double space leaving wide margins on both the sides.
- First page of mss should contain only the title of the paper, name(s) of author(s) and name and address of Organization(s) where the work has been carried out along with the affiliation of the authors.

Continued on back inner cover...

Nature Environment and Pollution Technology

Vol. 23, No. (1), December 2024

CONTENTS

The Journal is Currently Abstracted and Indexed In:

- CNKI Scholar (China National Knowledge Infrastructure)
- Scopus Cite Score (2022) 0.90
- Scopus®, SJR (2022) 0.191
- Index Copernicus (2022) = 128.35
- Indian Science Abstracts, New Delhi, India
- Chemical Abstracts, U.S.A.
- Pollution Abstracts, U.S.A.
- Elsevier Bibliographic Databases
- Paryavaran Abstract, New Delhi, India
- WorldCat (OCLC)
- Zoological Records
- CAB Abstracts, U.K.
- British Library
- Electronic Social and Science Citation Index (ESSCI)
- Connect Journals (India)
- Indian Citation Index (ICI)
- CrossRef (DOI)
- Indian Science
- EBSCO: Environment Index™
- ProQuest, U.K.
- JournalSeek
- Google Scholar
- DOAJ
- Research Bible (Japan)
- Zetoc
- J-Gate
- SHERPA/RoMEO
- Environment Abstract, U.S.A.
- Centre for Research Libraries
- Directory of Science
- Elektronische Zeitschriftenbibliothek (EZB)
- AGRIS (UN-FAO)
- CSA: Environmental Sciences and Pollution Management
- Ulrich's (Refereed) database
- Access to Global Online Research in Agriculture (AGORA)
- UDL-EDGE (Malaysia) Products like i-Journals, i-Focus and i-Future
- Present in UGC-CARE List (Group II)

www.neptjournal.com

Nature Environment and Pollution Technology

EDITORS

Nature Environment and Pollution Technology
An International Quarterly Scientific Journal

p-ISSN: 0972-6268
(Print copies up to 2016)
e-ISSN: 2395-3454

Vol. 23 | No. 1 | pp. 1-15 | 2024

Original Research Paper

https://doi.org/10.46488/NEPT.2024.v23i01.001

Open Access Journal

Exploring the Trend of Aerosol Optical Depth and its Implication on Urban Air Quality Using Multi-spectral Satellite Data During the Period from 2009 to 2020 over Dire Dawa, Ethiopia

Teshager Argaw Endale*†, Gelana Amente Raba*, Kassahun Ture Beketie and Gudina Legese Feyisa****
*College of Natural and Computational Sciences, Department of Physics, Haramaya University, Dire Dawa, Ethiopia
**Center of Environmental Sciences, Addis Ababa University, Addis Ababa, Ethiopia
†Corresponding author: Teshager Argaw Endale; tesh.phy08@gmail.com; abnereth15@gmail.com

Nat. Env. & Poll. Tech.
Website: www.neptjournal.com

Received: 12-05-2023
Revised: 08-07-2023
Accepted: 01-08-2023

Key Words:
Atmospheric aerosol
Aerosol optical depth
Air quality
Model validation
Multi-spectral sensor

ABSTRACT

This study focuses on atmospheric aerosols, especially aerosol optical depth (AOD), over Dire Dawa, Ethiopia, from 2009 to 2020. At first, a correlation between the four satellite sensors and AERONET was made for validation purposes and to determine the sensor that best represents Dire Dawa. Intercomparisons were also made among the four satellite sensors. After all statistical tests, annual, seasonal, and decadal trend analyses were made. The validation results indicated that the AOD of MODIS-terra showed the best correlation with AERONET with R^2 (0.78), RMSE (0.03), and MBE of 0.02 and represented the area better than the rest. The inter-comparison of AOD retrieved from multi-spectral satellite sensors showed a positive and satisfactory correlation between MODIS-Terra and OMI. Only MODIS-Aqua showed a linearly increasing mean annual AOD with R^2 = 0.43. In three seasons (summer, autumn, and spring), AOD showed linear increments over the 12 years, with R^2 ranging between 0.3 and 0.5. The three seasons also had nearly identical AODs of 0.23-0.28. However, winter had the lowest value of 0.2. MODIS-terra, out of the four sensors, exhibited increasing decadal tendency over the 2009-2020 period. Monthly analysis revealed that August had the highest AOD (0.265), and January had the lowest (0.14). The value of AOD obtained from this study over Dire Dawa shows a higher value during all seasons except during winter. Thus, this study gives a glimpse into the use of multi-spectral satellite sensors to monitor air quality over a semi-arid urban region.

INTRODUCTION

Both natural and anthropogenic, atmospheric aerosols are amongst the major climate-forcing agents recognized globally (IPCC 2013). They play a major role in the Earth's climate system; weather, regional or global climate 'influence the Earth's radiation budget and affect the regional hydrological cycle (Ramanathan et al. 2001). Aerosols can both directly and indirectly change the radiation budget (Jung et al. 2019). Air quality is affected by aerosol. Aerosol dynamics in the atmosphere are closely correlated with regional meteorology and their emission sources. Aerosol ties alter throughout time and space as a result of their short lifetime and a number of dynamic processes, including transport, deposition, convection, and others. The high variation of aerosol properties poses significant challenges for comprehending aerosol observed by satellite remote sensing and modeling aerosol transport (Eck et al. 2008).

To some extent, the local air pollution level can be estimated using AOD, one of the basic optical metrics among aerosol properties. An exceedingly clean atmosphere has an AOD value of 0.01, whereas one that is quite cloudy has a value of 0.4. Aerosol is also widely utilized as an obscure but significant indicator of climate change and radiation equilibrium of the atmosphere (Wang et al. 2020, Weizhi et al. 2021). AOD exerts a great influence on climate regionally and globally since it affects atmospheric radiation, transmission, and water circulation (Rosenfeld et al. 2007). In the conventional sense, one way of AOD acquisition is by field exploration; this fails to meet the requirements of the regional study, and neither demonstrates spatial continuity. This is because of restrictions faced by the ground survey on allocating observation posts. Advancement in satellite remote-sensing techniques has opened new corridors for monitoring and mapping of air pollution over large regions. At present, remote sensing (R.S.) technology is a crucial mode for testing and supervising aerosol based on the

strength of AOD (Badarinath et al. 2011, Ge et al. 2011). Over the last decade, the Moderate Resolution Imaging Spectroradiometer is one example of a satellite sensor (MODIS) carried on both Aqua and Terra platforms (Levy et al. 2013), the Multiangle Imaging Spectroradiometer (MISR) and the Ozone Monitoring Instrument (OMI) (Levelt et al. 2006) have investigated the atmosphere by characterizing physical and chemical properties of aerosols using observations and retrieval algorithms.

Dire Dawa is the most vulnerable city to extreme climate events like drought, high flash floods, and high temperatures (Gezahegn et al. 2021). Frequent dust storms also occur in the area, especially during certain months of the year. Moreover, growing industrialization and expanding urbanization are contributing to more emissions of carbon monoxide, sulfates, and nitrates in the air (Oluwasinaayomi et al. 2018). Since no ground-based air-pollution monitoring instrument is available, the trend of AOD long-term data retrieved from multi-spectral satellite sensors. The present study has three main objectives. The first is to extensively evaluate MODIS Aqua, MODIS-Terra, MISR, and OMI satellites and to make an inter-comparison of the data obtained from the satellite sensors. This inter-comparison of multiple sensors is needed from time to time because errors and biases are present in retrieval algorithms due to instrument calibration, sampling, and algorithm accuracy. The second objective is to assess the temporal variation of AOD, i.e., decadal, seasonal, and annual variations over Dire Dawa. This helps to explore the magnitude and dispersion of AOD loading on the temporal scale in the study area. The third objective is to explore the AOD Mann-Kendall trend test. This study also attempted to identify the convenient satellite suitable for estimating AOD, which can reveal the status of air quality in a specific region, by inter-comparing AOD data sets retrieved from MODIS-Aqua, MODIS-Terra, MISR, and OMI with ground-based, AERONET, observations in Addis Ababa.

MATERIALS AND METHODS

Description of the Study Area

This study was carried out at the base of Dengego Mountain in Dire Dawa City, in the country's eastern region, 927°' and 949°'N latitude and 4138°' and 4219°'E longitude. Although the majority of the city is located at about 1200 m a.s.l., the height inside the city's boundaries spans from 960 m in the northeast to 2450 m in the southwest (Oluwasinaayomi et al. 2018). The average wind speed is about 2.67 $m.s^{-1}$, and relative humidity records indicate 49.13 ± 6.25. Dire Dawa is located about 515 km east of Addis Ababa, the capital city of Ethiopia, 55 km from Harar, and 313 km from Port of Djibouti. East Hararghe administrative zone of Oromiya Regional State borders Dire Dawa in the south and southeast and the Shinele zone of Somali Regional State in the north, east, and west. The major towns surrounding the city of Dire Dawa are Shinile, Gildessa, Hurso, Kulubi, Kombolcha, and Ejersa Goro. The total area of the Dire Dawa is about 128,802 ha. The city is a favored strategic position for both commercial and industrial activities. It is the main gateway for the country's trade route to Djibouti. The city is known for being an industrial and commercial center, comprising food-processing plants, textile and cement factories, and the second-largest open market in the country. In terms of population, Dire Dawa is the second biggest city in Ethiopia, next to Addis Ababa, with over 400,000 inhabitants (Oluwasinaayomi et al. 2018).

The high inflow of vehicles coupled with fast population growth has contributed to the problem of road traffic congestion (Belachew & Zeleke 2015). This is also the cause for the increase of air pollutants such as NO_2, CO_2, SO_2, CO, etc., which at some locations exceed the annual average level set in the ambient air quality standard (Knife, 2017).

The temperature trend indicates that the city exhibited a warming trend (Gezahegn et al. 2021). Oluwasinaayomi et al. (2018), analysis states that the maximum temperature has been rising at a rate of roughly 0.67°C per decade. The increase in land surface temperature appears to have been caused by a shift in land use and land cover due to urbanization, settlement development, and the building of additional homes in the city. Fig 1. depicts a map of the study region.

Satellite Data Processing and Analysis

Data sources: The data used in this study (AOD daily data from 2009 to 2020) were obtained from widely used satellite sensors for semi-arid regions, namely, MODIS Aqua, MODIS-Terra, MISR, and OMI except for MISR, which has only data available up to 2017. For validating the AOD data retrieved using the above sensors, the only available ground-based instrument, AERONET of Addis Ababa University, Ethiopia, was used. The description for each sensor was presented under sections 2.2.1, 2.2.2, 2.2.3, and 2.2.4, respectively.

MODIS-Aqua and MODIS-Terra: The moderate resolution imaging Spectro-radiometer (MODIS) is a remote sensing instrument on board by the National Aeronautics and Space Administration's (NASA's) Earth Observing Systems (EOS), Terra, and Aqua satellites launched in 1999 and 2002, respectively. MODIS operates at an altitude of 705 km and makes radiance observations in 36 spectral channels in the wavelength range of 410–1440 nm at a spatial resolution ranging from 250 m to 1 km with a 2300 km wide swath

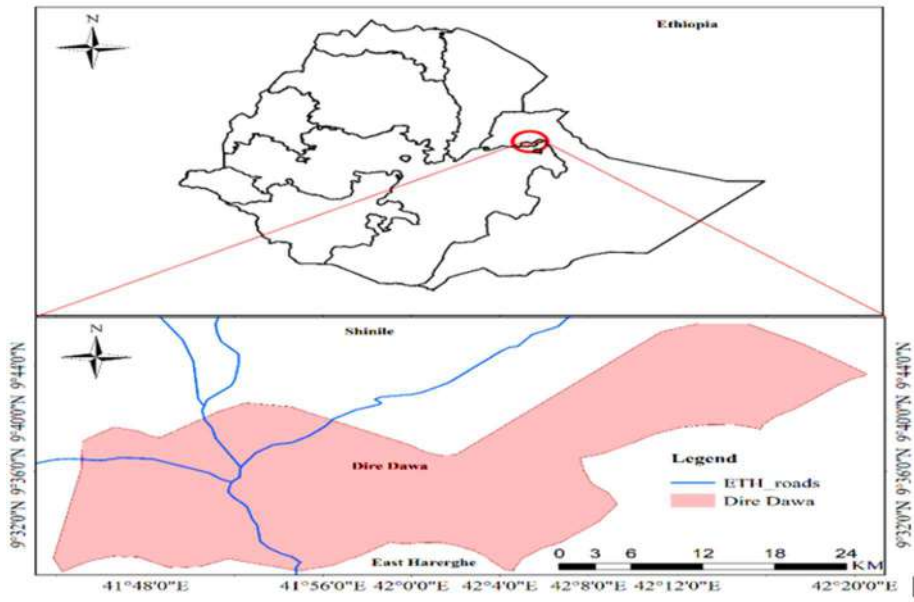

Fig. 1: Map of the study area of Dire Dawa.

and almost daily global coverage. Overland, MODIS AOD uncertainty is 0.05 ± 0.15. Hsu et al. (2013) give MODIS aerosol retrieval details.

To retrieve aerosol optical properties (e.g., AOD information) over bright-reflecting surfaces such as desert and urban areas deep blue (D.B.) algorithm is used (Hsu et al. 2013). The blue channel is used since it provides low surface reflectance over the desert surface and can get the expected AOD information (Hsu et al. 2013). In this study, the website (http://disc.sci.gsfc.nasa.gov/giovanni) retrieved aerosol data from MODIS Aqua and Terra with collection 6, and a resolution of 1º x 1º was used.

MISR data: The Multiangle Imaging Spectro Radiometer (MISR) instrument measures tropospheric aerosol characteristics through the acquisition of global multiangle imagery on the daylight side of Earth. MISR applies nine charge-coupled devices (CCDs), each with four independent line arrays positioned at nine view angles spread out at nadir, 26.1, 45.6, 60.0, and 70.5. In each of the nine MISR cameras, images are obtained from reflected and scattered sunlight in four bands – blue, green, red, and near-infrared – with a center wavelength value of 446, 558, 672, and 867 nm, respectively. The combination of viewing cameras and spectral wavelengths enables MISR to retrieve aerosols AOD over high-reflectivity surfaces like deserts.

In this study, we use Level 2 (version 0023) AOD at 558 nm (green band) measured by the MISR instrument with a 17.6 km resolution aboard the Terra satellite. The MISR data of 0.5°×0.5° has been rescaled by assigning equal weight to each sub-grid, after which 1°×1° resolution was obtained. MISR Level 2 aerosol retrievals use only data that pass angle-to-angle smoothness and spatial correlation tests (Martonchik et al. 2002).

OMI data: OMI was launched in July 2004 on NASA's EOS-Aura satellite, which is also part of the A-train constellation. It has a nadir-viewing imaging spectrometer that measures the top of the atmosphere (TOA) upwelling radiances between the visible and ultraviolet solar spectrum (270-500 nm), with a spatial resolution of approximately 0.5 nm (Levelt et al. 2006). The expected uncertainty in AOD retrieval is around ±30% AOD or 0.10, whichever is more significant over Land (Ahn et al. 2014). This study utilized 500 nm observations with high-quality retrievals (Final Algorithm Flags = 0) from 2009 to 2020. The data was accessed from a website (http://disc.sci.gsfc.nasa.gov/giovanni).

AERONET data: AERONET is a well-organized, ground-based robotic network of more than 300 sites around the globe that uses a sky radiometer and sun photometer for aerosol measurements (Holben et al. 1998). The spectral ranges for the direct sun between 340–1020 nm and diffuse sky 440–1020 nm radiances are employed by a sun-photometer to take AERONET measurements. Ramachandran and Sumita (2013) reported that continuous data may be safely obtained from ground-based measurements of various aerosol characteristics over a particular location. In the present study, a level 1.5 sun photometer retrieved from AOD500 data from December 2020 to June 2021 was acquired from

AEROENT. The data was accessed from websites (http://aeronet.gsfc.nasa.gov/).

Data Validation

To validate AOD data retrieved from MODIS-Aqua, MODIS-Terra, and OMI, AERONET-AOD daily data from December 2020 to June 2021 were utilized. Analysis was performed based on data availability. Validation against AERONET and inter-comparison were made with the data of the three satellite sensors except for MISR, which did not have data from December 2020 to June 2021. The data was downloaded from the AERONET website (http://aeronet.gsfc.nasa.gov/). A summary of the sensors' wavelengths, product types, and resolutions is given in Table 1.

Procedure in Data Validation

Validation of satellite-derived AOD involves comparison with ground-based measurements. Such comparison helps in determining uncertainties in satellite measurements and the development of improved algorithms (Cheng et al. 2012). AOD data validation in the period from 2009 to 2020, we compared results obtained from MODIS-Aqua, MODIS-Terra, MISR, and OMI, with AERONET.-Satellite sensors retrieve AOD at different wavelengths: MODIS at 470, 550, and 660 nm, MISR at 446, 558, 667, and 862 nm, and OMI at 342.5, 388.0, 442.0, 463.0, 483.5, and 500.0 nm. For increased accuracy in the validation, the AERONET-based AOD wavelength is interpolated logarithmically to each of the satellite-derived AOD using the Ångström power law. If AOD and Ångström exponent at one wavelength are known, then AOD at a different wavelength can be computed as:

$$\mathrm{AOD_a} = \mathrm{AOD_b}\left(\frac{\mathrm{a}}{\mathrm{b}}\right)^{-\alpha}$$

Variables a and b assume the values 550 nm and 555 nm for MISR and 500 nm (each) for OMI and AERONET, respectively. These wavelength ranges were selected since they are close to the average between the standard wavelengths of various sensors (440 nm to 865 nm).

Statistical Techniques

In this study, after AOD data were retrieved using multi-spectral satellite sensors for 12 years (i.e., 2009 to 2020) a statistical test parameter such as linear regression: intercept, slope, R^2 (determination coefficient), and other statistical parameters such as MBE (mean bias), MAE (mean percentage error), Relative mean bias (RMB) and RMSE (root-mean-square), Mean absolute percentage error (MAPE) (Tripathi et al. 2005, Floutsi et al. 2016). The accuracy of each of the algorithms was further assessed using EE (Remer et al. 2005, Kristjánsson et al. 2014), defined as the confidence envelopes for each of the AOD retrieval algorithms.

The coefficient of the residual mean (CRM), Coefficient of Efficiency (C.E.), and a 1:1 line is required to see whether the regression line falls above, below, or if it crosses this line (Mengistu & Amente 2020). In addition, the Mann-Kendall non-parametric test (Taotao et al. 2016) was used to observe the temporal trends. All the necessary Mann-Kendall test parameters were determined along with Sen's slope using Python programming.

RESULTS AND DISCUSSION

Validation of AOD with AERONET and Intercomparisons of AOD Data of the Satellite Sensors

Validation of MODIS-Aqua, MODIS-Terra, MISR, and OMI over Dire Dawa

Ground-based observations are used to validate satellite aerosol products both globally and regionally. Daily AOD values of the four sensors were compared with ground-based interpolated AERONET-AOD for Dire Dawa during 2020-2021. Fig. 2 shows the regression results between daily-averaged AODs for MODIS-Aqua, MODIS-Terra, and OMI with AERONET at 550 nm.

As observed in Fig. 2, even if the AOD results of all three sensors showed a positive correlation with that of

Table 1: Summary of data sets (Satellite and ground observation) used for the study from 2009 to 2020.

Sensor	Product Type	Parameters	Resolution		Data used	Remark
			Temporal	Spatial		
MODIS-Aqua(550nm)	MYD08D3V6.1	AOD, D.B.	Daily	1°	2009-2020	
MODIS-Terra(550nm)	MOD08D3V6.1	AOD, D.B.	Daily	1°	2009-2020	
MISR (555nm)	MIL3DAEV4	AOD	Daily	0.5°	2009-2017	NDA beyond 2017
OMI (500nm)	OMAERUVdv003	AOD	Daily	1°	2009-2020	
AERONET (500nm)		AOD	Daily	1°	Dec.2020-June2021	NDA before 2020

NDA= No data available

AERONET, the best correlation was observed between MODIS-Terra and AERONET (R^2~ 0.71 for linear fit without intercept and 0.78 (for linear fit with intercept).

The linear fit between MODIS-Aqua and AERONET gave R^2~ 0.52 for both with and without intercept. Besides, all points fell within P.B. of 95% Confidence Interval (CI), and the slopes of all the plots are also close to 1. Tables 2a and 2b show the statistical accuracy of the linearly fitted (with and without intercept) for the three sensors.

As seen in Table 2a, all three sensors showed positive linear correlations with AERONET data. Out of the three, MODIS-Terra exhibited the best correlation with AERONET in terms of R^2 (=0.78), RMSE (0.03), good R^2 and slope, and MBE of 0.02. Overall, the AOD data of this sensor could be taken as the best representation of Dire Dawa AOD. Using curve fit without intercept, MODIS Terra again outperformed the rest since it exhibited the highest R^2 (=0.72) and E.E. (82.2%), good R^2 and slope, MBE close to zero (0.02), and the fit line is close to the 1:1 line with very slight overestimation. Previous research by Levy et al. (2010) identified a calibration problem with the MODIS that would affect AOD time series analysis and reported some difficulties with the satellite-based AOD retrievals over Land. For instance, according to Levy et al. (2013), MODIS tends to overestimate AOD over bright land surfaces, including urban areas, relative to AERONET. In this respect, this paper also shows agreement with their studies since, despite the positive correlation, both MODI sensors showed slight overestimation.

The close agreement of the two fitted lines (with and without intercept) indicates a good correlation between sensors' and AERONET data. Since the air distance between Addis Ababa (location of AERONET data) and Dire Dawa is not greater than 300 km, it is safe to use the AOD of the best sensor (which in this case is MODIS terra) to represent Dire Dawa's AOD.

As shown in Table 2b, by the 1:1 line, all three sensors showed slight overestimation since they are all above the 1:1 line). By CE, MODIS-Aqua was good; MODIS-Terra was satisfactory, and OMI demonstrated poor performance. However, the effectiveness of the model by R^2 and slope was satisfactory and good for both MODIS-Aqua and

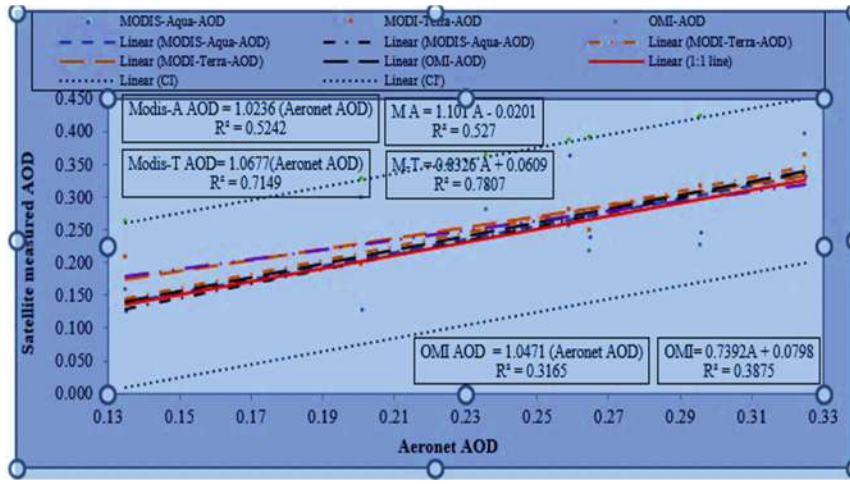

Fig. 2: Validation of AOD data retrieved from MODIS-Aqua, MODIS-Terra, and OMI sensors with AERONET over Dire Dawa. The linear curve fits were made with (right-side equations) and without intercepts (left-side equations).

Table 2a: Statistical parameters, model tendencies, and performance tests of the three AOD regression models over Dire Dawa (linear fits with intercepts).

A vs Sensor	Statistical parameters				Model tendency by			Model performance by				
	R^2	Slope	Intercept	RMSE	CRM	Slope (%)	1:1 line	CE	R^2 & slope	MBE	MAPE (%)	PB
M-A vs A	0.527	1.101	0.020	0.06	CA (-0.02)	OE (10.1)	SOE	G (0.94)	S & G	SOE (0.005)	VG (9)	API
M-T vs A	0.781	0.893	0.061	0.03	CA (-0.08)	UE (10.7)	SOE	S (0.69)	G & G	SOE (0.02)	VG (9.8)	API
OMI vs A	0.388	1.047	0.080	0.05	SUE (0.9)	OE (26.1)	SOE	P (0.04)	S & G	SOE (0.02)	VG (8)	API

A = AERONET, M-A = MODIS-Aqua, M-T = MODOS-Terra, CA = close agreement, SOE= slight overestimation), SUE = slight underestimation, U.E. = underestimation, S = satisfactory, G = Good, P = Poor, VG = very good, P.B. = 95% prediction bound, and API= All points included in P.B. Numbers in brackets under 'slope' represent the percent O.E. or U.E. while the ones under RMSE represent the percent error of AOD.

Table 2b: Statistical parameters, model tendencies, and performance tests of the three AOD regression models over Dire Dawa. (Linear fit without intercept).

A vs Sensor	Statistical parameters				Model tendency by			Model performance by				
	R^2	Slope	EE (%)	RMSE	CRM	Slope (%)	1:1 line	CE	R^2 & slope	MBE	MAPE (%)	PB
M-A vs A	0.52	1.023	71.4	0.06	CA (-0.02)	OE (2.3)	SOE	G (0.94)	S&G	SOE (0.005)	VG (9)	API
M-T vs A	0.72	1.067	82.2	0.03	CA (-0.08)	OE (6.7)	SOE	S (0.69)	G&G	SOE (0.02)	VG (9.8)	API
OMI vs A	0.32	1.047	59.6	0.05	SUE (0.9)	OE (4.7)	SOE	P (0.04)	S&G	SOE (0.02)	VG (8)	API

A = AERONET, M-A = MODIS-Aqua, M-T = MODOS-Terra, CA = close agreement, SOE= slight overestimation), SUE = slight underestimation, U.E. = underestimation, S = satisfactory, G = Good, P = Poor, VG = very good, P.B. = 95% prediction bound, and API= All points included in P.B. Numbers in brackets under 'slope' represent the percent O.E. or U.E. while the ones under RMSE represent the percent error of AOD.

OMI sensors, whereas MODIS-Terra demonstrated good performance for both R^2 and slope. The RMSE statistical test indicator showed values (of 0.06, 0.03, 0.05) that are close to zero, but MODIS Terra exhibited the least value. The E.E. values are all 60% or more. Here again, MODIS-Terra showed a superior value of 82%, followed by MODIS-Aqua. A study by Ashraf (2018) on MODIS, MISR, and AERONET climatology comparison across the Middle East and North Africa showed the performance of MODIS to be similar over the entire region, with ~68% of AOD within the confidence range. In this study, all the points are almost within the confidence interval. Gupta et al. (2018) found that 62.5 and 68.4 % of AODs retrieved from Terra MODIS and Aqua MODIS, respectively, fall within previously published expected error bounds of ± (0.05 + 0.2 × AOD), with the coefficient of determination (R^2) of ≥ 0.5), which is in agreement with this study. In the study by Bibi (2015) where they made intercomparisons of MODIS, MISR, OMI, and validation against AERONET, they obtained results similar to this study. The study of Kazuhisa et al. (2022) revealed that the localized uncertainties, particularly surrounding a humid coastal city, are exacerbated by heterogeneous surface reflectance, mixed aerosol optical characteristics, and strong meteorological variability, and as Dire Dawa is located in such a location this might affect the variation of AOD retrieval among the sensors.

Inter-comparison of MODIS-Aqua, MODIS-Terra, MISR, and OMI

Fig. 3(a) shows the inter-comparisons of data sets retrieved over Dire Dawa by the four sensors from 2009 to 2020.

As shown in Fig. 3a – 3f, the linear curve fits are done with intercepts (dashed lines) and without intercepts (solid lines). Considering the linear curve with intercepts, none (except the fit between MODIS T and OMI) gave even satisfactory correlations, as seen from the R^2 values. However, the slopes can be considered good. The tabular values of model tendencies and performance

Table 3a: Statistical parameters, model tendencies, and performance tests of the three AOD regression models over Dire Dawa for the linear fit with intercept.

Correlation	Statistical parameters				Model tendency by			Model performance by				
	R^2	Slope	Intercept	RMSE	CRM	Slope [%]	1:1 line	MBE	CE	R^2 & slope	MAPE [%]	PB
M-A vs M-T	0.24	0.347	0.148	0.068	UE(0.02)	U.E. (65.3)	Mixed	UE(-0.02)	S (0.38)	P & P	G (19.96)	MPI
M-A vs OMI	0.14	0.335	0.174	0.081	OE(-0.06)	U.E. (66.5)	Mixed	UE(-0.05)	P (-0.15)	P & P	S (30.94)	MPI
M-A vs MISR	0.07	0.238	0.183	0.151	OE(-0.03)	U.E. (76.2)	Mixed	O.E. (0.19)	P (-0.24)	P & P	G (13.79)	MPI
M-T vs OMI	0.33	0.719	0.088	0.060	OE(-0.09)	U.E. (28.1)	Mixed	UE(-0.02)	G (0.95)	S & G	G (19.78)	MPI
M-T vs MISR	0.04	0.299	0.173	0.147	UE(0.2)	U.E. (70.1)	Mixed	OE(0.05)	G (0.93)	P & P	S (21.82)	MPI
OMI vs MISR	0.02	0.156	0.200	0.159	OE(-0.02)	U.E. (84.4)	Mixed	UE(-0.07)	P (-0.88)	P & P	S (24.54)	MPI

M-A = MODIS-Aqua, M-T = MODOS-Terra, SUE = slight underestimation, P.O. = perfect overlap, SO = slight overlap, O.E. = overestimation, SOE = slight overestimation, MPI = most points included in P.B.

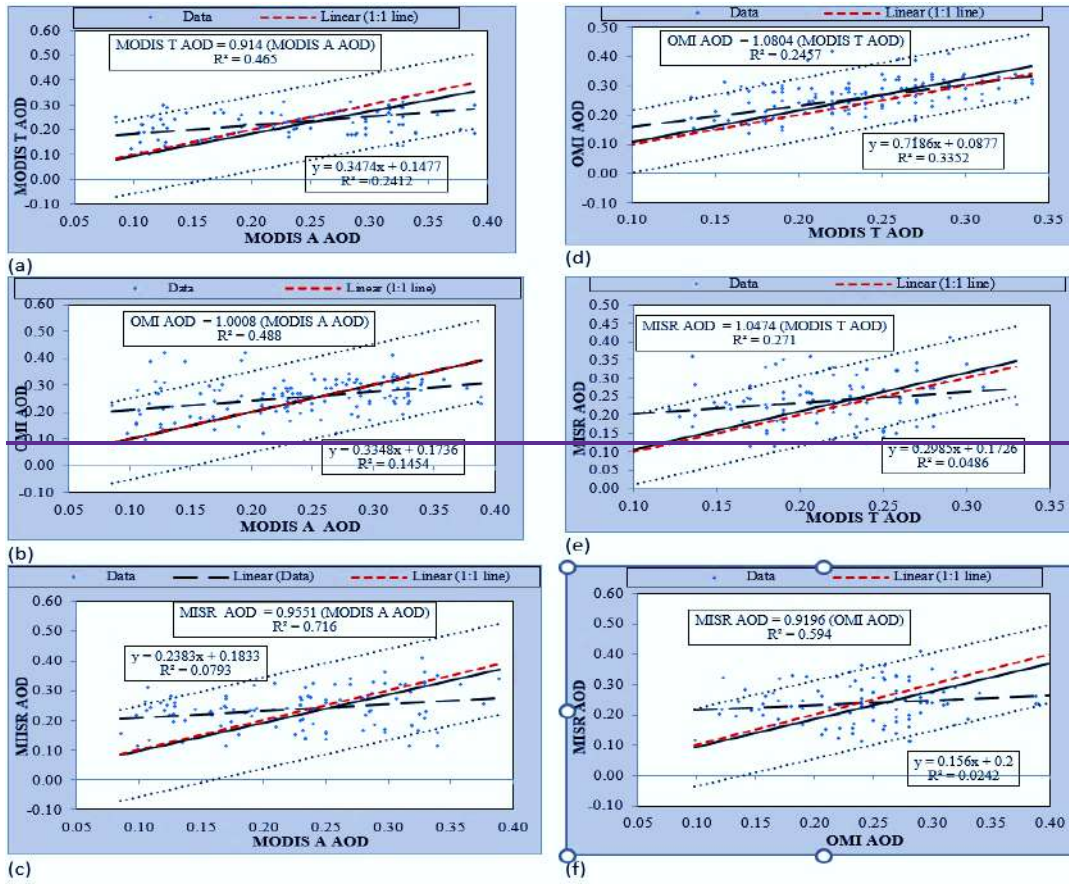

Fig. 3: Comparisons between (a) MODIS-Aqua vs MODIS-Terra, (b) MODIS-Aqua vs OMI, (c) MODIS-Aqua vs MISR, (d) MODIS-Terra vs OMI, (e) MODIS-Terra vs MISR (f) OMI vs MISR. The linear fit equation with and without intercept and coefficient of determination (R^2) are also given.

Table 3b: Statistical parameters, model tendencies, and performance tests of the three AOD regression models over Dire Dawa for fit line without intercept.

Correlation	Statistical parameters			Model tendency by				Model performance by			
	R^2	Slope	RMSE	CRM	Slope [%]	1:1 line	MBE	CE	R^2 & slope	MAPE [%]	PB
M-A vs M-T	0.465	0.914	0.068	UE(0.02)	UE (8.6)	SUE	UE(-0.02)	S (0.38)	S & G	G (19.96)	MPI
M-A vs OMI	0.488	1.001	0.081	OE(-0.06)	O.E. (0.1)	P.O.	UE(-0.05)	P (-0.15)	S & G	S (30.94)	MPI
M-A vs MISR	0.716	0.955	0.151	OE(-0.03)	UE (4.5)	SO	OE (0.19)	P (-0.24)	G & G	G (13.79)	MPI
M-T vs OMI	0.246	1.080	0.060	OE(-0.09)	O.E. (8.0)	O.E.	UE(-0.02)	G (0.95)	P & G	G (19.78)	MPI
M-T vs MISR	0.271	1.047	0.147	UE(0.28)	OE (4.7)	SOE	OE(0.05)	G (0.93)	P & G	S (21.82)	MPI
OMI vs MISR	0.594	0.920	0.159	OE(-0.02)	U.E. (8.0)	SUE	UE(-0.07)	P (-0.88)	S & G	S (24.54)	MPI

M-A = MODIS-Aqua, M-T = MODOS-Terra, SUE = slight underestimation, PO = perfect overlap, SO = slight overlap, OE = overestimation, SOE = slight overestimation, MPI = most points included in PB

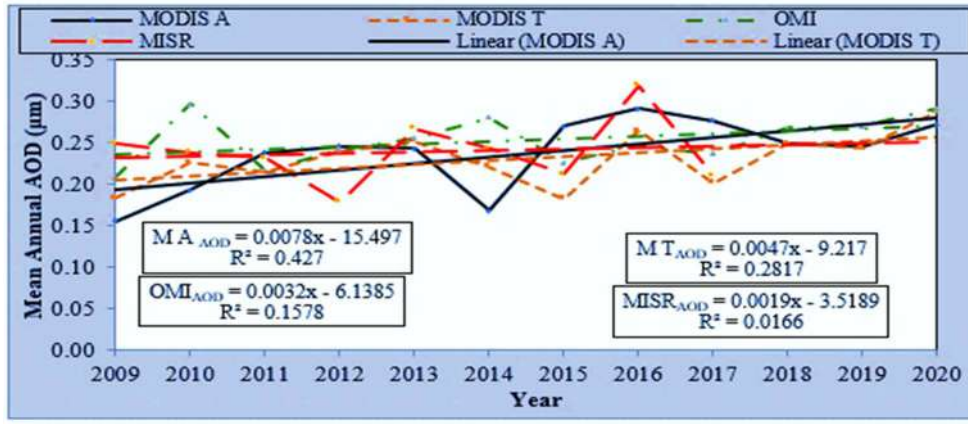

Fig. 4: Annual distribution of AOD retrieved using MODIS-Aqua (M A), MODIS-Terra (M T), OMI, and MISR from 2009 to 2020.

tests for the fitted line with intercept are shown in Table 3a.

The study of Ashraf (2019) revealed that Both MISR and MODIS provide a decent representation of the AOD climatology, in the Middle East and North Africa. Moreover, the study of Kazuhisa et al. (2022) revealed that the localized uncertainties, particularly surrounding a humid coastal city, are exacerbated by heterogeneous surface reflectance, mixed aerosol optical characteristics, and strong meteorological variability. As Dire Dawa is located in such a location, this might affect the variation of AOD retrieval among the sensors.

The fit line without intercept (though not as effective as the one with intercept) can show us the nature of the

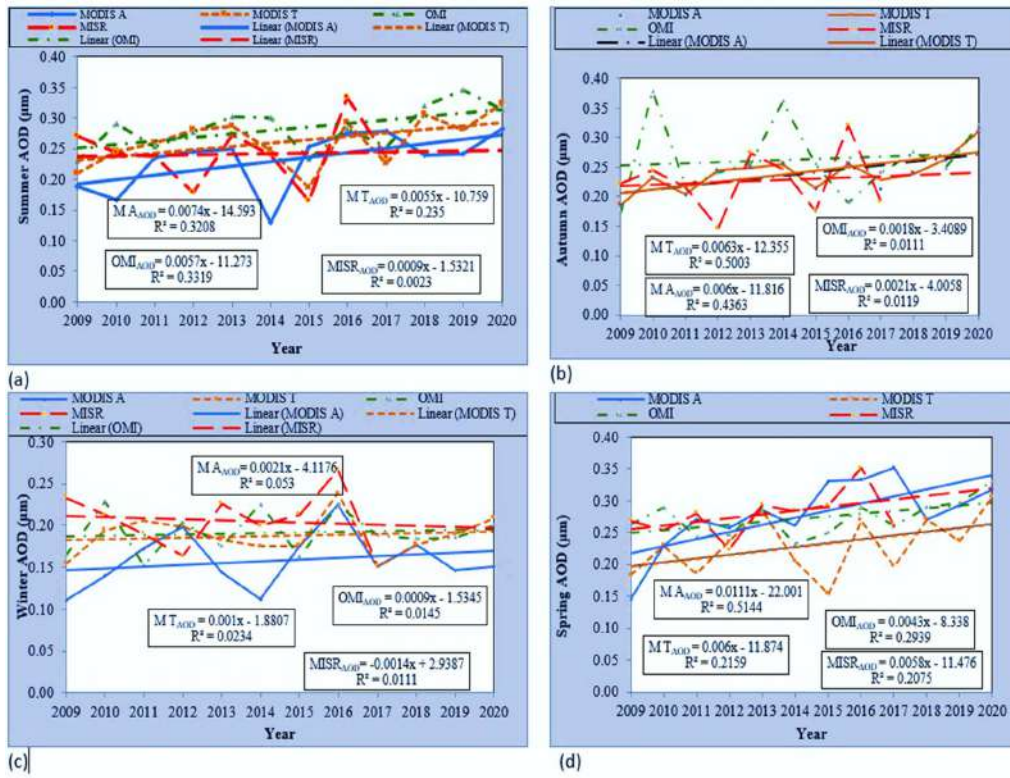

Fig. 5: Seasonal AOD retrieved from MODIS-Aqua, MODIS-Terra, MISR, and OMI in (a) summer, (b) autumn, (c) winter, and (d) spring seasons for the period of 2009 to 2020 over Dire Dawa.

correlations, as shown in Table 3b. In this case, there is no crossing of the fit line and the 1:1 line since the fit line is forced to pass through the origin (0, 0) point. This makes all the slopes within the acceptable limit and four out of the six R^2 values in the satisfactory range. The 95% prediction bound (P.B.) is shown in all the figures for this fit line, indicating most of the data points included within the bound. In this case, best fits were obtained between MODIS-Aqua and MISR AOD. However, this curve fit hides the correct tendency and nature of the correlation between the data points of the sensors.

Trend Analysis of AOD Data

Annual Variability of AOD Over Dire Dawa

The long-term linear AOD trend analysis was made using MODIS-Aqua, MODIS-Terra, OMI, and MISR over Dire Dawa from 2009 to 2020. The results are shown in Fig. 4.

In the figure, all the results revealed linearly increasing trends, though only that of MODIS aqua seems to have a satisfactory positive correlation. Such a positive trend of MODIS aqua exhibits a change in aerosol concentration of approximately 0.78% per year, which is the value of the slope of the MODIS_Terra equation. That of MODIS Terra comes to 0.47% per year. The difference between the two is 0.31%. Taking the value of MODIS terra as a representative for Dire Dawa, it takes around 40 years to double the current value of AOD of 0.20.

Ashraf (2019), in his study of dust-dominated sites in China, observed positive trends between MODIS-Terra, MODIS-Aqua, and MISR, unlike the weak correlations observed in this study. Based on these studies, highly concentrated aerosols in a certain region may indicate the occurrence of secondary particles resulting from industrial and urban pollutants, as well as biomass burning from various agricultural activities. In Dire Dawa, the increasing annual trend is not vivid at this time, perhaps due to the buffering effect of the surroundings or the offsetting effect of one season by another.

Seasonal Variability of AOD Over Dire Dawa

To see the yearly variability of AOD, seasonal differences were determined by dividing the year into four seasons, namely, summer (June - August), autumn (September - November), Winter (December - February), and spring (March-May). Using the data of a specific season and plotting the trends over 12 years helps to visualize the change season-wise. The plots of each season are shown in Figs. 5a-5d.

Three of the four sensors (M A, M T, and OMI) data showed slightly positive AOD trends during the summer season over the twelve years. The linear fits are satisfactory for M A and OMI. This season is one of the rainy seasons for the area and is therefore marked by increased water vapor and cloud cover in the atmosphere. The precipitation cleans the atmosphere and is responsible for reducing the AOD in the air. Despite that, the increase is by 0.74%/y for M A and 0.57%/y for OMI, which is close to the value of M T (0.53%/yr). The increase in AOD concentration over the years for this season may indicate a change in climates, such as a decline in rainfall, or it can be linked with increased urbanization, industrial expansion, and the like. Both MODIS sensors indicated satisfactory increasing trends for autumn, with 0.6%/y for M A and 0.63% for M T. The result, in this case, is close to that of the summer season.

None of the sensors' data depicted any trend in winter. Winter is when the atmosphere is clear (no clouds, no precipitation, and very small water vapor in the atmosphere). The temperature is relatively cooler, and the wind is also calmer. Despite changes such as increased land use/cover over the 12 years, the fact that AOD concentration remained constant during this season over the 12 years indicates that there is something that offsets the increment.

Increasing temperatures cause the local wind to produce thermal variations because of unequal heating, and the temperature difference leads to increased turbulence. The cooler temperature, calmer wind, and the lack of pollens (dormancy time of plants) in the winter decrease the number of aerosol particles that get into the atmosphere. Even the few particles that are airborne experience limited upward movement because of a lack of turbulence in the atmosphere. Besides, these particles take less time to return to the ground. These reasons seem to be the causes for the reduced AOD in the winter.

Almost all of the sensors indicated linearly increasing AOD trends over the 12 years for the spring season. The fits are satisfactory for M A with an increment of 1.11%/y and almost satisfactory for M T with a trend of 0.43%/y. Spring is a windy time and is also known for its short rainy season for Dire Dawa. The wind occasionally covers the city in the form of a dust storm, increasing the number of dust particles in the atmosphere, while the rain does the reverse (cleaning the atmosphere). The increment is, however, attributed to the increasing trend of wind over recent years, especially from the eastern side of the city, carrying with it dust particles picked from arid areas.

The seasonality of AOD is evident and can be connected to the frequent sandstorms that occur in the early spring, as reported by Li et al. (2021). Che et al. (2012) observed minimum AOD concentration in winter. The average AOD during the rainy season (spring and summer) is the largest, according to an analysis of seasonal fluctuations in the four

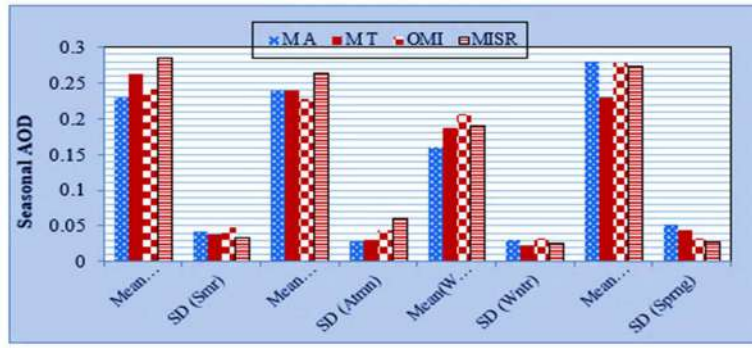

Fig. 6: Twelve-year mean and standard deviations of AOD of the four seasons shown for the four sensors.

Table 4: The summary of AOD trend analysis using the M.K. test and Sen's slope estimator in Dire Dawa from 2009 to 2020.

Sensor	Period P		Mann-Kendall trend test parameters				Decision
			Z	Tau()	Sein's slope		
MODIS-Aqua	Annual		0.019	2.337	0.530	0.008	Trend(increasing)
	Season	Summer	0.024	2.263	0.515	0.007	Trend (increasing)
		Autumn	0.011	2.537	0.576	0.006	Trend(increasing)
		Winter	0.271	1.100	0.258	0.001	No trend
		Spring	0.007	2.674	0.606	0.013	Trend(increasing)
MODIS-Terra	Annual		0.115	1.577	0.364	0.006	No trend
	Season	Summer	0.064	2.537	0.576	1.851	No trend
		Autumn	0.011	2.537	0.576	0.0 059	No trend
		Winter	0.732	0.343	0.091	0.00 075	No trend
		Spring	0.086	1.714	0.394	0.0063	Trend(increasing)
MISR	Annual		0.754	-0.003	-0.313	-0.111	No trend
	Season	Summer	0.602	-0.521	-0.167	-0.001	No trend
		Autumn	0.917	0.104	0.056	0.003	No trend
		Winter	0.754	-0.313	-0.111	-0.003	No trend
		Spring	0.251	1.147	0.333	0.006	No trend
OMI	Annual		0.115	0.005	1.577	0.005	No trend
	Season	Summer	0.054	1.925	0.439	0.006	No trend
		Autumn	0.451	0.754	0.182	0.004	No trend
		Winter	0.837	0.206	0.061	0.002	No trend
		Spring	0.039	2.062	0.470	0.004	Trend(increasing)

periods. This is likely because updrafts emerge as local surfaces warm up. In addition, wind speeds hasten the movement of mobile dunes; the accumulation of upward air and related dust on natural surfaces results in the highest AOD concentrations in the wet season, and low AOD values in winter are due to fewer sandstorms, snowfall, and decreased winter wind and dust activity (Li et al. 2021, Humera et al. 2017). The high AOD in summer is associated with coarse particles, and the lower AOD in Winter is associated with fine particles. The winter season shows low AOD values due to the presence of clouds, so aerosols act as a cloud condensation nucleus along with low wind speed, and therefore, the amount of aerosol dust reduction leads to low AOD values. As reported by Asmarech & Jaya (2021), the main cause of AOD in the winter due to large emissions of smoke and soot due to biomass burning. Biomass burning is also a frequent source of atmospheric pollution and poor air quality (Li et al. 2015).

Even though there are no remarkable differences in AOD among the seasons, the spring season exhibited the highest (0.20 - 0.35) and winter the lowest (0.15 – 0.22). Summer

and autumn had similar AOD concentrations of 0.20 - 0.29 (Fig. 6). As shown in Fig. 6, in terms of seasonal mean OMI recorded (0.284 ± 0.034) in the summer season > MODIS-Aqua (0.28 ± 0.051) observed in spring season > MISR (0.278 ± 0.033) recorded in spring season > MODIS-Terra (0.262 ± 0.039) observed in the summer season. On the other hand, the maximum AOD value was observed in the spring season (0.352) from MODIS-Aqua, and the minimum AOD value was obtained in the winter season (0.011) with the MISR sensor. The study revealed that the AOD values in spring and summer are significantly higher than those in autumn and winter.

During the wet season, due to a higher temperature, soil moisture is evaporated, and heated soil due to high wind velocities, which can increase AOD values, and a higher concentration of water vapors leads to a higher AOD (Alam et al. 2014; Filonchyk et al. 2019). High temperature and humidity are favorable conditions that increase gas to the particle conversion process and the hygroscopic growth of aerosol. In contrast, the low value of AOD in the dry season, particularly the winter season, is caused by the low surface temperature, which results in the weak production of mineral dust derived from the soil surface (Li et al. 2015).

Trend Analysis of AOD Using the Mann-Kendall Trend Test

The M.K. analysis shown in Table 4 is calculated for annual and seasonal AOD trends at a significant level of 0.05 for all four sensors.

As shown in Table 4, by comparing the P-value with alpha (5%). When the P-value is less than 0.05, there is a significant positive AOD trend.

Based on this test, only MODIS-Aqua showed a positive increasing trend in the annual period and during the summer, autumn, and spring seasons. From Sen's slope, the annual magnitude is 0.008 y^{-1} and 0.007, 0.006, and 0.013 per year for the three seasons, respectively. Aside from MODIS aqua, MODIS-terra and OMI showed increasing trends with Sen's slopes of 0.006 and 0.004, respectively. Similarly, the study of Arfan et al. (2017) revealed that the increasing AOD trends (95% statistical significance) are evident in spring (0.009 y^{-1}), summer (0.019 y^{-1}), and autumn (0.005 y^{-1}), but not in winter (0.003 y^{1}). As shown in Table 4 above, it is observed that increasing AOD trend values were observed during the wet season (spring and summer), and this is due to the increase in convective activities that enhance wind speed and surface temperature. The speed of wind initiated and facilitated the movement of copious amounts of soil dust aerosols into the atmosphere from the surface of dry ground of the arid and semi-arid regions, as reported by Asmarech & Jaya (2021) in their study on AOD over selected areas of Northern Ethiopia. The study of Oluwasinaayomi et al. (2018) revealed that in Dire

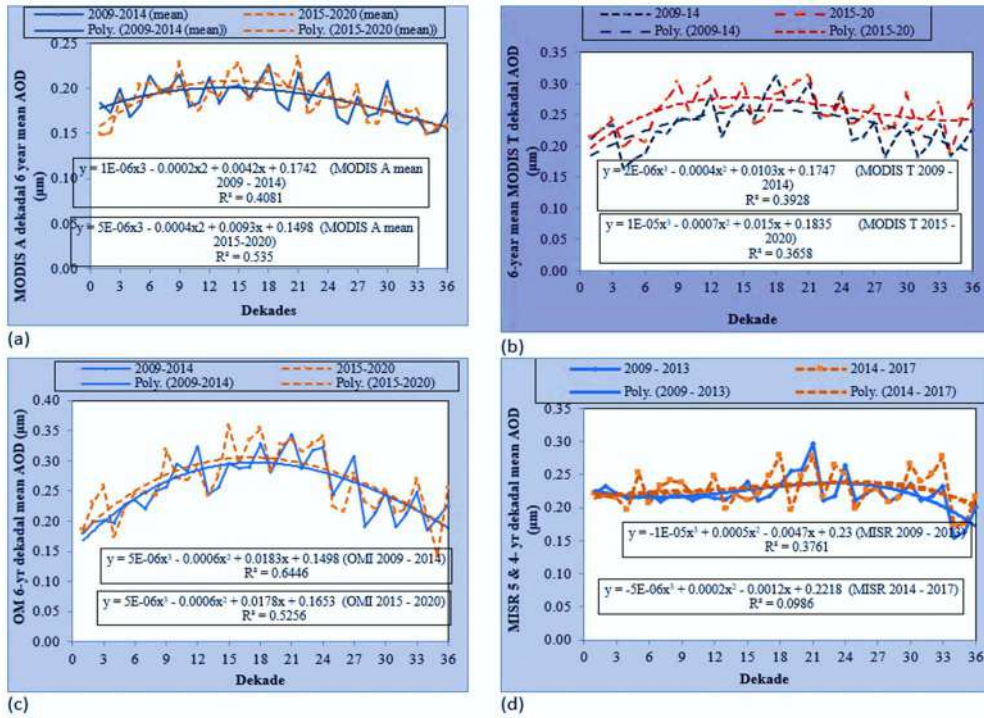

Fig. 7: AOD means decadal distribution retrieved using (a) MODIS-Aqua, (b) MODIS-Terra, (c) MISR (d) OMI from 2009 to 2020 over Dire Dawa.

Table 5: Mean monthly and standard deviation from 2009 to 2020 over Dire Dawa.

Sensor	Monthly mean AOD values											
	Sept.	Oct.	Nov	Dec.	Jan.	Feb	March	April	May	June	July	Aug.
MODIS-A	0.259±0.05	0.226±0.04	0.212±0.05	0.158±0.05	0.134±0.03	0.183±0.03	0.28±0.05	0.28±0.06	0.277±0.05	0.245±0.07	0.291±0.05	0.297±0.05
MODIS-T	0.253±0.03	0.233±0.04	0.234±0.03	0.234±0.03	0.14±0.03	0.188±0.03	0.224±0.04	0.248±0.04	0.218±0.04	0.26±0.04	0.262±0.04	0.265±0.04
OMI	0.277±0.04	0.279±0.06	0.235±0.09	0.212±0.04	0.144±0.03	0.219±0.05	0.263±0.04	0.283±0.03	0.273±0.03	0.273±0.04	0.293±0.05	0.285±0.03
MISR	0.219±0.06	0.224±0.04	0.236±0.05	0.18±0.04	0.222±0.05	0.218±0.05	0.305±0.02	0.300±0.05	0.217±0.05	0.241±0.07	0.257±0.04	0.247±0.06

Dawa, the poor air quality outcomes are further compounded by rural-urban migration, increasing population, poor land use planning and management, poverty, soil degradation, loss of vegetation cover, expansion of informal settlement, and inadequate waste management system.

Dekadal Trend of AOD over Dire Dawa from 2009 to 2020

At first, an attempt was made to see the variability of AOD every ten days throughout 2009 – 2020. Then, we found that trends were identical for 2009–2014 and 2015 -2020. Thus, we divided the period into two parts and analyzed the trends as shown in Fig. 4a – 4d. In the first period (2009-2014), MISR data from 2009-2013 were included. During the second period (2015 to 2020), MISR data was incomplete and thus excluded.

The 12 years were divided into two because there is a kind of cyclic behavior. Since there are three decades in a month, a total of 36 decades were considered for the six years. The plots of the two six years were done on the same axes for curve fitting purposes and to see changes that have taken place over the 12 years. The peaks of both curves occurred around the 18^{th} decade (3^{rd} year). In all four curves, the minimum occurred at the beginning and the end of the 6^{th} year. That means the minimum occurred in 2009, 2015, and 2020. The maximum occurred in 2011 and 2017. The maximum AOD was around 0.21 for MODIS aqua, 0.28 for MODIS terra, 0.30 for OMI, and 0.23 for MISR. OMI and MODIS terra showed a higher range of 0.17 – 0.28, while MODIS aqua and MISR exhibited similar ranges of 0.18 – 0.23. This reveals that the results of all four sensors are close to each other as far as AOD data is concerned.

As illustrated in Fig.7, MODIS-Terra AOD showed an increment from the first 6 years (2009 – 2014) to the second six years (2015 – 2020). This shows changes in Dire Dawa in terms of urbanization, land use/land cover, and climate change, such as an increase in temperature or reduction of rainfall. Such change was not observed with MODIS –Aqua AOD. OMI exhibited a very subdued change. MISR did not clearly show such a change, perhaps due to incomplete data, sensor retrieval performance, and surface reflectance. The cause could be linked to meteorological phenomena such as abundant rainfall (for the low times) and dry periods for the high AOD times. Besides, the sand particles in the desert areas and dust on bare surfaces increase the amount of particulate matter in the atmosphere. On a large scale, this leads to maximum AOD values.

Mean Monthly Distribution of AOD

Mean monthly AOD concentrations were obtained from the daily data. In this study, the mean AOD for the 12 months from 2009 to 2020 was processed in a unified manner, and the

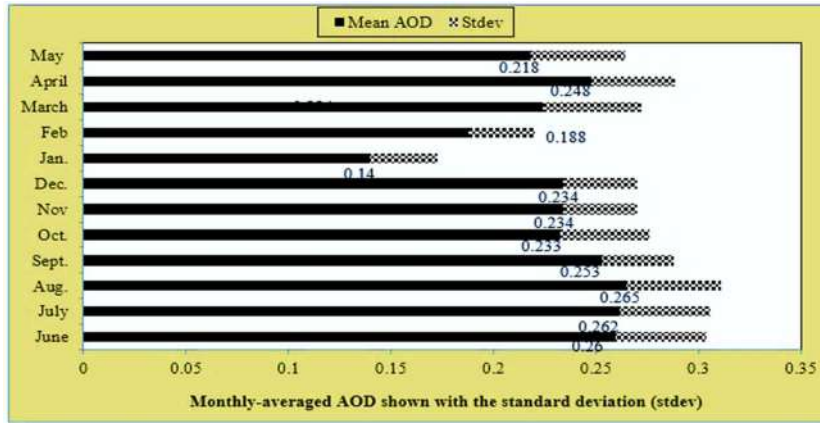

Fig. 8: Monthly-averaged MODIS-terra AOD of Dire Dawa for 2009 -2020 shown with the standard deviation (stdev).

results are shown in Table 5. The result shows that the AOD value retrieved using the MODIS-Aqua, MODIS-Terra, MISR, and OMI ranged from 0.14 to 0.305. As shown in Table 5, the mean monthly AOD was in the range of 0.134 – 0.297 for MODIS-Aqua, 0.14–0.265 for MODIS –Terra, 0.144 – 0.293 for OMI and 0.18 – 0.305 for MISR sensor. Since MODIS-terra represents Dire Dawa AOD better than the other sensors, the monthly-averaged AOD of this sensor is shown for all the months in Fig. 8.

Fig 8 shows that in the spring season (MAM) and summer season (JJA), AOD distribution recorded relatively higher values than the rest of the months. September, April, and August months exhibited higher AODs, while January exhibited the least. The variability within each month seems to be proportional to the mean AOD itself since the standard deviations were higher when mean AODs were higher and lower when the mean AODs were lower (e.g., January and February). One possibility why AOD is highest in August has something to do with more water vapor in the atmosphere, which is to be expected since these are the times when the dust and black cloud events occur in the region. Since aerosol particles serve as nucleation centers for condensation, the more the condensation, the more the aerosol particles are trapped in water vapors.

On the contrary, in January, there is very low water vapor in the atmosphere, resulting in less AOD. The monthly mean values of (MODIS) aerosol optical depth (AOD) at 550 nm examined by Marey et al. (2011) on aerosol climatology over the Nile Delta based on MODIS, MISR, and OMI sensors showed significant monthly variability of AOD to be maximum in April or May (~0.5) and a minimum in December and January (~0.2). Similarly, in the study made by Asmarech and Jaya (2021), the monthly mean seasonal variations of AOD show a maximum value in (June, July, and August). A minimum value in (December, January, and February) in their study on AOD variability over the Northern part of Ethiopia and Djibouti using MODIS sensor. The study further revealed that the aerosol distribution over Ethiopia is highly variable spatially and temporally.

CONCLUSIONS

The comparison of AOD with AERONET indicated that all three sensors showed a positive linear correlation with AERONET data, but MODIS-Terra exhibited the best representation. The inter-comparisons of AOD retrieved from multi-spectral satellite sensor show that the linear curve with intercept, none (except the fit between MODIS Terra and OMI) gave even satisfactory correlations as seen from the R^2 values. From the linear curve fit without intercept, MODIS-Aqua and MISR AOD revealed better correlations. This cross-comparison of several sensors is occasionally required since bias and mistakes in retrieval methods are present because of instrument calibration, sampling, and algorithm correctness.

Out of the annual trends of the four sensors, only the one with MODIS-aqua showed a satisfactory increasing linear trend. Season-wise, MODIS-aqua and OMI exhibited satisfactory increasing linear trends in summer, autumn, and spring. No trend was observed in winter. This shows that the seasonal data give better information about the AOD trend of the area than the annual. The three seasons exhibited almost similar AOD values, while the winter season showed the least. The month of lowest AOD was January, whereas August was the highest, and there seems to be a link between AOD and the amount of water vapor in the atmosphere. As far as decadal AOD is concerned, MODIS-terra (which best represents AOD over Dire Dawa) revealed the difference between the years 2009-2014 and 2015-2020 (increasing trend). Overall, the study shows an increasing AOD trend over Dire Dawa during the 12 years (2009 - 2020). This study

further concludes that MODIS-Terra can be a suitable sensor for AOD data retrieval over bright surfaces & semi-arid areas in Dire Dawa, Ethiopia. The AOD values were observed to be higher in summer (June to August) than during the rest of the months due to the predominance of coarse dust and sea salt particles and possibly also due to the higher water vapor content of the atmosphere due to high summer temperatures, which encourages the growth of aerosols.

Additionally, it was observed that significant AOD levels occurred in October, which may be related to crop harvesting and the ensuing plumes from biomass burning. From January through April, the AOD rises, then falls until December, and April is the month with the highest AOD. The springtime and summertime dust aerosols might be associated with the major contributors to AOD variations in addition to high meteorological parameters variability (wind speed, temperature, rainfall, relative humidity, etc.) and emissions from biomass burning, vehicles, and factories. This study also revealed that the deterioration of the air environment was more prominent and severe. The study's findings are significant in that they serve as a guide for satellite retrieval end users on which airborne over a specific geographic area and AOD range, sensors might offer accurate data. Satellite data such as MODIS, MISR, and OMI provide useful complementary information to investigate the optical and physical characteristics of aerosol.

The AOD collected over Dire Dawa showed notable discrepancies in aerosol variations and trends, which may be related to dust emissions, biomass burning, fossil fuel combustion, and socioeconomic practices. By lowering the burden of disease linked to air pollution and assisting in the short and long-term mitigation of climate change, policies to reduce air pollution offer a win-win strategy for both climate and health. In the past, satellite remote sensing of air quality was largely limited to monitoring at low temporal resolution (e.g., monthly). Advances in satellite sensors and modeling techniques enable shifts in research direction toward operational monitoring and forecasts of air quality and incorporation of multiple data sources to improve monitoring and forecast skills. These efforts will, consequently, improve our responses to public health problems and broader intercountry issues on air pollution. Moreover, this provides tangible information that can be helpful for policymakers, urban air quality monitors, communities, researchers, and all other stakeholders concerned with preventing and monitoring air quality. Therefore, these studies have important implications for climate systems and take a mitigation approach to monitor air quality over urban regions.

Further work is required to quantitatively understand the contributing factors from a natural and anthropogenic source responsible for AOD variability so that regulations can target specific factors of high priority/importance. These studies also provide us with more specific information about the functionality of particular sensors at the local and regional levels. The study also strongly recommends making use of a synergy of remote sensing and ground-installed devices, such as sun photometers, to monitor the status of air quality on a daily, decadal, monthly, annual, and seasonal basis over polluted urban areas.

ACKNOWLEDGMENT

We would also like to express our gratitude to NASA for providing MODIS, MISR, and OMI aerosol products, all of which are available from the GES DISC at NASA Goddard. Finally, the authors would like to express their sincere gratitude to the Center of Environmental Sciences at Addis Abeba University for providing the remote sensing equipment and training that helped to better complete this study.

REFERENCES

Ahn, C.O., Torres, O. and Jethva, H. 2014. Assessment of OMI near-UV aerosol optical depth over land. J. Geophys. Res.Atmos., 119: 2457-2473. doi:10.1002/2013JD020188.

Alam, K., Khan, R., Ali, S., Ajmal, M., Khan, G., Muhammad, W. and Ali, M. 2014. Variability of aerosol optical depth over Swat in Northern Pakistan based on satellite data. Arab. J. Geosci., 8(1); 547-555.

Ashraf, F. 2019. Comparative analysis of MODIS, MISR, and AERONET climatology over the Middle East and North Africa, Ann. Geophys., 37: 49–64. https://doi.org/10.5194/angeo-37-49.

Ashraf, F. 2018. Comparative analysis of MODIS, MISR, and AERONET climatology over the Middle East and North Africa. Ann. Geophys. Discuss., 1: 79. https://doi.org/10.5194/angeo-2018-79

Asmarech, E. and Jaya, P.R. 2021. Daily and seasonal variation of aerosol optical depth and angstrom exponent over Ethiopia using MODIS Data. Pollution, 8(1): 315-329. DOI: 10.22059/POLL.2021.316010.971.

Badarinath, K.V.S, Goto, D., Kharol, S.K., Mahalakshmi, D.V., Sharma, A.R. and Nakajima, T. 2011. Influence of natural and anthropogenic emissions on aerosol optical properties over a tropical urban site. Atmos. Res., 100: 111-120.https://doi.org/10.1016/j.atmosres.2011.01.003.

Belachew, M. and Zeleke, D.A. 2015. Statistical analysis of road traffic car accident in Dire Dawa Administrative City, Eastern Ethiopia. Sci. J. Appl. Math. Stat., 3(6): 250-256.

Bibi, M. 2015. Intercomparison of MODIS, MISR, OMI, and CALIPSO aerosol optical depth retrievals for four locations on the Indo-Gangetic plains and validation against AERONET data. Atmos. Environ., 111: 113-126.

Che H., Wang Y., Sun J. Zhang X., Zhang X. and Guo J. 2012.Variation of aerosol optical properties over Taklimakan Desert of China.Aerosol and Air Quality Research, 13(2): 777-785. DOI 10.4209/aaqr.2012.07.0200.

Cheng, T., Chen, H., Gu, X., Yu, T., Guo, J. and Guo, H. 2012. The inter-comparison of MODIS, MISR, and GOCART aerosol products against AERONET data over China. J. Quant. Spectrosc. Radiat. Transf., 113: 2135-2145. http://dx.doi.org/10.1016/j.jqsrt.2012.06.016.

Eck, T.F., Holben, B.N., Reid, J.S., Sinyuk, A., Dubovik, O., Smirnov, A., Giles, D., O'Neill, N.T., Tsay, S.C., Ji, Q., Al Mandoos, A., Ramzan Khan, M., Reid, E.A., Schafer, J.S., Sorokine, M., Newcomb, W.

and Slutsker, I. 2008. Spatial and temporal variability of column-integrated aerosol optical properties in the southern Arabian Gulf and United Arab Emirates in summer. J. Geophys Res., 113: 01204. doi:10.1029/2007JD008944.

Filonchyk, M., Yan, H., Zhang, Z., Yang, S., Li, W. and Li, Y. 2019. Combined use of satellite and surface observations to study aerosol optical depth in different regions of China. Sci. Rep., 9: 66-74, http://doi.org/10.1038/s41598-019-42466-6.

Floutsi, A.A., Korras-Carraca, M.B., Matsoukas, C., Hatzianastassiou, N., Biskos, G. 2016. Climatology and trends of aerosol optical depth over the Mediterranean basin during the last 12years (20022014) based on Collection 006 MODIS-Aqua data. Science of The Total Environment, 551-552: 292303. doi:10.1016/j.scitotenv.2016.01.192

Ge, J.M., Huang, J.P., Su, J., Bi, J.R. and Fu, Q. 2011. Short wave radiative closure experiment and direct forcing of dust aerosol over northwestern China. Geophys. Res. Lett., 38: 4975. https://doi.org/10.1029/2011GL049571

Gezahegn, B. T., Elias, F.M. and Aklile, A.E. 2021. Trends in daily temperature and precipitation extremes over Dire-Dawa, 1980-2018. J. Environ. Earth Sci., 11(9): 45-76.

Gupta P., Lorraine A., Remer, Robert C., Levy, and Shana M. 2018. Validation of MODIS 3 km land aerosol optical depth from NASA's EOS Terra and Aqua missions. Atmos. Meas. Tech., 11: 31453159. https://doi.org/10.5194/amt-11-3145-2018

Holben, B., Eck, T., Slutsker, I., Tanré, D., Buis, J., Setzer, A., Vermote, E., Reagan, J., Kaufman, Y., Nakajima, T., Lavenu, F., Jankowiak, I. and Smirnov, A. 1998. AERONET – A federated instrument network and data archive for aerosol characterization. Remote Sens. Environ., 66: 1-16.

Hsu, N.C., Jeong, M.J., Bettenhausen, C., Sayer, A.M., Hansell, R., Seftor, C.S., Huang, J. and Tsay, S.C. 2013. Enhanced deep blue aerosol retrieval algorithm: The second generation. J. Geophys. Res. Atmos., 118: 9296-9315.

Humera, B., Khan, A., Farrukh, C., Samina, B., Imran, S. and Thomas, B. 2017. Intercomparison of MODIS, MISR, OMI, and CALIPSO aerosol optical depth retrievals for four locations on the Indo-Gangetic plains and validation against AERONET data. Atmos. Environ., 11: 113-126. http://dx.doi.org/10.1016/j.atmosenv.2015.04.013.

IPCC. 2013. Contribution of Working Group I to the Fifth 4 Assessment Report of the Intergovernmental Panel on Climate Change. In Stocker, T.F., Qin, D., Plattner, G.K., Tignor, M., Allen, S.K., Boschung, J., Nauels, A., Xia, Y., Bex, V. and Midgley, P.M. (eds), Climate Change 2013: The Physical Science Basis, Cambridge University Press, Cambridge, UK and New York, NY, pp. 15324-15335. https://doi.org/10.1017/CBO9781107415324.

Jung, J., Souri, A.H., Wong, D.C., Lee, S., Jeon, W., Kim, J. and Choi, Y. 2019. The impact of the direct effect of aerosols on meteorology and air quality using aerosol optical depth assimilation during the KORUS AQ campaign. J. Geophys. Res. Atmos., 124: 8303-8319. https://doi.org/10.1029/2019JD030641.

Kazuhisa, T., Hiroshi, M., Tadahiro, H. and Mayumi, Y. 2022. Aerosol Optical Properties of Extreme Global Wildfires and Estimated Radiative Forcing with GCOM-C SGLI, Egusphere, https://doi.org/10.5194/egusphere-2022-21.

Knife, M. 2017.Evaluation of air pollutant levels in Dire-Dawa City, Ethiopia. Int. J. Environ. Sci. Nat. Resour., 7(3): 555711.

Kristjánsson, J.E., Muri, H., Boucher, O., Huneeus, N., Kravitz, B. and Robock, A. 2014. J. Geophys. Res. Atmos., 119: 1-17. http://dx.doi.org/10.1002/2013JD021060.

Levelt, P.F., Hilsenrath, E., Leppelmeier, G.W., van den Oord, G.H.J., Bhartia, P.K., Taminnen, J., de Haan, J.F. and Veefkind, J.P. 2006. Science objectives of the ozone monitoring instrument. IEEE Trans. Geosci. Remote Sens., 44(5): 1093-1101.

Levy, R.C., Remer, L.A., Kleidman, R.G., Mattoo, S., Ichoku, C., Kahn, R. and Eck, T.R. 2010. Global evaluation of the collection of 5 MODIS dark-target aerosol products over land. Atmos. Chem. Phys., 10: 10399-10420. doi:10.5194/acp-10-10399-201.

Levy, R.C., Mattoo, S., Munchak, L.A., Remer, L.A., Sayer, A.M., Patadia, F. and Hsu, N.C. 2013. The Collection 6 MODIS aerosol products over Land and ocean. Atmos. Meas. Tech., 6: 2989-3034. https://doi.org/10.5194/amt-6-2989-2013.

Li, J., Ge, X., He, Q. and Abbas, A. 2021. Aerosol optical depth (AOD): Spatial and temporal variations and association with meteorological covariates in Taklimakan desert, China. Peer J., 9: e10542. DOI 10.7717/peerj.10542.

Li, S., Wang, T., Xie, M., Han, Y. and Zhuang, B. 2015. Observed aerosol optical depth and angstrom exponent in the urban area of Nanjing, China. J. Atmos. Environ., 123: 350-356.

Marey, H.S., Gille, J.C., El-Askary, H.M., Shalaby, E.A. and El-Raey, M.E. 2011. Aerosol climatology over the Nile Delta based on MODIS, MISR, and OMI satellite data. Atmos. Chem. Phys., 11: 10637-10648, doi:10.5194/acp-11-10637.

Martonchik, J.V., Diner, D.J., Kahn, R.A., Ackerman, T.P., Verstraete, M.M., Pinty, B. and Gordon, H.R. 2002. Techniques for the retrieval of aerosol properties over land and ocean using multiangle imaging. Geosci. Remote Sens. IEEE Trans., 36: 1212-1227.

Mengistu, A. and Amente, M. 2020. Reformulating and testing Temesgen: Melesse's temperature-based evapotranspiration estimation method. Heliyon, 6: 02954. https://doi.org/10.1016/j.heliyon.2019.e02954.

Oluwasinaayomi, F.K., Muluneh, W., Abshare, M. and Samuel Babatunde, A. 2018. Analysis of air quality in Dire Dawa, Ethiopia. J. Air Waste Manag. Assoc., 68(8): 801-811. https://doi.org/10.1080/10962247.2017.1413020.

Ramachandran, M. and Sumita, G. 2013. Aerosol optical properties over South Asia from ground-based observations and remote sensing: A review. Climate, 1: 84-119; doi:10.3390/cli1030084 Open Acess.

Ramanathan, V., Crutzen, P. J., Kiehl, T. and Rosenfeld, D. 2001. Aerosols, climate, and the hydrologic cycle. Science, 294: 2119-2124.

Remer, L.A., Kaufman, Y.J., Tanré, D., Mattoo, S., Chu, D.A., Martins, J.V., Li, R.R., Ichoku, C., Levy, R.C., Kleidman, R.G., Eck, T.F., Vermote, E. and Holben, B.N. 2005. The MODIS aerosol algorithm, products, and validation. J. Atmos. Sci., 62: 947-973. http://dx.doi.org/10.1175/JAS3385.1.

Rosenfeld, D., Dai, J., Yu, X., Yao, Z., Xu, X., Yang, X. and Du, C. 2007. Inverse relations between amounts of air pollution and orographic precipitation. Science, 315: 1396. https://doi.org/10.1126/science.1137949PMID:17347436.

Taotao, C., Guimin, X., Lloyd, T. Wilson, W. and Daocai, C. 2016. Trend and cycle analysis of annual and seasonal precipitation in Liaoning, China. Adv. Meteorol., 70: 563. http://dx.doi.org/10.1155/2016/5170563.

Tripathi, S. N., Dey, S., Chandel, A., Srivastava, S., Singh, R. P., and Holben, B. N. 2005. Comparison of MODIS and AERONET derived aerosol optical depth over the Ganga Basin, India, Ann. Geophys., 23: 10931101, https://doi.org/10.5194/angeo-23-1093-2005.

Wang, S., Cohen, J.B., Lin, C. and Deng, W, 2020. Constraining the relationships between aerosol height, aerosol optical depth, and total column trace gas measurements using remote sensing and models. Atmos. Chem. Phys., 20(23): 15401-15426. https://doi.org/10.5194/acp-20-15401.

Weizhi, D., Jason Blake, C., Shuo, W. and Chuyong, L. 2021. Improving the understanding between climate variability and observed extremes of global NO_2 over the past 15 years. Environ. Res. Lett., 16(5): 054020. https://doi.org/10.1088/1748-9326/abd502.

ORCID DETAILS OF THE AUTHORS

Teshager Argaw Endale: https://orcid.org/0000-0003-0117-358X

Nature Environment and Pollution Technology
An International Quarterly Scientific Journal

p-ISSN: 0972-6268
(Print copies up to 2016)
e-ISSN: 2395-3454

Vol. 23 | No. 1 | pp. 17-32 | 2024

Original Research Paper

https://doi.org/10.46488/NEPT.2024.v23i01.002

Open Access Journal

Effects of Glyphosate on the Environment and Human Health

L. A. García-Villanueva*†, V. H. Cuapio-Ortega*, I. Y. Henández-Paniagua, G. Fernández-Villagómez*, J. Rodrigo-Ilarri***, M. E. Rodrigo-Clavero***, G. L. Andraca-Ayala**, G. B. Hernández-Cruz* and S. Banda-Santamaría***

*Engineering Faculty, UNAM, Civil Engineering and Geomatics Division, Department of Sanitary and Environmental Engineering, Ciudad de México, México

**Institute of Atmospheric Sciences and Climate Change, UNAM, Department of Environmental Sciences, Ciudad de México, México

***Instituto de Ingeniería del Agua y Medio Ambiente (IIAMA), Universitat Politècnica de València (UPV), Spain

†Corresponding author: L.A. García-Villanueva; lagvillanueva@ingenieria.unam.edu

Nat. Env. & Poll. Tech.
Website: www.neptjournal.com

Received: 21-06-2023
Revised: 25-07-2023
Accepted: 03-08-2023

Key Words:
Glyphosate
Pesticide
Human health
Toxicity

ABSTRACT

Glyphosate is a herbicide of a wide spectrum that alters the production of amino acids in plants, leading to their death. Due to its properties, it is used to eliminate weeds that interfere with human activity. The intensive use of this herbicide in the past decades has led to its frequent encounter in the environment as it has been detected in water, animals, and food destined for human consumption. Its impact on human health and the rest of living organisms has not been fully explored, given that many authors enter into contradictions with one another, specifically surrounding the role of surfactants in the commercial presentation of herbicides. The use of pesticides can have significant impacts on ecosystems, threatening bio-cultural diversity due to genetic contamination from transgenic crops. The effectiveness of Glyphosate-based herbicides in weed control is diminishing due to weed tolerance. However, the use of herbicides remains prevalent in large-scale crops due to the challenges of organic food production. In addition, the probable conflict of interest by the agrochemical industry does not bring a full picture with respect to the actions that world governments should take. Banning GLP-based herbicides may lead to the use of other pesticides, in which the long-term impacts will require further studies. The motivation for this research is the review of the latest advances of glyphosate in the world, considering the use and prohibitions of this herbicide, its interaction with water and soil, as well as the effects on both the environment and health. The search for information for this paper was carried out in the Mendeley, Elsevier, and Springer databases by filtering by the suitable keywords.

INTRODUCTION

Glyphosate (GLP) is currently the most used herbicide worldwide (Singh et al. 2020, Martins-Gomes et al. 2022). It was patented in 1970 by the Monsanto company, and since 1974, it has started to be commercialized as an active ingredient of the product Roundup®. This formula has been tested in more than 100 crops and more than 130 countries (Cruz 2013). It is a non-selective herbicide of a wide range (which means that it can be used in any crop that can tolerate it) and is post-emergent, of which its chemical formula is $C_3H_8NO_5P$, it is a weak organic acid, consisting of a glycine molecule and a phosphonomethyl molecule (MamaCoca 2000). The yearly sales of GLP represent 11% of the total agrochemical products worldwide. It is found in 750 commercial presentations, and its use has increased since the introduction of GMOs and the patent release in 2000 (CIBIOGEM 2019).

PATHWAYS OF TRANSFORMATION, LOCATION, AND EXPOSURE

Transgenic Crops and Their Role in the Use of Glyphosate-Based Herbicides

The herbicidal activity of GLP is based on its capacity to block the pathway of the enzyme Shikimato (a common route to biosynthesize aromatic compounds primarily in bacteria and plants) by inhibiting the enzyme 5-enolpyruvylshikimate-3-phosphate synthase (EPSPS). Due to the inexistence of these amino acids, the synthesis of proteins in vegetable cells stops, ceasing its growth, which leads to its death (CIBIOGEM 2019).

Transgenic crops are defined by the transfer of foreign genes of animal, vegetable, microbial, or viral origin to cultivated plant species (Chaparro 2011). The bacteria

Agrobacterium tumefaciens has been used to confer the gene that gives the crop tolerance to GLP, codifying an enzyme (EPSPS) that is not affected by the herbicide (Villalba 2009). The use of GMOs is widely spreading around the world, and their use puts their wild predecessors at risk of "transgenic contamination" through the spread of genetic material via pollination (Ribeiro 2020). For example, in Argentina, practically 100% of soy, 100% of cotton, and up to 98% of corn that gets cultivated on a yearly basis is a product of transgenic crops (ArgenBio 2021). Mexico imports more than one-third of its national corn consumption, and this comes primarily from the United States, a country in which more than 40% of the crops coming from this grain are of transgenic origin (Ribeiro 2020). In Uruguay, almost 100% of soy crops make use of RR (Roundup Ready) soy seeds, those of which contain a gene of the *Agrobacterium* sp. A bacteria that brings forth GLP resistance. In the United States, at least 50% of corn and cotton seeds and approximately 80% of canola seeds contain transgenic RNA (Ribeiro 2020).

The sum of these two factors, together with the demand of the population and industry, as well as the unrelenting interest of medium and large companies to increase production in order to supply the necessary crops on a global scale, has encouraged the excessive use of herbicides as a common practice in the development and production of large-scale agriculture. This is without considering the potential for long-term environmental and health damage.

Glyphosate Transport and Interaction in Soil

GLP shows a high potential for soil adsorption, therefore restricting its transport in the soil (Gandhi et al. 2021). Recent studies state that the sorption capacity of GLP is quite higher than that of other pesticides, reducing the risk of leaching (Hagner et al. 2015). Consequently, significant amounts of GLP residues have been found in soil samples, as indicated by (Aparicio et al. 2013, Gunarathna et al. 2018).

A global analysis using a large dataset from different countries shows that residues of GLP and its degradation product aminomethylphosphonic acid (AMPA) have been found on the soil surface (30 cm) and in the root zone (30-100 cm). The observed GLP residues' concentration can be correlated with the annual doses of application. (Maggi et al. 2020).

Despite the information previously stated, (Kremer & Means 2009) does not discard the possibility of GLP lixiviation; this is due to the fact that the herbicide is applied with a mix of fertilizers that may contain phosphorus, which may compete with GLP molecules during the adsorption in soils leaving GLP available for lixiviation.

In addition, (Hernández 2019) indicates that an increase in pH leads to an increase of the negative charges present in both the soil and GLP molecule, which encourages electrostatic repulsion, making the molecule prone to lixiviation.

For this reason, it is important to understand the processes involved in the potential pathways of dispersion of this contaminant where it causes adverse effects on any natural system. Studies of GLP leaching and impact are being developed in Mexico and other countries to propose control and management solutions.

Glyphosate Transport and Interaction in Water

In general, the surface water in agricultural areas is more susceptible to agrochemical contamination through surface run-off, direct overspray, and spray drift (Lutri et al. 2020, Cruz 2013). Groundwater pollution with herbicides is generally lower in groundwater reservoirs than in surface water reservoirs due to degradation in the unsaturated zone (Mueller & Senseman 2015). Nevertheless, several studies have demonstrated the potential for leaching and vertical transport to groundwater (Lupi et al. 2015, Okada et al. 2016).

Several recent reports suggest that water supplies in areas having intensive agricultural activities might be at high risk of contamination by GLP (Cengiz et al. 2017). In agricultural areas and groundwater of Mexico, GLP concentrations have been detected and associated with sampling sites in proximity to GLP-resistant soybean fields (Rendon-von Osten & Dzul-Caamal 2017).

In Sanchís et al. (2012), the authors analyzed GLP in Spain's groundwater, confirming that, despite the low mobility of this compound, the herbicide is capable of migrating towards the unconfined aquifer.

GLP residues have also been detected in groundwater samples from Argentina (Okada et al. 2018, Alonso et al. 2018), Ireland (McManus et al. 2017), Canada (Van Stempvoort et al. 2016), Australia (Davis et al. 2013), China (Geng et al. 2021). All studies show that the presence of GLP in groundwater depends fundamentally on the characteristics of the soil and the form of application of the herbicide. It has been established that GLP is accumulated for periods longer than 4 years when leached into groundwater (Okada et al. 2019).

Flows of surface water, such as run-off and stream discharge, are dispersal media for GLP and AMPA residues, leading to potential long-range ecosystem contamination within watersheds and along rivers (Maggi et al. 2020). Some recent studies have detected the presence of GLP in surface water (Gunarathna et al. 2018, Mac Loughlin et al.

2020, Mörtl et al. 2013) and even in marine environments (Mercurio et al. 2014, Skeff et al. 2015).

Government agencies should have programs for the control and monitoring of contaminants, as they play a crucial role in the proper management of risk in both agricultural and urban areas potentially contaminated by agrochemicals. Similarly, research into the interaction of GLP with water should continue, taking into account the hydrogeochemistry of any area of interest.

Glyphosate Persistence

GLP has a half-life in aquatic mediums of 2 to 91 days (Singh et al. 2020b). This information coincides with that of Duarte et al. (2003), for they mention that in a study conducted in Canada, the persistence of GLP was 12-60 days in pond water. In soils, (Singh et al. 2020b) report that the half-life of the herbicide is 2 to 251 days. The persistence of GLP in pond sediments is evidenced by a study conducted in Missouri in which bottom sediments were studied, resulting in an average life of the herbicide of 120 days. However, more than one year of half-life was attributed to sediments of Oregon and Michigan (Duarte et al. 2003).

Mercurio et al. (2014) conducted studies with coastal seawaters sampled from the Great Barrier Reef containing native bacteria from this ecosystem (taking into consideration that these intervene in the degradation of the herbicide). These results indicate that the half-life of GLP at 25°C in low light conditions is 47 days, increasing to 267 days in darkness at 25°C and 315 in darkness at a temperature of 31°C. According to these authors, the information previously stated suggests that the persistence of GLP in seawater is moderate when kept in low-light conditions but highly persistent in conditions of complete darkness.

Torrado (2018) referenced studies that speak of a large GLP persistence in soils, considering that the initial degradation is faster than the subsequent degradation. This author indicated that persistence of 249 days had been found in agricultural soils and from 259 to 296 days in eight forestal sites in Finland, while 335 days in Canada and from 1 to 3 years in 11 forestal sites in Sweden. The same author mentions that the half-life of GLP might be between 3 to 22.8 years.

The persistence of LPG in both water and soil indicates the possible existence of bioaccumulation processes in natural systems, creating a pathway of exposure that is not only immediate but may persist even when the agrochemical is no longer used in a given area.

Mechanisms for the Degradation of Glyphosate and Its Metabolites

GLP transforms into AMPA as soon as it comes into contact with water while maintaining the toxic aspects of its precursor (Poiger et al. 2017) and lengthening its half-life (Gandhi et al. 2021). Microbial pathways primarily achieve the degradation of GLPand. It is the population of *Pseudomonas* spp. that influences the most in this process, which results in the main metabolite of GLP ($C_3H_8NO_5P$) known as AMPA (CH_6NO_3P), which's chemical structure is depicted in Fig. 1 (Martínez et al. 2012).

The microbial biodegradation of GLP can be performed in water, solids, and aquatic sediments through the rupture of the C-N bond, which produces AMPA. In the same way, the AMPA is biologically degraded, releasing carbon dioxide. This reaction thrives under aerobic conditions (WHO 2005). Schuette (1998) revised the degradation pathways of GLP, focusing on conditions of forest environments; in Fig. 2, the proposed pathway is presented by the author.

Besides AMPA, have been identified the presence of metabolites like N-methylamino-methylphosphonic acid, glycine, N,N-dimethylaminomethylphosphonic acid,

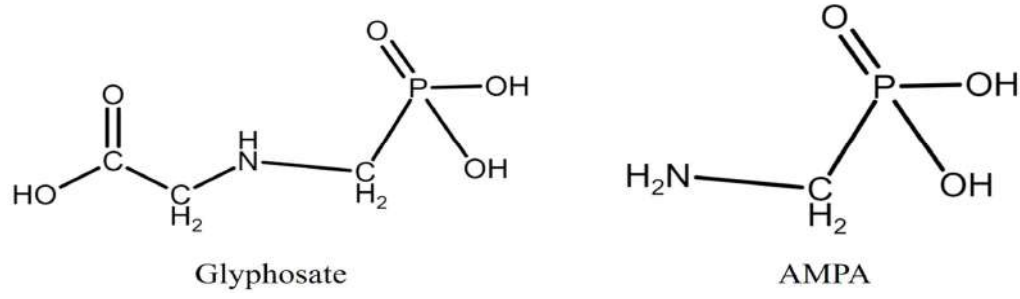

Fig. 1: Molecules of GLP and its metabolite AMPA, adapted from (You et al. 2013).

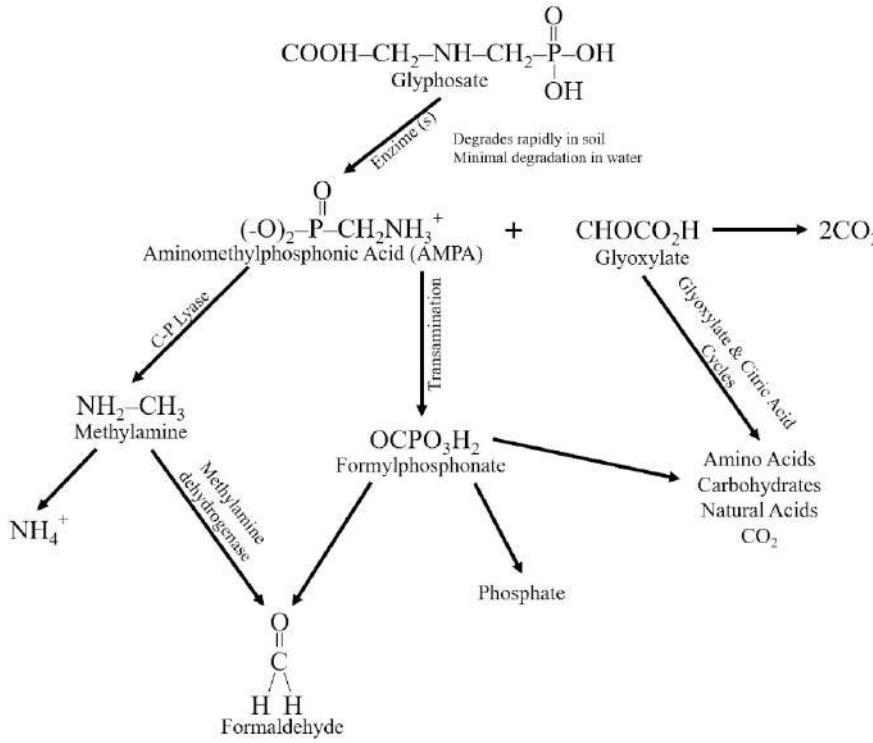

Fig. 2: GLP degradation pathways, Adapted from (Schuette 1998).

hydroxymethylphosphonic acid, and two other unknowns that all together do not exceed 1% of initial reactive (MamaCoca 2000).

EFFECTS ON THE ENVIRONMENT AND HEALTH

Effects of Glyphosate on Vegetation

Several studies indicate that pesticides and fertilizers are major factors that can affect the flora of natural and semi-natural habitats adjacent to agricultural fields; these studies have unanimously documented that sub-lethal herbicide doses reduce and delay plant flowering of non-target vegetation, resulting in overall declines of plant species richness within agricultural areas (Strandberg et al. 2021). Recent research even studies the long-term GLP persistence in perennial forest plants beyond one year after treatment (Botten et al. 2021).

The effects of low doses of GLP and sowing seasons on the macronutrient and micronutrient contents in the leaves and grains of common beans have specifically been studied (Pacheco de Almeida Prado Bortolheiro & de Almeida Silva 2021). Other studies have observed concentrations of GLP in legumes (Jarrell et al. 2020) or cereals (Cruz & Murray 2021, Xu et al. 2019).

Therefore, the constant use of GLP has been associated with an increase in herbicidal resistance by weeds associated with soy, corn, and cotton crops. At least 69 countries have informed their corresponding environmental authorities about the presence of some pesticide-resistant weeds (Bonny 2020).

Effects on Soil Microbial Activity

It has been detected that GLP that is applied on soil can interfere with the synthesis of some compounds related to microbial growth, therefore affecting the communities present in this medium, even though the prolonged exposure to the herbicide has led to certain bacteria taking advantage of GLP molecules and the intermediates in the degradation process, to obtain C, N, P, and energy for its growth (Boccolini 2019, Hernández 2019, Johnsen et al. 2001).

De María (2004) expressed that in fungi, bacteria, and plants, the pathway of the Shikimico acid is present, which means that bacteria are also susceptible to GLP effects. This fact may impact the soil biodiversity, like in the particular case of *Bradyrhizobium* sp. (genus of bacteria, many of which are nitrogen-fixing bacteria), given that the presence of GLP inhibits their growth, affecting the symbiotic nitrogen fixation as well.

In addition to what was previously stated, pesticides have the potential to encourage the development of certain microbial communities in soil. It is known that GLP can

promote the growth of fungal pathogens like *Fusarium* sp., which can harm other life forms. The fungi are capable of causing harm to the crops, poisoning the soils, and causing congenital disabilities in humans (Duarte et al. 2003).

Hussain et al. (2009) warned that pesticides that are applied to soils can influence chemical reactions such as the mineralization of organic material, nitrification and denitrification, ammonification, redox reactions, methanogenesis, and a decrease in soil enzymatic activity, which may serve as key indicators of soil health.

It is therefore important to propose solutions aimed at the use of other methods of crop care and conservation, the formulation of new agrochemicals, and the appropriate treatment of water and soil in areas without agricultural production that have been affected by LPG.

Remediation Techniques

Degradation of GLP can be achieved using abiotic and biotic means, like absorption, photolysis, thermolysis, and biodegradation with catabolic enzymes (Singh et al. 2020b). GLP degradation is accomplished mainly by various soil microorganisms (Sun et al. 2019).

The site exposure history and nutrient amendment would substantially alter the biodegradation of GLP and AMPA, showing that ammonium and phosphate, which are key ingredients in fertilizers, can enhance GLP biodegradation (Maggi et al. 2020). A complicating factor here is that phosphate can decrease GLP adsorption to the soil, thus increasing the risk of transport by run-off to rivers, aquifers, and ecosystems that have less GLP pre-exposure (Bento et al. 2018).

Despite the natural biodegradation of GLP, large volumes of wastewater with high concentrations of complex organics such as formaldehyde, GLP, and GLP from GLP manufacturing are difficult to degrade before reaching treatment plants; a novel technique being studied to remove GLP from wastewater is Supercritical water oxidation (SCWO) (Li et al. 2021).

Another recent remediation technique is a blend of photocatalysts with UV light that has come into the limelight for their ability to treat pollutants like pesticides. The photocatalytic degradation can break GLP down into non-toxic compounds like CO_2, water, and inorganic ions (Singh et al. 2020a). This mechanism depends on the photocatalytic oxidation reaction triggered by highly reactive oxidation and hydroxyl radicals (Xu et al. 2011). The benefits of photocatalysis comprise cost-effectiveness, stability, and non-toxicity, whereas its manipulation in situ is a critical disadvantage, this degradation method proved to be optimal for removing GLP in sewage treatment (Wang et al. 2016).

Many of these treatments require large investments, both financial and infrastructure. Thus, there is a growing interest in low-cost alternative techniques, and the use of polymeric membranes is a potentially attractive option because they are cheap, easy to produce, and have good adsorption characteristics (Carneiro et al. 2015).

An eco-friendly strategy like bioremediation would be another promising alternative to overcome the environmental and health risks derived from GLP use and its residues. Therefore, it has become essential to study GLP biodegradation driven by microbial degraders; numerous studies have revealed microbial capacity as a robust and useful tool in bioremediation (Singh et al. 2020b).

In this research, some investigations study wild plants tolerant to GLP and identify those microorganisms associated with the rhizosphere that could have the capacity to degrade GLP (López-Chávez et al. 2021).

The ideal plant for phytoremediation can adapt to the contaminated site, grow fast, produce a large amount of biomass, and develop a deep and extensive root system. Furthermore, it produces high levels of xenobiotic-degrading enzymes. It should be competitive with other plants, accumulate large amounts of pollutants, and be efficient in transferring them from the roots to the aerial parts of the plant (Del Buono et al. 2020).

The extension of this field of knowledge can be directed towards the study of real cases to assess environmental toxicity, as well as the comparison of different treatment alternatives, without neglecting the current need for environmental policy and regulation of herbicides.

Glyphosate's Toxicity on Animal Species

GLP's toxicity has been evidenced in several animal species with contradictory results (Salazar-López & Aldana Madrid 2011), Indicates that the presence of GLP in an aquatic medium leads to a delay in fish and algae growth, prevents sea urchin hatchings, and induces histopathological changes in tilapia gills. Mann & Bidwell (1999) affirm that GLP Isopropylamine in water is practically non-toxic, as it did not present mortality among four Australian frog species.

With contradictory results to those previously presented, Relyea (2012) conducted a study with wood frogs (*Rana sylvatica* or *Lithobates sylvaticus*), leopard frogs (*R. pipiens* o *L. pipiens*), and American toads (*Bufo americanus* o *Anaxyrus americanus*) exposing them to different concentration levels of the commercial product formulation Roundup Original Max®. This author concluded that GLP-based herbicides

could cause high mortality rates in the three different tadpoles of the amphibian species, decreasing the growth of wood and leopard frogs. In addition, the researcher identified morphological changes in these two species at this stage of their metamorphic process.

Relyea (2005) researched the impact of pesticides and herbicides on the biodiversity of an aquatic community that consisted of algae and 25 animal species. The Roundup® product decreased species richness by 22% and eliminated two tadpole species.

Krüger et al. (2014), found GLP in the lungs, liver, kidney, brain and intestinal wall of danes piglets. The pigs presented atrophy in ears and legs, cranial and spinal deformities, and one even showed a hole in its skull, and another one showed one huge eye and another that hadn't developed. The authors indicated that a higher number of studies were required to prove or exclude the role of the herbicide in the previously stated deformities.

In a study using zebrafish (*Danio rerio*), Roy et al. (2016) exposed this species' embryos to GLP, and the results indicated that the herbicide is toxic to the fish's heart development.

Although GLP is considered to be a pesticide that shows low toxicity to animals (Duke & Powles 2008), an increasing number of studies have shown that GLP has various sublethal effects on the honeybee gut microbiota, foraging behavior, developmental processes, and antioxidant pathways (Magal et al. 2019, Tan et al. 2022, Motta et al. 2018, Rossi et al. 2020).

Aparecida et al. (2013) refer to estuary contamination by sediments with herbicide residues (mostly diuron, atrazine, hexazinone, and ametrine) dragged by rivers. A fact that makes them partially responsible for the "regressive death" of mangroves. In addition to what has been previously stated, the authors indicate that herbicide contamination in seawater could influence the health of the Great Barrier Reef.

The effects of GLP on little animals have been studied recently. These studies analyze the effects of GLP on plankton (Sabio y García et al. 2020), fishes (Díaz-Martín et al. 2021, Bernardi et al. 2022), and mice (Thanomsit et al. 2022, Ait Bali et al. 2017). Larger mammals have also shown disorders associated with GLP, like cows (Wrobel 2018), piglets (Qiu et al. 2020), and hares (Martinez-Haro et al. 2022). Even large marine animals like manatees are exposed to GLP (De María et al. 2021).

It is also necessary to take into account the possible presence of this herbicide in livestock feed since it can affect both productivity and health (Sørensen et al. 2021). GLP residues have been found in soybeans and corn, which play an important role in animal nutrition (Pöppe et al. 2019). GLP exposure on an animal's per kg basis is 4 to 12 times higher than that of humans (Zhao et al. 2018).

It would be interesting to determine the relationship between the doses given in the various studies mentioned above and the concentrations reported in different environments and ecosystems in order to get a true picture of the current and future damage that could be caused throughout a food chain.

Acute Exposure of Animals to Glyphosate

GLP oral administration in bunnies, rats, and sheep indicated absorption of the minor gastrointestinal tract lower than 30%-36%. This chemical compound settled primarily in the bones; in rats, GLP did not go through any important biotransformation as it presented the AMPA as the only metabolite at a concentration between 0.2% and 0.3% of the initial applied dosage. (FAO/WHO 1994). A study conducted by the WHO (2005) indicated that rats absorb approximately 20% of the AMPA and that most of it is eliminated through urine.

Pandey et al. (2019) exposed male adult rats to a dosage of the Roundup® product formulation ranging from 0 $mg.kg^{-1}$ to 250 $mg.kg^{-1}$ for 14 days; these results suggest that the herbicide that was administered via oral route propitiated hepatic inflammation and can lead to the development of fatty liver disease.

Dallegrave et al. (2003) conducted a study with pregnant rats in which a dosage of the herbicide Roundup®, commercially distributed in Brazil, was administered 500 $mg.kg^{-1}$, 750 $mg.kg^{-1}$, and 1000 $mg.kg^{-1}$ of weight from day 6 to 15 of the gestation period. The rats that were treated with 1000 $mg.kg^{-1}$ presented a 50% mortality. The researchers conducted a cesarean operation on the 21st day of pregnancy. They found bone alterations in 15.4%, 33.1%, and 57.3% of the treated fetus with 500 $mg.kg^{-1}$, 750 $mg.kg^{-1}$, and 1000 $mg.kg^{-1}$, respectively.

Chronic Exposure of Animals to Glyphosate

In rats, it has been shown that prolonged exposure (lasting 26 months) to GLP in a dosage of up to 32 $mg.kg^{-1}$ of weight significantly increases the presence of tumors in interstitial cells (in charge of testosterone production) (WHO 2005).

Mesnage et al. (2017), in a study that lasted 2 years in which rats were administered a dosage of GLP equivalent to 4 $ng.kg^{-1}$ of corporal weight per day, concluded that chronic exposure to the herbicide may result in renal and hepatic damage with possible health implications within animal and human populations.

A sub-chronic exposure in rats (12 months) to GLP-based herbicides from juvenile age until adult, with a dosage ranging from 250 $mg.kg^{-1}.day^{-1}$ to 500 $mg.kg.day^{-1}$, induced a decrease in corporal weight and locomotive activity in addition to an increase in anxiety levels and behavior that may be interpreted as depression which suggests that the chronic exposure of rats to these herbicides may cause neurobehavioral changes (Ait Bali et al. 2017).

Despite the previously stated information, Agostini et al. (2020) mentioned that the chronic effects of GLP remain practically unexplored, indicating that more studies are necessary to shed light on the subject.

Human Exposure Pathways to the Glyphosate

GLP use, according to the WHO (2005), represents diverse risks to human health. The first one of these risks comes from direct contact with the skin or through inhaling, even though these risks are directly related to the workers who apply the product and the populations surrounding the application area. It would be expected that the most significant risk would come from food destined for human consumption that is exposed either directly or indirectly to GLP, such as animals, cereals, and legumes.

Peillex & Pelletier (2020) mentioned that GLP and its metabolite AMPA have been detected in soil, water, plants, food, and animals in addition to human urine, blood, and breast milk. These authors indicate that the urine of workers exposed to GLP can expect concentration levels that range from 0.26 $\mu g.L^{-1}$ to 73.5 $\mu g.L^{-1}$ and 0.16 $\mu g.L^{-1}$ to 7.6 $\mu g.L^{-1}$ in the general population.

Therefore, it is necessary to carry out research aimed at monitoring the long-term effects on human health, the care and protection of workers directly exposed to LPG, and the development of public policies focused on monitoring and regulating safe food for the population.

Glyphosate and its Metabolites in Water and Food Destined for Human Consumption

The main source of chronic exposure to GLP is food. Residues of GLP have been found in crops, drinking water, and tissues of animals that are destined for human consumption (Gandhi et al. 2021, González Ortega & Hagman Aguilar 2018, Hernández 2019).

Toccalino et al. (2012) mentioned in a study focused on water wells used for public supply in the United States that herbicides were among the most common organic contaminants. In another study conducted in the agricultural zone of Hopelchen, Mexico, GLP was detected in 90% of underground water samples (with a concentration ranging from 1.41$\mu g.L^{-1}$ to 0.44 $\mu g.L^{-1}$); in the three studied communities, the herbicide was present in purified water (with a max concentration of 0.44 $\mu g.L^{-1}$) and in bottled water which was sold by industry in Merida (this last one presented lower levels of GLP, with a concentration of 0.35 $\mu g.L^{-1}$) (Rendon-von Osten & Dzul-Caamal 2017). In human urine, GLP was found at a max concentration of 0.47$\mu g.l^{-1}$ (WHO 2005).

In summation, the GLP concentrations concerning human consumption exceeded the limits of 0.1 $\mu g.L^{-1}$ established by the European Union (Mesnage et al. 2017) without exceeding those established by the Mexican Official Standard, NOM-201-SSA1-2015.

Effects on Human Health

GLP and AMPA, its main degradation metabolite, are known to persist in the environment and can be found in house dust (Curwin et al. 2005), soil, air, surface water, and groundwater (Bai & Ogbourne 2016, Cosemans et al. 2022). One of the main concerns in relation to GLP is the possible effects induced on human health; they are mainly indirectly exposed to GLP through contaminated food, posing a potential long-term threat to human health (Cosemans et al. 2022, Louie et al. 2021).

Concerning the deaths caused by pesticides, the International Organization of Consumers Union informed that every four hours, a worker in the agricultural sector dies due to acute intoxication. This is equivalent to 10,000 deaths per year and up to 375,000 intoxication cases in the same time period (Idrovo 2000). The WHO shows that nearly 1,000,000 intoxication cases due to pesticides arose in the eighties, and 70% of these cases happened in a work environment (Campuzano et al. 2017). Peillex & Pelletier (2020) indicated that dermal ingestion and inhalation are the main pathways by which GLP enters the human body.

Several studies reported associations between GLP exposure and different health disorders (Cosemans et al. 2022) including i) cancer (Franke et al. 2021, Leon et al. 2019), ii) decrease in gestation time (Lesseur et al. 2022), iii) effects on lactation (Ruiz et al. 2021), iv) respiratory diseases (Pandher et al. 2021, Hoppin et al. 2008), and v) neurological diseases (von Ehrenstein et al. 2019). Laboratory studies have demonstrated the absorption of GLP in the human gastrointestinal tract and absorption of GLP via dermal route, ingestion, and inhalation (Torretta et al. 2018). Recent studies show immune-endocrine alterations induced by GLP (Muñóz et al. 2021, Maddalon et al. 2021). Other researchers emphasize the importance of human biomonitoring studies as a measure of internal exposure (Connolly et al. 2020, Ferreira et al. 2021, Faniband et al. 2021).

Peillex & Pelletier (2020) mentioned a correlation between GLP-based herbicides and a major frequency of spontaneous abortions, premature labor, and diverse deformities like harelip and Down syndrome. In Colombia, Camacho & Mejía (2017) compared health records and aerial fumigation records of the GLP herbicide to tackle the illicit cocaine crop. The results indicated that exposure to these pesticides relates to the increase in the number of spontaneous abortions and medical consultations concerning dermatological and respiratory illnesses.

The use of transgenic seeds and the GLP herbicide could worsen the current situation concerning bacterial antibiotic resistance, a fact that represents one of the biggest threats to humanity in the future (OMS 2020). In a study, bacteria *Escherichia coli* and *Salmonella enterica* serovar Typhimurium were exposed to the Roundup formula, which found an increase in the bacteria's resistance to antibiotics like Kanamicina and Ciprofloxacina (Kurenbach et al. 2015).

In light of this information, there is an urgent need to promote a conscious collaboration between decision-makers in government, society, the health sector, and agribusiness to address the challenges posed by GLP contamination, always keeping public health at the forefront.

Effects on Human Cells

Agostini et al. (2020) mentioned the presence of multiple studies conducted in the last 40 years regarding healthy and tumoral cells, in which many alterations were found due to GLP exposure to formulations that contain it as an active ingredient with highly varied effects depending on the type of cell, the commercial formulation of GLP used, exposure time, dosage, and the applied methodology.

Ledoux et al. (2020) indicate that it has been shown that GLP causes damage to the DNA of human mammary epithelial cells placental and umbilical cord cells, and induces effects regarding the mortality of sperm.

Neurological and Neurobehavioral Alterations

Exposure to pesticides used in agriculture has been associated with the risk of developing Parkinson's (Gorell et al. 1998). Burchfield et al. (2019) reference multiple authors that relate the inhibition of mitochondria with Parkinson's disease. In addition, they indicate that the classic toxins used for the research regarding this disease exert their toxicity through similar mechanisms to those of the herbicide.

Burchfield et al. (2019) evaluated the toxicity of the Touchdown® herbicide, which contains GLP as an active ingredient. They made use of the nematode *Caenorhabditis elegans,* treating it with the agrochemical for 30 minutes. The obtained results from the oxygen consumption indicated mitochondrial inhibition, a decrease in ATP levels, and an increase in hydrogen peroxide levels in comparison to those of the control groups.

In addition, it has been reported that GLP, as well as its AMPA metabolite, decreases the activity of the acetylcholinesterase enzyme, which ends the neurotransmisor effect of the Acetylcholine. (Van Bruggen et al. 2018). The changes in the concentration levels of this enzyme or its properties relate to Alzheimer's, Parkinson's, and Miastenia gravis diseases. (Sánchez & Salceda 2008).

Possible Effects on Gut Flora

In animals, GLP can damage the microbial communities present in the intestine and can unleash a negative effect on the animal; an example of this is that of bacteria in charge of lactic acid production that can be generally affected by GLP present in foods and water. These produce antibiotics and are suppressors of the bacteria *Clostridium botulinum,* a pathogenic microorganism in animals. (Van Bruggen et al. 2018).

Rueda-Ruzafa et al. (2019) referenced the close relationship that exists between the digestive system and the central nervous system. In addition, they mention the effects of GLP on the human body concerning the intestinal dysbiosis induced by the herbicide. As an example of the relationship between the nervous and digestive systems, the authors indicate that the intestinal microbial density in autistic children is different from that of healthy children, given that those who have the disorder show a decrease in beneficial bacteria (*Bifidobacterium*). Despite what was previously stated, the authors concluded that more studies are necessary to clarify the role that GLP plays in the development of behavioral disorders.

Effects of Inert Compounds Included in Commercial Formulations on Human Health

With frequency, commercial herbicides that contain GLP as an active ingredient include surfactants, which are compounds that reduce the tension between two phases present in a molecule. These can increase the dermic absorption and the neurotoxic effects, genotoxins, and endocrines, in addition to decreasing mobility and increasing the environmental persistence of the herbicide (Cruz 2013). Some studies affirm that the surfactants that accompany the GLP (at least in the case of Roundup®) are the ones that show the major toxicological effects (Burger & Fernández 2004). The surfactant polyoxy-ethylene-amine (POEA), according to Brausch et al. (2007), is extremely toxic to aquatic organisms, capable of inhibiting the growth of the

crustacean *Daphnia Magna* and causing similar effects on other organisms.

The surfactant POEA is derived from the grease of animal origin present in commercial formulations of herbicides like Roundup®. This herbicide is composed of 41.5% GLP and 16% POEA (Vargas 2018), even though the content of POEA may vary between 6% and 18%, according to its commercial presentation (Méndez 2015).

The POEA may contain as an impurity 1-4 dioxane, to which a carcinogenic capacity is attributed in animals, and kidney and liver damage in humans (Salazar López & Aldana Madrid 2011), according to the same authors, Folmar et al. (1979), used the herbicide Roundup® and technical grade GLP in fishes and aquatic invertebrates concluding that it is the surfactant of the commercial presentation (Roundup®), that plays the role of the primary toxic agent.

Martínez et al. (2007) showed in vitro studies with human mononuclear blood cells that the commercial presentation of the herbicide Roundup® has greater cytotoxicity (cellular toxicity) than the technical grade GLP, which suggests that the additives of the commercial formulations play an important role in the toxicity that is attributed to the herbicide.

Kaczewer (2002) exposed the participation of polyacrylamide, included in commercial presentations such as Roundup (an additive that reduces the derivatization of GLP to AMPA during its sprinkling and acts as a surfactant). This additive, in addition to GLP in adequate conditions of light and temperature, contributes to the release of acrylamide. This last compound is a potent neurotoxin that affects the male reproductive function and causes congenital deformities and animal cancer.

Out of the GLP biotransformation, the metabolite glioxilite surges; in rats, Ford et al. (2017) showed that this compound could inhibit enzymes in charge of oxidizing fatty acids in the liver; in addition, treating the rats with GLP increases the levels of triglycerides and cholesteryl esters. In the same way, Duarte et al. (2003) mentioned that in the formulation of Roundup®, the surfactant present is between 20 to 70 times more toxic to fish than the technical grade GLP. Torrado (2018) cites a study in which the Rodeo® formulation, which has GLP as an active ingredient in addition to surfactants AL77 and Optima, was compared with Roundup® in cocaine crops and resulted in being four times more toxic.

Aparecida et al. (2013) stated in a study conducted with commercial formulations of GLP and their effects on the proliferation, survival, and differentiation of one mammal cellular line (fibroblastos 3T3-L1), concluding that the herbicide inhibits cellular proliferation and induces the apoptosis (death or destruction of the cell aiming to control its growth or development). Despite what was previously stated, Agostini et al. (2020) indicated that in blood cells, it has been found that the formulation Roundup® is weakly mutagenic.

In view of the above, the regulation of LPG and herbicides should be updated and, if necessary, tightened, taking into account the different products and combinations of this compound with different additives in order to make them safer for health. For this to be possible, research into the adverse effects of these agrochemicals must continue.

CASE STUDY: GLYPHOSATE PROHIBITION

Position of International Agencies

In 1985, the Environmental Protection Agency of the United States (USEPA) classified GLP as a possible class C carcinogen (there is evidence suggesting its potential carcinogenic effect) due to the presence of renal tumors in rats. Subsequently, in 1986, the same agency requested from a scientific panel an evaluation regarding the toxicity of GLP. This latter one concluded that the renal tumors in rats previously mentioned are, in reality, an increase in the adenomas (benign tumors). In 1991, in light of a new review, the USEPA changed the rank from class C to E, "Evidence of non-carcinogenicity for humans." A similar conclusion was reached by the same agency in 2015, given that, after their third review, the agency concluded that GLP "is not likely to be carcinogenic for humans." (Pedemonte 2017, EPA 2016).

In 2020, the USEPA declared that GLP does not represent a risk to humans as long as it is used in accordance with the instructions provided (WSDA 2020, Mayer 2021).

In 2015, the International Agency for Research on Cancer (IARC) classified GLP in the 2A group as a "probable carcinogen" due to the idea that the GLP-based formulations are probably carcinogenic to humans, primarily for linfoma no Hodgkin (type of cancer that forms in the lymphatic system) (Weisenburger 2021).

The European Food Safety Authority (EFSA) mentioned in 2015 that it was unlikely that GLP represented a carcinogenic danger to humans. The Food and Agriculture Organization of the United Nations (FAO) concluded in 2016 that it is unlikely that GLP represents a carcinogenic risk in humans through dietary exposure (EPA 2016).

Glyphosate Prohibition

In Colombia, through the 1214 resolution established in 2015, the sprinkling of GLP was suspended, making it one

of the first countries in Latin America to take into account the negative effects of GLP as advertised by the WHO (Campuzano et al. 2017). Vietnam banned the registry, import, and use of products containing GLP in 2021. Meanwhile, the European Union, in 2017, renewed its GLP license for 5 more years, even though some countries that form part of it opposed the renewal. France announced its prohibition on all of its uses, including agricultural uses, by 2022, and Germany has plans to ban it by the end of 2023 (Ramírez 2021).

In Mexico, a decree was presented on December 31, 2020, at the Diario Oficial de la Federación, which states in its first article the gradual substitution of the use, acquisition, distribution, promotion, and importation of GLP and agrochemical products that contain it as an active ingredient for sustainable alternatives and culturally adequate that have the capacity to maintain production and that are safe for the environment and human beings, contributing to the biocultural diversity. This decree contemplates a period for the fulfillment of the previously stated objectives, starting at the decree's publication up until January 31, 2024. Despite what has been previously stated, in Mexico, there are authorized pesticides whose active ingredients (specifically 140 pesticides) are banned or not authorized by other countries, of which 65 are extremely dangerous according to the criteria established by the FAO and the WHO (Bejarano 2017).

Many authors dispute the decree released by the Mexican Government. (Alcántara-de la Cruz et al. 2021), Established a skeptical position regarding the Mexican government has decreed about application of technology and alternative methods focused on weed control since they established that successful cases have been conducted internationally in an almost exclusive manner and that their regional reach is limited. Also, the authors indicate that the prohibition of GLP may promote the use of other herbicides with similar or greater negative environmental impacts. Adding on to what has been previously stated, Bejarano (2017) mentioned that agricultural activity highly depends on pesticide use and that even with their use, the country is still unable to achieve auto-sufficient corn production, as one-third of the total national demand is imported. A crop that is basic in the Mexican diet.

According to Meftaul et al. (2021), GLP presents low toxicity compared with other herbicides, even though they do not dismiss its possible impact on human health and the fact that some microorganisms develop a resistance to it while others (beneficial aquatic and ground microorganisms) suffer prejudgemental effects. In addition, the weed's herbicide resistance and the probable negative impact on aquatic and land organism communities of great ecological importance make this a controversial subject.

Possible Conflict of Interest by the Agrochemical Industry

In 2015, the Monsanto Company obtained nearly 4,760 million dollars and 1,900 million in gross profits because of herbicide sales. These benefits are mainly due to their Roundup® formulation (Chatsko 2016).

Burtscher et al. (2017) mentioned the participation of the International Agency for Research on Cancer (IARC), which classified GLP in 2015 as a possible carcinogen, threatening many companies' great businesses dedicated to herbicide production like Monsanto. In 2012, the same authors indicated that the authorized use of GLP as an active ingredient was about to expire, for which the companies of the agrochemical industry (Monsanto being one of them) responded by creating the "Glyphosate Task Force" which was financed by the agrochemical industry in charge of GLP based herbicide production with the objective of supporting the substance's safety.

Williams et al. (2000) suggested in a study that Monsanto backed up that GLP is not a carcinogen and does not present any risks to human health. Williams et al. (2012) indicated in a Monsanto-sponsored review that GLP does not affect reproductive health (in humans and/or animals), establishing that the toxicity presented in the studies can be attributed to surfactants that are a part of commercial presentations. Kier & Kirkland (2013) (Monsanto ex-employee and company consultant, respectively) indicated that GLP and the commercial formulations that contain it as an active ingredient pose a genotoxic risk that is insignificant under normal human exposure conditions. All of what was previously stated was described in accordance with Burtscher et al. (2017).

Burtscher et al. (2017) indicated that the studies and reviews sponsored by the industry that defend GLP safety present manipulations including "apparently calculated omissions," "incorrect representation of facts," "irrelevant data to confuse and deny scientific evidence," "distort and/or hide inconvenient facts and manipulate evidence to support their own arguments."

Acquavella et al. (2016) and Williams et al. (2016a) arrived at the upcoming conclusion: "Our review did not find any support in the epidemiological literature that backs up a causation between GLP and linfoma no Hodgkin." Brusick et al. (2016) mentioned in a review that: "GLP, the commercial formulations, and AMPA do not represent a genotoxic risk, and the data does not support the monograph of the IARC's genotoxicity." Chang & Delzell (2016), based on a review, conclude that: "No cause relationship between GLP exposure and any type of linfoma no Hodgkin risk was established."

Solomon (2016) indicates in a review that: "the IARC's GLP classification as a possible human carcinogen was conducted without a detailed exposure evaluation." Williams et al. (2016a) exposed in a review that: "the data does not support the IARC's conclusion regarding the GLP as a probable human carcinogen." Williams et al. (2016b) concluded in a review that: "GLP is not a carcinogen in laboratory animals." According to Weisenburger (2021), every review that was previously mentioned emerges from the pesticide industry's sponsorship to oppose the evaluation of the IARC in 2015.

Despite what has been previously mentioned, Bayer (current property of the Monsanto company) reached a massive settlement/agreement in which 11 billion dollars will be paid in the U.S. to those who claim to suffer from cancer, especially linfoma no Hodgkin due to repeated herbicide exposures after tens of thousands of lawsuits were filed regarding cancer (Ramírez 2021, Forbes México 2018, Ximénez 2020)

CONCLUSIONS

The available literature of the past century displays contradictory stands regarding the role played by GLP-based herbicides on human and environmental health.

Diverse authors have identified the toxicological potential of the "inert compounds" present in commercial formulations, establishing that, in some cases, these are more harmful than GLP. The studies that use technical grade GLP (pure compound) conclude with the frequency that the herbicide does not represent any important risks; meanwhile, other studies that use commercial formulations that contain GLP as an active ingredient advise about the negative effects that these other substances may induce.

In many reviews, the presence of probable conflicts of interest has been evidenced due to the author's relationship with the GLP-based herbicide industry, many of which have supported the substance's safety based on its use. Because of what was previously stated, it is necessary to conduct studies that are not influenced by economic interests, especially coming from the agrochemical industry.

The continuous study and monitoring of environmental impacts due to GLP is relevant since the development of the flora and fauna adjacent to the areas where this herbicide is used may be negatively altered. In addition, due to the transport of contaminants, concentrations of GLP have been found in distant aquatic systems, which could establish an important impact on high-valued ecosystems. Related to the soil, the natural processes that take place can be altered, causing a decrease in bacterial growth or, on the contrary, promoting the development of certain pathogenic agents.

Due to the presence of GLP fixed in organs and bones of animals, there are several results on the effects on fauna, altering the development and diversity of species, causing changes in morphology, generating diseases, and even mortality in certain groups. It is recognized that further studies are needed to explore the effects of GLP in animals since their level of exposure is even higher than in humans.

GLP is one of the most common organic pollutants present in multiple resources used by humans, which makes it a threat to current and long-term health. The main route of human exposure is ingestion through food since there are records of GLP concentrations in foods such as crops, natural and purified water, as well, as animal tissue. Other routes of exposure are dermal contact and inhalation, which has led to the presence of this contaminant in blood, urine, and breast milk.

Exposure to GLP is associated with diseases in various stages of human development, as well as alterations to the neurological, immune, and endocrine systems. There is a relationship between the presence of GLP and problems in gestation and birth; additionally, the increase in antibiotic resistance of some bacteria due to the presence of GLP presents a new panorama of challenges for humanity. In addition, some authors mention the need to conduct studies in susceptible human populations, such as children or people with special genetic traits, and others that contemplate the mix of contaminants (including agrochemicals).

Regardless of the negative impacts that may come from the use of herbicides, it remains true that a big part of large-scale crops is favored by the use of these pesticides, which in some way has made us dependent on the use of these substances, given that production of organic foods comes with important difficulties and their large scale application tends to not be viable, even though the use of GLP based herbicides seems to be reaching an end in its use to control weeds given that many weed species have developed a tolerance to these types of herbicides.

The GLP-based herbicide ban may promote the use of other pesticides, with impacts that can only be determined with certainty by long-term studies. GLP, regardless of becoming the most widely used herbicide, has been used for almost 5 decades (since its first appearance in the Roundup® product in 1974) and has not yet reached a scientific consensus regarding its impact on the environment and human health.

Without a doubt, the subject of herbicides encompasses many diverse aspects of human life, from health, environment, economy, and culture, which means that the subject cannot be approached through a reductive analysis.

STATEMENTS AND DECLARATIONS

This work is part of the research project "Programa de Apoyo a Proyectos de Investigación e Innovación Tecnológica (PAPIIT) IN107622" supported by "Dirección General de Asuntos del Personal Académico (DGAPA)" and "Universidad Nacional Autónoma de México (UNAM)."

REFERENCES

Acquavella, J., Garabrant, D. and Marsh, G. 2016. Glyphosate epidemiology expert panel review: a weight of evidence systematic review of the relationship between glyphosate exposure and non-Hodgkin's lymphoma or multiple myeloma. Crit. Rev. Toxicol., 46: 28-43. https://doi.org/10.1080/10408444.2016.1214681

Agostini, L.P., Dettogni, R.S. and dos Reis, R.S. 2020. Effects of glyphosate exposure on human health: Insights from epidemiological and in vitro studies. Sci. Total Environ., 705: 135808. https://doi.org/10.1016/j.scitotenv.2019.135808

Ait Bali, Y., Ba-Mhamed, S. and Bennis, M. 2017. Behavioral and immunohistochemical study of the effects of subchronic and chronic exposure to glyphosate in mice. Front. Behav. Neurosci., 11: 146. https://doi.org/10.3389/fnbeh.2017.00146

Alcántara-de la Cruz, R., Cruz-Hipolito, H.E., Domínguez-Valenzuela, J.A. and De Prado, R. 2021. Glyphosate ban in Mexico : potential impacts on agriculture and weed management. Pest Manag. Sci., 77: 3820-3831. https://doi.org/10.1002/ps.6362

Alonso, L.L., Demetrio, P.M., Agustina Etchegoyen, M. and Marino, D.J. 2018. Glyphosate and atrazine in rainfall and soils in agroproductive areas of the Pampas region in Argentina. Sci. Total Environ., 645: 89-96. https://doi.org/10.1016/j.scitotenv.2018.07.134

Aparecida, M., Campos Ventura-Camargo, B. and Miyuki, M. 2013. Toxicity of herbicides: Impact on aquatic and soil biota and human health. Curr. Res. Herb., 16: 11-27

Aparicio, V.C., De Gerónimo, E. and Marino, D. 2013. Environmental fate of glyphosate and aminomethylphosphonic acid in surface waters and soil of agricultural basins. Chemosphere, 93: 1866-1873. https://doi.org/10.1016/j.chemosphere.2013.06.041

ArgenBio 2021. Transgenic Crops. https://www.argenbio.org/cultivos-transgenicos. Accessed 1 Feb. 2022.

Bai, S.H. and Ogbourne, S.M. 2016. Glyphosate: environmental contamination, toxicity and potential risks to human health via food contamination. Environ. Sci. Pollut. Res., 23: 18988-19001. https://doi.org/10.1007/s11356-016-7425-3

Bejarano, F. 2017. Los plaguicidas altamente peligrosos en México. México

Bento, C.P.M., Commelin, M.C. and Baartman, J.E.M. 2018. Spatial glyphosate and AMPA redistribution on the soil surface driven by sediment transport processes: A flume experiment. Environ. Pollut., 234: 1011-1020. https://doi.org/10.1016/j.envpol.2017.12.003

Bernardi, F., Lirola, J.R., Cestari, M.M. and Bombardelli, R.A. 2022. Effects on reproductive, biochemical and genotoxic parameters of herbicides 2,4-D and glyphosate in silver catfish (*Rhamdia quelen*). Environ. Toxicol. Pharmacol., 89: 103787. https://doi.org/10.1016/j.etap.2021.103787

Boccolini, M. 2019. Bacterial groups in a typical arguido with glyphosate application: influence on nitrogen bacteria. Sci. Floor, 37: 225-237.

Bonny, S. 2020. Herbicide-tolerant transgenic crops and resistant weeds, overview and agro-economic impacts. Agric. Econ., 7: 23-36.

Botten, N., Wood, L.J. and Werner, J.R. 2021. Glyphosate remains in forest plant tissues for a decade or more. For. Ecol. Manage., 493: 119259. https://doi.org/10.1016/j.foreco.2021.119259

Brausch, J.M., Beall, B. and Smith, P.N. 2007. Acute and sub-lethal toxicity of three POEA surfactant formulations to Daphnia magna. Bull. Environ. Contam. Toxicol., 78: 510-514. https://doi.org/10.1007/s00128-007-9091-0

Brusick, D., Aardema, M. and Kier, L. 2016. Genotoxicity expert panel review: Weight of evidence evaluation of the genotoxicity of glyphosate, glyphosate-based formulations, and aminomethylphosphonic acid. Crit. Rev. Toxicol., 46: 56-74. https://doi.org/10.1080/10408444.2016.1214680

Burchfield, S.L., Bailey, D.C. and Todt, CE. 2019. Acute exposure to a glyphosate-containing herbicide formulation inhibits Complex II and increases hydrogen peroxide in the model organism Caenorhabditis elegans. Environ. Toxicol. Pharmacol., 66: 36-42. https://doi.org/10.1016/j.etap.2018.12.019

Burger, M. and Fernández, S. 2004. Exposure to the herbicide glyphosate: Clinical toxicological aspects. Rev. Méd. Urug., 20: 1141

Burtscher, H., Clausing, P. and Robinson, C. 2017. Glyphosate and cancer: Buying science. How industry strategized (and regulators colluded) in an attempt to save the world's most widely used herbicide from a ban. https://www.global2000.at/sites/global/files/Glyphosate_and_cancer_Buying_science_EN_0.pdf. Accessed 1 Jul 2022

Camacho, A. and Mejía, D. 2017. The health consequences of aerial spraying illicit crops: The case of Colombia. J. Health Econ., 54: 147-160. https://doi.org/10.1016/j.jhealeco.2017.04.005

Campuzano, C., Feijoó, L. and Manzur, K. 2017. Effects of glyphosate poisoning in the agricultural population: Topic review. Rev. CES Salud Pública. 121-133

Carneiro, R.T.A., Taketa, T.B. and Gomes Neto, R.J. 2015. Removal of glyphosate herbicide from water using biopolymer membranes. J. Environ. Manag., 151: 353-360. https://doi.org/10.1016/j.jenvman.2015.01.005

Cengiz, M., Basancelbi, O. and Kitis, Y. 2017. Glyphosate residues in drinking waters and adverse health effects. Turkish J. Occup. Environ. Med. Saf., 2: 247-258.

Chang, E. and Delzell, E. 2016. Systematic review and meta-analysis of glyphosate exposure and risk of lymphohematopoietic cancers. J. Environ. Sci. Health Part B, 51: 402-434. https://doi.org/10.1080/03601234.2016.1142748

Chaparro, A. 2011. Cultivos transgénicos: Entre los riesgos biológicos y los beneficios ambientales y económicos. Acta Biol. Colomb., 16: 231-251.

Chatsko, M. 2016. How Much Money Does Monsanto Make From Roundup? https://www.fool.com/investing/2016/05/26/how-much-money-does-monsanto-make-from-roundup.aspx

CIBIOGEM. 2019. Monograph on glyphosate. https://conacyt.mx/cibiogem/images/cibiogem/comunicacion/MONOGRAFIA_SOBRE_GLIFOSATO_19.pdf. (Accessed 30 Jan 2022)

Connolly, A., Coggins, M.A. and Koch, H.M. 2020. Human biomonitoring of glyphosate exposures: State-of-the-art and future research challenges. Toxics, 8: 152. https://doi.org/10.3390/toxics8030060

Cosemans, C., Van Larebeke, N. and Janssen, B.G. 2022. Glyphosate and AMPA exposure in relation to markers of biological aging in an adult population-based study. Int. J. Hyg. Environ. Health, 240:113895. https://doi.org/10.1016/j.ijheh.2021.113895

Cruz, J.G. 2013. Glifosato : Uso , efecto y regulación en calidad del agua. Univ. Nac. Autón. de México

Cruz, J.M. and Murray, J.A. 2021. Determination of glyphosate and AMPA in oat products for the selection of candidate reference materials. Food Chem., 342: 128213. https://doi.org/10.1016/j.foodchem.2020.128213

Curwin, B.D., Hein, M.J., Sanderson, W.T. 2005. Pesticide contamination inside farm and nonfarm homes. J. Occup. Environ. Hyg., 2: 357-367. https://doi.org/10.1080/15459620591001606

Dallegrave, E., Mantese, F.D. and Coelho, R.S. 2003 The teratogenic potential of the herbicide glyphosate-Roundup® in Wistar rats. Toxicol. Lett., 142: 45-52. https://doi.org/10.1016/S0378-4274(02)00483-6

Davis, A.M., Thorburn, P.J and Lewis, S.E. 2013. Environmental impacts of irrigated sugarcane production: Herbicide run-off dynamics from farms and associated drainage systems. Agric. Ecosyst. Environ., 180: 123-135. https://doi.org/10.1016/j.agee.2011.06.019

De María, M., Silva-Sanchez, C. and Kroll, K.J. 2021. Chronic exposure to glyphosate in Florida manatee. Environ. Int., 152: 106493. https://doi.org/10.1016/j.envint.2021.106493

De María, N. 2004. Efecto del glifosato sobre la simbiosis "Lupinus Albus-Bradyrhizobium" SP. ("Lupinus"). Univ. Complutense de Madrid.

Del Buono, D., Terzano, R., Panfili, I. and Bartucca, M.L. 2020. Phytoremediation and detoxification of xenobiotics in plants: herbicide-safeners as a tool to improve plant efficiency in the remediation of polluted environments. A mini-review. Int. J. Phytoremed., 22: 789-803. https://doi.org/10.1080/15226514.2019.1710817

Díaz-Martín, R. D., Carvajal-Peraza, A., Yáñez-Rivera, B. and Betancourt-Lozano, M. 2021. Short exposure to glyphosate induces locomotor, craniofacial, and bone disorders in zebrafish (*Danio rerio*) embryos. Environ. Toxicol. Pharmacol., 87: 103700. https://doi.org/10.1016/j.etap.2021.103700

Duarte, W., Barragán, I. and Mocha, P. 2003. Effects of glyphosate (GP) with emphasis on aquatic organisms: Literature Review. Orinoquia, 7: 70-100

Duke, S.O. and Powles, S.B. 2008 Glyphosate: a once-in-a-century herbicide. Pest Manag. Sci., 64: 319-325. https://doi.org/10.1002/ps.1518

EPA. 2016 Glyphosate Issue Paper: Evaluation of Carcinogenic Potential. https://www.epa.gov/sites/default/files/2016-09/documents/glyphosate_issue_paper_evaluation_of_carcincogenic_potential.pdf. Accessed 5 May 2022

Faniband, M.H., Norén, E., Littorin, M. and Lindh, C.H. 2021. Human experimental exposure to glyphosate and biomonitoring of young Swedish adults. Int. J. Hyg. Environ. Health, 231: 113657. https://doi.org/10.1016/j.ijheh.2020.113657

FAO/WHO 1994. Environmental Health Criteria 159 Glyphosate. http://apps.who.int/iris/bitstream/handle/10665/40044/9241571594-eng.pdf?sequence=1

Ferreira, C., Duarte, S.C. and Costa, E. 2021. Urine biomonitoring of glyphosate in children: Exposure and risk assessment. Environ. Res., 198: 111294. https://doi.org/10.1016/j.envres.2021.111294

Forbes México. 2018. Bayer Buys Monsanto in the Most Expensive Operation in German History. https://www.forbes.com.mx/bayer-compra-monsanto-en-la-operacion-mas-costosa-de-la-historia-alemana/. Accessed 4 Jun 2022.

Ford, B., Bateman, L.A. and Gutierrez-Palominos, L. 2017. Mapping proteome-wide targets of glyphosate in mice. Cell Chem. Biol., 24: 56-63.

Franke, A.A., Li, X., Shvetsov, Y.B. and Lai, J.F. 2021. Pilot study on the urinary excretion of the glyphosate metabolite aminomethylphosphonic acid and breast cancer risk: The Multiethnic Cohort study. Environ. Pollut., 277: 116848. https://doi.org/10.1016/j.envpol.2021.116848

Gandhi, K., Khan, S. and Patrikar, M. 2021. Exposure risk and environmental impacts of glyphosate: Highlights on the toxicity of herbicide co-formulants. Environ. Challenges, 4: 100149. https://doi.org/10.1016/j.envc.2021.100149

Geng, Y., Jiang, L. and Zhang, D. 2021. Glyphosate, aminomethylphosphonic acid, and glufosinate-ammonium in agricultural groundwater and surface water in China from 2017 to 2018: Occurrence, main drivers, and environmental risk assessment. Sci. Total Environ., 769: 144396. https://doi.org/10.1016/j.scitotenv.2020.144396

González Ortega, E. and Hagman Aguilar, E. 2018. The herbicide glyphosate and its use in agriculture with genetically modified organisms. Inst. Nac. Ecol. Y Cambio Climático, 52: 1–21.

Gorell, J.M., Johnson, C.C. and Rybicki, B.A. 1998. The risk of Parkinson's disease with exposure to pesticides, farming, well water, and rural living. Neurology, 50: 1346-1350. https://doi.org/10.1212/WNL.50.5.1346

Gunarathna, S., Gunawardana, B. and Jayaweera, M. 2018. Glyphosate and AMPA of agricultural soil, surface water, groundwater, and sediments in areas prevalent with chronic kidney disease of unknown etiology, Sri Lanka. J. Environ. Sci. Heal. Part B, 53: 729-737. https://doi.org/10.1080/03601234.2018.1480157

Hagner, M., Hallman, S.and Jauhiainen, L. 2015. Birch (Betula spp.) wood biochar is a potential soil amendment to reduce glyphosate leaching in agricultural soils. J. Environ. Manage., 164: 46-52. https://doi.org/10.1016/j.jenvman.2015.08.039

Hernández, K. 2019. Microbial degradation of the herbicide glyphosate in agricultural soils of the Argentine Pampas Region. Univ. Nac. de Mar del Plata, 16: 663.

Hoppin, J.A., Umbach, D.M. and London, S.J. 2008. Pesticides and atopic and nonatopic asthma among farm women in the Agricultural Health Study. Am. J. Respir. Crit. Care Med., 177: 11-8. https://doi.org/10.1164/rccm.200706-821OC

Hussain, S., Siddique, T. and Saleem, M. 2009. Chapter 5 Impact of Pesticides on Soil Microbial Diversity, Enzymes, and Biochemical Reactions. pp 159-200

Idrovo, A. 2000. Surveillance of Pesticide Poisoning in Colombia. http://www.scielo.org.co/pdf/rsap/v2n1/0124-0064-rsap-2-01-00036.pdf

Jarrell, Z.R., Ahammad, M.U. and Benson, A.P. 2020. Glyphosate-based herbicide formulations and reproductive toxicity in animals. Vet. Anim. Sci., 10: 100126. https://doi.org/10.1016/j.vas.2020.100126

Johnsen, K., Jacobsen, C., Torsvik, V. and Sørensen, J. 2001. Pesticide effects on bacterial diversity in agricultural soils - a review. Biol. Fertil. Soils, 453-443 :33. https://doi.org/10.1007/s003740100351

Kaczewer, J. 2002. Toxicology of glyphosate: risks to human health. https://www.produccionanimal.com.ar/sanidad_intoxicaciones_metabolicos/intoxicaciones/27-toxicologia_del_glifosato.pdf. (Accessed 5 May 2022)

Kier, L.D. and Kirkland, D.J. 2013. Review of genotoxicity studies of glyphosate and glyphosate-based formulations. Crit. Rev. Toxicol., 43: 283-315. https://doi.org/10.3109/10408444.2013.770820

Kremer, R.J. and Means, N.E. 2009. Glyphosate and glyphosate-resistant crop interactions with rhizosphere microorganisms. Eur. J. Agron., 31: 153-161. https://doi.org/10.1016/j.eja.2009.06.004

Krüger, M., Schrödl, W. and Pedersen, I. 2014. Detection of glyphosate in malformed piglets. J. Environ. Anal. Toxicol., 04: https://doi.org/10.4172/2161-0525.1000230

Kurenbach, B., Marjoshi, D. and Amábile-Cuevas, C.F. 2015. Sublethal exposure to commercial formulations of the herbicides dicamba, 2,4-dichlorophenoxyacetic acid, and glyphosate cause changes in antibiotic susceptibility in Escherichia coli and *Salmonella enterica* serovar typhimurium. MBio, 6:112. https://doi.org/10.1128/mBio.00009-15

Ledoux, M.L., Hettiarachchy, N. and Yu, X. 2020. Penetration of glyphosate into the food supply and the incidental impact on the honey supply and bees. Food Control, 109: 106859. https://doi.org/10.1016/j.foodcont.2019.106859

Leon, M.E., Schinasi, L.H. and Lebailly, P. 2019. Pesticide use and risk of non-Hodgkin lymphoid malignancies in agricultural cohorts from France, Norway, and the USA: a pooled analysis from the AGRICOH consortium. Int. J. Epidemiol., 48: 1519-1535. https://doi.org/10.1093/ije/dyz017

Lesseur, C., Pathak, K.V. and Pirrotte, P. 2022. Urinary glyphosate concentration in pregnant women in relation to length of gestation. Environ. Res., 203: 111811. https://doi.org/10.1016/j.envres.2021.111811

Li, J., Wang, S. and Li, Y. 2021. Supercritical water oxidation of glyphosate wastewater. Chem. Eng. Res. Des., 168: 122-134. https://doi.org/10.1016/j.cherd.2021.02.002

López-Chávez, M.Y., Alvarez-Legorreta, T. and Infante-Mata, D. 2021. The glyphosate-remediation potential of selected plant species in artificial wetlands. Sci. Total Environ., 781: 146812. https://doi.org/10.1016/j.scitotenv.2021.146812

Louie, F., Jacobs, N.F.B. and Yang, L.G.L. 2021. A comparative evaluation of dietary exposure to glyphosate resulting from recommended U.S. diets. Food Chem. Toxicol., 158: 112670. https://doi.org/10.1016/j.fct.2021.112670

Lupi, L., Miglioranza, K.S.B. and Aparicio, V.C. 2015. Occurrence of glyphosate and AMPA in an agricultural watershed from the southeastern region of Argentina. Sci. Total Environ., 536: 687-694. https://doi.org/10.1016/j.scitotenv.2015.07.090

Lutri, V.F., Matteoda, E. and Blarasin, M. 2020. Hydrogeological features affecting the spatial distribution of glyphosate and AMPA in groundwater and surface water in an agroecosystem. Córdoba, Argentina. Sci. Total Environ., 711: 134557. https://doi.org/10.1016/j.scitotenv.2019.134557

Mac Loughlin, T.M., Peluso, M.L., Aparicio, V.C. and Marino, D.J.G. 2020. Contribution of soluble and particulate-matter fractions to the total glyphosate and AMPA load in water bodies associated with horticulture. Sci. Total Environ., 703: 134717. https://doi.org/10.1016/j.scitotenv.2019.134717

Maddalon, A., Galbiati, V. and Colosio, C. 2021. Glyphosate-based herbicides: Evidence of immune-endocrine alteration. Toxicology, 459: 152851. https://doi.org/10.1016/j.tox.2021.152851

Magal, P., Webb, G.F. and Wu, Y. 2019. An environmental model of honey bee colony collapse due to pesticide contamination. Bull. Math. Biol., 81: 4908-4931. https://doi.org/10.1007/s11538-019-00662-5

Maggi, F., la Cecilia, D. and Tang, F.H.M. and McBratney, A. 2020. The global environmental hazard of glyphosate use. Sci. Total Environ., 717: 137167. https://doi.org/10.1016/j.scitotenv.2020.137167

MamaCoca. 2000. Plan de Manejo Ambiental Erradicación de Cultivos Ilicitos. Plan manejo Ambient. 3-4.

Mann, R.M. and Bidwell, J.R. 1999. The toxicity of glyphosate and several glyphosate formulations to four species of Southwestern Australian frogs. Arch. Environ. Contam. Toxicol., 36: 193-199. https://doi.org/10.1007/s002449900460

Martinez-Haro, M., Chinchilla, J.M. and Camarero, P.R. 2022. Determination of glyphosate exposure in the Iberian hare: A potential focal species associated with agrosystems. Sci. Total Environ., 823: 153677. https://doi.org/10.1016/j.scitotenv.2022.153677

Martínez, A., Reyes, I. and Reyes, N. 2007. Citotoxicidad del glifosato en células mononucleares de sangre periférica humana. Biomédica, 27: 594. https://doi.org/10.7705/biomedica.v27i4.176

Martínez, P., Bernal, J., Agudelo, E. and Bernier, S. 2012. Tolerancia y degradación del glifosato por bacterias aisladas de suelos con aplicaciones frecuentes de Roundup SL®. Pilquen, 12: 454

Martins-Gomes, C., Silva, T.L., Andreani, T. and Silva, A.M. 2022. Glyphosate vs. Glyphosate-Based Herbicides Exposure: A Review on Their Toxicity. J Xenobiotics, 12: 21-40. https://doi.org/10.3390/jox12010003

Mayer, K. 2021. Herbicides and Your Health. https://www.webmd.com/cancer/herbicide-glyphosate-cancer (Accessed 3 Apr 2022).

McManus, S.L., Coxon, C.E. and Mellander, P.E. 2017. Hydrogeological characteristics influencing the occurrence of pesticides and pesticide metabolites in groundwater across the Republic of Ireland. Sci. Total Environ., 601-602: 594-602. https://doi.org/10.1016/j.scitotenv.2017.05.082

Meftaul, I.M., Venkateswarlu, K. and Annamalai, P. 2021. Glyphosate use in urban landscape soils: Fate, distribution, and potential human and environmental health risks. J. Environ. Manage., 292: 112786. https://doi.org/10.1016/j.jenvman.2021.112786

Méndez, A. 2015. Aislamiento E Identificación De Bacterias Capaces De Degradar Glifosato. Universidad ICESI.

Mercurio, P., Flores, F. and Mueller, J.F. 2014. Glyphosate persistence in seawater. Mar. Pollut. Bull., 85: 385-390. https://doi.org/10.1016/j.marpolbul.2014.01.021

Mesnage, R., Renney, G. and Séralini, G.E. 2017. Multiomics reveal non-alcoholic fatty liver disease in rats following chronic exposure to an ultra-low dose of Roundup herbicide. Sci. Rep., 7: 39328. https://doi.org/10.1038/srep39328

Mörtl, M., Németh, G. and Juracsek, J. 2013. Determination of glyphosate residues in Hungarian water samples by immunoassay. Microchem. J., 107: 143-151. https://doi.org/10.1016/j.microc.2012.05.021

Motta, E.V.S., Raymann, K. and Moran, N.A. 2018. Glyphosate perturbs the gut microbiota of honey bees. Proc Natl Acad Sci., 115: 10305-10310. https://doi.org/10.1073/pnas.1803880115

Mueller, T.C. and Senseman, S.A. 2015. Methods related to herbicide dissipation or degradation under field or laboratory conditions. Weed Sci., 63: 133–139. https://doi.org/10.1614/WS-D-13-00157.1

Muñóz, J.P., Bleak, T.C. and Calaf, G.M. 2021. Glyphosate and the key characteristics of an endocrine disruptor: A review. Chemosphere, 270: 128619. https://doi.org/10.1016/j.chemosphere.2020.128619

Okada, E., Coggan, T. and Anumol, T. 2019. A simple and rapid direct injection method for the determination of glyphosate and AMPA in environmental water samples. Anal. Bioanal. Chem., 411: 715-724. https://doi.org/10.1007/s00216-018-1490-z

Okada, E., Costa, J.L. and Bedmar, F. 2016. Adsorption and mobility of glyphosate in different soils under no-till and conventional tillage. Geoderma, 263: 78-85. https://doi.org/10.1016/j.geoderma.2015.09.009

Okada, E., Pérez, D. and De Gerónimo, E. 2018. Non-point source pollution of glyphosate and AMPA in a rural basin from the southeast Pampas, Argentina. Environ. Sci. Pollut. Res., 25: 15120-15132. https://doi.org/10.1007/s11356-018-1734-7

OMS 2020. Resistance to Antibiotics.. https://www.who.int/es/news-room/fact-sheets/detail/resistencia-a-los-antibioticos. (Accessed 4 Jun 2022).

Pacheco de Almeida Prado Bortolheiro, F. and de Almeida Silva, M. 2021. Low doses of glyphosate can affect the nutrient composition of common beans depending on the sowing season. Sci. Total Environ., 794: 148733. https://doi.org/10.1016/j.scitotenv.2021.148733

Pandey, A., Dabhade, P. and Kumarasamy, A. 2019. Inflammatory effects of subacute exposure of Roundup in rat liver and adipose tissue. Science, 17: 155. https://doi.org/10.1177/1559325819843380

Pandher, U., Kirychuk, S. and Schneberger, D. 2021. Pulmonary inflammatory response from co-exposure to LPS and glyphosate. Environ. Toxicol. Pharmacol., 86: 103651. https://doi.org/10.1016/j.etap.2021.103651

Pedemonte, F. 2017. Problemática del uso del glifosato. Universidad Nacional Agraria la Molina.

Peillex, C. and Pelletier, M. 2020. The impact and toxicity of glyphosate and glyphosate-based herbicides on health and immunity. J. Immunotoxicol., 17: 163-174. https://doi.org/10.1080/1547691X.2020.1804492

Poiger, T., Buerge, I.J. and Bächli, A. 2017. The occurrence of the herbicide glyphosate and its metabolite AMPA in surface waters in Switzerland was determined with online solid phase extraction LC-MS/MS. Environ. Sci. Pollut. Res., 24: 1588-1596. https://doi.org/10.1007/s11356-016-7835-2

Pöppe, J., Bote, K. and Merle, R. 2019. Minimum inhibitory concentration of glyphosate and a glyphosate-containing herbicide in *Salmonella enterica* isolates originating from different time periods, hosts, and serovars. Eur. J. Microbiol. Immunol., 9: 35-41. https://doi.org/10.1556/1886.2019.00005

Qiu, S., Fu, H. and Zhou, R. 2020. Toxic effects of glyphosate on intestinal morphology, antioxidant capacity, and barrier function in weaned piglets. Ecotoxicol. Environ. Saf., 187: 109846. https://doi.org/10.1016/j.ecoenv.2019.109846

Ramírez, F. 2021. El herbicida glifosato y sus alternativas Serie

Informes Técnicos IRET N° 44. https://www.researchgate.com/publication/349533585_El_herbicida_glifosato_y_sus_alternativas_Serie_Informes_Tecnicos_IRET_N_44. Accessed 7 Apr 2022

Relyea, R. 2012. New effects of Roundup on amphibians: Predators reduce herbicide mortality; herbicides induce antipredator morphology. Ecol. Appl., 22: 634-647. https://doi.org/10.1890/11-0189.1

Relyea, R.A. 2005. The impact of insecticides and herbicides on the biodiversity and productivity of aquatic communities. Ecol. Appl., 15: 618-627. https://doi.org/10.1890/03-5342

Rendon-von Osten, J. and Dzul-Caamal, R. 2017. Glyphosate residues in groundwater, drinking water and urine of subsistence farmers from intensive agriculture localities: A survey in Hopelchén, Campeche, Mexico. Int. J. Environ. Res. Public Health, 14: 595. https://doi.org/10.3390/ijerph14060595

Ribeiro, S., 2020. Maíz, transgénicos y transnacionales. Ciudad de México.

Rossi, E., Melgarejo, L. and Mendonça, M. 2020. Abejas & Agrotóxicos: Recopilación sobre las evidencias científicas de los impactos de los agrotóxicos en las Abejas – Petición ante la Relatoría DESCA de la Comisión Interamericana de Derechos Humanos. https://conacyt.mx/cibiogem/images/cibiogem/Documentos-recopilatorios-relevantes/Abejas-y-agrotoxicos.pdf

Roy, N.M., Ochs, J. and Zambrzycka, E. anderson, A., 2016. Glyphosate induces cardiovascular toxicity in Danio rerio. Environ Toxicol Pharmacol., 46: 292-300. https://doi.org/10.1016/j.etap.2016.08.010

Rueda-Ruzafa, L., Cruz, F., Roman, P. and Cardona, D. 2019. Gut microbiota and neurological effects of glyphosate. Neurotoxicology, 75: 1-8. https://doi.org/10.1016/j.neuro.2019.08.006

Ruiz, P., Dualde, P. and Coscollà, C. 2021. Biomonitoring of glyphosate and AMPA in the urine of Spanish lactating mothers. Sci. Total Environ., 801: 149688. https://doi.org/10.1016/j.scitotenv.2021.149688

Sabio y García, C.A., Schiaffino, M.R. and Lozano, V.L. 2020. New findings on the effect of glyphosate on autotrophic and heterotrophic picoplankton structure: A microcosm approach. Aquat. Toxicol., 222: 105463. https://doi.org/10.1016/j.aquatox.2020.105463

Salazar-López, N.J. and Aldana Madrid, M.L. 2011. Glyphosate herbicide: Uses, toxicity and regulation. Biotecnia, 13: 23. https://doi.org/10.18633/bt.v13i2.83

Sánchez, G. and Salceda, R. 2008. Polyfunctional Enzymes: The case of Acetylcholinesterase. https://www.medigraphic.com/pdfs/revedubio/reb-2008/reb082b.pdf. Accessed 5 Mar 2022

Sanchís, J., Kantiani, L. and Llorca, M. 2012. Determination of glyphosate in groundwater samples using an ultrasensitive immunoassay and confirmation by online solid-phase extraction followed by liquid chromatography coupled to tandem mass spectrometry. Anal. Bioanal. Chem., 402: 2335-2345. https://doi.org/10.1007/s00216-011-5541-y

Schuette, J. 1998. Environmental Fate of Glyphosate. https://silo.tips/download/environmental-fate-of-glyphosate-jeff-schuette. Accessed 4 Feb 2022.

Singh, S., Kumar V. and Datta, S. 2020a. Glyphosate uptake, translocation, resistance emergence in crops, analytical monitoring, toxicity and degradation: a review. Environ. Chem. Lett., 18: 663-702. https://doi.org/10.1007/s10311-020-00969-z

Singh, S., Kumar V. and Gill, J.P.K. 2020b. Herbicide Glyphosate: Toxicity and Microbial Degradation. Int. J. Environ. Res. Public Health, 17: 7519. https://doi.org/10.3390/ijerph17207519

Skeff, W., Neumann, C. and Schulz-Bull, D.E. 2015. Glyphosate and AMPA in the estuaries of the Baltic Sea method optimization and field study. Mar. Pollut. Bull., 100: 577-585. https://doi.org/10.1016/j.marpolbul.2015.08.015

Solomon, K.R. 2016. Glyphosate in the general population and applicators: a critical review of studies on exposures. Crit. Rev. Toxicol., 46: 21-27. https://doi.org/10.1080/10408444.2016.1214678

Sørensen, M.T., Poulsen, H.D., Katholm, C.L. and Højberg, O. 2021. Review: Feed residues of glyphosate-potential consequences for livestock health and productivity. Animal, 15: 100026. https://doi.org/10.1016/j.animal.2020.100026

Strandberg, B., Sørensen, P.B. and Bruus, M. 2021. Effects of glyphosate spray-drift on plant flowering. Environ. Pollut., 280: 116953. https://doi.org/10.1016/j.envpol.2021.116953

Sun, M., Li, H. and Jaisi, D.P. 2019. Degradation of glyphosate and bioavailability of phosphorus derived from glyphosate in a soil-water system. Water Res., 163: 114840. https://doi.org/10.1016/j.watres.2019.07.007

Tan, S., Li, G. and Liu, Z. 2022. Effects of glyphosate exposure on honeybees. Environ. Toxicol. Pharmacol., 90: 103792. https://doi.org/10.1016/j.etap.2021.103792

Thanomsit, C., Saetiew, J. and Meemon, P. 2022. Optical coherence tomography as an alternative tool for evaluating the effects of glyphosate on hybrid catfish (Clarias gariepinus × Clarias macrocephalus). Toxicol. Rep., 9: 181-190. https://doi.org/10.1016/j.toxrep.2022.01.010

Toccalino, P.L., Norman, J.E. and Scott, J.C. 2012. Chemical mixtures in untreated water from public-supply wells in the U.S.-Occurrence, composition, and potential toxicity. Sci Total Environ., 431: 262-270. https://doi.org/10.1016/j.scitotenv.2012.05.044

Torrado, J. 2018. Determinación de los efectos negativos que causa la aplicación del glifosato como mecanismo de control de arvenses sobre la salud humana y de los animales. Universidad Nacional Abierta Y A Distancia (UNAD)

Torretta, V., Katsoyiannis, I., Viotti, P. and Rada, E. 2018. Critical Review of the Effects of Glyphosate Exposure to the Environment and Humans through the Food Supply Chain. Sustainability, 10: 950. https://doi.org/10.3390/su10040950

Van Bruggen, A.H.C., He, M.M. and Shin, K. 2018. Environmental and health effects of the herbicide glyphosate. Sci. Total Environ., 616-617: 255-268. https://doi.org/10.1016/j.scitotenv.2017.10.309

Van Stempvoort, D.R., Spoelstra, J. and Senger, N.D. 2016. Glyphosate residues in rural groundwater, Nottawasaga River Watershed, Ontario, Canada. Pest. Manag. Sci., 72: 1862-1872. https://doi.org/10.1002/ps.4218

Vargas, A. 2018. Efecto del Alquil-Amina-Polietoxilada (POEA) y CaCO3 en Plaractus Brachypomus (Cuvier, 1818) (Characiformes: Characidae).

Villalba, A. 2009. Resistencia a herbicidas. Glifosato. Ciencia, Docencia y Tecnol Univ Nac Entre Ríos Concepción del Uruguay, Argentina XX: 169-186

von Ehrenstein, O.S., Ling, C. and Cui, X. 2019. Prenatal and infant exposure to ambient pesticides and autism spectrum disorder in children: Population-based case-control study. BMJ, l9: 62. https://doi.org/10.1136/bmj.l962

Wang, S., Seiwert, B. and Kästner, M. 2016. (Bio)degradation of glyphosate in water-sediment microcosms: A stable isotope co-labeling approach. Water Res., 99: 91-100. https://doi.org/10.1016/j.watres.2016.04.041

Weisenburger, D.D. 2021. A Review and Update with Perspective of Evidence that the Herbicide Glyphosate is a Cause of Non-Hodgkin Lymphoma. Clin Lymphoma Myeloma Leuk. 21: 621-630. https://doi.org/10.1016/j.clml.2021.04.009

WHO 2005. Glyphosate and AMPA in Drinking Water. https://www.who.int/water_sanitation_health/dwq/chemicals/glyphosateampa290605.pdf? Accessed 4 Feb 2022

Williams, A.L., Watson, R.E. and DeSesso, J.M. 2012. Developmental and reproductive outcomes in humans and animals after glyphosate exposure: A critical analysis. J. Toxicol. Environ. Health Part B, 15: 39-96. https://doi.org/10.1080/10937404.2012.632361

Williams, G.M., Aardema, M. and Acquavella, J. 2016a. A review of the carcinogenic potential of glyphosate by four independent expert panels and comparison to the IARC assessment. Crit. Rev. Toxicol., 46: 3-20. https://doi.org/10.1080/10408444.2016.1214677

Williams, G.M., Berry, C. and Burns, M. 2016b. Glyphosate rodent carcinogenicity bioassay expert panel review. Crit. Rev. Toxicol., 46: 44-55. https://doi.org/10.1080/10408444.2016.1214679

Williams, G.M., Kroes, R., Munro, I.C. 2000. Safety Evaluation and Risk Assessment of the Herbicide Roundup and Its Active Ingredient, Glyphosate, for Humans. Regul Toxicol. Pharmacol., 31: 117-165. https://doi.org/10.1006/rtph.1999.1371

Wrobel, M.H. 2018. Glyphosate affects the secretion of regulators of uterine contractions in cows, while it does not directly impair the motoric function of myometrium in vitro. Toxicol. Appl., Pharmacol., 349: 55-61. https://doi.org/10.1016/j.taap.2018.04.031

WSDA. 2020. Glyphosate: Ecological Fate and Effects and Human Health Summary. https://agr.wa.gov/getmedia/1a7d9deb-18dd-4604-84fd-da3805750854/871-wsdaglyphosatesummary2020. Accessed 4 May 2022

Ximénez, P. 2020. Bayer Agrees to Pay $11 Billion to Victims of Roundup Herbicide in the United States. https://elpais.com/sociedad/2020-06-24/bayer-acepta-pagar-11000-millones-de-dolares-a-las-victimas-del-herbicida-roundup.html. Accessed 5 Jun 2022.

Xu, J., Smith, S. and Smith, G. 2019. Glyphosate contamination in grains and foods: An overview. Food Contr., 106: 106710. https://doi.org/10.1016/j.foodcont.2019.106710

Xu, X., Ji, F., Fan, Z. and He, L. 2011. Degradation of glyphosate in soil photocatalyzed by Fe3O4/SiO2/TiO2 under solar light. Int. J. Environ. Res. Public Health, 8: 1258-1270. https://doi.org/10.3390/ijerph8041258

You, Z., Li, M. and Lambrechts, E. 2013. Glyphosate and AMPA inhibit cancer cell growth by inhibiting intracellular glycine synthesis. Drug. Des. Devel. Ther., 91: 635. https://doi.org/10.2147/DDDT.S49197

Zhao, J., Pacenka, S. and Wu, J. 2018. Detection of glyphosate residues in companion animal feeds. Environ. Pollut., 243: 1113-1118. https://doi.org/10.1016/j.envpol.2018.08.100

ORCID DETAILS OF THE AUTHORS

S. Jawahar: https://orcid.org/0009-0004-7805-9501
L. A. García: https://orcid.org/0000-0003-3080-1282
I. Y. Hernández: https://orcid.org/0000-0001-6097-223X
G. Fernández: https://orcid.org/0000-0002-9748-4157
J. Rodrigo: https://orcid.org/0000-0001-8380-7376
M. E. Rodrigo: https://orcid.org/0000-0002-8611-0504
G. L. Andraca: https://orcid.org/0000-0002-7945-7294
G. B. Hernández: https://orcid.org/0000-0002-4463-5900
S. Banda-Santamaría: https://orcid.org/0009-0001-4844-9654

Nature Environment and Pollution Technology
An International Quarterly Scientific Journal

p-ISSN: 0972-6268
(Print copies up to 2016)
e-ISSN: 2395-3454

Vol. 23 | No. 1 | pp. 33-53 | 2024

Original Research Paper

https://doi.org/10.46488/NEPT.2024.v23i01.003

Open Access Journal

Study On Spatial Variations of Surface Water Quality Vulnerable Zones in Baitarani River Basin, Odisha, India

Abhijeet Das*†, J. Jerlin Regin, A. Suhasini*** and K. Baby Lisa******

*Department of Civil Engineering, C.V. Raman Global University (C.G.U), Bhubaneswar-752054, Odisha, India
**Department of Civil Engineering, St. Xavier's Catholic College of Engineering, Nagercoil, Tamil Nadu, India
***Department of Chemistry, St. Xavier's Catholic College of Engineering, Nagercoil, Tamil Nadu, India
****Department of Electronics and Communication Engineering, St. Xavier's Catholic College of Engineering, Nagercoil, Tamil Nadu, India
†Corresponding author: Abhijeet Das; das.abhijeetlaltu1999@gmail.com, abhijeetlaltu1994@gmail.com

Nat. Env. & Poll. Tech.
Website: www.neptjournal.com

Received: 05-07-2023
Revised: 20-08-2023
Accepted: 21-08-2023

Key Words:
Water quality
Baitarani river
Entropy
TOPSIS
Pollution
Anthropogenic activities

ABSTRACT

The stated goal of the research is to investigate the surface water quality of the Baitarani River in Odisha to ascertain its compatibility for various uses. Large, complex datasets generated during the one-year (2021-2022) monitoring program were collected from 13 locations and encompassed 22 parameters. To examine temporal and spatial fluctuations in and to interpret these datasets, MCDMs like TOPSIS and the Entropy-based Water Quality Index (EWQI) were utilized. The physical and chemical outcomes of the current experiment were compared to WHO standards. According to the analysis's results, turbidity and total coliform (TC) are indicators that have a greater impact on water quality in all locations during both seasons and are directly linked to home and agricultural non-point source pollution. As per EWQI interpretation, 30.77 % of the observations in PRM and POM fall under the poor category. The findings showed how anthropogenic activities have harmed St. 8, 11, 12, and 13 and require effective management. A quantifiable approach was also carried out to decide the efficacy of TOPSIS. Farming attributes, including SAR, % Na, RSC, MR, KI, and PI, were estimated to delineate the agriculturally practicable zones. This work can offer a reference database for the betterment of water quality.

INTRODUCTION

Water pollution is the accumulation of naturally occurring organic matter, which is a complex mixture of different organic molecules resulting primarily from aquatic life, soil, and terrestrial vegetation, as well as toxic chemicals that are available in higher concentrations than what is usually found in water and may be dangerous to the environment (Thakur et al. 2020, Das 2022a). These days, water quality has become a severe problem that has drawn attention from all around the world to preserve and safeguard them (Banda & Kumarasamy 2020). River water quality is being negatively impacted by a number of anthropogenic and natural processes, which is preventing rivers from being used for a variety of purposes (Das 2022b, 2023). It is also a significant issue in the governance and design of water resources (Akhtar et al. 2020). In addition, a rise in urbanization, building, agricultural, and industrial activities, as well as natural processes like bedrock weathering, volcanic and earth crust erosion as well as human-induced actions like wastes generated from coal combustion, metallurgy, mining, and metal smelting are all contributing factors (Meng et al. 2017, Jha et al. 2020, Jinisha et al. 2020). Additionally, it has a negative influence on surface and groundwater, as well as on human well-being (Meshram et al. 2022). Surface water quality has grown extremely important in recent decades, especially in emerging nations like India. It has also become a touchy subject (Bora et al. 2017, Singh et al. 2020a). Therefore, monitoring the level of components, their concentration, sources, and distribution is crucial to managing water resources and preventing water pollution (Usman et al. 2018, Hong et al. 2020). Surface water quality (WQ) monitoring experts confront a difficult problem when elucidating monitored data (Hong et al. 2016). Water Quality Indices (WQIs) were developed as a result, and they are quite user-friendly and simple to use in computing hardware (Shrestha & Basnet 2018). Horton (1965) made the first modern WQI suggestion. Since then, a number of studies have put out and used several indexes to categorize the water quality in the concerned area (Tiyasha et al. 2020), but there isn't a WQI that is universally recognized. WQI development

involves a lot of subjectivity and unpredictability (Landwehr 1979). Subjective disturbances would be reduced by assigning fixed weights based on the indices and using intrinsic information (Li et al. 2010). Shannon (1948) or information entropy may be used to explain this data. Researchers applied information entropy effectively in their work (Singh 2013, 2014, Talukder et al. 2017). The term "entropy-weighted water quality index (EWQI)" refers to the summation of respective parameter weights and rating scales based on quality, taking all the criteria and transforming them into a cumulatively calculated numerical score. These are an enhancement over traditional WQIs which generally focused on the Delphi technique. Another major feature is the Analytical Hierarchy Process (AHP) approach, along with the expert survey method (ESM), which is jointly dependent on the assigning of weights to the concerned or relevant parameters that depend upon individual judgments and expert advice (Gorgij et al. 2019, Singh et al. 2020b). Geographical Information System (GIS) is a crucial concept to understand geospatial details in today's world for surface WQ (Balamurugan et al. 2020). Scientists from several domains have developed the GIS in recent decades for geospatial investigation, case studies, and its blending technique (Burrough & McDonnell 1998). Inverse Distance Weighting was used to accomplish this (IDW). Large datasets can be quickly and affordably transformed into a variety of spatially distributed diagrams and projections, which show trends, correlations of indicators, and vital pollution sources (Reddy et al. 2019). In the Adyar River basin, Chennai, Tamil Nadu, India, for instance, Ramachandran et al. (2020) illustrated seasonal quality water based on drinking WQI in conjunction with GIS. They discovered that the quality was contaminated for human use in many parts of the area investigated. Researchers have assessed the possibilities of multi-objective decision-making strategies in stream restoration initiatives in addition to WQIs, including demand response, redressing management, renewable energy sources, and WQI ranking modifications (Yousefi et al. 2018). TOPSIS determined the overall rating of each sampling site's pollution level (Technique for Order of Preference by Similarity to Ideal Solution). It uses information entropy and aims to find the scenario that is the farthest away from the negative ideal solution (NIS) and closest to the positive ideal solution (PIS) (Hwang et al. 1993). For exhibiting the quality of surface water in terms of irrigation, agricultural indicators namely Sodium adsorption ratio (SAR), Permeability index (PI), Residual sodium carbonate (RSC), Kelley's (1963) index (KI), Percent sodium (% Na), Magnesium hazard (MH) ratio, Residual sodium bicarbonate (RSBC), and Potential salinity (PS) have been widely used (Brhane 2018). To demonstrate the caliber of the water evaluation of the Baitarani River in Odisha, India, which aims to determine the many causes responsible for the fluctuations in the water quality, the present study was undertaken in 2021–2022. 22 physiochemical water quality parameters were inspected during the detection period, i.e., Pre-monsoon (PRM) and Post-monsoon (POM). The time frame considered for analysis is 1-year. The novelty of this recent study is a result of the integration of EWQI, GIS, and MCDMs in the management and monitoring of water quality. To evaluate if surface water is suitable for irrigation, calculations of agricultural indices such as SAR, % Na, RSC, PI, KR, MR, RSBC, and PS are also taken into account.

MATERIALS AND METHODS

Description of Study Area

The planned study would focus on the Baitarani River basin, which is located between 21°0'0" and 22° latitude and 85°0'0" to 86°30'0" east longitude. Because agriculture predominates in this region, crops like rice, maize, wheat, groundnuts, vegetables, and green gram are grown all year round. Vegetables and rice (paddy) are the prominent food crops grown in the area. Additionally, it is a popular tourist site and has built 7200 small-scale manufacturing enterprises. Due to the abundance of alluvial soil in the area, several crops thrive there. The mean annual rainfall is 1628 mm, and summertime temperatures range from 30 to 36°C to 16 to 17°C in winter. The topography of the basin is undulating, with an average slope of between 0 and 2 percent. It has a surface area of approximately 8645 km^2 and an elevation range of 32 to 1181 m above mean sea level (MSL). Most of the human population in this basin depends upon agriculture for their livelihood, and it is majorly used for cultivation, production, and horticulture techniques. However, the river has experienced quick and unchecked development activities, including the installation of industries, building projects, and the use of agricultural and forest areas for further development purposes. The soils also experience mild to severe erosion as a result of the absence of integrated soil conservation and irrigation methods. Since they are of enormous ecological and environmental value, proper monitoring is required to implement plans for their preservation and restoration. Fig. 1 shows the map showing locations and river path of the Baitarani River in the State of Odisha.

Sample Collection, Preservation, and Analysis

The watershed was first surveyed to determine the sampling site's location and to explain the specific point and non-point sources of contamination. 13 locations were selected owing to

Fig. 1: Location of the study area with sampling points.

the research area's high population density, agricultural activity, and waste disposal facilities. A weighted bottle sampler was used to collect water samples in triplicate throughout the years 2021–2022. After collection, the bottles were firmly shut and maintained in a refrigerator at 4°C. The dilutions were performed using deionized water. By dilution, the stock solutions were made into standard solutions. When sampling and testing, quality assurance and quality control are effective ways to get more precise data. The analysis has adhered to quality control in accordance with the 20th edition under the norms of Standard Methods which is used for the Examination of Water and Wastewaters, issued by APHA (2017). For their correctness in interpreting chemical data, these variables were cross-checked depending upon the principle of ionic balance error (IBE), which is otherwise defined as IBE = [(cations - anions)/ (cations + anions)] × 100. The cations and anions are displayed in milligrams per liter ($mg.L^{-1}$). The IBE value should not go over the permissible threshold of 5%.

Data Processing

Inverse distance weighted approaches are the most widely used techniques for creating spatial distribution maps (IDW). Using ArcGIS, this method was utilized to produce spatial variation maps (Anand et al. 2020, Ram et al. 2021). Microsoft Excel 2016 with XLSTAT 2015 was used to undergo statistical and computational analysis.

Entropy-Weighted Water Quality Index (EWQI)

The evaluation of water quality frequently uses the EWQI (Marghade et al. 2019). The following are the steps taken in the EWQI calculation as per (Gorgij et al. 2017). The following formula, developed by Claude Shannon in 1948, calculates the information entropy (E) of each assessed parameter, and it is expressed as $E_n = -(1/\ln n) \sum_{i=1}^{m} Vij \times \ln Vij$, whereas the variable "n" stands for a number of locations, and V_{ij} is taken as the probability of occurrence on the basis of the normalized value of examined parameter 'j' within the i^{th} specimen. It is expressed as $V_{ij} = v_{ij} / \sum v_{ij}$. Entropy weights (W) are calculated using $W_j = (1-E_j)/\sum(1-E_j)$. Lastly, the conjunction of entropy weights with the quality rating scale results in the given equation, and it is stated as $EWQI = \sum W_j \times U_j$, where U_j talks about individual variable which denotes the ratio which explains as monitored value gets divided by its standard value (S_j) for that indicator and it expresses in the form of $U_j = (I_j/S_j) \times 100$. Waters with an EWQI of 50 or less are considered to have excellent quality, those between 50 and 100 are considered to be good, those between 100 and 150 are considered to be average, those between 150 and 200 are considered to be poor, and those greater than 200 are considered to have extremely poor quality.

Determination of Rank using the TOPSIS Method

While calculating the Euclidean distances between the

positive ideal solution (PIS) and the nearest ideal solution (NIS), TOPSIS, which is based on information entropy, seeks to find the alternative or scenario that is closest to each. It is a useful tool for decision-making processes and can be used in the ways listed below (Hwang et al. 1993): Employing matrix P, grades for the sampling areas and their parameters were assigned. The matrix is clearly expressed below:

$$P_{m*c} = \begin{matrix} P11 & P12 \ldots & P1c \\ : & \ldots Pij & : \\ Pm1 & \ldots & Pmc \end{matrix}$$

Where P_{ij} displayed the value of the i^{th} alternative for the j^{th} criterion, the following criteria weights were generated using information entropy approaches. It is expressed in the following equation: $q_{ij} = P_{ij} / (P_{ij} + \ldots\ldots\ldots + P_{mj})$; for all $j \in \{1\ldots., c\}$ And, $E_j = [-1/\ln (m)] \sum q_{ij} \times \ln q_{ij}$; for all $j \in \{1\ldots., c\}$, where $0 \leq E_j \leq 1$. It talks about an index with a greater entropy value having a higher variation. Therefore, the weight is calculated as $W_j = d/ (d_1 + \ldots\ldots. + d_j)$ and $d_j = 1\text{-}E_j$. The equation $V = [N]_{m*c} \times w_{c*c}$ represents the normalized weighted decision matrix. Two ideal solutions namely PIS and NIS were computed from PIS = $\{\max v_{ij} I\, v_{ij} \in V\} = (v_1^+, \ldots., v_c^+)$ & NIS = $\{\min v_{ij} I\, v_{ij} \in V\} = (v_1^-, \ldots., v_c^-)$. Finally, the Euclidean distance of individual alternative from the PIS (d_i^+) and NIS (d_i^-) was computed as: $d_i^+ = [\sum (v_{ij} - v_j^+)^2]^{0.5}$ & $d_i^- = [\sum (v_{ij} - v_j^-)^2]^{0.5}$. Proximity or closeness coefficients (C.C) of each and every alternative was calculated as $PS = d_i^- / (d_i^- + d_i^+)$. Finally, the possibilities were ordered by their closeness coefficients.

Irrigation Water Quality Parameters

The quality of irrigation water indicates the appropriateness for agricultural use. In light of this, Equations based on Subramani et al. (2019) were used and taken to calculate the agricultural parameters such as SAR, % Na, RSC, PI, KR, MH, RSBC, and PS, in which all the ions are addressed in meq.L^{-1}. An important salinity tool, namely the sodium adsorption ratio (SAR) index, measures the ratio of the ions Na^+, Ca^{2+}, and Mg^{2+} in a water sample. In this index, Sodium hazard can be easily understood by estimating SAR, and it is computed with the help of this equation suggested by Richard (1954) and Adimalla (2018). Hence, it is expressed as SAR = $Na^+ / 2\{(Ca^{2+} + Mg^{2+})/2\}^{0.5}$. According to the index, irrigation water falls into one of four categories: excellent (<10), good (10-18), doubtful (18-26), and unsuitable (>26). Another indication of the quality of irrigation water is the sodium percentage (%Na), or soluble sodium concentration. Na^+ reacts with the soil and causes particle blockage, which lowers permeability (Suresh & Kottureshwara 2009, Keesari et al. 2016). It can be estimated using the relationship shown below: Na% = $[Na^+ / (Ca^{2+} + Mg^{2+} + Na^+)] \times 100$. Fipps (2003) claims that irrigation with water that has a sodium concentration of more than 60% may result in Na+ build-ups in the soil, which will damage the soil's physical properties. The compound residual sodium carbonate (RSC) is a mixture of the ions Ca^{2+}, Mg^{2+}, and CO_3^{2-} and HCO_3^- (Zaki et al. 2018). It is a crucial parameter and is expressed as RSC = $(HCO_3^- + CO_3^{2-}) - (Ca^{2+} + Mg^{2+})$ to determine the appropriateness. It is dangerous to use water for irrigation that has an RSC index > 2.5 meq.L^{-1}. It is safe for cultivable crops when the RSC index is less than 1.25 meq.L^{-1} and somewhat suitable when the RSC index is between 1.25 and 2.5 meq.L^{-1} (Narsimha 2020). In order to improve agriculture, the permeability index (PI), a key measure, is used to examine the effectiveness of irrigation water in relation to the soil. The following formula is used to calculate this value, and it is expressed as PI = $[Na^+ + (HCO_3^-)^{0.5}/(Ca^{2+} + Mg^{2+} + Na^+)] \times 100$. Using the permeability index (PI), Doneen (1965) divided the irrigation water into three classes. Class I talks about 100% maximum permeability, hence, safe for irrigation). On the other hand, Class II represents 75% maximum permeability, and it comes under the slightly appropriate class. Ultimately, Class III belongs to 25% maximum permeability, which depicts that it is not safe for farming. Kelly (1963) suggested that the values of the Kelly Index (KI) ratio might be used to conveniently handle the Na^+ problem in irrigation water. Na^+ is in opposition to Ca^{2+} and Mg^{2+} ions in this combination. This is computed by a formula, i.e., KI = $Na^+ / (Ca^{2+} + Mg^{2+})$. When KR is less than 1, water is suitable for irrigation, and when KR is greater than 1, it is not suitable for irrigation. The soil structure is typically harmed by greater Mg^{2+} concentrations, which causes the water to absorb more Na^+ and salts and reduce crop yields (Keesari et al. 2018). The magnesium hazard (MH) is the harmful result of the excessive concentration of Mg^{2+} in the irrigation water. The index for calculating the index, developed by Paliwal (1972), is MH = $[Mg^{2+} / (Ca^{2+} + Mg^{2+})] \times 100$. Water with an MH of less than 50 is regarded as appropriate for irrigation. However, surface water with an MH of more than 50 is not useful for irrigation. Because extended watering reduces soil permeability owing to HCO_3^- precipitation, an index termed residual sodium bicarbonate (RSBC) will be used to assess the alkalinity risk. It is determined using the Kadam et al. (2021) -proposed equation, i.e., RSBC = $HCO_3^- - Ca^{2+}$. The index values of 5 meq.L^{-1} were deemed satisfactory by Ravikumar and Somashekar (2017). Plant growth may be impacted by concentrations higher than 10 meq.L^{-1}. The river's potential salinity (PS) is steadily rising each year and is now acknowledged as a significant issue for downstream water users (Kumarasamy et al. 2014). It is thought to be

equal to the Cl^- concentration plus 50 percent of the sulfate concentration (Ravikumar & Somashekar 2017). This is represented or calculated using an equation, i.e., $PS = Cl^- + (½ * SO_4^{2-})$.

RESULTS AND DISCUSSION

Using pH, one may determine if surface water is acidic or alkaline (Balamurugan et al. 2020). In PRM and POM, the pH values ranged from 7.3 to 9.7 $mg.L^{-1}$, indicating alkaline conditions that favor phytoplankton development. In accordance with the WHO's (2017) recommendation for the pH range (6.5-8.5) for standard drinking water quality. Because of the increased warmth and photosynthetic activity, some stations have detected higher pH levels in drinking water. Due to the presence of these suspended particles, also known as turbidity, which get deposited in the water, the purity of the water reduces. The WHO has set a turbidity permissibility limit of 5 NTU (Nephelometric Turbidity Unit) (Kumar & Puri 2012). During the PRM and POM seasons, the values in the current study range between 8.2-25.2 and 11.8-38.7. Due to the presence of organic and inorganic debris from sewage discharge and agricultural runoff, the value was found to be high in all-weather circumstances. TDS (total dissolved solids) is a measure of the total salt content dissolved in water. The recorded values during PRM and POM in the experiment varied from 74 to 178 and 97 to 247, respectively, showing that they were well within the limitations (500 $mg.L^{-1}$). Due to excessive TSS (total suspended solids), less light enters the water, and photosynthesis proceeds more slowly. These effects lower the DO (dissolved oxygen) level and lessen the clarity of the water. On the other hand, during the seasons, i.e., PRM and POM, the value ranged between 30-121 and 97-247. According to WHO (2017), the amount was significantly below the 500 $mg.L^{-1}$ minimum threshold for drinking and agricultural purposes. The dissolved and suspended component or saltiness of the water is measured by the EC (electrical conductivity). It was in the range of 96-318 and 121-393 during PRM and POM, which is well satisfying the WHO criteria of 2250 $\mu S.cm^{-1}$. Because it has an impact on the organisms that live in the water body, DO is a crucial indicator for evaluating the quality of surface water (Bu et al. 2019). For this study, the DO values were noticed as 4.78-8.01 in PRM and 5.03-7.69 in POM respectively. As a result, DO levels are optimal over the whole research region. Higher alkalinity in water, and vice versa, increases its ability to neutralize acids. According to WHO (2017), it shouldn't be more than 120 $mg.L^{-1}$. The values fall between 43-99 in PRM and 69-99 in POM. The reading was discovered to be within the acceptable limit (120 $mg.L^{-1}$) for the entire sampling season. BOD (biochemical oxygen demand) measures how much oxygen microorganisms utilize to break down organic materials (Siraj et al. 2010). The recorded BOD values varied in a span of 0.86-4.23 in PRM and 0.88-4.54 in POM, respectively. The value was found to be under the WHO guideline limit (5 $mg.L^{-1}$). According to Marko et al. (2014), TH (total hardness) results from the presence of Ca^{2+} (calcium) and Mg^{2+} (magnesium) ions in the river and ranges from 64 to 121 in PRM and 71 to 135 in POM. The findings in this investigation were below the 300 $mg.L^{-1}$ acceptable limit (WHO 2017). In addition, rock weathering and rock-water interactions were blamed for the bicarbonate (HCO_3^-) concentration. In the current work, the values for PRM and POM, respectively, varied from 41.92 to 87.55 and 55.64 to 91.46. Readings from all of the chosen locations indicated that concentrations were higher during the wet season than they were during the dry season. Gypsum leaching results in the naturally occurring presence of SO_4^{2-} (sulfate) in water. The observed values for PRM and POM are respectively 2.4-6.87 and 2.31-7.16. The concentration in the river was at a level that did not provide a health risk, and the current readings in the study region were below the norm of WHO criteria and taken as 250 $mg.L^{-1}$. The primary causes of NO_3^- (nitrate) contamination of surface water were residential trash disposal in open areas, sewage disposal, and chemical fertilizers (Panneerselvam et al. 2020). The NO_3^- readings ranged in the ongoing work, with a value of 0.65 to 4.15 $mg.L^{-1}$ during the PRM and POM periods, respectively. It is suggested that 45 $mg.L^{-1}$ is the desirable upper limit for human consumption (WHO 2017). All observations, though, fell within the permitted ranges for each sample site. An exceptionally high dosage of PO_4^{3-} (phosphate) could cause digestive issues (Pandit & Yousuf 2002). Its value during the study period varied between 0.25 and 1.04 in PRM and 0.31 and 1.17 in POM. The findings showed that all of the water samples were within the WHO (2017) recommended limits of 1.2 $mg.L^{-1}$ and could be consumed directly without further treatment. The main sources of Cl^- (chloride) in surface water include arid climate, household waste, septic tanks, leaks, and irrigation return flows (Sadat-Noori et al. 2014, Wu et al. 2011). Cl^- levels in PRM and POM ranged from 7.87 to 28.18 and 8.72 to 28.86, respectively; these values fall within the allowable range of 250 $mg.L^{-1}$. Ca^{2+} is crucial for the normal development of bones, bodily fluid balance, muscle contraction, and testicular descent (Heaney et al. 1982). The usual threshold for Ca^{2+} in drinking water is taken as 75 $mg.L^{-1}$ (WHO 2017). It varied between 14.83 and 28.72 for PRM and 14.03 and 29.74 for POM in the research area. All places have water with Ca^{2+} levels that are within WHO guidelines. Additionally, the increased Mg^{2+} in the irrigation water aids in the plant's uptake of Ca^{2+} or K^+,

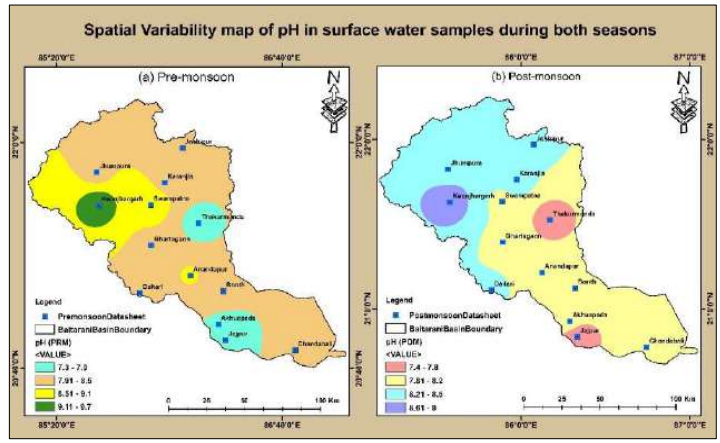

Fig. 2a: pH map.

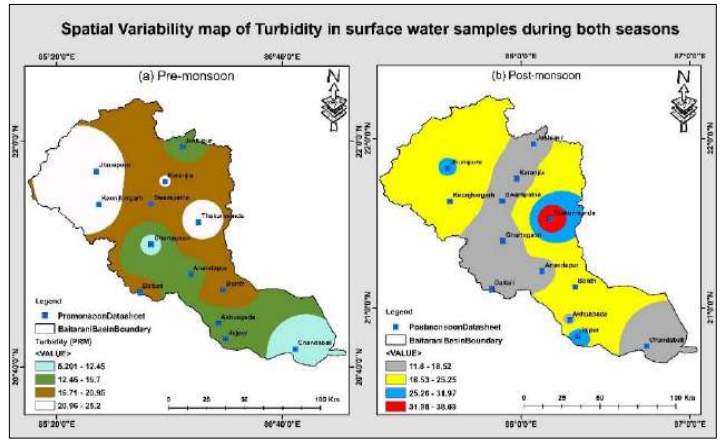

Fig. 2b: Turbidity map.

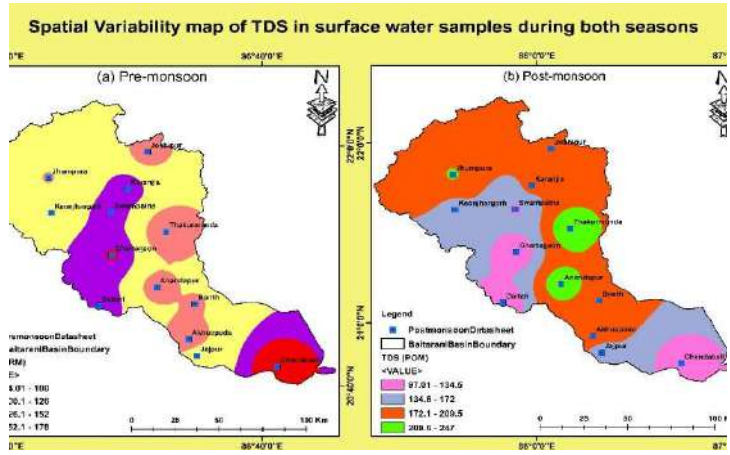

Fig. 2c: TDS map.

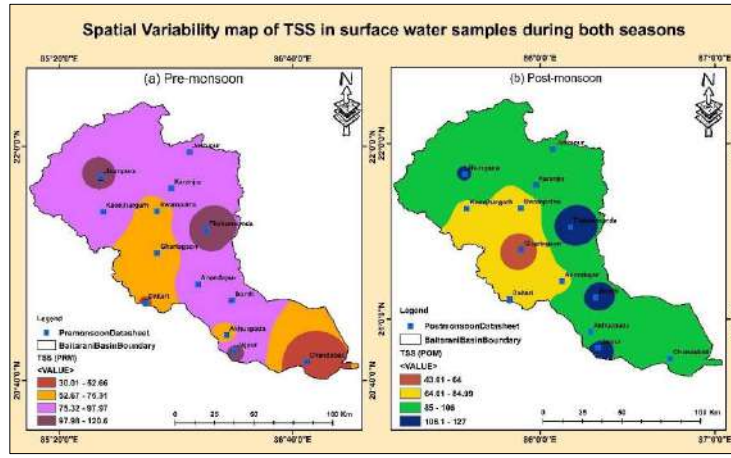

Fig. 2d: TSS map.

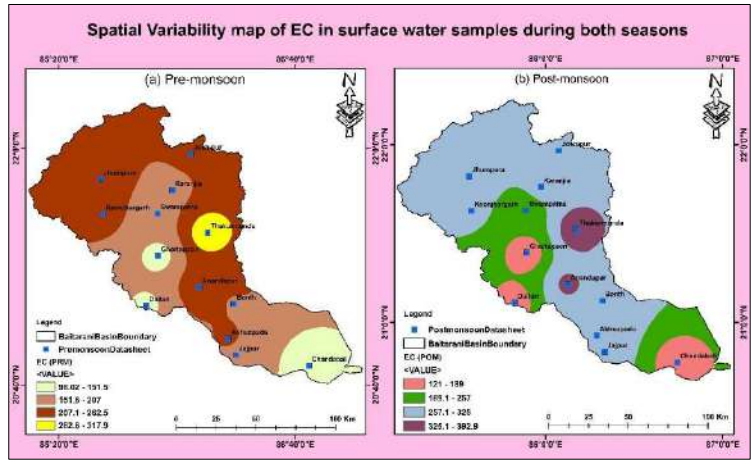

Fig. 2e: EC map.

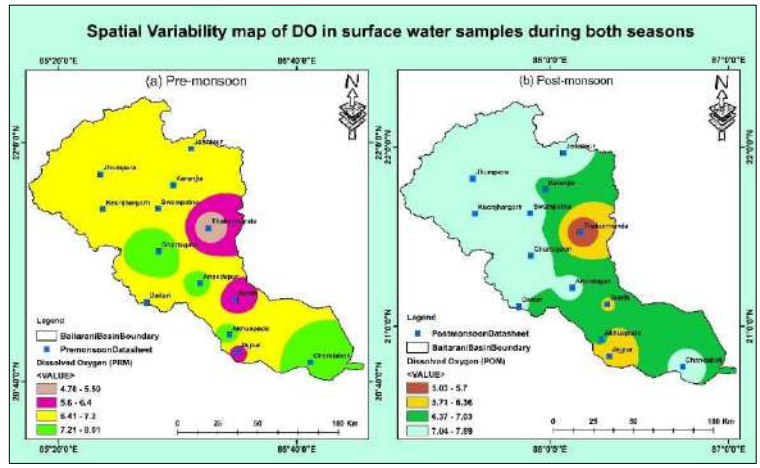

Fig. 2f: DO map.

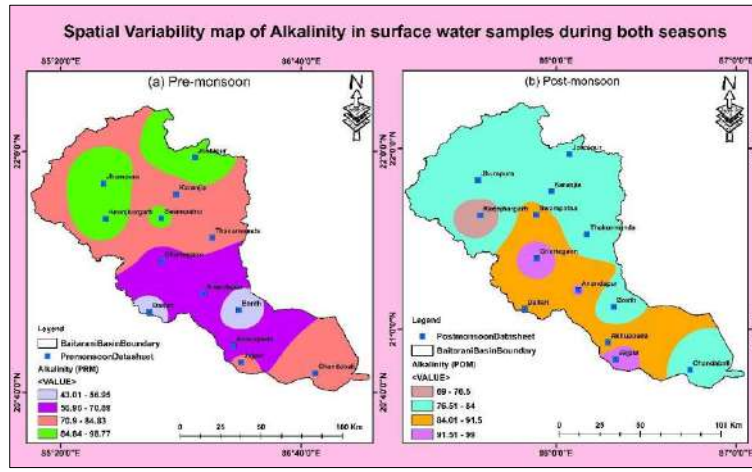

Fig. 2g: Alkalinity map.

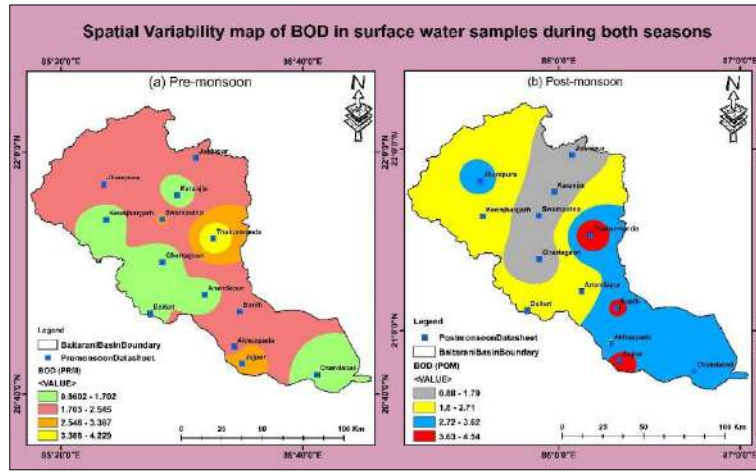

Fig. 2h: BOD map.

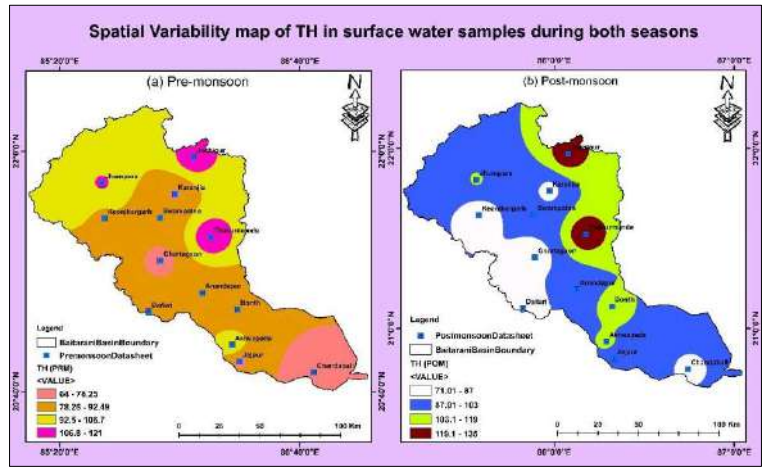

Fig. 2i: Total hardness (TH) map.

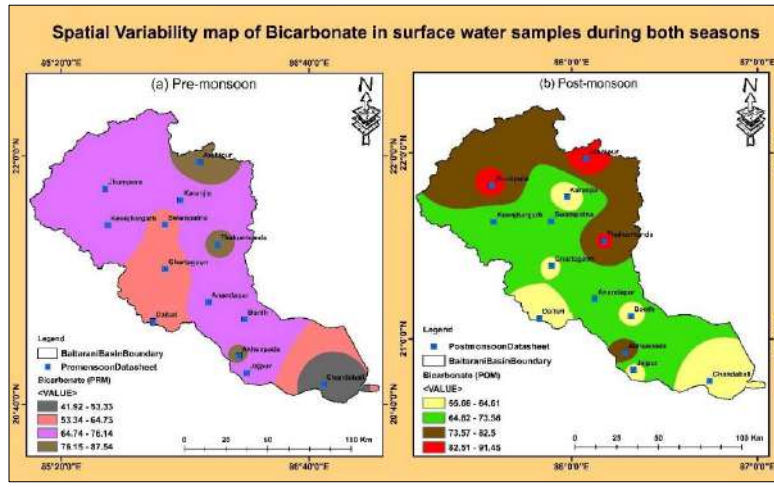

Fig. 2j: HCO_3^- map.

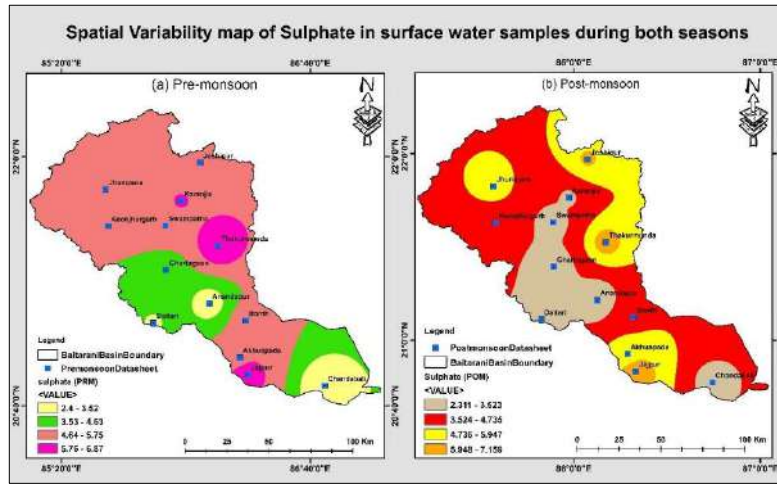

Fig. 2k: SO_4^{2-} map.

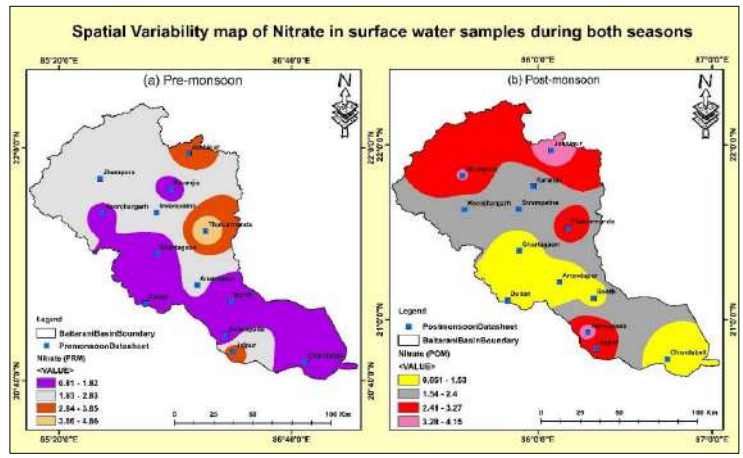

Fig. 2l: NO_3^- map.

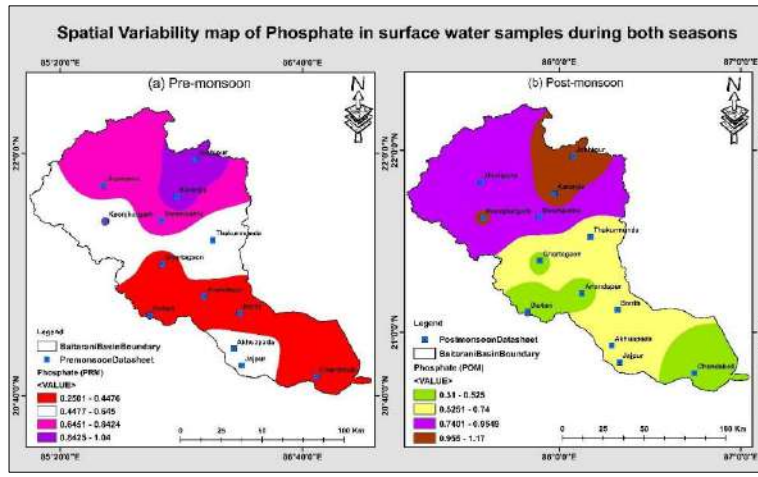

Fig. 2m: PO_4^{3-} map.

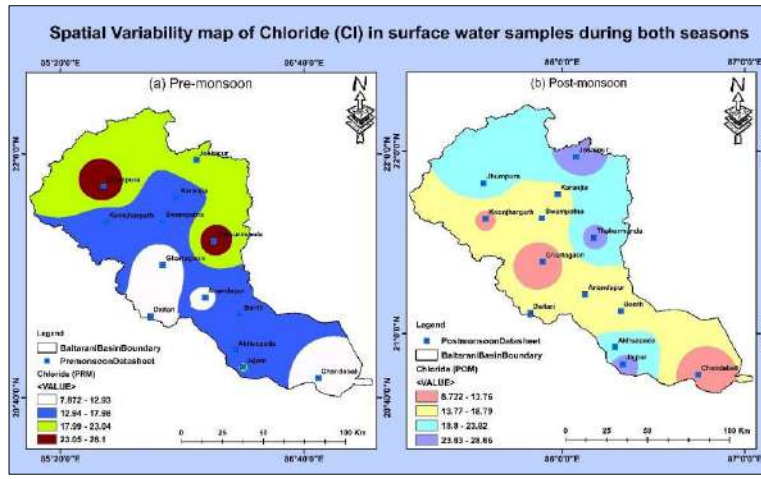

Fig. 2n: Cl^- map.

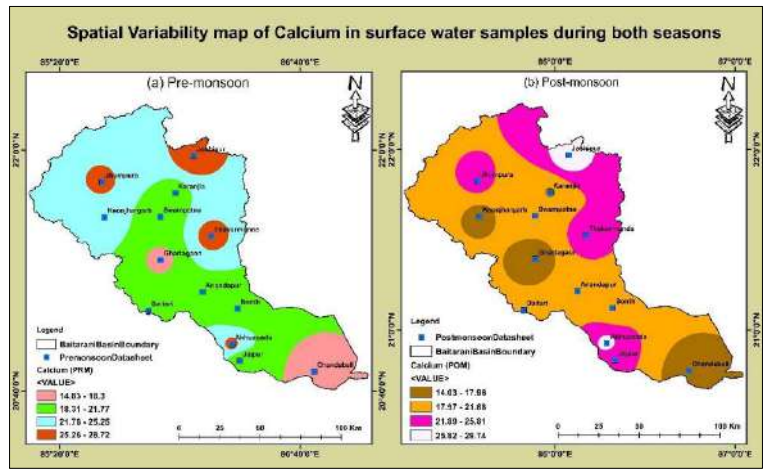

Fig. 2o: Ca^{2+} map.

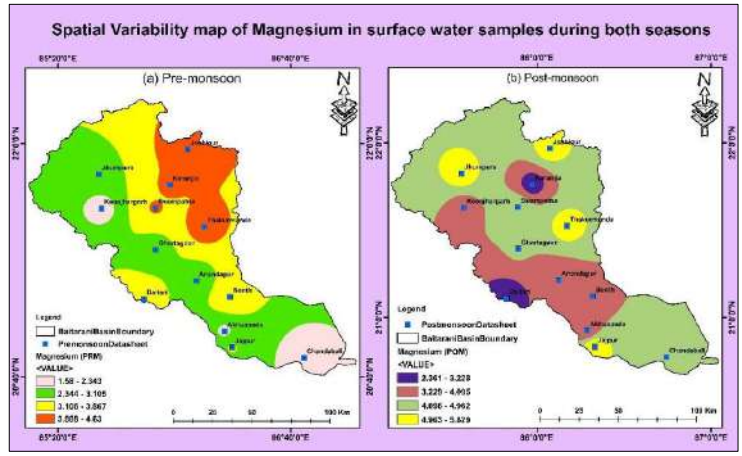

Fig. 2p: Mg^{2+} map.

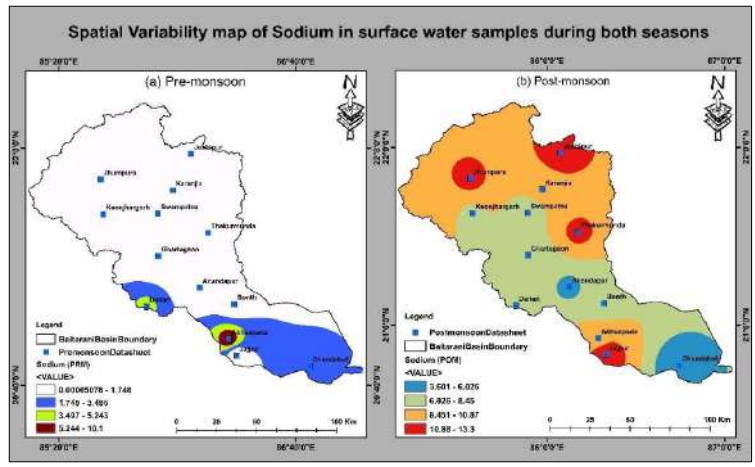

Fig. 2q: Na^{+} map.

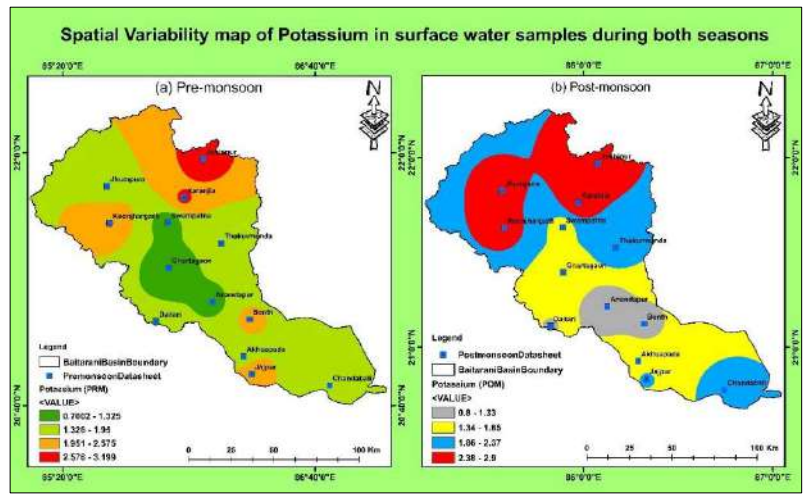

Fig. 2r: K^{+} map.

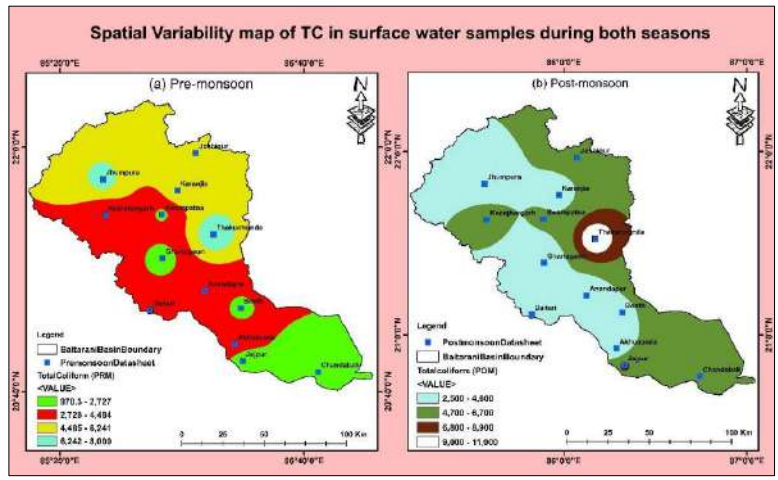

Fig. 2s: TC map.

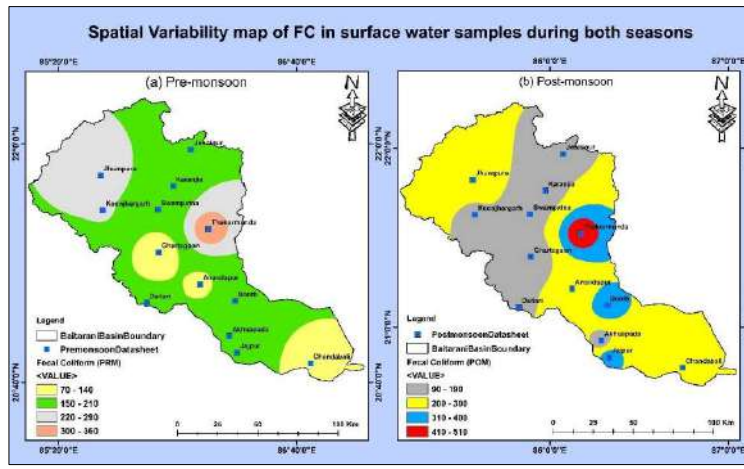

Fig. 2t: FC map.

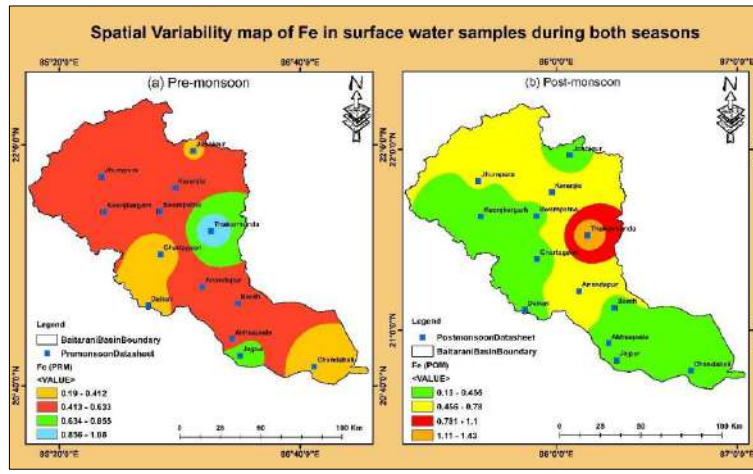

Fig. 2u: Fe^{2+} map.

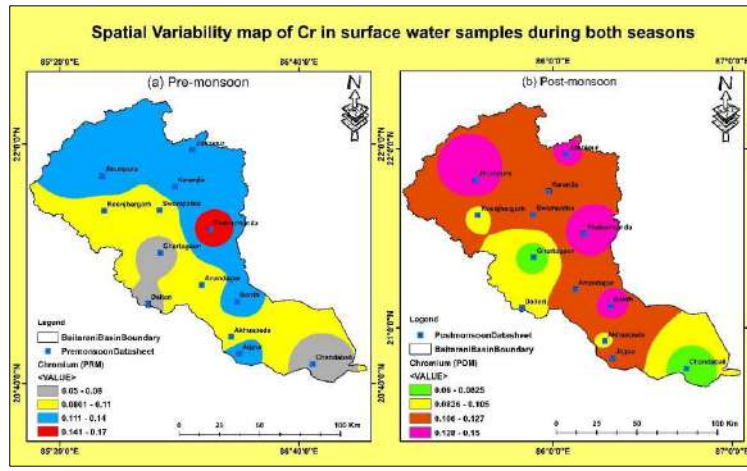

Fig. 2v: Cr^{2+} map.

which results in deficiencies in plant tissues (Bauder et al. 2011). Based on WHO norms, the allowable higher value for Mg^{2+} is 30 mg.L^{-1}. The Mg^{2+} concentration was below the maximum permitted level at all sampling locations, ranging from 1.58 to 4.63 in PRM and 2.36 to 5.83 in POM. The most significant element, Na^{+} (sodium), can be found in natural water (Haritash et al. 2016). According to WHO (2017), the limit for drinking water is 200 mg.L^{-1}. The values that were reported ranged from 3.6 to 13.30 in POM and 2 to 10.10 in PRM. The fertility of soils will decline with K^{+} (potassium) treatment under long-term farming. Consequently, this is a crucial component for improving irrigation (Li et al. 2019). The results found in the current analysis fell under the WHO threshold, and it is taken to be 12 mg.L^{-1} in the present study, the readings ranged from 0.7 to 2.20 for PRM and 0.8 to 2.9 for POM. In the study region, the value for PRM varied from 970 to 8000, and for TC (total coliform), it varied from 2500 to 11000 in POM. Most places that are close to industrial, municipal sewage systems, or hospitals have reported higher levels in the water. FC (fecal coliform) scores range from 70 to 360 in PRM and from 90 to 510 in the POM season, suggesting that all places are secure. In the current study, the concentration of Fe^{2+} (iron) in the river ranged from 0.19 to 1.08 in PRM and from 0.13 to 1.43 in POM season. Fe^{2+} is necessary for the transport of oxygen in the blood, but at high concentrations, it may result in hemochromatosis and DNA damage (Saleh & Al-Ruwih 1999). Except for St. 8 in PRM and St. 7 and 8 in the POM period, all water samples have concentrations below the permissible limit of 1.0 mg.L^{-1}. Water containing Cr^{2+} (chromium) lowers fatty acid and cholesterol levels and controls blood sugar and insulin levels. Cr^{2+} values (0.05-0.17 in PRM and 0.06-0.15 in POM) are below the 0.2 mg.L^{-1} criterion for drinking water in every sampling site in the research area. All units are in mg.L^{-1} for all indicators except pH (unitless) and EC in µS.cm^{-1}. As shown in Fig. 2a-v, spatial distribution maps were created for various parameters, which were performed in the Arc GIS 10.3 program, utilizing the inverse distance weighting (IDW) over the entire catchment to illustrate a link for enhancing water quality evaluations.

Some significant indices are used to assess the quality of river water used for irrigation, including SAR, % Na, RSC, MH, KI, PI, RSBC, and PS. A method called SAR is used to measure the proportion of Na^{+} to Ca^{2+} and Mg^{2+} ions in irrigation water, and it exhibits a maximum tendency to trigger a cation exchange reaction in soil (Singh et al. 2017). Implementing this index to the water samples reveals that during PRM and POM, recorded SAR values ranged from 0.09 to 0.39 and 0.15 to 0.46, suggesting excellent class with zero salinity. Fig. 3 depicts the interpolated map that was created. Na^{+} concentration has an impact on soil permeability. Hence, irrigation in the basin area could benefit from water grading depending on Na^{+} concentration. Fig. 4 illustrates the computed % Na findings for PRM and POM, which ranged from 12.56% to 28.43% and 15.73% to 29.76%, respectively. It has been found that most of the locations belong to excellent and good-quality zones. Higher Na percent (>10) is seen in some places, indicating that ion exchange and rock weathering from lithological units are dominant processes (Vasanthavigar et al. 2010). RSC is considered an efficient parameter for reviewing the suitability of water for irrigation/agriculture. Fig. 5 depicts the recorded range of RSC, which varies from -0.33-0.09 in PRM and -0.38-0.13 in POM. However, it is seen from the results that all locations belong to the zone of good water, which has an RSC value < 1.25 meq.L^{-1}. It is noted that water with a high MH ratio can impede the overall strong Ca^{2+} and Mg^{2+} ratio (Khanoranga & Khalid 2019, Das et al.

2023a). According to Fig. 6, the MH values vary from 11.92 to 25.81 for PRM and from 16.20 to 35.12 for POM. The findings show that all samples (100%) were appropriate for irrigation (MH<50). The surface water samples were used to compute the KI, which fluctuated between 0.10-0.35 and 0.14-0.36 during the PRM and POM seasons, respectively. Fig. 7 shows that 100% of the samples in the study region, which is less than unity, and infers that these samples are suitable for irrigation. Relying on the PI values seen in Fig. 8, the values for PRM and POM, respectively, varied from (41.8-65.7) % and (38-60.7) %. It implies that every place is classified as Class II or doubtful (25-75) percent. Based on RSBC, PRM and POM scores spanned from -0.16 to 0.29 and -0.09 to 0.34, respectively. The numbers are safe because they are far below the satisfactory value. In Fig. 9, the spatial variety of RSBC is clearly visible. According to the study region, the PS values varied from 6.05 to 2.83% in PRM and 7.38 to 25.81% in POM and are regarded as fair low. Fig. 10 demonstrates it clearly.

Additionally, EWQI assessed the water quality of Baitarani River, Odisha, in relation to the drinking water quality standard, and their results are displayed in Table 1. It is observed from the findings that TC holds the maximum entropy weight and is considered to have the highest influence on the water quality. The second-most important factor was NO_3^-. It was discovered that the calculated EWQI ranged from 46 to 199 in PRM and 42 to 199 in POM, respectively, and was rated as excellent to poor in both periods. In both seasons, St. 8 received the highest EWQI ratings and had high levels of turbidity, TC, FC, EC, TSS, BOD, TH, SO_4^{2-}, NO_3^-, Fe^{2+}, and Cr^{2+}.

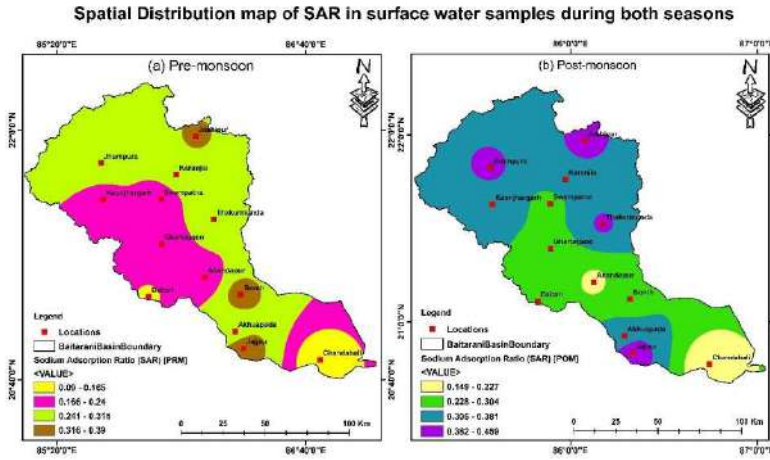

Fig. 3: Sodium adsorption ratio (SAR) map.

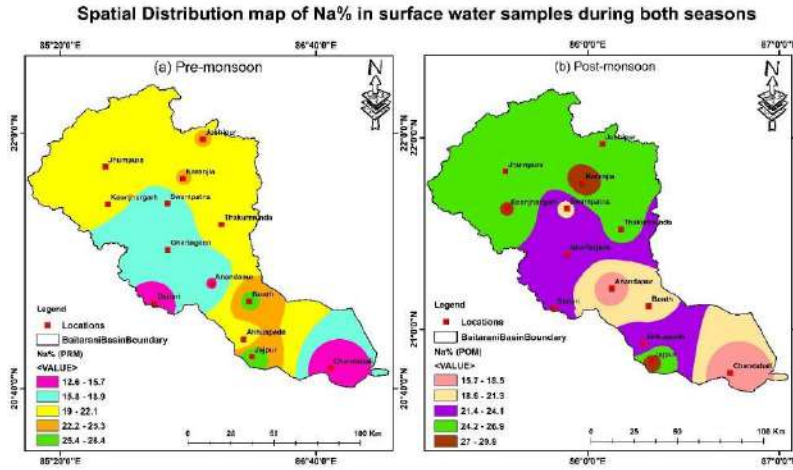

Fig. 4: Percent sodium (% Na) map.

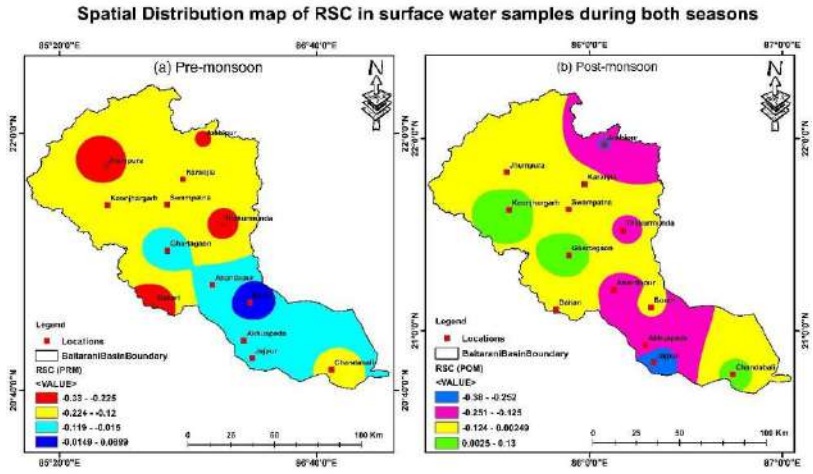

Fig. 5: Residual sodium carbonate (RSC) map.

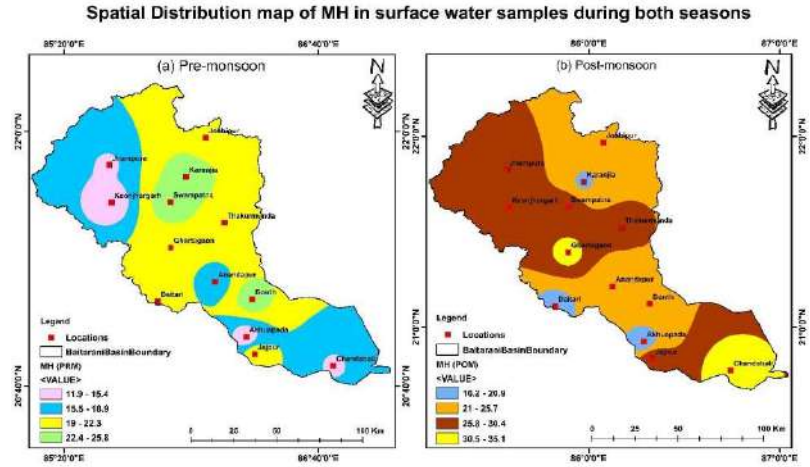

Fig. 6: Magnesium hazard (MH) map.

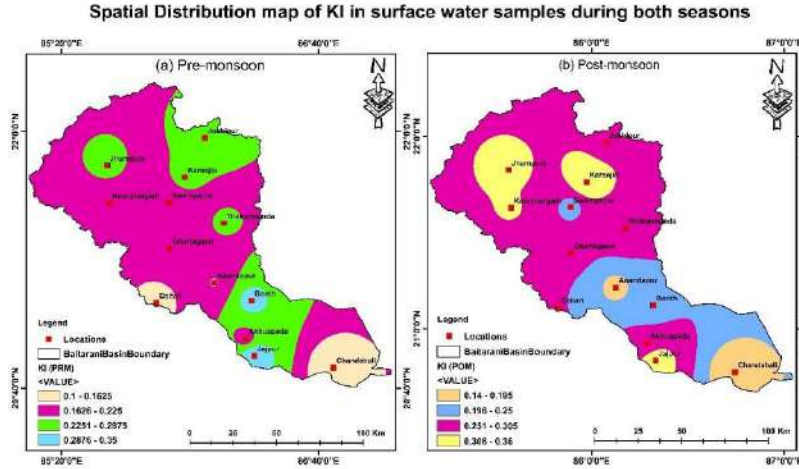

Fig. 7: Kelly's Index (KI) map.

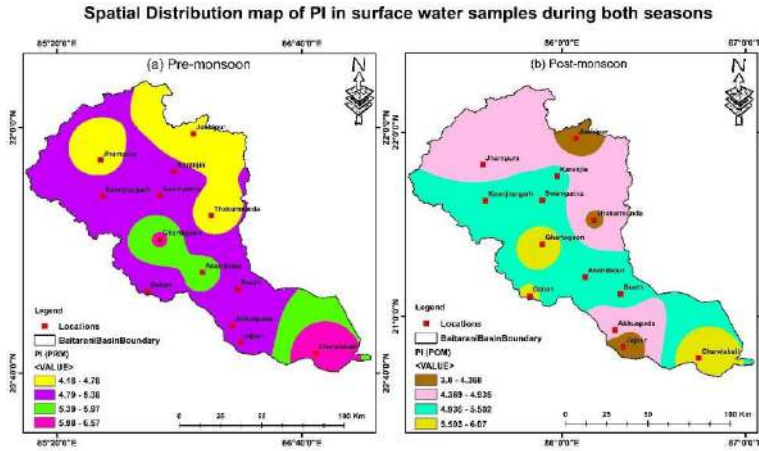

Fig. 8: Permeability Index (PI) map.

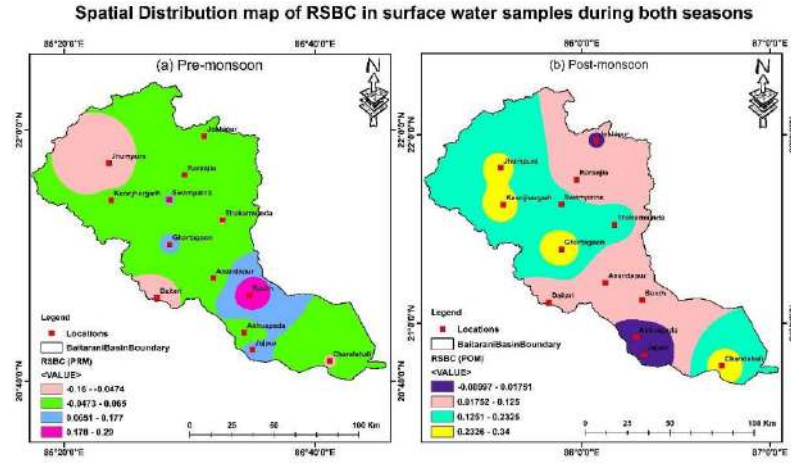

Fig. 9: Residual sodium bicarbonate (RSBC) map.

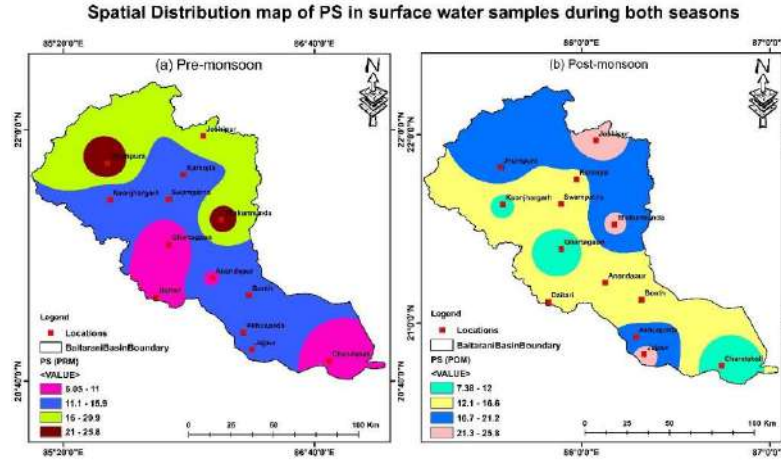

Fig. 10: Potential Salinity (PS) map.

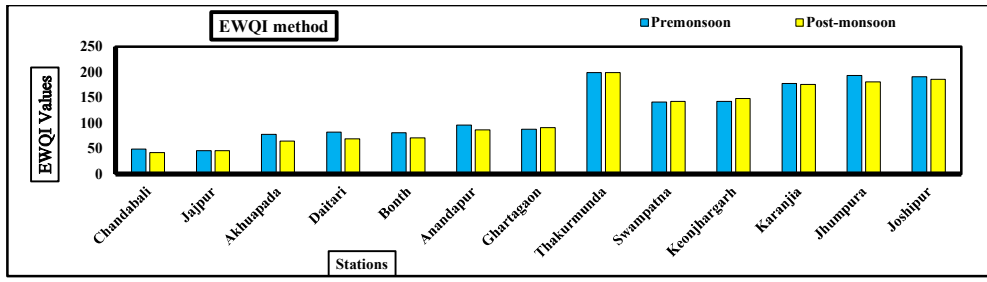

Fig. 11: EWQI classification.

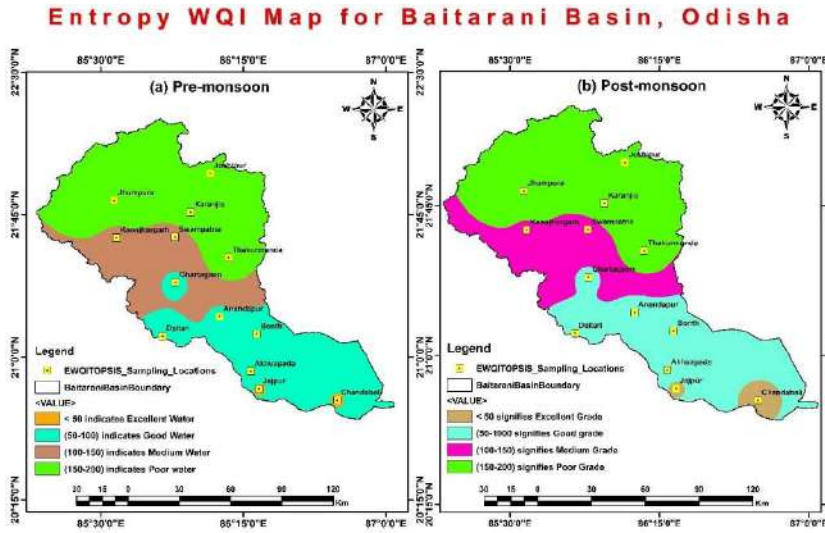

Fig. 12: Entropy WQI map.

Additionally, it is clear from the analysis at St. 8 that turbidity and TC had high values in comparison to their acceptable drinking water requirements (WHO 2017). Fig. 11 illustrates how the EWQI varies across the research area. The dispersal of the samples in percentage terms reveals that throughout the entire study area, Excellent water was found in 15.38% of samples, good water was found in 38.46%, Medium water was found in 15.38% of samples, and Poor water was found in 30.77% of samples in both periods. Fig. 12 depicts the interpolated map that was created. Results show that St. 8, 11, 12, and 13 in PRM and POM, which are described as having inadequate water, are extremely susceptible to activity caused by humans (Das et al. 2023b).

However, by assigning them their overall scores based on CC to PIS, the TOPSIS technique clearly indicates the relative pollution level. The rankings for CC and TOPSIS are shown in Table 2. The sampling location, St. 8, was the most contaminated compared to other locations during PRM and POM. Figs. 13 and 14 show the results of performance score and rank for both seasons. As the St. 8 had significant anthropogenic impacts, it was utterly unfit for drinking and irrigation purposes. Fig. 15 depicts the regional variation in output over the area. In order to draw drinking and irrigation water, TOPSIS ranks were therefore strongly identified as being substantially superior.

Table 1: EWQI in sampling locations of Baitarani River, Odisha.

Locations	Pre-monsoon (PRM)	Post-monsoon (POM)
St. 1	49	42
St. 2	46	46
St. 3	78	65
St. 4	82	69
St. 5	81	71
St. 6	96	87
St. 7	88	91
St. 8	199	199
St. 9	141	143
St. 10	143	148
St. 11	178	176
St. 12	194	181
St. 13	191	186

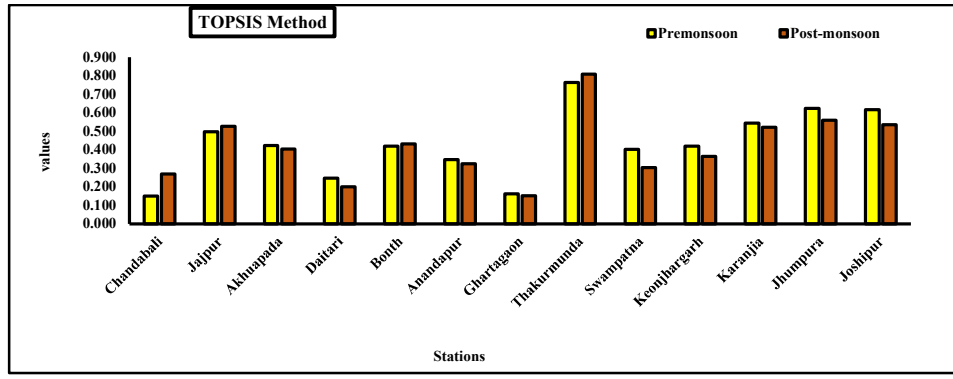

Fig. 13: Variability of TOPSIS ranks of concerned locations.

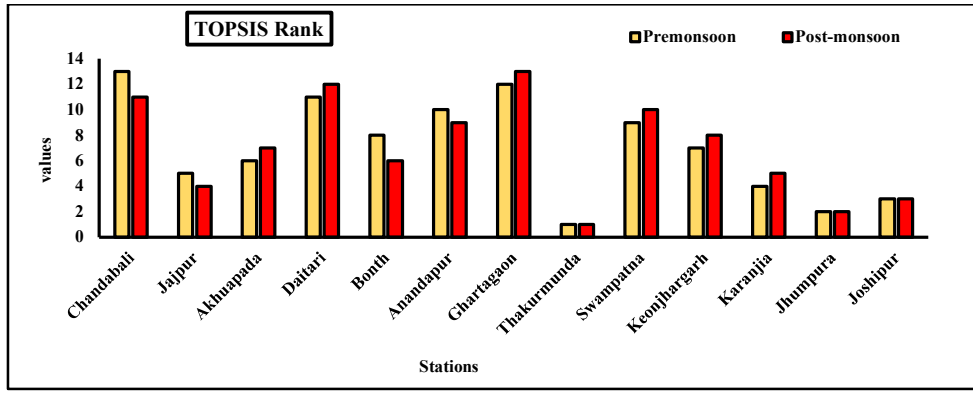

Fig. 14: Rank of all sampling sites during both seasons.

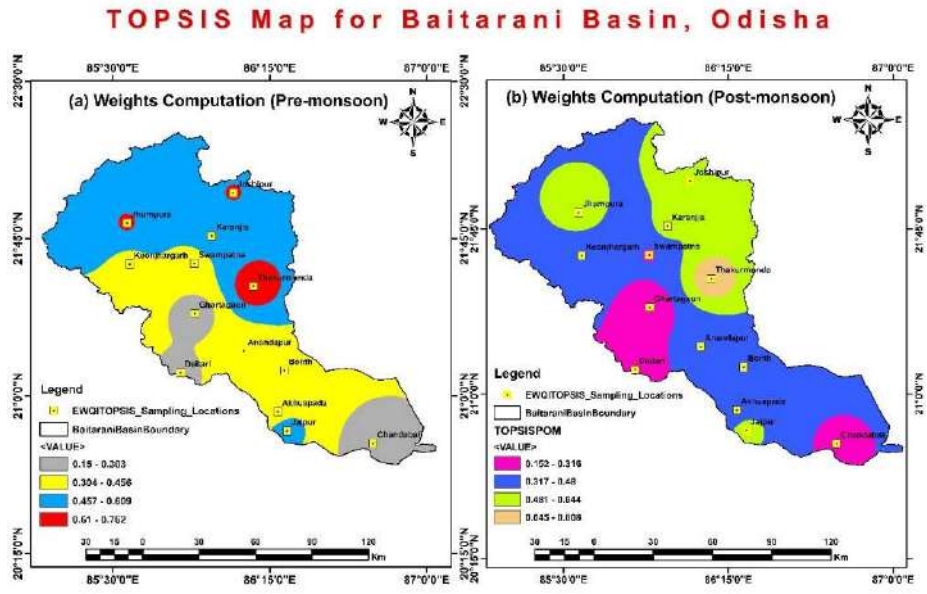

Fig. 15: TOPSIS spatial map.

Table 2: Closeness coefficients (C.C) and TOPSIS ranks of all the locations of the Baitarani River.

St. No.	Pre-monsoon (PRM)		Post-monsoon (POM)	
	C.C	Rank	C.C	Rank
St. 1	0.150	13	0.270	11
St. 2	0.497	5	0.525	4
St. 3	0.424	6	0.404	7
St. 4	0.247	11	0.199	12
St. 5	0.419	8	0.431	6
St. 6	0.347	10	0.325	9
St. 7	0.162	12	0.152	13
St. 8	0.762	1	0.808	1
St. 9	0.403	9	0.303	10
St. 10	0.419	7	0.364	8
St. 11	0.544	4	0.520	5
St. 12	0.623	2	0.559	2
St. 13	0.616	3	0.536	3

CONCLUSION

All living creatures rely on rivers as a natural resource. Thus, protecting the quality of the water is crucial for both the present and the future. In this study, a more effective method to measure water quality was developed using the TOPSIS method in conjunction with the entropy-based weight-determining method (EWQI), which explains and provides sufficient information on both geographical and seasonal variations for examining the compatibility of surface water for human intake and irrigation. By converting the dataset into corresponding unit data and numerical index values, the EWQI and TOPSIS models were shown to be effective methods for categorizing the differences in river water quality.

In order to evaluate the water quality, water samples were taken on a yearly basis over a period of one year (2021-2022) at 13 discharge locations that represent the stream's overall pollution load. The river's pH was found to remain comparatively higher, indicating an alkaline character in both seasons. In both seasons, adequate DO is present, which promotes good health of the aquatic ecosystem. The threshold limits are determined to be met for all the tested parameters. However, in both seasons and locations, the turbidity and TC concentrations were greater than the desirable limit for water for drinking. Throughout the period, i.e., both pre-monsoon and post-monsoon seasons, heavy rainfall-runoff discharge is the prominent cause of high turbidity. The removal of sediments from the river's bottom surface also caused a rise in turbidity, as well as related measures, including TC, TDS, and EC, in the majority of the stations. In PRM and POM, the recorded EWQI scores ranged from 46 to 199 and 42 to 199, respectively.

Based on the EWQI ratings, it is concluded that the water quality at all test sites ranges from excellent to poor. High EWQI levels indicate the water's toxicity at St. 8, 11, 12, and 13, which is the primary contributor to a number of health issues. Monitoring the treatment and disposal of sewage, industrial, and home waste is crucial during both seasons at these places in order to reduce water body pollution and prevent it from changing the chemical and physical makeup of drinkable water.

To characterize sampling locations, TOPSIS was further run with all measurable data included. This resulted in an overall rating of the sites based on their relative levels of pollution. According to the findings, St. 8 was the most contaminated location in both the periods compared to other places. The main causes are the effects of climate change, population growth that is occurring at a rapid rate, urbanization, and agricultural practices, all of which have a significant impact on human activities, including the quantity and quality of surface water resources.

All locations in the research region were determined to be suitable for irrigation water based on evaluations of SAR, % Na, RSC, MH, and KI values as indicators of irrigation water quality in both seasons. However, the PI of a river's water quality indicates doubt and should be controlled during both seasons because it could have dangerous consequences when used for irrigation. This was done in order to ascertain the water's suitability for agricultural usage. The TOPSIS ranking findings are consistent with the entropy method's results for calculating water quality, demonstrating its validity and application.

Based on the study's findings, it can be seen that combining these two models with irrigational indices can be used to find and separate the sources of surface water contamination, opening new possibilities for surface water protection and purification. In this context, it is predicted that decision-makers employed by agencies that safeguard water quality will discover the research findings to be of great value.

ACKNOWLEDGMENTS

The author extends their appreciation to C.V. Raman Global University (CGU), Bhubaneswar, Odisha, India, for providing the necessary equipment and lab facilities in order to carry out the research work. The authors gratefully acknowledge use of the services and facilities provided by State Pollution Control Board (S.P.C.B), Odisha, India.

REFERENCES

Adimalla, N. 2018. Groundwater quality for drinking and irrigation purposes and potential health risks Assessment: A case study from a semi-arid region of South India. Expos. Health, 18: 107. https://doi.org/10.1007/s12403-018-0288-8.

Akhtar, N., Syakir, M.I., Rai, S.P., Saini, R., Pant, N., Anees, M.T., Qadir, A. and Khan, U. 2020. Multivariate investigation of heavy metals in the groundwater for irrigation and drinking in Garautha tehsil, Jhansi District, India. Anal. Lett., 53(5): 774-794. https://doi.org/10.1080/00032719.2019.1676766

American Public Health Association (APHA). 2017. Standard Methods for the Examination of Water and Wastewater. Twenty-Third Edition. APHA, Washinton DC

Anand, B., Karunanidhi, D., Subramani, T., Srinivasamoorthy, K. and Suresh, M. 2020. Long-term trend detection and spatiotemporal analysis of groundwater levels using GIS techniques in the lower Bhavani River basin, Tamil Nadu, India. Environ. Dev. Sustain., 22(4): 2779-2800. https://doi.org/10.1007/s10668-019-00318-3

Balamurugan, P., Kumar, P.S., Shankar, K., Nagavinothini, R. and Vijayasurya, K. 2020. Non-carcinogenic risk assessment of groundwater in the southern part of Salem District in Tamil Nādu, India. J. Chilean Chem. Soc., 65(1): 4697-4707. https://doi.org/10.4067/S0717-97072020000104697

Banda, T.D. and Kumarasamy, M. 2020. A review of the existing water quality indices (WQIs). J. Phys. Opt., 2: 1-19.

Bauder, T.A., Waskom, R.M., Davis, J.G. and Sutherland, P.L. 2011. Irrigation water quality criteria. Colorado State Univ. Ext., 11: 525.

Bora, M. and Goswami, D.C. 2017. Water quality assessment in terms of water quality index (WQI): Case study of the Kolong River, Assam, India. Appl. Water Sci., 7(6): 3125-3135. https://doi.org/10.1007/s13201-016-0451-y

Brhane, G.K. 2018. Characterization of hydrochemistry and groundwater quality evaluation for drinking purposes in Adigrat area, Tigray, northern Ethiopia. Water Sci., 32(2): 213-229. https://doi.org/10.1016/j.wsj.2018.09.003

Burrough, P.A. and McDonnell, R.A. 1998. Principles of Geographical Information Systems. Oxford University Press, Oxford, p. 333.

Das, A. 2022a. Multivariate statistical approach for the assessment of water quality of Mahanadi basin, Odisha. Mater. Today: Proc., 65, A1-A11. https://doi.org/10.1016/j.matpr.2022.08.146

Das, A. 2022b. Water Criteria Evaluation for Drinking Purposes in Mahanadi River Basin, Odisha. Springer Nature, Singapore, pp. 237-260

Das, A. 2023. Assessment of potability of surface water and its health implication in Mahanadi Basin, Odisha. Mater. Today: Proc., 6: 65-35.

Das, A., Goya, A. and Soni, A. 2023b. Use of water quality indices and its evaluation to verify the impact of Mahanadi River basin, Odisha. AIP Conf. Proc., 2721(1): 040003. https://doi.org/10.1063/5.0153903

Das, A., Goyal, A. and Soni, A. 2023a. Deciphering surface water quality for irrigation and domestic purposes: A case study in Baitarani Basin, Odisha. AIP Conf. Proc., 2721(1): 040017. https://doi.org/10.1063/5.0153902

Doneen, L.D. 1965. Notes on water quality in Agriculture. Water Sci. Eng., 40: 1010.

Fipps, G. 2003. Irrigation water quality standards and salinity management strategies. Texas A&M University, Texas, pp. 1-17.

Gorgij, A.D., Wu, J. and Moghadam, A.A. 2019. Groundwater quality ranking using the improved entropy TOPSIS method: A case study in Azarshahr plain aquifer, east Azerbaijan. Iran Hum. Ecol. Risk Assess., 25(5): 176-190. https://doi.org/10.1080/10807 039. 2018.

Haritash, A.K., Gaur, S. and Garg, S. 2016. Assessment of water quality and suitability analysis of River Ganga in Rishikesh, India. Appl. Water, 14: 72-83.

Heaney, R.P., Gallagher, J.C., Johnston, C.C., Neer, R., Parfitt, A.M. and Whedon, G.D. 1982. Calcium nutrition and bone health in the elderly. Am. J. Clin. Nutr., 36(5): 986-1013. https://doi.org/10.1093/ajcn/36.5.986

Hong, T., Xie, Y., Yu, Q., Zhao, Y., Zhao, G. and Yang, L. 2016. Hydrochemical characteristics study and genetic analysis of groundwater in a key region of the Wumeng Mountain. Earth Environ., 44(1): 11-18. https://doi.org/10.14050/j.cnki.1672-9250.2016.01.002

Hong, Z., Zhao, Q., Chang, J., Peng, L., Wang, S., Hong, Y., Liu, G. and Ding, S. 2020. Evaluation of water quality and heavy metals in wetlands along the Yellow River in Henan Province. Sustainability, 12(4): 1300. https://doi.org/10.3390/su12041300

Horton, R.K. 1965. An index number system for rating water quality. J. Water Pollut. Control Fed., 37(3): 300-306.

Hwang, C.L., Lai, Y.J. and Liu, T.Y. 1993. A new approach for multiple objective decision making. Comput. Oper. Res., 20(8): 889-899. https://doi.org/10.1016/0305-0548(93)90109-V

Jha, M.K., Shekhar, A. and Jenifer, M.A. 2020. Assessing groundwater quality for drinking water supply using hybrid fuzzy-GIS-based water quality index. Water Res., 179: 1-16. https://doi.org/10.1016/j.watres.2020.115867

Jinisha, R., Jerlin Regin, J. and Maheswaran, J. 2020. A review on the emergence of single-chamber microbial fuel cell on wastewater treatment. IOP Conf. Ser. Mater. Sci. Eng., 983(1): 012002. https://doi.org/10.1088/1757-899X/983/1/012002

Kadam, A., Wagh, V., Patil, S., Umrikar, B. and Sankhua, R. 2021. Seasonal assessment of groundwater contamination, health risk, and chemometric investigation for a hard rock terrain of western India. Environ. Earth Sci., 80(5): 172. https://doi.org/10.1007/s12665-021-09414-y

Karunaidhi, D., Aravinthaswamy, P., Subramani, T., Jianhu, W. and Srinivasa Moorthy, K. 2019. Potential health risk assessment for fluoride and nitrate contamination in hard rock aquifers of Shanmuganadhi River basin, South India. Int. J. Hum. Health Risk Assess., 11: 212 https://doi.org/10.1080/10807.

Keesari, T., Ramakumar, K.L., Chidambaram, S. and Pethperumal, S. 2016. Understanding the hydro-chemical behavior of groundwater and its suitability for drinking and agricultural purposes in Pondicherry area, South India-A step towards sustainable development. Groundw. Sustain. Dev., 2-3: 143-153.

Kelley, W.P. 1963. Use of saline irrigation water. Soil Sci., 95(6): 385-391. https://doi.org/10.1097/00010694-196306000-00003

Khanoranga, M. and Khalid, S. 2019. An assessment of groundwater quality for irrigation and drinking purposes around brick kilns in three districts of Balochistan Province, Pakistan, through water quality index and multivariate statistical approaches. J. Geochem. Explor., 197: 14-26. https://doi.org/10.1016/j.gexplo.2018.11.007

Kumar, M. and Puri, A. 2012. A review of permissible limits of drinking water. Indian J. Occup. Environ. Med., 16(1): 40-44. https://doi.org/10.4103/0019-5278.99696

Kumarasamy, P., Arthur James, R.A., Dahms, H.U., Byeon, C.W. and Ramesh, R. 2014. Multivariate water quality assessment from the Tamiraparani river basin, Southern India. Environ. Earth Sci., 71(5): 2441-2451. https://doi.org/10.1007/s12665-013-2644-0

Landwehr, J.M. 1979. A statistical view of a class of water quality indices. Water Resour. Res., 15(2): 460-468. https://doi.org/10.1029/WR015i002p00460

Li, P., Qian, H. and Wu, J. 2010. Groundwater quality assessment based on improved water quality index in Pengyang County, Ningxia, Northwest China. J. Chem., 7(1): S209-S216.

Li, P., Tian, R. and Liu, R. 2019. Solute geochemistry and multivariate analysis of water quality in the Guohua phosphorite Mine, Guizhou Province, China. Exposure Health, 11(2): 81-94. https://doi.org/10.1007/s12403-018-0277-y

Marghade, D., Malpe, D.B., Subbarao, N. and Sunitha, B. 2019. Geochemical assessment of fluoride enriched groundwater and health implications from a part of Yavtmal District, India. Int. J Hum. Ecol. Risk Assess., 26(3): 673-694. https://doi.org/10.1080/10807039. 2018.1528862.

Marko, K., Al-Amri, N.S. and Elfeki, A.M.M. 2014. Geo-statistical analysis using GIS for mapping groundwater quality: A case study in the recharge area of Wadi Usfan, western Saudi Arabia. Arabian J. Geosci., 7(12): 5239-5252. https://doi.org/10.1007/s12517-013-1156-2

Meng, C.F., Song, X.Y., Zhao, W.J., Wang, M.H., Xia, L. and Fu, N. 2017. Health risk assessment and the pollutant source identification of the shallow groundwater in Xinxiang rural areas. J. Safety Environ., 17(5): 2024-2030.

Meshram, S.G., Singh, V.P., Kahya, E., Sepehri, M., Meshram, C., Hasan, M.A., Islam, S. and Duc, P.A. 2022. Assessing erosion-prone areas in a watershed using interval rough-analytical hierarchy process (IR-AHP) and fuzzy logic (FL). Stoch. Environ. Res. Risk Assess., 36(2): 297-312. https://doi.org/10.1007/s00477-021-02134-6

Narsimha, A. 2020. Spatial distribution, exposure, and potential health risk assessment from nitrate in drinking water from the semi-arid region of South India. Hum. Ecol. Risk Assess., 26: 310-314. https://doi.org/10.1080/10807, 039.2018.1508329.

Paliwal, K.V. 1972. Irrigation with saline water. Monogram, 2: 10

Pandit, A.K. and Yousuf, A.R. 2002. Trophic status of Kashmir Himalayan lakes as depicted by water chemistry. J. Res. Dev., 2: 1-12.

Panneerselvam, B., Paramasivam, S.K. and Karuppannan, S. 2020. A GIS-based evaluation of hydro-chemical characterization of groundwater in hard rock region, South Tamil Nadu, India. Arab J. Geosci., 13(17): 1-22.

Ram, A., Tiwari, S.K. and Pandey, H.K. 2021. Groundwater quality assessment using water quality index (WQI) under the GIS framework. Appl. Water Sci., 11: 1-20. https://doi.org/https://doi.org/10.1007/s13201-021-01376-7.

Ramachandran, A., Sivakumar, K. and Shanmugasundharamc, A. 2020. Evaluation of potable groundwater zone identification based on WQI and GIS techniques in Adyar River basin, Chennai, Tamilnadu, India. Acta Ecol. Sinica. https://doi.org/10.1016/j.chnaes.2020.02.006.

Ravikumar, P. and Somashekar, R.K. 2017. Principal component analysis and hydro-chemical facies characterization to evaluate groundwater quality in Varahi River basin, Karnataka state, India. Appl. Water Sci., 7(2): 745-755. https://doi.org/10.1007/s13201-015-0287-x

Reddy, M.B., Sunitha, V., Prasad, M., Sudarshan Reddy, Y. and Ramakrishna Reddy, M. 2019. Evaluation of groundwater suitability for domestic and agricultural utility in a semi-arid region of Anantapur, Andhra Pradesh State, South India. Groundw. Sustain. Dev., 9: 100262. https://doi.org/10.1016/j.gsd.

Richards, L.A. 1954. Diagnosis and improvement of saline and alkali soils. Soil Sci., 78(2): 160. https://doi.org/10.1097/00010694-195408000-00012

Roy, A., Keesari, T., Mohokar, H., Sinha, U.K. and Bitra, S. 2018. Assessment of groundwater quality in hard rock aquifer of central Telangana state for drinking and agriculture purposes. Appl. Water Sci., 8(5): 761. https://doi.org/10.1007/s13201-018-0761-3

Sadat-Noori, S.M., Ebrahimi, K. and Liaghat, A.M. 2014. Groundwater quality assessment using the Water Quality Index and GIS in Saveh-Nobaran aquifer, Iran. Environ. Earth Sci., 71(9): 3827-3843. https://doi.org/10.1007/s12665-013-2770-8

Saleh, A. and Al-Ruwih, F.S.M. 1999. Hydrogeochemical process operating within the main aquifers of Kuwait. J. Arid Environ., 42: 195-209.

Shannon, C.E. 1948. A mathematical theory of communication. Bell Syst. Tech. J. Sci., 27: 379-423.

Shrestha, A.K. and Basnet, N. 2018. An evaluation of physicochemical analysis and Water Quality Index of Ratuwa River of Damak, Jhapa, Nepal. Int. J. Recent Res. Rev., XI(2): 1-9.

Singh, A.K., Sathya, M., Verma, S. and Jayakumar, S. 2020a. Spatiotemporal variation of Water Quality Index in Kanwar wetland, Begusarai, India. Sustainable Water Resour. Manage., 6(3): 1-8. https://doi.org/10.1007/s40899-020-00401-y

Singh, G., Rishi, M.S., Herojeet, R., Kaur, L., Priyanka, K. and Sharma, K. 2020b. Multivariate analysis and geochemical signatures of groundwater in the agricultural-dominated taluks of Jalandhar district, Punjab, India. J. Geochem. Explor., 208: 106395. https://doi.org/10.1016/j.gexplo.2019.106395

Singh, S., Ghosh, N.C., Gurjar, S., Krishan, G., Kumar, S. and Berwal, P. 2017. Index-based assessment of the suitability of water quality for irrigation purposes under Indian conditions. Environ. Monit. Assess., 190(1): 29. https://doi.org/10.1007/s10661-017-6407-3

Singh, V.P. 2013. Entropy Theory and Its Application in Environmental and Water Engineering. Wiley & Sons, NY.

Singh, V.P. 2014. Entropy theory in hydraulic engineering: An introduction. Am. Soc. Civ. Eng.

Siraj, S., Yousuf, A.R., Bhat, F.A. and Parveen, N. 2010. The ecology of macrozoobenthos in Shallabugh wetland of Kashmir Himalaya, India. Eco. Nat. Environ., 2(5): 84-91.

Suresh, T. and Kottureshwara, N.M. 2009. Assessment of groundwater quality of borewells water of Hospet Taluka Region, Karnataka, India. Rasayan J. Chem., 2(1): 221-223. 10:455-474.

Talukder, B., Blay-Palmer, A., Hipel, K.W. and VanLoon, G.W. 2017. Elimination method of multi-criteria decision analysis (MCDA): A simple methodological approach for assessing agricultural sustainability. Sustainability, 9(2): 287. https://doi.org/10.3390/su9020287

Thakur, N., Rishi, M., Keesari, T., Sharma, D.A. and Sinha, U.K. 2020. Assessment of recharge source to springs in upper Beas basin of Kullu region, Himachal Pradesh, India using isotopic signatures. J. Radioanal. Nucl. Chem., 323(3): 1217-1225. https://doi.org/10.1007/s10967-019-06617-3

Tiyasha, S., Tung, T.M. and Yaseen, Z.M. 2020. A survey on river water quality modeling using artificial intelligence models: 2000-2020. J. Hydrol., 585: 124670. https://doi.org/10.1016/j.jhydrol.2020.124670

Usman, A., Dube, K., Shukla, S.P., Salaskar, P., Prakash, C., Sawant, P.B. and Singh, R. 2018. Water quality index as a tool for assessment of the status of an urban lake of Mumbai. Int. J. Curr. Microbiol. Appl. Sci., 7(4): 520-533. https://doi.org/10.20546/ijcmas.2018.704.061

Vasanthavigar, M., Srinivasamoorthy, K., Vijayaragavan, K., Ganthi, R.R., Chidambaram, S., Anandhan, P., Manivannan, R. and Vasudevan, S. 2010. Application of water quality for groundwater quality assessment: Thirumanimuttar sub-basin, Tamil Nadu, India. Environ. Monit. Assess., 171(1-4): 595-609. https://doi.org/10.1007/s10661-009-1302-1

World Health Organization. 2017. Guidelines for Drinking-Water Quality. World Health Organization, Washington DC.

Wu, J., Li, P. and Qian, H. 2011. Groundwater quality in Jingyuan County, a semi-humid area in Northwest China. J. Chem., 8(2): 787-793.

Yousefi, M., Yaseri, M. and Nabizadeh, R. 2018. Association of hypertension, body mass index and waist circumference with fluoride intake; water drinking in residents of fluoride endemic areas, Iran. Biol. Trace Elem. Res., 5: 11782-11788. https://doi.org/10.1007/s12011-018-1269-2

Zaki, S.R., Redwan, M., Masoud, A.M. and Abdel Moneim, A.A. 2019. Chemical characteristics and assessment of groundwater quality in Halayieb area, southeastern part of the Eastern Desert, Egypt. Geosci. J., 23(1): 149-164. https://doi.org/10.1007/s12303-018-0020-5.

ORCID DETAILS OF THE AUTHORS

Abhijeet Das: https://orcid.org/0000-0003-4599-5462

Nature Environment and Pollution Technology
An International Quarterly Scientific Journal

p-ISSN: 0972-6268
(Print copies up to 2016)
e-ISSN: 2395-3454

Vol. 23 | No. 1 | pp. 55-68 | 2024

Original Research Paper

https://doi.org/10.46488/NEPT.2024.v23i01.004

Open Access Journal

Wetland Ecosystem: Plant Species Diversity, Services, Degradation Drivers, and Community Perception in Sinana District, Oromia Region, Southeast Ethiopia

Kemalo Abdulmalik Boru*, Lalit Tukaram Ingale† and Kassahun Mulatu Lemt*****

*Department of Natural Resource Management, College of Agriculture and Natural Resource, Madda Walabu University, Bale Robe, Oromia, Ethiopia

**Environmental Science Department, College of Agriculture and Natural Resource, Mizan Tepi University, Mizan, Southwest, Ethiopia

***Department of Natural Resource Management, College of Agriculture and Natural Resource, Mizan Tepi University, Mizan, Southwest, Ethiopia

†Corresponding author: Lalit Tukaram Ingale; lalit.ingale17@gmail.com

Nat. Env. & Poll. Tech.
Website: www.neptjournal.com

Received: 03-07-2023
Revised: 18-08-2023
Accepted: 20-08-2023

Key Words:
Cultural service
Kedar wetland
Provisioning service
Regulating service
Species diversity
Species evenness

ABSTRACT

Wetlands are a vital source of biodiversity and ecosystem services. The study investigated the plant species diversity and assessed the perception of the ecosystem services of the area and drivers of wetland degradation in Sinana district, Southeast Ethiopia. Vegetation inventory, household surveys, focused group discussions, and key informant interviews were employed to gather information. A total of 45 sample plots laid along transacts were inventoried. A plot size of 5 m × 5 m (25 m^2) and 1 m × 1 m (1 m^2) nested within the major plot was used for shrubs and herbs, respectively. A total of 137 households were surveyed to collect socioeconomic data. The study identified 20 plant species belonging to 14 families. Family Cyperaceae was dominant within the studied wetland. The Shannon diversity (H=1.15) indicates that the wetland has low vegetation diversity with an uneven distribution (E=0.385) of vegetation. A total of 20 ecosystem services thought to be underprovisioning, regulating, and cultural services were identified. According to plaintiffs, major provision services are grazing livestock (77.4%), irrigation (76.6%), and harvesting of grass for fodder (68.6%). Important drivers of wetland degradation are a shortage of cropland (70.8%), lack of awareness (69.3%), upland land degradation (65.7%), and increasing population (62%). The main driver, a shortage of cropland, was the key driver, followed by a lack of awareness and upland land degradation. Therefore, the result heightened that the studied wetland is under serious degradation due to high human pressure associated with population growth and climate change. Thus, an appropriate wetland management strategy must be designed.

INTRODUCTION

Wetlands are the ecosystems or units of the landscape that are found within the interface between land and water, which are either fen, peatland, or water, whether natural or artificial, permanent or temporary, with water that is static or flowing, fresh, brackish or salt, including areas of marine water the depth of which at low water does not exceed six meters (Ramsar Convention Secretariat 2013). They are distributed everywhere around the globe and are estimated to cover approximately 6% of the worldwide land surface (Schuyt & Brander 2004), 4% of Africa (Lehner & Doll 2004, Zedler & Kercher 2005), and 2% of the total land mass of Ethiopia (Wondie 2010). The largest areas of wetlands are in Asia (32% of the worldwide area), North America (27%), Latin America, and the Caribbean (16%). Wetland areas in Europe (13%), Africa (10%), and Oceania (3%) are smaller (Davidson et al. 2018).

To date, no comprehensive documentation and studies of wetland characterizations have been made in Ethiopia. However, it is estimated that there are 58 major lakes and marshes and a total of 77 wetlands in Ethiopia, including lakes that cover a vicinity of 18,587 km^2, which is approximately 1.14% of the country's landmass (Karlsson 2015). Ethiopia is usually referred to as the water tower of Africa, with the whole annual volume of runoff water being approximately 110 billion cubic meters (USAID 2008). The wetlands of Ethiopia vary in attributes such as size, type, and location, and they represent a substantial microenvironment

in many parts of the country (Endalew 2015). Various varieties of wetlands are found to exist in Ethiopia, including alpine formations and riverine, lacustrine, palustrine, and floodplain wetlands (Abebe & Geheb 2003), except coastal and marine-related wetlands and extensive swamp-forest complexes (Dixon & Wood 2001). Ethiopian wetlands will be broadly grouped into four major categories supported by ecological zones, hydrological functions, geomorphologic formations, and atmospheric conditions. These categories are interspersed to create four key biomes, which also designate the climate in Ethiopia. These biomes are the Afro-tropical highlands, the Somali Masai, Sudan, Guinea, and the Sahelian Transition Zone groups (Tilahun et al. 1996, Wonderfrash 2003, Bezabih & Mosissa 2017).

Ethiopia, having variable topography and altitudinal range from 126 m below sea level to 4,620 m above water level, may be a country endowed with rich wetland resources (Yimer & Mengistou 2009). In Ethiopia, the wetland ecosystem covers 58 different types of wetlands, which offer enormous socioeconomic and environmental values despite these being under severe pressure and degradation. Due to improper extraction of uses and misconceptions forwarded to wetlands, the health of the wetlands is uninterruptedly declining from time to time, and their existence is suspected within the near future (Gebresllassie et al. 2014).

IMPORTANCE OF WETLAND ECOSYSTEMS

Ecologically, wetlands play critical ecosystem roles in biodiversity conservation, hydrological balance, and human welfare both through economic and sociocultural benefits (Ramsar 2007, Zeleke et al. 2015). The world's surface freshwater wetland is rich in species composition and is a habitat for over 40% of plant and animal species (Zedler & Kercher 2005). They are particularly important in Sub-Saharan African countries such as Ethiopia because they sustain agricultural livelihoods, mainly in areas with low or unpredictable rainfall and land scarcity where uplands have poor soil (Bezabih & Mosissa 2017, Menbere & Menbere 2018).

Wetlands offer natural resources and services to humankind. According to Hailu (2003), wetlands are used virtually by all households within the Western Wollaga and Illubabor zones in Ethiopia directly or indirectly. The most common uses are social/ceremonial reeds, medicinal plants, thatching reeds used for housing construction and granary roofing, domestic water supplies, dry season grazing land, water for livestock, and temporary crop-guarding huts of reeds, cultivation, and craft materials. The indirect uses of wetlands are because of their hydrological and ecological functions, which support various economic activities, life support systems, and human welfare. This includes groundwater recharge, flood control, nutrient cycling, erosion control, sediment traps, climate regulation, stream flow moderation, water filtration and purification, plant and fish products, biodiversity, wildlife habitat for nomadic wildlife, and pest control (Dugan 1990, McHugh et al. 2007).

Thus, understanding the standard of a wetland by measuring its biota is one of the direct tactics to preserve the biological diversity for extreme ecosystem service delivery (Fennessy et al. 2007). Information on plant species of a specific wetland is incredibly helpful for understanding wetland conditions and diagnosing the impacts of human interference on wetlands (Bijos et al. 2017, Woldemariam et al. 2018). It further helps in understanding appropriate ecological processes and developing suitable and sustainable conservation policies (Junk et al. 2013, Rosolen et al. 2015). Da Ponte et al. (2017) & Rahman et al. (2005) further stated that the community's perceptions of the importance of ecosystem services could make a valuable contribution toward successfully conserving natural resources such as wetlands protection and management.

COMPOSITION AND DIVERSITY OF WETLAND PLANTS

Wetland disturbance reduces plant species composition and relative abundances and facilitates opportunistic plant species establishment (Zedler & Kercher 2005, Handa et al. 2012, Battisti et al. 2016). EWNRA (2008) identified 36 plant species belonging to 18 families; the Cyperaceae, Combretaceae, and Asteraceae families were the widespread families. This showed that the wetlands of the study area were rich in plant diversity; however, further management intervention was required to scale back disturbance and ensure sustainable biodiversity conservation.

Wetland vegetation varies from wetland to wetland in numerous ways. Consistent with Mulatu et al. (2014), among wetland plant species of uncultivated sites of south Bench district, 7 plant species were dominant within the plant community, with a relative abundance of over two percent. These plant species were *Leersia hexandra* (46.35%), *Cyperus latifolius* (23.79%), *Thelypteris confluens* (3.96%), *Phyllanthus boehmii* (3.73%), *Persicaria glabra* (2.71%), *Dissotis canescens* (2.58%) and *Achyranthes aspera* (2.09%). These 7 plant species accounted for 85.21% of the community, while the remaining 22 species had a relative abundance of 2%, which accounted for 14.79%. The results revealed that important species such as *Leersia hexandra* and *Cyprus latifolius* decreased significantly due to cultivation.

The dominant plant species of the Tana wetland of the Amhara region of Ethiopia were reported by Wondie (2018). In addition, it specifies that the collective plant community similarity index in the midst of wetlands was mostly low (20%). The explanations for the low average percentage similarity are due to low plant diversity in some urban and agriculture-impacted wetlands.

DRIVERS OF WETLAND DEGRADATION

However, wetlands face a substantial threat due to human interaction, which indicates that approximately 50% of the world's wetlands have been lost since 1900 (Bezabih & Mosissa 2017, Hirpo 2018, Moges et al. 2018). Unregulated utilization of wetlands, including diversion of water for agricultural intensification, urbanization, dam construction, population pressures, food shortages, increased drainage and cultivation, and collection of sedges and reeds for roofing and housing, were identified as major drivers of wetland degradation in Ethiopia (Bezabih & Mosissa 2017, Menbere & Menbere 2018). Such drivers have resulted in wetland disturbances, degradation, and loss, which ultimately can cause the elimination of native plant species, encroachment of exotic species, and reduction of ecological and socioeconomic values of wetlands in Ethiopia (Collins 2005, Mulatu et al. 2014). Little awareness of the prominence of wetlands, or perhaps the prerequisite for their conservation and sustainable utilization, could be a delinquent in Ethiopia (Wondarfrash 2003).

The most common threats to wetlands are the results of a mixture of social, economic, and climatic factors, which have increased pressure on the natural resources in Ethiopian wetlands. Another constraint to the judicious use of African wetlands is the lack of knowledge by planners and natural resource managers of the advantages that they supply and the techniques by which they will be utilized in an exceedingly sustainable manner (Jogo & Hassan 2010). A large number of wetlands in Ethiopia are considered vulnerable zones; some are most exploited, mismanaged, and lose their regenerating capacity (Alemayehu 2006).

In 1999, the government increased its pressure on farmers to cultivate wetlands to make amends for more drought-induced food shortages (Dixon et al. 2008). Currently, wetland cultivation provides between 10 and 20% of the annual food needs of the region but will be as high as 100% during the summer months in some areas. Eucalyptus, banana, sugarcane, and Khat cultivation on the perimeters of wetlands and Teff cropping in wetlands have been identified as threats to the survival of those areas.

CONSEQUENCES OF WETLAND DEGRADATION

The consequences of wetland loss and degradation in Ethiopia's alterations of the hydrological regime of wetlands have significant physico-chemical and biological, ecological, and socioeconomic implications at a wider scale (Roggeri 1995, OECD 1996). In Ethiopia, the implications of wetland loss and degradation are enormous as well as directly affecting the livelihood base of rural communities, decrease and extinction of wild flora and fauna, loss of natural soil nutrients and water reservoirs, and their subsequent benefits (Bezabih & Mosissa 2017, Menbere & Menbere 2018). They have affected various traditional occupations, socioeconomic conditions, and cultural activities (Kumsa 2015). The drainage of wetlands in Illubabor Zones, southwest Ethiopia, has led to a variety of ecological and economic problems (Wood 2003).

In Ethiopia, wetland management is not efficiently harmonized and lacks acceptable policy support. Due to the absence of workable institutional arrangements and wetland management policies, sustainable management of wetlands and capacity building do not seem to be strengthened. As a result, the sector suffers from a shortage of skilled manpower that is capable of disseminating the concept of wise use of wetlands (Birhan et al. 2015, Seid 2017).

Wetlands in southeastern Ethiopia, particularly in the Sinana district, are ecologically, socially, and environmentally crucial for the realm. The enormous direct and indirect consequences of wetland loss and degradation are observed in the Kedar wetland. However, empirical evidence on the plant species diversity and ecosystem services of the wetland, and therefore the drivers for wetland degradation within the region and Sinana district, is not available. Thus, the target of the study was to investigate plant species diversity and assess the perception of people on ecosystem services and drivers of wetland degradation within the Sinana District of the Bale Zone, Southeast Ethiopia. As a result, the study attempts to fill this gap by providing scientific information useful to style an efficient management plan vital for sustainable management of wetlands.

MATERIALS AND METHODS

Description of the Study Area

This study was conducted in Sinana district, in Bale zone Oromia regional state. It is located approximately 430 km southeast of the capital of Ethiopia (Fig.1). Geographically, the study district is identified with the placement between 6°29′ to 7°10′ N latitude and 39°28′ to 39°57′ E longitude. The full area of the district is approximately 1168 km^2. The district has 20 rural and 4 urban kebeles, a total of 24 kebeles.

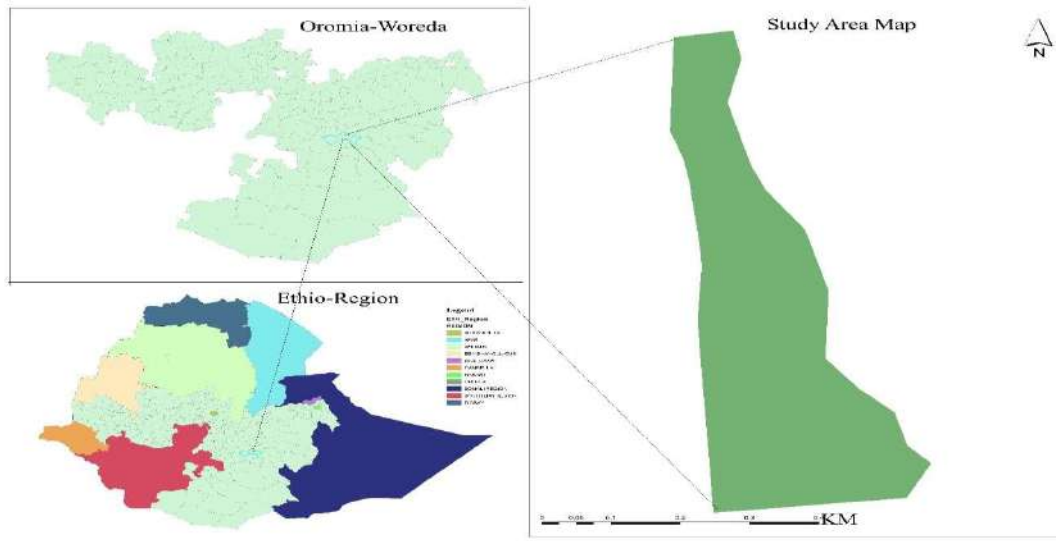

Fig. 1: Map of the study area.

The altitude of the district ranges from 1650 to 2950 m a.s.l. Of the entire area of the district, approximately 73.54% is plain land, 3.7% is hills, 9.6% is mountains, 12.3% is rugged, and 0.86% is gorge (Diriba & Kebede 2020).

The present study focused on the Kedar-Besaso wetland, which is one of the wetlands found within the Sinana district and has diverse ecological, economic, and environmental values within the area. It is located 9 km northeast of Robe town, the capital of the Bale Zone. The wetland covers approximately a region of approximately 30 ha and is found at longitudes 40°03′34″ and latitudes 07°08′24″. The elevation of the Kedar-Besaso wetland ranges from 2410 to 2420 m.a.s.l. The Kedar-Besaso wetland is an area made of land parcels owned by the community in common and individual agricultural tenure and used for grazing and drinking water by the community. The Kedar-Besaso wetland is categorized under swampy and freshwater wetlands fed by water sourced from perennial and seasonal water sources (Diriba & Kebede 2020). The annual average temperature is 16.5°C, whereas the minimum and maximum temperatures are 9°C and 23°C, respectively. The annual average rainfall is 1105mm, whereas the minimum and maximum rainfall are 1060 and 1150 mm, respectively (National Meteorological Agency of Ethiopia, 2012).

Farmers in this district experienced a mixed farming system of both livestock and major crops of wheat, barley, pulses, and oil crops. The rainfall pattern of the district is characterized by bimodal rainfall distribution. The district has two distinct seasons, i.e., autumn (belg), which extends from March to July, and summer (kiremt), which extends from August to January (Diriba & Kebede 2020). The presence of the Sinana Agricultural Research Center (SARC) and Oromia Seed Enterprise creates a decent opportunity for the farmers within the study area.

Research Methods

Site selection and household sample size: Aimed at wetland vegetation inventory, Kedar-Besaso wetland was selected purposively as this wetland is incredibly large, likewise a highly threatened wetland due to high pressure associated with urban expansion, improper water diversion for irrigation from the wetland, and pressure due to agricultural use and overgrazing. In addition, supported discussions with district experts and a preliminary survey, the wetland could represent the opposite surrounding wetlands situation within the study area in terms of the amount of disturbance and diversity of wetland use. Additionally, for the wetland vegetation inventory, three kebeles (smallest administrative unit) bordering the wetlands were selected purposively to review the perception of the community on the ecosystem services of wetlands and drivers of wetland degradation. Thus, two rural (Besaso & Shalo) and one urban (Nano Robe) kebele were selected. The household heads of every kebele were 8,458 (4,144 males and 4,314 females) from Nano Robe, 5,844 (2,982 males and 2,862 females) from Besaso and

Table 1: Site selection and household sample size.

Name of kebeles	Households (HH)	Sample size
Nano robe	8458	63
Besaso	5844	43
Shalo	4114	31
Total	18416	137

4114 (3,754 males and 360 females) from Shalo, with a total of 18,416 household heads (Table 1).

The sample size was determined using the formula developed by Cochran (1977) at a 95% confidence interval as follows:

$$n = \frac{Nz^2pq}{d^2(N-1)+pqz^2} \quad \ldots(1)$$

$$= \frac{18{,}416(1.96)^2(0.1 * 0.9)}{0.05^2(18{,}416-1)+0.1 * 0.9(1.96)^2}$$

$$= 137$$

Where n = sample size of household, P = 0.1 (proportion of the population to be included within the sample, that is, 10%), q = is 1-P, that is, (0.9), d = is that the degree of accuracy desired (0.05), N = a total number of housing units, Z = standardized normal variable and its value that corresponds to 95% confidence interval equals 1.96.

However, the numbers of household heads from each kebele were determined proportionally and obtained 63, 43, and 31 from Nano Robe, Besaso, and Shalo, respectively. Moreover, three key informants (KI) per kebele and a joint focus group discussion (FGD) composed of 8-10 farmers per group were used for data collection.

Data Collection

Vegetation data collection: A vegetation survey was conducted from August to September 2021 during the flowering season for many plants within the study area (Alemayehu & Solomon 2010). Before the vegetation inventory was conducted, wetland boundaries were delineated to the utmost extent of flooding or the sting of depressions to position transects and sampling plots. A transect-quadrant method was used to assess species composition (Shannon & Weiner 1949).

A vegetation inventory was conducted from the sampling plots lying along transects that were placed in the lower part of the wetland along the direction of water flow within the wetland. Sample plots of size five, 5 m × 5 m (25 m^2), and 1 m × 1 m (1 m^2) placed one in the middle, and four at each corner of the plot were used for shrubs/seedlings/sapling and herbaceous plants, respectively. Additionally, GPS readings and levels of disturbance were recorded for every main plot. A total of 45 sample plots lay along the transact and were inventoried. The gap between the transect line was 250 m, and between sampling, the plot was placed systematically at 100 m. Vegetation identification matching herbarium specimens and/or keying was completed using relevant flora identification texts, such as the Flora of Ethiopia and Eritrea (Hedberg et al. 2006). Vegetation samples were collected, pressed, and sent to the national capital, the University Herbarium, for added plant species identification, and further data were analyzed.

Socioeconomic data collection: The reconnaissance survey was dispensed to determine the practice of wetland resource use and other relevant information for designing data collection procedures.

Household survey: A household survey was carried out by employing a semi-structured questionnaire. The questionnaire was used to collect information on the background of respondents, the particular and potential use of wetlands, and drivers of wetland degradation. This household survey was conducted on 137 sample households permanently living within the area. The number of persons interviewed was 63, 43, and 31 in Nano robe, Besaso, and Shalo kebeles, respectively. We conducted the household interviews within the common language Afan Oromo, by translating the prepared questionnaire. An interview focused on each household's demographic and socioeconomic characteristics, perception of ecosystem services, and drivers of wetland degradation. Data were collected through questionnaires, and oral interviews were administered in August 2021 by three enumerators. The enumerators were knowledgeable and could speak, write, and browse both native and English languages. Additionally, the principal investigator provided the orientation and relevant information on a way to collect data and interrogate during the interviews.

Focus group discussion (FGD): The focus group discussion was steered in each kebele with a community representative consisting of 8-10 participants in each group. FGD was carried out to triangulate the information collected during the household survey and gain additional information, such as perceptions of respondents with reference to ecosystem service and drivers of change of the wetland, employing a guiding checklist.

Key informant interviews: The key informants consisted of representatives of relevant managers and agricultural extension of the village and natural resources management experts of the district. They were selected based on their knowledge of the wetland resources and people's dependency on and involvement in the management of the wetland. They were consulted to identify ecosystem services of the wetland, drivers of wetland degradation, and the history of wetland use and degradation. The key questions that were asked during interviews focused on the community's perceptions of ecosystem service and drivers of change within the wetland.

Data Analysis

Vegetation data analysis: Vegetation data were analyzed and summarized using diversity indices such as species

richness, Shannon and Wiener diversity (H'), and evenness (E). Diversity indices provide more information about community composition than simply species richness (i.e., the number of species present); they consider the relative abundances of various species and supply important information about the rarity and commonness of species in a community (Mueller-Dombis & Ellenberg 1974).

Shannon and Wiener diversity index (H'): Shannon & Wiener's (1949) index of species diversity was applied to quantify species diversity and richness. It is one of the foremost widely used methods in measuring the diversity of species and richness. The Shannon diversity index (H') was used to determine species diversity (Kent & Coker 1992) as follows:

$$H' = -\sum_{i=1}^{s} P_i \, lnP_i \quad \ldots(2)$$

Where H' is the Shannon and Wiener diversity index, S = total number of species within the sample, P_i = is the proportion of individuals of species, i = the proportion of total cover within the sample, and Ln = natural logarithm.

Evenness (E): Evenness or equitability was accustomed to quantifying the unique representation of a given species against a hypothetical community within which all species are equally common. The value of the evenness index falls between 0 and 1. The upper value of the evenness index indicates that the species were more evenly distributed within the given area of the study (Kent & Coker 1992). The evenness index was calculated using the formula:

$$J = \frac{H'}{lnS} \quad \ldots(3)$$

Where J = evenness, H' = Shannon-Wiener diversity index, S = total number of species within the sample, and ln = natural logarithm

Socioeconomic data analysis: Quantitative data obtained from interviews of households were first coded, categorized, and analyzed using descriptive analysis such as frequency analysis with Statistical Package for Social Sciences (SPSS) version 25 software. Data from the FGD and key informant interviews were summarized in narrative form. Ranking the drivers of wetland degradation perceived by respondents was computed with the principle of weighted average using the ranking index adopted by the previous researcher (Musa et al. 2006, Solomon et al. 2018) as follows:

$$\text{Index} = \frac{R_n C_1 + R_{n-1} C_2 + \cdots + R_1 C_n}{\sum (R_n C_1 + R_{n-1} C_2 + \cdots + R_1 C_n)} \quad \ldots(4)$$

Where: R_n = value given for the least ranked level (for example, if the least rank is 5th, then R_n = 5, R_{n-1} = 4, R_1 = 1, C_n = counts of the least ranked level (in the above example, the count of the 5th rank = Cn, and the count of the 1st rank = C_1. In addition, ranking methods were used to identify the dependence of households on wetland ecosystem services.

RESULTS

Vegetation Composition of the Wetland

A total of 20 herbaceous and grass plant species belonging to 14 families were identified in the studied wetland (Table 2). From a study site, the family Polygonaceae consists of three species, contributing 15%, followed by Cyperaceae, Apiaceae, Commelinaceae, and Asteraceae, each consisting of 2 species and comprising 40% of the study area plant species, while the remaining nine families, each had only 1 species each and covered 45% of the species composition.

Diversity of the Vegetation

The overall Shannon diversity (H') of the wetland was 1.15. According to Giliba et al. (2011), a diversity index value below 1.5 is low. Analysis was conducted by counting the abundance of every species. Thus, the studied wetland had low species diversity. This might have resulted from the high impact on the wetland due to agricultural expansion, overgrazing, irrigation water use, and urban waste disposal.

Table 2: Complete list of all identified plant species from the Kedar wetland.

Family Name	Name of species	Number of species	% Total
Polygonaceae	*Persicaria decipiens* *Persicaria glabra* *Rumex nepalensis*	3	15
Caryophyllaceae	*Drymaria cordata*	1	5
Apiaceae	*Cenetella asiatica* *Oenanthe palustris*	2	10
Commelinaceae	*Commelina forskalaei* *Commelina latifolia*	2	10
Asteraceae	*Galinsoga quadriradiata* *Ageratum conyzoides*	2	10
Convolvulaceae	*Ipomoea cordofana*	1	5
Cyperaceae	*Cyperus flavescent* *Cyperus aterrimu*	2	10
Labiatae	*Ajuga decumbence*	1	5
Poaceae	*Cynodon dactylon*	1	5
Onagraceae	*Ludwigia abyssinica*	1	5
Araliaceae	*Hydrocotyle umbellata*	1	5
Typhaceae	*Typha latifolia*	1	5
Araceae	*Colocasia esculenta*	1	5
Linderniaceae	*Lindernia rotundata*	1	5
Total		20	100%

The most frequent plant species within the studied wetland were *Typha latifolia*, *Commelina forsicalia*, *Cyperus aterrimu*, *Cyperus flavescent*, and *Colocasia esculenta*. Of the 48 plant species, 13 species, *Commelina forskalaei* (15.6%), *Leersia hexandra* (12.96%), *Digitaria sanguinalis* (12%), *Oplismenus spp*. (9.71%), *Digitaria temate* (8.02%), *Cyperus assimilis* (3.54%), *Phyllantus boehmii* (3.3%), *Rumex abyssinicus* (2.89%), *Cenetella asiatica* (2.6%), *Eragrostis ciliaris* (2.59%), *Achyranthes aspera* (2.44%), *Snowdenia polystachya* (2.16%) and *Polygala petitiana* (2.11%) with relative abundances over 2% accounted for 79.92% of the plant community in cultivated sites, of which 56.61% were upland plant species. On the other hand, wetland plant species such as *Thelypteris confluence*, *Cyperus mundtii*, *Leucas deflexa*, *Cyperus flavescens*, *Cyperus elegantulus*, *Sesbania dummeri, Fimbristylis dichotoma*, *Plectranthus argentatus*, *Aeschynomene schimperi*, *Sacciolepis rigens,* and *Triumfetta rhomboidea* species were not observed in the cultivated site.

Table 3: Characteristics of the respondents.

Variable	Category	Response rate	
		Number	Percentage [%]
Sex	Male	91	66.4
	Female	46	33.6
Age	20-29	38	27.7
	30-39	35	25.5
	40-49	33	24.1
	50-59	18	13.1
	Above 60	13	9.5
Marital status	Single	34	24.8
	Married	103	75.2
Level of education	None	6	4.4
	Primary	70	51.1
	Secondary	42	30.7
	Tertiary & Higher	19	13.9
Religion	Islamic	90	65.7
	Christian	47	34.3
Occupation	Government employed	25	18.2
	Farmers	74	54
	Merchants	38	27.7
Number of cattle	<5 cattle's	30	21.9
	5-10 cattle	42	30.7
	>10 cattle's	65	47.4
Size of farmland	<0.05 hectares	63	46
	<1hectares	50	36.5
	>2 hectares	24	17.5
Residence year	<5 years	14	10.2
	5-10 years	53	38.7
	>10 years	70	51.1

Community Perception of Ecosystem Services of the Wetland

Characteristics of the respondents: The results from Table 3 revealed that the majority (66.4%) of the respondents were male, and the remaining respondents were female. Regarding the age group, 27.7% of the respondents were aged between 20-29, followed by 30-39 (25.5%) and 40-49 (24.1%). The farmland size indicated that 46% had less than 0.05 ha of farm size, while 36.5% had less than 1 ha, and 17.5% had greater than 2 ha.

Perception of ecosystem services of the wetland: The study assessed the ecosystem services of a wetland, considering the actual and potential benefits through household surveys, FGDs, and key informant interviews. A total of 21 key ecosystem services categorized into provisioning, regulating, and cultural services were identified for the study area.

Provisioning service of the wetland: The most important provisioning services of the wetland are grazing, food through agriculture, fodder, and grass for various services, and water. The results also showed that the majority (77.4%) of the community used wetlands for grazing, followed by irrigation (76.6%), grasses for fodder (68.6%), and water for drinking livestock (48.2%) (Fig. 2). Communities produce different crops, vegetables, and fruits within the wetland and the surrounding upland during the dry season using water from wetlands as small-scale irrigation to secure household food needs and generate income.

Cyperus spp., locally called *Cheffe* (Afan Oromo), is usually used for roofing or thatching and adornment during holiday celebrations and regular coffee ceremonies. Approximately 56.2% of the households reported that they used *Cheffe* to form ornamental crafts, and 48.9% of them used a variety of wetland plant species as traditional medicines. FGD and key informants identified the foremost commonly used medicinal plants, including *Commelina latifolia*, *Ageratum conyzoides*, *Persicaria decipiens*, *Ludwigia abyssinica*, *Colocasia esculenta*, *Vernonia sp*., *Oenanthe palustris*, and *Lindernia rotundata*. For example, many sedges or *Cyperus* species are utilized in traditional medicines for the treatment of various diseases, e.g., stomach ache and bowel disorders, amenorrhea, bronchitis, tumors, communicable disease, pain and fever, diabetes, skin diseases, problems concerning the circulation of blood and reproductive organs (Mueller-Dombis & Ellenberg 1974).

Regulation service of the wetland: Regulating services were also important services perceived by respondents.

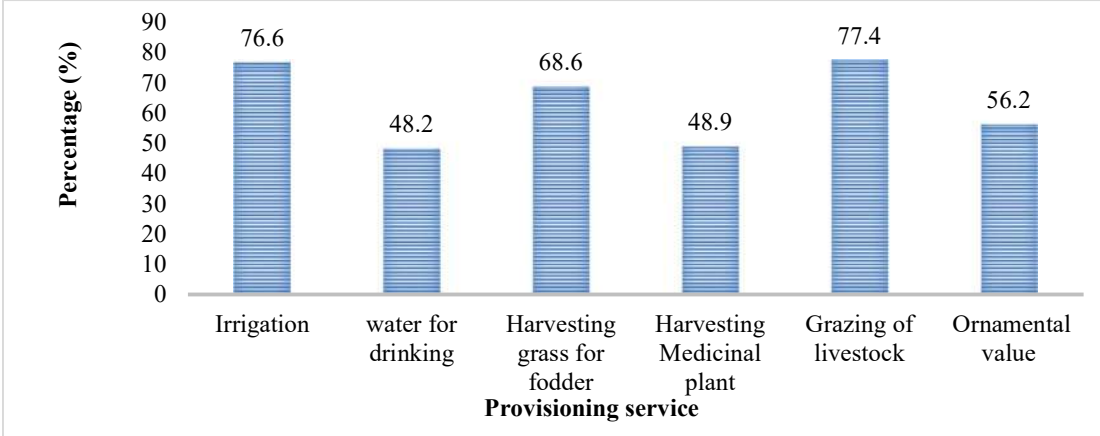

Fig. 2: Provisioning service within the studied wetland.

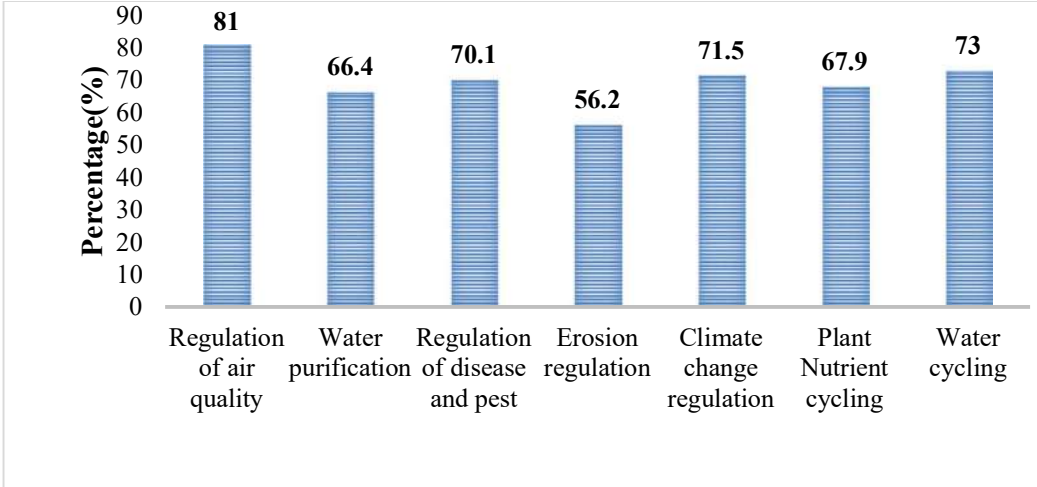

Fig. 3: Perception of the regulation services of the wetland.

Of the overall respondents, 81% believe that wetlands are important to controlling the air quality and condition of the encompassing area (Fig. 3). Seventy-three percent of them also believe that wetlands provide water cycling services, and 71.5% of them believe in climate change regulation. From households, 70.1% revealed that wetlands had served as a regulation of disease and pests.

The study respondents (66%) also believed that wetlands provide important regulation services in purifying water, followed by regulating soil erosion by 56%. Approximately 71% of households believed that wetlands could control the microclimate of the encircling area.

Cultural service of the wetland: Among the identified cultural ecosystem services, the aesthetic value was perceived by 81% of the households, followed by a sense of places and education and knowledge (77.4%) (Fig. 4). Educational and scientific value is also gained by appreciating natural biological processes in unimpacted environments. They also identified recreational values (76%), followed by cultural practice (74.5%). According to KIs Oromo, people had the tradition of celebrating *Erecha* within this wetland. Approximately 72% believed wetlands are the cultural heritage of their ancestors. During the FGD, they explained that cultural services, especially those associated with traditional ceremonies, were more important than other services.

Perceptions of drivers of wetland degradation: The respondents identify five important drivers of wetland degradation within the studied area: agricultural activity, shortage of cropland, lack of awareness, climate change, upland land degradation, and increasing population number. Among the identified drivers, shortage of cropland (70.8%)

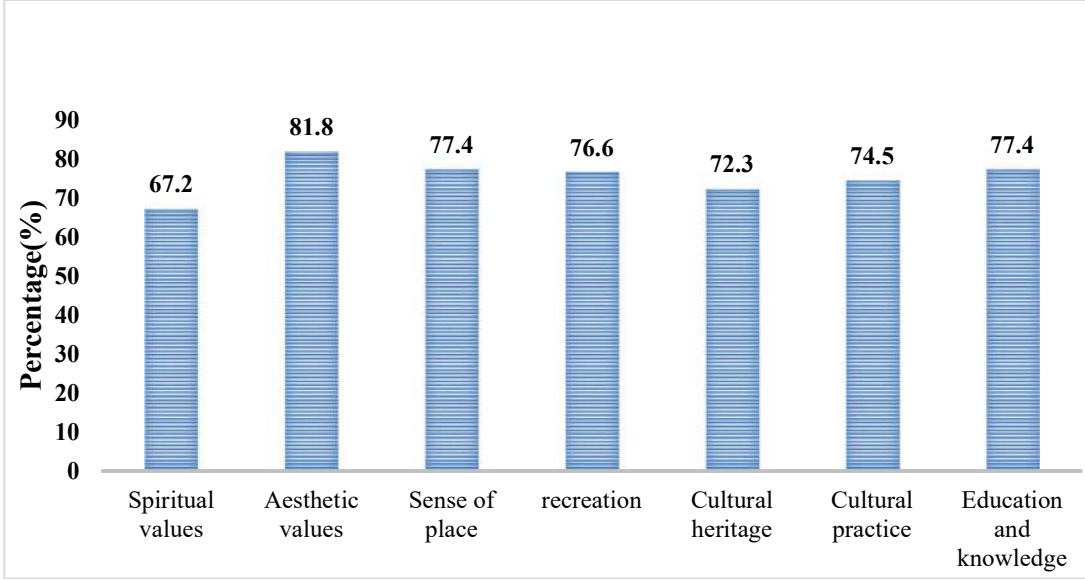

Fig. 4: Cultural service of the wetland.

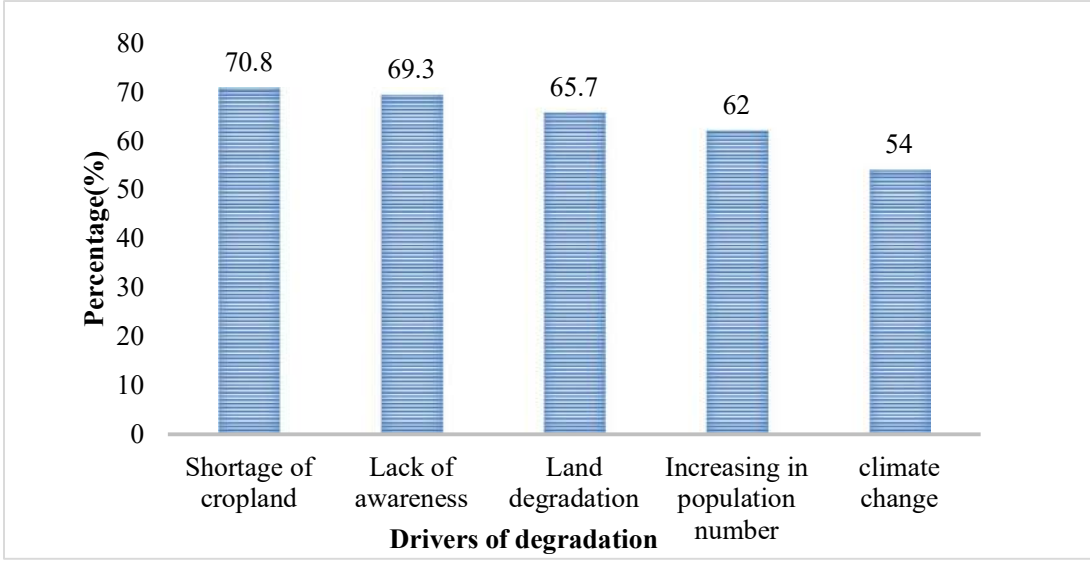

Fig. 5: Community perceptions of drivers of wetland degradation.

and lack of awareness (69.3%) were recognized as the major causes of wetland degradation, followed by upland land degradation (65.7%), increasing population (62%) and temperature change as causes of wetland degradation were perceived by 54% of the respondents (Fig. 5).

Lack of awareness that contributes to its share of wetland degradation within the study area: 69% of respondents believed it was a vital cause of wetland degradation. During the FGD and KI interviews, they mentioned that wetland management strategies practiced to date were not participatory and not integrated with awareness creation. Wetlands are taken as protected areas instead of using wetlands in a sustainable way (wise use strategy); therefore, the approach was not a win-win. Key informants also mentioned that the lack of a clear policy on wetlands is a crucial factor in wetland degradation. In some parts, wetlands are considered common land where no clear ownership is set; thus, their use is uncontrollable.

The present study respondents (62%) perceived that population growth is additionally a very important driver of

Table 4: Ranking of drivers of wetland degradation.

Drivers	Rank					Weight	Percent	Rank
	1	2	3	4	5			
Shortage of cropland	75	20	15	0	1	501	18.5	1
Lack of awareness	70	26	10	1	1	487	18.0	2
Land degradation	35	40	0	2	0	339	12.5	5
Population growth	64	12	9	15	2	427	15.7	3
Climate change	52	8	11	9	3	346	12.8	4

wetland degradation. According to the FGD, a shortage of lands for cultivation and grazing resulting from population growth directly increases the encroachment of the wetlands within the study area. They also mentioned that the conversion of grazing land-associated populations pushed them to search out grazing land within the wetlands. Restless upland cultivation to secure food for growing people and its cultivation without proper soil and water conservation increased soil erosion and siltation in wetlands, thereby endangering their ecological processes.

In the study area, 54% of households perceived global climate change as the driver of wetland degradation. The FGD identified that climate effects such as a shortage of rainfall, drought, changes within the length of the wet season, and lengthening within the dry period pushed the use of wetlands to avoid crop failure and death of cattle and their products. They also explained that they were captivated by the irrigation activity of crop production in wetlands during drought years.

Farmers also ranked the drivers of wetlands. The results from Table 4 revealed that a shortage of cropland is ranked first, followed by a lack of awareness. Both drivers are interlinked so that a farmer living around the studied wetland, as well as the neighboring areas, is forced to degrade the wetland to obtain additional croplands, generate income, and maintain their livelihoods.

DISCUSSION

In the present study, the plant families described from the studied wetland conform to the general pattern discussed for wetlands in other wetland areas in Ethiopia (EWNRA 2008). This finding agrees with Unbushe (2013), who described that the bulk of plant species within the wetlands of the Dabush swamp and other areas comprise Cyperaceae, Asteraceae, Onagraceae, Fabaceae, and Poaceae. However, in terms of dominancy, our results are different from those of Unbushe (2013), who found the highest number of species in the Poaceae family, while the findings of our study showed the highest number of species recorded within the family Polygonaceae. The variation is also because of the effect of agroecological differences and the level of wetland disturbance and degradation of vegetation. The findings during this work also showed that 55% of plant species were herbaceous, identical to the findings of Unbushe (2013), who found the dominance of herbaceous plants in wetlands.

Contrary to the present study, a study conducted by Mulatu et al. (2014) indicated that wetlands fraught with cultivation had more diversity than uncultivated (undisturbed) wetlands. Thus, the cause for low species diversity can be both the agroecological and wetland disturbance effects. The value of evenness (J) within the study area was 0.385. This implies that the distribution of wetland plant species was uneven because there was the dominance of some species within the studied wetland. This indicated that the wetlands were poor in plant diversity.

The species *Ageratum conyzoides*, *Commelina forsicalia*, and *Galinsoga* are typical upland weed species (Alvarez et al. 2012) that are present within the studied wetland, indicating that the wetland is changing its nature or degrading. A study conducted by Alvarez et al. (2012) and Mulatu et al. (2014) found that wetland drainage for the cultivation of wetlands promoted the invasion of upland weed species. Additionally, the species *Cyperus flavescent*, *Cyperus atterrimus*, and *Ludwigia abyssinica* were invasive, representing good indicators of impaired wetlands, and are common upland weeds in Eastern Africa (Alvarez et al. 2012). The presence of native wetland plant species such as *Cyperus flavescent*, *Cyperus atterrimus*, and *Ludwigia abyssinica* within the undisturbed part of the studied wetland indicated that part is under good wetland conditions (Gichuki et al. 2001, Mulatu et al. 2014).

Provisioning services are material benefits such as food, water, and other goods people directly obtain from the ecosystem (Millennium Ecosystem Assessment-MEA 2005). The dependence of humans on provisioning services is widely acknowledged, especially in developing countries, as people are highly dependent on natural resources (Bhatta et al. 2015, Oort et al. 2015). Communities produce different crops, vegetables, and fruits within the wetland and the surrounding upland during the dry season using water from

wetlands as small-scale irrigation to secure household food needs and generate income. Similar results were reported that rural communities in different parts of Ethiopia (Mulatu et al. 2014) and other parts of the planet (Hartel et al. 2014) used wetlands for dry-season agriculture.

Other studies revealed that wetlands have provided various services for several Ethiopian communities for hundreds of years. As an example, farmers in wetland areas drain wetlands for agricultural purposes, including the growth of crops, vegetables, and fruits (Hailu 2007, Mulatu et al. 2014). Such practices are common in many parts of the globe because wetlands with extensive agriculture but without fertilizer, herbicide, or pesticide application often provide additional services to food production, such as flood regulation and maintenance of water quality or biodiversity (Verhoeven & Setter 2009). Educational and scientific value is also gained by appreciating natural biological processes in unimpacted environments (Turpie et al. 2010).

The International Water Management Institute (2006) also reported that over 65% of residents within the Bumbwisudi wetland in Zanzibar used wetlands for irrigation for agriculture to support their livelihoods. The government of Ethiopia emphasizes small-scale irrigation practices to reinforce food security within the country (Awulachew et al. 2007). Experts from the Sinana district agriculture office also reported that the authorities were encouraging the cultivation of wetlands to fulfill food self-sufficiency targets. This can be similar to other Eastern African countries such as Rwanda (Gowa 2009) and Kenya (Gichuki et al. 2001), where the governments of the countries supported the transformation of wetlands for food production to mitigate food insecurity and improve the livelihoods of rural communities. Approximately 71% of households believed that wetlands could control the microclimate of the encircling area. The Ramsar Convention Secretariat (2006, 2007) also stated that wetlands could stabilize the climate, particularly patterns of temperature and rainfall, which are the first components of global climate change. Some studies (Hailu 2003, Hailu 2007, Ambelu et al. 2013) also supported the result by reporting that rural communities perceived appreciation for cultural services and regulating and supporting ecosystem services. This might be because regulating and supporting services seem to be more abstract and intangible than cultural services.

During the FGD, they explained that cultural services, especially those associated with traditional ceremonies, were more important than other services. A similar finding supported this result that wetlands are important in providing cultural services, including spiritual and aesthetic value to people (Turpie et al. 2010). A study conducted by Kindu et al. (2015) supported this, reporting that population growth, agricultural activity, shortage of cropland, and lack of awareness were the highest significant drivers of land degradation of wetlands within the Munessa-Shashemene, south-central highlands of Ethiopia.

Similarly, the expansion of crop production based on irrigation in and around the wetlands was a serious threat to the wetlands within the basin of Hawassa & Ziway wetlands through the employment of varied agrochemicals (pesticides, herbicides, fungicides, and fertilizers) to the nearby wetlands and terrestrial areas, which might be easily drained to wetlands and degrade the wetland (Hengsdijk et al. 2008).

Similar results were reported by Noriko et al. (2012), indicating that a shortage of cropland alone caused 73% of all wetland degradation in developing countries. Jogo & Hassan (2010) also suggested that improper use and waste discharge could potentially degrade wetlands and undermine their capacity to supply services in the future. In Ethiopia, the lack of a comprehensive wetlands policy and implementing the law, plus the absence of an establishment duly empowered to issue and implement wetland laws and coordinate management activities, is the underlying reason for the deterioration of the wetlands (Gebresllassie et al. 2014).

Rapid population growth is the fundamental cause of increased pressure on wetlands through on-site and off-site effects (Mequanent & Sisay 2015). Such impacts were serious in densely populated highlands of Ethiopia, such as around the shores of Lake Tana and a few of the valleys (Mequanent & Sisay 2015). Previous studies in other parts of the country also reported that population pressure is the major driver of wetland degradation (Hurni et al. 2005, Dessie & Kleman 2007, Kidane et al. 2012). This can be a typical survival strategy of rural populations during the events of degradation, drought, and rainfall variability across Africa (Campbell 1990).

CONCLUSIONS

Wetlands are a very important source of biodiversity and ecosystem services. The study identifies 20 plant species belonging to 14 families. Family Cyperaceae was dominant within the studied wetland. The overall Shannon diversity (H=1.15) indicates that the wetland has low vegetation diversity with an uneven distribution (E=0.385). The cause for the low diversity of vegetation is also the disturbances within the wetland and, thus, the agroecological effect within the world.

A total of 20 ecosystem services categorized under-provisioning, regulating, and cultural were identified. Among those major services are grazing livestock (77.4%),

regulation of air quality (81%), and aesthetic value (81.8%) near the wetland. The important drivers of the wetlands are a shortage of cropland (70.8%), lack of awareness (69.3%), upland land degradation (65.7%), and increasing population (62%). Among the foremost important drivers, the shortage of cropland was a key driver, followed by an absence of awareness and upland land degradation.

Therefore, the results illustrate that the studied wetland is degraded due to high human pressure associated with growth and global climate change. An appropriate wetland management strategy must be designed with awareness creation on wetland use, and community participation in wetland management should be implemented. Increasing the productivity of upland cropland through different mechanisms should be implemented to reduce the pressure on wetlands. Wetlands should be restored and rehabilitated whenever possible and can be conserved by ensuring their wise use. Further study on the impacts of wetland degradation is significant to supply scientific information for the conservation and sustainable use of wetland resources.

ACKNOWLEDGMENT

The authors are grateful to the Mizan Tepi University, Department of Natural Resource Management, College of Agriculture and Natural Resources, for offering us such an opportunity to conduct this research. The first author (Kemalo Abdulmalik Boru) is thankful to receive sponsorship grants from mutual agreement from Madda Walabu University and Mizan Tepi University, Ethiopia. The author would like to thank Mr. Feyisa Dadecho and Mr. Abdalgani Esmael for assisting in the study area for data collection and household data surveys. The authors also thank the editor for their constant support and the anonymous reviewers for their great help.

REFERENCES

Abebe, Y.D. and Geheb, K. (ed.). 2003. Wetlands of Ethiopia. Proceedings of a Seminar on the Resources and Status of Ethiopia's Wetlands, pp. 49-116.

Alemayehu, H. and Solomon, R. 2010. Challenges and opportunities for Chamo Lake wetland biodiversity, Ethiopia. J. Natcon. 22(3): 223-233.

Alemayehu, T. 2006. Groundwater Occurrence Hydrogeological Water Quality Aquifer in Ethiopia. Addis Ababa University, Ethiopia.

Alvarez, E., Alvaro, D. and Juan, S. 2012. Tree above-ground biomass allometries for carbon stocks estimation in the natural forests of Colombia. Forest Ecol. Manag., 267: 297-308. https://doi:10.1016/j.foreco.2011.12.013

Ambelu, A., Mekonnen, S. G. and Silassie, A. 2013. Physicochemical and biological characteristics of two Ethiopian wetlands. Wetlands, 33(4): 691-698. https://doiI.org/10.1007/s13157-013-0424-y

Awulachew, S.B., Yilma, A.D. and Loulseged, M. 2007. Water Resources and Irrigation Development in Ethiopia. International Water Management Institute, Colombo. IWMI Working Paper 123. International Water Management Institute (IWMI), Sri Lanka. 66p.

Ayalew, W. 2010. Current Land Use Practices and Possible Management Strategies in Shore Area, Wetland Ecosystem of Lake Tana: Towards Improving Livelihoods, Productivity and Biodiversity Conservation. In Seyoum M. Brook L (ed.), Management of Shallow Water Bodies for Improving Productivity and People's Livelihoods in Ethiopia. Addis Ababa University Printing Press, Addis Ababa, pp 9-16.

Ayalew, W. 2018. Ecological conditions and ecosystem services of wetlands in the Lake Tana area, Ethiopia. Ecohydrol. Hydrobiol., 18: 231-244. https://doi.org/10.1016/j.ecohyd.2018.02.002

Battisti, C., Poeta, G. and Fanelli, G. 2016. An Introduction to Disturbance Ecology: A Road Map for Wildlife Management and Conservation. Springer, Singapore.

Bezabih, B. and Mosissa, T. 2017. Review on distribution, importance, threats, and consequences of wetland degradation in Ethiopia. Inter. J. Water Res. Environ. Eng., 9(3): 64-71. https://doi:10.5897/IJWREE2016.0697

Bhatta, L.D., Oort, B.E.H.V. and Nigel, E. 2015. Ecosystem services and livelihoods in a changing climate: Understanding local adaptations in the Upper Koshi, Nepal. Int. J. Biodiv. Sci. Ecosys. Serv. Manag., 11(2): 145-155. https://doi.org/10.1080/21513732.2015.1027793

Bijos, N.R., Orlando, E.C.U. and de, R.B.M. 2017. Plant species composition, richness, and diversity in the palm swamps (Veredas) of Central Brazil. Flora, 236-237: 94-99 https://doi.org/10.1016/j.flora.2017.10.002

Birhan, M., Sahlu, S. and Getiye, Z. 2015. Assessment of challenges and opportunities of beekeeping in and around Gondar. AJE, 8(3): 127-131. https://doi:10.5829/idosi.aje.2015.8.3.95133.

Campbell, D.J. 1990. Strategies for coping with severe food deficits in rural Africa: A review of the literature. Food Foodways, 4: 143-162. https://doi.org/10.1080/07409710.1990.9961976

Cochran, W.G. 1977. Sampling Techniques. Third Edition. John Wiley & Sons, New York.

Collins, N.B. 2005. Wetlands: The Basics and Some More. Free State Department of Tourism, Environmental and Economic Affairs, Ethiopia.

Da Ponte, E., Kuenzer, C. and Parker, A. 2017. Forest covers loss in Paraguay and perception of ecosystem services: A case study of the upper Parana forest. Ecosyst. Services., 24: 200-212. https://doi.org/10.1016/j.ecoser.2017.03.009

Davidson, N.C., Fluet-Chouinard, E. and Finlayson, C.M. 2018. Global extent and distribution of wetlands: Trends and issues. Marine Freshwater Res., 69(4): 620-627. https://doi.org/10.1071/MF17019

Dessie, G. and Kleman, J. 2007. Pattern and magnitude of deforestation in the south-central Rift Valley region of Ethiopia. Mt. Res. Dev., 27(2): 162–168. https://doi.org/10.1659/mrd.0730

Dikaso, U. 2013. Wetland Vegetation Composition and Ecology of Abaya and Chamo in Southern and Finca'a Chomen and Dabus in Western Ethiopia. PhD dissertation Unpublished. Addis Ababa, Ethiopia. http://thesisbank.jhia.ac.ke/id/eprint/5999.

Diriba, L. and Kebede, T. 2020. Assessments of breeding practices, major constraints, and opportunities of sheep and goat production in Sinana district, Bale Zone, Ethiopia. J. Dairy, Veter. Animal Res., 9(3): 78-83.

Dixon, A.B. and Wood, A.P. 2001. Sustainable wetland management for food security and rural livelihoods in South-west Ethiopia: The interaction of local knowledge and institutions, government policies and globalization. http://www.wetlandaction.org/pdf/rwanda_seminar.pdf

Dixon, A.B., Wood, A.P. and Maconachie, R. 2008. Small swamp wetlands in southwest Ethiopia. In: Wood, A. and Van Halsema, G.E. (eds), Scoping Agriculture – Wetland Interactions: Towards a Sustainable Multiple Response Strategy (FAO Water Report 33). Food and Agriculture Organization of the United Nations, Rome, Italy, pp. 65-72.

Dugan, P.J. 1990. Wetland Conservation: A Review of Current Issues and Required Action. IUCN, Gland, Switzerland, pp.94-96 https://portals.iucn.org/library/node/6048

Endalew, M.T. 2015. A preliminary survey of Geray reservoir, Amhara national, regional state, west Gojjam, Jabitehnan woreda, Ethiopia: focus on wetland management. J. Coast. Life Med., 3(4): 307-311. https://oaji.net/articles/2015/2154-1445308778.pdf

Ethiopian Wetlands and Natural Resources Association (EWNRA). 2008. Baseline Study of Wetland in Kefa Zone, Alemgono, Gojeb-Gewata, and Garina. Ethiopian Wildlife and Natural Resource Association, Addis Ababa.

Fennessy, M.S., Jacobs, A.D. and Kentula, M.E. 2007. An evaluation of rapid methods for assessing the ecological condition of wetlands. Wetlands, 27: 543-560. https://doi.org/10.1672/0277-5212(2007)27[543:AEORMF]2.0.CO;2

Gebresllassie, H., Gashaw, T. and Mehari, A. 2014. Wetland degradation in Ethiopia: Causes, consequences, and remedies. J. of Environment and Earth Sci., 4(11): 40-49. https://core.ac.uk/download/pdf/234663476.pdf

Gichuki, J., Guebas, F.D. and Mugo, M. 2001. Species inventory and the local uses of the plants and fishes of the Lower Sondu Miriu wetland of Lake Victoria, Kenya. Hydrobiologia, 458: 99-106. https://doi.org/10.1023/A:1013192330498

Giliba, A.R., Boon, K.E. and Kayombo, J.C. 2011. Species composition, richness, and diversity in Miombo woodland of Bereku forest reserve, Tanzania. J. Biodiv., 2(1): 1-7. https://doi.org/10.1080/09766901.2011.11884724

Gowa, E. (ed.) 2009. Rwanda State of Environment and Outlook: Our Environment for Economic Development. Rwanda Environment Management Authority, Rwanda.

Hailu, A. 2003. Wetlands Research in Southwestern Ethiopia: The Experience of the Ethiopian Wetlands Research Programme. In Abebe, Y.D. and Geheb, K. (eds), Wetlands of Ethiopia: Proceeding of a Seminar on the Resources and Status of Ethiopia's Wetlands, IUCN, Addis Ababa, pp. 37-48

Hailu, A. 2007. Potential Wetland Resources of Ethiopia: Use and Threats. In: Mengistu, A.A. (ed), Proceedings of the Public Meetings on Harnessing the Water Resources of Ethiopia for Sustainable Development in the New Ethiopian Millennium Forum for Environment. Forum for Environment, Addis Ababa, pp. 1-11.

Handa, C., Aleverse, M. and Beker, M. 2012. Opportunistic vascular plant introduction agricultural wetland for East Africa. Int. J. Agric. Sci., 2(9): 810-830.

Hartel, T., Fischer, J. and Campeanu, C. 2014. The importance of ecosystem services for rural inhabitants in a changing cultural landscape in Romania. Ecol. Soc., 19(2): 42. http://dx.doi.org/10.5751/ES-06333-190242

Hedberg, I., Kelbessa, E. and Edwards, S. (ed.) 2006. Flora of Ethiopia and Eritrea: Gentianaceae to Cyclocheilaceae. Volume 5. Addis Ababa University, Addis Ababa and Uppsala. https://www.librarycat.org/lib/newcrossbooks/item/92607792

Hengsdijk, H., Meijerink, G. and Hellegers, P. 2008. Appraisal of Payment for Environmental Services Related to Water Management in the Central Rift Valley of Ethiopia. Water for Food and Ecosystem, Strategy and Policy Brief, Wageningen University, Ethiopia, p.4.

Hirpo, L.A. 2018. The effect of wetland degradation on fish production in Ethiopia. Inter. J. Adv. Res. Biol. Sci., 5(2) : 178-187. https://ijarbs.com/pdfcopy/feb2018/ijarbs18.pdf.

Hosonuma, N., Martin, H. and Veronique, D. 2012. An assessment of deforestation and forest degradation drivers in developing countries. Environ. Res. Lett., 7(4): 044009. http://dx.doi.org/10.1088/1748-9326/7/4/044009

Hurni, H., Tato, K. and Zeleke, G. 2005. The implications of changes in population, land use, and land management for surface runoff in the Upper Nile Basin area of Ethiopia. Mt. Res. Dev., 25(2): 147-154. https://doi.org/10.1659/0276-4741(2005)025%5B0147:TIOCIP%5D2.0.CO;2

International Water Management Institute. 2006. Working Wetlands: A New Approach to Balancing Agricultural Development with Environmental Protection. IWMI, Ethiopia.

Jogo, W. and Hassan, R., 2010. Balancing the use of wetlands for economic well-being and ecological security: the case of the Limpopo Wetland in southern Africa. Ecol. Econ., 69: 1869-1876. https://doi:10.1016/j.ecolecon.2010.02.021

Junk, W.J., Shuqing, A. and Finlayson, C. 2013. Current state of knowledge regarding the world's wetlands and their future under global climate change: A synthesis. Aqua. Sci., 75(1): 151-167. https://doi.org/10.1007/s00027-012-0278-z

Karlsson, J. 2015. Scoping Study of Water Resource Management in the Textile Industry in Ethiopia. Stockholm International Water Institute (SIWI), Stockholm, . 1-39.

Kent, M. and Coker, P. 1992. Vegetation Description and Analysis: A Practical Approach. CRC Press, Boca Raton, pp. 363. https://doi:10.2307/3451427

Kidane, Y., Stahlmann, R. and Beierkuhnlein, C. 2012. Vegetation dynamics, and land use and land cover change in the Bale Mountains, Ethiopia. Environ. Monit. Assess., 184(12): 7473-7489. https://doi:10.1007/s10661-011-2514-8

Kindu, M., Schneider, T. and Teketay, D. 2015. Drivers of land use/land cover changes in the Munessa-Shashemene landscape of the south-central highlands of Ethiopia. Environ. Monit. Assess., 187(7): 452.

Kumsa, A. 2015. GIS and Remote Sensing based analysis of population and environmental change: The case of Jarmet wetland and its surrounding environments in Western Ethiopia. Master Thesis. Addis Ababa University, Ethiopia.

Lehner, B. and Döll, P. 2004. Development and validation of a global database of lakes, reservoirs, and wetlands. J. Hydrol., 296(1-4): 1-22. https://doi.org/10.1016/j.jhydrol.2004.03.028

McHugh, O., McHugh, A.N. and Eloundou-Enyegue, P.M. 2007. Integrated qualitative assessment of wetland hydrological and land cover changes in a data-scarce dry Ethiopian highland watershed. Land Degrad. Dev., 18(6): 643-658. https://doi.org/10.1002/ldr.803

Menbere, I.P. and Menbere, T.P. 2018. Wetland ecosystems in Ethiopia and their implications in ecotourism and biodiversity conservation. J. Ecol. Nat. Environ., 10(6): 8096.

Mequanent, D. and Sisay, A. 2015, Wetlands potential, current situation and its threats in Tana sub-basin, Ethiopia. World J. Agric. Econ. Rural Devel., 1(2): 1-4.

Millennium Ecosystem Assessment. 2005. Ecosystems and Human Well-Being: Wetlands and Water Synthesis. World Resources Institute, Washington DC.

Moges, A., Beyene, A. and Triest, L. 2018. Imbalance of ecosystem services of wetlands and the perception of the local community towards their restoration and management in Jimma Highlands, Southwestern Ethiopia. Wetlands, 38: 1081-1095. https://doi.org/10.1007/s13157-016-0743-x

Mueller-Dombois, D. and Ellenberg, H. 1974. Aims and Methods of Vegetation Ecology. John Wiley and Sons, New York, p. 547.

Mulatu, K., Hunde, D. and Kissi, E. 2014. Impacts of wetland cultivation on plant diversity and soil fertility in South-Bench District, Southwestern Ethiopia. African J. Agric. Res., 9: 2936-2947. https://doi:10.5897/AJAR2013.7986.

Musa, L., Peters, K. and Ahmed, M. 2006. On-farm characterization of Butana and Kenana cattle, breed production systems in Sudan. Livest. Res. Rural Dev., 18: 1277-1288.

National Meteorological Agency of Ethiopia 2012. http://www.ethiomet.gov.et/other_forecasts/ten_daily_forecast.

OECD 1996. Guidelines for Aid Agencies for Improved Conservation and

Sustainable Use of Tropical and Sub-Tropical Wetlands: Sustainable Use of Wetlands. OECD, Paris, France. https://www.cbd.int/doc/guidelines/fin-oecd-gd-lns-wlands-en.pdf

Oort, B.V., Bhatta, L.D. and Baral, H. 2015. Assessing community values to support mapping of ecosystem services in the Koshi river basin, Nepal. Ecosyst. Serv., 13: 70-80. https://doi.org/10.1016/j.ecoser.2014.11.004.

Rahman, M.M., Islam, M.A. and Rahman, M.M. 2005. Final Technical Report on Knowledge, Attitude, and Practices. Center for Natural Resource Studies (CNRS), Dhaka, p. 1213.

Ramsar Convention Secretariat, 2006. The Ramsar Convention Manual: A Guide to the Convention on Wetlands (Ramsar, Iran, 1971), Fourth Edition. Ramsar Convention Secretariat, Gland, Switzerland.

Ramsar Convention Secretariat. 2007. Wise Use of Wetlands: A Conceptual Framework for the Wise Use of Wetlands. Ramsar Handbooks for the Wise Use of Wetlands. Third Edition. Ramsar Convention Secretariat, Gland, Switzerland.

Ramsar Convention Secretariat. 2013. The Ramsar Convention Manual: A Guide to the Convention on Wetlands (Ramsar, Iran, 1971)· Sixth Edition. Ramsar Convention Secretariat, Gland, Switzerland, pp. 6.

Roggeri, H. 1995. Tropical Freshwater Wetlands: A Guide to Current Knowledge and Sustainable Management: Developments in Hydrobiology. Kluwer Academic Publishers, Dordrecht, Boston, London, 83(4): 340-363. https://doi.org/10.1002/iroh.19980830403.

Rosolen, V., de Oliveira, D.A. and Bueno, G.T. 2015. Vereda and Murundu wetlands and changes in Brazilian environmental laws: Challenges to conservation. Wetl. Ecol. Manag., 23: 285-292. https://doi:10.1007/s11273-014-9380-4

Schuyt, K. and Brander, L. 2004. Living Waters: Conserving the Source of Life - The Economic Values of the World's Wetlands. WWF, Gland, Switzerland and Amsterdam, The Netherlands.

Seid, G. 2017. Status of wetland ecosystems in Ethiopia and required actions for conservation. J. of Res. Dev. Manage., 32: 92-100.

Shannon, C.E, and Weiner, W. 1949. The mathematical theory of communication. University of Illinois Press. https://monoskop.org/images/b/be/Shannon_Claude_E_Weaver_Warren_The_Mathematical_Theory_of_Communication_1963.pdf

Solomon, N., Hishe, H. and Annang, T. 2018. Forest cover change, key drivers and community perception in Wujig Mahgo Waren Forest of Northern Ethiopia. Land, 7(1): 32. https://doi.org/10.3390/land7010032

Tilahun, S., Edwards, S. and Tewolde, B.G.E. (ed.) 1996. Important Bird Areas of Ethiopia: A First Inventory. Ethiopia Wildlife and Natural History Society, Addis Ababa.

Turpie, J., Lannas, K. and Scovronick, N. 2010. Wetland Ecosystem Services and Their Valuation: A Review of Current Understanding and Practice. In Malan H (ed), Wetland Valuation. The Water Research Commission, Limpopo Province, pp. 1-132.

United States Agency for International Development (USAID). 2008. Ethiopian Biodiversity and Tropical Forests 118/119 Assessment. USAID, Biodiversity Analysis and Technical Support Team, Addis Ababa.

Verhoeven, J.T. and Setter, T.L. 2010. Agricultural use of wetlands: opportunities and limitations. Ann. Bot., 105(1): 155-163. https://doi:10.1093/aob/mcp172

Woldemariam, W., Mekonnen, T. and Morrison, K. 2018. Assessment of wetland flora and avifauna species diversity in Kafa zone, Southwestern Ethiopia. J. Asia-Pac. Biodiv., 11(4): 494-502. https://doi.org/10.1016/j.japb.2018.08.003.

Wonderfrash, M. 2003. Wetlands, Birds, and Important Bird Areas in Ethiopia. In Abebe, Y.D. and Geheb, K. (eds), Wetlands of Ethiopia. IUCN, Nairobi, pp. 3748.

Wood, A. 2003. Wetlands, gender, and poverty: some elements in the development of sustainable and equitable wetland management. Proceed. Conf. Wetl., 11: 65.

Yimer, H.D. and Mengistou, S. 2009. Water quality parameters and macroinvertebrates index of biotic integrity of the Jimma wetlands, Southwestern Ethiopia. J. Wetlands Ecol., 3: 77-93. https://doi.org/10.3126/jowe.v3i0.2265.

Zedler, J.B. and Kercher, S. 2005. Wetland resources: status, trends, ecosystem services, and restorability. Annual Rev. Environ. Res., 30: 39-74. https://doi.org/10.1146/annurev.energy.30.050504.144248.

Zeleke, A., Gadisa, T. and Gebremichael, G. 2015. Diversity and relative abundance of bird species of Sheko district, Bench Maji zone, Southwest Ethiopia. Int. J. Dev. Res., 5(4): 3975-3979.

ORCID DETAILS OF THE AUTHORS

Lalit Tukaram Ingale: https://orcid.org/0000-0003-0407-6064

Nature Environment and Pollution Technology
An International Quarterly Scientific Journal

p-ISSN: 0972-6268
(Print copies up to 2016)
e-ISSN: 2395-3454

Vol. 23 | No. 1 | pp. 69-86 | 2024

Original Research Paper

https://doi.org/10.46488/NEPT.2024.v23i01.005

Open Access Journal

Design and Modelling of Urban Stormwater Management and Treatment Infrastructure for Communities in Wuse, Abuja

O. J. Oyebode† and **A.M. Umar**
Civil and Environmental Engineering Department, Afe Babalola University, Ado-Ekiti Ekiti State, Nigeria
†Corresponding author: O. J. Oyebode; oyebodedare@yahoo.com

Nat. Env. & Poll. Tech.
Website: www.neptjournal.com

Received: 18-07-2023
Revised: 17-09-2023
Accepted: 18-09-2023

Key Words:
Stormwater management
Pollution
Civil infrastructure
Environmental sustainability

ABSTRACT

Effective stormwater management can be used to regulate water quantity and quality for environmental sustainability, flood control, pollution reduction and other advantages of civil engineering infrastructures. Pollution of the environment and contamination of water sources can emanate from improper stormwater management. This study used a small-scale model of rainwater harvesting to analyze the design and model of urban stormwater management and treatment infrastructure for the neighborhoods in Abuja. The water quality of the treated stormwater retrieved has improved as a result of the usage of memory foam, alum, and chlorine to filter out contaminants and pathogens. With the fictitious stormwater treatment model created for this study, average values of the physicochemical parameters were collected from the stormwater discharge after it had been filtered and treated. The use of potash alum has had a variety of effects on the water's quality. From 697 $mg.L^{-1}$ to 635 $mg.L^{-1}$, the total dissolved solids dropped. The DO dropped from 5.87 $mg.L^{-1}$ to 3.92 $mg.L^{-1}$ as well. Additionally, the turbidity rose from 4.42 FNU to 4.58 FNU, and the salinity rose from 0.7 PSU to 1.44 PSU, respectively. pH decreases from 19.78 to 15.17 $mg.L^{-1}$, BOD decreases from 8.35 to 6.51, and COD decreases from 2.55 to 1.9. Calcium hardness has decreased from 287 $mg.L^{-1}$ to 265.83 $mg.L^{-1}$. The conductivity increases marginally from 3.24 $ms.cm^{-1}$ to 3.82 $ms.cm^{-1}$. The Fe^{2+} and Zn^{2+} ions exhibit a little decrease from 0.143 $mg.L^{-1}$ to 0.055 $mg.L^{-1}$ and from 0.092 $mg.L^{-1}$ to 0.045 $mg.L^{-1}$, respectively. Due to inadequate or nonexistent drainage systems in the many states and villages throughout the country, stormwater run-off management and treatment in Nigeria have been a colossal failure. Effective stormwater management can be sustained by using legal and environmental laws.

INTRODUCTION

There are copious challenges facing urban stormwater management in most nations of the world**.** This results in several issues, including floods, which cost lives and destroy property. The vast majority of stormwater that is wasted can be used in the community in several ways, whether at homes, businesses, or industrial facilities. While stormwater serves as a backup water source for irrigation, toilet water tanks, car washing, laundry, fire sprinkler systems, and other uses, it is important to manage and reuse stormwater run-off in a way that conserves potable water. Stormwater is the term for the liquid that is created when it rains. If improperly managed and channeled, stormwater can produce flooding and water contamination, which can be a serious issue for a city. Stormwater can be appropriately harvested and purified to meet the demands of people in the community by a variety of ways of filtration and disinfection due to the substantial rise in the need for clean water for various means of consumption and usage by the people and the community. The primary objective of this research has historically been to recognize the critical relevance of planning and modeling infrastructure for the collection and treatment of urban stormwater that happens during rainfall in a town in Nigeria.

PAST STUDIES

The control of both the quantity and quality of water is known as stormwater management. To manage (and treat) contaminated rainwater, a variety of structural or engineering control devices and procedures (operational and procedural practices) are used. Stormwater. Water quality can be slightly improved, and floods can be decreased with the help of stormwater management. The network of pipelines, impermeable surfaces, storage ponds, and other devices used for stormwater management include several methods of reducing peak discharge (Borgaonkar & Marhaba 2021). For human activity and habitation, water availability is essential. Although there is more than enough water on the planet (1.5 × 10 metric tons) to feed all 5.5 billion people,

clean, drinkable water is not commonly accessible. The WHO attributes the great majority of natural disasters that afflict people to water or a lack thereof. Nano-drug delivery, the most recent development in drug delivery technology, provides distinctive physicochemical properties, prolonged physiological retention, and controlled release of medicinal chemicals for increased health benefits (Antoniraj et al. 2022). Many opportunities exist on the job site to evaluate the efficacy of interventions designed to enhance the mental health and quality of life of large populations (Atlantis et al. 2004). Total trihalomethanes in water (TTHMs) are byproducts of municipal water disinfection. Exposure to TTHM has been related to cancer and may harm fertility (Lewis et al. 2021). The main method used nowadays to disinfect domestic drinking water supplies in many places is chlorination. This procedure has been demonstrated to reduce the morbidity and mortality of aquatic infectious illnesses since the early 20th century (Cutler & Miller 2005).

Since there is a great deal of variation in potable water demand across different locations, the potential for potable water savings must be assessed for each area to determine the technical viability of adopting RWHS. While some nations are experiencing a water crisis, rainwater gathering can help these nations manage their sustainable water resources. Using rainwater harvesting systems is advised as a sustainable development approach for managing water resources in light of population increase and fast urbanization (Kolavani 2020). Given how heavily potable water demand is influenced by geography, it is important to assess the potential for potable water savings before determining whether it is technically feasible to adopt RWHS. While some nations are experiencing a water crisis, rainwater gathering can help these nations manage their sustainable water resources. Using rainwater harvesting systems is advised as a sustainable development approach for managing water resources in light of population increase and fast urbanization (Kolavani 2020). Using the application of EPA SWMM5, a mathematical model, engineering, and management alternatives can be used for stormwater management (Harshani & Wijesekera 2010).

In Nigeria, there is a severe lack of water, particularly in metropolitan areas, where the water poverty index (WPI) measures the amount of time (in minutes) required to gather a specific amount of water (in liters) for home use each day (Adewumi et al. 2011). Activities aimed at reducing pollution and controlling flooding call for careful management of available water resources, engineering evaluation, cutting-edge technology, and suitable hydraulic structural designs (Oyebode & Paul 2023). For environmental sustainability, pollution reduction, and public health (Oyebode et al. 2023), groundwater monitoring and engineering intervention are required. According to Oyebode & Waterway (2023), the characterization and management of greywater are significant environmental challenges in the majority of countries.

Rapid urbanization is well documented to have several negative consequences on the hydrological cycle due to a decrease in previous land and a decline in stormwater run-off water quality. For managing urban stormwater, there are a variety of software tools available, such as the Storm Water Drainage System Design and Analysis Program (DRAINS), Urban Drainage and Sewer Model (MOUSE), InfoWorks River Simulation (InfoWork RS), Hydrological Simulation Program-Fortran (HSPF), Distributed Routing Rainfall-Runoff Model (DR3M), Storm Water Management Model (SWMM), XP Storm Water Management Model (XPSWMM), MIKE-SWMM, Quality-Quanty Simulators (QQS), Storage, Treatment, Overflow, Run-off Model (STORM), and Hydrologic Engineering Centre-Hydrologic Modelling System (HEC-HMS) (Haris et al. 2016).

Enhancing urban water cycle management can lower greenhouse gas emissions and help cities adapt to climate change. Due to the necessity to control increased surface flow, stormwater in metropolitan areas has traditionally been collected and sent to sewage treatment plants. Over time, Green Infrastructure (GI) methods have been recognized as a viable approach to stormwater management (Jayasooriya & Ng 2014). The chance to achieve environmental sustainability is through stormwater management. To protect the environment and public health, medical waste management strives to enhance health (Oyebode et al. 2023). The weighted average water quality index (WAWQI) method was used to calculate the research area's water quality index, and the USEPA method was used to evaluate any potential health risks (Ogarekpe et al. 2023).

Wet ponds, dry ponds, infiltration trenches, artificial wetlands, permeable pavements, and others are common stormwater treatment techniques. The focus should be placed on evaluating and maintaining stormwater treatment procedures (Erickson et al. 2013). Stormwater control measure inspection and maintenance procedures are frequently unclear and applied inconsistently. Stormwater management methods and green infrastructure are becoming more and more popular for controlling urban hydrology and stormwater as urbanized places throughout the world struggle with growth pains and evolving views on urban development. When calculating life-cycle costs, a stormwater management measure's purpose must be maintained and should not be disregarded (Erickson et al. 2018). Urban areas' continued expansion and the public's growing understanding of stormwater's effects on the environment have stoked interest

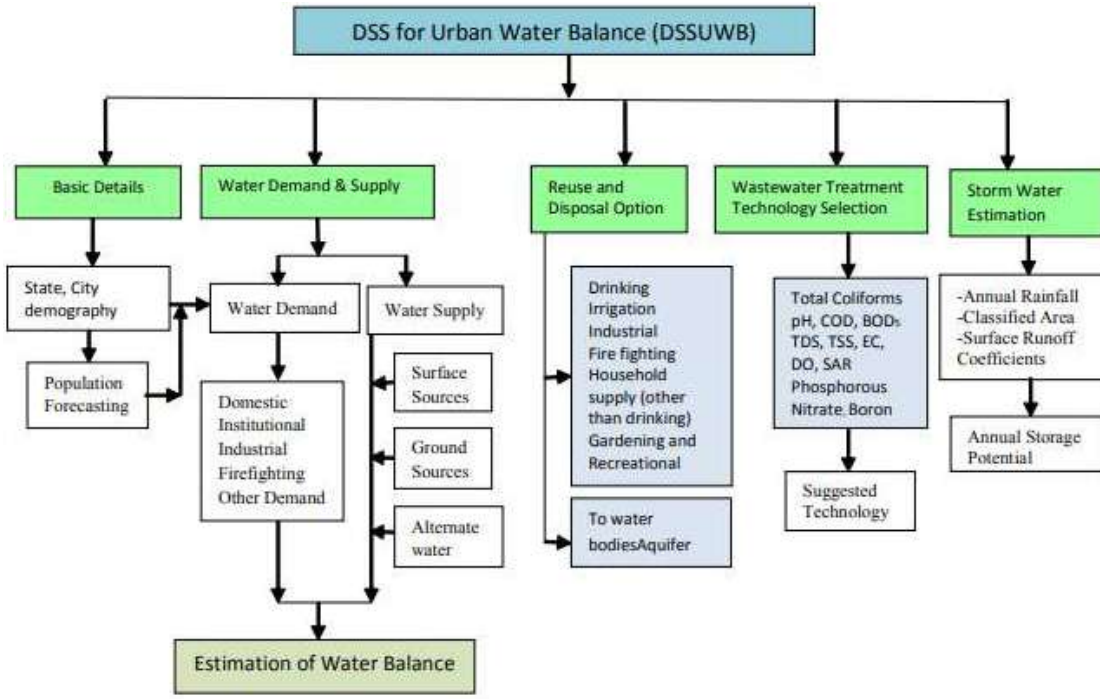

Source: (Maurya et al. 2018).

Fig. 1: Proposed framework for urban water balance.

in the receiving water bodies' quality. Several attempts have been made over the past two decades to improve urban drainage systems by using mitigation strategies to reduce the adverse effects of stormwater on the environment (Freni et al. 2010).

Many modules, including Basic Information, Water Demand and Supply, Reuse and Disposal Options, Wastewater Treatment Technology Selection, and Stormwater Management, make up the foundation for the proposed urban water balancing (Fig. 1).

Ecology has suffered as a result of the development brought on by rapid urbanization and industrialization. The quickly expanding industry discharged untreated effluent into the nearby bodies of water (Wanganeo et al. 2009). One of the best instruments for informing concerned consumers and decision-makers about water quality is the Water Quality Index. Water contamination is a significant economic and public health issue in addition to being an aesthetic one. The lake can be kept from degrading further by routinely monitoring the water quality. In many regions of the world, the depletion of freshwater resources has emerged as a significant issue of this century. Wastewater is increasingly posing a major challenge to the sustainability of urban environments in urban settings, in addition to the steadily rising demand for freshwater brought on by population growth and infrastructure development. This problem has an impact on both the environment and human health. Stormwater management is a common activity since it necessitates infrastructure for its execution. Calculating the yearly surface run-off is necessary for both centralized and decentralized collection schemes (Maurya et al. 2018).

According to the organization, natural disasters affected one-third of humanity throughout the twentieth century's last decade, with floods and droughts accounting for 86% of those affected. Drought is the leading cause of death because it frequently results in starvation. Because of the scarcity of drinkable water and the importance of water to human survival, individuals from all walks of life are scrambling to find a way out of this mess. River research has gradually increased in recent years due to the rising social awareness of the need to safeguard the environment of the water. This suggests that measuring water quality has a significant impact on human survival and growth. The potential of water to sequester carbon is directly influenced by its quality. Thus, it is crucial to comprehend the river water quality (Guojiao et al. 2023). Rural communities in developing countries face a slew of issues that wreak havoc on the quality of life there. One of these is the near-complete lack of public infrastructure and services, particularly drinkable water. In the year 2002, there were 1,099 million people without an appropriate water

supply, with 84 percent living in rural regions. The misrule and carelessness with which the government responds to emergencies are particularly shocking, given that water is a necessity and a critical life-sustaining element. As a result, the rural poor are at the mercy of the natural water cycle, which includes streams, ponds, rivers, and rain run-off from roofs. The poor's access to water through these sources is dependent on seasonal fluctuations, making it extremely difficult for them to obtain water during the dry season. People experiencing poverty are particularly affected by water-borne infections due to the unsanitary conditions of these sources of water.

Given the circumstances, the purpose of this work is to present a cost-effective and long-term management strategy for rain and run-off in rural areas and, by extension, metropolitan areas of developing Microbial diseases which are rampant in the poorest portions of most developing country cities, costing billions of dollars in wasted lives and sick employees, according to a recent World Bank report. When water sources are contaminated, and sanitation facilities are relatively low or non-existent, when rats, flies, and mosquitoes abound, typhoid, dysentery, and encephalitis are among the plagues of people experiencing poverty.

A stormwater treatment process is the method through which a stormwater treatment practice improves stormwater run-off quality, decreases run-off volume, decreases run-off peak flow, or any combination of the three. A dry pond, for example, collects stormwater and gently releases it to downstream receiving waters (in comparison to uncontrolled conditions). Because most contaminants in stormwater that are retained by a dry pond settle out while the stormwater run-off is held in the pond, sedimentation is the major treatment process of a dry pond. Because the treatment procedure is so crucial, this manual organizes stormwater treatment approaches by their major treatment phase. Table 1 indicates global diarrhoea disease and geo-helminthiases statistics for 1990. However, to comprehend stormwater processes, one must first investigate the composition of stormwater and the effects it has on the ecosystem.

Stormwater Treatment

A stormwater treatment method enhances the quality of stormwater run-off, lowers the volume of run-off, lowers the peak flow of run-off, or any combination of the three. Stormwater treatment techniques include source reduction, sand filters, infiltration basins and trenches, rain gardens, dry ponds, wet ponds, constructed wetlands, filter strips, swales, wet vaults, and subsurface sedimentation techniques. Stormwater treatment is the process of removing contaminants and poisons from surface water run-off before they enter a river, lake, or other body of water. Preventing pollution is usually preferable to treating it since it is challenging to get rid of it after it has gotten into the ecosystem. Even though no two stormwater projects are exactly alike, you must have confidence in your system and the experts that support it. (Erickson et al. 2013).

Since the 1970s, new stormwater development technologies such as detention and retention ponds, permeable surfaces, infiltration trenches, surface and subsurface groundwater recharge, and other source control measures have been created.

Constructed Wetlands

There are designed stormwater wetlands to reduce flood peaks, improve the water quality of surface run-off, and restore part of the city's natural habitat and birdlife, in addition to artificial wetlands (e.g., horizontal flow) for wastewater treatment. They can be used in conjunction with surface and subsurface groundwater recharge systems, as well as the treatment of soil aquifers. An illustration of this strategy is shown in (Fig. 2)

i. **Rainwater Harvesting**: Rainwater collecting is gaining popularity in urban areas because it delivers the dual benefits of preserving potable water and lowering stormwater run-off. When rainwater is collected and used to irrigate landscaped areas, the water is either evapotranspiration by vegetation or infused into the soil, helping to preserve the water balance that existed before development. Rain falling on a catchment surface, such as a roof, is collected and transported to a storage tank. This strategy is illustrated in (Fig. 3). The captured rainwater can be utilized for outside non-potable water purposes like irrigation and pressure washing or within the building to flush toilets and urinals with little pre-treatment (e.g., gravity filtration or first-flush

Table 1: Global diarrhoeal disease and geo-helminthiases statistics for 1990.

Disease	Number	Remarks
Diarrhea	4,073,920,110 cases	56% in children aged 0 to 4, 94% in developing countries
Ascariasis	61,847,000 persons with high-intensity infection	73% of children aged 5 to 14 all in developing countries
Trichuriasis	45,421,000 persons with high-intensity infection	79% of children aged 5 to 14 all in developing countries
Human hookworm infection	152,492,000 persons with high-intensity infection: 36.014,000 persons with anemia	72% of adults aged 15 to 44 all in developing countries

diversion). In rural areas, it is also a commonly utilized and effective strategy.

ii. **Green Roofs:** A thin layer of vegetation and growing medium is planted on top of a typical flat or sloped roof to create green roofs, also known as "living roofs" or "rooftop gardens." Green roofs are hailed as having numerous advantages for cities, including increased energy efficiency, reduced urban heat island effects, and the development of green space for passive recreation or aesthetic delight. For example, treated greywater can be used to irrigate green roofs or vertical gardens. They appeal to a water resources manager because of the benefits they provide in terms of water quality, water balance, and peak flow control. The green roof functions like a lawn or meadow in terms of hydrology, holding rainwater in the growth media and ponding regions.

iii. **Constructed Wetlands:** There are designed stormwater wetlands to reduce flood peaks, improve the water quality of surface run-off, and restore part of the city's natural habitat and birdlife, in addition to artificial wetlands (e.g., horizontal flow) for wastewater treatment (Oyebode et al. 2023). They can be used in conjunction with surface

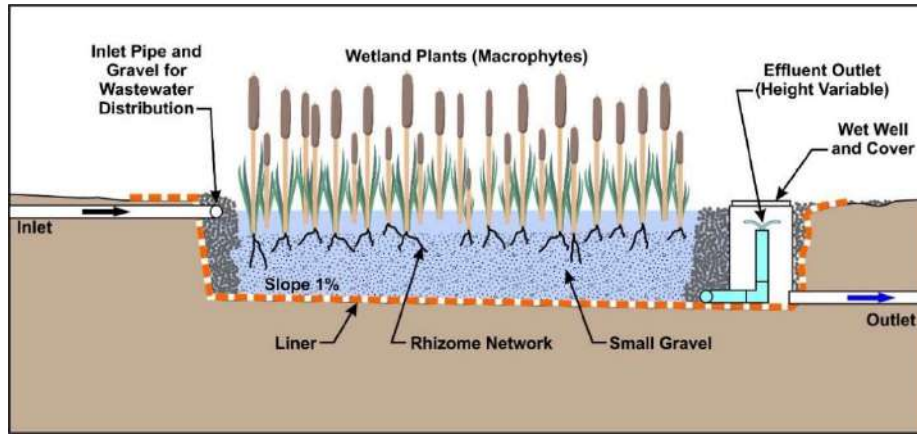

Fig. 2: Constructed wetland.

Fig. 3: Rainfall harvesting (William et al. 2023).

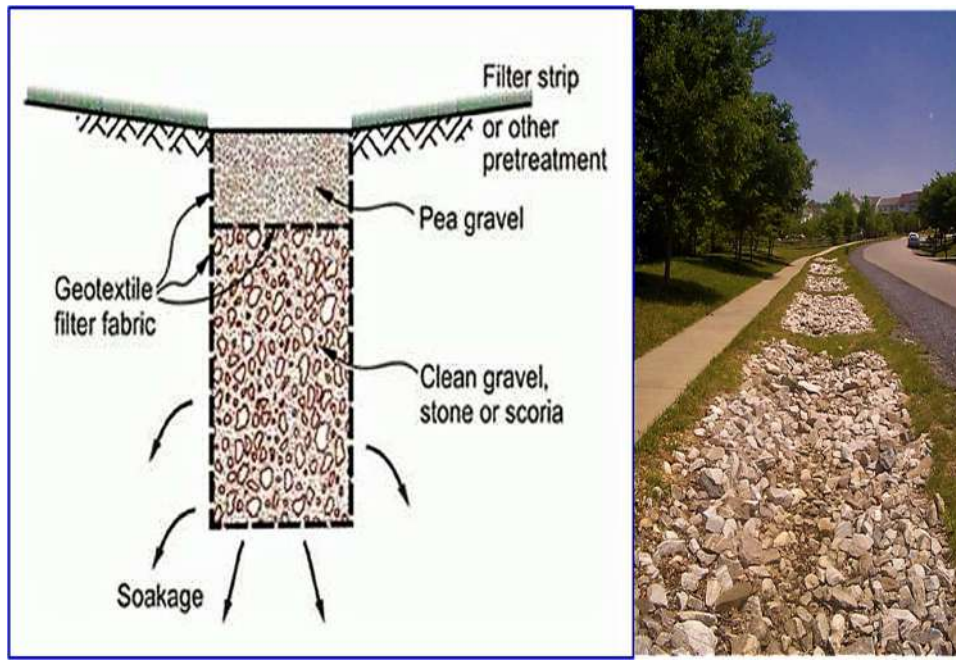

Fig. 4: Design of infiltration trenches.

and subsurface groundwater recharge systems, as well as the treatment of soil aquifers.

Infiltration Type Devices

1. **Infiltration Trenches:** Infiltration trenches (also known as soak pits) are shallow excavations filled with uniformly crushed stone to create underground reservoirs for rainwater run-off. The discharge gradually seeps into the subsoil and eventually into the water table through the trench's bottom. To prevent sediment entry, the walls and top are coated with geotextile. Trench designs can be altered to contain vegetation and other elements, forming a bio-filtration zone. They are frequently built alongside outdoor parking spaces or streets. Infiltration into the soil is used to treat the water. A design of this method is shown in (Fig. 4). However, where sediment concentration in run-off is high, there is a risk of clogging.
2. **Grass Filter Stripes:** Grass filter stripes (also known as grassed filters or filter stripes) are densely vegetated, evenly graded areas that treat surface flow from nearby impermeable areas. Grass filter strips lower run-off speeds, trap silt and other pollutants and provide a small amount of infiltration.
3. **Grassed Swales:** Open grassed channels in which stormwater flow is slowed and partially penetrated are known as grass swales (also known as vegetated swales). Water in the swale is slowed by check dams and vegetation, which allows sedimentation, filtering via the root zone and soil matrix, evapotranspiration, and infiltration into the underlying native soil. An example of this method is shown in (Fig. 5). For stormwater conveyance, simple grass channels or ditches have traditionally been employed, particularly for roadway drainage. Simple grass channel and roadside ditch design that utilize design characteristics such as improved geometry and check dams increase the pollutant removal and run-off reduction functions of enhanced grass swales.
4. **Pervious Pavements:** A permeable pavement surface with a stone reservoir beneath it is known as pervious pavement. The reservoir briefly collects surface run-off before infiltrating it into the subsoil or subsurface drainage, improving water quality in the process. Porous materials, such as ancient lime mortars and pervious pavements, are created from materials that are generally mono-graded. This correlates to a lack of "fine" components in the case of previous pavement. Pervious pavement is also known as "no-fines concrete" in some cases, and it is illustrated in (Fig. 6).
5. **Infiltration basin:** An infiltration basin (also known as an infiltration pond) is a structure built within highly permeable soils to store stormwater run-off temporarily (see also surface groundwater recharge).

Fig. 5: Enhanced grass swales feature check dams that temporarily pond run-off to increase pollutant retention and infiltration and decrease flow velocity.

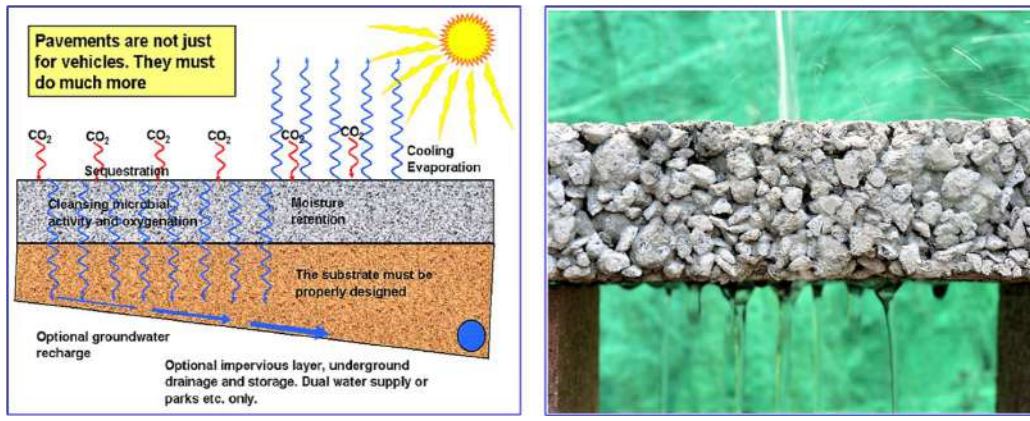

Fig. 6: A theoretical cross-section of porous pavement (left) and porous pavement during a demonstration.

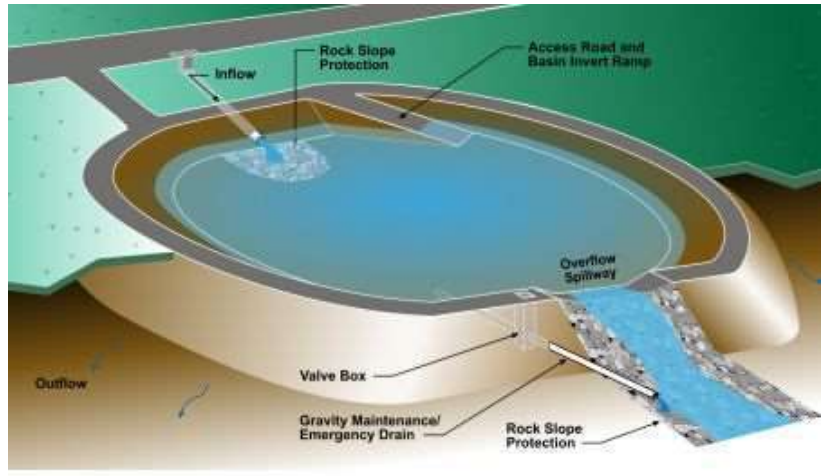

Fig. 7: Infiltration basin.

An example of an infiltration basin is shown in (Fig. 7). Infiltration basins, unlike detention basins, do not often have a structural outlet to release run-off from the stormwater quality design storm. Instead, an infiltration basin's outflow is routed into the surrounding soil. An infiltration basin and an extended detention basin can be coupled to provide additional run-off storage for stormwater quality and quantity management. The TSS clearance rate for infiltration basins has been set at 80%(Oyebode et al. 2023).

Costs to Consider

The costs of various systems are highly dependent on technology, topography, and specialist knowledge. Some are simple to implement, while others are more complicated and cost more. Stormwater management, on the other hand, prevents infrastructure damage and protects the people of urban and rural populations.

Health Aspects

Modern stormwater methods primarily include some ecological treatment effects, with the overall goal of protecting the public's health, welfare, and safety (by preventing water pollution) and property from flood dangers (by securely routing and discharging stormwater from developments)

Urban solid trash can be a hazard to public health as well as the proper operation of stormwater facilities. Domestic sewer connections to stormwater drainage systems, both legal and illegal, result in ancillaries such as retention basins becoming pollutant traps. These are washed out during high floods, resulting in water pollution.

High loads of fine particles can also clog infiltration systems, resulting in permanent ponding. This can lead to mosquito breeding, which is a significant issue in humid locations where malaria and other tropical diseases are prevalent.

Advantages of Stormwater Management

- The surface run-off will be properly drained.
- The ability to recharge groundwater and reuse precipitation and surface run-off for irrigation and household purposes
- Stormwater treatment would begin as soon as possible.
- Damage to infrastructures is avoided; flood prevention is achieved.
- Green and recreational places can be integrated into the urban landscape.

Disadvantages of Stormwater Management

- Expertise is necessary for planning, implementation, operation, and maintenance.
- Depending on the approach, a significant amount of work and effort is necessary.
- High sedimentation rates provide a risk of blocking the infiltration system.

MATERIALS AND METHODS

The method of approach taken for this project is to manage stormwater run-off by harvesting the rainfall using a detention tank (the collection point) to collect stormwater run-off from roofs of various buildings, filtering (using memory foam), and disinfecting the collected stormwater with the use of alum and chlorine as a means to kill all impure particles and bacteria in the water.

Processes

1. **Pre-analysis of influent run-off**: tests are carried out on the stormwater to determine the total suspended solids (TSS), total dissolved solids (TDS), and coliform present before proceeding with the filtration processes.
2. **The collection tank**: based on my analysis, stormwater run-off is channeled with the use of roof gutters from roofs after rainfall into the detention tank. The stormwater passes through a net at the top of the detention tank to remove impurities (like leaves, twigs, sticks, sand, and tree branches) and prevent them from entering the tank.
3. **The polyurethane foam**: the foam is located inside the detention tank, and the stormwater passes through the foam to filter out impurities and suspended solids before transferring to another tank for flocculation.
4. **Flocculation**: adding a certain amount of alum (potassium alum) to the volume of stormwater present for 30 min in the flocculation tank to clarify the water gathers tiny impurities (not visible) and turn them into flocs and make them settle at the bottom of the tank before transferring to another tank for chlorination. Alum dosages range from 5 mg per liter for generally clear water to 85 mg per liter for severely turbid waterways such as industrial effluent (Antoniraj et al. 2022). Potassium alum has a chemical formula of $K_2SO_4.Al_2(SO_4)_3 \cdot 24H_2O$.
5. **Chlorination**: the chlorine solution will be added to this final tank containing the stormwater to disinfect the water volume from various forms of bacteria and

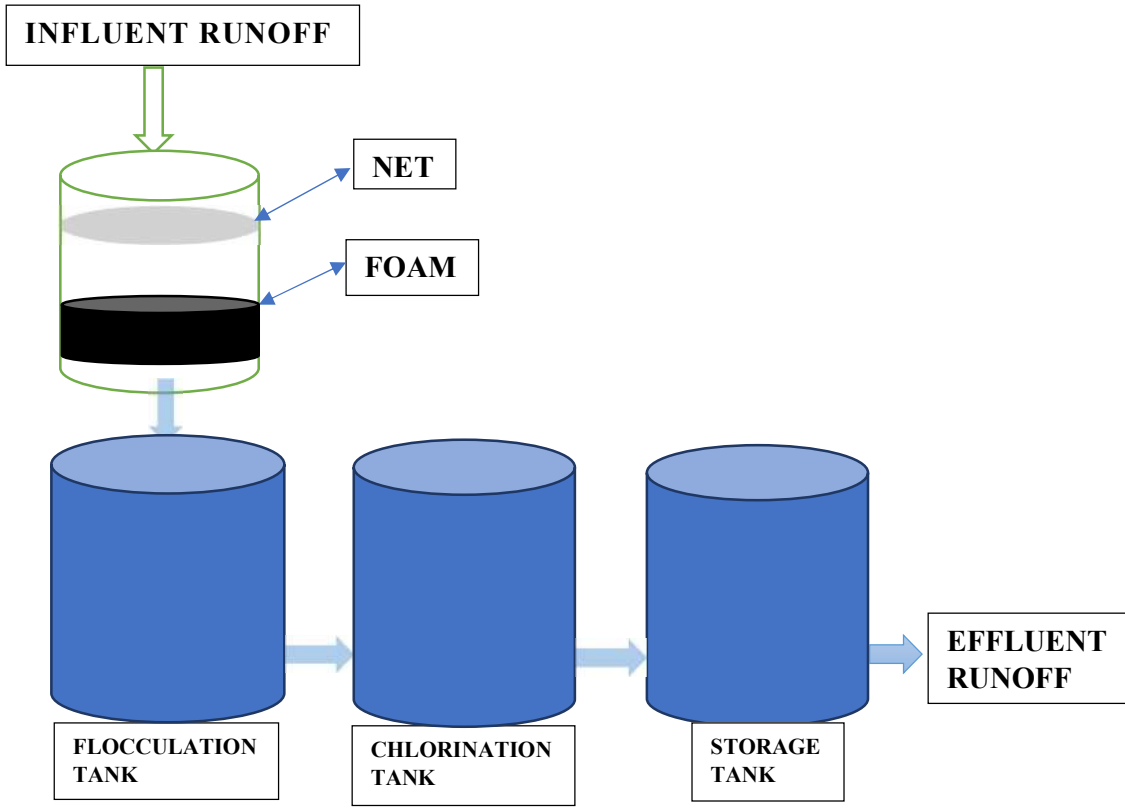

Fig. 8: Diagram of the stormwater treatment process.

germs, rendering it safe for usage. Chlorine levels in drinking water up to 4 milligrams per liter (mg.L^{-1} or 4 parts per million (ppm)) are deemed safe. Harmful health consequences are unlikely to occur at this level. For the chlorination tank, preparation of 0.5% chlorine solution: Grams/liter = [% dilute/% concentrate] × 1000.

6. **Post analysis of effluent run-off**: tests are carried out on the stormwater after the processes to determine the changes and improvement of the TSS and TDS before it can be rendered safe for distribution.
7. **Distribution**: after all the processes, the water is stored in the storage tank and can now be distributed for usage in various forms in the community at large. Fig. 8 presents details of this.

Apparatus

i. **Stormwater collection tank**: the volume of the tank used for the collection of influent stormwater run-off for this experiment is 18.9 liters.

ii. **Net**: a net with a mesh size of 1.2 mm (0.047 in) is used as the first stage of filtration to remove debris from the stormwater run-off.

iii. **Foam**: a polyurethane foam sheet is used as the second stage of filtration to remove smaller debris that may have escaped the net from the stormwater run-off.

Fig. 9, Fig. 10, and Fig. 11 present polyurethane foam, potash alum, and sodium hypochlorite, while Fig. 12 presents the model of the stormwater treatment system.

iv. **Flocculation tank**: after the run-off passes through the filters to the flocculation tank, alum is added to bring the colloidal particles out of suspension to sediment under the form of floc or flake.

v. **Chlorination tank**: after flocculation, the run-off is then released into the chlorination tank, where chlorine is added to disinfect the stormwater run-off and render it safe for usage in various forms.

vi. **Storage tank**: after all the processes have taken place, the water is stored in this tank to manage the distribution.

Relevance of the Method

After the process of filtration and treatment of stormwater run-off using this method, the effluent water can be used for:

i. Watering your garden.

Fig. 9: Polyurethane foam.

Fig. 10: Potash alum.

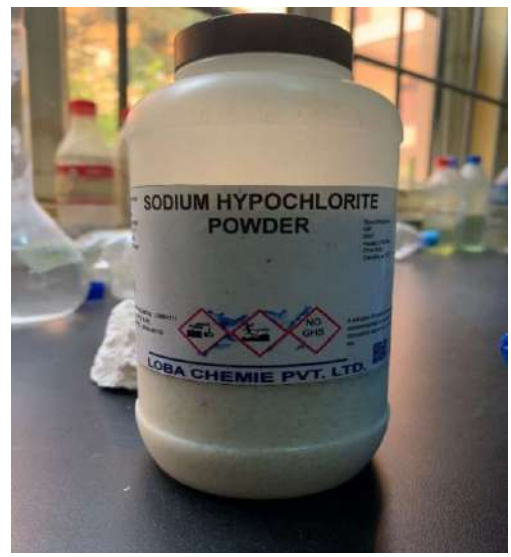

Fig. 11: Sodium hypochlorite.

Fig. 12: Model of the stormwater treatment system.

ii. Toilet flushing.

iii. Adding water to your swimming pool without using the mains water.

iv. Car and driveway cleaning.

v. Clothes cleaning.

Catchment Capacity

After calculating the catchment area of the roof and the annual rainfall, the estimated catchment capacity of that specific roof can be calculated using the following formulas:

Monthly Roof Catchment Capacity = Monthly rainfall (in millimeters) × Roof surface area (in square meters).

Annual Roof Catchment Capacity = Annual rainfall (in millimeters) × Roof surface area (in square meters).

RESULTS AND DISCUSSION

The average values of the physicochemical parameters obtained from the stormwater run-off after passing through the filtration and treatment process of the fabricated model of stormwater treatment used for this project. The use of potash alum has caused several modifications in the water quality. TDS is lowered to 635 $mg.L^{-1}$ from 697 $mg.L^{-1}$. Since then, the DO has dropped from 5.87 $mg.L^{-1}$ to 3.92 $mg.L^{-1}$. Additionally, the turbidity and salinity both increased from 4.42 FNU to 4.58 FNU and from 0.7 PSU to 1.44 PSU, respectively. From 8.35 to 6.51, 2.55 to 1.9 $mg.L^{-1}$, and 19.78 $mg.L^{-1}$ to 15.17 $mg.L^{-1}$, respectively, the pH, BOD, and COD were all reduced. It was discovered that the calcium hardness has decreased from 287 $mg.L^{-1}$ to 265.83 $mg.L^{-1}$. As the conductivity rises from 3.24 $ms.cm^{-1}$ to 3.82 $ms.cm^{-1}$, it does so slightly. From 0.143 $mg.L^{-1}$ to 0.055 $mg.L^{-1}$ and from 0.092 $mg.L^{-1}$ to 0.045 $mg.L^{-1}$, respectively, the Fe^{2+} and Zn^{2+} ions show a small drop.

The usage of potash alum and chlorine might have several negative health consequences, such as:

i. Digestive issues because the acidity increase can cause several digestion difficulties.

ii. Inhalation: If fine particles are breathed in while it is dissolved in water, it may irritate the respiratory system.

iii. Contact with the skin and eyes might irritate, including redness, itching, and discomfort.

The correct use of alum, according to the WHO and the Water Sanitation and Health (WSH), needs competence. As a result, a standard value for the application of potash alum for ordinary people is required, particularly in Nigeria, where there is a problem with inadequate stormwater management.

Pre-Analysis of Stormwater Run-Off

Table 2 presents various tests that were carried out on stormwater samples (Before treatment), while Table 3 presents the monthly average rainfall in Abuja. Fig. 13 presents information on annual rainfall.

Table 2: Combined Results compared to recommended standards.

TEST	Unit	Value 1	Value 2	Value 3	Average value
Total Dissolved Solids (TDS)	$mg.L^{-1}$	697	701	693	697
Dissolved Oxygen (DO)	$mg.L^{-1}$	5.76	5.84	6.02	5.873333333
Salinity	PSU	0.7	0.7	0.7	0.7
Turbidity	FNU	4.95	4.24	4.08	4.423333333
pH	-	8.3	8.36	8.4	8.353333333
Biochemical Oxygen Demand (BOD)	$mg.L^{-1}$	2.7	2.35	2.6	2.55
Chemical Oxygen Demand (COD)	$mg.L^{-1}$	20.35	20.5	18.5	19.78333333
Calcium Hardness	$mg.L^{-1}$	288	280	293	287
Conductivity	$ms.cm^{-1}$	3.12	3.31	3.29	3.24
Fe^{2+}	$mg.L^{-1}$	0.145	0.1	0.185	0.143333333
Zn^{2+}	$mg.L^{-1}$	0.065	0.105	0.105	0.091666667

Calculations and Estimates

Table 3: Monthly average rainfall in Abuja.

Months	Rainfall 1 (mm) source:(Climate-data.org, 2020)	Rainfall 2 (mm)source:(Spark, 2019)	Average Monthly Rainfall(mm)
January	2	0	1
February	6	2.5	4.25
March	20	17.5	18.75
April	57	75	66
May	138	132.5	135.25
June	205	160	182.5
July	269	207.5	238.25
August	326	245	285.5
September	290	225	257.5
October	144	105	124.5
November	11	10	10.5
December	1	0	0.5

Total Annual Rainfall = $\sum$(Average monthly rainfall) = 1,324.5mm.

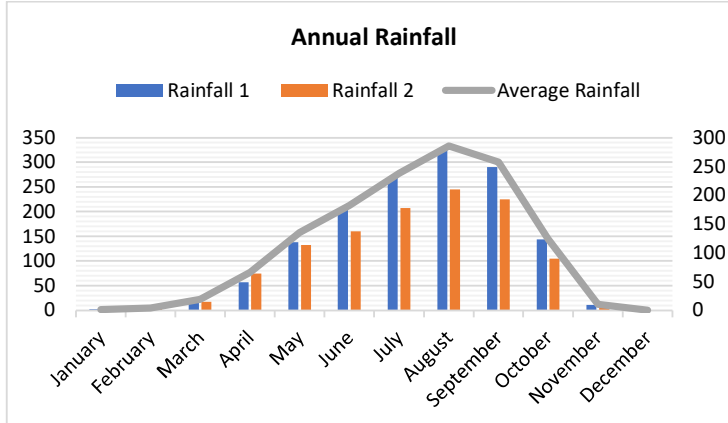

Fig. 13: Annual rainfall.

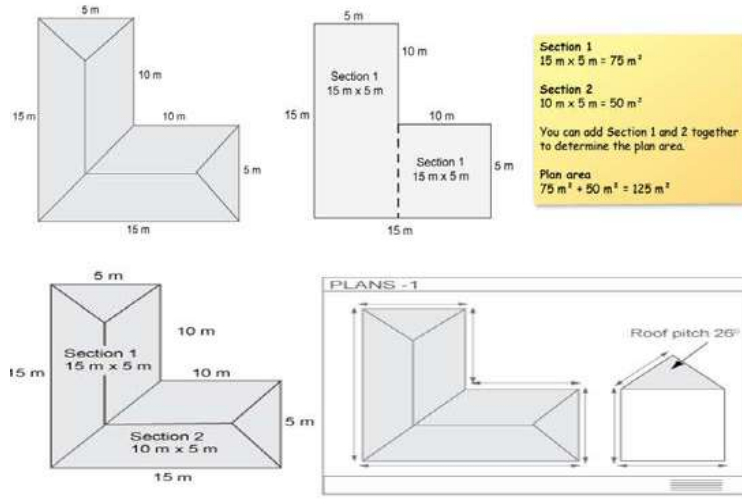

Fig. 14: The pitch roof details.

Table 4: Catchment area slope factor (F).

Roof slope degrees	Factor for the increased surface area of the roof (F)	Roof slope degrees	Factor for the increased surface area of the roof (F)	Roof slope degrees	Factor for the increased surface area of the roof (F)
0	1.00	22	1.20	44	1.48
1	1.01	23	1.21	45	1.50
2	1.02	24	1.22	46	1.52
3	1.03	25	1.23	47	1.54
4	1.03	26	1.24	48	1.56
5	1.04	27	1.25	49	1.58
6	1.05	28	1.27	50	1.60
7	1.06	29	1.28	51	1.62
8	1.07	30	1.29	52	1.64
9	1.08	31	1.30	53	1.66
10	1.09	32	1.31	54	1.69
11	1.10	33	1.32	55	1.71
12	1.11	34	1.34	56	1.74
13	1.12	35	1.35	57	1.77
14	1.12	36	1.36	58	1.80
15	1.13	37	1.38	59	1.83
16	1.14	38	1.39	60	1.87
17	1.15	39	1.40	61	1.90
18	1.16	40	1.42	62	1.94
19	1.17	41	1.43	63	1.98
20	1.18	42	1.45	64	2.03
21	1.19	43	1.47	65	2.07

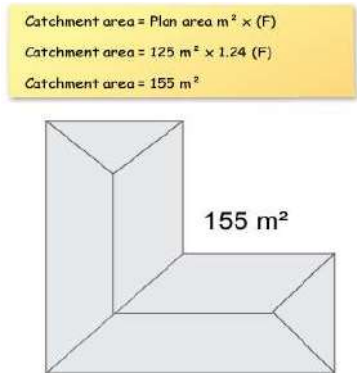

Fig. 15: Catchment area (Plumb 2010).

Catchment Area

For example, to determine the catchment area of stormwater for a roof drainage system of a house with an eaves gutter (Fig. 14):

We first divide the roof into simple shapes and determine its area by multiplying the length of the roof by the breadth of the roof will give you the catchment area of a building with a flat roof. When calculating the catchment area of a roof with a pitched roof, remember to factor in the pitch of the roof. The roof pitch is usually indicated on the plan by the architect. The pitch of this building's roof is 26°. The 'Catchment area – Slope factor (For eaves gutter alone) table (Table. 4) from AS/NZS 3500.3.2003 will be needed to determine the slope factor (F).

The roof, in this case, has a pitch of 26°. Therefore, the slope factor (F) is 1.24. By multiplying the plan area by the slope factor (F), you can now calculate the catchment area (Fig. 15).

Fig. 16 presents a typical Sustainable Urban Drainage Systems (SUDS) Decision Making. Also, Fig. 17 presented a map of Abuja Central Area and six area councils in Abuja.

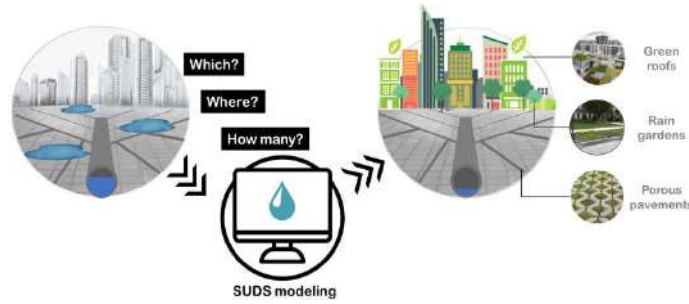

Source: (Ferrans et al. 2022).

Fig. 16: Sustainable Urban Drainage Systems (SUDS) decision making.

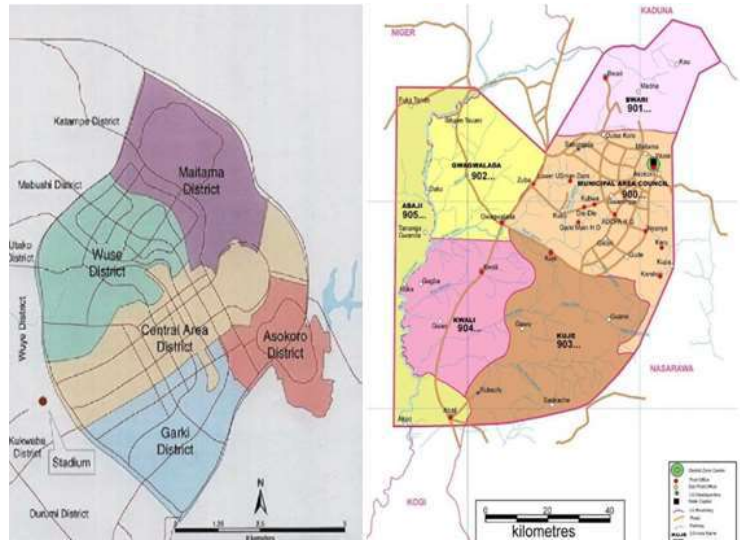

Source: (Afolabi & Raimi 2021).

Fig. 17: Map of Abuja Central Area and area Councils in Abuja, Nigeria.

Table 5: Monthly roof catchment capacity.

Months	Rainfall	Catchment	Monthly Roof Catchment Capacity (Liters)
January	1	155	155
February	4.25	155	658.75
March	18.75	155	2906.25
April	66	155	10230
May	135.25	155	20963.75
June	182.5	155	28287.5
July	238.25	155	36928.75
August	285.5	155	44252.5
September	257.5	155	39912.5
October	124.5	155	19297.5
November	10.5	155	1627.5
December	0.5	155	77.5

Table 6: Various Tests were carried out on Stormwater samples (After treatment).

Test	Unit	Value 1	Value 2	Value 3	Average Value
Total Dissolved solids (TDS)	$mg.L^{-1}$	654	620	632	635.3333333
Dissolved Oxygen (DO)	$mg.L^{-1}$	3.67	4.12	3.96	3.916666667
Salinity	PSU	1.26	1.56	1.51	1.443333333
Turbidity	FNU	4.51	4.57	4.66	4.58
pH	-	6.43	6.31	6.79	6.51
Biochemical Oxygen Demand (BOD)	$mg.L^{-1}$	1.9	1.75	2.05	1.9
Chemical Oxygen Demand (COD)	$mg.L^{-1}$	20.5	12	13	15.16666667
Calcium Hardness	$mg.L^{-1}$	268	263	266.5	265.8333333
Conductivity	$ms.cm^{-1}$	3.2	4.06	4.21	3.823333333
Fe^{2+}	$mg.L^{-1}$	0.055	0.065	0.045	0.055
Zn^{2+}	$mg.L^{-1}$	0.045	0.045	0.046	0.045333333

Table 7: Results compared to recommended standards.

Test	Units	Before Treatment Value	After Treatment Value	Recommended raw water criteria set by WHO
TDS	$mg.L^{-1}$	697	635.3	600 - 900
DO	$mg.L^{-1}$	5.87	3.92	6.5 - 8.0
Salinity	PSU	0.7	1.44	30 - 37
Turbidity	FNU	4.42	4.58	1.0 - 5.0
pH	~	8.35	6.51	6.5 - 8.5
BOD	$mg.L^{-1}$	2.55	1.9	<5.0
COD	$mg.L^{-1}$	19.78	15.17	<120
Calcium Hardness	$mg.L^{-1}$	287	265.83	0 - 150
Conductivity	$ms.cm^{-1}$	3.24	3.82	<0.4
Fe^{2+}	$mg.L^{-1}$	0.143	0.055	<0.3
Zn^{2+}	$mg.L^{-1}$	0.092	0.045	<5.0

Catchment Capacity

After calculating the catchment area of the roof and the annual rainfall, the estimated catchment capacity of that specific roof can be calculated using the following formulas:

Monthly Roof Catchment Capacity = Monthly rainfall (in millimeters) × Roof surface area (in square meters).

Annual Roof Catchment Capacity = Annual rainfall (in millimeters) × Roof surface area (in square meters).

Note: Roughly speaking, 1 millimeter of rain over 1 square meter of roof equals 1 liter of water. If the catchment area is 155 m^2, the monthly roof catchment capacity is as indicated in Table 5.

This is the amount of water that can be saved and reused by stormwater harvesting for every month of the year.

Therefore, if the Total Annual Rainfall = 1,324.5 mm while the catchment area is 155 m^2.

The Annual Roof Catchment Capacity = 1,324.5mm × 155m^2 = 205,297.5 liters. This is the amount of water that can be saved and reused over a year by stormwater harvesting.

Post-Analysis of Stormwater Run-Off

Table 6 presents various tests that were carried out on Stormwater samples (After treatment), while Table 7. Results compared to recommended standards.

Combined Results

The correct use of alum, according to the WHO and the Water Sanitation and Hygiene (WASH), needs competence. As a result, a standard value for the application of potash alum for ordinary people is required, particularly in Nigeria, where there is a problem with inadequate stormwater management.

CONCLUSIONS

For a clean environment and to reduce pollution, communities' urban stormwater management and treatment infrastructure must be designed and modeled. The typical values of the physicochemical parameters obtained from the stormwater run-off after it has been filtered and treated by the constructed stormwater treatment model utilized for this study. The water quality has changed in several ways as a result of the usage of potash alum. TDS is now 635 $mg.L^{-1}$ instead of 697 $mg.L^{-1}$. The DO was 5.87 $mg.L^{-1}$ and is now 3.92 $mg.L^{-1}$.

Moreover, the turbidity and salinity both increased from 4.42 FNU to 4.58 FNU and from 0.7 PSU to 1.44 PSU, respectively. BOD, COD, and pH all decrease from 8.35 to 6.51, 2.55 to 1.9, and 19.78 to 15.17 $mg.L^{-1}$, respectively. There is a decrease in calcium hardness, from 287 $mg.L^{-1}$ to 265.83 $mg.L^{-1}$.

As the conductivity rises from 3.24 $ms.cm^{-1}$ to 3.82 $ms.cm^{-1}$, it does so slightly. From 0.143 $mg.L^{-1}$ to 0.055 $mg.L^{-1}$ and from 0.092 $mg.L^{-1}$ to 0.045 $mg.L^{-1}$, respectively, the Fe2+ and Zn2+ ions show a small drop. Ecosystems become unstable as a result of nutrients and organic materials, and this can lead to biological disasters like algal blooms. To make sure that the stormwater treatment methods are running flawlessly and fulfilling their intended purposes, they should be frequently inspected and maintained. Inadequate equipment maintenance could lead to a decrease in the effectiveness of pollution removal or even an increase in pollutant loadings, worsening the effects down the line. According to the results of the above small-scale constructed model's effective treatment of the stormwater sample, the sample satisfies the WHO's suggested standards for raw water in terms of TDS, pH, turbidity, BOD, and COD. Since effluent water is primarily used for non-potable applications like car washing, gardening, toilet flushing, and laundry, these uses are considered safe. Stormwater management provides a means for achieving environmental sustainability. The use of green infrastructure techniques is now acknowledged as a successful stormwater management strategy. The Storm Water Drainage System Design and Analysis Program (DRAINS), the Urban Drainage and Sewer Model (MOUSE), InfoWorks River Simulation (InfoWork RS), the Hydrological Simulation Program-Fortran (HSPF), and many other software tools can be used to manage urban stormwater. It is legitimate to state that after treatment, rainwater can be used as raw water. One of the most difficult things is to get a reliable figure on water needs because it depends the availability, cost and the location. Rainwater harvesting is a decentralized and environmentally solution that can avert many environmental problems associated with centralized, conventional and large project approaches. To reach the highest level of sustainability, all stakeholders should be involved in the planning and implementation rainwater harvesting systems. The effectiveness of this method and data on water quality must be periodically monitored and updated for adequate pollution abatement and environmental sustainability.

RECOMMENDATIONS

Recommendations are the following:

More research and Water quality management are essential for ensuring that water resources and stormwater are safe and healthy for human consumption and other uses.

i. More research and water quality management are

essential for ensuring that water resources and stormwater are safe and healthy for human consumption and other uses.

ii. To ensure that the stormwater treatment methods are working properly and are in excellent operating condition, they should be frequently inspected and maintained. Inadequate equipment maintenance could lead to a decrease in the effectiveness of pollution removal or even an increase in pollutant loadings, worsening the effects down the line.

iii. Capacity building and community participation are essential for ensuring that stakeholders have the knowledge, skills, and tools necessary to manage water resources sustainably.

iv. The need for operating and maintaining the tanks should be made clearer to house owners. There is a need to verify that PVC or another corrosion-resistant material, such as the gutter, downpipe, and tank, are used. Add a gutter trap or a net to prevent leaves and branches from falling into the tank.

v. The rainwater tank should be tightly covered for safety reasons as well as to keep dust, run-off, and insects out of the tank.

vi. Since the initial cost of building a tank is the main barrier to adoption, a loan program or subsidy for homeowners to meet this cost should be implemented.

vii. In dry zone districts where the groundwater is both mineralized and polluted, drinking rainwater after proper treatment should be encouraged. It is believed that the high calcium and mineral content in the dry zone regions is to blame for the rising occurrence of renal illnesses.

viii. The generally great quality of rainwater should be made known to enable more people to consume it and use it for other varied communal reasons.

REFERENCES

Adewumi, I.K., Oyebode, O.J., Igbokwe, K.C. and Aluko, O.G. 2011. Water Footprints in Four Selected Breweries in Nigeria. In Finkbeiner, M. (ed), Towards Life Cycle Sustainability Management, Springer, Dordrecht, Netherlands, pp. 171-181.

Afolabi, A.S. and Raimi, M.O. 2021. When water turns deadly: Investigating source identification and quality of drinking water in Piwoyi Community of Federal Capital Territory, Abuja Nigeria.

Antoniraj, M.G., Dhayanandamoorthy, Y., Kumar., M., Kandasamy, R., Balan, D.J. and Devi, K.P. 2022. Design and evaluation of redox responsive disulfide containing resveratrol loaded nanocarrier anti-cancer activity in the MDA-MB-231 cell line. Mater. Today Commun., 32: 103873.

Atlantis, E., Chow, C.M., Kirby, A. and Singh, M.F. 2004. An effective exercise-based intervention for improving mental health and quality of life measures: A randomized controlled trial. Prevent. Med., 39(2): 424-434.

Borgaonkar, A.D. and Marhaba, T.F. 2021. Evaluation of Sustainability Strategies: A Water Quantity and Quality Perspective. In Ahuja, S. (ed), Handbook of Water Purity and Quality, Elsevier, The Netherlands, pp. 409-454.

Cutler, D. and Miller, G. 2005. The role of public health improvements in health advances: The twentieth-century United States. Demography, 42(1): 1-22.

Erickson, A.J., Taguchi, V.J. and Gulliver, J.S. 2018. The challenge of maintaining stormwater control measures: A synthesis of recent research and practitioner experience. Sustainability, 10(10): 3666.

Erickson, A.J., Weiss: T., Gulliver, J.S., Erickson, A.J., Weiss: T. and Gulliver, J.S. 2013. Stormwater Treatment Practices. In Erickson, A.J., Weiss, P.T. and Gulliver, J. (eds), Optimizing Stormwater Treatment Practices: A Handbook of Assessment and Maintenance, Springer, Cham, pp.35-51.

Ferrans, M., Torres, M.N., Temprano, J. and Sánchez, J.P.R. 2022. Sustainable urban drainage system (SUDS) modeling supporting decision-making: A systematic quantitative review. Sci. Total Environ., 806: 150447.

Freni, G., Mannina, G. and Viviani, G. 2010. Urban stormwater quality management: centralized versus source control. J. Water Resour. Plan. Manag., 136(2): 268-278.

Guojiao, L., Baohui, M. and Lehao, W. 2023. Water quality assessment of Wenyu River with variable weight cloud model. Nat. Environ. Pollut. Technol., 22(1): 16-36.

Haris, H., Chow, M.F., Usman, F., Sidek, L.M., Roseli, Z.A. and Norlida, M.D. 2016. Urban stormwater management model and tools for designing stormwater management of green infrastructure practices. IOP Conf. Ser. Earth Environ. Sci., 32(1): 012022.

Harshani, H.M.D. and Wijesekera, N.T.S. 2010. Application of stormwater management modeling for ungauged watersheds in urban areas: A case study of the Matara municipal council area.

Jayasooriya, V. M. and Ng, A.W.M. 2014. Tools for modeling of stormwater management and economics of green infrastructure practices: A review. Water, Air, and Soil Pollution, 225: 1-20.

Kolavani, N.J. 2020. Technical feasibility analysis of rainwater harvesting system implementation for domestic use. Sustain. Cities Soc., 62: 102340.

Lewis, A., McKeon, T.P., De Roos, A.J., Ravel, J., Elovitz, M.A. and Burris, H.H. 2021. Associations of public water system trihalomethane exposure during pregnancy with spontaneous preterm birth and the cervicovaginal microbial-immune state. Environ. Res., 199: 111288.

Maurya, S.P., Ohri, A. and Singh, K. 2018. Evaluation of urban water balance using decision support system of Varanasi City, India. Nat. Environ. Pollut. Technol., 17(4): 1219-1225.

Ogarekpe, N.M., Nnaji, C.C., Oyebode, O.J., Ekpenyong, M.G., Ofem, O.I., Tenebe, I.T. and Asitok, A.D. 2023. Groundwater quality index and potential human health risk assessment of heavy metals in water: A case study of Calabar metropolis, Nigeria. Environ. Nanotechnol. Monit. Manag., 19: 100780.

Oyebode, O.J. and Paul, F. 2023. Flood mitigation and pollution abatement in Kaduna metropolis through engineering assessment and analytical hierarchy process design. Nat. Environ. Pollut. Technol., 22(2): 641.

Oyebode, O.J., Okpala, C.C., Ajibade, S.M., Ogarekpe, N.M., Afolalu, S.A., Coker, A.O. and Adeniyi, A.T. 2023. Comparative assessment of medical waste management in multi-system and selected teaching hospitals in Ekiti State, Nigeria. Nat. Environ. Pollut. Technol., 22(2): 653-669.

Wanganeo, A., Shanker, A., Saha, T. and Ghosh, W. 2009. Physico-chemical characteristics of stormwater flow canal under the influence of tides. Nat. Environ. Pollut. Technol., 15(2): 141-128.

William, P., Oyebode, O. J., Ramu, G., Lakhanpal, S., Gupta, K. K. and Al-Jawahry, H. M. 2023. Framework for IoT Based Real-Time Monitoring System of Rainfall Water Level for Flood Prediction Using LSTM Network. In 2023 3rd International Conference on Pervasive Computing and Social Networking (ICPCSN) (pp. 1326-1321). IEEE.

ORCID DETAILS OF THE AUTHORS

O. J. Oyebode: https://orcid.org/0000-0003-2792-146X

Nature Environment and Pollution Technology
An International Quarterly Scientific Journal

p-ISSN: 0972-6268
(Print copies up to 2016)
e-ISSN: 2395-3454

Vol. 23 | No. 1 | pp. 87-97 | 2024

Original Research Paper

https://doi.org/10.46488/NEPT.2024.v23i01.006

Open Access Journal

Research Progress on in-situ Remediation of Typical Heavy Metals in Petroleum Hydrocarbon-contaminated Soil Enrichment by Plants

B. Yang*(**)†, Q. H. Xue*(**), C. T. Qu*(**), C. Lu*(**), F. F. Liu*(**), H. Zhang*, L. T. Ma*(**), L. Qi** and Y. T. Wang***

*Shaanxi Key Laboratory of Environmental Pollution Control Technology and Reservoir Protection for Oil and Gas Fields, Xi 'an Shiyou University, Xi 'an 710065, PR China
**School of Chemistry and Chemical Engineering, Xi 'an Shiyou University, Xi 'a 710065, PR China
***College of Chemistry and Material Weinan Normal University, Weinan 714099, PR China
†Corresponding author: Yang Bo; yangbo@xsyu.edu.cn

Nat. Env. & Poll. Tech.
Website: www.neptjournal.com

Received: 26-06-2023
Revised: 28-07-2023
Accepted: 03-08-2023

Key Words:
Phytoremediation
Hyperaccumulator
Heavy metals
Petroleum hydrocarbons

ABSTRACT

Petroleum hydrocarbon is one of the dangerous substances in the process of petroleum development, refining, processing, transportation, and production. In the related activities of the petroleum industry, the output is large, and improper treatment will cause pollution to the surrounding environment. It is an urgent problem to conduct harmless and resource treatment of petroleum hydrocarbon polluted soil. Plant enrichment, as an environmentally friendly and pollution-free technical means, has the advantages of low cost and small change to the soil environment and effectively solves the problems of excessive heavy metals in petroleum hydrocarbons through plant enrichment. In this paper, the development process of plant enrichment, remediation methods, and plant enrichment of typical heavy metals (Cd, Hg, Zn) in petroleum hydrocarbon-polluted soil were systematically introduced. Through investigation, the mechanism and influencing factors of plant enrichment of heavy metals in the presence of petroleum hydrocarbons were summarized and analyzed, and the possible development direction of plant enrichment technology in the future was prospected.

INTRODUCTION

In the process of petroleum development and processing, oily sludge mainly includes landing sludge, settling tank sludge, three-phase separator sludge, oil spill sludge from production accidents, etc. The composition is complex, including some hydrocarbon substances and heavy metals that are difficult to degrade (Qu et al. 2017, Chen et al. 2017, Zan et al. 2021, Ren et al. 2021). At present, some oil and gas fields in China have been subjected to different degrees of combined pollution of petroleum hydrocarbons and heavy metals. For example, the soil of a shale gas well in Changning contains two pollutants: petroleum hydrocarbons and heavy metals nickel (Ma et al. 2018). There are more than 10 kinds of heavy metal elements in the oil-polluted soil of the Yellow River Delta (Li 2019). These heavy metals are mainly in the form of compounds, which lead to the lack of available potassium, phosphorus, and other nutrient elements and their reduced availability, thus weakening the soil's ability to supply crops (Jiang et al. 2021). The complex interaction with organic pollutants in the soil may change the form, solubility, and bioavailability of pollutants, thereby inhibiting or promoting each other's repair efficiency (Freitas et al. 2016). Heavy metals and polycyclic aromatic hydrocarbons in petroleum are carcinogenic and mutagenic (Xu et al. 2012), posing a potential threat to human life and health (Yan et al. 2009, Wu et al. 2015). Therefore, the combined pollution of petroleum hydrocarbons and heavy metals has attracted great attention worldwide (Huang et al. 2016, Istrate et al. 2018).

Soil heavy metal remediation techniques include physical, chemical, and biological technologies. Among them, physical technologies include heat treatment (Khan et al. 2004), glass restoration (Zhang et al. 2022), guest soil and soil exchange (Ren & Liu 2021), etc. Chemical techniques include leaching (Chen et al. 2022), curing stabilization (Singh et al. 2020), electrokinetic repair (Gao et al. 2021), and Fenton oxidation (Xu et al. 2016). In the above techniques, Li et al. (2021) repaired soil contaminated by petroleum hydrocarbon and heavy metal cadmium complex by immobilizing microorganisms for 60 days, and the heavy metal Cd in soil changed from exchangeable and organically bound states to residual states. The degradation rate of petroleum hydrocarbons reached 51.25%. Xu Hongting et

al. (2019) used persulfate as an oxidant. They controlled the cathodic solution pH=4 treatment to remove Cu, Zn, Pb, and Ni in the soil with an average removal rate of 13.6%, 17.3%, 12.3%, and 17.1%, respectively. The average removal rate of total petroleum hydrocarbons was 96.2%. Although the repair efficiency of physical and chemical technology can reach 70%-90% (Yang et al. 2019, Li et al. 2020, Pan et al. 2021), it is also affected by other factors such as pH value, Zeta potential, and chemical properties, which are easy to destroy the physical and chemical properties of soil and cause secondary pollution (Hu et al. 2017, Gidudu & Chhirwa 2020, Diksha et al. 2022). Bioremediation is to remove soil pollutants through the ability of organisms to decompose toxic and harmful substances without changing the existing physical and chemical properties of soil (Ren & Liu 2021). These include phytoremediation technology (Liu et al. 2022), microbial remediation technology (Chishti et al. 2013), and animal remediation technology (Zhang et al. 2022). Among them, microorganisms have poor genetic stability and are prone to variation, and generally cannot remove all pollutants, and specific microorganisms can only degrade specific chemical substances. Once the state of the compound changes, it may not be degraded by the same microbial enzyme. In practical application, pollutants in soil have different forms and may be unstable. The adsorption and accumulation capacity of microorganisms for heavy metals is limited, and they have to compete with indigenous strains and are significantly affected by the environment (Xia 2019). The pollutants absorbed by animals during restoration may be released into the environment due to metabolism or death (Feng 2019), so phytoremediation technology has become one of the most popular technologies at present.

Phytoremediation refers to the use of plants to extract, fix, and degrade indigenous and foreign heavy metals in soil (USEPA 2000). To a certain extent, it makes up for the lack of microorganisms affected by climate and geological conditions and the low concentration of heavy metals in animals (Zhou et al. 2022). There are five main ways for phytoremediation of contaminated soil: plant extraction, plant volatilization, plant stabilization, root filtration, and plant degradation (Ye 2021). Phytoremediation techniques are shown in Table 1, and heavy metal remediation pathways are shown in Fig 1. Among them, plant extraction, plant stabilization, and root filtration are also collectively referred to as plant enrichment (Chen et al. 2013), which refers to the methods of fixing heavy metals on the surface of roots or absorbing them into the body and storing them in leaves, so as to gradually reduce or even eliminate the content of heavy metals in soil. As early as the 19th century, Baker et al. (1990) found that the distribution of *Alyssum bertolonii* in soil was significantly correlated with the contents of Ni, Cd, and Zn in soil, indicating the possibility of plant enrichment (Ingrouille & Smirnoff 1986). In the 1970s, relevant studies in China (Brooks et al. 1977) also used *Elsholtzia harchowensis* Sun distributed in copper mining areas of Anhui Province and parts of the middle and lower reaches of Hubei Province as an indicator plant for mineral exploration to further prove the existence of plant enrichment. Since then, studies on plant enrichment have gradually increased, and as a technical means to control contaminated soil, experimental studies, and field applications have been carried out in agriculture, petroleum, and other fields. Due to its improved plant tolerance and good environmental protection, it has attracted wide attention in recent years (Wei & Chen 2001, Shen 2012, Yao et al. 2019, Liu 2019, Mazeed et al. 2020, Yang et al. 2021). At present, researches on phytoremediation mainly focus on the soil surrounding mines and farmlands (Wang et al. 2018, Zhao et al. 2023), while there are few reports on heavy metals in oil-polluted soil because petroleum pollutants are easy to form mucous membranes on the surface of plant roots, hinder plant root respiration and nutrient absorption, and even cause root rot and plant death in severe cases. This affects the survival rate of plants (Luo 2022). Oil pollutants also significantly changed the original carbon, nitrogen, and phosphorus ratio of soil, increasing soil pH value and a significant decrease in organic matter content (Teng et al. 2015), thus changing the vertical distribution of soil nutrients and affecting the normal life activities of plants. In the oilfield site with serious soil heavy metal pollution, the detection rate and excess rate of heavy metals Cd and Zn are high (Tao 2000), the volatility of mercury (Hg) and the activity of exchangeable mercury in the soil are high, which are the three metals with serious pollution problems. However, in the process of phytoremediation of heavy metals, the interaction between petroleum hydrocarbons and heavy metals is still unknown (Li et al. 2012, Li et al. 2019, Ezekiel et al. 2021, Gong et al. 2022, Guo et al. 2022). Therefore, there is still a lot of room for the application of phytoremediation technology in the remediation of heavy metals in oil-contaminated soil.

In summary, aiming at the pollution problem of typical heavy metals (Cd, Hg, Zn) in the soil of crudely polluted sites, this paper systematically introduced the research progress of remediation of typical heavy metals in the soil of crudely polluted sites by plant enrichment and prospected the possible research development direction.

PLANT ENRICHMENT OF TYPICAL HEAVY METALS

In 1977, Brooks first proposed the concept of hyperaccumulator (Brooks et al. 1977), which refers to plants growing in the

natural environment with dry weight Ni content exceeding 1000 $mg \cdot kg^{-1}$. With the deepening of research, American scientist Chaney et al. proposed the idea of plant enrichment of heavy metals in soil in 1983, and people gradually shifted the treatment of heavy metal pollution to the restoration of hyperaccumulators (Guo et al. 2022). Although the concept of hyperaccumulator has been proposed and widely used for more than 40 years, there are still many controversies about its evaluation methods. The most common evaluation methods for hyperaccumulators have two aspects. On the one hand, it means that the absorption of heavy metals by the above-ground parts of plants is 100 times higher than that of ordinary plants.

On the other hand, plants with BCF (Bioconcentration Factors) greater than 1 or TF (Translocation Factor) greater than 1 will not affect normal life activities (Zeng et al. 2019). In the past two decades, nearly 70 species of heavy metal hyperaccumulators have been discovered in China, which have strong root absorption, transfer, and leaf detoxification fixation abilities (Cui & Li 2016, Huang et al. 2020). It is mainly distributed in the southern region and is relatively rare in the cold regions in the north. Most hyperaccumulators grow in metal mining areas where soil nutrients are scarce (An et al. 2015). Most of them are herbaceous plants, while a few are trees and shrubs (Guo et al. 2022). The

Table 1: Characteristics of phytoremediation.

Phytoremediation technology	Repair pathway	Mainly repair heavy metal types	Reference
Phytoextraction	Heavy metals are transferred through plant roots to plant stems and leaves and harvesting stems and leaves remove soil heavy metals. Fast growth, large biomass, strong resistance to disease, strong adaptability to the environment.	Pb, Cd, Ni, Cu, Cr, Hg, Zn, etc.	(Luo et al. 2020)
phytovolatilization	Plant roots release chemicals that react with heavy metals, or plants convert absorbed solid or liquid heavy metal compounds into gases that are released into the atmosphere.	Hg, Se, As, etc.	(Liu et al. 2019)
Phytostabilization	Plant roots absorb heavy metals in the soil, weaken the flow and migration capacity of heavy metals in the soil so that they are not used for biological use, and reduce the environmental pollution caused by heavy metals entering the groundwater.	As, Cd, Cr, Cu, Hg, Ni, Pb, Zn, etc.	(Ye 2021)
Phytofiltration	When the root system changes the rhizosphere environment of plants, the root system will secrete organic acids to change the form of heavy metals. Cadmium phosphate, zinc phosphate, and lead sulfate precipitate in root exudates to resist the toxicity of heavy metals. Insoluble phosphorus is the main form of extracellular metal precipitation.	As, Cd, Cr, Cu, Hg, Ni, Pb, Zn, etc.	(Salt et al. 1995)
Phytodegradation	Plant roots and related microorganisms are used to degrade pollutants in soil. Microorganisms change the physicochemical properties of heavy metals to affect their migration and transformation and reduce the content of heavy metals.	As, Cd, Cr, Cu, Hg, Ni, Pb, Zn, etc.	(Sabreena et al. 2022)

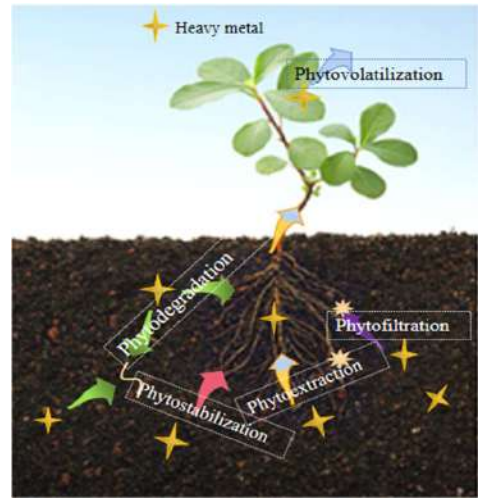

Fig. 1: Heavy metal remediation pathway.

Table 2: Related characteristics of Some hyperaccumulation plants.

Plant name	Sort	Repair metal	Repair effect/ground metal content	Reference
Chaetomitriopsis glaucocarpa	Herb	Zn	BCF>1	(Sun et al. 2018)
Hedwigia ciliata Ehrh. ex P. Beauv.				(Sun et al. 2018)
Sedum alfredii			19674 mg·kg^{-1}	(Long et al. 2002)
Arabis paniculate			77442 mg·kg^{-1}	(Tang et al. 2005)
Potentilla griffithii velutina			27600 mg·kg^{-1}	(Du 2005)
Picris divaricate			12472 mg·kg^{-1}	(Tang et al. 2005)
Sedum plumbizincicola			9609 mg·kg^{-1}	(Wu et al. 2012)
Symphytum officinale			17795 mg·kg^{-1}	(Zhang et al.2016)
Brassica juncea			18823 mg·kg^{-1}	(Zhang et al.2016)
Beta vulgaris cicla			159.79 mg·kg^{-1}	(Li et al. 2007)
Cardamine circaeoides			550 mg·kg^{-1}	(Liu et al. 2018)
Mirabilis jalapa			539.87 mg·kg^{-1}	(Zhou & Liu 2006)
Amaranthus tricolor			212 mg·kg^{-1}	(Fan 2007)
Euphobia thymifolia			202.086 mg·kg^{-1}	(Liu et al. 2006)
Emilia jaranica			404.23 mg·kg^{-1}	(Wang 2008)
Bidens pilosa			119.1 mg·kg^{-1}	(Sun et al. 2009)
Sonchus asper			387.5 mg·kg^{-1}	(Li et al. 2008)
Tagetes erecta			345.75 mg·kg^{-1}	(Lin 2008)
Artemisia argyi			105.59 mg·kg^{-1}	(Li et al. 2008)
Iva xanthifolia			474.30 mg·kg^{-1}	(Zhao et al. 2010)
Erigeron annuus			159.6 mg·kg^{-1}	(Cheng et al. 2010)
Cardamine hupingshanensis			131 mg·kg^{-1}	(Bai & Li 2012)
Sigesbeckia orientalis			192.92 mg·kg^{-1}	(Zhang et al. 2013)
Youngia erythrocarpa			317.87 mg·kg^{-1}	(Ning 2014)
Emilia sonchifolia			114.5 mg·kg^{-1}	(Zhou et al. 2014)
Galinsoga parviflora			205.62 mg·kg^{-1}	(Jin 2014)
Ageratum conyzoides			121.50 mg·kg^{-1}	(Sun et al. 2015)
Chenopodium ficifolium			179.73 mg·kg^{-1}	(Zhang et al. 2016)
Vinca major			190.82 mg·kg^{-1}	(Zhang et al. 2016)
Lolium perenne L.			BCF>1	(Jing et al. 2019a)
Sonneratia apetala Buchanan-Hamilton				(Peng et al. 2020)
Phytolacca americana L.		Hg		(Lu et al. 2004)
Euphorbia esula L.			35.1 mg·kg^{-1}	(Wang & Yi 2010)
Solanum nigrum		Cd	101.1 mg·kg^{-1}	(Wei et al. 2004)
Viola lucent			4825 mg·kg^{-1}	(Liu et al. 2003)
Lantana camara	Shurb		105.91 mg·kg^{-1}	(Sun et al. 2009)
Lonicera japonica			300 mg·kg^{-1}	(Liu et al. 2013)
Averrhoa carambola	Arbor		615 mg·kg^{-1}	(Lin 2010)

most typical hyperaccumulator in zinc-contaminated soil is *Sedum alfredii* (Zhou et al. 2021), *Solanum nigrum* (Wei et al. 2004), and *Viola lucens* (Liu et al. 2003) can be used as hyperaccumulators in cadmium-contaminated soil. *Euphorbia esula* L. can be used as a hyperaccumulator in mercury-contaminated soil (Wang & Yi 2010). The related characteristics of other hyperaccumulator plants are shown in Table 2. With the continuous breakthrough in the research of hyperaccumulator plants, a variety of hyperaccumulator plants that enrich typical heavy metals

have been discovered and should be used in experiments and markets.

Cadmium Enrichment

At present, there are more than 40 kinds of plants that can repair cadmium-contaminated soil, among which more than 10 species of hyperaccumulator plants (Shi et al. 2015, Wang et al. 2016, Jale et al. 2018). Researchers (Zhang et al. 2022) found that *Acacia auriculiformis A. Cunn. ex Benth.* had strong cadmium resistance to Cd under the condition of increasing CO_2 and N content. Compared with Cd alone, *Syzygium hainanense* Chang et Miau increased plant biomass more than double and decreased Cd concentration in leaves. This is because CO_2 and N offset the adverse effects of cadmium on the biomass of *C. hainanensis* by increasing the photosynthetic rate, N concentration, and efficiency of the stem water transport network. In addition to the two plants mentioned above, *Cinnamomum camphora* (L.) Presl and *Castanopsis hystrix* Hook respectively significantly increased the cadmium ion concentration in leaves under the same conditions compared with cadmium content alone (Zang et al. 2021). They were 162.1% and 338.0%, respectively, indicating that plants have species-specific ability to repair cadmium pollution. Chen et al. (2021) combined three consecutive crops of cabbage, ryegrass, and cabbage with two kinds of biochar (PBC, Poplar bark biochar) and thiourea-modified poplar bark biochar (TPBC, thiourea-modified poplar bark biochar)was used to repair CD-contaminated soil in situ. Compared with the control group, the residual cadmium in soil increased by 75.75%, and the cadmium in a weak acid-soluble state decreased by 160.62%. The combined remediation of biochar and fast-growing plants can reduce the bioavailability of cadmium and also overcome the problem of low efficiency and a long time of in-situ remediation.

Mercury Enrichment

At present, there are more than 20 species of hyperaccumulators that can repair mercury-contaminated soil (Shi et al. 2015). The bioenrichment coefficient and transport coefficient of *Pteris vittate*, *Miscanthus sinensis* and *Ipomoea nil* were all greater than 1. However, some research results are limited to polluted soil with medium and low concentrations. Wu et al. (2022) found that the content and distribution of heavy metals in sediments of the Pearl River Estuary tend to be consistent with oil pollution, and the total mercury content in sediments is 0.104 $mg \cdot kg^{-1}$. Mercury in soil mostly exists in residual and organic bonded states. However, exchangeable mercury accounts for 0.04%, but this part of mercury has high activity, and it is easy to form complex mercury with sulfides in soil and combine mercury with organic matter (Zhao et al. 2014). The physical and chemical properties of soil determine the existence form of mercury. In soil with pH<7, mercury is the most sensitive to organic matter, and in alkaline soil, mercury is mainly absorbed by clay minerals (Li et al. 2018, Jia et al. 2020). Researchers (Aleksandra et al. 2008) found that *Salix viminalis* E. L. Wolf absorbs and distributes mercury in a plant-stable manner, preferentially binding mercury in the cell wall of the outer part of the cortex and central cylinder and in the thin-walled nucleus, with the highest mercury content in the roots and maintaining a rich microbial population in the rhizosphere. However, the root system of *Artemisia salix* is mainly distributed in the upper layer of the soil, polluted by mercury, which was unfavorable to the stability of the soil.

Zinc Enrichment

At present, there are more than 20 species of hyperaccumulators that can repair zinc-contaminated soil, distributed in 4 to 6 families (Konrad et al. 2018). Zou Yanmei et al. (2019) found through plant extraction that the enrichment coefficient of *Phragmites australis* for heavy metals in polluted soil with a mass ratio of total petroleum hydrocarbons less than 200 $mg \cdot kg^{-1}$ was greater than 1, which was because of the low concentration of petroleum hydrocarbons as a carbon source improved the respiration and transpiration of the reed. Then, the heavy metals migrate to the rhizosphere surface with water to promote their absorption in the roots. However, when the mass ratio of total petroleum hydrocarbon in the soil is greater than 410 $mg \cdot kg^{-1}$, macromolecules with higher hydrophobicity and greater viscosity in petroleum will adsorb on the surface of reed roots, which will reduce respiration and transpiration. The heavy metal enrichment ability will decrease. This is consistent with the findings of Li (2019). Yu et al. (2022) found that *Bidens pilosa* L. and *Xanthium sibiricum* Patrin ex Widder not only showed better metal extraction ability but also showed higher sprout biomass after repeated extraction of plants. The extractable lead, cadmium, and zinc contents of diethylenetriamine pentaacetic acid (DTPA) in plant rhizosphere soil were decreased. Foreign researchers (Peter et al. 2015) evaluated the Zn repair potential of *Acalypha wilkesiana* Mull. Arg. by setting gradient experiments, and found that pH, phosphorus, and water content of polluted soil repaired by *Acalypha wilkesiana* increased, nitrogen and organic carbon content decreased, and the plants accumulated a large amount of zinc in stems and leaves compared with the roots. By evaluating the bioenrichment coefficient (BCF) and transport coefficient (TF), zinc levels in roots and stems indicate that more bioavailable zinc pools are transferred from roots to leaves and stems, which can be used as plants to repair zinc-contaminated soil.

ENRICHMENT MECHANISM

The enrichment of heavy metals by plants in the presence of petroleum hydrocarbons in soil depends on the effects of plant root exudes on soil and rhizosphere microorganisms (Wang & Wu 2021, Wang et al. 2022). Root exudates refer to the general term of organic compounds released by some plants to the rhizosphere environment through their roots during the growth and development process (Xue et al. 2017). At present, more than 200 root exudates, including sugars, organic acids, enzymes, auxin, and amino acids, are released from different parts of plant roots into the soil environment, which can provide carbon and nitrogen sources required for microbial activities, increase the activity of rhizosphere microorganisms by up to 100 times, and improve the phenomenon of reduced diversity of soil bacteria caused by heavy metals (Ali et al. 2013, He et al. 2020). Under the stimulation of heavy metals, plants usually secrete a large number of organic acids with low molecular weight, such as citric acid and oxalic acid (Carballeira et al. 2016), which activate the insoluble heavy metals in soil and change the presence state or REDOX state of organic pollutants in the environment through reduction, acidification, and complexation, to reduce the toxicity of organic matter (Wu et al. 2018). Reduce the toxicity of organic pollutants to plants, improve the tolerance of plants, and promote the absorption, transfer, and enrichment of organic pollutants by plants (Niu et al. 2009, ar et al. 2012). Rhizosphere microbial effect refers to the use of a large number of rhizosphere soil microorganisms (including bacteria, fungi, actinomyces, etc.) to affect the toxicity, morphology, and biological availability of soil pollutants through various modes of action (Xing et al. 2004, Shinjini et al. 2014, Li et al. 2016). Root exudates are carriers of material, energy, and information exchange between plants and soil microorganisms, and plant rhizosphere microorganisms are effective proof that root exudates promote rhizosphere microflora changes. Plant roots can provide nutrients such as amino acids, vitamins, and enzymes required by microorganisms. Nutrients (Compant et al. 2009) also significantly stimulate soil enzyme reactions, such as terpenes, phenols, and organic acids (Jean-Patrick et al. 2012), which will affect the soil microbial community structure and increase the content of organic matter in rhizosphere soil. It can change the adsorption capacity of rhizosphere soil to organic pollutants, significantly improve the activity of rhizosphere microorganisms, and indirectly promote the degradation of organic pollutants by rhizosphere microorganisms. Rhizosphere microorganisms can consume organic matter and mineral nutrients in root exudates, change the type and quantity of root exudates, form a concentration gradient in the rhizosphere region, and directly promote the release of root exudates (Canarini et al. 2019). The mechanism of phytoremediation of heavy metals is shown in Fig. 2. Therefore, the interaction between root exudes and rhizosphere microorganisms plays a positive role in the enrichment of heavy metals.

INFLUENCING FACTORS

Temperature

Temperature is one of the important factors in maintaining normal plant growth, and it also affects the physicochemical properties of petroleum hydrocarbon pollutants. At low temperatures, the viscosity of petroleum hydrocarbons increases, while the volatility of toxic and low molecular weight petroleum hydrocarbons decreases, resulting in slow degradation of plants and soil microorganisms (Mar 1975, Foght et al. 1996, Ajona & Vasanthi 2021). Although plant degradation of petroleum hydrocarbon pollutants has the

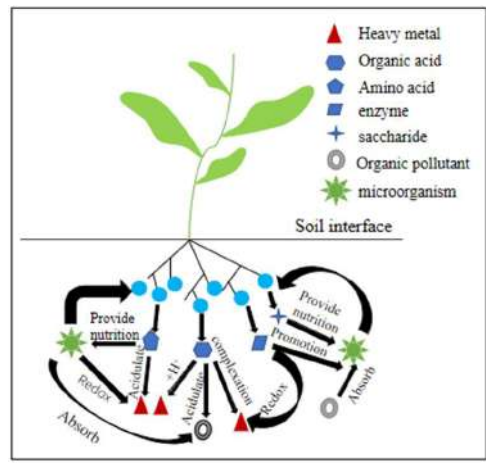

Fig. 2: Mechanism of phytoremediation of heavy metals.

highest degradation rate in the range of 30-40℃ (Bartha 1984, Cooney 1984), the degradation rate usually decreases with the decrease in temperature. Higher temperatures increase the solubility of petroleum hydrocarbons, reduce viscosity, and transfer long-chain normal alkanes from the solid phase to the water phase (Jackie et al. 2006, OkohAnthony 2006).

Temperature also affects the ability of plants to accumulate heavy metals by affecting the growth and development of plants and biomass. Different plants have different requirements for temperature. When the temperature is suitable, the growth and metabolism of aquatic plants are vigorous, and the enrichment ability of heavy metal ions is also enhanced accordingly. Experimental studies have shown (Pan & He 2006, He et al. 2022) that *Eichhornia crassipes* stop growing at 5℃, start growing at 13℃, and grow faster above 25℃. At that time, it has a strong heavy metal enrichment ability, and at 30℃, it grows fastest, at which time it has the strongest enrichment ability.

Soil pH

pH value is the main factor affecting the enrichment of heavy metals in plants. Depending on the nature of the heavy metal and the environment in which it exists, changing the pH of the environment can alter the bioavailability of the heavy metal. Generally, lowering the soil pH will increase the heavy metal content in the soil solution. In the living environment of plants, most heavy metals exist in insoluble states, and their solubility is controlled by pH value. Heavy metals precipitate with the increase of pH value in the environment, thus affecting the absorption and utilization of plants (Fang et al. 2022). When the pH value of the plant's living environment is lower than 6, the metal does not easily form hydroxide precipitation, and the ionic state is conducive to absorption. The experiment shows (Chen et al. 2019) that the higher the bioavailability of heavy metals in the living environment of plants, the stronger the absorption capacity of plants for heavy metals. This is because pH can affect not only the availability of heavy metals in a plant's environment but also the plant. In extremely acidic soil conditions, plants cannot survive. That is, there is no enrichment ability. Qiu et al. (2008) conducted experiments on Ni enrichment of *A. corsicum* and *A. murale* in the cruciferous family. They showed that the Ni absorption capacity of the two plants increased by two to three times when the pH value increased from 4.97 to 6.08. It may be that the decrease of H+ in soil relatively improves the absorption of metal ions by plant root complexes, or it may be that the decrease in the mobility of metal ions in soil and the weakening of the competitive adsorption between ions increase the absorption of Ni by roots (Urszula et al. 2004).

Oil Content

The removal rate of soil pollutants is one of the key indexes to directly evaluate the effect of phytoremediation. The concentration of oil pollution is the key environmental factor limiting the phytoremediation effect, and it is also the main evaluation index to determine the phytoremediation effect of tested plants in response to the stress of different oil pollution concentrations (Jing et al. 2019b). Wang et al. (2023) studied the repair effects of *Rudbeckia hirta* L. on petroleum hydrocarbons with different oil content. They found that soil with oil pollution concentration $\leq 6\%$ significantly promoted the plant height, root length, underground dry weight, root vigor, and root the head ratio of *Rudbeckia hirta* L. but significantly inhibited *Rudbeckia Hirta* L. when the oil pollution concentration was $\geq 8\%$. This is because the increase in the concentration of crude oil pollutants will significantly increase the soil viscosity and hydrophobicity (Qi et al. 2015), hinder the respiration of plant roots, and destroy plant root tissues through osmosis (Li et al. 2020), reduce soil water content in the micro-domain environment, limit the effective circulation of soil nutrients, and thus change soil biological and non-biological environmental factors.

The effect of heavy metals on plant growth shows the phenomenon of low promotion and high inhibition. That is, low concentrations of heavy metals can promote plant growth, and the amount of heavy metals accumulated by plants increases with the increase of heavy metal concentration (Li et al. 2008). Through experiments, Tang et al. (2018) and Wei et al. (2014) found that at low concentrations, Cr had a promoting effect on the chlorophyll content and biomass of wetland plants Reflorum and bamboo willow. With the increase of heavy metal concentration, plants can make corresponding physiological adjustments to the stress to alleviate or eliminate the damage caused by heavy metal stress to plants and maintain the normal growth of plants. However, plants' ability to relieve heavy metal stress has a certain threshold value. Under high concentrations of heavy metal stress, plants' ability to enrich heavy metal will decrease with the increase of metal concentration. This is because high concentration of toxic heavy metals has a destructive effect on plant cell structure, resulting in plant wilt and even death.

When heavy metals coexist with petroleum hydrocarbons, the effect of plant enrichment is different from that in the presence of a single pollutant, resulting in antagonistic or synergistic effects. The mechanism of this process is very complex, involving many factors such as the type, concentration, plant species, and tissue location of heavy metals and petroleum hydrocarbons, so further studies are needed.

CONCLUSION

With the continuous optimization and deepening of phytoremediation technology, these research results have significantly reduced the difficulty of remediation of heavy metals in soil contaminated by petroleum hydrocarbons and, at the same time, reduced the treatment cost and the possibility of secondary pollution. At present, most studies focus on single or multiple phytoremediation of a few heavy metals, and the understanding of the co-removal effect of petroleum hydrocarbons and heavy metals is still very limited, but this effect is the best solution for bioremediation of contaminated sites, especially when the heavy metal pollutant load is high. The amount of heavy metals in oily sludge is large, and the concentration is large. In order to strengthen the repair effect of plants on heavy metals, the following aspects can be considered:

(1) Strengthen the interaction between plants and various organisms to achieve the purpose of enrichment of heavy metals.

(2) At present, the application and development range of intercropping, intercropping, and rotation restoration models of hyperaccumulator is relatively narrow, so it is possible to explore the growth cycle of hyperaccumulator and enrich metals many times or transfer heavy metals from hyperaccumulator with a large amount of heavy metals in their bodies so that the hyperaccumulator can make secondary utilization.

(3) Explore the use of genetic engineering to improve hyperaccumulators to improve the metal enrichment ability of plants.

ACKNOWLEDGEMENTS

This research was supported by the Natural Science Basic Research Plan in Shaanxi Province of China (2023-JC-YB-129).

REFERENCES

Ajona, M. and Vasanthi, P. 2021. Bioremediation of petroleum contaminated soils – A review. Mater. Today: Proc., 45(p7): 7117-7122.

Aleksandra, S., Regina, G., Kucharski, R., Urszula, Z., Eugeniusz, M. and Laymon, G. 2008. Remediation aspect of microbial changes of plant rhizosphere in mercury-contaminated soil. Environ. Monit. Assess., 137(1-3): 101-109.

Ali, H., Khan, E. and Sajad, M.A. 2013. Phytoremediation of heavy metals-Concepts and applications. Chemosphere, 91(7): 869-881.

An, J., Gong, X.S. and Wei, S.H. 2015. Research progress on technologies of phytoremediation of heavy metal contaminated soils. Plant Physiol. J., 34(11): 3261-3270.

Bai, H.F. and Li, X.M. 2012. Cadmium accumulation in hyperaccumulator *Cardamine hupingshanensis*. Jiangsu J. Agric. Sci., 28(01): 76-79.

Baker, A.J.M. and Proctor, J. 1990. The influence of cadmium, copper, lead, and zinc on the distribution and evolution of metallophytes in the British Isles. Plant Syst. Evol., 173(1/2): 91-108.

Bartha, R. 1984. The treatment and disposal of petroleum wastes in petroleum microbiology. Petrol. Microbiol., 15: 553-578.

Brooks, R.R., Lee, J., Reeves, R.D. and Jafre, T. 1977. Detection of nickeliferous rocks by analysis of herbarium specimens of indicator plants. J. Geochem. Explor., 7(1977): 49-57.

Canarini, A., Kaiser, C., Merchant, A., Richter, A. and Wanek, W. 2019. Root exudation of primary metabolites: mechanisms and their roles in plant responses to environmental stimuli. Front. Plant Sci., 10(2019): 157.

Carballeira, T., Ruiz, I. and Soto, M. 2016. Effect of plants and surface loading rate on the treatment efficiency of shallow subsurface constructed wetlands. Ecol. Eng., 90(2016): 203-214.

Chen, F., Zhu, Y.F., Ma, J., Liu, J.N., Yu, H.C. and Zhang, S.L. 2021. In-situ remediation of Cd-contaminated soil around industrial sites by biochar combined with rank vegetation. J. China Coal Soc., 46(05): 1477-1486

Chen, G.C., Liu, Y.Q., Wang, R.M., Zhang, J.F. and Gary, O. 2013. Cadmium adsorption by willow root: the role of cell walls and their subfractions. Environ. Sci. Pollut. Res. Int., 20(8): 5665-5672.

Chen, H.C., Wu, K.J. and Li, R. 2019. Effects of exogenous organic acids on the characteristics of Cd accumulation of Salix variegata under Cd stress. Acta Ecol. Sin., 39(12): 4510-4518.

Chen, L., Zhang, X.M., Liu, F., Liu, X.B. and Ou, Y.P. 2017. Current situation and prospect of oil-contaminated site remediation.Appl. Chem. Ind., 46(03): 573-576.

Chen, M.Q., Ji, L.J., Sun, J., Xing, Y.L., Zhang, J.Z., Liu, P., Gu, Q., Li, S.P., Liu, Y.W. and Jiao, W.T. 2022. Progress in basic research and engineering application of washing/flushing technology for heavy metal contaminated soil remediation. Environ. Pollut. Control, 44(02): 238-243.

Cheng, G.L., Jiang, D.K., Li, S.Q., Zhao, L., Chen, Y.C., Zhang, Z.G., Chen, P., Yao, D.X. and Liu, J. 2010. Remediation of cadmium-contaminated soil by composite plants. Soil Biol. Biochem., 43(1): 712-728.

Chishti, Z., Hussain, S., Arshad, K.R., Khalid, A. and Arshad, M. 2013. Microbial degradation of chlorpyrifos in liquid media and soil. J. Environ. Manage., 114(2013): 372-380.

Compant, S., Clément, C. and Sessitsch, A. 2009. Plant growth-promoting bacteria in the rhizo- and endosphere of plants: Their role, colonization, mechanisms involved and prospects for utilization. Soil Biol. Biochem., 42(5): 669-678.

Cooney, J.J. 1984. Fate of Petroleum Pollutants In Freshwater Ecosystems. Springer, Cham.

Cui, L.Z. and Li, S.F. 2021. Remediation Technology and Application of Contaminated Soil. Beijing: Chem. Ind. Press.

Diksha, S., Ankita, G. and Moumita, C. 2022. A review on biosurfactant producing bacteria for remediation of petroleum contaminated soils. 3 Biotech., 12(9): 218.

Du, S.J. 2005. Study on Zinc Absorption and Enrichment Characteristics of *Potentilla grifithii*. Springer, Cham

Ezekiel, C.E., Osuji, L.C. and Onojake, M C. 2021. Use of alkyl polyglycosides in the remediation of heavy metals from hydrocarbon-contaminated soils. J. Global Ecol. Environ., 23-24.

Fan, H.L. 2007. Physiological Mechanism of Cadmium Accumulation in Amaranth. Chinese Academy of Agricultural Sciences, Beijing.

Fang, Z.G., Xie, J.T. and Yang, Q. 2022. Role and mechanism of low molecular-weight-organic acids in enhanced phytoremediation of heavy metal contaminated soil. Environ. Sci., 43(10): 4669-4678.

Feng, H. 2019. Discussion on microbial remediation technology of heavy metal contaminated soil. IOP Conf. Ser. Earth Environ. Sci., 358(2019): 022011.

Foght, J.M., Westlake, D.W., Johnson, W.M. and Ridgway, H.F. 1996. Environmental gasoline-utilizing isolates and clinical isolates of Pseudomonas aeruginosa are taxonomically indistinguishable by

chemotaxonomic and molecular techniques. Microbiology, 142(9): 2333-40.

Freitas, S.D.A.C. and Vieira, L.M., Rocha, V.R.M., Santos, P.T., Santos, V.R.A., Gomes, R.J.L., Soares, D.P.O.S. and Antonio, M.J. 2016. Cadmium and lead in seafood from the Aratu Bay, Brazil, and the human health risk assessment. Environ. Monit. Assess., 188(4): 259.

Gao, X.X., Liu, Y.X., Yuan, J., Kong, X., Bai, H. and Li, R.Y. 2021. Research progress on remediation technology for mercury-contaminated soil. Mod. Chem. Ind., 41(08): 63-67.

Gidudu, B. and Chirwa, E.M.N. 2020. The combined application of a high voltage, low electrode spacing, and biosurfactants enhances the bio-electrokinetic remediation of petroleum-contaminated soil. J. Cleaner Prod., 276.

Gong, J., He, L.S. and Li, Q. 2022. Species distribution and source analysis of heavy metals in surrounding soil typical petroleum sites. Environ. Sci., 43(12): 5710-5717.

Guo, S.M., Yu, H.B. and Yuan, L.Y. 2022. Research progress of screening of germplasm resources of heavy metal hyperaccumulator in recent 20 years in China. Asian J. Ecotoxicol., 17(02): 96-108.

Guo, W.J., Guo, H.X., Zhang, Y.Y., Gao, Y.P., Tian, T., Luo B., Lei, C.Y. and Ruan, Y. 2022. Distribution characteristics and ecological risk assessment of heavy metals in farmland around Changqing Oilfield. J. Environ. Occup., 39(05): 527-531+538.

He, J.Q., Li, S.Y., Wu, S.Y., Hu, J.Y., Wang, Y. and Wang, G.H. 2022. Review on phytoremediation of heavy metal polluted water. Appl. Chem. Ind., 51(06): 1804-1810.

He, Y.J., Sun, M.H. and Shen, Y.T. 2020. Research progress on the interaction mechanism between hyperaccumulators and heavy metals and its application. Rock Mineral Anal., 39(05): 639-657.

Hu, L.W., Chen, M., Yang, Q., Tao, M.X. and Yang, T. 2017. Present situation of heavy metal pollution in sediments and its remediation technologies. Environ. Eng., 35(12): 115-118+123.

Huang, R., Dong, M.L., Mao, P., Zhuang, P., Paz-Ferreiro, J., Li, Y.X., Li, Y.W., Hu, X.Y., Netherway, P. and Li, Z.A. 2020. Evaluation of phytoremediation potential of five Cd (hyper)accumulators in two Cd-contaminated soils. Sci. Total Environ., 721(prepublish): 137581.

Huang, R.X., Zhou, J.H., Yuan, Y.H., Tian, S.N., Hu, L., Luo, X., Tian, T.H. and Li, Z.X., 2016. A review of the remediation technologies of petroleum-contaminated soils. J. Nanchang Inst. Technol., 35(03): 48-54.

Ingrouille, M.J. and Smirnoff, N. 1986. Thlaspi caerulescens J. & C. Presl. (*T. alpestre* L.) in Britain. New Phytol., 102(1): 219-233.

Istrate, I.A., Cocârță, D.M., Wu, Z.C. and Stoian, M.A. 2018. Minimizing the health risks from hydrocarbon-contaminated soils by using electric field-based treatment for soil remediation. Sustainability, 10(1): 253.

Jackie, A., Jai, S.D. and Mein, F.J. 2006. Bioremediation of hydrocarbon-contaminated polar soils. Extremophiles: Life under extreme conditions. Biotechnology, 10(3): 171-179.

Jale, C., Ahmet, A. and Zeliha, L. 2018. Metal hyperaccumulating Brassicaceae from the ultramafic area of Yahyali in Kayseri province, Turkey. Ecol. Res., 33(4): 705-713.

Jean-Patrick, T., My, P.T.T., Diane, B. and Michel, S. 2012. Plant exudates promote PCB degradation by rhodococcal rhizobacteria. Appl. Microbiol. Biotechnol., 95(6): 1589-603.

Jia, W., Chen, J.Q. and Chang, J.J. 2020. Bioremediation of mercury contamination: A review. Environ. Eng., 38(05): 171-178.

Jiang, X.Y., Zhang, S.X., Yin X.X., Zhang, S.P., Li, D. and Wang, L.H. 2021. Research progress on heavy metals pollution and its control in the soil-crop system. Asian J. Ecotoxicol., 16(06): 150-160.

Jin, Q. 2014. Study on the changes of antioxidant enzyme activity and photosynthetic characteristics of Galinsoga parviflora, a cadmium-enriched plant, Sichuan Agric. Univ. J., 16: 25.

Jing, L.H., Chen, X.M., Xiao, W., Tian, J., Qi, Q., Xiao, S.Q., Yan, T.T. and Zhang, X.H. 2019a. Heavy metals contaminated soil and wastewater remediation by Ryegrass and microbial degradation of its enriched plant. Chin. J. Environ. Eng., 13(06): 1449-1456.

Jing, M.B., Zhou, T.L., Liang, J., Yang, R.Q. and Wu, S.S. 2019b. Response of four kinds of adaptable plants to ecological restoration of crude oil contaminated soil in Eastern Gansu Province. Bull. Soil Water Conserv., 39(01): 286-293.

Khan, F.I., Husain, T. and Hejazi, R. 2004. An overview and analysis of site remediation technologies. J. Environ. Manage., 71(2): 95-122.

Konrad, N., Rai, B.M., Adil, E.H., Sai, G.T., Wei, M.J., Fu, M.M. and Jiang, W.P. 2018. Variation in the angiosperm ionome. Physiol. Plant., 163(3): 306-322.

Li, B.L., Shao, C.Y., Chen, G. and Zhang, Z.J. 2018. New techniques for disposal of soil containing mercury. Chin. J. Soil Sci., 49(05): 1247-1253.

Li, F.Y., Zhang, Y., Li, X., Bai, J., Ma, X.P., Wang, J.J. and Wang, H.S. 2009. A method for repairing cadmium-polluted soil by using Compositaceae plants. Sustainability, 53: 1765

Li, L.J., Xie, T.T., Zhang, S.L., Yuan, Z.X., Liu, M.H. and Li, C.X. 2020. Characteristics of nutrient content and enzyme activity in the rhizosphere and bulk soils of four suitable plant species in the hydro-fluctuation zone of the Three Gorges Reservoir. Acta Ecol. Sin., 40(21): 7611-7620.

Li, R.W. 2019. Study on the migration and enrichment of heavy metals in the Yellow River delta under the background of petroleum hydrocarbon pollution., Univ. Chin. Acad. Sci. J., 12: 58.

Li, R.W., Zou, Y.M. and Wang, C.Y. 2019. Vertical distribution and influencing factors of heavy metals in oilfield soil in the Yellow River Delta. Environ. Chem., 38(11): 2583-2593.

Li, X., Liu, P., Xu, G.D., Cai, M.Z. and Chen, N. 2008. Study on phytopurification and phytoremediation of electroplating sewage by wetland plants. J. Zhejiang For. Sci. Technol., 2008(04): 16-21.

Li, X., Wang, Y.X., Luo, T., Wang L., Yong S.S., Zhang Y.H., Lan, S., Xie, Z.S. and Wang, H.Y. 2021. Remediation of petroleum hydrocarbon-cadmium co-contaminated soil by biochar-loaded microorganisms. Chin. J. Environ. Eng., 15(02): 677-687.

Li, X.P., Liu, X.Y. and Xu, C.L. 2016. Leaching characteristic of toxic metals in urban soil from Valley City by organic acid and soil bacteria. Acta Sci. Circumstantiae, 36(11): 4153-4163.

Li, Y., Fang, Q.X. and Zu, Y.Q. 2008. Accumulation characteristics of two ecotypes *Sonchus asper* (L.) Hill. To Cd. Acta Bot. Boreali-Occidentalia Sin., 2008(06): 1150-1154.

Li, Y.S., Sun, L.N., Sun, T.H. and Wang H. 2007. Cadmium hyperaccumulator *Beta vulgaris* varcicla L. and Its accumulating characteristics. J. Agro-Environ. Sci., 2007(04): 1386-1389.

Li, Y.T., Li, D., Lai, L.J. and Li, Y.H. 2020. Remediation of petroleum hydrocarbon contaminated soil by using activated persulfate with ultrasound and ultrasound/Fe. Chemosphere, 238(C): 124657.

Li, Y.X., Zheng, X.L. and Sun, J. 2012. Distributions and ecological assessment of heavy metals of Chengdao oilfield sea areas. Mar. Environ. Sci., 31(02): 190-194.

Lin, J.T. 2010. Study on the potential of Averrhoa carambola for repairing moderately cadmium-contaminated soil, Sun Yat-sen Univ. J., 1: 5-11.

Lin, W. 2008. Identification of hyperaccumulating ornamentals and strengthening technology of ecological remediation. Inst. Appl. Ecol., Chin. Acad. Sci., 3: 23-38.

Liu X.H., Gao, Y.T. and He, B. 2006. Application and method of super enrichment plant remediation of lead-contaminated soil. Soil Air Water, 15: 46-58.

Liu, G.Q., Gu, X.Z., Hu, Z.W. and Xu, J. 2022. Research progress of bioremediation technology for agricultural soil organic pollution. Jiangsu Agric. Sci., 50(01): 27-33.

Liu, W., Shu, W.S. and Lan, C.Y. 2003. *Viola baoshanensis*, a new cadmium superaccumulator. Chin. Sci. Bull., 47(19): 2046-2049.

Liu, W., Zhang, Y.B. and Jia, Y.M. 2019. Research progress of

phytoremediation and strengthening measures for heavy metals contaminated. Environ. Eng., 37(05): 29-33-44.
Liu, Y.F., Long, S.Q. and Shao, S.S. 2018. A study on hyperaccumulation of Se and Cd in *Cardamine violifolia*. Earth Environ., 46(02): 173-178.
Liu, Y.S. 2019. Effect of tetradecane concentration on phytoremediation of Cd-tetradecane compound contaminated soil, Shenyang Jianzhu Univ.
Liu, Z.L., He, X.Y. and Chen, W. 2013. *Lonicera japonica* Thunb. - a newly discovered Cd hyper-accumulator. Ecol. Environ. Sci., 22(04): 666-670.
Long, X.X., Ni, W.Z. and Fu, C.X. 2002. Sedum alfredii H: A new Zn hyperaccumulating plant first found in China. Chin. Sci. Bull., 47(19): 1634-1637.
Lu, Y.G., Huang, J.G., Teng, Y. and Luo, Y.S. 2004. Growth and uptake response to Ni by hyperaccumulator Plantain. J. Soil Water Conserv., 4(01): 108-110-114.
Luo, Q. 2022. Study on plant screening for remediation of oil-contaminated soil in Jianghan Oilfield, Yangtze Univ. J., 1: 1-10.
Luo, Y., Liu F. and Ren, J. 2020. Research progress on evaluation methods of phytoremediation effectiveness of soil contaminated with heavy metal. Appl. Chem. Ind., 49(03): 755-760.
Ma, Y.S., Li, X., Mao, H.M., Wang, B. and Wang, P.J. 2018. Remediation of hydrocarbon–heavy metal co-contaminated soil by electrokinetics combined with biostimulation. Chem. Eng. J., 353: 410-418.
Mar, X.1975. Effects of temperature and crude oil composition on petroleum biodegradation. Appl. Microbiol., 30(3): 396-403.
Mazeed, A., Lothe, N.B., Kumar, A., Sharma, S.K., Srivastav, S. and Verma, R.K. 2020. Evaluation of phytoaccumulation potential of toxic metals from sewage sludge by high-value aromatic plant geranium. J. Environ. Biol., 41(4): 761-769.
Ning, B. 2014. Study on the mechanism of Cd enrichment in Youngia erythrocarpa. Sichuan Agric. Univ. J., 1: 6.
Niu, Z.X., Sun, L.N. and Sun, T.H. 2009. Plant-microorganism combined remediation of heavy metals-contaminated soils: Its research progress. Chin. J. Ecol., 28(11): 2366-2373.
OkohAnthony, I. 2006. Biodegradation alternative in the cleanup of petroleum hydrocarbon pollutants. Biotechnol. Mol. Biol. Rev., 1(2): 38-50.
Pan, C.L. and He, J. 2006. Effect of hydrophyte on the treatment of wastewater with chromium. Environ. Sci. Surv., 6(03): 34-35+47.
Pan, Y.F., Tang, Z., Peng, X.Y. and Gao, P. 2021. Microbial remediation techniques for petroleum hydrocarbons contaminated soil: a review. Chem. Ind. Eng. Prog., 40(08): 4562-4572.
Peng, P.F., Li, X.L. and Yang, Q. 2020. Distribution and enrichment characteristics of heavy metal elements in Mangrove plant: *Sonneratia apetala*. Mar. Sci. Bull., 39(05): 609-616.
Peter, A.O., Olusegun, E.P., Bankole, O.S. and Abiodun, A.S. 2015. Remediation of Zinc zinc-contaminated soil using *Acalypha wilkesiana*. J. Global Ecol. Environ., 2(2): 82-89.
Qi, Y.C., Wang, J., Tong, Y.A., Hu, X.S., Liu, G.H. and Li, Y. 2015. Screening of weed plants for phytoremediation of petroleum-contaminated soils. Ecol. Sci., 34(01): 148-153.
Qiu, R.L., Liu, F.J., Wan, Y.B., Tang, Y.T. and Hu, P.J. 2008. Phytoremediation on nickel-contaminated soils by hyperaccumulators *Alyssum corsicum* and *Alyssum murale*. China Environ. Sci., 28(11): 6.
Qu, C.T., Li, J.L. and Zhu, S.D. 2017. Oil Sludge Treatment Technology of Oil Field. Petroleum Industry Press, Beijing.
Rajkumar, M., Sandhya, S., Prasad, M.N.V. and Freitas, H. 2012. Perspectives of plant-associated microbes in heavy metal phytoremediation. Biotechnol. Adv., 30(6): 1562-1574.
Ren, R., Su, H., Li, C.N. and Sun, Q.N. 2021. Research progress on the technology of recycling oily sludge. Appl. Chem. Ind., 50(04): 1044-1048.
Ren, Z.S. and Liu, S.H. 2021. Research progress on remediation of heavy metal contaminated soil. Bull. Chin. Ceram. Soc., 40(06): 2042-2051.
Sabreena, S.H., Ahmad, B.S., Vineet, K., Ahmad, G.B. and Fuad, A. 2022. Phytoremediation of heavy metals: An indispensable contrivance in green remediation technology. Plants, 11(9): 1255.
Salt, D.E., Blaylock, M., Kumar, N.P., Dushenkov, V., Ensley, B.D., Chet, I. and Raskin, I. 1995. Phytoremediation: a novel strategy for the removal of toxic metals from the environment using plants. Biotechnology, 13(5): 468-474.
Shen, Y.Y. 2012. Study on behavior characteristics of petroleum pollutants in soil and rhizosphere remediation of plants. Chang'an Univ. J., 1: 1-6.
Shi, R., Wu, X.F., Li, Y., Feng, C.L. and Li, Y.S. 2015. Plant species applied in phytoremediation of heavy metal contaminated soils. J. Cent. S. Univ. For. Tech., 35(04): 139-146.
Shinjini, M., Heli, J., Pauli, S., Cosme, L.Q., Pirjo, T., Pertti, P. and Kim, Y. 2014. Spatial patterns of microbial diversity and activity in an aged creosote-contaminated site. ISME J., 8(10): 2131-42.
Singh, D.S., Kaur, T.P. and Agniva, M. 2020. Remediation techniques for removal of heavy metals from the soil contaminated through different sources: a review. Environ. Sci. Pollut. Res. Int., 27(2): 1319-1333.
Sun, T.G., Xiong, Y., Guo, Y.C., Zhao, Y. and Yang, Z.H. 2018. Comparison analysis of enrichment ability of heavy metals for six bryophytes. Northern Horticulture, 2018(20): 91-95.
Sun, Y.B., Zhou, Q.X., Liu, R. and Ren, W.J. 2009. The invention relates to a method for repairing heavy metal polluted soil by using five-color plum, a cadmium superaccumulator. Sustainability, 12: 563-576
Sun, Y.Y., Xu, L.L., Feng, X.D. and Guan, P. 2015. Biomass, cadmium accumulation, and chlorophyll fluorescence parameters response of *Ageratum conyzoides* to different concentrations of cadmium stress. Guihaia, 35(05): 679-684.
Tang, Q., Zhu, S.X., Zhao, B., Yang, X.Q. and Gu, J.F. 2018. Physiological and biochemical responses of *Thalia dealbata* of wetland plants to Cr stress. Sci. Technol. Eng., 18(35): 108-115.
Tang, Y.T., Qiu, R.L., Zeng, X.W. and Fang X.H. 2005. A newfound Pb/Zn/Cd hyperaccumulator-Arabis Paniculata L. Acta Sci. Nat. Univ. Sunyatseni, 2005(04): 135-136.
Tao, S., Liu, Z. and Huang, K.M. 2000. Study on the species and the bioavailabilities of heavy metals in oil-polluted soil. China Environ. Sci., 20(01): 57-60.
Teng, T., Cai, T.J., Liu, J.X., Ju, C.Y., Wang, T.Y. and Duan, T.Y. 2015. Impacts of the Sino-Russia crude oil pipeline on nutrients and heavy metals in the soil of different *Larix gmelinii* Forests. J. Soil Water Conserv., 29(02): 94-99.
Urszula, K., Alex, P., Cananres, L, Cyrill, R., Scott, A.J. and Jenkins, R.R. 2004. The effect of pH on metal accumulation in two *Alyssum* species. J. Environ. Qual., 33(6): 2090-102.
USEPA. 2000. Introduction to phytoremediation. EPA 600/R-99/107. U.S. Environmental Protection Agency, Office of Research and Development, Cincinnati, Oh. USA.
Wang, J.C., Jing, M.B., Zhang, W., Zhang, G.S., Zhang, B.L. and Liu, G.X. 2023. Phytoremediation effect of Rudbeckia hirta on crude oil-contaminated soils in the Loess Plateau of eastern Gansu Province. Chin. J. Ecol., 42(04): 933-945.
Wang, L., Yang D., Li, Z.T., Fu, Y.H., Liu, X.M., Brookes, P.C. and Xu, J.M. 2018. A comprehensive mitigation strategy for heavy metal contamination of farmland around mining areas – Screening of low accumulated cultivars, soil remediation, and risk assessment. Environ. Pollut. 245(2018): 820-828.
Wang, M.X., Wan, Y.L., Dong, L. and Li, X. 2016. Research progress in phytoremediation of cadmium-contaminated soil. Environ. Pollut. Contr., 38(02): 111.
Wang, M.Y. and Yi, Y. 2010. A newly discovered mercury-enriched plant - Whey euphorbia. Jiangsu Agric. Sci., 10(02): 354-356.
Wang, T. and Wu, Q.M. 2021. Research progress on the mechanism of plant rhizosphere degradation of soil polychlorinated biphenyls. Environ. Sci. Technol., 44(04): 36-44.
Wang, Y., Feng, F.Y., Ge, J., Li, Y. and Yu, X.Y. 2022. Effects and

mechanisms of plant root exudates on soil remediation. Acta Ecol. Sin., 42(03): 829-842.

Wei, C.Y. and Chen, T.B. 2001. Hyperaccumulators and phytoremediation of heavy metal contaminated soil: a review of studies in China and abroad. Acta Ecol. Sin., 2001(07): 1196-1203.

Wei, J.L., Pan, L.H., Chen, Y.S. and Fan, H.Q. 2014. Physiological and ecological characteristics of *Cyperus malaccensis* to Cr^{6+} stress. Guihaia, 34(01): 89-94.

Wei, S.H., Zhou, Q.X., Wang, X., Zhang, K.S. and Guo, G.L. 2004. A newly discovered cadmium-accumulating plant called *Solanum nigrum* L. Chinese Sci. Bull., 2004(24): 2568-2573.

Wu, L.H., Li, Z., Ikuko, A., Liu, L., Han, C.L., Tomoyuki, M., Luo, Y.M. and Peter, C. 2012. Effects of organic amendments on Cd, Zn and Cu bioavailability in soil with repeated phytoremediation by *Sedum plumbizincicola*. Int. J. Phytoremediation, 14(10): 1024-38.

Wu, L.P., Bai, W.Y., Wen, K.J., Li, K. and Shuo, W. 2018. Heavy metals dissolution characteristics in incineration slag by leaching with simulated root system organic acids. Chin. J. Environ. Eng., 12(08): 2220-2230.

Wu, P., Liu, Y., Li, C.H., Xiao, Y.Y., Wang, T., Lin, L. and Xie, Y.F. 2022. Effects of heavy metals and oil in sediments of Pearl River Estuary on microbial community. Trans. Oceanol. Limnol., 44(01): 106-114.

Wu, Y., Yuan, J., Zhang, J., Li, F. and Bai, C.L. 2015. Removal of heavy metals from oily sludge by subcritical wet air oxidation. Environ. Prot. Chem. Ind., 35(03): 236-240.

Xia, L.F. 2019. Status of microbial remediation technology in petroleum-contaminated land. IOP Conf. Ser. Earth Environ. Sci., 300(5): 052050.

Xing, W.Q., Luo, Y.M., Li, L.P., Liu, S.L. and Ding, K.Q. 2004. Rhizosphere remediation from persistent organic pollutants and research approaches. Soils, 2004(03): 258-263.

Xu, D.Y., Cao, P.P., Le, W.X. and Hong, Y.J. 2016. Heavy metal migration and speciation changes of residual sludge during the Fenton oxidation processing. Chin. J. Environ. Eng., 10(10): 5893-5900.

Xu, H.T., Cang, L. and Song, Y. 2019. Influence exploration of conditions on the removal of PAHs and heavy metals by electrokinetic oxidation remediation in soil. Environ. Pollut. Contr., 41(01): 10-15+22.

Xu, P., Zeng G.M., Huang, D.L., Feng, C.L., Hu, S., Zhao, M.H., Lai, C., Wei, Z., Huang, C., Xie, G.X. and Liu, Z. F. 2012. Use of iron oxide nanomaterials in wastewater treatment: A review. Sci. Total Environ., 424(4): 1-10.

Xue, Y.J., Guo J., Zhao, M., Wang, R.Y., Hou, S.Z., Yang, Y., Zhong, B., Guo, H., Liu, C., Shen, Y. and Liu, D. 2017. Research progress of soil plant root exudates in heavy metal contaminated soil. J. Zhejiang Univ., 34(06): 1137-1148

Yan, Z.G., Ding, Q. and Li, F.S. 2009. Glossary of Contaminated Sites. Science Press, Beijing.

Yang, G.L., Zheng, M.M., Tan, A.J., Liu, Y.T., Feng, D. and Lv, S. M. 2021. Research on the mechanisms of plant enrichment and detoxification of cadmium. Biology, 10(6): 544.

Yang, Z., Liu, L.S., Liu, M.J., Liu, L.L., Yi, G.M., Jin, Q.Q., Lu, Y.P. and Yue, Y. 2019. Exploration of small-scale experimental conditions in thermal desorption remediation of petroleum-contaminated soil. Chin. J. Environ. Eng., 13(10): 2320-2327.

Yao, A.J., Ju, L., Ling, X.D., Liu, C., Wei, X.G., Qiu, H., Tang, Y.T., Morel, J.L., Qiu, R.L., Li, C. and Wang, S.Z. 2019. Simultaneous attenuation of phytoaccumulation of Cd and As in soil treated with inorganic and organic amendments. Environ. Pollut., 250(2019): 464-474.

Ye, C.Y. 2021. Research status of phytoremediation of soil heavy metal pollution. Mod. Agric. Sci. Technol., 2021(17): 169-170.

Yu, F.M., Tang, S.T., Shi, X.W., Liang, X., Liu, K.H., Huang, Y.Z. and Li Y. 2022. Phytoextraction of metal(loid)s from contaminated soils by six plant species: A field study. Sci. Total Environ., 804(2022): 150282-150282.

Zan, S., Lv, J., Li, Z., Cai, Y., Wang, Z. and Wang, J. 2021. Genomic insights into *Pseudoalteromonas* sp. JSTW was coping with petroleum-heavy metals combined with pollution. J. Basic Microbiol., 61(10): 947-957.

Zang, X.W., Luo, X.Z., Hou, E.Q., Zhang, G.H., Zhang, X.F., Xiao, M.J., Wen, D.Z. and Zhang, L.L. 2021. Effects of elevated CO_2 concentration and nitrogen addition on the chemical compositions, construction cost, and payback time of subtropical trees in Cd-contaminated mesocosm soil. Tree Physiol., 42(5): 1002-1015.

Zeng, C.Z., Yan, M.L. and Liu, Z.X. 2019. Heavy metal hyperaccumulator plants and their evolution: facts and controversies. Plant Physiol. J., 55(08): 1063-1074.

Zhang, S.R., Lin, H.C., Deng, L.J., Gong, G.S., Jia, Y.X., Xu, X.X., Li, T., Li, Y. and Chen, H. 2013. Cadmium tolerance and accumulation characteristics of Siegesbeckia orientalis L. Ecol. Eng., 51(3): 133-139.

Zhang, W.L., Zhang, Y., Liu, P., Duan, C.Q. and Liu, C.E 2022. Research progress of earthworm in phytoremediation of heavy metal contaminated soil. Environ. Sci. Technol., 45(08): 155-165.

Zhang, X., Ge, F. F., Wang, X. F., Wei, D., Liu, Y. X., Jin, C. X., Zheng, L. Q. and Cui, W. J. 2008. A method for repairing cadmium-polluted soil by using cadmium superaccumulator Chenopodiu Zhang, Z.Q., Li, R.H., Shen, F. and Sun, X.N. 2016. Remediation of soil or water polluted by heavy metals by using the super-enriched plant Comfrey. Geogr. Phys. Chem. Technol., 114: 561-573.

Zhang, X., Ge, F.F., Wang, X.F., Wei, D., Liu, Y.X., Jin, C.X., Zheng, L.Q. and Cui, W.J. 2008. A method for repairing cadmium-polluted soil by using cadmium superaccumulator Chenopodium. Sustainability, 16: 732-749.

Zhang, X.F., Liu, H., Luo, X.Z., Xiao, M.J., Xiang, P., Chen, M.H., Zhang, X.Q., Zhang, L.L., Ye, Q. and Wen, D.Z. 2022. Contrasting responses in growth, photosynthesis, and hydraulics of two subtropical tree species to cadmium contamination as affected by elevated CO2 and nitrogen addition. Sci. Total Environ., 837(2022): 155858.

Zhang, Y.S., Zhou, Z.K., Yang, S.J., Li, R., Li, L.X., Li, J.Y. and Fan X.L. 2022. Principles and technologies for remediation of heavy metal contaminated soil. Nonferr. Metals Extrac. Metall., 22(10): 124-134.

Zhao, J.T., Li, Y.Y., Gao, Y.X., Li, B., Li, Y.F., Zhao, Y.L. and Chai, Z. F. 2014. Study of mercury-resistant wild plants growing in the mercury mine area of Wanshan District, Guizhou Province. Asian J. Ecotoxicol., 9(05): 881-887.

Zhao, X.H., Ren, Z.G., Zu, Y.G. and Tao Y. 2010. Cadmium enrichment characteristics of invasive plant Pseudoxanthium. For. Eng., 26(04): 39-43.

Zhao, X.N., Yang, Z.F. and Yu, T. 2023. Review of heavy metal pollution and remediation technology in the soil of mining areas. Geol. China, 50(01): 84-101.

Zhou, K., Zhang, S.M., Sun, M.Y. and Wang, Z.F. 2021. Absorption and accumulation characteristics of Sedum alfredii on heavy metals Zn and Cd under stress. Shandong Agric. Sci., 53(08): 90-93.

Zhou, Q.X. and Liu, J.N. 2008. A method for repairing heavy metal polluted soil by using purple jasmine flower plants. Soil, 11: 81-96.

Zhou, R.R., Liu, W.T. and Zhou, Q.X. 2014. The invention relates to a method for repairing single or compound-contaminated soil with cadmium and lead by using super-accumulated flower red. Biol. Chem. Anal., 53: 2516

Zhou, X.S., Lou, X., Radnaeva, L.D., Nikitina, E. and Wang, H. 2022. Advances in heavy metal accumulation characteristics of plants in Soil. Asian J. Ecotoxicol., 17(03): 400-410.

Zou, Y.M., Li, R.W., Sun, Z.G. and Wang, C.Y. 2019. Accumulation and migration of 5 kinds of heavy metals in vegetative organs of Phragmites australis in the Yellow River delta under petroleum hydrocarbons pollution. Wetl. Sci., 17(04): 485-492.

Nature Environment and Pollution Technology
An International Quarterly Scientific Journal

p-ISSN: 0972-6268
(Print copies up to 2016)
e-ISSN: 2395-3454

Vol. 23 | No. 1 | pp. 99-110 | 2024

Original Research Paper

https://doi.org/10.46488/NEPT.2024.v23i01.007

Open Access Journal

Growth and Immunity Performance of Nile Tilapia (*Oreochromis niloticus*) Challenged by Toxicity of Bio-Insecticide with Active Ingredients Eugenol and Azadirachtin

Ayi Yustiati*†, Alifia Ajmala Palsa*, Titin Herawati*, Roffi Grandiosa*, Ibnu Bangkit Bioshina Suryadi* and Ichsan Nurul Bari**

*Department of Fisheries, Faculty of Fisheries and Marine Science, Universitas Padjadjaran, West Java, Indonesia
**Department of Agrotechnology, Faculty of Agriculture, Universitas Padjadjaran, West Java, Indonesia
†Corresponding author: Ayi Yustiati; yustiati@yahoo.com

Nat. Env. & Poll. Tech.
Website: www.neptjournal.com

Received: 04-06-2023
Revised: 28-08-2023
Accepted: 01-09-2023

Key Words:
Nile tilapia
Bio-insecticide
Eugenol
Azadirachtin
Immunity performance

ABSTRACT

This study aims to determine the maximum concentration and the long-term effects after exposure to a bio-insecticide with active ingredients eugenol and azadirachtin on the survival rate, immunity, and growth of Nile tilapia. The method used in this study was experimental, using a completely randomized design (CRD) with six treatments and three replications. Fishes were exposed to eugenol and azadirachtin at concentrations 10, 20, 30, 40, and 50% of LC_{50} value for 14 days, followed by 14 days of maintenance to see the effect on growth. The results showed that 66 $mg.L^{-1}$ treatment was a concentration that did not interfere with the survival rate of Nile tilapia, which was 86.7%. The number of leukocytes increased on the third day by the highest increase in 66 $mg.L^{-1}$ treatment at 12.01×10^4 $cells.mm^{-3}$. Meanwhile, erythrocytes decreased, with the highest decrease in 66 $mg.L^{-1}$ treatment at 1.13×10^6 $cells.mm^{-3}$. The average growth rate in fish slowed down with increasing concentrations of exposure, with the lowest average growth in length and absolute weight in the 66 $mg.L^{-1}$ treatment was 0.57 cm and 1.68 g.

INTRODUCTION

Pesticides are one of the most toxic contaminants entering the aquatic environment (Yang et al. 2021). Farmers usually use chemical pesticides to eradicate these pests because many are sold in the market and are very effective in eradicating pests (Astuti & Widyastuti 2016). Various aquatic organisms are physiologically affected by pesticides produced by the agricultural industry. For this reason, there is concern about releasing pesticides into aquatic environments worldwide. Chronic exposure to toxic substances in fish in the aquatic environment causes morphological, biochemical, and physiological cell changes (Fernandes et al. 2013). However, over time, bio-pesticides have become an alternative trend of choice for overcoming bio-pest problems because they can reduce environmental pollution and are relatively cheaper than chemical pesticides (Wiratno & Trisawa 2013). According to the Indonesian Ministry of Agriculture, the use of pesticides continues to increase yearly, with the most used being insecticides.

Among bio-insecticides, several plant families with the potential as a source of bio-insecticides are Meliaceae, Annonaceae, Piperaceae, Asteraceae, and Zingiberaceae (Prijono 1999). Neem seeds (*Azadirachta indica* A. Juss) and clove oil are known to be used as bio-insecticides to control insects (Deyashi et al. 2016). Neem seed extract and clove oil contain several active compounds that can act as contact poisons, such as azadirachtin and eugenol. Azadirachtin is a secondary metabolite of the triterpenoid group, which has long been used as an active ingredient in bio-insecticide from the neem plant (Deyashi et al. 2016). Meanwhile, 80% of the eugenol content was obtained from the extraction of the clove plant (*Eugenia caryophyllata* Thunb) in the form of clove oil or essential oil (Hadi 2013).

The extensive use of chemical insecticides has become essential to current agricultural practices (Deyashi et al. 2016). Using insecticides in the agricultural sector can produce waste and enter water bodies through agricultural irrigation. Jannah and Yusnita (2020) state that insecticides are persistent, and their residues can remain in the water, soil, and fish body tissues. Irrigation water is used for agricultural activities, usually also used for aquaculture activities. Nile tilapia cultivation can be done in semi-intensive ponds, intensive ponds, and even in rice fields. So, if the location of the aquaculture pond is located in an agricultural area, the

insecticide can enter and cause harmful effects on the life of aquatic organisms.

According to Pramleonita et al. (2018), Nile tilapia has a reasonably high tolerance for changes in its environment. In addition, Nile tilapia is also recommended by the USEPA (United States Environmental Protection Agency) as a toxicological test animal because it is widespread, easy to cultivate, can tolerate unfavorable environments, and is easy to maintain in the laboratory (Radiopoetra 1996). Water pollution due to insecticide use can be determined through toxicity tests. The use of experimental animals to conduct toxicity tests is a form of aquatic toxicology research whose role is to determine the level of toxicity of insecticide at specific concentrations.

The active compounds of bio-insecticide with active ingredients eugenol and azadirachtin are organic chemical compounds that can disrupt the environmental balance of fish in aquaculture ponds. In addition, the bio-insecticide has yet to be circulated in the community, and its toxicity to fish has yet to be discovered. Therefore, it is necessary to carry out further research to determine the long-term effect of post-exposure bio-insecticide with active ingredients of eugenol and azadirachtin on the survival rate, immunity, and growth of Nile tilapia.

MATERIALS AND METHODS

Chemicals

The bio-insecticide used has active ingredients of eugenol 20 $g.L^{-1}$ and azadirachtin 0.02 $g.L^{-1}$ that are in liquid form and have a volume of 500 mL/bottle. The bio-insecticide used has yet to be circulated among the public and is still in the testing phase. So, it doesn't have a trademark yet.

Animal Collection and Acclimatization

Freshwater teleost, *Oreochromis niloticus* (Nirwana Nile tilapia) fingerlings size 5-6 cm from the Cibiru Fish Fingerling Center, Bandung City, Indonesia. The experiments are performed following local/national guidelines for experimentation on animals. They were acclimatized in the hatchery for three days at 28 – 30°C. The fish are fed commercially available fish food with a 39 – 41% protein content.

Insecticide Preparation

Bio-insecticide was measured using a 200 µL micropipette. Each treatment, namely B treatments (13.2 $mg.L^{-1}$), C (26.4 $mg.L^{-1}$), D (39.6 $mg.L^{-1}$), E (52.8 $mg.L^{-1}$), and F (66 $mg.L^{-1}$), then put into a 1.5 mL Eppendorf tube and closed tightly. Then, affix a marker label.

Determination of LC_{50} Value

Fish were saved by twelve aquariums (six treatments and two replications). While the other ten fish were in the experimental group, the first group functioned as the control group. Fish from the experimental groups were exposed for 96 hours to eugenol and azadirachtin at various concentrations (50, 75, 100, 125, 150, and 175 $mg.L^{-1}$) prepared from the stock solution. Fish mortality in various concentrations was measured in 24, 48, 72, and 96 hours, and dead animals were removed immediately. Using the software, the LC_{50} values for 24, 48, 72, and 96 hours were calculated by converting mortalities (% values) into probit scale. Eugenol and azadirachtin were supplied at various safe concentrations (10, 20, 30, 40, and 50%) following the measurement of the LC_{50}.

Experimental Procedure

This research was conducted for 28 days by observations in the first 14 days and the next 14 days. This study used eighteen aquariums measuring 60 × 29.5 × 35.5 cm^3 as containers. Nile tilapia fingerlings used as many as 20 fish/aquarium with a volume of 40 L of water. The feeding rate was 3% of the weight of fish biomass by giving it three times a day at 08.00, 12.00, and 16.00 Western Indonesia Time. The commercial feed used contains 39-41% protein. To maintain water quality, siphoning off 10% of the maintenance container is carried out every once in three days in the afternoon. Meanwhile, on the 14 days, the water is changed.

The research method was experimental by completely randomized design (CRD) with six treatments and three replications. The concentrations used were 0%, 10%, 20%, 30%, 40%, and 50% of the LC_{50} of bio-insecticide for Nile tilapia. The following are the treatments used:

A Treatment: 0 $mg.L^{-1}$ (control)

B Treatment: 13.2 $mg.L^{-1}$ (10% of LC_{50})

C Treatment: 26.4 $mg.L^{-1}$ (20% of LC_{50})

D Treatment: 39.6 $mg.L^{-1}$ (30% of LC_{50})

E Treatment: 52.8 $mg.L^{-1}$ (40% of LC_{50})

F Treatment: 66 $mg.L^{-1}$ (50% of LC_{50})

Data Analysis

Data analysis on survival and growth rates used an analysis of variance (ANOVA) with an F test at a 95% confidence level. If a significant difference exists, a follow-up test with Duncan's multiple range test will be carried out at the 95% confidence level. Data analysis on leukocytes and erythrocytes was analyzed descriptively and quantitatively.

Macroscopic symptom data, feed response, and shock response were analyzed descriptively and qualitatively. Meanwhile, water quality data were analyzed descriptively and quantitatively and compared based on the Indonesian National Standard.

RESULTS

LC_{50} Values of Eugenol and Azadirachtin

The LC_{50} values of eugenol and azadirachtin in Nile tilapia are presented in Table 1; bio-insecticide of eugenol and

Table 1: The LC_{50} values of eugenol and azadirachtin in Nile tilapia following 96 h exposure

Confidence Limits							
	Probability	95% Confidence Limits for Concentration			95% Confidence Limits for log (Concentration)[b]		
		Estimate	Lower Bound	Upper Bound	Estimate	Lower Bound	Upper Bound
PROBIT[a]	.010	59.233	.534	87.182	1.773	-.273	1.940
	.020	65.063	1.052	92.251	1.813	.022	1.965
	.030	69.057	1.616	95.712	1.839	.208	1.981
	.040	72.221	2.231	98.467	1.859	.349	1.993
	.050	74.902	2.899	100.820	1.874	.462	2.004
	.060	77.263	3.621	102.915	1.888	.559	2.012
	.070	79.393	4.398	104.831	1.900	.643	2.020
	.080	81.351	5.233	106.619	1.910	.719	2.028
	.090	83.173	6.127	108.312	1.920	.787	2.035
	.100	84.886	7.081	109.933	1.929	.850	2.041
	.150	92.363	12.831	117.502	1.965	1.108	2.070
	.200	98.773	20.391	125.036	1.995	1.309	2.097
	.250	104.625	29.978	133.476	2.020	1.477	2.125
	.300	110.176	41.660	143.969	2.042	1.620	2.158
	.350	115.582	55.117	158.339	2.063	1.741	2.200
	.400	120.956	69.368	179.589	2.083	1.841	2.254
	.450	126.394	82.890	212.067	2.102	1.919	2.326
	.500	131.985	94.493	261.065	2.121	1.975	2.417
	.550	137.822	103.987	332.920	2.139	2.017	2.522
	.600	144.018	111.847	436.754	2.158	2.049	2.640
	.650	150.715	118.657	587.664	2.178	2.074	2.769
	.700	158.110	124.903	812.338	2.199	2.097	2.910
	.750	166.498	130.977	1161.161	2.221	2.117	3.065
	.800	176.363	137.258	1738.962	2.246	2.138	3.240
	.850	188.602	144.227	2798.588	2.276	2.159	3.447
	.900	205.216	152.763	5117.303	2.312	2.184	3.709
	.910	209.443	154.813	5923.656	2.321	2.190	3.773
	.920	214.134	157.041	6945.614	2.331	2.196	3.842
	.930	219.414	159.494	8275.653	2.341	2.203	3.918
	.940	225.464	162.243	10066.596	2.353	2.210	4.003
	.950	232.569	165.394	12590.053	2.367	2.219	4.100
	.960	241.202	169.124	16379.101	2.382	2.228	4.214
	.970	252.256	173.760	22642.483	2.402	2.240	4.355
	.980	267.739	180.024	34841.845	2.428	2.255	4.542
	.990	294.093	190.180	68790.241	2.468	2.279	4.838

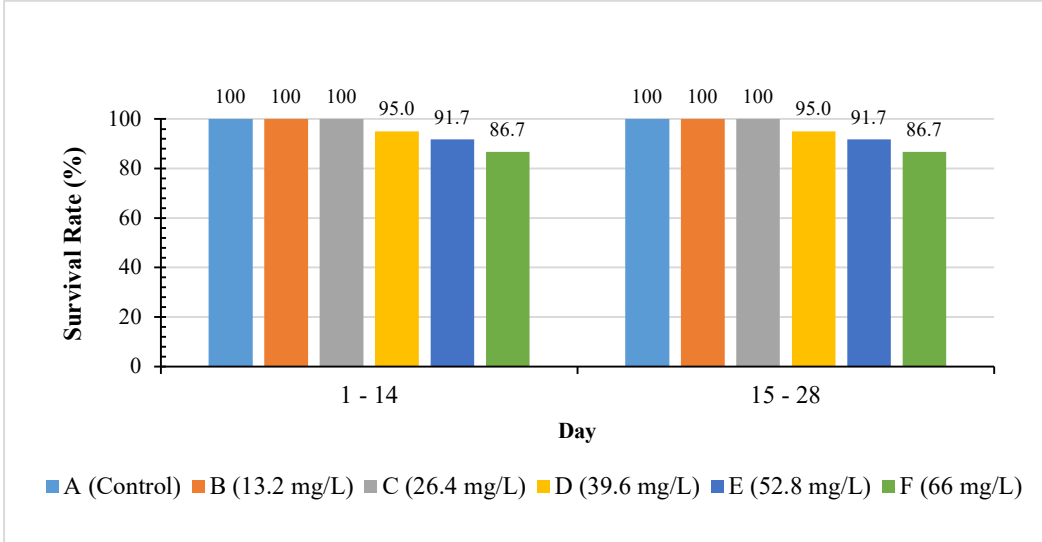

Fig. 1: The survival rate of Nile tilapia exposed to bio-insecticide with active ingredients eugenol and azadirachtin in the first 14 days and the second 14 days.

azadirachtin displayed relatively low toxicity to Nile tilapia, with an $LC_{50\text{-}96h}$ of 132 $mg.L^{-1}$.

Survival Rate (SR)

The survival rate of Nile tilapia was observed from the first day to the 14th day and continued from the 15th day to the 28th day, which can be seen in Fig. 1.

In the first 14 days of observation, the effects of eugenol and azadirachtin on survival rate in Nile tilapia was seen after 24 h exposure that there was death on 39.6, 52.8, and 66 $mg.L^{-1}$ treatments. The survival rate of Nile tilapia was significantly decreased at 66 $mg.L^{-1}$ treatment compared to the controls. Given that eugenol and azadirachtin survival rate changes in Nile tilapia, we hypothesized that the higher

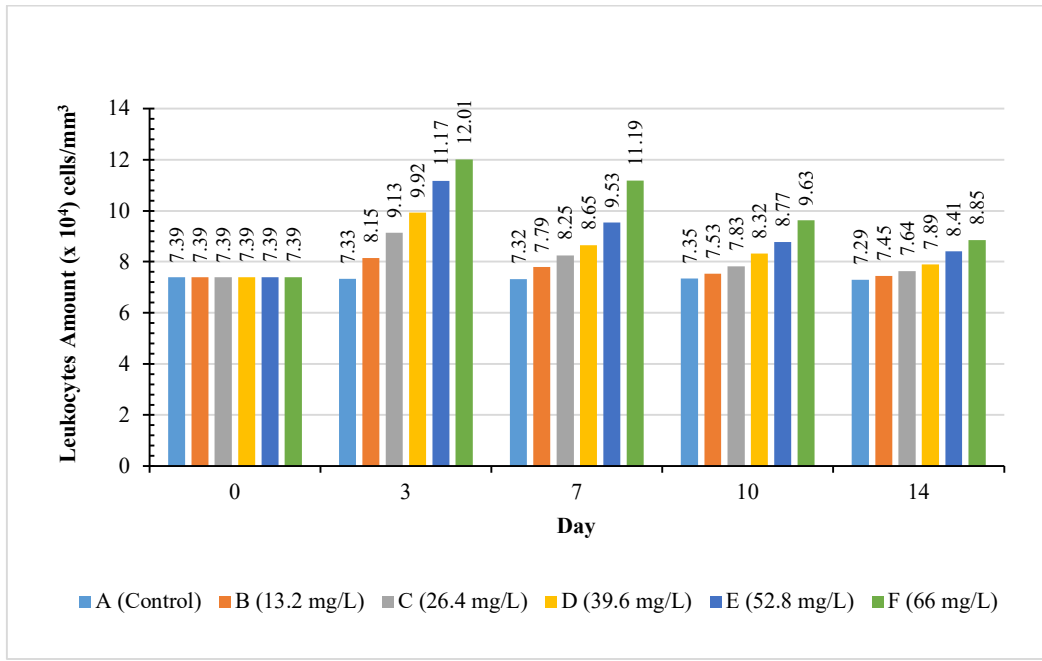

Fig. 2: The average number of Nile tilapia leukocytes in the first 14 days of observation with five times data collection.

the exposure concentration of bio-insecticide, the lower the survival rate of the tested fish. In the following 14 days of observation, there were no deaths in the test fish.

White Blood Cells (Leukocytes)

Based on Fig. 2, the leukocyte value in the treatment exposed to bio-insecticide experienced a maximum increase on the third day, with the highest increase in 66 mg.L^{-1} treatment at 12.01×10^4 cells.mm^{-3}. If compared to the control group, there was a significant decrease in this treatment. The increase in the number of leukocytes was higher than the control treatment can be used as a reference that fish health is being disturbed. On the seventh day, the leukocyte count of fish from each treatment decreased until the 14th day.

Red Blood Cells (Erythrocytes)

The number of erythrocytes in Nile tilapia exposed to bio-insecticide with the active ingredients eugenol and azadirachtin is still within the normal range for the number of erythrocytes in Nile tilapia but decreased compared to the control treatment. On the third day, it was seen that there was a maximum decrease in the number of erythrocytes in the treatment exposed to bio-insecticide, with the most significant decrease in 66 mg.L^{-1} treatment at 1.13×10^6 cells.mm^{-3}. On the seventh day, the number of erythrocytes in Nile tilapia exposed to bio-insecticide with the active ingredients eugenol and azadirachtin began to increase until the 14th day. The increase in erythrocytes on the seventh day is the initial stage of healing in fish by producing erythrocytes. The graph of the erythrocytes in Nile tilapia exposed to bio-insecticide with the active ingredients eugenol and azadirachtin can be seen in Fig. 3.

Length Growth (L_m)

Based on Fig. 4, the highest mean absolute length was in the control treatment at 1.88 cm. Conversely, 66 mg.L^{-1} treatment at 0.57 cm was the lowest length growth average. Length value absolute tended to decrease with increasing concentration of treatment. Exposure to bio-insecticide with active ingredients eugenol and azadirachtin significantly affected the length of growth of Nile tilapia fingerlings.

Weight Growth (W_m)

Based on Fig. 5, it is known that the highest average absolute weight growth was in the control treatment at 3.65 g. In the treatment exposed to bio-insecticide with the active ingredients eugenol and azadirachtin, the weight growth of Nile tilapia fingerling slowed down with the high concentration of the bio-insecticide given, with the lowest weight growth occurring in 66 mg.L^{-1} treatment at 1.68 g. The stunted growth of Nile tilapia can be seen in Fig. 6, the blackish digestive organs of the fish, presumably accumulated residues of bio-insecticide with the active ingredients eugenol and azadirachtin.

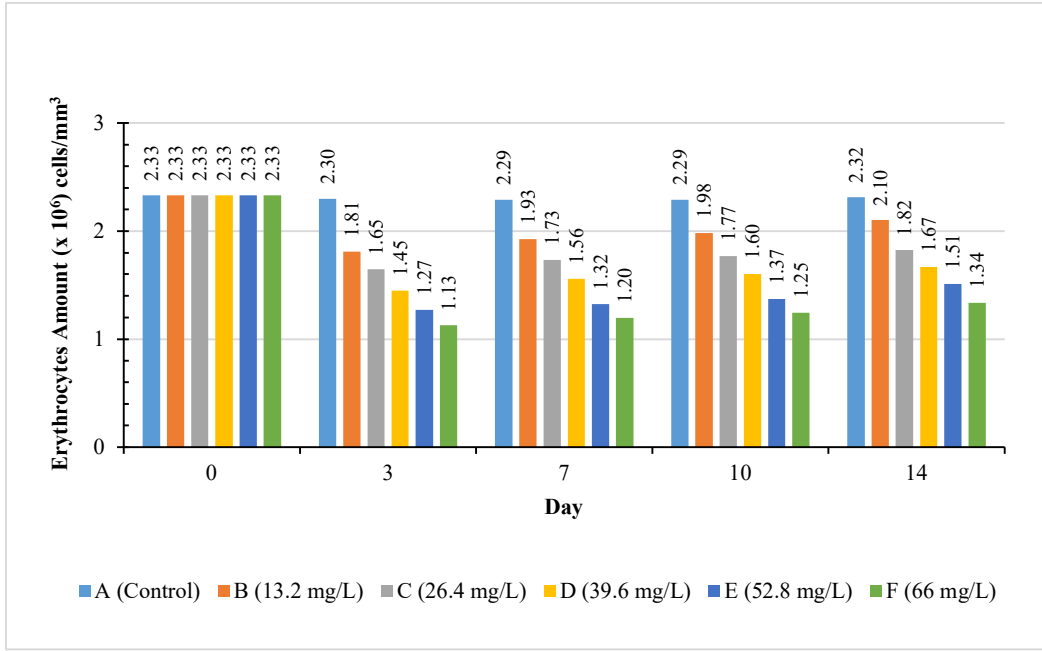

Fig. 3: The average number of Nile tilapia erythrocytes in the first 14 days of observation with five times data collection.

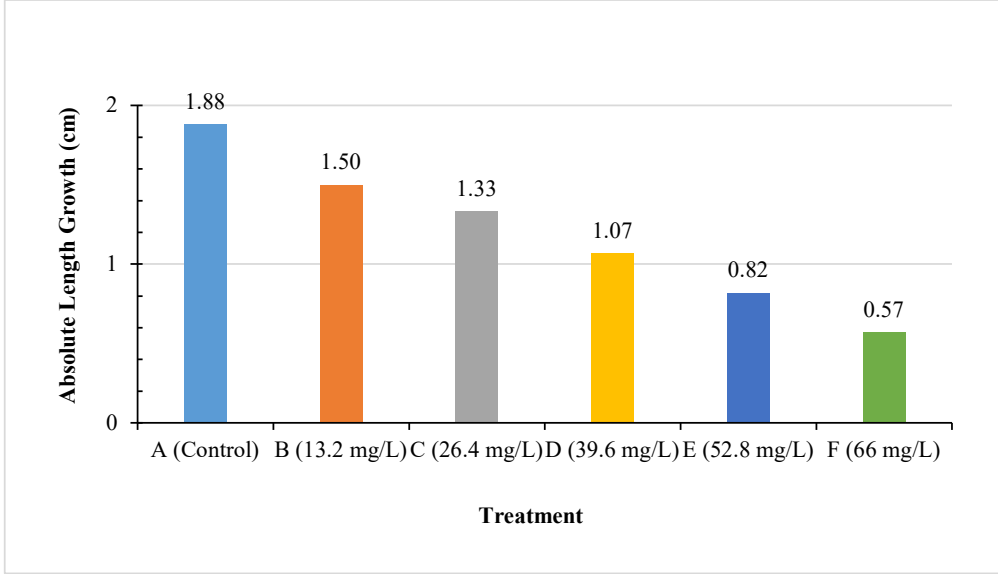

Fig. 4: The results of observing the growth in absolute length of Nile tilapia exposed to bio-insecticide with active ingredients eugenol and azadirachtin, which are carried out once a week.

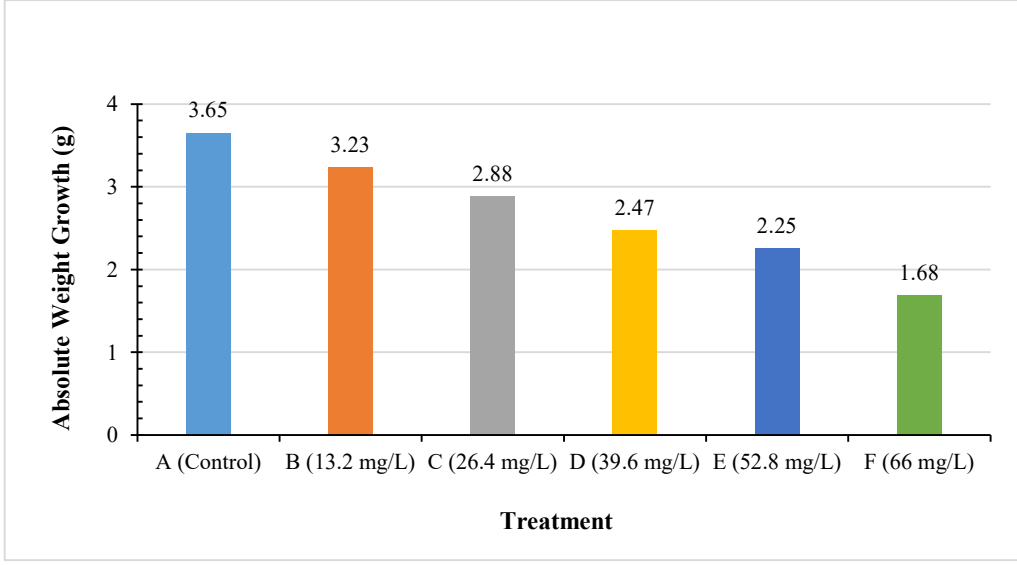

Fig. 5: The results of observing the growth in absolute weight of Nile tilapia exposed to bio-insecticide with active ingredients eugenol and azadirachtin, which are carried out once a week.

Macroscopic Symptoms

Observations of macroscopic symptoms were observed from the first until the 14th day. Based on Fig. 7, macroscopic symptoms on the morphology of the fish's body were shown on the first day, incredibly shortly after exposure to bio-insecticide with the active ingredients eugenol and azadirachtin, the color of the Nile tilapia's fins faded, and the body produced much mucus. In this 14th-day test, macroscopic symptoms in fish were not very visible (only showed mild symptoms).

Feed Response

Based on Table 2, the 39.6, 52.8, and 66 mg.L^{-1} treatments decrease appetite, especially on the first and second day, although not drastically. Then, gradually back to normal on the third day. Meanwhile, feed response in 13.2 and 26.4

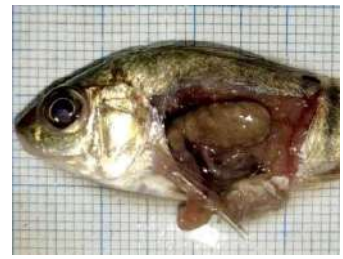

Healthy fish

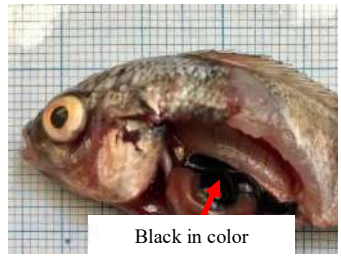

6 hours of death

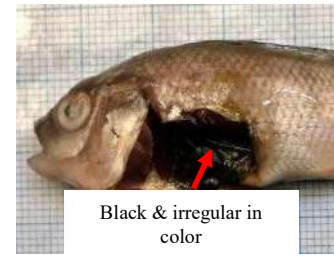

24 hours of death

Fig. 6: Digestive conditions of Nile tilapia exposed to bio-insecticide with active ingredients eugenol and azadirachtin for the first 14 days.

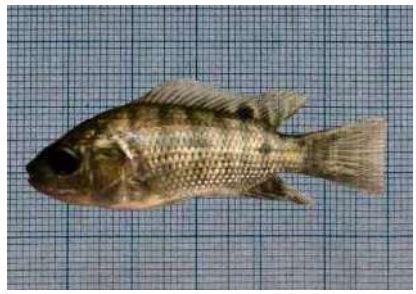

Healthy fish

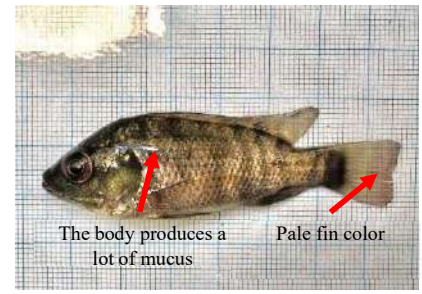

Fish exposed to bio-insecticide

Fig. 7: Macroscopic symptoms of Nile tilapia visible during 14 days of rearing after exposure to bio-insecticide with active ingredients eugenol and azadirachtin.

mg.L^{-1} treatments showed that Nile tilapia feed response did not slow down.

Shock Response

Based on Table 3, the shock response of Nile tilapia in 52.8 and 66 mg.L^{-1} treatments on the first day shows that fish tend to be more passive and less responsive to shock. This is presumably due to exposure to toxicants, which causes the fish's metabolism to decrease, causing slower movements and less responsiveness to shocks. The activity of the fish gradually improved on the second day, and it was seen that in 52.8 mg.L^{-1} treatment in all replicates, > 80% of the fish responded to the shock given. In the control treatment, 13.2, 26.4, and 39.6 mg.L^{-1} treatments, the fish's shock response tended to be stable and active from the first day of exposure to the 14th day.

Water Quality

During the first 14 days of rearing, the water temperature was 28-32°C. The temperature range for the first 14 days of maintenance is known to be not much different from the maintenance for the next 14 days. The range of pH values of all treatments during the first 14 days of maintenance was in the range of 6.5-6.8. Meanwhile, the maintenance for the next 14 days was in the range of 6.6-6.7. The dissolved oxygen measurements showed that the lowest dissolved oxygen content was 4.8 mg.L^{-1}. Meanwhile, the highest dissolved oxygen value was 5.6 mg.L^{-1}. The results of water

Table 2: Response of Nile tilapia feed exposed to bio-insecticide with active ingredients eugenol and azadirachtin from the first day to the 14th day.

Treatment	Repeat	Day													
		1	2	3	4	5	6	7	8	9	10	11	12	13	14
A	1	+++	+++	+++	+++	+++	+++	+++	+++	+++	+++	+++	+++	+++	+++
	2	+++	+++	+++	+++	+++	+++	+++	+++	+++	+++	+++	+++	+++	+++
	3	+++	+++	+++	+++	+++	+++	+++	+++	+++	+++	+++	+++	+++	+++
B	1	+++	+++	+++	+++	+++	+++	+++	+++	+++	+++	+++	+++	+++	+++
	2	+++	+++	+++	+++	+++	+++	+++	+++	+++	+++	+++	+++	+++	+++
	3	+++	+++	+++	+++	+++	+++	+++	+++	+++	+++	+++	+++	+++	+++
C	1	+++	+++	+++	+++	+++	+++	+++	+++	+++	+++	+++	+++	+++	+++
	2	+++	+++	+++	+++	+++	+++	+++	+++	+++	+++	+++	+++	+++	+++
	3	+++	+++	+++	+++	+++	+++	+++	+++	+++	+++	+++	+++	+++	+++
D	1	++	+++	+++	+++	+++	+++	+++	+++	+++	+++	+++	+++	+++	+++
	2	+++	+++	+++	+++	+++	+++	+++	+++	+++	+++	+++	+++	+++	+++
	3	++	+++	+++	+++	+++	+++	+++	+++	+++	+++	+++	+++	+++	+++
E	1	++	++	+++	+++	+++	+++	+++	+++	+++	+++	+++	+++	+++	+++
	2	++	+++	+++	+++	+++	+++	+++	+++	+++	+++	+++	+++	+++	+++
	3	++	+++	+++	+++	+++	+++	+++	+++	+++	+++	+++	+++	+++	+++
F	1	++	++	+++	+++	+++	+++	+++	+++	+++	+++	+++	+++	+++	+++
	2	++	++	+++	+++	+++	+++	+++	+++	+++	+++	+++	+++	+++	+++
	3	++	+++	+++	+++	+++	+++	+++	+++	+++	+++	+++	+++	+++	+++

Description: (+++) fish respond to feed in under 30 seconds, (++) fish respond to feed in 31 - 90 seconds, (+) fish respond to feed in 91 - 180 seconds, (-) fish do not eat the feed given

Table 3: Response of Nile tilapia shock exposed to bio-insecticide with active ingredients eugenol and azadirachtin from the first day to the 14th day.

Treatment	Repeat	Day													
		1	2	3	4	5	6	7	8	9	10	11	12	13	14
A	1	+++	+++	+++	+++	+++	+++	+++	+++	+++	+++	+++	+++	+++	+++
	2	+++	+++	+++	+++	+++	+++	+++	+++	+++	+++	+++	+++	+++	+++
	3	+++	+++	+++	+++	+++	+++	+++	+++	+++	+++	+++	+++	+++	+++
B	1	+++	+++	+++	+++	+++	+++	+++	+++	+++	+++	+++	+++	+++	+++
	2	+++	+++	+++	+++	+++	+++	+++	+++	+++	+++	+++	+++	+++	+++
	3	+++	+++	+++	+++	+++	+++	+++	+++	+++	+++	+++	+++	+++	+++
C	1	+++	+++	+++	+++	+++	+++	+++	+++	+++	+++	+++	+++	+++	+++
	2	+++	+++	+++	+++	+++	+++	+++	+++	+++	+++	+++	+++	+++	+++
	3	+++	+++	+++	+++	+++	+++	+++	+++	+++	+++	+++	+++	+++	+++
D	1	+++	+++	+++	+++	+++	+++	+++	+++	+++	+++	+++	+++	+++	+++
	2	+++	+++	+++	+++	+++	+++	+++	+++	+++	+++	+++	+++	+++	+++
	3	+++	+++	+++	+++	+++	+++	+++	+++	+++	+++	+++	+++	+++	+++
E	1	++	+++	+++	+++	+++	+++	+++	+++	+++	+++	+++	+++	+++	+++
	2	+++	+++	+++	+++	+++	+++	+++	+++	+++	+++	+++	+++	+++	+++
	3	++	+++	+++	+++	+++	+++	+++	+++	+++	+++	+++	+++	+++	+++
F	1	++	+++	+++	+++	+++	+++	+++	+++	+++	+++	+++	+++	+++	+++
	2	++	++	+++	+++	+++	+++	+++	+++	+++	+++	+++	+++	+++	+++
	3	++	+++	+++	+++	+++	+++	+++	+++	+++	+++	+++	+++	+++	+++

Description: (+++) > 80% of fish respond to shock, (++) > 60% of fish respond to shock, (+) 30 - 60% of fish respond to shock, (-) < 30% of fish respond to shock.

Table 4: Water quality (temperature (°C), dissolved oxygen (mg.L^{-1}), and (pH)).

Treatment	3rd, 7th, 10th, and 14th day			21st and 28th day		
	Temperature [°C]	pH	DO [mg.L^{-1}]	Temperature [°C]	pH	DO [mg.L^{-1}]
A	30 – 32	6,5 – 6,7	5,1 – 5,6	30 – 32	6,6 – 6,7	5,3 – 5,5
B	28 – 30,5	6,5 – 6,8	4,8 – 5,6	29 – 31	6,6 – 6,7	5,4 – 5,6
C	28,5 – 31	6,5 – 6,7	4,9 – 5,4	29,5 – 31	6,6 – 6,6	5,2 – 5,4
D	28,5 – 31	6,6 – 6,7	5,1 – 5,5	29 – 31	6,7 – 6,7	5,3 – 5,5
E	28 – 31	6,5 – 6,7	5,0 – 5,4	28,5 – 30,5	6,6 – 6,6	5,3 – 5,4
F	28,5 – 31	6,6 – 6,7	5,0 – 5,4	28,5 – 31	6,7 – 6,7	5,2 – 5,4
Optimal (INS 2009)	25 - 30	6,5 - 8,5	≥ 5	25 - 30	6,5 - 8,5	≥ 5

quality measurements (temperature, dissolved oxygen (DO), and potential of hydrogen (pH)) are still within the optimal range because it is so controllable according to the demands of a completely randomized design (CRD); there should be no other factors other than exposure to bio-insecticide with active ingredients eugenol and azadirachtin. Water quality during research can be seen in Table 4.

DISCUSSION

Based on this study, bio-insecticides with active ingredients eugenol and azadirachtin are compounds with a low toxicity level to Nile tilapia fingerlings because the $LC_{50\text{-}96h}$ value shows > 100 mg.L^{-1}, which is 132 mg.L^{-1}. These results follow the criteria determined by the USEPA that the $LC_{50\text{-}96h}$ toxicity value of > 100 mg.L^{-1} in the aquatic environment is classified as a low toxicity category (Kinasih et al. 2013). It is also supported by the results of the first 14 days of observation that the lowest survival rate value at 66 mg.L^{-1} exposure (50% LC_{50}) was 86.7% which showed that it was still relatively good for the survival rate of Nile tilapia but caused the most deaths with the same symptoms as in exposure 39.6 and 52.8 mg.L^{-1}. This follows the quality standards of the Indonesian national average that the survival rate value of good Nile tilapia has a percentage of ≥ 75%. In contrast, at exposures of 13.2 and 26.4 mg.L^{-1}, there were no deaths, and the clinical symptoms were not significant. This shows that the higher the concentration of bio-insecticide given, the lower the survival rate of the test fish. It is known that on the following 14 days of observation, there were no deaths in Nile tilapia after exposure to bio-insecticides, which was allegedly due to water changes. Hence, the fish's living media supported everyday life. In addition, Nile tilapia is a fish that easily adapts to its environment. This is supported by the statement of Sibagariang et al. (2020) that Nile tilapia is a freshwater fish that easily adapts to unfavorable environments.

Environmental pollution due to the extensive use of pesticides without proper management has a broad impact on the potential survival rate of aquatic animals, especially fish (Mishra & Devi 2014). This situation is caused by the function of the gills and organs directly related to the fish's living environmental media starting to experience damage due to insecticide contamination. Fish are exposed to chemical contaminants due to direct integumentary contact through the mouth and respiration through the gills (Shah & Parveen 2020). Some of these toxic chemicals persist in the environment for a long time and can affect physiology (cause damage to tissues) (Mishra & Devi 2014). The gills cannot supply oxygen adequately to the body (Ihsan et al. 2021). However, in lower concentrations, this toxic complex can cause increased tissue damage and reduce fish survival rate (Yancheva et al. 2022). In summary, it can be concluded that in a short-term trial by Georgieva et al. (2021), gills are more severely affected as the principal organs that come into direct contact with poisons when pollution occurs in the aquatic environment. As explained by Fernandes (2019), gills are a crucial entry point for dissolved pollutants due to their extensive surface area, and morphological characteristics support the absorption of contaminants in fish.

According to the research results of Georgieva et al. (2021), the significant impact of the pesticides used can have a long-lasting effect on the liver through the bloodstream. The fish's respiration rate reflects metabolic activity and responses due to changes in the surrounding environment, which can indicate adjustment capacity (Yancheva et al. 2022). Fish can reflect a direct response to toxic substances contained in water by changing their physiological response, such as the intensity of respiration rate (Yancheva et al. 2022). Similar to the results obtained, Nile tilapia exposed to bio-insecticide with active ingredients eugenol and azadirachtin experienced a lack of oxygen supply compared to the control group. These results can generally be attributed to respiratory distress caused by the limited access to oxygen to the fish's gills. This condition was also one of the factors causing the decrease in the number of erythrocytes compared to the control after exposure to bio-insecticide with the active ingredients eugenol and azadirachtin. Ikeda

(1970) stated that a decrease in metabolic rate decreased the number of fish erythrocytes. A decrease in the number of erythrocytes indicates the occurrence of kidney disorders and fish suffering from anemia (Wedemeyer & Yasutake 1977). Possibly, anemia occurs due to reduced oxygen binding in the blood due to disruption of the fish's respiratory organs, so the release of erythrocytes in the blood circulation is minor. According to Matofani et al. (2013), hemoglobin is closely related to erythrocytes; the lower the hemoglobin level, the fish is suspected of having anemia because it is closely related to the oxygen-holding capacity in the blood.

The clinical symptoms shown by the fish were when they were exposed to bio-insecticide with the active ingredients eugenol and azadirachtin, in which the fish soared to the surface, hanging from the surface to take in oxygen, and the fish's body produced much mucus. This study's results align with Yancheva et al. (2022) that excessive mucus secretion may result from a defensive response and avoidance to minimize irritation caused by the tested pesticides. According to Uchenna et al. (2022), mucosal cells can efficiently capture toxic substances and help prevent the entry of harmful substances into the gills so that the release of mucus can reduce the entry of various toxic compounds into the circulatory system. Epidermal mucus functions as a physiological and immunological first line of defense to maintain normal physiological status in teleost fish (Santoso et al. 2020). However, mucus in the fish's body can be a problem if much mucus is produced because it can inhibit gas exchange through the gills (Ihsan et al. 2021). Exposure to toxic substances can cause stress to fish and alter mucus production, harming fish (Reverter et al. 2018). In line with the statement of Santoso et al. (2020), fish that are stressed due to exposure to chemical pollutants secrete more mucus as a barrier and inhibit the diffusion of chemicals.

Based on visual observations immediately after exposure to bio-insecticides with the active ingredients eugenol and azadirachtin, there were changes in the behavior of Nile tilapia, such as irregular swimming patterns, whirling, and tending to tilt. According to the research results of Ihsan et al. (2021), fish exposed to chlorpyrifos inhibit metabolic processes in the body, causing fish to experience stress. The percentage of stressed goldfish with inactive and solitary fish tended to decrease with the time the insecticide was exposed. After being exposed to the insecticide chlorpyrifos, the common symptoms exhibited by goldfish are unusual swimming movements with irregular movements or classified as panic by moving in all directions. The next day, there was death in the fish, and the living conditions were more passive, silent, and solitary on the bottom or on the surface and getting weaker. So, it can be seen that the longer the fish are exposed to insecticides, the lower the movement of the fish's body (Ihsan et al. 2021). Fish infected with the insecticide chlorpyrifos generally experience a decrease in movement, which is thought to be because the chlorpyrifos has affected the nervous system and interfered with muscle movement, causing the fish to weaken and move erratically (Ihsan et al. 2021). Strange or abnormal fish movements are caused by a lack of coordination between the nervous system and muscles (Ihsan et al. 2019). According to Sellamuthu (2014), eugenol is also a phenol compound that has an alcohol group, so it can weaken and disrupt the nervous system. Based on this, it is known that the active compound of eugenol has a strong enough effect on weakening the nervous system in exposed Nile tilapia so that the fish give an abnormal response to their physiological system. Meanwhile, the cause of fish showing a whirling swimming pattern is caused by damage to the midbrain (metencephalon), which is responsible for regulating the body's balance in water (Hardi et al. 2011). The brain plays a regulatory role in fish physiology and is the most critical organ in fish toxicology, especially when pesticides are involved in the nervous system's workings (Mishra & Devi 2014).

Stress on fish due to exposure to contaminants, besides affecting the clinical symptoms, can also affect the number of leukocytes. This is supported by Lestari et al. (2017) that high leukocyte counts are due to stress on fish due to poor and polluted water quality. Based on the research journal Singh & Srivastava (2010), leukocytes play a significant role in the body's defense mechanism, which consists of lymphocytes (producing antibodies), granulocytes, and monocytes (as phagocytes to save injured tissue). The innate immune response is a frontline defense and a robust response, but it can be altered by pesticides (Li et al. 2013). The increase in the number of leukocytes higher than the control treatment can be used to reference that fish health is being disturbed due to exposure to bio-insecticides with active ingredients eugenol and azadirachtin. The increase in leukocytes in fish exposed to insecticides provides essential information about the general physiology and health status of fish under investigation (Singh & Srivastava 2010). It is known that fish exposed to triazophos 5 and 10% $LC_{50\text{-}96h}$ show significant reductions in various immune functions (Chandra et al. 2021).

Disruption of the homeostatic and physiological mechanisms of the fish body can cause lasting effects on inhibited growth and productivity of fish, which is characterized by fish's appetite loss (Royan et al. 2014). The decrease in appetite and the startle response in fish is thought to be due to the effects of exposure to the active ingredients eugenol and azadirachtin, which cause the fish's

metabolism to decrease so that their movements slow down and are less responsive when they are shocked. This is supported by the statement of Wardhana and Wijaya (2015) that essential oils have the potential to inhibit eating activity. Meanwhile, the feed response in treatments 13.2 and 26.4 $mg.L^{-1}$ showed that the Nile tilapia feed response did not slow. This shows that bio-insecticide with active ingredients eugenol and azadirachtin at exposure to these concentrations does not affect the fish's sense of smell and sight, so the fish can respond to feed in under 30 seconds. This statement is supported by the results of Suryadi et al. (2021), which stated that a fungicide with the active ingredient *Bacillus amyloliquefaciens* did not interfere with the sense of smell and sight of Nile tilapia and carp in responding to feed.

This research showed that the growth in length and absolute weight of Nile tilapia exposed to bio-insecticide with active ingredients eugenol and azadirachtin slowed down as the bio-insecticide exposure increased. The inhibition of fish growth is thought to be due to reduced oxygen supply due to disruption of the respiratory organs. Aquatic biota need oxygen in burning food to carry out activities, such as swimming, growth, reproduction, etc. (Ihsan et al. 2021). Therefore, a lack of oxygen in the fish's body can disrupt fish life, including slowing growth (et al. 2019). Similar to the results of Hafiz et al. (2018) on the toxicity of the herbicide isopropylamine glyphosate on the growth of catfish fingerlings, which showed that the highest growth was in the control treatment of 5.76 ± 1.40^{b} and the lowest in the 30% LC_{50} treatment (2.90×10^{-1} $mL.L^{-1}$) of 3.73 ± 1.51^{a}. The effect of pesticides on fish can occur indirectly (sublethal effects), which can inhibit growth (Hafiz et al. 2018). This was also stated by Damayanti & Abdulgani (2013) that behavioral abnormalities in fish, when exposed to organophosphates, can fail to store energy for metabolic processes.

The stunted growth of Nile tilapia can be seen in Fig. 6, the blackish digestive organs of the fish, presumably due to the accumulation of bio-insecticide residues with the active ingredients eugenol and azadirachtin. Thus, both directly and indirectly, the work function of the digestive organs of fish is disrupted and affects its growth. Exposure to toxic pesticides causes energy obtained from feed to be focused more on the adaptation and maintenance of damaged body tissue than on its growth (Mason 1979). Thus, the higher the concentration of exposure to bio-insecticide with the active ingredients eugenol and azadirachtin, it is suspected this will cause an imbalance between the amount of feed that enters as energy and energy output for survival rate. This is what causes the feed to be less effective for the growth of Nile tilapia.

CONCLUSIONS

The recommended concentration of bio-insecticide with active ingredients eugenol and azadirachtin is 66 $mg.L^{-1}$ (50% LC_{50}), which is a concentration that does not interfere with the survival rate of Nile tilapia. In addition, it is necessary to conduct field tests to compare the doses sprayed on plants with a concentration of bio-insecticide getting into the waters.

The number of leukocytes increased on the third day, with the highest increase in 66 $mg.L^{-1}$ treatment at 12.01×10^{4} $cells.mm^{-3}$. Meanwhile, the number of erythrocytes decreased, with the largest decrease in 66 $mg.L^{-1}$ treatment at 1.13×10^{6} $cells.mm^{-3}$.

Fish feed response decreased on the first and second days, then gradually increased on the 3rd day. Meanwhile, the fish startle response decreased on the first day and gradually became active again on the third day.

The highest absolute length growth was in the control treatment at 1.88 cm, and the lowest absolute length growth was in the 66 $mg.L^{-1}$ treatment at 0.57 cm. Meanwhile, the highest absolute weight growth was in the control treatment at 3.65 g, and the lowest absolute weight was in the 66 $mg.L^{-1}$ treatment at 1.68 g.

REFERENCES

Astuti, W. and Widyastuti, C.R. 2016. Environmentally friendly organic pesticide to eradicate vegetable plant pests. Eng. J. Technol. Appl. Learn., 14(2): 115-120.

Chandra, R.K., Bhardwaj, A.K. and Tripathi, M.K. 2021. Evaluation of triazophos induced immunotoxicity of spleen and head kidney in freshwater teleost, *Channa punctata*. Comp. Biochem. Physiol. Part C Toxicol. Pharmacol., 245(109029): 1-7.

Damayanti, M.M. and Abdulgani, N. 2013. The effect of exposure to the sub-lethal insecticide diazinon 600 EC on the rate of oxygen consumption and growth rate of tilapia fish (Oreochromis mossambicus). ITS Sci. Arts J., 2(2): 207-211.

Deyashi, M., Misra, K.K., Bhattacharya, S.S. and Chakraborty, S.B. 2016. Acute toxicity of a neem seed kernel-based biopesticide, nimbecidine plus on an edible freshwater crab, *Varuna litterata* (Fabricius, 1798). Int. J. Adv. Res. Biol. Sci., 3(10): 122-130.

Fernandes, M.N., Paulino, M.G., Sakuragui, M.M., Ramos, C.A., Pereira, C.D.S. and Henrique, H.S. 2013. Organochlorines and metals induce changes in the mitochondria-rich cells of fish gills: An integrative field study involving chemical, biochemical and morphological analyses. Aqua. Toxicol., 126: 180-190.

Fernandes, M.N. 2019. The Histology of Fishes: Gills Respiration and Ionic-Osmoregulation. CRC Press, Florida, pp. 246-266.

Georgieva, E., Yancheva, V., Stoyanova, S., Velcheva, I., Iliev, I., Vasileva, T., Bivolarski, V., Petkova, E., Laszlo, B., Nyeste, K. and Antal, L. 2021. Which is more toxic? Evaluation of the short-term toxic effects of chlorpyrifos and cypermethrin on selected biomarkers in common carp (*Cyprinus carpio*, Linnaeus 1758). Toxics, 9(6): 125.

Hadi, S. 2013. Extraction of clove flower essential oil (clove oil) using n-hexane and benzene solvents. J. Renew. Nat. Mater., 1(2): 25-30.

Hafiz, F., Prasetiyono, E. and Syaputra, D. 2018. Toxicity of herbicides

containing the active ingredient isopropylamine glyphosate on the growth of catfish seeds (Clarias gariepinus Burchell, 1822). Oceanol. Limnol. Eng., 3(3): 235-244..

Hardi, E.H., Pebrianto, C.A. and Saptiani G. 2014. Toxicity of extracellular and intracellular product of *Pseudomonas* sp. in Tilapia (*Oreochromis niloticus*). J. Veteriner, 15(3): 312-322.

Ihsan, T., Edwin, T. and Yanti, R.D. 2019. The effect of sublethal exposure of chlorpyrifos to Nile tilapia (*Oreochromis niloticus*): A case study of Twin Lakes of West Sumatra, Indonesia. Nat. Environ. Pollut. Technol., 18(4): 1399-1403.

Ihsan, T., Edwin, T., Paramita, D. and Frimeli, N. 2021. The effect of chlorpyrifos exposure on carp fish at Twin Lakes of West Sumatra Indonesia. IOP Conf. Ser. Earth Environ. Sci., 623(1): 012002.

Ikeda, T. 1970. Relationship between Respiration Rate and Body Size in Marine Plankton Animals as a Function of the Temperature of Habitat. Hokkaido University, Hokkaido, Japan.

Jannah, W. and Yusnita. 2018. Acute toxicity test (LC50) of herbicide with the active ingredient paraquat dichloride against tilapia (Oreochromis niloticus Trewavas) in experimental tanks. J. Indon. Educ., 1(2): 44-50.

Jiao, W., Han, Q., Xu, Y., Jiang, H., Xing, H. and Teng, X. 2019. Impaired immune function and structural integrity in the gills of common carp (*Cyprinus carpio* L.) caused by chlorpyrifos exposure through oxidative stress and apoptosis. Fish Shellfish Immunol., 86: 239-245.

Kinasih, I., Supriyatna, A. and Rusputa, R.N. 2013. Toxicity test of babadotan leaf extract (*Ageratum conyzoides* Linn) on common carp (*Cyprinus carpio* Linn.) as a non-target organism. J. Istek., 7: 121-32.

Lestari, E., Setyawati, T.R. and Yanti, A.H. 2019. Hematological profile of snakehead fish (Channa striata Bloch, 1793). J. Protobiont., 8(2): 1-7.

Li, X., Liu, L., Zhang, Y., Fang, Q., Li, Y. and Li, Y. 2013. Toxic effects of chlorpyrifos on lysozyme activities, the contents of complement C_3 and IgM, and IgM and complement C_3 expressions in common carp (*Cyprinus carpio* L.). Chemosphere, 93(2): 428-433.

Mason, C.F. 1979. Biology of Fresh Water Pollution. Longman, London.

Matofani, A.S., Hastuti, S. and Basuki, F. 2013. Blood profile of tilapia kunti (*Oreochromis niloticus*) injected by *Streptococcus agalactiae* with different density. J. Aquacul. Manag. Technol., 2(2): 64-72.

Mishra, A. and Devi, Y. 2014. Histopathological alterations in the brain (optic tectum) of the freshwater teleost *Channa punctatus* in response to acute and subchronic exposure to the pesticide chlorpyrifos. Acta Histochem., 116(1): 176-181.

Pramleonita, M., Yuliani, N., Arizal, R. and Wardoyo, S.E. 2018. Physical and chemical parameters of water pond for black Nile tilapia fish (*Oreochromis niloticus*). J. Sains Nat. Univ. Nusa Bangsa, 8(1): 24-34.

Prijono, D. 1999. Prospek dan Strategi Pemanfaatan Insektisida Alami dalam PHT. Pusat Kajian Pengendalian Hama Terpadu. Institut Pertanian Bogor. Bogor.

Radiopoetra. 1996. Kualitas Air untuk Ikan Hias Air Tawar. Proyek Buku Terpadu. Jakarta.

Reverter, M., Tapissier-Bontemps, N., Lecchini, D., Banaigs, B. and Sasal, P. 2018. Biological and ecological roles of external fish mucus: A review. Fishes, 3(41): 1-19.

Royan, F., Rejeki, S. and Haditomo, AH.C. 2014. The effects of different salinity on blood profile parameters of tilapia (*Oreochromis niloticus*). J. Aquacul. Manag. Technol., 3(2): 109-117.

Santoso, H.B., Suhartono, E., Yunita, R. and Biyatmoko, D. 2020. Epidermal mucus as a potential biological matrix for fish health analysis. Egypt. J. Aqua. Biol. Fish., 24(6): 361-382.

Sellamuthu, R. 2014. Eugenol. Encyclop Toxicol., 2: 539-541.

Shah, Z.U. and Parveen, S. 2020. A Review on pesticide pollution in the aquatic ecosystem and a review on pesticide pollution in aquatic ecosystems and probable adverse effects on fish. Pollution Research, 39(2): 309-321.

Sibagariang, D.I.S., Pratiwi, I.E., Saidah, M. and Hafriliza, A. 2020. Pola pertumbuhan ikan nila (*Oreochromis niloticus*) hasil budidaya masyarakat di Desa Bangun Sari Baru Kecamatan Tanjung Morawa. J. Jeumpa, 7(2): 443-449.

Singh, N.N. and Srivastava, A.K. 2010. Hematological parameters as bioindicators of insecticide exposure in teleosts. Ecotoxicology, 19: 838-854.

Suryadi, I.B.B., Bari, I.N. and Lal, T.M. 2021. Sublethal effects of fungicide *Bacillus amyloliquefaciens* on tilapia (*Oreochromis niloticus*) and common carp (*Cyprinus carpio*) fingerlings. J. Akuak. Rawa Indon., 9(2): 185-199.

Uchenna, U.B., Uka, A. and Obiahu, O.H. 2022. The impact of sub-lethal concentrations of glyphosate on growth and haematology of African catfish under aquatic ecological micro-climate. Environ. Chem. Ecotoxicol., 4: 164-170.

Wardhana, A.H. and Wijayam, V. 2015. Biolarvacidal test of essential oil of wangi root (*Vetiveria ziznoides*) and nilam leaf (*Pogostemon cablin*) against larvae causing myiasis, *Chrysomya bezziana*. Animal Husband. Veter. Technol., 11: 408-415.

Wedemeyer, G.A. and Yasutake, W.T. 1977. Clinical Methods for the Assessment of the Effect of Environmental Stress on Fish Health. US Fish and Wildlife Service, NY, pp. 89.

Wiratno, S. and Trisawa, I.M. 2013. Research progress, formulation, and utilization of botanical pesticides. J. Litbang Pertan., 32(4): 150-155.

Yancheva, V., Georgieva, E., Velcheva, I., Iliev, I., Stoyanova, S., Vasileva, T., Bivolarski, V., Todorova-Bambaldokova, D., Zulkipli, N., Antal, L. and Nyeste, K. 2022. Assessment of the exposure of two pesticides on common carp (*Cyprinus carpio* Linnaeus, 1758): are the prolonged biomarker responses adaptive or destructive? Comp. Biochem. Physiol. Part C Toxicol. Pharmacol., 261: 109446.

Yang, C., Lim, W. and Song, G. 2021. Immunotoxicological effects of insecticides in exposed fishes. Comp. Biochem. Physiol. Part C Toxicol. Pharmacol., 247: 109064.

Nature Environment and Pollution Technology
An International Quarterly Scientific Journal

p-ISSN: 0972-6268
(Print copies up to 2016)
e-ISSN: 2395-3454

Vol. 23 | No. 1 | pp. 111-124 | 2024

Original Research Paper

https://doi.org/10.46488/NEPT.2024.v23i01.008

Open Access Journal

Ecological Regeneration of Wetland: Case Study of Kanwar Lake, Begusarai

Sameen Fatma† and Md. Danish
Department of Architecture and Planning, National Institute of Technology, Patna-800005, Bihar, India
†Corresponding author: Sameen Fatma; sameenf.phd22.ar@nitp.ac.in

Nat. Env. & Poll. Tech.
Website: www.neptjournal.com

Received: 07-05-2023
Revised: 05-07-2023
Accepted: 14-07-2023

Key Words:
Pollution
Industrial development
Encroachment
Water quality
Waste disposal

ABSTRACT

The wetlands are the partially water-submerged environments that are highly productive, and support fauna and flora species in significant numbers that are dependent for their survival on the organic production of wetlands. Kanwar Lake is situated about 22 kilometers to the northwest of Begusarai. The Gandak River, a tributary of the Ganges, meanders across the area, creating the largest oxbow lake in Asia. It is a natural body of water that is significant on many different levels, including ecological, floral, faunal, geomorphological, and zoological. In 1989, the state government of Bihar designated Kanwar as a protected area for avian species. It has been considered a Ramsar site since 1987, but the wetland was not one of the 13 designated sites. In 1984, the lake's area was 6,786 hectares (ha), but by 2004, it had shrunk to 6,043.825 ha. Only 2,032 hectares remained of the original lake area by 2012. Wealthy farmers and locals have rapidly colonized the lake bed. Lake biodiversity has declined as weeds have grown across the wetland. Widespread deforestation, overgrazing, unsustainable agricultural methods and over-exploitation of biomass for wood, fodder, and timber have stripped the land of its natural vegetative cover and exacerbated erosion. The research deals with the ecological study of the area and how urbanization has caused impacts on it. It focuses on how this has caused the deterioration of the lake and the measures for restoring the lake ecology, safeguarding the trend of urbanization. After analyzing the major key issues and analyzing the issues at the edge of the lake and around the Manjhaul, some of the major findings conclude that there is a need for stormwater management of the whole city, restoration of Kanwar wetland, and industrial control around the lake.

INTRODUCTION

The wetlands are environments that are highly productive, and support fauna and flora species in significant numbers that are dependent for their survival on the organic production of wetlands (Desta et al. 2012). These wetlands, which were earlier used for hunting and fishing, are taken as wastelands and are used for residential, industrial development, and agricultural land by draining and filling (Patrick 1994). Despite having great ecological importance, they are continuing to be degraded, and the main reason is anthropogenic activities (Johnson 2012). These are vulnerable and fragile ecosystems that are in alarming condition and are extinguished because of intensive agricultural and industrial practices (Gattenlöhner et al. 2004). Reviving the wetland will include the functions of re-establishment and natural site reconstruction, which have been degraded and are losing their identity as vital ecosystems (Johnson 2012).

With a surface area of 67.37 km^2 and a distance of 22 km from Begusarai, Kanwar Lake in Bihar is Asia's largest freshwater oxbow lake. The Gandak River, a tributary of the Ganges, meanders across the area, creating the largest oxbow lake in Asia (Sharma 1993). It is approximately three times the size of the Bharatpur Sanctuary. It is an important, extremely ecological, floral, faunal, geomorphological, and natural water body. On Tuesday, June 20, 1989, the state government of Bihar designated Kanwar as a protected area for avian species (Singh et al. 2021). It has been considered a Ramsar site since 1987, but the wetland was not one of the 13 designated as having international significance in 2002. According to a 2007 study (Ambastha et al. 2007), in recent years, the Ramsar Convention has come to govern internationally significant wetlands (Chandra et al. 2023). Every year, birds from all across Central Asia and the Himalayan areas come here to spend the winter. The marsh also provides a large number of plant and animal life throughout the year (Prasad 2016). The government has designated 15,000 acres as a wetland in the region. The lake's depth and surface area expand during the rainy season thanks to runoff from neighboring communities, including Jaimanglagarh, Rajour, Parora, Narainpur, Sonbasa, Kumbhi, and others. Still, the lake significantly decreases in size during the dry seasons of winter and summer. In 1984, the lake's area was 6,786 hectares (ha), but by 2004, it had shrunk

to 6,043.825 ha. As of 2012, the lake's area was down to about 2,032 hectares.

Kanwar Lake provides a haven for numerous endangered, fragile, and near-threatened species, including the Oriental white-backed vulture (Kumar 2013). Up until the 1980s, the lake served as a major stopover for migrating birds. However, poachers and trappers have taken control in modern times, drastically reducing bird populations. Birds in an area may be in danger from poisonous chemicals used in farming. To prevent more land transactions, this wetland is essential. Large amounts of silt washing into the lake have reduced its depth. Each year, about 3.8 centimeters of silt are added to the lake. Lake biodiversity has declined as weeds have grown across the wetland. Widespread deforestation, overgrazing, unsustainable agricultural methods, and over-exploitation of biomass for wood, fodder, and timber have stripped the land of its natural vegetative cover and exacerbated erosion. Wealthy farmers and locals have rapidly colonized the lake bed (Kumar & Vardhan Pandey 2017). The lake is bordered on the west and south by the Burigandak River and on the north and east by the N.E. Railway line from Samastipur to Khagaria. The lake was created by a cut in the Burigandak River's meander, which occurred in the vast plains of a deep alluvial region. The average rainfall is 1000-1800 mm. The island of Jai Manglagadh, also known as Monkey Island, is located in the southeast corner of the lake and covers about 34 square kilometers. Fig. 1 depicts the lake area and the adjoining island Jai Manglagadh, and the nearby subdivision of Manjhaul.

The historical significance of the Jaimangla temple on the Kanwar lake's bank is well known. A number of artifacts from the distant past have been discovered in the region. Artifacts from the Post Suguna period, including terracotta, glazed ware, an iron sickle, and more, were unearthed. Many coins from the Tuglak period were also unearthed there. Not only have these artifacts been found in the fort town, but so have a large number of cannon balls. An ancient temple dedicated to the goddess "Jaimangal" (also known as Durga or Bhavani) is located within the walls of the fort of the same name. Because of this, the hill known as "Jaimangal Temple and Jaimangal Fort" on the shore of the lake is rich in history. Several significant archaeological artifacts have been discovered in the area, including a Northern Blackware vessel, a terracotta head, and pieces of idols carved from Cherts and Basalts. In addition, the earthen seals discovered at the sites indicated that they belonged to the Gupta period, which ruled from approximately 400 to 600 AD. Several archaeological finds, including Northern Black ware,

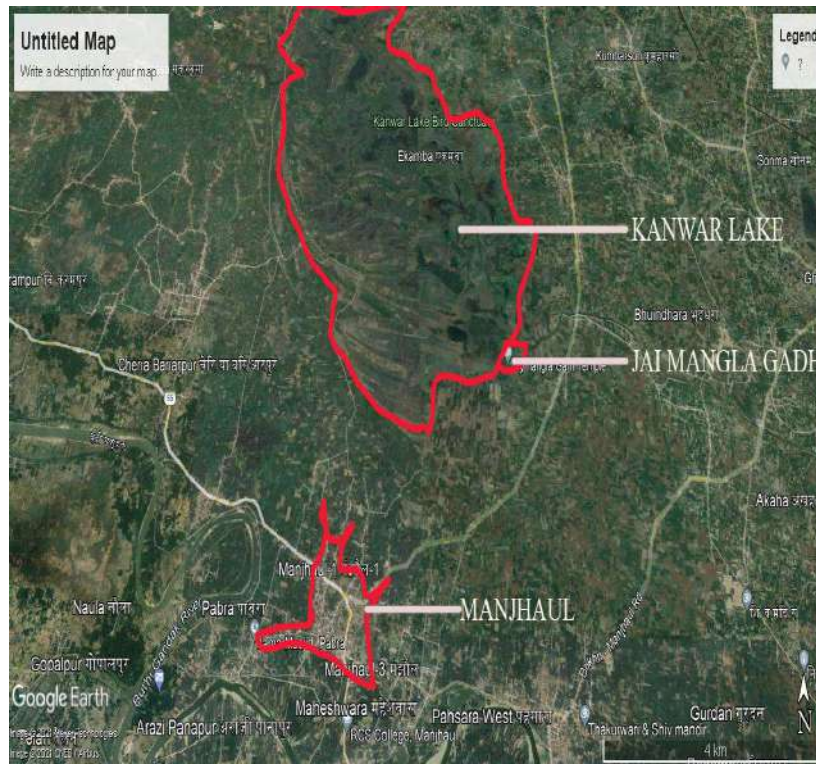

(Source: Google Earth).

Fig. 1: Settlements of Jaimanglagadh, Manjhaul subdivision, and Kanwar lake.

Terracotta heads, and fragments of idols made of Cherts and Basalts, have been discovered in the region. These structures belonged to the Gupta dynasty when they were constructed (about 400-600 AD; the earthen seal confirms this).

MATERIALS AND METHODS

The case of Kanwar Lake was taken, and a detailed analysis was done, finding the issues that are leading to its degradation. The analysis is done with the identification of wetland functions and values and the working of the wetland. Further, with the data collection and site study, which included understanding the conditions of the place, sampling, interviews, surveys, observations, maps were generated, and the urban layer analysis and morphological layer analysis were done to identify the current situation on the ground in the year 2021. Further, the issues have been identified with different tools like Chord diagrams, cause and effect diagrams, issue mapping, and issue impact matrix. Further, a vision is provided with proposals for the regeneration.

RESULTS

Ecological Evolution and Shrinking of Kanwar Lake

It has shrunk by 66% since 2004, with just 30% of the initial coverage area remaining, as measured in 1984. Loss of natural vegetation cover due to deforestation, overgrazing, unsustainable agricultural practices and excessive biomass harvesting for fuel, feed, and lumber. Due to the widespread use of chemical fertilizers, pesticides and herbicides in nearby farm fields, the wetland's water quality has drastically declined. Untargeted hunting has historically harmed the winter vacationing population. The wetland currently has no legal boundaries. This creates a rivalry between the two groups, the Sahnis, and the farmers. Sahnis depend on fishing for a living, and they want the wetland to be flooded all year so they can fish all year.

The ecological history of the Kanwar Lake is as follows:

1801- Village survey

1895- Verdict of Calcutta High Court for fishing and trapping rights

1962- Cleaning of drainage canal

1965-66- More cultivation and more crops due to cleaning of the drainage canal. More land came out of submergence, but the canal silted soon

1972- Bird capturing prohibited

1986- Fishing, buying, selling, and poaching on land was banned under the Wildlife Protection Act of 1972

1987- Flood: A dam on river Bagmati collapsed upstream. The flood again cleaned the drainage canal.

1989- 20 June - declaration of Kanwar Lake bird sanctuary

1992-93 Survey of land after creation of Bird sanctuary

1994-95 Cleaning of weeds in the drainage canal

Biodiversity in Lake

The ecological diversity of plants, birds, fish, and some ordinary creatures in Kanwar Lake is highly rich. There have also been found about 106 macrophytes, phytoplankton and hydrophytes. Some 60 of the 106 known bird species were migratory birds, whereas the remainder were common or local. About 120 species of macrophytes are known to exist in and around the lake. Rather than some of the native trees, internal shrubs and grasses are abundantly found on the Jaimanglagarh Island with plantings of forest departments, such as Arjun (Terminalia arhuna) and Sisso (Dalbergia sissoo) (Prasad 2016). Sometimes, these trees are good for birds as they protect them. Some varieties of fish, insects, mollusks etc. are also prevalent. Although the lake region has decreased as a result of land invasions for agricultural and residential uses, which adversely affects organisms, some of them are endangered because of many human activities interfering with their life cycle.

Flora and Fauna

It has an abundance of plant and animal life, including many different kinds of Imili, Neem, Bamboo, Sohar, Babool, Sissoo, Khajur, Shirish, etc. (Prasad 2016). Fig. 2 depicts the existing flora in the area. More than 40 kinds of fish can be found in the waters of Kanwar Lake, which visitors to the Kanwar Lake Bird Sanctuary frequently spot. Reptiles such as the Indian Cobra, Indian Krait, Tortoise, Water Snake, Dhaman, and many sorts of Lizards; mammals such as the Musk Deer, Palm Squirrel, Leopard, Himalayan Black Bear, Common Mongoose, Rhesus Macaque, Indian Fox, Barking Deer, Jackal, Nilgai (Prasad 2016) and more. As depicted in Fig. 3 beautiful birds such as the Crested Serpent Eagle, Yellow Throated Sparrow, Purple Rumped Sunbird, Magpie Robin, Tailor Bird, Red Wattled Lapwing, Black Winged Kite, Long Billed Vulture, Black Drongo, Jungle Babbler, Swallow, Oriental White-Backed Vulture, Painted Snipe, Bush Lark, Spotted Owlet, Palm Civet, and others can be spotted here.

Usage of Lake

Lakes are an extremely valuable habitat for both humans and animals. Even though most wetland-related activities are shared rather evenly among different communities, some

(Source: Author)

Fig. 2: Image showing the different types of Flora present at the lake.

(Source: Author)

Fig. 3: Image showing the different types of fauna present at the lake.

do differ slightly. These communities depend heavily on agriculture and livestock for subsistence as shown in Fig. 4, with a range of 21.4–43.3 percent of annual income going towards fodder sourced from the Kanwar Lake. This means that the people of the villages in the vicinity of Kanwar Lake use the wetland system there mostly to grow feed for their animals. Grazing animals are common in these regions because they were once utilized to cultivate fodder.

Conversely, fish are plentiful in a wetland ecosystem. Again, a sizeable percentage of the locals use this marsh for fishing (13.3-25.0%, to be exact) as shown in Fig. 5. The majority of homes also participate in plant processing and other derivatives businesses in addition to these mainstay industries. Khajahnpur, closest to the Kanwar wetland system, has the highest concentration of this kind of activity, but it is widespread throughout the region. The settlements almost equally share in the use of Kanwar Lake's wetland environment. The obvious inference is that the majority of the local population relies on agricultural and animal processing. As a result, the Kanwar Lake wetland system is highly valued in the area. The locals of Jai Mangla Gadh island also utilize this body of water to

(Source: Author)

Fig. 4: Image denoting the agricultural activity in the lake.

(Source: Author)

Fig. 5: Image denoting the fishing activity in the lake.

clean their dishes and laundry. The villagers use the lake as a washroom and for drinking water. The sewage waste has been disposed of in the lake of the sub-urban settlement of Manjhaul.

DISCUSSION

Functions and Values of Kanwar Lake

Functions: Relying on breeding and migrating birds and mammals for food, water, and shelter, production of sugarcane, rice and mustard, surface water nitrogen and phosphorus removal via biogeochemical cycling. Instead of releasing it into the atmosphere as carbon dioxide, which would have a warming effect on the planet's temperatures, peat bogs sequester carbon inside their line and preserve (peat) plant biomass. Growth of primary producers and consumers. Hydrological cycling revives stores and releases water in various ways.

Values: Recreational value for bird watching, photography and hunting fish, Societal value as habitats for fish, wildlife and plants. Primary habitats of wetlands depend on them for survival. Seasonal inhabitants of food, water and cover are plentiful. Cultural value as it has a temple on the island with great significance from the Gupta dynasty. Economic value for commercial fish catch and crops like rice and sugarcane. Too much surface runoff carrying pollutants and

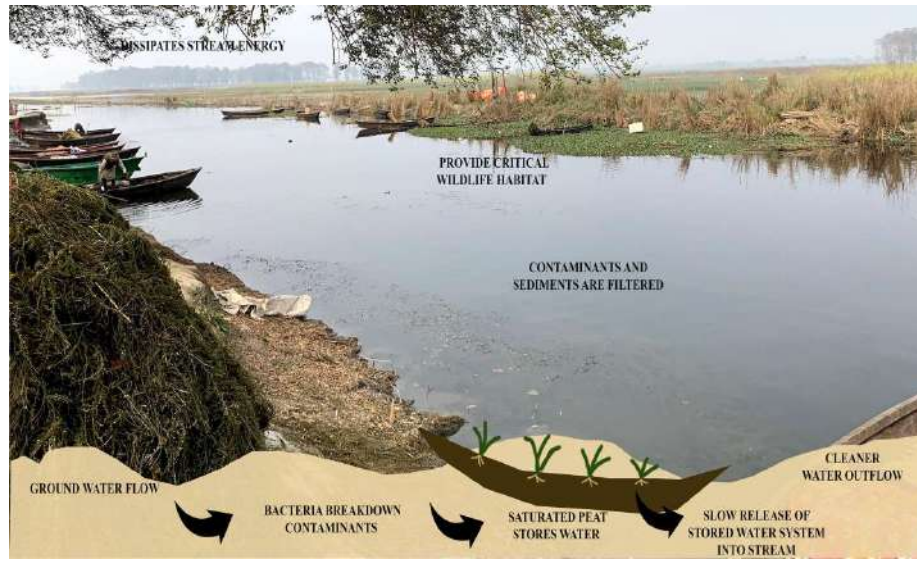

(Source: Author)

Fig. 6: Image showing the Working of Kanwar wetland as its disruption is the cause of degradation.

sediments degrading the lake. Educational value as diversity for research opportunities.

Working at Kanwar Wetland

The wetland values have dissipating energy, which lessens the speed of the stream. It acts as a natural sponge that recharges groundwater, controls erosion, absorbs water, provides wildlife habitat, breaks contaminants, and filters it. Fig. 6 depicts the working of the wetland where due to the lost connection from the canal, the freshwater is not released and thus hampers the working of the wetland.

Morphological Study

In land cover and land use, the cropland increased from 2005 to 2016 on a larger scale, the wetland has been decreasing with a decrease in fallow land and the plantation is increasing trend. Fig. 7 depicts the existing built use of sub-division Manjhaul which is majorly residential, as about 95% is residential. The only commercial buildings are found on the primary road and this road has only commercial and mixed-use buildings on it. Few mixed-use and commercial buildings can be found in the Manjhaul market lane. Some public semi-public buildings can be found throughout the division. All the villages that surround the Kanwar Lake including the Jai Manglagadh Island are residential. Medium-rise buildings can be found mostly in the Manjhaul settlement, and a good amount of low-rise buildings are also found. Mostly low-rise buildings are found in the adjoining villages and few medium-rise buildings can be found and the Jai Manglagadh Island has low-rise buildings. Talking about the road hierarchy, three types of roads are found: the primary road, i.e. is. 10-15m, the secondary road, i.e., 4-6m, and the tertiary road, i.e., 1.5-2.5m wide. The whole site has 73% unbuilt area and 27% built-up area. On the site, two types of open spaces are found, which are the green areas and the agricultural land. A good amount of green areas are found in the Manjhaul settlement and green areas and a good amount of agricultural land are found in the Kanwar Lake.

Habitat of Birds

Five kinds of habitat are found in the Kanwar Lake which are depicted in Fig. 8.

1. **Open water:** The Podicipedidae, Phalacrocoracidae, Threskiornithidae, Anatidae, Rallidae, Jacanidae, Strigidae and Alcedinidae are habitats for birds found in the open water.
2. **Floating macrophytic vegetation:** Phalacrocoracidae, Threskiornithidae, Rallidae, Laridae, Alcedinidae and Sturnidae are the habitats of birds found in floating macrophytic vegetation.
3. **Phragmites and marginal emergent plants:** Aradeidae, Ciconidae, Threskiornithidae, Anatidae, Jacanidae, Haemantopidae, Rostratulidae, Recurvirostridae, Glareolidae and Laridae are the habitats of birds found in phragmites and marginal emergent plants.
4. **Marginal terrestrial vegetation:** Aradeidae, Accipetridae, Phasnidae, Apodidae, Dicruridae, Upupidae and Sturnidae are the habitats of birds found in marginal terrestrial vegetation.

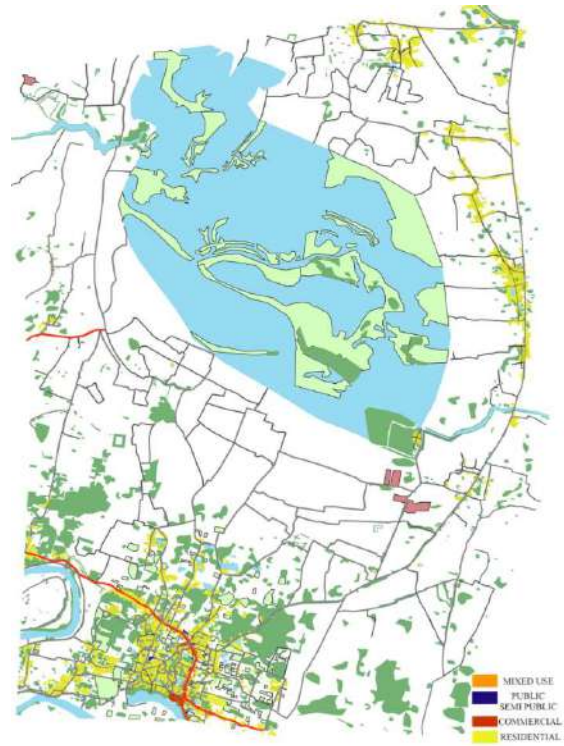

(Source: Author)

Fig. 7: Map showing the built use, which majorly shows the residential area.

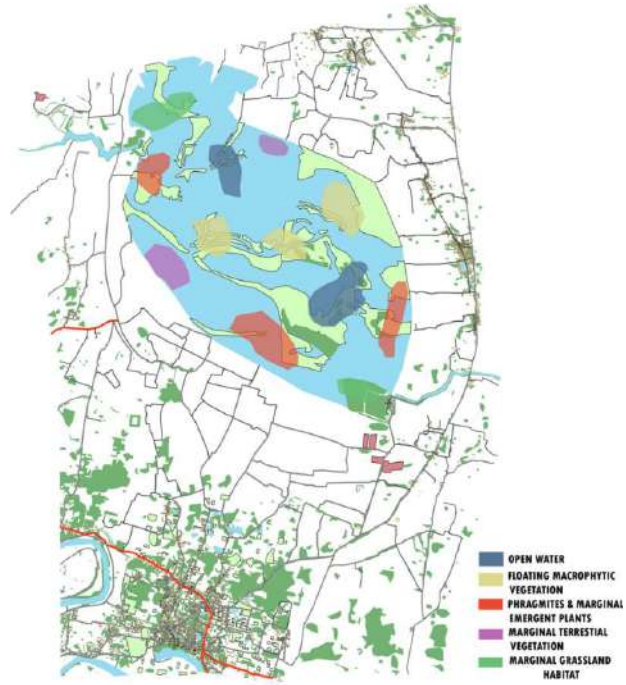

(Source: Author)

Fig. 8: Map depicting the five types of habitats in the lake.

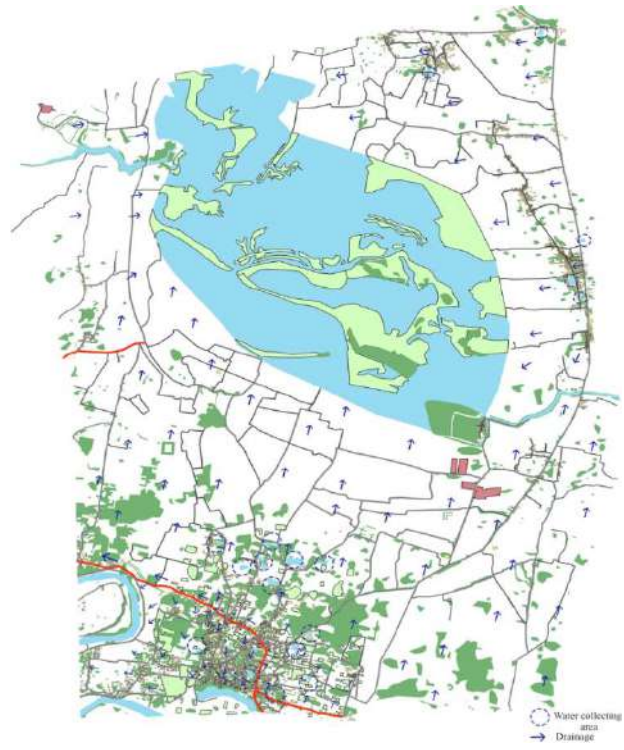

(Source: Author)

Fig. 9: Map depicting the drainage flow, which is towards the north of the lake.

5. **Marginal grassland habitat:** Aradeidae, Ciconidae, Accipetridae, Rostratulidae, Glareolidae, Apodidae, Dicruridae, Upupidae and Sturnidae are the habitats of birds found in marginal grassland habitats.

Drainage of the City

The drainage of the city is towards the north and goes into Kanwar Lake as depicted in Fig. 9. The Manjhaul settlement has a partial drainage system on the primary road but lacks in the other parts and all the overflow drainage goes directly into the Kanwar Lake. The ponds are present in the city and all the overflow waters are collected in those ponds and then overflow into the Kanwar Lake.

Activities in and Around the Lake

Fig. 10 depicts the detailed activities in and around the lake while showcasing the depth of the lake. The crops found around the lake area are sugarcane, rice (paddy crop), and mustard, but only sugarcane and rice plantations can be found in the lake area. Fishing activities can be found in some front parts of the lake area, while the fishermen are found living in the Jai Manglagadh area and the adjacent Rajouri village. The grazing grounds are found next to the lake, as the villagers are using it for their cattle grazing. The farmers who practice agriculture live in the nearby villages, and industries are found near the lake, which disposes of waste in the lake. At the Jai Manglagadh island, the Kabar Mahotsav is organized every year for the upliftment of the local people to showcase their talent and discuss the issues related to Kanwar Lake. The market area is far away from the lake and is the main Manjaul market, which is 7 km away from the lake. The water depth of the lake varies from 10 feet to 6 feet. The central part of the lake has the highest water depth of 10 feet and the starting and ending parts has the lowest water depth.

Issues Leading to the Dying of the Lake

The issues that are leading to the deterioration and shrinking of the lake are the presence of agricultural activity happening in the lake area and the dead remains of the left-over plants that are decayed in the water. The people have made embankments on the canal to restrict the flow of water so that they can practice fishing activity in the lake, and this closing of canals leads to floods in the nearby areas. Kanwar Lake has a good quantity of snails in the water and the shells of snails are thrown at the side of the lake as waste, leading to deterioration of the side and water quality. The waste from the sub-division Manjahul and Jai Mangla Gadh is thrown at the lake site,

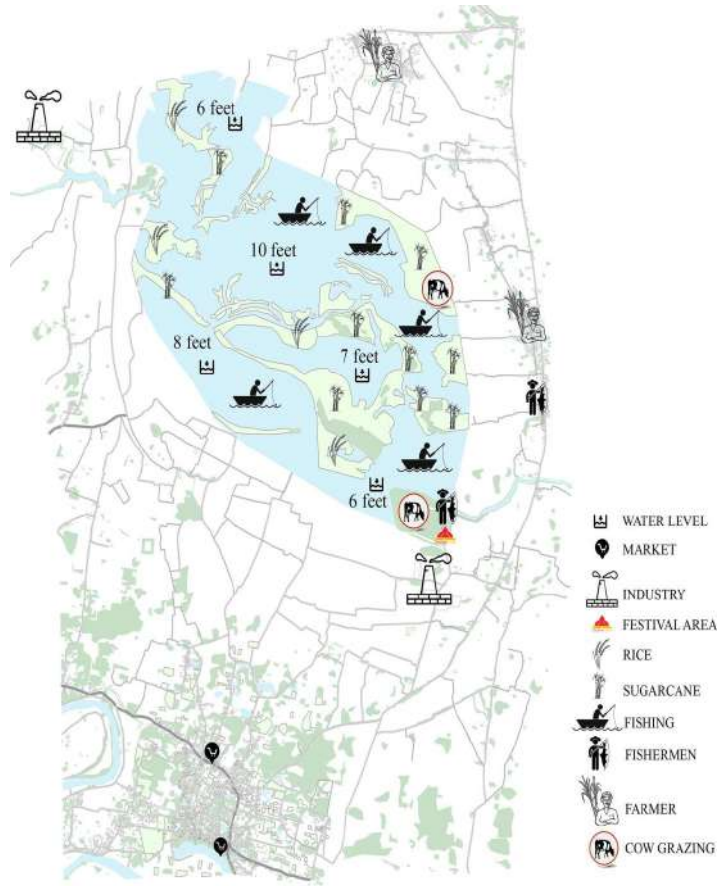

(Source: Author)

Fig. 10: Map depicting the different activities taking place in and around the lake.

deteriorating the water quality. The dead remains of the plants can be found floating in the lake, which is deteriorating the water of the lake. The lake is used as a washroom by the nearby villagers and for washing clothes, utensils, and themselves. Overfishing activity has led to the loss of biodiversity, and the agriculture and water quality have led to the loss of habitats. The overgrazing on the sides of the lake led to the loss of habitats. There are factories present on the edges of the lake surface whose remains are discharged into the lake, polluting and leading to its shrinkage. The waste generated by the tourists at the Jai Mangla Gadh temple area is directly thrown into the lake, and because of this, water cannot be found in the area and the lake is degrading. The eutrophication is taking place in the river. The sewage wastewater of the sub-urban settlement Manjhaul and Jai Mangla Gadh village is flushed into the lake, hence leading to its contamination. The issues are mapped in the Fig. 11.

The major issues found in the area are industrial development, agriculture, human disturbance, pollution, weather and climate change, and trapping and hunting.

Fig. 12 depicts the detailed issues found in the area which are threatening the lake. Industrial development includes extraction of soil from the lake, brick kiln and their wastes dumped in the lake and alcohol production discharge. Agriculture includes the deterioration of water quality, extinction of birds and decaying of remains of crop cultivated. The human disturbance includes embankments by fishermen, boating and encroachment of land for cultivation and tourism at Jai Manglagadh Island. Pollution includes sewage disposal from the village, Sewage flow of settlement Manjhaul, dumping of waste, washing of clothes, bathing, and Agriculture waste. Weather and climate change which includes shrinking of lakes, shrinking of habitats and floods. Trapping and hunting, which includes fishing and hunting of migratory birds.

Fig. 13 depicts the factors by which the habitats were affected like eutrophication, siltation, degraded water quality, etc. which caused the changes in habitats leading to habitat shrinkage.

The below-mentioned causes and effects have been

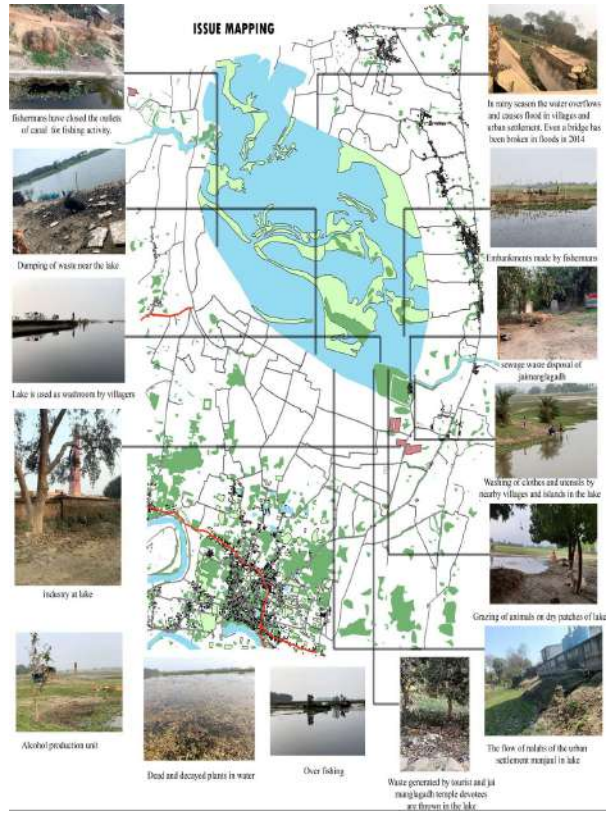

Fig. 11: Issues mapping.

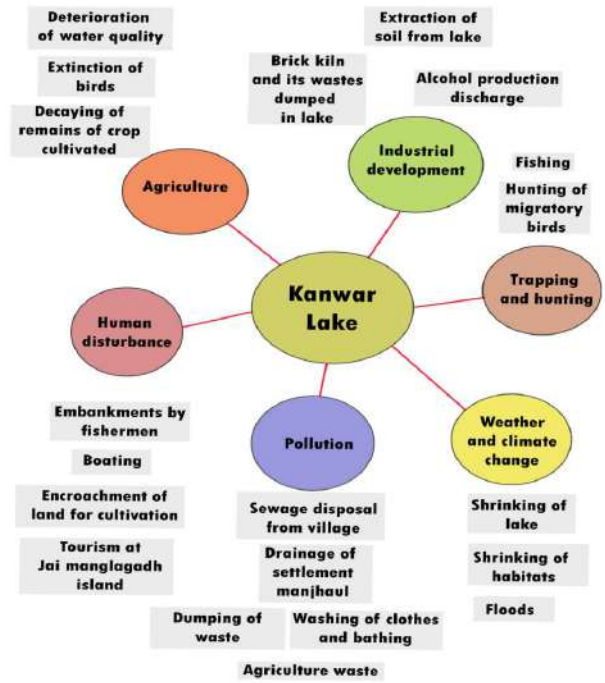

Fig. 12: Image showing the major issues threatening the lake.

identified from the cause-and-effect diagram showcased in the Figs. 14, 15 and 16.

The lake was shrinking because of the disposal of waste, encroachment, use of agricultural pesticides and extraction of soil. The changing of habitats was because of eutrophication, human presence, decayed vegetation, reduced water levels, hunting, and encroachment. The shrinking of habitats was because of water quality, heavy siltation, extensive deforestation, encroachment, unsustainable agriculture practices and reduced water quality. The canal dried because the inlets were blocked, intentionally choking the canals by fishermen's embankments and accumulation of sand. There is no development in the area because of lack of leadership, no interest in government, land conflict between landlord and fishermen, and dispute over ownership. Degradation of lakes is because of the disposal of sewage, fishing, decaying of crops, extraction of soil, embankments and encroachments, and industrial discharge.

The water quality results in the shrinkage of habitats, shrinkage of lakes, change in habitats, loss of biodiversity, loss of migratory birds, extinction of birds and loss of wetlands and more marshy land. The pollution results in water quality degradation, extinction of birds, health disorders, and loss of biodiversity. Industrial development leads to the shrinkage of lakes and water pollution. Agriculture activity leads to shrinkage, change in habitats, loss of Lake Biodiversity, and water pollution. Human intervention like grazing leads to the degradation of shallow water habitats, and waste disposal leads

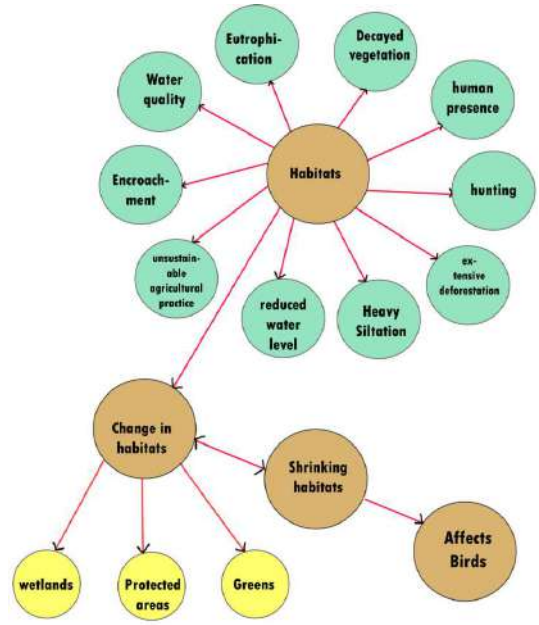

(Source: Author)

Fig. 13: Image showing the reasons for the change in habitats and its effect.

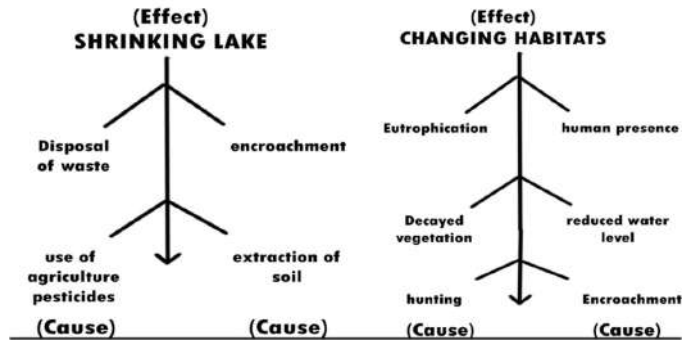

Fig. 14: Cause and effect of shrinking of the lake and changing of habitats.

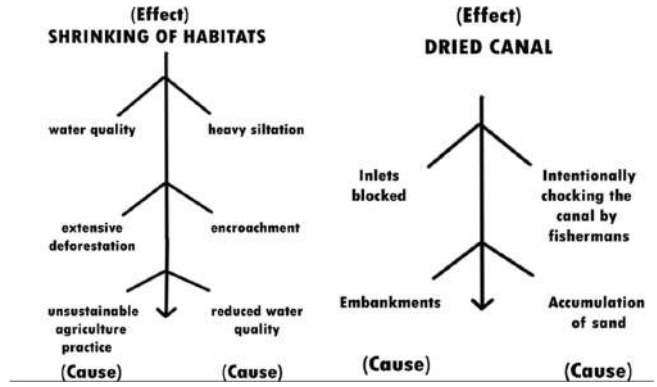

Fig. 15: Cause and effect of shrinking of habitats and drying of the canal.

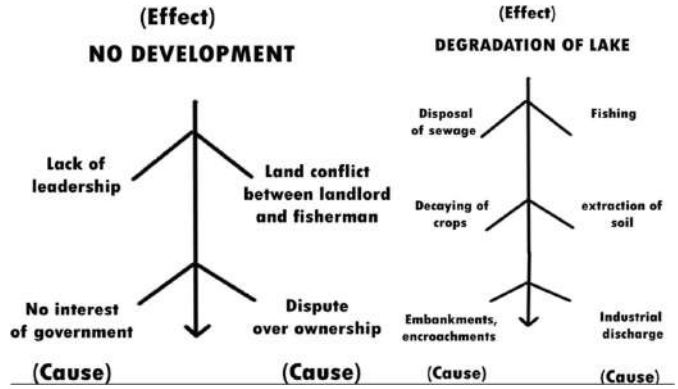

Fig. 16: Cause and effect of no development taking place and degradation of lake.

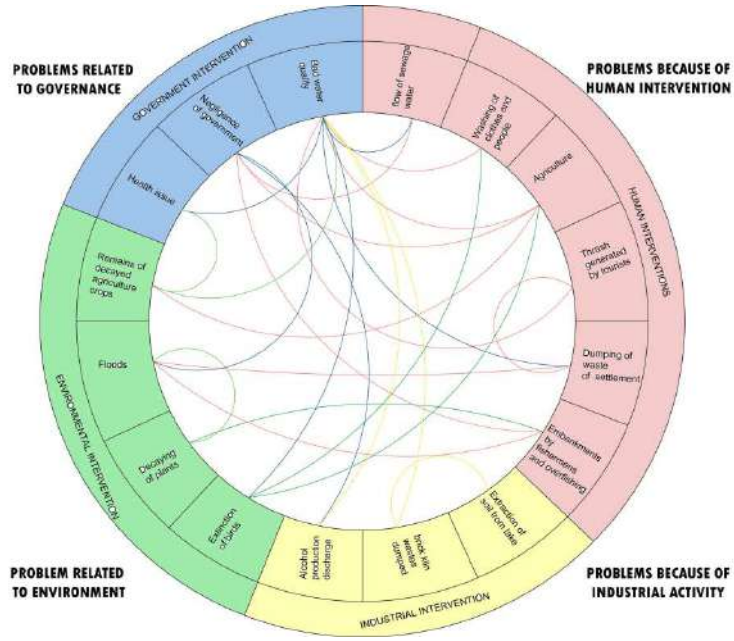

Fig. 17: Chord diagram depicting the issues which are majorly human intervention, government negligence, environmental and industrial intervention.

Table 1: Issues and their impact in the lake.

Issues	Impact
Water quality	Shrinkage of habitat
	Shrinkage of lake
	Change in habitats
	Loss of biodiversity
	Loss of migratory birds
	Extinction of birds
	Loss of wetland and more marshy land
Pollution	water quality degradation
	Extinction of birds
	Health disorders
	Loss of biodiversity
Industrial development	Shrinkage of lake
	Water pollution
Agriculture	Shrinkage of lake
	Change in habitats
	Loss of lake biodiversity
	Water pollution
Human intervention	
Grazing	Degradation of shallow water habitats
Waste disposal	Degradation of water quality and weed infestation
Fishing	Floods
	Contamination of water
	Trapping
	Degradation of lake
Encroachment	Floods
	Shrinkage of lake
	Change in habitats

to the degradation of water quality and weed infestation. The major issues were identified by linking all the listed problems in the form of a chord diagram by dividing the issues of the area into four broader sections as mentioned in Fig. 17. A detailed issue impact matrix explains the issues and the impacts they had on the lake and the surrounding area showcased in the Table 1.

CONCLUSIONS

Hence, the detailed analysis of Kanwar Lake has been studied with respect to morphology, ecology, terms of values and functions, etc, and various issues have been identified with the help of different tools. The major issues that came across were because of agriculture, human disturbances, industrial development, pollution, trapping and hunting, and weather and climate change. These issues led to degraded water quality and caused the shrinking of the lake, shrinking of habitats in the lake, change in habitats, loss in biodiversity, loss of migratory birds, extinction of birds, health disorders, etc. Agriculture and fishing activity was very prominent and were one of the major reasons for the dying of the lake. The sewage flow of the urban settlement Manjhaul flows in the lake, which degrades the water quality.

After analyzing the major key issues and analyzing the issues at the edge of the lake and around the Manjhaul, some of the major findings conclude there is a need for stormwater management of the whole city, restoration of Kanwar wetland, and industrial control around the lake. Some recommendations are provided below with the vision to conserve and revive the lake ecology by providing better infrastructure and livelihood to upgrade the economy and tourism of the region.

1. Decontamination of the water and protection of wetlands by regulating the use of water quality standards and revival of the canal for the functioning of the watershed and minimizing flooding.
2. Regulation of industrial development around the lake through policy and master plan
3. Demarcation of sanctuary area and regulation of land use practice and restoration of hydrological connectivity and creation of buffer zone for eco-restoration.
4. Improvement of the human habitations like drinking water, sanitation and solid waste management with proper drainage channels for settlements and Promotion of ecological and cultural tourism with proper waste management
5. Community involvement and active participation for restoration and Promotion and recognition of economic values of wetland ecosystem services and biodiversity and enforcement of land control regulation.
6. Buffer zone to be provided across the lake so that filtered water gets into the lake with the provision of cropland to reduce the agricultural activity in the lake.
7. Further, for recreation and water purification, Wetland Parks and floating wetlands should be provided. For the development of the area, community centers and restaurants should be provided for tourists.

ACKNOWLEDGMENT

We are also thankful to the Ministry of Education, Government of India, for generous funding to the Department of Architecture and Planning, National Institute of Technology, Patna, Bihar.

REFERENCES

Ambastha, K., Hussain, S.A. and Badola, R. 2007. Resource dependence and attitudes of local people toward conservation of Kabartal wetland: A case study from the Indo-Gangetic plains. Wetlands Ecol, Manag., 15(4): 287-302. https://doi.org/10.1007/s11273-006-9029-z

Chandra, K., Bharti, D., Kumar, S., Raghunathan, C., Gupta, D., Biswajit, A. and Chowdhury, R. 2023. Ramsar wetlands of India. Rec. Surv. India, 123(1S): 1-15. DOI: 10.26515/rzsi/v123/i1S/2023/172458

Desta, H., Lemma, B. and Fetene, A. 2012. Aspects of climate change and its associated impacts on wetland ecosystem functions: A review. J. Am. Sci., 8(10): 81.

Gattenlöhner, U., Marion, H.R. and Sabine Jantschke, E. 2004. Reviving Wetlands – Sustainable Management of Wetlands and Shallow Lakes. Global Nature Fund, Germany, pp. 1-136.

Johnson, B.A. 2012. Ecological Restoration of the Wairio Wetland, Lake Wairarapa: Water Table Relationships and Cost-Benefit Analysis of Restoration Strategies. Master Thesis. Victoria University of Wellington, Kelburn, Wellington, New Zealand, pp. 1-24

Kumar, M. 2013. Resource inventory analysis of Kabartal wetland. Int. J. Res. Hum. Social Sci., 8(1): 13-26.

Kumar, R. and Vardhan Pandey, V. 2017. Kanwar Lake: A Dying Wetland Ecosystem. International Conference on Environment and Ecology, ICCE, 27-29 March 2017, St. Xavier's College, Ranchi, Confederation of Indian Universities, New Delhi, pp. 111-127.

Patrick, W.H. 1994. From wastelands to wetlands. J. Environ. Qual., 23(5): 892-896.

Prasad, B. 2016. The World's Largest Oxbow Lake Kanwar Lake. WISA, South Asia, pp. 1-163.

Sharma, U.P. 1993. Origin, geomorphology and current trends of terrestrialisation of Kawar Lake (Begusarai), Bihar: A typical wetland system of India. SIL Proceed., 25(2): 804-810. https://doi.org/10.1080/03680770.1992.11900255

Singh, A.M., Sathya, M., Verma, S. and Agam Kumar, S.J. 2021. Assessment of anthropogenic pressure and population attitude for the conservation of Kanwar Wetland, Begusarai, India. In: Singh, P., Singh, R., Singh, V.K. and Bhadouria, R. (eds), Pollutants and Water Management, Wiley, NY, pp. 22-46.

Nature Environment and Pollution Technology
An International Quarterly Scientific Journal

p-ISSN: 0972-6268
(Print copies up to 2016)
e-ISSN: 2395-3454

Vol. 23 | No. 1 | pp. 125-137 | 2024

Original Research Paper

https://doi.org/10.46488/NEPT.2024.v23i01.009

Open Access Journal

Need for an Evolved Groundwater Justice in Rural Areas of Uttar Pradesh, India

V. S. Tari*, N. Siddiqui, D. Rathi***, N. N. Siddiqui** and D. K. Wahyuni*†**

*Department of Biology, Faculty of Science and Technology, Universitas Airlangganiversitas Airlangga, Jl. Sukarno Hatta, Surabaya, 60115, East Java, Indonesia

**Vinayaka Mission's Law School (VMLS), Chennai, India

***School of Law, CHRIST (Deemed to be University), Delhi NCR, India

†Corresponding author: D. K. Wahyuni; dwi-k-w@fst.unair.ac.id

Nat. Env. & Poll. Tech.
Website: www.neptjournal.com

Received: 11-07-2023
Revised: 25-08-2023
Accepted: 02-09-2023

Key Words:
Groundwater
Legal reform
Sustainability
Groundwater justice
Co-evolution

ABSTRACT

As groundwater is the primary element of life, countries all over the world are experimenting with legal reforms. The degree to which law reforms combine justice and sustainability is a crucial question. In response to this question, the present article focuses on a case study of Uttar Pradesh, India. Our response is based on a content analysis of the Uttar Pradesh Groundwater (Management and Regulation) Act, 2019, and the Uttar Pradesh Groundwater (Management and Regulation) Rules, 2020. Three conclusions emerged from our investigation. First, the 2019 Groundwater Act and the 2020 Draft Groundwater Rules are primarily motivated by concerns about resource sustainability, particularly in areas where the water table is steadily declining. Still, neither the 2019 Groundwater Act nor the 2020 Draft Groundwater Rules propose any proactive groundwater justice measures. Second, we suggest that some locally defined basic elements are critical in supporting sustainability and – to a lesser extent – groundwater justice. These characteristics include a community's ability to (1) recognize a crisis and show a willingness to address it; (2) establish a rule-bound community groundwater resource; (3) demonstrate leadership and a sense of community; and (4) make use of awareness, information, and knowledge. Our third conclusion is that there is a need for community practices and state-led groundwater law to co-evolve; this co-evolution has the potential to create groundwater arrangements that support both groundwater justice and sustainability.

INTRODUCTION

Water is a very crucial compound of life for survival. Our ancient philosophers believed that the entire universe is made up of five major elements, viz. Air (*Vayu*), Water (*Jal*), space (*Aakash*), Fire (*Tej*), Earth (Soil), etc (Tari 2015). Groundwater resource is hidden in pores and cracks under the ground through percolating from the earth's surface or due to geological activities like volcanic activities or sedimentation (Velis et al. 2017, Fetter 2001, CR, 2012).

However, man is the most intelligent animal on this planet, and he is always in search of the easiness of life. For that, he is continuously modifying nature in a way that he can get a better life today without thinking about its future consequences, and it is so-called "Development." In 1987, due to awareness and research in various fields, it was recommended by the Bruntland Commission Report that the development should be sustainable, i.e., "Development that meets the needs of the present without compromising the ability of future generation to meet their own needs" (Keeble 1988). As water is crucial for any development, there is a need to think about respective sustainability development goals (Tari et al. 2022, Tari & Patil, 2017b, 2017a). Groundwater sustainability can be broadly defined as the "Continuous availability of groundwater of sufficient quality and quantity for ecosystem functions and future generations" (Velis et al. 2017).

The biosphere consists of three major spheres namely lithosphere, atmosphere, and hydrosphere (Fig. 1). For development purposes, man is using all possible reservoirs from the biosphere (Tari 2015). Fig. 1 depicts that all three spheres are major reservoirs for raw materials used in the development. Out of that hydrosphere is our major concern due to the importance and vulnerability of major water resources, i.e., groundwater on the 'Earth.'

A variety of human activities, as well as natural sources, can pollute groundwater; they render it hazardous and unsuitable for human consumption. The soil can allow substances from the surface of the land to pass through

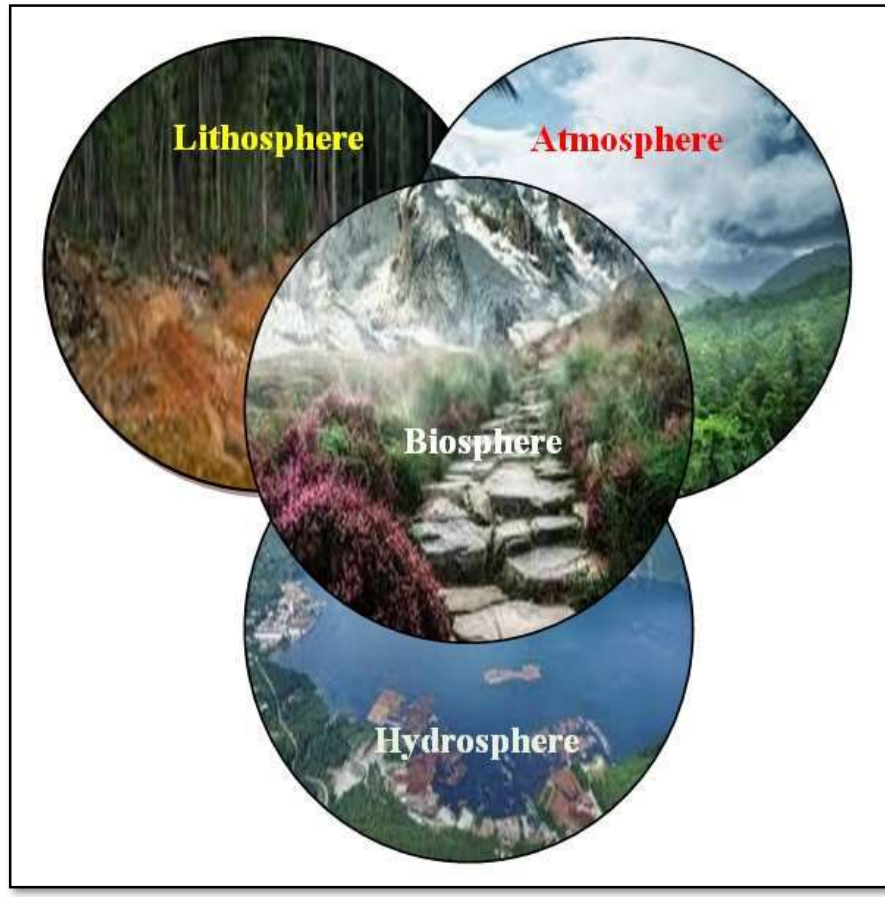

Fig. 1: Structure of biosphere.

it and end up in the groundwater. For instance, chemicals and fertilizers may enter groundwater sources. Used motor oil, hazardous materials from mining sites, and road salt may also leak into the groundwater. Furthermore, harmful compounds from underground storage tanks, leaking landfills, and untreated septic tank waste have the potential to pollute groundwater. Its depletion is very serious and needs immediate attention because groundwater is the only source of drinking water, particularly in rural areas.

GROUNDWATER: ISSUES AND CHALLENGES IN INDIA

Groundwater is prominently used as a source of drinking water for the majority of the world's population. Besides that, it also helps to provide nutrients and stabilizes relative temperature (Kløve et al. 2011). Therefore, the management of this precious resource is a major environmental concern. The movement of water under the ground is significantly slow, particularly at a speed of 0.01-10 $m.day^{-1}$ under natural conditions. The residence time (time required in storage) ranges from 10 to 1000s years (Foster 2013, Gleeson et al. 2012). The depletion of groundwater stock was considered a major indicator of water scarcity. Poor drinking water quality, a lack of water supply, deteriorated surface water systems, expensive cleaning expenses, high prices for alternative water suppliers, and/or significant health issues can all arise from groundwater contamination. The effects of polluted surface water or contaminated groundwater are frequently severe. For instance, crucial shellfish habitats have been destroyed in estuaries affected by high nitrogen levels from groundwater sources.

Groundwater contamination makes it impossible for the region to support plant, human, and animal life. Both the local population and the value of the land decline. It also has the impact of making industries that rely on groundwater for product production less stable. As a result, the impacted areas' companies would have to import water from other places, which might be expensive. Additionally, the water's low quality might cause them to shut down. In rural areas, a large portion of groundwater is going towards

irrigation. Apart from irrigation, groundwater is significantly used in other developmental sectors such as industrial, food production and security, commercial, climate change adaptation activities, recreation, hydrological carbon dioxide sequestration, hydrological resilience, health, food and energy production, and hydrological energy access (Velis et al. 2017, Gramont 2011).

Overexploitation for intensive irrigation and other developmental activities can lead to depletion in water tables, aquifer drying, saltwater intrusion, groundwater contamination, water logging, increasing water salinity, etc (Singh & Singh 2002). Overexploitation is not the only problem with groundwater, besides that, deterioration in groundwater quality is another serious problem with groundwater. The assessment of the water problem was comprehensively reported by Balasubramanian (2015) and Singh & Singh (2002). The planet Earth has 71% water. Hence, it is called a blue planet. The physical distribution of water is shown in Table 1 (Water Science School 2019). Socio-economic dependency on groundwater is well explained by Burke (2001).

From data regarding the physical distribution of water (Table 1), it is clear that freshwater is only 2.5% of the total world's water. However, only 30.1% of total freshwater is groundwater, which can be used for other essential activities of life, i.e., domestic and development. The groundwater is indiscriminately used probably due to low cost and easily available technologies for extraction (Moench 2003, Cuadrado-Quesada & Joy 2021). Therefore, aquifers are rapidly declining, and the quality of water is continuously deteriorating because of pollution with time. The serious deterioration of groundwater resources in India will be addressed by Cuadrado-Quesada and Joy (2021).

Table 1: Physical distribution of world's water (Compiled by authors).

Sr. No.	Source	Percentage (%)
1.	Saline Water	97
1.1	World's Ocean	96.5
1.2	Other Saline	0.9
2.	Fresh Water	2.5
2.1	Ground Water	30.1
2.2	Ice and snow	68.7
2.3	Surface / Other fresh water	1.2
2.3.1	Waters in living organism	0.26
2.3.2	Atmosphere	3
2.3.3	Rivers	0.49
2.3.4	Soil Moisture	3.8
2.3.5	Marshes and Swamps	2.6
2.3.6	Lakes	20.9
2.3.7	Ground ice and Permafrost	60

(Source: Water Science School 2019, Balasubramanian 2015)

Boelens & Vos (2018) stated that the current status of groundwater resources is quite alarming as far as the global need for water is concerned. The most extracted raw material in the world is 'Groundwater.' However, the global withdrawal rate is 800-1000 km3/year, which exceeds the withdrawal rate of oil by a factor of 20 (Margat & van der 2013). India is one of the largest groundwater consumer countries in the world (Vijay Shankar et al. 2011). Groundwater management has to be done with the notion that groundwater is our common property (Vijay Shankar et al. 2011).

GROUNDWATER STATUS IN RURAL INDIA

Indian economy is significantly dependent on the agriculture sector. Therefore, India is the biggest consumer of groundwater for agricultural purposes (Shah 2009). The data, according to the 2001 Census, shows increasing numbers of groundwater irrigation structures, viz. wells, tube wells, etc. (Indian Agricultural Statics 2008). Tube wells account for 50% compared to all other irrigation structures. However, the number of tube wells rapidly increased after 1995 (Vijay Shankar et al. 2011) (Government of India 2001). Eventually, every fourth homeowner owns at least one groundwater irrigation structure in rural parts of India (Shah 2009).

The tube wells percentage dramatically increased from merely 1% as of 1960-61 to 40% as of 2006-07. The surface water has declined as of the 1950s from 60% to 30% in the first decade of the twenty-first century (Government of India 2001). According to the Government of India (2001), Punjab, Haryana, and Uttar Pradesh are states having 57% of tube wells in India. The major groundwater anarchy identified from census data is regarding tube wells, which depict that, on average, there are 27, 21.5, and 14.1% of tube wells /sq. m. of net sown area in Punjab, Uttar Pradesh, and Haryana, respectively (Vijay Shankar et al. 2011). According to the National Aeronautics and Space Administration (NASA) assessment from 2002 to 2008, three states, namely Punjab, Haryana, and Rajasthan, lost about 109 km3 of water, leading to a decrease in the groundwater table to 0.33 m/annum (Rodell 2009).

The contamination of pollutants such as arsenic and fluoride is increasing with a decrease in groundwater levels. Consequently, such water is not fit for human consumption and farming. The continuous increase in salinity and water logging events are making soil unproductive, thereby directly affecting the productivity and profitability of farmers (Singh & Singh 2002).

Table 2: Comparison of categorization of state-wise groundwater resource assessment 2017 and 2020 (Compiled by authors).

Sr.No.	State	Categorization (2017)	Categorization (2020)
1.	Andaman and Nicobar Islands	Safe / Saline	Safe
2.	Andhra Pradesh	Over-exploited/ Semi-critical/ Critical/ Safe/ Saline	Over-exploited/ Semi-critical/ Critical/ Safe/ Saline
3.	Arunachal Pradesh	Safe	Safe
4.	Aassam	Safe	Safe
5.	Bihar	Over-exploited/ Semi-critical/ Critical/Safe	Over-exploited/ Semi-critical/ Critical/Safe
6.	Chandigarh	Semi-critical	Semi-critical
7.	Chattisgarh	Semi-critical/ Critical/ Safe	Semi-critical/ Critical/ Safe
8.	Dadra and Nagar Haveli	Safe	Safe
9.	Daman and Diu	Critical/ Safe	Over-exploited/ Safe
10.	Delhi	Over-exploited/ Semi-critical/ Critical/ Safe	Over-exploited/ Semi-critical/ Critical/ Safe
11.	Goa	Safe	Safe
12.	Gujrat	Over-exploited/ Semi-critical/ Critical/ Safe/ Saline	Over-exploited/ Semi-critical/ Critical/ Safe/ Saline
13.	Haryana	Over-exploited/ Semi-critical/ Critical/ Safe	Over-exploited/Semi-critical/ Critical/Safe
14.	Himachal Pradesh	Over exploited	Safe
15.	Jammu and Kashmir	Safe	Safe
16.	Jharkhand	Over-exploited/ Semi-critical/ Critical/ Safe	Over-exploited/ Semi-critical/ Critical/ Safe
17.	Karnataka	Over-exploited/ Semi-critical/ Critical/ Safe	Over-exploited/ Semi-critical/ Critical/ Safe
18.	Kerala	Semi-critical/ Critical/ Safe	Semi-critical/ Critical/ Safe
19.	Ladakh	Safe	Safe
20.	Lakshdweep	Semi-critical/ Safe	Semi-critical/ Safe
21.	Madhya Pradesh	Over-exploited/ Semi-critical/ Critical/ Safe	Over-exploited/ Semi critical/ Critical/ Safe
22.	Maharashtra	Over-exploited/ Semi-critical/ Critical/ Safe/ Saline	Over-exploited/ Semi-critical/ Critical/ Safe/ Saline
23.	Manipur	Safe	Safe
24.	Meghalaya	Safe	Safe
25.	Mizoram	Safe	Safe
26.	Nagaland	Safe	Safe
27.	Odisha	Semi-critical/ Safe/ Saline	Semi-critical/ Safe/ Saline
28.	Punjab	Over-exploited/ Semi critical/ Critical/ Safe	Over-exploited/ Semi-critical/ Critical/ Safe
29.	Rajasthan	Over-exploited/ Semi-critical/ Critical/ Safe/ Saline	Over-exploited/ Semi-critical/ Critical/ Safe/ Saline
30.	Sikkim	Safe	Safe
31.	Tamilnadu	Over-exploited/ Semi-critical/ Critical/ Safe/ Saline	Over-exploited/ Semi-critical/ Critical/ Safe/ Saline
32.	Telangana	Over-exploited/ Semi-critical/ Critical/ Safe	Over-exploited/ Semi-critical/ Critical/ Safe
33.	Tripura	Safe	Safe
34.	Puducherry	Over-exploited/ Semi-critical/ Saline	Critical/ Saline/Safe
35.	Uttar Pradesh	Over-exploited/ Semi-critical/ Critical/ Safe	Over-exploited/ Semi-critical/ Critical/ Safe
36.	Uttarakhand	Semi-critical/ Safe	Semi-critical/ Safe
37.	West Bengal	Semi-critical/ Critical/ Safe	Semi-critical/ Critical/ Safe

Source: Central Ground Water Board (CGWB), Ground Water Assessment Report 2017 and 2020

Table 3: Categorization of assessment units from 2004-2020.

Sr. No.	Categorization of blocks	2004	2009	2011	2013	2017	2020
	Total assessed units	5723	5842	6607	6584	6881	6965
1.	Safe	4078	4277	4503	4519	4310	4427
2.	Semicritical	550	523	697	681	972	1057
3.	Critical	226	169	217	253	313	270
4.	Over exploited	839	802	1071	1034	1186	1114
5.	Saline	30	71	92	96	100	97

Source: (Central Ground Water Board 2021)

The comparison of state-wise groundwater resource categorization was assessed from Central Ground Water Board (CGWB) data (Table 2). As we can see in Table 2 there are only 12-14 states out of 37 with a safe category of groundwater in all blocks of the respective state in India in the year 2017 to 2020. However, some blocks of states are facing the dangerous situation of over-exploited, semi-critical, critical, and saline categories of groundwater (Table 2). However, the issue of assessment of groundwater is important because it was found that groundwater potential data estimated by CGWB are showing deviation from real-time examined data at regional levels. There are some incidents found that CGWB levels are showing high readings (Singh 2001).

As we can see in table no. 3 there are numerous units with a safe groundwater level. However, over-exploited blocks are also more in numbers, and these are increasing over the years, which is a dangerous situation for sustainability and water security in the future. Furthermore, Vijay Shankar et al. (2011) illustrated the comparative status of groundwater development from CGWB data. They found that there is a big challenge to groundwater resources in India as extreme exploitation is being done, viz. Punjab (145%), Haryana (109%), and Rajasthan (125%) can be considered unsustainable groundwater levels. Whereas Uttar Pradesh (75%), Gujarat (76%), and Tamil Nadu (85%) are considered states of India that are fast reaching threshold limits because of the quantitative depletion of groundwater to unsustainable groundwater levels. Almost all districts from Punjab, Haryana, and Rajasthan are in the unsafe category. However, 72% of Tamil Nadu and 50% of Uttar Pradesh and Karnataka districts are in the unsafe category (Vijay Shankar et al. 2011). The extreme decline of water levels, i.e., 1-2 meters per year, is found in some parts of India, viz. North Gujarat, Coimbatore, and Madurai districts of Tamil Nadu, South Rajasthan, Kolar district of Karnataka, Royalseema in Andhra Pradesh, Punjab, Haryana, and Uttar Pradesh (Singh & Singh 2002). However, in Madhya Pradesh, a long-term decline in groundwater level has been reported, i.e., 13.05 meters (Saksena 2000).

This kind of scenario will create non-accessibility of groundwater to poor farmers because of the increased cost of drilling tube wells and lifting groundwater, predominantly in groundwater-irrigation areas. Therefore, if these trends remain unchecked without proper management, then India will certainly face a major water crisis in the coming decades. It is a warning bell for researchers, geologists, and the government to investigate it as a major environmental concern.

The overexploitation of groundwater is a major problem for managers in groundwater-irrigated areas. However, large areas in the major canal periphery are suffering from waterlogging and associated salinity or alkalinity problems (Singh & Singh 2002). Singh (1993) reported that in some peripheral areas of the canal, the water table is rising high, i.e., 1m per year. Based on past development, it was reported that near about 1 million to 2 million hectares per year are brought under irrigation areas in India. However, it was assumed from data that 3% of the area would sooner or later become saline or waterlogged, and the rate of spread of water logging or salinization in irrigated areas in upcoming years would be about 30,000-60,000 ha per year (Singh 1998). This problem is a big challenge for engineers and managers to manage irrigation commands.

The Central Ground Water Board and state groundwater agencies in India, where each of them built up its monitoring network, are largely responsible for groundwater quality monitoring. However, there are concerns about how adequate the scientific data they provide is:

- The monitoring station network is not thick enough. Analysis of the quality of the water leaves out important factors that can be used to identify heavy metals, pesticides, and other harmful effluent contamination.
- There are few civil society organizations capable of doing the professionally demanding, technologically complex, and frequently politically sensitive duties required to provide the scientific data that is now accessible, notably the data on pollution.

The Indian Easement Act 1882 states that "every owner of

land has the right to collect and dispose within his limits of all water under the land which does not pass in a defined channel and all water on its surface which does not pass in a defined channel," is frequently cited as the first legal reference to groundwater in India. This suggests that groundwater would have the same status as surface water flowing via a specified channel whenever it is discovered to do so. However, the Indian Easement of 1882 created a connection between the landowner and the right to groundwater. According to the constitutional requirements, "Water" is a state subject, and state governments are ultimately responsible for managing water resources. The complicated natural occurrence of groundwater in various hydrogeological contexts, its wide-ranging significance as a socioeconomic good, and difficulties with ownership have made it extremely difficult to manage groundwater scientifically. India's pollution watchdogs are the Central Pollution Control Board (CPCB) and the State Pollution Control Boards (SPCBs).

Therefore, in 1970, the Central Government created a Model Ground Water Control and Regulation Bill and sent it to all States to persuade them to adopt groundwater law as well as to ensure some degree of uniformity in the Acts of various States. Later, the Model Bill was updated in 1992, 1996, and 2005. The Model Bill's central idea is the creation of State Ground Water Authorities, which will have the authority to "Notify" a region for groundwater management and issue licenses for well-drilling in certain notified regions. Small and marginal farmers were excused from obtaining a permit for well drilling under the 1992 Model Bill. Users must register if they are already users.

There is little doubt that the country's current groundwater situation shows the necessity for a paradigm shift in the nation's groundwater law system. Initially, it is necessary to sever the connection between groundwater and landowner created by the Indian Easement Act of 1886, which is still in effect today. In the current system, groundwater rights belong to landowners, and landless people, who make up more than 30% of the population, are denied access to this essential right, even though groundwater serves as their primary supply of drinking and living water. The Supreme Court has declared that the public trust in (surface) water. Given that groundwater is a communal resource by its very nature, the public trust theory should also safeguard it.

Moreover, it ignores the fact that groundwater resources are more regional than surface water resources, making local management more efficient. Decentralization, as introduced in the 73rd and 74th amendments to the Indian Constitution in 1992, has granted municipalities in urban areas and Panchayati Raj Institutions in rural regions certain water-related authorities. Furthermore, there will be an increasing opportunity for user conflicts of interest when groundwater is put under more stress. The case of Hindustan Coca-Cola Beverages v. Perumatty Gram Panchayat, involving the Coca-Cola bottling facility in Plachimada, Kerala, is the most well-known (2005). The fact that the current groundwater regulation restricts additional extraction in previously "over-exploited" regions while making no plans to address the current water security is another disadvantage. No groundwater law incorporates the prevention and precautionary principles acknowledged in the Environment (Protection) Act of 1986 but more lately in the National Green Tribunal Act of 2010. To stop the bad practices connected with Permit Raj, the groundwater control system should adopt the transparency principles of the Right to Information Act, 2005. It's also necessary to review the Central Ground Water Authority's function. CGWA's advising function now only entails helping the states establish regulations for rainwater gathering.

Official recognition of the need for a new legal framework led the former Planning Commission to develop a draft Model Bill for the Conservation, Protection, and Regulation of Ground Water in 2011 (Model Bill for the Conservation, Protection, and Regulation of Ground Water 2011). The draft Model Bill advocated ending the century-old connection between property ownership and groundwater by designating groundwater as a common pool resource and designating the State as the public trustee of groundwater. It establishes the right to water and introduces the utilization of groundwater as a priority. Gram Panchayats and Municipalities, the lowest levels of democratic administration, were given the authority to manage aquifers wisely, followed by blocks, districts, and the State Ground Water Advisory Council. The regulatory structure outlined in the draft Model Bill from 2011 has too many agencies engaged, which would result in unwelcome bureaucratic red tape. Simplifying the institutional framework is necessary. To make groundwater legislation a revised and practical legal framework, it should sufficiently emphasize various groundwater management measures, such as micro irrigation, recycling, and reuse of groundwater. Therefore, a new review of the Model Ground Water Bill is necessary.

Even though monitoring the quality of rivers' water and groundwater has only lately come under their jurisdiction. However, "non-point" pollution from agriculture is not covered by monitoring. There are issues with the institutional design. The SPCBs carry out the combined tasks of enforcing pollution control standards and monitoring pollution. However, the possibility that consistent WQM and its correct distribution might call into question the Boards' legitimacy as an enforcement body deters them from effectively carrying

out the first duty. The agency also lacks the administrative framework and legal authority to hold polluters accountable.

As a result, the agency is less successful in upholding pollution control standards. Polluters are deterred from doing so by the fact that the cost of pollution is far lower than the cost of remediation, while the Boards are not required to carry out environmental management programs. The most frequent cause of groundwater pollution is pumping-activated geo–geo-hydrochemical processes. The only real way to stop contamination after it has begun is to completely stop pumping. However, this is highly challenging because irrigated agriculture and livelihoods are dependent on groundwater in India for millions of rural communities. Pumping would be prohibited by any legal or regulatory action, which would deprive communities of their historical rights. Landowners have a de facto right to draw groundwater from beneath their property even though de jure rights in groundwater are unclear. Although nitrate pollution can be effectively reduced by using fertilizers in the recommended quantities, rotating crops, applying fertilizer at the right times, and using organic manure instead of chemical fertilizers, neither fertilizer use nor the disposal of animal waste is subject to any institutional regulations.

COMMUNITY PRACTICES IN RURAL REGIONS OF INDIA

In rural India, there is more agricultural area. Hence, community practices in rural regions of India are more crucial in the vulnerability of groundwater. Some major reasons for groundwater depletion are slowly and gradually increasing pressure on aquifers, race for drilling and pumping of the groundwater, non-regulated groundwater extraction, large population, which leads to an increase in water consumption per capita, etc. According to the Planning Commission (2007), the sustainable yield management goal is 'average withdrawals should not exceed long-term water recharge' as far as groundwater management is concerned. For the betterment of future resources, this limit should not be crossed. As far as the agriculture sector is concerned, it is estimated that groundwater is a more convenient option for irrigation purposes because it is available at the point on the field under which farmers require minimum conveyance infrastructure. It also helps to save the cost of field management and ultimately increases profitability. Consequently, intensive irrigation has increased over time (Singh & Singh 2002).

In the western parts of India, people are supported by local Non-Governmental Organizations that have initiated a massive well recharge movement, which is particularly based on the principle of 'Water on your roof stays on your roof; water on your field stays on your field, and water in your village stays in your village.' However, Villagers have modified some 3,00,000 wells and open bore wells to divert rainwater runoff to them. These villagers, with the help of NGOs, have also constructed thousands of check dams, ponds, and other rainwater harvesting and water table recharging structures on self-help principles (Shah 2000).

Artificial recharge of groundwater reservoirs is an acceptable strategy for better management of the groundwater to counter overexploitation of the reservoirs. It helps prevent declining water levels of aquifers, storage of surplus surface water, and monsoon runoff protects saltwater intrusion in the aquifer, etc. Artificial recharge can be achieved by rainwater harvesting (RWH) and aquifer recharging with imported water. Chaddha D. K. 2000 opined that the potential of groundwater storage that can be used is 160 billion Cubic Meters (BCM). However, RWH is a more economical, technical, and feasible option for water management in rural as well as urban areas in India. The Ministry of Water Resources has started a program for rainwater harvesting and groundwater recharge, and for that, around 450 million Indian rupees were allotted in the 9th plan. The 'Khadins' of Rajasthan and 'Tankas' of western Gujarat are more crucial for groundwater recharge in the relevant parts of India (Shah 2000). Though CGWB and other governmental authorities are imposing pressure on groundwater recharge projects, it is essential to be very careful, especially in the urban parts of India, while planning and designing for the same activity. Because there are possibilities of entry of many pollutants such as toxic chemicals, bacteria, other total dissolved solids along with recharged water, etc. (Singh & Singh 2002). The series (over the period) analysis and comparative analysis were carried out by Zhai et al. (2021) to verify the existence of an increasing effect through laboratory leaching tests, and the impacts of aquatic chemical environment conditions like pH were also studied. However, they found that the increase of organic chemicals in the groundwater was one of the reasons for the release of 'Fe' and 'Mn' (Zhai et al. 2021).

CASE STUDY OF UTTAR PRADESH AND ITS RURAL REGIONS

Uttar Pradesh (UP) is occupying the Upper and Middle Ganga Plain. It is confined between the Himalayas in the north, the plateau region of the Bundelkhand in the South, and the Yamuna River on the west side. The UP is situated in north India and surrounded by Bihar and Jharkhand in the east, Uttarakhand and Nepal on the north side, Madhya Pradesh and Rajasthan in the south, and Haryana and Delhi on the west side. The state of Uttar Pradesh lies between North latitude 23°52'12" and 30°24'30" and East longitude

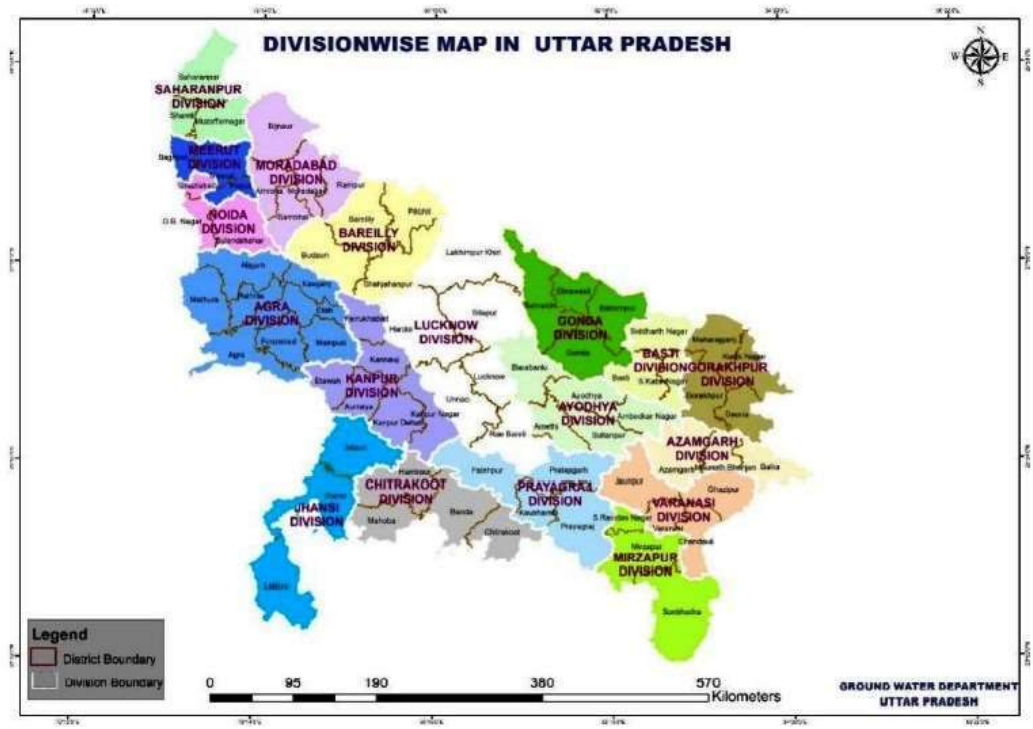

(Source: Groundwater Department UP and Central Ground Water Board Lucknow 2021)

Fig. 2: Administrative boundaries of Uttar Pradesh.

77°05'38" and 84°38'30". It covers an area of 2,41,710 sq km. Whereas, administratively, Uttar Pradesh (Fig. 2) has been divided into 18 divisions, 75 districts, 340 tehsils, and 826 blocks (Groundwater Department UP & Central Ground Water Board Lucknow, 2021). According to the *Census* in 2011, the urban population of UP state is 39.9 million, and that of the rural region is 159.7 million. The most important concern is about 67% of the population living in rural areas and directly or indirectly dependent on agricultural produce for their livelihood. However, farm income can account for more than 20% of the income of a household (Census 2011).

Some of the Union territories/states are facing a relentless problem of groundwater level decline in India viz. Madhya Pradesh, Tamil Nadu, Uttar Pradesh, Gujarat, Rajasthan, Haryana, Punjab, Karnataka, Pondicherry, Maharashtra, and Delhi (NCR). In some districts of west Uttar Pradesh, groundwater levels are being declined to 0.66 m per year. Saksena R. S. 2000 opined that nearly 20% of the areas in Uttar Pradesh located outside the canal periphery have shown a decline in the groundwater table by 7 meters during the period 1972-85. However, in Tamil Nadu, the groundwater level has declined by 10 to 50m in some districts of the state in the last 40-50 years (Saksena 2000). The Central Ground Water Board has already started artificial recharge studies in the overexploited regions of Punjab, Maharashtra, Haryana, Uttar Pradesh, Jammu, Kashmir, etc. (Singh & Singh 2002).

The extractable Groundwater resources found as of March 2020 were 66.88 BCM (Billion Cubic meters). However, net groundwater availability for future use is 21.53 (Table 4). The dynamic groundwater status assessment of Uttar Pradesh was carried out by Ground Water Department UP and Central

Table 4: The dynamic groundwater status of Uttar Pradesh as of March 2020.

Uttar Pradesh (2020)		in Bcm
Ground water Recharge	Recharge from rainfall	39.05
	Recharge from other sources	33.15
	Total annual ground water recharge	72.2
Total Natural Discharges		5.32
Annual extractable ground water Resources		66.88
Current Annual ground water Extraction	Irrigation	41.29
	Domestic	4.74
	Total	46.03
Annual GW Allocation for domestic use as of 2025		5.38
Net Ground Water Availability for future use		21.53
Stage of groundwater Extraction (%)		68.83%

(Source: Groundwater Department UP and Central Ground Water Board Lucknow 2021)

Ground Water Board Lucknow in 2021. The working group assessed more than 836 units i.e., 10 urban cities having more than 10 lakh population were included in the assessment units. However, they have categorized assessed units viz. Safe, Semi-critical, Critical, Overexploited, etc. Out of 836 units, 544, 177, 49, and 66 units were found to be safe, semi-critical, critical, and overexploited groundwater resources, respectively (As of March 2020).

GROUNDWATER REGULATION IN UTTAR PRADESH

Groundwater is still a necessity in Uttar Pradesh as it accounts for not only their drinking use but also for their irrigational purposes. Therefore, because it has tremendous use in Uttar Pradesh, the laws regulating the usage of the same should be very sturdy in meeting the problems faced at present. However, all the rules that regulate the groundwater in Uttar Pradesh are based on the principles that were in use during the British colonial period. There have been proposals by the Central Government to regulate the groundwater regime in India since the 1970s. However, it is also not sufficient to meet the current needs of groundwater depletion.

The legal framework for groundwater used today finds its origin in the nineteenth century which has been later confirmed in the Indian Easements Act 1882 during the British period. That period observes a series of judgments given concerning the use, accessibility, and depletion of groundwater resources. In the case of *Chasemore v Richards*, the groundwater that had no definite course and percolated through the underground strata would not be covered under the same rules and regulations that cover the water flowing in rivers and streams. This ruling gave a lot of leverage to the landowners who could use the groundwater at their convenience, and it was also upheld in another case of *Acton v Bundell*, where it had been clearly stated that since the landowners had complete control, neighbors' claim could not be considered for the same. There has been a constant need to draft sturdy groundwater regulations owing to the reduced groundwater tables and mismanagement. The government addressed the issue by formulating a Groundwater Development and Management Model Bill, 1970 for the states to adopt, which has also been revised in 1992, 1996, and 2005. The States have been slow in adopting the regulations for groundwater conservation. However, all the States or Union Territories that have adopted the groundwater regulations find their base in the model bill by the government. The league has also followed Uttar Pradesh by formulating the Uttar Pradesh Groundwater Conservation, Protection, Development (Management. Control and Regulation) Bill, 2010 (hereinafter Uttar Pradesh Groundwater Bill).

The groundwater Bill suggests various measures and ways to curb the exploitation of groundwater. The few major highlights of the Bill would be as follows:

1. It aims to set up a Uttar Pradesh Groundwater Authority, which shall be empowered to declare areas as critical, semi-critical, and over-exploited to regulate the groundwater in the areas accordingly.
2. This Authority shall be under the direct control and supervision of the State Government.
3. It provides for the setting up of various associations, such as resident welfare and water users in both urban and rural areas, for reducing the exploitation of groundwater in those areas.
4. The Act places civil servants regulating the groundwater along with a member from a non-governmental organization and a member who has expertise in technology from the National Institute of Hydrology in Roorkee.
5. The Local level authorities do not have any direct power as the Bill does not propose their power directly. However, they shall be responsible for assisting the higher-level authorities in terms of capacity building, looking into how the Bill is being violated, etc., in their area.
6. There are also various other proposals that the Bill suggests making, such as the provision of service providers. These service providers shall be responsible for inspecting the amount of groundwater being withdrawn by the users and have a check on the rainwater harvesting and recharge measures adopted and their efficiency in general.
7. The Bill also proposes to register the drilling agencies in order to curb the exploitation of groundwater resources.
8. The consumers of groundwater residing in critical areas are supposed to get registered by applying for a certificate of registration. The consumers using groundwater resources for industrial or commercial use also must apply for a certificate of registration.
9. The Bill also proposes for a different level of pumps to be allowed or regulated in rural, critical, or over-exploited areas. The level of pumps allowed depends on the category the area falls into.
10. The rural areas are permitted to pump 7.5hp without any regulation. However, pumps above this compulsorily must be self-regulated with the help of established water associations.
11. The semi-critical areas have a stricter mechanism than the above-mentioned one. In the urban areas, it accounts

for pumping of only up to 0.5 hp, which will have to be regulated by the local bodies in those areas.

12. No well can be constructed by any entity in over-exploited areas in order to save the further curbing of groundwater resources in that area.
13. Therefore, it can be said that the UP Groundwater Bill finds its base in the Model Bill laid down by the government. It does distinguish users of groundwater and categorizes different areas into different levels based on the level of groundwater in that area. However, this Bill does not prove to be an effective measure to curb all the problems related to groundwater in Uttar Pradesh.

Demarcation has been laid down between the surface and groundwater as it is completely based on the scientific data and understanding of groundwater, which does not lay down a demarcation with surface water. Therefore, the landowners are vested with immense powers to freely use the groundwater without any proper regulation. The landless groundwater users are not even included in the purview of this Bill, which makes it socially inequitable in all forms.

The Bill does not include in its purview the fundamental right to water of the citizens by not including in its ambit the landless owners, which makes it derogatory or inconsistent with part III of the Constitution. The Bill focuses only on the personal level issues that the landowners and their neighbors could face, which therefore makes it redundant to tackle the groundwater problems at the aquifer level and take a holistic approach to the environmental degradation of the groundwater resources. The Bill has proposed too many institutions at different levels but has no binding mechanism to make these institutions answerable to one single entity. This scattered system of accountability and answerability will lead to redundancy in the working of these institutions.

Therefore, there is a dire need not only for regulation to regulate the groundwater sources but also to bring in essential reforms for the deteriorating effect of groundwater resources. A few of the possible ways in which it could be achieved are as follows:

1. A unitary nature of water regulation is appreciated, which shall include in its purview of regulation not only the groundwater but also the surface water, which shall enable a holistic way of preserving our water resources.
2. Proper respect for the fundamental rights of the landless people should be given as it leads to the violation of their rights. Everyone has basic needs, and water is one of the most essential in them and, therefore, should not be denied in any manner whatsoever.
3. Any unreasonable use of water resources that becomes a threat to the aquifer should be curbed and properly regulated.

THE UTTAR PRADESH GROUNDWATER (MANAGEMENT AND REGULATION) ACT, 2019

The enactment of the Uttar Pradesh Groundwater (Management and Regulation) Act in 2019 was a decisive response to the critical issues stemming from uncontrolled extraction of groundwater, declining water levels, and contamination affecting both urban and rural areas of Uttar Pradesh. This comprehensive legislation introduces a multifaceted approach to promote responsible and sustainable management of the state's groundwater resources. The key provisions and notable aspects of the Act are as follows:

1. **Formation of Committees:** The Act establishes a range of committees at various administrative levels, including Gram Panchayat, Block Panchayat, Municipal, and District levels. These committees are vested with the crucial responsibility of effectively managing and regulating groundwater resources. Their primary roles encompass devising strategies for the protection and conservation of groundwater.
2. **Groundwater Security Plans:** At the heart of the Act lies the emphasis on developing and implementing Groundwater Security Plans. These plans, created at both the Gram Panchayat and Block Panchayat levels, are designed to ensure prudent groundwater management and tailored solutions to region-specific challenges.
3. **State Groundwater Management and Regulatory Authority:** A pivotal aspect of the Act is the establishment of the Uttar Pradesh State Groundwater Management and Regulatory Authority (SGWMRA). This authoritative body is tasked with providing guidelines, identifying regulated areas, and offering expert advice to the government on effective water conservation practices.
4. **Registration and Regulation:** The Act mandates the registration of existing users engaged in commercial, industrial, infrastructural, and bulk groundwater usage, covering both notified and non-notified areas. Additionally, the Act imposes restrictions on the construction of new wells in notified areas and closely monitors the extraction, sale, and distribution of groundwater.
5. **Fees and Penalties:** Noteworthy are the specified penalties for non-compliance outlined in the Act, encompassing fines and potential imprisonment. The

Act differentiates between various user categories, imposing more severe penalties for repeat offenders and those found guilty of polluting groundwater resources.

6. **Rainwater Harvesting and Environmental Safeguarding:** The Act places a strong emphasis on sustainable practices, encouraging actions such as rainwater harvesting, self-regulation, groundwater replenishment, and measures to prevent waterlogging. It underscores the importance of adopting suitable technologies and designs to achieve these objectives.
7. **Impact Assessment and Transparency:** Transparency is a fundamental aspect of the Act. Authorities are required to conduct thorough assessments of the social and environmental impacts of their initiatives. This commitment to transparency extends to the proactive disclosure of information related to impact assessments.
8. **Groundwater Grievance Authority:** The Act introduces the establishment of a dedicated Groundwater Grievance Authority responsible for addressing concerns related to groundwater management and regulation.
9. **Groundwater Fund:** A significant feature of the Act is the creation of a Groundwater Fund designated for various activities aimed at effective groundwater management. This encompasses conservation measures and initiatives to enhance efficiency.
10. **Governmental Powers and Exemptions:** Acknowledging diverse scenarios and requirements, the Act empowers the state government to formulate implementation rules and offers flexibility in granting exemptions under specific circumstances.

In summary, the Uttar Pradesh Groundwater (Management and Regulation) Act of 2019 represents a substantial stride in addressing the challenges arising from unchecked groundwater exploitation, dwindling water levels, and contamination. Through the establishment of a structured framework for responsible groundwater management, the Act endeavors to ensure water security for both urban and rural areas. Moreover, its overarching goal is to safeguard the environment while promoting equitable access to this indispensable resource. (U.P. Act No. 13 2019)

UTTAR PRADESH GROUND WATER (MANAGEMENT AND REGULATION) RULES, 2020

Core principles play a pivotal role in shaping well-crafted public policies regarding water resources. These principles provide the bedrock for achieving consistency in approaches when dealing with the planning, development, and management of water resources. The fundamental tenets are delineated as follows:

1. **Integrated and Environmentally Sound Perspective:** Effective planning, development, and management of water resources should be underpinned by holistic and environmentally sustainable viewpoints. These perspectives should encompass state and national contexts while factoring in the human, social, and economic requisites. This ensures a judicious and conscientious utilization of resources.
2. **Equity and Social Justice:** The principle of equity and social justice should guide the allocation of water resources. This principle guarantees the fair distribution of water resources, taking into account the diverse needs of various societal segments.
3. **Informed Decision Making and Good Governance:** Informed decision-making is of paramount importance in attaining goals related to equity, social justice, and sustainability. Thus, it is imperative to uphold practices of good governance that facilitate well-informed decisions for the greater benefit of the community.
4. **Community Resource and Public Trust Doctrine:** It is crucial to treat water as a communal asset held in trust by the state in adherence to the public trust doctrine. This approach seeks to realize equitable and sustainable development, as well as ensuring food security and livelihood opportunities for all.
5. **Right to Safe Water and Sanitation:** Unrestricted access to safe and hygienic drinking water and sanitation services is an inherent human right necessary for a dignified and fulfilling life. Consequently, these essentials should hold precedence over other water uses.
6. **Balancing Human Needs and Economic Considerations:** Beyond the primary requirement of safe drinking water and sanitation, it is prudent to consider water as an economic commodity to incentivize resource conservation and efficient utilization.
7. **Ecological Considerations:** Acknowledging water's vital role in maintaining ecosystems, ecological factors should be thoughtfully integrated into water management decisions.
8. **River Basin as a Planning Unit:** All facets of the water cycle, encompassing evapotranspiration, precipitation, runoff, rivers, lakes, soil moisture, and groundwater, are interconnected. Thus, the river basin should serve as the foundational hydrological unit for planning endeavors.
9. **Integrated Approach to Quantity and Quality:** The interrelation between water quality and quantity

underscores the need for a comprehensive management approach. This entails integrating wider environmental management strategies, including economic incentives and penalties, to curtail pollution and wastage.

10. **Addressing Climate Change Impact:** It is imperative to account for the influence of climate change on water resource availability while making well-informed water management decisions.

To sum up, these guiding principles constitute a framework for shaping effective policies related to water resources. By aligning policies with these principles, governments can secure the sustainable, equitable, and efficient use of water resources, concurrently ensuring environmental preservation and meeting society's indispensable needs (Khan et al. 2021).

SUGGESTIONS AND RECOMMENDATIONS

- **Review of methodology:** The management of groundwater is solely dependent on the available data of groundwater assessment. However, methodologies used for the collection of valid data are crucial for monitoring, implementation, and decision-making.
- **Mapping of aquifers:** Aquifer mapping and groundwater quality assessment at proper scale in every identified hydro-geological block is important for further management of aquifers.
- **Domestic water security:** Prioritization and management of domestic groundwater security by applying proper strategies suggested by government authorities or legal frameworks.

CONCLUSION

The therapeutic options operate according to physics and chemistry principles. As a result, maintaining a set of predetermined operating parameters is crucial to maintaining their efficiency. This would require competent technical personnel, which is largely lacking, for system operations as well as routine maintenance. To be efficient and cheap, most of the drinking water treatment technologies must be tested in local communities. It is crucial that water pipes do not cross sewage or are not immersed in sewage places in communities where clearer water delivery networks provide clean drinking water. There is a chance that sewage will mingle with pipe water in the communities because the sewage channels are open. Despite the overwhelming effort, we hope that one day, all rural regions will have subsurface drainage systems that will lessen the number of organic particles that might contaminate groundwater.

Rural water supply programs are now being conducted in rural regions under the Water and Sanitation Department. The program's goals are to offer access to clean drinking water through tap connections and to ensure that every home builds a latrine to prevent open defecation. Talking specifically about U.P. (our case study) and the legal dimensions, then, the legalities of groundwater have not been addressed in the Bill. This also reflects the need to relook at the laws and policies from a state-specific lens.

Common people are reporting the poor quality of the water. Institutions and civil society must be reinforced so they can react swiftly to issues with water quality. This is made possible by increased awareness of the types of groundwater pollution, the potential dangers to groundwater quality in their area, the degree of susceptibility, the negative impacts of utilizing polluted water, and feasible preventive actions. In turn, they could exert pressure on the line agencies to deliver. Strengthening civil society organizations is crucial since groundwater quality fluctuations are frequently erratic. Because of the high expenses and technical expertise required, it is very challenging for monitoring agencies to set up an intricate network of WQM stations. Additionally, people's willingness to pay for water is closely correlated with their knowledge of and awareness of the negative effects of consuming contaminated or polluted water. By creating a crucial database on groundwater quality, reputable and technically proficient NGOs may significantly contribute to the development of civil society.

REFERENCES

Acton v Blundell. 1843. 12 Meeson and Welsby 324 (Court of Exchequer Chamber, 1 January 1843).

Balasubramanian, A. 2015. The World's Water: Technical Report. Centre for Advanced Studies in Earth Science, University of Mysore.

Boelens, R. and Vos, J. (Eds.). 2018. Water justice. Cambridge University Press.

Burke, J.J. 2001. Groundwater and Society: Resources, Tensions and Opportunities. United Nations, New York.

Census. 2011. Retrieved from http://www.censusindia.gov.in/2011census/dchb/2732_PART_B_DCHB_RATNAGIRI.pdf

Central Ground Water Board & Board. 2021. National Compilation on Dynamic Ground Water Resources of India, 2020. https://cgwb.gov.in/sites/default/files/MainLinks/2021-08-02-GWRA_India_2020.pdf

Central Ground Water Board 2020. Groundwater resource assessment Report. https://cgwb.gov.in/cgwbpnm/public/uploads/documents/16879324231614740340file.pdf

Chaddha, D.K. 2000. Groundwater recharge: option for groundwater management. J. Transp. Infrastruct., 7(4): 44-57.

Cuadrado-Quesada, G. and Joy, K.J. 2021. The need for co-evolution of groundwater law and community practices for groundwater justice and sustainability: Insights from Maharashtra, India. Water Altern., 14(3): 717-733.

Fetter, C.W. 2001. Applied Hydrogeology. Prentice Hall, NJ.

Fitts, C.R. 2012. Groundwater Science. Second Edition. Elsevier, The Netherlands.

Foster, S. 2013. Groundwater: A global focus on the local resource. Curr. Opin. Environ. Sustain., 5(6): 685-695.

George Chasemore v Henry Richards. 1859. VII House of Lords Cases 349 (House of Lords, 27 July 1859).

Gleeson, T., Wada, Y. and Bierkens, M.F. 2012. Water balance of global aquifers revealed by groundwater footprint. Nature, 488(7410): 197-200. doi: 10.1038/nature11295.

Government of India. 2001. Minor Irrigation Census, Report on Census of Minor Irrigation Schemes (1993-94). Minor Irrigation Division, Ministry of Water Resources, New Delhi.

Gramont, H.M. 2011. Towards A Joint Management of Transboundary Aquifer Systems. UNESCO, Paris.

Ground Water Department UP & Central Ground Water Board Lucknow. 2021. Dynamic Ground Water Resources. https://upgwd.gov.in/MediaGallery/ESTIMATIONREPORT_2020.pdf

Indian Agricultural Statics 2008. Ministry of Agriculture. Retrieved from http://dacnet.nic.in/eands/latest_2008

Keeble, B.R. 1988. The Brundtland Report: Our Common Future. Med. War, 4(1): 17-25. doi: 10.1080/07488008808408783.

Khan, S.A., Puthucherril, T.G. and Paul, S.R. (Eds.). 2021. Groundwater Law and Management in India: From an Elitist to an Egalitarian Paradigm. Springer, Singapore

Kløve, B., Ala-aho, P., Bertrand, G., Boukalova, Z., Ertürk, A., Goldscheider, N., Ilmonen, J., Karakaya, N., Kupfersberger, H., Kvœrner, J., Lundberg, A., Mileusnić, M., Moszczynska, A., Muotka, T., Preda, E., Rossi, P., Siergieiev, D., Šimek, J., Wachniew, P., Angheluta, V., Widerlund, A. and Ala-Ah, P.O.A. 2011. Groundwater-dependent ecosystems. Part I: Hydroecological status and trends. Environ. Sci. Pol., 14(7): 770-781. doi: 10.1016/j.envsci.2011.04.002.

Margat, J. and van der G.J. 2013. Groundwater Around the World: A Geographic Synopsis. Taylor & Francis Group, London.

Model Bill for the Conservation, Protection, and Regulation of Groundwater 2011. Retrieved from http://www.planningcommission.nic.in/aboutus/committee/wrkgrp12/wr/wg_model_bill.pdf

Moench, M. 2003. Groundwater and Poverty: Exploring the Connections. In Llamas, E. and Ramon, M. (eds), Intensive Use of Groundwater: Challenges and Opportunities, AA Balkema Publishers, Cape Town, pp. 441-456.

Phillipe Cullet, Groundwater Regulation Uttar Pradesh: Beyond 2010 Bill. International Environmental Law and Research Centre. Retrieved from https://www.ielrc.org/content/p1202.pdf

Planning Commission 2007. Groundwater Management and Ownership: Report of the Expert Group. GoI, New Delhi.

Rodell, M. 2009. Satellite-based Estimates of Groundwater Depletion in India. Nature J., 460: 999-1002.

Saksena, R.S. 2000. Conjunctive Use of Surface and Groundwater. Indian National Committee on Hydrology, National Institute of Hydrology, Roorkee, Uttarakhand.

Shah, T. 2000, August. Mobilising social energy against environmental challenge: Understanding the groundwater recharge movement in Western India. In: Natural Resources Forum, 24(3): 197-209).

Shah, T. 2009. India's groundwater irrigation economy: The challenge of balancing livelihoods and environment. Quarterly Journal of Central Ground Water Board, pp.21-37.

Singh, D.K. 2001. Water Resources Development and Management Strategies for Rajgarh Block of Mirzapur District. Water Technology Centre, Indian Agricultural Research Institute.

Singh, D.K. and Singh, A.K. 2002. Groundwater situation in India: Problems and perspective. Water Resour. Dev., 18(4): 536-580. doi: 10.1080/0790062022000017400.

Singh, O.P. 1993. Drainage Problems and Design Criteria for Land Drainage Systems.: Sustainable Irrigation in Saline Environment, Central Soil Salinity Research Institute, Karnal, Haryana.

Singh, O.P. 1998. Salinity and Waterlogging Problems on Irrigation Commands. Agricultural Salinity Management in India, Central Soil Salinity Research Institute, Karnal, Haryana.

Tari, V. 2015. Earth, Man, and Environment. In Patil, P. (ed), Definition, Principles and Scope of Environment. DPS Publishing House, New Delhi, pp. 1-20.

Tari, V.S. and Patil, P.Y. 2017a. Challenge of contamination of pesticides for Alphonso in Ratnagiri District, Maharashtra, India. Res. J. Chem. Environ., 21(12),:54-64.

Tari, V.S. and Patil, P.Y. 2017b. Transfer of heavy metal in the soil to plant from a pesticide-contaminated area (mango orchards) of Ratnagiri District, Maharashtra, India. Res. J. Chem. Environ., 1(1): 26-32.

Tari, V.S., Gupta, R. and Siddiqui, N. 2022. Impact of Climate Change on Upper Ganga Ramsar Site of UP, India. In: Rathore, A. (ed), Handbook of Research on Monitoring and Evaluating the Ecological Health of Wetlands. IGI Global, Pennsylvania, US. pp. 92-105. doi: 10.4018/978-1-7998-9498-8.ch006.

Velis, M., Conti, K.I. and Biermann, F. 2017. Groundwater and human development: synergies and trade-offs within the context of the sustainable development goals. Sustain, Sci., 12(6): 100

Vijay Shankar, P.S., Kulkarni, H. and Krishnan, S. 2011. India's groundwater challenge and the way forward. Econ. Polt. Week., 46(2): 37-45.

Water Science School 2019. U.S. Geological Survey's (USGS), Water Science School. https://www.usgs.gov/special-topics/water-science-school

Zhai, Y., Han, Y., Xia, X., Li, X., Hong, Y.T. and Lu, J.W. 2021. Anthropogenic organic pollutants in groundwater increase releases of Fe and Mn from aquifer sediments. Water, 13(1920): 1-15. doi: https://doi.org/10.3390/w13141920.

Nature Environment and Pollution Technology
An International Quarterly Scientific Journal

p-ISSN: 0972-6268
(Print copies up to 2016)
e-ISSN: 2395-3454

Vol. 23 | No. 1 | pp. 139-150 | 2024

Original Research Paper

https://doi.org/10.46488/NEPT.2024.v23i01.010

Open Access Journal

An Eco-friendly *Mangifera indica* Leaves Extract Corrosion Inhibitor for Stainless Steel in Acidic Medium

Dharampal Bajaj and Pratiksha D. Khurpade†
School of Chemical Engineering, Dr. Vishwanath Karad MIT World Peace University, Pune-411038, India
†Corresponding author: Pratiksha D. Khurpade; pratiksha.khurpadekale@mitwpu.edu.in

Nat. Env. & Poll. Tech.
Website: www.neptjournal.com

Received: 13-06-2023
Revised: 05-07-2023
Accepted: 15-07-2023

Key Words:
Green corrosion inhibitor
Mangifera indica leaf extract
Adsorption isotherm
Acidic media

ABSTRACT

Corrosion of metals and alloys is one of the most frequent problems encountered in chemical and process industries. Inefficient corrosion control measures typically lead to an increased risk of unplanned downtime, huge economic loss, environmental damage, and health and safety hazards. Hence, it is essential to develop environment-friendly and cost-effective corrosion inhibitors over existing toxic anticorrosive agents. The main objective of this work is to examine the efficacy of eco-friendly ethanolic extract of *Mangifera indica* leaves (MIL) in different concentrations as a green corrosion inhibitor for stainless steel (SS-316L) under an acidic environment. The inhibition efficiency of *Mangifera indica* leaves extract in 1 M hydrochloric acid (HCl) was evaluated by conventional weight loss method along with adsorption isotherm analysis. Chemical compounds present in leaf extract and changes in surface morphology of SS-316L samples were assessed using Fourier Transform Infrared spectroscopy (FTIR) and Field Emission Scanning Electron Microscopy (FE-SEM) provided with elemental analysis. The results of the weight loss method revealed that the inhibition efficiency increases with increasing MIL extract concentration due to higher surface coverage. The highest inhibition efficiency of almost 63.43% in 14 days and minimum corrosion rate of 0.433 mm per year was obtained for SS-316 L in 1.0 M HCl with 1000 ppm concentration. The adsorption of MIL extract on SS-316L surface followed Freundlich adsorption isotherm, and the obtained value of free Energy of adsorption (ΔG°_{ads} = – 9.20 kJ.mol^{-1}) indicates the physical adsorption mechanism. The developed regression-based models can predict the corrosion rate as a function of inhibitor concentration and exposure time with good accuracy (>80%). Thus, the present findings demonstrate that *Mangifera indica* L. leaves extract can suitably be applied as an inexpensive, non-toxic, biodegradable, efficient green corrosion inhibitor for the protection of stainless steel in acidic media.

INTRODUCTION

Corrosion of metals and alloys is the primary concern in chemical and process industries, and mitigating it necessitates a tremendous amount of capital. The serious consequences of corrosion are irreparable damage to equipment, sudden failures leading to fire and explosion, and the release of toxic products that are harmful to the environment and also to human health. It can cause disruptions in operations, such as plant shutdowns and even loss of production, resulting in severe economic losses (Loto et al. 2020). According to the National Association of Corrosion Engineers (NACE International) IMPACT Report 2016, the global corrosion cost was estimated at $ 2.5 trillion (USD) per year, which is equivalent to 3.5% of the 2020 world Gross Domestic Product (GDP). In India, it costs 4.2% of the country's GDP and thus necessitates the appropriate measures for the prevention and control of corrosion (Impact Report 2016).

Stainless steel is one of the most widely used metal alloys in chemical process industries, oil and gas industries, construction industries, and many more due to their unique properties such as excellent corrosion resistance, high strength and toughness, durability, attractive appearance, recyclability and cost-effectiveness as compared to other metals (Aslam et al. 2022). SS-316L is among the most commonly used grades of the stainless-steel family of the 300 series. It is an iron-based alloy with 16 to 18% chromium content and other alloying elements. The addition of chromium imparts excellent corrosion resistance to SS-316 against many aggressive solutions via the formation of a thin passive film of chromium oxide covering the surface in the presence of an oxidizing environment. This film acts as a barrier that prevents the diffusion of corrosive ions into the metal surface, thus protecting it from corrosion attacks. However, stainless steel is unable to resist corrosion attack by an aggressive acid environment, namely hydrochloric acid, as

it breaks down the chromium oxide layer covering the surface, followed by localized corrosion (Simescu-Lazar et al. 2023). Hydrochloric acid (HCl) is widely used in various industrial processes such as acid pickling of steel and iron, chemical cleaning, descaling as well and oil well acidification and, thus, results in serious corrosion issues due to deterioration of passive film (Shamsheera et al. 2022, Oguike 2014).

Various methods such as cathodic protection, galvanizing, and the use of protective coatings and paints have been used in industries for corrosion control of metal surfaces for a long time (Veedu et al. 2019, Buchheit 2018). However, the usage of organic and inorganic inhibitors is considered one of the practical approaches to minimize corrosion (Aslam et al. 2022, Umoren et al. 2016). The corrosion inhibitor is a chemical substance which, in addition to even small amounts to the corrosive solution, decreases the rate of corrosion (Zhou et al. 2023). Some synthetic organic inhibitors are 1, 3-azole, pyridines, and fatty amides, whereas phosphates and chromates belong to inorganic inhibitors that have been used as efficient corrosion inhibitors (Salleh et al. 2021). These inhibitors resist the corrosion effectively because of the presence of heteroatoms such as C, N, O, or S (electronegative groups) and pi-electrons in their structures that facilitate their physical or chemical adsorption over the metal surface (having empty *d* orbitals), thereby isolating the surface from corrhibitor.

In past few years, various green inhibitors from plant origins, such as Pomegranate leaves, Marigold flowers, Neem leaves, Hibiscus leaves, Jackfruit pectin, etc. have been investigated by many researchers for metal and metal alloy corrosion against acidic medium (Shamsheera et al. 2022, Gaidhani et al. 2020, Abboud et al. 2016, Mourya et al. 2014, Sharma et al. 2009). Very recently, Pal & Das (2023) investigated the corrosion inhibition activity of extract from kitchen waste of onion peel against aggressive hydrochloric acid and sulfuric acid media for boiler-quality Stainless Steel. Their research revealed good inhibition efficiency of onion peel extract in both the acidic media (Pal & Das 2023). These literature reports demonstrated that plant extracts are rich sources of organic constituents with heteroatoms such as nitrogen, oxygen, and sulfur, which are responsible for their excellent corrosion-resistive activity. These compounds can be extracted from leaves, stems, or fruit peels using simple aqueous or ethanolic extraction processes, which are not only cost-effective but environmentally benign as well.

Limited literature is available on the evaluation of *Mangifera indica* leaf extract as a corrosion inhibitor on stainless steel (SS-316L) surface in HCl solution (Veedu et al. 2019, da Rocha et al. 2010). Veedu et al. (2019) have utilized extracts of mango leaf extract as corrosion inhibitors for commercial steel in marine environments. In contrast, another work used aqueous extracts of orange, mango, passion fruit, and cashew peel against corrosion of carbon steel in an HCl medium (da Rocha et al. 2010).

Mangifera indica (also known as mango) is a tropical fruit crop that belongs to the Anacardiaceae family. India ranks first in area and production of mangoes in the world, and most importantly, it is abundantly available throughout the whole year in India. Extracts obtained from different parts of the mango tree are rich in phytochemicals such as mangiferin, phenolic acids, benzophenones, flavonoids, ascorbic acid, terpenoids, carotenoid, etc., and thus possess anti-cancer, anti-inflammatory, anti-diabetic, anti-oxidant and anti-microbial activity (Mirza et al. 2021). In spite of the great potential of mango leaves in the food and pharmaceutical industries, less importance was given to it in the corrosion protection research area. Additionally, all the above-mentioned corrosion inhibition studies in the literature are based on mild steel or carbon steel in an acid environment. However, till now, no research work has been reported on the investigation of *Mangifera indica* for SS-316L metal in an acid environment. Therefore, there is a need for systematic study and development of an effective green corrosion inhibitor from *Mangifera indica* for SS-316L metal in an HCl environment.

The main objective of the present work is to synthesize a green corrosion inhibitor using ethanolic extract of *Mangifera indica* leaves and evaluate its anti-corrosion activity on stainless steel (SS-316L) in an acidic medium (1 M hydrochloric acid solution). A direct quantitative weight loss method was employed to estimate corrosion rate and inhibition efficiency at different concentrations of MIL extract. Fitting adsorption isotherm models evaluated adsorption and thermodynamics parameters, and the mechanism of inhibitor adsorption on the SS-316L surface was studied. Additionally, Fourier Transform Infrared spectroscopy (FTIR), Field Emission Scanning Electron Microscopy (FE-SEM), along Energy Dispersive spectroscopy (EDS) were utilized to provide additional insights into the corrosion inhibition mechanism of MIL extract. Later, multivariate regression-based models were developed to predict corrosion rate as a function of inhibitor concentration and exposure time. The novelty of this paper is the use of *Mangifera indica* leaves on SS-316 corrosion for the first time and the development of a mathematical model to predict the corrosion rate as a function of important process parameters. The findings of the present study demonstrated that MIL extract can be utilized as an efficient, non-toxic, cost-effective, and biodegradable anticorrosive material for stainless steel protection in reducing acid applications.

MATERIALS AND METHODS

Materials

Fresh *Mangifera indica* leaves (also known as mango leaves) were collected from a mango tree situated in local Pune, India, in November. Ethanol (C_2H_5OH, 98%), acetone (CH_3COCH_3, Merck company) & hydrochloric acid (HCl, 37%, Merck company) of AR grade were used for the synthesis of mango leaf extract and corrosive test solution for the study without any purification. Stainless steel (SS-316L) coupons of chemical composition (wt. %): C = 0.014%, Si = 0.75%, Mn = 1.26%, P = 0.041%, S = 0.006%, Cr = 17.34%, Mo = 2.10%, Ni = 10.12% and balance is Fe were sourced locally and tested following ASTM A 276/ 276 M method by Industrial metal test lab located at Mumbai. Coupons dimensions were in the range of 30 mm × 9 mm ×1.9 mm with a 5 mm drilled hole. Glass bottles were used to conduct the corrosion study.

Mangifera Indica Leaves (MIL) Extract Preparation

Mangifera indica leaves were washed with plenty of water to remove the extraneous material like dust particles and then dried in the hot air oven at 80°C for 3 h. To prepare the extract, dried mango leaves were ground to a fine powder (approx. 15 g) and extracted in 150 ml ethanol for 4 h in the agitated round bottom flask at ambient temperature. The obtained mixture was then filtered, and excess ethanol was removed by rotavapor at 85 °C to get the MIL extract.

Specimen Coupon's Preparation

Before the experiment, SS-316L coupons of rectangular shape were mechanically abraded with emery paper grade 200. After that, these coupons were washed with water to remove the dust and then rinsed with acetone. After washing, coupons were dried & kept in a desiccator to avoid contamination before corrosion studies.

Solution Preparation

1 M HCL solution, which acts as a corrosive environment, was prepared from 37% analytical grade HCL solution using distilled water. Prepared 1M HCL solution was kept in glass bottles with different concentrations of MIL extract of 0 ppm, 200 ppm, 400 ppm, 600 ppm, 800 ppm, and 1000 ppm. Anti-corrosive properties of each concentration of MIL extract have been tested on sample coupons using the weight loss method.

Weight Loss Measurement

Experiments were conducted to investigate the degree of metal corrosion in acidic solutions using standard weight loss methods reported in the literature (Bhardwaj et al. 2021). For weight loss measurement studies, the weight of each SS-316L coupon was recorded twice before the immersion test. The stainless-steel coupons were then immersed in 1M HCl as corrosive media without and with MIL extract of different concentrations ranging from 200 to 1000 ppm for 14 days. After specified periods, samples were removed from the acid solutions, followed by cleaning and drying. After that, the specimen samples were again weighed (recorded twice) to obtain the loss in weight upon exposure to test solutions (1M HCl) with and without MIL extract, and average values are reported here.

The rate of corrosion for both uninhibited and inhibited systems was calculated using the following equation (1),

$$C_R(\text{cm/h}) = \frac{\text{weight loss}}{\text{area} \times \text{time}} = \frac{(W_0 - W)}{(\rho \times A \times t)} \quad \ldots(1)$$

where, C_R is the corrosion rate in $cm.h^{-1}$. (which is later converted to $mm.yr^{-1}$.), W_0 and W denotes the weight of SS-316L coupons before and after immersion in acidic medium (g), ρ is the density of material in g/cm^3 (7.86 $g.cm^{-3}$ for steel), A represents the surface area of coupons in cm^2, t represents time of exposure in hrs.

The percentage inhibition efficiency (% IE) of the mango leaf extract as green corrosion inhibitor on SS-316L specimens in the presence of acidic (HCl) medium was computed using equation (2) as,

$$\text{IE \%} = \frac{\text{Corrosion rate without inhibitor} - \text{Corrosion rate with MIL inhibitor}}{\text{Corrosion rate of uninhibited system}} \times 100$$

$$\text{IE (\%)} = \frac{C_{Ro} - C_{Ri}}{C_{Ro}} \times 100 \quad \ldots(2)$$

where, C_{Ro} and C_{Ri} are the corrosion rates of immersed SS-316L coupons in acidic corrosive media and the corrosive solution containing varying concentrations of MIL extract as a green corrosion inhibitor, in ($mm.yr^{-1}$.), respectively.

The concentration of green corrosion inhibitor used and surface coverage with green corrosion inhibitor provided to SS-316L were the main components of this study. Surface coverage (θ) of MIL extract was calculated using the following equation (3)

$$\theta = \frac{C_{Ro} - C_{Ri}}{C_{Ro}} \quad \ldots(3)$$

Characterization of MIL Extract and Metal Specimens

Fourier transform infrared spectroscopy was utilized to identify the functional groups present in mango leaf extract, which are responsible for the anti-corrosive effect. The FTIR analysis was performed using Bruker ALPHA II Model

(available at Central Instrumentation Facility, Savitribai Phule Pune University, Pune) in the range of 500-4000 cm^{-1}.

The Field Emission Scanning Electron Microscopy (of Carl Zeiss make, (model ULTRA 55) available at the Indian Institute of Technology (IIT) Bombay was used to obtain the changes in surface morphology of corroded SS-316L samples. The samples were cut into 5.0 × 5.0 × 3.0 mm for SEM analysis. In addition, energy dispersion spectroscopy (EDS) analysis was performed for the same samples to get the elemental concentration. Two-dimensional images of different resolutions were taken for detailed analysis. For SEM and EDS analysis, SS-316L coupons immersed in the absence of MIL extract and with 600 ppm and 1000 ppm MIL extract were selected for the study.

Adsorption Isotherm Study

Adsorption isotherms are generally used to predict the adsorption behavior of green corrosion inhibitor (MIL extract) on the SS-316L surface. Different isotherms, such as Freundlich, Langmuir, Temkin, and Flory Huggins adsorption isotherms, etc., are widely used in previous studies to characterize the corrosion inhibition study (Ogunleye et al. 2020). In this study, Langmuir and Freundlich's isotherms were utilized for the adsorption study because of their simplicity, and their model parameters give complete information related to the corrosion inhibition study.

Langmuir isotherm model is described by Eqn. (4) as

$$C\left(\frac{1-\theta}{\theta}\right) = \frac{1}{K_{ads}} \quad \ldots(4)$$

In general, Eqn. (4) is linearized to obtain Eqns. (5 or 6) as follows

$$\frac{C}{\theta} = \frac{1}{K_{ads}} + C \quad \ldots(5)$$

$$\log\left[\frac{\theta}{(1-\theta)}\right] = \log K_{ads} + \log C \quad \ldots(6)$$

where C is the concentration of MIL inhibitor in g/L θ represents the fraction of the metal surface covered with the inhibitor calculated using Eqn. (3), and K_{ads} is the equilibrium adsorption constant in $L.g^{-1}$.

The plot of (C/θ) versus C or log [θ/(1-θ)] versus log C gives a straight line with a unit slope, which obeys Langmuir isotherm**.** The correlation coefficient (R^2) close to 1 indicates best-fit isotherm model. The value of K_{ads} is estimated from the reciprocal of the intercept of the linear fit of the plot (C/θ) versus C.

In addition, data obtained from the weight loss study was used to fit the Freundlich adsorption isotherm model is expressed as

$$\theta = K_{ads}\, C^n \quad \ldots(7)$$

It is expressed in linear form as

$$\log\theta = \log K_{ads} + n \log C \quad \ldots(8)$$

where n denotes the slope of the straight-line fit of the graph log θ vs. log C (Freundlich isotherm) The intercept yields the value of the equilibrium constant of adsorption, K_{ads}.

The standard adsorption free energy ΔG^0_{ads} is related to the obtained equilibrium constant (K_{ads}) from isotherm models as presented in Eqn. (9). It is used to represent the feasibility and nature of adsorption, such as physisorption or chemisorption.

$$\Delta G^0_{ads} = -2.303\, RT \log\,(55.5 \times K_{ads}) \quad \ldots(9)$$

where, ΔG^0_{ads} is a change in standard Gibb's free Energy ($kJ.mol^{-1}$), K_{ads} represents the adsorption equilibrium constant obtained from the isotherm plot, *55.5* denotes molar heat of adsorption of water in solution (Akinbulumo et al. 2020), R denotes universal gas constant, and T is the absolute temperature (K). The value of $\Delta G^0_{ads} \leq -20$ kJ mol^{-1} is associated with the physisorption mechanism and $\Delta G^0_{ads} \geq -40$ $kJ.mol^{-1}$ indicates chemical adsorption (Bhardwaj et al. 2021, Akinbulumo et al. 2020).

RESULTS AND DISCUSSION

Weight Loss Analysis

The weight loss method is widely used for quantitative

Table 1: Results of weight loss method of SS-316L coupons immersed in 1 M HCl solution without and with MIL extract after 14 days of immersion.

Concentration of MIL extract [ppm]	Weight Loss after 14 days [g]	Corrosion rate C_R [$mm.yr^{-1}$]	% Inhibition efficiency	Surface coverage [θ]
Blank (or 0 ppm)	0.259	1.184	-	-
200	0.250	1.145	3.33	0.0333
400	0.219	1.094	7.61	0.0761
600	0.173	0.702	40.68	0.4068
800	0.121	0.585	50.59	0.5059
1000	0.105	0.433	63.42	0.6342

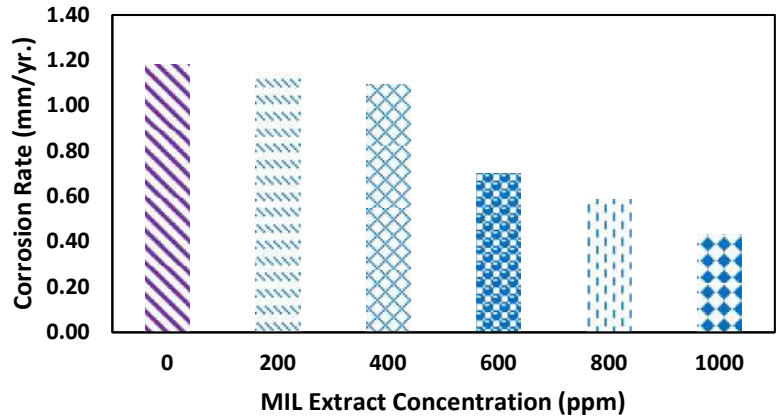

Fig. 1: Bar diagram of Corrosion rate (mm/yr.) of SS-316L after immersion in 1M HCl medium without and with MIL extract at different concentrations for 14 days.

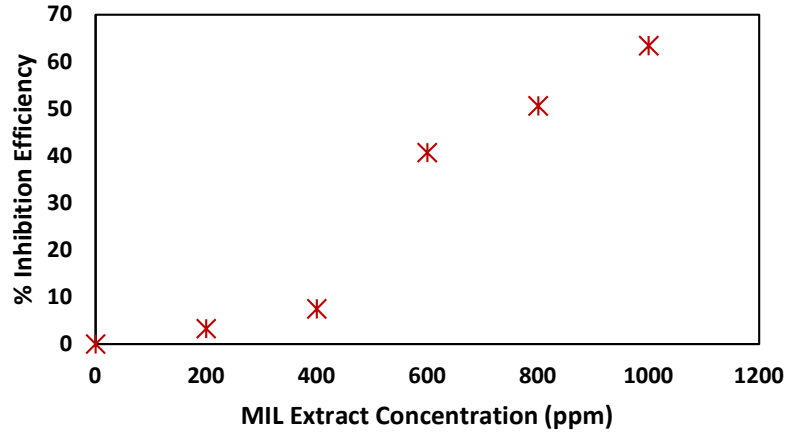

Fig. 2: Percentage inhibition efficiency of SS-316L after immersion in 1M HCl medium without and with MIL extract at different concentrations for 14 days.

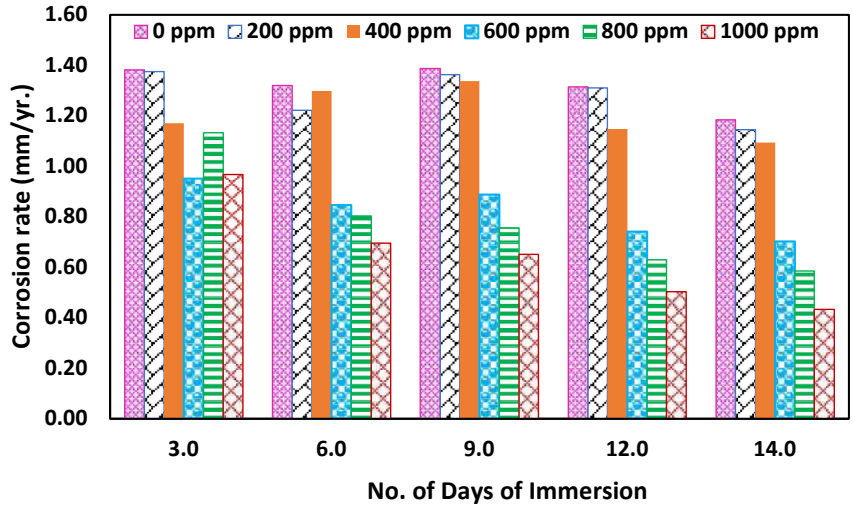

Fig. 3: Variation of Corrosion rate (mm/yr.) of SS-316L with time and variation of MIL extract concentrations.

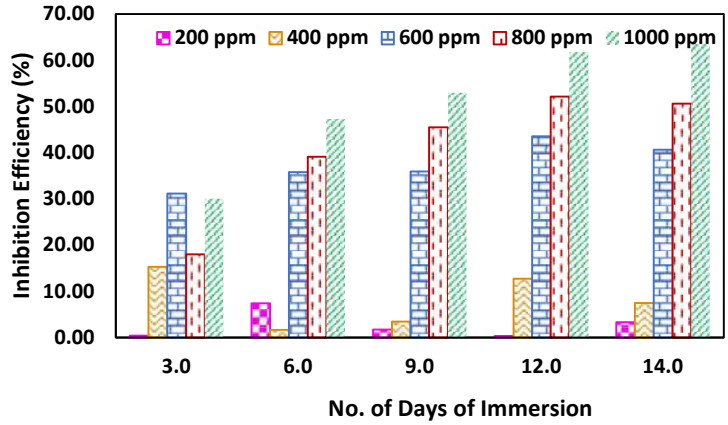

Fig. 4: Variation of Inhibition efficiency of SS-316L with time and different concentrations of MIL extract in 1 M HCl.

evaluation of metal corrosion inhibition as it utilizes simple and easy-to-measure parameters, i.e., loss in weight of the metal after exposure to a corrosive medium. The corrosion rate and percentage inhibition efficiency of SS-316L coupons obtained from the systematic weight loss experimental runs for various concentrations of MIL extract ranging from 200 to 1000 ppm after 14 days of immersion in acidic corrosive media are exhibited in Table 1 and Figs. 1 and 2, respectively. The presented data in Table 1 indicated that weight loss after 14 days of immersion in 1M HCl with 1000 ppm of MIL extract is 0.105 g as compared to a greater weight loss of 0.259 g in the absence of an inhibitor. Figs. 1 and 2 depict that the value of the corrosion rate of SS-316L decreases with an increase in the concentration of MIL extract, resulting in an increase in inhibition efficiency after immersion in 14 days. It is seen from the plots that inhibition efficiency is less than 50% up to 600 ppm MIL extract, and after that, it increases significantly with an increase in inhibitor concentration. The maximum % corrosion inhibition efficiency of 63.42% and minimum corrosion rate (0.433 $mm.yr^{-1}$.) were obtained using 1000 ppm of MIL extract.

Similarly, detailed result analysis of variation of corrosion rate ($mm.yr^{-1}$.) and inhibition efficiency (%) with time (3, 6, 9, 12, and 14 days) and MIL extract concentrations (0, 200, 400, 600, 800 and 1000 ppm) are shown in Figs. 3 and 4, respectively. Analysis of figures reveals the impact of the MIL extract on corrosion rate as well as in inhibition efficiency with time. This finding implies that mango leaf extract forms a protective film on the SS-316L surface and thus gives a significant reduction in corrosion rate and

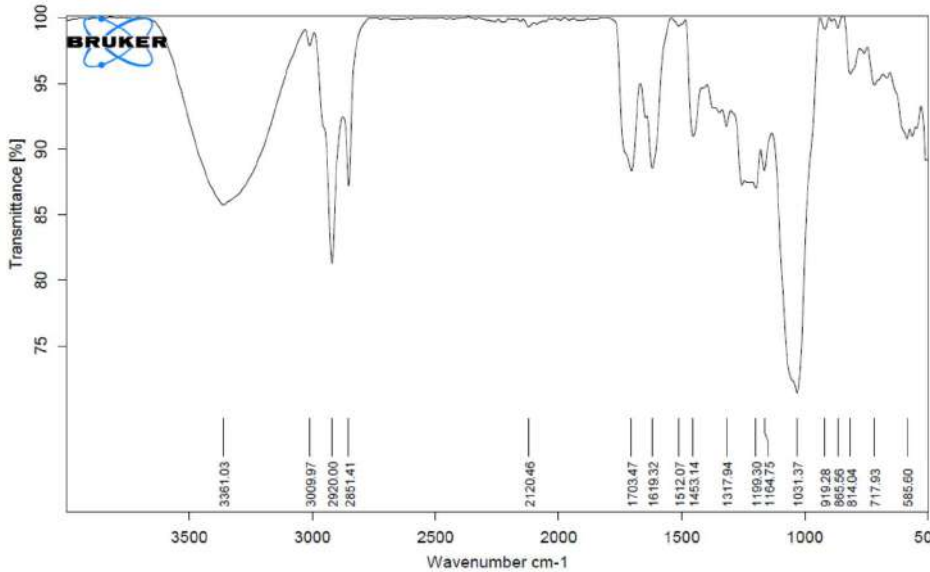

Fig. 5: FTIR spectrum of *Mangifera indica* Leaf extract.

increment in inhibition efficiency in an acid environment. This corrosion inhibition film of MIL extract on SS-316L can be attributed to the presence of many active functional groups in organic components of MIL extract, such as gallic acid, mangiferin iriflophenone, etc., and thus, may act as inhibitors to protect the metal surface. Results presented in Table 1 also show that maximum surface coverage was obtained at 1000 ppm of MIL extract. Previous investigations showed a similar trend of corrosion rate and inhibition efficiency of green inhibitors for mild steel corrosion in an acidic (HCl) environment (Shamsheera et al. 2022, Akinbulumo et al. 2020). Overall, it can be concluded that this MIL extract acts as an efficient green corrosion inhibitor for stainless steel grade SS-316L in a hydrochloric acid medium.

FTIR Analysis

The FTIR spectrum of the mango leaf extract was conducted, and the results are reported in Fig. 5. The spectra of mango leaf extract depict a broad peak at wavenumber 3361.03 cm^{-1} exhibits O-H bond stretching vibration of phenolic compounds and alcohols. Three peaks of aromatic ring C-H bond stretching were observed at 3009.97 cm^{-1}, 2920 $cm^{-1,}$ and 2851.41 cm^{-1}. Further, the peak of O-H/C-H bending of the phenol group appeared at 1317.94 $cm^{-1,}$ and C=C bond stretching in the aromatic ring was confirmed at 1453.14 and 1512.07 cm^{-1}. Three peaks at 1619.32, 1703.47 $cm^{-1,}$ and 1031.37 cm^{-1} with medium to strong intensity were attributed to the presence of stretching vibration of carbonyl groups (C=O and C-O). These peaks are identical to the FTIR spectrum of mango leaf extract reported by Veddu et al., 2019 and Ramezanzadeh et al., 2019. Hence, previous findings and present results revealed the presence of various functional groups in MIL extracts such as gallic acid (3,4,5-Trihydroxybenzoic acid), mangiferin (C 2-β-d-glucopyranosyl-1,3,6,7-tetrahydroxyxanthone) and iriflophenone (4-hydroxyphenyl) -(2,4,6-tri hydroxyphenyl) methanone) etc. (Ramezanzadeh et al. 2019, Veedu et al. 2019). This FTIR analysis confirms the corrosion inhibition activity is mainly due to the presence of heteroatoms in the synthesized MIL extract that can easily adsorb on metal surfaces and thus act as a protective film to inhibit stainless steel corrosion. Further investigation using SEM and EDS analysis along with adsorption isotherm analysis was conducted to infer more information about the protective layer formation of synthesized green corrosion inhibitor on the SS-316L surface.

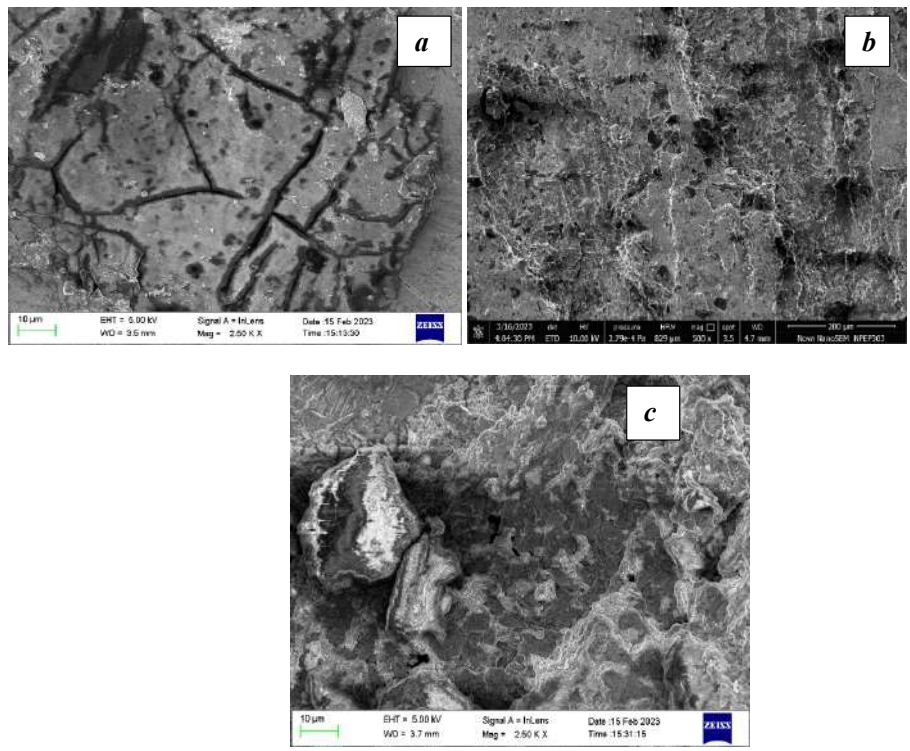

Fig. 6: FE-SEM image of SS-316L coupons immersed in 1 M HCl solutions (*a*) without MIL extract, (*b*) with 600 ppm MIL extract, (*c*) with 1000 ppm MIL extract.

Scanning Electron Microscopic Analysis

The surface morphology of SS-316L coupons exposed to 1 M HCl solution without and with MIL extract (1000 and 600 ppm concentration) was evaluated using FE-SEM images. FE-SEM image for SS-316L coupon immersed in 1 M HCl solution without inhibitor is displayed in Fig. 6 a, and with 600 and 1000 ppm MIL extract are presented in Figs. 6 b and c, respectively. It is seen from the FE-SEM image that the SS-316L sample immersed in 1M HCl solution without MIL extract inhibitor has a rough and corroded texture on the surface (Fig. 6 a), indicating the severe corrosion of the specimen. Figs. 6 b and c exhibited the formation of the protective layer of MIL extract (white film observed) but with some localized pitting corrosion (black spots). This deposition of inhibitor film on the surface indicated the covering of the ML extract on the metal specimen surface, which prevents contact of corrosive media with the surface. Therefore, the damage to the SS-316L surface is noticeably less in the presence of an inhibitor (Figs. 6 b and c). Many

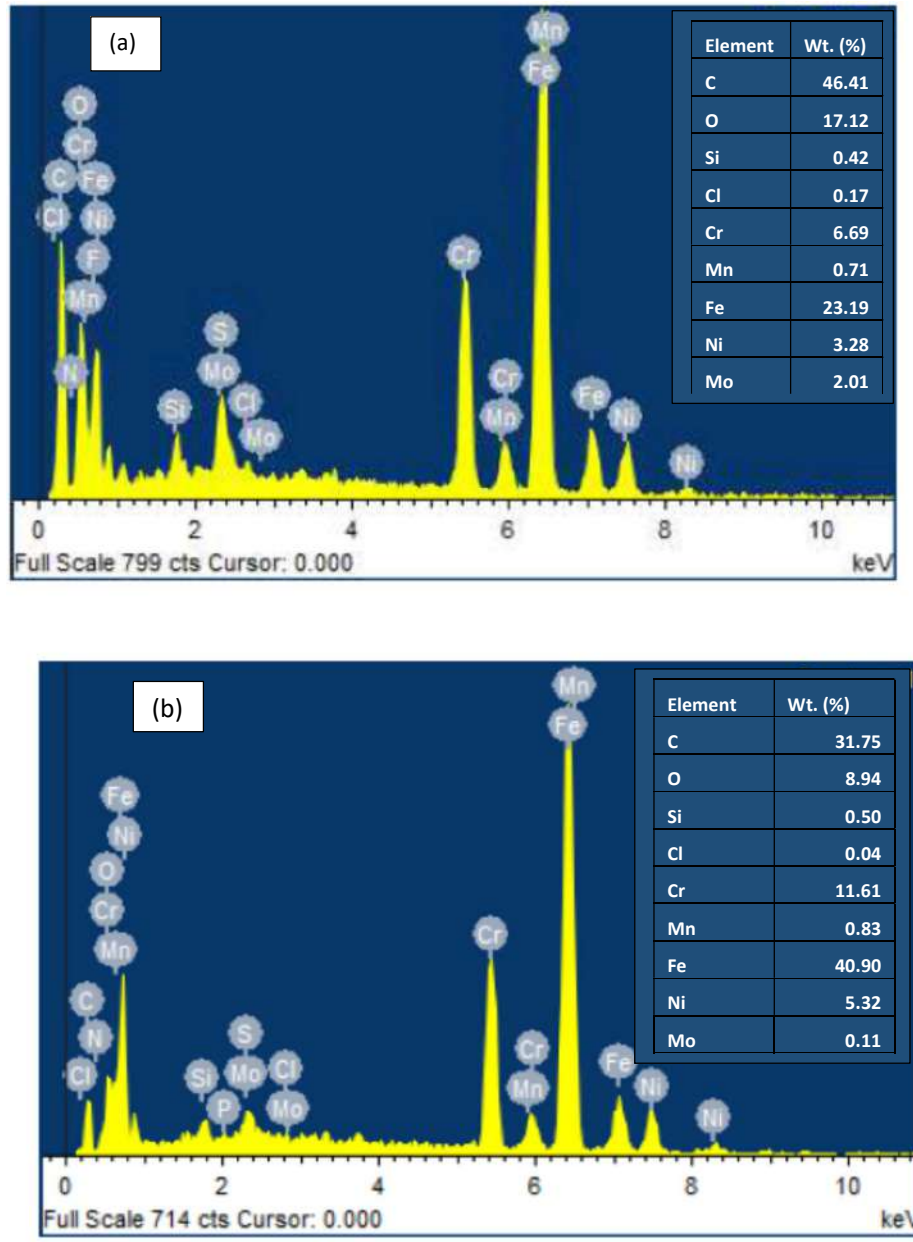

Fig. 7: EDS spectrum of SS-316L coupons after 14 days of immersion in 1M HCl (*a*) without MIL inhibitor (*b*) with 1000 ppm MIL inhibitor.

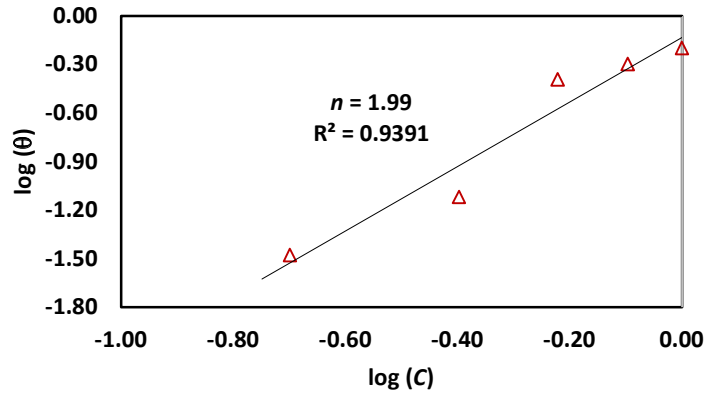

Fig. 8: Freundlich Adsorption Isotherm of MIL inhibitor.

cracks and pits were observed on the surface of the sample due to corrosion in the absence of an inhibitor, and localized pitting was observed at a low concentration of 600 ppm of inhibitor, as exhibited in Fig. 6 b. Compared to a specimen immersed in 1000 ppm, the metal coupon immersed in 600 ppm is more corroded but less than the bare specimen. Thus, it can be concluded that bare stainless steel is hard to resist the corrosion of acid. In contrast, the protected surface, due to the layering of the inhibitor (Figs. 6 b and c), provides more corrosion resistance. The present results are confirmed with similar results of corrosion inhibition reported by Ramezanzadeh et al. (2019) with *Mangifera indica* leaf extract on the mild steel surface.

Subsequently, EDS analysis was performed to determine the elemental analysis of metal specimens in the absence and presence of an inhibitor. EDS spectrum of SS-316L coupons after 14 days of immersion in 1M HCl without MIL inhibitor and with 1000 ppm MIL inhibitor are presented in Fig. 7 a and b, respectively. It is important to note that the addition of an inhibitor forms a protective film on the metal surface to protect it from an HCl attack. This resulted in a higher content of Fe, Cr, Ni, and Mn and less carbon, chlorine, and oxygen content in the presence of 1000 ppm MIL inhibitor than blank solution, as exhibited in Fig. 7 b. Conversely, as evident from Fig. 7 a, higher amounts of C, O, and Cl species and less percentage of Fe were obtained with uninhibited samples, indicating the formation of corrosion products on the surface. This reveals that in the absence of an inhibitor, the inherent protective film of chromium oxide is unable to resist the attack by HCl, resulting in increased pitting and even crack formation (Fig. 6 a). These findings illustrated that the organic compounds with heteroatoms present in the MIL extract help to evade the contact of stainless-steel surface with corrosive media and, hence, increased inhibition efficiency (Table 1).

In contrast, without MIL extract, the corrosion rate of stainless steel in an acidic solution was significantly enhanced. These results are consistent with the observed trend from the weight loss method, FTIR, and SEM analysis. Hence, the morphological characterization confirmed the formation of the anticorrosive film of MIL extract on the SS-316L surface and thus resisted the acid corrosion efficiently.

Adsorption Study

The result obtained from the fitting of various isotherms provides detailed insight into the adsorption mechanism and inhibition activity of the MIL extract at the interface between the corrosive medium and SS-316L surface. Firstly, the Langmuir isotherm plot was plotted between C/θ versus C based on Eqn. (5), but the fitting of the experimental data results in a poor fit with a low R^2 value, and hence, results are not reported here.

Later, Freundlich isotherm was plotted with obtained experimental data of log (θ) versus log (C) for MIL extract after 14 days and displayed in Fig 8. Freundlich isotherm parameters n and equilibrium adsorption constant K_{ads} were evaluated from the slope and intercept of the same plot. Fig. 8 depicts the best fit of the Freundlich adsorption isotherm model to experimental data with an R^2 value of 0.94 and an obtained value of n from the slope of the graph close to 2. This fitting of Freundlich adsorption isotherm confirmed the development of multilayer adsorption (i.e., physisorption) of MIL extract at heterogenous sites on the SS-316L surface, which is the main assumption of the Freundlich equation. In contrast, Langmuir isotherm assumes monolayer adsorption on homogeneous sites and, thus, results in poor fitting for the present data.

Furthermore, the obtained K_{ads} value from the intercept of the best-fit line at 298 K is 0.7389 $L.g^{-1}$, showing effective adsorption of MIL extract on the SS-316L surface, which indicates better protection of metal specimen and hence efficient anti-corrosion nature of synthesized green corrosion inhibitor. The obtained value of free Energy

of adsorption (ΔG°_{ads}) from Eqn. (9) is – 9.20 kJ.mol^{-1} at 298 K (< – 20 kJ.mol^{-1}), indicating adsorption of MIL extract on SS-316L surface is spontaneous, feasible, and via physisorption mechanism as a result of electrostatic interaction between the charged metal and the inhibitor molecule. The obtained results showed good agreement with the previous investigation of corrosion inhibition study using leaves and stem extracts of Sida Acuta with values of free Energy of adsorption at 303 K (ΔG°_{ads} = – 10.6 kJ.mol^{-1}) and K_{ads} value of 1.22 L.g^{-1} by Umoren et al. (2016). So, it can be concluded from the obtained ΔG°_{ads} values that the MIL adsorbed physically on the SS-316L surface for the development of protective layers against corrosion.

Mathematical Model Development for Prediction of Corrosion Rate

In this study, two mathematical models (linear and quadratic) based on multivariate regression analysis were developed for the estimation of the corrosion rate for SS-316L against 1 M HCl. The experimental data of the corrosion study obtained in this work were utilized to develop the models, which comprise inhibitor concentration and exposure time as the input parameters and corrosion rate as the out parameter. The effect of individual variables and the interaction between them was considered in both models.

Multivariate regression is a standard statistical method used to estimate the relationship between the one dependent variable of interest (also known as a response variable, i.e., the targeted output) and multiple independent variables (called predictor variables).

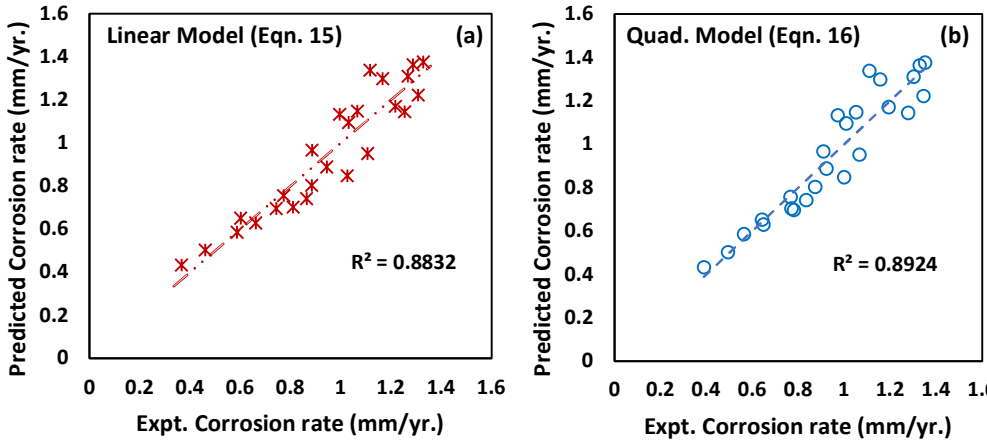

Fig. 9: Predicted corrosion rate using (a) linear model eqn. 15 (b) quadratic model eqn. 16 versus experimental corrosion rate.

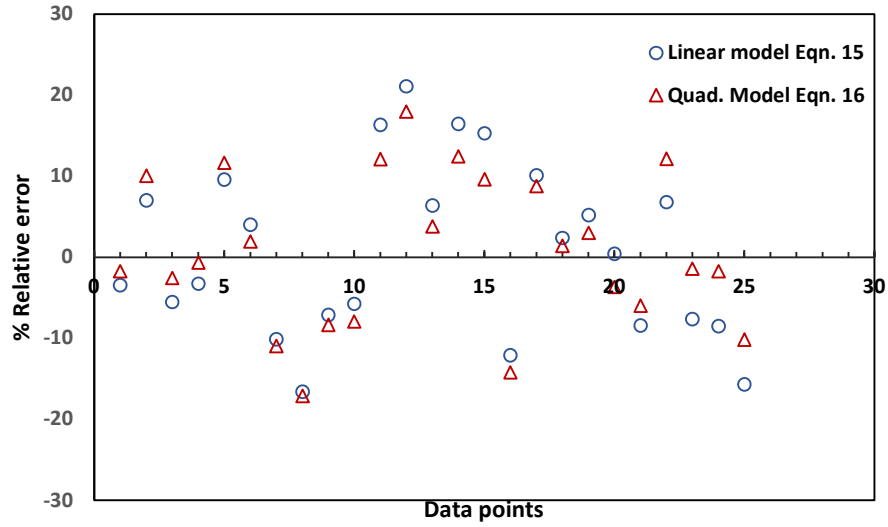

Fig. 10: % Relative error for the relevant data points using (o) linear and (Δ) quadratic model.

Multivariable linear model was developed in the form mentioned below:

$$C_R = a_0 + a_1 \times C + a_2 \times t + a_3 \times C \times t + \varepsilon \quad \ldots(10)$$

Similarly, the developed multivariable quadratic model can be expressed by the following equation:

$$C_R = a_0 + a_1 \times C + a_2 \times t + a_3 \times C^2 + a_4 \times t^2 + a_5 \times C \times t + \varepsilon \quad \ldots(11)$$

where C_R represents corrosion rate, C denotes inhibitor concentration, and t is exposure time, a_0, a_1, a_2, a_3, a_4 and a_5 are model parameters, and ε is residuals between predicted and experimental values.

The optimal parameters a_0, a_1, a_2, a_3, a_4 and a_5 of proposed models (Eqns. 10 and 11) that best fit the data points were estimated using a least square method that minimizes the square of residuals (SSR).

$$SSR = \sum_{i=1}^{n} \varepsilon_i^2 = \sum_{i=1}^{n} \left(Y_i - \sum_{j=1}^{k} a_j X_{ij}\right)^2 \quad \ldots(12)$$

In this equation, n is the number of experiments, Y represents the experimental output (C_R) and X denotes the experimental inputs (C and t).

To evaluate the efficiency and accuracy of the developed regression-based models, two statistical parameters, namely percentage relative error and coefficient of determination, were utilized.

Performance of the Developed Models Using Statistical Error Analysis

To measure the efficiency and accuracy of the developed model, two statistical metrics, namely percentage relative error and coefficient of determination, were used. Percentage relative error or percentage error that represents the relative deviation of predicted corrosion rate from the experimental value.

$$E_i = \left(\frac{(C_R)_{Pred.} - (C_R)_{expt.}}{(C_R)_{expt.}}\right) \times 100, i = 1, 2, \ldots, n \quad \ldots(13)$$

The coefficient of determination indicates how close the model's predicted value is to the actual experimental value.

$$R^2 = 1 - \frac{\sum_{i=1}^{n}\left[(C_R)_{Pred.} - (C_R)_{expt.}\right]^2}{\sum_{i=1}^{n}\left[(C_R)_{Pred.} - \overline{(C_R)}_{expt.}\right]^2} \quad \ldots(14)$$

If the value of R^2 is close to unity means the model is best fitted to experimental values.

The optimal parameters were computed using multivariate regression using EXCEL, and overall linear and quadratic models are represented by Eqns. 15 and 16 as follows:

$$C_R = 1.43 - 0.0004 \times C + 0.00343 \times t - 5.1 \times 10^{-5} \times C \times t \quad \ldots(15)$$

$$C_R = 1.507 - 0.00088 \times C + 0.01302 \times t + 3.98 \times 10^{-7} \times C^2 - 0.00056 \times t^2 \quad 5.1 \times 10^{-5} \times C \times t \quad \ldots(16)$$

Fig. 9 a and b depict the linear and quadratic model predicted results of corrosion rate (using Eqns. 15 and 16) versus experimental corrosion rate data. As depicted in Fig. 9 a and b, the predicted corrosion rate using multivariate regression linear and quadratic models exhibits good agreement with experimental data. However, as evident in Fig. 9 b, the quadratic model exhibits slightly better performance than the linear model by achieving higher coefficient of determination values of 0.89 as compared to the linear model (R^2 = 0.88). Finally, the percentage relative deviation from the multivariate linear and quadratic regression models versus the relative data index is illustrated in Fig. 10. As can be seen in this figure, the maximum percentage relative error is higher in the linear model (21%) as compared to the quadratic model (17%). These results reveal that the quadratic model predicts corrosion rate with a higher accuracy of 82% as compared to the linear regression model with an accuracy of 79%.

CONCLUSIONS

The corrosion resistivity of eco-friendly *Mangifera indica* leaves extract on the surface of stainless steel (SS-316L) in hydrochloric acid solution was evaluated using weight loss, adsorption isotherm, FTIR spectroscopy, Scanning electron microscopic and Energy dispersive spectroscopic techniques. Weight loss analysis reveals that *Mangifera indica* leaf extract efficiently inhibits corrosion of stainless steel (SS-316L) in 1 M HCl media with inhibition efficiency of 63.42% at 1000 ppm MIL concentration. The enhancement in inhibition efficiency and detraction in the corrosion rate of SS-316L was obtained with an increase in MIL extract concentration and immersion time. Furthermore, FTIR analysis confirmed the presence of functional groups with heteroatoms (electron donating) in the MIL extract, which exhibited the corrosion-resistant effect against the hydrochloric acid solution. Detailed analysis using SEM and EDS further confirmed the severely corroded metal surface in the absence of MIL extract. The results of the corrosion behavior of MIL extract at different concentrations obtained using weight loss measurements are in good agreement with those obtained from FTIR, SEM, and EDS analysis. The Freundlich adsorption isotherm fits well with the data, clearly indicates the multilayer adsorption of organic constituents

present in MIL extract, which implies physisorption on the surface of stainless steel. The obtained negative value of ΔG^{o}_{ads} indicates corrosion reaction is spontaneous in an acidic solution. Lastly, the developed multivariate regression-based models can predict corrosion rate with a relative percentage error of less than 21%. Hence, it can be concluded that *Mangifera indica* leaf extract can be utilized as an eco-friendly, low-cost, and efficient green corrosion inhibitor in the hydrochloric acid environment for stainless steel (SS-316L) as a substitute for existing toxic and costly corrosion inhibitors.

REFERENCES

Abboud, Y., Tanane, O., El Bouari, A., Salghi, R., Hammouti, B., Chetouani, A. and Jodeh, S. and 2016. Corrosion inhibition of carbon steel in hydrochloric acid solution using pomegranate leaf extracts. Corros. Eng. Sci. Technol., 565-557 :(8)51. http://dx.doi.org/10.1179/1743278215Y.0000000058.

Akinbulumo, O.A., Odejobi, O.J. and Odekanle, E.L. 2020. Thermodynamics and adsorption study of the corrosion inhibition of mild steel by Euphorbia heterophylla L. extract in 1.5 M HCl. Results Mater., 5: 100074. https://doi.org/10.1016/j.rinma.2020.100074.

Aslam, R., Mobin, M., Zehra, S. and Aslam, J. 2022. A comprehensive review of corrosion inhibitors employed to mitigate stainless steel corrosion in different environments. J. Mol. Liq., 364: 119992. https://doi.org/10.1016/j.molliq.2022.119992

Bhardwaj, N., Sharma P. and Kumar V. 2021. Triticum aestivum extract as corrosion inhibitor for stainless steel (SS-410) in acidic media: Experimental and theoretical study. Curr. Res. Green Sustain. Chem., 4: 100189.

Buchheit, R.G. 2018. Corrosion Resistant Coatings and Paints, In Kutz, M. (ed), Handbook of Environmental Degradation of Materials, Third Edition, William Andrew Publishing, NY, pp. 449-468. https://doi.org/10.1016/B978-0-323-52472-8.00022-8.

da Rocha, J.C., da Cunha Ponciano Gomes, J.A. and D'Elia, E. 2010. Corrosion inhibition of carbon steel in hydrochloric acid solution by fruit peel aqueous extracts. Corros. Sci., 52: 2341-2348. https://doi.org/10.1016/j.corsci.2010.03.033

Gaidhani, K.Y., Khurpade, P.D. and Nandi, S. 2020. Hibiscus leaves extract: A green corrosion inhibitor. J. Indian Chem, Soc., 97: 865-869.

Impact Report. 2016. Assessment of Global Cost of Corrosion. http://impact.nace.org/economic-impact.aspx. Accessed 23 Mar 2023.

Loto, R.T., Loto, C.A. and Akinyele, M. 2020. Effect of ginger, pomegranate, and celery extracts on zinc electrodeposition, surface morphology, and corrosion inhibition of mild steel. Alex. Eng. J., 59(2): 933-941. https://doi.org/10.1016/j.aej.2020.03.014.

Mirza, B., Croley, C.R., Ahmad, M., Pumarol, J., Das, N., Sethi, G. and Bishayee, A. 2021. Mango (*Mangifera indica* L.): A magnificent plant with cancer-preventive and anticancer therapeutic potential. Crit. Rev. Food Sci. Nutri., 2151-2125 :(13)61. https://doi.org/10.1080/10408398.2020.1771678

Mourya, P., Banerjee, S. and Singh, M.M. 2014. Corrosion inhibition of mild steel in acidic solution by Tagetes erecta (marigold flower) extracts as a green inhibitor. Corros. Sci., 85: 352-363. https://doi.org/10.1016/j.corsci.2014.04.036

Oguike, R.S. 2014. Corrosion studies on stainless steel (FE6956) in hydrochloric acid solution. Adv. Mater. Phys. Chem., 4: 153-163. http://dx.doi.org/10.4236/ampc.2014.48018

Ogunleye, O.O., Arinkoola, A.O., Eletta, O.A, Agbede, O.O., Osho, Y.A., Morakinyo, A. F. and Hamed, J.O. 2020. Green corrosion inhibition and adsorption characteristics of Luffa cylindrica leaf extract on mild steel in a hydrochloric acid environment. Heliyon, 6: e03205. https://doi.org/10.1016/j.heliyon.2020.e03205.

Pal, A. and Das, C. 2023. Novel use of kitchen waste: protection of boiler quality steel from corrosion in acidic media using onion waste. Chem. Paper, 77: 1107-1127. https://doi.org/10.1007/s11696-022-02549-7

Patricia, E.A., Fiori-Bimbi, M.V., Adriana, N., Silvia, A.B. and Claudio, A.G. 2018. Rollinia occidentalis extract as green corrosion inhibitor for carbon steel in HCl solution. J. Ind. Eng. Chem., 25: 92-99. https://doi.org/10.1016/j.jiec.2017.09.012

Ramezanzadeh, M., Bahlakeh, G., Sanaei, Z. and Ramezanzadeh, B. 2019. Corrosion inhibition of mild steel in 1 M HCl solution by ethanolic extract of eco-friendly *Mangifera indica* (mango) leaves: Electrochemical, molecular dynamics, Monte Carlo and ab initio study. Appl. Surf. Sci., 463: 1058-1077. https://doi.org/10.1016/j.apsusc.2018.09.029.

Salleh, S.Z., Yusoff, A.H., Zakaria, S.K., Taib, M.A.A., Seman, A.A., Masri, M.N., Mohamad, M., Mamat, S., Sobri, S.A., Ali, A. and Teo, P.T. 2021. Plant extracts as green corrosion inhibitor for ferrous metal alloys: A review. J. Clean. Prod., 304: 127030. https://doi.org/10.1016/j.jclepro.2021.127030.

Sharma, S.K., Mudhoo A., Jain G. and Khamis E. 2009. Corrosion inhibition of neem (*Azadirachta indica*) leaves extract as a green corrosion inhibitor for zinc in H_2SO_4. Green Chem. Lett. Rev., 2(1): 47-51. https://doi.org/10.1080/17518250903002335.

Simescu-Lazar, F., Slaoui, S., Essahli, M., Bohr, F., Lamiri, A., Vanoye, L. and Chopart, J.P. 2023. *Thymus satureoides* oil as green corrosion inhibitor for 316L stainless steel in 3% NaCl. Exper. Theoret. Stud. Lubri., 11(56): 56-63. https://doi.org/10.3390/lubricants11020056.

Shamsheera, K.O., Prasad, A.R., Arshad, M. and Joseph, A. 2022. A sustainable method of mitigating acid corrosion of mild steel using jackfruit pectin (JP) as green inhibitor: Theoretical and electrochemical studies. J. Indian Chem. Soc., 99: 100271. https://doi.org/10.1016/j.jics.2021.100271.

Umoren, S.A., Eduok, U.M., Solomon, M.M. and Udoh, A.P. 2016. Corrosion inhibition by leaves and stem extracts of *Sida acuta* for mild steel in 1 M H2SO4 solutions investigated by chemical and spectroscopic techniques. Arab. J. Chem., 9: S209-S224. http://dx.doi.org/10.1016/j.arabjc.2011.03.008

Veedu, K.K., Kalarikkal, T.P., Jayakumar, N.N. and Gopalan, N.K. 2019. Anticorrosive performance of *Mangifera indica* L. leaf extract-based hybrid coating on steel. ACS Omega, 4(6): 10176-10184. https://doi.org/10.1021/acsomega.9b00632.

Zhou, X., Dong, O., Wei, D., Bai, J., Xue, F., Zhang, B., Ba, Z. and Wang, Z. 2023. Smart corrosion inhibitors for controlled release: A review. Corros. Eng. Sci. Technol., 204-190 :(2)58. https://doi.org/10.1080/1478422X.2022.2161122.

ORCID DETAILS OF THE AUTHORS

Pratiksha D. Khurpade: https://orcid.org/0000-0002-6658-4614

Nature Environment and Pollution Technology
An International Quarterly Scientific Journal

p-ISSN: 0972-6268
(Print copies up to 2016)
e-ISSN: 2395-3454

Vol. 23 | No. 1 | pp. 151-160 | 2024

Original Research Paper

https://doi.org/10.46488/NEPT.2024.v23i01.011

Open Access Journal

Will Development and Temperature be Reconciled?

Faradiba Faradiba*†, St. Fatimah Azzahra, Endah Yuniarti***, Lodewik Zet****, Tris Kurniawati Laia* and Rini Wulandari*****

*Physics Education Study Program, Universitas Kristen, Indonesia
**Chemistry Education Study Program, Universitas Kristen, Indonesia
***Aviation Engineering Study Program, Universitas Dirgantara, Marsekal, Suryadarma, Indonesia
****BPS-Statistics, Indonesia
†Corresponding author: Faradiba Faradiba; faradiba@uki.ac.id

Nat. Env. & Poll. Tech.
Website: www.neptjournal.com

Received: 13-07-2023
Revised: 08-08-2023
Accepted: 23-08-2023

Key Words:
Rural development
Air pollution
Temperature increase
Multiple correspondence analysis
Instrumental variables method

ABSTRACT

The country's advancement is fueled by regional growth. It frequently has many detrimental effects in its application, including contamination. Climate, notably temperature, is negatively impacted by the ensuing pollution. This study uses the Multiple Correspondence Analysis (MCA) method to measure the pollution index, followed by the instrumental variable (IV) method to calculate the effect of development on pollution and temperature. Rural data from Podes 2018 is among the data used in this investigation. The findings of this study show that developed and developing areas are where the negative pollution index forms the most frequently. The construction and the resulting pollution index have a negative impact on temperature. The development process should pay attention to environmental aspects to anticipate worse temperature changes in the coming period.

INTRODUCTION

The issue of global warming has become a tough task for implementation in fighting these problems. Apart from having to pursue measurable development achievements in socio-economic indicators, the government is asked to maintain the environmental conditions of the local area and those around it (Faradiba & Lodewik 2020, Wood & DeClerck 2015, Zhang et al. 2017). Global warming that has occurred has begun to be felt in various aspects of life, so the country has made efforts through various regulations to combat these problems (Bahrami et al. 2022, De Schryver et al. 2009, Houillon & Jolliet 2005, Peters et al. 2011).

The simplest global warming can be felt through weather conditions that are getting warmer every day. This phenomenon occurs because humans will compare the current temperature conditions with the conditions some time ago (Faradiba 2021, Foster & Rahmstorf 2011, Hansen et al. 2006, Li et al. 2011). To increase comfort in activities, people often take shortcuts by using an Air Conditioner (AC). Community use of air conditioning will disrupt the ozone layer and later will have a negative impact on global air temperature (Bolaji & Huan 2013, Busakhin 2022). On the other hand, without realizing it, the development carried out by the government will have an impact on the surrounding environment (Jalil & Feridun 2011). Exploration of natural resources will disturb the balance of the ecosystem (Mogborukor 2014, Wilkinson et al. 2013). Significant development accelerations can be achieved when the country's focus has shifted from primary economic activities to secondary and tertiary economies. It is known that the primary economy promotes sectors based on nature. The signal of a shift in economic activity is thought to be due to the lack of natural resources in the local area.

The transition of economic activity in developed regions tends to be based on the industrial sector. The industrial sector will have greater added value. However, the residual waste caused by industrial processes is also very worrying (Li & Randak 2009, Zhang et al. 2016). The waste disposal can be in the form of liquid, solid, and gas, all of which will disrupt the nature-based economic sector. This problem is usually resolved through the concentration of industrial areas located from residential areas and fields where agricultural businesses are located (Reni et al. 2022).

The phenomenon that occurs in Indonesia today is that many people have switched professions from the agricultural sector to the non-agricultural sector. This supports the

economic theory, which states that people will leave the primary sector and switch to other sectors (Inglehart 2018). Based on Fig. 1, it is known that economic progress, as measured by the rural development index, is still centered on the island of Java. This condition is in contrast to the areas in eastern Indonesia, which are still largely underdeveloped. The difference between Java Island and eastern Indonesia is not only visible from the conditions of development, but the consequences of natural ecosystems are also important. The natural ecosystems in eastern Indonesia tend to be well preserved compared to Java Island (Marshall & Beehler 2012, Sindhu 2017). The current condition shows that most of the villages are catching up, especially in areas that are left behind in developing areas.

Based on Fig. 2, natural conditions that are still natural can be seen from the temperature conditions in eastern Indonesia. The temperature in Indonesia is relatively low when compared to other regions. Extreme conditions can be seen in areas on the island of Java. Java Island has a relatively high temperature level in almost all regions (Kameswara & Suharjit 2023). Extreme conditions can also be seen in East Kalimantan Province. East Kalimantan Province is a province outside Java Island that has significant economic activity in supporting the Indonesian economy.

The phenomenon between development followed by pollution and having an impact on air temperature is like the two blades (Hamed et al. 2013, Senthilkumar 2019). On the one hand, the government wants socio-economic problems in the community through economic activities, but on the other hand, there are things that need to be sacrificed. Many studies have concluded that economic progress as measured by GDP will have an impact on temperature at both the country and provincial levels. This research will determine the impact of development instrumented with a pollution index and its impact on increasing air temperature. Additionally, the Multiple Correspondence Analysis (MCA) technique will be used to assess the pollution index in this study. This research makes use of many rural-level indicators, including

Fig. 1: Distribution of Rural Development Index and transition of development acceleration.

Fig. 2: Average temperature by Province 2018.

the development index and the pollution index. The village development index employed has taken into account a variety of factors, including government, economics, health, and education (BPS 2019). The pollution index built includes all pollution felt by rural communities.

MATERIALS AND METHODS

This research makes use of information from BPS-Statistics Indonesia's Village Potential 2018 findings, which include information on 75,436 villages. The pollution index will be created in this study to assess the level of pollution in rural regions. Additionally, this study makes use of data from the Rural Development Index that takes into account numerous features of a community. For this investigation, the BMKG-Meteorology, Climatology, and Geophysics Agency provided temperature data.

Multiple Correspondence Analysis (MCA)

Based on research findings from Yokota et al. (2017), the Multiple Correspondence Analysis (MCA) approach is used in this study (Yokota et al. 2017) to create the pollution index. By using this technique, category indices have been measured (Abdi & Valentin 2007, Asselin & Anh 2008, Rodrigues et al. 2016). Each of the *K* variables in the computation has a level of *Jk*, where *J* is the total of all *Jk*. Included are as many observations as *I* can count. The letter *X* stands for the $I \times J$ matrix. Two sets of factor scores will be generated by doing a correspondence analysis on the indicator matrix: one for the rows and one for the columns. Scaling the variance of these component scores to coincide with the relevant eigenvalues is a typical procedure. The breakdown of a single value in the following equation yields the factor score:

$$D_r^{-\frac{1}{2}}(Z - rc^T)D_c^{-\frac{1}{2}} = P\Delta Q^T \quad \ldots(1)$$

(Where an eigenvalue matrix is a diagonal matrix with a single value). The following equation is used to get the row and column factor scores, respectively:

$$F = D_r^{-\frac{1}{2}} P\Delta \qquad G = D_c^{-\frac{1}{2}} Q\Delta \quad \ldots(2)$$

The following equation may be used to indicate the distance squared between rows and columns:

$$d_r = diag\{FF^T\} \qquad d_c = diag\{GG^T\} \quad \ldots(3)$$

Instrumental Variable (IV)

The model has an endogeneity problem; hence, this inquiry will continue using the Instrumental Variable (IV) method. According to Wooldridge (2016), instrumental variable analysis provides a solution to the endogeneity problem. The Ordinary Least Square (OLS) estimator will be biased and inconsistent in the absence of a critical variable. Say there is a simple regression equation that appears as follows:

$$y = \beta_0 + \beta_i x + u \quad \ldots(4)$$

The relevance instrument is the name given to this supposition. The variable *z* is referred to as the instrument or instrumental variable for the variable *x*. Additionally, the so-called endogenous variable x elevates the subsequent regression equation:

$$x = \pi_0 + \pi_i x + z + v \quad \ldots(5)$$

The IV technique, according to Gujarati and Porter (2009), is completed in two steps. The first step is to use regression equation (2) to estimate the value of the variable *x*, represented by the symbol x. The next step is to insert the value of the variable x into equation (1) and run OLS regression. This second stage estimate is an unbiased and consistent estimator from the IV approach. These models will be developed for this study:

Preliminary model

$$Pollution_{index} = \alpha + \beta_1 rural\ development_{index} + \beta_2 GDRP_{per\ capita} + \beta_i X_i + \varepsilon \quad \ldots(6)$$

Temperature OLS model

$$Temperature = \alpha + \beta_1 pollution_{index} + \beta_i X_i + \varepsilon \quad \ldots(7)$$

Temperature IV model

$$\text{Temperature} = \alpha + \beta_1 \widehat{pollution}_{\text{index}} + \beta_i X_i + \varepsilon \quad \ldots(8)$$

RESULTS AND DISCUSSION

Fig. 3 demonstrates that the number of villages on Kalimantan Island with a negative index as a percentage is larger than the number of villages on other islands. Pollution is a concern in the community, as shown by negative signs. The index value is more negatively skewed in areas where pollution is more pervasive. Pollution levels are quite low in the islands of Bali, Nusa Tenggara, Papua, Maluku, and Papua. This phenomenon is seen in almost every instance of pollution and pollution aggregation in general.

Based on Fig. 4, it is known that, in comparison to other development categories, villages with a negative index in the independent category have a comparatively large number. This tendency may be seen in the overall pollution index as well as the water, soil, and air pollution indices.

Based on Fig. 5, it is known that the soil pollution index has the highest level of severity when compared to the water

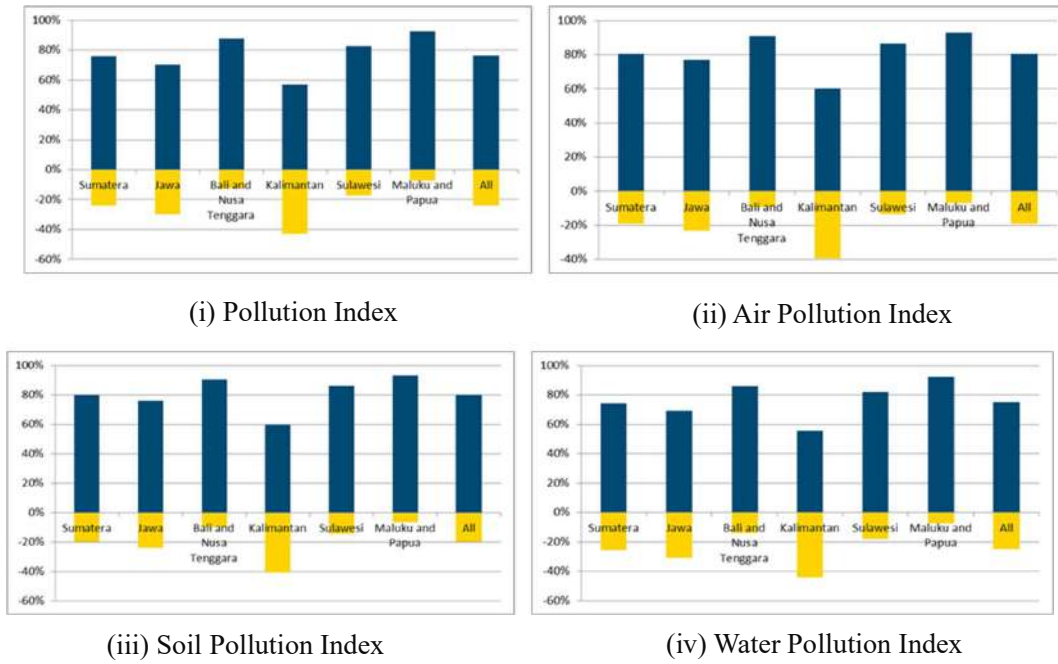

(i) Pollution Index (ii) Air Pollution Index

(iii) Soil Pollution Index (iv) Water Pollution Index

Fig. 3: Index Distribution by Island 2018.

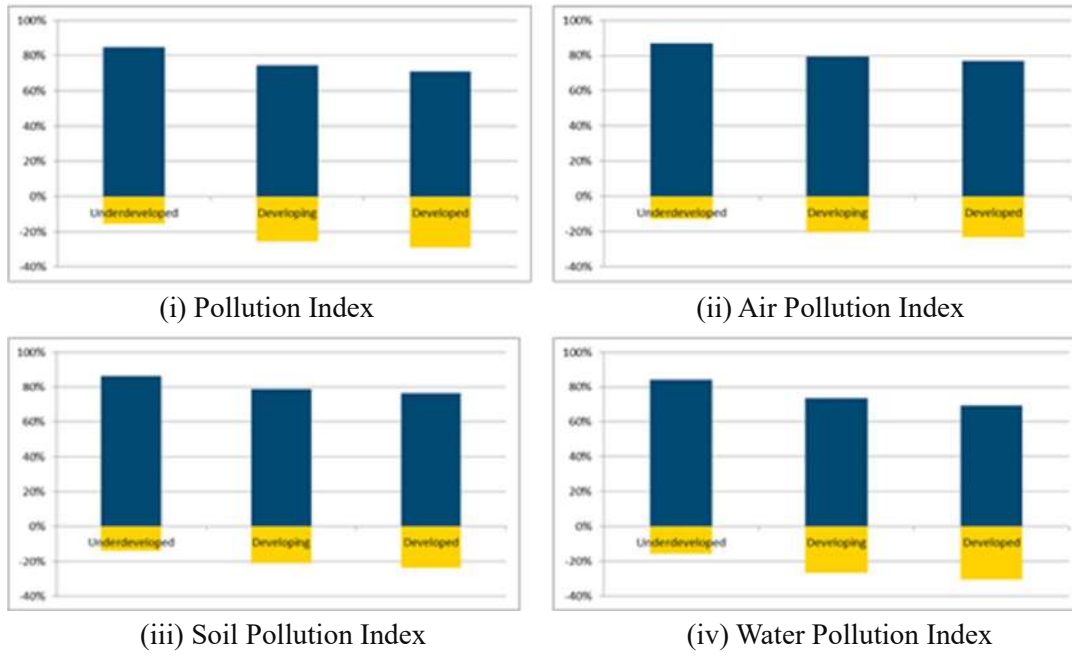

(i) Pollution Index (ii) Air Pollution Index

(iii) Soil Pollution Index (iv) Water Pollution Index

Fig. 4: Index distribution by development category 2018.

pollution index and air pollution index. From the index calculation results, it is known that the soil pollution index has a dominant negative contribution to the formation of the overall pollution index. A higher negative pollution index indicates a deeper level of severity.

If you pay attention in stages, the level of pollution is getting higher, starting from the category of underdeveloped development, developing, to being developed. Air pollution is the type of pollution that has the highest index level.

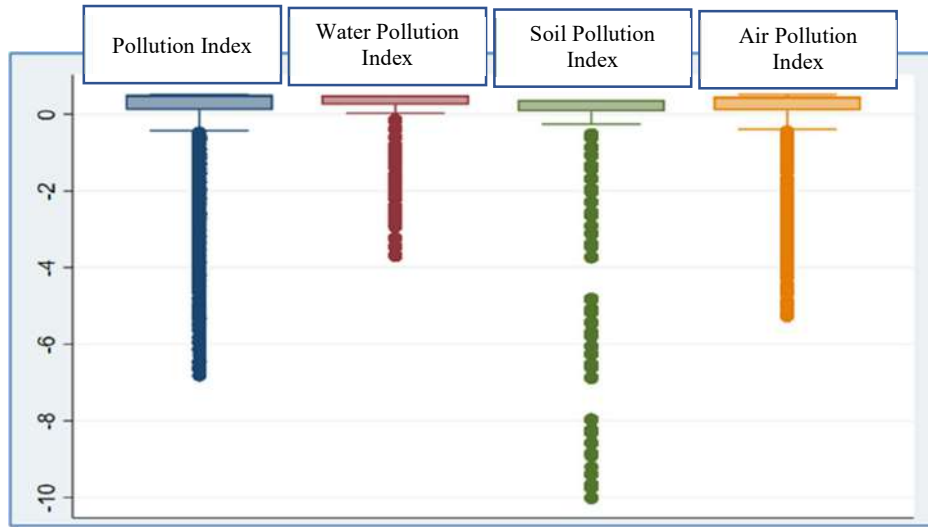

Fig. 5: Pollution Index by Type.

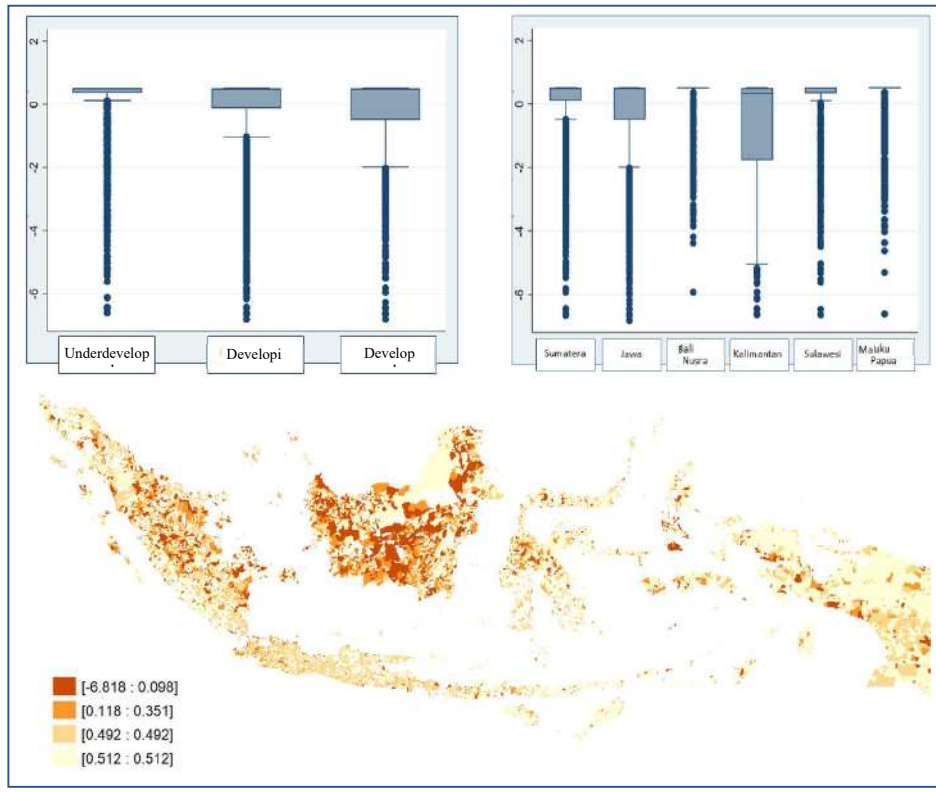

Fig. 6: Distribution of Pollution Index.

The pollution index, based on Fig. 6, if classified according to the development category, the developing category has the largest average negative index when compared to other development categories. This phenomenon can be seen from the size of the squares in the negative area. Rural with underdeveloped categories have the smallest average negative index. If classified according to the major islands in Indonesia, Java, and Kalimantan have an average index range that dominates in negative areas. Good conditions can be seen in Maluku and Papua Islands.

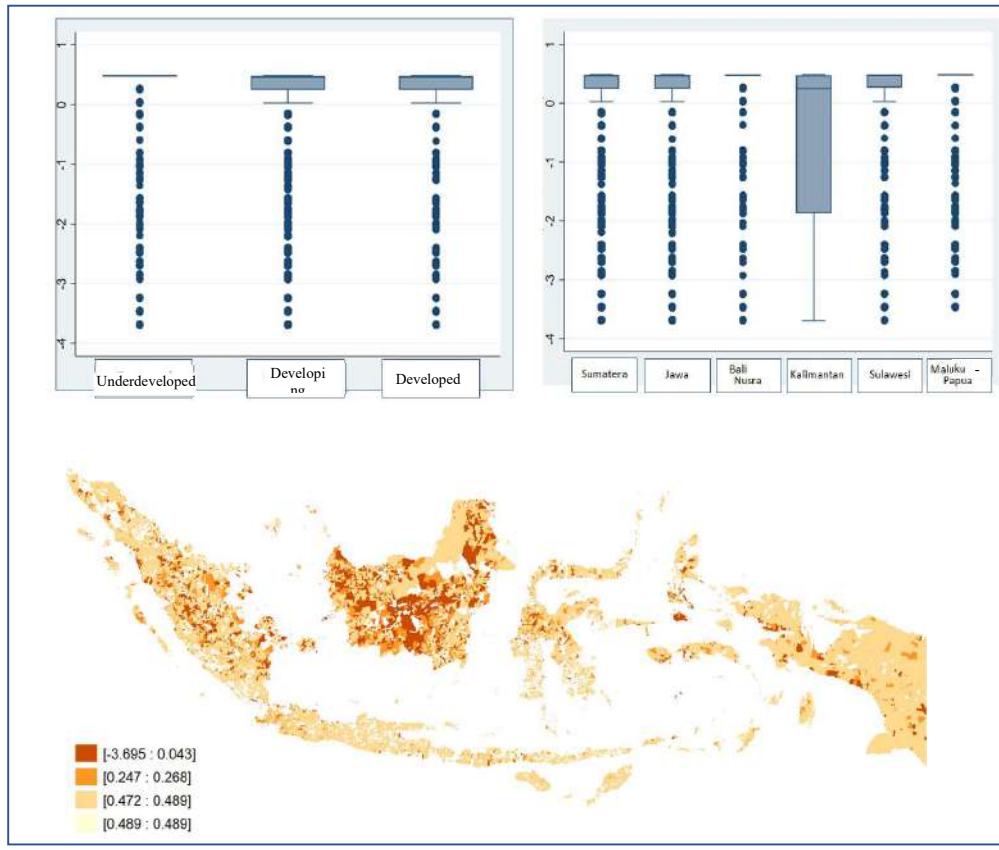

Fig. 7: Distribution of Water Pollution Index.

On the islands of Maluku and Papua, no average grouping is seen in negative areas. This phenomenon is because there is no domination box found in negative areas. If classified according to villages in Indonesia, Kalimantan Island has the largest negative index. The distribution of the negative index can be seen in areas that are, in fact, urban areas or areas close to the economic center or government center. The distribution of the created negative index totaled -6.818.

Based on Fig. 7, the water contamination index usually has positive index ranges across all development categories. The box size sees this in the area above 0. Comparing Kalimantan Island to the other major Indonesian islands, the average index range is mostly negative. Sumatra, Java, and Sulawesi are all in excellent condition.

The negative zones in the islands of Papua, Maluku, Nusa Tenggara, and Bali do not have an average grouping. Negative sections on these islands lack a dominance box, which accounts for this peculiarity. When classified as rural in Indonesia, Kalimantan Island has the highest negative index. The distribution of the negative index caused by water pollution has a maximum value of -3.695.

Based on Fig. 8, the soil contamination index usually has positive index ranges for all development categories. The box size sees this in the area above 0. Compared to the other major Indonesian islands, Kalimantan Island has an average index range that predominates in the negative zone. Sumatra, Java, and Sulawesi are all in excellent condition. The negative zones in the islands of Papua, Maluku, Nusa Tenggara, and Bali do not have an average grouping. Negative sections on these islands lack a dominance box, which accounts for this peculiarity. When compared to Indonesian communities, Kalimantan Island has the highest negative index. The water contamination-related negative index distribution achieves a value of -10.020.

Based on Fig. 9, in the air pollution index, all development categories have an index range that is mostly positive in underdeveloped areas. This can be seen from the box size in the area above 0. In developing and developed areas, the grouping occurs in the negative area. This indicates that most of the indexes are in the negative range. If classified according to the major islands in Indonesia, Sumatra, Java, and Kalimantan have an average index range that dominates in negative areas. Good conditions can be seen on the island

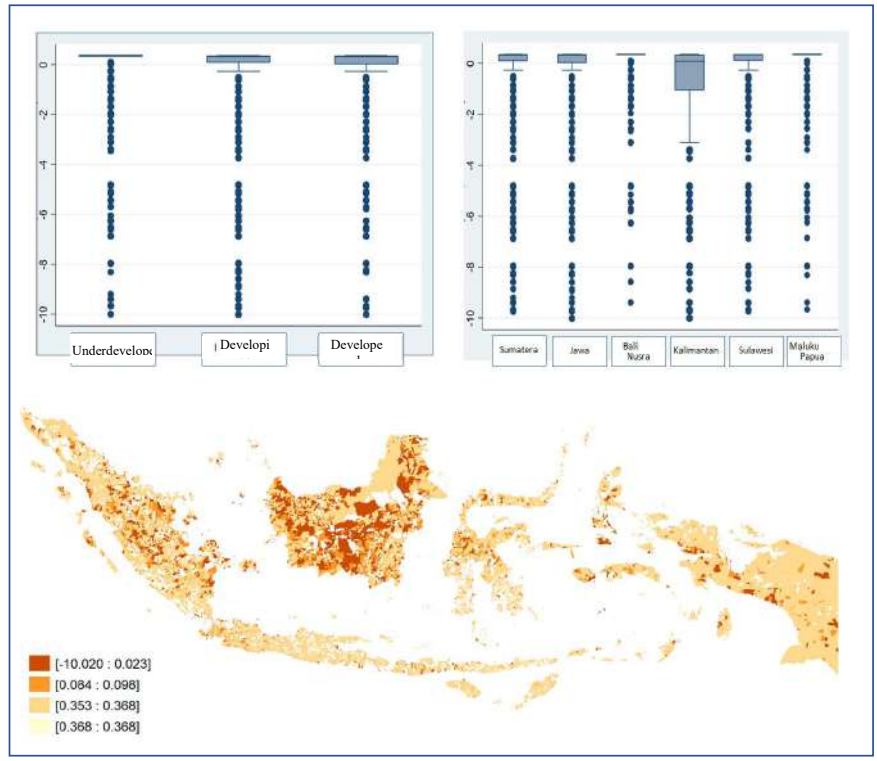

Fig. 8: Distribution of Soil Pollution Index.

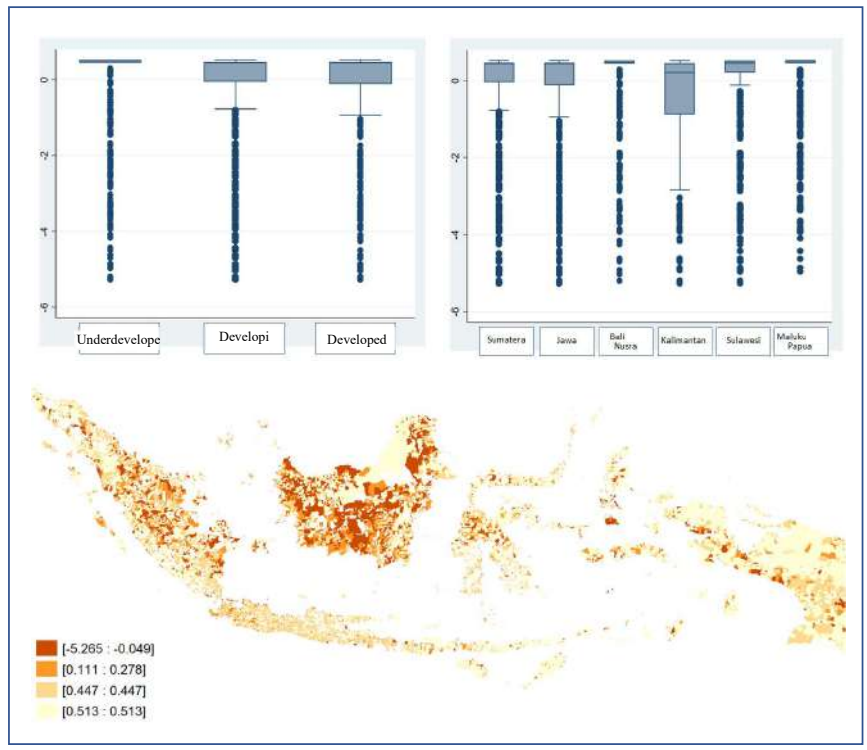

Fig. 9: Distribution of Air Pollution Index.

Table 1: General estimation results for first stage IV on the pollution index.

Variable	Country	Suma-tera	Jawa	Bali and Nusa Tenggara	Kali-mantan	Sulawesi	Maluku and Papua
(1)	(2)	(3)	(4)	(5)	(6)	(7)	(8)
Rural development index	-0.0088***	-0.0049***	-0.0030***	-0.0098***	0.0024	-0.0023**	-0.0016***
GRDP per capita	-0.2108***	-0.2536***	-0.1610***	-0.3492***	-0.1881	-0.1910***	-0.0957***
R^2	0.0189	0.0130	0.0029	0.0440	0.0047	0.0068	0.0087
Observation	75,436						

Source: Stata 16 (processed) processing results

Note: The dependent variable in the model is the pollution index. The instrument variables in the model are the village development index and GRDP per capita. Significance level notation *** p <1%, ** p <5%, and * p <10%.

Table 2: Estimation results of OLS and IV in general at temperature.

Variable	Bali and Nusa Tenggara		Kalimantan		Sulawesi	
	OLS	IV	OLS	IV	OLS	IV
(1)	(8)	(9)	(10)	(11)	(12)	(13)
Pollution index	0.0295***	0.3410***	0.0042**	1.1144***	0.0035	-0.0190
R^2	0.0779	< 0.0001	0.0009	< 0.0001	0.0001	0.0065
Observation	75,436					

Variable	Country		Sumatera		Jawa	
	OLS	IV	OLS	IV	OLS	IV
(1)	(2)	(3)	(4)	(5)	(6)	(7)
Pollution index	0.0605***	0.5810***	0.0059**	-0.0587	0.1230***	2.6880***
R^2	0.0047	< 0.0001	0.0003	< 0.0001	0.0078	< 0.0001
Observation	75,436					

Variable	Maluku and Papua	
	OLS	IV
(1)	(14)	(15)
Pollution index	0.0302***	0.2688***
R^2	0.0108	< 0.0001
Observation	75,436	

Source: Stata 16 (processed) processing results

Note: The dependent variable in the model is temperature. The independent variable in the model is the pollution index. The instrument variables in the model are the village development index and GRDP per capita. Significance level notation *** p <1%, ** p <5%, and * p <10%.

of Sulawesi because there is a grouping of positive index ranges. There is no average grouping in negative regions in the islands of Bali, Nusa Tenggara, Maluku, and Papua. This anomaly is caused by the absence of a domination box in negative areas on these islands. The biggest negative index is seen on Kalimantan Island when compared to Indonesian communities. Water contamination creates a distribution of the negative index that reaches a value of -5.265.

The impact of the instrument factors on the relevant variable is shown in Table 1. From these findings, it may be inferred that growth in Indonesia has a detrimental effect on pollution in general, both nationally and throughout the archipelago. Additionally, the direction and importance of per capita GRDP as a control variable are the same. The islands of Bali and Nusa Tenggara saw the highest development effect, whereas Maluku and Papua experienced the least.

Table 2 shows how the pollution index affects temperature. According to the calculations, pollution has a beneficial effect on temperature both nationally and throughout the Indonesian archipelago. The island of Java is where development has had the most impact, whereas Bali and Nusa Tenggara have witnessed the least change.

As a factor for the success of a region, development is often used as an indicator that can be compared between regions. However, development turns out to have bad impacts, especially on environmental aspects and indirect impacts on climate change. Climate change that has occurred has prompted environmental experts to urge the public and the government to continue to maintain the purity of nature as a legacy for future generations. The climatic impact that is most felt is the higher temperature in the last decade.

From this research, it is known that the greatest pollution is seen in developed and developing areas, followed by underdeveloped areas. Underdeveloped areas tend to be still natural, so the pollution index formed for all types of pollution tends to be good. This is different from the developed and developing regions, which have a relatively large negative index. The negative index that is formed can be described as the developed and developing regions having more pollution than the underdeveloped areas. According to earlier studies' findings, pollution levels in developed regions would be greater than those in undeveloped ones. (Hoffmann 2019, Kumar et al. 2015, Mayer 1999).

When linked to the development that occurs, the entire region confirms that development will cause significant pollution. This Indonesian phenomenon is consistent with studies done in other nations and is seen in rural regions (Brauer et al. 2002, Gan et al. 2020, Gehring et al. 2010). The development carried out by each region often explores the natural resources that are around it so that it has an impact on the ecosystem. In the short term, the most felt is the progress of the area and the welfare of the surrounding community. However, in the long term, this will be eroded by the negative impacts that arise, especially on environmental factors.

Pollution that occurs in developed areas is often found in several countries. The government must anticipate the bad impacts caused by the development that occurs. The government can endeavor to reinforce the rules relating to the exploration of natural resources that have an impact on the environment. Thus, in practice, the progress of an area is not only measured through development alone but through the environmental impacts that occur.

From the results of the regression calculation in this study, it is known that development has a negative impact on temperature conditions. These results are visible both nationally, as well as on most islands in Indonesia. This result reaffirms that the recent climate change is the impact of development. The results of this study are in line with several previous studies that have linked development with temperature (Ding et al. 2007, Horne et al. 2019, Melicher et al. 2019). The global warming that occurs will certainly have a negative impact on human life, especially the livelihoods of most Indonesians as farmers. The yields were no longer as expected due to the long drought.

It takes coordination between the government, investors, and the community to be able to anticipate the negative impacts of development on pollution and temperature. It is hoped that with good coordination, the development process can run, and the environmental ecosystem can be maintained. This study still uses temperature data at the provincial level. In further research, temperature data at the village level are needed to produce more representative research results.

CONCLUSION

Environmental activists and the government are always trying to control climate change that is happening. The climate change that most people feel is increasing global warming. This phenomenon adversely affects various community activities. Through research, it is known that the development that occurs has a negative impact on the temperature in Indonesia. This result occurs in most archipelagic regions in Indonesia. It takes various efforts from the government and society to anticipate worse events because development often takes precedence over environmental aspects.

ACKNOWLEDGMENTS

In an effort to speed up village development, the Directorate General of Higher Education, Research and Technology (Ditjen Diktiristek) provided funding for the study "Exploration and Potential Impacts of Development on Increasing Regional Temperatures in Support of Community Service to Society 2023." The outcomes of the study served as the foundation for this journal paper, written by Faradiba and the Team. The whole responsibility for the contents rests with the author.

REFERENCES

Abdi, H. and Valentin, D. 2007. Multiple correspondence analysis. Encycl. Measure Stat., 2(4): 651-657.

Asselin, L.M. and Anh, V.T. 2008. Multidimensional Poverty and Multiple Correspondence Analysis. In Kakwani, N. (ed), Quantitative Approaches to Multidimensional Poverty Measurement. Springer, Cham, pp. 80-103.

Bahrami, A., Awn, R.F., Corona, J. and Eriksson, B. 2022. How aware and active is the Swedish building and real estate sector in climate-smart concrete? Int. J. Eng. Trends and Technol., 70(1): 126-138.

Bolaji, B.O. and Huan, Z. 2013. Ozone depletion and global warming: Case for the use of natural refrigerant: A review. Renew. Sustain. Energy Rev., 18: 49-54.

BPS. 2019. Indeks Pembangunan Desa 2018.

Brauer, M., Hoek, G., Van Vliet, P., Meliefste, K., Fischer, P. H., Wijga, A., Koopman, L. P., Neijens, H. J., Gerritsen, J. and Kerkhof, M. 2002. Air pollution from traffic and the development of respiratory infections and asthmatic and allergic symptoms in children. Am. J. Resp. Crit. Care Med., 166(8): 1092-1098.

Busakhin, A.V. 2022. Smoke ventilation differential pressure system. Int. J. Eng. Trends Technol., 70(2): 449-454. / https://doi.org/10.14445/22315381/IJETT-V70I7P246

De Schryver, A.M., Brakkee, K.W., Goedkoop, M.J. and Huijbregts, M.A.J. 2009. Characterization Factors for Global Warming in Life Cycle Assessment Based on Damages to Humans and Ecosystems. ACS Publications, Washington, DC.

Ding, Y., Ren, G., Zhao, Z., Xu, Y., Luo, Y., Li, Q. and Zhang, J. 2007. Detection, causes, and projection of climate change over China: An overview of recent progress. Adv. Atmos. Sci., 24(6): 954-971.

Faradiba, F. 2021. Analysis of intensity, duration, and frequency of rain daily on Java Island using the Mononobe method. J. Phys. Conf, Ser., 1783:, 1-7.

Faradiba, F. and Lodewik, Z. 2020. The impact of climate factors, disaster, and social community in rural development. J. Asian Fin. Econ. Bus., 7(9): 707-717.

Foster, G. and Rahmstorf, S. 2011. Global temperature evolution 1979-2010. Environ. Res. Lett., 6(4): 44022.

Gan, T., Liang, W., Yang, H. and Liao, X. 2020. The effect of economic development on haze pollution (PM2. 5) based on a spatial perspective: Urbanization as a mediating variable. J. Clean. Prod., 266: 121880.

Gehring, U., Wijga, A.H., Brauer, M., Fischer, P., de Jongste, J.C., Kerkhof, M., Oldenwening, M., Smit, H.A. and Brunekreef, B. 2010. Traffic-related air pollution and the development of asthma and allergies during the first 8 years of life. Am. J. Resp. Crit. Care Med., 181(6): 596-603.

Gujarati, D.N. and Porter, D. 2009. Basic Econometrics. Mcgraw-Hill, NY, p. 719.

Hamed, M.. Jassim, M. and Yousif Abdulla Aziz Kurdi, F.H.I.A. 2013. Pollution issues in Iraqi Kurdistan region. Int. J. Eng. Trends Technol., 4(5): 2050-2058.

Hansen, J., Sato, M., Ruedy, R., Lo, K., Lea, D.W. and Medina-Elizade, M. 2006. Global temperature change. Proceed. Nat. Acad. Sci., 103(39): 14288-14293.

Hoffmann, B. 2019. Air Pollution in Cities: Urban and Transport Planning Determinants and Health in Cities. In Nieuwenhuijsen, M. and Khreis, H. (eds), Integrating Human Health into Urban and Transport Planning, Springer, Cham, pp. 425-441.

Horne, C.R., Hirst, A.G., Atkinson, D., Almeda, R. and Kiørboe, T. 2019. Rapid shifts in the thermal sensitivity of growth but not development rate cause temperature–size response variability during ontogeny in arthropods. Oikos, 128(6): 823-835.

Houillon, G. and Jolliet, O. 2005. Life cycle assessment of processes for the treatment of wastewater urban sludge: energy and global warming analysis. J. Clean. Prod., 13(3): 287-299.

Inglehart, R. 2018. Culture Shift in Advanced Industrial Society. Princeton University Press, Princeton.

Jalil, A. and Feridun, M. 2011. The impact of growth, energy and financial development on the environment in China: A cointegration analysis. Energy Econ., 33(2): 284-291.

Kameswara, A.S.P. and Suharjito, M. 2023. Analysis of flood disaster risk factors with geographic information system (GIS) and analytical hierarchy process (AHP) methods in Bekasi City, West Java, Indonesia. Int. J. Eng. Trends Technol., 71(4): 371-386. https://doi.org/10.14445/22315381/IJETT-V71I4P233

Kumar, P., Morawska, L., Martani, C., Biskos, G., Neophytou, M., Di Sabatino, S., Bell, M., Norford, L. and Britter, R. 2015. The rise of low-cost sensing for managing air pollution in cities. Environ. Int., 75: 199-205.

Li, Y., Johnson, E.J. and Zaval, L. 2011. Local warming: Daily temperature change influences belief in global warming. Psychol. Sci., 22(4): 454-459.

Li, Z.H. and Randak, T. 2009. Residual pharmaceutically active compounds (PhACs) in the aquatic environment-status, toxicity, and kinetics: a review. Veter. Med., 54(7): 295-314.

Marshall, A.J. and Beehler, B.M. 2012. Ecology of Indonesian Papua, Part Two.

Mayer, H. 1999. Air pollution in cities. Atmos. Environ., 33(24-25): 4029-4037.

Melicher, D., Wilson, E.S., Bowsher, J.H., Peterson, S.S., Yocum, G.D. and Rinehart, J.P. 2019. Long-distance transportation causes temperature stress in the honey bee, Apis mellifera (Hymenoptera: Apidae). Environ. Entomol., 48(3): 691-701.

Mogborukor, J.O.A. 2014. The impact of oil exploration and exploitation on water quality and vegetal resources in a rain forest ecosystem of Nigeria. Mediterr. J. Social Sci., 5(27): 1678.

Peters, G.P., Aamaas, B., Lund, M., Solli, C. and Fuglestvedt, J.S. 2011. Alternative "global warming" metrics in life cycle assessment: A case study with existing transportation data. Environ. Sci. Technol., 45(20): 8633-8641.

Reni, O.T., Sumbangan, B. and Farouk Maricar, R.T.L. 2022. Spatial distribution of livestock wastewater pollution and its treatment in Saddang watershed. Int. J. Eng. Trends Technol., 70(11): 106-116. https://doi.org/10.14445/22315381/IJETT-V70I11P211

Rodrigues, L., Grave, R., de Oliveira, J.M. and Nogueira, C. 2016. Study on homophobic bullying in Portugal using multiple correspondence analysis (MCA). Rev. Latin. Psicol., 48(3): 191-200.

Senthilkumar, M.K. 2019. Effect of average air temperature and relative humidity on global radiation. Int. J. Eng. Trends and Technol., 67(3): 52-57.

Sindhu, C.P.A. 2017. Numerical modeling of urban air temperature. Int. J. Eng. Trends Technol., 53(2): 95-99.

Wilkinson, C., Saarne, T., Peterson, G.D. and Colding, J. 2013. Strategic spatial planning and the ecosystem services concept–a historical exploration. Ecology and Society, 18(1).

Wood, S.L.R. and DeClerck, F. 2015. Ecosystems and human well□being in the Sustainable Development Goals. Wiley Online Library.

Wooldridge, J.M. 2016. Introductory Econometrics: A Modern Approach. Nelson Education, Toronto, Canada.

Yokota, K., Watanabe, K., Wachi, T., Otsuka, Y., Hirama, K. and Fujita, G. 2017. Crime linkage of sex offenses in Japan by multiple correspondence analysis. J. Invest. Psychol. Offend. Profil., 10: 1468. https://doi.org/10.1002/jip.1468

Zhang, X., Warner, M.E. and Homsy, G.C. 2017. Environment, equity, and economic development goals: Understanding differences in local economic development strategies. Econ. Dev. Quart., 31(3): 196-209.

Zhang, Y., Feng, G., Zhang, M., Ren, H., Bai, J., Guo, Y., Jiang, H. and Kang, L. 2016. Residual coal exploitation and its impact on sustainable development of the coal industry in China. Energy Policy, 96: 534-541

ORCID DETAILS OF THE AUTHORS

Faradiba Faradiba: https://orcid.org/0000-0002-9375-8501
Lodewik Zet: https://orcid.org/0000-0002-9020-5282

Nature Environment and Pollution Technology
An International Quarterly Scientific Journal

p-ISSN: 0972-6268
(Print copies up to 2016)
e-ISSN: 2395-3454

Vol. 23 | No. 1 | pp. 161-172 | 2024

Original Research Paper

https://doi.org/10.46488/NEPT.2024.v23i01.012

Open Access Journal

Evaluation of the Contaminated Area Using an Integrated Multi-Attribute Decision-Making Method

A. Mohamed Nusaf * and R. Kumaravel **†

*Department of Mathematics, College of Engineering and Technology, SRM Institute of Science and Technology, Kattankulathur-603203, Tamil Nadu, India

**Department of Career Development Centre, College of Engineering and Technology, SRM Institute of Science and Technology, Kattankulathur-603203, Tamil Nadu, India

†Corresponding author: R. Kumaravel; kumaravr@srmist.edu.in

Nat. Env. & Poll. Tech.
Website: www.neptjournal.com

Received: 15-06-2023
Revised: 25-07-2023
Accepted: 27-07-2023

Key Words:
Analytical hierarchy process
Air pollution
Decision analysis
Entropy
Multi-attribute decision-making
VIKOR model

ABSTRACT

Air pollution affects public health and the environment, creating great concern in developed and developing countries. In India, there are numerous reasons for air pollution, and festivals like Diwali also contribute to air contamination. Determining the polluted region using several air contaminants is significant and should be analyzed carefully. This study aims to analyze the air quality in Tamil Nadu, India, during the Diwali festival from 2019 to 2021, based on multiple air pollutants. The study models the impact of air pollution as a Multi-Attribute Decision-Making (MADM) problem. It introduces a hybrid approach, namely the Analytical Hierarchy Process-Entropy-VIseKriterijumska Optimizacija I Kompromisno Resenje (AHP-Entropy-VIKOR) model, to analyze and rank the areas based on the quality of air. A combined approach of AHP and entropy is employed to determine the weights of multiple air pollutants. The VIKOR approach ranks the areas and identifies the areas with the worst air quality during the festival. The proposed model is validated by performing the Spearman's rank correlation with two existing MADM methods: Combinative Distance Based Assessment (CODAS) and Weighted Aggregates Sum Product Assessment (WASPAS). Sensitivity analysis is carried out to assess the effects of the priority weights and the dependency of the pollutants in ranking the regions. The highest air pollution level during the festival was seen in Cellisini Colony (2019), Rayapuram (2020), T. Nagar and Triplicane (2021) in their respective year. The results demonstrate the consistency and efficiency of the proposed approach.

INTRODUCTION

Detrimental atmospheric substances contaminate the air and affect human health and the environment. It arises from various sources, including industrial emissions, transportation, and agricultural activities (Suresh et al. 2021). According to the State of Global Air Report (SGA 2020), air pollution causes around 7 million deaths annually, making it the fourth largest risk factor for death worldwide. Air pollution is a significant public health concern in India because many cities are ranked among the most polluted globally (Verma et al. 2020). Even festivals such as Bhogi and Diwali significantly contribute to air pollution in India. This study focuses on the Diwali festival, known as the "festival of lights." Diwali is celebrated in many parts of the world and is a major festival in India. It is usually celebrated in October or November and marks the victory of good over evil and light over darkness. During the festival, people light fireworks and burn lamps and candles to honor the festival. These rituals enhance the level of sulfur dioxide, nitrogen oxides, particulate matter, and other air pollutants. The consequences of these air pollutants are severe. It causes respiratory and cardiovascular diseases, chronic obstructive pulmonary disease, and many more (Mandal et al. 2022). Creating efficient methods for evaluating air quality based on multiple pollutants to tackle the air pollution issue is crucial. Many studies have employed mathematical methods that convert multiple air pollutant concentrations into a single value, offering a clear representation of the air quality (CPCB 2022, Kumaravel & Vallinayagam 2012, Dionova et al. 2020, Zeydan & Pekkaya 2021).

The sources of these pollutants are diverse and interconnected. Therefore, the present study employed a hybrid MADM model that simultaneously offers ranking and analysis to assist decision-makers in addressing real-time issues involving independent attributes. The main aim of the current research is to formulate a hybrid model that

suggests a strategy for enhancing air quality. MADM is a branch of Operations Research that assists in evaluating decision alternatives against a performance attribute by a single decision-maker or a group of decision-makers. Various decision-making methodologies such as AHP, ELECTRE, PROMETHEE, TOPSIS, and VIKOR exist to facilitate efficient decision-making (Tzeng & Huang 2011). Many methods include attribute weights during the aggregation process. Various weighting techniques have been developed to assign weights to the attribute. These methodologies fall into two categories: subjective and objective weighting methods. The subjective methods determine weights according to the preferences of decision-makers. The most popular subjective weighting methods are the AHP and the best-worst method. The objective methods determine attribute weights using mathematical models and neglecting the decision maker's subjective judgment information. The most popular objective weighting methods are entropy and standard deviation (Zardari et al. 2015). The utilization of these methodologies is broad and far-reaching (Abdul et al. 2022, Chundi et al. 2022, Dev et al. 2022, Hasanzadeh et al. 2023, Morkunas & Volkov 2023, Shahnazari et al. 2021, Siew et al. 2021, Stanković et al. 2021).

In air quality assessment, Chen et al. (2019) employed VIKOR and DANP to analyze the potential improvement strategies for air quality in Kaohsiung, Taiwan. Ozkaya & Erdin (2020) utilized TOPSIS and VIKOR methods to evaluate sustainable forest and air quality management and the current situation in European countries. Lin et al. (2021) proposed an air quality assessment method that considers several pollutants using Entropy and TOPSIS. Xu & Chernikov (2021) applied a combined Entropy-TOPSIS-PROMETHEE method to assess air quality in several cities in China. Torkayesh et al. (2022) employed the Best-Worst Method and the Measurement of Alternatives and Ranking According to the Compromise Solution method to conduct a comparative analysis of air pollutants in 22 European countries. The objective was to provide a reference for regional and national strategies aimed at enhancing environmental sustainability.

The literature showed that several studies presented air quality assessment as a significant MADM problem due to its dependency on multiple quality indicators. Several studies adopted different approaches for the assessment of air quality. No study has presented the combined AHP-Entropy weighting approach for assessing weights based on air pollutants. Thus, this study incorporates the combined AHP-Entropy weighting approach with VIKOR, named the AHP-Entropy-VIKOR method, to determine the air quality and rank the areas. The rest of the paper is structured as follows: study area and data collection represent the considered alternatives, attributes, and statistical data. The methodology section focuses on the algorithms of the methods. The research findings are summed up and validated using Spearman's rank correlation, and sensitivity analysis is determined in the results and discussion section. Finally, the article is concluded in conclusion.

Study Area and Data Collection

This study aims to assess the air quality and to identify the most contaminated region during the Diwali festival in the 26 zones of Tamil Nadu, India, as depicted in Table 1, and the ambient air pollutants Sulphur dioxide (SO_2), Nitrogen dioxide (NO_2), and Particulate matter (PM_{10} microns $\leq 10\,\mu g\backslash m^3$ and $PM_{2.5}$ microns $\leq 2.5\,\mu g\backslash m^3$) have been selected as the attribute to evaluate the air quality using the proposed model.

The concentration of these pollutants during the Diwali festival from 2019 to 2021 was procured from the Tamil

Table 1: The considered areas of Tamil Nadu during the Diwali festival.

State	District	Regions	Abbreviation
Tamil Nadu	Chennai	Besant Nagar	BSN
		T.Nagar	TNR
		Nungambakkam	NGM
		Triplicane	TRP
		Sowcarpet	SCT
	Coimbatore	Gowndampalayam	GDM
		Collectorate Office	COO
	Cuddalore	Imperial Road	IMR
		Pudupalayam	PDP
	Madurai	Thirunagar	THN
		Birla Vishram	BVM
	Salem	Sri Saradha Balamandhir School	SBC
		Siva Tower	SVT
	Tirunelveli	Pettai	PET
		Vannarpettai	VPT
	Trichy	Ramalinga Nagar	RMN
		Gandhi Market	GNM
	Vellore	Gandhi Nagar	GNN
		Sidco Industrial Estate	SIE
	Dindigul	Rajagopal Iyangar	RGI
	Hosur	ESI Hospital	ESI
		Inel Transit House	ITH
	Thoothukudi	Raju Nagar	RNR
		Cellisini Colony	CCY
	Tiruppur	Kumaran Complex	KMC
		Rayapuram	RPM

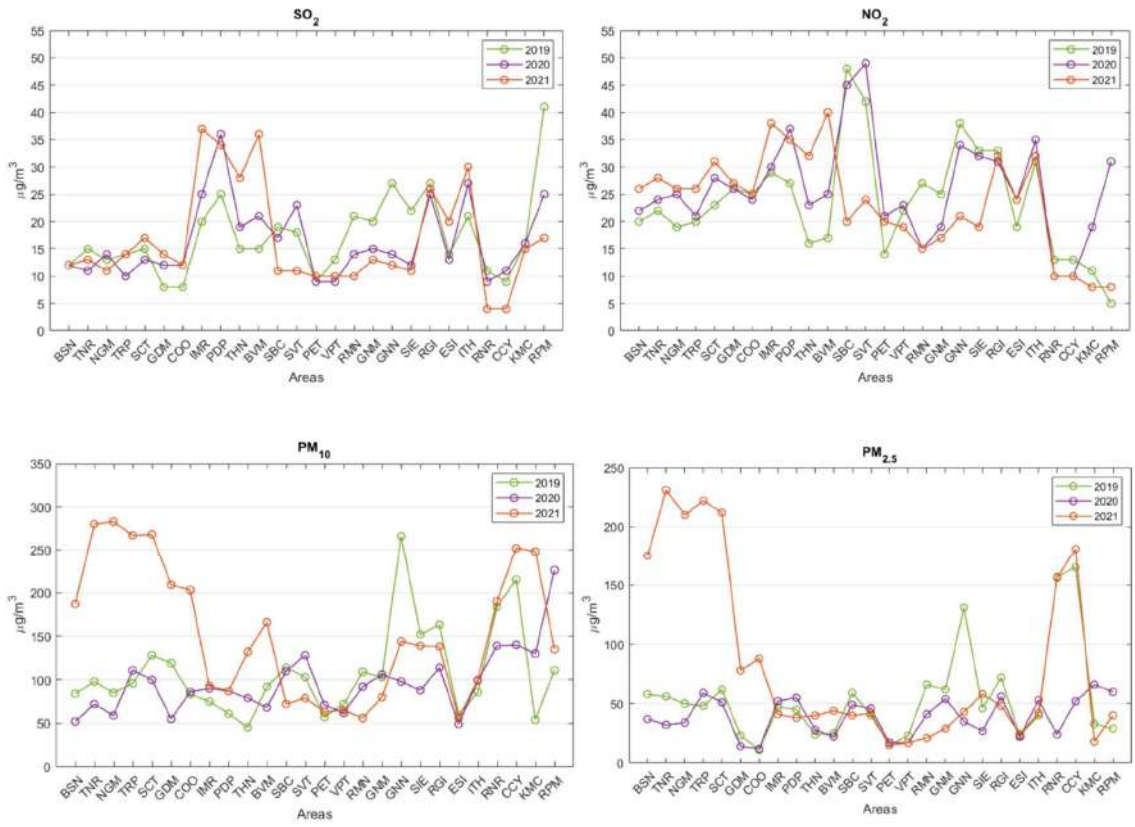

Fig. 1: Data distribution of each pollutant.

Nadu Pollution Control Board (TNPCB 2022) in Chennai. The data distribution for the four contaminants is presented in Fig. 1.

Descriptive statistics of the pollutants studied in the community of Tamil Nadu have been carried out. Table 2 shows a statistical summary of these data, including measures of central tendency and variability in the form.

The maximum concentration values of SO_2 and NO_2 in 2019, 2020, and 2021 were within the permissible limits, with values ranging from 36 µg.m^{-3} to 49 µg.m^{-3} However, all three years exceeded the average daily limit of 100 µg.m^{-3} for PM_{10}, with maximum values ranging from 226 µg.m^{-3} to 283 µg.m^{-3} Similarly, all three years exceeded the average limit of 60 µg.m^{-3} for $PM_{2.5}$, with maximum values ranging from 66 µg.m^{-3} to 231 µg.m^{-3} It is worth noting that

Table 2: Summary statistics of the air pollutant concentrations.

Year	2019				2020				2021			
Pollutants	SO_2	NO_2	PM_{10}	$PM_{2.5}$	SO_2	NO_2	PM_{10}	$PM_{2.5}$	SO_2	NO_2	PM_{10}	$PM_{2.5}$
Count	26	26	26	26	26	26	26	26	26	26	26	26
Average *[µg.m^{-3}]*	17.23	23.77	108.23	54.23	16.31	26.27	96.58	39.04	16.62	23.58	153.54	82.81
Standard dev. *[µg.m^{-3}]*	7.31	9.86	51.75	39.59	6.85	9.14	37.23	16.32	9.35	8.88	77.58	74.45
Coeff. of variation %	42%	41%	48%	73%	42%	35%	39%	42%	56%	38%	51%	90%
Minimum *[µg.m^{-3}]*	8	5	45	11	9	10	49	12	4	8	56	15
Maximum*[µg.m^{-3}]*	41	48	266	165	36	49	226	66	37	40	283	231
Range *[µg.m^{-3}]*	33	43	221	154	27	39	177	54	33	32	227	216
Stnd. Skewness	1.41	0.55	1.54	1.81	1.23	0.56	1.66	-0.15	1.05	-0.16	0.37	1.06
Stnd. Kurtosis	3.17	0.42	2.57	2.98	1.14	0.82	4.73	-1.34	0.09	-0.57	-1.26	-0.56

large standard deviations were found for PM_{10} in all years, indicating significant variations in the concentration levels within the studied regions. Additionally, the coefficient of variation for $PM_{2.5}$ was higher in 2019 and 2021, suggesting more variability in the concentration levels of this pollutant during those years. Furthermore, the skewness values indicate the distribution characteristics of the contaminants. $PM_{2.5}$ exhibited higher skewness values in 2019 and 2021, indicating a skewed distribution. PM_{10} showed higher skewness in 2020. These observations highlight the elevated levels of particulate matter, specifically PM_{10} and $PM_{2.5}$, during the Diwali festival period. The results emphasize the need for effective measures to reduce and control particulate matter pollution, as it poses a significant health risk to the population.

MATERIALS AND METHODS

This study aims to fill the gap in the limited application of MADM methods in air quality assessment. We propose a hybrid approach that combines the AHP and Entropy weighting techniques to prioritize the attributes (parameters) in the decision-making process. The VIKOR method evaluates and ranks the alternatives (areas) and identifies the most polluted region. The flowchart in Fig. 2 presents the methodology of the proposed AHP-Entropy-VIKOR model.

Initial Decision Matrix

A MADM decision matrix $A = [a_{ij}]_{p\times k}$ consists of p alternatives and k attributes as presented in equation (1).

$$A = \begin{bmatrix} a_{11} & a_{12} & \cdots & a_{1k} \\ a_{12} & a_{22} & \cdots & a_{2k} \\ \vdots & \vdots & \vdots & \vdots \\ a_{p1} & a_{p2} & \ldots & a_{pk} \end{bmatrix} \quad \ldots(1)$$

Here, $a_{ij}\ (1 \le i \le p,\ 1 \le j \le k)$ i indicates the performance ratings of i^{th} alternative to the j^{th} attribute for the initial data shown in Fig. 1.

Weighting Methods

The weights assigned to the attributes can be determined through alternative data or expert opinions. This study adopts standard weighting methods, including the AHP and Entropy methods.

AHP

Saaty (1990) developed the AHP in 1977 to assign relative importance to options based on their comparison on a ratio scale. Fig. 3 depicts the decision hierarchy utilized in the AHP method to determine the most polluted region.

The relative significance of each attribute is ranked based on the ratio scales presented in Table 3.

The paired comparison matrix $P = [p_{ij}]_{p\times k}$ Utilized in this analysis to determine the weight of each attribute is displayed in equation 2.

$$P = \begin{bmatrix} 1 & 3 & 0.33 & 0.20 \\ 0.33 & 1 & 0.20 & 0.14 \\ 3 & 5 & 1 & 0.33 \\ 5 & 7 & 3 & 1 \end{bmatrix} \quad \ldots(2)$$

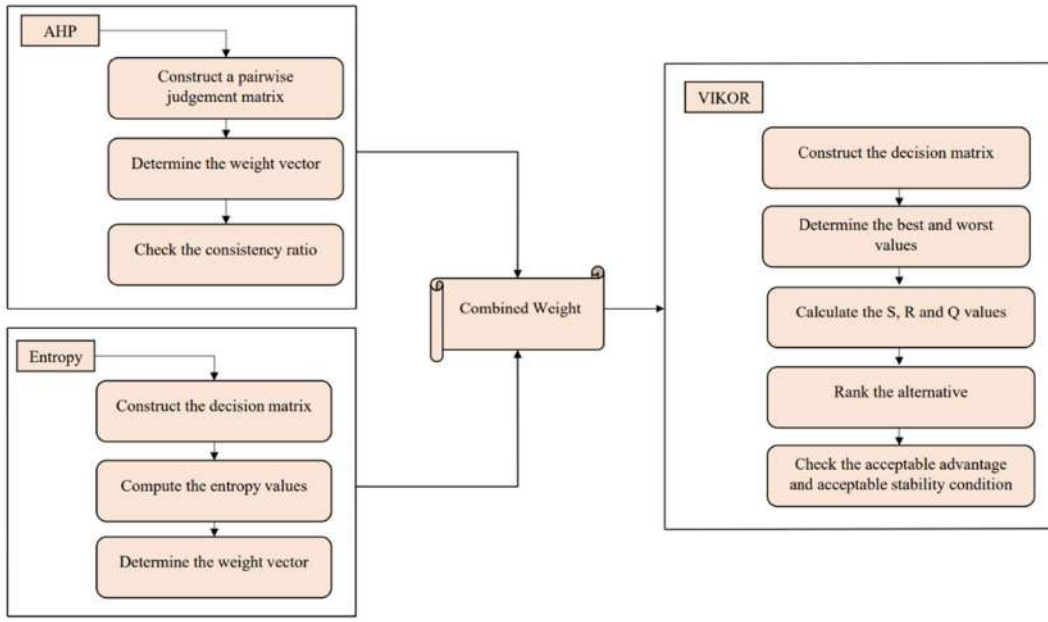

Fig. 2: AHP-Entropy-VIKOR Model.

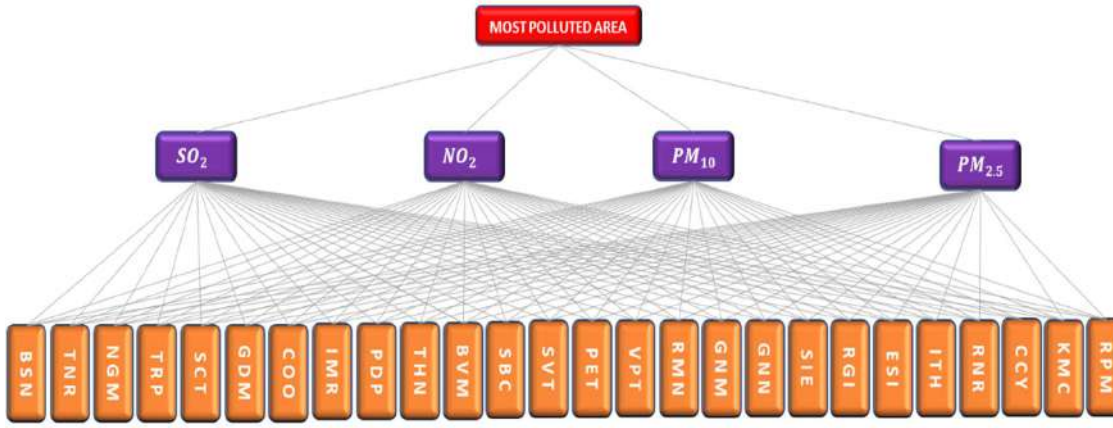

Fig. 3: Decision hierarchy of alternatives and attributes.

Table 3: Ratio Scale.

Numerical Rating	1	3	5	7	9	2,4,6,8
Importance	Equal importance	Moderate importance	Strong Importance	Very strong importance	Extreme Importance	Intermediate Values

We require the vector $\alpha = [\alpha_1, \alpha_2, \ldots, \alpha_k]$, which represents the weight of each attribute in matrix P. To obtain the vector α from P, divide each column of P by its sum to receive a new column in P, referred to as P_{norm}. The weight α_i is estimated by taking the mean values in the i^{th} row of P_{norm}.

The Consistency Index (C.I.) and Consistency Ratio (C.R.) are calculated using equations (3) and (4), respectively. The Random Index (R.I.) value for a 4 × 4 matrix is 0.9.

$$C.I. = \frac{\lambda_{max} - n}{n-1} \quad \ldots(3)$$

Here, $\lambda_{max} = \frac{1}{n}\sum_{i=1}^{p} \frac{P\alpha_i^T}{\alpha_i}$

$$C.R. = \frac{C.I}{R.I} \quad \ldots(4)$$

The C.R. value must be lower than 0.1 for the results to be considered.

Entropy

The entropy method, a weighting approach introduced by Shannon (1948), has been selected to assign relative significance to the various attributes. The algorithm for the entropy method is as follows:

Step 1: Using the following formula, normalize the decision matrix by substituting each a_{ij} by n_{ij}.

$$n_{ij} = \frac{a_{ij}}{\sum_{i=1}^{p} a_{ij}} \quad (1 \le i \le p, 1 \le j \le k) \quad \ldots(5)$$

Step 2: Calculate the entropy value e_j of j^{th} attribute by

$$e_j = -h\sum_{i=1}^{p} n_{ij} \ln n_{ij} \quad \left(h = \frac{1}{\ln p}, \quad 1 \le i \le p, 1 \le j \le k\right) \quad \ldots(6)$$

Step 3: Determine the degree of diversification of the j^{th} attribute

$$v_j = 1 - e_j \quad (1 \le j \le k) \quad \ldots(7)$$

Step 4: Calculate the weight of the attributes using

$$\beta_j = \frac{v_j}{\sum_{j=1}^{k} v_j} \quad (1 \le j \le k) \quad \ldots(8)$$

Combined Weights

This study employs a hybrid approach to maximize the advantages of both the AHP and Entropy methods by combining the relative importance of each attribute. The final weight of each attribute w_j is calculated as follows:

$$w_j = \frac{\alpha_j \beta_j}{\sum_{j=1}^{k} \alpha_j \beta_j} \quad \ldots(9)$$

Where α_j represents the weight assigned to the j^{th} attribute determined through the AHP approach and β_j represents the weight assigned to the j^{th} attribute determined through the Entropy method.

VIKOR

Opricovic and Tzeng (2004) developed the VIKOR method to rank and select a range of alternatives in a conflicting attribute. It provides a multi-attribute ranking index based on the closeness measure to the ideal solution. The algorithm for the VIKOR method is as follows:

Step 1: The best f_i^* and worst f_i^- values for each attribute can be determined using equation (10) for the benefit attribute and equation (11) for the non-benefit attribute.

$$f_j^* = max_i f_{ij},\ f_j^- = min_i f_{ij} \quad \ldots(10)$$

$$f_j^* = min_i f_{ij},\ f_j^- = max_i f_{ij} \quad \ldots(11)$$

Step 2: The S_i and R_i values can be calculated using equations (12) and (13), respectively.

$$S_i = \sum_{j=1}^{k} w_j \frac{(f_j^* - f_{ij})}{(f_j^* - f_j^-)} \quad \ldots(12)$$

$$R_i = max_j \left[w_j \frac{(f_j^* - f_{ij})}{(f_j^* - f_j^-)} \right] \quad \ldots(13)$$

Step 3: The Q_i values can be calculated using equation (14).

$$Q_i = \frac{v(S_i - S^*)}{(S^- - S^*)} + (1 - v)\frac{(R_i - R^*)}{(R^- - R^*)} \quad \ldots(14)$$

where $S^* = min_i S_i,\ S^- = max_i S_i,\ R^* = min_i R_i,\ R^- = max_i R_i$. The parameter v serves as a weight for the strategy of maximum group utility, while $1 - v$ is the weight of individual regret. Typically, $v = 0.5$ is taken in this calculation.

Step 4: The alternatives are ranked based on the lowest value of Q. The alternative with the lowest value of Q is considered the best-ranked alternative.

Step 5: If the following two conditions are satisfied, a compromise solution can be proposed with an alternative A^1, which is ranked the highest based on the measure Q

C1: Acceptable advantage:

$$Q(A^2) - Q(A^1) \geq DQ$$

where A^2 is the second-ranked alternative according to Q and $DQ = \frac{1}{(p-1)}$ (p is the number of alternatives).

C2: Acceptable stability in decision-making:

The alternative A^1 must also be the best ranked according to S or/and R.

If one of the conditions is not satisfied, then a set of compromise solutions is proposed, which consists of the following:

- The alternatives A^1 and A^2 if only condition 1 is true or
- The set of alternatives $A^1, A^2, \ldots, A^p$ if condition 1 is false; A^p is determined by $Q(A^p) - Q(A^1) < DQ$.

RESULTS AND DISCUSSION

An endeavor has been undertaken to identify the most contaminated region by employing the proposed AHP-Entropy-VIKOR model based on the air pollutant concentration in diverse parts of Tamil Nadu. The AHP calculates the attribute's subjective weights through a pairwise comparison matrix in equation (2). The determined weights are $\alpha_j = [0.122\ 0.057\ 0.263\ 0.558]$. After constructing the pairwise comparison matrix, it is imperative to assess its consistency. The obtained Eigenvalue λ_{max},is 4.119, and the consistency ratio is 0.04, less than the permissible value of 0.1, indicating good consistency in the judgments made. The Entropy technique uses the initial data to calculate the objective weights of the attribute. The resulting weight, β_j, as determined by equation (8), is represented in Table 4.

Table 4: Entropy weights of the attributes.

Year	β_1	β_2	β_3	β_4
2019	0.167	0.177	0.206	0.450
2020	0.266	0.201	0.221	0.312
2021	0.206	0.108	0.181	0.506

Table 5: Final weights of the attributes.

Year	w_1	w_2	w_3	w_4
2019	0.061	0.030	0.161	0.748
2020	0.118	0.041	0.210	0.630
2021	0.070	0.017	0.132	0.782

A hybrid weighting approach is adopted to derive more moderate weights, incorporating the AHP and Entropy methods. The final weights w_j of the attributes calculated by equation (9) are presented in Table 5.

Using the VIKOR approach, the best and worst values of all attributes from the initial data are identified, and then the VIKOR parameters. S_i, R_i,and Q_i are determined by applying equations (12), (13), and (14) These values are represented and ranked in Table 6. Following the methodology, two conditions are verified to determine the most suitable alternative in the VIKOR method.

By verifying the conditions, it can be inferred that the alternatives satisfied the requirements for acceptable advantage and stability in 2019 and 2020. As a result, CYY and RPM have ranked as the most contaminated regions in their respective years. However, in 2021, while the acceptable stability condition is fulfilled, the acceptable advantage condition is not. Consequently, TNR and TRP are identified as the most polluted areas among alternatives. COO was the least polluted area in the years 2019 and 2020. For the year 2021, PET was the least polluted area. However, since the TNPCB result (TNPCB 2022) was based on the breakpoint concentration of these pollutants and obtained through the maximum aggregation operator, the ranking of these twenty-six areas was slightly different. The result is represented in Fig. 4.

According to the TNPCB results, Cellisini Colony, Rayapuram, and T. Nagar were the worst polluted areas in 2019, 2020, and 2021, respectively, and Thirunagar, ESI Hospital, and Ramalinga Nagar were considered the least contaminated area in 2019, 2020, and 2021. For the most

Table 6: Ranks of the VIKOR parameters.

Areas	2019				2020				2021			
	S_i	R_i	Q_i	Rank	S_i	R_i	Q_i	Rank	S_i	R_i	Q_i	Rank
BSN	0.725	0.520	0.693	9	0.679	0.339	0.577	15	0.319	0.203	0.247	6
TNR	0.718	0.529	0.696	10	0.716	0.397	0.652	17	0.059	0.051	0.001	1
NGM	0.762	0.558	0.743	12	0.694	0.374	0.618	16	0.138	0.076	0.062	4
TRP	0.762	0.568	0.750	13	0.361	0.137	0.199	5	0.098	0.048	0.021	2
SCT	0.666	0.500	0.644	6	0.447	0.175	0.287	10	0.124	0.069	0.050	3
GDM	0.873	0.690	0.904	21	0.939	0.607	0.979	25	0.652	0.554	0.668	9
COO	0.958	0.748	0.997	26	0.928	0.630	0.993	26	0.625	0.517	0.628	8
IMR	0.764	0.573	0.755	14	0.393	0.163	0.243	8	0.799	0.688	0.839	13
PDP	0.777	0.583	0.769	15	0.307	0.165	0.191	4	0.821	0.698	0.858	17
THN	0.916	0.685	0.926	23	0.720	0.444	0.697	18	0.802	0.691	0.843	15
BVM	0.876	0.680	0.899	20	0.792	0.514	0.804	21	0.747	0.677	0.803	11
SBC	0.666	0.515	0.654	8	0.423	0.198	0.293	11	0.879	0.691	0.885	20
SVT	0.773	0.607	0.784	16	0.407	0.234	0.314	12	0.866	0.684	0.873	19
PET	0.964	0.728	0.986	25	0.904	0.572	0.926	23	0.977	0.782	1.000	26
VPT	0.901	0.690	0.920	22	0.912	0.572	0.931	24	0.969	0.774	0.991	25
RMN	0.647	0.481	0.618	5	0.583	0.292	0.476	13	0.962	0.760	0.977	24
GNM	0.674	0.500	0.648	7	0.406	0.143	0.232	7	0.912	0.731	0.930	22
GNN	0.198	0.165	0.123	3	0.626	0.362	0.565	14	0.824	0.680	0.848	16
SIE	0.707	0.578	0.724	11	0.742	0.455	0.721	19	0.776	0.626	0.784	10
RGI	0.563	0.452	0.547	4	0.317	0.133	0.168	3	0.774	0.662	0.808	12
ESI	0.911	0.690	0.926	24	0.851	0.514	0.841	22	0.925	0.749	0.950	23
ITH	0.787	0.607	0.793	17	0.357	0.152	0.210	6	0.809	0.684	0.842	14
RNR	0.178	0.060	0.035	2	0.753	0.490	0.759	20	0.411	0.271	0.344	7
CCY	0.121	0.059	0.000	1	0.416	0.163	0.257	9	0.284	0.181	0.213	5
KMC	0.868	0.641	0.866	19	0.233	0.114	0.099	2	0.854	0.771	0.926	21
RPM	0.804	0.660	0.842	18	0.137	0.070	0.000	1	0.836	0.691	0.862	18

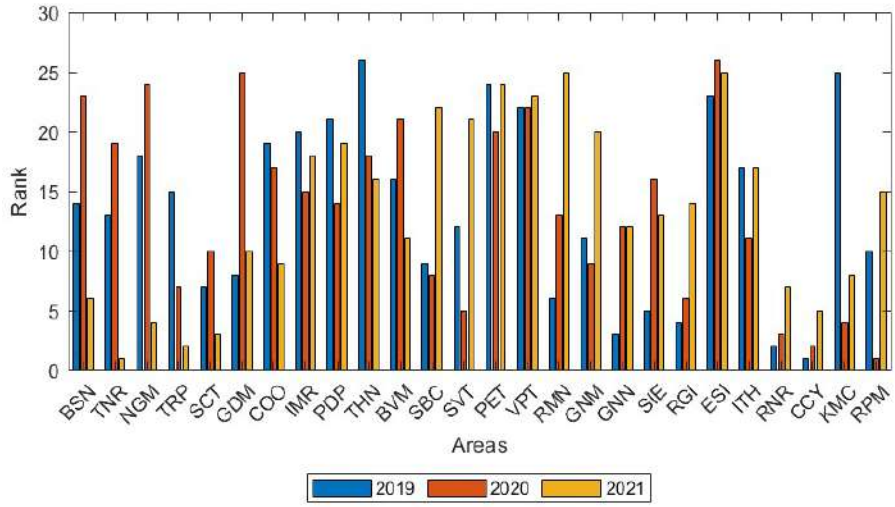

Fig. 4: TNPCB Ranking.

polluted area, the result obtained from AHP-Entropy-VIKOR is similar to the TNPCB result.

Comparison with MADM Methods

The present study validates the methodology by conducting a comparison between the proposed VIKOR approach and two established MADM approaches: Combinative Distance Assessment (CODAS) (Keshavarz et al. 2016) and Weighted Aggregated Sum Product Assessment (WASPAS) (Zavadskas et al. 2012). Both techniques are applied to the same dataset to rank the areas and determine the most polluted area in Tamil Nadu. The ranking outcomes of these methods are illustrated in Table 7.

From Table 7, the CODAS and WASPAS results indicate that Cellisini Colony, Rayapuram, and T. Nagar were ranked as one of the twenty-six areas of Tamil Nadu. Pettai and Collectorate Office was ranked as the least polluted area for 2019 by CODAS and WASPAS, respectively. Gowndampalayam (2020) and Pettai (2021) were ranked as the least polluted areas from CODAS and WASPAS methods in their respective year.

Moreover, a statistical test called Spearman's rank correlation test is employed to examine the interrelationship between the rankings derived from the proposed VIKOR model and the rankings obtained from CODAS and WASPAS methods. Spearman's coefficient assesses the significance of correlation among two or more rankings. The ranking of two datasets (A_1 and A_2) is calculated using the following equation:

$$\rho = 1 - \frac{6\sum d_i^2}{n(n^2-1)} \quad \ldots(15)$$

Here, n represents the number of alternatives and d^2 denotes the squared difference between the two rankings. The resulting ρ value indicates the relationship between the

Table 7: Ranking of CODAS and WASPAS.

Year	2019		2020		2021	
Methods	CODAS	WASPAS	CODAS	WASPAS	CODAS	WASPAS
BSN	9	11	15	15	6	6
TNR	10	9	17	17	1	1
NGM	12	12	16	16	4	4
TRP	13	13	5	6	2	2
SCT	6	6	10	12	3	3
GDM	20	21	26	26	9	9
COO	25	26	25	25	8	8
IMR	14	14	8	7	13	13
PDP	15	15	4	4	17	17
THN	23	24	18	18	15	14
BVM	21	20	21	21	11	11
SBC	8	7	11	10	21	20
SVT	16	16	12	8	19	19
PET	26	25	23	23	26	26
VPT	22	22	24	24	25	25
RMN	5	5	13	13	24	24
GNM	7	8	7	9	22	22
GNN	3	3	14	14	16	16
SIE	11	10	19	19	10	10
RGI	4	4	3	3	12	12
ESI	24	23	22	22	23	23
ITH	17	17	6	5	14	15
RNR	2	2	20	20	7	7
CCY	1	1	9	11	5	5
KMC	19	19	2	2	20	21
RPM	18	18	1	1	18	18

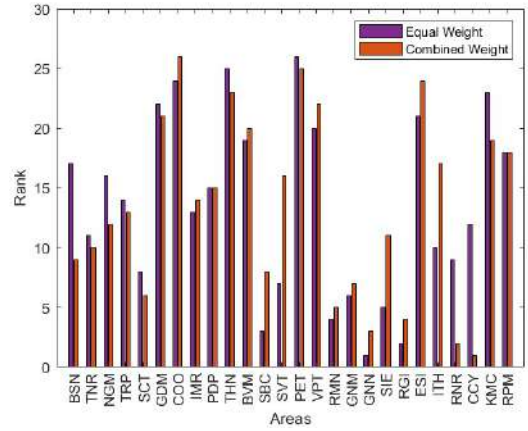

(a) Ranking for the year 2019 using equal and combined weight

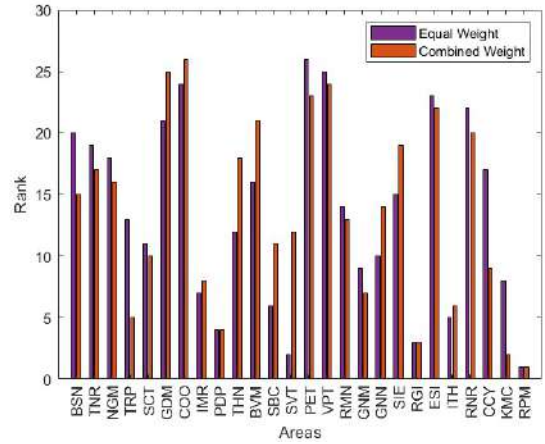

(b) Ranking for the year 2020 using equal and combined weight

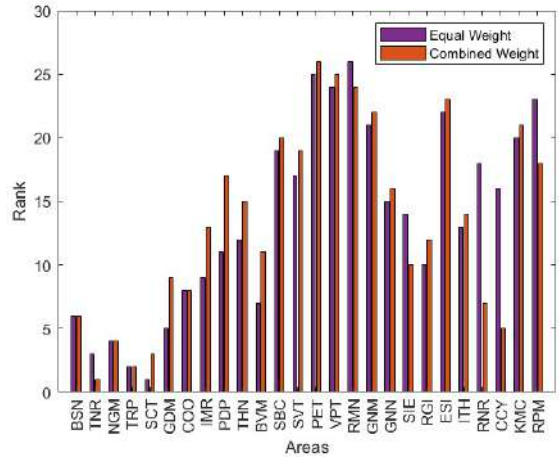

(c) Ranking for the year 2021 using equal and combined weight

Fig. 5: Sensitivity analysis for scenario 1.

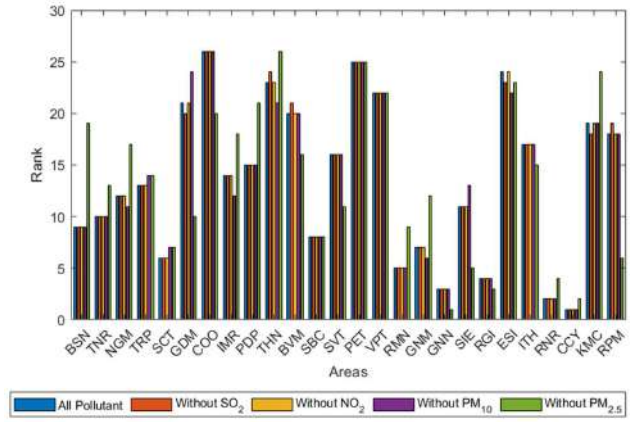

(a) Variations in the rank for the year 2019

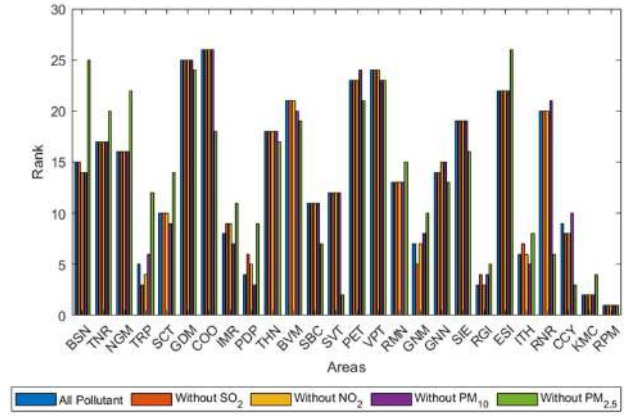

(b) Variations in the rank for the year 2020.

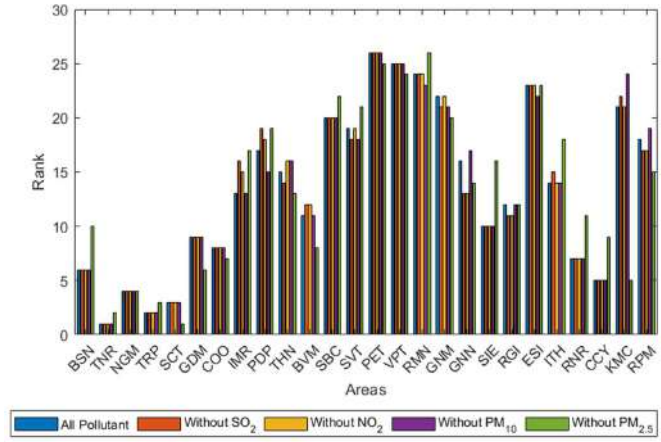

(c) Variations in the rank for the year 2020.

Fig. 6: Sensitivity analysis for scenario 2.

two sets. The value closer to +1 signifies a strong positive relationship, whereas the value nearer to – 1 indicates a strong negative relationship.

From the ranks obtained from AHP-Entropy-VIKOR, CODAS, and WASPAS, the correlation is determined using the equation (15). The Spearman's rank correlation among the AHP-Entropy-VIKOR approach with CODAS and WASPAS methods in 2019 is 0.999 and 0.997; in 2020, it is 0.999 and 0.988; in 2021, it is 0.999 and 0.999 respectively. It is also observed that the correlation between the AHP-Entropy-VIKOR is a little higher with CODAS when compared with WASPAS. However, Spearman's rank correlation indicates a strong positive correlation between the methods.

Sensitivity Analysis

A sensitivity analysis is carried out to examine the effect of priority weights on the ranking of regions and to identify the impact of a specific air pollutant on air quality. The sensitivity analysis in the present study considers two scenarios:

- The priority weights have changed.
- Reduction of pollutants

Scenario 1

This scenario presents the changes in the weights of the attributes and the comparison between the 2 cases:

Case 1: By applying a combined AHP-Entropy approach.

Case 2: Equal weights are considered for all attributes.

Fig. 5 depicts the ranking of the areas that vary while applying the AHP-Entropy approach and the equal weight approach. It can be seen that the ranking of the areas changes in many places when using equal weights across the years. In 2019, all the area ranks were changed, whereas in 2020, PDP, RGI, and RPM are the only areas where the rank is unchanged. In 2021, BSN, NGM, and COO attained the same rank, and the ranks of other areas were changed when applying the equal weight approach.

When evaluating any decision-making problem, the weights of the attributes are vital. Air has different concentrations of multiple pollutants. So, scenario 1 indicates that computing the pollutant's weights is essential while finding the most polluted region.

Scenario 2

In this case, sensitivity analysis removes air pollutants one at a time to observe how they affect the ranking of contaminated places. This sensitivity analysis gives information on the pollutant that significantly impacts air quality and the contaminant that affects the region's rank. For the study, SO_2 is eliminated first, NO_2 second, then PM_{10} finally $PM_{2.5}$ is eliminated, and Fig. 6 illustrates the area's ranking after removing the pollutant.

This scenario represents the impact of a particular pollutant and changes in ranking while eliminating each pollutant. When eliminating the air pollutant SO_2, NO_2, and PM_{10} the ranks of the areas are not affected, but while eliminating the pollutant $PM_{2.5}$ it causes a significant change in rank across the years. This sensitivity case concludes the effect of the pollutant $PM_{2.5}$ causes more impact while ranking the most polluted areas. The air quality of these areas can be improved by reducing the sources that emit the air pollutant $PM_{2.5}$.

CONCLUSION

This study identified the most polluted area in Tamil Nadu during the Diwali festival in 2019-2021 by implementing the AHP-Entropy-VIKOR model. Four different pollutants were considered, and their weights were determined using AHP and Entropy methods to attain the advantage from both the subjective and objective weight approach. The study encompassed 26 different areas in Tamil Nadu as alternatives and ranked them through the proposed model based on the priority weights attained from the combined AHP and entropy methods. The results indicated that Cellisini Colony (CYY) in Thoothukudi and Rayapuram (RPM) in Tiruppur were the most polluted areas in 2019 and 2020, respectively. However, due to the failed condition in the year 2021, T. Nagar and Triplicane in Chennai were the most contaminated areas in that year. The proposed model has many advantages, like less complexity and computation of air pollutant weights using subjective and objective weight concepts.

Furthermore, the validation of the proposed decision support system is checked through Spearman's rank correlation with the other two existing MADM approaches, CODAS and WASPAS. The result proved the consistency and strong correlation in the ranking of the proposed approach. Sensitivity analysis is also carried out to identify the importance of specific air pollutants on overall air quality and to determine whether the pollutant's weight affects the ranks of the city. The first analysis provided the ranks of the area to illustrate that the priority weights of the pollutants are vital in ranking the areas, and the second analysis indicated that the pollutant has more impact on the area's rank. These results might help government agencies in making the right decisions. In the future, the present work can be enhanced by incorporating more pollutants and factors like temperature, humidity, and wind to analyze the air quality.

ACKNOWLEDGEMENT

The authors thank the Tamil Nadu Pollution Control Board (TNPCB, Chennai) for providing the air pollution monitoring data during the Diwali festival in Chennai.

REFERENCES

Abdul, D., Wenqi, J. and Tanveer, A. 2022. Prioritisation of renewable energy sources for electricity generation through AHP-VIKOR integrated methodology. Renew. Energy, 184: 1018-1032.

Central Pollution Control Board (CPCB). 2022. National Air Quality Index. Retrieved from https://app.cpcbccr.com/ccr/

Chen, K.H., Yien, J.M., Chiang, C.H., Tsai, P.C. and Tsai, F.S. 2019. Identifying key sources of city air quality: A hybrid MCDM model and improvement strategies. Appl. Sci., 9(7): 1414.

Chundi, V., Raju, S., Waim, A.R. and Swain, S.S. 2022. Priority ranking of road pavements for maintenance using analytical hierarchy process and VIKOR method. Innov. Infrastruct. Solut., 7: 1-17.

Dev, S., Aherwar, A. and Patnaik, A. 2020. Material selection for automotive piston components using the entropy-VIKOR method. Silicon, 12: 155-169.

Dionova, B.W., Mohammed, M.N., Al-Zubaidi, S. and Yusuf, E. 2020. Environment indoor air quality assessment using fuzzy inference system. ICT Exp., 3)6): 185-194.

Hasanzadeh, R., Mojaver, P., Khalilarya, S. and Azdast, T. 2023. Air co-gasification process of LDPE/HDPE waste based on thermodynamic modeling: Hybrid multi-criteria decision-making techniques with sensitivity analysis. Int. J. Hydrog. Energy, 48(6): 2145-2160.

Keshavarz Ghorabaee, M., Zavadskas, E.K., Turskis, Z. and Antucheviciene, J. 2016. A new combinative distance-based assessment (CODAS) method for multi-criteria decision-making. Econ. Comput. Econ. Cybern., 50(3): 25-44.

Kumaravel, R. and Vallinayagam, V. 2012. Fuzzy inference system for air quality in using Matlab. Chennai, India. Environ. Dev., 7(1): 181-184.

Lin, H., Pan, T. and Chen, S. 2021. Comprehensive evaluation of urban air quality using the relative entropy theory and improved TOPSIS method. Air Qual. Atmos. Health, 14: 251-258.

Mandal, J., Chanda, A. and Samanta, S. 2022. Air pollution in three megacities of India during the Diwali festival amidst the COVID-19 pandemic. Sustain. Cities Soc., 76: 103504.

Morkunas, M. and Volkov, A. 2023. The progress of the development of climate-smart agriculture in Europe: Is there cohesion in the European Union? Environ. Manage., 7: 1-17.

Opricovic, S. and Tzeng, G.H. 2004. Compromise solution by MCDM methods: A comparative analysis of VIKOR and TOPSIS. Eur. J. Oper. Res., 156(2): 445-455.

Ozkaya, G. and Erdin, C. 2020. Evaluation of sustainable forest and air quality management and the current situation in Europe through operation research methods. Sustainability, 12(24): 10588.

Saaty, T.L. 1990. How to make a decision: The analytic hierarchy process. Eur. J. Oper. Res., 48(1): 9-26.

Shahnazari, A., Pourdej, H. and Kharage, M.D. 2021. Ranking of organic fertiliser production from solid municipal waste systems using analytic hierarchy process (AHP) and VIKOR models. Biocatal. Agric. Biotechnol., 32: 101946.

Shannon, C.E. 1948. A mathematical theory of communication. Bell Syst. Tech. J., 27(3): 379-423.

Siew, L.W., Hoe, L.W., Fai, L.K., Bakar, M.A. and Xian, S.J. 2021. Analysis of the e-learning method in Malaysia with the AHP-VIKOR model. Int. J. Inf. Educ. Technol., 11(2): 52-58.

Stanković, J.J., Popović, Ž. and Marjanović, I. 2021. Assessing smartness and urban development of the european cities: An integrated approach of entropy and VIKOR. In: Topcu, Y.I., Özaydın, Ö., Kabak, Ö. and Önsel Ekici, Ş. (eds), Multiple Criteria Decision Making: Contributions to Management Science, Springer, Cham, pp. 64-101.

State of Global Air Report (SGA). 2020 available at https://www.stateofglobalair.org/sites/default/files/documents/2022-09/soga-2020-report.pdf

Suresh, S., Modi, R., Sharma, A.K., Arisutha, S. and Sillanpää, M. 2021. Pre-COVID-19 pandemic: effects on air quality in the three cities of India using fuzzy MCDM model. J. Environ. Health Sci. Eng., 16: 1-11.

Tamil Nadu Pollution Control Board (TNPCB). 2019-2021 Diwali festival data. Retrieved from https://tnpcb.gov.in/aqisurvey.php (accessed 19-12-2022)

Torkayesh, A.E., Alizadeh, R., Soltanisehat, L., Torkayesh, S.E. and Lund, P.D. 2022. A comparative assessment of air quality across European countries using an integrated decision support model. Socio-Econ. Plan. Sci., 81: 101198.

Tzeng, G.H. and Huang, J.J. 2011. Multiple Attribute Decision Making: Methods and Applications. CRC Press, Boca Raton, Florida.

Xu, F. and Chernikov, A.S. 2021. Real-time air quality assessment based on the EM-TOPSIS-PROMETHEE integrated assessment method. IOP Conf. Ser. Earth Environ. Sci., 864(1): 012058.

Zardari, N.H., Ahmed, K., Shirazi, S.M. and Yusop, Z.B. 2015. Weighting methods and their effects on multi-criteria decision-making model outcomes in water resources management. Springer.

Zavadskas, E.K., Turskis, Z., Antucheviciene, J. and Zakarevicius, A. 2012. Optimisation of weighted aggregated sum product assessment. Elektron. Elektrotech., 122(6): 3-6.

Zeydan, Ö. and Pekkaya, M. 2021. Evaluating air quality monitoring stations in Turkey by using multi-criteria decision making. Atmos. Pollut. Res., 12(5): 101046.

ORCID DETAILS OF THE AUTHORS

A. Mohamed Nusaf: https://orcid.org/0000-0002-5507-9807
R. Kumaravel: https://orcid.org/0000-0003-0873-4757

Nature Environment and Pollution Technology
An International Quarterly Scientific Journal

p-ISSN: 0972-6268
(Print copies up to 2016)
e-ISSN: 2395-3454

Vol. 23 | No. 1 | pp. 173-181 | 2024

Original Research Paper

https://doi.org/10.46488/NEPT.2024.v23i01.013

Open Access Journal

Recent Progress of Novel Porous Materials in Wastewater Treatment

Deqi Kong*, Hua Chen*, Zhen Xiang and Bin Wang***†**
*Sichuan Institute of Building Research CO., Ltd., Chengdu, 610084, China
**Sichuan Huashi Overseas Investment & Engineering CO., Ltd., Chengdu, 610081, China
***Faculty of Quality Management and Inspection & Quarantine, Yibin University, Yibin, China
†Corresponding author: Bin Wang; binwang17711@163.com

Nat. Env. & Poll. Tech.
Website: www.neptjournal.com

Received: 06-04-2023
Revised: 31-05-2023
Accepted: 06-06-2023

Key Words:
Porous materials
Wastewater treatment
Adsorption
Pollutants

ABSTRACT

Unavoidably, the expansion of industry causes the release of numerous heavy metals, radionuclides, and organic pollutants into the environment. Due to these pollutants, the extremely toxic, highly carcinogenic chemicals provide a serious risk to people and aquatic life. Wastewater pollutants must be removed to safeguard the ecology. A huge specific surface area, multiple binding sites, a plethora of functional groups, variable pore size, and simplicity of surface modification are just a few advantages of porous materials. They are considered viable candidate materials for the efficient and selective removal of contaminants from aqueous solutions in a range of difficult circumstances due to their benefits. This work reviews the characteristics, methods of functionalization, and ways of modification of many novel porous materials in recent years. The use of these porous materials in the treatment of wastewater was examined. The development potential of porous materials is finally summed up.

INTRODUCTION

Urbanization and the rapid advancement of industrial technology have greatly improved people's quality of life, but they have also brought up new environmental issues, including widespread concern over water contamination (Mestre & Carvalho 2019, Osorio et al. 2016).

These encompass natural dyes, personal care products (PPCPs), endocrine disruptors, and some non-biodegradable Persistent organic pollutants (POPs) from the fabric industry (Michael et al. 2013). In particular, antibiotics in PPCPs, such as xanthamine antibiotics (SAs), are widely used to treat bacterial infections in humans, plants, and livestock, and most of them can't be totally metabolized (Doretto et al. 2014). More than 10 types of SA have been detected in rivers, sediments, groundwater, and soils in many countries, including the United States, the United Kingdom, China, and Australia (Verlicchi et al. 2012). Studies have proven that the concentrations of common sulfonamide Sulfamethoxazole (SMZ) in wastewater are in the vary of 100-2500 $ng.L^{-1}$, and these in floor water are in the range of 60-940 $ng.L^{-1}$, the concentration detected in drinking water used to be about 12 $ng.L^{-1}$ (Padhye et al. 2014). Although SMZ is launched at low stages and does not have direct poisonous results on humans, it can affect microbial communities and ecosystems, posing a long-term chance of elevated drug resistance and the manufacturing of resistant genes (Rodriguez-Escales & Sanchez-Vila 2016). Therefore, it is imperative to undertake some environmentally friendly techniques to do away with organic pollution from water.

The common strategies of natural wastewater remedy are adsorption, chemical precipitation, biofilm method, electrochemical method, photocatalytic technique, and so on (Reza et al. 2017). Adsorption, biofilm, and other techniques can correctly treat natural pollutants in water, but these techniques are via using some substances to adsorb natural pollution to its surface. This manner belongs to the transfer of pollution process, easy to cause the use of substances on the environment again pollution. Therefore, it is common for post-use materials to be similarly processed, which will result in a bigger cost. Chemical precipitation and electrochemical methods are additionally frequent methods in the therapy of organic pollution in water. Still, in the method of reaction, it is handy to produce toxic and unstable metabolites, which will have negative outcomes on animal and human health. In recent years, photocatalytic technological know-how has received massive interest due to the fact it is a clean and efficient water pollution treatment method. Through the photocatalyst is excited by light, the light power is transformed into chemical energy, and the chemical response happens with the target so as to achieve the purpose of the cure of pollutants. Photocatalytic

science has been extensively used in wastewater sterilization, degradation of organic pollution in water, and photocatalytic cracking of water hydrogen production and different fields.

Porous substances have the advantages of a large, unique floor area, many binding sites, ample purposeful groups, controllable pore dimensions, and convenient floor modification. It is viewed as a manageable candidate material for efficient and selective removal of contaminants from aqueous solutions underneath complicated conditions. In this work, the properties, functionalization, and modification strategies of new porous materials such as porous natural polymer, metal-organic frameworks, MXene, and covalent organic frameworks are reviewed and discussed. As shown in Fig. 1, this work critiques the application of four porous materials in the therapy of heavy metallic ions, radionuclide contaminants, and natural pollutants from aqueous solution. It presents beneficial education for the lookup of wastewater therapy and material development.

SYNTHESIS OF NOVEL POROUS MATERIALS

Metal-organic Frameworks

The technical constraints of conventional porous materials and nano-based materials for environmental applications have been acknowledged, and metal-organic frameworks (MOFs) have been identified as a promising alternative. MOFs are uniformly organized porous materials made of positively charged metal ions and organic ligands that act as bridges. Because of the special chemical flexibility provided by their metallic centers and organic linkers, their shape and porosity can be rationally tailored. Different MOFs can be created through inventive synthetic design using a variety of metal clusters and organic linkers.

The utilization of MOFs in numerous fields, together with sensors, catalysis, electricity storage, separation, storage, drug transport systems, nonlinear optics, and many others. Their feasibility toward wastewater cure for a number of pollution (e.g., heavy metallic ions, pesticides, volatile organic pollutants (VOCs), and other hazardous chemicals) has been evaluated.

A magnetic zirconium-based metal-organic framework nanocomposite was created by Far et al. (2020) using a simple solvothermal process, and it was previously employed as an adsorbent to remove direct and acid dyes from aqueous solution. The examined direct and acid dyes were absorbed by the dendrimer-functionalized magnetic composite at rates of 173.7 and 122.5 $mg.g^{-1}$, respectively, which was previously higher than that of the available magnetic adsorbents. This research offers fresh perspectives on the creation and application of hybrid magnetic adsorbents, as

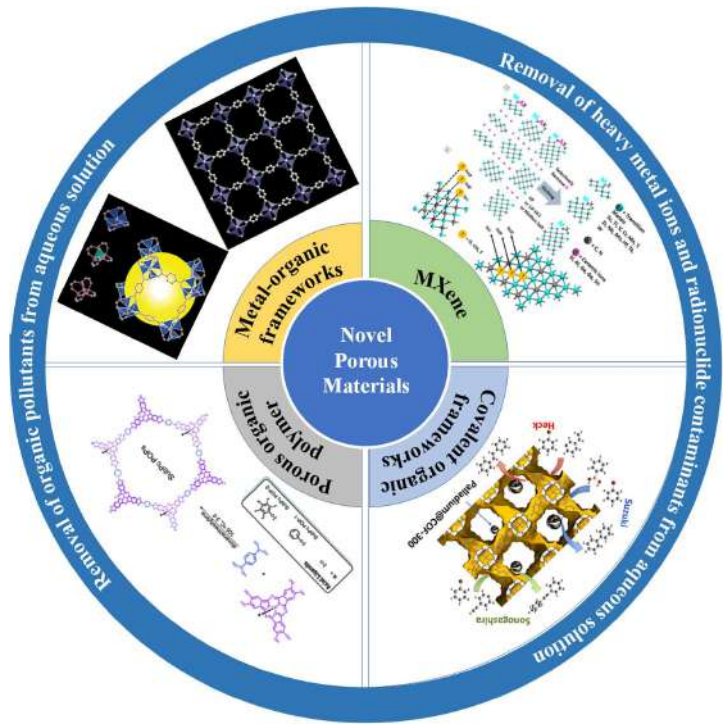

Fig. 1: Schematic illustration of the application of four porous substances in the treatment of heavy metallic ions, radionuclide contaminants, and natural pollution from aqueous solution (Gonçalves et al. 2016, Wu & Jiang 2023, Eder et al. 2017, Li et al. 1999).

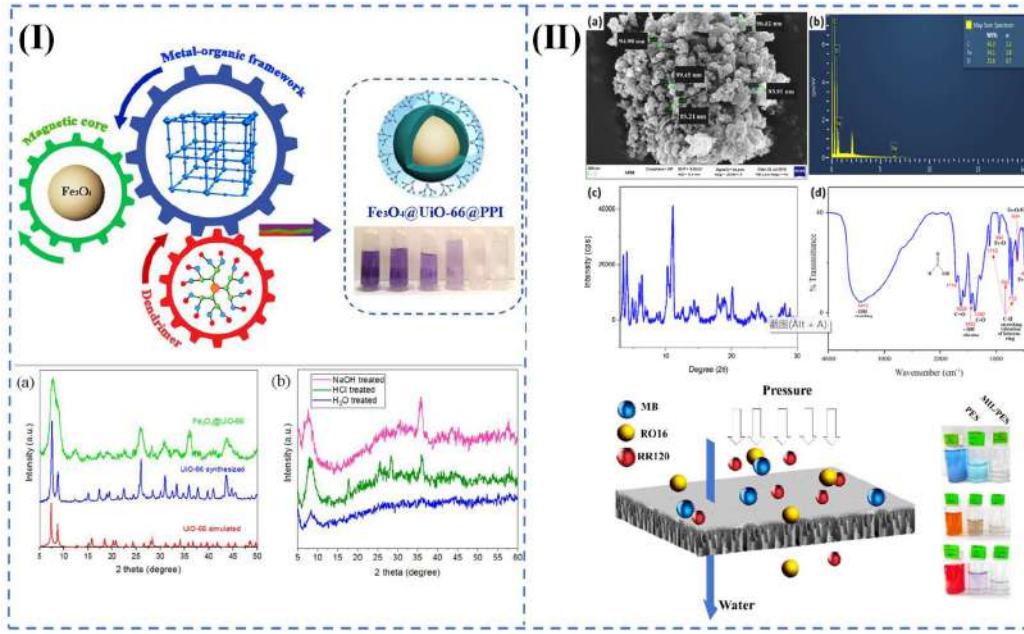

Fig. 2: (I) Fe_3O_4@UiO-66 nanocomposite's XRD patterns before and after a stability test, as well as the adsorption of the dye AB92, (II) FESEM picture, EDX, XRD, and FTIR of MIL-100(Fe), as well as the polymeric membrane modified with Fe-MOF nanoparticles rejecting both cationic and anionic dyes.

depicted in Fig. 2 (I), that combine the synergistic properties of nanoporous metal-organic frameworks and dendrimers with a wide range of functional corporations.

Johari et al. (2021) fabricated a hybrid flat sheet combined matrix membranes by blending polyethersulfone (PES) with an exclusive weight percentage of ferric-based metal-organic framework (Fe-MOF). The results showed that the Fe-MOF/PES membranes had first-rate rejections ($>98.5\%$) for cationic and anionic dyes, and the permeation flux was as high as 165.68 $L.m^{-2}h^{-1}$. Fig. 2 (II) depicts a schematic illustration of the preparation.

MXene

MXenes has a layered structure resembling graphene. It has garnered a lot of interest due to its distinct structure, exceptional physical chemistry characteristics, and great

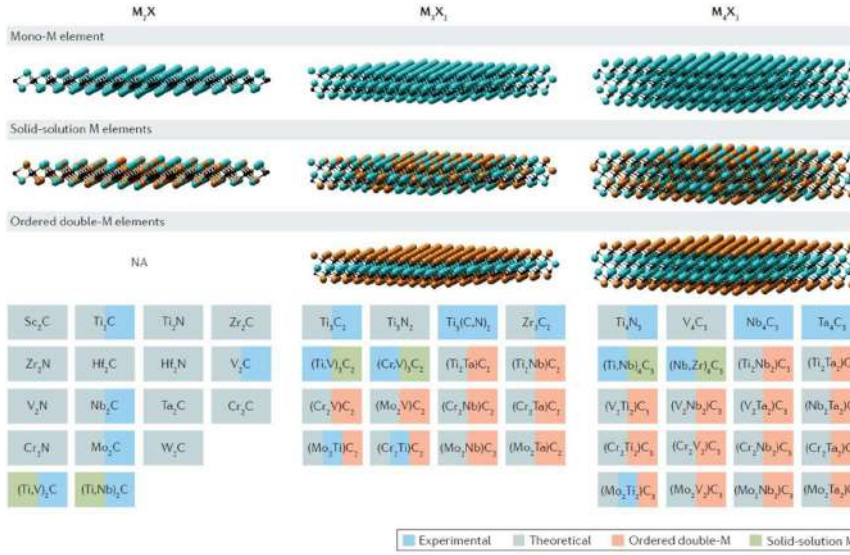

Fig. 3: Mxene model diagram with different structures (Naguib et al. 2011).

carrier mobility. MXenes' surface functional groups and elemental composition both have a significant impact on the properties of electron dispersion and carrier transport. It is possible to modify the surface functional groups and electrical characteristics, opening the door to the creation of composite catalysts based on MXenes and the subsequent production of more effective catalysts.

MXene is a substance made of transition metal carbides and nitrides with the chemical formula $M_{N+1}X_nT_x$ (n = 1-3) (Tariq et al. 2018, Folorunso et al. 2021), where M stands for transition metal elements belonging to the IIIA and Iva families, such as Ti, Sc, Cr, V, Zr, Nb, Mo, Hf, and Ta; X is either C or N; and T_x is the surface functional groups -O, -OH, and -F. As shown in Fig. 3, the solid solution structures of at least two metals are $(Ti, V)_2C$, $(Cr_2Ti)_3C_2$, and $(Nb, Zr)_4C_3$. MXene contains three molecular formulas, M_4X_3, M_3X_2, and M_2X_1, which are stacked alternatively in the form of $[M\text{-}X]_nM$. Bimetallic structure $(Mo_2Ta)C_2$, $(Cr_2V)C_2$, and $(Mo_2Ta_2)C_3$ that is ordered.

MXene has been extensively used in recent years in the domains of energy storage (Naguib & Gogotsi 2015), electromagnetic shielding (Shahzad et al. 2016), biosensors (Shi et al. 2019), water purification (Ihsanullah 2020), electrocatalysis and photocatalysis (Wang & Lee 2020) due to its properties of having a large specific surface area, metal conductivity, and tunable energy band. Particularly, it has been demonstrated that MXene is a highly effective co-catalyst whose conductivity is on par with noble metals.

Chen et al. (2019) organized the composite with excessive catalytic pastime via loading MoS_2 on MXene lamellar through the hydrothermal method. Under visible light conditions, the hydrogen generation rate reached 9679 $\mu mol \cdot g^{-1} \cdot h^{-1}$, as shown in Fig. 4 (I). My Tran (et al. 2021) produced MXene by Al-selective etching of Ti_3AlC_2 MAX phase with HF. The mainly F-terminated $Ti_3C_2T_x$ MXene was shown to be an effective methylene blue (MB) adsorbent in wastewater. Surprisingly, the mainly F-terminated MXene absorbed 92% of MB in 20 µM of MB aqueous solution in 5 minutes. Furthermore, the MXene was largely recyclable, allowing for recurrent use. Fig. 4 (II) depicts a schematic illustration of the preparation.

Covalent Organic Frameworks

Covalent organic frameworks (COF) are a novel class of porous materials that have received a lot of research (Bukhari et al. 2023). COF is highly organized via reversible reactivity, in contrast to conventional short-range covalent polymers joined by irreversible condensation. By using pre-designed structures, COF may perform specialized tasks in contrast to typical porous crystalline materials like zeolite and metal-organic framework (MOF). They are architecturally diversified, low-density materials with the advantages of excellent thermal stability and permanent porosity (da Silva et al. 2023).

Cote et al. (2005) produced COF for the first time in 2005. Following it, there were numerous COFs. These characteristics of organic porous polymers make them suitable for use in optoelectronics, sensing (Martínez-Perinan et al. 2022), drug delivery, adsorption, separation (Dautzenberg et al. 2023), catalysis (Pachfule et al. 2018), energy storage, and drug delivery. COF, as a powerful metal-

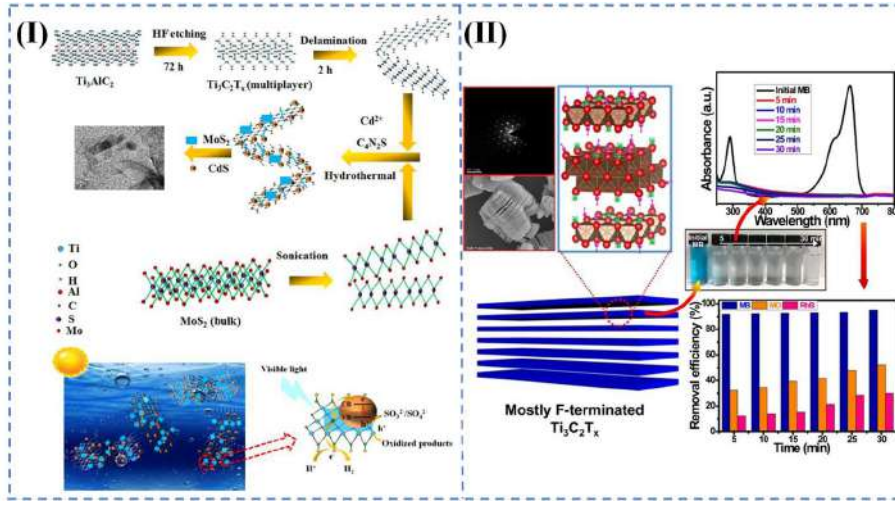

Fig. 4: (I) The schematic illustration for the preparation of CdS-MoS_2-MXene by hydrothermal method and the mechanism of the CdS-MoS_2-Mxene catalyst under visible light, (II) the structures of $Ti_3C_2T_x$ MXene and the adsorption performance for MB.

free photocatalyst and as a contaminant-removal adsorbent, is very challenging.

Ruidas et al. (2023) prepared a C_6-TRZ-TPA COF by segregation of donor-acceptor moieties with the extended Schiffbase condensation between tris(4-formylphenyl)amine and 4, 4′, 4″ - (1, 3, 5-triazine-2, 4, 6-triyl)trianiline. The COF had a Brunauer-Emmett-Teller (BET) surface area of 1058 $m^2 \cdot g^{-1}$, and it had a pore volume of 0.73 $cc.g^{-1}$. The COF has been investigated as a potent metal-free photocatalyst for wastewater treatment and as an adsorbent for iodine extraction, and it could be used to harness solar energy for environmental cleanup. Fig. 5 (I) displays a schematic illustration of the preparation.

El-Mahdy et al. (2020) created the bifluorenylidene-based covalent organic frameworks (COFs) BFTB-PyTA, BFTB-BFTB, and BFTB-BCTA using one-pot polycondensations of BFTB-4CHO with PyTA-$4NH_2$, BFTB-$4NH_2$, and BCTA-$4NH_2$. These three COFs have outstanding crystallinities, high specific surface areas, and exceedingly high thermal stabilities. Rhodamine B (RhB), a tiny dye molecule, was exceptionally well-adsorbed by the COFs in water, outperforming all previously reported COFs, conjugated polymers, activated carbons, and other typical nanoporous adsorbents with maximum adsorption capacities of up to 2127 $mg.g^{-1}$, as shown in Fig. 5 (II).

Porous Organic Polymer

Porous materials have completed the transition from traditional inorganic hybrid materials to porous organic materials, realizing the cross-fertilization of inorganic and organic chemistry, showing the vigorous development of porous materials and broad application prospects. As an important branch of porous materials, porous organic polymer (Pops) materials have developed rapidly in recent years. According to the different structures and synthesis strategies, POPs can be classified into covalent organic building block materials, super-connected polymers, self-microporous polymers, conjugated microporous polymers, porous aromatic skeletal materials, and covalent triazine organic skeletal materials. Depending on the diversity of organic chemistry, there are many pathways for the synthesis of Pops, including Yamamoto coupling, Suzuki coupling, Sonogashira-Hagihara cross-coupling, oxidative polymerization, imine condensation, nitrile trimerization, and solvate-thermal radical polymerization reactions.

Comparison of organic-inorganic hybrid materials such as metal oxide inorganic porous materials and metal-organic skeletal compounds. The advantages of Pops are outstanding: the molecular chain consists of only light elements, and the skeleton density is low. The structural units are designed and synthesized by organic reactions and are easy to functionalize. Covalent bonds connect the structural units and have highly stable physicochemical properties for use in high-temperature, high-pressure, humid, or acidic environments. The structural units are mostly rigid aromatic structures that resist large surface tensions during drying and prevent pore collapse, resulting in permanent pore structures.

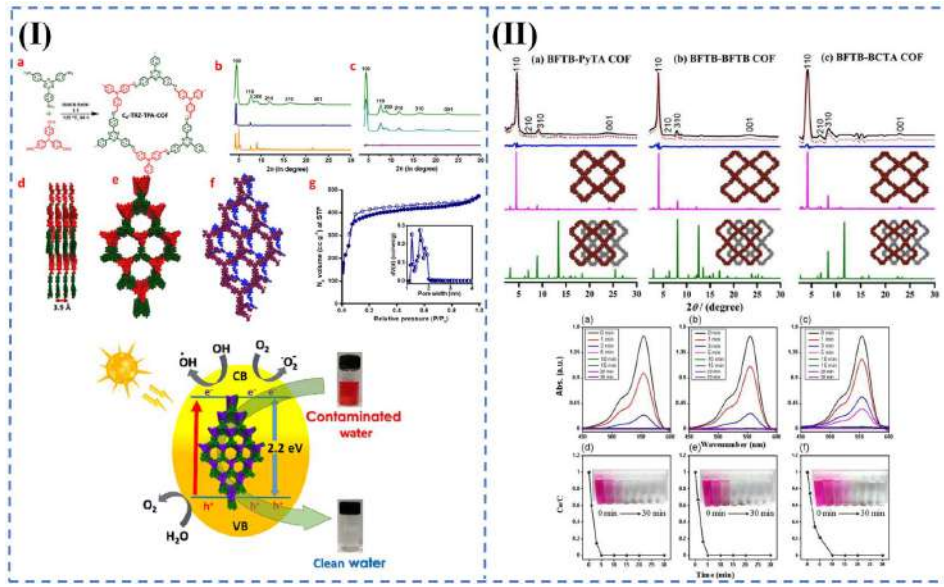

Fig. 5: (I) A schematic illustration of the preparation of C6-TRZ-TPA COF and their properties characterizations, (II) PXRD spectrum of the BFTB-PyTA, BFTB-BFTB, and BFTB-BCTA COFs and their adsorption results of RhB solution.

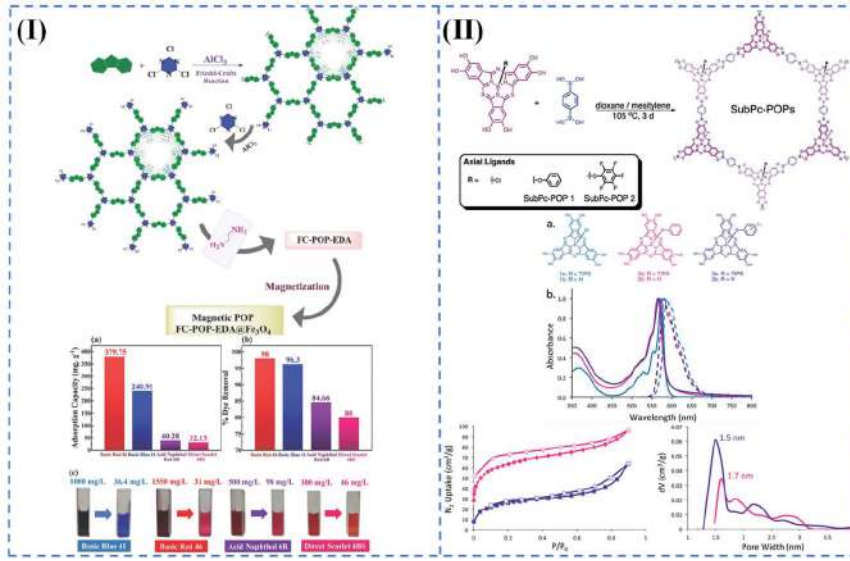

Fig. 6: (I) Preparation of FC-POP-EDA@ Fe_3O_4 and the dye removal effect, (II) preparation of the SubPc-POPs and the structures of monomers.

An accessible binding site-containing magnetic POP(FC-POP-EDA@Fe_3O_4) with amino functionality was created by Taheri and Dinari (2022). The mesoporous FC-POP-EDA@ Fe_3O_4 structure has a specific surface area of 402.11 $m^2.g^{-1}$ and well-defined crystallinity. Compared to anionic dyes, it showed better adhesion toward cationic dyes. For the synthesized POP, basic red 46, basic blue 41, direct scarlet 4BS, and acid naphthol 6B, respectively, had maximal adsorption capacities of 379.75, 240.9, 32.13, and 40.28 $mg.g^{-1}$. The findings show that FC-POP-EDA@Fe_3O_4 is an effective adsorbent for the selective filtration of cationic dyes from textile effluent. Fig. 6 (I) displays a schematic illustration of the preparation.

The creation and evaluation of two SubPc-based porous organic polymers (POPs) were described by Eder et al. (Eder 2017). The SubPc-POPs have reasonable surface areas, and in the solid state, their Q-bands are considerably redshifted. Fig. 6 (II) displays a schematic illustration of the preparation.

APPLICATIONS OF POROUS MATERIALS IN WASTEWATER TREATMENT

Removal of Heavy Metal Ions and Radionuclide Contaminants from Aqueous Solutions

Heavy metals are significant environmental pollutants that have a high chemical toxicity, are easily absorbed by humans and ecosystems, and constitute a major threat to both human health and the environment's ecological balance. By incorporating heavy metal ion adsorption sites into the pore structure of porous organic polymers by synthetic design, it is conceivable for porous organic polymers to function as efficient adsorbents for heavy metal ions.

Common heavy metal and radionuclide pollutants (such as Cd^{2+}, Cu^{2+}, Hg^{2+}, Pb^{2+}, U(VI), etc) in the water environment are difficult to degrade. As kinds of porous materials, they have been widely used in the removal of heavy metals in water environments in Table 1.

Nuclear energy can significantly lessen the strain of the energy problem in today's society because it has a high energy density and is a low-carbon energy source. Uranium, a crucial resource for the growth of nuclear energy, directly affects the long-term viability of the industry. On the other hand, uranium and its derivatives are highly polluted, radioactive, and poisonous.

A wide range of conventional materials, such as mineral clays, oxide aerogels, hydroxylapatite, metal sulfides, carbon-based materials, and hybrid materials based on graphene oxide (GO), have been created for the adsorption of toxic/radioactive metal ions. However, the following areas still have certain restrictions: Poor adsorption selectivity, slow adsorption kinetics, weak recyclability, difficulty in repeated treatment, poor environmental stability, complex material preparation process, difficulty in producing quickly on a large scale, and low maximum adsorption capacity of the adsorbent are all to be considered. To get over the constraints of present practical applications, it is critical to create novel materials for the manufacture of adsorbents.

New porous materials, such as covalent organic frameworks (COF) and metal-organic frameworks (MOF), have broad application prospects in the fields related to

Table 1: Removal of heavy metal ions and radionuclide contaminants from aqueous solution by porous materials.

Pollutant	Material	$S_{BET}/S_{Langmuir}$ [$m^2.g^{-1}$]	C_0 [$mg.L^{-1}$]	Q_{max} [$mg.g^{-1}$]	Removal rate [%]	Reference
Cr(VI)	ZIF-8	-	2.5	0.15	0.1	(Niknam Shahrak et al. 2017)
	Walnut shell biochar	-	110	-	93	(Kokab et al. 2021)
	MS-HMS-PL	414.5	-	257.67	-	(Soltani et al. 2020)
	Chitosan-g-PNVCL/ZIF-8 nanofibers	-	500	495.6	49.6	(Bahmani et al. 2019)
Hg(II)	FT-MOF	-	10	-	99.95	(Mon et al. 2017)
	Magnetic bentonite (M-B)	206.71	50	26.18	99.52	(Zou et al. 2018)
	Sulfurized magnetic biochar (SMBC)	337.5	-	8.93	-	(Hsu et al. 2021)
	Th-1	610	-	125.0	-	(Modak et al. 2019)
	Th-2	750	-	145.0	-	
	Th-3	480	-	128.0	-	
Pb(II)	UiO-66	1578	100	-	4	(Saleem et al. 2016)
	AT-MAC	-	-	310.9	99.5	(Waly et al. 2021)
	TMU-4	-	0.1	237	-	(Tahmasebi et al. 2015)
U(VI)	MIL-101-CMPO	2365	30	5.32	-	(De Decker et al. 2017)
	CMPO-functionalised polymers	-	-	26.7	-	(Annam et al. 2018)
	Polymer-coated polyacrylinitrile	20.9	50	33.0	-	(Aly et al. 2017)

environmental protection because of their excellent chemical stability, designability, and porosity. As kinds of porous materials, they have been widely used in the removal of heavy metal ions and radionuclide contaminants from aqueous solution in Table 1.

Removal of Organic Pollutants from Aqueous Solution

Textile, leather, plastic, paper, cosmetics, pharmaceuticals, printing, and other industries utilize organic dyes extensively. Dye waste that is inappropriately disposed of into the water cycle will unavoidably harm the aquatic ecosystem because dyes are non-degradable and carcinogenic. Adsorption is currently thought to be one of the most efficient ways to get rid of organic dyes. Still, conventional adsorbents like activated carbon, zeolite, and natural fiber have several drawbacks, including poor selectivity, poor reusability, and so on.

More and more people are becoming interested in porous polymers. They have the benefits of a high specific surface area, low mass, low density, high thermal stability, and high water stability when compared to other porous materials. There have been numerous types of organic porous polymers developed over the past ten years, and they can be classified into two groups based on their structural makeup: crystalline organic porous polymers and amorphous organic porous polymers. Covalent organic framework materials (COFs) are a common example of crystalline organic porous polymers. Hypercrosslinked polymers (HCPs), self-microporous polymers (PIMs), conjugated microporous polymers (CMPs), and other such materials are examples of amorphous organic porous polymers. As kinds of porous materials, they have been widely used in the removal of organic pollutants from aqueous solutions in Table 2.

Table 2: Removal of organic pollutants from aqueous solution by porous materials.

Pollutant	Material	$S_{BET}/S_{Langmuir}$ [$m^2.g^{-1}$]	C_0 [$mg.L^{-1}$]	Q_{max} [$mg.g^{-1}$]	Removal rate [%]	Reference
Organic dye	ZIF-67@Fe_3O_4@ESM	1263.9	10,15,20	208.33	-	(Mahmoodi et al. 2019)
	COFs	-	-	-	99	(Pan et al. 2019)
	TPOP–SO_3H	1002	-	97.1	-	(Li et al. 2019)
Phenolic compound	CNTs–PDMS	-	-	25 $mg.g^{-1}$ for 4-NP	-	(Turco et al. 2018)
	DPP	513.9	-	254.2	78.9	(Liu et al. 2022)
	FPP	772.8	-	339.4	81.9	
	R-g-Ch	-	-	188.6 $mg.g^{-1}$ for phenol	-	(Heydaripour et al. 2019)

CONCLUSIONS AND PERSPECTIVES

Porous materials are viewed as potential candidate materials for the effective and selective removal of contaminants from aqueous solutions under challenging circumstances because of their advantages of having a large specific surface area, numerous binding sites, abundant functional groups, controllable pore size, and convenient surface modification.

In this work, a sizable number of published literatures that are crucial to the adsorption process, such as pH value, temperature, and others, are reviewed. Another crucial element influencing the effectiveness of adsorption is the chemical and physical makeup of the adsorbents. Adsorbents having a lot of functional groups and a high specific surface area can improve this process. Future studies should focus on modification and composite materials, as well as ways to increase stability, decrease cost, evaluate toxicity, and increase adsorption capacity. There is still much to learn about how to regulate the synthesis conditions to create organic porous polymers with a greater specific surface area. The application of organic porous polymers in environmental remediation will be a significant area of research in the future.

ACKNOWLEDGMENTS

This work was supported by the Sichuan Science and Technology Program (2023JDZH0025) and the Sailing Plans Project of Yibin University (2021QH015).

REFERENCES

Aly, Z., Scales, N., Davis, J. and Lumpkin, G. 2017. Mesoporous polymer-coated PAN beads for environmental applications: fabrication, characterization, and uranium adsorption studies. J. Radioanal. Nucl. Chem., 311(1): 43-57.

Annam, S., Brahmmananda, C.V.S., Sivaraman, N., Sivaramakrishna, A. and Vijayakrishna, K. 2018. Carbamoylmethylphosphine oxide functionalized porous crosslinked polymers towards a sequential separation of uranium (VI) and thorium (IV). React. Funct. Polym., 131: 203-210.

Bahmani, E., Koushkbaghi, S., Darabi, M., ZabihiSahebi, A., Askari A. and Irani, M. 2019. Fabrication of novel chitosan-g-PNVCL/ZIF-8 composite nanofibers for adsorption of Cr(VI), As(V), and phenol in single and ternary systems. Carbohyd. Polym., 224: 115148.

Bukhari, S., Ahmed, N., Amjad, M., Hussain, M., Elsherif, M., Ejaz H. and Alotaibi, N. 2023. Covalent organic frameworks (COFs) as multi-target multifunctional frameworks. Polymers, 15(2): 267.

Chen, R., Wang, P., Chen, J., Wang C. and Ao, Y. 2019. Synergetic effect of MoS_2 and MXene on the enhanced H_2 evolution performance of CdS under visible light irradiation. Appl. Surf. Sci., 473: 11-19.

Cote, A., Benin, A., Ockwig, N., O'Keeffe, M., Matzger A. and Yaghi, O. 2005. Porous, crystalline, covalent organic frameworks. Science, 310(5751): 1166-1170.

da Silva, V. D., Zalewska, K., Petrovski, Z., Buarque, C.D., Branco L.C. and Esteves P.M. 2023. Covalent organic frameworks as promising materials for the removal of metal and organic pollutants from water. Mater. Today Sustain., 21: 100279.

Dautzenberg, E., Li, G. and Louis, C. 2023. Aromatic amine-functionalized covalent organic frameworks (COFs) for CO_2/N_2 separation. ACS Appl. Mater. Interf., 15(4): 5118-5127.

De Decker, J., Folens, K., Clercq, J., Meledina, M., Tendeloo, G., Laing, G. and Voort, P. 2017. Ship-in-a-bottle CMPO in MIL-101(Cr) for selective uranium recovery from aqueous streams through adsorption. J. Hazard, Mater., 335: 1-9.

Doretto, K., Peruchi, L. and Rath, S. 2014. Sorption and desorption of sulfadimethoxine, sulfaquinoxaline, and sulfamethazine antimicrobials in Brazilian soils. Sci. Tot. Environ., 476-477: 406-414.

Eder, G., Walker, B. and McGrier, P. 2017. Subphthalocyanine-based porous organic polymers. RSC Adv., 7(47): 29271-29274.

El-Mahdy, A., Zakaria, M., Wang, H., Chen, T., Yamauchi, Y. and Kuo, S. 2020. Heteroporous bifluorenylidene-based covalent organic frameworks displaying exceptional dye adsorption behavior and high energy storage. J. Mater. Chem. A, 8(47): 25148-25155.

Far, H., Hasanzadeh, M., Nashtaei, M., Rabbani, M., Haji, A. and Moghadam, B. 2020. PPI-dendrimer-functionalized magnetic metal-organic framework (Fe_3O_4@MOF@PPI) with high adsorption capacity for sustainable wastewater treatment. ACS Appl. Mater. Interf., 12(22): 25294-25303.

Folorunso, O., Kumar, N., Hamam, Y., Sadiku R. and Ray, S. 2021. Recent progress on 2D metal carbide/nitride (MXene) nanocomposites for lithium-based batteries. FlatChem., 29: 100281.

Gonçalves, R., de Oliveira, A., Sindra, H., Archanjo, B., Mendoza, M., Carneiro, L., Buarque, C. and Esteves, P. 2016. Heterogeneous catalysis by covalent organic frameworks (COF): $Pd(OAc)_2$@COF-300 in cross-coupling reactions. ChemCatChem., 8(4): 743-750.

Heydaripour, J., Gazi, M., Oladipo, A. and Gulcan, H. 2019. Porous magnetic resin-g-chitosan beads for adsorptive removal of phenolic compounds. International J. Biol. Macromol., 123: 1125-1131.

Hsu, C., Cheng, Y., Huang, Y., Atkinson J. and Hsi, H. 2021. A novel synthesis of sulfurized magnetic biochar for aqueous Hg(II) capture as a potential method for environmental remediation in water. Sci. Tot. Environ., 784: 147240.

Ihsanullah, M. 2020. Potential of MXenes in water desalination: Current status and perspectives. Nano-Micro Lett., 12(1): 72.

Johari, N., Yusof, N., Lau, W., Abdullah, N., Salleh, W., Jaafar, J., Aziz, F. and Ismail, A. 2021. Polyethersulfone ultrafiltration membrane incorporated with ferric-based metal-organic framework for textile wastewater treatment. Sep. Purif. Technol., 270: 118819.

Kokab, T., Ashraf, H., Shakoor, M., Jilani, A., Ahmad, S., Majid, M., Ali, S., Farid, N., Alghamdi, R., Al-Quwaie, D. and Hakeem, K. 2021. Effective removal of Cr(VI) from wastewater using biochar derived from walnut shell. Int. J. Environ. Res. Pub. Health, 18(18): 9670.

Li, H., Eddaoudi, M., O'Keeffe M. and Yaghi, O. 1999. Design and synthesis of an exceptionally stable and highly porous metal-organic framework. Nature, 402(6759): 276-279.

Li, Y., Wang, H., Zhao, W., Wang, X., Shi, Y., Fan, H., Sun H. and Tan, L. 2019. Facile synthesis of a triptycene-based porous organic polymer with a high efficiency and recyclable adsorption for organic dyes. J. Appl. Poly., 136(39): 47987.

Liu, Y., Zhou, X., Jin, C., Liu, Gg., Liu Z. and Kong, Z. 2022. Efficient and rapid removal of typical phenolic compounds from water with biobased porous organic polymers. Indust. Crops Prod., 184: 114971.

Mahmoodi, N., Taghizadeh, M., Taghizadeh, A., Abdi, J., Hayati B. and Shekarchi, A. 2019. Bio-based magnetic metal-organic framework nanocomposite: Ultrasound-assisted synthesis and pollutant (heavy metal and dye) removal from aqueous media. Appl. Surf. Sci., 480: 288-299.

Martinez-Periñan, E., Martinez-Fernandez, M., Segura, J. and Lorenzo, E. 2022. Electrochemical (bio)sensors based on covalent organic frameworks (COFs). Appl. Surf. Sci., 22(13): 4758.

Mestre, A. and Carvalho, A. 2019. Photocatalytic degradation of pharmaceuticals carbamazepine, diclofenac, and sulfamethoxazole by semiconductor and carbon materials: A review. Science, 24(20): 3702.

Michael, I., Rizzo, L., McArdell, C., Manaia, C., Merlin, C., Schwartz, T., Dagot, C. and Fatta-Kassinos, D. 2013. Urban wastewater treatment plants as hotspots for the release of antibiotics in the environment: A review. Water Res., 47(3): 957-995.

Modak, A., Das, S., Chanda, D., Samanta, A. and Jana, S. 2019. Thiophene containing microporous and mesoporous nanoplates for separation of mercury from aqueous solution. New J. Chem., 43(8): 3341-3349.

Mon, M., Qu, X., Ferrando-Soria, J., Pellicer-Carreño, I., Sepúlveda-Escribano, A., Ramos-Fernandez, E., Jansen, J., Armentano, D. and Pardo, E. 2017. Fine-tuning of the confined space in microporous metal-organic frameworks for efficient mercury removal. J. Mater. Chem. A, 5(38): 20120-20125.

My Tran, N., Ta, Q., Sreedhar, A. and Noh, J. 2021. $Ti_3C_2T_x$ MXene playing as a strong methylene blue adsorbent in wastewater. Appl. Surf. Sci., 537: 148006.

Naguib, M. and Gogotsi, Y. 2015. Synthesis of two-dimensional materials by selective extraction. Account. Chem. Res., 48(1): 128-135.

Naguib, M., Kurtoglu, M., Presser, V., Lu, J., Niu, J., Heon, M., Hultman, L., Gogotsi, Y. and Barsoum, M. 2011. Two-dimensional nanocrystals produced by exfoliation of Ti_3AlC_2. Science, 23(37): 4248-4253.

Niknam Shahrak, M., Ghahramaninezhad, M. and Eydifarash, M. 2017. Zeolitic imidazolate framework-8 for efficient adsorption and removal of Cr(VI) ions from aqueous solution. Environ. Sci. Pollut. Res., 24(10): 9624-9634.

Osorio, V., Sanchís, J., Abad, J., Ginebreda, A., Farré, M., Pérez, S. and Barceló, D. 2016. Investigating the formation and toxicity of nitrogen transformation products of diclofenac and sulfamethoxazole in wastewater treatment plants. J. Hazard. Mater., 309: 157-164.

Pachfule, P., Acharjya, A., Roeser, J., Langenhahn, T., Schwarze, M., Schomäcker, R., Thomas, A. and Schmidt, J. 2018. Diacetylene functionalized covalent organic framework (COF) for photocatalytic hydrogen generation. J. Am. Chem. Soc., 140(4): 1423-1427.

Padhye, L., Yao, H., Kung'u, F. and Huang, C. 2014. Year-long evaluation on the occurrence and fate of pharmaceuticals, personal care products, and endocrine-disrupting chemicals in an urban drinking water treatment plant. Water Res., 51: 266-276.

Pan, F., Guo, W., Su, Y., Khan, N., Yang, H. and Jiang, Z. 2019. Direct growth of covalent organic framework nanofiltration membranes on modified porous substrates for dyes separation. Sep. Purif. Technol., 215: 582-589.

Reza, K., Kurny, A. and Gulshan, F. 2017. Parameters affecting the photocatalytic degradation of dyes using TiO_2: A review. Appl. Water Sci., 7(4): 1569-1578.

Rodriguez-Escales, P. and Sanchez-Vila, X. 2016. Fate of sulfamethoxazole in groundwater: Conceptualizing and modeling metabolite formation under different redox conditions. Water Res., 105: 540-550.

Ruidas, S., Chowdhury, A., Ghosh, A., Ghosh, A., Mondal, S., Dinga Wonanke, A., Addicoat, M., Das, A., Modak, A. and Bhaumik, A. 2023. Covalent organic framework as a metal-free photocatalyst for dye degradation and radioactive iodine adsorption. Langmuir, 52: 1162.

Saleem, H., Rafique, U. and Davies, R. 2016. Investigations on post-synthetically modified UiO-66-NH_2 for the adsorptive removal of heavy metal ions from aqueous solution. Micropor. Mesopor. Mater., 221: 238-244.

Shahzad, F., Alhabeb, M., Hatter, C., Anasori, B., Hong, S., Koo, C. and Gogotsi, Y. 2016. Electromagnetic interference shielding with 2D transition metal carbides (MXenes). Science, 353(6304): 1137-1140.

Shi, X., Wang, H., Xie, X., Xue, Q., Zhang, J., Kang, S., Wang, C., Liang, J. and Chen, Y. 2019. Bioinspired ultrasensitive and stretchable MXene-based strain sensor via nacre-mimetic microscale "brick-and-mortar" architecture. ACS Nano, 13(1): 649-659.

Soltani, R., Marjani, A., Soltani, R. and Shirazian, S. 2020. Hierarchical multi-shell hollow micro-meso-macroporous silica for Cr(VI) adsorption. Sci. Rep., 10(1): 9788.

Taheri, N. and Dinari, M. 2022. Amino-functionalized magnetic porous organic polymer for the selective removal of toxic cationic dyes from textile wastewater. New J. Chem., 46(23): 11174-11184.

Tahmasebi, E., Masoomi, M., Yamini, Y. and Morsali, A. 2015. Application of mechanosynthesized azine-decorated zinc(II) metal-organic frameworks for highly efficient removal and extraction of some heavy metal ions from aqueous samples: A comparative study. Inorg. Chem., 54(2): 425-433.

Tariq, A., Irfan Ali, S., Akinwande, D. and Rizwan, S. 2018. Efficient visible-light photocatalysis of 2D-MXene nanohybrids with Gd^{3+}- and Sn^{4+}-codoped bismuth ferrite. ACS Omega, 3(10): 13828-13836.

Turco, A., Monteduro, A., Mazzotta, E., Maruccio, G. and Malitesta, C. 2018. An innovative porous nanocomposite material for the removal of phenolic compounds from aqueous solutions. Nanotechnology, 8(5): 334.

Verlicchi, P., Al Aukidy, M. and Zambello, E. 2012. Occurrence of pharmaceutical compounds in urban wastewater: Removal, mass load, and environmental risk after a secondary treatment: A review. Sci. Tot. Eniron., 429: 123-155.

Waly, S., El-Wakil, A., Abou El-Maaty, W. and Awad, F. 2021. Efficient removal of Pb(II) and Hg(II) ions from aqueous solution by amine and thiol-modified activated carbon. J. Saud. Chem. Soc., 25(8): 101296.

Wang, H. and Lee, J. 2020. Recent advances in structural engineering of MXene electrocatalysts. J. Mater. Chem. A, 8(21): 10604-10624.

Wu, T. and Jiang, D. 2023. Computational studies of MXenes. MRS Bull., 48(1): 499.

Zou, C., Liang, J., Jiang, W., Guan, Y. and Zhang, Y. 2018. Adsorption behavior of magnetic bentonite for removing Hg(ii) from aqueous solutions. RSC Adv., 8(48): 27587-27595.

Nature Environment and Pollution Technology
An International Quarterly Scientific Journal

p-ISSN: 0972-6268
(Print copies up to 2016)
e-ISSN: 2395-3454

Vol. 23 | No. 1 | pp. 183-191 | 2024

Original Research Paper

https://doi.org/10.46488/NEPT.2024.v23i01.014

Open Access Journal

An Overview of the Need for Circular Economy on Electric Vehicle Batteries

S. Padmanabhan*†, C. Joel, S. Mahalingam***, J. R. Deepak****, T. Vinod Kumar***** and Deborah Raj******

*School of Mechanical and Construction, Vel Tech Rangarajan Dr.Sagunthala R&D Institute of Science and Technology, Chennai, India

**Department of Mechanical Engineering, Easwari Engineering College, Chennai, India

***Department of Mechanical Engineering, Sona College of Technology, Salem, India

****School of Mechanical Engineering, Sathyabama Institute of Science and Technology, Chennai, India

*****Department of Mechanical Engineering, Vels Institute of Science, Technology & Advanced Studies (VISTAS), Chennai, India

******Department of Communication, Madras Christian College, Chennai, India

†Corresponding author: S. Padmanabhan; padmanabhan.ks@gmail.com

Nat. Env. & Poll. Tech.
Website: www.neptjournal.com

Received: 06-08-2023
Revised: 05-09-2023
Accepted: 22-09-2023

Key Words:
Circular economy
Battery
Environment
Pollution
Recycle
Electric vehicles
E-waste

ABSTRACT

Batteries are a widely utilized and simple method for powering electronic devices, particularly given the prevalence of individuals traveling to all gadgets. The escalating adoption of electric vehicles and portable electronic devices has led to a surge in the demand for lithium-ion batteries. Consequently, this has given rise to supply uncertainties in acquiring essential minerals such as lithium and cobalt, along with concerns about the proper disposal of dead batteries. The existing methods for battery recycling exhibit variations based on the individual chemistries of the batteries, hence influencing both cost factors and greenhouse gas emissions. Simultaneously, there exists a possibility for repurposing depleted batteries for low-tier energy storage applications. The absence of legislation pertaining to the secure storage and handling of waste streams contributes to the accumulation of refuse in exposed environments and the release of hazardous substances from landfills. In addition, contemporary battery manufacturing methods necessitate the utilization of innovative substances, such as ionic liquids for electrolytes and nanostructures for cathodes, to enhance the energy characteristics and longevity of batteries. The presence of uncertainties regarding the accurate assessment of the environmental consequences associated with novel battery chemicals has the potential to impede efforts aimed at recycling and containment. The objective of this analysis is to consolidate the existing knowledge regarding battery pollutants, both those that are recognized and those that remain uncertain, and to assess their potential environmental impacts. Additionally, this research aims to examine the current strategies and methods employed for the recycling of batteries in the circular economy.

INTRODUCTION

Electric vehicles (EVs) are widely recognized for their environmentally beneficial characteristics and extended durability. The increasing popularity of electric cars in India and other regions can be attributed, in part, to their significantly lower emissions when compared to conventional automobiles and trucks that rely on fossil fuels. However, critics contend that the purported advantages in terms of pollution reduction are often overstated, while the challenges associated with battery management are disregarded. However, the efficacy of the nation's battery recycling system might be enhanced by many advantages, opportunities, and challenges. Approximately 60% of the total cost of manufacturing an electric vehicle battery can be attributed to the expenditure on raw materials. However, the costs associated with EV battery disposal can be significantly reduced by the implementation of a comprehensive recycling system. Let us consider the potentialities and challenges within this particular domain (Velázquez-Martínez et al. 2019, Pražanová et al. 2022).

The researcher identified a significant lack of awareness among end users, authorities, and recyclers regarding the health dangers, environmental impacts, and regulatory measures pertaining to e-waste. The researcher delineated a triad of straightforward procedures that, when implemented collectively, have the potential to substantially modify public behavior with regard to a certain matter. Effective e-waste

management has three essential components: sensitization. The recognition of electronic devices as discarded items, the acquisition of knowledge regarding the proper handling of electronic waste, and the acknowledgment of the increasing significance of e-waste management as a pressing issue that necessitates attention. Nevertheless, a significant obstacle to the effective management of electronic trash (e-waste) is the lack of awareness and education among the entire population of India (Chandramauli 2020).

With the growing significance of sustainability among many stakeholders, such as customers, investors, regulators, and employees, automakers are acknowledging the imperative for future generations of automotive products to achieve success in both commercial and environmental aspects. To promote sustainability, efforts are being made to better both the products and manufacturing processes. The company's current product line exhibits enhanced fuel efficiency, increased utilization of recycled materials, and the incorporation of sustainably sourced resources like wood and leather. To mitigate the carbon emissions associated with its manufacturing operations, the company is adopting various strategies, including the utilization of renewable energy sources, optimization of energy consumption, and reduction of waste generation and water consumption (Velázquez-Martínez et al. 2019, Harper et al. 2023).

The researcher brought forth a comprehensive analysis of the challenges and potential remedies associated with the effective handling and control of electronic trash in the Indian context. The research delineated the pertinent techniques and challenges involved in tackling this emerging concern from an Indian vantage point. Various stakeholders, including manufacturers, assemblers, importers, recyclers, consumers, and government agencies, collectively contribute to the comprehensive process of e-waste collection and recycling. The introduction of electronic garbage further compounds the issue of handling solid waste in India, hence adding a layer of complication. The creation of standards is crucial for ensuring the appropriate disposal and recovery of valuable elements from electronic waste. In the process of producing state-of-the-art electronic devices, it is imperative to strategically consider the future decommissioning of these technologies (Joseph 2007, Skinner et al. 2010).

In the Indian context, it is prevalent for customers to prolong the retention of obsolete electronic devices, choosing to engage in repair or inheritance practices rather than engaging in disposal activities. There is a widely accepted agreement over the hesitancy to promptly discard electronic garbage as a commodity (Turaga et al. 2019). Due to the implementation of regulations in 2012, pollution control boards have been assigned the responsibility of collating inventories of electronic waste that are specific to their respective states. The aggregation of sales data on electronic equipment at the national level is crucial for accurately calculating e-waste volumes. This poses a challenge in creating inventories at the state level. Electronic garbage sometimes referred to as e-waste, is generated through both domestic means and illicit importation, primarily originating from affluent economies. Limited information is available regarding the composition and volume of electronic garbage (e-waste) that is imported into the nation. A comprehensive understanding of the production, content, and flow of waste is important to develop effective systems for the collection, transportation, and processing of waste materials (Li et al. 2019, Chandramauli 2020).

When considering the circular economy, it is important to anticipate the potential challenges that may arise if industries experience significant growth. It is possible that the processes and methods that have been effective at smaller sizes could become burdensome when dealing with larger volumes. The increasing difficulty of implementing a circular economy for batteries can be attributed to a convergence of various long-term trends. Firstly, the declining price of new batteries poses a challenge. Additionally, advancements in battery formulation result in future batteries containing components that have diminishing value, hence exerting pressure on recyclers' profit margins. This observation suggests that the suitability of technologies and processes may vary between industries with different characteristics, such as high material value and low volume, versus low material value and high volume (Leung 2019, Deshwal et al. 2022).

The constant sourcing of e-waste volumes that provide economies of scale poses a hindrance to the entry of private enterprises aiming to establish e-waste management systems within the formal sector. When private firms are uncertain about their ability to obtain adequate amounts of e-waste, they may deem it unprofitable to allocate resources toward the development of efficient recycling systems for electronic trash. Moreover, these marketplaces present substantial challenges in terms of accessing and disseminating information. The market may face obstacles stemming from a limited understanding of effective recycling techniques, which can be attributed to the industry's very nascent stage of development. Furthermore, the limited awareness among customers regarding the management of electronic trash is a barrier to achieving optimal market efficiency. This can be attributed, at least partially, to the lack of trustworthiness in the already accessible information. The establishment of more robust electronic waste (e-waste) marketplaces may require a heightened involvement of public policy (Skinner et al. 2010, Kang et al. 2013).

Within conventional waste management, a sequential arrangement of alternatives exists for the prioritized handling of waste streams. In the initial scenario, it is advisable to minimize waste in its entirety. However, in cases where waste is unavoidable, the conventional hierarchy of options, listed in order of preference, would typically include reuse as the primary choice, followed by remanufacture. If neither of these options is feasible, recycling with energy recovery would be the next preferred alternative, with disposal being considered as a last resort. Numerous waste management hierarchies have been suggested in addressing battery waste, wherein the majority advocate for the incorporation of reuse as a fundamental component. The concept of reuse can be categorized into two distinct forms: direct reuse, which occurs within the primary application, and secondary reuse, which takes place in a different application.

Moreover, the concept of reuse in the primary context can be further categorized based on the preservation of the donor battery's integrity, referred to as direct reuse, or the necessity of remanufacturing, known as indirect reuse (Ali et al. 2021). The objective of this analysis is to consolidate the existing knowledge regarding battery pollutants, both those that are recognized and those that remain uncertain, and to assess their potential environmental impacts. Additionally, this research aims to examine the current strategies and methods employed for the recycling of batteries in the circular economy.

CIRCULAR ECONOMY ASPECT OF EV BATTERY

The concept of the circular economy has garnered significant interest from policymakers and commercial players as it pertains to the important matter of resource efficiency and material circularity. The fundamental tenets of the circular economy revolve around the elimination of waste and pollution, with particular emphasis on the final stage of a product's life cycle. Additionally, the principles involve prolonging the use of products and materials, specifically during the middle phase of their life cycle, and promoting the restoration of natural ecosystems. This restoration is primarily focused on achieving environmental sustainability and reducing the reliance on material consumption and production patterns. This entails addressing the initial stages of a product's life cycle, such as material extraction for the technical cycle and the utilization of bio-based materials for the biological cycle. Furthermore, the principles advocate for the use of non-toxic materials and the adoption of renewable energy sources. The economic tool in question aims to promote a deceleration, restriction, and closed-loop approach to current patterns of material consumption while also emphasizing bolstering social and environmental objectives (Velázquez-Martínez et al. 2019, Selvi & Ritha 2022).

The implementation of circular economy techniques pertaining to electric vehicle (EV) batteries is of utmost importance to mitigate resource depletion, diminish environmental consequences, and optimize the value of these very valued energy storage devices. One potential approach to enhance the longevity of batteries involves the optimization of their design to prioritize durability and facilitate reparability. The implementation of modular designs, which provide the convenient replacement of specific components such as cells or modules, has the potential to enhance the overall lifespan of batteries and mitigate the necessity for total replacements (Ahuja et al. 2020).

This study aims to develop systematic procedures for the refurbishment and remanufacturing of utilized electric vehicle batteries. Once batteries have concluded their operational lifespan in-car applications, they may still retain a significant amount of capacity suitable for stationary energy storage or other uses that require less demanding energy requirements. One potential application for repurposing used electric vehicle batteries is their utilization in various energy storage capacities, including grid stability, integration of renewable energy sources, and backup power systems. The utilization of "second-life" applications has the potential to enhance the longevity of batteries prior to their ultimate recycling process (Olsson et al. 2018, Koller et al. 2021).

The objective is to devise effective recycling methodologies that can extract valuable elements, including lithium, cobalt, nickel, and other metals, from depleted electric vehicle batteries. These materials have the potential for utilization in the production of novel batteries or alternative commodities, hence mitigating the requirement for primary resources. The implementation of closed-loop supply chains entails the adoption of a system wherein manufacturers assume the responsibility of reclaiming used batteries, engaging in the recycling process to extract valuable elements, and subsequently utilizing these materials in the production of new batteries. This approach serves to decrease the dependence on primary resources and mitigate the generation of excess waste. The objective is to enhance consumer consciousness regarding the ecological ramifications of electric vehicle batteries and to advocate for the implementation of eco-labeling mechanisms that emphasize items adhering to circular economy principles. This approach aims to foster responsible patterns of consumption and disposal (Richa et al. 2017, EY 2022).

Governments possess the ability to encourage the adoption of circular economy practices through policy instruments, such as extended producer responsibility, which imposes a legal obligation on producers to assume

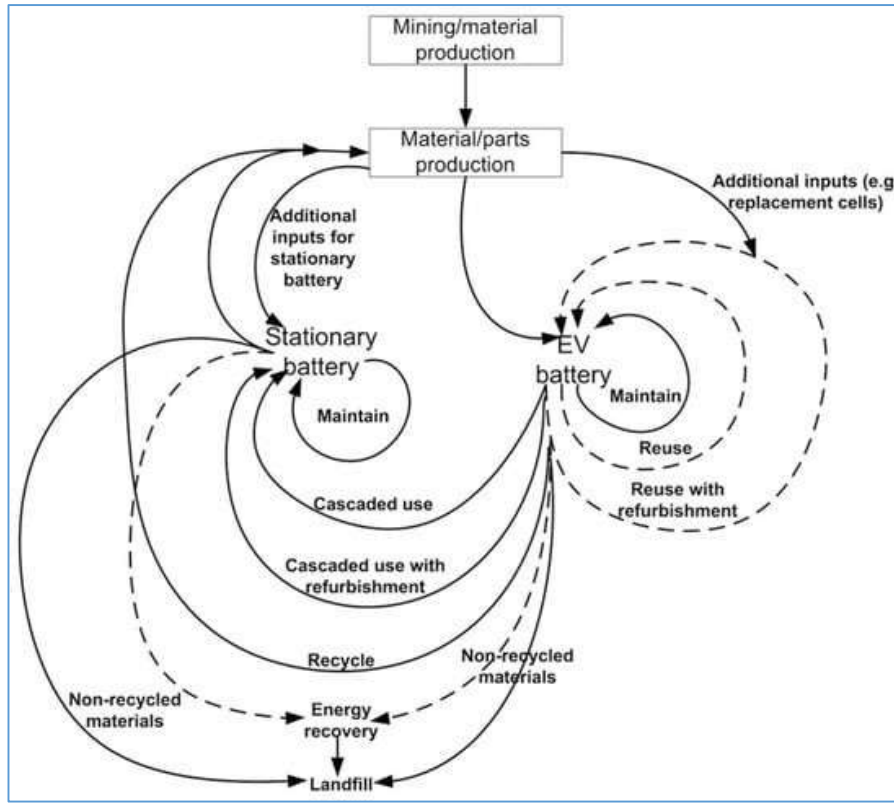

Fig. 1: Recycling opportunities on EV battery (Wang et al. 2014, Richa et al. 2017).

responsibility for the proper management of their products at the end of their life cycle. The implementation of circular economy solutions has the potential to effectively mitigate the environmental impact associated with electric car batteries while simultaneously optimizing their economic and environmental worth for their entire lifespan (Li et al. 2019).

A waste management hierarchy (Fig. 1), influenced by the principles of a circular economy, was put out for the treatment of end-of-life lithium-ion batteries derived from electric vehicles. The application of life cycle eco-efficiency criteria was utilized to assess the potential trade-offs, both environmental and economic, that could arise from the management of end-of-life electric vehicle battery packs in the community, in accordance with the circular economy hierarchy. Nevertheless, the advantages of retired electric vehicle lithium-ion batteries are significantly amplified when they are repurposed for stationary energy storage, resulting in the elimination of less efficient lead-acid batteries. The utilization of reuse and cascaded usage has the potential to generate cost savings for electric vehicle owners and the utility sector. However, it is important to note that the exact extent of the economic advantages in the future remains unpredictable due to the lack of knowledge regarding the future pricing of battery systems. Despite the numerous advantages, existing waste policies lack emphasis on circular economy techniques such as battery reuse and cascaded usage. While loop-closing battery recycling offers significant benefits in terms of metal recovery, its profitability may be compromised in the presence of persistently high recycling costs. Considerable focus has been directed towards the implementation of landfill disposal bans for batteries. However, empirical findings suggest that a more comprehensive approach involving direct and cascaded reuse, followed by recycling, can yield significantly higher reductions in eco-toxicity loads compared to relying just on landfill bans. The results emphasize the significance of conducting life cycle and eco-efficiency analyses to determine the specific stage within a circular economy hierarchy that yields the most environmental advantages (Wang et al. 2014, Richa et al. 2017).

The value chain commences with the stages of design and manufacture (Fig. 2). Following the initial usage cycle, an assessment is conducted to evaluate the state of the battery's health and capacity. This evaluation aims to determine whether the battery is suitable for repurposing in an alternative vehicle or stationary application or if it

necessitates immediate recycling. If the potential for a subsequent existence exists, the battery undergoes a process of restoration. The techniques involved in refurbishment can vary depending on the specific battery and its intended purpose (Olsson et al. 2018).

ANALYZING PROSPECTS FOR ELECTRIC VEHICLE BATTERY

The assessment of opportunities in battery recycling mostly revolves around the anticipated worth of $300 billion for India's electric vehicle industry by the year 2030. The lithium-ion battery (LIB) has emerged as the most optimal choice among many battery types for numerous applications. The prevailing types of lithium-ion batteries (LIBs) employed in electric vehicles are lithium, nickel, manganese, and cobalt (LNMC) batteries, as well as lithium iron phosphate (LFP) batteries. The durability of these batteries extends up to a span of eight to ten years. Nevertheless, it is not recommended to use them in electric vehicles (EVs) once their energy-generating capability diminishes below 80%. Alternatively, these batteries can still be utilized in stationary applications, such as the storage of renewable energy and other purposes that do not necessitate their mobility (Dobó et al. 2023).

The preliminary suggestions on battery waste management have been published by the Indian government to mitigate the improper handling and disposal of lithium-ion batteries (LIBs). Based on the stipulations outlined in these rules, producers must assume responsibility for the complete life cycle of a utilized battery, encompassing the stages of collection, recycling, and ultimate disposal. The government provides financial incentives to encourage investments in LIB recycling (Turaga et al. 2019). A limited number of companies have initiated experimental programs for the recycling of lithium-ion batteries. By employing pyro and hydrometallurgical methods, a recovery rate of 90% was achieved for the initial material. The materials that have been successfully recovered exhibit a high level of purity, reaching up to 99%. This exceptional purity renders them very suitable for utilization in the production of new batteries (Deshwal et al. 2022). The cost of recycling Lithium-Ion Batteries is considerable, and currently, there is limited policy support for this practice. The existing technological infrastructure of the government is insufficient for the effective collection, storage, and recycling of lithium-ion battery waste. Legislation and regulatory measures for the handling, recycling, and proper disposal of decommissioned lithium-ion batteries have yet to be implemented. To achieve cost-effective large-scale deployment in renewable and other stationary applications, it is imperative to establish standards for the second-use utilization of outmoded electric vehicle batteries (Skinner et al. 2010, Abubakar et al. 2022).

The implementation of a circular economy within the domestic electric vehicle (EV) and storage industries is expected to yield significant advantages. In alignment with the government's objective of Aatma Nirbhar Bharat, the utilization of recycled materials derived from outdated

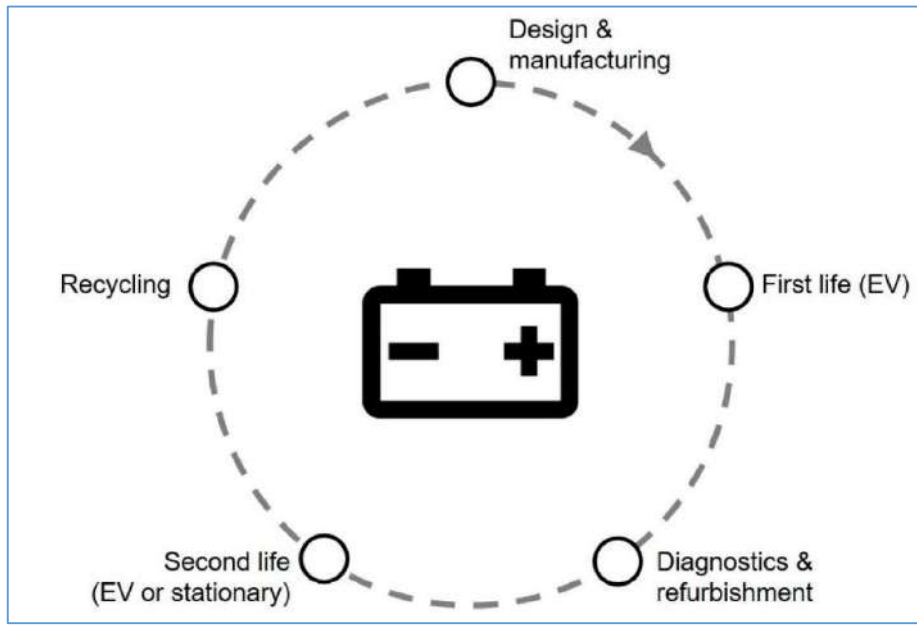

Fig. 2: EV Battery Value Chain (Olsson et al. 2018).

batteries would enable India to achieve a production capacity of 60 GWh LIB cells by the year 2030. This would result in a reduced reliance on imports and create new economic opportunities for makers of lithium-ion cells. According to a recent study, the adoption of recycled materials has the potential to significantly reduce carbon dioxide (CO2) emissions, with a potential reduction of up to 90 percent. (Pražanová et al. 2022, EY 2022).

EV Battery Recycling Opportunity

Unfortunately, there isn't a recycling infrastructure in India that can handle large volumes of waste. Used batteries are just dumped in landfills without any sort of processing. The elements lithium (which may react spontaneously with moisture to produce explosions), nickel, and cobalt are all present in LIBs.

A type of rechargeable battery used in electric cars, lithium-ion batteries store and release energy as needed. The batteries used in anything from motorcycles to semis and city buses are essentially interchangeable. Yet, their make-up and size change from vehicle to vehicle according to the quantity of electricity needed to operate them. The proper handling of dead batteries in electric vehicles is not well-known or practiced. New data, however, shows that recycling is the smartest and most practical choice in this scenario (Melchor-Martínez et al. 2021). As the electric vehicle industry is expected to develop rapidly (about 35% by 2026), so too will the need for batteries. A mandated recycling method for the safe disposal and recycling of EV batteries is required by certain current laws (E-waste (Management and Handling) Rules, 2011, E-waste (Management and Handling) Regulations, 2016, and E-waste (Management) Amendment Rules, 2018) (Melchor-Martínez et al. 2021, Wagner-Wenz et al. 2023).

Batteries can perform their function thanks to their capacity to gradually transform chemical energy into electrical energy. The chemical energy is held within the battery, and the battery will not start producing electrical power until it is first connected to an electronic device. The chemicals that are necessary for this process, including lead, lithium, mercury, and cadmium, can, unfortunately, be dangerous due to their poisonous, corrosive, or other harmful properties (Li et al. 2019, Wang et al. 2023). Due to the stringent rules that are placed on the production of batteries, it is highly unlikely that the normal usage of batteries would injure us because the potentially harmful chemicals are safely contained within the battery itself. Yet, once their chemical energy has been expended and they are no longer functional, batteries can present challenges when it comes time to dispose of them. The majority of the time, people throw away their used batteries in their regular garbage, which increases the likelihood that the batteries will end up in a landfill. These batteries will start to degrade over time, and the components that make them up are known to have a potentially harmful effect on the surrounding environment over a period of time (Lv et al. 2018).

Disposal of Batteries and the Health of Humans

Batteries can have a detrimental effect on the surrounding environment, which in turn can affect human health. It should go without saying that the harsh chemicals contained within batteries are harmful to human beings; yet, in today's world, it is quite unusual that we will come into direct touch with these chemicals from a battery itself unless the battery has been destroyed. Yet, when batteries that have been thrown away do damage to the environment, we run the danger of accidentally coming into touch with the chemicals that are released into the environment. (Noudeng et al. 2022). It is recognized that certain of the chemicals and hazardous metals found in batteries are carcinogens, which simply means that they have the potential to cause cancer in humans. Yet, it can be challenging to assess the full impact that improper disposal of batteries has on public health. Batteries pose a potential threat to human health if they are disposed of in landfills regularly since doing so raises the risk of cancer and other major health problems (Borthakur 2015, Noudeng et al. 2022, Dobó et al. 2023).

When a battery has reached the end of its useful life, it could appear to be a simple matter to dispose of it in the garbage at home. On the other hand, this indicates that the battery will very definitely be dumped in a landfill, where it will pose a threat to both the health of people and the environment. Instead, you should make sure that outdated batteries are recycled appropriately. If you are unclear about where to take your used batteries, it is best to check with your local government. Every town has various processes for dealing with the disposal of electronic waste, so if you are unsure of where to take them, it is best to check with your local government (Li et al. 2019, Selvi & Ritha 2022). In certain cases, electronic businesses will collect used batteries to send them for safe recycling; this means that all you have to do to recycle your old batteries is drop them off at the store in question. In a similar vein, users may frequently submit their old mobile phones to the maker or carrier of their new cell phone so that the company can recycle the devices. Batteries for automobiles are sometimes taken in by auto dealerships as well as repair businesses (Ordoñez et al. 2016, Pražanová, Knap & D.I. Stroe 2022, Wang et al. 2023).

ENVIRONMENTAL IMPACT OF EV BATTERY

The transportation of batteries results in supplementary

Table 1: Comparing the emissions of EVs and ICE vehicles (Ricardo Energy & Environment 2020).

Vehicle	Estimated lifecycle Emissions (tonnes CO_2)	Proportion of Emission in Productions	Estimated Emissions in production (tonnes CO_2)
Petrol Vehicle	24	23%	5.6
Hybrid Vehicle	21	31%	6.5
Battery Vehicle	19	46%	6.8

environmental expenses, hence amplifying their carbon footprint in comparison to that of internal combustion engine (ICE) vehicles. According to a study conducted in 2021 that compared the emissions of electric vehicles (EVs) and internal combustion engine (ICE) vehicles, it was determined that the production process accounts for 46% of carbon emissions associated with EVs. In contrast, it accounts for a comparatively lower 26% of emissions in ICE vehicles. Approximately 3,628.74 kilograms of carbon dioxide are emitted throughout the production process of a solitary electric vehicle, and it would necessitate eight years of driving before the yearly reduction in emissions would be sufficient to offset the original emissions. The data presented in Table 1 was obtained from the Lifecycle Analysis of UK Road Vehicles conducted by Ricardo (Ricardo Energy & Environment 2020).

The release of chemicals from batteries into aquatic habitats is related to the potential for the release of harmful substances. The improper or negligent treatment of used batteries can result in the discharge of corrosive liquids and dissolved metals that are harmful to both plants and animals. This can happen when the batteries are broken down into their parts. Batteries should not be disposed of in landfills in an improper manner since this might lead to the discharge of harmful compounds into the groundwater and into the environment (Abubakar et al. 2022, Shakil et al. 2022, Dodd et al. 2023).

Pollutants released into the atmosphere undergo photochemical reactions that result in the production of hazardous compounds, such as ozone, along with other dangerous gases and particle substances. Thermal inversions, which are common in major cities, can lead to a hazardous accumulation of photochemical smog, which is well-documented as a leading contributor to the mortality rate of humans. The concentration of acidic chemicals in atmospheric particles is what causes the acidification of the air. These particles, which are left behind by rain, affect the soil as well as the organisms that live there. As a result of their lower contribution to overall air pollution, rechargeable batteries have a smaller impact on these environmental consequences than their disposable counterparts (Lv et al. 2018, Noudeng et al. 2022). The manufacture, transportation, and distribution of batteries all require the use of natural resources, which contributes to the quickening of the rate at which natural resources are being depleted. Because fewer rechargeable batteries are required to produce the same amount of energy as disposable batteries, the usage of rechargeable batteries results in a reduction in the amount of non-renewable natural resources consumed (Roy et al. 2021).

The influence of growing levels of greenhouse gases is to blame for the rise in the global average surface temperature. The production of batteries, as well as their transportation, both result in the release of exhaust and other pollutants into the atmosphere, which contributes to the phenomenon known as the greenhouse effect. Rechargeable batteries are better for the environment than single-use batteries since they may be used several times before being thrown away. This is because the production of rechargeable batteries and the transportation of these batteries results in less emissions of greenhouse gases. (Noudeng et al. 2022; Wagner-Wenz et al. 2023)

Reduce Impact on the Environment

If you want to have as little of a negative influence as possible on the surrounding environment, you should think about powering your electronic equipment using rechargeable batteries. When compared with the usage of many single-use batteries, the generation of the same quantity of energy using a rechargeable battery results in the consumption of a significantly lower amount of non-renewable natural resources. In addition, the long-term cost of using rechargeable batteries is typically lower than the cost of using standard batteries. Rechargeable batteries may have a higher up-front cost, but in the long run, they can save you money since you won't need to buy as many single-use batteries in the future. This will allow you to get a faster return on your investment (Ordoñez et al. 2016, Li et al. 2019).

When rechargeable batteries are utilized, there will be a reduction in the amount of single-use batteries that end up at recycling centers, which is beneficial because recycling facilities frequently make use of natural resources. When it comes to trash, it is important to keep in mind the "three Rs": reducing, reusing, and recycling. Recycling is essential to the process of shielding the environment from the negative effects of hazardous trash. Still, we can do even more to safeguard it if we cut back on the quantity of rubbish that

we generate in the first place. By reusing the same battery over and over again, you may dramatically cut down on the amount of trash you produce when you use rechargeable batteries (Roy et al. 2021, Islam & Iyer-Raniga 2022, Wagner-Wenz et al. 2023).

CONCLUSION

The development of electric vehicle infrastructure in India is now in its nascent stage, although it is gradually gaining traction. India presently accounts for approximately 7% of the global carbon emissions, equivalent to over 2.5 billion metric tons. Vehicles utilizing internal combustion engines contribute about 40% of India's total pollution. In light of these circumstances, it is imperative to promptly launch a significant effort to promote the use of electric vehicles as a means to mitigate the escalating levels of pollution. The imperative to mitigate the impacts of climate change has necessitated a global shift towards a low-carbon economy, hence prompting a transformation in international climate policy. Around 20 states in India have formulated a comprehensive electric vehicle policy at the state level, aiming to expedite the nation's complete transition from internal combustion engine vehicles to EVs. Nevertheless, the absence of adequate rules for the appropriate storage and administration of waste streams results in the accumulation of refuse in public areas, potentially leading to the leakage of hazardous chemicals from landfills.

Furthermore, the utilization of novel materials, such as ionic liquids for electrolytes and nanostructures for cathodes, has the potential to augment the energy efficiency and longevity of batteries. The limited understanding of the actual environmental impact of emerging battery chemistries may provide further obstacles to recycling and containment endeavors. The escalation of fuel prices and the growing emphasis on environmentally sustainable energy sources are two significant catalysts propelling the demand for alternative fuels. Climate change is widely acknowledged by major nations as a significant issue, prompting active efforts to identify timely solutions. This recognition further reinforces the impetus for transitioning to electric vehicles (EVs) while ensuring the safe recycling of batteries.

REFERENCES

Abubakar, A., Zangina, A.S., Maigari, A.I., Badamasi, M.M., Ishak, M.Y., Abdullahi, A.S. and Haruna, J.A. 2022. Pollution of the heavy metal threat posed by e-waste burning and its assessment of human health risk. Environ. Sci. Pollut. Res., 29(40): 61065-61079.

Ahuja, J., Dawson, L. and Lee, R. 2020. A circular economy for electric vehicle batteries: driving the change. J. Prop. Plan. Environ. Law, 12(3): 235-250.

Ali, H., Khan, H.A. and Pecht, M.G. 2021. Circular economy of Li batteries: Technologies and trends. J. Energy Stor., 40: 102690.

Borthakur, A. 2015. Generation and Management of Electronic Waste in India: An Assessment from Stakeholders' Perspective. J. Dev. Soc., 31(2): 220-248.

Chandramauli, A. 2020. Comparison study of electronic waste management in India & Switzerland. Int. J. Adv. Eng. Res. Dev., 4(10): 485-492.

Deshwal, D., Sangwan, P. and Dahiya, N. 2022. Economic Analysis of Lithium Ion Battery Recycling in India. Wirel. Pers. Commun., 124(4): 3263-3286.

Dobó, Z., Dinh, T. and Kulcsár, T. 2023. A review on recycling of spent lithium-ion batteries. Energy Rep., 9: 6362-6395.

Dodd, M., Amponsah, L.O., Grundy, S. and Darko, G. 2023. Human health risk associated with metal exposure at Agbogbloshie e-waste site and the surrounding neighborhood in Accra, Ghana. Environ. Geochem. Health, 45(7): 4515-4531.

EY 2022. Electrifying Indian Mobility. https://assets.ey.com/content/dam/ey-sites/ey-com/en_in/topics/automotive-and-transportation/2022/ey-electrifying-indian-mobility-report.pdf

Harper, G.D.J., Kendrick, E., Anderson, P.A., Mrozik, W., Christensen, P., Lambert, S., Greenwood, D., Das, P.K., Ahmeid, M. and Milojevic, Z. 2023. Roadmap for a sustainable circular economy in lithium-ion and future battery technologies. J. Phys. Energy, 5(2): 21501.

Islam, M.T. and Iyer-Raniga, U. 2022. Lithium-Ion Battery Recycling in the Circular Economy: A Review. Recycling, 7(3): 116-126.

Joseph, K. 2007. Electronic Waste Management in India: Issues and Strategies. Center for Environmental Studies, Anna University, Chennai.

Kang, D.H.P., Chen, M. and Ogunseitan, O.A. 2013. Potential environmental and human health impacts of rechargeable lithium batteries in electronic waste. Environ. Sci. Technol., 47(10): 5495-5503.

Koller, J., Oechsle, O. and Hellmich, C. 2021. A battery circular economy ? Definition, significance, and end-of-life strategies. World Sci., 16: 321-336.

Leung, A.O.W. 2019. Environmental Contamination and Health Effects Due to E-waste Recycling. Elseiver, The Netherlands.

Li, H., Dai, J., Wang, A., Zhao, S., Ye, H. and Zhang, J. 2019. Recycling and Treatment of Waste Batteries. IOP Conf. Ser. Mater. Sci. Eng., 612(5): 1101-1121.

Lv, W., Wang, Z., Cao, H., Sun, Y., Zhang, Y. and Sun, Z. 2018. A critical review and analysis of the recycling of spent lithium-ion batteries. ACS Sustain. Chem. Eng., 6(2): 1504-1521.

Melchor-Martínez, E.M., Macias-Garbett, R., Malacara-Becerra, A., Iqbal, H.M.N., Sosa-Hernández, J.E. and Parra-Saldívar, R. 2021. Environmental impact of emerging contaminants from battery waste: A mini-review. Case Stud. Chem. Environ. Eng., 3: 14-22.

Noudeng, V., Quan, N.V. and Xuan, T.D. 2022. A future perspective on waste management of lithium-ion batteries for electric vehicles in Lao PDR: Current status and challenges. Int. J. Environ. Res. Public Health, 19(23): 1-22.

Olsson, L., Fallahi, S., Schnurr, M., Diener, D. and Van Loon, P. 2018. Circular business models for extended EV battery life. Batteries, 4(4): 516-526.

Ordoñez, J., Gago, E.J. and Girard, A. 2016. Processes and technologies for the recycling and recovery of spent lithium-ion batteries. Renew. Sustain. Energy Rev., 60: 195-205.

Pražanová, A., Knap, V. and Stroe, D.I. 2022. Literature review, recycling of lithium-ion batteries from electric vehicles. Energies, 15(3): 1-29.

Ricardo Energy & Environment. 2020. Determining the environmental impacts of conventional and alternatively fuelled vehicles through LCA. Retrieved from https://op.europa.eu/sv/publication-detail/-/publication/1f494180-bc0e-11ea-811c-01aa75ed71a1

Richa, K., Babbitt, C.W. and Gaustad, G. 2017. Eco-Efficiency Analysis of a Lithium-Ion Battery Waste Hierarchy Inspired by Circular Economy. J Ind Ecol., 21(3): 715-730.

Roy, J.J., Cao, B. and Madhavi, S. 2021. A review on the recycling of spent lithium-ion batteries (LIBs) by the bioleaching approach. Chemosphere, 282: 130944.

Selvi, P. and Ritha, W. 2022. A green inventory model for the battery. Waste Manag., 6(3): 7949-7955.

Shakil, S., Nawaz, K. and Sadef, Y. 2022. Evaluation and environmental risk assessment of heavy metals in the soil released from e-waste management activities in Lahore, Pakistan. Environ. Monit. Assess., 195(1): 89.

Skinner, A., Dinter, Y., Lloyd, A. and Strothmann, P. 2010. The Challenges of E-Waste Management in India: Can India draw lessons from the EU and the USA? Asien, 117: 7-26.

Turaga, R.M.R., Bhaskar, K., Sinha, S., Hinchliffe, D., Hemkhaus, M., Arora, R., Chatterjee, S., Khetriwal, D.S., Radulovic, V., Singhal, P. and Sharma, H. 2019. E-Waste management in India: Issues and strategies. Vikalpa, 44(3): 127-162.

Velázquez-Martínez, O., Valio, J., Santasalo-Aarnio, A., Reuter, M. and Serna-Guerrero, R. 2019. A critical review of lithium-ion battery recycling processes from a circular economy perspective. Batteries, 5(4): 5-7.

Wagner-Wenz, R., van Zuilichem, A.J., Göllner-Völker, L., Berberich, K., Weidenkaff, A. and Schebek, L. 2023. Recycling Routes of Lithium-Ion Batteries: A Critical Review of the Development Status, the Process Performance, and Life-Cycle Environmental Impacts. Springer International Publishing, Singapore.

Wang, X., Gaustad, G., Babbitt, C.W. and Richa, K. 2014. Economies of scale for future lithium-ion battery recycling infrastructure. Resour. Conserv. Recycl., 83: 53-62.

Wang, Y., Zhai, Q. and Yuan, C. 2023. Analysis of direct recycling methods for retired lithium-ion batteries from electric vehicles. Procedia CIRP, 116: 702-707.

ORCID DETAILS OF THE AUTHORS

S.Padmanabhan: https://orcid.org/0000-0003-4813-975X

Nature Environment and Pollution Technology
An International Quarterly Scientific Journal

p-ISSN: 0972-6268
(Print copies up to 2016)
e-ISSN: 2395-3454

Vol. 23 | No. 1 | pp. 193-201 | 2024

Review Research Paper

https://doi.org/10.46488/NEPT.2024.v23i01.015

Open Access Journal

An Overview of Anaerobic Digestion of Cow Dung

V. M. Nekhubvi*†

*Department of Science Foundation, Faculty of Science, Engineering and Agriculture, University of Venda, South Africa

†corresponding author: V. M. Nekhubvi; vhutshilo.nekhubvi@univen.ac.za

Nat. Env. & Poll. Tech.
Website: www.neptjournal.com

Received: 16-04-2023
Revised: 06-06-2023
Accepted: 07-06-2023

Key Words:
Mono-substrate digestion
Household size digesters
Single-stage digestion systems
Biogas digester start-up
Feedstock

ABSTRACT

In the past decade, governments and development agencies have contributed significantly to society through anaerobic digestion technology (ADT). Anaerobic digestion technology (ADT) has become an important tool in the fight against global poverty and environmental issues, leading to positive change in communities around the world. The technology works as a wet or dry process, depending on its classification. The process is complex and yields multiple benefits, such as creating a natural fertilizer that can be used to help crops grow, as well as generating renewable energy sources. It is common knowledge that many household-sized digesters installed in different areas are one-stage digesters. One-stage digesters do not require a separate pre-treatment stage before the digestion process. This makes them simpler and more cost-effective to install and operate than traditional two-stage digesters. Thus, some drawbacks are associated with these systems since they feed on just one type of feedstock. Many researchers fail to adequately address interactions critical to ADT's operation, including interactions among growth factors and operating parameters. In a single-stage and one-substrate digester, researchers commonly neglect to study the digester feeding and operational conditions. Anaerobic digestion was the subject of this review, covering research conducted between 2001 and 2022. The study identified a significant drawback associated with mono-digestion and single-stage digestion. The findings illustrate that mono-substrate and single-stage digestion are worthwhile approaches, even though they have their challenges. However, adding a further digestion stage can significantly improve biogas production.

INTRODUCTION

Anaerobic digestion technology (ADT) for biogas production provides solutions to the increasing problems associated with energy production (Sawyerr et al. 2019). As global energy consumption increases due to population growth, more biogas projects are urgently needed (Abanades et al. 2021). Anaerobic digestion technology (ADT) has received financial assistance from development donors and government agencies. It is mainly used in rural households because feedstock is readily available (Roubík et al. 2018, Pandey et al. 2021, Lohani et al. 2021). By reducing dependence on fossil fuels and creating jobs, biogas energy can be an essential part of the future of renewable energy technologies (Begum & Nazri 2013). In the long term, greenhouse gas (GHG) emissions will be reduced (Anukam et al. 2019), thus reducing global warming (Sadeleer et al. 2020). Roubík et al. (2018) found that households without biogas emit more greenhouse gases than households with biogas. Several applications for raw biogas include heating, cooking, and lighting (Black et al. 2021). In Contrast to raw biogas, it is possible to convert it into biomethane that can be used for electricity generation or transportation (Gaby et al. 2017, Abanades et al. 2021). A volume of purified biogas has an energy equivalent to 1.1 liters of gasoline or 0.97 liters of natural gas, according to (Rajendran et al. 2012). Anaerobic digestion (AD) plants requiring small-scale conversion of biogas require a higher power consumption than large-scale plants (0.25-0.5 kWh per $1m^3$ of biogas) (Li et al. 2017). Depending on the methane (CH_4) content, which varies between 50 and 65% (Li et al. 2017), the value of raw biogas' calorific value ranges between 5.5 - 7.5 $kWh.m^{-3}$ (Okonkwo et al. 2018). Khan et al. (2018) reported a biogas density of 1.15 $kg.m^{-3}$ and a calorific value of 11.06 $kWh.m^{-3}$. Methane content is determined by the material used to feed the digester. A recent study suggests that all agricultural waste can be converted into biogas (Łochyńska & Frankowski 2018). An examination of the CH_4 yield of the feedstock is crucial for assessing the economic viability of a biogas investment (Kozłowski et al. 2018). In the study by Anderman et al. (2015), participants showed that they spent significantly less time

cooking and collecting firewood in households with biogas. Biogas production is highly influenced by two key aspects of AD: feeding and operating conditions (Ignatowicz et al. 2021, Nsair et al. 2020). Therefore, this review focuses on the factors related to feeding the digester, with pH and temperature regulation. Furthermore, the influence of these components on biogas production's efficiency and productivity is evaluated to gain a comprehensive understanding of the subject.

DIGESTER FEEDING

To feed the digester, the substrate is fed into the biogas digester immediately after mixing it with water. This helps to ensure that the substrate is evenly distributed and that the bacteria in the digester can access it quickly and efficiently to produce biogas. It has been found that the feeding of biogas digesters varies depending on the availability of substrates. The main substrates for biogas digesters are organic matter such as food waste, agricultural waste, and animal manure. The biogas digester can be fed more frequently if these substrates are abundant. If not, then the biogas digester must be fed less often. Wang et al. (2021) have shown three types of feeding mixtures (singular, binary, and ternary). A singular process uses one feedstock, a binary process uses two, and a ternary process uses three.

In most cases, mono and co-mixtures of feedstocks are the most common, with singular feedstocks falling under mono and binary or ternary feedstocks falling under co-mixture. In addition to ternary mixtures of feedstocks, Kim et al. (2019) have also demonstrated applying such a method using agricultural and food wastes and dairy manure from a small anaerobic digester. Castano et al. (2014) used a 1:1 ratio waste mixture to feed the digester. During the experiment, the digester was fed three times per week. The mixture was effective, as biogas production increased significantly with the addition of the waste mixture. Obileke et al. (2020) used cow dung with water at a 1:1 (waste: water) ratio before digestion. Ramaswamy & Vemareddy (2015) fed a 1 m^3 biogas digester with a mixture of cow dung and a water ratio of 1:10. When it comes to the feeding of the digester. It may be fed more than once per day (Achu Nges et al. 2012). This will help ensure that the digester runs at optimal efficiency and performance. In essence, it is the inoculum-to-substrate ratio (I/S) that is usually fed more than once in anaerobic digestion as the substrate alone may present some difficulties, such as changing the properties of the substrate (Parra-Orobio et al. 2016), in addition to differences in the amounts of three main organic components: carbohydrates, lipids, and proteins (Khadka et al. 2022). Ofosu & Aklaku (2010) considered biogas production from lipids attractive because they are reduced organic materials with high methane yields. It has been suggested by a recent research study published by Rivas Solano et al. (2016) that the use of a single substrate (e.g., livestock manure) is not commendable because some substrates have a low methane yield compared to others (Song et al. 2021). Therefore, it is important to consider the relative methane yield of each substrate when selecting the optimal mix for anaerobic digestion. Biogas production is inadequate with the digestion of cow manure alone (Elsayed et al. 2022). Again, Mata-Alvarez et al. (2014) highlight some drawbacks associated with the anaerobic digestion of single substrates. It has been established that using manure only results in low performance (Mao et al. 2015). Specifically, they noted that nitrogen imbalance and ammonia inhibition were major causes since livestock manure contains a high nitrogen content, such as goat manure (1.01%), chicken manure (1.03%), and dairy manure (0.35%), and swine manure (0.24%). When selecting feedstock, factors such as availability, cost, biogas yields, and environmental benefits should be considered (Bhatnagar et al. 2022).

Furthermore, feedstock selection should be tailored to the specific requirements of the biogas production process for optimal results. In a technical study on household digesters, Tumutegyereize et al. (2017) established a baseline for future research on factors influencing their adoption, use, and management decisions of biogas technology. Cow dung dominated the feedstock list. However, if the mixing ratios are used appropriately, the risk of the anaerobic digestion system failing is eliminated because if the feed material is too diluted, it will be washed out, and then system failure will occur (Kim et al. 2019). Cow dung and water composition must be in the right proportion.

Consequently, it is essential to ensure that all components are correctly balanced to optimize biogas production. This will eliminate the risk of system failure and establish a successful biogas production plant. Berhe et al. (2017) showed that the most effective promotional tool is an efficient biogas digester, while satisfied users are the best advocates for biogas technology.

ANAEROBIC DIGESTION OPERATION

Due to its simplicity of operation and the diversity of materials used as feedstock, anaerobic digestion (AD) is a widely researched technology (Bhatnagar et al. 2022). The organic materials are broken down in a digester or lagoon to produce biogas and fertilizer through wet and dry processes. Elsharkawy et al. (2019) categorized AD as dry and wet. Dry AD processes waste with a total solid content greater than 20%, and wet AD processes waste with less than 10% TS content. Uddin et al. (2021) indicated that the

solid content of a dry AD system is between 20 and 40%. The study by Kassongo et al. (2022) said that AD reactors are categorized as wet (≤ 10% TS), semi-dry (10-20% TS), and dry (≥20% TS) systems. The anaerobic digestion process applies immediately after the mixture substrate has been poured into the digester. The core of AD operation is feedstock disintegration, digestion, and operational conditions. According to their feed arrangement, anaerobic digestion operations are categorized into batch, continuous, and combined digestion (He et al. 2022). A batch mode can be used for anaerobic degradation, inoculum activity, and inhibition (Raposo et al. 2011). Achu Nges et al. (2012) showed that it is possible to predict full-scale methane yield using a batch mode approach. In a batch mode, complex organic matter is fed once in the digester (Uddin et al. 2021). Continuous mode operation is when the digester feeds more than once a day. Anaerobic digesters can be configured as single-stage, two-stage, or multi-stage reactors. The steps of hydrolysis/acidogenesis and acetogenesis/methanogenesis occur in either the same or separated digesters (Rabii et al. 2019).

Feedstock Disintegration

It has been well-documented that different bacteria respond to diverse environmental conditions in an assembly-line manner, involving four biochemical steps: hydrolysis, acidogenesis, acetogenesis, and methanogenesis (Filer et al. 2019). Interestingly, each of the above biochemical sequential steps is executed by different microbe species with various characteristics, growth rates, and substrate affinities (Duan et al. 2017).

Hydrolysis

Hydrolysis transforms complex carbohydrates, fats, and proteins into soluble monomers and dimers, including sugars (glucose, sucrose, and fructose), fatty acids, and amino acids (Rajendran et al. 2012). Hydrolysis is often considered a simple first-order process due to the vast variations in substrate composition and is not applicable in all situations (Mani & Sundaram 2016). This is because some compounds are resistant to hydrolysis or may undergo other reactions that are more favorable under certain conditions. For example, hydrocarbons (compounds consisting of hydrogen and carbon atoms) are generally not susceptible to hydrolysis because they do not contain any functional groups that can be readily hydrolyzed. The hydrolysis of particulate matter has been identified as the rate-limiting step in AD (Mani & Sundaram 2016) when the particulate matter cannot degrade readily or in systems with high loading rates. During the hydrolysis process, it is essential to maintain uniform mixing and temperature within the digester system. The extracellular hydrolytic enzymes produced by the bacteria can have intimate contact with complex organics without limiting the overall stabilization reaction (Mani & Sundaram 2016). The rate of the hydrolysis process is determined by the particle size, along with the pH value (Ziemiński & Frąc 2012). This negative relationship between solids' size and the rate of the hydrolysis process can, therefore, affect the overall performance of the entire process. It is important to note that the adverse effects of large solids are minimized by conducting expensive pre-treatments to disintegrate and dissolve the substrates before AD. Approximately 20 to 40% of the total process costs are attributed to pre-treatments to improve hydrolysis (Menzel et al. 2020). Even though some organic substrates are particulate, some tend to dissolve quickly when immersed in water (Panico et al. 2014). Hydrolytic microorganisms are favored to grow in slightly acidic conditions (Menzel et al. 2020). Myint et al. (2007) developed a mathematical model for the hydrolysis and acidogenesis reactions of anaerobic digestion of cattle manure. However, due to its poor statistical significance, they did not account for pH's influence on the hydrolysis rate from the linear regression. The process of hydrolysis can be viewed from a chemical perspective (Anukam et al. 2019);

$$(C_6H_{10}O_5)n + n\,H_2O \rightarrow n\,C_6H_{12}O_6 + nH_2 \quad \ldots(1)$$

Where $C_6H_{10}O_5$ stands for cellulose via the addition of water (H_2O) to form glucose ($C_6H_{12}O_6$) as the primary product and give off hydrogen (H_2). A first-order kinetic model can accurately predict hydrolysis involving concentrated degradable organic materials (Mani & Sundaram 2016);

$$\frac{dS}{dt} = -k_{hyd}s \quad \ldots(2)$$

where S is the volatile solids (VS) concentration, k_{hyd} is the first-order coefficient, and t is time in days. Batch experiment data can be fitted to a first-order equation to find hydrolysis rate coefficients (Moestedt et al. 2015). Eqn (2) shows that the observed conversion rate of hydrolysis is affected by the amount of solid substrate in the reaction chamber (Guo et al. 2021). Integrating Equation (2) yields the following result.

$$InS = -k_{hyd}t + b \quad \ldots(3)$$

This is where b is the constant of integration. (ln S) can be plotted against t to find the slope ($-k_{hyd}$) and intercept b. The hydrolysis rate coefficients increase with a rise in temperature, which translates to (Luo et al. 2012);

$$Ink = \frac{E_a}{RT} + InA \quad \ldots(4)$$

A stands for the pre-exponential factor, E_a ($Jmol^{-1}$) is the energy of activation of a reaction, $T(K)$ is the absolute temperature, and R is the gas constant($J{\cdot}K^{-1}{\cdot}mol^{-1}$). The

slope of the line predicted by the Arrhenius equation can be used to calculate the activation energy. Kothari et al. (2018) showed that the following expression could be used to find the activation parameter enthalpy;

$$\Delta H = Ea - RT \quad \ldots(5)$$

Where $\Delta H(Jmol^{-1})$ is the enthalpy of a body at a specific temperature, $T(K)$ and R represent the gas constant ($J{\cdot}K^{-1}{\cdot}mol^{-1}$), respectively. Based on what has been found so far, hydrolysis is a bottleneck stage that requires higher temperatures to accelerate degradation. Hydrolysis requires breaking the glycosidic bonds that link the monomers together. This requires higher temperatures to increase the reaction rate and make it more efficient. In general, AD is run at three temperature levels: psychrophilic (<20°C), mesophilic (20-43°C, and thermophilic (50-60°C (Nie et al. 2021). In unheated digesters, heat is generated by solar radiation in mesophilic or psychrophilic conditions. This heat is then utilized to produce the necessary temperature for anaerobic digestion, with the optimum temperature depending on the type of microorganisms in the digester. Methane yields can be increased with thermophilic digestion temperatures. Rapid hydrolysis, however, can result in the accumulation of ammonia and volatile fatty acids, which can lower pH and methane productivity (Kassongo et al. 2022).

In contrast, Ahring et al. (2001) reported a lower methane yield at 65°C than 55°C. Thermophilic temperatures are widely employed in large-scale digesters (Ahring et al. (2001). This is because thermophilic bacteria are more efficient at breaking down organic matter, such as animal and food wastes, into biogas than other types of bacteria. Furthermore, thermophilic temperatures reduce pathogen risk in biogas, making it safe to use. Anaerobic digestion on a large-scale digester is most effectively accomplished by a continuous two-stage configuration consisting of a thermophilic first and a mesophilic second stage.

Cow Dung as Feedstock for Anaerobic Digestion

Due to its availability and as an inexpensive source of organic material rich in methane-producing bacteria, cow dung is the most common feedstock used in household biogas digesters in rural areas. Cow dung is lignocellulosic and has enough nutrients, making it a low-cost input with valuable outputs through the AD process (Zeb et al. 2022). It has carbohydrates, lipids, fats, and proteins (Saady & Massé 2015). So, cow dung consists of 1.6-23.5% cellulose, 1.4-12.8% hemicellulose, and 2.7-13.9% lignin (Zeb et al. 2022). In India, fixed dome biogas digesters are fed only animal manure (Khan & Martin 2016). Akbulut et al. (2021) showed that a family-size biogas digester could produce biogas volumes like 3,816.85 $m^3.a^{-1}$ from only cow manure. The investigation results of the study by Baba and Nasir (2012) showed that cow dung might be one of the feedstocks for efficient biogas production and waste treatment. Fresh cow dung is estimated to have 28% water Sruthy et al. (2017). However, Raja et al. (2021) and Szymajda et al. (2021) showed that fresh cow dung has approximately 80% water. Haryanto et al. (2018) reported an average of 80.12% of water in fresh cow dung. For AD to generate biogas energy, fresh cow dung is mixed with water at a widely used ratio of 1:1 (Baba & Nasir 2012).

Physiochemical Properties of Cow Dung

Cow dung, also known as cow manure, is a mixture of organic and inorganic materials excreted by cows. The physicochemical properties of cow dung can vary depending on several factors, including the age and breed of the cow and its diet. It is estimated that the composition of cow dung consists of 1.8-2.4% N_2, 1.0-1.2% P_2O_5, 0.6-0.8% K, and 50-75% organic humus (Ogur & Irungu 2013). As a feedstock for digesters, cow dung must have a sure consistency, including a total solids (TS) or dry matter (DM) content, volatile solids (VS) or organic solids, moisture, pH, particle size, and chemical oxygen demand (COD) (Wang et al. 2019). Feedstocks with bulk solids are said to adversely affect anaerobic digestion performance (Yi et al. 2014). Low TS content can result in low biogas yield and reduced process efficiency. Thus, optimizing the feedstock's TS content is important for optimal process performance. Generally, a 6-10% TS content is considered optimal for AD performance. However, the optimal TS content may vary depending on the feedstock and AD system. Conducting a series of experiments to determine the optimal TS content for a given feedstock and AD system is recommended. The total solids (TS) can be determined after the feedstock is heated to 105°C for at least an hour and then cooled; the total solids (TS) can be determined. The total solids (TS) contain both organic and inorganic substances. This can be expressed mathematically as follows:

$$TS = \frac{[Weight\ after\ heating\ to\ 105°C]}{\text{Weight before heating}} \times 100 \quad \ldots(6)$$

The researchers in Nsair et al. (2020) mentioned that the size of the dry matter (DM) during wet fermentation plays an essential role. The researchers considered the dry weight value to be less than 15% during wet fermentation. A research study conducted by Triolo et al. (2013) suggested that 10% DM would be best. The dry matter value can estimate how much volatile solid is in the slurry. As an alternative, volatile solids (VS) are found when the dry matter is heated to 550°C. Equation (7) describes the volatile solids (VS).

$$\text{VS (\% of TS)} = \frac{[(Weight\ after\ heating\ to\ 105\ ^0C - Weight\ after\ heating\ to\ 550\ ^0C)]}{\text{Weight before heating}} \times 100 \quad \ldots(7)$$

Volatile solids (VS) are a mixture of biodegradable and nonbiodegradable organic matter in livestock manure (Appuhamy et al. 2018). This mixture can differ in its content and composition between types of livestock and even between different manure sources of the same animal species. Based on Saady and Massé (2015) study, a significant portion of the VS in dairy manure is lignocellulosic biomass. The VS content of cow dung will vary depending on what the cow feeds on. When a laboratory or pilot-scale anaerobic digestion or large-scale anaerobic digestion is performed, the total solids (TS) or volatile solids (VS) are often used to calculate the biogas yield results (Bedoić et al. 2020).

The Stoichiometric C: N Ratio of Cow Dung

The carbon to nitrogen (C: N) ratio of cow dung is an important parameter to consider in biogas production because it affects the rate and efficiency of the anaerobic digestion process. A ratio between 20:1 and 30:1 is ideal for producing flammable gases for any substrate. This range provides the necessary nutrients for the microorganisms involved in the anaerobic digestion process. As a result, when the C: N ratio is outside this range for more efficient biogas production, it will need to be co-digested (or mixed) with another substrate with a moderate C: N ratio (Zainudeen et al. 2021). There is evidence that the best C: N ratio in methane fermentation is 25:1-30:1. However, operating conditions, such as temperature, may affect the depletion of carbon and nitrogen, resulting in inhibitory effects on the process (Wang et al. 2014). According to Table 1, at least 28:1 and 20:1 ratios are suitable for anaerobic digestion. Therefore, adhering to these ratios is imperative for successful anaerobic digestion.

Organic Loading Rate

The OLR measures how much VS the digester can receive and how it influences the biogas production rates (Nsair et al. 2020, Haryanto et al. 2018). The organic loading rate depends on the types of feedstocks used; therefore, it can be considered a VS loading rate (kgVS.m^{-3}.day). The OLR is defined in mathematical terms using Equation (8) (Nsair et al. 2020):

Table 1: A comparison of the stoichiometric ratio (C/N) of cow manure.

C	N	C:N	Reference
43.08	1.53	28.16	(Fajobi et al. 2022)
47.83	3.95	12.10	(Aravani et al. 2022)
45.47 ± 0.03	2.94 ± 0.09	15.45 ± 0.12	(Zhang et al. 2022)
-	1.16 ± 0.08	16.26 ± 0.14	(Rahman et al. 2021)
-	-	20.6	(Dhungana et al. 2022)
-	-	41.43	(Bella & Rao 2022)

$$OLR = \frac{m_{cd} C_{OM}}{V_D} \quad \ldots(8)$$

Where m_{cd} is the amount of mass of feedstock that is consumed in a given period (kg d^{-1}), C_{OM} is the proportion of dry organic matter in the digester (%), and V_D is the digester's volume (m^3). It is noteworthy that (Bedoić et al. 2020) defined OLR using Equation (9).

$$OLR = \frac{Q}{V_D} \quad \ldots(9)$$

The feedstock volumetric flow rate is Q, and V_D is the digester's volume. This equation only focuses on the ratio of fresh feedstock to water without considering total VS, COD, or BOD. Jaeger and Blanchard (2022) reported using a digester with an 8 m^3 and a practical volume of 6 m^3, fed with 3.8 kgVS.m^{-3}day. Some authors refer to OLR as the COD loading rate. Researchers refer to OLR as the COD loading rate because the OLR is directly related to the COD concentration of the wastewater being treated. By knowing the COD concentration and the flow rate of the wastewater, the OLR can be calculated. OLR is important in wastewater treatment because it is a key factor affecting the treatment process's performance and efficiency. High OLRs can cause operational issues such as poor treatment efficiency, reactor instability, and accumulation of toxic compounds, while low OLRs can result in underutilization of the treatment capacity. Therefore, measuring OLR and COD loading rates is important for designing, optimizing, and operating biogas digester systems.

This is especially true for those operating wastewater treatment plants (Khan et al. 2022). As shown by Ünyay et al. (2022), an increase in OLR dramatically reduces methane yield, so finding the optimal OLR for a given digester configuration is imperative. In a study by Obileke et al. (2020), the organic loading rate was recommended to be between 1.6 and 4.8 kgVS.m^{-3} per day. Some authors have misrepresented the OLR units in their works. In their paper, Menacho et al. (2022) represent OLR as a flow rate to refer to the studies of others who expressed OLR in terms of (gVS.day^{-1}) and (gCOD.day^{-1}) as the reference for their validation tests. However, the flow rate is not a suitable unit of measure for expressing OLR. There was another error in the representation of the organic loading rate in the study by Ansar (2022), which mentioned a rate of 3.06 kg.m^{-3}day^{-1} for organic loading. To help prevent confusion, the organic loading rate should be distinguished from the volumetric flow rate(VFR) or just the volumetric loading rate. Volumetric flow rate (VFR) is a measure of the volume of fluid that flows through a system per unit of time. It is typically expressed in units of m^3.h^{-1} or m^3.day^{-1}. It is considered that the organic loading rate (OLR) is the main parameter in

determining the design in the continuous AD (Rocamora et al. 2020).

The Flow Rate of the Substrate

Equation (10) describes the total volumetric flow rate ($m^3.day^{-1}$) to the digester as the ratio of the overall feeding mass rate ($kg.day^{-1}$) and the density of the feedstock ($kg.m^{-3}$) (Wresta et al. 2015).

$$Q = \frac{(m_f + m_w)}{\rho_{f+w}} \quad \ldots(10)$$

Where m_f, m_w, and p_{f+w} stand for the feedstock mass, water mass, and the density of the mixture of water and feedstock, respectively. The volumetric flow rate is the most used by households when feeding the digester.

Hydraulic Retention Time

The hydraulic retention time (HRT) is determined based on the feedstock flow rate (Tan et al. 2021). The HRT is an important parameter in the design and operation of biogas plants as compared to other parameters. It refers to the amount of time that the substrate (organic matter) remains in the digester, which affects the rate of biogas production (Obileke et al. 2021). It is emphasized that HRT is an important parameter that should be reviewed regularly for AD processes to be stable. The given Equation (11) below is one of the formulas that Kesharwani & Bajpai (2021) used to define HRT mathematically.

$$HRT = \frac{V_D}{Q} \quad \ldots(11)$$

Where Q ($m^3.day^{-1}$) is the volumetric flow rate fed to the digester of volume V_D (m^3). Variations in HRT have ranged between 20 and 100 days (Rajendran et al. 2012). In contrast, Nsair et al. (2020) have shown that the HRT varied from 0.75 to 60.00 days, with the optimal period of 16 to 60 days. Uddin et al. (2021) stated that a minimum of 10 days of HRT is necessary to ensure that bacteria are not washed away during the process. HRT is chosen according to the digester volume, digestion processes, and feedstock temperature. Using wet mass substrate instead of mass substrate VS in the OLR expression, HRT is equivalent to an inverse of OLR (Lissens et al. 2001).

Interestingly, OLR is directly related to HRT (Ruile et al. 2015). Experimentation and system performance monitoring typically determine the optimal HRT for a particular biogas plant. This involves gradually increasing or decreasing the HRT and monitoring the biogas production and process stability until the optimal HRT is achieved.

Challenges and Recommendations

Despite the worldwide popularity of the anaerobic digestion of cow dung, it still has some disadvantages, such as inhibition of the process, feedstock variability, process instability system design and management, and low biogas production due to the high C: N ratio. Addressing these challenges requires a thorough understanding of anaerobic digestion's biological and chemical processes and the factors that can impact system performance. Careful management of feedstock, process conditions, and system design can help optimize biogas production and reduce environmental impacts. Based on the literature reviewed AD, the following recommendations are made. Manure from livestock, especially cow dung, should be considered in waste management and biogas production. To maximize biogas production, the addition of other organic substrates and co-substrates, such as crop residues, should be considered.

Moreover, mono-digestion should be promoted and not neglected to combat the high nitrogen content in livestock manure. Mono-digestion is a process in which manure is fermented only once to produce biogas. This process helps to reduce the amount of nitrogen in manure, which can then be used as fertilizer and reduces the environmental impact of livestock farming. Overall, mono-digestion can be a useful strategy for optimizing the anaerobic digestion process and improving the efficiency and effectiveness of biogas production. However, it is important to carefully select the appropriate substrate and optimize the process conditions to ensure optimal performance.

CONCLUSIONS

Based on anaerobic digestion technology published between 2001 and 2022 in research articles searched for information about biogas feeding and digestion. The information was then used to draw insights into biogas feeding trends and anaerobic digestion technology over the past two decades. According to the review findings, the conclusion is that several factors can affect the digester stability and biogas production rate. These factors begin with volatile solids content. The volatile solids content is critical because it affects the number of microorganisms available for digestion. This directly impacts the production of biogas. In addition, the pH and temperature of the slurry inside the digester, as well as the amount of nutrients and oxygen, can also affect the stability and biogas production rate. In addition, digesters are fed differently depending on feedstock availability. Thus, the composition of the feedstock, including the volatile solids content, will directly impact the amount of biogas produced. Recent research shows that co-digesting feedstock is helpful because mono-substrates fed into AD systems present drawbacks like a low hydrolysis rate that leads to insufficient biogas production. This is because when a variety

of substrates are co-digested, the microbial community within the AD system can more efficiently break down the feedstock and convert it into biogas.

Additionally, the complexity of the microbial community can be increased by adding more substrates, which can lead to better biogas production. Following recent research, keeping uniform mixing and temperature, particle size, and pH controls how fast organic matter hydrolyses in AD. Feedstocks that need pre-treatment before hydrolysis are expensive to process and account for 20-40% of the total process cost. Pre-treatment of feedstocks is necessary to break down the complex organic matter into simpler compounds, which then can be hydrolyzed. This pre-treatment step is energy and time-consuming and, therefore, expensive.

REFERENCES

Anderman, T., DeFries, R.S., Wood, S.A., Remans, R.A., Richie, U.E. and Shujayath, E. 2015. Biogas cook stoves for healthy and sustainable diets? A case study in Southern India. Front. Nutr., 2(28): 1-12

Abanades, S., Abbaspour, H., Ahmadi, A., Das, B., Ehyaei, M., Esmaeilion, F., El Haj Assad, M., Hajilounezhad, T., Jamali, D., Hmida, A., Ozgoli, H.A., Safari1, S., AlShabi, M. and Bani-Hani, E.H. 2021. A critical review of biogas production and usage with legislation framework across the globe. Int. J. Environ. Sci. Technol., 19: 3377-3400.

Achu Nges, I., Escobar, F., Fu, X. and Björnsson, L. 2012. Benefits of supplementing an industrial waste anaerobic digester with energy crops for increased biogas production. Waste Manag, 32(1): 53-59.

Ahring, B. K., Ibrahim, A.A. and Mladenovska, Z. 2001. Effect of temperature increase from 55 to 65 degrees C on performance and microbial population dynamics of an anaerobic reactor treating cattle manure. Water Res., 35(10): 2446-2452.

Akbulut, A., Arslan, O., Arat, H. and Erbaş, O. 2021. Important aspects for the planning of biogas energy plants: Malatya case study. Case Stud. Thermal Eng., 26:1-22.

Ansar, A. 2022. Assessment of laboratory scale cylindrical sequencing batch reactor for the treatment of abattoir effluent. Innov. Infrastruct. Sol., 7(100): 121-146.

Anukam, A., Mohammadi, A., Naqvi, M. and Granström, K. 2019. A review of the chemistry of anaerobic digestion: Methods of accelerating and optimizing process efficiency. Processes, 7: 504.

Appuhamy, J.A.D.R.N., Moraes, L.E., Wagner-Riddle C., Casper D.P. and Kebreab E. 2018. Predicting manure volatile solid output of lactating dairy cows. J. Dairy Sci., 101(1): 820-829.

Aravani, V.P., Tsigkou, K., Papadakis, V.G. and Kornaros, M. 2022. Biochemical methane potential of most promising agricultural residues in northern and southern Greece. Chemosphere, 296: 611.

Baba, S.U.I.A. and Nasir, I. 2012. Anaerobic digestion of cow dung for biogas production. J. Eng. Appl. Sci., 7(2): 169-172.

Bedoić, R., Ćosić, B., Pukšec, T. and Duić, N. 2020. Anaerobic digestion of agri-food by-products. Am. Soc. Agric. Biol. Eng., 16: 545.

Begum, S. and Nazri, A. H. 2013. Energy Efficiency of Biogas Produced from Different Biomass Sources. IOP Conf. Ser. Earth Environ. Sci., 16: 1-4.

Bella, K. and Rao, V. P. 2022. Anaerobic co-digestion of cheese whey and septage: Effect of substrate and inoculum on biogas production. J. Environ. Manag., 308: 116.

Berhe, T.G., Rahwa, G.T., Grmanesh, A.D. and Lemlem, S. M. 2017. Biogas plant distribution for rural household sustainable energy supply in Africa. Energy Pol. Res., 4(1): 10-20.

Bhatnagar, N., Ryan, D., Murphy, R. and Enright, A.M. 2022. A comprehensive review of green policy, anaerobic digestion of animal manure and chicken litter feedstock potential – Global and Irish perspective. Renew. Sustain. Energy Rev.,154.

Black, M.J., Roy, A., Twinomunuji, E., Kemausor, F., Oduro, R., Leach, M., Sadhkhan, J. and Murphy, R. 2021. Bottled biogas: An opportunity for clean cooking in Ghana and Uganda. Energies, 14(13): 1-14.

Castano, J.M., Martin, J.F. and Ciotola, R. 2014. Performance of a small-scale, variable temperature fixed dome digester in a temperate climate. Energies., 7(9): 651.

Dhungana, B., Marsolek, M. and Lohani, S.P. 2022. Anaerobic co-digestion of food waste with livestock manure at ambient temperature: A biogas based circular economy and sustainable development goals. Sustainability, 14(6): 1-16.

Duan, Z., Bournazou, M N.C. and Kravaris, C. 2017. Dynamic model reduction for two-stage anaerobic digestion processes. Chem. Eng. J., 327: 1102-1116.

Elsayed, M., Andres , Y. and Blel, W. 2022. Anaerobic co-digestion of linen, sugar beet pulp, and wheat straw with cow manure: Effects of mixing ratio and transient change of co-substrate. Biomass Conv. Bioref., 11: 25.

Elsharkawy, K., Elsamadony, M. and Afify, H. 2019. Comparative analysis of common full-scale reactors for dry anaerobic digestion process. E3S Web Conf., 83: 1-6.

Fajobi, M.O., Lasode, O.A., Adeleke, A.A., Ikubanni P.P. and Balogun, A.O. 2022. Investigation of physicochemical characteristics of selected lignocellulose biomass. Sci. Rep., 12: 64.

Filer, J., Ding, H.H. and Chang, S. 2019. Biochemical Methane Potential (BMP) Assay Method for Anaerobic Digestion Research. Water.,11:1-29.

Fu, Y., Luo, T., Mei, Z., Li, J., Qiu, K. and Ge, Y. 2018. Dry Anaerobic Digestion Technologies for Agricultural Straw and Acceptability in China. Sustainability, 10(12): 4588.

Gaby, J.C., Zamanzadeh, M. and Horn, S.J. 2017. The effect of temperature and retention time on methane production and microbial community composition in staged anaerobic digesters fed with food waste. Biotechnol. Biofuels, 10: 61.

Guo, H., Oosterkamp, J.M., Tonin, F., Hendriks, A., Nair, R., van Lier, J.B. and Kreuk, M. 2021. Reconsidering hydrolysis kinetics for anaerobic digestion of waste-activated sludge applying cascade reactors with ultra-short residence times. Water Res., 202: 4652.

Haryanto, A., Triyono, S. and Wicaksono, N.H. 2018. Effect of loading rate on biogas production from cow dung in a semi-continuous anaerobic digester. Int. J. Renew. Energy Develop., 7(2): 93-100.

He, W., Zhang, L., Liu, H., Zhang, Y., Fu, B., Zhang, X. and Jiang, Q. 2022. CO_2 sequestration mediated by wollastonite in anaerobic digestion of sewage sludge: From sequence batch to semi-continuous operation. Chemosphere, 287(3): 645.

Ignatowicz, K., Piekarski, J. and Kogut, P. 2021. Influence of selected substrate dosage on the process of biogas installation start-up in real conditions. Energies, 14: 1-11.

Jaeger, A. and Blanchard, R.E. 2022. Techno-economic analysis of an enhanced anaerobic digester in the Andean area of Peru. Int. J. Energy Environ. Eng., 13: 805-819.

Kassongo, J., Shahsavari, E. and Ball, A.S. 2022. Substrate-to-inoculum ratio drives solid-state anaerobic digestion of unamended grape marc and cheese whey. PLoS ONE, 17(1): 545.

Kesharwani, N. and Bajpai, S. 2021. Pilot scale anaerobic co-digestion at tropical ambient temperature of India: Digester performance and techno-economic assessment. Bioresour. Technol. Rep., 15: 641.

Khadka, A., Parajuli, A., Dangol, S., Thapa, B., Sapkota, L., Carmona-Martínez, A.A. and Ghimire, A. 2022. Effect of the substrate to inoculum ratios on the kinetics of biogas production during the mesophilic anaerobic digestion of food waste. Energies, 15: 834

Khan, E U. and Martin, A.R. 2016. Review of biogas digester technology in rural Bangladesh. Renewable and Sustainable Energy Reviews., 62: 247-259.

Khan, N.A., Bokhari, A., Mubashir, M., Klemeš, J.J., Morabet, R.E., Khan, R.A., Alsubih, M., Azam, M., Saqib,S., Mukhtar, A., Koyande, A. and Show, P.L. 2022. Treatment of hospital wastewater with submerged aerobic fixed film reactor coupled with tube-settler. Chemosphere, 28(3): 114.

Khan, S.I., Aftab, S., Chaudhry, T.A. and Younis, M.N. 2018. Production of biogas by the co-digestion of cow dung and crop residue at the University of the Punjab Lahore, Pakistan. Afr. J. Environ. Sci. Technol., 12(2): 91-95.

Kim, J., Baek, G., Kim, J. and Lee, C. 2019. Energy production from different organic wastes by anaerobic co-digestion: Maximizing methane yield versus maximizing synergistic effect. Renew. Energy, 136(C): 683-690.

Kothari, R., Ahmad, S., Pathak, V.V., Pandey, A., Singh, S., Kumar, K. and Tyagi, V.V. 2018. Experiment-based thermodynamic feasibility with co-digestion of nutrient-rich biowaste materials for biogas production. Biotechnology, 8(1): 34.

Kozłowski, K., Dach, J., Lewicki, A. and Cieślik, M. 2018. Laboratory simulation of an agricultural biogas plant start-up. Chem. Eng. Technol., 41(4): 74.

Lissens, G., Vandevivere, P., De Baere, L., Biey, E.M. and Verstrae, W. 2001. Solid waste digestors: Process performance and practice for municipal solid waste digestion. Water Science and Technology., 44(8): 91-102.

Li, Y., Liu, H., Yan, F., Su, D., Wang, Y. and Zhou, H. 2017. High-calorific biogas production from anaerobic digestion of food waste using a two-phase pressurized biofilm (TPPB) system. Bioresource Technology, 224: 56-62.

Łochyńska, M. and Frankowski, J. 2018. The biogas production potential from silkworm waste. Waste Manag., 79: 564-570.

Lohani, S.P., Dhungana, B., Horn, H. and Khatiwada, D. 2021. Small-scale biogas technology and clean cooking fuel: Assessing the potential and links with SDGs in low-income countries – A case study of Nepal. Sustain. Energy Technol. Assess., 46: 1-14.

Luo, K., Yang, Q., Li, X., Yang, G., Liu,Y., Wang, D., Zheng, W. and Zeng, G. 2012. Hydrolysis kinetics in anaerobic digestion of waste-activated sludge enhanced by - amylase. Biochem. Eng. J., 62: 17-21.

Mani, S. and Sundaram, J. 2016. Process simulation and modeling: Anaerobic digestion of complex organic matter. Biomass and Bioenergy, 93: 158-167.

Mao, C., Feng, Y., Wang, X. and Ren, G. 2015. Review on research achievements of biogas from anaerobic digestion. Renew. Sustain. Energy Rev., 45: 540-555.

Mata-Alvarez, J., Dosta, J., Romero-Güiza, M.S., Fonoll, X., Peces, M. and Astals, S. 2014. A critical review of anaerobic co-digestion achievements between 2010 and 2013. Renew. Sustain. Energy Rev., 36: 412-427.

Menacho, W.A., Mazid, A.M. and Das, N. 2022. Modeling and analysis for biogas production process simulation of food waste using Aspen Plus. Fuel, 309: 7459.

Menzel, T., Neubauer, P. and Junne, S. 2020. Role of microbial hydrolysis in anaerobic digestion. Energies, 13: 6.

Mkiramwen, L.L. 2012. The impact of biogas conversion technology for economic development: A case study in Kilimanjaro Region. Int. Schol. Res. Notices, 5: 1-9.

Moestedt, J., Malmborg, J. and Nordell, E. 2015. Determination of methane and carbon dioxide formation rate constants for semi-continuously fed anaerobic digesters. Energies, 8: 645-655.

Mullo, A.S., Sanchez, W.E., Salazar, F.W., Chacha, J.M. and Flores, A. 2018. Implementation of a cattle manure biodigester for the production of gas for single-family use. E3S Web Conf., 57: 01003 (2018).

Myint, M., Nirmalakhandan, N. and Speece, R.E. 2007. Anaerobic fermentation of cattle manure: Modeling of hydrolysis and acidogenesis. Water Res., 41(2): 323-332.

Nie, E., He, P., Zhang, H., Hao, L., Shao, L. and Lü, F. 2021. How does temperature regulate anaerobic digestion? Renew. Sustain. Energy Reviews, 150: 1414-1422.

Nsair, A., Onen Cinar, S., Alassali, A., Abu Qdais, H., Kuchta, K. 2020. Operational Parameters of Biogas Plants: A Review and Evaluation Study. Energies., 13(15): 3761.

Nwokolo, N., Mukumba, P., Obileke, K. and Enebe, M. 2020. Waste to energy: A focus on the impact of substrate type in biogas production. Processes, 8(10): 1224.

Obileke, K., Mamphweli, S., Meyer, E.L., Makaka, G. and Nwokolo, N.L. 2020. Design and Fabrication of a Plastic Biogas Digester for the Production of Biogas from Cow Dung. Journal of Engineering., 1-11.

Obileke, K., Nwokolo, N., Makaka, G., Mukumba, P. and Onyeaka, H. 2021. Anaerobic digestion: Technology for biogas production as a source of renewable energy: A review. Energy Environ., 32(2): 191-225.

Ofosu, M.A. and Aklaku, E.D. 2010. Determining the optimum proportion of shea waste in an anaerobic co-fermentation process. J. Sci. Technol., 30(1): 119-128.

Ogur, E. and Irungu, P. 2013. Design of a biogas generator. Int. J. Eng. Res. Appl., 3(6): 630-635.

Okonkwo, U.C., Onokpite, E. and Onokwai, A. O. 2018. Comparative study of the optimal ratio of biogas production from various organic wastes and weeds for digester/restarted digester. J. King Saud Univ. Eng. Sci., 30(2): 123-129.

Pandey, P., Pandey, A., Yan, L., Wang, D., Pandey, V., Meikap, B.C., Huo, J., Zhang, R. and Pandey, P.K. 2021. Dairy waste and potential of small-scale biogas digester for rural energy in India. Appl. Sci., 11(22): 10671.

Panico, A., D'Antonio, G., Esposito, G., Frunzo, L., Iodice, P. and Pirozzi, F. 2014. The effect of substrate-bulk interaction on hydrolysis modeling in the anaerobic digestion process. Sustainability, 6(12): 8348-8363.

Parra-Orobio, B.A., Torres-Lozada, P. and Marmolejo-Rebellón, L.F. 2016. Influence of the mixing ratio on the anaerobic co-digestion of municipal biowaste with domestic wastewater sludge on methane production. DYNA, 83(199): 86-93.

Rabii, A., Aldin, S., Dahman, Y. and Elbeshbishy, E. 2019. A review of anaerobic co-digestion with a focus on the microbial populations and the effect of multi-stage digester configuration. Energies, 12(6): 15-26.

Rahman, M.D., Azizul Haque, M.D., Ahsan Kabir, A.K.M., Abul Hashem, M.D., Abul Kalam Azad, M.D. and Bhuiyan, M.K. 2021. Efficacy of biogas production from different types of livestock manures. Int. J. Smart Grid, 5(4): 158-166.

Raja, M.K.M.M., Manne, R. and Devarajan, A. 2021. Benefits of cow dung: A human ignored gift. J. Nat. Remed., 2: 15-46.

Rajendran, K., Aslanzadeh, S. and Taherzadeh, M.J. 2012. Household biogas digesters: A review. Energies, 5: 2911-2942

Ramaswamy, J. and Vemareddy, P.S. 2015. Production of biogas using small-scale plug flow reactor and sizing calculation for biodegradable solid waste. Renew Wind Water Solar, 2(6): 545.

Raposo, F., De la Rubia, M.A., Fernández-Cegrí, V. and Borja, R. 2011. Anaerobic digestion of solid organic substrates in batch mode: An overview relating to methane yields and experimental procedures. Renew. Sustain. Energy Rev., 16: 861-877.

Rivas Solano, O., Faith Vargas, M. and Guillén Watson, R. 2016. Biodigesters: chemical, physical, and biological factors related to their productivity. Tecnol. en Marcha., 23(1): 39-46.

Rocamora, I., Wagland, S.T., Villa,R., Simpson, E.W., Fernández, O. and Yadira Bajón-Fernández, Y.B. 2020. Dry anaerobic digestion of

organic waste: A review of operational parameters and their impact on process performance. Bioresour. Technol., 62: 299.

Roubík, H., Mazancová, J., Le Dinh, P., Dinh Van, D. and Banout, J. 2018. Biogas quality across small-scale biogas plants: A case of Central Vietnam. Energies, 11(7): 1794.

Ruile, S., Schmitz, S., Mönch-Tegeder, M. and Oechsner, H. 2015. Degradation efficiency of agricultural biogas plants: A full-scale study. Bioresour. Technol., 178: 341-349.

Saady, N.M.C. and Massé, D.I. 2015. Impact of organic loading rate on psychrophilic anaerobic digestion of solid dairy manure. Energies, 8(3): 16-32.

Sadeleer, I. d., Brattebø, H. and Callewaert, . P., 2020. Waste prevention, energy recovery or recycling - Directions for household food waste management in light of circular economy policy. Resources, Conservation & Recycling., 160.

Sawyerr, N., Trois, C. and Workneh, T. 2019. Optimization of biogas yield through co-digestion of cassava biomass, vegetable and fruits waste at mesophilic temperatures. International J. Renew. Res., 9(2): 771-782.

Song, Y.J., Oh, K.S., Lee, B., Pak, D.W., Cha, J.H. and Park, J.G. 2021. Characteristics of biogas production from organic wastes mixed at optimal ratios in an anaerobic co-digestion reactor. Energies, 14(20): 6812.

Sruthy, B., Anisha, G.K., Gibi, M.M. and Sruthi, G.R. 2017. An experimental investigation on the strength of concrete made with cow dung ash and glass fiber. Int. J. Eng. Res. Technol., 6(3): 492-495.

Szymajda, A., Łaska, G. and Joka, M. 2021. Assessment of cow dung pellets as a renewable solid fuel in direct combustion technologies. Energies, 14: 15-26.

Tan, J.B., Jamali, N.S., Tan, W.E., Che Man, H. and Zainal Abidin, Z. 2021. Techno-economic assessment of on-farm anaerobic digestion system using attached-biofilm reactor in the dairy industry. Sustainability., 13(4): 2063.

Triolo, J.M., Ward, A.J., Pedersen, L. and Sommer, S.G. 2013. Characteristics of animal slurry as a key biomass for biogas production in Denmark. Biomass Sustain., 16: 307-326.

Tumutegyereize, P., Ketlogetswe, C., Gandure, J. and Banadda, N. 2017. Technical evaluation of uptake, use, management and future implications of household biogas digesters: A case of Kampala City peri-urban areas. Comput Water Energy Environ. Eng., 6(2): 111-116.

Uddin, M.N., Siddiki, S.K.Y.A., Mofijur, M., Djavanroodi, F., Hazrat, M.A., Show, P.L., Ahmed, S.F. and Chu, Y. 2021. Prospects of bioenergy production from organic waste using anaerobic digestion technology: A mini-review. Front. Energy Res., 9: 15-26.

Ünyay, H., Yılmaz, F., İbrahim, A.B., Perendeci, N.A., Çoban,I. and Şahinkaya, E. 2022. Effects of organic loading rate on methane production from switchgrass in batch and semi-continuous stirred tank reactor system. Biomass Bioenergy, 156: 106306.

Wang, H., Aguirre-Villegas, H.A., Larson, R.A. and Alkan-Ozkaynak, A. 2019. Physical properties of dairy manure pre- and post-anaerobic digestion. Appl. Sci., 9: 16-25.

Wang, J. 2014. Decentralized biogas technology of anaerobic digestion and farm ecosystem: opportunities and challenges. Front. Energy Res., 2(10): 1-12.

Wang, X., Lu, X., Li, F. and Yang, G. 2014. Effects of temperature and carbon-nitrogen (c/n) ratio on the performance of anaerobic co-digestion of dairy. PLoS ONE, 9(5): 16-23.

Wang,Y.,Yang, L., Li, Y., Fu, L., Yuan, C., Yao, L. and Luo, J. 2021. Reactor performance and economic evaluation of singular, binary, and ternary mixing of feedstocks for anaerobic digestion. Environ. Technol., 42(2): 318-328.

Wang, Z., Jiang, Y., Wang, S., Zhang, Y., Hu, Y., Hu, Z., Wu, G., Zhan, X. 2020. Impact of total solids content on anaerobic co-digestion of pig manure and food waste: Insights into shifting of the methanogenic pathway. Waste Management, 114: 96-106.

Wresta, A., Andriani, D., Saepudin, A. and Sudibyo, H. 2015. Economic analysis of cow manure biogas as an energy source for electricity power generation in small-scale ranch. Energy Proced., 68: 122-131.

Yi, J., Dong, B., Jin, J. and Dai, X. 2014. Effect of increasing total solids contents on anaerobic digestion of food waste under mesophilic conditions: performance and microbial characteristics analysis. PloS one, 9(7): 1-10.

Zainudeen, M., Kwarteng, M., Nyamful, A., Mohammed, L. and Mutala, M. 2021. Effect of temperature and pH variation on anaerobic digestion for biogas production. Ghana J. Agric. Sci., 56(2): 1-13.

Zeb, I., Yousaf, S., Ali, M., Yasmeen, A., Khan, A., Tariq, J., Zhao, Q., Abbasi. A., Ahmad, R., Khalil, T., Yaqoob, A. and Bil, M. 2022. In-situ microaeration of anaerobic digester treating buffalo manure for enhanced biogas yield. Renew. Energy, 181(C): 843-850.

Ziemiński, K. and Frąc, M. 2012. Methane fermentation process as anaerobic digestion of biomass: Transformations, stages, and microorganisms. African Journal of Biotechnology, 11(18): 4127-4139.

ORCID DETAILS OF THE AUTHORS

V. M. Nekhubvi: https://orcid.org/0009-0004-7805-9501

Nature Environment and Pollution Technology
An International Quarterly Scientific Journal

p-ISSN: 0972-6268
(Print copies up to 2016)
e-ISSN: 2395-3454

Vol. 23 | No. 1 | pp. 203-213 | 2024

Original Research Paper

https://doi.org/10.46488/NEPT.2024.v23i01.016

Open Access Journal

Application of Arc-SWAT Model for Water Budgeting and Water Resource Planning at the Yeralwadi Catchment of Khatav, India

R. S. Sabale*(**)†, S. S. Bobade*, B. Venkatesh* and M. K. Jose*****

*Department of Civil Engineering, Pimpri Chinchwad College of Engineering & Research, Ravet, Pune-412101, India
**Visvesvaraya Technological University, Belagavi, Karnataka-590018, India
***Hard Rock Regional Centre, National Institute of Hydrology, Belagavi, Karnataka-590019, India
†Corresponding author: R. S. Sabale; ranjeetsabale123@gmail.com

Nat. Env. & Poll. Tech.
Website: www.neptjournal.com

Received: 03-06-2023
Revised: 19-07-2023
Accepted: 26-07-2023

Key Words:
Arc-SWAT model
Surface water modeling
Irrigation
Agriculture
Water budget

ABSTRACT

Every facet of life, including human habitation, economic development, food security, etc., depends on water as a valuable resource. Due to the burgeoning population and rapid urbanization, water availability needs to be simulated and measured using hydrologic models and trustworthy data. To fulfill this aim, the SWAT model was processed in this work. The SWAT model was formulated to estimate the hydrological parameters of Yeralwadi using meteorological data from IMD (India Meteorological Department) for the period 1995-2020. The observed discharge data was collected from the HDUG Nasik group and used in the calibration and validation of the Model. The SWAT model was corrected & validated through the SUFI-II algorithm in SWAT-CUP to get a better result. The model's sensitivity is checked by using statistical parameters like Nash-Sutcliffe Efficiency (NSE) and a coefficient of determination (R^2). NSE values were 0.72 and 0.80 in calibration and validation, and R^2 were 0.80 & 0.76 in calibration and validation, respectively, indicating the acceptance of the model. Results show that 40.6% of the total yearly precipitation was lost by evapotranspiration. The estimated total discharge from the Yeralwadi catchment was 55.6%, out of which 41.2% was surface runoff and 14.4% was baseflow. The other 17.8% was made up of percolation into confined and unconfined aquifers, which served as soil and groundwater storages. The surface runoff is influenced by Curve number (CnII), SOL_AWC, ESCO, and base flow was influenced by ALPHA-BF and GW_REVAP. This study will be useful to water managers and researchers to develop sustainable water resource management and to alleviate the water scarcity issues in the study basin.

INTRODUCTION

Water is not a luxurious thing but is necessary for all living beings. It plays a very important role in the survival of all living beings. Moreover, relatively substantial amounts of water are necessary for both to function properly; hence, it is more important to study the water requirement (Singh 2014). Water availability has an impact on domestic and international relations, economic success, quantity of food supply, relocation of people, and habitats for humans and other animals. The connection between issues concerning water availability & supply for groundwater-dependent irrigation systems has lately come up in various discussions (Dovie & Kasei 2018). Water resources are under a lot of pressure due to rapid economic development, burgeoning population (Samimi et al. 2020), as well as global climate change (Ross 2018), particularly in arid, semiarid, and water-scarce regions (Prabhanjan et al. 2015). The regional and season-wise water distribution across the basins is influenced by factors like land use, prevailing cropping patterns, locations of water applicants, and water usage timing (Du et al. 2022). There is limited availability of water resources in many arid region and semi-arid regions, which influences the potential demand for it.

It is a need of the 21st century to estimate and understand the water metrics and how to manage it sustainably. Most water resource projects are influenced due to climate change (Dovie & Kasei 2018). Therefore, throughout the globe, researchers are working on water budgeting by quantifying the water by taking into account different water users like domestic, industrial, agricultural, and public use (Ridoutt et al. 2009, Vairavamoorthy et al. 2008). Use of hydrologic models like ArcSWAT (Sabale et al. 2023, Sabale & Jose 2021, 2022, 2023), MODFLOW (Abdalla 2009, Baalousha 2016), MIKE (Kaleris & Langousis 2017) and HEC-RAS with accurate data sets proves very efficient in hydrological modeling. These GIS-based Agro-hydrological models

required the following data as inputs: meteorological data, socio-economic data, Infrastructure and technological data, and agricultural information to quantify the availability of water in the study basin.

The cropping pattern and water usage at one sector affect the water consumption and outputs from another sector, e.g., the water discharge downstream of the river is decreased by irrigation along river basins. Although the water resources are overwhelmed due to climate change and over-demand from different water users, such minute approaches will aid in the sustainable development of water resources. The heuristic rainfall-runoff models are formulated by (Oki et al. 2001) to better understand and simulate the changes in water use caused by anthropogenic activities. Through numerical simulations and testing of different management scenarios, the computing power of those models allows users to better understand and estimate the attributes of water resources (Ninija Merina et al. 2019). Users can evaluate the hydrological relationships in river basins using these numerical models, which combine several empirical equations and fundamentals of science (Neitsch et al. 2002, 2005).

The most precise and practically applicable way to predict water availability and its distribution in the study basin under various demand and operating scenarios is to use hydrologic models. SWAT model, which is an agro-hydrological, process-based, and semi-distributed model, is used to represent both runoff generation processes and their influence on the hydrology of the study area. Authors have tried these models to correlate water use and water availability to ascertain the long-term effect of an environmental change on the hydrologic response of the basin (Liu et al. 2013, Neitsch et al. 2002, Saraf & Regulwar 2018).

This study aims to predict the volume of water available in the Yeralwadi catchment using the SWAT hydrological model. The meteorological data to process the SWAT model was taken from the India Meteorological Department (IMD). Also, the available observed hydro-meteorological data from the HDUG group was used to correct and validate the SWAT model. The outcomes of this work will provide information to researchers, decision-makers, and water policymakers about the water resources in the Yeralwadi catchment, as well as to adapt the best practices (BMPs) for boosting sustainable agricultural output and ensuring food security.

MATERIALS AND METHODS

Materials Used

The present work is devoted to ascertaining the application of the ArcSWAT model for the estimation of water availability at the Yeralwadi basin of Khatav taluka of Maharashtra in India. The selected study area is almost dry and semi-arid, as declared by CGWB, with issues like water scarcity, secondary soil salinization, and waterlogging in a few places. By processing the SWAT, authors are interested in estimating the water available, and according to that, irrigation scheduling and best management practices for the acceleration of sustainable development of water resources are suggested.

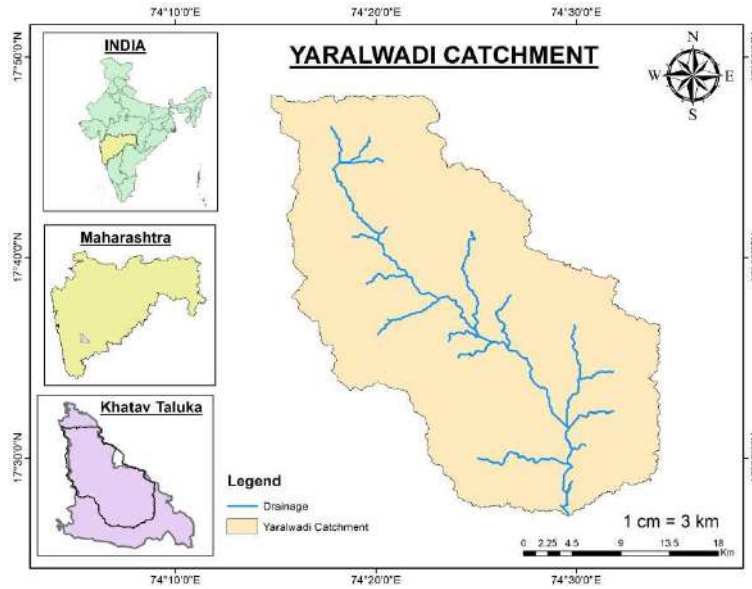

Fig. 1: Index map of the study area.

Study Area

Fig. 1 shows an index map of the study area, i.e., Yeralwadi catchment, which is located in Khatav taluka (17.5279° N, 74.4893° E) of Satara district in the state of Maharashtra. Khatav taluka is a semi-arid region and measures geographically 1358 sq. km. In the present work, the SWAT model was processed on a 790 sq. km area. Yerala River is one of the major tributaries of the Krishna River flowing through the study basin. The study area receives an average annual rainfall of 560 mm (CGWB 2017). Moreover, the average temperature ranges from 13°C to 40°C, and the average wind speed observed in the study area is 7 $Km.hr^{-1}$. In general, the topographical distribution of the Yeralwadi catchment is characterized by moderate flatlands with slopes ranging from 0% to 3%, 3% to 15%, and more than 15%, representing 18.22%, 73.73%, and 8%, respectively.

The land use of the study area comprises maximum agricultural use, and most of the land is barren. The prevailing crops observed in the study area are Paddy, Jowar, Soyabin, and Sugarcane. The Ner Dam, Yeralwadi Dam, and Mayani Lake are prominent surface water sources in the study area.

Input Data Formulation

Digital elevation model (DEM): To process SWAT, the inputs are provided as meteorological data, digital elevation model (DEM), Soils, and Landuse Land cover details. The meteorological data for the period 2000 to 2020 was taken from IMD and NASA websites. The daily data like rainfall (mm), maximum and minimum temperature (°C), relative humidity (%), wind speed ($Km.hr^{-1}$), and solar radiation were collected for Ambavade (Khatav) station. The Digital Elevation Model (DEM) for the Yeralwadi area was taken from the USGS database with 30 m resolution (Fig. 2). The soil map was prepared by using FAO soils, and Landuse map was processed using the image classification tool in ArcSWAT with the maximum likelihood option. The Landsat-8 images are used for 2018-2019 to process the LULC map.

Land use (LULC) map: This map depicts the physical characteristics and usage of the basin, like forest area, built-up, and barren land. It describes how the area is being used (Fig. 4). In this work, to process the SWAT model, the LULC data for (2018-2020) was downloaded from the earth-explorer website, and the precaution has

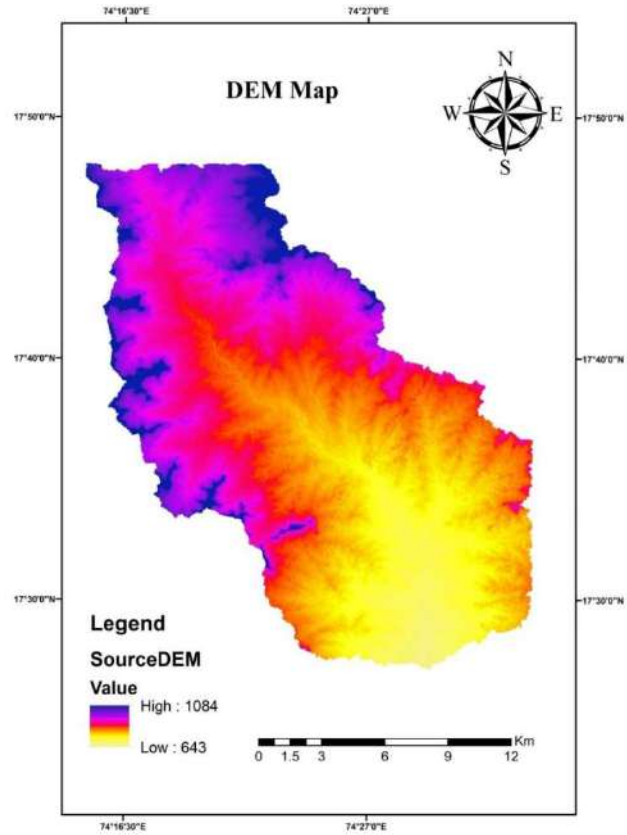

Fig. 2: Digital Elevation Model (DEM).

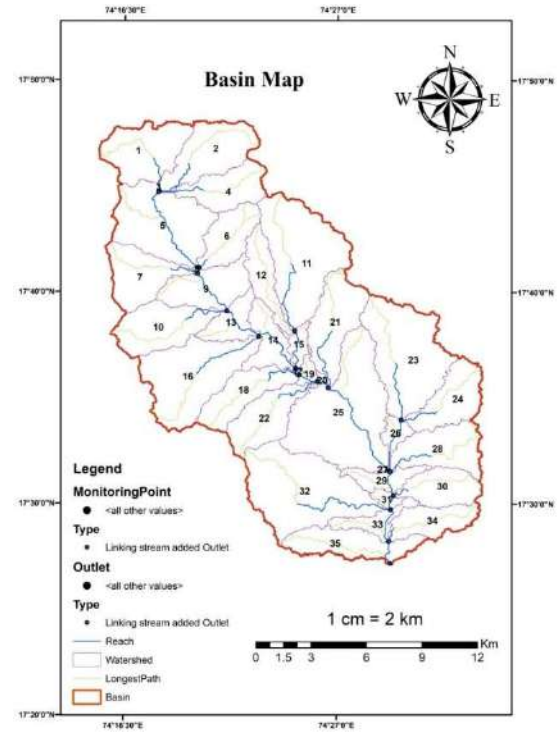

Fig. 3: Basin map.

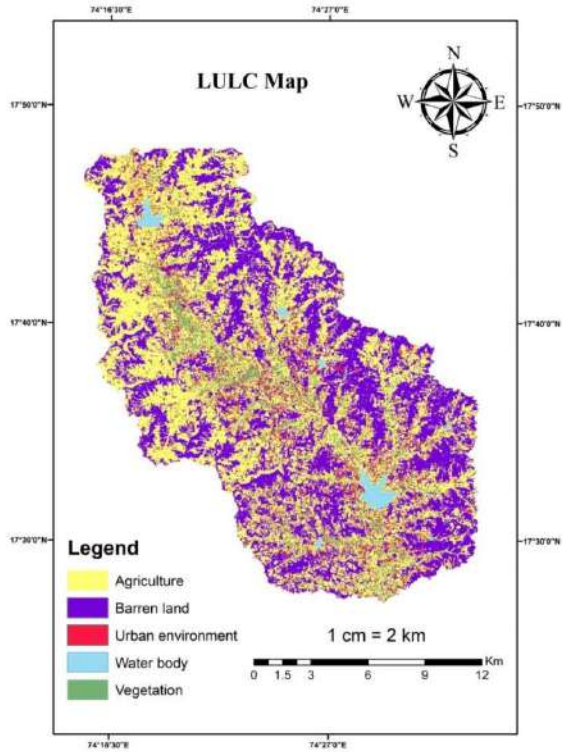

Fig. 4: The LULC map.

Table 1: Land use details of the study area.

LULC Details	Area [ha]	% Watershed Area
Agriculture	37824.67	48.50
Barren Land	30077.14	38.57
Residential low density	4829.70	6.19
Water	961.40	1.23
Forest	4293.72	5.51

been taken that selected data having clouds less than 10%. For the present work, the land use land cover map for the Yeralwadi basin was formulated using image classification in ArcSWAT-2012 and using Landsat-8 imagery. In the present work, the Land is being used as agricultural land 48.50%, Barren land 38.57%, Water bodies 1.23%, dense Forest 5.51%, and Low density residential built area 6.19% (Table 1). From LULC attributes, it is observed that such land use land cover is more vulnerable to soil erosion, and the reservoirs downstream are more susceptible to siltation.

Soils in the study area: Highly accurate soil data are more important to process the SWAT model (Stadnyk & Holmes 2023). The SWAT Model has built information on soils from the world and Indian continents. In the present work, the soil data was taken from the Soil Survey Department of India (NBSSLUP) to a scale of 1:250,000 (Kumar et al. 2015). The soil data was accessible in a detailed format, and that gives the soil texture profile. Then, in the SWAT model, it was digitized for further processing (Dutta & Sen 2018). Fig. 5 depicts the soil types found in the study region. The four types of soil were found in the study area. Table 2 shows the percentages of soil.

Methodology Adopted

In this work, the semi-distributed model SWAT, which the US Agriculture Research Department developed, was used (Arnold et al. 1998, Kim et al. 2008, Neitsch et al. 2002). The SWAT is a GIS-based, semi-distributed, physical model that simulates the rainfall-runoff process and also predicts the hydrological parameters (Eini et al. 2023). The SWAT model is highly efficient, and it is capable of running over a long period. The model uses

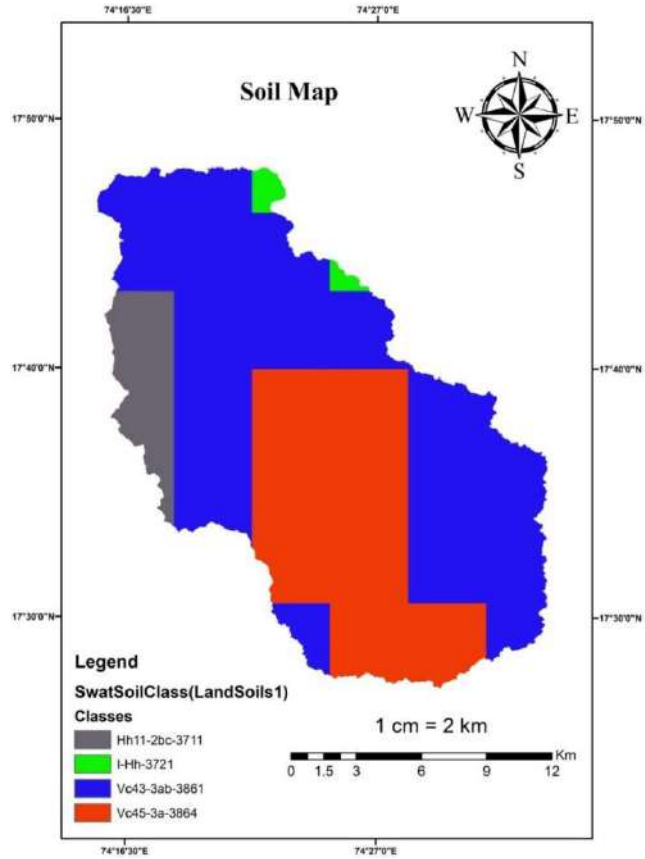

Fig. 5: Soil map.

GIS-based information like digital elevation. Land uses land cover (LULC) of the study area, climate data, and soil data to process and yield simulated results in terms of water available, loss of water, transportation of nutrients and pesticides, etc. The basic principle that governs the SWAT model is as given below (Eq. 1) (Jajarmizadeh et al. 2017),

$$SH_t = S_0 + \sum_{i=1}^{t}(P_{day} - R_{Surf} - Q_{Seep} - E_0 - Q_{gw}) \quad \ldots(1)$$

Where,

SHt = soil humidity (mm), S_0 = soil base humidity (mm), t = Time period (days), P_{day} = Precipitation volume (mm), R_{surf} = surface runoff, E_0 = evapotranspiration (mm), Qseep = seepage of water from the soil into deep layers, Qgw = underground runoff (mm).

SWAT Model

ArcSWAT - 2012 version was used to set up the surface water model (Fig. 6). In the first step, using digital elevations, the whole study area is delineated into the number of sub-basins. The delineation process provides the information as sub-watersheds, main reach, lateral reach, and slope (Fig. 3). The sub-basins are again divided into smaller homogenous units called HRU (Hydrological Response Units) (Santhi et al. 2001). The HRUs are smaller portions having unique slopes, types of soil, and land use patterns. In the present study, after delineation, the catchment is divided into 35 sub-basins (Fig. 3) consisting of 196 HRUs. The four types of soil were found in the catchment, as given in Table 2.

The model's performance statistics were reviewed, and using water balance ratios, the water availability of the catchment was calculated.

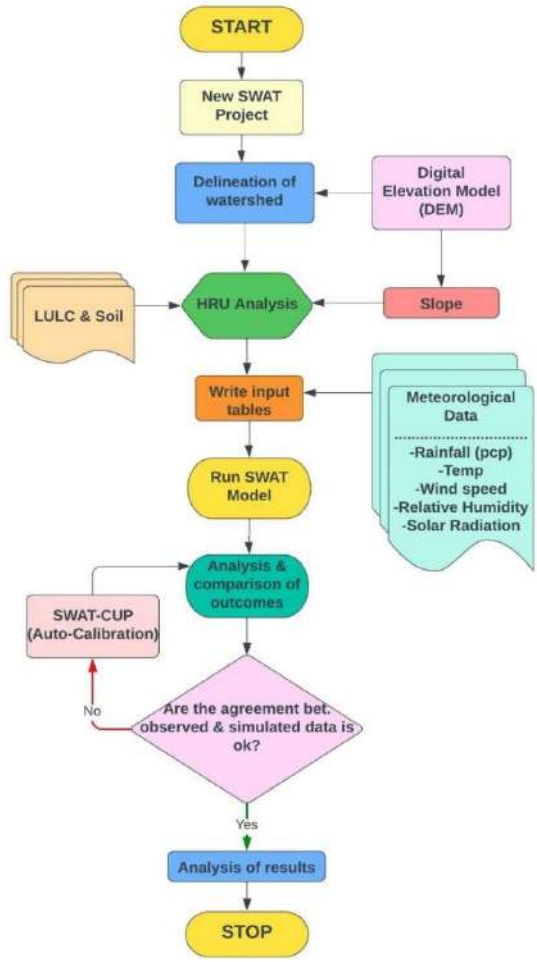

Fig. 6: Flow chart-SWAT Model.

Table 2: Detail of Soils.

Sr. No.	Class of Soil	Name of Soil	% of Soil
1.	Hh11-2bc-3711	Clay_Loam	7.3%
2.	I-Hh-3721	Loam	1.2%
3.	Vc43-3ab-3861	Clay	58.07%
4.	Vc45-3a-3864	Clay	33.30%

Calibration of SWAT

The calibration of the model consists of the systematic approach to adjust the model's parameters until the results show good agreement with observed field data (Zomorodian et al. 2017). Eq. (2) presents the calibration of the SWAT model (Beven 2006) (Fig. 7).

$$q(x,t) = M(\Theta,x,t) + \varepsilon(x,t) \quad \ldots(2)$$

Where,

q(x,t)- Volume of flow at time 't'

M (Θ,x,t)- Volume of flow at different parameters

ε (x,t)- error at a specific time.

Both manual and automatic calibration was carried out, with the parameters adjusted as necessary to fit the data collected (Guzman et al. 2015). The SWAT CUP tool was used for the calibration of the SWAT model with the SUFI-2 algorithm. Multiple iterations were performed to re-adjust the parameters to best match the observed values. The SWAT model was calibrated by using observed stream flow data from the year 2003 to 2012. However, the SWAT model is capable of a two-way calibration-validation and is reliable in modeling watersheds in the tempo-spatial aspect (Grusson et al. 2017, 2018). As a result, the calibration period of 2003–2012 was chosen, and it was contrasted with the same period of river flows. The R^2 value for calibration was observed at 0.80, and NSE was 0.72.

Validation of SWAT

After the calibration process, SWAT model validation involves putting the calibrated model to the test by observed field data (a few set of data that is not utilized in the calibration process) with the model predictions while maintaining the values of all input parameters (Moradi-Jalal et al. 2007). In the present work, to validate the model, the discharge data from the years 2013 to 2016 were used (Fig. 8). The R^2 value obtained during validation is 0.76, and NSE was 0.80.

RESULTS AND DISCUSSION

The following hydrological parameters (Table 3) were assessed to ascertain their sensitivity during the calibration and validation process. After trial and error, it was observed that the CN II, i.e., initial Soil Conservation System Number, SURLAG, and ESCO (The soil evaporation compensation factor) were highly sensitive parameters as their rank is higher. Initially, CN II was given by model was 90, but after the calibration process, CN II was best fitted to 78. The ESCO, EPCO, ALPHA_BF, SLSUBBSN, and groundwater delay time (GW_DELAY) these factors significantly affect the calibration process.

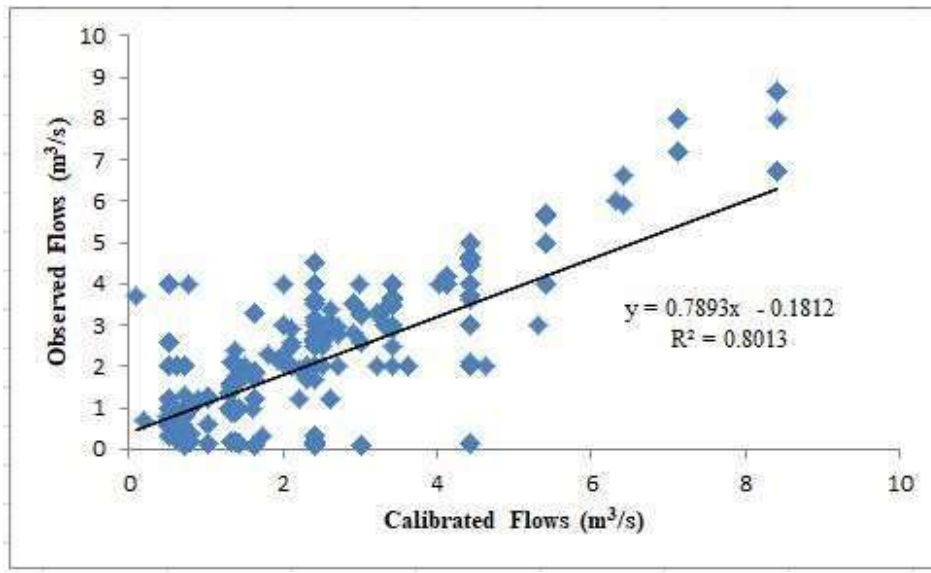

Fig. 7: Calibration of SWAT Model.

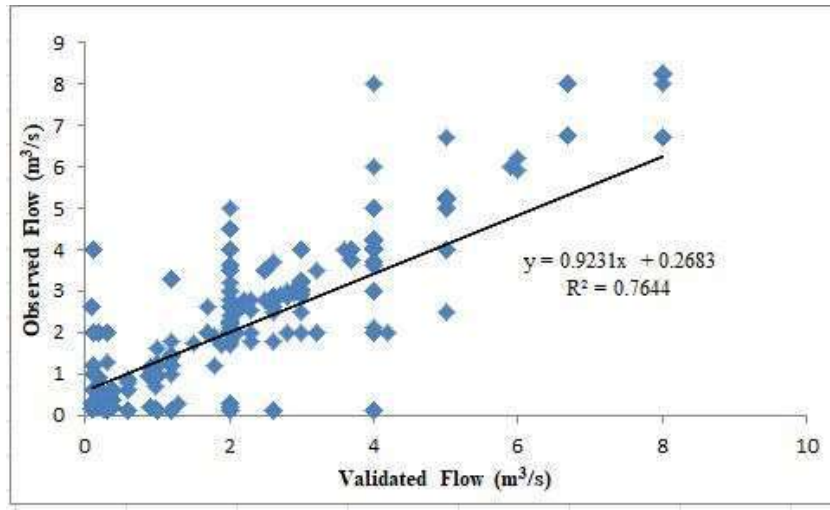

Fig. 8: Validation of SWAT Model.

Hydrology of Study Area

Fig. 10 shows the hydrological presentation of the study area. The average actual evapotranspiration of the study area is 398.4 mm, and precipitation is 978 mm. Table 4 explains the hydrological parameters in the calibration and validation process. The surface runoff from the basin was observed as 403.46 mm. The results show that the total sediment yield from the basin was 64.3 $x10^5$ $ton.ha^{-1}$ for the period of (2010-2020). Moreover, the sub-basins numbers 33, 34 & 35 are more prone to soil erosion & they must be treated for control of soil erosion.

Model Performance

For the present work to carry out calibration and validation, the SWAT-CUP tool with the SUFI II algorithm was used. Statistical parameters like NSE (Nash-Sutcliffe efficiency) and coefficient of determination (R^2) (Eq.4) were used to check the sensitivity of the work. The NSE is a widely used tool to determine the residual variance of hydrological models, and its formula is given by Eq.(3),

$$NSE = 1 - \left\{ \frac{\sum_{i=1}^{n} \left(Y_i^{obs} - Y_i^{sim}\right)^2}{\sum_{i=1}^{n} \left(Y_i^{obs} - Y_i^{mean}\right)^2} \right\} \quad \ldots(3)$$

Table 3: Ranges of parameter and their values used in the sensitivity analysis.

Abbreviations	Details of Parameters	Range	SWAT Values	Final Values
ALPHA_BF.gw	Baseflow factor (days)	0-1	0.045	0.01
CN.mgt	Initial SCS CN II value	35-98	90.97	78
ESCO.hru	Soil evaporation compensation factor	0-1	0.94	0.4
GW_DELAY.gw	Groundwater delay (days)	0-500	41	41
GWQMN.gw	Depth of water in the shallow aquifer	0-5000	1200	1280
REVAPMN.gw	Threshold depth of water in the shallow aquifer for "revap" to occur (mm)	0-1000	740	856
SURLAG.hru	Surface runoff lag time in the HRU (days)	0.05-24	3	0.5

Table 4: Assessment of hydrological parameters.

Parameters	Values in Calibration [mm]	%	Values in Validation [mm]	%	Average	%
Rainfall	978.7	100	992.3	100	985.5	100
Evapotranspiration	398.4	40.7	412.3	41.6	405.35	41.15
Lateral Flow	3.3	0.3	4.1	0.4	3.7	0.35
Surface Runoff	403.46	41.22	421.6	42.48	412.53	41.85
Deep Aquifer recharge	8.66	0.8	6.98	0.7	7.82	0.75
Shallow Aquifer storage	173.14	17.6	159.36	16.1	166.25	16.85
Return Flow	140.72	14.31	124.36	12.5	132.54	13.40

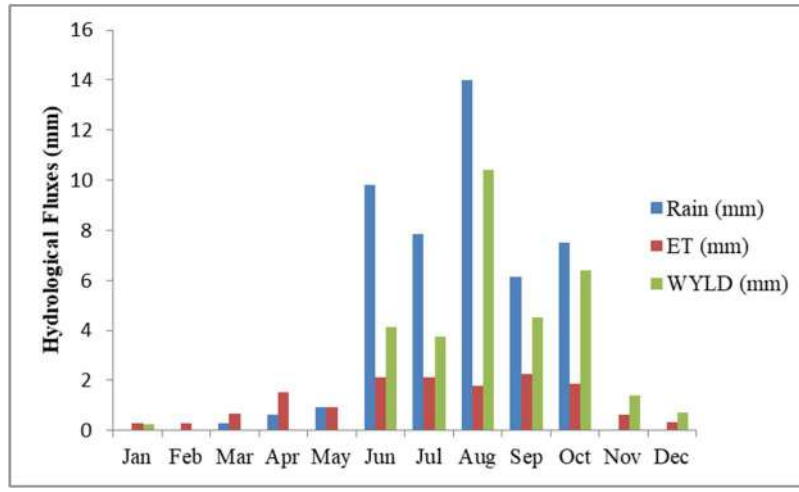

Fig. 9: Water budget.

Where, Y^{obs}= Observed data

Y^{sim} = Simulated data and Y^{mean} = Mean observed data

$$R^2 = \frac{[\sum_{i=1}^{n}(Oi-\overline{O})(Pi-\overline{P})]}{\sum_{i=1}^{n}\left[(Oi-\overline{O})\ \sum_{i=1}^{n}(Pi-\overline{P})^2\right]} \quad \ldots(4)$$

Water Budget

In the water budgeting of the study basin (Fig. 9), the SWAT model is calibrated and validated; the outputs of water balance are presented in (Table 5). The findings show that there is no significant variation between the two models.

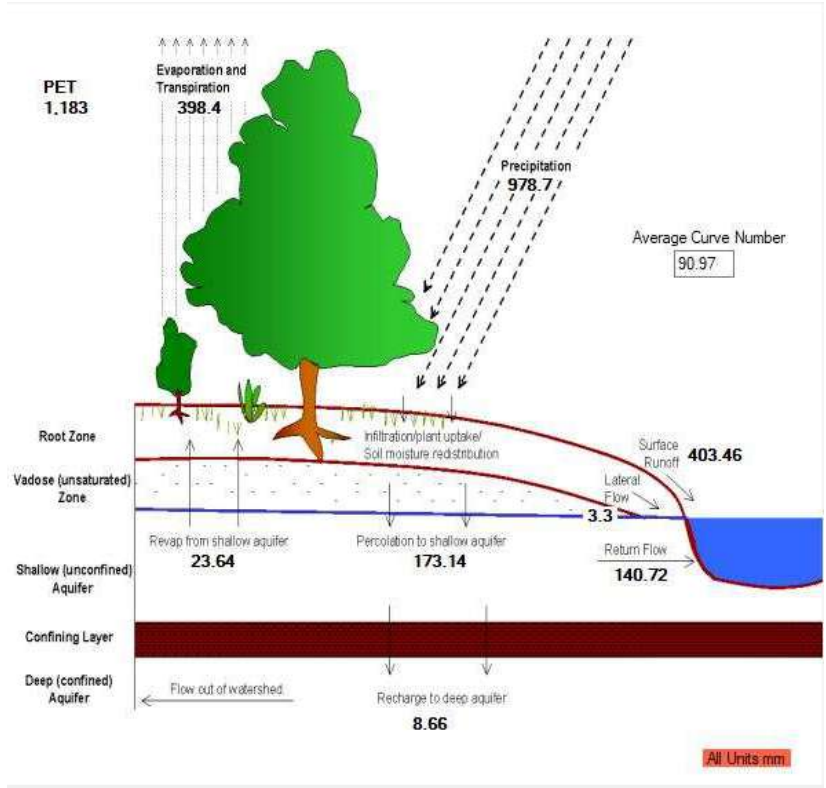

Fig. 10: Hydrology of the study area.

A few previous works (Moriasi et al. 2007) used both calibrated and verified data in their analysis and found that the results were not significantly different. The Yeralwadi area has an annual rainfall of about 978 mm. The major loss of water happens in terms evapotranspiration process and is one of the highly influencing hydrological components that accounts for 400 mm of water, i.e., 40.07% of total rainfall. The previous work (Kaleris & Langousis 2017, Kumar et al. 2015) has estimated the rate of evapotranspiration as the highest component within the catchment responsible for water loss. Moreover, the reasons for this higher loss are prevailing high temperatures, low precipitation, and low relative humidity trends.

Finally, the yearly total discharge was calculated to be 544.18 mm, or 55.6% of the annual precipitation (41.2% from surface runoff and 14.4% from baseflow). Moreover, the estimated percolations of the shallow and deep aquifers were 173.14 mm and 8.66 mm, or 17% and 0.8% of the annual precipitation, respectively. It was observed that despite a decade and separation of time between the calibration (2003-2012) and validation (2013-2016), the outcomes showed that the basin properties had not changed appreciably over more than a decade, as depicted in Fig. 10.

Available Water

The findings indicate that evapotranspiration accounts for around 40.07 % of the catchment's water loss. The remaining percentage is divided between the percolation tank and outflow (surface runoff, lateral flow, and return flow). By comparing the discharge metrics (Table 5), the surface runoff from the basin is greater than 40%. Moreover, the maximum rainfall was observed in July & August, which yields a high volume of runoff as maximum soil gets saturated, as shown in the hydrograph (Fig. 9), which aids the flood situation in the study basin. This scenario shows that there is a higher possibility that basin water users rely on surface runoff by storing excess water at the time of high flood season and utilizing it in the water deficit period.

The amount of water that percolates into the soil depends on its water-bearing capacity. It is crucial for calculating the amount of soil water that may be used to replenish aquifers. Around 173.14 mm means 17.69% of total rainfall volume is going to infiltrate shallow aquifers, and about 1% is added to deep aquifers. The shallow aquifer recharge is divided into 14.3% water loss as return flow that feeds the basin outlet. So, it is observed that the water table is at a low level, which holds a sufficient volume of water that can be utilized for irrigation. This scenario is validated by taking wells in shallow aquifers.

Table 5: Performance indicators used.

Statistical Parameters	During Calibration	During Validation
Coefficient of Determination (R^2)	0.80	0.76
Nash-Sutcliffe Efficiency (NSE)	0.72	0.80

Monthly average values for a few hydrologic components were calculated and are shown in Fig. 7. The rate of evapotranspiration progressively rises as seasons get wetter. During the dry season, it falls gradually. It also showed that the Yeralwadi catchment has a high water yield.

CONCLUSIONS

In current research work, the SWAT model was processed to estimate the surface water available in the Yeralwadi basin. The simulation work shows good statistical values for the Nash-Sutcliffe Efficiency (NSE > 0.8) and correlation coefficients R^2 (0.80) (Table 5). The model's performance was satisfactory (Table 6). The findings significantly increased our understanding of the water availability in the watershed, especially the surface runoff and the percolation tank. The shallow aquifer (depth up to 80 Feet) contains more water, which may be acquired for use with less input cost during the dry season. The findings also demonstrated the possibility for surface runoff that made up the majority of the total flow to be captured in well-designed water harvesting structures such as dams and ponds that may be used for irrigation and a variety of other uses during the dry seasons. Also, the SWAT model is able to estimate the sediment load transported from the basin, so vulnerable basins for soil erosion are also identified by SWAT.

ACKNOWLEDGMENT

The authors are thankful to the National Institute of

Table 6: Values/range of statistical parameters. (Moriasi et al. 2007, Nash & Sutcliffe 1970).

Performance ratings	NSE	R^2	Percentage bias [%]	
			Sediment	Flow
Very good	0.75-1	0.75 -1.00	< ± 15	< ± 10
Good	0.65-0.75	0.65-0.75	± 15 to ± 30	± 10 to ± 15
Satisfactory	0.50-0.65	0.50-0.65	± 30 to ± 55	± 15 to ± 25
Unsatisfactory	< 0.50	< 0.50	> ± 55	> ± 25

Hydrology, Belagavi, and PCETs Pimpri Chinchwad College of Engineering & Research, Ravet, Pune for their continuous support. Also, the authors extend gratitude to all those researchers, scientists, and authors who are doing great research work in this field.

REFERENCES

Abdalla, O.A.E. 2009. Groundwater modeling in semiarid central Sudan: Adequacy and long-term abstraction. Arab. J. Geosci., 2(4): 321-335.

Arnold, J.G., Srinivasan, R., Muttiah, R.S. and Williams, J.R. 1998. Large area hydrologic modeling and assessment part I: Model development. J. Am. Water Resour. Assoc., 34(1): 73-89.

Baalousha, H.M. 2016. Development of a groundwater flow model for the highly parameterized Qatar aquifers. Model. Earth Syst. Environ., 2(2): 141.

Beven, K. 2006. A manifesto for the equifinality thesis. J. Hydrol., 320(1-2): 18-36.

CGWB 2017. Aquifer maps and groundwater management plan. Report of Central Ground Water Board.

Dovie, D.B.K. and Kasei, R. A. 2018. Hydro-climatic stress, shallow groundwater wells, and coping in Ghana's White Volta basin. Sci. Total Environ., 636: 1268-1278.

Du, E., Tian, Y., Cai, X., Zheng, Y., Han, F., Li, X., Zhao, M., Yang, Y. and Zheng, C. 2022. Evaluating Distributed Policies for Conjunctive Surface Water-Groundwater Management in Large River Basins: Water Uses Versus Hydrological Impacts. Water Resour. Res., 14: 361-368.

Dutta, S. and Sen, D. 2018. Application of SWAT model for predicting soil erosion and sediment yield. Sustain. Water Resour. Manag., 4(3): 447-468.

Eini, M.R., Massari, C. and Piniewski, M. 2023. Satellite-based soil moisture enhances the reliability of agro-hydrological modeling in large transboundary river basins. Sci. Total Environ., 16: 873.

Guzman, J.A., Moriasi, D.N., Gowda, P.H., Steiner, J.L., Starks, P.J., Arnold, J.G. and Srinivasan, R. 2015. A model integration framework for linking SWAT and MODFLOW. Environ, Model. Software, 73: 103-116.

Jajarmizadeh, M., Sidek, L.M., Harun, S. and Salarpour, M. 2017. Optimal calibration and uncertainty analysis of SWAT for an arid climate. Air Soil Water Res., 10: 111-121.

Kaleris, V. and Langousis, A. 2017. Comparison of two rainfall–runoff models: effects of conceptualization on water budget components. Hydrol. Sci. J., 62(5): 729-748.

Kim, N.W., Chung, I. M., Won, Y.S. and Arnold, J.G. 2008. Development and application of the integrated SWAT-MODFLOW model. J. Hydrol., 356(1-2): 1-16.

Kumar, S., Raghuwanshi, N.S. and Mishra, A. 2015. Identification and management of critical erosion watersheds for improving reservoir life using hydrological modeling. Sustain. Water Resour. Manag., 1(1): 57-70.

Liu, L., Cui, Y. and Luo, Y. 2013. Integrated modeling of conjunctive water use in a canal-well irrigation district in the lower Yellow River Basin, China. J. Irrig. Drain. Eng., 139(9): 775-784.

Moradi-Jalal, M., Bozorg Haddad, O., Karney, B. W. and Mariño, M. A. 2007. Reservoir operation in assigning optimal multi-crop irrigation areas. Agric. Water Manag., 90(1-2): 149-159.

Moriasi, D.N., Arnold, J.G., Van Liew, M.W. and Bingner, R.L. 2007. Model evaluation guidelines for systematic quantification of accuracy in watershed simulations. Trans. ASABE, 50(3): 885-900.

Nash, J.E. and Sutcliffe, J.V. 1970. River flow forecasting through conceptual models: part I. A discussion of principles. J. Hydrol., 10(3): 282-290.

Neitsch, S.L., Arnold, J.G., Kiniry, J.R., Srinivasan, R. and Williams, J.R. 2002. Soil and Water Assessment Tool User's Manual. TWRI Report TR-192.

Neitsch, S.L., Arnold, J.G., Kiniry, J.R. and Williams, J.R. 2005. Soil and Water Assessment Tool: Theoretical Documentation Version 2005. Agricultural Research Service Blackland Research Center, Temple, Texas, USA.

Ninija Merina, R., Sashikkumar, M.C., Danesh, A. and Rizvana, N. 2019. Modeling technique for sediment evaluation at the reservoir (South India). Water Resour., 46(4): 553-562.

Oki, T., Agata, Y., Kanae, S., Saruhashi, T., Yang, D. and Musiake, K. 2001. Assessment of global water resources using integrative total flow paths. Hydrol. Sci. J., 46(6): 983-995.

Prabhanjan, A., Rao, E.P. and Eldho, T.I. 2015. Application of SWAT model and geospatial techniques for sediment-yield modeling in ungauged watersheds. J. Hydrol. Eng., 20(6): 1-6.

Ridoutt, B.G., Eady, S.J., Sellahewa, J., Simons, L. and Bektash, R. 2009. Water footprinting at the product brand level: case study and future challenges. J. Clean. Prod., 17(13): 1228-1235.

Ross, A. 2018. Speeding the transition towards integrated groundwater and surface water management in Australia. J. Hydrol., 567: e1-e10.

Sabale, R. and Jose, M. 2021. Hydrological modeling to study the impact of conjunctive use on groundwater levels in the command area. J. Indian Water Works Assoc., 53(3): 190-197.

Sabale, R. and Jose, M. 2022. Optimization of conjunctive use of surface and groundwater by using LINGO and PSO in water resources management. Innov. Infrastruct. Solut., 7(1): 545.

Sabale, R. and Jose, M. K. 2023. Conjunctive use modeling using SWAT and GMS for sustainable irrigation in Khatav, India. Lect. Notes Civ. Eng., 16: 373-386.

Sabale, R., Venkatesh, B. and Jose, M. 2023. Sustainable water resource management through conjunctive use of groundwater and surface water: A review. Innov. Infrastruct. Solut., 8(1): 1-12.

Samimi, M., Mirchi, A., Moriasi, D., Ahn, S., Alian, S., Taghvaeian, S. and Sheng, Z. 2020. Modeling arid/semi-arid irrigated agricultural watersheds with SWAT: Applications, challenges, and solution strategies. J. Hydrol., 590: 125418.

Santhi, C., Arnold, J.G., Williams, J.R., Dugas, W.A., Srinivasan, R. and Hauck, L.M. 2001. Validation of the SWAT model on a large river basin with point and nonpoint sources. J. Ame. Water Resour. Assoc., 37(5): 1169-1188.

Saraf, V.R. and Regulwar, D.G. 2018. Impact of climate change on runoff generation in the Upper Godavari River Basin, India. J. Hazard. Toxic Radio. Waste, 22(4): 04: 221.

Singh, A. 2014. Conjunctive use of water resources for sustainable irrigated agriculture. J. Hydro., 519: 1688-1697.

Stadnyk, T.A. and Holmes, T.L. 2023. Large scale hydrologic and tracer aided modeling: A review. J. Hydro., 9: 177.

Vairavamoorthy, K., Gorantiwar, S.D. and Pathirana, A. 2008. Managing urban water supplies in developing countries - Climate change and water scarcity scenarios. Phys. Chem. Earth, 33(5): 330-339.

Zomorodian, M., Lai, S.H., Homayounfar, M., Ibrahim, S. and Pender, G. 2017. Development and application of coupled system dynamics and game theory: A dynamic water conflict resolution method. PLoS ONE, 12(12): 650.

ORCID DETAILS OF THE AUTHORS

R. S. Sabale: https://orcid.org/0000-0003-4944-4625
S. S. Bobade: https://orcid.org/0000-0001-7839-1855

Nature Environment and Pollution Technology
An International Quarterly Scientific Journal

p-ISSN: 0972-6268
(Print copies up to 2016)
e-ISSN: 2395-3454

Vol. 23 | No. 1 | pp. 215-223 | 2024

Original Research Paper

https://doi.org/10.46488/NEPT.2024.v23i01.017

Open Access Journal

Enhanced Solar Photovoltaic Power Production Approach for Electric Vehicle Charging Station: Economic and Environmental Aspects

J. Techo*, S. Techo, A. Palamanit***, E. Saniso****, A. A. Chand***** and P. Prasannaa******†**

*Division of Industrial Technology, Faculty of Agricultural Technology and Industrial Technology, Nakhon Sawan Rajabhat University, 398 Sawanwithi Road, Mueang Nakhon Sawan, Nakhon Sawan 60000, Thailand

**Microbial Diversity and Bioproducts Research Unit, Mahidol University, Nakhonsawan Campus, Nakhonsawan 60130, Thailand

***Biomass Energy and Sustainable Technologies (BEST) Research Center, Energy Technology Program, Department of Specialized Engineering, Faculty of Engineering, Prince of Songkla University, 15 Kanjanavanich Rd., Hat Yai, Songkhla 90110, Thailand

****Industrial Physics Program, Faculty of Sciences Technology and Agriculture, Yala Rajabhat University, 133 Tesaban 3 Road, Amphur Muang, Yala 95000, Thailand

*****School of Information Technology, Engineering, Mathematics and Physics (STEMP), The University of the South Pacific, Suva, Fiji

******Department of Mechanical Engineering, AMET University, Chennai, Tamil Nadu, India

†Corresponding author: P. Prasannaa; prasannaina@gmail.com

Nat. Env. & Poll. Tech.
Website: www.neptjournal.com

Received: 23-05-2023
Revised: 27-06-2023
Accepted: 06-07-2023

Key Words:
EV charging station
Solar energy
Economic analysis
Carbon-free

ABSTRACT

In recent years, Electric Vehicles (EVs) are contributing a major share in Thailand and benefit the environment. Most of the EV charging stations are sourced from solar energy as it becomes a carbon-free source of energy production. Secondly, Thailand is rich in solar irradiance, and higher irradiance leads to higher power production. On the other hand, in tropical conditions, solar Photovoltaic (PV) module temperature increases following the solar irradiance due to high ambient temperature, resulting negative impact on the efficiency and lifespan of photovoltaic (PV) modules. Further, to increase PV power production, in this study, different rates of cooling strategies are proposed. The study found that reducing the temperature by 5% to 25% resulted in increased average power outputs of 5947.94W, 6021.43W, 6094.92W, 6168.41W, and 6241W, respectively. Notably, 25% of the cooling rate achieved higher production. However, it is lower than the nominal power production. Following that, economic analysis and environmental impacts are analyzed for Thailand's EV charging station using a different cooling rate of PV module. Overall, it is concluded that, depending on the economic viability of the EV charging station, cooling technology can be applied, and it will benefit the EV charging station both economically and environmentally. To further enhance the solar PV power production approach for EV charging stations in Thailand, it is imperative to prioritize future endeavors towards optimizing cooling technology, integrating energy storage, and implementing supportive policies.

INTRODUCTION

Electric vehicles (EVs) offer a promising alternative to fossil fuels in the transportation sector due to their increased energy efficiency and reduced local pollutants. However, the challenge remains to meet the energy demands of charging EV batteries using clean and renewable energy sources. Solar photovoltaic (PV) modules convert light photons into electricity and are a widely accepted future renewable energy technology (Velmurugan et al. 2020a, Bayrak et al. 2020, Homlakorn et al. 2023). However, PV module efficiency decreases as the cell temperature exceeds the optimal operating temperature. However, this can be addressed by adopting external cooling techniques (Prasannaa et al. 2021, Rajseakar et al. 2019, Velmurugan et al. 2021).

Active cooling techniques involve the use of pumps or fans to keep a flow of air or water over the front or rear of the PV panel, leading to higher PV performance rates than passive techniques (Teo et al 2012, Velmurugan et al 2022a, Velmurugan et al 2021). However, this method incurs higher expenditures associated with system upkeep and power

usage. Various studies have investigated the effectiveness of cooling techniques, including spraying water on the PV module's rear surface, using rectangular heat exchangers affixed to the rear, and forced air cooling (Velmurugan et al. 2022b). Colt et al. (2016) discovered that spraying water on the back surface of a PV module resulted in a 32% decrease in module temperature and a 57% increase in electrical efficiency. In a study conducted by Baloch et al. (2015), the performance of a PV module equipped with a rectangular heat exchanger (RHX) attached to the PV module's back surface was compared to that of a module without cooling. The maximum efficiency for cooling with an RHX was found to be 13.07%, compared to 7.82% for modules without cooling. Sajjad et al. (2019) explored the use of forced air cooling to improve PV module performance and compared their findings to those of uncooled modules. The results showed that adopting air cooling technology led to higher electrical efficiency and power ratios, with respective improvements of 7.2% and 6%.

In comparison, passive cooling techniques rely on the three fundamental heat transfer mechanisms of convection, conduction, and radiation. They can be improved by combining phase change materials (PCMs) and PV panels into a single module (Velmurugan et al. 2020b, Velmurugan et al. 2020c, Velmurugan et al. 2018). PCM-enclosed PV systems have been found to reduce PV module temperature and increase PV module efficiency. Hasan et al. (2015) utilized phase change material (RT25) with internal fins to regulate the temperature rise of a PV system. They investigated the thermal performance of different internal fin arrangements and discovered that incorporating PCM into the PV system resulted in a cell temperature below 29°C during the ambient temperature of 23°C. Nada et al. (2018) examined the effectiveness of pure PCM and PCM combined with Al_2O_3 nanoparticles and compared them with a conventional PV module. Three identical PV modules were used in the experiment, with two of them connected to the chosen PCMs and one serving as a reference. Their findings revealed that the PV temperature was reduced by 10.6°C and 8.1°C, respectively, and the PV module efficiency increased by 13.2% and 5.7%, respectively.

The above literature studies have shown that the most effective method of reducing the temperature of PV modules was through active cooling, resulting in a temperature reduction of 20 to 38% (Velmurugan et al. 2022a, Alktranee & Péter 2023, Agyekum et al. 2021). Meanwhile, the passive cooling method, which can reduce the temperature of the PV module most significantly, achieved a range of 15 to 30% (Nižetić et al 2021, Ali 2020, Hudișteanu et al 2021). In this study, general cooling systems are proposed with a cooling rate of 5-25 % with an incremental of 5 % rather than determining the particular cooling strategies.

- Depending on the EV charging station's economical strength, any existing cooling methods can be adopted.
- This study highlights the importance of using a variable rate of cooling strategies to improve the PV system power production.
- Further, the economic and environmental analysis are performed and compared with the nominal PV systems operation mode.

MATERIALS AND METHODS

In this study, different cooling rates are performed for the 15.5 kWp solar PV system and EV charging station. The last three years of meteorological data are downloaded from the NASA Powerlac open source to understand the nature of Thailand's solar potential. Further, different rates of PV module cooling power production and economic analysis are conducted, and the outcomes are compared by analyzing the environmental aspects to determine the necessity of PV module cooling under tropical climatic conditions in the northern part of Thailand. Fig. 1 shows the schematic view of the present study.

Electrical Power Output

The electrical power output of the 15.5 kWP solar PV system is calculated using the meteorological data of 2022. PV module electrical power outputs are the product of the maximum voltage and current obtained from the PV module using Eq (1) (Velmurugan et al. 2020a).

$$P = IV_o = \left[I_{ph} - I_s \left(e^{\frac{q(V+IR_s)}{NKT}} - 1 \right) - \frac{V + IR_s}{R_{sh}} \right] V_o \ldots (1)$$

Where,

$$I_s = I_{or} \left(\frac{T}{T_r} \right)^3 \left[\left(\frac{1}{T_r} - \frac{1}{T} \right) e^{\left(\frac{qE_g}{N} \right)} \right]$$

In the above-given equation, I_{ph} represents the photo-generated current, and I_s represents the saturation current. The elementary electron charge is denoted by q. The Boltzmann constant is represented by K(1.38×10^{-23} J/K), T represents the absolute temperature, T_r represents the reference temperature, and R_s arises from the resistance of the metallic contacts and the ohmic resistance of the material. R_{sh} is derived from the current leakage across the p-n junction or at the edges of the cell.

Economic Analysis

Net present value: A major component of analyzing the effects of investment and flow direction is the net present

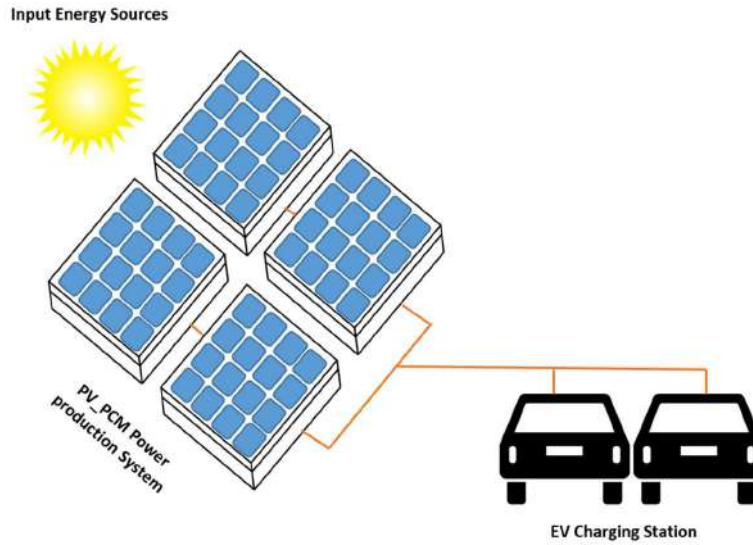

Fig. 1: Schematic view of study.

value (NPV), as expressed in Eq. (2). The overall capital investment, interest rate, discount rate, and the cost of running and maintaining the cooling system are all likely to be significant determinants of NPV (Nijmeh et al. 2020).

$$\text{Net present value (NPV)} = \sum_{t}^{T} \frac{C_t}{(1+r)^t} - C_0 . \quad ..(2)$$

Where C_t is the total cash with respect to the system lifespan, r is the interest or discount rate, which is often considered less than 5%, t is the total lifespan of the system, and C_0 is the cost of the capital investment.

Profitability index: The profitability index (PI) is directly proportional to the ratio of net present value and the initial investment cost of the cooling system, as expressed in Eq. (3) (Kijo-Kleczkowska et al. 2022). The profitability index is expected to be at least unity, which means the system is yielding no loss or yielding benefit. If the PI is less than 1, the total investment cost was not recouped during the system's lifespan.

$$\text{Profitability Index (PI)} = \frac{\text{NPV}}{\text{Capital investment}} \quad \ldots(3)$$

Payback period: The payback period is often analyzed in the economic analysis, which shows the payback time for the invested project, which is derived by capital investment and annual cash flow length as expressed in Eq. (4) (Souayfane et al. 2019).

$$\text{Payback period} = \frac{\text{Total investment}}{\text{Annual cash flow}} \quad ...(4)$$

Environmental Analysis

The reduction of CO_2, PM2.5, and NOx emissions associated with the use of PV systems is a significant benefit to the environment and public health. However, it is important to consider the entire lifecycle of the system, including production, operation, and disposal. In this study, we analyze the environmental impact of the enhanced solar PV power production approach with different cooling rates. The reduction in greenhouse gas emissions and other particulate matter associated with combustion processes can have significant positive impacts on air quality and public health.

RESULTS AND DISCUSSION

Meteorological and PV Module Temperature

The temperature of a photovoltaic (PV) module is affected by several factors, including ambient temperature, solar irradiation, relative humidity, and wind speed. Among these factors, ambient temperature has the most significant impact on the rise in PV module temperature. In Thailand, the climate is characterized by hot and humid conditions, with long, hot summers and mild winters. During the summer months of March to June, the PV module temperature can peak at 72°C, with an average temperature range of 58-65°C. In contrast, the moderate winter season lasts from November to February, and the peak temperature during this period is 61°C, with an average temperature range of 53-57°C. These temperature variations can affect the performance of PV systems in higher order.

Fig. 2(a-c) depicts weather data and operating temperatures of a photovoltaic (PV) system situated in Thailand. The

PV system's thermal stress is correlated with the ambient temperature, as demonstrated in Fig.2(a-c). This indicates that when the ambient temperature increases, so does the PV temperature. The impact of wind speed on the convection heat loss and gain from a PV surface is demonstrated in the same figure. The wind speed varies between 3.2 m/s and 7.2 m/s throughout the year, and the energy incident on the PV is determined by total daily irradiation. Total daily insolation and solar irradiation are highest during the summer and lowest during the winter. The average solar irradiation ranges from 679 W/m^2 to 975 W/m^2. Between winter and summer, a difference of 30.35% is noted. Relative humidity varies throughout the year due to seasonal changes in temperature and moisture content in the air. During summer, the average relative humidity is 54% and can reach a maximum of 82%. Warmer air has a higher capacity to hold moisture, so the relative humidity tends to be lower.

In contrast, during winter, the relative humidity ranges from 80% to 94%. Colder air has a lower capacity to hold moisture, resulting in higher relative humidity levels as the air becomes saturated more easily. These variations in temperature and moisture content contribute to the fluctuation of relative humidity throughout the year. Ambient temperature and relative humidity have an inverse relationship; when the ambient temperature rises, relative humidity drops, and vice versa.

PV Module Power Profile Under Variable Cooling

Fig. 3 illustrates the power production for 2022. The solar irradiance was followed without any temperature loss, resulting in nominal electrical power generation. However, real-time power conversion was greatly affected by the TPV rise, leading to an average actual power output of 5874.46 W, which is less than the average nominal power of 6600.27 W. The power loss is the difference between the nominal and actual power, and the maximum power loss in the system was found to be 725.81 W. To address this issue, researchers have used PCM and sensible materials as cooling materials to reduce the module temperature by 15 to 30%. The purpose of this study was to determine the maximum power production achievable by reducing the module temperature by 5% to 25%. The findings indicated that a reduction in temperature ranging from 5% to 25% resulted in an average power output of 5947.94W, 6021.43W, 6094.92W, 6168.41W, and 6241.90W, respectively. Without a cooling system, the maximum actual energy output was 26617kWh. However, with the implementation of a PV temperature reduction system, the energy output was enhanced, resulting in 26950kWh, 27283kWh, 27616kWh, 27949kWh, and 28282kWh for temperature reductions of 5%, 10%, 15%, 20%, and 25%, respectively. Notably, a 25% reduction in temperature led to a maximum energy output that was 1665kWh higher than that of a PV system without cooling.

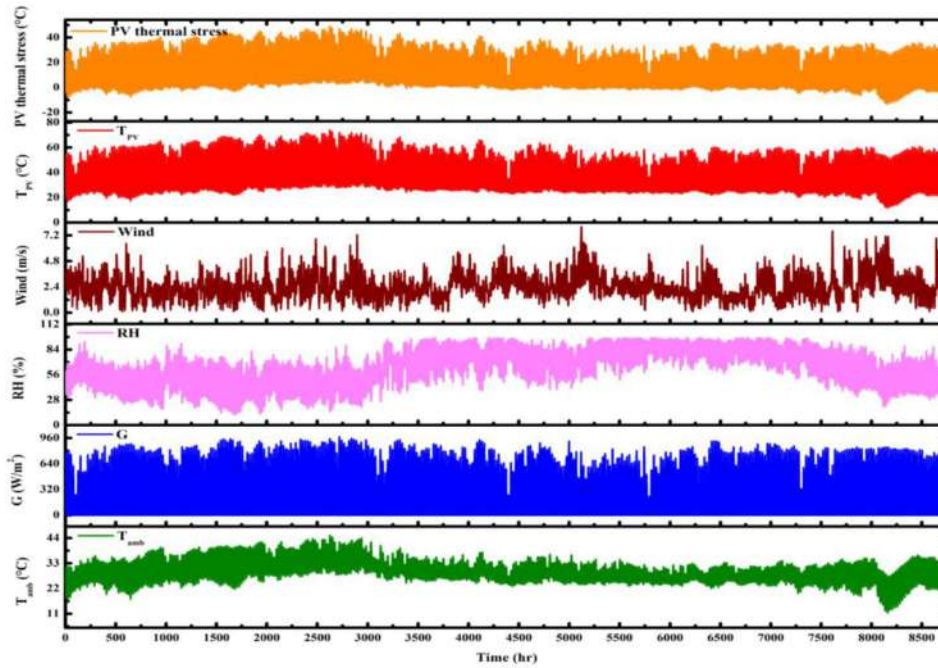

(a)

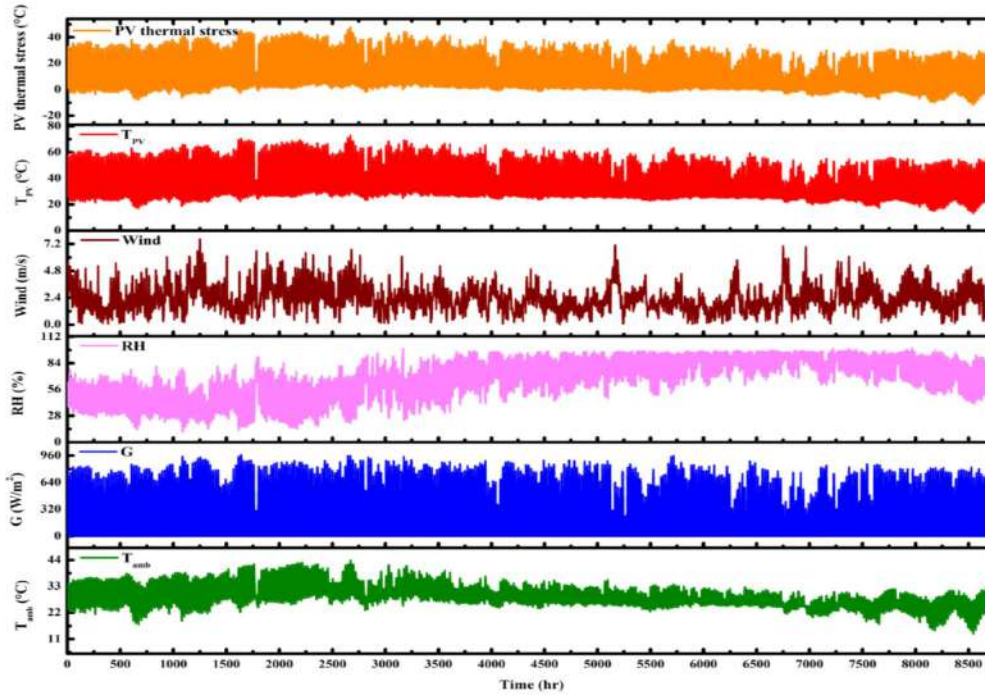

(b)

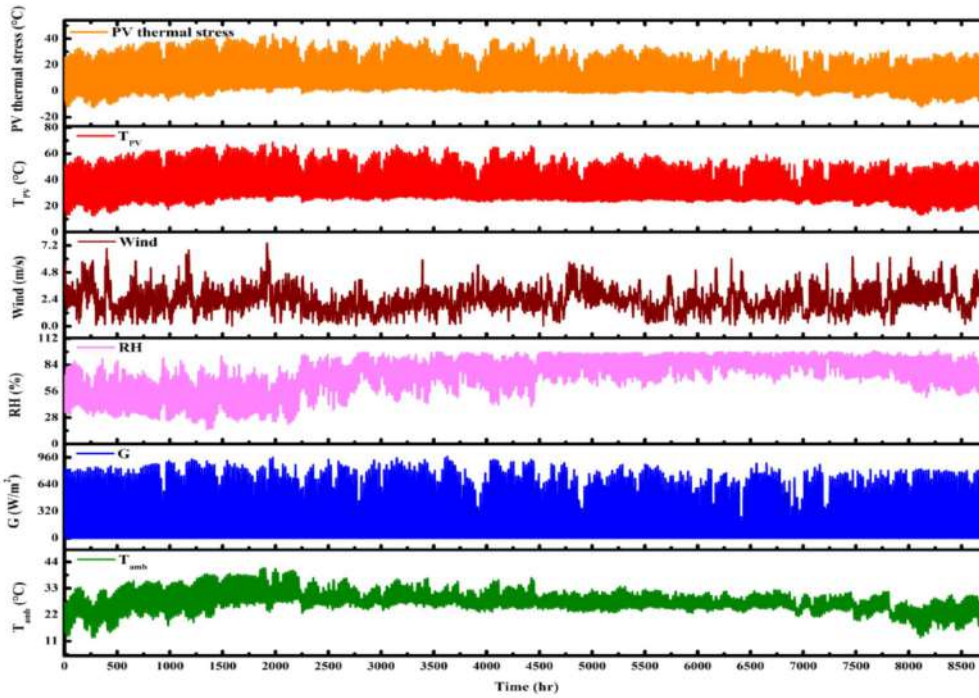

(c)

Fig. 2: Meteorological, PV module temperature and stress profile for (a) 2020, (b) 2021, and (c) 2022.

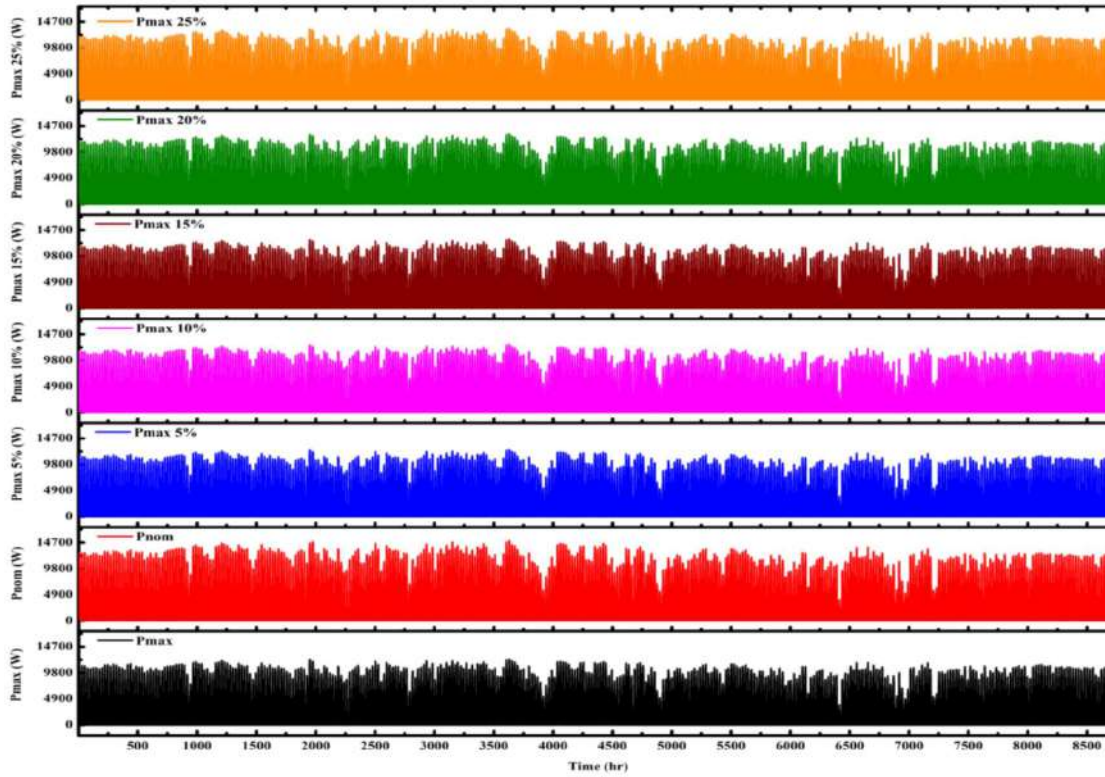

Fig. 3: PV module power profile under variable cooling for the year 2022.

Economic Analysis

The economic study is performed for a different cooling rate of 15.5 kWp in a solar system, as shown in Fig.4. Net Present Value (NPV) is a financial metric that calculates the present value of future cash flows for an investment or project using a discount rate. The NPV for a traditional PV system is 1410191.07, while for a PV cooling system with temperature reductions of 5%, 10%, 15%, 20%, and 25%, shows the NPV of 26108.39, 52202.72, 78297.06, 104391.4, and 130485.7 which is higher than the traditional PV system, indicating a positive return on investment.

The payback period for cooling methods with a 15.5 kWp PV system depends on various factors, including initial costs, energy savings, and electricity costs. It is found that a shorter payback period of 4.44, 4.39, 4.34, 4.29, and 4.24 years is attained as compared to conventional PV, which has a payback period of 4.5 years because the higher power output of the 15.5 kWP solar system with a cooling model generates higher power resulting in higher revenue attained.

The profitability index (PI) is a financial metric that evaluates the potential profitability of an investment. The PI increases linearly as the module temperature decreases, with a 25% reduction leading to a PI of 2.56 for the PV-PCM system. PI greater than 1 indicates a positive return on investment, with higher values indicating greater profitability. The savings for a 5% to 25% temperature reduction in a PV-PCM system range from 1.17% to 7.36%, which is 7.36% higher than conventional PV modules for a 25% temperature reduction.

Environmental Analysis

Cooling the PV module plays a significant role in reducing CO_2 emissions, which contribute to climate change. By reducing the temperature of PV modules, the efficiency of the solar cells is improved. This means that more electricity can be generated with the same amount of irradiance. This increased efficiency leads to a reduction in CO_2 emissions per unit of electricity generated. Fig. 5 shows that 5%, 10%, 15%, 20%, and 25% of module temperature reductions resulted in 13475, 13475, 13808, 13974, and 14141 kg of CO_2 reduction, respectively.

In addition to directly reducing PM2.5 concentrations, cooling the PV module can also indirectly reduce PM1.5 emissions by decreasing the demand for electricity from fossil fuel sources, which are major contributors to PM2.5 emissions. This indirect effect can have a significant impact, particularly in areas where fossil fuels are heavily used.

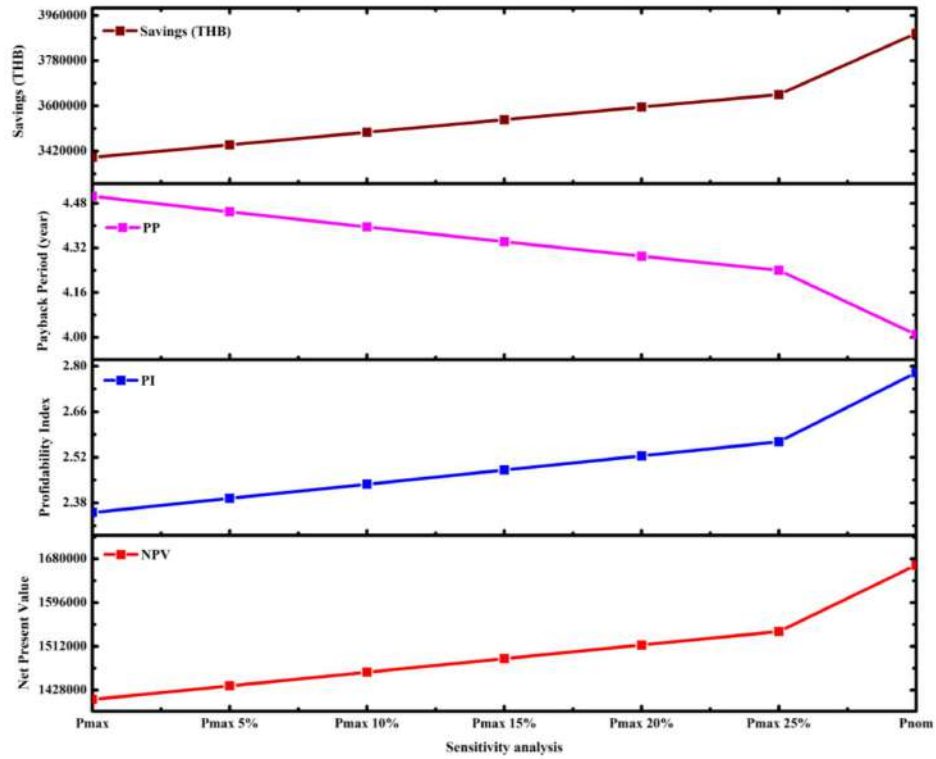

Fig. 4: Economic analysis of 15.5 kWp solar PV-powered EV charging station.

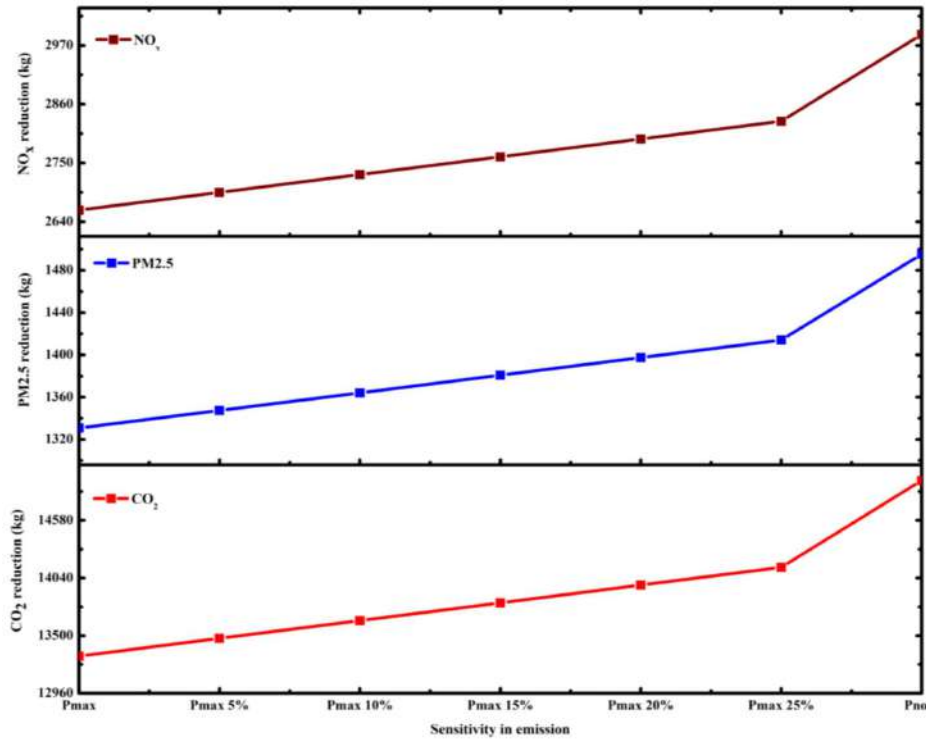

Fig. 5: Environmental Analysis of 15.5 kWp solar PV-powered EV charging station.

Based on Fig. 5, reducing module temperature by 25% results in a reduction of 1414 kg of PM2.5.

NOx refers to a group of nitrogen oxide gases produced by combustion processes, such as those used in power plants and transportation. NOx is a significant air pollutant and contributes to a range of environmental and health problems, including acid rain, smog, and respiratory diseases. Reducing NOx emissions is a crucial goal for improving public health and promoting a cleaner and more sustainable environment. Overall, cooling the PV modules will reduce NOx emissions and promote a cleaner and more sustainable environment. According to Fig. 5, module temperature reduction results in reductions of 2695 kg, 2728 kg, 2761 kg, 2794 kg, and 2825 kg in NOx, respectively.

CONCLUSION

This investigation aimed to assess the technical and economic feasibility of the improved PV power production by reducing the module temperature by 5-25%. The study evaluated the impact of different cooling rates on a 15.5 kWp solar PV system to recommend the EV charging station in tropical conditions of Thailand. The results showed that a 25% reduction in PV module temperature led to an increase of 1665kWh in energy production, surpassing the energy output of a PV system without cooling. Furthermore, the economic analysis of Net Present Value (NPV), Profitability Index (PI), and Payback Periods (PP) indicated a positive return on investment, suggesting that cooling technology is a feasible and economically viable option. In addition to the economic benefits, the reduction of greenhouse gas emissions, PM2.5, and NOx emissions can have significant positive impacts on the environment and public health.

In conclusion, the study suggests that the application of cooling technology can be beneficial for the EV charging station, both economically and environmentally. However, the decision to implement the cooling technology must be based on the economic viability of the EV charging station. Future efforts should focus on optimizing cooling technology, integrating energy storage, and implementing supportive policies to further enhance the solar PV power production approach for EV charging stations in Thailand.

REFERENCES

Agyekum, E.B., Kumar, S.P., Alwan, N.T., Velkin, V.I., Shcheklein, S.E. and Yaqoob, S.J. 2021. Experimental investigation of the effect of a combination of active and passive cooling mechanisms on the thermal characteristics and efficiency of solar PV modules. Inventions, 6(4): 63.

Ali, H.M. 2020. Recent advancements in PV cooling and efficiency enhancement integrating phase change materials based systems: A comprehensive review. Solar Energy, 197: 163-198.

Alktranee, M. and Péter, B. 2023. Energy and exergy analysis for photovoltaic modules cooled by evaporative cooling techniques. Energy Rep., 9: 122-132.

Baloch, A.A.B., Bahaidarah, H.M.S., Gandhidasan, P. and Al-Sulaiman, F.A. 2015. Experimental and numerical performance analysis of a converging channel heat exchanger for PV cooling. Energy Convers. Manage., 103: 14-27.

Bayrak, F., Oztop, H.F. and Selimefendigil, F. 2020. Experimental study for the application of different cooling techniques in photovoltaic (PV) panels. Energy Convers. Manage., 212: 112789.

Colt, G. 2016. Performance evaluation of a PV panel by rear surface water active cooling. 2016. Int. Conf, Appl. Theort.. Electr., 16: 1474.

Hasan, A., McCormack, S.J., Huang, M.J., Sarwar, J. and Norton, B. 2015. Increased photovoltaic performance through temperature regulation by phase change materials: Materials comparison in different climates. Sol. Energy, 115: 264-276.

Homlakorn, S., Velmurugan, K., Suksri, A. and Wongwuttanasatian, T. 2023. Comparative study for photovoltaic cooling using metal mesh inserted eutectic phase change material enclosure. Case Stud. Therm. Eng., 45: 103024.

Hudișteanu, S.V., Țurcanu, F.E., Chereches, N.C., Popovici, C.G., Verdeș, M. and Huditeanu, I. 2021. Enhancement of PV Panel Power Production by Passive Cooling Using Heat Sinks with Perforated Fins. Appl. Sci., 11(23): 11323.

Kijo-Kleczkowska, A., Bruś, P. and Więciorkowski, G. 2022. Profitability analysis of a photovoltaic installation - A case study. Energy, 261: 125310.

Nada, S.A., El-Nagar, D.H. and Hussein, H.M.S. 2018. Improving the thermal regulation and efficiency enhancement of PCM-Integrated PV modules using nanoparticles. Energy Convers. Manage., 166: 735-743.

Nijmeh, S., Hammad, B., Al-Abed, M. and Bani-Khalid, R. 2020. A technical and economic study of a photovoltaic–-phase change material (PV-PCM) system in Jordan. Jordan J. Mech. Ind. Eng., 14: 371-379.

Nižetić, S., Jurčević, M., Čoko, D. and Arıcı, M. 2021. A novel and effective passive cooling strategy for photovoltaic panels. Renew. Sustain. Energy Rev., 145: 111164.

Prasannaa, P., Ramkumar, R., Sunilkumar, K. and Rajasekar, R. 2021. Experimental study on a binary mixture ratio of fatty acid-based PCM integrated to PV panel for thermal regulation on a hot and cold month. Int. J. Sustain. Energy, 40(3): 218-234.

Rajasekar, R., Prasannaa, P. and Kumar, R. 2019. Efficiency of Solar PV Panel by the Application of Coconut Fibres Saturated by Earthen Clay Pot Water. Environ. Technol., 42: 1-12.

Sajjad, U., Amer, M., Ali, H.M., Dahiya, A. and Abbas, N. 2019. Cost-effective cooling of photovoltaic modules to improve efficiency. Case Stud. Thermal Eng., 14: 100420.

Souayfane, F., Biwole, P.H., Fardoun, F. and Achard, P. 2019. Energy performance and economic analysis of a TIM-PCM wall under different climates. Energy, 169: 1274-1291.

Teo, H.G., Lee, P.S. and Hawlader, M. 2012. An active cooling system for photovoltaic modules. Appl. Energy, 90: 309-315.

Velmurugan, K., Karthikeyan, V., Korukonda, T.b., Kuppusamy, M., Emsaeng, K., Sukchai, S., Sirisamphanwong, C., Wongwuttanasatian, T., Madurai Elavarasan, R., Haes Alhelou, H. and Subramaniam, U. 2020b. Experimental Studies on PV Module Cooling with Radiation Source PCM Matrix. IEEE Access, PP: 1-1.

Velmurugan, K., Karthikeyan, V., Korukonda, T.B., Poongavanam, P., Nadarajan, S., Kumarasamy, S., Wongwuttanasatian, T. and Sandeep, D. 2020c. Experimental studies on photovoltaic module temperature reduction using eutectic cold phase change material. Solar Energy, 209: 302-315.

Velmurugan, K., Karthikeyan, V., Sharma, K., Korukonda, T.B., K, V., Balasubramanian, D. and Wongwuttanasatian, T. 2022b. Contactless phase change material based photovoltaic module cooling: A statistical

approach by clustering and correlation algorithm. J. Energy Storage, 53: 105139.

Velmurugan, K., Kumarasamy, S., Wongwuttanasatian, T. and Seithtanabutara, V. 2021. Review of PCM types and suggestions for an applicable cascaded PCM for passive PV module cooling under tropical climate conditions. J. Cleaner Prod., 293: 126065.

Velmurugan, K., Madurai Elavarasan, R., De, P., Karthikeyan, V., Korukonda, T.B., Arockia Dhanraj, J., Emsaeng, K., Chowdhury, M., Techato, K., Khier, B. and Attia, E.A. 2022a. A review of heat batteries based PV module cooling: Case studies on performance enhancement of large-scale solar PV system. Sustainability, 14: 1-65.

Velmurugan, K., Sirisamphanwong, C. and Sukchai, S. 2018. Investigation on Thermal Absorptivity of PCM Matrix Material for Photovoltaic Module Temperature Reduction. Key Eng. Mater., 777: 97-101.

Velmurugan, K., Sirisamphanwong, C., Sukchai, S., Sahoo, S.K. and Wongwuttanasatian, T. 2020a. Reducing PV module temperature with radiation-based PV module incorporating composite phase change material. J. Energy Storage, 29: 101346.

ORCID DETAILS OF THE AUTHORS

J. Techo: https://orcid.org/0009-0004-3937-3709
S. Techo: https://orcid.org/0000-0002-7346-6050
A. Palamanit: https://orcid.org/0000-0003-2833-9754
E. Saniso: https://orcid.org/0000-0002-3665-1580
A.A. Chand: https://orcid.org/0000-0002-1478-0680
P.Prasannaa: https://orcid.org/0000-0001-8972-5785

Nature Environment and Pollution Technology
An International Quarterly Scientific Journal

p-ISSN: 0972-6268
(Print copies up to 2016)
e-ISSN: 2395-3454

Vol. 23 | No. 1 | pp. 225-233 | 2024

Original Research Paper

https://doi.org/10.46488/NEPT.2024.v23i01.018

Open Access Journal

Integrated Riverside Development Along Adyar River, Chennai

S. Indhu Kirthika† and R. Shanmuga Priyan

Department of School of Planning, Architecture and Design Excellence, Hindustan Institute of Technology and Science, Chennai, India

†Corresponding author: Indhu Kirthika S.; ar.kirthika98@gmail.com

Nat. Env. & Poll. Tech.
Website: www.neptjournal.com

Received: 29-05-2023
Revised: 18-07-2023
Accepted: 26-07-2023

Key Words:
Riverside planning
River zoning and regulation
Integrated riverside development
River front development

ABSTRACT

Integrated Riverside Development (IRD) is a planning approach that aims to achieve sustainable development of urban areas located along riverbanks. To implement this IRD with controlled regulations, the study is focused on developing a comprehensive riverside development and river zoning regulatory framework that integrates all five main elements, with particular emphasis on economic, ecological, and social factors, in order to reduce encroachment and pollution in the study area. The objectives of the study include analyzing the current land use, recreational parks, encroachments, pollution levels, sewage disposal patterns, and solid waste dumping zones in the study area, as well as studying the socio-economic and eco-environmental aspects of the area. Additionally, identifying and analyzing the major threats to the river and developing a river zoning regulatory framework using the land use matrix technique is also included in the study objectives. The study area (Adyar River) was chosen based on social, ecological, and economic factors, and data was collected through surveys and from government offices. Using the land use matrix method, proposals for riverside development were made, and the zones were classified into development-prohibited, development-restricted, and development-optimized zones. The zones were classified based on the calculated values of Eco sensitivity for each of the three zones. Proposals were then given based on these classified zones, and the levels of development potential were determined. The proposed zoning regulatory framework is expected to have a significant impact in reducing further encroachments and improving connectivity between the city and the river. By considering socio-economic, ecological, and environmental aspects, the study recommends appropriate zoning regulations for riverfront developments that promote sustainable growth.

INTRODUCTION

Rivers have long been a human settlement's lifeline. Humans originally plowed the very first lines along the rivers, creating the groundwork for the development of cities (Barve & Sen 2011). Rivers were important elements of the social fabric and have rapidly changed due to shifts in their usage, urbanization pressures, and the declining health of river systems. Then came the era of environmental protection and the rebirth of rivers through a much more comprehensive instrument: river rejuvenation and urban riverfront development to focus on all the physical, social, cultural, and heritage dimensions of the river that fills urban settlements once more. The challenge in recent years has been integrating waterways with urban areas (Barve & Sen 2011). Riverfront development is a way to integrate the river into the growth of the urban fabric that is environmentally favorable. Rivers are being rediscovered in cities all around the world with the idea of integrated riverside development (IRD), which encompasses physical, social, economic, ecological, and management aspects (Vriddhi 2017). Integrated riverside development (IRD) is a planning approach that focuses on the sustainable development of urban areas located along riverbanks (Gharge 2016). The aim of IRD is to improve the overall quality of life for residents, as well as to protect and enhance the natural environment of the river and its surroundings. Integrated riverside development (IRD) can be implemented with zoning regulations to ensure sustainable development and meet the needs of the local community. Zoning regulations can help create mixed-use zones, set height, and setback requirements, preserve green spaces, and promote sustainability. They play a critical role in the success of IRD projects by ensuring that the development is in line with the overall goals of the project.

It has been determined that according to the literature review and case study, there are safety concerns (Darshini & Lathia 2019), weak regulations for riverside construction, environmental problems like channelization, declining water quality, elimination of riparian vegetation, etc. and flooding

problems (Bhavna & Vimwala 2015) These aforementioned problems will be addressed by integrating 3 factors of riverfront's economic, social, and ecological components (Xuejun Duan 2021). The research gap identified from the literature review and case studies was the lack of zoning restrictions for riverfront planning in both national and international contexts. This gap presents significant challenges in achieving sustainable riverfront development. Therefore, the research aims to address these difficulties by taking into account the parameters identified from the literature review and case studies.

The aim is to develop a comprehensive regulatory framework for riverside development and river zoning to reduce encroachment and pollution in the study area. To achieve this goal, several objectives were framed. Firstly, the current land use, proportion of recreational parks, encroachments, pollution levels, sewage disposal patterns, and solid waste dumping zones in the study area were analyzed to determine the river regulation zoning. Secondly, the socio-economic and eco-environmental aspects of the study area were studied. Thirdly, the major threats to the river were identified and analyzed. Finally, a river zoning regulatory framework was developed using the land use matrix technique. The zoning regulatory framework will have a significant impact on reducing further encroachments, and it will facilitate better connectivity between the city and the river. By considering socio-economic, ecological, and environmental aspects, the study can recommend appropriate zoning regulations for riverfront developments that promote sustainable growth. This will help to create a balance between the developmental needs of the city and the conservation of the river for future generations. The integrated development of riversides involves various factors such as social, economic, environmental, and infrastructural aspects. However, due to the time constraints and the specific aim of the study, the research is limited to analyzing the socio-economic and eco-environmental factors only.

MATERIALS AND METHODS

The site for this study was selected based on three main factors: social, ecological, and economic. In the secondary data collection stage, a reconnaissance survey was conducted, and a base map was prepared and identified the parameters for the socioeconomic and ecological factors. The primary

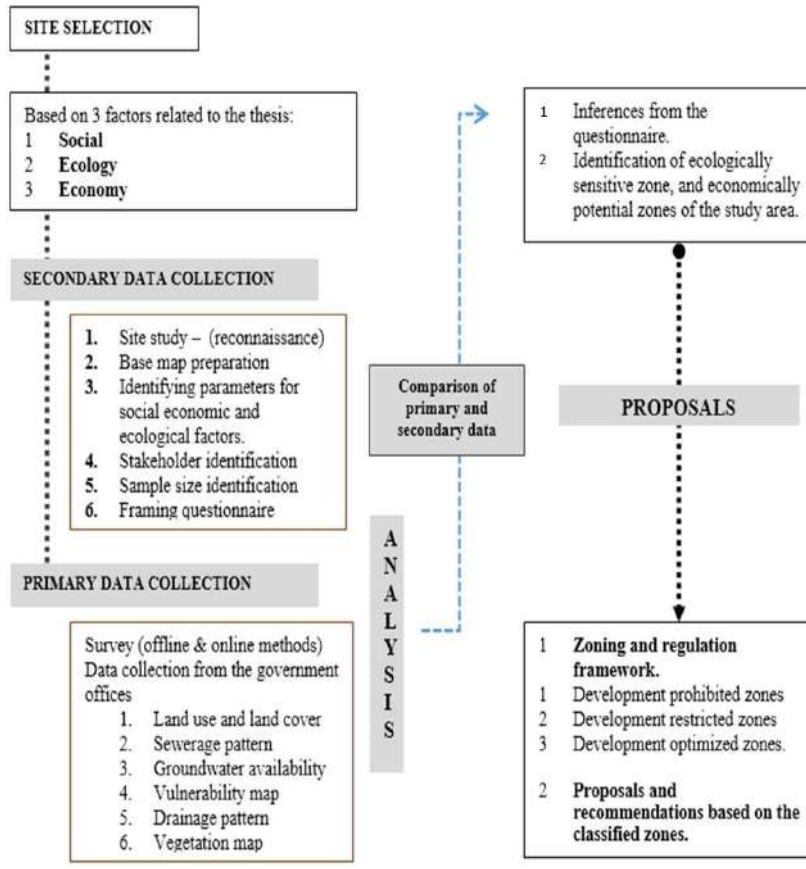

Fig. 1: Methodology flow chart.

data collection was conducted through surveys, both online and offline methods, and data was collected from government offices. Both primary and secondary data were then compared and analyzed to draw inferences. The proposals for riverfront development were made using the land use matrix method (Barve & Sen 2011), and the zones were classified into development-prohibited, development-restricted, and development-optimized zones (Xuejun Duan 2021). This zoning framework has the potential to reduce further encroachments along the river and to better connect the city and the river, thus contributing to the sustainable development of the area (Fig. 1).

Study Area

Chennai is a major city in southern India, located on the east coast of the country in the state of Tamil Nadu. The selected study area is the Adyar River, which is located in the city of Chennai, Tamil Nadu, India. Its latitude and longitude coordinates are approximately 13.0059° N, 80.2566° E. The Adyar River has great significance for the people of Chennai, as it is a major source of water for the city and also serves as a natural habitat for various aquatic species. The selected study area covers an area of 11.9 sq. km. It includes a 7.6 km stretch of the Adyar River, along with settlements situated within 500 m on either side of the river. The Adyar River is located in the southern part of Chennai, the capital city of the Indian state of Tamil Nadu. The river originates from the Chembarambakkam Lake in the west. It flows for approximately 42 km, and it is divided into two main stretches - the upstream stretch from Malaipattu to Guindy and the downstream stretch from Guindy to the estuary before emptying into the Bay of Bengal in the east. The soil type in the Adyar River basin is predominantly sandy and clayey. The climate of the Adyar River basin is tropical, with a hot and humid summer season and a mild winter season. The average annual rainfall in the Adyar River basin is approximately 1,300 mm. Adyar River has good connectivity to major roads and public transportation in Chennai.

As per the 2011 census, the study area has a total population of 3.5 lakhs. The study area is divided into wards for convenience to take survey and analysis. In each ward, 25 samples will have been taken, resulting in a total of 198 samples for the entire study area.

Analysis

Socio-economic analysis: The study area, including the Adyar and Kodambakkam zones, is characterized by various socio-economic factors, including occupation, education, income, and housing conditions. The Adyar zone has witnessed a high influx of Migrants due to the availability of employment opportunities and housing options. However, there is a disparity in the quality of housing between different areas, with the Thideer Nagar and Malligai Poonagar slums having a significant number of kutcha houses. The settlements along the riverbanks are primarily informal, with open defecation being common in the Adyar and Kodambakkam areas. Solid waste management is also a significant issue, with only a small fraction of waste being collected from doorsteps and the common disposal areas not being regularly cleaned. These factors highlight the need for efforts to improve housing conditions, provide services equitably, and develop effective solid waste management systems in the study area.

Eco-environmental analysis: Environmental and ecological aspects are crucial in the zoning of rivers to ensure sustainable use and conservation of the river ecosystem. River zoning regulations can minimize human activities that can negatively impact the river and its surroundings, thereby protecting the long-term health and well-being of both the river and the communities that depend on it. In the surveyed Adyar and Kodambakkam zones, the majority of the water supply comes from community water schemes, water boards, and bore wells. In contrast, surface water is relied on by those living along the river banks, especially in slums. The water quality of the Adyar River is extremely poor in all three zones, with the Adyar zone being the most severely impacted. Poor water quality has significant health impacts, including the spread of illnesses among those living in the surrounding areas. The Adyar zone is also highly affected by waterlogging and flooding incidents during the monsoon season and cyclones, causing severe damage to property and infrastructure, disrupting transportation and communication, and potentially leading to loss of life.

Threats and Suggestions

The Adyar River in Chennai, India, is facing severe environmental and ecological issues due to human activities. The river is polluted with domestic waste and plastic, indicating improper waste disposal by people living along the riverbanks. Urbanization and encroachments have significantly reduced the river's width, leading to sediment displacement, habitat loss for aquatic species, and an increased risk of flooding. Communities living near the Adyar River are concerned about the negative impacts of solid waste disposal and sewage on the river's health. They are urging the government to implement stricter waste disposal laws and build more sewage treatment plants. The direct discharge of urban wastewater, irregular solid waste dumps, and conversion of agricultural lands into commercial or residential plots due to urbanization are all contributing factors to the declining quality of river water.

Land Use Matrix Method

The Land Use Matrix Method is a commonly used approach in urban planning and land management to determine the best possible use of land within a certain area. In the context of the Adyar River, this method has been used to classify different zones along the river into development-prohibited, development-restricted, and development-optimized zones based on factors such as ecological sensitivity and economic development potential.

The land use matrix method involved the identification of vacant lands within a 3 km radius on both sides of the study area. These vacant lands were then analyzed based on ecological and economic development potential factors (Gharge 2016). For ecologically sensitive zones, parameters such as proximity to nature reserve zones, flood plains, and CRZ zones were considered. On the other hand, the economic development potential zone was analyzed based on the waterway grade and transport conditions (Xuejun Duan 2021)

The assessment of ecological sensitivity represents the evaluation of the environmental vulnerabilities and ecological functions of nature reserve zones, flood plains, and coastal regulation zones. This assessment helps to ensure the preservation of the integrity, stability, and interconnectedness of these areas. Similarly, the economic development potential assessment represents the value of the riverside in terms of socio-economic development. This includes consideration of factors such as waterway grade and transport conditions to determine the suitability of the area for future development (Xuejun Duan 2021) (Fig. 2).

Assessment Method for Ecological Sensitivity in Land Use Matrix Method

Ecological sensitivity is assessed based on the proximity of the identified vacant lands to the selected parameters, such as nature reserve zones, flood plains, and CRZ zones. Compliance with national standards is also an essential consideration.

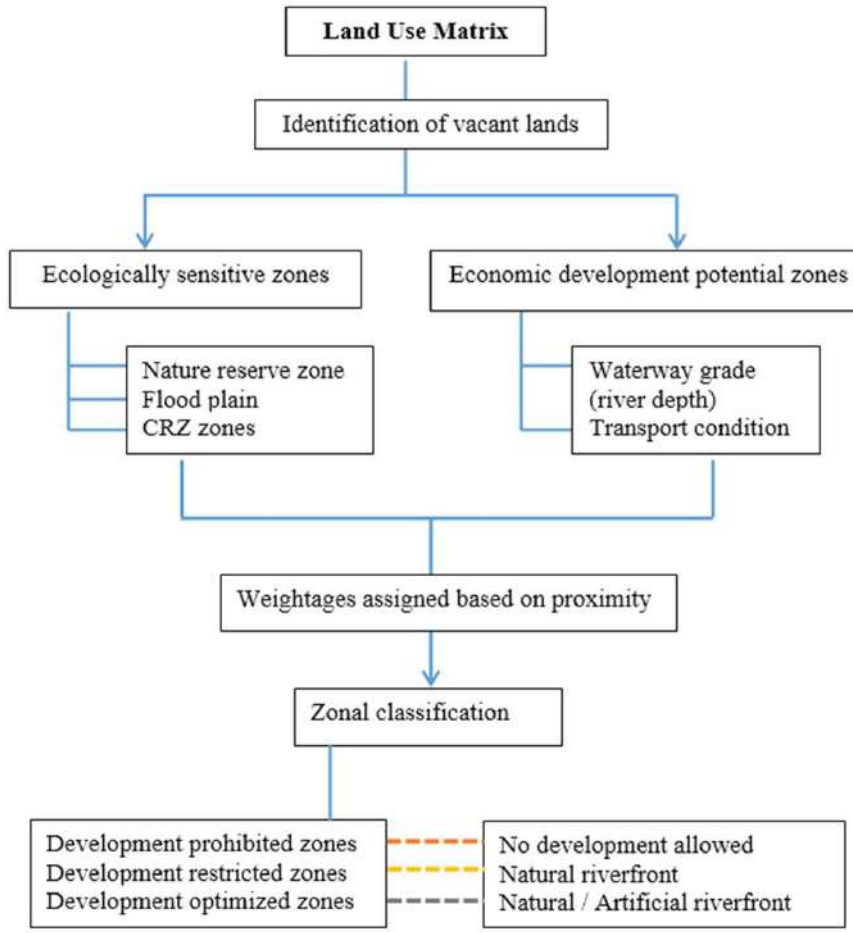

Fig. 2: Land use matrix methodology.

Table 1: Eco-sensitive zones assessment.

Proximity to nature reserve zones	proximity to floodplain zones	proximity to CRZ zones	Weightage
< 1km	< 500 m	< 100 m	1
1km to 3km	500 m to 1km	100 m to 500 m	2.5
>3 km	>1 km	>500m	5

The evaluation of vacant land in proximity to nature reserve zones, flood plains, and coastal regulation zones is critical in determining its potential for development. For nature reserve zones, a buffer of at least 1 km is recommended, with a weightage of 1 assigned to land within this distance, indicating low potential for development. A weightage of 2.5 is provided for distances between 1 km and 3 km, signifying minimal development potential. Land located beyond 3 km is assigned a weightage of 3, indicating higher potential for development. For flood plains, a minimum buffer zone of 500 m from the high flood plain is recommended. A weightage of 1 is assigned to land within this distance, with a weightage of 2.5 provided for distances between 500 m and 1 km and a weightage of 5 assigned for distances greater than 1 km. Regarding the proximity of vacant land to the CRZ zone, a buffer of 100 meters is recommended. A weightage of 1 is assigned for distances less than 100 meters, a weightage of 2.5 for distances between 100 meters to 500 meters, and a weightage of 5 for land located beyond 500 meters. These weights indicate the development potential of the land, with a higher weightage indicating a greater potential for development. (Table 1)

Assessment Method for Development Potentials

Development potentials of the study area are assessed with the two parameters: depth of the river and transport condition. To identify the river depth, the study area is divided into three zones, from TVK Bridge to Kotturpuram Bridge (zone1), Kotturpuram Bridge to Maraimalai Adigalar Bridge (zone 2), and Maraimalai Adigalar Bridge to Ekatuthangal Bridge(zone 3). The river depth was calculated and given a weightage as shown in the table. Proposals for public squares and recreational parks will be given in areas with lower river depth, while proposals for boating activities will be made in areas with higher river depth (Fig. 3).

Furthermore, to assess the transportation conditions and accessibility of the study area, the entire river stretch, which is 7.9 km in length, was divided into sections of 500 m radius, placed adjacently along the river. The weightage for each section was determined based on the availability of public transport modes within the 500 m radius. The weightage system evaluates the availability of public transport modes based on proximity, with a score of 5 if all three modes are available, 2.5 for two modes, and 1 for one mode (Table 2).

Table 2: Economic development potential assessment.

Distance interval	Waterway grade (depth of the river)	Transport conditions and accessibility based on the availability of public transport. (bus stops/ stands, railway stations, metro stations) if,	Weightage
500 m	< 5m	Single mode	1
	5m - 10 m	double mode	2.5
	> 10 m	Three modes	5

Zonal Classification

The zonal classification is done with the output values of the land use matrix as given in Fig. 2. It is further classified

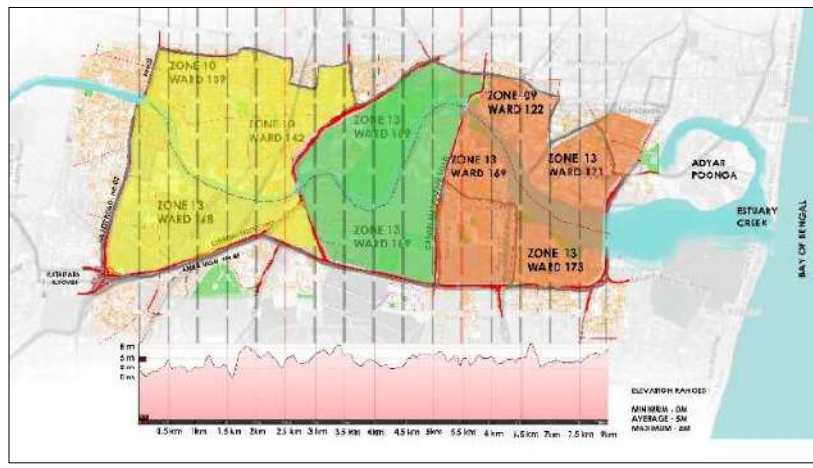

Fig. 3: Waterway grade mapping.

into 3 zones: development prohibited, development restricted zone, and development optimized zones calculated from the eco-sensitivity. With the output of development potential zone values, the proposals will be given (Table 3).

RESULTS AND DISCUSSION

The zones were classified based on the calculated values of Eco sensitivity for each of the three zones (Table 4). This classification revealed that Zone 1 should be designated as a development-prohibited zone, while Zone 2 is development-optimized, and Zone 3 is development-restricted. Proposals were then given based on these classified zones, and the levels of development potential were determined with the waterway grade and transport condition parameters (Tables 5 & 6). It was found that Zone 1 has a lower potential for development, while Zone 2 has medium potential, and Zone 3 has a higher potential for future development (Table 7).

Table 3: Zonal classification.

Zone	Eco Sensitivity Level	Development Potential Level	Proposal
Development prohibited zones	High	Any level	No development allowed
Development restricted zones	Low/ Medium	High/ Medium	Natural riverfront
Development optimized zones	Low	High	Artificial riverfront
	Low	Low/ Medium	Natural riverfront

Based on the zoning plan (Table 3*)*, it was determined that no developments should be allowed in Zone 1, which is designated as a development-prohibited zone. For Zones 2 and 3, the recommendation is to preserve the natural riverfront, considering both the ecological sensitivity and development potential of the areas (Table 8).

Table 4: Eco-sensitive zone matrix results.

ECOLOGICALLY SENSITIVE ZONES (Based on proximity)									
Zone	Vacant Land	Nature reserve zones -Guindy National Park (Kms)	Weightage	Floodplain (m)	weightage	CRZ zones (m)	weightage	Added weightage	Eco sensitivity level
z1	v1	1.69	2.5	177	1	200	2.5	6	23
z1	v2	1.52	2.5	100	1	19	1	4.5	
z1	v3	1.5	2.5	160	1	70	1	4.5	
z1	v15	2.08	2.5	200	1	160	2.5	6	
z1	v17	2.45	2.5	920	2.5	400	2.5	7.5	
z1	v11	5	5	3235	5	2400	5	15	
z1	v26	0.15	1	1990	5	1200	5	11	
z1	v27	0.15	1	2000	5	1200	5	11	
z1	v28	4.9	3	3150	5	2900	5	13	
z1	v29	4.63	3	2300	5	2300	5	13	
z2	v12	2.45	2.5	320	1	320	2.5	6	6.4
z2	v21	0.75	1	450	1	1645	5	7	
z2	v22	1.45	2.5	10	1	200	2.5	6	
z3	v4	2.16	2.5	563	2.5	3430	5	10	9.75
z3	v5	1.89	2.5	209	1	3300	5	8.5	
z3	v6	1.66	2.5	1006	5	3890	5	12.5	
z3	v7	1.75	2.5	1540	5	3984	5	12.5	
z3	v8	1	2.5	923	2.5	3460	5	10	
z3	v9	1.45	2.5	40	1	2752	5	8.5	
z3	v10	0.9	1	40	1	2442	5	7	
z3	v13	3	2.5	115	1	3160	5	8.5	
z3	v14	1.78	2.5	240	1	3085	5	8.5	
z3	v18	2.21	2.5	15	1	2787	5	8.5	
z3	v19	1.5	2.5	20	1	2665	5	8.5	
z3	v20	1.9	2.5	10	1	2690	5	8.5	
z3	v16	0.3	1	609	2.5	1912	5	8.5	
z3	v23	1.17	2.5	3057	5	4600	5	12.5	
z3	v24	1.13	2.5	2350	5	4036	5	12.5	
z3	v25	0.8	1	2516	5	4090	5	11	

Table 5: Economic development - Waterway grade results.

ECONOMIC DEVELOPMENT POTENTIAL - WATERWAY GRADE				
Zone	Distance interval	River depth points	Average for weightage values	River depth average
zone 1	0 - 0.5 km	2m + 2m + 5m	8	6.5
	0.5 km - 1 km	2m + 2m + 2m	3	
	1 km - 1.5 km	5m + 2m + 2m	7	
	1.5 km -2 km	2m + 5m + 8m	8.5	
	2 km -2.5 km	5m + 5m + 2m	6	
zone 2	2.5 km - 3 km	5m + 5m + 5m	7.5	6.9
	3 km - 3.5 km	6m + 6m + 8m	10	
	3.5 km -4 km	5m + 2m + 5m	6.5	
	4 km - 4.5 km	2m + 2m + 2m	3	
	4.5 km - 5 km	5m + 5m + 5m	7.5	
zone 3	5 km - 5.5 km	5m + 5m + 6m	7.5	7.7
	5.5 km - 6 km	5m + 5m + 5m	7.5	
	6 km - 6.5 km	5m + 4m + 5m	6	
	6.5 km - 7 km	5m + 8m + 5m	10	
	7 km - 7.5 km	4m + 4m + 4m	7.5	
	7.5 km - 8 km	5m + 6m + 6m	7.5	

Table 6: Economic development - transport accessibility condition.

ECONOMIC DEVELOPMENT POTENTIAL - TRANSPORT AND ACCESSIBILITY CONDITION					
Distance Interval (500 m Radius (r) from the River)	Bus Station	Railway Station	Metro Station	Weightage (Based on the availability of No. of Modes)	Development Potential Level
r0	1	0	0	1	1.5
r1	1	2	0	2.5	
r2	3	0	0	1	
r3	1	0	0	1	1.75
r4	3	0	1	2.5	
r5	2	0	0	1	1
r6	3	0	0	1	

Table 7: Development potential level.

ECONOMIC DEVELOPMENT POTENTIAL			
Zone	Waterway grade average	Transport and accessibility conditions average	Development potential level
zone 1	6.5	1.5	8
zone 2	6.9	1.75	8.65
zone 3	7.7	1	8.7

Table 8: Zoning classification and proposals.

Zone	Eco sensitivity level	Weightage	Zones classified based on Eco eco-sensitivity	Development potential level	Weightage	Proposal
Development prohibited zones	High	23	ZONE 1	Any level	8	No development allowed
Development restricted zones	Low/ Medium	9.75	ZONE 3	High/ Medium	8.7	Natural riverfront
Development optimized zones	Low	6.4	ZONE 2	High	Nil	Artificial riverfront
	Low			Low/ Medium	8.65	Natural riverfront

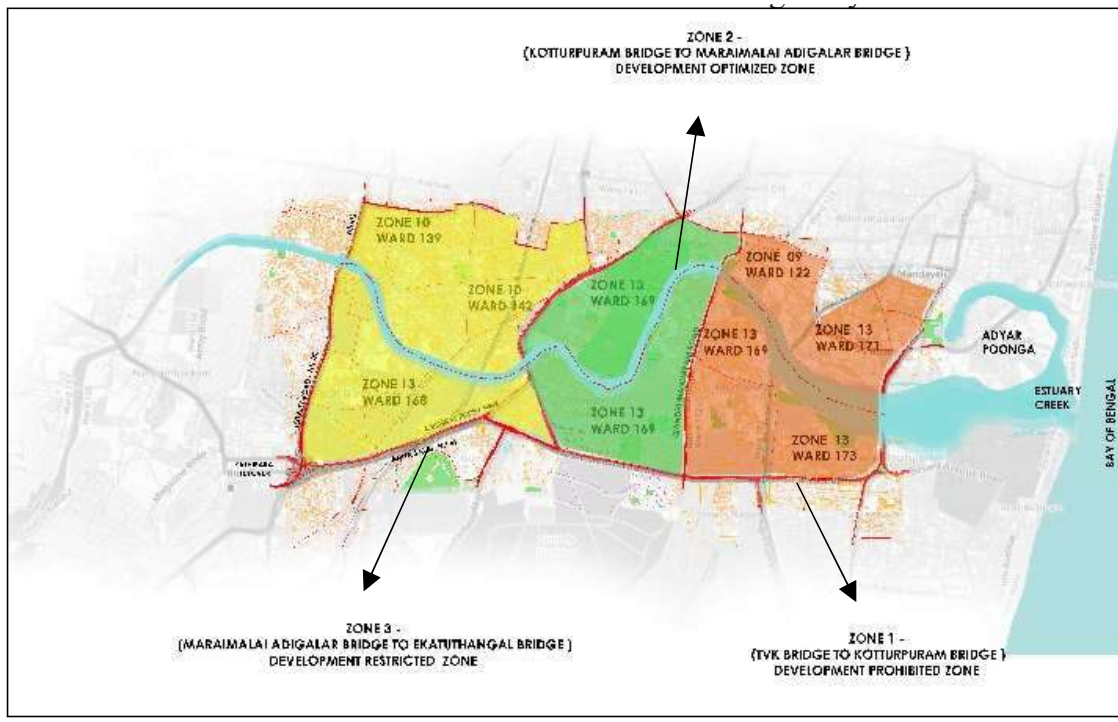

Fig. 4: Zone classification.

The classified zones and the proposal have been mapped and are displayed in Fig. 4. The development prohibited zone is depicted in orange, the development optimized zone is shown in green, and the development restricted zone is indicated in yellow. This approach aims to protect the environment while also promoting development in suitable locations.

CONCLUSION

The zones were classified based on the calculated values of Eco sensitivity for each of the three zones. The output value of Eco sensitivity shows that Zone 1 (TVK Bridge to Kotturpuram Bridge) has a higher level of Eco sensitivity. In contrast, Zone 2 (Kotturpuram Bridge to Maraimalai Adigalar Bridge) has a lower Eco-sensitivity value. Zone 3 (Maraimalai angular Bridge to Ekatuthangal Bridge) has a medium Eco sensitivity level with values of 23, 9.75, and 6.4, respectively. Based on the Eco sensitivity level, Zone 1 is classified as a development-prohibited zone, Zone 2 comes under development-optimized zones, and Zone 3 comes under development-restricted zones.

Further, with the output values of development potential, proposals were given. The results of the development potential show that Zone 1 has a low potential with a value of 8, Zone 2 has a low potential with a value of 8.65, and Zone 3 has a medium potential level with a value of 8.7. Thus, the zonal classification suggests that no further developments should be allowed in Zone 1, and in Zones 2 and 3, developments should be based on the natural riverfronts.

In prohibited zones (zone 1), Hospitals, nursing homes, and housing likely to have occupants who may not be sufficiently mobile to avoid injury or death during a flood, Police stations, fire stations, vehicle and equipment storage facilities, and emergency operations centers that are needed for flood response activities before, during, and after the flood, STP /WTP/Power plant and stations: bus depot were not allowed to construct. In development-optimized zones (zone 2), developments like Open-air theatres, indoor recreational uses, dwellings, waterfront tourism development projects, Co- cooperative markets, public toilets, libraries, and more than G+1 buildings were allowed to be constructed in this zone. In the restricted zone (zone 3), Parks /gardens/ playgrounds, sports facilities, Burial crematoria, and ground and only up to G +1 buildings only allowed to be constructed in this zone.

The recommendations and proposals were based on the classified zones. Several recommendations can be implemented to address the challenges faced by the Adyar River. These include increasing the capacity of the existing sewerage system and constructing new Sewage Treatment Plants (STPs) to ensure proper treatment of sewage,

relocating slum areas that are prone to flood danger to safer areas, enforcing Development Control Regulations (DCR) for any new development along the riverfront, implementing proper regulations for solid waste management, and undertaking regular cleaning and maintenance of the river by a separate river maintenance team. These recommendations can help maintain the water quality of the river, reduce pollution, prevent further Encroachments, and improve the overall quality of life of the residents.

By implementing the above recommendations, the river's ecological and social values can be restored. The findings of this study will be useful for policymakers and urban planners in formulating and implementing effective zoning regulations for the future growth of riverside areas. Integrated development of riversides involves a range of factors, including social, economic, environmental, infrastructural, physical, and management aspects. However, due to time constraints and the study's specific aim, the research analyzed only the socio-economic and eco-environmental factors. By including both physical and management parameters, the project can achieve a more comprehensive and holistic approach towards riverside development, leading to better outcomes in terms of economic, environmental, and social benefits.

REFERENCES

Bhavna, M. and Vimawala, S. 2015. Waterfront and its relationship to the city structure. Int. J. Res. Sci. Innov., 3(1): 2321-2705.

Darshini, M. and Lathia, S. 2019. Women's safety and public spaces: Lessons from the Sabarmati riverfront, India. Urban Plan., 4(2): 1214-1218

Gharge, M.C. 2016. Integrated riverfront development: A case study of Pune**.** Int. J. Res. Civ. Eng. Architect. Des., 4(3): 2347-2855.

Barve, S. and Sen, S. 2011. Riverside restoration: City Planner's viewpoint: A case of Mutha riverfront Pune. Water Resour. Manag., 145: 1743-3541.

Vriddhi, R. 2017. Riverfront development in Indian cities: The missing link. GSTF J. Eng. Technol., 5: 126. DOI: 10.5176/2251-3701_4.2.196.

Xuejun Duan, C. 2021. Assessing ecological sensitivity and economic potentials and regulation zoning of the riverfront development along the Yangtze River. China. J. Clean. Prod., 291: 125963.

Nature Environment and Pollution Technology
An International Quarterly Scientific Journal

p-ISSN: 0972-6268
(Print copies up to 2016)
e-ISSN: 2395-3454

Vol. 23 | No. 1 | pp. 235-243 | 2024

Original Research Paper

https://doi.org/10.46488/NEPT.2024.v23i01.019

Open Access Journal

Selection of White-Rot Fungi for Decolorization of Palm Oil Mill Effluent and Evaluation of Biodegradation and Biosorption Processes

Sanhathai Ridtibud*, Nuttika Suwannasai, Apichaya Sawasdee***†, Verawat Champreda****(*****), Cherdchai Phosri******, Sarper Sarp*******, Nipon Pisutpaisal*(********) and Siriorn Boonyawanich*(********)**

*Department of Agro-Industrial, Food and Environment Technology, Faculty of Applied Science, King Mongkut's University of Technology North Bangkok, Bangkok, 10800, Thailand

**Department of Microbiology, Faculty of Science, Srinakharinwirot University, 114 Sukhumvit 23, Watthana, Bangkok, 10110, Thailand

***Program in Innovation of Environmental Management, College of Innovative Management, Valaya Alongkorn Rajabhat University Under the Royal Patronage Pathumthani 13180, Thailand

****BIOTEC-JGSEE Integrative Biorefinery Laboratory, Innovation Cluster 2 Building, Thailand Science Park, Phaholyothin Road, Khlong Luang, Pathumthani 12120, Thailand

*****Biorefinery Technology and Bioproducts Research Group, National Center for Genetic Engineering and Biotechnology, 113 Thailand Science Park, Phaholyothin Road, Khlong Luang, Pathumthani 12120, Thailand

******Department of Biology, Faculty of Science, Nakhon Phanom University, 124 Moo 12, Ard-Samart Subdistrict, Muang District, Nakhon Phanom, 48000, Thailand

*******Centre for Water Advanced Technologies and Environmental Research (CWATER), College of Engineering, Swansea University, Swansea SA1 8EN, UK

********The Biosensor and Bioelectronics Technology Centre, King Mongkut's University of Technology, North Bangkok, Bangkok, 10800, Thailand

†Corresponding author: Apichaya Sawasdee; apichaya.s@vru.ac.th

Nat. Env. & Poll. Tech.
Website: www.neptjournal.com

Received: 27-05-2023
Revised: 09-07-2023
Accepted: 01-08-2023

Key Words:
Biodegradation
Biosorption
White-rot fungi
Palm oil mill effluent
Decolorization

ABSTRACT

Ten species of white-rot fungi were evaluated for their ability to decolorization of palm oil mill effluent. The highest decolorization efficiency was found with *Trametes elegans* (PP17-06), followed by *Ganoderma* sp.2 (PW17-06) and *Ganoderma* sp.2 (PW17-177), respectively. *T. elegans* was further evaluated for the long-term performance of decolorization for 24 d. The optimal retention time for the decolorization was 8 d, with a color removal efficiency of 47.7%. Beyond 18 d of incubation, decolorization efficiency was reduced due to the autolysis of enzymes. During the biodegradation process, manganese peroxidase enzyme activities reached a maximum of 36.03 $U.L^{-1}$. However, no significant laccase and lignin peroxidase activities were observed. *T. elegans* was also assessed for decolorization performance through biosorption on mycelial biomass. The synthesis of the enzyme was prevented by exposing the mycelium to $HgCl_2$. Within an optimal contact time of 2 d, decolorization efficiency reached 12.5% with ADMI reduction from 4259.0 (±20.1) ADMI to 3727 (±104.04) ADMI. Results indicate that the adsorption capacity was reached at this time, and no significant color removal can be achieved by biomass. Results obtained in this study showed the potential of *T. elegans* in decolorizing palm oil mill effluent.

INTRODUCTION

Palm oil is gaining high demand in developing countries as a high-quality oil source for cooking. Due to the increasing demand, the palm oil industry is expanding across countries in Asia, Africa, and Latin America (Mohammad et al. 2021). Palm oil mill effluent (POME) is a major environmental concern due to the high amount of organic compounds resulting in high concentrations of biological oxygen demand (BOD) and chemical oxygen demand (COD) (Saad 2020). Treatment of POME is necessary before discharge into the natural water bodies. Currently, various chemical, physical, and biological methods, such as coagulation, adsorption, anaerobic biodegradation, aerobic biodegradation, and advanced oxidation processes, are used in treating wastewater from palm oil mills (Sani et al. 2020).

Biological treatment methods are widely applied to remove organic carbon concentrations. However, despite bacteria's ability to easily remove most biodegradable compounds, benzene, and aromatic structures are difficult to degrade using bacteria. POME usually has a dark brownish color due to the presence of various color compounds such as phenolic, carotene, lignin, and pectin (Abdulsalam et al. 2018, 2020, Saad 2020). The COD of 1586 mg.L^{-1}, total solid of 3840 mg.L^{-1}, suspended solid of 2170 mg.L^{-1}, total phenol of 43 mg.L^{-1}, and color value of 2417 PtCo were reported in the effluent of the final anaerobic pond (Rakamthong & Prasertsan 2011). Achieving satisfactory color removal using aerobic or anaerobic bacteria is challenging (Rakamthong & Prasertsan 2011). On the other hand, chemical and physical treatment methods are expensive compared to biological systems (Kutty et al. 2019).

White-rot fungi provide a promising solution in decolorizing various types of industrial wastewater due to their ability to degrade lignocellulose compounds by producing ligninolytic enzymes such as laccase, manganese peroxidase (MnP), and lignin peroxidase (LiP) (Fang et al. 2020, Grelska & Noszczyńska 2020, Zhang et al. 2017). The white-rot fungus of *Trametes hirsuta* AK04 was reported removal efficiencies between 78 and 98% for ten phenolic compounds (Phenol, gallic acid, protocatechuic acid, 4-hydroxybenzoic acid, 4-hydroxyphenylacetic acid, caffeic acid, ferulic acid, syringic acid, p-coumaric acid, and vanillic acid) that can be found in POME. It was also reported that the presence of glucose and yeast extract in the fungi growth medium could enhance the degradation rates of phenolics (Kietkwanboot et al. 2020). *Phanerochaete chrysosporium* ATCC 24725 mycelium achieved a decolorization efficiency of 83.4% in 3 d and a phenol removal efficiency of 61.22% in 6 d using the decanter effluent as the supplement nutrient source for the final effluent of a palm oil mill (Rakamthong & Prasertsan 2011).

In addition to the color removal by biodegradation of compounds through enzyme activities, fungi can remove color by biosorption. White-rot fungus, *Haematonectria haematococca* BwIII43, showed a sorption capacity of 247.47 and 161.00 mg.g^{-1} for Alizarin Blue Black B and alkali lignin, respectively (Rybczyńska-Tkaczyk & Korniłłowicz-Kowalska 2016). The biosorption capacities were correlated with the molecular structure of dye compounds, and the ionic radius of dyes was found to be influenced by the biosorption capabilities (Maurya et al. 2006).

The application of white-rot fungi in the decolorization of POME has not been widely investigated in previous studies. There is a lack of studies to characterize the mechanisms involved in the decolorization of POME. Therefore, this study investigated the biodegradation and biosorption processes involved in the decolorization of POME. To characterize the biodegradation, enzyme activities of isolated fungi were monitored. To determine the biosorption capacities, mycelial growth was prevented by exposing it to the $HgCl_2$ solution. Thus, the enzyme biodegradation process ceased, and color removal mainly occurred through the biosorption of biomass. American Dye Manufacturing Index (ADMI) weighted ordinate method was used to measure the color of wastewater.

MATERIALS AND METHODS

Palm Oil Mill Effluent

POME was collected from the effluent of a palm oil mill after the treatment in the final aeration pond at Suksomboon Group, Chonburi, Thailand. The wastewater was kept at a temperature of 4°C and sterilized by autoclaving at 121°C and 15 psi for 15 min before use. The composition of glucose yeast extract (GYE) medium was supplemented in POME with concentrations (g.L^{-1}) of 10.0 glucose, 1.0 K_2HPO_4, 0.5 $MgSO_4 \cdot 7H_2O$, 0.5 KCL, 0.01 $FeSO_4 \cdot 7H_2O$, and 1.75 NH_4NO_3 (Vaithanomsat et al. 2010). However, the original color of POME was not changed when GYE medium was added.

Fungal Culture and Inoculum Preparation

The seven species, including ten strains of white-rot fungi as listed in Table 1, were obtained from the Department of Microbiology, Faculty of Science, Srinakharinwirot University, Thailand. These fungi species were originally collected from mixed deciduous and deciduous dipterocarp forests in the northeastern provinces of Nakhon Phanom, Sakon Nakhon, Udon Thani, and Chaiyaphum in Thailand.

Table 1: The seven species (ten strains) for the decolorization of palm oil mill effluent.

Species	Strains	GenBank Accession No.*
Coriolopsis aspera	NP17-02	MK589289
Ganoderma lingzhi	PW17-43	MK589272
Ganoderma sp.2	PW17-06, PW17-154, and PW17-177	MK589273, MK589275, and MK589276
Microporus sp.1	PP17-04	MK589279
Microporus sp.2	PP17-17 and PP17-20	MK589281 and MK589282
Trametes elegans	PP17-06	MK589285
Pseudolagarobasidium sp.	PP17-33	MK589289

*The accession numbers are unique identifiers assigned to a record in GenBank (NCBI Nucleotide database).

Fungi were cultured in potato dextrose agar (PDA). The PDA contained (L^{-1} of distilled water) potatoes 200 g, glucose 20 g, and agar 15 g. Cultures were preserved on the PDA medium at 4°C. Preserved cultures were incubated in a fresh PDA medium for 7 d at room temperature to prepare inoculums for experiments.

Evaluation of Decolorization Efficiencies of Isolated Fungi

From 7-day-old cultures, five active fungal mycelial plugs (5 mm in diameter) from each species were extracted and inoculated into Erlenmeyer flasks containing 50 mL of POME. An abiotic control experiment was also conducted without adding any fungal inoculum. The flasks were placed on an orbital shaker and incubated at 150 rpm and room temperature for 5 d. To measure the ADMI, samples were filtered through the Whatman filter paper (grade 1).

Based on the decolorization results obtained in the preliminary investigation, the fungal isolate that showed the highest decolorization efficiencies for POME was selected for further experiments. The incubation was conducted for 24 d to assess the decolorization efficiencies and enzyme activities.

Evaluation of Biosorption Capabilities of Fungi Biomass

The fungal biomass was immersed in 0.7% (w/v) $HgCl_2$ solution for 30 min during shaking. After that, the fungal biomass was filtered and rinsed with sterile distilled water. A piece of mycelium that was exposed to $HgCl_2$ was placed on the PDA medium to ensure no synthesis of fungal enzymes (Argumedo-Delira et al. 2021). Then, the fungal biomass was inoculated to 50 ml POME and shaken for 24 d at room temperature. Samples from POME were taken every two days to measure ADMI. The color removal efficiencies by biosorption were calculated. The experiment was conducted in triplicates.

Analytical Methods

Color: The color was determined in the ADMI unit using a spectrophotometer (Hach DR3900). A wavelength range of 320–1100 nm was applied, and the manufacturer's instructions were followed for the 2120 F. ADMI Weighted-Ordinate Spectrophotometric Method (APHA 23rd, 2017).

Laccase, manganese peroxidase, and lignin peroxidase assays: Samples of enzymes obtained from the POME were analyzed for the laccase, MnP, and LiP activities. Laccase enzyme activity was assessed by monitoring the oxidation of 2,2'-Azino-bis-3-ethylbenzthiazoline-6-sulphonic (ABTS) acid at a wavelength of 420 nm (Extinction coefficient; ε = 36,000 $M^{-1}.cm^{-1}$) (Machado & Matheus 2006). MnP enzyme activity was determined by monitoring the oxidation of 2,6-dimethoxyphenol (DMP) at a wavelength of 469 nm (ε = 10,000 $M^{-1}.cm^{-1}$) (Silva et al. 2014). The oxidation of veratryl alcohol (3,4-dimethoxybenzyl alcohol) to veratraldehyde in the presence of H_2O_2 at a wavelength of 310 nm (ε = 9300 $M^{-1}.cm^{-1}$) was monitored to determine the LiP enzyme activity (Tien & Kirk 1988). One unit (U) of the activity of ligninolytic enzymes is defined as the amount of enzyme that transforms 1 µmol of substrate per minute (Thamvithayakorn et al. 2019).

Other parameters measured: Gravimetric analysis was used to determine biomass generation. The weight of the dry biomass was measured after drying the samples at 50 °C for 24 h in a temperature controller. A pH meter (PH100 EXTECH ExStik) was used to monitor the changes in pH during the treatment period.

Calculations

Color removal efficiencies and rate: The percentage of color removal (CR%) was calculated using the color value measured from the control at the beginning of the experiment ($ADMI_0$) and the color value measured from the fungi-inoculated samples at the end of the retention time of T ($ADMI_T$). The color removal efficiencies were calculated according to equation (1).

$$Color\ removel\ efficiency\ (\%) = \frac{ADMI\ (T_0) - ADMI\ (T_5)}{ADMI\ T_0} \times 100 \quad \ldots(1)$$

Where ADMI (T_0) is the Color from control at T_0 and ADMI (T_5) is = Color from treatment at T_5.

Enzyme activity: Enzyme activity (U L^{-1}) was calculated using followed the equation (2)

$$Enzyme\ activity = \frac{\Delta Abs \times V \times D \times 10^3}{\varepsilon \times V \times t} \quad \ldots(2)$$

Where ΔAbs is the difference between the absorbance value before and after the reaction, V is the total amount of substance in the reaction (ml), D is the dilution level, ε is the absorbance constant (M^{-1} cm^{-1}), v is the volume of the crude extracted enzyme (ml), and t is curing time (min).

Biomass growth rate: Biomass growth rate (BM_r) was calculated according to the equation (3)

$$Biomass\ growth\ rate\ (BM_r) = \frac{BM_{C2} - BM_{C1}}{T_2 - T_1} \quad \ldots(3)$$

Where BM_{C1} and BM_{C2} are biomass concentrations measured at time T_1 and T_2, respectively.

Statistical analysis: The mean value (± standard deviation) of three independent replicates was calculated for all parameters measured during the experiments. One-way

analysis of variance (One-way ANOVA) method was used for the statistical analysis at 0.05 probability level.

RESULTS

Preliminary Selection of Fungal Strains for Decolorization of Palm Oil Mill Effluent

The decolorization efficiencies obtained with isolated fungi are illustrated in Fig. 1. No color removal was found with three fungal species, *Ganoderma lingzhi* (PW17-43), *Coriolopsis aspera* (NP17-02), and *Microporus* sp.2 (PP17-20). The highest decolorization efficiencies of 58.0 and 49.1% were detected with *T. elegans* and *Ganoderma* sp.2 (PW17-06), respectively. Other species showed decolorization efficiencies between 12.11-23.78% during the retention time of 5 d.

Long-term Performance Evaluation of *T. Elegans* for Decolorization, Enzyme Production, Biomass Generation, and pH Changes

The variations of ADMI and pH are shown in Fig. 2a. Color removal efficiencies and enzyme activities with respect to time are plotted in Fig. 2b. The initial color (at 0 d) of POME was 4506 (±143.54) ADMI. No significant changes in the ADMI were observed until 6 d. Hence, no decolorization efficiencies were obtained. However, the color rapidly decreased to 2356 (±361.01) ADMI at 8 d. During this period (between 6 to 8 d), the color removal rate was 900 ADMI d^{-1}. As a result, a decolorization efficiency of 47.7(±6.94) % was reached at 8 d in POME. The MnP enzyme activities were gradually increased during the initial period and reached 34.63 (±6.07) $U.L^{-1}$ at 6 d. The rapid decolorization after 6 d could be attributed to enzyme production. The initial pH of 7.18 (±0.02) was decreased to 3.24 (±0.19) at 8 d with the decolorization of POME.

However, no significant changes in decolorization efficiencies were observed within the duration of 8 to 18 d. Similarly, pH in the POME was not significantly varied during this period. The MnP enzyme activities were also decreased, suggesting that the color removal was attributed to the MnP enzymatic biodegradation. The highest MnP production was 36.03 $U.L^{-1}$ in 10 d. MnP was not found on day 18, and color values tended to decrease. The color observed in POME at 14 d is shown in Fig. 3. It was within the period that fungi achieved the highest decolorization efficiencies. The dark brownish color found in the original POME was observed in the abiotic control. The biotic experiments showed a comparatively light brownish color. The original color of the fungal biomass observed at 0 d was changed to a dark brownish color when inoculated to the POME, as shown in Fig. 4. Thus, these observations indicate that fungi were in charge of the biosorption of color compounds.

The variation of fungal biomass concentration with respect to time is presented in Fig. 4. The initial biomass concentration was 0.55 (±0.07) $g.L^{-1}$. No biomass growth was observed until 6 d. At 8 d, a biomass concentration of 2.29 (±0.49) g L^{-1} was detected. During the period between 6 to 8 d, the biomass growth rate was 0.57 $g.L^{-1}.d^{-1}$. Similarly, higher decolorization rates were observed during this period, as

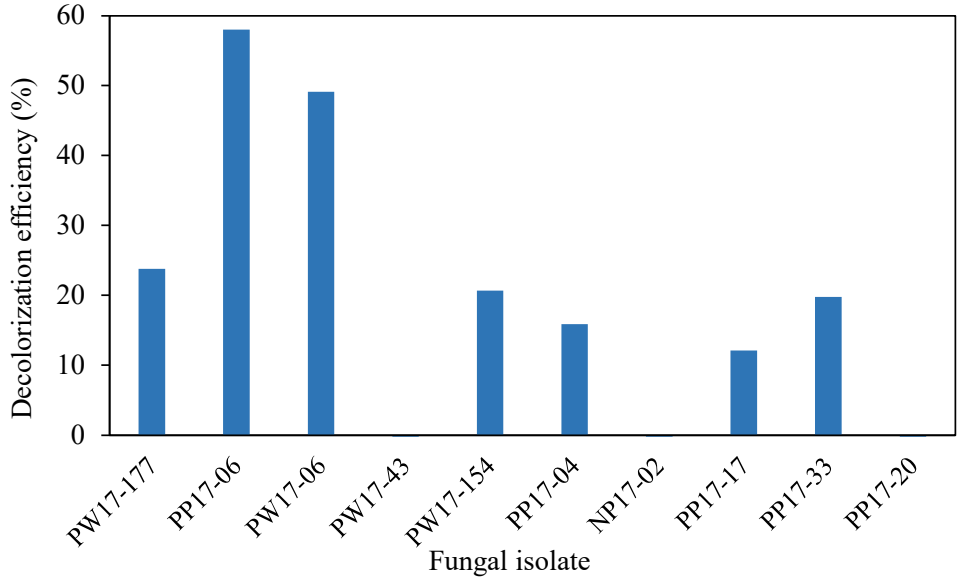

Fig. 1: The decolorization efficiencies of 10 isolated fungi after 5 d of incubation in palm oil mill effluent (POME).

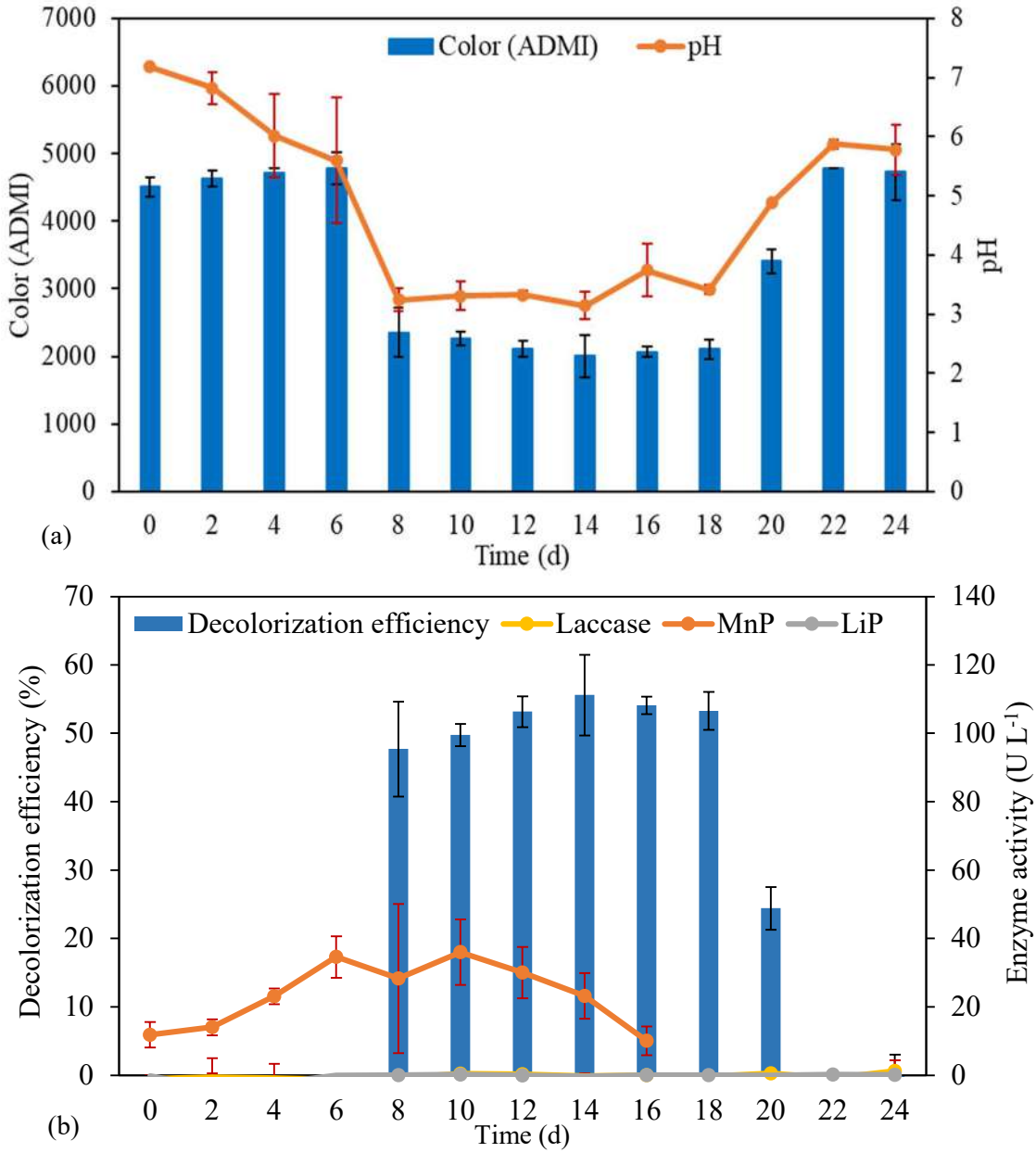

Fig. 2: Variations of (a) color and pH and (b) decolorization efficiency and enzyme activities with respect to time using *T.elegans*. The respective color of the column or line chart is used in the letters. A comparison of means of enzyme activities is provided only for MnP. Bars indicate the standard deviation of the mean (±SD).

discussed above. Thus, the decrease in color could be attributed to the consumption of color compounds in the POME during fungal biomass growth. However, despite no significant changes in color after 8 d, the biomass concentration gradually increased and reached a peak of 7.24 (±0.79) $g.L^{-1}$ at 18 d.

Evaluation of Biosorption Capabilities of *T. elegans* Biomass

The variations of color and decolorization efficiency with respect to time are illustrated in Fig. 5. The initial color measured in the POME was 4259.0 (±20.1) ADMI. It was reduced to 3727 (±104.04) ADMI at the optimal time of 2 d, reaching a corresponding decolorization efficiency of 12.50 (±2.44) %. After 2 d, no significant increase in the decolorization efficiency was detected.

DISCUSSION

Various color removal efficiencies were obtained with

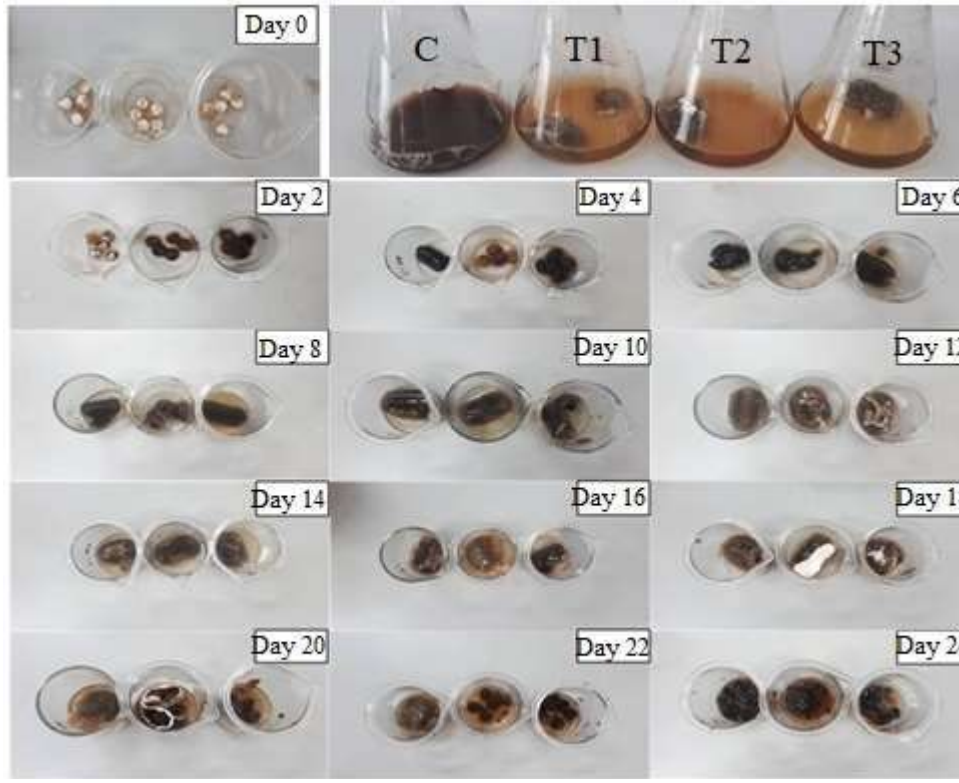

Fig. 3: Visual appearance observed in *T.elegans* biomass during the palm oil mill effluent (POME) treatment period of 24 d. A comparison of color observed in POME at 14 d is shown in the upper right corner. C is the abiotic control. T1, T2, and T3 are biotic triplicates inoculated with *T.elegans*.

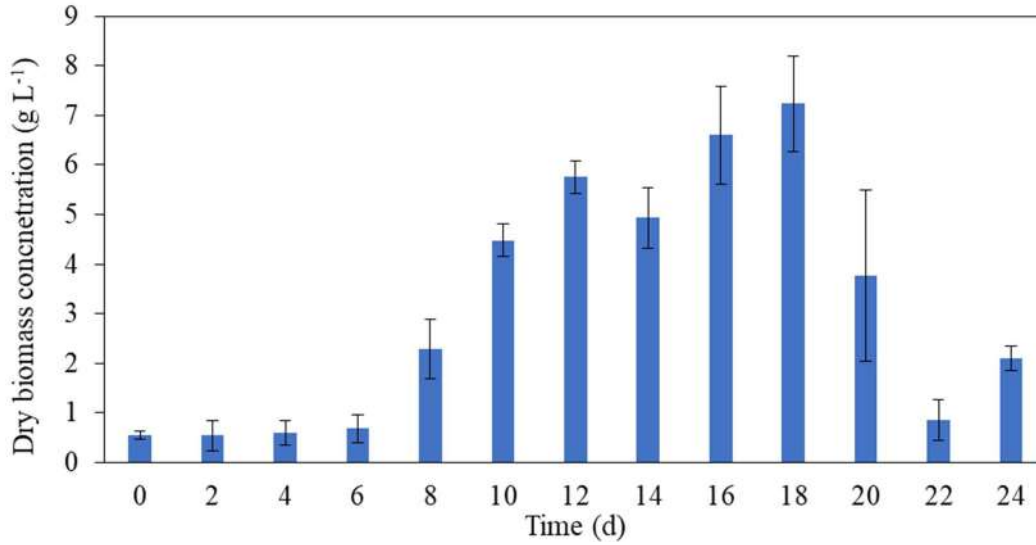

Fig. 4: Variations of dry *T.elegans* biomass concentration with respect to time. Bars indicate the standard deviation of the mean (±SD).

different strains of fungi. In degrading a certain compound, the biological activities of different species can be varied (Sagar et al. 2020). Thus, the compounds available in POME could be easily degraded by some fungi species, while the degradation process could be hindered in other species. Among the ten isolated fungi, seven isolates of white-rot fungi were able to decolorize POME. Results indicate that the ligninolytic enzymes, including laccase and manganese

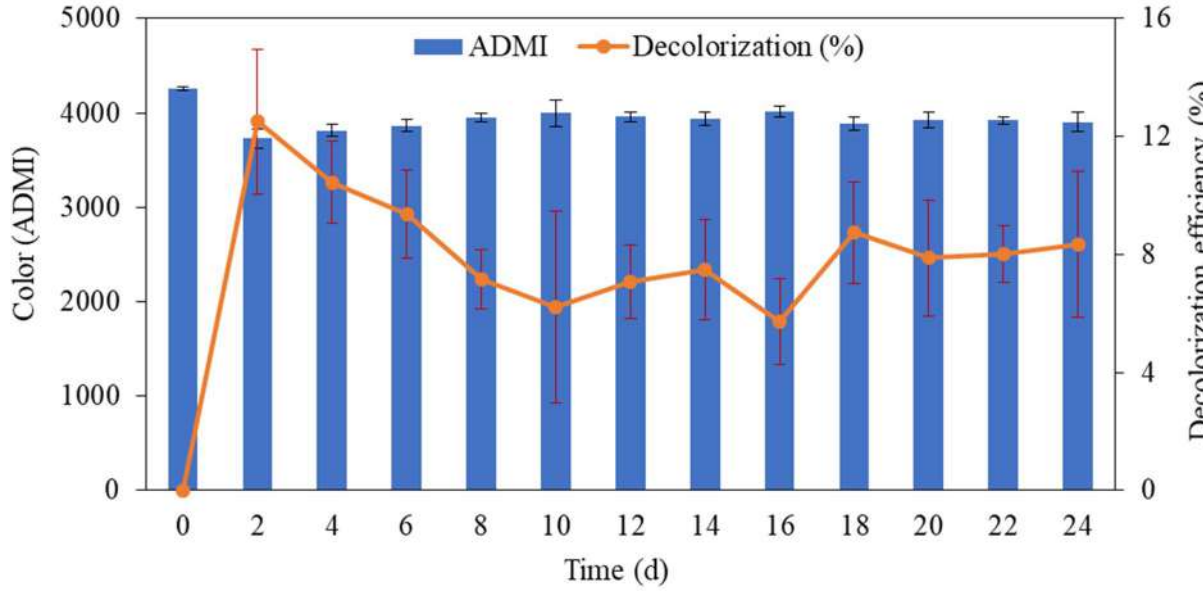

Fig. 5: Variations of color and decolorization efficiency with respect to time in treating palm oil mill effluent through biosorption on *T.elegans* biomass. Bars indicate the standard deviation of the mean (±SD).

peroxidase (MnP), can degrade color compounds that are unable to reduce during aerobic or anaerobic treatment (Raghukumar et al. 1996, Srinivasan & Viraraghavan 2010). Thus, white-rot fungi provide a promising solution for the further treatment of POME. However, the removal efficiencies were not satisfactory during 5 d of treatment time. To evaluate the decolorization performance in long-term applications, *T.elegans*, which showed the highest decolorization efficiency, was further tested for an extended period of 24 days.

However, extending the retention time did not elevate the decolorization efficiencies. The optimum retention time for the color removal was 8 d. After 18 d, decolorization efficiency was decreased. A similar phenomenon was reported with *Aspergillus flavus* and *Penicillium canescens* reaching maximum decolorization efficiencies of 97 and 92% at 7 d. No elevation in decolorization efficiency was reported, further extending the retention period to 14 d (Hefnawy et al. 2017). *Aspergillus* 2BNL1 and *Aspergillus* 1AAL1 reported maximum decolorization efficiencies between 81–95% at an optimal retention time of 1 d, while *Lentinus edodes* UEC2019 reached similar levels at 3 d (Souza et al. 2005). When the retention time increases, available nutrients in the growth medium are insufficient for the growth of fungi. As a result, the enzyme digests its enzymes, which is referred to as autolysis, releasing intracellular chromophore compounds. These compounds can further increase the color of the growth medium (Souza et al. 2014, 2005).

In this study, the highest decolorization efficiency reached by *T.elegans* was 55.61 (±5.89) %. Decolorization efficiencies reported with different types of wastewater are summarized in Table 2. In decolorizing POME, *Trametes hirsuta* AK 04, which was immobilized onto oil palm fibers, reached decolorization efficiencies up to 87.1% after 8 d of incubation. It was reported immobilized fungi are more resistant to inhibitory compounds in POME than in the mobilized bacteria (Kietkwanboot et al. 2015).

Despite no significant changes monitored in color between the period of 8-18 d, the fungal biomass concentration gradually increased and reached the maximum of 7.24 (±0.96) $g.L^{-1}$ at 18 d. POME contains various compounds that are added through the processes of palm oil production. Easily biodegradable compounds were utilized by fungi during the initial period, contributing to the color removal. However, some compounds in POME were reluctant to fungal biodegradation. Thus, these compounds still existed in the POME, contributing to the color in the later period. However, despite no degradation of color compounds occurring, the fungal biomass was gradually increased due to the consumption of other compounds. Generally, the fungal biodegradation process occurs through primary and secondary metabolisms. Fungi utilized a co-substrate such as glucose in the primary metabolisms. In the secondary metabolisms, laccase, MnP, and LiP enzymes carry out the color degradation (Pazarlıoğlu et al. 2005, Pedroza et al. 2007, Ramsay et al. 2005). In this study, POME was enriched by 10 $g.L^{-1}$ of glucose to enhance the decolorization process.

Table 2: Decolorization efficiencies reported with different types of wastewater using fungi.

Fungal species	Wastewater	Treatment system	T[a] [d]	DE[b] [%]	Reference
Trametes Hirsuta AK 04	Palm oil mill effluent	Two-stage biological process	8	87.1	Kietkwanboot et al. (2015)
Phanerochaete flavido-alba	Olive oil mill wastewater	Laboratory-scale bioreactor	18.75	70	Blánquez et al. (2002)
Pleurotus ostreatus	Apple processing residues	Packed-bed reactor	1	50	Iandolo et al. (2011)
Aspergillus flavus F10	Pulp mill effluent	Biological treatment	10	66.32	Barapatre and Jha (2016)
Fibrodontia sp. RCK783S	Pulp mill effluent	NR*	5	52.2-54.8	Kreetachat et al. (2016)
Penicillium glabrum Pg1	Textile wastewater	Packed bed bioreactor	3	98.2	Arikan et al. (2019)
Phanerochaete velutina	Textile wastewater	NR*	14	55	Zafiu et al. (2021)
Saccharomyces cerevisiae	Synthetic melanoidin wastewater	Packed bed bioreactor	0.25	70	Tsiakiri et al. (2020)
T. elegans	Palm oil mill effluent	Laboratory-scale reactor	8	47.72	This study

a: Treatment time, b: Decolorization efficiency, NR*: Not reported

In this study, the isolated fungi showed significantly high MnP production compared to laccase. These findings indicate that the laccase and LiP enzymes were not active during the biodegradation of color compounds. The redox potential of laccase is lower compared to MnP. Thus, laccase degrades compounds with low redox potential. MnP enzyme can oxidize more recalcitrant aromatic compounds due to the higher redox potential (Fang et al. 2018, 2020). The higher MnP production could be attributed to the presence of recalcitrant aromatic compounds in the POME.

In addition to the enzymatic biodegradation of color compounds, part of the color removal could be attributed to the biosorption of fungal biomass. In the next experiment, fungal biomass was exposed to $HgCl_2$ to kill the mycelium and avoid the further synthesis of fungal enzymes. Thus, biosorption can act as a mechanism in the decolorizing of POME. In this study, the optimum decolorization through biosorption occurred at 2 d. Further increase in the contact time did not enhance the color removal. Similar behavior was observed (Kabbout & Taha 2014) with *Aspergillus fumigatus*. Biosorption of methylene blue reached a maximum of 71% at 210 min. After that, no significant increase in biosorption occurred.

CONCLUSIONS

T.elegans showed decolorization of palm oil mill effluent utilizing both biodegradation and biosorption mechanisms. The optimal retention period for the color removal by biodegradation was 8 d, reaching a decolorization efficiency of 47.4%. MnP enzymes were useful in degrading complex color compounds. A decolorization efficiency of 12.5% was achieved during the optimal contact time of 2 d during biosorption on fungal biomass. Despite fungi showing the potential for decolorization of palm oil mill effluent, the decolorization efficiencies were not satisfactory. The treated palm oil mill effluent was not sufficient to the purified levels that can be discharged into natural water bodies. Fungi-based decolorization can be coupled with other advanced treatment technologies to develop more efficient, sustainable, and economical methods.

ACKNOWLEDGEMENT

We would like to acknowledge financial support from King Mongkut's University of Technology, North Bangkok (KMUTNB-65-IP-03; KMUTNB-66-KNOW-18; KMUTNB-FF-65-67).

REFERENCES

Abdulsalam, M., Che Man, H., Islam Adris, A., Zainal Abidin, Z. and Faezah Younos, K. 2018. The pertinence of microwave irradiated coconut shell bio-sorbent for wastewater decolorization: Structural morphology and adsorption optimization using the response surface method (RSM). Int. J. Environ. Res. Public. Health., 15(10): 1-19.

Abdulsalam, M., Man, H.C., Abidin, Z.Z., Yunos, K.F. and Idris, A.I. 2020. Decolorization of Palm Oil Mill Effluent by Klebsiella Pneumonia ABZ11: Remediation Efficacy and Statistical Optimization of Treatment Conditions. Front. Microbiol., 11:675.

APHA. 2017. Standard Methods for the Examination of Water and Wastewater. Twenty-Third Edition. American Public Health Association, Washington DC.

Argumedo-Delira, R., Gómez-Martínez, M.J. and Uribe-Kaffure, R. 2021. Trichoderma biomass as an alternative for removal of Congo red and Malachite green industrial dyes. Appl. Sci., 11(1): 448.

Arikan, E.B., Isik, Z., Bouras, H.D. and Dizge, N. 2019. Investigation of immobilized filamentous fungi for treatment of real textile industry wastewater using up-flow packed bed bioreactor. Bioresour. Technol. Rep., 7: 100197.

Barapatre, A. and Jha, H. 2016. Decolorization and biological treatment of pulp and paper mill effluent by lignin-degrading fungus Aspergillus flavus strain F10. Int. J. Curr. Microbiol. Appl. Sci., 5: 19-32.

Blánquez, P., Caminal, G., Sarrà, M., Vicent, M.T. and Gabarrell, X. 2002. Olive oil mill wastewater decoloration and detoxification in a bioreactor

by the white rot fungus Phanerochaete flavido-alba. Biotechnol. Prog., 18(3): 660-662.

Fang, W., Zhang, P., Zhang, X., Zhu, X., Lier, J.B.V. and Spanjers, H. 2018. White rot fungi pretreatment to advance volatile fatty acid production from solid-state fermentation of solid digestate: Efficiency and mechanisms. Energy, 162: 534-541.

Fang, W., Zhang, X., Zhang, P., Morera, X.C., Lier, J.B.V. and Spanjers, H. 2020. Evaluation of white rot fungi pretreatment of mushroom residues for volatile fatty acid production by anaerobic fermentation: Feedstock applicability and fungal function. Bioresour. Technol., 297: 122447.

Grelska, A. and Noszczyńska, M. 2020. White rot fungi can be a promising tool for the removal of bisphenol A, bisphenol S, and nonylphenol from wastewater. Environ. Sci. Pollut. Res. Int., 27(32): 39958-39976.

Hefnawy, M.A., Gharieb, M.M., Shaaban, M.T. and Soliman, A.M. 2017. Optimization of culture condition for enhanced decolorization of direct blue dye by *Aspergillus flavus* and *Penicillium canescens*. J. Appl. Pharm. Sci., 7: 083-092.

Iandolo, D., Amore, A., Birolo, L., Leo, G., Olivieri, G. and Faraco, V. 2011. Fungal solid state fermentation on agro-industrial wastes for acid wastewater decolorization in a continuous flow packed-bed bioreactor. Bioresour. Technol., 102(16): 7603-7607.

Kabbout, R. and Taha, S. 2014. Biodecolorization of textile dye effluent by biosorption on fungal biomass materials. Phys. Procedia., 55: 437-444.

Kietkwanboot, A., Chaiprapat, S., Müller, R. and Suttinun, O. 2020. Biodegradation of phenolic compounds present in palm oil mill effluent as single and mixed substrates by Trametes hirsuta AK04. J. Environ. Sci. Health Part A., 55(8): 989-1002.

Kietkwanboot, A., Tran, H. and Suttinun, O. 2015. Simultaneous dephenolization and decolorization of treated palm oil mill effluent by oil palm fiber-immobilized trametes hirsuta strain AK 04. Water Air Soil Pollut., 226.

Kreetachat, T., Chaisan, O. and Vaithanomsat, P. 2016. Decolorization of pulp and paper mill effluents using wood rotting fungus Fibrodontia sp. RCK783S. Int. J. Environ. Sci. Dev., 7: 321-324.

Kutty, S.R.M., Almahbashi, N.M.Y., Nazrin, A.A.M., Malek, M.A., Noor,, A., Baloo, L. and Ghaleb, A.A.S. 2019. Adsorption kinetics of color removal from palm oil mill effluent using wastewater sludge carbon in column studies. Heliyon, 5(10): e02439.

Maurya, N.S., Mittal, A.K., Cornel, P. and Rother, E. 2006. Biosorption of dyes using dead macro fungi: Effect of dye structure, ionic strength, and pH. Bioresour. Technol., 97(3): 512-521.

Mohammad, S., Baidurah, S., Kobayashi, T., Ismail, N. and Leh, C.P. 2021. Palm oil mill effluent treatment processes: A review. Processes, 9(5): 739.

Pazarlıoğlu, N.K., Sariişik, M. and Telefoncu, A. 2005. Laccase: Production by Trametes versicolor and application to denim washing. Process Biochem., 40(5): 1673-1678.

Pedroza, A., Mosqueda, R., Alonso-Vante, N. and Rodríguez-Vázquez, R. 2007. Sequential treatment via Trametes versicolor and UV/TiO2/RuxSey to reduce contaminants in wastewater resulting from the bleaching process during paper production. Chemosphere, 67: 793-801.

Raghukumar, C., Chandramohan, D., Michel, F.C. and Redd, C.A. 1996. Degradation of lignin and decolorization of paper mill bleach plant effluent (BPE) by marine fungi. Biotechnol. Lett., 18(1): 105-106.

Rakamthong, C. and Prasertsan, P. 2011. Decolorization and phenol removal of anaerobic palm oil mill effluent by Phanerochaete chrysosporium ATCC 24725. TIChE International Conference, Hatyai, Songkhla, Thailand, 10-11 Nov 2011.

Ramsay, J.A., Mok, W.H.W., Luu, Y.S. and Savage, M. 2005. Decoloration of textile dyes by alginate-immobilized trametes versicolor. Chemosphere, 61(7): 956-964.

Rybczyńska-Tkaczyk, K. and Korniłłowicz-Kowalska, T. 2016. Biosorption optimization and equilibrium isotherm of industrial dye compounds in novel strains of microscopic fungi. Int. J. Environ. Sci. Technol., 13(12): 2837-2846.

Saad, S. 2020. Removal color from palm oil mill effluent (POME): Electrocoagulation method vs microfiltration using nanofiber membrane. Int. J. Electrochem. Sci., 11283-11293.

Sagar, S., Sharma, I., Thakur, M. and Tripathi, A. 2020. Decolorization and degradation of Sunset Yellow-FCF and Acid Orange-7 by wild white rot fungi Trametes elegans and Trametes Versicolor and their extracellular ligninolytic enzymes. Int. J. Sci. Technol. Res., 9 (01): 2255-2271.

Sani, S., Dashti, A.F. and Adnan, R. 2020. Applications of Fenton oxidation processes for decontamination of palm oil mill effluent: A review. Arab. J. Chem., 13(10): 7302-7323.

Souza, É., Souza, J.V., Silva, F.T. and Brazil de Paiva, T.C. 2014. Treatment of an ECF bleaching effluent with white-rot fungi in an air-lift bioreactor. Environ. Earth Sci., 72(4): 1289-1294.

Souza, J.V., Silva, E.S., Silva, F.T. and Teresa C.B. 2005. Fungal treatment of a delignification effluent from a nitrocellulose industry. Bioresour. Technol., 96(17): 1936-1942.

Srinivasan, A. and Viraraghavan, T. 2010. Decolorization of dye wastewaters by biosorbents: A review. J. Environ. Manage., 91(10): 1915-1929.

Thamvithayakorn, P., Phosri, C., Pisutpaisal, N., Krajangsang, S., Whalley, A.J.S. and Suwannasai, N. 2019. Utilization of oil palm decanter cake for valuable laccase and manganese peroxidase enzyme production from a novel white-rot fungus, Pseudolagarobasidium sp. PP17-33. Biotech., 9(11): 417.

Tien, M. and Kirk, T.K. 1988. Lignin peroxidase of Phanerochaete chrysosporium. In: Methods in Enzymology. Academic Press, 161: 238-249.

Tsiakiri, E.P., Sompatzi, E., Voukia, F., Sotiropoulos, S. and Pantazaki, A.A. 2020. Biocatalytic and bioelectrolytic decolorization of simulated melanoidin wastewaters by Saccharomyces cerevisiae cells suspended and conjugated on silica and alumina. J. Environ. Chem. Eng., 8(5): 104078.

Vaithanomsat, P., Apiwatanapiwat, W., Petchoy, O. and Cheschant, J. 2010. Decolorization of reactive dye by white-rot fungus *Datronia* sp. KAPI0039. Kasetsart. J. Nat. Sci., 44: 879-890.

Zafiu, C., Part, F., Ehmoser, E.K. and Kahkonen, M.A. 2021. Investigations on inhibitory effects of nickel and cobalt salts on the decolorization of textile dyes by the white rot fungus *Phanerochaete velutina*. Ecotoxicol. Environ. Saf., 215: 112093.

Zhang, A., Wang, G., Gong, G. and Shen, J. 2017. Immobilization of white rot fungi to carbohydrate-rich corn cob as a basis for tertiary treatment of secondarily treated pulp and paper mill wastewater. Ind. Crops Prod., 109: 538-541.

ORCID DETAILS OF THE AUTHORS

Apichaya Sawasdee: https://orcid.org/0000-0001-5947-5797

Nature Environment and Pollution Technology
An International Quarterly Scientific Journal

p-ISSN: 0972-6268
(Print copies up to 2016)
e-ISSN: 2395-3454

Vol. 23 | No. 1 | pp. 245-253 | 2024

Original Research Paper

https://doi.org/10.46488/NEPT.2024.v23i01.020

Open Access Journal

Urban Indian Environment in the Context of a Pandemic

Abhijith. S.*, Akshara S. N.* and P. P. Nikhil Raj†**

*Department of Computer Science and Engineering, Amrita School of Computing, Coimbatore, Amrita Vishwa Vidyapeetham, India

**Department of Chemical Engineering and Materials Science, Amrita School of Engineering, Amrita Vishwa Vidyapeetham, Coimbatore, India

†Corresponding author: P. P. Nikhil Raj; cb.en.u4cse19102@cb.students.amrita.edu; pp_nikhilraj@cb.amrita.edu

Nat. Env. & Poll. Tech.
Website: www.neptjournal.com

Received: 09-06-2023
Revised: 19-07-2023
Accepted: 27-07-2023

Key Words:
COVID-19
Air Quality Index
Population
Urban environment

ABSTRACT

The spread of the Coronavirus disease 2019 (COVID-19) has impacted human life severely since November 2019. The urban centers in the world, especially, were highly affected by the diseases. Several socioeconomic and environmental factors probably enhanced the spread of the pandemic and consequent mortality. Many studies examining environmental factors, such as air quality, in urban centers indicate the roles of those factors in the spread of diseases and consequent mortality. However, other socioeconomic factors that directly or indirectly elevate the mass death of people are seldom studied. The present study explores the socioeconomic factors and air quality influencing COVID-19 deaths in urban India. We randomly selected 19 Indian cities and collected each city's socioeconomic and air quality data from reliable and open sources. The data were analyzed using multivariate data analysis techniques using R statistics. The results showed significant positive relationships, population, and total area of the urban centers.

INTRODUCTION

The world has witnessed the intensity of the Severe Acute Respiratory Syndrome Coronavirus 2 (SARS-COV-2), also known as COVID-19, since November 2019. So far, the pandemic (declared by the World Health Organization on March 11, 2020) has led to the deaths of more than six million people around the globe (covid19.who.int). The virus is highly versatile and mutating (Balachandran et al. 2022). Its known transmission modes include contact, droplet, airborne, fomite, fecal-oral, bloodborne, mother-to-child, and animal-to-human transmission (www.who.int). The environmental setup is also a crucial factor in determining the spread. Since the Coronavirus attacks the respiratory tract, people exposed to highly polluted air and suffering from respiratory ailments (Subbarao et al. 2020) and people with other comorbidities, heart diseases, lung cancer, etc., are highly vulnerable to COVID-19 infection. People living in urban centers with considerably low air quality are also of prime concern (Conticini et al. 2020, Cao et al. 2020). For example, the highest cases of COVID-19 deaths reported in urban areas in China, South Korea, Iran, and northern Italy were exacerbated by poor air quality (Jiang et al. 2020, Gupta et al. 2021). The spread of the disease in a region is also linked to its geographical location, economy and public awareness. It is also associated with the region's health systems' capacity, readiness and ability to curtail the spread (Kejela 2020). At an individual level, community consciousness, age, and social (in fact, physical distancing) distancing are other significant factors influencing the spread of the disease (Raj & Azeez 2020, Lakshmi & Suresh 2020, Priya et al. 2021).

Regarding the Air Quality Index in 2020, the air quality in world cities, in general, is almost five times above the WHO exposure recommendations (WHO 2021). Six major pollutants, Carbon Monoxide, Lead, Nitrogen Oxide, Ozone, Particulate matter (PM), and Sulphur dioxide, are highly likely to affect a population's short and long-term health. Of the PMs (PM_{10} and $PM_{2.5}$), $PM_{2.5}$ is considered the most lethal; chronic exposure to $PM_{2.5}$ increases the risk of acute respiratory diseases among the older population (Benmarhnia 2020) since that can penetrate the bronchi deeper (www.who.int). As per a recent report by the European Environment Agency, around 0.30 million premature deaths in urban areas of 27 European countries were due to high $PM_{2.5}$. Vehicular emission (25%) followed by agriculture (22%), domestic fuel burning (20%), natural dust and salt (18%), and industrial activities (15%) significantly contribute to PMs (PM_{10}, $PM_{2.5}$, etc.) in cities (Karagulian et al. 2015).

Due to the poor air quality, approximately 1.24 million people lose their lives in India annually (Balakrishnan et al. 2019). It is reported that high pollution levels in the ambient

air contribute to respiratory dysfunctions among urban dwellers (Balakrishnan et al. 2014, Venkataraman et al. 2018, Khilnani & Tiwari 2018). In 2019, air pollution accounted for 17.8 % of total mortality in India, of which 5% of deaths were attributed to PM pollution. However, the deaths due to household air pollution decreased from 74.2 million in 1990 to 0.61 million in 2019, around 64.2% of the total death cases (Pandey et al. 2021). In India, it is reported that the primary sector contributing significantly to ambient air quality is the transport sector, which substantially contributes (7-43%) to ambient air PM (Gurjar et al. 2016). Khilnani & Tiwari (2018) reported that the ambient air pollution in the major city centers of the country is showing an alarmingly rising trend.

From different studies carried out by the Central Pollution Control Board (CPCB), it has been found that 46 Indian cities are severely polluted (Nasir et al. 2016). It is widely known that most Indian metro cities are highly polluted, with 14 out of 20 Indian cities examined being shortlisted as among the world's most air-polluted cities (Sikarwar & Rani 2020). As a fast-developing country (fifth-largest economy in terms of nominal GDP), India has an active industrial sector and fossil fuel-based power plants. From 2010 to 2015, it was observed that the emission of CO_2 gas significantly increased in most parts of the country (Girdhar et al. 2021).

Air pollution is one of the significant outcomes of the current economic development model (Aditya et al. 2022). While the developed nations were historically massive emitters, the rapidly growing economies are increasingly contributing to air pollution since high emission level of air-polluting gasses like CO_2 is usual evils in the current economic development model. WHO and OECD reported that Europe's economic cost of premature death and disability from air pollution in 2015 was nearly USD 1.6 trillion (Manjula 2018). The adverse effects of air pollution are diverse, including social and psychological (Chen & Jin 2019, Heissel et al. 2022). Studies have also shown that a 10% rise in $PM_{2.5}$ caused a 2.4% fall in the price of houses in China during 2005-2013 (Sivarethinamohan et al. 2021). Present-day economic developmental models are committed to the financial growth calculated in terms of the Gross Domestic Productivity of a region and that, most times, fail to ensure the socioeconomic welfare of the people, except perhaps by the trickle-down effect. The major cities in developing countries like India are deprived of scientific urban planning and crucial amenities required for overall welfare, face urban chaos, and are highly vulnerable to natural and human-made disasters. Inadequacy of clean drinking water, clean air, green space, hygienic living conditions, hospitals, and other life-sustaining institutions in urban centers increases the vulnerability.

There is an inverse relationship between the quality of air and the COVID-19 mortality rate (Naqvi et al. 2021). For instance, it has been proven that PM can act as a carrier for SARS-COV-2 (Setti et al. 2020, Borisova & Komisarenko 2021, Pivato et al. 2021). The finer ones ($PM_{2.5}$) have a higher potential to spread the virus (Nor et al. 2021). However, such studies have not considered other possible socioeconomic factors influencing the COVID-19 death toll in urban centers. In that context, the present study examines the relationships between various socioeconomic factors and air quality that influenced the COVID-19 death in Indian cities.

MATERIALS AND METHODS

For the present study, we have selected 19 Indian cities based on the data available. These cities were Hyderabad, Visakhapatnam, Surat, Bangalore, Kochi, Bhopal, Indore, Jabalpur, Mumbai, Nagpur, Nashik, Pune, Jaipur, Chennai, Coimbatore, Kolkata, Delhi, Patna and Meerut (Fig. 1). These city centers in the corresponding districts are ascribed to be highly populous areas surrounded by less populated rural or sub-urban settlements. These city centers act as the centers of each district's economic, social, and administrative processes. In this study, the district-level COVID-19 death rate reported till 17 March 2022 was collected from the National Center for Disease Control under the Ministry of Health and Family Welfare, Government of India (https://www.ncdc.gov.in/Mortality/Home.html). We used the district-level data to represent the COVID-19 death cases of the cities since there were no reliable data available exclusively on the city-level COVID-19 death cases. Further, we assumed that the district-level data primarily represent the death cases reported from the urban centers; it is known that in India, rural COVID-19 death cases were not reported during the first wave and seldom reflected during the second wave (Jha et al. 2022).

The air quality data relating to SO_2, NO_2, and PM_{10} for ten years (2008-2019) corresponding to each of those cities was collected from the Indian Institute of Tropical Meteorology (IITM) (https://cpcb.nic.in/annual-report.php). Using the average values of SO_2, NO_2, and PM_{10}, the AQI for each city was calculated using the AQI matrix provided by the Central Pollution Control Board at https://app.cpcbccr.com/ccr_docs/AQI%20-Calculator.xls. The city's socioeconomic data, area, population, population density, per capita income, and the number of hospitals and hospital beds were collected from https://www.indiastat.com/, the annual death rates from https://crsorgi.gov.in/annual-report.html, and the GDP of the cities from https://ca.finance.yahoo.com/photos/the-top-15-indian-cities-by-gdp-1348807591slideshow.html.

Since there are no routine and exhaustive censuses conducted by the Census of India (Government of India) for 2021, we used the population data for the earlier 3 census periods, 1991, 2001, and 2011, and estimated the current population, making use of the growth trend and the well-known equation is given below:

$$PN = P_0(1 + \frac{r}{100})^t$$

Where *PN* is the projected population for the year *t*,

P_0 is the initial population

r is the population growth rate, and *t* is the years.

The growth rate was calculated using the equation

$$r = \{(P_n - P_0/P_0)100\}/N$$

Where *N* is the projected year.

Since there are no updated data on the number of hospitals and the total number of hospital beds available, we used the census data available for the years 2001 and 2011 procured from the office of the registrar general and census commissioner, India https://censusindia.gov.in/census.website/data/census-tables. While comparing the data between 2001 and 2011, we found that for some cities, there was a decrease in the number of hospitals and bed availability; hence, we used the latest census data (i.e. 2011) for the analysis.

Multiple correlation analysis was done to reveal the relationships among the variables. Multiple linear regression analysis was carried out to check the affinity of each variable to the COVID death rate since multiple regression analysis is a widely used simple model to predict an outcome variable (Y) from a group of predictor variables (X_n). In general, multiple regressions can be represented by the following equation:

$$\{Y = B_0 + B_1X_1 + B_2X_2 + \ldots B_nX_n + E\}$$

Where,

Y is the dependent predicted variable.

B_0 is the Y-intercept or value of Y when X values are 0.

B_1, B_2, and B_n are the regression coefficients for X_1, X_2, and X_n, respectively.

E is the residual standard deviation.

We used the R statistical package (Rstudio 2022.07.2) for all the analyses.

RESULTS AND DISCUSSIONS

The per capita income was highest in Surat, followed by Delhi and Mumbai, with the lowest per capita income in Jabalpur. The number of hospitals was highest in Mumbai, followed by Jabalpur, and the lowest number of hospitals in Jaipur. Mumbai has the highest number of hospital beds

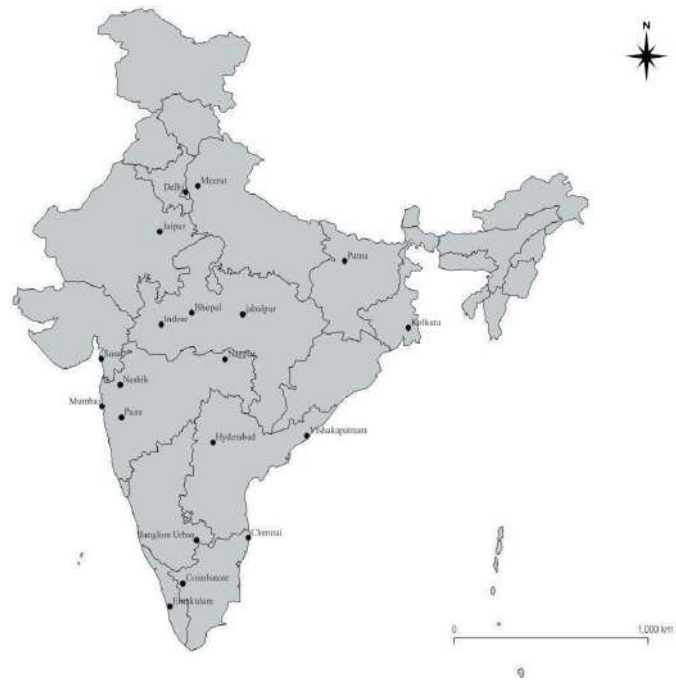

Fig. 1: Map of India showing the location of the 19 selected cities for the study.

available, followed by Jabalpur and Kochi, and the lowest was in Meerut. Among the 19 cities, the projected population is highest in Bangalore, followed by Mumbai, Delhi, Surat, Hyderabad, Pune, Jaipur, Chennai, Kolkata, Nagpur, Indore, Nashik, Patna, Visakhapatnam, Bhopal, Meerut, Jabalpur, Coimbatore, and Kochi. According to the population projection, Bangalore surpasses all other cities, including Mumbai and Delhi, due to Bangalore's consistently higher population growth rate, escalated possibly by immigration. The decadal population growth between 1991 and 2011 in Bangalore is more than five million. The immigration of highly skilled workers due to employment opportunities in the ICT sector, in the city, growing at an incredible pace (Narayana 2011) the "livability" of the city, mainly infrastructure amenities, climate, etc., could be the other factors for the population growth in Bangalore. It is important to note that, as suggested by the projection, the tier-2 cities in India, like Surat, Pune, and Jaipur, surpass the tier-1 cities, such as Chennai and Kolkata, in population. Sikarwar (2020) studied the population trend in Kolkata city and found that after 1971, the city's population showed a trend that, after 2001, slanted toward negative growth.

Moreover, cities like Bangalore (Ramachandra 2018) and Hyderabad (Das 2015) showed significant spatial growth during the last decade after the census in 2011. Among the cities, the GDP of Mumbai is the highest, followed by Delhi, Kolkata, and Bangalore. Jabalpur has the lowest GDP level among the cities.

The correlation analysis shows that all variables except the number of hospital beds positively correlate to the COVID-19 death rate in cities. GDP, population, the average death rate of the cities, and the concentration of NO_2 levels in the air are significantly correlated with the death rates. Although the number of hospital beds negatively correlated with the death rate, it is insignificant; very rational in that higher bed availability, a capital stock (Ravaghi et al 2020), and reflected better access to inpatient health care. Similarly, the SO_2, PM_{10}, Air Quality Index, per capita income, number of hospitals, urban area, and population density are positively correlated with the COVID-19 death rate of the cities but do not show any significant trend (Table 1).

The multiple regression analysis results between the COVID-19 death rate in the city with the other variables, NO_2, SO_2, PM_{10}, GDP, population, and normal death, of the cities indicated a positive impact. In contrast, AQI, income per capita, number of hospitals, number of hospital beds, area of the city, and the population density of the city show a negative relationship with the death rate. Of this, notably, only the population and area of the city have a significant level of predictability on the COVID-19 death in the city. From the model, COVID-19 deaths in the city can be estimated by the formula:

COVID death = $5.8 \times 103 + 0.0016 \times$ Population $- 21.9 \times$ Area, and the model is significant (Adjusted R-squared: 0.7126: p-value of F-statistic: 0.03; Table 2).

There is a significant positive correlation between the COVID-19 death rate and the population (r= 0.68; p=0.0564). Among the selected cities, COVID-19 death was reported highest in Delhi, followed by Pune, Mumbai, and Bangalore, all densely populated megacities in India. The lowest number of personal losses due to COVID-19 was reported in Jabalpur. According to some studies, COVID-19 death cases were higher in cities with denser populations in Algeria (Kadi & Khelfaoui 2020). It has to be noted that in highly populated cities such as Kolkata, Chennai, Surat, and Hyderabad, the reported cases are fewer, which might be due to imprecise statistics or deliberate under-reporting by the authorities to reduce the instances (Jha et al. 2022, Anand et al. 2021, Lancet 2020). It is also reported that there is a lack of reporting the COVID-19 death cases in the older age group in India (Lewnard et al. 2022).

While checking for the significant correlation between the population and other variables, it is found that only two variables that relate to the city's economic status, the GDP and per capita income, are significantly and positively correlated with the population. In India, it is documented that the rural-to-urban mass migration for employment in the non-agriculture sector has increased many folds during the post-globalization of the Indian market economy (Siggel 2010). The city's urban centers offer many opportunities for people from the rural agricultural sector. Due to many factors, including higher input costs, insufficient returns, and an inadequate labor force, the rural agriculture sector has become unprofitable. The immigration of the poor rural labor eventually increased city centers' GDP and per capita income. Among the selected cities, the country's commercial capital, Mumbai, scores the highest GDP, followed by Delhi and Kolkata, and the GDP of Jabalpur is the lowest.

Similarly, the per capita income of Jabalpur is the lowest among the studied cities; Surat has the highest per capita income among these cities. It is reported that there is a direct connection between the availability of transportation networks with COVID-19 spread (Zhu & Guo 2021). The air transportation networks significantly increased epidemics' spread in general (Colizza et al. 2006). In the case of COVID, due to global and local air travel, cities with higher GDP have a chance of higher spread since it is there that global investment and consequent travelers would be high, as reflected by the initial spread in cities like Mumbai and Delhi.

Table 1: Correlation matrix of the variables (Pearson correlation coefficients - r).

	CD	NO	SO	PM	AQI	IC	GDP	NH	NB	P	ND	AR	DEN
CD	1.00												
NO	0.53*	1.00											
SO	0.26	0.22	1.00										
PM	0.26	0.57*	-0.20	1.00									
AQI	0.27	0.59*	-0.17	1.00	1.00								
IC	0.30	0.16	0.30	0.06	0.08	1.00							
GDP	0.78*	0.43	-0.05	0.35	0.35	0.35	1.00						
NH	0.28	0.01	-0.11	-0.01	0.02	0.14	0.60	1.00					
NB	-0.02	-0.25	-0.25	-0.23	-0.21	0.05	0.25	0.77*	1.00				
P	0.68*	0.30	0.02	0.34	0.36	0.63*	0.75*	0.46	0.19	1.00			
ND	0.83*	0.45	-0.01	0.37	0.36	0.39	0.88*	0.31	0.04	0.79*	1.00		
AR	0.45	0.20	-0.03	0.13	0.16	0.34	0.51	0.35	0.17	0.77*	0.59*	1.00	
DEN	0.33	0.25	0.17	0.38	0.39	0.62*	0.43	0.15	-0.04	0.57*	0.47	0.04	1.00

CD: COVID deaths, NO = NO_2, SO = SO_2, PM = PM_{10}, AQI = Air Quality Index, IC = Percapita income, GDP = GDP of the city, NH = Number of Hospitals, NB = Number of Hospital Beds, P = Total Population, ND = Annual death in number, AR = Urban area, and DEN = Population density.

The highly populated cities in India are the country's economic hubs and industrial centers. Emissions, vehicular, and power generation are also higher in megacities due to higher per capita vehicle availability and higher energy consumption by diverse sectors. Further, household carbon emission is also a crucial issue in India (Beig et al. 2021). All these activities are closely related to air quality, and exposure to highly polluted air is one of the primary reasons of chronic respiratory illness of people, which is a potential factor significantly hiking the chances of death in COVID-affected individuals (Schraufnagel et al. 2019).

Especially since people suffering from other respiratory diseases exposed to air pollution are considered highly vulnerable to COVID-19 death due to comorbidities (Naqvi et al. 2021). Metro cities such as Delhi, Kolkata, and Mumbai are considered the most polluted areas in the world regarding air pollutants (Guttikunda & Nishadh 2022, Guttikunda et al. 2014). As per the recent report by IQAir (https://www.iqair.com/), based on the average annual PM_{10} concentration, Delhi stands fourth most highly polluted city in the world, followed by Meerut, Patna, Kolkata, Jaipur, Mumbai, Indore, Visakhapatnam, Bhopal, Jabalpur, Pune, Nashik, Hyderabad, Bengaluru, Chennai, and Kochi. However, IQAir does not document the air quality for Surat, Coimbatore, and Nagpur.

A significant positive relationship between AQI and COVID-19 death has been reported by various researchers globally (Wu et al. 2020, Zhu et al. 2020, Conticini et al. 2020). A significant correlation is seen between industrial pollutants like $PM_{2.5}$ and COVID-19 deaths in metropolitan and industrial cities in India, as Travaglio et al. (2020) observed. While examining the disability-adjusted life years (DALYs) of the people living in Delhi and Mumbai in 2015, Maji et al. (2017b) found that for the low AQI, the mortality rate increased more than double the mortality observed during 1995 for both the cities. Kolluru et al. (2022) examined the significant relationship between air quality and the COVID spread during the second wave in Delhi. The present study also demonstrates a positive relationship between COVID-19 death and the AQI of cities, but it is not statistically significant. However, there is a significant correlation between the concentration of NO_2 in the urban air and COVID-19 death. The insignificance of AQI's relation with death might be due to the insignificance of the other variables, SO_2 and $PM_{10,}$ in determining the AQI of the city, possibly for the inaccuracy in the measurement of the parameters available in these official data sets.

Studies have already proved that prolonged exposure to high concentrations of NO_2 in the atmosphere can lead to other ailments (Ogen 2020), such as hypertension, diabetes (Shin et al. 2020), and other ischemic heart diseases (Qiu et al. 2013). A significant positive correlation between the average annual death rate and the COVID-19 death rate was observed in the present study. It is reported that 12.5% of India's average normal death rate is due to diseases associated with high exposure to poor air quality (Guttikunda & Goel 2013). Further, Maji et al. (2017a) concluded that poor air quality directly influences the annual mortality rate in Delhi alone. As mentioned earlier, it is reported that people exposed to poor AQI are highly vulnerable to mortality due to COVID-19 (Naqvi et al. 2021). Further, the present results indicate that the country still lacks monitoring infrastructure and high-resolution pollution concentration maps relating

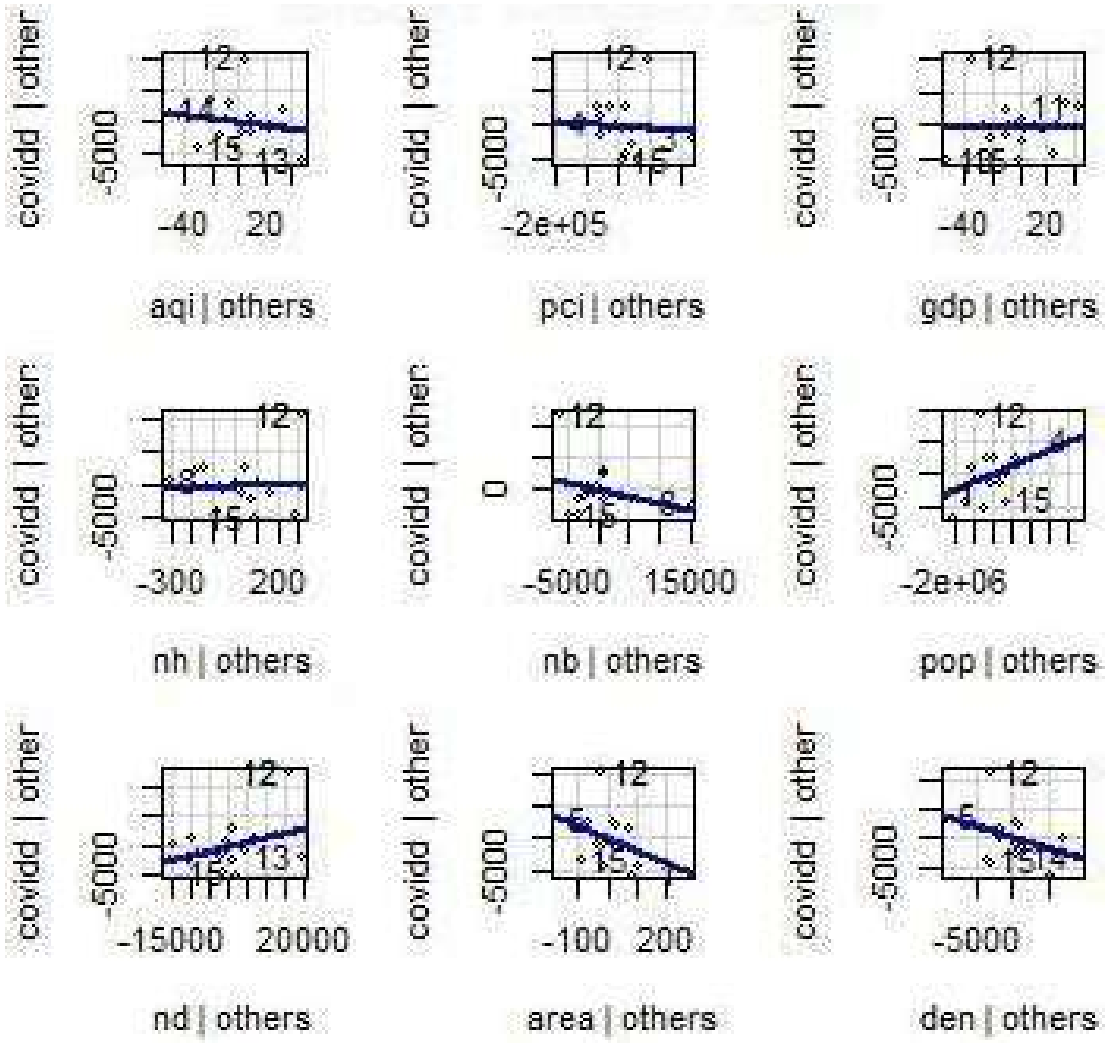

Fig. 2. Added variable plot for potential drivers for COVID death in urban India. AQI, per capita income, number of hospitals, number of hospital beds, the total area of the city, and population density showcase a negative relationship. Population and average annual death show a positive relationship, whereas per capita income, GDP, and the number of hospitals are almost neutral in association with COVID-19 deaths.

to urban India's real-time air quality assessment (Agrawal et al. 2021).

It must be noted that all megacities are at the top of the list while checking the number of hospitals and hospital beds in the cities. However, when it comes to the per capita availability of hospital facilities, cities including megacities, is very low. It has been found that the average death rate before the COVID-19 scenario shows no significant correlation between the per capita availability of hospital facilities and the annual death rate among the cities.

This again shows that the number of hospital facilities needs to be improved for the population. The number of hospital beds per the census data includes private and public hospitals; in India, it is clear that for most of the population, accessing private facilities is still a financial concern (Duggal 2007). Recent studies on the Indian healthcare system in the wake of the COVID-19 pandemic also reveal the fact that the privatization of medical facilities has become a financial, geographical, administrative, and logistic burden for the middle and low-income groups, the majority of the population in the country (Bhaduri 2020). The government's role has been highly restricted to financial aid for private parties (Chandwani 2021), while the government promotes the privatization of even such essential facilities.

It is worth noting that the present study does not testify to the inverse relationship between AQI and COVID-19 death, as reported by many others mentioned in the text. We presume this may be due to a shortage of data with adequate

Table 2: Multiple regression analysis results.

Parameter	Estimate	Std.Error	t value	Pr(>|t|)
(Intercept)	5.89E+03	1.04E+04	0.569	0.5902
NO_2	1.07E+02	1.00E+02	1.068	0.3264
SO_2	3.69E+02	2.13E+02	1.733	0.1338
PM_{10}	3.80E+01	2.99E+02	0.127	0.9028
AQI	-8.65E+01	4.09E+02	-0.211	0.8395
Income per capita	-1.24E-02	1.10E-02	-1.122	0.3049
GDP	6.18E+00	3.91E+01	0.158	0.8795
Hospital	-1.31E+00	5.32E+00	-0.247	0.8134
Hospital beds	-1.22E-02	2.22E-01	-0.055	0.9579
Population	1.59E-03	6.73E-04	2.359	*0.0564
Normal death	1.23E-01	1.06E-01	1.155	0.292
Area	-2.19E+01	9.85E+00	-2.222	*0.068
Density	-4.17E-01	2.20E-01	-1.899	0.1063

Significance codes: '*' 0.1
Multiple R-squared: 0.9042, Adjusted R-squared: 0.7126
F-statistic: 4.719 on 12 and 6 DF, p-value: 0.03406

precision and the sampling points not being statistically representative. The Added variable plot (Fig. 2) between drivers and COVID-19 deaths in urban India also indicates the absence of precise data. For example, as per Fig. 2, COVID-19 death is negatively influenced by the AQI of the respective cities, which is unreasonable according to the general understanding (Naqvi et al. 2021). Similarly, the negative relationship between the city's population density and COVID-19 deaths, as shown in the plot, is illogical since the disease spread is likely to be enhanced by physical closeness among the people (Kadi & Khelfaoui 2020). As mentioned earlier, data reliability is one of the major lacunae in countries like India, which is one of the major limitations of this type of study. It may be noted that the Death and Birth Registration Authority accepts the inadequacy of reliable data on mortality in India (Basu & Adair 2021).

CONCLUSION

Several studies from various parts of the globe documented the regional AQI in urban city centers and its influence in spreading the COVID-19 epidemic. However, we hypothesized that several more underlying socioeconomic factors influence the spread of COVID-19. The present study evaluates COVID-19 in urban India by examining the socioeconomic factors and the AQI of 19 randomly selected urban centers. Our results showcased that the COVID death positively correlates with AQI, population, population density, the average annual death rate in the city, the total area of the urban centers, income per capita, and GDP; and the correlation is significant for GDP, population and average annual death rate of the city. It is also found that among the factors determining the AQI, the concentration of NO_x is significantly correlated with COVID-19 death. COVID-19 death in cities is negatively correlated with the number of hospital beds in the city. The multiple regression analysis among the selected variables also showed significant positive relationships between COVID-19 death and the population and the total urban area in the city. The study also concluded that the lack of reliable data is a major lacuna while examining the crucial drivers of COVID-19 death in urban India.

REFERENCES

Aditya N.S., Nair, A.Y. and Veni, S. 2022. Determining the Effect of Correlation between Asthma/Gross Domestic Product and Air Pollution. In 2022 International Conference on Wireless Communications Signal Processing and Networking (WiSPNET) (pp. 44-48). IEEE

Agrawal, G., Mohan, D. and Rahman, H. 2021. Ambient air pollution in selected small cities in India: Observed trends and future challenges. IATSS Res., 45(1): 19-30.

Anand, A., Sandefur, J. and Subramanian, A. 2021. Three new estimates of India's all-cause excess mortality during the COVID-19 pandemic.

Balachandran, S., Moni, M., Sathyapalan, D.T., Varghese, P., Jose, M.P., Murugan, M.R., Rajan, C., Saboo, D., Nair, S.S., Varkey, R.A. and Balachandran, P. 2022. A comparison of clinical outcomes between vaccinated and vaccine-naive patients of COVID-19 in four tertiary care hospitals of Kerala, South India. Clinical Epidemiology and Global Health, 13: 100971.

Balakrishnan, K., Cohen, A. and Smith, K.R. 2014. Addressing the burden of disease attributable to air pollution in India: the need to integrate across household and ambient air pollution exposures. Environ. Health Persp., 122(1): A6-A7.

Balakrishnan, K., Dey, S., Gupta, T., Dhaliwal, R.S., Brauer, M., Cohen, A.J., Stanaway, J.D., Beig, G., Joshi, T.K., Aggarwal, A.N. and Sabde, Y. 2019. The impact of air pollution on deaths, disease burden, and life expectancy across the states of India: The global burden of disease study 2017. Lancet Planet. Health, 3(1): e26-e39.

Basu, J.K. and Adair, T. 2021. Have inequalities in the completeness of death registration between states in India narrowed during two decades of civil registration system strengthening? Int. J. Equity Health, 20(1): 1-9.

Beig, G., Korhale, N., Rathod, A., Maji, S., Sahu, S.K., Dole, S., Latha, R. and Murthy, B.S. 2021. On modeling the growing menace of household emissions under COVID-19 in Indian metros. Environ. Pollut., 272: 115993.

Benmarhnia, T. 2020. Linkages between air pollution and the health burden from COVID-19: methodological challenges and opportunities. Am. J. Epidemiol., 189(11): 1238-1243.

Bhaduri, S.D. 2020. Post-COVID healthcare reform in India: What to expect? J. Family Med. Primary Care, 9(11): 5427.

Borisova, T. and Komisarenko, S. 2021. Air pollution particulate matter as a potential carrier of SARS-CoV-2 to the nervous system and/or neurological symptom enhancer: Arguments in favor. Environ. Sci. Pollut. Res., 28(30): 40371-40377.

Cao, Y., Chen, M., Dong, D., Xie, S. and Liu, M. 2020. Environmental pollutants damage airway epithelial cell cilia: Implications for the prevention of obstructive lung diseases. Thoracic Cancer, 11(3): 505-510.

Chandwani, R. 2021. Stakeholders in the Indian Healthcare Sector. Vikalpa, 46(2): 65-70.

Chen, S. and Jin, H. 2019. Pricing for the clean air: Evidence from the Chinese housing market. J. Clean. Prod., 206: 297-306.

Colizza, V., Barrat, A., Barthélemy, M. and Vespignani, A. 2006. The role of the airline transportation network in the prediction and predictability of global epidemics. Proceed. National Acad. Sci., 103(7): 2015-2020.

Conticini, E., Frediani, B. and Caro, D. 2020. Can atmospheric pollution be considered a co-factor in extremely high levels of SARS-CoV-2 lethality in Northern Italy? Environ. Pollut., 261: 114465.

Das, D. 2015. Hyderabad: Visioning, restructuring and making of a high-tech city. Cities, 43: 48-58.

Duggal, R. 2007. Healthcare in India: changing the financing strategy. Social Pol. Admin., 41(4): 386-394.

Girdhar, A., Kapur, H., Kumar, V., Kaur, M., Singh, D. and Damasevicius, R. 2021. Effect of COVID-19 outbreak on urban health and environment. Air Qual. Atmos. Health, 14(3): 389-397.

Gupta, A., Bherwani, H., Gautam, S., Anjum, S., Musugu, K., Kumar, N., Anshul, A. and Kumar, R. 2021. Is air pollution aggravating COVID-19 lethality? Exploration in Asian cities using statistical models. Environ. Dev. Sustain., 23(4): 6408-6417

Gurjar, B.R., Ravindra, K. and Nagpure, A.S. 2016. Air pollution trends over Indian megacities and their local-to-global implications. Atmos. Environ., 142: 475-495.

Guttikunda, S. and Nishadh, K.A. 2022. Evolution of India's PM2.5 pollution between 1998 and 2020 using global reanalysis fields coupled with satellite observations and fuel consumption patterns. Environ. Sci. Atmos., 15: 541.

Guttikunda, S.K. and Goel, R. 2013. Health impacts of particulate pollution in a megacity—Delhi, India. Environ. Dev., 6: 8-20.

Guttikunda, S.K., Goel, R. and Pant, P. 2014. Nature of air pollution, emission sources, and management in the Indian cities. Atmos. Environ., 95: 501-510.

Heissel, J.A., Persico, C. and Simon, D. 2022. Does pollution drive achievement? The effect of traffic pollution on academic performance. J. Hum. Resour., 57(3): 747-776.

Jha, P., Deshmukh, Y., Tumbe, C., Suraweera, W., Bhowmick, A., Sharma, S., Novosad, P., Fu, S.H., Newcombe, L., Gelband, H. and Brown, P. 2022. COVID mortality in India: National survey data and health facility deaths. Science, 375(6581): 667-671.

Jiang, Y., Wu, X.J. and Guan, Y.J. 2020. Effect of ambient air pollutants and meteorological variables on COVID-19 incidence. Infect. Contr. Hosp. Epidemiol., 41(9): 1011-1015.

Kadi, N. and Khelfaoui, M. 2020. Population density, a factor in the spread of COVID-19 in Algeria: statistic study. Bull. National Res. Centre, 44(1): 1-7.

Karagulian, F., Belis, C.A., Dora, C.F.C., Prüss-Ustün, A.M., Bonjour, S., Adair-Rohani, H. and Amann, M. 2015. Contributions to cities' ambient particulate matter (PM): A systematic review of local source contributions at global level. Atmos. Environ., 120: 475-483.

Kejela, T. 2020. Probable factors contributing to the fast spread of the novel Coronavirus (COVID-19) in Ethiopia. J. Infect. Dis. Epidemiol., 6: 169.

Khilnani, G.C. and Tiwari, P. 2018. Air pollution in India and related adverse respiratory health effects: past, present, and future directions. Curr. Opinion Pulm. Med., 24(2): 108-116.

Kolluru, S.S.R., Nagendra, S.M., Patra, A.K., Gautam, S., Alshetty, V.D. and Kumar, P. 2022. Did unprecedented air pollution levels cause a spike in Delhi's COVID cases during the second wave? Stoch. Environ. Res. Risk Assess., 15: 1-16.

Lakshmi, P.S. and Suresh, M. 2020. Factors influencing the epidemiological characteristics of pandemic COVID-19: A TISM approach. Int. J. Healthcare Manag., 13(2): 89-98.

Lancet, T. 2020. COVID-19 in India: the dangers of false optimism. Lancet (London, England), 396(10255): 867.

Lewnard, J.A., Mahmud, A., Narayan, T., Wahl, B., Selvavinayagam, T.S. and Laxminarayan, R. 2022. All-cause mortality during the COVID-19 pandemic in Chennai, India: an observational study. Lancet Infect. Dis., 22(4): 463-472.

Maji, K.J., Dikshit, A.K. and Deshpande, A. 2017b. Disability-adjusted life years and economic cost assessment of the health effects related to PM2.5 and PM10 pollution in Mumbai and Delhi, India, from 1991 to 2015. Environmental Science and Pollution Research, 24(5): 4709-4730.

Maji, S., Ahmed, S., Siddiqui, W.A. and Ghosh, S. 2017a. Short-term effects of criteria air pollutants on daily mortality in Delhi, India. Atmos. Environ., 150: 210-219.

Manjula, P.M. 2018. Economics and air pollution analysis of Chennai city. Int. Rev. Bus. Econ., 1(3): 17.

Naqvi, H.R., Mutreja, G., Shakeel, A. and Siddiqui, M.A. 2021. Spatio-temporal analysis of air quality and its relationship with major COVID-19 hotspot places in India. Remote Sens. Appl. Soc. Environ., 22: 100473.

Nasir, H., Goyal, K. and Prabhakar, D. 2016. Review of air quality monitoring: A case study of India. Indian J. Sci. Technol., 9(44): 1-7.

Nor, N.S.M., Yip, C.W., Ibrahim, N., Jaafar, M.H., Rashid, Z.Z., Mustafa, N., Hamid, H.H.A., Chandru, K., Latif, M.T., Saw, P.E. and Lin, C.Y. 2021. Particulate matter (PM2. 5) as a potential SARS-CoV-2 carrier. Scientific Reports, 11(1): 1-6.

Ogen, Y. 2020. Assessing nitrogen dioxide (NO2) levels as a contributing factor to Coronavirus (COVID-19) fatality. Science of the Total Environment, 726: 138605.

Pandey, A., Brauer, M., Cropper, M.L., Balakrishnan, K., Mathur, P., Dey, S., Turkgulu, B., Kumar, G.A., Khare, M., Beig, G. and Gupta, T. 2021. Health and economic impact of air pollution in the states of India: The global burden of disease study 2019. Lancet Planet. Health, 5(1): e25-e38.

Pivato, A., Amoruso, I., Formenton, G., Di Maria, F., Bonato, T., Vanin, S., Marion, A. and Baldovin, T. 2021. Evaluating the presence of SARS-CoV-2 RNA in the particulate matter during the peak of COVID-19 in Padua, northern Italy. Sci. Total Environ., 784: 147129.

Priya, V., Samyuktha, S., Fernandez, S., Biju, A., Anand, G.S., Venniyoor, V., Mathew, K.A. and Marwaha, V. 2021. Knowledge, attitude, and practice towards COVID-19 among social media users in an engineering college in South India. J. Commun. Dis., 3(2): 35-42.

Qiu, H., Yu, I.T.S., Wang, X., Tian, L., Tse, L.A. and Wong, T.W. 2013. Season and humidity dependence of the effects of air pollution on COPD hospitalizations in Hong Kong. Atmos. Environ., 76: 74-80.

Raj, P.P.N. and Azeez, P.A. 2020. Economic Growth, the Pandemic, and the Convalescing Nature. Retrieved from https://businesseconomics.in/economic-growth-pandemic-and-convalescing-nature.

Ravaghi, H., Alidoost, S., Mannion, R. and Bélorgeot, V.D. 2020. Models and methods for determining the optimal number of beds in hospitals and regions: A systematic scoping review. BMC Health Services Res., 20(1): 1-13.

Schraufnagel, D.E., Balmes, J.R., Cowl, C.T., De Matteis, S., Jung, S.H., Mortimer, K., Perez-Padilla, R., Rice, M.B., Riojas-Rodriguez, H., Sood, A. and Thurston, G.D. 2019. Air pollution and noncommunicable diseases: A review by the Forum of International Respiratory Societies' Environmental Committee, Part 2: Air pollution and organ systems. Chest, 155(2): 417-426.

Setti, L., Passarini, F., De Gennaro, G., Barbieri, P., Licen, S., Perrone, M.G., Piazzalunga, A., Borelli, M., Palmisani, J., Di Gilio, A. and Rizzo, E. 2020. Potential role of particulate matter in the spreading of COVID-19 in Northern Italy: first observational study based on initial epidemic diffusion. BMJ Open, 10(9): e039338.

Shin, S., Bai, L., Oiamo, T.H., Burnett, R.T., Weichenthal, S., Jerrett, M., Kwong, J.C., Goldberg, M.S., Copes, R., Kopp, A. and Chen, H. 2020. Association between road traffic noise and incidence of diabetes

mellitus and hypertension in Toronto, Canada: a population□based cohort study. J. Am. Heart Association, 9(6): e013021.
Siggel, E. 2010. The Indian informal sector: the impact of globalization and reform. Int. Lab. Rev., 149(1): 93-105.
Sikarwar, A. and Rani, R. 2020. Assessing the immediate effect of COVID-19 lockdown on air quality: A case study of Delhi, India. Journal of Environmental Geography, 13(3-4): 27-33.
Sikarwar, A. 2020. Falling population growth and subsequent land use pattern: A study of Kolkata. In Chattopadhyay, A. and Ghosh, S. (eds), Population Dynamics in Eastern India and Bangladesh, Springer, Singapore, pp. 383-392.
Sivarethinamohan, R., Sujatha, S., Priya, S., Gafoor, A. and Rahman, Z. 2021. Impact of air pollution in health and socioeconomic aspects: review on future approach. Mater. Today Proceed., 37: 2725-2729.
Subbarao, K. and Mahanty, S. 2020. Respiratory virus infections: understanding COVID-19. Immunity, 52(6): 905-909.
Travaglio, M., Yu, Y., Popovic, R., Selley, L., Leal, N.S. and Martins, L.M. 2021. Links between air pollution and COVID-19 in England. Environ. Pollut., 268: 115859.
Venkataraman, C., Brauer, M., Tibrewal, K., Sadavarte, P., Ma, Q., Cohen, A., Chaliyakunnel, S., Frostad, J., Klimont, Z., Martin, R.V. and Millet, D.B. 2018. Source influence on emission pathways and ambient PM 2.5 pollution over India (2015-2050). Atmos. Chem. Phys., 18(11): 8017-8039.
World Health Organization (WHO). 2021. New WHO Global Air Quality Guidelines Aim to Save Millions of Lives from Air Pollution. Retrieved from https://www.who.int/news/item/22-09-2021-new-who-global-air-quality-guidelines-aim-to-save-millions-of-lives-from-air-pollution (accessed October 1, 2021)
Wu, X., Nethery, R.C., Sabath, M.B., Braun, D. and Dominici, F. 2020. Exposure to air pollution and COVID-19 mortality in the United States: A nationwide cross-sectional study. MedRxiv, 11: 225.
Zhu, P. and Guo, Y. 2021. The role of high-speed rail and air travel in the spread of COVID-19 in China. Travel Med. Infect. Dis., 42: 102097.
Zhu, Y., Xie, J., Huang, F. and Cao, L. 2020. Association between short-term exposure to air pollution and COVID-19 infection: Evidence from China. Sci. Total Environ., 727: 138704.

ORCID DETAILS OF THE AUTHORS

P. P. Nikhil Raj: https://orcid.org/0000-0002-5104-4607

Nature Environment and Pollution Technology
An International Quarterly Scientific Journal

p-ISSN: 0972-6268
(Print copies up to 2016)
e-ISSN: 2395-3454

Vol. 23 | No. 1 | pp. 255-263 | 2024

Original Research Paper

https://doi.org/10.46488/NEPT.2024.v23i01.021

Open Access Journal

The Suitability of Fe_3O_4/Graphene Oxide Nanocomposite for Adsorptive Removal of Methylene Blue and Congo Red

Viet Cao*†, Phuong Anh Cao, Duy Linh Han**, Minh Tuan Ngo***, Truong Xuan Vuong**** and Hung Nguyen Manh***

*Faculty of Natural Sciences, Hung Vuong University, Nguyen Tat Thanh Street, Viet Tri 35120, Phu Tho, Vietnam
**Joint Russia-Vietnam Tropical Science and Technology Research Center, 63 Nguyen Van Huyen, Hanoi 122100, Vietnam
***Department of Manufacturing Engineering, Faculty of Mechanical Engineering, Thai Nguyen University of Technology, Thai Nguyen 250000, Vietnam
****Faculty of Chemistry, TNU-University of Science, Thai Nguyen City 24000, Vietnam
†Corresponding author: Viet Cao; caoviet@hvu.edu.vn

Nat. Env. & Poll. Tech.
Website: www.neptjournal.com

Received: 22-06-2023
Revised: 15-07-2023
Accepted: 02-08-2023

Key Words:
Fe_3O_4/GO nanocomposite
Methylene blue
Congo red
Adsorption

ABSTRACT

In this study, Fe_3O_4/GO nanocomposite was synthesized by hydrothermal method and tested for its efficiency in removing methylene blue (MB) and congo red (CR) from water. The synthesized nanocomposite was characterized using Fourier-transform infrared spectroscopy (FTIR), X-ray diffraction (XRD), and scanning electron microscopy (SEM). The optimal values for MB and CR removal were determined to be pH 6.0, an adsorbent weight of 50.0 mg, and a contact time of 10 min. The adsorption isotherms of the contaminants on the nanocomposite were analyzed using the Freundlich model, indicating a heterogeneous distribution of active sites on the adsorbent surface. The highest adsorption capacity of MB and CR is 135.1 and 285.7 $mg.g^{-1}$, respectively. Moreover, Fe_3O_4/GO nanocomposite recycled five cycles with proper adsorption capacity. Overall, the Fe_3O_4/GO nanocomposite holds great promise for efficient and sustainable water treatment, providing safe and clean water globally.

INTRODUCTION

Water pollution is a significant environmental and health problem, with various sources of contamination, including industrial and domestic waste, agricultural practices, and natural disasters such as floods and landslides (Akhtar et al. 2021, Luo et al. 2022, Peters & Meybeck 2000). Dyes play a significant role as pollutants in wastewater, posing a considerable threat to human health due to their persistent and non-biodegradable properties. Dyes are categorized based on the charge of their chromophore group, namely cationic, anionic, and non-ionic dyes, the latter being insoluble in water (Maheshwari et al. 2021). Congo red (CR) is a well-known anionic diazo dye widely used in the textile industry, laboratory research, and staining applications. On the other hand, methylene blue (MB) is a basic dye applied widely by textile and paper industries to scientific research and medical practices. This versatile dye has exceptional color stability and water solubility (Heo et al. 2022, Lachheb et al. 2002). Both MB and CR dyes pose severe risks to human health, including gastrointestinal illnesses, skin diseases, and even cancer (Halim et al. 2015, Thattil & Leema Rose 2019). Therefore, developing efficient and sustainable water treatment technologies is essential for ensuring access to safe and clean water.

In recent years, nanotechnology has emerged as a promising water treatment approach due to nanoparticles' unique properties (Gehrke et al. 2015, Qu et al. 2013, Theron et al. 2008). Nanoparticles have a high surface-to-volume ratio, enhancing their reactivity and allowing for the development of more efficient and effective water treatment technologies (Cele 2020, Saikia et al. 2019, Vaghari et al. 2016).

The Fe_3O_4/graphene oxide (Fe_3O_4/GO) composite has received considerable attention among the various nanoparticles due to its excellent adsorption and photocatalytic properties (Ouyang et al. 2015, Yao et al. 2012). Fe_3O_4 nanoparticles possess magnetic properties, which enable easy separation of the nanocomposite from treated water using an external magnetic field. GO has a large specific surface area and high reactivity, making it an ideal support material for

Fe_3O_4 nanoparticles. Studies on the removal of CR and MB from aqueous solution based on Fe_3O_4/GO nanoparticles and their adsorption mechanism are still lacking.

In this study, Fe_3O_4/GO nanocomposite was synthesized and tested for its efficiency in removing two contaminants, namely methylene blue (MB) and congo red (CR), from water. Different experimental factors, such as pH, the weight of the adsorbent, and the contact time, were investigated to determine their impact on the adsorption efficiency of Fe_3O_4/GO nanocomposites. Additionally, the viability of recycling the material to maintain its adsorption capacity for MB and CR was evaluated.

MATERIALS AND METHODS

Materials and Chemicals

The materials used in this study include methylene blue ($C_{16}H_{18}ClN_3S$), congo red ($C_{32}H_{22}N_6Na_2O_6S_2$), iron(II) chloride tetrahydrate ($FeCl_2.4H_2O$), iron(III) chloride hexahydrate ($FeCl_3.6H_2O$), graphite, sodium hydroxide (NaOH), hydrochloric acid (HCl), sulfuric acid (H_2SO_4), hydrogen peroxide (H_2O_2), potassium permanganate ($KMnO_4$), and sodium nitrate ($NaNO_3$). All chemicals were purchased from Sigma-Aldrich (St. Louis, MO, USA) and Merck (Darmstadt, Germany). Deionized (DI) water was used in all experiments.

Instrumentation

The equipment used in this study includes a magnetic stirrer, pH meter, ultraviolet-visible (UV-Vis) spectrophotometer (Genesys 10s, USA), and centrifuge (Hettich Zentrifugen, Germany). The adsorptions of MB and CR were measured at 665 nm, 498 nm, and 510 nm, respectively. The morphology and structure of the Fe_3O_4/GO composite were characterized using scanning electron microscopy (SEM) (TM 4000 plus Hitachi) and X-ray diffraction (XRD) (MiniFlex 600 Rigaku) employing CuK_α (λ=1.5418 Å, 2Θ/steps = 0.03 °/step). Fourier transform infrared spectroscopy (FTIR) in the range 4000 to 400 cm^{-1} was carried out using FT/IR-4600 Jasco. The surface area was observed by Brunauer–Emmett–Teller (Micromeritics Tristar II 3020). Magnetic measurements were made using a vibrating sample magnetometer (VSM) at room temperature.

Synthesis of Fe_3O_4/GO Nanocomposite

To synthesize GO, natural graphite powder was subjected to a modified Hummer's method (Zaaba et al. 2017). In brief, 3 g graphite powder was added to 42 mL H_2SO_4 98% and cooled under vigorous stirring. $KMnO_4$ was added steadily and kept at a temperature of up to 35°C, vigorous stirring for 30 min. DI water was added slowly, and the mixture was kept under 50°C, stirring for 1 h. The mixture was washed with H_2O_2, HCl, and DI water and dried under vacuum at 50°C.

To synthesize Fe_3O_4/GO, 5,79 g of $FeCl_2.4H_2O$ and 8,1 g of $FeCl_3.6H_2O$ were dissolved in 200 mL of DI water and homogenized solution of dispersed graphene oxide with ultrasonic vibration. Afterward, a vigorous stirring process was employed to add NaOH until the pH reached approximately 12. Subsequently, the mixture was heated to 150°C in a Teflon-lined autoclave for 7 h. The resulting mixture was then separated by centrifugation, followed by multiple washes with ethanol and water. Finally, it was dried at 80°C for 12 h.

Procedure

Batch adsorption studies were conducted to evaluate the Fe_3O_4/GO nanocomposite's efficiency for removing MB and CR from samples. In each experiment, a known amount of the Fe_3O_4/GO nanocomposite was added to a 50 mL aqueous solution of the contaminant with an initial concentration of 10 to 500 $mg.L^{-1}$. The solution was ultrasonic vibration for 5 min and stirred for 30 min. After that, the solution was kept at room temperature. The Fe_3O_4/GO nanocomposite was separated from the solution by magnetic separation and centrifugation, and the residual concentration of the contaminant was measured using a UV-Vis spectrophotometer. The efficiency of adsorbate removal (*AR*) and adsorption capacity of equilibrium () was calculated using the following equation:

$$AR\ \% = \frac{C_0 - C_t}{C_0} x100$$

$$q_e = \frac{V(C_0 - C_t)}{m}$$

Where C_0 is the initial concentration, C_t is the MB or CR concentration at time t, respectively. m is the amount of used adsorbents, V is the solution volume.

RESULTS AND DISCUSSION

Characterization of Fe_3O_4/GO Nanocomposite

Fig. 1 displays the Fourier-transform infrared (FTIR) spectra of the adsorbent in the range of 400-4000 cm^{-1}. The peak at about 582 cm^{-1}, which indicates the vibration of the Fe-O bond, corresponds to the formation of Fe_3O_4 in the adsorbent (Cao et al. 2014, Nguyen et al. 2020). The peak at 1384 and 1052 cm^{-1} were assigned to the two stretching vibration bands related to the C–O bond attached to the hydroxyl and carboxyl groups, respectively. Additionally, stretching

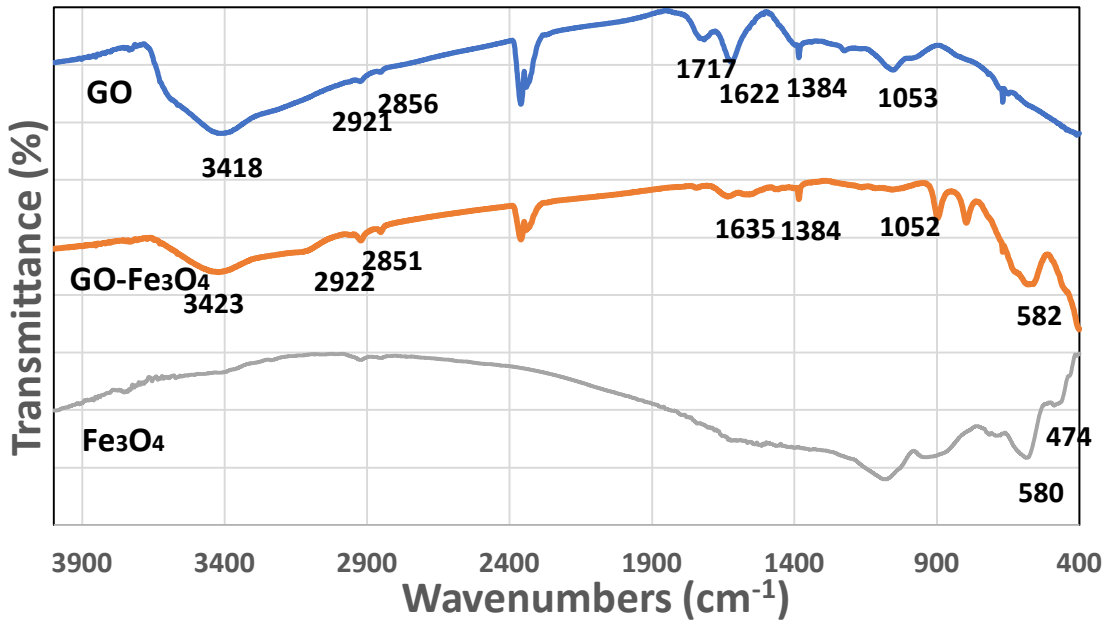

Fig. 1: FTIR spectra of the Fe_3O_4/GO nanocomposite.

vibrations of C=C are identified at 1635 cm^{-1}. The stretching vibration bands related to the C = O bond of the carboxyl group can be seen at 1717 cm^{-1}. The stretching vibration of the O-H bond was observed as a strong vibration in the range of around 3423 cm^{-1}. These findings aligned with previous studies (Cui et al. 2015, Liu et al. 2014, Ye et al. 2014). Consequently, these findings confirm the successful synthesis of the Fe_3O_4/GO adsorbent, in which all functional groups act as sites for adsorption and substantially contribute to capturing MB and CR from the samples.

The X-ray diffraction (XRD) patterns of the Fe_3O_4/GO are shown in Fig. 2. The peaks can be seen at $2\theta = 30.1^o$ (220), 35.5^o (311), 43.1^o (400), 53.1^o (422), 57.1^o (511), and 62.5^o (440). By comparing the angle pattern observed in the XRD analysis with the standard Fe_3O_4 compound card (JCPDS file no. 190629), it could be concluded that the composite being studied was consistent with the magnetite phase (He & Gao 2011). These findings provide crucial information on the crystallographic properties of Fe_3O_4/GO, which was essential in understanding the adsorption behavior of the nanocomposite.

Fig. 3 displays SEM images of Fe_3O_4/GO nanocomposite samples captured at different magnifications. The images reveal that spherical magnetic nanoparticles ranged in size from 30 to 100 nm and were located on the surface of GO. The adsorption-desorption isotherm is shown in Fig. 4. The specific surface area of Fe_3O_4/GO nanocomposite is 604.57

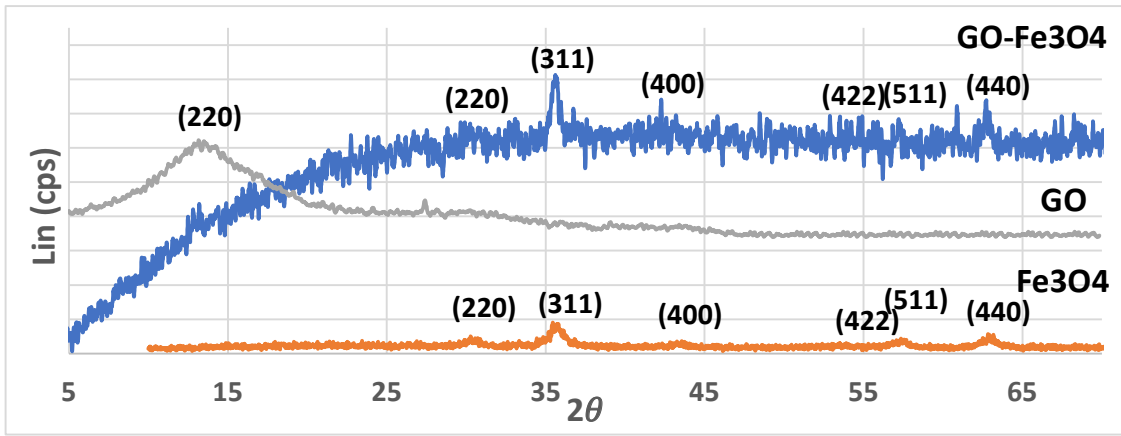

Fig. 2: XRD patterns of the Fe_3O_4/GO nanocomposite.

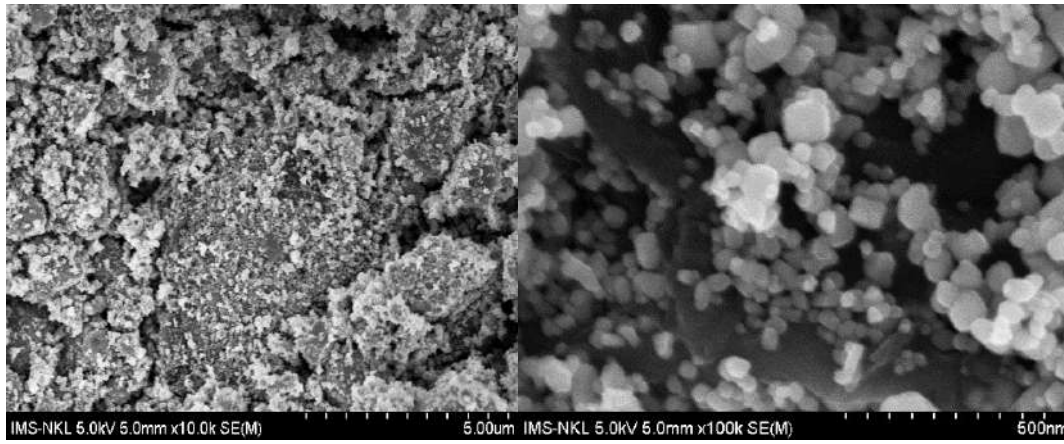

Fig. 3: SEM image of Fe_3O_4/GO nanocomposite.

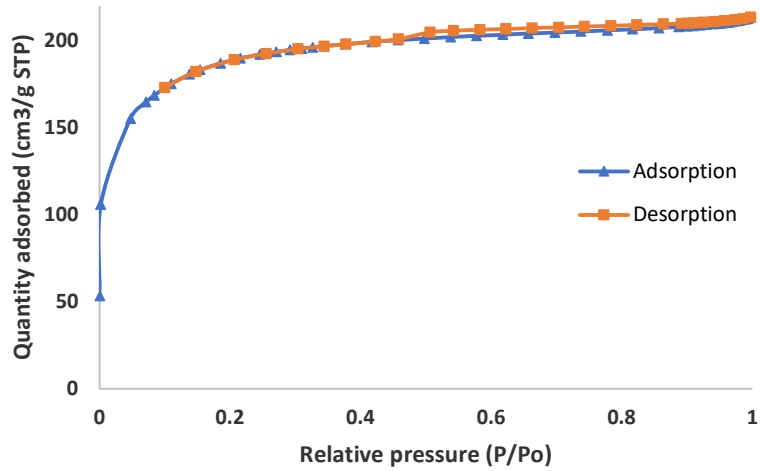

Fig. 4: N_2 adsorption and desorption isotherms of Fe_3O_4/GO nanocomposite.

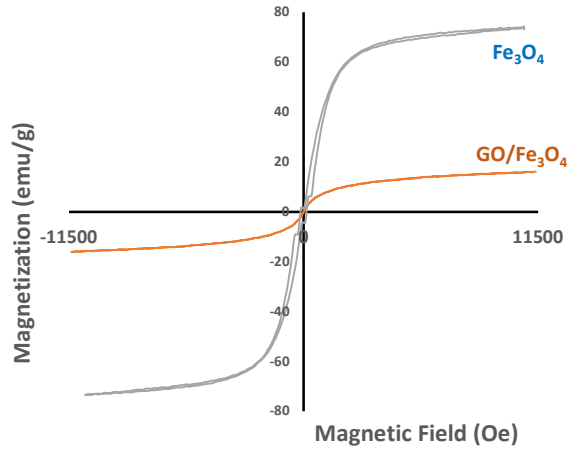

Fig. 5: Magnetic hysteresis loop of Fe_3O_4/GO nanocomposites and Fe_3O_4.

$m^2.g^{-1}$, which is higher than the reported values (Liu et al. 2012, Mahvi et al. 2021).

Fig. 5 presents the magnetization hysteresis curves of Fe_3O_4/GO, which were measured under room temperature conditions. The saturation magnetization of Fe_3O_4/GO was determined to be 15.91 $emu.g^{-1}$, demonstrating a lower value compared to that of Fe_3O_4 (73.55 $emu.g^{-1}$). This reduction in saturation magnetization can be attributed to the lower concentration of Fe_3O_4 within Fe_3O_4/GO, which was caused by the presence of the non-magnetic component GO. The graph in Fig. 5 reveals that the remanence magnetization and coercivity values of Fe_3O_4/GO were remarkably low, indicating that Fe_3O_4/GO exhibited superparamagnetic behavior at room temperature. The superparamagnetic properties of Fe_3O_4/GO suggest that it could be readily separated from water by applying a magnetic field. Furthermore, upon removal of the magnetic field, Fe_3O_4/GO can disperse effectively within a reaction solution.

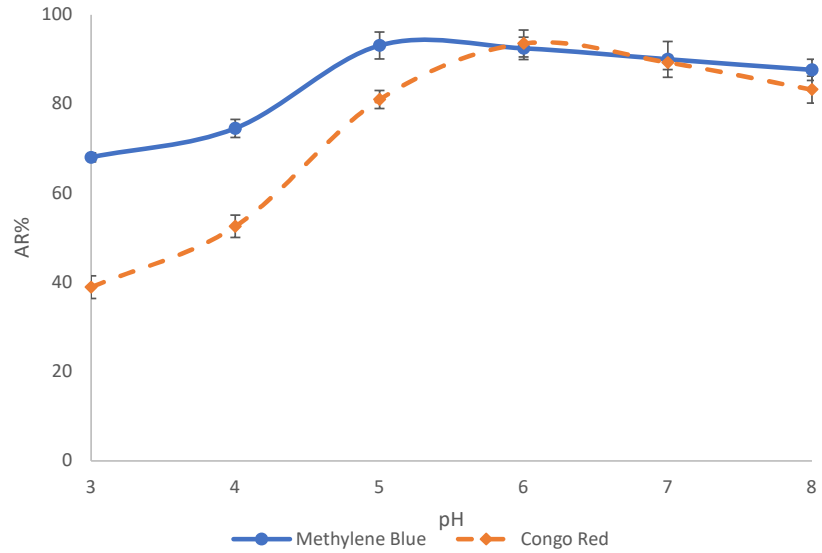

Fig. 6: Influence of pH on the removal of MB and CR.

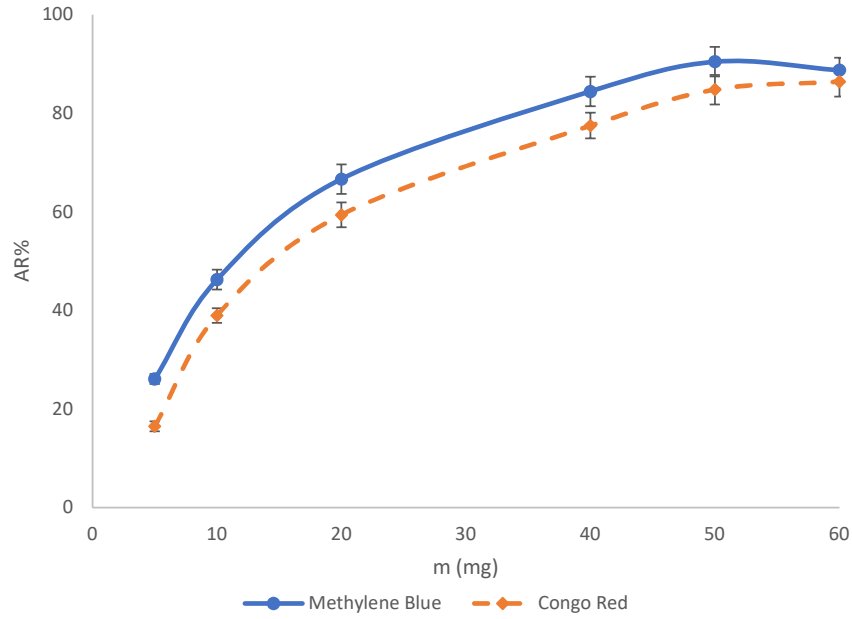

Fig. 7: Influence of the amount of adsorbent (m) on the removal of MB and CR.

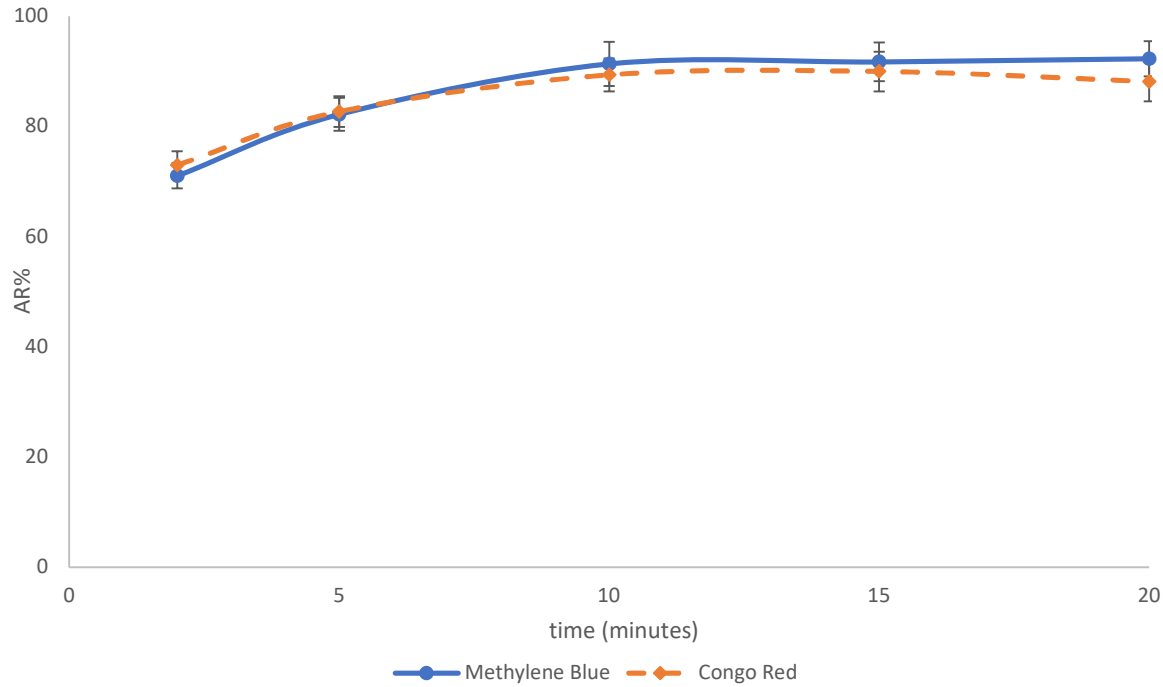

Fig. 8: Influence of the time (min) on the removal of MB and CR.

Factors Affecting the Adsorption Efficiency

The adsorption recovery of MB and CR was studied over a pH range of 3.0 to 8.0. Fig. 6 shows that the maximum adsorption was obtained at pH 6.0 for MB and CR. The pH_{pzc} value of Fe_3O_4/GO was 6.2 (Mahvi et al. 2021, You et al. 2019). At pH 6.0 below the pH_{pzc}, the surface of the adsorbent was positively charged. The pKa values of MB and CR are 3.8 and 4.5, respectively. Therefore, at a solution's pH above pKa, the MB and CR exist in anionic speciations. The recovery of MB and CR through adsorption could be attributed to the electrostatic attraction between the adsorbent's surface and the analytes. Comparable findings have been documented in existing literature (Cheng et al. 2019, Yousef & El-Eswed 2009, Yu et al. 2016). Therefore, a pH of 6.0 was used for MB and CR as the optimal pH value.

The adsorption recovery can be influenced by the amount of adsorbent used. The quantities of the adsorbent (ranging from 5.0 to 60.0 mg) affected the retrieval of MB and CR was examined. This was accomplished by introducing varying amounts of the nanocomposite into the sample solutions. As depicted in Fig. 7, an increase in the amount of adsorbent resulted in a higher recovery due to the availability of additional adsorption sites. However, once the extraction of the analytes reached saturation, further increases in the adsorbent amount did not lead to a proportional increase in extraction, resulting in wastage. The best results were obtained when 50.0 mg of the adsorbent was utilized in the following experiments.

In addition to the adsorbent amount, the contact time (ranging from 2.0 to 20.0 min) played a significant role in the adsorption process of the Fe_3O_4/GO nanocomposite. Fig. 8 illustrates the effect of time on the removal of MB and CR. The results demonstrate that initially, the adsorption of both dyes increased with longer times due to the availability of more active adsorption sites. However, the recovery eventually reached a constant value as the number of accessible active adsorption sites decreased. Therefore, a contact time of 10.0 min was chosen for subsequent experiments.

Furthermore, it was carefully selected a desorbing agent that fulfilled specific criteria: it had to be cost-effective, environmentally friendly, effective in desorption, and not cause any damage to the structure of the adsorbent. Fe_3O_4/GO nanocomposite used is dispersed in weak acidic environments, 20 mL of distilled water and acetic acid, ultrasound vibration for 5 min, then washed with magnets. This process is repeated 2 times. Next, wash the material with distilled water twice at 40°C, then wash with ethanol at 40°C. Finally, the material is dried at 60°C overnight. The ability of the adsorbent to be reused was assessed, and Fig. 9 illustrates that even after undergoing five cycles, the adsorbent maintained effective adsorption recovery, demonstrating its suitability for repeated utilization.

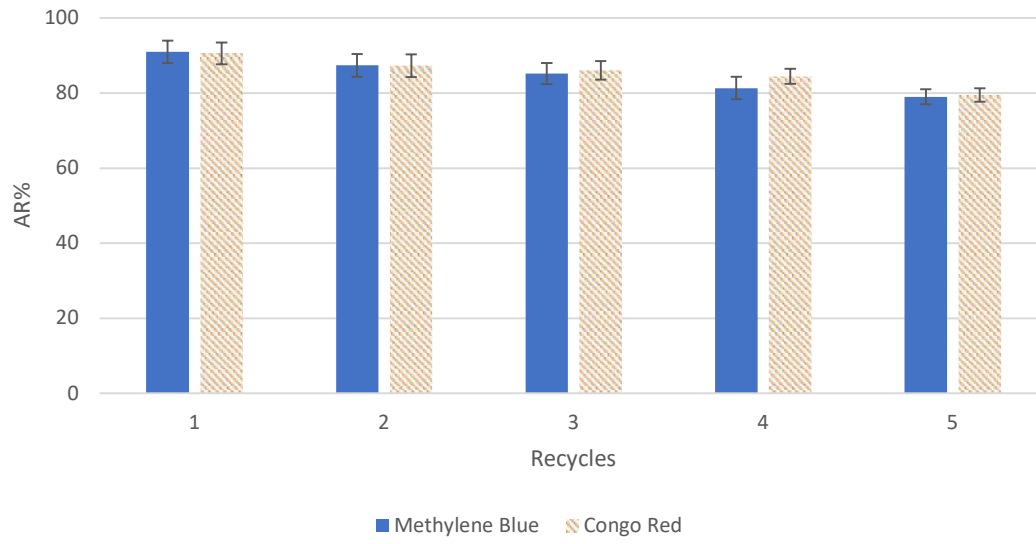

Fig. 9: Reusability study of Fe_3O_4/GO nanocomposite (pH = 6.0, time 10 min and amount of adsorbent 50.0 mg).

The adsorption process is driven by the affinity between the adsorbate and the surface of the adsorbent, and it continues until the system reaches dynamic equilibrium. Adsorption isotherms can describe the relationship between the adsorbate and the adsorbent surface. The Langmuir model (1) is suitable for analyzing monolayer adsorption, while the Freundlich model (2) applies to heterogeneous surfaces and multilayer adsorption.

$$\frac{C_e}{q_e} = \frac{1}{q_m K_L} + \frac{C_e}{q_m} \quad ...(1)$$

$$\ln q_e = \ln K_F + (1/n) \ln C_e \quad ...(2)$$

Where C_e is the equilibrium concentration ($mg.L^{-1}$); q_e is the amount of adsorbed analyte per unit mass of the adsorbent, and q_m is the maximum adsorption capacity ($mg.g^{-1}$); K_L is the Langmuir constant ($L.mg^{-1}$) related to the energy of adsorption; is the adsorption intensity; K_F and $1/n$ Are Freundlich constants related to adsorption capacity and intensity of adsorption, respectively.

Table 1: Parameters and the correlation coefficients fitted by Langmuir and Freundlich models of MB and CR onto Fe_3O_4/GO nanocomposite.

		Methylene Blue	Congo Red
Langmuir model	q_m [$mg.g^{-1}$]	135.1	285.7
	K_L [$L.mg^{-1}$]	0.0316	0.0071
	R^2	0.9075	0.9246
Freundlich model	K_F [$mg.g^{-1}$]	1.531	0.486
	N	1.31	0.96
	R^2	0.9897	0.9877

Table 1 presents the key parameters, including n, K_F, K_L, and q_m, along with the determination coefficient (R^2) of the adsorption models. The outcomes suggest that the experimental data aligns well with the Freundlich model within the investigated range, as indicated by its higher R^2 value compared to the Langmuir model for three analytes. This observation could be attributed to the uneven distribution of active sites on the surface of the adsorbent. The favorable isotherm of the Freundlich model may be

Table 2: Comparison of maximum adsorption capacity of Fe_3O_4/GO and other adsorbents.

Adsorbents	Maximum adsorption capacity (mg/g)		References
	MB	CR	
Wheat shells (WHS)	16.56	-	(Bulut & Aydın 2006)
Halloysite nanotubes (HNTs)	84.32	-	(Zhao & Liu 2008)
Graphene	153.85	-	(Liu et al. 2012)
Activated biochar (CO_2–biochar)	161	-	(Franciski et al. 2018)
Zn-Fe_2O_4 nanospheres	-	16.58	(Rahimi et al. 2011)
Maghemite nanoparticles (γ-Fe2O3)	-	208.33	(Afkhami & Moosavi 2010)
Anilinepropylsilica xerogel (SiAn)	-	22.62	(Pavan et al. 2008)
Unmodified fly ash	-	22.12	(Harja et al. 2022)
Fe_3O_4/GO	135.1	285.7	This work

attributed to the low oxidation degree(Yan et al. 2014). According to Langmuir isotherm, the maximum monolayer adsorption capacity of MB and CR at equilibrium is 135.1 and 285.7 $mg.g^{-1}$, respectively.

Table 2 compares the ability to adsorb MB and CR using Fe_3O_4/GO and other adsorbents. The findings indicate that Fe_3O_4/GO performed exceptionally well as an adsorbent, showing a comparatively higher adsorption capacity for MB and CR than the other materials tested.

CONCLUSIONS

Overall, the results of this study indicate that the Fe_3O_4/GO nanocomposite is an effective adsorbent for removing MB and CR from water. A composite material, Fe_3O_4/GO, was synthesized and employed to capture MB and CR from a sample. The adsorbent proved to be highly effective for both MB and CR. By optimizing the conditions, the pH level of 6.0, an adsorbent quantity of 50.0 mg, and an adsorption time of 10.0 min were identified as the ideal values. Equilibrium data for the adsorption of both substances were gathered using the Langmuir and Freundlich models, two different isotherm models. The determination coefficient of the Freundlich model surpassed that of the Langmuir model. The maximum capacity for monolayer adsorption was 135.1 $mg.g^{-1}$ for MB and 285.7 $mg.g^{-1}$ for CR. These results indicated that the proposed adsorbent possessed exceptional adsorption capabilities. Moreover, the adsorbent could be reused up to five times without declining performance, leading to cost savings.

ACKNOWLEDGMENTS

This work was supported by Hung Vuong University through the project "Synthesis of Fe_3O_4/graphene oxide nanocomposite for the treatment of organic contaminants". We would like to thank the peer reviewers for their valuable suggestions and comments that improved this paper.

REFERENCES

Afkhami, A. and Moosavi, R. 2010. Adsorptive removal of Congo red, a carcinogenic textile dye, from aqueous solutions by maghemite nanoparticles. J. Hazard. Mater., 174(1-3): 398-403.

Akhtar, N., Syakir Ishak, M.I., Bhawani, S.A. and Umar, K. 2021. Various natural and anthropogenic factors responsible for water quality degradation: A review. Water, 13(19): 456

Bulut, Y. and Aydın, H. 2006. A kinetics and thermodynamics study of methylene blue adsorption on wheat shells. Desalination, 194(1): 259-267.

Cao, C., Xiao, L., Chen, C., Shi, X., Cao, Q. and Gao, L. 2014. In situ preparation of magnetic Fe3O4/chitosan nanoparticles via a novel reduction-precipitation method and their application in adsorption of reactive azo dye. Powder Technol., 260: 90-97.

Cele, T. 2020. Preparation of nanoparticles. Eng. Nanomater. Saf., 5: 11-21.

Cheng, J., Sun, Z., Yu, Y., Li, X. and Li, T. 2019. Effects of modified carbon black nanoparticles on plant-microbe remediation of petroleum and heavy metal co-contaminated soils. Int. J. Phytoremed., 21(7): 634-642.

Cui, L., Wang, Y., Gao, L., Hu, L., Yan, L. and Wang, Y. 2015. EDTA functionalized magnetic graphene oxide for removal of Pb(II), Hg(II), and Cu(II) in water treatment: Adsorption mechanism and separation property. Chem. Eng. J., 281: 1-10.

Franciski, M.A., Peres, E.C., Godinho, M., Perondi, D., Foletto, E.L. and Oliveira, M.L.S. 2018. Development of CO2-activated biochar from solid wastes of a beer industry and its application for methylene blue adsorption. Waste Manag., 78: 630-638.

Gehrke, I., Geiser, A. and Somborn-Schulz, A. 2015. Innovations in nanotechnology for water treatment. Nanotechnol. Sci. Appl., 8: 1-17.

Halim, A.A., Han, K.K. and Hanafiah, M.M. 2015. Removal of methylene blue from dye wastewater using river sand by adsorption. Nat. Environ. Pollut. Technol., 14(1): 89-94.

Harja, M., Buema, G. and Bucur, D. 2022. Recent advances in the removal of Congo Red dye by adsorption using industrial waste. Sci. Rep., 12(1):1-18.

He, H. and Gao, C. 2011. Synthesis of Fe3O4/Pt nanoparticles decorated carbon nanotubes and their use as magnetically recyclable catalysts. J. Nanomater, 19: 35.

Heo, J.W., An, L., Chen, J., Bae, J.H. and Kim, Y.S. 2022. Preparation of amine-functionalized lignins for the selective adsorption of Methylene blue and Congo red. Chemosphere, 295: 313.

Lachheb, H., Puzenat, E., Houas, A., Ksibi, M., Elaloui, E. and Guillard, C. 2002. Photocatalytic degradation of various types of dyes (Alizarin S, Crocein Orange G, Methyl Red, Congo Red, Methylene Blue) in water by UV-irradiated titania. Appl. Catal. B Environ., 39(1): 75-90.

Liu, L., Zhang, Y., He, Y., Xie, Y., Huang, L. and Wang, Y. 2014. Preparation of montmorillonite-pillared graphene oxide with increased single- and co-adsorption towards lead ions and methylene blue. RSC Adv., 5(6): 3965-3973.

Liu, T., Li, Y., Du, Q., Sun, J., Jiao, Y. and Liu, Y. 2012. Adsorption of methylene blue from aqueous solution by graphene. Coll. Surf. B Biointerf., 90(1): 197-203.

Luo, P., Mu, Y., Wang, S., Zhu, W. and Mishra, B.K. 2022. Exploring sustainable solutions for the water environment in Chinese and Southeast Asian cities. Ambio., 51(5): 1199-1218.

Maheshwari, K., Agrawal, M. and Gupta, A.B. 2021. Dye Pollution in Water and Wastewater. In: Muthu, S.S. and Khadir, A. (eds), Novel Materials for Dye-Containing Wastewater Treatment, Springer, Singapore, pp. 1-25.

Mahvi, A.H., Balarak, D. and Bazrafshan, E. 2021. Remarkable reusability of magnetic Fe_3O_4-graphene oxide composite: A highly effective adsorbent for Cr(VI) ions. Int. J. Environ. Anal. Chem., 5: 1-21.

Nguyen, V.H., Van, H.T., Nguyen, V.Q., Dam, X. and Hoang, L.P. 2020. Magnetic Fe_3O_4 nanoparticle biochar derived from Pomelo peel for reactive red 21 adsorption from aqueous solution. J. Chem., 2: 1-11.

Ouyang, K., Zhu, C., Zhao, Y., Wang, L., Xie, S. and Wang, Q. 2015. Adsorption mechanism of magnetically separable Fe3O4/graphene oxide hybrids. Appl. Surf. Sci., 355: 562-569.

Pavan, F.A., Dias, S.L.P., Lima, E.C. and Benvenutti, E.V. 2008. Removal of Congo red from aqueous solution by anilinepropylsilica xerogel. Dye Pigm., 76(1): 64-69.

Peters, N.E. and Meybeck, M. 2000. Water quality degradation effects on freshwater availability: Impacts of human activities. Water Int., 25(2): 185-193.

Qu, X., Alvarez, P.J.J. and Li, Q. 2013. Applications of nanotechnology in water and wastewater treatment. Water Res., 47(12): 3931-3946.

Rahimi, R., Kerdari, H., Rabbani, M. and Shafiee, M. 2011. Synthesis, characterization and adsorbing properties of hollow Zn-Fe_2O_4 nanospheres on removal of Congo red from aqueous solution. Desalination, 280(1-3): 412-418.

Saikia, J., Gogoi, A. and Baruah, S. 2019. Nanotechnology for water remediation. In: Dasgupta, N., Ranjan, S. and Lichtfouse, E. (eds), Environmental Nanotechnology, Volume 2, Springer, Cham, pp. 195-211.

Thattil, P.P. and Leema Rose, A. 2019. Photodegradation of Congo red dye via simple and effective air oxidation using copper(II) chloride and sunlight. Nat. Environ. Pollut. Technol., 18(4): 1243-1248.

Theron, J., Walker, J.A. and Cloete, T.E. 2008. Nanotechnology and water treatment: Applications and emerging opportunities. Crit. Rev. Microbiol., 34(1): 43-69.

Vaghari, H., Jafarizadeh-Malmiri, H., Mohammadlou, M., Berenjian, A. and Anarjan, N. 2016. Application of magnetic nanoparticles in smart enzyme immobilization. Biotechnol. Lett., 38(2): 223-233.

Yan, H., Tao, X., Yang, Z., Li, K. and Yang, H. 2014. Effects of the oxidation degree of graphene oxide on the adsorption of methylene blue. J. Hazard. Mater., 268: 191-198.

Yao, Y., Miao, S., Liu, S., Ma, L.P., Sun, H. and Wang, S. 2012. Synthesis, characterization, and adsorption properties of magnetic Fe_3O_4@ graphene nanocomposite. Chem. Eng. J., 184: 326-332.

Ye, N., Xie, Y., Shi, P., Gao, T. and Ma, J. 2014. Synthesis of magnetite/ graphene oxide/chitosan composite and its application for protein adsorption. Mater. Sci. Eng., 45: 8-14.

You, N., Wang, X.F., Li, J.Y., Fan, H.T., Shen, H. and Zhang, Q. 2019. Synergistic removal of arsanilic acid using adsorption and magnetic separation technique based on Fe_3O_4@graphene nanocomposite. J. Ind. Eng. Chem., 70: 346-354.

Yousef, R.I. and El-Eswed, B. 2009. The effect of pH on the adsorption of phenol and chlorophenols onto natural zeolite. Coll. Surf. A Physicochem. Eng. Asp., 334(1-3): 92-99.

Yu, L., Chen, J., Liang, Z., Xu, W., Chen, L. and Ye, D. 2016. Degradation of phenol using Fe_3O_4-GO nanocomposite as a heterogeneous photo-Fenton catalyst. Sep. Purif. Technol., 171: 80-87.

Zaaba, N.I., Foo, K.L., Hashim, U., Tan, S.J., Liu, W.W. and Voon, C.H. 2017. Synthesis of graphene oxide using modified hummers method: Solvent influence. Procedia Eng., 184: 469-477.

Zhao, M. and Liu, P. 2008. Adsorption behavior of methylene blue on halloysite nanotubes. Micropor. Mesopor. Mater., 112(1-3): 419-424.

Nature Environment and Pollution Technology
An International Quarterly Scientific Journal

p-ISSN: 0972-6268
(Print copies up to 2016)
e-ISSN: 2395-3454

Vol. 23 | No. 1 | pp. 265-273 | 2024

Original Research Paper

https://doi.org/10.46488/NEPT.2024.v23i01.022

Open Access Journal

Competitive Adsorption of Cd(II) and Zn(II) on Biochar, Loess, and Biochar-loess Mixture

Y. W. Li, B. W. Zhao†, L. Wang, Y. Q. Li, T. Wang, Y. H. Jia and M. L. Zhao
School of Environmental and Municipal Engineering, Lanzhou Jiaotong University, Lanzhou 730070, China
†Corresponding author: B.W. Zhao; baoweizhao@mail.lzjtu.cn

Nat. Env. & Poll. Tech.
Website: www.neptjournal.com

Received: 28-06-2023
Revised: 10-08-2023
Accepted: 20-08-2023

Key Words:
Cd(II)
Zn(II)
Biochar
Competitive adsorption
Loess

ABSTRACT

Combined heavy metal contamination in soil is a common phenomenon. Biochar amendment into the soil is considered to be an alternative for immobilization remediation of soil contaminated with heavy metals due to its adsorption and alkalization. However, much attention has been paid to the adsorption and immobilization of single heavy metals by biochar. In this paper, the competitive adsorption of Cd(II) and Zn(II) on biochar derived from cotton straw and pig manure at 500℃ (BCS500 and BPM500), loess and biochar-loess mixtures were investigated using the batch equilibrium method. The results showed that the adsorption capacities of biochars, loess, and biochar-loess mixtures to Cd(II) and Zn(II) in the mixed Cd-Zn systems increased with the increase of initial metal concentrations of Cd(II) and Zn(II). The adsorptive capacities of BCS500 and BPM500 to Cd(II) in mixed Cd-Zn system were 33% and 35% less than those in the single Cd(II)systems, while the adsorptive capacities to Zn(II) were 62% and 56% less than those in the single Zn(II) systems. The adsorptive capacities of loess to Cd(II) and Zn(II) in mixed Cd-Zn systems were 29% and 55% less than those in the single metal systems. The adsorptive capacities of loess-BCS500 (LBCS) and loess-BPM500 (LBPM) to Cd(II) in mixed Cd-Zn system were 40% and 38% less than those in the single Cd(II) systems, while the adsorptive capacities to Zn(II) were 63% and 60% less than those in the single Zn(II)systems. Moreover, the competitive adsorptive capacity of Cd(II) is greater than that of Zn(II). It can be seen that when heavy metal pollution with similar nature of multiple elements exists in soil, the amount of adsorbent should be increased to resist the possible weakened adsorption caused by competitive adsorption in order to guarantee an effective absorption treatment.

INTRODUCTION

Heavy metals, due to their extreme toxicity and non-biodegradable characteristics, are an unceasing threat to the environment (Mukherjee et al. 2022), making their pollution a major environmental hazard. Due to heavy metal-contaminated soil is often characterized by its accumulative nature and difficulty in recovery, thus posing an effective risk to both human health and the ecosystem (Sharma et al. 2022). Heavy metals are rarely found in single contamination in nature, and evidence suggests that one heavy metal pollution usually accompanies another one (Syed et al. 2022). Studies have shown that in recent years, high concentrations of cadmium (Cd) and zinc (Zn) have often been observed together (Peng et al. 2022). Research has demonstrated that Cd, one of the most hazardous heavy metals, is especially abundant in many agricultural regions (Liu et al. 2022), as well as areas contaminated by both point and non-point pollution sources. While Zn is an essential nutrient for plants, it can still be harmful when present at exceedingly high concentrations (Valkova et al. 2022, McStay et al. 2022, Sellami et al. 2022). It has been proved that the danger posed by Cd-Zn co-contamination is even greater than that by a single one of them. As a result, remediation of soils contaminated with two or more heavy metals, e.g., Cd-Zn, would be more complex (Li et al. 2022a).

Biochar is a green and environmentally friendly soil remediation agent that can effectively immobilize heavy metals in the soil (Wu et al. 2022). In addition, biochar has the potential to improve soil quality in multiple ways, from changing the physical characteristics to altering the chemical composition (Mensah et al. 2022), which elevates crop growth, thereby increasing food production. To date, numerous researches have suggested the potential and feasibility of using biochar to adsorb and fixation of heavy metals in the soil (Xu et al. 2020). Reports have shown that the bioavailable concentrations of Pb, Cu, Cd, and Zn in contaminated soil decreased significantly when different amounts of biochar were applied, and this reduction increased

with application amounts of biochar. Studies conducted by Xu et al. (2013) found that when peanut straw biochar was added to loess soil with a heavy metal, it had a dramatic effect on the adsorption of Cu, Pb, and Cd. Specifically, the adsorption capacity of Cu, Pb, and Cd increased by 98%, 97%, and 193%, respectively, compared to the control group without peanut straw charcoal. Bhadoria et al. (2022) prepared three biosorbents and investigated their adsorption effects on Cd(II) and Zn(II) under different conditions. The batch studies conducted showed that, in comparison to Zn(II) ions, much higher amount of Cd(II) ions was adsorbed onto all three adsorbents. Wang (2016) conducted adsorption experiments on Cd(II) or Zn(II) separately, exploring the adsorption capacity of either single metal on loess, biochar, and loess with biochar. Although a great deal of research has been curated regarding the adsorption and immobilization of heavy metals on biochar, investigations on such processes are predominantly focused on single heavy metal ions. To elaborate, most studies have failed to consider the interactions among different heavy metal ions, limiting the applicability of such findings (Wang et al. 2019, Praneeth et al. 2022). The interaction between different kinds of heavy metals and soil with biochar remains inadequate.

Taking the abovementioned issues into account, the adsorption capacities of Cd(II) and Zn(II) on biochar, loess, and a combination of biochar-loess were compared through an isothermal adsorption experiment. The objectives of this experiment were to study the adsorption interaction between two metals in a Cd(II)-Zn(II) composite system and to compare the findings with single heavy metal adsorption tests; researchers can validate the interaction mechanism between Cd(II) and Zn(II). The findings from this investigation can offer a theoretically valid basis for remediating loess soil through the use of biochar and offer useful insights regarding the development and utilization of adsorption immobilization technology for soils contaminated by heavy metals.

MATERIALS AND METHODS

Materials

The stock solutions of Cd(II) were prepared by $Cd(NO_3)_2{\cdot}4H_2O$, and the stock solutions of Zn(II) were prepared by $Zn(NO_3)_2{\cdot}6H_2O$. Cotton (*Gossypium* sp. L.) straw (CS) for preparation of biochar (BCS) was collected from farmland around Kuerle City, Xinjiang. Pig manure (PM) for preparation of biochar (BPM) was sampled from a farm in Lanzhou, Gansu Province. The CS was washed with tap water, then air-dried and cut into a size of 10 cm. The CS pieces were put in an oven and dried overnight at 80°C and removed after drying. The PM was air-dried to pick up the adulterants, and the big pieces were smashed, passed through a 40 mesh sieve, and stored in a dryer.

The CS or PM powder was mixed evenly and put into the crucible, and then the powder was compacted and sealed. The powder was pyrolyzed in a muffle furnace (SX_2 series, Shanghai Jiazhan Instrument Equipment Co., Ltd., China) with limited oxygen for 6 hours, and the pyrolysis was performed at 500°C. Then, the powder was taken out after cooling to room temperature, ground evenly in a mortar, passed through an 80 mesh sieve, and treated with 1 $mol.L^{-1}$ HCl. The powder was rinsed with de-ionized water until the solution was neutral. After being dried at 70 °C~80 °C, the biochars were put into brown jars and marked as BCS500 and BPM500, respectively.

Loess was sampled from 0-20 cm of topsoil on the hill near Lanzhou Jiaotong University. Large stones, withered leaves, and plant roots in loess were eliminated, passed through a 3 mm sieve, mixed evenly, and passed through an 80 mesh sieve for use.

Characterization of Biochar and Loess

Biochar pH value was determined using the method of national standard (GB/T 12496.7-1999, China). The percentages of C, H, N, and S in biochar were determined by the Vario El elemental analyzer (Vario EL cube, Elementar, Germany). Then, the aromaticity and polar size of biochar samples were inferred by the values of H/C and (O+N)/C. Ash was determined by the method of national standard (GB/T 12496.3-1999, China). The loess pH was determined with a pH meter (PHS-3E, Shandong Ouleibo Co., Ltd. China), with soil: water = 1:5 v:v, and electrical conductivity (EC) was determined with a Conductivity meter (DDS-11A, Hangzhou Aolilong Instrument Co., Ltd. China), with soil: water = 1:5 v:v. The soil cation exchange capacity (CEC) was determined by the $Ca(OAc)_2$ method (National Standard NY/T1121.5-2006, China). Soil organic matter was resolved by potassium dichromate oxidation-spectrophotometry (National Standard HJ615-2011, conversion factor 1.724, China). The drying weighing method was used to determine soil water content. The soil bulk weight was determined by the ring knife method (GB/T 50123, China).

The Brunauer–Emmett–Teller (BET) pore size and surface area distribution of the samples were determined using an ASAP 2020 M rapid BET surface area/pore analyzer (Micromeritics, USA). The external morphological characteristics of the biochar samples were inspected by a JSM-5600 LV scanning electron microscope (JEOL Ltd., Japan). Qualitative testing of surface functional groups utilized a Nexus 870 Fourier transform infrared spectrometer (Nicolet, USA). The mineral phase components of the

samples were determined by a Rigaku, D/max2200 p X-ray diffraction analyzer (Micromeritics, USA).

Adsorption Experiment Design

To test competitive adsorption, the influence of the initial concentration of heavy metals on adsorption capacity was mainly studied. Cd(II) with concentrations of 10, 30, 50, 80, 100, 200, and 300 mg.L^{-1} were combined with Zn(II) with the same concentrations at a mass concentration ratio of 1:1, and the mixed system (containing 0.01 mol.L^{-1} $NaNO_3$) was used for batch isothermal adsorption experiments. Biochar, loess, and loess with biochar (LBCS and LBPM) (the mass ratio of biochar to loess was 1:10) were weighed as 0.100 g respectively into a 50 mL conical flask, and 20 mL of Cd(II)-Zn(II) solution with a fixed pH value was added. The initial concentrations of solutions were adjusted to 10, 30, 50, 80, 100, 200, and 300 mg.L^{-1}, respectively. The solution was put into an air bath shaker (THZ-82, Jiangsu JintanYoulian Instrument Research Institute, China) at 25 °C and oscillated for 24 hours at 150 r.min^{-1}. Then solution was passed through a 0.45 μm filter membrane to remove contaminating particles. Following dilution and volume adjustments, concentrations of Cd(II) and Zn(II) were determined in the filter solution. All tests were performed three times in parallel.

Analysis and Calculation Methods

Concentrations of Cd(II) and Zn(II) were determined at wavelength 228.8 nm and 213.9 nm by Atomic absorption spectrophotometer (Varian Spectrum AA110/220, USA). The flame type was acetylene air. The adsorption capacity of adsorbents for Cd(II) and Zn(II) was calculated by the following formula:

$$Q_e = \frac{(C_0 - C_e) \cdot V}{m} \quad \ldots(1)$$

Where C_0 and C_e refer to initial and equilibrium concentrations of Cd(II) and Zn(II) (mg.L^{-1}); m is the mass of adsorbent in the conical bottle (g); Q_e is the adsorption capacity of adsorbent for Cd(II) and Zn(II) (mg.g^{-1}); V is the solution volume (L).

The Freundlich isothermal adsorption model and Langmuir isothermal adsorption model were used to fit the experimental data. The equations are as follows:

Freundlich: $$\ln Q_e = \ln K_f + 1/n \cdot \ln C_e \quad \ldots(2)$$

Langmuir: $$\frac{C_e}{Q_e} = \frac{1}{(b \cdot Q_m)} + \frac{C_e}{Q_m} \quad \ldots(3)$$

where K_f and n refer to Freundlich isothermal equation constants; C_e is the solution concentration at equilibrium (mg/L); Q_e is the adsorption capacity of adsorbent to Cd(II) or Zn(II) at equilibrium time (mg/g); Q_m is maximum adsorption amount (mg/g); and b is the affinity of influential point positions on adsorbent surfaces to Cd(II) and Zn(II) (L.mg^{-1}).

RESULTS AND DISCUSSION

Characterization of Biochars and Loess

The basic physicochemical properties of loess, BCS500, and BPM500 are shown in Table 1. It can be observed that the two biochars differ expressively in terms of yield and ash content. Notably, BPM500 exhibited higher values in both respects compared to BCS500.

Table 1 indicates that the pH values of biochars are weakly acidic, and that of loess is weakly basic. Research has shown that the pH of biochar could lie anywhere in the range of 4 to 12 (Lehmann et al. 2007). Carbon (C) stands out as being the highest element in BCS500 and BPM500, with the levels of O, H, N, and S decreasing in succession. The (O+N)/C and H/C ratios are typically utilized to evaluate the

Table 1: Basic physicochemical properties of biochar and loess.

	pH	Element content [%]					Element ratio			Yield and ash content [%]	
		C	H	O	N	S	O/C	H/C	(O+N)/C	Yield	Ash
BCS500	5.77	48.7	4.25	13.3	3.48	0.962	0.273	0.0873	0.345	34.5	29.3
BPM500	4.46	12.5	0.585	27.8	1.33	0.325	2.22	0.0468	2.33	65.8	47.5
	pH	Organic matter [mg.g^{-1}]		CEC [cmol.kg^{-1}]		EC [ms]		Bulk density [g.cm^{-1}]		Water content [%]	
loess	8.35	9.56		5.40		0.929		1.31		13.8	

Table 2: BET surface areas and porosity of biochar and loess.

Sample	BET surface area [m^2.g^{-1}]	t–pLot micropore area [m^2.g^{-1}]	Single-point total hole volume[cm^3.g^{-1}]	t–pLot micropore volume [cm^3.g^{-1}]	BET average aperture (Å)
Loess	8.032	2.0706	0.021799	0.000023	108.562
BCS500	28.74	15.307	0.053207	0.000480	46.7488
BPM500	22.65	8.4990	0.026750	0.000289	68.3823

polarity and aromaticity of biochars, and it can be seen that BCS500 has a higher degree of aromaticity, while BPM500 appears to be more polar and hydrophilic (Jia et al. 2013, Chen et al. 2011).

The order of BET-specific surface areas is BCS500 > BPM500 > loess (Table 2). Compared to biochar, the microporous area of loess is only a quarter of the specific surface area, which suggests that the porosity of biochar is more abundant and pronounced. Nonetheless, the data on average pore size reveal some noteworthy discrepancies. The BET average aperture of BCS500 and BPM500 is significantly smaller than that of loess. From the above analysis, it can be preliminarily judged that the physical adsorption performance of BCS500 is passing beyond that of BPM500 and loess. However, since physical adsorption only accounts for a small part of the adsorption mechanism, the adsorption process is more of the effect of chemical groups in the adsorbent. The adsorption capacity of biochar and loess cannot be judged correctly yet.

Fig. 1 shows the scanning electron microscope images of loess, BPM500, and BCS500 at 500x magnification. The structure diagram provides a direct insight into the microscopic morphology and morphological characteristics of each adsorbent. Fig. 1(a) paints a vivid picture of loess; its edges are sharp and irregular, its surface is smooth, and the particles exhibit varying sizes with no visible pore structure. Additionally, their distribution is not uniform, and spacing is wide. Fig. 1(b) illustrates how the BPM500 particles are tightly bound together, exhibiting diverse morphologies, such as jagged layers, flocculent solids resembling honeycombs, rough surfaces, and large pores.

Additionally, irregular massive solids with sharp edges and corners, smooth veneers, and no layered or porous structures are also present. It can be seen from Fig. 1(c) that highly dispersed and disordered tissues are closely spaced with the layers of the middle square, such as adherence to its surface, and there are some layer breakage and collapse phenomena on the side of the layers. The pore structure is obvious, and the micropore is more mesoporous with a larger specific surface area, which is consistent with the pore size analysis.

Fig. 2 displays the infrared spectra of two biochars and loess, along with some of the important oxygen-containing functional groups that can be deduced by examining the specific absorption peak positions in the respective spectra. Analyzing the infrared spectra of loess in Fig. 2(a), it is evident that the absorption peaks near 3617.9 cm^{-1} and 3417.3 cm^{-1} are attributed to -OH stretching vibrations, while the weak absorption peaks near 2854.2 cm^{-1} correspond to the absorption vibration of the -CH functional group. Fig. 2(b) shows the

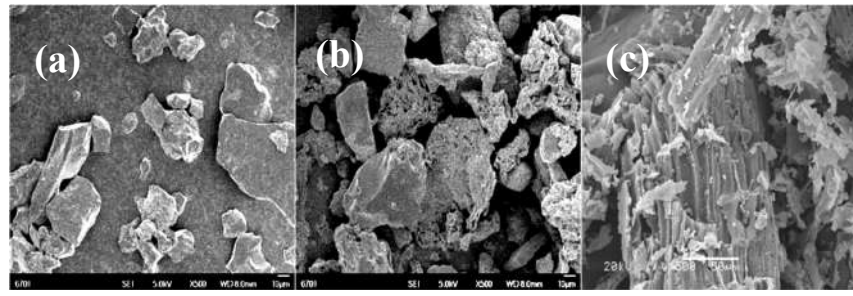

Fig. 1: Photomicrograph from scanning electron microscope for loess (a), BPM500 (b), and BCS500 (c).

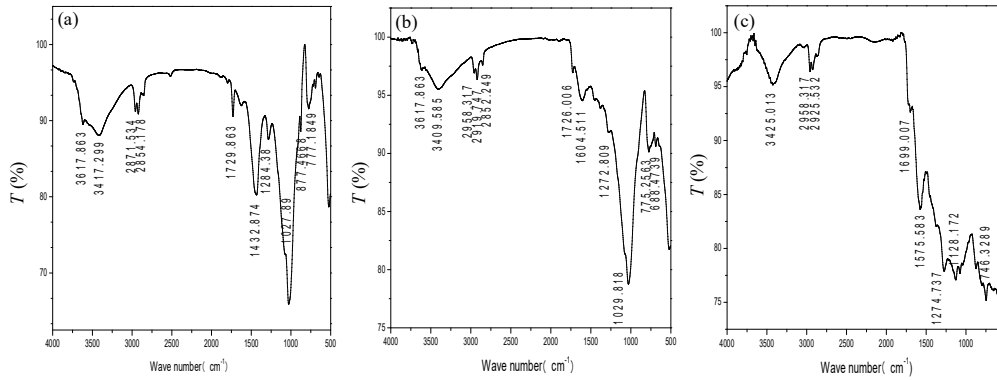

Fig. 2: FTIR spectra for loess (a), BPM500 (b), and BCS500 (c).

infrared spectrum of BPM500, in which the absorption peaks at 3409.59 cm^{-1} and 3617.86 cm^{-1} are attributed to the stretching vibration of hydroxy-OH, and three peaks near 2919.75 cm^{-1} represent the aliphatic CH_2 absorption. The absorption peak near 1604.51 cm^{-1} is speculated to be caused by the C=O stretching vibration. Fig. 2(c) shows the infrared spectrum of BCS500, in which the peak at 3425.01 cm^{-1} is caused by the phenolic hydroxy -OH vibration.

Similarly, the absorption peaks at 2958.32 cm^{-1} and 2925.53 cm^{-1} are attributed to the typical -CH stretching vibration peaks in alkanes. The peak at 1575.58 cm^{-1} is generated by the antisymmetric stretching vibration of -COO- in the carboxyl of C=O stretching vibration in the lactone group (Uchimiya et al. 2010). Interpreting the infrared spectra of the three adsorbents, it can be concluded that, despite their varying raw materials, the characteristic absorption peaks of their oxygen-containing functional groups remain almost identical.

X-ray diffraction (XRD) is a valuable tool for analyzing the microscopic structure of crystalline substances in samples. In Fig. 3, various biochars and loess are examined using XRD to illustrate their distinct patterns. Fig. 3(a) reveals that the XRD pattern of loess comprises a prominent peak at 2θ=26.62° with a narrow spectral line and regular peak shape. This characteristic is indicative of the sample having large grains coupled with a nearly faultless and uniform crystal structure, which is further evidenced through software analysis suggesting that the peak originates from quartz. In Fig. 3(b), it can be noted that the XRD spectrum of BPM500 and loess are quite alike. The crystal structure is orderly, and the main peak of SiO_2 in quartz structure can still be seen at 2θ= 25°-30°. Contrastingly, a drastically different pattern is observed for BCS500 in Fig. 3(c). It is found that there is no characteristic peak of quartz SiO_2 in BCS500, and there is a diffraction peak of wider graphite phase carbon in the range of 2θ= 10°-30°.

Effect of Initial Metal Concentration on Adsorption

The adsorption capacities of adsorbents for Cd(II) and Zn(II) are shown in Fig. 4 and Fig. 5 when the initial concentrations of the two metal ions change equally. The diagram demonstrates a clear relationship between the adsorption capacity of adsorbent and initial metal concentration in the mixed system. As the initial metal concentration increases from 10 $mg.L^{-1}$ to 300 $mg.L^{-1}$, the adsorption capacity of BCS500, BPM500, loess, LBCS, and LBPM to Cd(II) increases respectively from 1.23, 0.74, 1.01, 0.99, and 1.03 $mg.g^{-1}$ to 9.32, 5.58, 5.78, 6.71, and 6.24 $mg.g^{-1}$. Concurrently, the corresponding adsorption capacity for Zn(II) is propounded from 0.76, 0.38, 0.76, 0.69, and 0.76 $mg.g^{-1}$ to 6.26, 6.71, 12.3, 10.2, and 9.04 $mg.g^{-1}$. Wang et al. (2016) conducted the adsorption experiments on single Cd(II) or Zn(II) and explored the adsorption capacities of loess, biochar, LBPM, and LBCS to Cd(II) or Zn(II) on these metals individually. As the initial concentration of Cd(II) and Zn(II) increases from 10 $mg.L^{-1}$ to 300 $mg.L^{-1}$, a remarkable difference in the adsorption capacities of BCS500, LBCS, BPM500, LBPM, and loess is observed, with the former rising from 1.43, 1.46, 1.25, 1.37, and 1.33 $mg.g^{-1}$ to 13.69, 12.26, 8.52, 10.03, and 8.23 $mg.g^{-1}$ respectively and the latter from 1.12, 1.91, 0.97, 1.95, and 1.97 $mg.g^{-1}$ to 16.61, 27.76, 15.34, 24.36, and 27.51 $mg.g^{-1}$. The ability of the adsorbents to adsorb Zn(II) was more substantial than that of Cd(II). The amount of Cd(□) adsorbed by BCS500 and LBCS in both single and mixed Cd-Zn systems is remarkably greater than that of BPM500 and LBPM, suggesting that in the face of Cd(II) pollution in the environment, BCS500 may be the more preferential choice. In the mixed Cd-Zn system, the adsorption amount of BPM500 on Zn(II) is marginally higher than that of BCS500. There is also a slight discrepancy observed between the adsorption capacities of BPM500 and LBPM in comparison to those of BCS500 and LBCS. Nonetheless, the distinction in their performance is not substantial, allowing us to select either BPM500 or BCS500

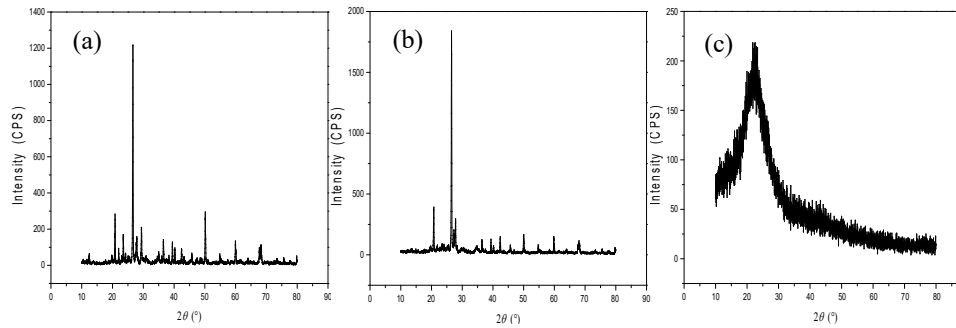

Fig. 3: XRD spectra for loess (a), BPM500 (b), and BCS500 (c).

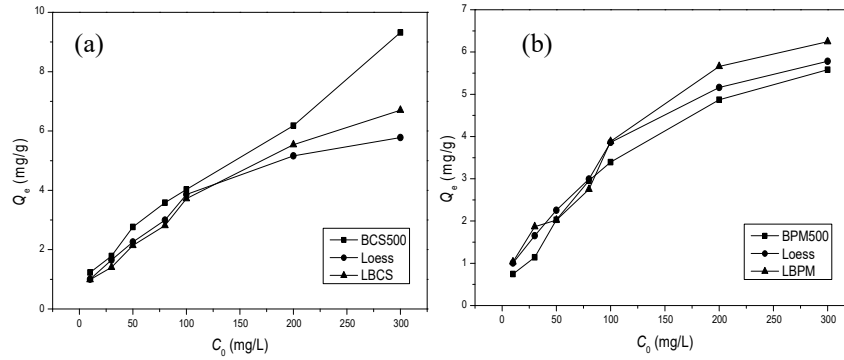

Fig. 4: Effect of initial concentration of metal ions on adsorption of Cd(II) onto BCS500, loess, and LBCS (a), and Cd(II) onto BPM500, loess, and LBPM(b).

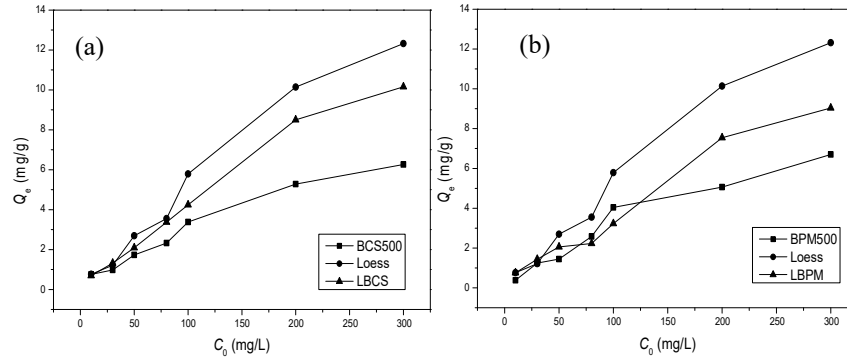

Fig. 5: Effect of initial concentration of metal ions on adsorption of Zn(II) onto BCS500, loess, and LBCS (a), and Zn(II) onto BPM500, loess, and LBPM (b).

depending on their economic utility and convenience when dealing with zinc-related pollution in the environment.

Comparing the adsorption capacities of Cd(II) and Zn(II) when placed in single metal systems and hybrid metal systems, the results show that BCS500, BPM500, loess, LBCS, LBPM experienced a reduction of 33%, 35%, 29%, 45%, and 38% respectively when exposed to Cd(II). As for Zn(II), the adsorption capacities of these materials were reduced by 62%, 56%, 55%, 63%, and 60%. It is clear that the adsorption capacity of adsorbing Zn(II) in the hybrid metal systems decreased more compared with the single metal system. Furthermore, the competitive adsorption capacity

Table 3: Isotherm parameters of adsorption of Cd(II) and Zn(II) onto biochars, loess and loess with biochar in Cd(II)-Zn(II) system.

Adsorbent	Langmuir			Freundlich		
	Q_m [mg.g^{-1}]	b [L.mg^{-1}]	R^2	K_f[L·mg^{-1}]	n	R^2
BCS500 (Cd)	4.79	0.0832	0.776	0.487	1.98	0.957
BPM500 (Cd)	4.27	0.0311	0.879	0.243	1.76	0.974
Loess (Cd)	4.24	0.0584	0.881	0.461	2.20	0.984
LBCS (Cd)	4.06	0.0580	0.797	0.355	1.94	0.968
LBPM (Cd)	4.27	0.0622	0.859	0.442	2.12	0.969
BCS500 (Zn)	3.42	0.0409	0.776	0.259	1.89	0.869
BPM500 (Zn)	9.45	0.00529	0.749	0.171	1.66	0.982
Loess (Zn)	6.81	0.0192	0.805	0.250	1.54	0.879
LBCS (Zn)	6.31	0.0178	0.868	0.225	1.60	0.944
LBPM (Zn)	4.56	0.0303	0.849	0.232	1.70	0.919

of Cd(II) surpassed that of Zn(II) when they were placed in these special conditions.

Langmuir and Freundlich's equations were utilized to fit the data collected by Cd(II) and Zn(II) under equal competition. As summarized in Table 3, the correlation coefficients R^2 of the two isothermal equations demonstrate that the adsorption isotherms of biochar and loess for Cd(II) and Zn(II) follow the Freundlich equation under mixed metal conditions, yielding R^2 values that greatly surpassed 0.8565. At the initial concentration of 200 $mg.L^{-1}$, the adsorption of BCS500, BPM500, loess, LBCS, and LBPM to Cd(II) and Zn(II) exceeded the fitting value calculated by the Langmuir formula, indicating that the adsorption of both metals by biochar, loess, and biochar-loess mixture mainly occurs through multi-molecular layer adsorption, which is similar to the fitting result of single metal systems. The maximum adsorption capacity of both Cd(II) and Zn(II) was reduced, and the adsorption capacity of Zn(II) was reduced more obviously under mixed Cd-Zn system compared with Wang's (2016) experimental results under the single system. The results showed that the two heavy metals showed antagonistic adsorption on the surface of biochar, loess, and biochar-loess mixture, that is, mutual inhibition and competition.

Interaction Principle of Cd(II) and Zn(II) on Adsorbent

Biochar, loess, and biochar-loess mixture exhibited more adsorptive effects on Cd(II) and Zn(II) in single metal systems, and the sorption capacity for Zn(II) surpassed that of Cd(II) (Wang 2016). Furthermore, the sorption order for biochar to Cd(II) was BCS500, followed by BPM500. While considering Zn(II), BCS500 surpassed BPM500 again. However, loess was observed to be more effective at adsorbing Zn(II). It is evident that Cd(II) and Zn(II) display varying selectivity for adsorbents. Amongst these results, BCS500 had the most effective adsorption effect on Zn(II). This might be because the hydroxyl and carboxyl groups contained in BCS not only present surface complexation but also a chemical hydrogen bonding effect on Zn(II) (Li et al. 2022b). In addition, an additional degree of physical adsorption was added to optimize its adsorption capacity. Investigating the mixed Cd-Zn system, it seems that Cd(II) has greater competitive adsorption capacity when compared to Zn(II). This can be attributed to the actuality that the adsorption capacity for cations of the same valence mainly depends on the hydration radius of the cation, meaning that the larger the ion radius, the easier it is to be adsorbed.

Consequently, the ionic radius of Cd(II) is 0.97 Å (Ahmed et al. 2022), whereas the radius of Zn(II) is only 0.74 Å (Li et al. 2008). And the hydration radii of $Cd(H_2O)$ and $Zn(H_2O)$ are 4.29 Å and 4.30 Å. The large hydration radius of Zn(II) results in overwhelming competitive adsorption capacity. At the same time, compared to a single metal system, the adsorption capacity of the adsorbent for both Cd(II) and Zn(II) has been significantly reduced, indicating a form of antagonistic adsorption between the two heavy metals on the surface of biochar, loess, and loess with biochar (Guo et al. 2019, Cui et al. 2021). This can be ascribed to the fact that Cd(II) and Zn(II) have similar chemical properties (Cutillas-Barreiro et al. 2014), leading to binding site competition when they coexist.

Nevertheless, Niu (2016) explore the equilibrium adsorption of Cd(II) and Zn(II) by alluvial clay on the basalt slope. Discovered in both single and binary systems was that the adsorption of Zn(II) was higher than that of Cd(II) due to the more substantial competitive ability of Zn(II). This could potentially be linked to the smaller ion radius of Zn(II).

As for Cd(II), the adsorption mechanism of biochars was physical adsorption as well as ion exchange of hydroxyl, lactone, and phenolic groups on the surface. For Zn(II) were mainly because of the surface complexation of acidic oxygen-containing functional groups and the role of chemical hydrogen bond (Wang 2016). In the mixed Cd(II)-Zn(II) system, the adsorption capacity of biochar, loess, and loess with biochar to both heavy metals showed a decreasing trend compared with the single metal system, and the adsorption capacity of Zn(II) decreased more significantly. At varying initial concentrations, the reduction of Zn(II) adsorption was much more substantial than that of Cd(II), signifying that the competitive adsorption capacity of Cd(II) is greater than that of Zn(II). This suggests that adsorbent has a greater preferential selectivity towards Cd(II). Overall, when several ions coexist, the competitive adsorption capacity is linked to the nature of the ions themselves (Liu et al. 2020). In a research conducted by Sposito et al. (1982), the ion radius and ionization potential of specific heavy metals were found to have a direct correlation with their capacity to form covalent bonds, ultimately influencing their stability in forming strong complexes. It was ultimately determined that the order of effectiveness was Pb(II) > Cd(II) > Cu(II) > Ni(II) > Zn(II). The work by McBride (1994) determined that electronegativity could be used to assess the sequence of adsorption and suggested that the order of heavy metal adsorption by adsorbent is Cu(II) > Ni(II) > Pb(II) > Cd(II) > Zn(II). The larger the charge-diameter ratio, the stronger the hydrogen bond is formed. The hydrolysis constant of the heavy metals is also taken into consideration; the larger the ion radius, the more likely it is for them to be adsorbed.

CONCLUSIONS

Under the Cd-Zn system, the adsorption capacities of both

Cd(II) and Zn(II) were shown to be lower than what was observed in single metal systems. The decrease of Zn(II) concentration decreased more than that of Cd(II), indicating that the two metals have mutual inhibition under the Cd-Zn system. This competitive effect became more and more prominent as the concentration of the two metals in the activated solution increased. In the Cd-Zn system, it is apparent that the competitive adsorption capacity of Cd(II) was greater than that of Zn(II) due to their similar chemical properties, which yielded an antagonistic adsorption behavior. Therefore, it is necessary to increase the amount of adsorbent when there is antagonistic adsorption in the system in order to ensure the desired adsorption effect.

ACKNOWLEDGEMENT

This work was financially supported by the National Nature Science Foundation of China (51766008, 22166022) and the Basic Top-notch Talent Training Plan of Lanzhou Jiaotong University (2022JC10).

REFERENCES

Ahmed, M.M.N., Bodowara, F.S., Zhou, W., Penteado, J.F., Smeltz, J.L. and Pathirathna, P. 2022. Electrochemical detection of Cd(ii) ions in complex matrices with nanopipets. RSC Advances, 12(2): 1077-1083. https://doi.org/10.1039/D1RA07655H

Bhadoria, P., Shrivastava, M., Khandelwal, A., Das, R., Langyan, S., Rohatgi, B. and Singh R. 2022. Preparation of modified rice straw-based bio-adsorbents for the improved removal of heavy metals from wastewater. Sustain. Chem. Pharm., 29: 100742. https://doi.org/10.1016/j.scp.2022.100742

Chen, X., Chen, G., Chen, L., Chen, Y., Lehmann, J., McBride, M.B. and Hay, A.G. 2011. Adsorption of copper and zinc by biochars produced from pyrolysis of hardwood and corn straw in aqueous solution. Bioresour. Technol., 102(19): 8877-8884. https://doi.org/10.1016/j.biortech.2011.06.078

Cui, X., Zhang, J., Pan, M., Lin, Q., Khan, M.B., Yang, X., He, Z., Yan, B. and Chen, G. 2021. Double-edged effects of polyvinyl chloride addition on heavy metal separation and biochar production during pyrolysis of Cd/Zn hyperaccumulator. J. Hazard. Mater., 416: 125793. https://do016/j.jhazmat.2021.125793

Cutillas-Barreiro, L., Ansias-Manso, L., Fernández-Calviño, D., Arias-Estévez, M., Nóvoa-Muñoz, J.C., Fernández-Sanjurjo, M.J., Álvarez-Rodríguez, E. and Núñez-Delgado, A. 2014. Pine bark as bio-adsorbent for Cd, Cu, Ni, Pb, and Zn: batch-type and stirred flow chamber experiments. J. Environ. Manag., 144: 258-264. https://doi.org/10.1016/j.jenvman.2014.06.008

Guo, J.M., Yang, J.X., Yang, J., Chen, T.B., Li, H.E., Xu, T.B., Zhou, X.Y., Ye, Y. and Yu, B. 2019. Interaction of Cd and Zn affecting the root morphology and accumulation of heavy metals in *Sedum aizoon*. Huanjing Kexue, 40(1): 470-479. https://doi.org/10.1007/10.13227/j.hjkx. 201805055

Jia, M., Wang, F., Bian, Y., Jin, X., Song, Y., Kengara, F.O., Xu, R. and Jiang, X. 2013. Effects of pH and metal ions on oxytetracycline sorption to maize-straw-derived biochar. Bioresour. Technol., 136: 87-93. https://doi.org/10.1016/j.biortech.2013.02.098

Lehmann, J. 2007. A handful of carbon. Nature, 443: 143-144. https://doi.org/10.1038/447143a

Li, M.O., Xiao, X., Liu, R., Chen, C. and Huang, L. 2008. Structural characterization of zinc-substituted hydroxyapatite prepared by hydrothermal method. J. Mater. Sci. Med., 19: 797-803. https://doi.org/10.1007/ s10856-007-3213-4

Li, W., Qiu, Z., Ma, Y., Zhang, B., Li, L., Li, Q., He, Q. and Zheng, Z. 2022a. Preparation and characterization of ginger peel polysaccharide–Zn (II) complexes and evaluation of anti-inflammatory activity. Antioxidants, 11(12): 2331. https://doi.org/10.3390/antiox11122331

Li, Y., Xin, J. and Tian, R. 2022b. Physiological defense and metabolic strategy of Pistia stratiotes in response to zinc-cadmium co-pollution. Plant Physiology and Biochemistry, 178: 1-11. https://doi.org/10.1016/j.plaphy.2022.02.020

Liu, Y., Chen, Z., Xiao, T., Zhu, Z., Jia, S., Sun, J., Ning, Z., Gao, T. and Liu, C. 2022. Enrichment and environmental availability of cadmium in agricultural soils developed on Cd-rich black shale in southwestern China. Environ. Sci. Pollut. Res., 29(24): 36243-36254. https://doi.org/10.1007/s11356-021- 18008-x

Liu, Y., Han, J., Dong, S., Li, Y., Liu, S., Zhou, Q., Chen, C. and Alessi, D.S., Konhauser, K.O. and Zhao, H. 2020. Competitive adsorption of heavy metals by anaerobic ammonium-oxidizing (anammox) consortia. Chemosphere, 258: 127289. https://doi.org/10.1016/j.chemosphere.2020.127289

McBride, M.B. 1994. Environmental Chemistry of Soils. Oxford University Press, New York.

McStay, A.C., Walser, S.L., Sirkovich, E.C., Perdrial, N. and Richardson, J.R. 2022. Nutrient and toxic elements in soils and plants across ten urban community gardens: Comparing pXRF and ICP-based soil measurements. J. Environ. Qual., 51(3): 439-450. https://doi.org/10.1002/jeq2.20346

Mensah, A.K., Marschner, B., Shaheen, S.M. and Rinklebe, J. 2022. Biochar, compost, iron oxide, manure, and inorganic fertilizer affect the bioavailability of arsenic and improve the soil quality of an abandoned arsenic-contaminated gold mine spoil. Ecotoxicol. Environ. Saf., 234: 113358. https://doi.org/10.1016/j.ecoenv.2022.113358.

Mukherjee, A.G., Wanjari, U.R., Renu, K., Vellingiri, B. and Gopalakrishnan, A.V. 2022. Heavy metal and metalloid-induced reproductive toxicity. Environ. Toxicol. Pharmacol., 92: 103859. https://doi.org/10.1016/j.etap.2022.103859

Niu, Z.R. 2016. Competitive Adsorption Behavior of Zn^{2+} and Cd^{2+} onto the Basaltic Diluvial-Colluvium Clay. China University of Geosciences, Beijing.

Peng, J., Zhang, S., Han, Y., Bate, B., Ke, H. and Chen, Y. 2022. Soil heavy metal pollution of industrial legacies in China and health risk assessment. Sci. Tot. Environ., 816: 151632. https://doi.org/10.1016/j.scitotenv.2021. 151632.

Praneeth, S., Zameer, A., Zhang, N., Dubey, B.K. and Sarmah, A.K. 2022. Biochar admixture cement mortar fines for adsorptive removal of heavy metals in single and multimetal solution: Insights into the sorption mechanisms and environmental significance. Sci. Tot. Environ., 839: 155992. https://doi.org/10.1016/j.scitotenv.2022.155992.

Sellami, S., Zeghouan, O., Dhahri, F., Mechi, L., Moussaoui, Y. and Kebabi, B. 2022. Assessment of heavy metal pollution in urban and peri-urban soil of Setif city (High Plains, eastern Algeria). Environ. Monit. Assess., 194(2): 126. https://doi.org/10.1007/s10661-022-09781-4.

Sharma, A., Kapoor, D., Gautam, S., Landi, M., Kandhol, N., Araniti, F., Ramakrishnan, M., Satish, L., Singh, V.P., Sharma, P., Bhardwaj, R., Tripathi, D.K. and Zheng, B. 2022. Heavy metal induced regulation of plant biology: Recent insights. Physiol. Plant., 174(3): e13688. https://doi.org/10.1111/ppl.13688.

Sposito, G., Lund, L.J. and Chang, A.C. 1982. Trace metal chemistry in arid‐zone field soils amended with sewage sludge: I. Fractionation of Ni, Cu, Zn, Cd, and Pb in solid phases. Soil Sci. Soc. Am. J., 46(2): 260-264. https://doi.org/10.2136/sssaj1982.03615995004600020009x

Syed, Z., Sogani, M., Rajvanshi, J. and Sonu, K. 2022. Microbial biofilms

for environmental bioremediation of heavy metals: A review. Appl. Biochem. Biotechnol., 5: 1-19. https://doi.org/10.1007/s12010-022-04276-x

Uchimiya, M., Lima, I.M., Klasson, K.T., Chang, S., Wartelle, L.H. and Rodgers, J.E. 2010. Immobilization of heavy metal ions (Cu^{II}, Cd^{II}, Ni^{II}, and Pb^{II}) by broiler litter-derived biochars in water and soil. J. Agric. Food Chem., 58(9): 5538-5544. https://doi.org/10.1021/jf9044217.

Valkova, E., Atanasov, V., Tzanova, M., Atanassova, S., Sirakov, I., Velichkova, K., Marinova, M.H., and Yakimov K. 2022. Content of Pb and Zn in sediments and hydrobionts as ecological markers for pollution assessment of freshwater objects in Bulgaria: A review. Int. J. Environ. Res. Public Health, 19(15): 9600. https://doi.org/10.3390/ijerph19159600.

Wang, L. 2016. Preparation, Characterization and Effect and Mechanism of Biochar on the Adsorption of Cd(II), Zn(II) in Loess. Lanzhou Jiaotong University, Lanzhou.

Wang, L., Wang, Y., Ma, F., Tankpa, V., Bai, S., Guo, X. and Wang, X. 2019. Mechanisms and reutilization of modified biochar used for removal of heavy metals from wastewater: A review. Sci. Tot. Environ., 668: 1298-1309. https://doi.org/10.1016/j.scitotenv.2019.03.011.

Wu, D., Peng, W., Yu, X., Yu, X., Dong, X., Lai, M., Liang, Z., Xie, S., Jacobs, D.F. and Zeng, S. 2022. Biochar alleviating heavy metals phytotoxicity in sludge-amended soil varies with plant adaptability. Environ. Res., 215: 114248. https://doi.org/10.1016/j.envres.2022.114248.

Xu, W., Shafi, M., Penttinen, P., Hou, S., Wang, S., Ma, J., Zhong, B., Guo, J., Xu, M. and Ye, Z. 2020. The bioavailability of heavy metals in contaminated soil is affected by different mass ratios of biochars. Environ. Technol., 41(25): 3329-3337. https://doi.org/10.1080/21622515.2019.1609096.

Xu, X., Cao, X., Zhao, L., Wang, H., Yu, H. and Gao, B. 2013. Removal of Cu, Zn, and Cd from aqueous solutions by the dairy manure-derived biochar. Environ. Sci. Pollut. Res., 20: 358-368. https://doi.org/10.1007/s11356-012-0873-5.

Nature Environment and Pollution Technology
An International Quarterly Scientific Journal

p-ISSN: 0972-6268
(Print copies up to 2016)
e-ISSN: 2395-3454

Vol. 23 | No. 1 | pp. 275-285 | 2024

Original Research Paper

https://doi.org/10.46488/NEPT.2024.v23i01.023

Open Access Journal

Effectiveness of Cadmium on Biochemical Shift of Pea Plant Treated with Mycorrhiza and Putrescine

Prasann Kumar*†, Shipa Rani Dey* and Debjani Choudhury**

*Department of Agronomy, School of Agriculture, Lovely Professional University, Jalandhar-144411, Punjab, India

**Department of Plant Pathology, School of Agriculture, Lovely Professional University, Jalandhar-144411, Punjab, India

†Corresponding author: Prasann Kumar; prasann0659@gmail.com

Nat. Env. & Poll. Tech.
Website: www.neptjournal.com

Received: 07-06-2023
Revised: 05-08-2023
Accepted: 19-08-2023

Key Words:
Antioxidant
Bioaccumulation
Cadmium
Enzymes
Glomus
Putrescine
Mycorrhiza

ABSTRACT

Heavy metals like cadmium (Cd), mercury (Hg), bismuth (Bi), and arsenic (As) are potent and harmful poisonous sources that cause havoc on health conditions for the population of the world. However, the response of our crop species to these potent heavy metals-related toxicity is still left to be fully understood. It is a matter of great concern, as we are heavily dependent on crop species like rice, wheat, peas, etc. Our study here aims to learn about the defensive mechanism of *Pisum sativum* L. aided with putrescine and mycorrhiza against the stress created by Cd-related toxicity. We quantified physiological parameters such as the membrane-related injury and stability index. We further measured the total free proline content, lipid peroxidation content, and SOD activity. We executed our quantitative experiments on the stressed pea plants due to the exogenously applied Cd-toxicity in the presence and absence of mycorrhiza and putrescine. Insights of our significant results will improve the understanding of readers of the role of mycorrhiza and putrescine in improvising the tolerance level of a pea plant over Cd-related toxicity.

INTRODUCTION

Cadmium metal pollution has become a major issue all over the world. Cadmium has been released into the environment as a result of its mobilization from ores and subsequent processing for various applications (Glowacka et al. 2019). As the level of industrialization rises, causing disruptions in natural biological cycles, the problem of heavy metals in soil and water pollution becomes a major threat (El-Amier et al. 2019). Heavy metals, unlike biological substances, are largely non-biodegradable and accumulate in the environment. The accumulation of heavy metals in soils and waters endangers both human health and the environment. As living organisms progress from lower trophic levels to higher trophic levels, these elements accumulate, and their concentrations increase in their body tissues (a biomagnification phenomenon). Heavy metals in soil have toxicological effects on soil microbes, which may result in a decrease in their number and activity (Khan et al. 2010). Soil fungi in terrestrial plant mycorrhizae can form a symbiotic relationship with the host plant, providing nutrients and water in exchange for carbon for survival (Kumar & Dwivedi 2014, Kumar & Dwivedi 2018a, 2018b). According to various research studies, mycorrhizae have beneficial effects on host plant growth under various stresses such as drought, salinity, heavy metal stress, and so on (Emamverdian et al. 2015). Many more mechanisms that increase fungal tolerance and host plant mechanisms under heavy metal stress must be clarified (Kumar & Dwivedi 2018a, 2018b, 2018c, Beshamgan et al. 2019). Because of the fantastic ability of mycorrhizae in the morphological and physiological developing mechanism, the fungal mycorrhizal has improved effects on plant growth as well as on the environment under heavy metal stress (Kumar et al. 2016 a, b, Alzahrani & Raddy 2019). Heavy metal stress is one of the most important stresses that harm plant growth and the environment due to its high toxicity (Nahar et al. 2016, Kumar et al. 2018a, 2018b, 2018c, 2018d). The biological mechanism is one of the most important methods for mitigating heavy metal stress, in which soil microbes such as Arbuscular Mycorrhizal, endophytic bacteria, and plant growth-promoting rhizobacteria are used for mitigating the hostile effects of heavy metal stress on plant growth as well as in maintaining the environment (Pathak et al. 2017, Taie et al. 2019). The various bioremediation details

mechanisms in which fungal association with the host flora has the expression of stress genes, glomalin production, and the phylogeny of fungal in different parts of the mycorrhizal plant under heavy metal toxicity (Soudek et al. 2016). The presence of cadmium harms plants growth and the environment (Abdelhameed & Metwally 2019). Different microbes in the soil are the most effective tool for increasing plant efficiency and improving environmental conditions (Cui et al. 2019). Microbes such as mycorrhizae, endophytic bacteria, and plant growth-promoting rhizobacteria increase plant growth as well as environmental properties under various stresses (Glick 2003). Nowadays, heavy metal is a serious stress, in addition to all other stresses that reduce plant efficiency and the environment. Based on their density (>5 $g.cm^{-3}$), the 53 elements are classified as heavy metals in the periodic table Holleman and Wiberg (1985). The primary function of the essential heavy metal is enzymatic catabolization, electron transfer, and DNA and RNA metabolism (Zenk 1996, Jamal et al. 2002). Heavy metals such as lead, arsenic, chromium, and others are sources of contamination that have negative effects on plants and the environment. The high concentration of heavy metals has an impact on plant metabolism, soil microbes, ecosystems, and the food chain (Opik et al. 2006, Friedlova 2010). The main source of heavy metal concentration in the environment is the increasing rate of industrialization and urbanization, as well as improper waste disposal. Excess herbicide use, fertilization, and sludge are all anthropogenic activities that contribute to heavy metal contamination in the environment. Still, the mining process is the most common source of trace elements (Whitmore 2006). If the concentration of heavy metals exceeds their permissible limits, it has negative effects on microbial activities as well as in plants and has an impact on the environment (Miransari 2011). The presence of a high concentration of heavy metal alters the structure of enzymes, protein structure, and essential element substitutes. The structure of the plasma membrane is also altered, reducing its permeability and functionality. Cadmium (Cd), for example, is a harmful and severely toxic heavy metal; even at levels as low as 0.1 mg to 0.2 mg, Cd is ranked seventh in the world's crust as the most toxic element (Kumar et al. 2011a, 2011b). Many anthropogenic practices, such as the use of sewage water for agriculture and continuous phosphorus processing, increased the amount of cadmium in farm soil (Tai et al. 2016). Cadmium toxicity is also increasing in the agricultural sector as a result of the constant use of phosphorus (Kumar et al. 2013). Cadmium is bioavailable and, as a metalorganic complex, easily transported within plants. Cadmium competed for absorption sites, preventing plants from absorbing phosphorus and other mineral nutrients. Several studies concluded that mycorrhizal fungi affect the growth and development of plants grown in heavy metal-contaminated waste sites (Kumar et al. 2018a, 2018b). Mycoremediation is a sub-remediation technique under Bioremediation. Mycoremediation is composed of two words: Myco and Remediation, where Myco means fungus and remediation means to cure. Various fungi are used in the Mycoremediation process to clean the environment of pollution and other toxic effluents (Miransari 2011, 2016, Miransari et al. 2009). Various studies have explained the calming effect of Arbuscular Mycorrhiza (AM) on various forms of stress, such as heat, salinity, and heavy metals. Any of these pathways demonstrates how fungi mitigate the negative effects of stress on plant growth and the surrounding ecosystem: (1) an increase in nutrient and water consumption, (2) an increase in plant hormonal output, (3) other microbial interactions on the soil, (4) an increase in sodium absorption of heavy metals, and (5) modification of the roots of fungal-based plants (Miransari 2011, Kumar 2018).

Putrescine (Put) is a polyamine (PA) that influences the growth and development of plants, especially stress responses, as well as apoptosis and programmed death in plants (Kumar et al. 2012, Kumar et al. 2019). At optimal and cellular pH levels, PAs are small, positively charged aliphatic amines that bind negatively charged molecules such as reactive oxygen species and provide the shielding impact in the cell (Kumar & Dwivedi 2018, Kumar et al. 2018a, 2018b, 2018c). Given the history of heavy metal contamination in medicinal plants, there is an urgent need for systematic control of toxic heavy metals in plants used as economic crops (Kumar & Pathak 2019).

Our systematic approach to understanding the defense mechanism of *Pisum sativum* L. against Cd-toxicity aimed to learn a few key inherent physiological factors that are traceable in a stressed pea plant. Plants have a well-established tolerance mechanism of antioxidant enzyme systems that can tolerate the potential toxicity of ROS to cope with ROS-induced oxidative stress. An antioxidant defense system involving the sequential and simultaneous action of several enzymes is one of the protection mechanisms adopted by plants. Those noticeable factors are total free proline, membrane stability index, membrane injury index, lipid peroxidation, and Superoxide dismutase activity. We discussed our significant findings regarding these key factors in the presence and absence of mycorrhiza and putrescine, which works. We established here in favor of improvising tolerance level for pea plant.

MATERIALS AND METHODS

The pot experiment was performed with a genotype of a pea, Arkel, in our well-designed shared polyhouse. Disease-free

and healthy, bold seeds of Pea and Arkel were obtained from the Punjab Agriculture University, Ludhiana. The endomycorrhiza *Glomus mosseae* was obtained from the Tata Energical Research Institute, New Delhi. The cadmium in the form of cadmium nitrate ($Cd(NO_3)_2$) was obtained from the LPU block 26-401 laboratory and purchased from Merck Life Science, a vibrant science technology company. Similarly, Putrescinehas have been obtained from the LPU block 26-401 laboratory of Crop Physiology.

A few seeds of *Pisum sativum* L. were sowed in each pot containing enriched soil with a capacity of 14 kg. Targeted pots were inoculated with Endomycorrhiza *Glomus* species, and followed by heavy metal stress in the plant was created by exogenously applied cadmium nitrate in the soil of those pots. One best concentration of cadmium nitrate based on initial screening was selected, i.e., 100 ppm per pot of soil. Furthermore, putrescine was added to a foliar sample at an interval of 15 days at an optimized concentration of 10 ppm. The temporal observations were made after sowing seeds at three stages such as 30, 60, and 90 days after sowing (DAS). Ten treatments, including a control, were executed. For each treatment, three replicas were carried out. The detailed plan of treatments was: T1= Control; T2: Cadmium nitrate (100ppm); T3: Control + Mycorrhiza (*Glomus* sp., AMF); T4: Control + Putrescine (5 ppm); T5: Control + Putrescine (10 ppm); T6: Cadmium nitrate (100 ppm) + Putrescine (5ppm); T7: Cadmium nitrate (100 ppm) + Putrescine (10ppm); T8: Cadmium nitrate (100 ppm) + Mycorrhiza (*Glomus* sp., AMF); T9: Cadmium nitrate + Mycorrhiza (*Glomus* sp., AMF) + Putrescine (5 ppm); T10 : Cadmium nitrate (100 ppm) + Mycorrhiza (*Glomus* sp., AMF) + Putrescine (10 ppm).

Estimation of Free Proline (µg.mL^{-1})

The estimation of free proline was measured as suggested by Bates et al. (1973). In short, tissue was removed with sulphosalicylic acid, and proteins were precipitated as a protein-sulphosalicylic acid system. Under the acidic environment, the extracted proline was allowed to react with ninhydrin to create a red color. The 100 mg plant test content was homogenized with mortar and pestle in 10 mL of sulphosalicylic acid (3%). The mixture was centrifuged at 6000 rpm for 10 min, and the supernatant was collected. 2.0 mL of the extract was mixed with 2 mL of glacial acetic acid and ninhydrin reagent in the test tube. The reaction mixture was kept for ~30 min in a water bath at 100°C until the brick red color developed, and then it was allowed to cool down. 5 mL of toluene was added to this reaction mixture, and afterward, it was transferred to the separation funnel. The absorbance of the separated content was shown at 520 nm using a toluene-free spectrophotometer. Proline (10 mg) was dissolved in 3% aqueous sulphosalicylic acid and finally diluted up to 100 mL afterward. The aliquots of 0.2, 0.4, 0.6, 0.8, and 1.0 mL were taken into various test tubes for the spectra measurement, and the volume increased to make up to 2 mL by adding 3% aqueous sulphosalicylic acid.

Estimation of Membrane Stability Index and Injury Index (%)

Membrane stability index (MSI) and membrane injury index (MII) were quantified using the methodology defined by Premchandra et al. (1990). Solute leakage (electrolyte leakage) assessment from cells and the measurement of MSI can indirectly help us to measure the damage to the membrane. The stimulating effect of stress on the leakage of electrolytes could be attributed to plasma membrane injury, too. The MSI and MII were measured by putting 200 mg of leaves in two sets of 10 mL of double-distilled water. One set was heated in a warm water bath at 40°C for 30 min and measured electrical conductivity (C1). The second set was boiled at 100°C for 10 min in a boiling water bath, and the electrical conductivity (C2) was measured. The electrical conductivity in both cases was measured using a conductivity meter (ME977-C, Max Electronics, India). The equations for the measurement of MSI and MII are mentioned below;

$$MSI = 100\left[1 - \frac{C1}{C2}\right]$$

$$MII = 100\left[\frac{C1}{C2}\right]$$

Estimation of Lipid Peroxidation [Malondialdehyde (MDA) Content]

Heath and Packer (1968) originally developed the estimation of Lipid Peroxidation. By measuring the amount of malondialdehyde (MDA) content, lipid peroxidation was estimated. A 5 mL solution of 5% trichloroacetic acid (TCA) was applied to decrease the volume of collected and processed leaf tissues into small pieces. The homogenates were then moved to fresh tubes, which were centrifuged for 15 min at 12,000 rpm at room temperature. Applied in a 20% TCA solution, the same amounts of supernatant, and 0.5% thiobarbituric acid (TBA) to a fresh tube and boiled at 100^{o}C for 25 min. The tubes were placed in the ice bath and then centrifuged for 5 minutes at 10,000 rpm at room temperature. The supernatant absorption was measured at 532 nm, and the absorption was removed at 600 nm for non-specific turbidity, while 0.5% TBA was used blank in a 20 percent solution for TCA. The sum of the MDA-TBA complex (red pigment) was measured as 155 M^{-1} cm^{-1} from the extinction coefficient. Measurements were taken from

the values of MDA material. The results were reported as MDA g^{-1} fresh weight (FW) µmoles.

Estimation of Superoxide Dismutase (SOD) Activity

Superoxide dismutase (SOD) enzyme activity was calculated as exactly described in Dhindsa et al. (1981). SOD's assay is based on inhibiting EDTA, L-methionine, and nitro-blue tetrazolium formazan formation. Leaf extracts (100 mg) are homogenized with an extraction buffer of 5 mL (0.1 M phosphate buffers, 0.5 mM EDTA pH 7.5). In a cooling centrifuge (REMI, C-24), the homogenate was centrifuged at 10,000 g for 10 min. The supernatant was collected after centrifugation, and this supernatant was used as a source of enzymes. The sample pipelines for each particular enzyme contain three mL of a reaction mixture, which should be 0.1 M of 1.5 M sodium carbonate, 0.2 mL of 200 mm methionine, 0.1 mL of 2.25 mM NBT, 0.1 metric mL of 3 mm EDTA, 1.5 mL of 100 mm potassium phosphate solution, 1 ml of distilled water and 0.1 mL of enzyme extract. Two tubes have been taken as a monitor without removing the enzyme. The reaction was initiated by adding 0.1 mL of riboflavin (60 µM) to all test tube sets and placing the 2 tube sets (one in which enzyme was added and the other in which enzyme was not added) below a light source of two 15 min fluorescent lamps. A black cloth switching off the light and covering the tube sets halted the reaction. The set of tubes developed the maximum color without an enzyme extract. A non-irradiated set in which a light source was not supplied, but enzyme extract was kept in the dark, and therefore, color did not develop and served as blank. Using a spectrophotometer (Elico, SL 196), the absorption of all test tube sets was measured at 560 nm. Enzyme unit (EU) was calculated as per the formula given below:

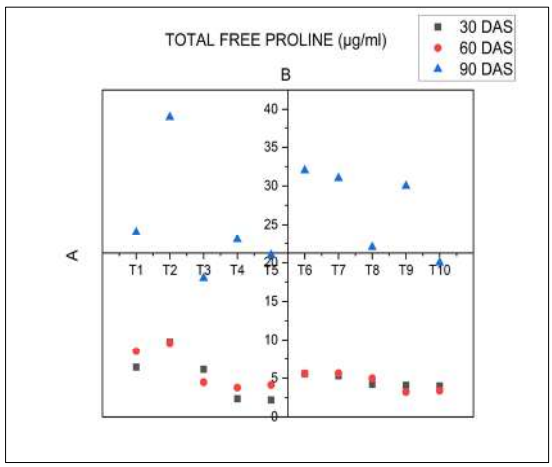

Fig. 1: Scatter central plot of Total Stability Index.

EU = Absorbance without enzyme in light - (Absorbance with an enzyme in light - Absorbance in Dark)/Absorbance without enzyme in light/2

The EU was expressed on a per gm fresh weight basis as well as based on per mg protein (specific activity).

Statistical Analysis

The mean values were calculated from three replicates. The data were analyzed statistically by applying the technique of analysis of variance for a completely randomized design and significance to be tested by using the Duncan Multiple Range Test (DMRT) with the help of Statistical Package for the Social Sciences (SPSS). Critical difference for treatments means-tested at a 5% level of significance.

RESULTS AND DISCUSSION

Estimation of Total Free Proline

In Arkel, a pea variety, under cadmium imparted stress, the total free proline [EU g^{-1} Fresh Weight] was measured (Table 1, Fig. 1). The average total free proline content was observed to increase significantly from 34.28% to 11.52%, and 38.46% at intervals of 30, 60, and 90 days after sowed (DAS) respectively when the pea plant was subjected to heavy metal-related stress applied in 2nd set of experimental condition (T2) relative to the controlled experiment (T1) (Table 1**,** Fig. 1). Exogenous application of endomycorrhiza in soil (T3) demonstrated the mitigating impact by reducing

Table 1: Total free proline of pea after different treatments.

Treatments	30DAS	60DAS	90DAS
T1	$6.42^{b} \pm 0.13$	$8.52^{b} \pm 0.23$	$24^{d} \pm 0.39$
T2	$9.77^{a} \pm 0.11$	$9.63^{a} \pm 0.09$	$39^{a} \pm 0.48$
T3	$6.14^{b} \pm 0.03$	$4.47^{de} \pm 0.28$	$18^{h} \pm 0.09$
T4	$2.34^{e} \pm 0.10$	$3.78^{fg} \pm 0.03$	$23^{de} \pm 0.07$
T5	$2.19^{e} \pm 0.11$	$4.12^{ef} \pm 0.09$	$21^{fg} \pm 0.13$
T6	$5.58^{c} \pm 0.17$	$5.57^{c} \pm 0.16$	$32^{b} \pm 0.17$
T7	$5.29^{c} \pm 0.05$	$5.63^{c} \pm 0.07$	$31^{bc} \pm 0.28$
T8	$4.18^{d} \pm 0.10$	$4.97^{d} \pm 0.15$	$22^{ef} \pm 0.06$
T9	$4.09^{d} \pm 0.05$	$3.21^{h} \pm 0.10$	$30^{c} \pm 0.74$
T10	$4.01^{d} \pm 0.09$	$3.38^{gh} \pm 0.04$	$20^{g} \pm 0.42$

Note: DAS = Days after sowing. Data are in the form of mean± SEM. Significance at $P \leq 0.05$ using SPSS ver. 22. T1= Control; T2: Cadmium nitrate (100ppm); T3: Control + Mycorrhiza (*Glomus* sp., AMF); T4: Control + Putrescine (5 ppm); T5: Control + Putrescine (10 ppm); T6: Cadmium nitrate (100 ppm) + Putrescine (5ppm); T7: Cadmium nitrate (100 ppm) + Putrescine (10ppm); T8: Cadmium nitrate (100 ppm) + Mycorrhiza (*Glomus* sp., AMF); T9: Cadmium nitrate + Mycorrhiza (*Glomus* sp., AMF) + Putrescine (5 ppm); T10 : Cadmium nitrate (100 ppm) + Mycorrhiza (*Glomus* sp., AMF) + Putrescine (10 ppm)

the total free proline content by 37.15%, 53.58% and 53.84% relative to the condition of T2 at 30, 60 and 90 DAS, respectively (Table 1, Fig. 1). When it was compared to T2, the exogenous application of putrescine (T6) showed a mitigating effect by decreasing total free proline by 42.88%, 42.15%, and 17.94% on proposed DAS, respectively. Significantly, the average total free proline content was noticed a reduction by 77.58%, 57.21%, and 46.15% at 30, 60 and 90 DAS, respectively, when a higher dose of putrescine (T5) was applied compared to the experimental condition of T2 (Table 1, Fig. 1). Similarly, the total free proline output was observed with a substantial decline of 45.85%, 41.53%, and 20.51% at the proposed DAS when we compared the data between T7 and T2. Moreover, the average total free proline content was noticed to decrease significantly by 57.21%, 48.39%, and 43.58% in comparison to that of T2 when we administered a higher dose of putrescine in T8 (Table 1, Fig. 1). Interestingly, the combination of putrescine and mycorrhiza in the treatment of T9 showed a decreasing level of the average total free proline content by 58.13%, 66.66% and 23.07% at 30, 60, and 90 DAS treatment, respectively. The substantial total free proline content was decreased by 58.95%, 64.90%, and 48.71% in T10, concerning T2, respectively. The total free proline content in the treatment of T4 was observed to decrease significantly at the suggested DAS by 76.04%, 60.74%, and 41.02%, respectively, in comparison to that of T2. The putrescine impact (5ppm) was more active at 30 DAS, and the mycorrhiza + putrescine (5ppm) was more successful at 60 DAS. Therefore, it is clear that proline synthesis in the plant may be a result of any kind of injury, either through heavy metal. Biosynthesis of proline accelerated when the plants are treated with toxic heavy metal content. Exposure to cadmium causes toxicity within the plant (a kind of stress); consequently, proline is synthesized and helps to protect the plant. The external application of putrescine with 5 ppm was found to be a potent mitigating agent to combat the effect of cadmium toxicity (Zengia & Munzuroglu 2005). Mycorrhiza may reduce the transfer of heavy metals to the target plant or the end of the aerial component from roots. The resistance to heavy metals improves with enhanced nutritional intake and P. The roots of the colonized target plant may store heavy metals in the root and the fungal hyphae, preventing them from spreading to the plant tip or aerial portion. A ceasing movement of heavier metals in the fungal hyphae emerges from the very critical process of the fungus that protects the main plant from the bad impact of heavy metals. The vesicles, arbuscular, and vacuoles may be the source of the aggregation of heavy metals. It prevents the entry of cadmium into the plants. The research has shown the rise in the concentration of Cu in the vacuoles of spores and the accumulation of Cd vacuoles of the hyphae of *Glomus intraradices* under the stress of heavy metals. This type of storage structure can develop tolerance towards the stress in the target plant fungi. The cell wall of the fungi is a perfect site for heavy metal binding as it has carboxyl, hydroxyl, and free amino acids for heavy metal absorption. The appearance of the cell wall and thickness can observe this type of absorption ability. As an example, the species of fungus, which belongs to the family Glomeraceae, does not possess thick hyphae because their diameter lies between the range of 0.8 to 4.5 µm and the hyphae cell wall is equal to 1.2 µmto the maximum (Kumar & Dwivedi 2018a, 2018b, 2018c).

Membrane Stability Index [MSI] [%]

In pea variety Arkel under cadmium stress, the impact of polyamine (putrescine), mycorrhiza, and their combination on MSI (%) was examined. Table 2 documented the MSI.

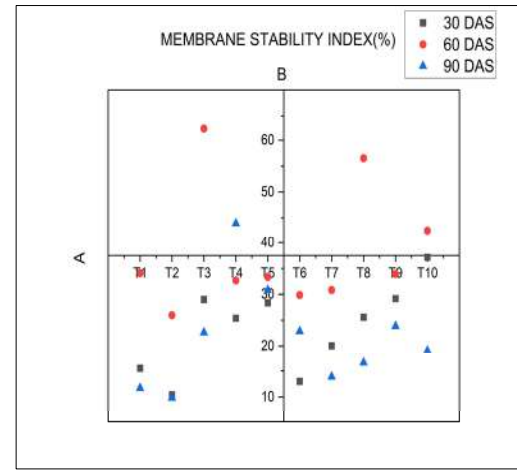

Fig. 2: Scatter central plot of Membrane Free Proline.

Table 2: Membrane Stability Index of pea after different treatments.

Treatments	30DAS	60DAS	90DAS
T1	$15.49^{e} \pm 0.40$	$34.1^{d} \pm 0.41$	$11.71^{fg} \pm 0.38$
T2	$10.41^{g} \pm 1.18$	$25.97^{g} \pm 0.48$	$9.85^{g} \pm 0.80$
T3	$28.98^{b} \pm 0.16$	$62.24^{a} \pm 0.95$	$22.63^{c} \pm 0.46$
T4	$25.4^{c} \pm 0.21$	$32.66^{de} \pm 0.29$	$43.96^{a} \pm 0.37$
T5	$28.35^{b} \pm 0.46$	$33.34^{d} \pm 0.511$	$30.80^{b} \pm 1.27$
T6	$13.01^{f} \pm 0.34$	$29.84^{f} \pm 0.04$	$22.88^{c} \pm 0.70$
T7	$20.08^{d} \pm 1.86$	$30.83^{ef} \pm 0.53$	$13.87^{f} \pm 0.54$
T8	$25.58^{b} \pm 0.38$	$56.52^{b} \pm 1.25$	$16.57^{e} \pm 1.41$
T9	$29.19^{b} \pm 0.16$	$33.91^{d} \pm 0.47$	$23.88^{c} \pm 0.69$
T10	$37.13^{a} \pm 0.31$	$42.54^{c} \pm 0.61$	$19.1^{d} \pm 0.46$

Note: Symbols as per Table 1.

It is clear that, when subjected to heavy metal stress (T2) at 30, 60 and 90 DAS intervals, the mean MSI decreased significantly by 32.79%, 23.84%, and 15.88% relative to control (T1) (Table 2, Fig. 2). Exogenous application of endomycorrhiza in soil (T3) shows the mitigation impact by growing MSI by 64.07%, 58.27%, and 56.47% relative to T2 at 30, 60, and 90 DAS (Table 2, Fig. 2). The exogenous application of putrescine (T6) shows the increasing MSI by 19.98%, 12.96%, and 56.94% at 30, 60, and 90 DAS. Similarly, when T5 was compared with T2, the mean MSI increased significantly by 63.28%, 22.10%, and 68.02% (Table 2, Fig. 2). Likewise, the MSI increased significantly to 48.15%, 15.76%, and 28.98% at the suggested DAS (T7) (Table 2, Fig. 2). The average MSI increased significantly compared to T8 by 63.57%, 54.05%, and 40.55% when treated with a higher dose of putrescine compared to T2. Combining putrescine and mycorrhiza in treatment, T9 significantly increases the MSI at the planned DAS by 64.33%, 23.41%, and 58.75%, respectively. Compared with T2, T10 improved substantial MSI by 71.96%, 38.96%, and 48.42%, respectively. The MSI was observed to rise significantly in T4 by 59.01%, 20.48%, and 77.59%, respectively, relative to T2 in the original DAS (Table 2, Fig. 2). Therefore, putrescine's effect on 30 DAS at 10 ppm + mycorrhiza, just mycorrhiza at 60 and 90 DAS, Putrescine (5 ppm) shows the best-mitigating impact in improved MSI words. AMF increases anti-oxidant activity and has often helped reduce exposure to oxidative stress. The thickness of the hyphae of fungus from the family of Gigasporaceae is higher than 20 µm of the average diameter. The research work has shown that a greater amount of heavy metals can be maintained by the thinner hyphae if compared with the hyphae with a greater thickness. This is due to the greater surface area in the thinner hyphae. Research work has shown that in mycorrhiza plants, the cortex of the root retains a much greater amount of heavy metals, which include Fe, Zn, and Niand. Various species of mycorrhizal fungus also have the variable ability to absorb heavy metals (Cabral et al. 2015). The important mechanism that can convert mycorrhizal plants into heavy metal-absorbing plants is the larger production of glutathione-derived peptides and phytochelatins; only higher plants create these. As a result, these plants will have the ability to chelate metalloids and heavy metals (Garg & Pandey 2015)

From all the parameters that help in determining the mitigating effects of the heavy metal stress of mycorrhizal fungi, the ability of AM fungus to mitigate heavy metals from the soils that are polluted is unique. Some of the mycorrhizal fungi can be better than other species of fungus when compared (Kumar et al. 2018d). Heavy metal allocation to various parts of the target plant by AM fungi also varies because some heavy metals can be accumulated at the aerial parts while some are at the roots of the plant (Kumar et al. 2018).

Membrane Injury Index [MII] [%]

It is evident (Table 3, Fig. 3) that when exposed to heavy metal stress (T2) at 30, 60, and 90 DAS intervals, the average MII was significantly increased by 5.67%, 10.98%, and 2.06% compared to the control (T1). Exogenous application of endomycorrhiza in soil (T3) demonstrated the impact of mitigation by reducing the MII by 20.72%, 48.99%, and 14.17% relative to T2 at 30, 60 and 90 DAS. Relative to T2, putrescine (T6) exogenous application had a beneficial impact on potential DAS by reducing MII by 2.90%, 5.22%, and 14.45% (Table 3, Fig. 3). The average MII was significantly reduced when treated with a higher dose of putrescine (T5) compared to T2 by 20.02%, 9.95%, and 23.24%. Similarly, the MII declined dramatically to

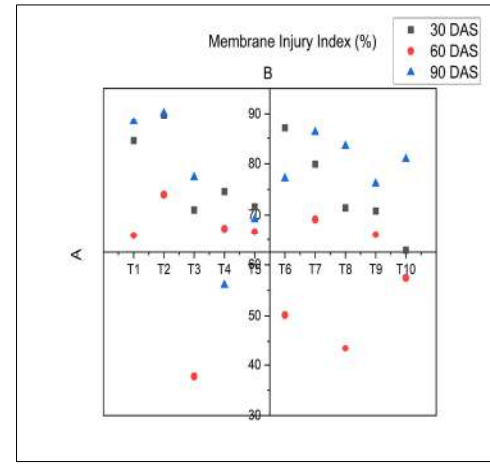

Fig. 3: Scatter central plot of Membrane Injury Index.

Table 3: Membrane Injury Index of pea after different treatments.

Treatments	30DAS	60DAS	90DAS
T1	$84.51^{c} \pm 0.40$	$65.9^{ab} \pm 0.41$	$88.29^{ab} \pm 0.38$
T2	$89.59^{a} \pm 1.19$	$74^{a} \pm 0.48$	$90.15^{a} \pm 0.80$
T3	$71.02^{f} \pm 0.17$	$37.76^{c} \pm 0.98$	$77.37^{e} \pm 0.47$
T4	$74.6^{e} \pm 0.21$	$67.34^{ab} \pm 0.29$	$56.04^{g} \pm 0.38$
T5	$71.65^{f} \pm 0.45$	$66.66^{ab} \pm 0.48$	$69.19^{f} \pm 1.21$
T6	$86.99^{b} \pm 0.35$	$50.16^{bc} \pm 16.85$	$77.12^{e} \pm 0.74$
T7	$79.92^{d} \pm 1.91$	$69.17^{ab} \pm 0.54$	$86.13^{b} \pm 0.54$
T8	$71.42^{f} \pm 0.39$	$43.48^{c} \pm 1.22$	$83.43^{c} \pm 1.43$
T9	$70.81^{f} \pm 0.17$	$66.09^{ab} \pm 0.47$	$76.12^{e} \pm 0.70$
T10	$62.87^{g} \pm 0.32$	$57.45^{abc} \pm 0.59$	$80.9^{d} \pm 0.47$

Note: Symbols as per Table 1.

10.79%, 6.56%, and 4.45% at the suggested DAS in T7 (Table 3, Fig. 3). The median MII decreased dramatically when administered with a higher dose of putrescine compared to T8 by 20.28%, 41.26%, and 7.45% relative to T2 (Table 3, Fig. 3). Combining putrescine and mycorrhiza in treatment T9 by decreasing MII at the proposed DAS by 20.96%, 10.72%, and 15.56%(Table 3, Fig. 3). The T10was compared with the T2 treatment, and significant MII decreased by 29.82%, 22.39%, and 10.26%, respectively (Table 3, Fig. 3). The MII was observed to decrease significantly in this therapy (T4) by 16.73%, 9.03%, and 37.83%, respectively, relative to T2 in the original DAS (Table 3, Fig. 3). In terms of enhanced MII, the effect of putrescine at 10 ppm + mycorrhiza on 30 DAS, only mycorrhiza at 60 and 90 DAS, Putrescine (5 ppm) shows the best mitigating effect. Some fungal species are not tolerant under heavy metal stress. Still, one of the most important fungal species, named Glomeraceae, is the dominant species, which can tolerate and be used in the inoculation of the host plant under heavy stresses due to some special morphological as well as physiological potential of fungal species having the fast growth to produce the spores (Lenoir et al. 2016). In the contaminated soil, the fungal can prevent the plants from absorbing the heavy metal as well as by restricting the interaction of host plants with heavy metals. The fungal grows even in contaminated soil and can have a positive interaction with terrestrial plants, which are used for bioremediation (Cabaral et al. 2015). When the stress conditions, germination spore stages, colonization, hyphal growth, and sporulation are harmfully affected by the stress conditions, it results in the reduction of fungi as well as the growth of roots of host plants (Zhu et al. 2012). Under heavy metal stress, there is the production of reactive oxygen species hydrogen peroxide, radical of hydroxyl, and superoxide anion radicals due to the induction of activities of antioxidants, which affects the cellular structure and their activities (Apel & Hirt 2004, Fobert & Despres 2005). From the different research, it was reported that the Glomus species are the best and able to mitigate the effect of various stresses like salinity as well as drought (Sanchez-Castro et al. 2012). The fungal growth is very fast, and they colonize rapidly around the roots of host plants and provide resistance to the host plant to withstand the heavy metal stress (Mohammad et al. 2003). The growing pollutants harm the lipids of the mycorrhizal fungi membrane, which is essential for the establishment of symbiotic relations with host plants (Calonne et al. 2012).

Under the stress of copper, fungi overexpressed glomalin production, and fungi were protected from the negative effect of arsenic and helped to fix the proteins of fungus (Ferrol et al. 2009).

Under the conditions of stress, growing the mycorrhizal pant by indigenous isolation was an appropriate method and producing stress-tolerant fungi in stressful ecosystems such as toxic areas and saline stress conditions. The fungi increase the environmental quality and act as bioindicators as well as help transfer pollutants by making an interface between soil and plants (Lenoir et al. 2016). In detail, these mechanisms of mycorrhizal fungi are used for avoiding the stresses, i.e., (1) various gene expressions, (2) morphological transformation, (3) formation of various molecules and proteins like chaperone, trehalose, and antioxidants, etc., (4) compartmentalization, and (5) transportation of contaminants.

Lipid Peroxidation [MDA]

It is clear that (Table 4, Fig. 4) when subjected to heavy metal stress (T2) at 30, 60, and 90 DAS periods, the mean MDA content increased significantly by 69.45 percent, 40.86 percent, and 42.76 percent relative to control (T1) (Table 4,

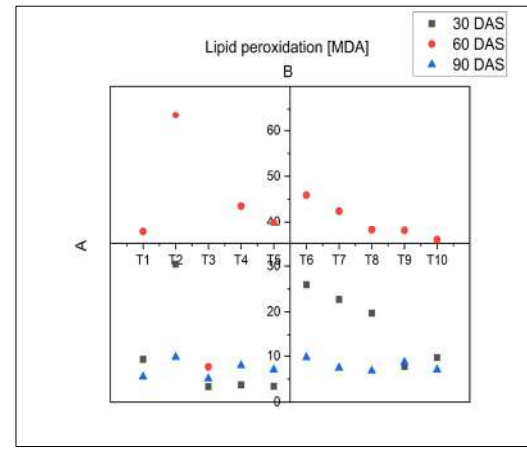

Fig. 4: Scatter central plot of Lipid Peroxidation (MDA Content).

Table 4: MDA content of pea after different treatments.

Treatments	30DAS	60DAS	90DAS
T1	$9.3^{a} \pm 0.14$	$37.58^{ef} \pm 0.09$	$5.5^{f} \pm 0.17$
T2	$30.45^{a} \pm 0.36$	$63.55^{a} \pm 0.82$	$9.78^{ab} \pm 0.15$
T3	$3.35^{g} \pm 0.23$	$7.66^{g} \pm 0.31$	$5.11^{f} \pm 0.11$
T4	$3.76^{g} \pm 0.26$	$43.47^{c} \pm 0.49$	$7.98^{cd} \pm 0.39$
T5	$3.45^{g} \pm 0.23$	$39.83^{d} \pm 0.57$	$7.05^{de} \pm 0.45$
T6	$25.94^{b} \pm 0.76$	$45.88^{b} \pm 0.40$	$9.72^{a} \pm 0.25$
T7	$22.73^{c} \pm 0.13$	$42.37^{c} \pm 0.47$	$7.45^{de} \pm 0.18$
T8	$19.73^{d} \pm 0.36$	$37.97^{e} \pm 0.39$	$6.82^{e} \pm 0.32$
T9	$7.75^{f} \pm 0.28$	$37.82^{e} \pm 0.66$	$8.67^{bc} \pm 0.30$
T10	$9.68^{e} \pm 0.19$	$35.82^{f} \pm 0.40$	$7.06^{de} \pm 0.28$

Note: Symbols as per Table 1.

Fig. 4). Exogenous application of endomycorrhiza in soil (T3) demonstrated the mitigating impact by reducing the MDA content by 88.98%, 87.94%, and 46.82% relative to T2 at 30, 60, and 90 DAS (Table 4, Fig. 4). Compared to T2, putrescine (T6) exogenous application showed a mitigating effect on the proposed DAS by decreasing MDA by 14.81%, 27.80%, and 3.22% (Table 4, Fig. 4). Across 88.66%, 37.32%, and 26.63%, when administered with a higher dose of putrescine (T5) relative to T2, the mean MDA concentration was significantly reduced (Table 4, Fig. 4). Furthermore, the MDA amount decreased significantly to 25.35%, 33.32%, and 22.47% at the suggested DAS was associated with T7 (Table 4, Fig. 4). The average MDA content decreased significantly when treated with a higher dose of putrescine compared to T8 by 35.20%, 40.25%, and 29.03% compared to T2 (Table 4, Fig. 4). The use of putrescine and mycorrhiza in T9 treatment decreased by 74.54%, 40.48%, and 9.71%, respectively (Table 4, Fig. 4). As T10 was associated with T2 therapy, substantial MDA content decreased by 68.21%, 43.63%, and 26.53%, respectively (Table 4, Fig. 4). The amount of MDA in this therapy (T4) was observed to decrease significantly by 87.65%, 31.59%, and 16.96%, respectively, relative to T2 in the original DAS (Table 4, Fig. 4). ROS is potentially harmful to cell membranes, resulting in membrane lipid oxidation (lipid peroxidation). Malondialdehyde (MDA) is one of the lipid peroxidation end breakdown products and can be used as an in vivo lipid peroxidation predictor. To defend against oxidative stress, a network of antioxidant enzymes such as superoxide dismutase (SOD) and catalase (CAT) has evolved multiple scavenging mechanisms to regulate the rate of ROS. Scientists studied the impact on *Brassica rapa* of treatment with selenium dioxide, putrescine, and cadmium chloride. The experiment showed that the treatment of selenium dioxide and cadmium chloride produced stress in turnip plants, thus inducing enhanced MDA and anthocyanin content into maximized development of ROS and inhibiting chlorophyll biosynthesis. The application of SeO_2 and putrescine improved antioxidant function and fostered better growth of crops.

Fungus of mycorrhiza is responsible for the production of a suitable environment for the activities of microbes present in soil and their growth by raising the amount of organic matter in soil and increasing the activities and growth of roots (Silva et al. 2006; Khan et al. 2000). Hence, the use of mycorrhiza fungi was an appropriate technique for soil bioremediation. If mycorrhiza fungi were used with growth hormones, then bioremediation would work with greater effectiveness. The single spores of fungi help to produce and grow the vast hyphae network. If hosted plants existed. Bioremediation of polluted areas is possible by a single use of mycorrhizal fungi (Cabral et al. 2010, Declerck et al. 2005, Mugnier & Mosse 1987)

There is two most important mechanisms upon which the mycorrhizal fungal works to mitigate the effect of heavy metal under the contaminated soil named as phytostabilization and phytoextraction. When the mycorrhizal fungi uptake the heavy metal from the contaminated soil it has a couple of hyphae physiological mechanism, which includes protein expression like metallothionein as well as glomalin, heavy metal retention by the spores of fungal, in cellular membrane heavy metal complexation, molecular gene expression which results in the phytostabilization activation process (Behra 2014, Yang et al. 2014). When the symbiosis occurs between the mycorrhizal fungi and the hyperaccumulating plants, it results in increasing the absorption and the translocation of heavy metals, which leads to phytoextraction. Different plant parts, like herbaceous as well as corn plants, undergo the process of phytostabilization, and phytoextraction has been

Table 5: SOD activity of pea after different treatments.

Treatments	30DAS	60DAS	90DAS
T1	$0.57^{c} \pm 0.025$	$0.16^{de} \pm 0.004$	$0.39^{e} \pm 0.019$
T2	$0.85^{a} \pm 0.012$	$0.74^{a} \pm 0.025$	$1.35^{a} \pm 0.060$
T3	$0.3^{g} \pm 0.012$	$0.03^{f} \pm 0.002$	$0.37^{e} \pm 0.037$
T4	$0.58^{c} \pm 0.008$	$0.33^{c} \pm 0.004$	$0.78^{b} \pm 0.021$
T5	$0.4^{f} \pm 0.025$	$0.44^{b} \pm 0.016$	$0.55^{cd} \pm 0.002$
T6	$0.4^{f} \pm 0.025$	$0.35^{c} \pm 0.009$	$0.82^{b} \pm 0.026$
T7	$0.51^{cd} \pm 0.016$	$0.41^{b} \pm 0.014$	$0.61^{c} \pm 0.023$
T8	$0.72^{b} \pm 0.029$	$0.18^{d} \pm 0.008$	$0.59^{cd} \pm 0.025$
T9	$0.48^{de} \pm 0.021$	$0.13^{e} \pm 0.004$	$0.52^{cd} \pm 0.004$
T10	$0.43^{ef} \pm 0.012$	$0.15^{de} \pm 0.012$	$0.50^{d} \pm 0.004$

Note: Symbols as per Table 1.

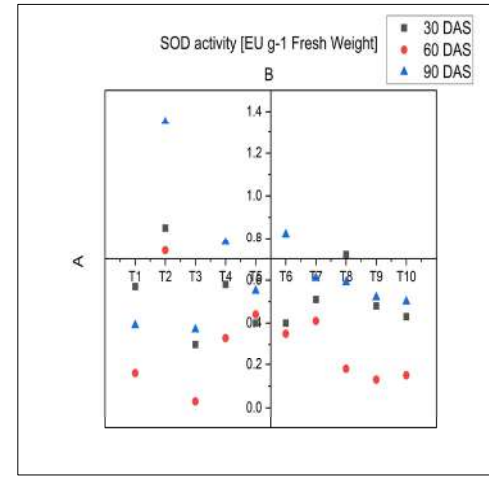

Fig. 5: Scatter central plot of SOD activity.

found in different research conducted by scientists (Soares & Siqueira 2008). The mechanism's efficiency or ability depends upon different parameters like the production of biomass, the growth rate of the plant, as well as the tolerance power of the plants to withstand the heavy metal stress even at higher concentration levels, and the heavy metal bioavailability.

SOD Activity [EU g^{-1} Fresh Weight]

The mean SOD output increased significantly at 32.94%, 78.37%, and 70.14% when subjected to heavy metal stress (T2) relative to control (T1) at 30, 60, and 90 DAS intervals (Table 5, Fig. 5). Exogenous application of endomycorrhiza in soil (T3) demonstrated the mitigation impact by minimizing SOD production by 64.70%, 94.59%, and 72.22% relative to T2 at 30, 60, and 90 DAS (Table 5, Fig. 5). Compared to T2, putrescine (T6) exogenous application showed a mitigating effect on the proposed DAS by decreasing SOD activity by 52.94%, 52.70%, and 40.74% (Table 5, Fig. 5). The median SOD output was significantly reduced by 52.94%, 40.54%, and 58.51% when administered with a higher dose of putrescine (T5) relative to (T2) compared to T2 (Table 5, Fig. 5). Likewise, the SOD behavior decreased significantly with 40.0%, 44.59%, and 54.81% at the proposed DAS in T7 (Table 5, Fig. 5). The median SOD output decreased dramatically when administered with a higher dose of putrescine relative to T8 by 15.29%, 75.67%, and 56.29% compared to T2 (Table 5, Fig. 5). The combination of putrescine and mycorrhiza in the T9 treatment decreased by 43.52%, 82.43%, and 61.48% in the proposed DAS treatment (Table 5, Fig. 5). Comparing T10 treatment with T2 treatment, significant SOD activity decreased by 49.41%, 79.72%, and 62.96%, respectively (Table 5, Fig. 5). The SOD activity was found to decrease significantly in this treatment (T4) by 31.76%, 55.40%, and 42.22%, respectively, compared to T2 in the proposed DAS (Table 5, Fig. 5). Mycorrhiza has thus been found to have a greater impact on SOD behavior with 30, 60 & 90 DAS (Table 5, Fig. 5). ROS is likely to damage the cell membranes, resulting in oxidative lipid degradation (lipid peroxidation). Superoxide dismutase (SOD) is a metal enzyme that catalyzes the oxygen and H_2O_2 dispersion of superoxide radicals. It is well known that various environmental stresses frequently lead to increased production of ROS since SOD was proposed to be important in the resistance of plant stress and provide the first line of defense from the toxic effects of high ROS concentrations. The experiment was carried out, suggesting that the growth of plant roots and shoots was decreased when *Pisum sativum* L. was treated with different Cd concentrations. The protein, which is produced by mycorrhizal fungi, is a glycoprotein, glomalin, that helps in soil particle binding, and hence, properties of the soil are improved and able for heavy metal binding in the soil (Wu et al. 2014). Wu et al. (2014), reported that the AM fungi glomalin protein (Wu et al. 2014) produces the absorption of heavy metals in nickel and lead in the soil by organic matter. As chromium is highly toxic both for human health and for plants, mycorrhizal fungi have less efficacy in mitigating the levels of Cr in the contaminated soil rhizosphere. Hence, the function of mycorrhizal fungi is not further studied in one of its remedial techniques. It requires more study of that specific metal (Gil-Cardeza et al. 2014). It is important to be aware that the effects of mycorrhizal fungal phylogenesis on heavy metals' biological remediation have been questioned (He et al. 2014). Under the stress of heavy metal, he conducted an experiment in which the effect of phylogenetics on plant growth of the host plant of Glomeraceae and in glomerate was evaluated. From the result, it was found that both the phylogenetic mycorrhizal fungi have positive effects on the growth of the host plants under heavy metal stress and the variation in different concentrations of heavy metal. Glomerate has also been reported to be more favorable for the host plant's growth under heavy metal stress, whereas non-Glomeraceae mycorrhizal fungi were better for host plants under no-stress conditions. The fungus response of glomeraceae depends on different plant species, as plant growth of legumes is better than that of nonlegumes under heavy metal stress. As a result, the use of legumes, in combination with glomeraceae, was indicated to have a more beneficial way of heavy metal bioremediation. When phosphorus is applied by the exogenous to improve the nutrition of host plants, the effects of heavy metal contamination using mycorrheatic fungi are mitigated (Wu et al. 2016a, 2016b). It was concluded that the mycorrhizal fungi could enhance the growth of a plant by increasing the absorption of nutrients such as phosphorus and by immobilizing chromium from the roots of the host plants with fungi. The test also showed that the chromium is stabilized and distributed in the roots of host plants. As a result, mycorrhiza fungal roots can adsorb chromium, which reduces the translocation of chromium to aerial parts of the host plant.

CONCLUSION

The use of putrescine and mycorrhiza outperformed SOD's antioxidant activity, as well as MDA, proline, and membrane injury. The impact of putrescine was more active at 30 DAS. In contrast, the application in combination with mycorrhiza was more active at 60 DAS for the possible reduction of toxicity through improved cell stability and reduced injury. In all days of intervals, mycorrhiza was found to have a greater impact on superoxide dismutase behavior. We learned that

polyamines such as putrescine as well as mycorrhiza glomus offer significant protective mechanisms against Cd-toxicity in peas through their protective role in plants, mediated by balancing the enzymatic and non-enzymatic antioxidants. This study gave us insights into the efficient and balancing role of putrescine and mycorrhiza glomus in minimizing the damage done by Cd contamination. Importantly, we are confident that this defensive work could be extended to other heavy metals-related toxicity, but that needs a serious assessment in future work.

ACKNOWLEDGMENTS

P.K., S.R.D. and D.C. gratefully acknowledge the support provided by Lovely Professional University.

REFERENCES

Apel, K. and Hirt, H. 2004. Reactive oxygen species: metabolism, oxidative stress, and signal transduction. Ann. Rev. Plant Biol., 55: 373-399.

Abdelhameed, R.E. and Metwell, R.A. 2019. Alleviation of cadmium stress by Arbuscular mycorrhizal symbiosis. Int. J. Phytoremed., 21(7): 663-671.

Alzahrani, Y. and Raddy, M.M. 2019. Composed to antioxidants and polyamines, the role of maize grain-derived biostimulants in improving cadmium tolerance in wheat plants. Eco. Environ. Saf., 182: 109378.

Bates, L.S. 1973. Rapid determination of free proline for water-stress studies. Plant Soil, 39: 205-207.

Behra, K. 2014. Phytoremediation, Transgenic Plants, and Microbes. In: Lichtfouse, E. (ed), Sustainable Agriculture Reviews, Springer, Cham, pp. 65-85.

Beshamgan, E.S., Sharifi, M. and Zarinkamar, F. 2019. Crosstalk among polyamines, phytohormones, hydrogen peroxide, and phenylethanoid glycosides responses in Scrophulariastriata to Cd stress. Plant Physiol. Biochem., 143: 129-141.

Cui, G., Ai, S., Chen, K. and Wang, X. 2019. Arbuscular mycorrhiza augments cadmium tolerance in soybeans by altering the accumulation and partitioning of natural elements and related gene expression. Eco. Environ. Saf., 171: 231-239.

Calonne, M., Sahraoui, A.L.H. and Campagnac, E. 2012. Propiconazole inhibits the sterol 14a-demethylase in *Glomus irregular,* like in phytopathogenic fungi. Chemosphere, 87: 376-383.

Cabral, L., Siqueira, J. and Soares, C. 2010. Retention of heavy metals by arbuscular mycorrhizal fungi mycelium. Química Nova, 33: 25-29.

Cabral, L., Soares, C. and Giachini, A. 2015. Arbuscular mycorrhizal fungi in phytoremediation of contaminated areas by trace elements: mechanisms and major benefits of their applications. World Microbiol. Biotechnol., 31: 1655-1664.

Declerck, S., Strullu, D. and Fortin, J. 2005. In Vitro Culture of Mycorrhizas. Springer, New York.

Dhindsa, R.S., Plumb□Dhindsa, P. and Thorpe, T.A. 1981. Leaf senescence: correlated with increased levels of membrane permeability and lipid peroxidation and decreased levels of superoxide dismutase and catalase. J. Exper. Bot., 32**:** 93-101.

Emamverdian, A., Ding, Y., Mokhberdoran, F. and Xie, Y. 2015. Heavy metal stress and some mechanisms of plant defense response. Sci. World J., 15:18.

El-Amier, Y., Elhindi, K., El-Hendawy, S., Al-Rashed, S. and Abd-ElGawad, A. 2019. Antioxidant system and biomolecule alteration in Pisum sativum under heavy metal stress and possible alleviation by 5-aminolevulinic acid. Mole, 24(22): 4194.

Fobert, P.R. and Despres, C. 2005. Redox control of systemic acquired resistance. Currents Opinion of Plant Biology, 8: 378-382.

Ferrol, N., González-Guerrero, M. and Valderas, A. 2009. Survival strategies of arbuscular mycorrhizal fungi in Cu-polluted environments. Phytoche. Rev., 8: 551-559.

Friedlova, M. 2010. The influence of heavy metals on soil biological and chemical properties. Soil Water Res., 5: 21-27.

Glick, B.R. 2003. Phytoremediation: synergistic use of plants and bacteria to clean up the environment. Biotechnol. Adv., 21: 383-393.

Gil-Cardeza ML,Ferri A, Cornejo P. et al.(2014). Distribution of chromium species in a Cr-polluted soil: the presence of Cr (III) in glomalin-related protein fraction. Sci. Total Environ., 493: 828-833.

Garg, N. and Pandey, R. 2015. Effectiveness of native and exotic arbuscular mycorrhizal fungi on nutrient uptake and ion homeostasis in salt-stressed *Cajanus cajan* L. (Millsp.) genotypes. Mycorrhiza, 25: 165-180.

Glowacka, K., Źróbek-Sokolnik, A., Okorski, A. and Najdzion, J. 2019. The effect of cadmium on the activity of stress-related enzymes and the ultrastructure of pea roots. Plants, 8(10): 413.

Holleman, A. and Wiberg, E. 1985. Lehrbuch der AnorganischenChemie. Nabu Press, Berlin

He, L., Yang, H. and Yu, Z. 2014. Arbuscular mycorrhizal fungal phylogenetic groups differ in affecting host plants along with heavy metal levels. J. Environ. Sci., 26: 2034-2040.

Heath, R.L. and Packer, L. 1968. Photoperoxidation in isolated chloroplasts. I. Kinetics and stoichiometry of fatty acid peroxidation. Arch. Biochem. Biophys., 125**:** 189-198.

Jamal, A., Ayuba, N. and Usmana, M. 2002. Arbuscular mycorrhizal fungi enhance zinc and nickel uptake from contaminated soil by soybean and lentil. Intl. J. Phyto., 4: 205-221.

Khan, A., Kuek. C. and Chaudhry, T. 2000. Role of plants, mycorrhizae, and phytochelatorsen heavy metal contaminated land remediation. Chemos, 41: 197-207.

Kumar, P., Mandal, B. and Dwivedi, P. 2011a. Heavy metal scavenging capacity of Menthaspicata and Allium cepa. Med. Plant Int. J. Phytomed. Rel. Ind., 3(4): 315-318.

Kumar, P., Mandal, B. and Dwivedi, P. 2011b. Heavy metals scavenging of soils and sludges by ornamental plants. J. Appl. Horticul., 13(2): 144-146.

Kumar, P., Dwivedi, P. and Singh, P. 2012. Role of polyamine in combating heavy metal stress in *Stevia rebaudiana* Bertoni under in vitro conditions. Intl. J. Agricul. Environ. Biotechnol., 5(3):193-198.

Kumar, P., Mandal, B. and Dwivedi, P. 2013. Phytoremediation for defending heavy metal stress in weed flora. Intl. J. Agricul. Environ. Biotechnol., 6(4): 647.

Kumar, P. and Dwivedi, P. 2014. Phytoremediation of Cadmium through Sorghum. Daya Publishing House, New Delhi, pp. 311-342.

Kumar, P. Dwivedi, P. and Hemantaranjan, A. 2016a. Short-term Responses of Crops Under Mercury Contamination at Hazardous Waste Sites: Plant Stress Tolerance Physiological and Molecular Strategies, Scientific Publishers, p.149.

Kumar, P., Dwivedi, P. and Hemantaranjan, A. 2016b. Physiological and biochemical properties of Gliricidia: Its cultivation is scope for remunerative venture for farmers. Plant Stress Toler. Physiol. Mol. Strat., 1: 359.

Kumar, P. and Dwivedi, P. 2018a. Putrescine and glomus mycorrhiza moderate cadmium actuated stress reactions in Zea mays L. by means of extraordinary reference to sugar and protein. Vegetos Int. J. Res., 31(3): 74-77.

Kumar, P. and Dwivedi, P. 2018b. Ameliorative Effects of Polyamines for Combating Heavy Metal Toxicity in Plants Growing in Contaminated Sites with Special Reference to Cadmium. CRC Press, Taylor & Francis Group, UK, pp. 404.

Kumar, P. and Dwivedi, P. 2018c. Cadmium-induced alteration in leaf

length, leaf width, and their ratio of glomus-treated sorghum seed. J. Pharmacog. Phytochem., 7(6): 131-148.

Kumar, P., Kumar, S. and Naik, M. 2018a. Glomus and putrescine-based mitigation of cadmium-induced toxicity in maize. J Pharma Phytochem., 7(5): 2384-2386.

Kumar, P., Misao, L. and Jyoti, N. 2018b. Polyamines and mycorrhiza-based mitigation of cadmium-induced toxicity for plant height and leaf number in maize. Intl J Che. Stud., 6(5): 2491-2494.

Kumar, P., Pathak, S., Kumar, M. and Dwivedi, P. 2018c. Role of secondary metabolites for the mitigation of cadmium toxicity in sorghum grown under mycorrhizal inoculated hazardous waste site. In: Kumar, N. (ed), Biotechnological Approaches for Medicinal and Aromatic Plants, Springer, Singapore, pp. 199-212.

Kumar, P. 2018 Signal Transduction in Plant With Respect to Heavy Metal Toxicity: An Overview. CRC Press, Taylor & Francis Group, p. 394.

Kumar, P., Mandala, H., Kumar, P.S., Johnson, Y., Nada, J., Mohit, N. and Sunil, K. 2018d. Effect on chlorophyll a/b ratio in cadmium contaminated maize leaves treated with putrescine and mycorrhiza. Annals Biol., 34(3): 281-283.

Kumar, P. and Pathak, S. 2019. Responsiveness index of sorghum (Sorghum bicolor (L.) Moench) grown under cadmium-contaminated soil treated with putrescine and mycorrhiza. Bangla. J. Bot., 48(1): 139-143.

Kumar, P., Siddique, A., Thongbam, S., Chopra, P. and Kumar, S. 2019. Cadmium-induced changes in total starch, total amylose, and amylopectin content in putrescine and mycorrhiza-treated sorghum crop. Nature Environ. Pollut. Technol., 18(2): 525-530.

Pathak, S., Kumar, P., Mishra, P.K. and Kumar, M. 2017. Mycorrhiza-assisted approach for bioremediation with special reference to biosorption. Pollut. Res., 36(2): 330-333.

Premachandra, G.S., Saneoka, H. and Ogata, S. 1989. Nutrio-physiological evaluation of polyethyleneglycol test of cell membrane stability in maize. CT-op Sci., 29: 1287-1292.

Lenoir, I., Fontaine, J. and Sahraoui, A. 2016. Arbuscularmycorrhizal fungal responses to abiotic stresses: A review. Photochem, 123: 4-15.

Mugnier, J. and Mosse, B. 1987. Vesicular-arbuscular mycorrhizal infection in transformed root-inducing T-DNA roots grown axenically. Phytopathology, 77: 1045-1050.

Mohammad, M., Hamad, S. and Malkawi, H. 2003. The population of arbuscular mycorrhizal fungi in the semi-arid environment of Jordan is influenced by biotic and abiotic factors. J Arid Environ., 53: 409-417.

Miransari, M., Bahrami, H.A. and Rejali, F. 2009. Effects of arbuscular mycorrhiza, soil sterilization, and soil compaction on wheat (*Triticum aestivum* L.) nutrients uptake. Soil Till. Res., 104: 48-55.

Miransari, M. 2011. Hyperaccumulators, arbuscular mycorrhizal fungi, and stress of heavy metals. Biotechnol. Adv., 29: 645-653.

Miransari, M. 2016. Soybean production and heavy metal stress. In: Miransari M (ed) Abiotic and biotic stresses in soybean production. Soybean production. Elsevier, Amsterdam, pp. 197-216.

Nahar, K., Rahman, M., Hasanuzzaman, M., Alam, M.M., Rahman, A., Suzuki, T. and Fujita, M. 2016. Physiological and biochemical mechanisms of spermine-induced cadmium stress tolerance in mung bean (*Vigna radiata* L.) seedlings. Environ. Sci. Pollut. Res., 23(21): 21206-21218.

Opik, M., Moora, M. and Liira, J. 2006. Composition of root-colonizing arbuscular mycorrhizal fungal communities in different ecosystems around the globe. J. Ecol., 94: 778-790.

Silva, S., Siqueira, J. and Soares, C. 2006. Mycorrhizal fungi influence on Brachiaria grass growth and heavy metal extraction in contaminated soil. Pesq. Agr. Bras., 41: 1749-1757.

Soares, C. and Siqueira, J. 2008. Mycorrhiza and phosphate protection of tropical grass species against heavy metal toxicity in multi-contaminated soil. Biol. Fert. Soils, 44: 833-841.

Sajedi, N.A., Ardakani, M.R. and Rejali, F. 2010. Yield and yield components of hybrid corn (*Zea mays* L.) as affected by mycorrhizal symbiosis and zinc sulfate under drought stress. Physiol. Mol. Biol. Plants, 16: 343-351.

Sanchez-Castro, I., Ferrol, N. and Barea, J. 2012. Analyzing the community composition of arbuscular mycorrhizal fungi colonizing the roots of representative shrubland species in a Mediterranean ecosystem. J. Arid. Environ., 80: 1-9.

Soudek, P., Ursu, M., Petrova, S. and Vanek, T. 2016. Improving crop tolerance to heavy metal stress by polyamine application. Food Chem., 213: 223-229.

Taie, H.A., El-Yazal, M.A.S., Ahmed, S.M. and Raddy, M.M. 2019. Polyamines modulate growth, antioxidant activity, and genomic DNA in heavy metal-stressed wheat plants. Environ. Sxien. Pollut. Res., 26(2): 22338-22350.

Tai, Y., Li, Z. and Mcbride, M.B. 2016. Natural attenuation of toxic metal phytoavailability in 35-year-old sewage sludge-amended soil. Environmental monitoring and assessment, 188(4): 241.

Whitmore, A. 2006. The emperor's new clothes: Sustainable mining? J. Clean. Prod., 14: 309-314.

Wu, Z., McGrouther, K. and Huang, J. 2014. Decomposition and the contribution of glomalin-related soil protein (GRSP) in heavy metal sequestration: A field experiment. Soil Biol. Biochem., 68: 283-290.

Wu, S., Zhang, X. and Chen, B. 2016a. Chromium immobilization by extraradical mycelium of arbuscular mycorrhiza contributes to plant chromium tolerance. Environ. Exper. Bot., 122: 10-18.

Wu, S., Zhang, X. and Sun, Y. 2016b. Chromium immobilization by extra- and intraradical fungal structures of arbuscular mycorrhizal symbioses. J. Hazard. Mater., 316: 34-42.

Yang, W., Zhang, T. and Li, S. 2014. Metal removal from and microbial property improvement of multiple heavy metals contaminated soil by phytoextraction with a cadmium hyperaccumulator *Sedum alfredii* H. J. Soils Sed., 14: 1385-1396.

Zenk, M.H. 1996. Heavy metal detoxification in higher plants: A review. Gene, 179: 21-30.

Zhu, X., Song, F. and Liu, S. 2012. Arbuscular mycorrhizae improve photosynthesis and water status of *Zea mays* L. under drought stress. Plant Soil Environ., 58: 186-191.

Nature Environment and Pollution Technology
An International Quarterly Scientific Journal

p-ISSN: 0972-6268
(Print copies up to 2016)
e-ISSN: 2395-3454

Vol. 23 | No. 1 | pp. 287-294 | 2024

Original Research Paper

https://doi.org/10.46488/NEPT.2024.v23i01.024

Open Access Journal

Analysis and Characterization of Municipal Solid Wastes Generated in Ifugao State University Potia Campus: A Basis For Planning of Waste Management

P. Latugan, J. J. Carabacan, G. Bonicillo, J. Cayog, M. Q. Eyawa, M. T. Cairel and J. M. Ngohayon†

*Ifugao State University, Potia Campus, Potia, Alfonso Lista, Ifugao, Philippines

†Corresponding author: J. M. Ngohayon; engrjoelngohayon@gmail.com

Nat. Env. & Poll. Tech.
Website: www.neptjournal.com

Received: 17-07-2023
Revised: 22-08-2023
Accepted: 23-08-2023

Key Words:
Municipal solid waste
Waste composition
Waste volume
Waste management

ABSTRACT

The end of the COVID-19 pandemic resulted in the total return of students and employees in Ifugao State University Potia Campus, a higher education institution located in Potia, Alfonso Lista, Ifugao, Philippines. However, the return of the pre-pandemic operations on campus caused problems in managing the generated municipal solid wastes. Hence, an analysis and characterization of the generated municipal solid wastes was conducted to determine important data that can be used for future waste management planning. The generated municipal solid wastes were gathered from the various waste generators within the campus for five consecutive days. The total generated municipal solid waste on the campus was about 140.10 kg.day^{-1}, most of which was contributed by the canteens (20.86%). The generated municipal solid wastes were dominated by biodegradable waste (48.65%) and recyclable waste (37.26%). In addition, most of the generated municipal solid wastes were related to people's food and beverage consumption behavior. The total volume of the MSW generated daily was about 5.647 m^3. It is recommended that the campus create and enforce its waste management plan to specifically address the aforementioned characteristics of the generated municipal solid wastes.

INTRODUCTION

The COVID-19 pandemic has brought about several changes to the municipal solid waste (MSW) generation. Because of the restrictions brought about by the pandemic, most people were forced into confinement within the safety of their homes. As such, the bulk of MSW generation in communities has shifted from institutional, industrial, and commercial to residential, as evident in several studies (Ngohayon & Tulagan 2022, Roy et al. 2021, Sinha et al. 2020). Post-pandemic, people are free to go anywhere after the restrictions were lifted, given the lowered risk of contracting COVID-19. As such, the MSW generation is expected to change again. Hence, it is important to develop or improve existing waste management plans to address the changes in the MSW generation.

The Ifugao State University (IFSU) Potia Campus, a higher education institution in the municipality of Potia, Alfonso Lista, Ifugao, Philippines, had similarly experienced the aforementioned effects of the COVID-19 pandemic. Because of the pandemic, all the students were sent home, while only a few employees were allowed to work under a rotational schedule. Since the pandemic has ended, the campus population has grown to about 3900 people. Of this number, about 4.6% constitutes the employees, while the rest are the students (IFSU Potia Campus Human Resource and Development Office & Registrar's Office, personal communication, January 18, 2023). With this increase in population, it is also expected that there will be changes in the MSW generation within the campus.

Currently, the campus is experiencing the following problems regarding MSW management: (1) No engineered and centralized MSW storage facility exists. While there is a designated temporary storage location for the generated MSW before its collection and disposal, the capacity is insufficient, and other environmental factors were not considered. This is evident by the many tattered trash bags and littered trash around the storage location, ravaged by scavenging animals or the heavy rain. (2) Lack of proper waste segregation among the campus constituents. This is primarily due to insufficient trash cans designated for each type of waste. Hence, people would unthinkingly dump waste in the nearest available trash can. This can also be attributed to the lack of environmental awareness among the people. Therefore, even if there are some designated trash cans for each type of waste, waste segregation is still not adequately practiced, as evidenced by the prevalence of mixed waste. (3) The lack of treatment facilities. The

campus has no compost pits to dispose of its biodegradable wastes. Hence, biodegradable wastes were thrown into the ravines. In addition, there are no recycling facilities nor any market for recycled products within the community. Thus, the recyclable wastes are also being disposed of in the community's sanitary landfill. (4) Lack of institutional policies to address the generated MSW. While national laws and local ordinances exist, they do not specifically cater to the type of MSW generated on campus. Hence, this also contributes to the prevalence of the aforementioned problems in MSW management.

Clearly, there is a need for the campus to plan an MSW management that can effectively address these aforementioned problems. To do that, it is important to determine the current MSW generation data of the campus. Hence, this study was conducted to determine important MSW generation data, including the MSW generation rate, the amount of generated MSW, the composition of generated MSW, and the volume of generated MSW. The campus can use the results obtained from the study to develop policies for managing its generated MSW. In addition, future researchers can use the study results as a basis for developing interventions, such as projects and campaigns to reduce MSW generation or even utilize the generated MSW.

MATERIALS AND METHODS

The study followed a descriptive research design to determine the MSW generation data of the IFSU Potia Campus. The waste analysis and characterization (WACS) approach used in the study was based on the study of Ngohayon & Tulagan (2022).

The data gathering was conducted in IFSU Potia Campus (shown in Fig. 1). The buildings and areas inside the campus were grouped according to the waste generator classification of EcoGov (2011): (1) Institutional waste generators where people often do office work, meetings, classes, laboratory activities, and to some extent, eating and cleaning. (2) Commercial waste generators, particularly food establishments, where people often do cooking, eating, and cleaning. (3) Recreational waste generators where people often do sports activities and maintenance. The campus leases several agricultural lots. However, these were not included as one of the waste generators as the generated agricultural wastes from these areas are the responsibility of the lessee and not the institution. The summary of the inventory of the waste generators within the institution is listed in Table 1.

Before the data gathering, the generated MSW from the previous days was collected to ensure that each waste generator had empty trash cans. In addition, the various focal persons for each waste generator were briefed for their assistance during the waste collection.

Data were gathered for five consecutive working days from February 20 to February 24, 2023. The institution was working under normal operations during the data gathering such that there were no celebrations, general cleaning, examination, or natural disasters during the aforementioned dates. Empty trash cans with readable labels for each type of waste were distributed in each designated waste generator.

Table 1: The inventory of the waste generators within the IFSU Potia Campus.

Waste Generators	Waste Generator Category*	No. of Buildings/ Area	Daily No. of People**
Administration Building (Admin)	Institutional	1	180[A]
Library	Institutional	1	800[B]
Research, Development, Extension, and Training Office (RDET)	Institutional	1	10[A]
College of Education (COE)	Institutional	1	738[A]
College of Criminal Justice Education (CCJE)	Institutional	1	1303[A]
College of Health Sciences (CHS)	Institutional	1	239[A]
College of Business Management (CBM)	Institutional	1	230[A]
College of Engineering and Technology (CET)	Institutional	1	188[A]
College of Agriculture and Sustainable Development (CASD)	Institutional	1	634[A]
College of Advanced Education (CAE)	Institutional	1	200[B]
Canteen	Commercial	6	2000[B]
Sports Ground	Recreational	1	500[B]

* Based on the waste generator category of EcoGov (2011)

** [A] based on the data provided by IFSU Potia Campus' Registrar's Office and Human Resource and Development Office, [B] based on personal communication with the management/focal person

Fig. 1: The map of the IFSU Potia Campus.

Table 2: Description of the types of waste used in the characterization of the generated MSW.

Category*	Description*	Sample Waste Recovered from the Study
Biodegradable	Waste that can be easily decomposed and can be turned into compost once it is exposed to various agents of decomposition.	food waste, soiled office paper waste, used paper food containers
Recyclables	Wastes which are in relatively good condition enough to be recovered and converted into new products.	plastic cups, plastic bottles, plastic cutleries, office papers, cans, textiles
Residual	Wastes that cannot be recycled anymore due to several factors such as market demand, technological limitations, costs, and quality of recycled products, among others. These are immediately transported to the sanitary landfills for disposal.	plastic straws, sando bags, polystyrene food containers, laminated food packaging (composites), ashes, soot, and dirt
Special	Household hazardous waste.	Used face masks

*Source: National Solid Waste Management Commission 2018

The trash cans were strategically placed so students and employees could easily see them. Trash bags were put inside the deployed trash cans at around 8:00 AM and collected and replaced with new trash bags at exactly 8:00 AM the following day. The MSW collected from each waste generator was brought to the Science Research Laboratory on campus for analysis and characterization.

A calibrated weighing scale was used to measure the total mass of the collected MSW from each waste generator. The generation rate for each waste generator was then calculated using the formula (Kawai & Tasaki 2016):

$$\text{Generation Rate} = \frac{\text{Total Mass of MSW}}{\text{No. of Waste Generator per Sample}}$$

properly segregated according to MSW classification in Table 2. Furthermore, the biodegradable wastes were further segregated into soiled office paper, used paper food containers, and food waste. In addition, the recyclable wastes were further segregated into plastic cups, plastic bottles, plastic cutleries, papers, cans, and textiles.

The masses of each of the segregated wastes were measured using a calibrated weighing scale. The composition of each type of waste was calculated using the formula (Miguel et al. 2016):

$$\%\ \text{type of waste} = \frac{\text{Mass of Type of Waste}}{\text{Total Mass of MSW}} \times 100$$

After measuring the masses, the volumes of each segregated waste were measured using a calibrated container. After obtaining the data from the five-day sampling, the average daily generation rate, waste composition, and volume of generated MSW were computed.

RESULTS AND DISCUSSION

MSW Generation Rate and MSW Generated Daily

The summary of the calculated MSW generation rate and the MSW generated daily from the various waste generators in the IFSU Potia Campus is shown in Table 3. Overall, the campus generated approximately 140.10 kg of MSW daily. This is a significant increase from the reported MSW generation rate (7.40 kg.day^{-1}) among the institutions, including the IFSU Potia Campus, in Potia, Alfonso Lista, Ifugao, Philippines back in 2020 (Ngohayon & Tulagan 2022). This increase in MSW generation can be attributed to the total return of the students and the employees on campus after the COVID-19 pandemic ended.

Among the institutional waste generators, COE had the highest MSW generation (16.63 kg.day^{-1}). This can be attributed to the relatively high daily number of people (738) within its premises compared to most institutional waste generators. This is supported by several studies (Khajuria et al. 2010, Liu et al. 2019), which have shown that population directly affects MSW generation, such that the more consumers are present, the more MSW is generated. This trend may also be why CASD, which had a relatively high daily number of people (634), had a relatively high MSW generation (13.96 kg.day^{-1}). In contrast, RDET, which had the least daily number of people (10), had a relatively low MSW generation (2.84 kg.day^{-1}). However, this was not the case for CCJE, which had the highest daily number of people (1303) among the institutional waste generators, as it generated relatively lower MSW (8.37 kg.day^{-1}) than COE and CASD. This can be attributed to the overcrowding situation in CCJE. Since the CCJE building is relatively small, this forced the people, especially the students, to go elsewhere (mainly in the nearby canteen areas) while waiting for the start of their classes.

While CHS, CBM, CET, and CAE had relatively low daily numbers of people, they generated relatively high amounts of MSW. This is because their buildings are the central locations of the laboratories on campus, where various

Table 3: The MSW generation rate and the MSW generated daily in IFSU Potia Campus.

Waste Generators*	MSW Generation Rate (kg/day/building)	No. of Buildings/ Areas	MSW Generated**	
			kg/day	(%)
Admin[A]	8.17	1	8.17	5.83
Library[A]	2.35	1	2.35	1.67
RDET[A]	2.84	1	2.84	2.03
COE[A]	16.63	1	16.63	11.87
CCJE[A]	8.37	1	8.37	5.99
CHS[A]	12.32	1	12.32	8.79
CBM[A]	8.65	1	8.65	6.18
CET[A]	10.55	1	10.55	7.53
CASD[A]	13.96	1	13.96	9.96
CAE[A]	6.60	1	6.60	4.71
Canteen[B]	4.87	6	29.22	20.86
Sports Ground[C]	20.43	1	20.43	14.58
Total			140.10	100

* A - institutional, B - commercial, C - recreational

** MSW Generated Daily = MSW Generation Rate × No. of Buildings/Areas

laboratory activities are being done in addition to the usual classroom activities. Hence, these additional activities may have contributed to the MSW generated. Similarly, the Admin Building also had a relatively low daily number of people (180) yet produced relatively high amounts of MSW (8.17 kg.day^{-1}). This can be attributed to the fact that it is the central building of the campus, where most office work is being done, and is the most visited building among the employees and sometimes the students within a day. While the library had a relatively high daily number of people (800), it did not generate that much MSW (2.35 kg.day^{-1}). This is because, unlike the rest of the waste generators, fewer activities were allowed, and more restrictions were imposed on its premises. For example, only the staff were allowed to dine inside, while the students could not bring food or drinks.

The six canteens under the commercial waste generator category had the highest MSW generation (29.22 kg.day^{-1}) since they had the highest daily numbers of people (2000) within the campus. This is reasonable as employees and students often visit these canteens for breakfast, lunch, and snacks. This is consistent with the results of the study of Nguyen et al. (2021) and Pandey et al. (2016), which also showed that university canteens and cafeterias generated more waste than the institutional areas in their respective university study sites.

The sports ground, under the recreational center category, had the second highest MSW generation (20.43 kg.day^{-1}). These can be attributed to several factors: (1) Typically, sporting events gather spectators in the area, which increases the MSW generation (Atchariyasopon 2017). (2) Unlike the other identified waste generators on the campus, the sports grounds span the largest area (as shown in Fig. 1). Hence, there are more areas to cover for maintenance. Because of this, there is relatively more MSW generated from the cleaning activities. (3) The sports ground also doubles as an area for drying harvested grains (mainly corn). Hence, these additional activities can also contribute to the generated MSW in the area. (4) The sports ground also has a dormitory that exclusively houses the Reserve Officers' Training Corps (ROTC) students tasked with maintaining and guarding the sports ground. Typically, these residential areas inside the universities generate many MSW round-the-clock (Arazo 2015), further contributing to the MSW generation in the sports ground.

Composition of Generated MSW

The summary of the MSW composition from the waste generators is shown in Table 4. Overall, the IFSU Potia Campus produced mostly biodegradable wastes (48.65%),

Table 4: The composition of the generated MSW in the IFSU Potia Campus.

Waste Generator*	Biodegradable (%)			Recyclable (%)						Residual (%)	Special (%)
	Soiled Office Papers	Used Paper Food Containers	Food Waste	Plastic Cups	Plastic Bottles	Plastic Cutleries	Office Papers	Cans	Textiles		
Admin[A]	20.39	3.73	23.17	2.51	17.81	1.90	18.97	0.00	0.00	10.41	1.10
Library[A]	14.96	10.68	5.13	1.35	44.23	2.69	12.82	0.00	0.00	8.12	0.02
RDET[A]	18.63	8.78	42.91	2.97	4.88	5.12	6.87	0.00	0.00	9.80	0.05
COE[A]	10.59	17.69	14.75	6.21	32.78	2.67	1.98	1.68	1.92	8.21	1.53
CCJE[A]	5.36	8.34	16.97	4.41	49.91	1.07	3.93	0.00	0.00	7.50	2.50
CHS[A]	12.57	6.13	20.58	6.81	19.26	3.51	9.43	1.77	3.22	15.60	1.11
CBM[A]	22.09	11.92	17.77	3.59	28.25	1.74	6.95	4.05	0.00	3.01	0.64
CET[A]	11.40	13.38	10.96	3.72	37.92	1.86	3.72	0.00	0.00	15.34	1.72
CASD[A]	1.57	4.55	23.12	7.03	42.01	0.28	5.04	3.31	0.34	12.32	0.43
CAE[A]	19.71	13.04	7.96	6.52	30.03	5.34	0.61	0.00	0.00	10.92	5.87
Canteen[B]	20.15	4.28	28.27	10.10	14.31	5.01	1.33	0.36	0.00	15.96	0.23
Sports Ground[C]	3.09	3.70	61.92	1.32	9.79	0.25	8.76	0.73	0.00	9.06	1.38
Total	15.24	6.46	26.95	7.43	21.30	3.46	3.88	0.86	0.33	13.25	0.84
Grand Total	48.65			37.26						13.25	0.84

* A - institutional, B - commercial, C - recreational

closely followed by recyclable wastes (37.26%), then residual wastes (13.25%), and special wastes (0.84%). In the study of Ngohayon & Tulagan (2022), it was found that the generated MSW from the institutions (including IFSU Potia Campus) within Potia, Alfonso Lista, Ifugao, Philippines in 2020 was also primarily dominated by biodegradable wastes. On the other hand, their study had relatively more residual than recyclable wastes. The higher residual wastes back then may be attributed to the changes in the consumption behavior of the people brought about by the COVID-19 pandemic, such as (1) the avoidance of people reusing or recycling potentially contaminated materials and immediately discarding them as residuals and (2) the rise of online shopping which increased the residual packaging wastes. Hence, after the COVID-19 pandemic had ended, the new changes in consumption behavior might have influenced these changes in the MSW composition.

Among the various types of wastes, it can be seen that those related to food and beverage consumption dominated the overall MSW generated: (1) food wastes and (2) food packaging wastes, including used paper food containers, plastic bottles, plastic cups, plastic cutleries, and the majority of the residual wastes (plastic straws, sando bags, polystyrene food containers, and laminated food packagings).

Food waste is a common, notorious occurrence, especially in the canteens and cafeterias of schools and universities. Food waste may arise from various wasteful behaviors: (1) On the food preparation side, it can include the overproduction of cooked meals, over-purchasing, and ineffective food planning and management, among others (Filho et al. 2023). (2) On the food consumption side, it can include reasons such as the consumers not liking the food or that the servings are too big to finish, among others (Acheson 2023). However, the current study did not assess if the obtained food wastes were generated from the preparation of the food or food leftovers. Hence, future studies should look into this aspect to develop a food waste reduction or utilization project to address the generated food waste.

While there were already initiatives in reducing plastic food packaging through the use of biodegradable paper food containers, it was still not enough as most of the aforementioned food packaging wastes were made up of non-biodegradable plastic materials. To reduce the plastic bottle and plastic cup waste, the campus can enforce a policy that limits or even bans the use and selling of these receptacles. Instead, the campus should encourage the use of refillable water receptacles. To supplement this, the campus can also look into installing water dispensers and water bottle refilling stations within the campus. This is supported by several studies (The Travel Foundation 2011, United Nations Environment Programme & World Travel & Tourism Council 2021, Willis et al. 2019, University of Michigan-Dearborn 2022), which have shown positive effects upon the use of installed water dispensers and water bottle refilling stations, particularly with the decreased in the use of single-use water bottles and the increase in awareness and positive outlook among the users.

Plastic cutleries can also be reduced by banning them while promoting wooden cutleries and/or encouraging people to bring their reusable cutleries. This is evident in the study of Marazzi et al. (2020), which found that using wooden and reusable cutleries can help reduce tonnes of plastic cutlery waste. Furthermore, future studies can also look into the production of edible tableware, which recently gained traction in several countries (Natarajan et al. 2019). In particular, future studies could look into fabricating edible tableware made of locally available raw materials in the community.

Among the generated residual wastes, some notable ones related to food and beverage consumption were plastic straws, sando bags, polystyrene food containers, and laminated food packaging (composites). Several straw alternatives can be explored, such as bamboo straws, wheat straws, polylactic acid (PLA) straws, and stainless-steel straws, which offer several efficient and environmentally friendly benefits compared to plastic straws (Qiu et al. 2022). Cotton tote bags can be an excellent alternative to sando bags used in carrying items as they are reusable and washable (Iheukwumere et al. 2020). On the other hand, for sando bags used as simple food packaging, banana leaf packaging can be explored since these are cheap, biodegradable, have antioxidant and antibacterial properties (Rikasa & Mufeez 2023, Pratama & Junianto 2021), and are ubiquitous in the community. Moreover, people can bring their reusable lunch boxes to reduce further reliance on paper food containers, sando bags, and polystyrene food containers. For laminated food packaging (composites), commonly used in commercial food products such as chips, cookies, instant noodles, and nuts, among others, there is still no systematic separation and recycling process available in the country (World Wide Fund Philippines 2020). Hence, these always end up in sanitary landfills. To reduce the generation of these types of waste, the canteens on campus can look into offering a variety of food products that do not use any laminated food packaging. Instead, they can be served using the previously mentioned food packaging alternatives.

Typically, institutional units have highly recyclable office papers due to various office works such as printing, note-taking, and crafting, among others (Ngohayon & Tulagan 2022). However, this was not the case for the campus, as

Table 5: The volume of generated MSW daily in IFSU Potia Campus.

Waste Generator*	Daily Volume (m^3/day)				Total
	Biodegradable	Recyclable	Residual	Special	
Admin[A]	0.091	0.200	0.059	0.002	0.352
Library[A]	0.062	0.068	0.032	0.001	0.163
RDET[A]	0.069	0.039	0.025	0.001	0.134
COE[A]	0.303	0.296	0.115	0.011	0.725
CCJE[A]	0.093	0.134	0.027	0.011	0.265
CHS[A]	0.136	0.212	0.204	0.004	0.556
CBM[A]	0.216	0.125	0.019	0.002	0.362
CET[A]	0.166	0.244	0.081	0.007	0.498
CASD[A]	0.076	0.275	0.109	0.001	0.461
CAE[A]	0.174	0.116	0.070	0.015	0.375
Canteen[B]	0.473	0.402	0.273	0.001	1.149
Sports Ground[C]	0.194	0.278	0.130	0.005	0.607
Total	2.053	2.389	1.144	0.061	5.647

* A - institutional, B - commercial, C - recreational

its overall recyclable office papers were only about 3.88%. This can be attributed to the prevalent mixing of the various types of waste within the campus - the supposedly recyclable office paper wastes get mixed with other waste types and are soiled by food scraps and other liquids. Hence, the soiled office paper waste (15.24%) was classified as biodegradable. Therefore, it is recommended that strict compliance to waste segregation be enforced and followed to prevent the soiling of recyclable office paper waste.

It should be noted that there are currently no recycling projects on the campus or in the community. Similarly, this is also the case for special wastes that do not have a dedicated hazardous waste disposal facility. Because of these, both the recyclables and special wastes are being treated as residual wastes, bringing the residual wastes to a total of 51.35%. Thus, about half of the campus's generated MSW were disposed of in the community's sanitary landfill.

The Volume of Generated MSW Daily

The summary of the calculated volumes of generated MSW daily per type of waste and per waste generator in the IFSU Potia Campus is shown in Table 5. The generated MSW from the canteen had the largest volume because it is also the top waste generator, as previously discussed. Although the biodegradable wastes had the highest mass contribution, as previously shown, this did not translate to having the largest volume. Instead, the recyclable wastes garnered the largest volume. This is because recyclable wastes, such as office paper wastes and plastic containers, typically have lower densities than biodegradable wastes (Bowan & Tierobaar 2014).

The total volume of the generated MSW daily on the campus is approximately 5.647 $m^3.day^{-1}$. This is significantly higher than the generated MSW from institutions (including IFSU Potia Campus) in 2020, which was only 0.11 kg.day-1 (Ngohayon & Tulagan 2022). Similarly, the increase in the volume of generated MSW daily in the present study can be attributed to the increase in the number of people within the campus as both the employees and the students have fully returned after the COVID-19 pandemic has ended.

CONCLUSIONS

About 140.10 kg of MSW is generated within the IFSU Potia Campus daily. Among the various waste generators, the canteens generated the highest MSW. It was also found that the daily number of people, the type of activities, and the area size may influence the amount of MSW generated among the various waste generators on the campus. The overall composition of the generated MSW was dominated by biodegradable waste (48.65%), closely followed by recyclable waste (37.26%), then residual waste (13.25%), and special waste (0.84%). In addition, most of the generated MSW was found to be related to food and beverage consumption, such as food waste and packaging waste. It was also found that the waste composition of the generated MSW in IFSU Potia may be influenced by people's consumption and waste segregation behavior. The volume of the MSW generated daily was about 5.647 m^3. Among the types of waste, recyclable wastes

contributed the most, closely followed by biodegradable wastes, then residual wastes. It was also found that the density of the waste may influence its volume.

While there are available national laws and local ordinances, they are not being strictly implemented, which resulted in the irresponsible usage of various single-use plastic products and the mixing of various types of waste within the campus. Hence, it is recommended that the campus create and enforce its waste management plan to specifically address the type of MSW generated within its area. It can include the development of policies that ban specific types of materials, such as single-use plastic products, and promote more eco-friendly alternatives. To supplement this, the campus can also organize a periodic awareness campaign among its constituents and develop knowledge resources such as videos and infographics that can be distributed online.

ACKNOWLEDGEMENT

The authors would like to acknowledge the whole IFSU Potia Campus for participating in this study and sharing the vision for improving MSW management within the campus. The authors would also like to acknowledge the assistance provided by the College of Education and the Research Department of the campus.

REFERENCES

Acheson, C. 2023. Food Waste: The Student Perspective: Why do students waste food, and what can be done about it? In Zero Waste Scotland. https://www.zerowastescotland.org.uk/resources/food-waste-student-perspective

Arazo, R.O. 2015. Compositions of solid wastes generated from a school campus. Int. J. Res. Eng. Technol., 4(10): 545.

Atchariyasopon, K. 2017. Sustainable solid waste management in sports events: A case study of football matches in Thailand. J Popul. Soc. Sci., 25(1): 145-152.

Bowan, P.A. and Tierobaar, M. T. 2014. Characteristics and Management of Solid Waste in Ghanaian Markets - a Study of WA Municipality Characteristics And Management Of Solid Waste In Ghanaian Markets - A Study Of WA Municipality. Civil and Environmental Research, 6(January 2014):114-119.

EcoGov. 2011. Waste Analysis and Characterization Study: A Manual. Second Edition. Philippine Environmental Governance Project, Diliman, Quezon City, The Philippines.

Filho, W.L., Ribeiro, P.C.C., Setti, A.F.F., Azam, F.M.S., Abubakar, I.R., Castillo-Apraiz, J., Tamayo, U., Özuyar, P., Frizzo, K. and Borsari, B. 2023. Toward food waste reduction at universities. Environ. Dev. Sustain., 16: 124.

Iheukwumere, S.O., Nkwocha, K.F., Tonnie-Okoye, N. and Umeh, P.P. 2020. A look at plastic bags and alternatives. J. Geogr. Meteorol. Environ., 3(1): 27-35.

Kawai, K. and Tasaki, T. 2016. Revisiting estimates of municipal solid waste generation per capita and their reliability. J. Mater. Cyc. Waste Manag., 18(1): 1-13.

Khajuria, A., Yamamoto, Y., & Morioka, T. 2010. Estimation of municipal solid waste generation and landfill area in Asian developing countries. J. Environ. Biol., 31(5): 649-654.

Liu, J., Li, Q., Gu, W. and Wang, C. 2019. The impact of consumption patterns on the generation of municipal solid waste in China: Evidence from provincial data. Int. J. Environ. Res. Pub. Health, 16(10): 1-19.

Marazzi, L., Loiselle, S., Anderson, L. M., Rocliffe, S. & Winton, D. J. 2020. Consumer-based actions to reduce plastic pollution in rivers: A multi-criteria decision analysis approach. PLOS ONE, 15(8): e0236410.

Miguel, M.G., Paixao Filho, J.L.D., Benatti, J.C.B., Leme, M.A.D.G., Mortatti, B.C., Gabrielli, G., Elaiuy, M.L C., Pereira, S.Y. and Teixeira, E.N. 2016. Gravimetric composition of municipal solid waste disposed of in a large-scale experimental cell in Southeastern Brazil. Int. J. Environ. Waste Manag., 17(2): 128.

Natarajan, N., Vasudevan, M., Vivekk-Velusamy, V. and Selvaraj, M. 2019. Eco-friendly and edible waste cutlery for a sustainable environment. Int. J. Eng. Adv. Technol., 9: 615-624.

National Solid Waste Management Commission. 2018. Ecological Solid Waste Management [Brochure]. https://nswmc.emb.gov.ph/wp-content/uploads/2016/06/6.ESWM-for-HH.pdf

Ngohayon, J.M. and Tulagan, J. 2022. Analysis and characterization of municipal solid wastes generated in a community in the Northern Philippines. Nature Environ. Pollut. Technol., 21(5): 2291-2297.

Nguyen, D.B., Phu, S.T.P., Dinh, C.L. and Usami, M. 2021. Practical solid waste management system in a campus in Danang City, Vietnam. Chemical Engineering Transactions, 89(2021).

Pandey, U.P., Banerjee, R., Mumtaj, N. and Izhar, T. 2016. Evaluation of solid waste collection and segregation: A case study of Integral University Campus, Lucknow. Int. J. Emerg. Technol. Eng. Res., 4(5): 10-15.

Pratama, R.L. and Junianto, M. 2021. Banana leaves as a natural food packaging: A review. Glob. Sci. J., 9(12): 55-65.

Qiu, N., Sha, M. and Xu, X. 2022. Evaluation and future development direction of paper straw and plastic straw. IOP Conference Series: Earth and Environmental Science, 1011(1): 012029.

Rikasa, A.M. and Mufeez, M.S.M. 2023. Banana Leaf Food Packaging: An Alternative and Ecofriendly Solution for Food Industry in Sri Lanka. Multisectoral Approaches to Accelerate Economic Transformation in the Face of Crisis in Sri Lanka.

Roy, P., Mohanty, A.K., Wagner, A., Sharif, S., Khalil, H. and Misra, M. 2021. Impacts of COVID-19 outbreak on the municipal solid waste management: Now and beyond the pandemic. ACS Environ., (1): 32-45.

Sinha, R., Michelsen, J.D., Akcura, E. and Njie, L. 2020. COVID-19's Impact on the Waste Sector. International Finance Corporation, Washinton, DC.

The Travel Foundation. 2011. Plastics reduction in the hotel industry in Cyprus - Travel Foundation. Travel Foundation. Retrieved from https://www.thetravelfoundation.org.uk/casestudy/plastics-reduction-in-the-hotel-industry-in-cyprus/ (accessed July 15, 2023)

United Nations Environment Programme & World Travel & Tourism Council. 2021. Rethinking Single-Use Plastic Products in Travel & Tourism: Impacts, Management Practices and Recommendations. https://wedocs.unep.org/20.500.11822/36324 (accessed July 15, 2023)

University of Michigan-Dearborn. 2022. Campus Water Bottle Filling Stations: Putting a Dent in Single-Use Plastic. Retrieved from https://umdearborn.edu/news/campus-water-bottle-filling-stations-are-putting-dent-single-use-plastic (accessed July 15, 2023)

Willis, K., Hardesty, B.D., Vince, J. and Wilcox, C. 2019. The success of water refill stations reducing Single-Use plastic bottle litter. Sustainability, 11(19): 5232.

World Wide Fund Philippines 2020. EPR Scheme Assessment for Plastic Packaging Waste in the Ph. WWF, Phillippines.

ORCID DETAILS OF THE AUTHORS

J. M. Ngohayon: https://orcid.org/0000-0002-1230-5931

Nature Environment and Pollution Technology
An International Quarterly Scientific Journal

p-ISSN: 0972-6268
(Print copies up to 2016)
e-ISSN: 2395-3454

Vol. 23 | No. 1 | pp. 295-309 | 2024

Original Research Paper

https://doi.org/10.46488/NEPT.2024.v23i01.025

Open Access Journal

Mapping and Quantifying Integrated Land Degradation Status of Goa Using Geostatistical Approach and Remote Sensing Data

V. G. Prabhu Gaonkar*, **F. M. Nadaf****† and Vikas Kapale*****

*Department of Geoinformatics, Goa University, Parvatibai Chowgule College, Margao, Goa, India
**Department of Geography, DPM's Shree Mallikarjun & Shri Chetan Manju Desai College, Canacona, Goa, India
***Indian Institute of Technology, Kanpur, India
†Corresponding author: F. M. Nadaf; fmnadaf@gmail.com

Nat. Env. & Poll. Tech.
Website: www.neptjournal.com

Received: 17-06-2023
Revised: 18-08-2023
Accepted: 17-11-2023

Key Words:
Land degradation
RUSLE model
Erodibility
Erosivity
Cover management
Land use land cover

ABSTRACT

Globally, land degradation is becoming a grave concern. Over the years, conditions such as drought, extreme weather events, pollution, changes in land use land cover, and desertification have intensified and led to land degradation, affecting both ecological and economic processes. Equally, during the last two centuries, population and urbanization have amplified manifold and increased the demand for additional food and shelter, resulting in alteration in land use land cover, over-grazing, and over-cultivation, loss of nutrient-rich surface soil, greater runoff from the more impermeable subsoil, and reduced water availability. Geographically, Goa is a highly diversified state. It is sandwiched between the West Coast and the Western Ghats. The state is blessed with beaches, mangroves, backwaters, wetlands, wildlife sanctuaries, evergreen forests, barren lands, and other vital ecosystems. The State of Goa, on average, receives more than 3000 millimeters of rainfall annually with high surface runoff. Using both primary and secondary data, this study sought to investigate and quantify the state's land degradation. Secondary data came from satellites and other sources, while primary data came from field observation and ground truthing. Land degradation factors related to soil loss and the spatial pattern of soil erosion are predicted and evaluated using the Revised Universal Soil Loss Equation (RUSLE) method. Landsat-8 OLI-TIRS images were utilized to decide land use and cover (C factor), while DEM information was utilized to assess (LS factor). A soil map and rainfall data were collected to acquire a better understanding of soil erodibility (K factor) and rainfall erosivity (R factor). The kriging interpolation technique was used to gain a deeper comprehension of land degradation.The purpose of this paper is to comprehend the concept of integrated land degradation and how it affects the environment of Goa. Using remote sensing data and geostatistical methods, the study creates a comprehensive map of land degradation in the region by identifying and analyzing the various forms of land degradation in Goa. The paper also looks at how rainfall and the amount of land cover affect the rate of soil erosion in Goa. According to the findings, intense rainfall makes the eastern part of Goa particularly susceptible to soil erosion, and bare soil has a greater potential for erosion than vegetated land. The paper concludes that comprehensive land degradation mapping can be a useful tool for developing efficient land management strategies to preserve soil and encourage sustainable development in the region.

INTRODUCTION

Land debasement is the crumbling of land's quality and ability to support human and ecological frameworks. Over the years, it has become a critical environmental problem affecting the quality of soil, water, and air and threatens food security and economic development (El-Gammal et al. 2015, Ewunetu et al. 2021, Flores-Renteria et al. 2016, Kawy & Darwish 2019, Nkonya et al. 2016, Balasubramani et al. 2015, Odorico et al. 2011, Taylor & Millar 2009, Ravi et al. 2009). Land degradation arises from various factors, including human activities, climate change, erosion, and deforestation (Yolanda & Mart 2021).

The phenomenon of Integrated Land Degradation is intricate and results from a blend of natural and anthropogenic variables. In recent times, there has been growing apprehension regarding the scale and intensity of land degradation and its repercussions on both ecological systems and human welfare (Prabhu Gaonkar et al. 2022). Land degradation affects billions of people worldwide, directly or indirectly. It can potentially harm rural livelihoods,

reduce ecosystem productivity, alter vegetation composition, and overuse soil resources (D'Odorico & Ravi 2023).

Land degradation, desertification, and soil erosion pose a significant threat to sustainable development, particularly in regions with low rainfall, low soil fertility, and high poverty rates (IPCC 2019). Based on global land degradation patterns, roughly 24% of the world's land area experiences moderate to high levels of degradation. The most severe levels of degradation are observed in Africa and Asia (Bai et al. 2008). India is the most severely affected by land degradation (Obalum et al. 2012, Almouctar et al. 2021).

The United Nations Environment Programme (UNEP) emphasizes the significance of an integrated land degradation assessment to tackle the various causes and consequences of land degradation in a methodical and comprehensive approach, which considers the social, economic, and environmental dimensions of the problem (Vi & World 1950). Integrated Land Degradation is a complex and multifaceted issue that requires a holistic and integrated approach to address

Since the 1930s, scientists have employed land degradation assessment to forecast and identify control erosion methods (Allafta & Opp 2021, Ayalew 2015, Dutta et al. 2015). At various levels, including global, regional, and local, numerous approaches have been employed to quantify land degradation (Allafta & Opp, 2021, Auerswald 1992, Ayalew 2015, Dutta et al. 2015, Jarašiunas et al. 2020, Quiquampoix 2008, Thapa 2020, Wagari & Tamiru 2021). Numerous models have been created to estimate rates of soil loss to enhance comprehension (Amiya et al. 2019, Poesen et al. 2003).

Several methodologies and equations for risk assessment or predictive evaluation of soil degradation are prevalent (Angima et al. 2003, Hoyos 2005, Peng & Shao 2009, Prasannakumar et al. 2011, Quarishi 2014, Zhao et al. 2012). Using old field-based approaches, meticulously mapping and monitoring the spatial distribution of soil loss across enormously large zones is a difficult, costly, and time-consuming task (Allafta & Opp 2021, Prasannakumar et al. 2011). On the contrary, at the regional scales, erosion models, such as USLE/RUSLE, SEMMED, WEPP, ANSWERS, EUROSEM, LISEM, SWAT, AGNPS, and SWRRB, have distinct characteristics and different applications (Blackley et al. 2015, Boggs et al. 2001, Dabral et al. 2008, Golijanin et al. 2022, Ismail & Ravichandran 2008, Jazouli et al. 2019, Lu & Li 2004).

Remote sensing technology linked with Geographic Information System (GIS) is widely used and recognized as a remarkable and effective method for analyzing land degradation (Anand et al. 2018, Ara et al. 2021, Chen et al. 2021, Jazouli et al. 2019, Selvakumar 2018). Various models were developed to study land degradation, such as the Erosion potential method, the Modified Universal Soil Loss Equation, and the Revised Soil Loss Equation Model (Golijanin et al. 2022). Numerous current works and research studies have employed the RUSLE approach in conjunction with GIS (Tosic et al. 2011, Blackley et al. 2015, Kouli & Soupios 2009, Lanorte et al. 2019, Milentijević et al. 2021, Polykretis et al. 2020, Prasannakumar et al. 2011a, Swarnkar et al. 2017, Yuksel et al. 2008, Golijanin et al. 2022).

The Revised Universal Soil Loss Equation (RUSLE) is a widely used model in Geographical Information Systems (GIS) for predicting soil erosion and assessing the impact of land use activities on soil loss (NSW 2021). The RUSLE model considers multiple factors that contribute to soil erosion, including slope gradient, soil type, land cover, climate, and land management practices. The model uses a set of algorithms to calculate the erosion risk for each cell in a given geographic area.

Land degradation is a growing concern in the small coastal state of Goa in India. Goa is a global tourist destination that has been rapidly expanding in recent years, putting immense pressure on the land. In recent years, Goa has been facing multiple forms of land degradation that are threatening not only its environment but also its social and economic well-being. Urbanization, changes in land use, land cover, deforestation, and mining activities have led to soil erosion, loss of soil fertility, and depletion of groundwater resources. Hence, this chapter attempts to examine the extent of land degradation that has occurred in the State of Goa using the RUSLE model.

OBJECTIVES

The key objectives of this study include

1. To understand the concept of integrated land degradation and its impact on Goa's environment.
2. To identify and analyze the different types of land degradation occurring in Goa using remote sensing data.
3. To apply geostatistical techniques to create a comprehensive map of land degradation in Goa.
4. To quantify the extent of land degradation in Goa and determine the spatial distribution of different types of land degradation.

AREA OF INVESTIGATION

Goa is a small coastal state located on the west coast of India. Goa is known for its natural beauty, vibrant culture, and tourism industry. The eco-geography of Goa is unique, with a diverse range of ecosystems, flora, and fauna. The

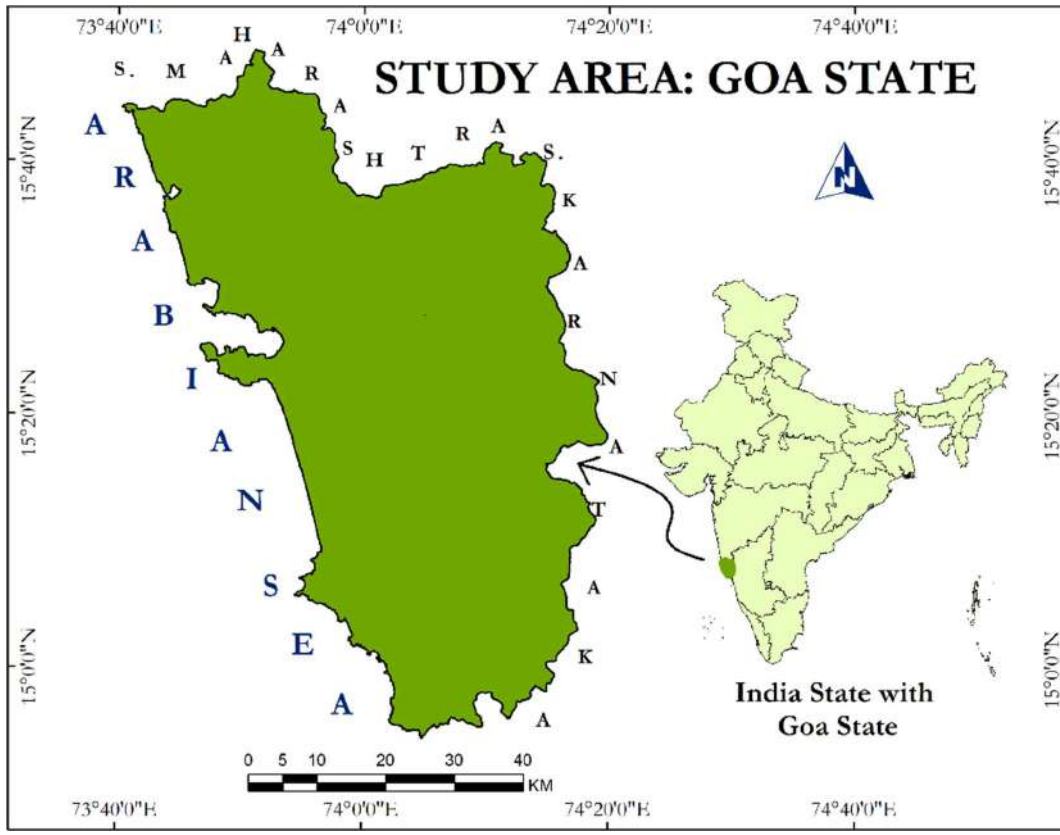

Fig. 1: Map of the study area: Goa.

state is blessed with numerous hills, sandy beaches, rocky cliffs, rivers, waterfalls, estuaries, mangroves, forests, and that attract millions of visitors from all over the world.

Mathematically, Goa extends amidst the parallels of 1400‘45°” to 1559‘47°” North latitudes and 7354‘40°” to 7411‘20°” east of meridians (Prabhu Gaonkar et al. 2022) (Fig. 1). It covers a geographical expanse of 3702 sq. km. It tolerates pressure of 1,458,545 persons (2011, Census). The State of Goa is 105 km long and 65 km wide. To the north, Goa is bordered by Maharashtra, while to the south lies Karnataka, and on the western side, it is surrounded by the blue waters of the Arabian Sea.

Goa’s territory has been classified into four physiographic divisions by the Geological Survey of India, which are:

1. Western Ghats Region (700-1000 Meters above Sea Level)

2. Foot Hill Region of Western Ghats (300-700 Meters above Sea Level)

3. Undulating Terrain (10-300 Meters above Sea Level)

4. Coastal Plains (0-10 Meters above Sea Level)

The eco-geography of Goa is under threat from various human activities, including mining, deforestation, urbanization, and tourism. Mining activities in the state have led to soil erosion, water pollution, and loss of biodiversity. Deforestation, primarily for commercial purposes, has led to soil degradation and loss of forest cover. Urbanization, particularly in the coastal areas, has led to the destruction of natural habitats and the loss of biodiversity. The tourism industry, which is a major source of revenue for the state, has also put pressure on the state’s natural resources, including water, land, and forests.

MATERIALS AND METHODS

This study is the result of primary and secondary data sources. Primary data were collected from field observations and ground-truthing, while the secondary data were derived from the following sources (Table 1).

There are several steps involved in the RUSLE model implementation methodology. The creation of the input parameter database is the first step. Using measurements taken in the field of the rates of soil erosion, the second step is to calibrate the model. The third step involves applying the equations to the database’s input parameters to determine the

Table 1: Databased used for RUSLE model.

Sr. No.	Data Type	Description	Sources
1.	Satellite Data	https://earthexplorer.usgs.gov_	LANSAT OLI for the year 2021 was grouped into 7 classes
2.	Digital elevation model	https://earthexplorer.usgs.gov	SRTM with 30m resolution
3.	Rainfall Data	Indian Meteorological Department, Goa-India	Rainfall data from 12 rain gauge stations for 30 years
4.	Soil Data	Directorate of Mines and Geology, Goa-India	The study area's soil map is categorized into seven classes based on the texture of the soil.

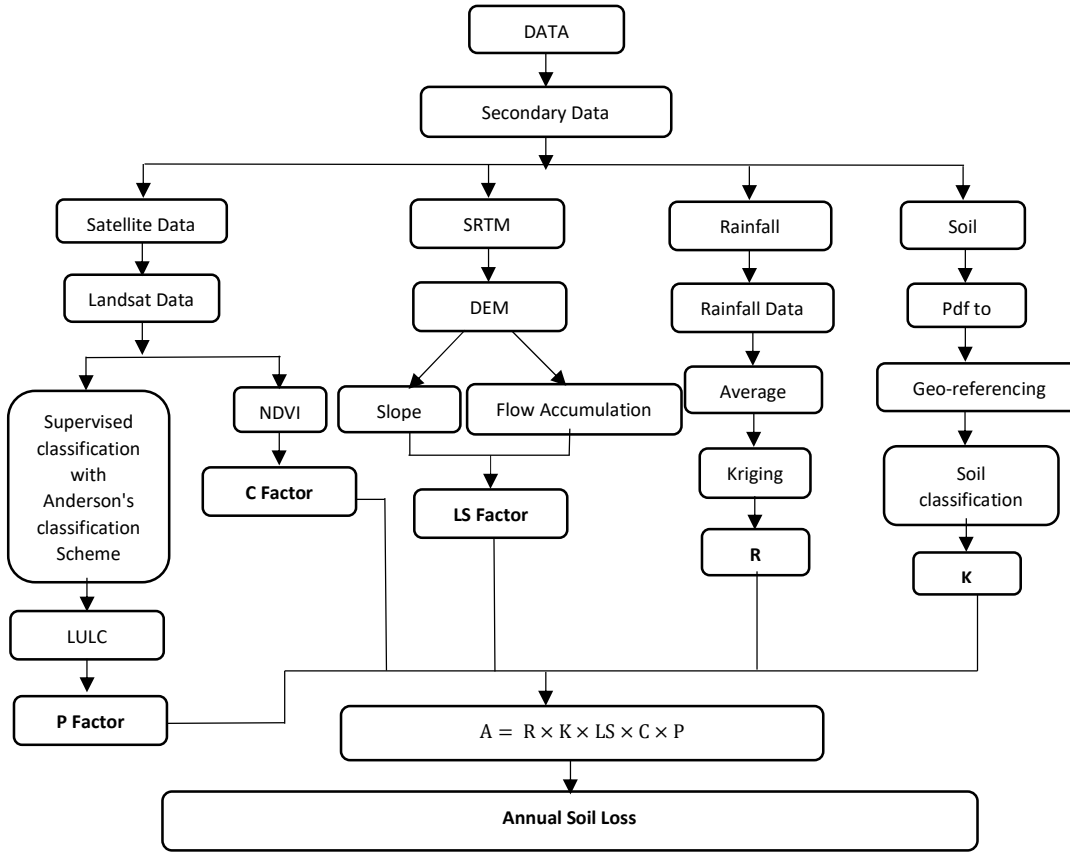

Fig. 2: Methodology chart.

risk of soil erosion for each cell. The fourth step is to look over the results and figure out where soil erosion is most likely. The development of management plans to lessen the likelihood of soil erosion in these locations is the final step (Fig. 2).

The RUSLE model employs a set of algorithms to calculate the erosion risk of each cell within a specific geographical area. By utilizing a GIS environment, the output of the RUSLE model can be showcased to exhibit the risk of soil erosion across a given landscape (Jarašiunas et al. 2020, Terranova et al. 2009). The RUSLE model uses five parameters to determine the average yearly soil loss measured in tons per hectare (Benavidez et al. 2018, Ganasri & Ramesh 2016, Ghosh et al. 2022, Kulimushi et al. 2021, Negese et al. 2021, Tayebi et al. 2019, Terranova et al. 2009, Thomas et al. 2018a).

$$A = R \times K \times LS \times C \times P \quad \ldots(1)$$

Where A signifies the average soil loss, R stands for rainfall-runoff erosivity, K for soil erodibility, LS for slope length and slope steepness, C for cover management, and P for conservation practices (Abdul Rahaman et al. 2015, Prasannakumar et al. 2012, Thomas et al. 2018b). Dimensionless parameters include LS, C, and P factors (Prasannakumar et al. 2011b). The data inputs for the RUSLE model used in this study were obtained from

various sources. Rainfall data was sourced from the Indian Meteorological Department, while soil data was acquired from the Directorate of Mines and Geology in Goa. Landsat-8 OLI-TIRS data and elevation data were retrieved from the GLOVIS website to determine slope length, slope steepness, and conservation practices. To create a soil erosional map, the raster outputs of all parameters were processed using the "Raster Calculator" tool, found within the "Spatial Analyst tools" in the ArcGIS 10.8 edition. By incorporating information on rainfall, elevation, soil, and land use/land cover, the study was able to estimate soil loss within the state of Goa.

RESULTS AND DISCUSSION

Rainfall-Runoff Erosivity (R Factor)

A thorough evaluation of rainfall erosivity is essential to comprehend hydrological and geomorphological processes as it denotes the potential of rainfall to erode soil (Yassoglou et al. 2017). The computation of the R-factor is a challenging undertaking that heavily depends on multiple factors, including the length, volume, intensity, energy, and size of raindrops, as well as the precipitation pattern and ensuing runoff rates (Farhan & Nawaiseh 2015, Jarašiunas et al. 2020). Rainfall probability can be determined using rainfall

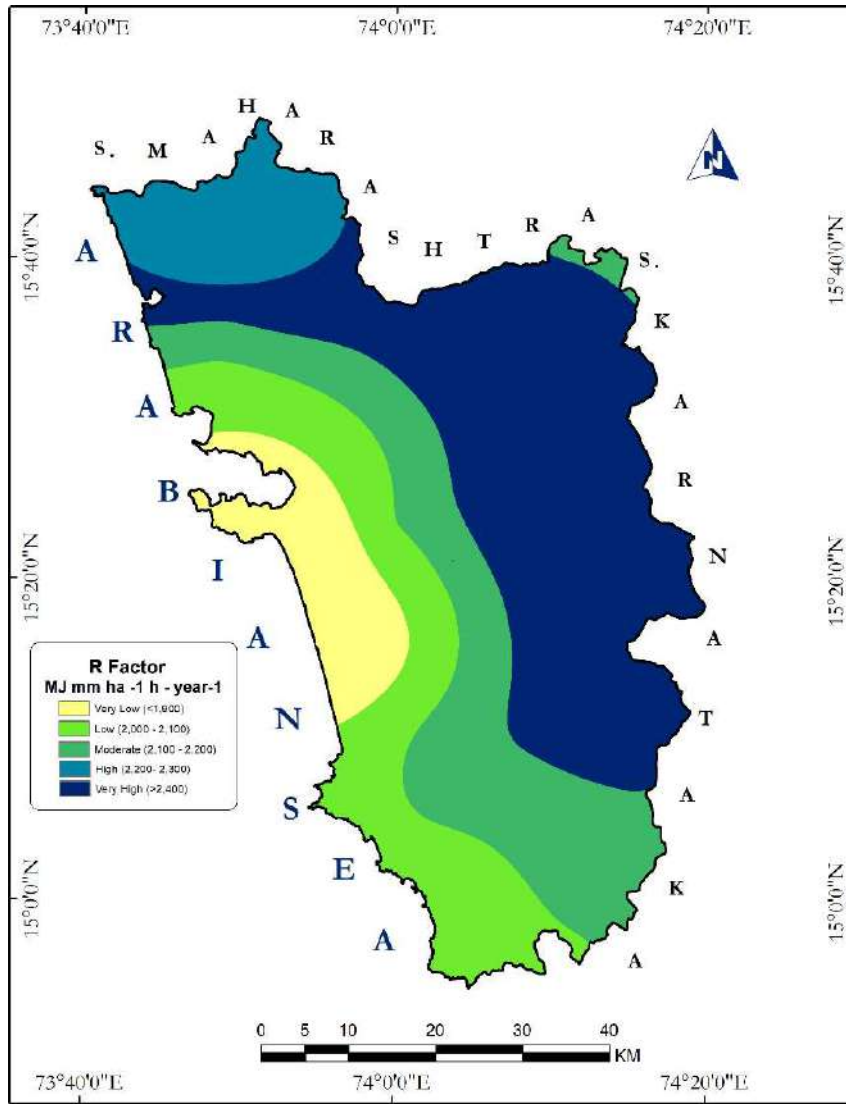

Fig. 3: The study area map depicting R- Factor: Rainfall erosivity.

Table 2: Taluka-wise rainfall distribution, Goa.

Station	Average of 1971-2020	Actual Rainfall in 2021	Station	Average of 1971-2020	Actual Rainfall in 2021
Tiswadi (Panaji)	2904.6	3935.7	Sanguem (Sanguem)	3687.9	4438.5
Bardez (Mapusa)	2990	4041.2	Dharbandora (Dharbandora)	NA	NA
Pernem (Pernem)	NA	5247.6	Ponda (Ponda)	3453.3	4361.6
Bicholim (Sanquelim)	NA	4304.3	Canacona (Canacona)	NA	3836.6
Sattari (Valpoi)	4160.9	4499.3	Quepem (Quepem)	3617.1	4457.8
			Salcete (Margao)	3040	3242.8
			Mormugao (Mormugao)	2719.6	3206.6
North Goa	3351.8	4252.1	South Goa	3212.55	3768.2
			Goa	3277.8	3995.1

Source: Indian Meteorological Department, Goa

intensity (Amellah & el Morabiti, 2021). Multiple research papers have employed the average annual precipitation data to calculate the R-factor in the study area using the same methodology (Abdul Rahaman et al. 2015, Prasannakumar et al. 2011a, 2011b, Swarnkar et al. 2017, Taylor 2009, Thomas et al. 2018a).

$$R = P * 0.5 \quad \ldots(2)$$

The symbol R represents yearly precipitation data. To determine the precipitation levels for the year 2021, data was obtained from the Indian Meteorological Department, drawing from average data from 12 different locations. This data was subsequently converted into raster format using "multi-dimensional tools" and "Make NetCDF Raster layer" in ArcGIS 10.8. The modified raster layer was then transformed into points using "Conversion Tools." Finally, a rainfall map of the study area was produced using the statistical tool "Kriging" found within the "Spatial Analyst Tools" in ArcGIS 10.8, utilizing the collected points (Allafta & Opp 2021, Jarašiunas et al. 2020).

The coastal region of western India receives a significant amount of rainfall, making it one of the highest precipitation-receiving areas in the country. During the monsoon season from June to September, over 90% of the annual rainfall is concentrated in this region (Nandargi & Gupta, 2018, Patwardhan & Asnani 2000). Study shows that there is a swift surge in precipitation along the Arabian Sea coast in close proximity to the Western Ghats' maximum elevation line (Patwardhan & Asnani 2000). Our study also reveals the same (Fig. 3 & Table 3).

The average annual rainfall in Goa is more than 3200 mm, with some variations depending on the region (Table 2). It is an observed fact that rainfall can have a significant impact on erosion. When it rains, water runs off the ground, causing soil erosion as it carries away topsoil, sediments, and other materials. The more intense the rainfall, the greater the potential for soil erosion.

The R factor for Goa varies depending on the location and the season. Though the western parts of Goa, including the coastal areas, receive less rainfall than the eastern parts of the state, it experiences cyclones and intense storms during the monsoon season, which can increase the erosive power of rainfall.

Rainfall erosivity is a critical factor in determining the potential for soil erosion. High rainfall erosivity leads to increased soil erosion rates, which can have negative impacts on soil fertility, water quality, and ecological health. As per the data presented in (Table 3), it is clear that almost half of

Table 3: Area of R- R-Factor: Rainfall erosivity.

Sr. No	Intensity	Area in Sq. Km.	Area in %
1.	Very Low	327.70	8.85
2.	Low	710.77	19.20
3.	Moderate	839.20	22.66
4.	High	323.83	8.74
5.	Very High	1501.39	40.55
	Total	3702.00	100.00

Goa's total geographical area (i.e., 50%) is categorized as having high and very high rainfall erosivity indicating that a significant portion of Eastern Goa is vulnerable to high levels of soil erosion due to intense rainfall. Additionally, around 22.66% of the total area of Central Goa is under moderate erosivity, which experiences moderate rainfall, indicating moderate soil erosion, while roughly 28% of the area falls under the category of very low-to-low rainfall erosivity. This suggests that western Goa experiences less intense rainfall, resulting in lower levels of soil erosion.

Cover Management (C Factor)

The C-factors are critical parameters for crop management, as they are closely linked to land-use types and reduction factors in soil erosion (Jazouli et al. 2019, Nigel & Rughooputh 2010, Rabia 2016). However, the majority of Indian crops lack C-factors, necessitating the use of values discovered by previous research (Almagro et al. 2019, Karaburun 2010, Solanky et al. 2018, Zhou 2009) to evaluate the impact of cropping and management strategies on soil erosion rates in agricultural regions. The C-factor is a dimensionless factor ranging from 0 to 1, with 0 indicating completely non-erodible conditions in areas with high green vegetation cover, while 1 indicates greater soil loss due to extensive tillage, leaving a smooth surface that generates significant runoff and makes the soil susceptible to erosion. NDVI spectral indices are calculated using the following equation:

$$\text{NDVI} = \frac{NIR-RED}{NIR+RED} \quad \ldots(3)$$

Where band 5 of OLI is the reflectance of near-infrared, while Red is the reflectance of the visible red band that is band 4 of OLI. The equation was used to compute the geographical distribution of the C factor (Chinthaparthi & Student 2007, Fathizad et al. 2014, Ganasri & Ramesh 2015, UNCCD 2017, Wischmeier 1959).

$$C = exp\left[-\propto \frac{NDVI}{\beta - NDVI}\right] \quad \ldots(4)$$

Land Use Land Cover (LULC) influences soil erosion rates. Different land cover types have varying soil erodibility. For example, a field with bare soil has a higher C factor than a field with vegetation cover because bare soil is more susceptible to erosion. The study area consists of five main

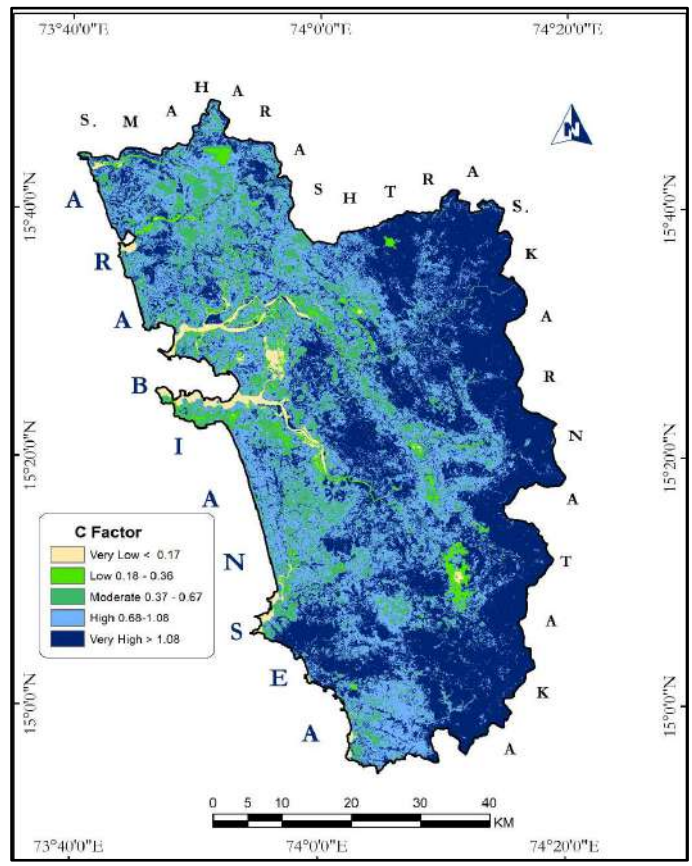

Fig. 4: The study area map depicting C- Factor: Cover Management.

Table 4: Area of C- Factor: Cover Management.

Classes	Area in Sq. Km.	Area in %
Very Low	1734.75	46.86
Low	1263.83	34.13
Moderate	524.68	14.17
High	101.38	2.73
Very High	77.36	2.09
Total	3702.00	100.00

LULC types, namely Vegetation, Flooded Vegetation, Agriculture, Built-up, and Barren land. Previous literature was consulted to determine the appropriate C factor values for each of these classes. The C factor values ranged from the lowest value of 0 assigned to the waterbody class to the highest value of 1 assigned to the Vegetation, Flooded Vegetation, Built-up, and Barren land classes. The Agriculture class was assigned a C factor value of 0.5.

It is evident from (Table 4) that the largest C factor class is "Very Low," covering almost half (46.86%) of the study area, followed by "Low" at 34.13%. These two classes indicate that the majority of the study area has a low susceptibility to soil erosion, which is a positive indication

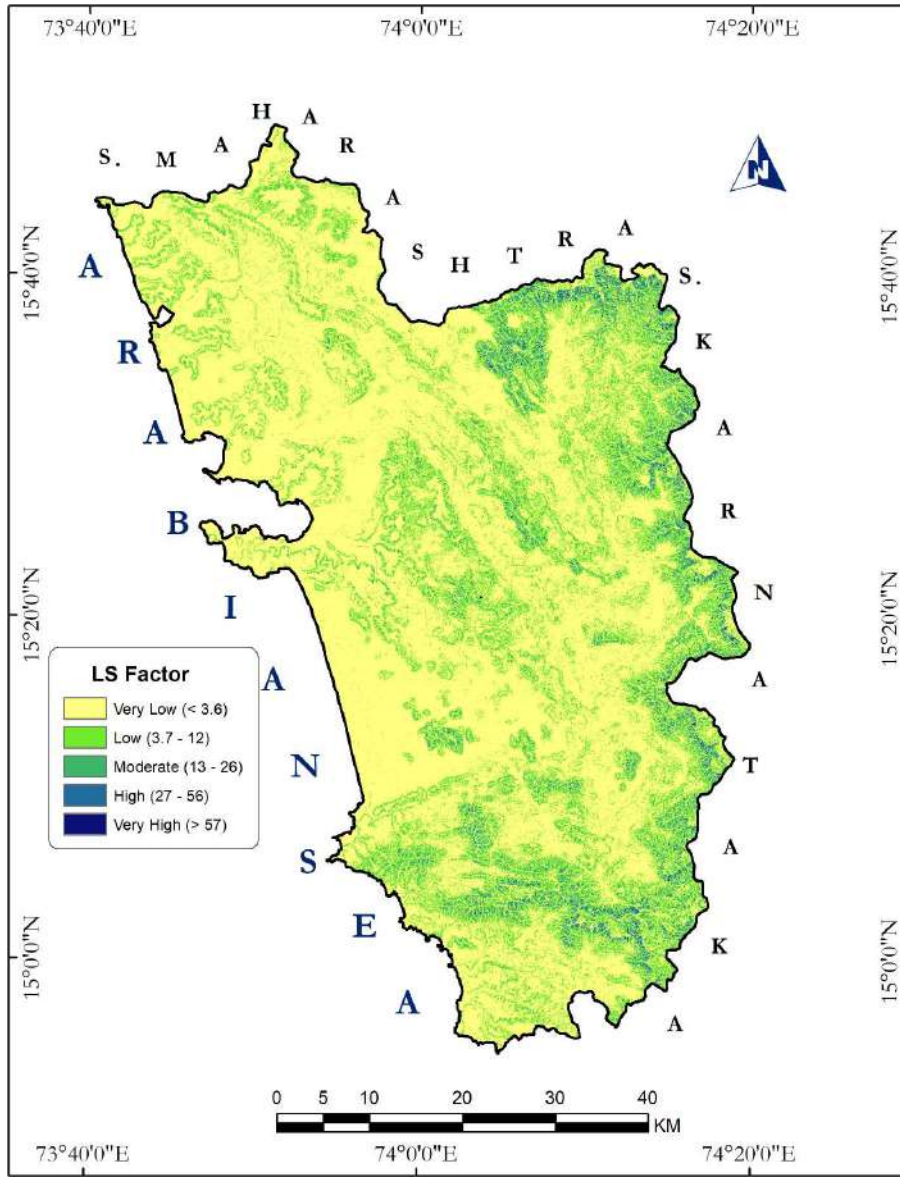

Fig. 5: The study area map depicting LS- Factor: Soil slope length.

for sustainable land management practices.

The "Moderate" class covers a smaller area of 14.17%, suggesting that some parts of the study area have moderate susceptibility to soil erosion. Meanwhile, the "High" and "Very High" classes have a combined area of only 4.82%, indicating that the study area has a relatively low susceptibility to severe soil erosion.

Slope Steepness and Slope Length (LS Factor)

The LS factor was computed in ArcGIS using a Digital Elevation Model (DEM) (Jarašiunas et al. 2020, Jazouli et al. 2019). It combines the effects of slope length (L) and steepness (S) on soil erosion in RUSLE. Steeper and longer slopes generate higher overland flow velocities, leading to greater runoff and increased potential for soil loss (Wagari & Tamiru 2021). The LS parameter, which is the product of L and S, quantifies the terrain's impact on erosion (Jarašiunas et al. 2020, Lastoria et al. 2008). As the slope steepness increases, the runoff velocity and erosivity also increase. The values for L and S were obtained using ArcGIS Spatial Analyst tools. Other studies computed the LS factor using the same method by collecting 30 M SRTM datasets (Fayas et al. 2019, Moore & Burch 1986, Prasannakumar et al. 2011, UNCCD 2017). This approach was also followed for the study region.

$$LS = (Flow\ accumulation \times Cell\ size/22.13)^{0.4} \times (Sin\ slope/0.0896)^{1.3} \quad \ldots(5)$$

The LS factor plays a crucial role in the RUSLE Model since it accounts for the impact of topography on soil erosion. By incorporating slope length and steepness, the LS factor can effectively pinpoint areas that are more susceptible to soil loss and prioritize conservation measures to mitigate erosion.

In the study area, the "Very Low" and "Low" LS-factor classes dominate, covering almost 70% and 21.67% of the area, respectively. These classes indicate that the majority of the study area comprises gentle slopes and short slope lengths, which are less prone to soil erosion.

The "Moderate" LS-factor class covers a relatively smaller area of 6.29%, suggesting that some parts of the study area have moderate slope steepness and length, which may increase the risk of soil erosion. Meanwhile, the "High" and "Very High" classes combined only occupy 2.25% of the study area, indicating that the number of steep and long slopes highly vulnerable to soil erosion is limited.

Overall, the distribution of LS-factor classes suggests that the study area is relatively less susceptible to soil erosion due to the preponderance of gentle slopes and short slope lengths. However, it is important to note that certain parts of the area with moderate slope steepness and length may still be at risk and require conservation measures to reduce soil loss.

Soil Erodibility (K Factor)

Soil erodibility (K) is a metric that indicates the vulnerability of soil or surface material to erosion, sediment transportability, and the volume and speed of runoff for a given amount of rainfall under typical conditions (Zhao et al. 2012). The K factor is determined based on the inherent characteristics of soil, including physical, chemical, and mineralogical properties, which all contribute to soil erosion (Franzluebbers 2010, Fu et al. 2006, Pal & Chakrabortty 2019, Phinzi & Ngetar 2019). For instance, soils with a loamy texture, which are medium-grained and have a tendency to disintegrate and runoff, often exhibit high K values (Yuksel et al. 2008).

The K factor map was generated using the soil texture map obtained from the Directorate of Mines and Geology, Goa. The area of investigation was divided into six primary textural classifications of soils, and the corresponding K values were determined from different sources (Abdul Rahaman et al. 2015, Polykretis et al. 2020, Wagari & Tamiru 2021).

The K value of soil is dependent on its location and texture. Clayey soil has low K values due to its high resistance to separation, while sandy soil, which is coarse-grained, also has low K values and low runoff potentials. Conversely, loamy, fine loamy type, and fine mixed soils have high K values, as they are more prone to disintegration

Table 5: Area of LS- Factor: Soil Slope Length.

Classes	Area in sq. km	Area in %
Very Low	2584.06	69.80
Low	802.04	21.66
Moderate	232.8	6.28
High	59.55	1.60
Very High	23.55	0.63
Total	3702.00	100.00

Table 6: Depicting K values.

Sr.No.	Soil Texture Type	K Values
1.	Clayey	0.0402
2.	Loamy	0.26
3.	Fine Loamy	0.07
4.	Fine Loamy Typic	0.39
5.	Fine Mixed	0.43
6.	Sandy	0.20

Table 7: Showing the area of K- Factor: Soil Erodibility.

Classes	Area in sq. km	Area in %
Very Low	102.41	2.76
Low	2101.15	56.75
Moderate	325.47	8.79
High	54.20	1.46
Very High	1118.76	30.22
Total	3702.00	100

and generate more runoff. In the study area, six major soil texture classes were identified, including clayey, loamy, fine loamy, fine loamy type, fine mixed, and sandy.

The lowest K value is < 0.01, which is for the waterbody, while the highest K value (> 0.2) is located near the coastal belt to the mid-region of the study area. The fine mixed soil, which has a K value of 0.43 (Table 6), is classified as a very high class and is located in the eastern part of the state of Goa.

Table 7 indicates that the majority of the study area falls under the "Low" K factor class, covering 56.76% of the total area. The "Very High" K factor class covers 30.22% of the study area, indicating that a significant portion of the area is prone to soil erosion due to its soil texture. The "Moderate" and "High" K factor classes cover relatively smaller areas, indicating that only a few parts of the study area have soil textures that are more susceptible to soil erosion.

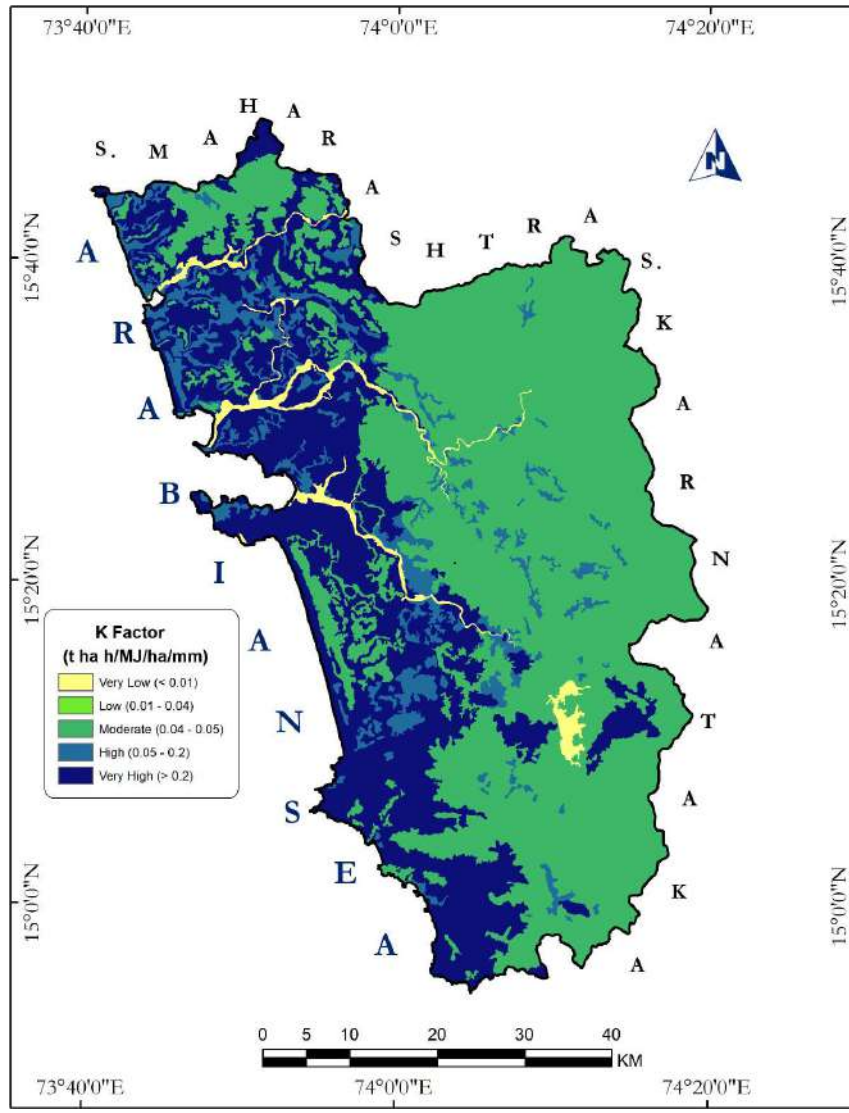

Fig. 6: The study area map depicting K- Factor: Soil erodibility.

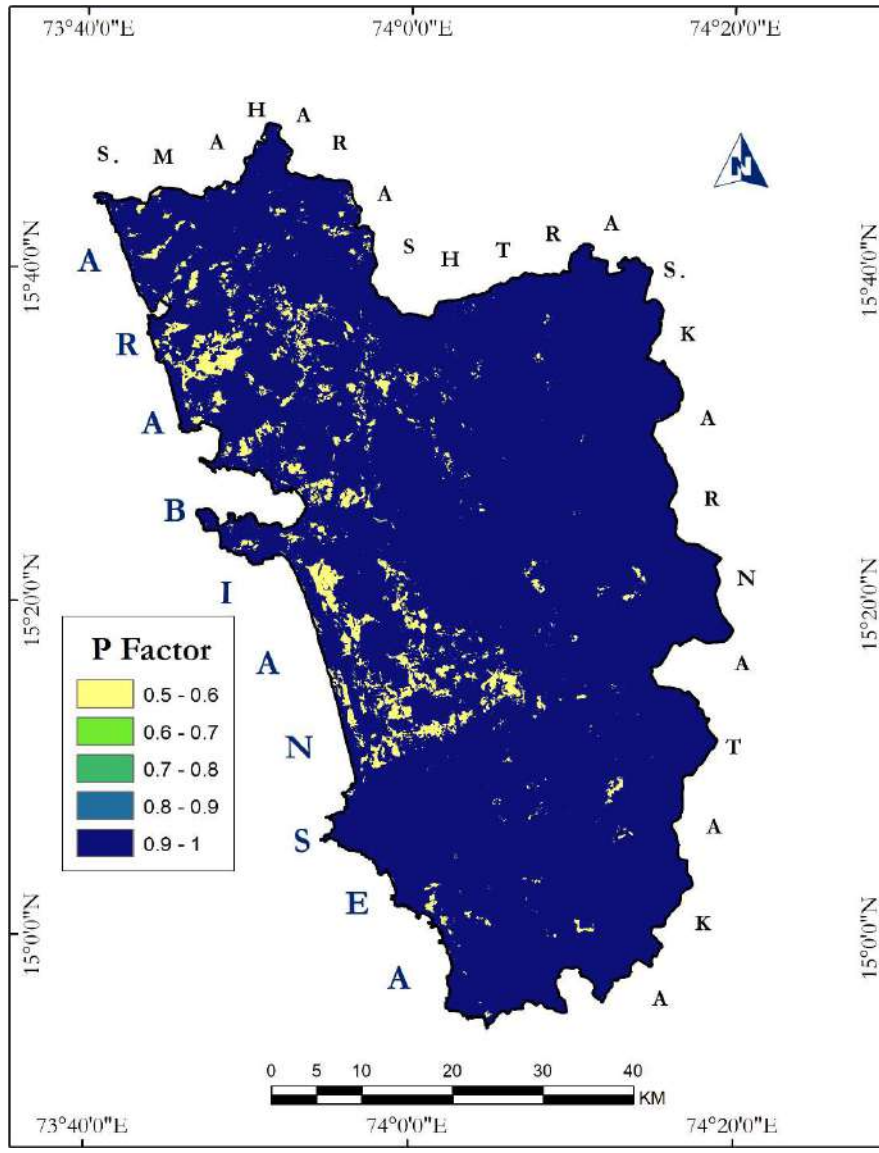

Fig. 7: The study area map depicting P- Factor: Conservation practice.

Conservation Practice (P Factor)

Erosion control measures, represented by the P factor (Naqvi et al. 2012), have an impact on the yearly soil loss in the research area. The support practice factor (Boggs et al. 2001, Karydas & Sekuloska 2009, Lee 2004, Yassoglou et al. 2017) indicates the effectiveness of measures that reduce water runoff volume and pace, as well as soil erosion. The P factor ranges from 0 to 1, with values close to 0 indicating good conservation practices and values close to 1 indicating poor conservation practices (Mohan & Kumaraswamy 2015, Periyasamy 2017). Land-use land-cover classes are used to determine the P factor, and the same process was used to determine the study area's P factor. No conservation activities receive the highest values, while the most effective conservation practices receive the lowest values.

The P factor is influenced by the terrain slope, with values ranging from 0 to 1. A value close to 0 indicates strong conservation behavior, while a value close to 1

Table 8: The area of P- Factor: Conservation practice.

Sr. No.	Area in sq. km	Area in %
1.	204.52	5.52
2.	3497.48	94.47
Total	3702.00	100.00

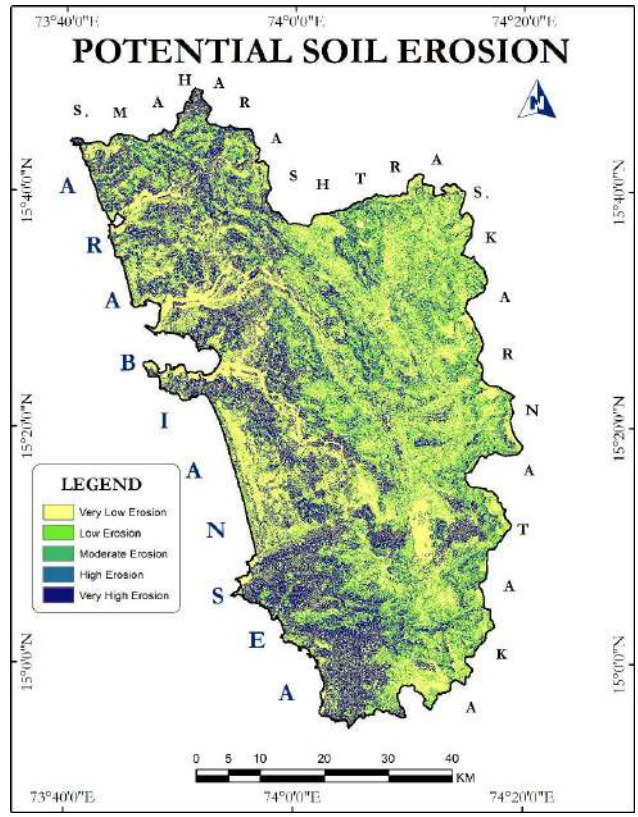

Fig. 8: RUSLE-based soil erosion rate estimated for the state of Goa.

indicates poor conservation practice. Within the study area, a P factor value of 0.5 pertains solely to a limited number of patches distinguished by the yellow color, indicating good conservation practices. Conversely, patches marked in blue represent bad conservation practices. Only 5.524% of the area is classified as being under the good conservation category, while the remaining 94.475% falls under the bad conservation category (Table 8).

RUSLE-based Soil Erosion Rate Estimation

The study area's potential soil erosion was evaluated using five key parameters, namely Rainfall Erosivity (R factor), Slope Steepness and Slope Length (LS factor), Soil Erodibility (K factor), Conservation Practice (P factor), and Cover Management (C factor). Figs. 3 to 7 illustrate the outputs of each parameter. The R factor indicates that higher rainfall intensity corresponds to higher erosion potential. The LS factor helps to understand slope steepness, where steeper slopes result in higher runoff and erosion. The C factor helps us understand the effects of Land Use Land Cover (LULC) on soil loss rates. The K factor describes soil's vulnerability to the rate of runoff and erosion, with soils that generate large runoff having the highest K values.

Based on the RUSLE-based soil erosion rate estimated for the state of Goa (Fig. 8), the entire State is classified into five categories based on its erosion risk such as very low, low, moderate, high, and very high.

The largest area falls under the "very low" erosion risk category, which comprises 48.03 percent (1778.20 sq. km) of the total area. This is followed by the "very high" erosion risk category, which comprises 24.35 percent (901.69 sq. km) of the total area (Table 9).

The "low" and "moderate" erosion risk categories each comprise a smaller proportion of the total area, with 14.68 percent (543.61 sq. km) and 8.81 percent (326.27 sq. km), respectively. The "high" erosion risk category is the smallest, comprising only 4.11 percent (152.20 sq. km) of the total area (Table 9).

CONCLUSION

Overall, the findings of this study provide valuable insights into the potential soil erosion in the state of Goa, which can be used to develop effective soil conservation strategies. By identifying the areas with the highest erosion

Table 9: The area of potential soil erosion.

Classes	Area in sq. km	Area in %
Very Low	1778.20	48.03
Low	543.61	14.68
Moderate	326.27	8.81
High	152.20	4.11
Very High	901.69	24.35
Total	3702	100

risk, policymakers can prioritize the implementation of conservation practices and cover management strategies to reduce soil loss rates. Additionally, these results can be used to inform land use planning decisions and ensure sustainable land use practices in the region.

It is important to note that the study's results are based on modeling and estimation techniques and are subject to some degree of uncertainty. Therefore, further research is needed to validate these findings and assess the effectiveness of soil conservation measures in mitigating erosion rates. Nonetheless, the study provides a solid foundation for understanding the potential soil erosion in the state of Goa. It highlights the importance of sustainable land use practices to protect the region's soil resources.

REFERENCES

Abdul Rahaman, S., Aruchamy, S., Jegankumar, R. and Abdul Ajeez, S. 2015. Estimation of annual average soil loss, based on RUSLE model in Kallar watershed, Bhavani Basin, Tamil Nadu, India. ISPRS Annals, 2(2W2): 207-214.

Allafta, H. and Opp, C. 2021. GIS-based multicriteria analysis for flood-prone areas mapping in the transboundary Shatt Al-Arab basin, Iraq-Iran. Geomatics Nat. Hazards Risk, 12(1): 2087-2116.

Almagro, A., Thomé, T.C., Colman, C.B., Pereira, R.B., Marcato Junior, J., Rodrigues, D.B.B. and Oliveira, P.T.S. 2019. Improving cover and management factor (C-factor) estimation using remote sensing approaches for tropical regions. Int. Soil Water Conserv. Res., 7(4): 325-334.

Almouctar, M.A.S., Wu, Y., Zhao, F. and Dossou, J.F. 2021. Soil erosion assessment using the RUSLE model and geospatial techniques (Remote Sensing and GIS) in South-Central Niger (Maradi Region). Water, 13(24), p.3511.

Amellah, O. and el Morabiti, K. 2021. Assessment of soil erosion risk severity using GIS, remote sensing, and RUSLE model in Oued Laou Basin, Morocco. Soil Sci. Ann., 72(3): 1-11.

Amiya, G., Saha, S. and Pourghasemi, H.R. 2019. Soil erosion assessment using the RUSLE model and its validation by the FR probability model. Geocarto Int., 35(15): 1750-1768.

Anand, J., Gosain, A.K. and Khosa, R. 2018. Prediction of land use changes based on Land Change Modeler and attribution of changes in the water balance of the Ganga basin to land use change using the SWAT model. Sci. Total Environ., 644: 503-519.

Angima, S.D., Stott, D.E., O'Neill, M.K., Ong, C.K. and Weesies, G.A. 2003. Soil erosion prediction using RUSLE for central Kenyan highland conditions. Agric. Ecosyst. Environ., 97(1-3): 295-308.

Ara, S., Alif, M.A.U.J. and Islam, K.M.A. 2021. Impact of tourism on LULC and LST in a coastal island of Bangladesh: A geospatial approach on St. Martin's island of Bay of Bengal. J. Indian Soc. Remote Sensing, 49(10): 2329-2345.

Bai, Z.G., Dent, D.L., Olsson, L. and Schaepman, M.E. 2008. Global Assessment of Land Degradation and Improvement: Identification by Remote Sensing. GLADA Report No. 5. Food and Agriculture Organization and World Soil Information, The Netherlands.

Balasubramani, K., Veena, M., Kumaraswamy, K. and Saravanabavan, V. 2015. Estimation of soil erosion in a semi-arid watershed of Tamil Nadu (India) using revised universal soil loss equation (RUSLE) model through GIS. Modeling Earth Systems and Environment, 1(3): 1-17. https://doi.org/10.1007/s40808-015-0015-4

Benavidez, R., Jackson, B., Maxwell, D. and Norton, K. 2018. A review of the (revised) Universal Soil Loss Equation ((R) USLE): With a view to increasing its global applicability and improving soil loss estimates. Hydrol. Earth Syst. Sci., 22(11): 6059-6086. https://doi.org/10.5194/hess-22-6059-2018

Blackley, R., Sbrocchi, C., Steinfeld, C., Grundy, M., Biggs, A. and Silburn, M. 2015. Geographical systems approach to the assessment of soil erosion using the RUSLE model. AREAWP No. 5/2015. Queensland, pp. 63-74.

Boggs, G., Devonport, C., Evans, K. and Puig, P. 2001. GIS-based rapid assessment of erosion risk in a small catchment in the wet/dry tropics of Australia. Land Degrad. Dev., 12(5): 417-434.

Chen, H., Chen, C., Zhang, Z., Lu, C., Wang, L., He, X., Chu, Y. and Chen, J. 2021. Changes of the spatial and temporal characteristics of land-use landscape patterns using multi-temporal Landsat satellite data: A case study of Zhoushan Island, China. Ocean Coast. Manage., 213: 105842.

Chinthaparthi, S. and Student, P. 2007. Detection and future prediction of coastal changes in Chennai using remote sensing and GIS techniques. Int. J. Innovative Res. Sci., Eng. Technol., 3297(2): 2319-8753.

Dabral, P.P., Baithuri, N. and Pandey, A. 2008. Soil erosion assessment in a hilly catchment of North Eastern India using USLE, GIS, and remote sensing. Water Resour. Manage., 22(12): 1783-1798.

D'Odorico, P. and Ravi, S. 2023. Land degradation and environmental change. In: Biological and environmental hazards, risks, and disasters, pp. -359 367. Elsevier. https://doi.org/10.1016/B978-0-12-394847-2.00014-0

Dutta, D., Das, S., Kundu, A. and Taj, A. 2015. Soil erosion risk assessment in Sanjal watershed, Jharkhand (India) using geo-informatics, RUSLE model, and TRMM data. Modeling Earth Syst. Environ., 1(4): 1-9.

El-Gammal, M.I., Ali, R.R. and Abou Samra, R.M. 2015. GIS-based land degradation risk assessment of Damietta Governorate, Egypt. Egyptian J. Basic Appl. Sci., 2(3): 183-189.

Ewunetu, A., Simane, B., Teferi, E. and Zaitchik, B.F. 2021. Mapping and quantifying comprehensive land degradation status using spatial multicriteria evaluation technique in the headwaters area of upper Blue Nile river. Sustainability, 13(4): 1-28.

Farhan, Y. and Nawaiseh, S. 2015. Spatial assessment of soil erosion risk using RUSLE and GIS techniques. Environ. Earth Sci., 74(6): 4649-4669.

Fathizad, H., Karimi, H. and Alibakshi, S.M. 2014. The estimation of erosion and sediment by using the RUSLE model and RS and GIS techniques: A case study: Arid and semi-arid regions of Doviraj, Ilam Province, Iran. Int. J. Agric. Crop Sci., 34: 604.

Fayas, C.M., Abeysingha, N.S., Nirmanee, K.G.S., Samaratunga, D. and Mallawatantri, A. 2019. Soil loss estimation using the RUSLE model to prioritize erosion control in the Kelani river basin in Sri Lanka. Int. Soil Water Conserv. Res., 7(2): 130-137.

Flores-Renteria, D., Rincon, A., Valladares, F. and Curiel Yuste, J. 2016. Agricultural matrix affects differently the alpha and beta structural and functional diversity of soil microbial communities in a fragmented Mediterranean holm oak forest. Soil Biol. Biochem., 92: 345-436.

Franzluebbers, A.J. 2010. Principles of soil conservation and management. Vadose Zone Journal, 9(1): 199. https://doi.org/10.2136/vzj2009.0110br

Fu, G., Chen, S. and McCool, D.K. 2006. Modeling the impacts of no-till practice on soil erosion and sediment yield with RUSLE, SEDD, and

ArcView GIS. Soil Till. Res., 85(1-2): 38-49. https://doi.org/10.1016/j.still.2004.11.009

Ganasri, B.P. and Ramesh, H. 2016. Assessment of soil erosion by RUSLE model using remote sensing and GIS: A case study of Nethravathi Basin. Geosci. Front., 7(6): 953-961. https://doi.org/10.1016/j.gsf.2015.10.007

Ghosh, A., Rakshit, S., Tikle, S., Das, S., Chatterjee, U., Pande, C.B., Alataway, A., Al-Othman, A.A., Dewidar, A.Z. and Mattar, M.A. 2022. Integration of GIS and remote sensing with RUSLE model for estimation of soil erosion. Land, 12(1): 116. https://doi.org/10.3390/land12010116

Golijanin, J., Nikolić, G., Valjarević, A., Ivanović, R., Tunguz, V., Bojić, S., Grmuša, M., Lukić Tanović, M., Perić, M., Hrelja, E. and Stankov, S. 2022. Estimation of potential soil erosion reduction using GIS-based RUSLE under different land cover management models: A case study of Pale Municipality, B and H.. Front. Environ. Sci., 10: 1-13. https://doi.org/10.3389/fenvs.2022.945789

Hoyos, N. 2005. Spatial modeling of soil erosion potential in a tropical watershed of the Colombian Andes. CATENA, 63(1): 85-108. https://doi.org/10.1016/j.catena.2005.05.012

IPCC. 2019. Climate Change and Land: An IPCC Special Report on Climate Change, Desertification, Land Degradation, Sustainable Land Management, Food Security, and Greenhouse Gas Fluxes in Terrestrial Ecosystems. https://www.ipcc.ch/srccl/ (accessed 13 July 2023)

Ismail, J. and Ravichandran, S. 2008. RUSLE2 model application for soil erosion assessment using remote sensing and GIS. Water Resour. Manag., 22(1): 83-102. https://doi.org/10.1007/s11269-006-9145-9

Jarašiunas, G., Świtoniak, M. and Kinderienė, I. 2020. Dynamics of slope processes under changing land use conditions in young morainic landscapes, Western Lithuania. Int. Agrophys., 1(34): 43-55. https://doi.org/10.31545/intagr/116404

Jazouli, A.E., Barakat, A., Khellouk, R., Rais, J. and Baghdadi, M.E. 2019. Remote sensing and GIS techniques for prediction of land use land cover change effects on soil erosion in the high basin of the Oum Er Rabia River (Morocco). Remote Sens. Appl. Soc. Environ., 13: 361-374. https://doi.org/10.1016/j.rsase.2018.12.004

Karaburun, A. 2010. Estimation of C factor for soil erosion modeling using NDVI in Buyukceece watershed. Ozean J. Appl. Sci., 3(1): 77-85. http://ozelacademy.com/OJAS_v3n1_8.pdf

Karydas, C.G., Sekuloska, T. and Silleos, G.N. 2009. Quantification and site-specification of the support practice factor when mapping soil erosion risk associated with olive plantations in the Mediterranean island of Crete. Environ. Monit. Assess., 149(1-4): 19-28. https://doi.org/10.1007/s10661-008-0179-8

Kawy, W.A.M.A. and Darwish, K.M. 2019. Assessment of land degradation and implications on agricultural land in Qalyubia Governorate, Egypt. Bull. National Res. Centre, 43(1): 1-14. https://doi.org/10.1186/s42269-019-0102-1

Kouli, M., Soupios, P. and Vallianatos, F. 2009. Soil erosion prediction using the Revised Universal Soil Loss Equation (RUSLE) in a GIS framework, Chania, northwestern Crete, Greece. Environmental Geology, 57(3): 483-497. https://doi.org/10.1007/s00254-008-1318-9

Kulimushi, L.C., Choudhari, P., Mubalama, L.K. and Banswe, G.T. 2021. GIS and remote sensing-based assessment of soil erosion risk using RUSLE model in South-Kivu province, Eastern Democratic Republic of Congo. Geomat. Natural Hazards Risk, 12(1): 961-987. https://doi.org/10.1080/19475705.2021.1906759

Lanorte, A., Cillis, G., Calamita, G., Nolè, G., Pilogallo, A., Tucci, B. and De Santis, F. 2019. Integrated approach of RUSLE, GIS, and ESA Sentinel-2 satellite data for post-fire soil erosion assessment in Basilicata region (Southern Italy. Geomatics, Natural Hazards and Risk, 10(1): 1563-1595. https://doi.org/10.1080/19475705.2019.1578271

Lastoria, B., Miserocchi, F., Lanciani, A. and Monaceli, G. 2008. An estimated erosion map for the {Aterno-Pescara} river basin. Europ. Water, 21: 29-39.

Lee, S. 2004. Soil erosion assessment and its verification using the universal soil loss equation and geographic information system: A case study at Boun, Korea. Environ. Geol., 45(4): 457-465. https://doi.org/10.1007/s00254-003-0897-8

Lu, D. and Li, G. 2004. Brazilian Amazonia : Mapping Soil Erosion Risk in Rondo Using RUSLE. Remote Sens. GIS, 5: 499-512.

Milentijević, N., Ostojic, M., Fekete, R., Kalkan, K., Ristic, D., Bacevic, N.R., Stevanovic, V. and Pantelic, M. 2021. Assessment of soil erosion rates using revised universal soil loss equation (RUSLE) and GIS in Bačka, Serbia. Pol. J. Environ. Stud., 30(6), 5175-5184. https://doi.org/10.15244/pjoes/135617

Moore, D. and Burch, G.J. 1986. DIVISION S-6. The physical basis of the length-slope factor in the universal soil loss. Soil Conserv., 50: 1294-1298.

Nandargi, S.S. and Gupta, V.K. 2018. Spatial and temporal distribution of rainfall and rainy days over the Goa State J. Energy Resour. Conv., 1(1): 1-17.

Naqvi, H.R., Mallick, J., Devi, L.M. and Siddiqui, M.A. 2012. Multi-temporal annual soil loss risk mapping employing Revised Universal Soil Loss Equation (RUSLE) model in Nun Nadi Watershed, Uttrakhand, India. Arab. J. Geosci., 6(10): 4045-4056. https://doi.org/10.1007/s12517-012-0661-z

Negese, A., Fekadu, E. and Getnet, H. 2021. Potential soil loss estimation and erosion-prone area prioritization using RUSLE, GIS, and remote sensing in Chereti watershed, Northeastern Ethiopia. Air Soil Water Res., 14: 81. https://doi.org/10.1177/11786221209858l4

Nigel, R. and Rughooputh, S.D.D.V. 2010. Soil erosion risk mapping with new datasets: An improved identification and prioritization of high erosion risk areas. CATENA, 82(3): 191-205. https://doi.org/10.1016/j.catena.2010.06.005

Nkonya, E., Mirzabev, A. and Braun, J.V. 2016. Economics of Land Degradation and Improvement: A Global Assessment for Sustainable Development. Springer, Cham. https://doi.org/10.1007/978-3-319-19168-3

NSW 2021. Southern NSW, Australia. https://www.health.nsw.gov.au/lhd/Pages/snswlhd.aspx

Obalum, S.E., Buri, M.M., Nwite, J.C., Hermansah, Y., Igwe, C.A. and Wakatsuki, T. 2012. Soil degradation: Induced decline in productivity of sub-Saharan African soils: The prospects of looking downwards the lowlands with the Sawah eco-technology. Appl. Environ. Soil. Sci., 20: 1-10. https://doi.org/10.1155/2012/673926

Odorico, P.D., Okin, G.S. and Bestelmeyer, B.T. 2011. A synthetic review of feedback and drivers of shrub encroachment in arid grasslands. Ecohydrology, 5(5); 520-530. https://doi.org/10.1002/eco.259

Pal, S.C. and Chakrabortty, R. 2019. Simulating the impact of climate change on soil erosion in a sub-tropical monsoon-dominated watershed based on RUSLE, SCS runoff, and MIROC5 climatic model. Adv. Space Res., 64(2): 352-377. https://doi.org/10.1016/j.asr.2019.04.033

Patwardhan, S.K. and Asnani, G.C. 2000. Meso-scale distribution of summer monsoon rainfall near the Western Ghats, India. Int. J. Climatol., 20(5): 575-581. https://doi.org/10.1002/(SICI)1097-0088(200004)20:5<575::AID-JOC509>3.0.CO;2-6

Peng, X.Y. and Shao, J.E. 2009. Assessment of soil erosion using RUSLE and GIS: A case study of the Maotiao River watershed, Guizhou Province, China. Water, 145: 1643-1652. https://doi.org/10.1007/s00254-008-1261-9

Periyasamy, R. 2017. Estimation of soil erosion vulnerability in Perambalur Taluk, Tamil Nadu, using revised universal soil loss equation model (RUSLE) and geo-information technology. Sustainability, 11: 139-152

Phinzi, K. and Ngetar, N.S. 2019. The assessment of water-borne erosion at catchment level using GIS-based RUSLE and remote sensing: A review. Int. Soil Water Conserv. Res., 7(1): 27-46. https://doi.org/10.1016/j.iswcr.2018.12.002

Poesen, J., Nachtergaele, J., Verstraeten, G. and Valentin, C. 2003. Gully erosion and environmental change: Importance and research needs. CATENA, 50(2-4): 91-133. https://doi.org/10.1016/S0341-8162(02)00143-1

Polykretis, C., Alexakis, D.D., Grillakis, M. and Manaudakis, S. 2020. Assessment of intra-annual and interannual variabilities of soil erosion in Crete Island (Greece) by incorporating the dynamic "nature" of R and C factors in RUSLE. Remote Sens., 12(15): 2439.

Prabhu Gaonkar, V.G., Nadaf, F.M., Balajiraokapale, V. and Gaonkar, S.M. 2022. Analyzing spatiotemporal changes in land surface temperature of coastal Goa using LANDSAT satellite data BT. In: Chatterjee, U., Akanwa, A.O., Kumar, S., Singh, S.K. and Roy, A.D. (eds.), Ecological Footprints of Climate Change: Adaptive Approaches and Sustainability, Springer International Publishing, Cham, pp. 517-541. https://doi.org/10.1007/978-3-031-15501-7_20

Prasannakumar, V., Shiny, R., Geetha, N. and Vijith, H. 2011a. Spatial prediction of soil erosion risk by remote sensing, GIS and RUSLE approach: A case study of Siruvani river watershed in Attapady valley, Kerala, India. Environ. Earth Sci., 64(4): 965-972. https://doi.org/10.1007/s12665-011-0913-3

Prasannakumar, V., Vijith, H., Abinod, S. and Geetha, N. 2012. Estimation of soil erosion risk within a small mountainous sub-watershed in Kerala, India, using Revised Universal Soil Loss Equation (RUSLE) and geo-information technology. Geosci. Front. 3(2): 209-215. https://doi.org/10.1016/j.gsf.2011.11.003

Prasannakumar, V., Vijith, H., Geetha, N. and Shiny, R. 2011b. Regional scale erosion assessment of a sub-tropical highland segment in the Western Ghats of Kerala, South India. Water Resources Management, 25(14): 3715-3727. https://doi.org/10.1007/s11269-011-9878-y

Quarishi, A.M.F. 2014. Soil erosion risk prediction with RS and GIS for the northwestern part of Hebei province, China. J. Appl. Sci., 12: 669. https://doi.org/10.3923/jas.2003.659.669

Quiquampoix, H. 2008. Enzymes and proteins, interactions with soil-constituent surfaces. Encycloped. Earth Sci. Ser., 8: 210-216. https://doi.org/10.1007/978-1-4020-3995-9_189

Rabia, A.H. 2016. Mapping Soil Erosion Risk Using Rusle, Gis, and Remote Sensing Techniques. The 4th International Congress of ECSSS, EUROSOIL, 2-6 July 2012, Bari, Italy,

Ravi, S., D'Odorico, P., Wang, L., White, C.S., Okin, G.S., Macko, S.A. and Collins, S.L. 2009. Post-fire resource redistribution in desert grasslands: A possible negative feedback on land degradation. Ecosystems, 12(3): 434-444. https://doi.org/10.1007/s10021-009-9233-9

Selvakumar, N.N.R. 2018. Influence of land use changes on spatial erosion pattern, a time series analysis using RUSLE and GIS: The cases of Ambuliyar sub-basin, India. Acta Geophysica, 2. https://doi.org/10.1007/s11600-018-0186-2

Solanky, V., Sangeeta, S. and Katiyar, S.K. 2018. Land surface temperature estimation using remote sensing data. Hydrol. Model., 16: 343-351. https://doi.org/10.1007/978-981-10-5801-1_24

Swarnkar, S., Malini, A., Tripathi, S. and Sinha, R. 2017. Assessment of uncertainties in soil erosion and sediment yield estimates at ungauged basins: An application to the Garra River basin, India. Hydrol. Earth Syst. Sci., 22(4): 2471-2485.

Tayebi, S., Mohammadi, H., Shamsipoor, A., Tayebi, S., Alavi, S.A. and Hoseinioun, S. 2019. Analysis of land surface temperature trend and climate resilience challenges in Tehran. Int. J. Environ. Sci. Technol., 16(12): 8585-8594. https://doi.org/10.1007/s13762-019-02329-z

Taylor, M.S. 2009. Innis Lecture: Environmental crises: Past, present, and future. Canad. J. Econ., 42(4): 1240-1275. https://doi.org/10.1111/j.1540-5982.2009.01545.x

Taylor, N. and Millar, H. 2009. Long bugs to short plants: The Lon protease in protein stability and thermotolerance. New Phytol., 181: 505-508.

Terranova, O., Antronico, L., Coscarelli, R. and Iaquinta, P. 2009. Soil erosion risk scenarios in the Mediterranean environment using RUSLE and GIS: An application model for Calabria (southern Italy. Geomorphology, 112(3–4): 228-245. https://doi.org/10.1016/j.geomorph.2009.06.009

Thapa, P. 2020. Spatial estimation of soil erosion using RUSLE modeling: A case study of Dolakha district, Nepal. Environ. Syst. Res., 9(1): 177. https://doi.org/10.1186/s40068-020-00177-2

Thomas, J., Joseph, S. and Thrivikramji, K.P. 2018a. Assessment of soil erosion in a tropical mountain river basin of the southern Western Ghats, India, using RUSLE and GIS. Geosci. Front., 9(3): 893-906. https://doi.org/10.1016/j.gsf.2017.05.011

Thomas, J., Joseph, S. and Thrivikramji, K.P. 2018b. Estimation of soil erosion in a rain shadow river basin in the southern Western Ghats, India using RUSLE and transport limited sediment delivery function, 6. 2018. Int. Soil Water Conserv. Res., 6(2): 111-122. https://doi.org/10.1016/j.iswcr.2017.12.001

Tian, Y.C., Zhou, Y.M., Wu, B.F. and Zhou, W.F. 2009. Risk assessment of water soil erosion in the upper basin of Miyun Reservoir, Beijing, China. Environ. Geol., 57(4): 937-942. https://doi.org/10.1007/s00254-008-1376-z

Tosic, R., Dragicevic, S., Kostadinov, S. and Dragovic, N. 2011. Assessment of soil erosion potential by the USLE method: Case study, Republic of Srpska-BiH. Fresenius Environ. Bull., 20(8): 1910-1917.

United Nations Convention to Combat Desertification (UNCCD) 2017. The Global Land Outlook. UNCCD & Partners, Bonn, Germany, pp. 1-340.

Vi, V. and World, T.A. 1950. Encyclopedia of World History. Ancient World, 1: 1-3.

Wagari, M. and Tamiru, H. 2021. RUSLE model based annual soil loss quantification for soil erosion protection: A case of Fincha catchment, Ethiopia. Air Soil Water Res., 14: 234. https://doi.org/10.1177/11786221211046234

Wischmeier, W.H. 1959. A rainfall erosion index for a universal soil-loss equation. Soil Sci. Sci. Am. J., 23(3): 246-249. https://doi.org/10.2136/sssaj1959.03615995002300030027x

Yassoglou, N., Tsadilas, C. and Kosmas, C. 2017. Land Degradation and Desertification. In Yassoglou, N., Tsadilas, C. and Kosmas, C. (eds), The Soils of Greece, Springer, Cham, pp. 87-96. https://doi.org/10.1007/978-3-319-53334-6_10

Yolanda, S. and Mart, A. 2021. Remote sensing calculation of the influence of wildfire on erosion in high mountain areas. *Agronomy*, *11*(8): 1459.

Yuksel, A., Gundogan, R. and Akay, A.E. 2008. Using the remote sensing and GIS technology for erosion risk mapping of Kartalkaya dam watershed in Kahramanmaras, Turkey. Sensors, 8(8): 4851-4865. https://doi.org/10.3390/s8084851

Zhao, W.W., Fu, B.J. and Chen, L.D. 2012. A comparison between soil loss evaluation index and the C-factor of RUSLE: A case study in the Loess Plateau of China. Hydrol. Earth Syst. Sci., 16(8): 2739-2748. https://doi.org/10.5194/hess-16-2739-2012

ORCID DETAILS OF THE AUTHORS

V. G. Prabhu Gaonkar: https://orcid.org/0000-0002-2252-8274
F M Nadaf: https://orcid.org/0000-0002-5846-4591
Vikas Kapale: https://orcid.org/0000-0002-3069-6542

Nature Environment and Pollution Technology
An International Quarterly Scientific Journal

p-ISSN: 0972-6268
(Print copies up to 2016)
e-ISSN: 2395-3454

Vol. 23 | No. 1 | pp. 311-319 | 2024

Original Research Paper

https://doi.org/10.46488/NEPT.2024.v23i01.026

Open Access Journal

Effective Utilization of Bio and Industry Wastes to Produce Thermal Insulation Concrete: A Novel Solution for Energy-Saving Buildings

Jerlin Regin*, Maria Rajesh Antony†, Raya Said Mohammed Al-Zaabiya**, May Darwish Ali Al Balushi**, Hamdah Ali Ahmed Al Shehhi**, Nooralsnaa Abdallah Mohammed Al-Farsi** and Athari Khalifa Handi Al-Saadi****

*Department of Civil Engineering, St. Xavier's Catholic College of Engineering, Chunkankadai, India

**Civil Engineering Department, University of Technology and Applied Sciences-Shinas, Sultanate of Oman

†Corresponding author: Maria Rajesh Antony; rajesh.amaladhas@shct.edu.om

Nat. Env. & Poll. Tech.
Website: www.neptjournal.com

Received: 05-07-2023
Revised: 24-08-2023
Accepted: 02-09-2023

Key Words:
Thermal insulation concrete
Energy saving buildings
Sustainable materials
Recycling
Waste materials

ABSTRACT

The research addressed the effective and sustainable ways to enhance the thermal insulation properties of concrete without compromising its structural integrity. Traditional methods of enhancing thermal insulation in buildings, such as using thick layers of insulation materials, can be costly and may not always be practical in certain settings. Additionally, the disposal of waste materials such as date palm fiber, shopping plastic bags, and thermocol beads presents an environmental challenge. Therefore, this study aims to investigate the potential use of these waste materials as additives in concrete to improve its thermal insulation properties while also providing a sustainable solution for waste disposal. Date palm fiber is a natural material that is widely available in the Gulf region. Plastic bags are a huge waste from the shops every day, and from the packing materials, this thermocol is a huge waste product. We have to recycle it very efficiently to protect the environment. Three types of special materials, such as thermocol beads (30%), date palm fiber (3%) & shopping plastic bag fiber (3%), were tested in this research. Thermocol beads, when used, reduce their strength and increase the thermal resistance of concrete, while date palm fiber and shopping bag waste fiber, when used, increase the strength of concrete and also increase the thermal resistance of concrete, so it is an excellent reinforcing material and thermal barrier for shopping plastic bags fiber and date palm fiber. Based on this research result, when thermocol beads are used, they prevent heat by 42 percent, while when added with date palm fiber and plastic fiber, they also block heat by an average of 30% percent; thus, all three ingredients are considered excellent thermal insulation material. The reduction in thermal conductivity was attributed to the formation of air voids and the low thermal conductivity of the waste materials. The density of the concrete decreased with the addition of the waste materials. The study suggests that the incorporation of date palm fiber, shopping bag waste fiber, and thermocol beads can be an effective way to enhance the thermal insulation properties of concrete while also providing an environmentally sustainable solution for waste disposal. It will boost green energy technology in the construction industry.

INTRODUCTION

Insulating concrete is an important way to reduce energy consumption and lower greenhouse gas emissions. The use of waste materials in concrete production is also an effective way to reduce the environmental impact of construction. By combining these two approaches, it is possible to create a more sustainable and energy-efficient building material.

Many different types of waste materials can be added to concrete to enhance its thermal insulation properties, including agricultural waste, sawdust, and fly ash. These materials are often readily available and inexpensive, making them an attractive option for builders and contractors. Enhancing thermal insulation in concrete by adding bio and industry wastes is a novel solution for energy-saving buildings that have the potential to reduce energy consumption and lower greenhouse gas emissions in the construction industry. The idea is to use waste materials to create a more sustainable and energy-efficient building material.

Concrete is one of the most commonly used building materials in the world, but it has a high thermal conductivity, which means it can allow heat to escape easily (Hagishima & Tanimoto 2013). This makes it an inefficient material for building insulation, and as a result, a lot of energy is wasted on heating and cooling buildings. To solve this problem, builders have traditionally used various types of insulating materials, such as fiberglass and foam, to improve the

insulation properties of concrete. However, these materials can be expensive and harm the environment. By adding waste materials to concrete, it is possible to create a more sustainable and cost-effective insulation solution (Karakurt et al. 2010). Agricultural waste, sawdust, and fly ash are all examples of waste materials that can be added to concrete to enhance its thermal insulation properties. These materials are often readily available and inexpensive, making them an attractive option for builders and contractors (Holt & Raivio 2005)

Agricultural waste, such as rice husks, wheat straw, and corn cobs, can be used as lightweight aggregate in concrete production. When added to concrete, it creates pockets of air that improve the insulation properties of the material. Sawdust is another waste material that can be added to concrete to improve its insulation properties. When sawdust is added to concrete, it creates small voids that trap air and reduce thermal conductivity. Fly ash, a by-product of coal-fired power plants, is another waste material that can be added to concrete to improve its insulation properties. When fly ash is added to concrete, it reduces the amount of cement needed, which lowers the carbon footprint of the concrete. It also improves the insulation properties of the material by creating a more porous structure (Asan 1998)

The study investigates the effects of using rice husk ash and sawdust ash as partial replacements for cement in concrete. The results show that both materials can significantly improve the thermal insulation properties of concrete (Asan & Sancaktar 1998). The study evaluates the sustainability of lightweight concrete made with agricultural and industrial waste aggregates. The results show that the use of waste materials in concrete production can significantly reduce the environmental impact of construction and improve building energy efficiency (Asan 2000, 2006). The review article discusses the potential of using various industrial waste by-products, such as fly ash, blast furnace slag, and silica fume, as thermal insulation materials in sustainable construction. The authors conclude that these waste materials have the potential to improve building energy efficiency and reduce environmental impact (Hlaváček et al. 2015). The study investigates the thermal properties of lightweight concrete produced with wood sawdust and polyurethane foam wastes. The results show that this type of concrete has excellent thermal insulation properties and can significantly reduce energy consumption in buildings (Petrov & Schlegel 1994). The study investigates the thermal insulation performance of concrete with rice husk ash. The results show that rice husk ash can significantly improve the thermal insulation properties of concrete (Shi et al. 2020, Singh et al. 2011). The review article discusses the use of various industrial waste materials, such as fly ash, blast furnace slag, and silica fume, as insulation materials in buildings. The authors conclude that these waste materials have the potential to reduce energy consumption and improve building sustainability (Real et al. 2016). The study investigates the thermal insulation properties of concrete with sawdust as an aggregate. The results show that sawdust concrete has excellent thermal insulation properties and can significantly reduce energy consumption in buildings (Jayamaha et al. 1996). The study investigates the development of lightweight concrete using various industrial waste materials, such as fly ash, blast furnace slag, and bottom ash. The results show that these waste materials can be effectively used to produce lightweight concrete with good thermal insulation properties (Petrov & Schlegel 1994).

The research focuses on developing energy-efficient hygrothermal bio-composites by incorporating industrial and hazardous waste materials. These composites aim to provide effective thermal insulation. The work likely involves characterizing the mechanical, thermal, and hygrothermal properties of these bio-composites to assess their suitability for energy-saving applications in construction (Muhammad et al. 2020). The study presents a novel approach to creating a thermal insulation composite using a compression method. It combines industrial solid wastes and expanded polystyrene beads, aiming to enhance thermal efficiency. The research explores a sustainable solution for repurposing waste materials and improving building insulation (Guopu et al. 2021). The research offers a comprehensive review of sustainable bio-based insulation materials for energy-efficient buildings. It examines various natural and renewable materials that can enhance thermal performance while minimizing environmental impact.

Overall, the use of waste materials in concrete production can help reduce the environmental impact of construction and create a more sustainable and energy-efficient building material. By enhancing the thermal insulation properties of concrete through the addition of waste materials, it is possible to reduce energy consumption and lower greenhouse gas emissions in the construction industry.

MATERIALS AND METHODS

The materials and methods for enhancing thermal insulation in concrete by adding date palm fiber, plastic waste fiber, and thermocol beads are as follows:

Materials

i. Cement
ii. Aggregates (such as sand, gravel, or crushed stone)
iii. Water

iv. Date palm fiber

v. Plastic waste fiber

vi. Thermocol beads

The physical properties of cement, sand, aggregate, water, date palm fiber, plastic bag waste fiber, and thermocol beads (Fig. 1 and 2), along with the corresponding experimental test results and relevant code standards, are given below,

i. Cement:
   - Physical Properties: Fineness - 350 $m^2.kg^{-1}$, initial setting time - 35 min, specific gravity – 3.10.
   - Code Standards: ASTM C150

ii. Sand:
   - Physical Properties: Water absorption–1 %, fineness modulus–2.7, specific gravity – 2.8.
   - Code Standards: ASTM C33 (concrete aggregates)

iii. Coarse Aggregate:
   - Physical Properties: Fineness modulus –6.5, specific gravity – 2.8, absorption – 1%.
   - Code Standards: ASTM C33 (concrete aggregates)

iv. Water:
   - Physical Properties: Density – 1000 $kg.m^{-3}$, pH – 7.0, chloride content -990ppm.
   - Code Standards: ACI 318 (American Concrete Institute)

v. Date Palm Fiber:
   - Physical Properties: Fiber length – 50 mm, diameter - 200 µm, tensile strength – 300 Mpa, moisture content – 12%
   - Code Standards: ASTM C1116 (fiber-reinforced concrete), ASTM D638 (standard for tensile testing).

vi. Plastic Bag Waste Fiber:
   - Physical Properties: Fiber length – 50 mm, diameter - 200 µm, tensile strength – 600 Mpa, moisture content – 5%
   - Code Standards: ASTM C1116 (fiber-reinforced concrete), ASTM D638 (standard for tensile testing).

vii. Thermocol Beads:

Fig. 1: Date palm fiber concrete.

Fig. 2: Thermocol beads concrete.

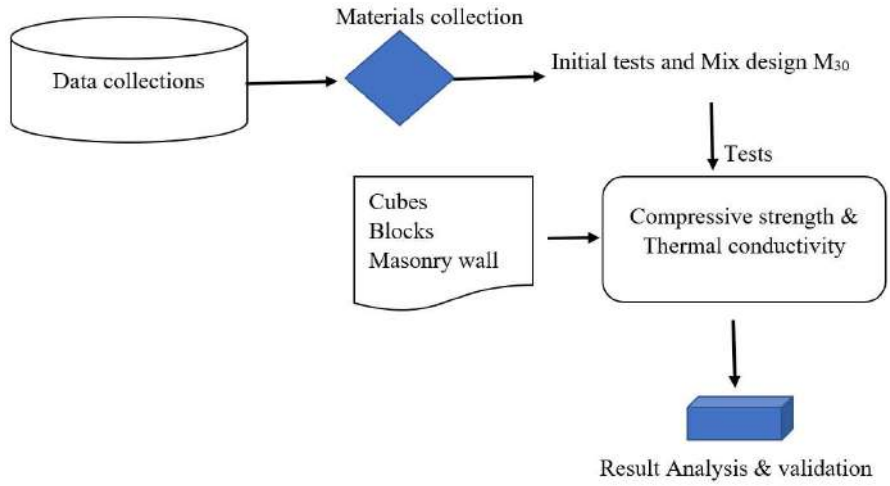

Fig. 3: Road map for the research program.

- Physical Properties: density – 20 kg.m^{-3}, compressive strength – 150 kpa, thermal conductivity –0.05 W.m^{-1}.K^{-1}, water absorption –2%
- Code Standards: ASTM C578

Methods

- Determine the appropriate proportion of each waste material to be added to the concrete mix. This can be determined through trial mixes or by consulting previous research studies.
- Prepare the waste materials for use. The date palm fiber should be cleaned, dried, and chopped into small pieces. The plastic waste fiber should be cleaned and shredded. The thermocol beads should be cleaned and separated from any impurities.
- Mix the cement, aggregates, water, and waste materials in the appropriate proportions. The mixing process should ensure that the waste materials are evenly distributed throughout the mix.
- Pour the mixed concrete into the desired mold or form.
- Allow the concrete to cure according to the manufacturer's instructions.
- Test the thermal insulation properties of the concrete using appropriate testing methods such as thermal conductivity measurements or infrared thermography.
- Compare the thermal insulation performance of the concrete with and without the added waste materials to determine the effectiveness of the insulation.

It is important to note that the specific materials and methods used may vary depending on the specific waste materials being used and the desired insulation performance (Fig. 3). Additionally, safety precautions should be taken when handling waste materials to protect workers and the environment. The addition of date palm fiber, plastic waste fiber, and thermocol beads to concrete can have positive effects on its thermal insulation properties. It may provide a sustainable solution for energy-saving buildings.

The experimental research on enhancing thermal insulation in concrete by adding date palm fiber, shopping plastic bag fiber, and thermocol beads has identified several reasons or causes for the improvements observed. These include:

- **Reduced thermal conductivity:** The addition of date palm fiber, shopping plastic bag fiber, and thermocol beads to concrete has been shown to reduce its thermal conductivity. This is because these materials have low thermal conductivity and act as insulators, which reduces the amount of heat that can pass through the concrete.
- **Increased thermal resistance:** The addition of these materials to concrete has also been shown to increase its thermal resistance. This means that the concrete is better able to resist heat transfer, which helps to keep buildings warmer in winter and cooler in summer.
- **Improved mechanical properties:** The addition of date palm fiber and shopping plastic bag fiber to concrete mixtures has been shown to improve its compressive strength and reduce its weight. This is because these fibers reinforce the concrete, making it stronger and more durable.
- **Sustainable approach:** Using waste materials such as date palm fiber, shopping plastic bag fiber, and

thermocol beads in concrete mixtures is a sustainable construction approach. This approach not only reduces waste but also reduces the need for new raw materials, which can help to reduce the environmental impact of the construction industry.

In summary, the research has identified that the addition of date palm fiber, shopping plastic bag fiber, and thermocol beads to concrete can improve its thermal insulation properties mechanical properties, and promote sustainable construction practices.

Experimental Setup

The primary measure of the thermal conductivity of date palm fiber concrete requires an experimental setup that allows for controlled temperature conditions and accurate measurement of heat transfer through the material. The overall arrangement of the various components and measuring instruments used in the setup is shown in Fig. 4. Moreover, the photographic view of the setup and the heat flow pattern are given in Fig. 5. Here is an outline of the basic steps and components required for such an experiment:

RESULTS AND DISCUSSION

Compressive Strength Results

Fig. 6 shows the results of a compressive strength test conducted on a concrete cube containing various percentages of thermocol beads, date palm fiber, and shopping plastic fiber. Based on the comparison of the optimal % substitutions in numerous experimental tests. The compressive strength values of thermocol beads (30%), date palm fiber (3%), and shopping plastic bags (3%) were compared. When comparing, the additive of 3% shopping plastic bag fiber produced the highest result, which was 30.25 $N.mm^2$. For these tests, all concrete is deemed to be M_{30} grade. Conventional concrete (CC) compressive strength was 27.25 $N.mm^{-2}$. In all of these comparisons, the strength of the thermocol beads was too low (18.8 $N.mm^{-2}$), while

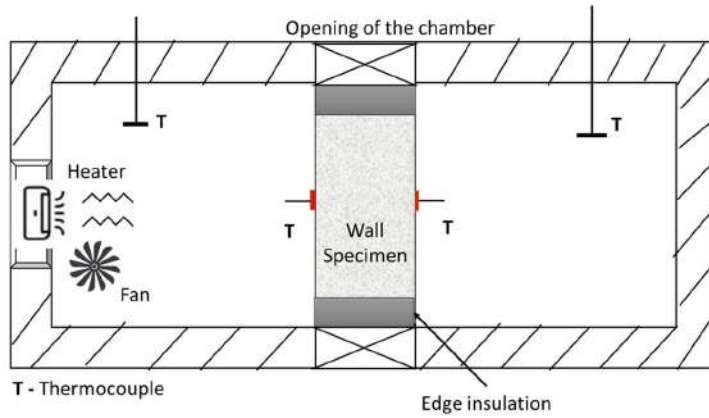

Fig. 4: Thermal conductivity experimental setup.

Fig. 5: Testing setup for finding Thermal conductivity of green masonry wall.

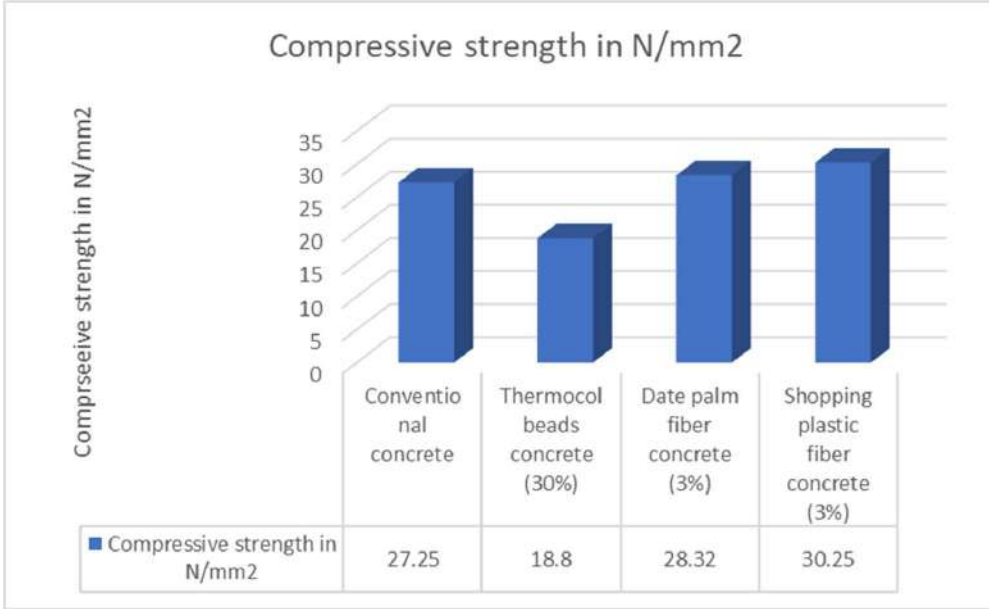

Fig. 6: Compressive strength of cube with various % of thermocol beads.

the strength of the shopping plastic bags was higher (30.25 N.mm^{-2}). When comparing these strengths to traditional concrete, shopping plastic fiber has a 10% higher percentage, date palm fiber has a 4% higher percentage, and thermocol beads have a 31% lower percentage.

Measurement of Thermal Conductivity

The thermal conductivity (k) of green and conventional concrete and slab units are determined using the thermal conductivity setup developed at UTAS-Shinas. A thermal conductivity setup is used to measure the rate of heat flow and temperature variation in and out of wall/slab units. The results of the tested concrete and wall units are shown in Fig. 7. Based on the experimental study, it was found that thermocol beads have better thermal conductivity than conventional concrete. The presence of air pockets and voids in the concrete results in a reduction in weight and a reduction in thermal conductivity.

The following equation has been used to determine the thermal conductivity of structural models.

$$\text{Thermal conductivity (k)} = \frac{Q\,\Delta X}{A\,(T_2 - T_1)}$$

Here, k represents thermal conductivity, Q represents the rate of power, ΔX represents the thickness of the wall, T_2 represents the outer wall surface

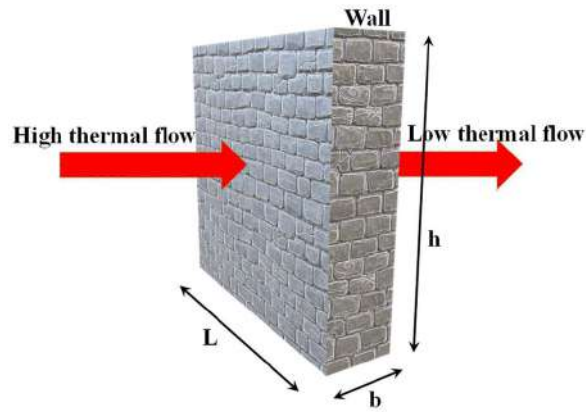

Fig. 7: Thermal flow measurement.

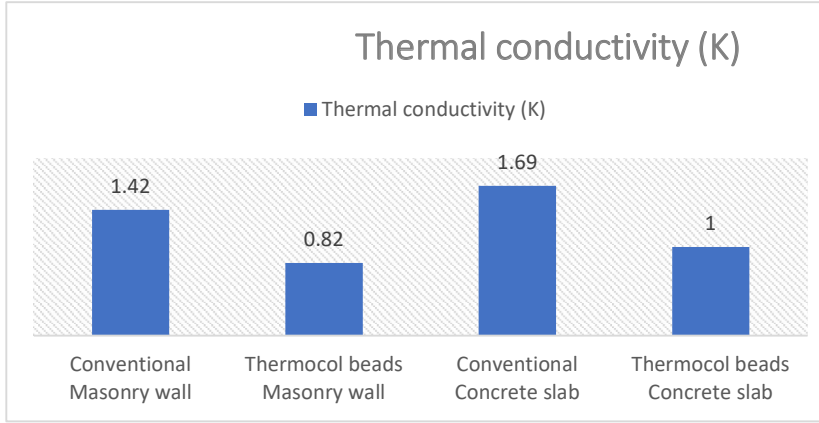

Fig. 8. Comparison of thermal conductivity between thermcol beads and CC.

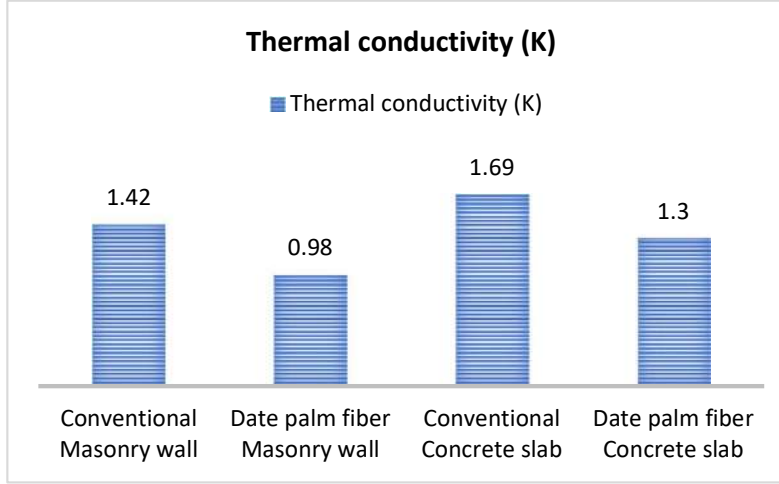

Fig. 9: Comparison of thermal conductivity between date palm fiber and CC.

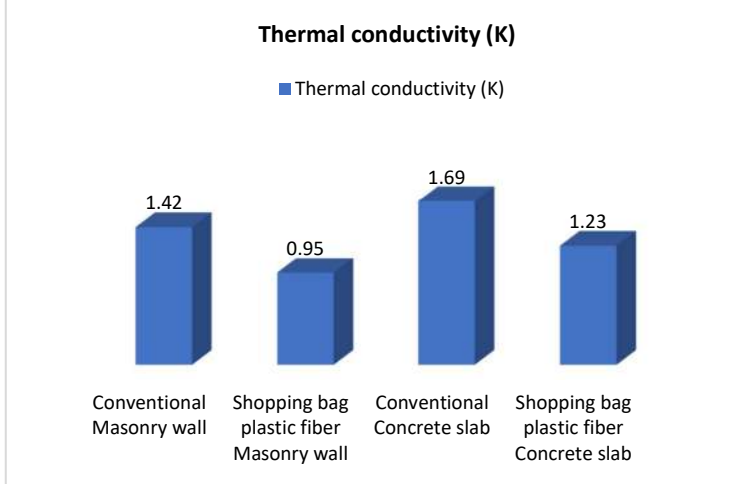

Fig. 10: Comparison of thermal conductivity between shopping plastic bag fiber and CC.

temperature, and T_1 represents the inner wall surface temperature.

Fig. 8 shows that thermocol beads wall and concrete have 42.3%, 41% higher thermal resistance than conventional wall and concrete, which was tested from the thermal conductivity setup and measured for a long duration every five min. interval. Fig. 8 shows that the value is the average value of the entire time of the experiment.

Fig. 9 shows that thermocol beads wall and concrete have 30.1%, 23% higher thermal resistance than conventional wall and concrete, which was tested from the thermal conductivity setup and measured for a long duration with every 5 min interval. Fig. 9 shows that the value is the average value of the entire time of the experiment.

Fig. 10 shows that thermocol beads wall and concrete have 33% and 27.2% higher thermal resistance than conventional wall and concrete, which was tested from the thermal conductivity setup and measured for a long duration with every 5 min interval. Fig. 10 shows that the value is the average value of the entire time of the experiment.

The research demonstrates the successful utilization of date palm fiber, shopping plastic bags, and thermocol beads in producing thermal insulation concrete. The results show that incorporating these waste materials into concrete mixtures enhances the composite‘s thermal performance and energy-saving potential. Date palm fiber improves mechanical properties and contributes to sound insulation. Plastic bags and thermocol beads contribute to lightweight and low thermal conductivity. The study justifies these materials‘ effectiveness in creating an innovative and sustainable solution for energy-efficient buildings, offering waste reduction, improved insulation, and enhanced construction possibilities.

CONCLUSION

Based on the experimental research conducted, it can be concluded that the addition of date palm fiber, shopping plastic bag fiber, and thermocol beads to concrete can significantly enhance its thermal insulation properties. The highest compressive strength of concrete was found when 3% shopping plastic fiber was added and produced the highest result of 30.25 $N.mm^{-2}$. According to the findings of thermal resistance, increasing the date palm fiber, plastic fiber, and thermocol beads % results in an increase in heat resistance. Comparing all these trials, thermocol beads have higher thermal resistance than CC, such as concrete and wall, 42.3% and 41%, respectively. The study found that the thermal conductivity of concrete decreased with the addition of these materials, increasing thermal resistance and insulation performance. The results also showed that the addition of date palm fiber and shopping plastic bag fiber in concrete mixtures improved its compressive strength and reduced its weight. This suggests that these fibers can also enhance the mechanical properties of concrete. Furthermore, the use of these materials in concrete mixtures is a sustainable approach to construction because they are recyclable and reusable waste materials. This makes them a cost-effective and environmentally friendly solution for enhancing the thermal insulation properties of buildings.

In conclusion, the experimental research supports the notion that the addition of date palm fiber, shopping plastic bag fiber, and thermocol beads to concrete is a novel and effective solution for enhancing thermal insulation in buildings and reducing energy consumption. This approach can also promote sustainable construction practices and reduce the environmental impact of the construction industry.

ACKNOWLEDGMENT

The authors are thankful to the management of the University of Technology and Applied Sciences-Shinas, Sultanate of Oman, and the Head of the Engineering and Civil Engineering Section for their continuous support and encouragement in carrying out this research.

REFERENCES

Asan, H. 1998. Effects of wall's insulation thickness and position on time lag and decrement factor. Energy Build., 28(3) 299-305.

Asan, H. 2000. Investigation of wall's optimum insulation position from maximum time lag and minimum decrement factor point of view. Energy Build., 32(2): 197-203.

Asan, H. 2006. Numerical computation of time lags and decrement factors for different building materials. Build. Environ., 41(5): 615-620.

Asan, H. and Sancaktar, Y.S. 1998. Effects of wall's thermophysical properties on time lag and decrement factor. Energy and Buildings, 28(2): 159-166.

Guopu, S., Liu, T., Li, G. and Wang, Z. 2021. A novel thermal insulation composite fabricated with industrial solid wastes and expanded polystyrene beads by compression method. J. Clean. Prod., 279: 123420.

Hagishima, A. and Tanimoto, J. 2003. Field measurements for estimating the convective heat transfer coefficient at building surfaces. Build. Environ., 38(7): 873-881.

Hlaváček, P., Šmilauer, V., Škvára, F., Kopecký, L. and Šulc, R. 2015. Inorganic foams made from alkali-activated fly ash: Mechanical, chemical and physical properties. J. Europ. Ceramic Soc., 35(2): 703-709.

Holt, E. and Raivio, P. 2005. Use of gasification residues in aerated autoclaved concrete. Cem. Concr. Res., 35(4): 796-802.

Jayamaha, S.E.G., Wijeysundera, N.E. and Chou, S.K. 1996. Measurement of the heat transfer coefficient for walls. Build. Environ., 31(5): 399-407.

Karakurt, C., Kurama, H. andTopcu, I.B. 2010. Utilization of natural zeolite in aerated concrete production. Cem. Concr. Comp., 32(1): 1-8.

Muhammad, R.A., Chen, B., Haque, A. and Shah, S.F.A. 2020. Utilization of industrial and hazardous waste materials to formulate energy-efficient hygrothermal bio-composites, J. Clean. Prod., 250: 119469.

Petrov, I. and Schlegel, E. 1994. Application of automatic image analysis

for the investigation of autoclaved aerated concrete structure. Cem. Concr. Res., 24(5): 830-840.

Real, S., Gomes, M.G., Rodrigues, A.M. and Bogas, J.A. 2016. Contribution of structural lightweight aggregate concrete to the reduction of thermal bridging effect in buildings. Construct. Build. Mater., 121: 460-470.

Shi, J., Liu, B., Liu, Y., Wang, E., He, Z., Xu, H. and Ren, X. 2020. Preparation and characterization of lightweight aggregate foamed geopolymer concretes aerated using hydrogen peroxide. Construct. Build. Mater., 256: 119442.

Singh, R., Bhoopal, R.S. and Kumar, S. 2011. Prediction of effective thermal conductivity of moist, porous materials using an artificial neural network approach. Build. Environ., 46(12): 2603-2608.

Nature Environment and Pollution Technology
An International Quarterly Scientific Journal

p-ISSN: 0972-6268
(Print copies up to 2016)
e-ISSN: 2395-3454

Vol. 23 | No. 1 | pp. 321-330 | 2024

Original Research Paper

https://doi.org/10.46488/NEPT.2024.v23i01.027

Open Access Journal

A Facile Method for Synthesis of α-Fe_2O_3 Nanoparticles and Assessment of Their Characterization

Paramjeet Dhull*, Rajesh Kumar Lohchab*†, Mikhlesh Kumari*, Kulbir Singh, Anil Kumar Bhankhar*** and Shaloo******

*Department of Environmental Science and Engineering, Guru Jambheshwar University of Science and Technology, Hisar-125001, Haryana, India

**Department of Civil Engineering, MM Engineering College, Maharishi Markandeshwar (Deemed to be University), Mullana (Ambala), 133207, Haryana, India

***Department of Bio and Nanotechnology, Guru Jambheshwar University of Science & Technology, Hisar-125001, Haryana, India

****Water Technology Centre, ICAR-Indian Agricultural Research Institute, New Delhi-110012, India

†Corresponding Author: Rajesh Kumar Lohchab; rajeshlohchab@gmail.com

Nat. Env. & Poll. Tech.
Website: www.neptjournal.com

Received: 20-06-2023
Revised: 13-08-2023
Accepted: 19-08-2023

Key Words:
α-Fe_2O_3 nanoparticles,
Hematite
XRD
SEM-EDX
Raman spectroscopy
BET

ABSTRACT

Recently, magnetic nanomaterials have gained much attention from researchers because of their various unique physical and chemical properties and usage in a wide range of technological aspects. In this study, the synthesis of α-Fe_2O_3 nanoparticles was performed by a simple co-precipitation method. The synthesis of α-Fe_2O_3 nanoparticles was carried out by mixing ferric nitrate and oxalic acid in an aqueous solution followed by evaporation, resulting in the solution's dried form. The synthesized nanoparticles were analyzed by XRD, FTIR, Raman spectra, SEM-EDX, DSC, BET, and Zeta potential for detailed examination of the morphology, structure, and other physicochemical characteristics. The XRD results confirmed that the nanoparticles formed were Hematite (α-Fe_2O_3) after the evaluation of obtained spectra compared to the Joint Committee on Powder Diffraction Standards Database (JCPDS). The FTIR spectra showed various bonds among functional groups, O-H bending, Fe-O group, and within-vibration bonds. The phase study of the α-Fe_2O_3 nanoparticles was performed by using Raman spectroscopy. SEM depicted a sphere-like or rhombohedral (hexagonal) structure, and the EDX spectrum confirmed the peaks of iron and oxygen.

INTRODUCTION

Nanotechnology, engineering, and manufacturing art of working and functionating matter at the nanoscale (1–100 nm) has emerged as an attractive option in the field of engineering and environmental science. Nanotechnology has a great beneficial potential in a wide range of fields (Lo et al. 2012) like biomedicine (Ebrahiminezhad et al. 2016), biotechnology, enzyme and protein immobilization, biosensors (Morais et al. 2009), wastewater treatment, bioremediation of heavy metals (Xu et al. 2022), optics, ceramics, electronics (Rao et al. 2000) and environmental remediation (Villanueva et al. 2009). It has been considered that nanoparticles, mainly metal oxides, are working more effectively and efficiently as adsorbents for cleaning environmental pollution because of their smaller size, large surface area, and zero generation of secondary pollutants. They can penetrate deeper contamination zones where microparticles cannot (Gurlhosur & Sreekanth 2018). Nanotechnology has been touted as a modern technology that helps in outstripping various physical and chemical property barriers of different materials in nano-forms (Masoomi et al. 2010). The synthesis of nanomaterials can be attempted by different methods like photochemical reduction, chemical reduction, spray-pyrolysis, electrodeposition, hydrothermal, co-precipitation, sol-gel, and microemulsion (Bozkurt 2020).

In recent times, iron oxide nanoparticles have attracted great attention due to their excellent thermodynamic properties, strong environmental toxicity, resistance to biological toxicity and corrosion, high stability, strong redox potential, and absorption abilities (Liu et al. 2019). Due to their unique physical properties as compared to clump material, magnetic nanoparticles have gained significant interest. The properties of a nanomaterial are greatly influenced by surface morphology, phase, and microstructure as compared with those of clump materials. However, these parameters are dependent on the quality and purity of the

phase of the synthesized nanomaterial (Qureshi et al. 2022). As a result, the importance of single-phase material can not be emaciated as it is vital for the specific measurement of different physical properties (magnetic and electrical, etc.) (Terayama et al. 2018).

Iron oxide is a renowned conventional semiconductor with a negative temperature resistance coefficient (Terna et al. 2021). The quest to prepare a homogenous mixture of iron nanoparticles has led researchers to develop various practices for the manufacturing process of iron oxide nanoparticles, such as chemical precipitation, sol-gel process, pulsed layer ablation, electro-spinning and solvent precipitation, hydrothermal, combustion technique, etc. (Farahmandjou & Soflaee 2015, Ganguli & Tokeer 2007, Subaihi & Naglah 2022). The pathway used for the synthesis of nanomaterial greatly influences the standardized physicochemical characterization of magnetite nanoparticles by affecting the crystallinity, structure, and surface area (Chircov & Vasile 2022). However, there is still a major challenge in the development of a simple and more efficient method for the synthesis of pure and homogenous magnetite particles with high dispersion and narrow-size dispensation (Terayama et al. 2018). There are two familiar crystalline phases of iron oxide (Fe_2O_3), i.e., the γ-phase has a cubic structure, maghemite, and the α-phase has a rhombohedral structure, hematite (Wang et al. 2013). The process of calcination performs the conversion of γ-phase to α-phase when the temperature reaches 400°C, and this forms α-Fe_2O_3 nanoparticles with significant grain growth (Farahmandjou & Soflaee 2015). The α-phase is considered to be the most important polymorph existing as hematite with a rhombohedral-centered hexagonal structure and a close-packed oxygen lattice (Basavegowda et al. 2017). Hematite (α-Fe_2O_3), the most stable form of iron oxide, is one of the most environment-friendly semiconductors having a band gap energy of Eg = 2.1 eV (Cao et al. 2003). It is conventionally used for gas sensors, catalysts, fine ceramics, electrodes, magnetic materials, photocatalytic activity, red pigment, and anticorrosion protective paints (Farahmandjou & Soflaee 2015). While synthesizing iron nanoparticles, some important factors must be considered, such as the size and shape of nanoparticles, intrinsic properties, surface charge and surface coating, non-toxicity, and their stability in the aqueous environment (Chircov & Vasile 2022). Therefore, the choice of a suitable synthesis method offers the ability to control the shape, size, stability, and surface coating of the nanoparticles (Ansari et al. 2022). The salt (precursor) and reactants ratio used in the chemical

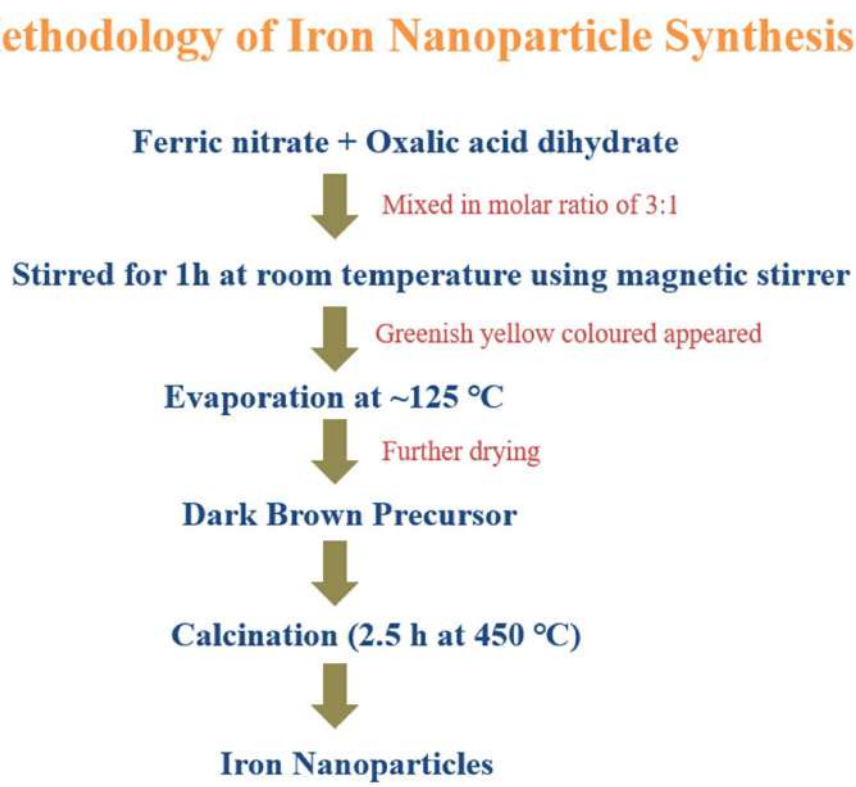

Fig. 1: Flow diagram of α-Fe_2O_3 nanoparticles synthesis.

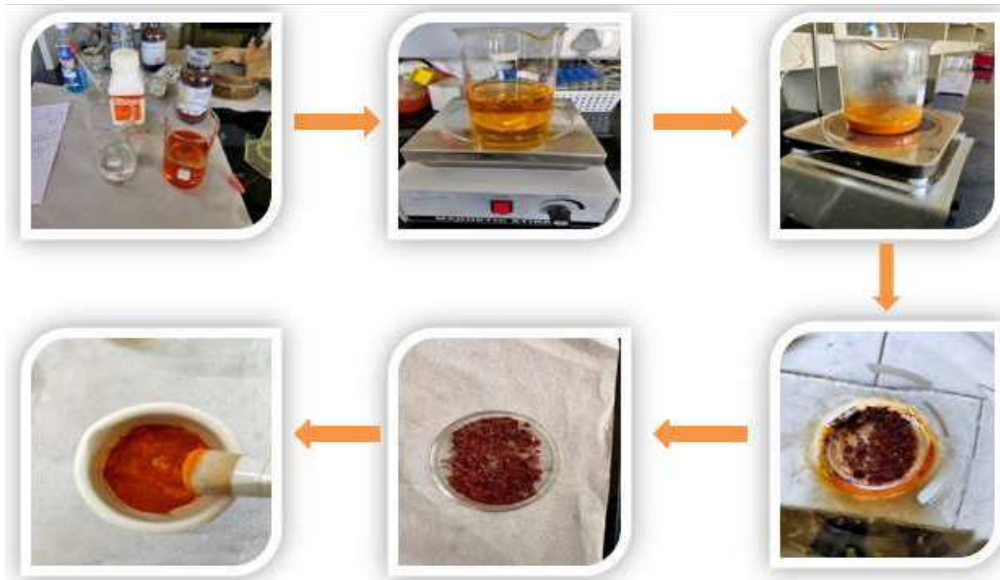

Fig. 2: Pictorial representation of methodology of α-Fe_2O_3 nanoparticles synthesis.

methods of iron nanoparticle synthesis greatly influences its composition, size, shape, and ionic strength. The mixing rate and the temperature provided during the process, along with the agitation provided, also influence the properties of the iron nanoparticles formed (Aragaw et al. 2021).

In the present study, iron oxide nanoparticles were synthesized by a simple chemical method. Analytical grade chemicals (Ferric nitrate and Oxalic acid) were used as the initial compounds, along with water as a solvent for the synthesis of nano-sized, single-phase hematite (α-Fe_2O_3). The morphological and structural characterization was performed by SEM-EDX, FTIR, XRD and Raman spectroscopy, DSC, BET, and Zeta potential.

MATERIALS AND METHODS

Synthesis Procedure of α-Fe_2O_3 Nanoparticles

The whole process of iron nanoparticle synthesis was used according to Pant et al. (2009). The whole procedure of α-Fe_2O_3 synthesis is represented in the form of a flow diagram in Fig. 1. The chemicals used for the synthesis of α-Fe_2O_3 were ferric nitrate anhydrous and oxalic acid dehydrates of analytical grade without any further purification. Nano powder synthesis process was carried out by mixing ferric nitrate and oxalic acid aqueous solutions in a molar ratio of 3:1 and stimulated at room temperature for one hour with the help of a magnetic stirrer (Fig. 2). Evaporation of this mixture was done by heating on a hot plate at temperature ~ 125°C and a greenish yellow colored precursor was formed. Further drying of the precursor formed was performed for about 1 h until the color changed from greenish yellow to dark brown. The dark brown precursor was ground to make iron oxide powder, followed by calcination for 2 and a half hours at temperatures ranging from 250-450°C.

Characterization of Synthesized α-Fe_2O_3 Nanoparticles

The prepared α-Fe_2O_3 nanoparticles were characterized with the help of instruments like XRD, SEM-EDS, FTIR, Raman spectrometer, and BET for structure and surface morphological properties and size specification of the synthesized α-Fe_2O_3 nanoparticles. An X-ray diffractometer was used to record spectra of the synthesized α-Fe_2O_3 nanoparticles for identifying the structural phase and to estimate particle size. The model used for the analysis was the Rigaku Miniflex-II diffractometer, Japan. Scanning electron microscopy (SEM) was used for morphological structure analysis of synthesized α-Fe_2O_3 nanoparticles by using an instrument with model number JSM 7610 F+, JEOL, Japan, operated at an accelerating voltage of 15kV. EDS measurement was done for the estimation of the chemical composition of the prepared sample's weight and atomic percentage. The BET analysis was performed by using Micromeritics Gemini V2.00.

The Raman spectra were recorded by a Raman spectrometer (Alpha 300, WITec Focus Innovations with an Excitation laser line of 632 nm from a He-Ne laser) at room temperature. Fourier transform infrared (FT-IR) spectra were recorded by using Spectrum Two, PerkinElmer in a range of 400 cm^{-1} to 4000 cm^{-1} wavenumbers for identifying the chemical bonds along with the functional group of the

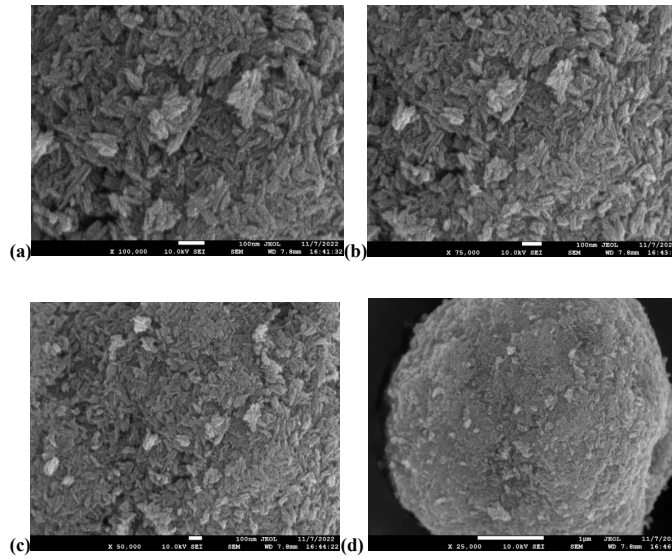

(e)

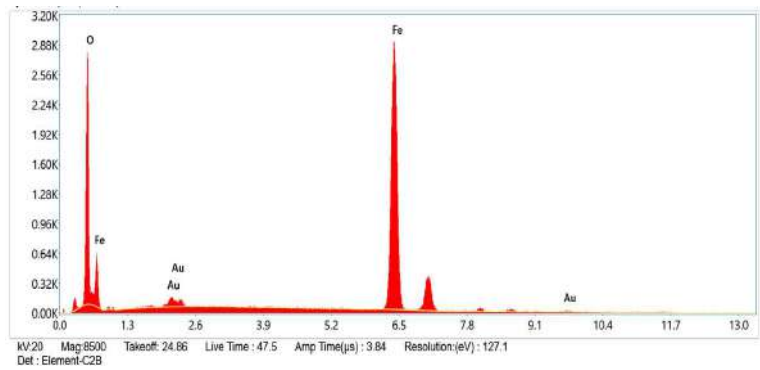

(f)

Element	Weight (%)	Atomic (%)	Error (%)	R	A	F
O K	30.9	62.0	9.9	0.8401	0.1836	1.0000
Fe K	64.8	37.3	2.5	0.9256	0.9593	1.0322
Au L	4.3	0.7	34.4	0.9660	0.9541	1.0231

Fig. 3: SEM-EDS analysis of α-Fe_2O_3 nanoparticles. (a) SEM image of α-Fe_2O_3 nanoparticles at 100000 X magnification; (b) SEM image of α-Fe_2O_3 nanoparticles at 75000 X magnification; (c) SEM image of α-Fe_2O_3 nanoparticles at 50000 X magnification; (d) SEM image of α-Fe_2O_3 nanoparticles at 25000 X magniIation; (e) depiction of EDS peaks of the elements in α-Fe_2O_3 nanoparticles; (f) Weight percentage of the elements in α-Fe_2O_3 nanoparticles.

synthesized α-Fe_2O_3 nanoparticles. Differential Scanning Calorimetry (DSC) was used for differential scanning calorimetry examination and the thermal stability of α-Fe_2O_3 nanoparticles between 0-500°C under a nitrogen atmosphere with an increase in temperature of 10°C.min^{-1}. The model used was Discovery 25/TA Instruments Waters. Zeta potential was measured with a Malvern Zeta analyzer.

RESULTS AND DISCUSSION

SEM-EDX Analysis

A scanning electron microscope (SEM) is a type of microscope that provides high-resolution images of any sample or object by scanning it with a focused beam of electrons across the surface and detecting backscattered electron signal with up to ~50000 X magnifications (Nahari et al. 2022). Energy-dispersive X-ray spectroscopy (EDX or EDXS), also known as Energy dispersive X-ray analyzer (EDA) or energy dispersive X-ray microanalysis (EDXM), is an analytical technique used to provide the elemental analysis, quantitative composition, and chemical composition of a sample (Sayed & Polshettiwar 2015). Scanning Electron Microscopy was used for the qualitative analysis of surface morphology and structure of calcined α-Fe_2O_3 nanoparticles (Fig. 3). In Fig. 3(a-d), α-Fe_2O_3 nanoparticles images at different magnifications at the nanoscale are shown. The assembly of α-Fe_2O_3 nanoparticles was compact, having a spherical or rhombohedral (hexagonal) structure. The synthesis of α-Fe_2O_3 nanoparticles had a diameter in the range of 9 nm-12.5 nm.

Energy dispersive spectroscopy (EDS) of α-Fe_2O_3 prepared by the simple chemical method is depicted in Fig. 1, which confirms the presence of iron and oxygen elements with their weight percentage in the synthesized sample. The presence of gold (Au) is because of the gold coating on the sample during the SEM analysis. The peaks of iron and oxygen are shown in the EDS graph with fewer other elements as impurities. The atomic percentage of iron and oxygen in the sample was 37.3% and 62%, respectively. The weight percentage of iron and oxygen was 64.8% and 30.9%, respectively, as shown in Fig. 3(f).

FTIR Analysis

Fourier Transformed Infrared Spectroscopy (FTIR) was used to investigate the functional groups of the synthesized α-Fe_2O_3 nanoparticles. Fig. 4 depicts the infrared spectrum of the synthesized α-Fe_2O_3 nanoparticles. The spectrum represents various kinds of chemical bonds and their functional groups present in the synthesized α-Fe_2O_3 sample. The broader band located at 3409.78 cm^{-1} wavenumbers is assigned to the O–H stretching vibration, which indicates a hydrogen bond and confirms the presence of the hydroxyl (-OH) group (Weldegebrieal & Sibhatu 2021). The stretching and bending vibration peak located at 1631.12 cm^{-1} wavenumbers represents the H-O-H bond of adsorbed water (Subaihi & Naglah 2022).

The spectrum of α-Fe_2O_3 confirmed the presence of the aromatic C-H in-plane bend stretching vibrations observed at peaks 1023.80 cm^{-1} and 1093.22 cm^{-1} (Khoshnam et al. 2021). The absorption bands at 446.42 cm^{-1} and 531.26 cm^{-1}

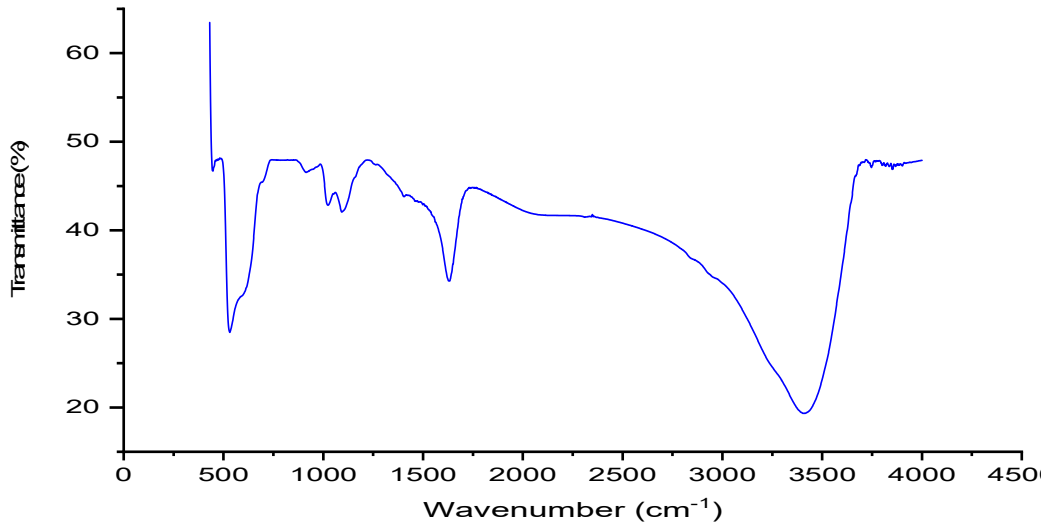

Fig. 4: Fourier Transformed Infrared Spectroscopy (FTIR) analysis of α-Fe_2O_3 nanoparticles.

signify the vibrations of the Fe-O stretching bond, which confirms the presence of α-Fe_2O_3 (Khoshnam et al. 2021).

XRD Analysis

X-ray diffraction (XRD) examination of peaks of the synthesized α-Fe_2O_3 nanoparticles was studied and shown in Fig 5. The synthesized iron oxide nanoparticles were identified as α-Fe_2O_3 (Hematite) on evaluation of the obtained spectra against the Joint Committee on Powder Diffraction Standards Database (JCPDS) manual. With the increase in temperature, the diffraction peak intensity of the samples also increases and decreases in the peak width at half maximum, indicating an improvement in crystallinity (Gurlhosur & Sreekanth 2018). The XRD pattern of the sample shows the high crystallinity of the α-Fe_2O_3 sample.

The peaks at 2θ were obtained at 30.46°, 35.86°, 43.46°, 57.46° and 63.14° as per ASTM standard for α-Fe_2O_3 nanoparticles. The peaks obtained are typical of hematite and are in relevance with (Shah 2023.), which obtained α-Fe_2O_3 nanoparticles using glucose and sucrose fuels. The XRD peaks are good indicators of the rhombohedral hematite, related to the R3c space group with unit cell parameters of a = 5.038 Å and c = 13.772 Å. Moreover, the XRD results also showed more intense and sharper peaks, which indicates the high crystalline nature of the α-Fe_2O_3 (Benhammada et al. 2020, Khoshnam et al. 2021).

Raman Analysis

Raman spectroscopy is a significant non-destructive tool to investigate the chemical and structural composition of a wide range of materials. It has been regarded as the appropriate technique for the characterization of nano-sized substances since it allows the identification of slight vibrations of nonmaterial (Benhammada et al. 2020). To further clarify the phase of the rhombohedral particles, Fig. 6 shows the Raman spectrum of the synthesized α-Fe_2O_3 nanoparticles. The spectrum of synthesized α-Fe_2O_3 nanoparticles shows three strong peaks around 227, 289, and 401 cm^{-1} and two weak bands at 494 and 601 cm^{-1}. The results are in accordance with Kumar et al. (2023). Also, the two strong peaks at 227 and 289 cm^{-1} can be attributed to the A_1g and E_g Raman modes of α-Fe_2O_3 nanoparticles, which are very near to 224 and 287 cm^{-1} peaks obtained by (Rohilla et al. 2023, Abad et al. 2020). The different vibrational modes of the material are presented.

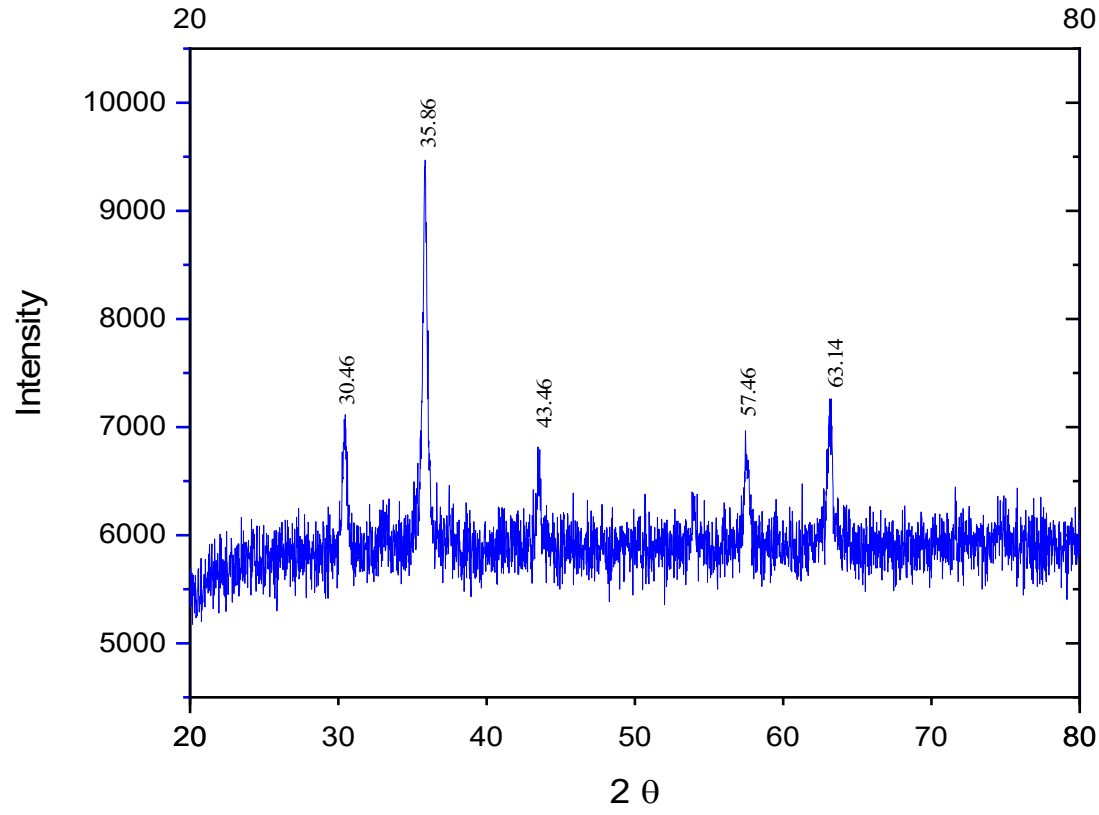

Fig. 5: X-ray Diffraction (XRD) pattern of synthesized α-Fe_2O_3 nanoparticles.

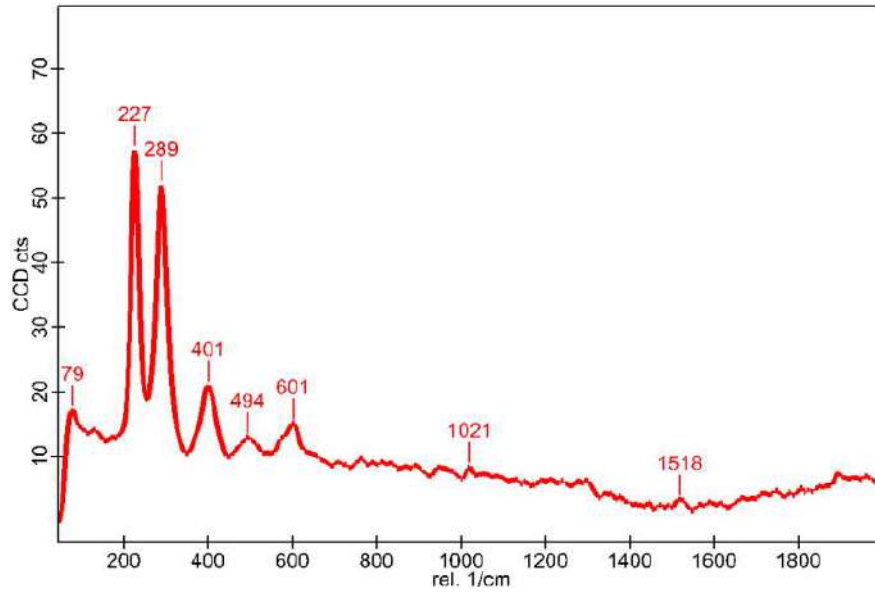

Fig. 6: Raman spectroscopy of synthesized α-Fe_2O_3 nanoparticles.

DSC Analysis

In Differential Scanning Calorimetry (DSC) analysis, the relationship between heat flow (W/g) and temperature (°C) is analyzed for the synthesized α-Fe_2O_3 nanoparticles. The DSC results are depicted in Fig. 7. The two main peaks observed were an endothermic peak at a temperature of 156.62°C with normalized enthalpy of 121.10 $J.g^{-1}$ and an exothermic peak at a temperature of 332.37°C with normalized enthalpy of 35.105 $J.g^{-1}$. The endothermic peak is associated with a phase change in the sample, which indicates that the degradation of the sample can occur at a small range of temperatures. An exothermic peak at 332.37°C showed a big step change, which indicates the stability of the sample and phase transition started. These peaks are related to the transformation of the amorphous phase to crystalline Fe_2O_3 and its transformation to α-Fe_2O_3 nanoparticles (Bozkurt 2020). The DSC profile confirms the purity of the α-Fe_2O_3 nanoparticle synthesized.

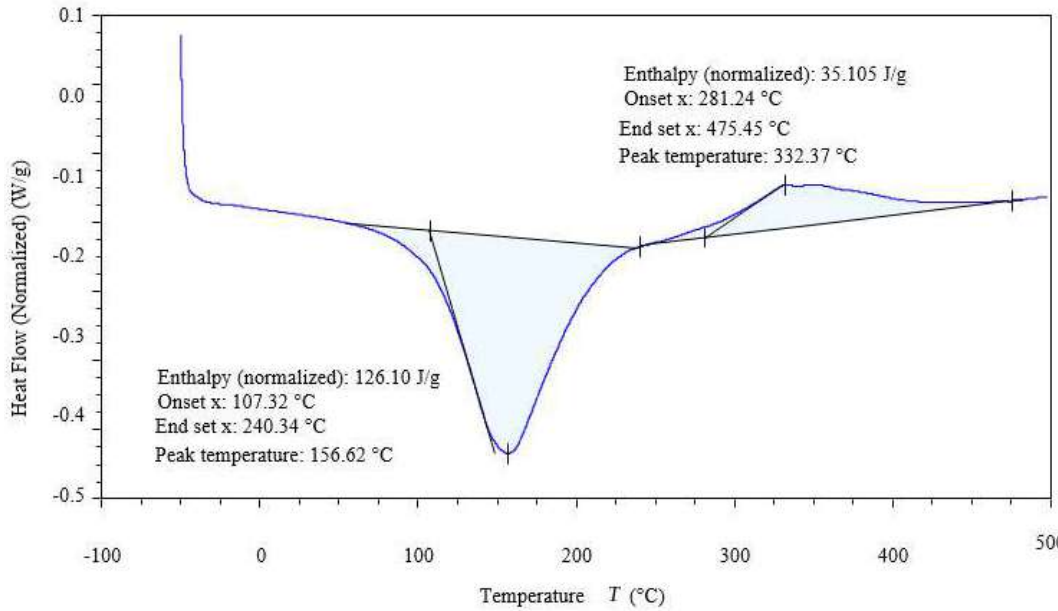

Fig. 7: Differential Scanning Calorimetry (DSC) graph of α-Fe_2O_3 nanoparticles.

Table 1: Zeta potential deviation and parameters.

		Mean [mV]	Area [%]	Standard deviation
Zeta potential [mV]	-15.0	Peak 1: –15.0	100.0	3.29
Zeta deviation [mV]	3.15	Peak 2: zero	zero	Zero
Conductivity [mS.cm^{-1}]	0.320	Peak 3: zero	zero	Zero
Quality of the result	Good			

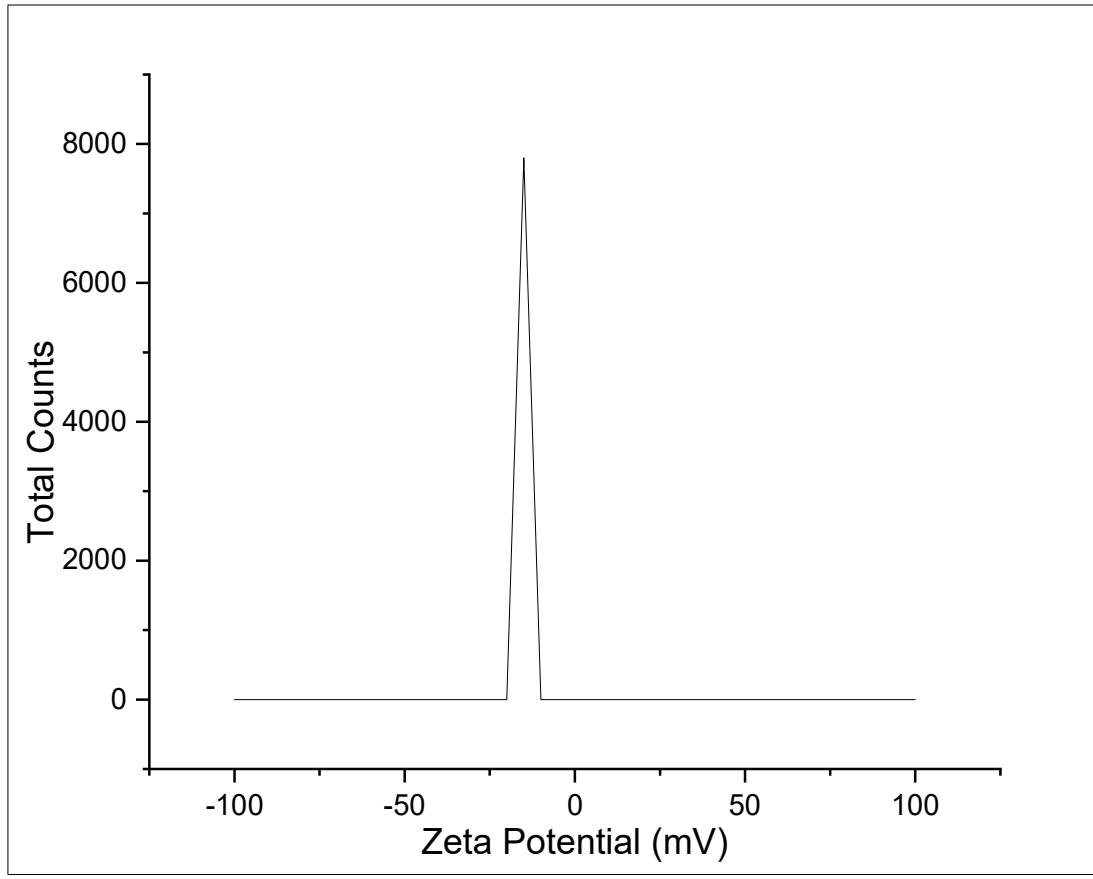

Fig. 8: Zeta potential of synthesized α-Fe_2O_3 nanoparticles.

Zeta Potential

Size is one of the most important factors in describing nanoparticle (NP) properties, although to distinguish NPs from bulk materials, substantial discussion exists on the size threshold (Lakshminarayanan et al. 2021). ζ-potential is the electrokinetic potential difference between the diffusing medium and compact layer of fluid in which nanoparticles are immersed (Kongsat et al. 2021). ζ-potential measurements were performed for the assessment of colloidal and dispersion stability. At a low ζ-potential value, dispersions in due course are cumulative because of the van der Waals force. Thus, NPs with a high absolute value of ζ-potentials are supposed to have stable dispersions, whereas those with lower values lean toward accumulation (Colla et al. 2012, Nourafkan et al. 2017). ζ-potential is used to measure the stability (ζ-potential values with greater than +30 mV and less than −30 mV) of nanoparticles in an aqueous solution. ζ-potential was measured using water as a dispersant, with a refractive index of 1.330, a dispersant dielectric constant of 78.5, and a viscosity (cP) of 0.8872. A ζ-potential of −15 mV was measured for the synthesized α-Fe_2O_3 nanoparticles, as shown in Fig. 8 and ζ-potential deviation and parameters are given in Table 1. Thus, the synthesized α-Fe_2O_3 nanoparticles are supposed to have stable dispersal potential. These negative potential charge values suggest that α-Fe_2O_3 nanoparticles can be good adsorbents for various applications.

Table 2: BET surface area of α-Fe_2O_3 nanoparticles as reported by various studies.

Method of NP synthesis	BET surface area [$m^2.g^{-1}$]	References
Chemical synthesis	79.2	(Maji et al. 2012)
Chemical synthesis	90.71	(Waseem et al. 2014)
Chemical synthesis	105.1	(Zhang et al. 2012)

BET Analysis

The N_2 adsorption-desorption isotherm characteristics were used to estimate the porous structure of the α-Fe_2O_3 nanoparticles. The BET surface area of the α-Fe_2O_3 nanoparticles was calculated as 132.9304 $m^2.g^{-1}$, which is significantly higher than the values previously reported by various chemical methods (Table 2). The pore volume of α-Fe_2O_3 nanoparticles was measured as 0.379642 $cm^3.g^{-1}$. The greater specific surface area and microporous characteristics of α-Fe_2O_3 nanoparticles would be advantageous for prospective catalytic/adsorptive usage of this substance in a variety of environmental applications.

CONCLUSION

The iron oxide nanoparticles were synthesized by a simple co-precipitation method at 450°C. The experimental design uses the simplest approach for the preparation of the α-Fe_2O_3 nanoparticles. The characterizations observed showed confirmation of the preparation of good quality α-Fe_2O_3 nanoparticles. The BET surface area of the α-Fe_2O_3 nanoparticles was 132.9304 $m^2.g^{-1}$, which is significantly higher than the other studies reported so far. The XRD spectrum confirms the rhombohedral (hexagonal) structure of α-Fe_2O_3 with highlighted peaks at 30.46°, 35.86°, 43.46°, 57.46° and 63.14°. Further, SEM also confirms the sphere-like or rhombohedral (hexagonal) shape of the characteristic nanoparticles. Moreover, the presence of iron and oxygen is confirmed by SEM-EDS. FTIR provided good quality peaks between the range of 400 cm^{-1} to 4000 cm^{-1} wavenumbers, which represented various kinds of chemical bonds and their functional groups. This also confirmed the presence of the α-Fe-O stretching mode of α-Fe_2O_3 nanoparticles. The Raman spectroscopy showed the phase change in synthesized α-Fe_2O_3 nanoparticles. The DSC analysis showed two peaks, i.e., endothermic and exothermic, confirming the phase transition and stability of the synthesized α-Fe_2O_3 nanoparticles. This further suggests that these nanoparticles can be useful in the absorption process used for wastewater treatment and enhancement of microbial diversity during anaerobic digestion, which ultimately helps in the increment of biogas production and many more applications.

REFERENCES

Abad, Z.A.K., Nemati, A., Khachatourian, A.M. and Golmohammad, M. 2020. Synthesis and characterization of rGO/Fe_2O_3 nanocomposite as an efficient supercapacitor electrode material. J. Mater. Sci. Mater. Electron., 31: 14998-15005. https://doi.org/10.1007/s10854-020-04062-7.

Ansari, M.J., Kadhim, M.M., Hussein, B.A., Lafta, H.A. and Kianfar, E. 2022. Synthesis and stability of magnetic nanoparticles. BioNanoSci., 12(2): 627-638. https://doi.org/10.1007/S12668-022-00947-5.

Aragaw, T.A., Bogale, F.M. and Aragaw, B.A. 2021. Iron-based nanoparticles in wastewater treatment: A review on synthesis methods, applications, and removal mechanisms. J. Saudi Chem. Soc., 25(8): 101280. https://doi.org/10.1016/j.jscs.2021.101280.

Basavegowda, N., Mishra, K. and Lee, Y.R. 2017. Synthesis, characterization, and catalytic applications of hematite (α- Fe_2O_3) nanoparticles as reusable nanocatalyst. Adv. Nat. Sci. Nanosci. Nanotechnol., 8(2): 025017. https://doi.org/10.1088/2043-6254/aa6885.

Benhammada, A., Trache, D., Kesraoui, M., Tarchoun, A.F., Chelouche, S. and Mezroua, A. 2020. Synthesis and characterization of α- Fe_2O_3 nanoparticles from different precursors and their catalytic effect on the thermal decomposition of nitrocellulose. Thermochim. Acta., 686: 178570. https://doi.org/10.1016/j.tca.2020.178570.

Bozkurt, G. 2020. Synthesis and characterization of α- Fe_2O_3 nanoparticles by microemulsion method. Erzincan Univ. J> Sci. Technol., 13: 890-897. https://doi.org/10.18185/erzifbed.742160.

Cao, D., He, P. and Hu, N. 2003. Electrochemical biosensors utilizing electron transfer in heme proteins immobilized on Fe_3O_4 nanoparticles. Analyst, 128(10): 1268-1274. https://doi.org/10.1039/B308242C.

Chircov, C. and Vasile, B.S. 2022. New Approaches in Synthesis and Characterization Methods of Iron Oxide Nanoparticles. In Huang, X.L.E. (eds), Iron Oxide Nanoparticles. Intechopen, NY, pp. 78-104. DOI: 10.5772/intechopen.101784.

Colla, L., Fedele, L., Scattolini, M. and Bobbo, S. 2012. Water-based Fe_2O_3 nanofluid characterization: thermal conductivity and viscosity measurements and correlation. Adv. Mech. Eng., 4: 674947. https://doi.org/10.1155/2012/674947.

Ebrahiminezhad, A., Bagheri, M., Taghizadeh, S.M., Berenjian, A. and Ghasemi, Y. 2016. Biomimetic synthesis of silver nanoparticles using microalgal secretory carbohydrates as a novel anticancer and antimicrobial. Adv. Nat. Sci.: Nanosci. Nanotechnol., 7: 015018. https://doi.org/10.1088/2043-6262/7/1/015018.

Farahmandjou, M. and Soflaee, F. 2015. Synthesis and characterization of α- Fe_2O_3 nanoparticles by simple co-precipitation method. Phys. Chem. Res., 3: 191-196. https://doi.org/10.22036/PCR.2015.9193.

Ganguli, A.K. and Tokeer, A. 2007. Nanorods of iron oxalate synthesized using reverse micelles: Facile route for α-Fe_2O_3 and Fe_2O_4 nanoparticles. J. Nanosci. Nanotechnol., 7: 2029-2035. https://doi.org/10.1166/jnn.2007.763.1.

Gurlhosur, S.H. and Sreekanth, B. 2018. Synthesis characterization of iron oxide (α-Fe2O3) nanoparticles and its application in photocatalytic reduction of cadmium (II). Int. J. Eng. Res. Technol., 7: 388-393. https://doi.org/10.14419/ijet.v7i3.34.19234.

Khoshnam, M., Farahbakhsh, J., Zargar, M. and Mohammad, A.W. 2021. α-Fe_2O_3/graphene oxide powder and thin film nanocomposites as peculiar photocatalysts for dye removal from wastewater. Sci. Rep., 11(1): 20378. https://doi.org/10.1038/s41598-021-99849-x.

Kongsat, P., Kudkaew, K., Tangjai, J., O'Rear, E.A. and Pongprayoon, T. 2021. Synthesis of structure-controlled hematite nanoparticles by a surfactant-assisted hydrothermal method and property analysis. J. Phys. Chem. Solids, 148: 109685. https://doi.org/10.1016/j.jpcs.2020.109685.

Kumar, P., Mathpal, M.C, Inwati, G.K., Kumar, S., Duvenhage, M., Roos, W.D. and Swart, H.C. 2023. Study of defect-induced chemical modifications in spinel zinc-ferrites nanostructures by in-depth XPS

investigation. Magnetochemistry, 9(1): 20. https://doi.org/10.3390/magnetochemistry9010020.

Lakshminarayanan, S., Shereen, M.F., Niraimathi, K.L. and Brindha, P. 2021. One-pot green synthesis of iron oxide nanoparticles from Bauhinia tomentosa: Characterization and application towards synthesis of 1, 3 diolein. Sci. Rep., 11(1): 1-13. https://doi.org/10.1038/s41598-021-87960-y.

Liu, M., Huang, W., Wang, Z., Wu, S. and Liu, R. 2019. A novel rapid-combustion process for the preparation of magnetic α-Fe2O3 nanoparticles. AIP Adv., 9: 0-6. https://doi.org/10.1063/1.5126660.

Lo, H.M., Chiu, H.Y., Lo, S.W. and Lo, F.C. 2012. Effects of micro-nano and non-micro-nano MSWI ashes addition on MSW anaerobic digestion. Bioresour. Technol., 114: 90-94. https://doi.org/10.1016/j.biortech.2012.03.002.

Maji, S.K., Mukherjee, N., Mondal, A. and Adhikary, B. 2012. Synthesis, characterization and photocatalytic activity of α- Fe_2O_3 nanoparticles. Polyhedron, 33: 145-149. https://doi.org/10.1016/j.poly.2011.11.017.

Masoomi, M.Y., Mahmoudi, G. and Morsali, A. 2010. Sonochemical syntheses and characterization of new nanorod crystals of mercury (II) metal-organic polymer generated from polyimine ligands. J. Coord. Chem., 63: 1186-1193. https://doi.org/10.1080/00958971003721226.

Morais, V.A., Verstreken, P., Roethig, A., Smet, J., Snellinx, A., Vanbrabant, M., Haddad, D., Frezza, C., Mandemakers, W., Vogt-Weisenhorn, D., Van Coster, R., Wurst, W., Scorrano, L. and De Strooper, B. 2009. Parkinson's disease mutations in PINK1 result in decreased Complex I activity and deficient synaptic function. EMBO Mol. Med., 1: 99-111. https://doi.org/10.1002/emmm.200900006.

Nahari, M.H., al Ali, A., Asiri, A., Mahnashi, M.H., Shaikh, I.A., Shettar, A.K. and Hoskeri, J. 2022. Green synthesis and characterization of Iron nanoparticles synthesized from aqueous leaf extract of Vitex leucoxylon and its biomedical applications. Nanomaterials, 12(14): 2404. https://doi.org/10.3390/nano12142404.

Nourafkan, E., Asachi, M., Gao, H., Raza, G. and Wen, D. 2017. Synthesis of stable iron oxide nanoparticle dispersions in high ionic media. J. Ind. Eng. Chem., 50: 57-71. https://doi.org/10.1016/j.jiec.2017.01.026.

Pant, P., Naik, B.D. and Ghosh, N.N. 2009. Synthesis of α- Fe_2O_3 nanopowder by simple chemical method. Mater. Technol., 24(4): 213-216. https://doi.org/10.1179/175355509X387183.

Qureshi, A.A., Javed, S., Javed, H.M.A., Jamshaid, M., Ali, U. and Akram, M.A. 2022. Systematic investigation of structural, morphological, thermal, optoelectronic, and magnetic properties of high-purity hematite/magnetite nanoparticles for optoelectronics. Nanomaterials, 12: 1635. https://doi.org/10.3390/nano12101635.

Rao, C.N.R., Kulkarni, G.U., Thomas, P.J. and Edwards, P.P. 2000. Metal nanoparticles and their assemblies. Chem. Soc. Rev., 29: 27-35. https://doi.org/10.1039/A904518J.

Rohilla, M., Saxena, A. and Tyagi, Y.K. 2023. Facile synthesis of rGO/Fe_2O_3 nanocomposite and its combination with aerosol forming composite for ultra-fast fire extinguishment. J. Mater. Sci., 1-16. https://doi.org/10.1007/S10853-022-08130-7.

Sayed, F.N. and Polshettiwar, V. 2015. Facile and sustainable synthesis of shaped iron oxide nanoparticles: Effect of iron precursor salts on the shapes of iron oxides. Sci. Rep., 5(1): 9733. https://doi.org/10.1038/srep09733.

Shah, R.K., 2023. Efficient photocatalytic degradation of methyl orange dye using facilely synthesized α- Fe_2O_3 nanoparticles. Arab. J. Chem., 16(2): 104444. https://doi.org/10.1016/j.arabjc.2022.104444.

Subaihi, A. and Naglah, A.M. 2022. Facile synthesis and characterization of Fe_2O_3 nanoparticles using L-lysine and L-serine for efficient photocatalytic degradation of methylene blue dye. Arab. J. Chem., 15: 103613. https://doi.org/10.1016/j.arabjc.2021.103613.

Terayama, K., Yamashita, T., Oguchi, T. and Tsuda, K. 2018. Fine-grained optimization method for crystal structure prediction. NPJ Comput. Mater., 4: 32. https://doi.org/10.1038/s41524-018-0090-y.

Terna, A.D., Elemike, E.E., Mbonu, J.I., Osafile, O.E. and Ezeani, R.O. 2021. The future of semiconductors nanoparticles: Synthesis, properties and applications. MSEB, 272: 115363. https://doi.org/10.1016/j.mseb.2021.115363.

Villanueva, A., Cãete, M., Roca, A.G., Calero, M., Veintemillas-Verdaguer, S., Serna, C.J., Del Puerto Morales, M. and Miranda, R. 2009. The influence of surface functionalization on the enhanced internalization of magnetic nanoparticles in cancer cells. Nanotechnology, 20: 115103. https://doi.org/10.1088/0957-4484/20/11/115103.

Wang, B., Wei, Q. and Qu, S. 2013. Synthesis and characterization of uniform and crystalline magnetite nanoparticles via oxidation-precipitation and modified co-precipitation methods. Int. J. Electrochem. Sci., 8: 3786-3793.

Waseem, M., Munsif, S. and Rashid, U. 2014. Physical properties of α-Fe_2O_3 nanoparticles fabricated by modified hydrolysis technique. Appl. Nanosci., 4: 643-648. https://doi.org/10.1007/s13204-013-0240-y.

Weldegebrieal, G.K. and Sibhatu, A.K. 2021. Photocatalytic activity of biosynthesized α- Fe_2O_3 nanoparticles for the degradation of methylene blue and methyl orange dyes. Optik, 241: 167226. https://doi.org/10.1016/j.ijleo.2021.167226.

Xu, W., Yang, T., Liu, S., Du, L., Chen, Q., Li, X., Dong, J., Zhang, Z., Lu, S., Gong, Y., Zhou, L., Liu, Y. and Tan, X. 2022. Insights into the synthesis, types and application of iron nanoparticles: The overlooked significance of environmental effects. Environ. Int., 158: 106980. https://doi.org/10.1016/j.envint.2021.106980.

Zhang, G.Y., Feng, Y., Xu, Y.Y., Gao, D.Z. and Sun, Y.Q. 2012. Controlled synthesis of mesoporous α- Fe_2O_3 nanorods and visible light photocatalytic property. Mater. Res. Bull., 47: 625-630. https://doi.org/10.1016/j.materresbull.2011.12.032.

Nature Environment and Pollution Technology
An International Quarterly Scientific Journal

p-ISSN: 0972-6268
(Print copies up to 2016)
e-ISSN: 2395-3454

Vol. 23 | No. 1 | pp. 331-339 | 2024

Original Research Paper

https://doi.org/10.46488/NEPT.2024.v23i01.028

Open Access Journal

Water Resource Impacts of Irrigation: The Case of the Main Irrigation Canal from the M'Pourie Plain to Rosso in Mauritania

Mewgef El Ezza dite Hanane Djieh Cheikh Med Fadel*(**)† B. A. Dick(***), E. C. S'Id****, M. B. Ammar**, Y. M. Sidi**, L. S. Mohamed*(**), A. Semesdy***, M. L. Yehdhih* and M. Fekhaoui***

*Geo-Biodiversity and Natural Patrimony Laboratory, Scientific Institute, Mohamed V University, Rabat, Morocco, 4 Av. Ibn Batouta, BP 1014 RP, Rabat, Morocco

**Research Unit of the Water, Pollution, Environment, University of Nouakchott, Av. 5265+F22, BP 880, Nouakchott, Mauritania

***National Laboratory for the Quality Control of Medicines, Mauritania

****Research Unit: Membrane, Material, Environment and Aquatic Environment (2MEMA)/FST, University of Nouakchott, Av. 5265+F22, BP 880, Nouakchott, Mauritania

†Corresponding author: Mewgef El Ezza dite Hanane Djieh Cheikh Med Fadel; hananedieh@gmail.com

Nat. Env. & Poll. Tech.
Website: www.neptjournal.com

Received: 26-07-2023
Revised: 09-09-2023
Accepted: 10-09-2023

Key Words:
Water resource
Irrigation water quality
Irrigation
M'Pourie plain

ABSTRACT

An important factor in determining agricultural production is the availability of irrigation water in the main canal of the M'Pourie plain. This factor affects both the intensification of crops and the size of the irrigation areas. The main Senegal River canal in Rosso, Mauritania, runs across the Plaine of M'Pourie. This study aims to assess the physicochemical quality of the water used for irrigation and agriculture in the main irrigation canal on the M'Pourie plain. The measurements were made from 2021 to 2022, and the following physical and chemical parameters were monitored: pH, temperature, electrical conductivity, salt content, calcium, magnesium, sodium, and potassium; ammonium bicarbonate; chloride; nitrite; nitrate; nitrogen; sulfate; and sodium adsorption ratio (SAR). These measurements were analyzed using volumetric, spectroscopic, and spectrophotometric methods. After conducting statistical analysis and comparing the results with Moroccan quality standards for surface water utilized in irrigation, it has been discovered that the average pH value is 7.51, indicating a neutral state. However, the average nitrite and ammonium values exceed Moroccan standards at 5.16 $mg.L^{-1}$ and 0.41 $mg.L^{-1}$, respectively. The water's low mineralization is attributed to its low electrical conductivity, with an average of 52.2 $\mu S.cm^{-1}$. Based on the analysis of the Senegal River water used for irrigation in the M'Pourie plain, it has been determined that its sodium adsorption ratio and electrical conductivity classify it as belonging to class C1S1. This indicates that the water has low salinity and is excellent for irrigation, with a low risk of alkalinization.

INTRODUCTION

In many countries, the water demand now surpasses the available supply. As the world's population continues to increase, natural water shortages are becoming more frequent (Gu et al. 2019, Hussain et al. 2019). Studies indicate that by 2025, an estimated 3.5 million people worldwide may face water shortages (Guterres 2017). As a result, researchers are exploring unconventional water resources to alleviate this issue. Irrigation is identified as the main consumer of freshwater, accounting for around 80% of total freshwater use for agricultural land (Rizzo et al. 2020). It is forecast to increase by a further 15% by 2030 (Guterres 2017, World Bank 2017), which will exacerbate water crises in regions already facing shortages, such as North Africa and the Middle East, in the coming decades, a proportion of over 40% of the world's population is expected to face water stress or water scarcity, which will have a significant impact on water security (Elgallal et al. 2016). On May 25, 2020, the European Commission published a new regulation establishing minimum requirements for the reuse of water for agricultural irrigation purposes, which came into force. However, the corresponding new guidelines will be implemented from June 26, 2023, and will facilitate water reuse within the European Union (Becerra-Castro et al. 2015). According to recent statistics, agriculture consumes the largest share of water compared to industry and domestic needs (Becerra-Castro et al. 2015). It uses more than 70% of total withdrawals.

Mauritania, a Sahelian country, experiences frequent droughts and unpredictable weather patterns. It receives

minimal rainfall and has a high rate of sunshine, resulting in a scarcity of water resources. Despite these challenges, the Senegal River is a vital source of freshwater for Mauritania. The river is extensively used for drinking water and irrigation of farms along both banks. It is a crucial natural resource for the country and the sub-region, playing a significant role in socio-economic development. Unfortunately, due to population growth, human activities, and the impact of climate change in this region, the quality of the river's water is deteriorating (World Bank 2017). The issue of water quality in the Senegal River is a crucial social, economic, political, and scientific concern regarding irrigation development. The primary source of water for irrigation in Mauritania is the river's runoff. The goal of this study is to monitor the physical and chemical quality of the Senegal River's water and evaluate its appropriateness for irrigation purposes.

Additionally, this research aims to assess the impact of the river's water on the primary irrigation canal of the M'Pourie plain in Rosso, Mauritania. We analyzed various parameters, including Temperature, pH, Conductivity, Dissolved Salt Content, Chloride, Sulfate, Bicarbonates, Calcium, Magnesium, Sodium, Potassium, Ammonium, Nitrogen, Nitrate, and Nitrite. Additionally, our study aims to estimate the possible effects of the primary irrigation canal on the water resources of the M'Pourie plain in Rosso, Mauritania.

MATERIALS AND METHODS

Study Area

The study was conducted at the M'Pourie plain in Rosso (Trarza), which is the primary agricultural zone in Mauritania. It was established in the 1980s as a pilot farm and covers an expansive 1,500 hectares. The plain features a machinery department and a pumping station from the Senegal River valley, and it's divided into three brigades. The cooperatives manage 850 hectares, while the remaining area covers 1,500 hectares. The Trarza region, where the plain is located, is between latitudes 16°30' and 18°30' and longitudes 14° and 16°, with a total surface area of 33,000 km². The region is renowned for its intensive agricultural activity. To gather water samples, we selected nine sites along the edge of the primary canal of the M'Pourie plain.

Sampling

During the 2021-2022 period, sampling was carried out at nine sites along the main M'Pourie canal, with four sites in the middle of the canal (SP, CP1, CP2, CP3), four on the left bank (CST3-1-1, CS3-2-1, CS3-1, and (CS1), and one site on the right bank (CS2-1). Sampling sites were l The sampling sites, which were selected due to their proximity to pollution sources and accessibility, were situated 100 meters apart from each other. They were named as follows: Canal Principal1 (CP1), Canal Secondaire1 (CS1), Canal Principal2 (CP2), Canal Secondaire2 (CS2), Canal Principal3 (CP3), Canal Secondaire 3-1 (CS3-1), Canal Secondaire3-2 (CS3-2), Canal Secondaire Tertiaire 3-1 (CST3-1), and Station de Pompage (SP). Samples were collected in one-liter plastic bottles and kept at a temperature of 4 degrees Celsius. The analyses were conducted at the laboratory of the Water-Pollution-Environment unit, located at the

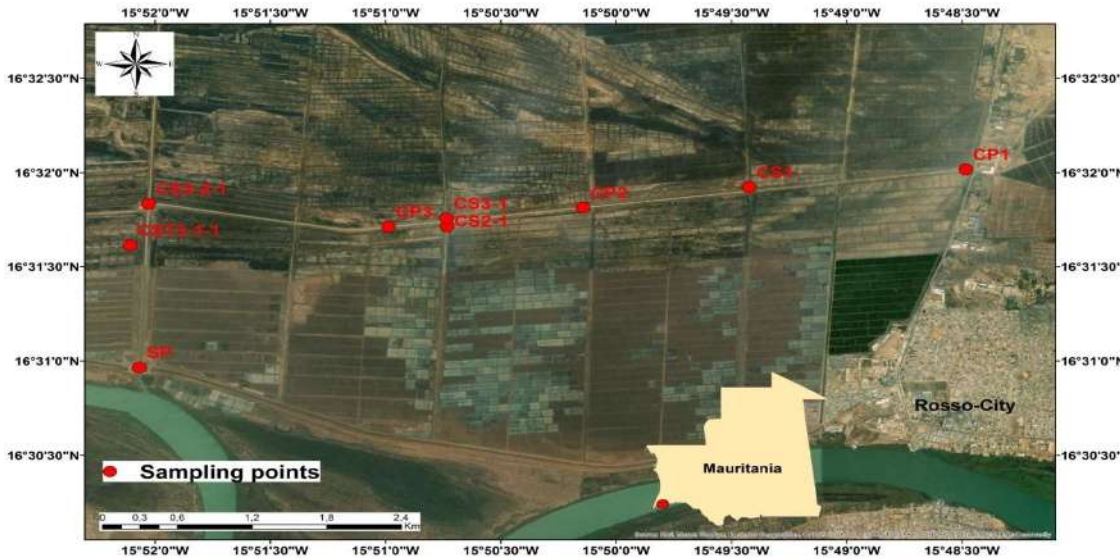

Fig. 1: Sampling sites for the main irrigation canal on the M'Pourie plain.

Table 1: Overview of physico-chemical parameters at various sites.

Parameters	CP1	CS1	CP2	CS2	CP3	CS3-1	CS3-2	CS3T-1	SP	Average	STANDARDS	
											MOROCCO	FAO
Temperature (°C)	29.5	29.3	29.1	29.1	29.1	29.1	29.1	29.1	29.1	29.1	35°C	--
pH	8.40	7.71	7.66	7.42	7.37	7.45	7.27	6.90	7.41	7.51	6.5 -8.4	6.5 -8.4
Conductivity µS/cm	50	60	50	50	50	50	50	60	50	52,22	8700	< 750
Total dissolved salt [mg.L^{-1}]	25	30	25	25	25	25	25	30	25	26,11	--	--
Calcium [mg.L^{-1}]	8.81	8.81	3.20	4.80	6.41	4.80	7.21	7.21	7.21	6.49	--	--
Magnesium [mg.L^{-1}]	2.43	3.40	4.80	3.88	2.91	4.86	1.91	2.91	2.43	3.28	--	--
Sodium [mg.L^{-1}]	18	19	18	21	20	21	18	21	19	17,44	69	--
Potassium [mg.L^{-1}]	2	4	5	6	5	2	4	5	5	4,22	--	--
Ammonium [mg.L^{-1}]	0.26	0.35	0.49	0.17	0.93	0.18	0.24	0.78	0.32	0.41	--	--
Nitrite [mg.L^{-1}]	2.64	4.12	6.43	1.15	13.69	1.32	2.31	11.22	3.63	5.16	--	--
Nitrate [mg.L^{-1}]	3.52	5.50	8.58	1.54	18.26	1.76	3.08	14.96	4.84	6.88	50	5.0 – 30
Nitrogen [mg.L^{-1}]	0.80	1.25	1.95	0.35	4.15	0.40	0.70	3.40	1.10	1.56	--	--
Sulfate [mg.L^{-1}]	38	17	37	8	90	20	14	69	4	33	250	--
Bicarbonates [mg.L^{-1}]	67.10	61.00	61.00	67.10	79.30	54.90	54.90	61.00	42.70	61.00	518	< 91,5
Chloride [mg.L^{-1}])	31.95	28.40	24.85	24.85	28.40	28.40	28.40	28.40	28.4	28.01	350	< 142

Faculty of Science and Technology of the University of Nouakchott.

Analysis Methods

After collecting the samples, we used a HANNA HI 9024 pH meter to measure temperature and pH levels. The HANNA HI 8733 conductivity meter is used to measure electrical conductivity (EC). To determine the levels of nitrates (NO_3^-), nitrites (NO_2^-), ammonium (NH_4^+), and sulfates (SO_4^{2-}), we utilize a UV-visible spectrophotometer (WEG 7100). Meanwhile, the presence of calcium (Ca^{2+}), magnesium (Mg^{2+}), chloride (Cl^-), and bicarbonates (HCO_3^-) are determined through the volumetric method in the presence of selective media. Additionally, we quantify the levels of sodium (Na^+) and potassium (K^+) using a Corning-type flame photometer. Lastly, the sodium adsorption ratio (SAR) is calculated using the following formula: $SAR= [Na^+]/\{(Ca^{++}+Mg^{++})/2\}^{1/2}$, where the concentrations of Na^+, Ca^{2+}, and Mg^{2+} ions are expressed in meq.L^{-1}.

RESULTS AND DISCUSSION

Assessment of Water Quality in the Main Irrigation Canal on the M'Pourie Plain

A comparison was made between the quality parameters of irrigation water at M'Pourie, measured at nine different sampling sites, and other studies on surface water quality used for irrigation. The study evaluated 15 parameters of M'Pourie irrigation water from nine distinct locations. Table 1 displays the results obtained for each physico-chemical parameter, which were compared to Moroccan and FAO standards. The analysis of physico-chemical parameters varied across the different samples tested.

pH and Temperature Evaluations

The pH values observed across different samples, ranging from 6.9 to 8.40 (as depicted in Fig. 1), adhere to the Moroccan regulations for ensuring the quality of water used for irrigation. The pH levels being close to neutral are advantageous for irrigation purposes. Notably, similar pH results have been reported by (Kahimba et al. 2016, N'diaye et al. 2014, Nsiala Kimfuta 2012).

Furthermore, the mean temperature value recorded in Fig. 1 is 29.1°C, which is consistent with the Moroccan regulations for water quality intended for irrigation. This temperature value is in line with what was reported by (Nsiala Kimfuta 2012).

Evaluation of Conductivity and TDS

Fig. 2 displays the conductivity values, with the maximum value being 60µS.cm^{-1} and the minimum value being 50

$\mu S.cm^{-1}$. These findings are comparable to those discovered by (Nsiala Kimfuta 2012). However, our results are lower than those obtained by (Kahimba et al. 2016). These observations indicate that the Senegal River water utilized for irrigation has poor mineralization. The average TDS value (Fig. 3) of 26.11 $mg.L^{-1}$ aligns with Moroccan and FAO standards. These values are also similar to those found by (Nsiala Kimfuta 2012), indicating that the Senegal River water used for irrigation has relatively low mineralization.

Chloride, Sulfate and Bicarbonate Evaluations

Fig. 4 displays the levels of sulfate, chloride, and bicarbonate. The research conducted on nine sites indicates that the sulfate and bicarbonate levels adhere to the regulations set by Morocco. The average sulfate value is 33 $mg.L^{-1}$, which aligns with the findings of (Akil et al. 2014). Moreover, the average chloride value is 28.01 $mg.L^{-1}$, consistent with the standards set by Moroccan and FAO. These outcomes are comparable to (N'diaye et al. 2014) research**.**

Calcium and Magnesium Evaluations

The calcium concentration values displayed in Fig. 5 are 6.49 $mg.L^{-1}$, which is unacceptable. Good-quality irrigation water should contain calcium levels ranging from 20 to 400 $mg.L^{-1}$, as per (Rodier 2009). It is worth noting that the magnesium value of 3.28 $mg.L^{-1}$ is lower than that obtained by (Nsiala Kimfuta 2012).

Sodium and Potassium Evaluations

According to Fig. 6, it can be observed that the irrigation water sampling sites exhibit an average sodium level of 17.44 $mg.L^{-1}$ and an average potassium level of 4.22 $mg.L^{-1}$. There appear to be no errors in the data presented**.**

Evaluations of Nitrogen Elements

The water samples taken from various watercourses showed significant concentrations of nitrogenous elements. These concentrations were found to exceed the quality standards set by Morocco for irrigation water, as shown in Fig. 7. Table 1 reveals that the nitrite concentrations ranged from 1.15 $mg.L^{-1}$ to 13.69 mg/L^{-1} across the nine sampled sites, exceeding the Moroccan standard limits. Our findings align with those of Mounjid et al. (2014) and are higher than those of Akatumbila et al. (2016). Nitrate levels were within

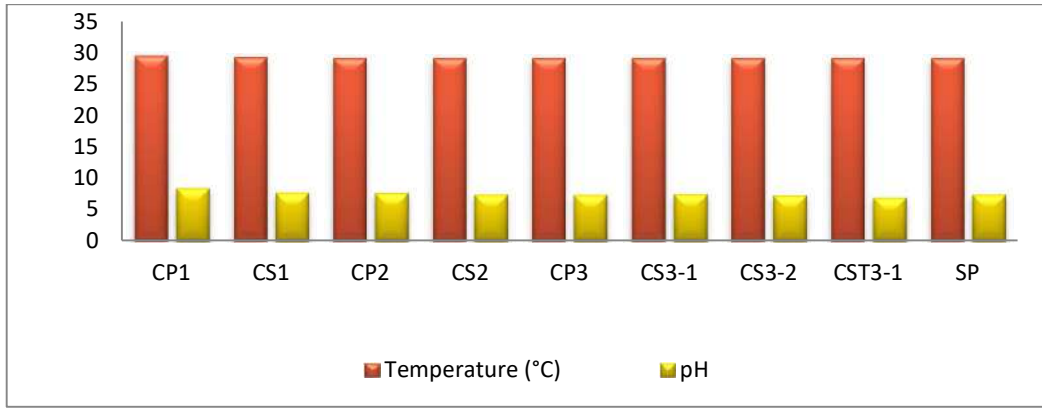

Fig. 1: pH and temperature evaluations.

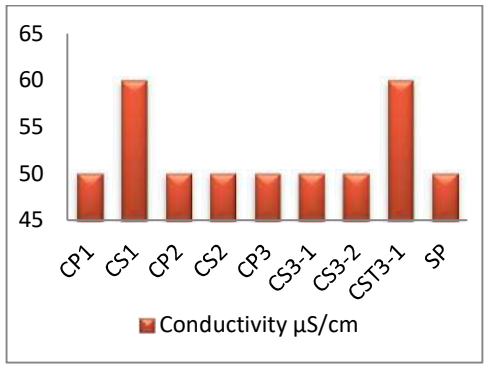

Fig. 2: Evaluation of conductivity.

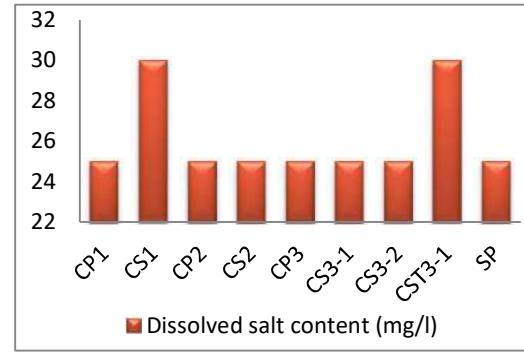

Fig. 3: Evaluation of TDS.

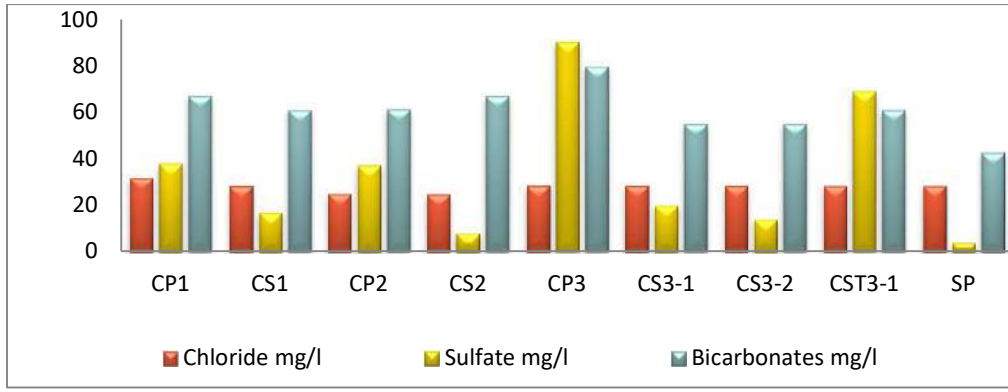

Fig. 4: Chloride, sulfate and bicarbonate values.

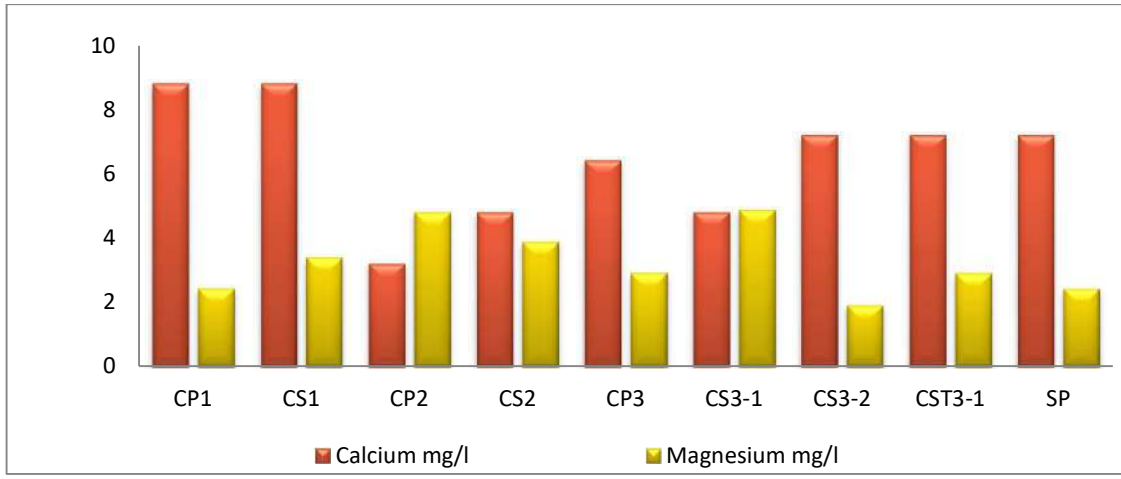

Fig. 5: Calcium and magnesium evaluations.

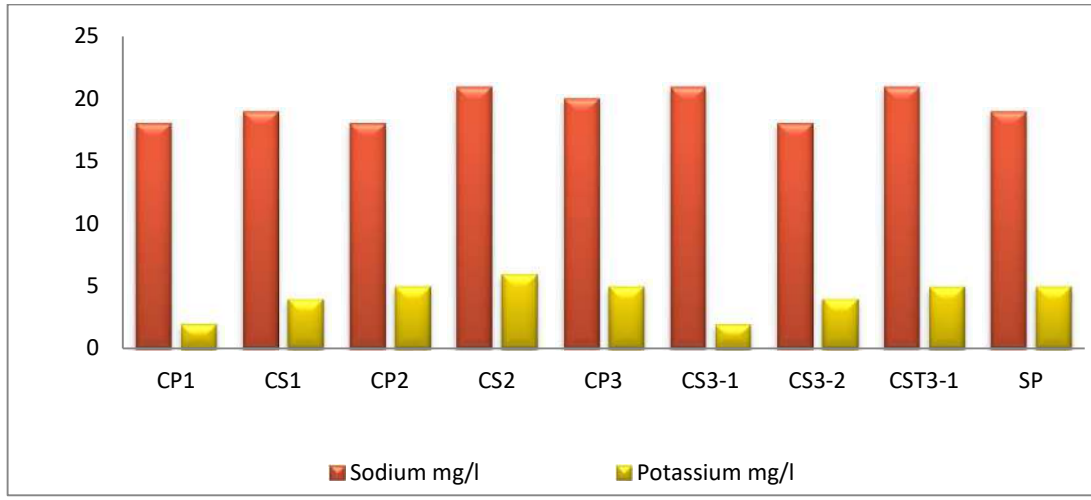

Fig. 6: Sodium and potassium evaluations.

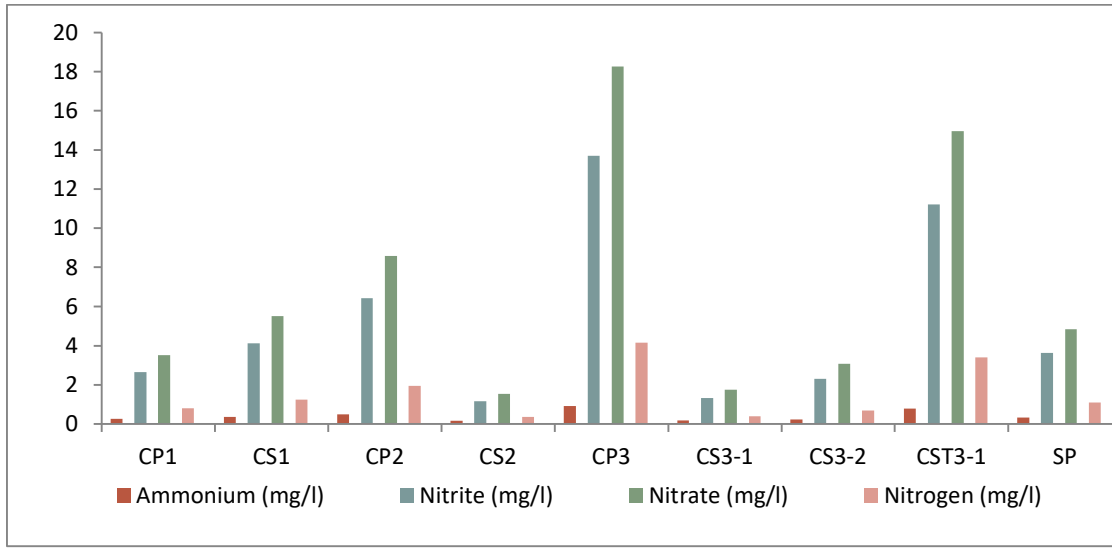

Fig. 7: Evaluations of azotic elements (ammonium, nitrites, nitrates, and nitrogen).

Table 2: The physical-chemical irrigation parameters in meq.L^{-1}.

Parameters	Symbol	Unit	CP1	CS1	CP2	CS2	CP3	CS3-1	CS3-2	CS3T-1	SP
Conductivity	CE	µS.cm^{-1}	50	60	50	50	50	50	50	60	50
Calcium	Ca^{2+}	Méq.L^{-1}	0.44	0.44	0.16	0.24	0.32	0.24	0.36	0.36	0.36
Magnesium	Mg^{2+}	méq.L^{-1}	0.19	0.27	0.38	0.31	0.23	0.38	0.15	0.23	0.19
Sodium	Na^{+}	méq.L^{-1}	1.56	1.65	1.56	1.83	1.74	1.83	1.56	1.86	1.65
Potassium	K^{+}	méq.L^{-1}	0.05	0.10	0.12	0.15	0.12	0.05	0.10	0.12	0.12
Sodium Adsorption Ratio	SAR	-------	3.92	4.16	3.92	4.61	4.38	4.61	3.92	4.68	4.16

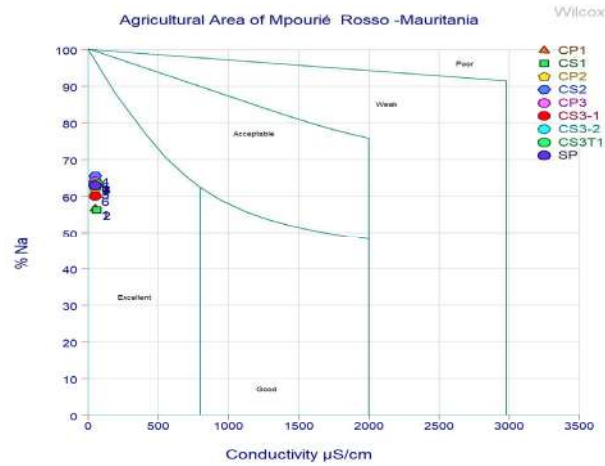

Fig. 8: Evaluation of the salinity of M'Pourie waters.

Moroccan standards, but the values obtained were higher than those found by Pwema (2014). The ammonium levels obtained across the nine sites were similar to those found by Diallo et al. (2011), but our results were higher than those obtained by Akatumbila et al. (2016).

Water Quality in the Main Canal of the M'Pourie Plain for Irrigation Purposes

When analyzing irrigation water, temperature (25 degrees) and SAR are two crucial variables to consider. The classification

system developed by Scientist Richards is widely used for assessing salinity-alkalinity risks, with 16 classes available. However, it should be noted that this method alone does not provide information on the risk of salinization or sodification. To assess these risks, it's important to consider electrical conductivity and SAR, both of which are useful indicators for soil salinization and alkalinization.

The M'Pourie plain's irrigation water has a salt adsorption ratio (SAR) ranging from 3.92 to 4.68, with an average of 4.26 (Table 2). All samples previously tested had sodium adsorption ratios below 10, indicating that there is no accumulation of sodium (Goula et al. 2007) (Fig. 8).

The US Salinity Laboratory has created a quality scale for irrigation water to mitigate its negative impact on soil and plants. The scale is based on electrical conductivity and SAR.

Irrigation Water Classifications in Relation to Conductivity and SAR

The determination of the chemical quality of water for its use in irrigation is based on the knowledge of the chemical characteristics of several variables particularly salinity and the sodium adsorption ratio (SAR) to determine the suitability of these waters in irrigation.

The results of the conductivity and SAR analysis show a spatial typology of stations which are characterized by low-risk water, excellent water quality with an absence of strong alkalinization (S1) at very high risk, poor water quality, and a very strong alkalization of waters (Tables 3, 4 and Fig. 9).

Table 3: Irrigation water quality scale based on electrical conductivity (Harivandi 1999).

Conductivity (Ce)	Water classes	Interpretation
Ce < 250µS.cm^{-1}	C_1	Low risk
250µS.cm^{-1} < Ce <[750µS.cm^{-1}]	C_2	Medium risk
750µS.cm^{-1} < Ce <[2250µS.cm^{-1}]	C_3	High risk
2250µS.cm^{-1} < Ce <[5000µS.cm^{-1}]	C_4	Very high risk

Table 4: Irrigation water quality scale in relation to SAR.

SAR	Water classes	Interpretation
0 < SAR <=10	S_1	excellent at low risk of alkalinization
10 < SAR <18	S_2	good with acceptable alkalinization hazards
18 < SAR <26	S_3	medium qualities with a high risk of alkalinization
SAR > 26	S_4	poor qualities with high alkalization risks

Source: (Durand 1982)

The water from stations S3 and S4 cannot be used except for very tolerant crops; otherwise, the water is unusable, because it is very dangerous on poorly drained soils and can present a danger to a certain extent on most crops.

The US Salinity Laboratory (14) scale of analysis results shows that irrigation water from the M'Pourie plain is class C1S1, i.e. irrigation water with low salinity and excellent alkalinity (Fig. 9).

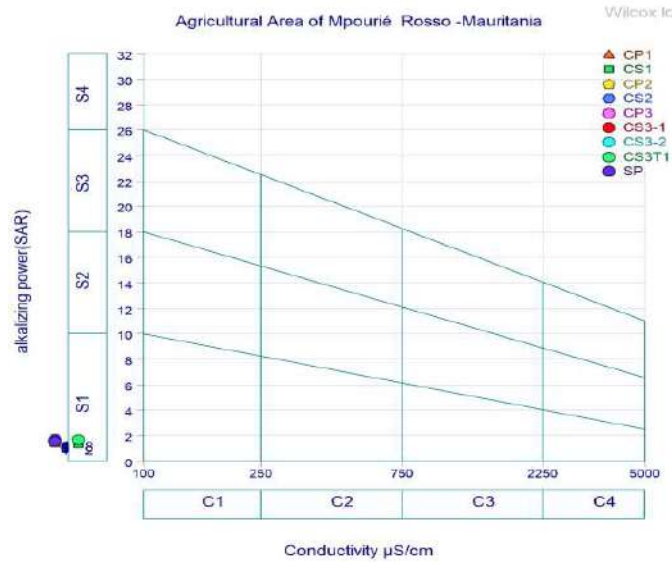

Fig. 9: SAR /Conductivity assessment.

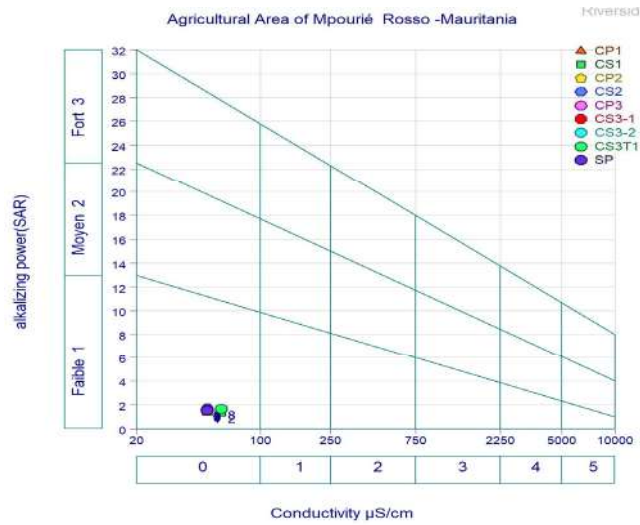

Fig. 10: RIVERSIDE diagram.

Riverside Diagram Classification

Taking into account this classification and after plotting all the water points from the various campaigns on the Richards diagram, according to the SAR/conductivity cross-index, we were able to identify the presence of the following class: C1S1 (Fig. 9 and Fig.10)

CONCLUSION

Our study aimed to evaluate the quality of Senegal River water utilized for agriculture in the M'Pourie plain located in Rosso. This is a crucial matter considering the increasing need for surface water due to the expanding agricultural practices. The water quality findings from the M'Pourie plain in Rosso deliver significant insights, particularly with regard to pH levels that fall within the acceptable range. The low mineralization confirms that the water is ideal for irrigation, and the salinity effect indicates the absence of permeability issues linked to overall salinity. The excessive use of fertilizers and other products in agricultural areas has resulted in high nitrite and ammonium levels in the irrigation water of the M'Pourie plain. However, the nitrate values meet the toxicity standards and do not pose any general problems for irrigation.

Moreover, the levels of sodium, sulfate, bicarbonate, and chloride are within Moroccan standards. The sodium adsorption ratio and electrical conductivity indicate that the Senegal River water used for irrigation in the M'Pourie plain is categorized as class C1S1, indicating low-salinity, excellent water with a low risk of alkalinization. While the waters of the Senegal River, especially those of the main M'Pourie canal, are generally suitable for irrigation, the concerned authorities must keep a check on them and update them regularly.

REFERENCES

Akatumbila, L., Mabiala, M., Lubini, A., Pwema, K. and Musibono, E.A. 2016. Contribution to the evaluation of the physico-chemical quality of water: The case of the Gombe urban river of Kinshasa-city in the Democratic Republic of Congo. Larhyss J., 6: 7-29.

Akil, A., Hassan, T., Fatima, E.H., Lahcen, B. and Abderrahim, L. 2014. Study of the physicochemical quality and metallic contamination of surface waters in the Guigou watershed, Morocco. Eur. Sci. J., 10: 45-63.

Becerra-Castro, C., Lopes, A.R., Vaz-Moreira, I., Silva, E.F., Manaia, C.M. and Nunes, O.C. 2015. Wastewater reuse in irrigation: A microbiological perspective on implications in soil fertility and human and environmental health. Environ. Int., 75: 117-135.

Diallo, A.D., N'Diaye, A.D. and Sid, M.O. 2011. Variability of nitrates, nitrites and ammonium in irrigation and drainage water: case of the M'Pourié plain in Rosso (Mauritania). Sci. Lib., 3: 56-63.

Durand, J.H. 1982. Irrigable Soils: Pedological Study, 399 pp.

Elgallal, M., Fletcher, L. and Evans, B. 2016. Assessment of potential risks associated with chemicals in wastewater used for irrigation in arid and semiarid zones: A review. Agric. Water Manage., 177: 419-431.

Goula, B., Kouame, I.K., Coulibaly, L., Gnagne, T., Savane, I. and Djoman, P.D. 2007. Characterization of activated sludge effluent from a food factory with a view to its use as water for watering lawns in a humid tropical zone. Rev. Sci. Eau., 20(3): 299-307.

Gu, X., Xiao, Y., Yin, S., Liu, H., Men, B., Hao, Z., Qian, P., Yan, H., Hao, Q., Niu, Y., Huang, H. and Pei, Q. 2019. Impact of long-term reclaimed water irrigation on the distribution of potentially toxic elements in soil: An in-situ experiment study in the North China Plain. Int. J. Environ. Res. Public Health, 16: 649.

Guterres, A. 2017. Sustainable Development Goals Report 2017. United Nations, Department of Economic and Social Affairs, NY.

Harivandi, A. 1999. Interpreting turfgrass irrigation Water test results. Water J. Calif., 11: 33-46.

Hussain, M.I., Muscolo, A., Farooq, M. and Ahmad, W. 2019. Sustainable use and management of non-conventional water resources for rehabilitation of marginal lands in arid and semiarid environments. Agric. Water Manage., 221: 462-476.

Kahimba, F.C., Ali, R.M. and Mahoo, H.F. 2016. Evaluation of irrigation water quality for paddy production at Bumbwisudi rice irrigation scheme, Zanzibar. Tanz. J. Agric. Sci., 7: 114-119.

Mounjid, J., Cohen, N., Fadlaoui, S., Belhouari, A. and Oubraim, S. 2014. Contribution to the evaluation of the physico-chemical quality of the Merzeg watercourse (peri-urban Casablanca, Morocco). Larhyss J., 31-51.

N'diaye, A.D., Salem, K.M.M. and El, M.B. 2014. Contribution to the study of the Spatio-temporal evolution of the physicochemical quality of water from the right bank of the Senegal River. Biol.Sci. Pharm. Res., 1(2): 016-021.

Nsiala Kimfuta, C. 2012. Contribution to the Geochemical Study of the Waters of the N'Djili River Watershed East of Kinshasa, Democratic Republic of Congo. Unpublished Doctoral Dissertation. Free University, Brussels.

Pwema, K. 2014. Food Ecology, Reproduction, and Modes of Adaptation of Five Species of Labeo Cuvier, 1817 in Lentic and Rapid Environments at Pool Malebo in the Congo River. Doctoral Thesis. University of Kinshasa.

Rizzo, L., Gernjak, W., Krzeminski, P., Malato, S., McArdell, C.S., Perez, J.A.S., Schaar, H. and Fatta-Kassinos, D. 2020. Best available technologies and treatment trains to address current challenges in urban wastewater reuse for irrigation of crops in EU countries. Sci. Total Environ., 710: 136312.

Rodier, J. 2009. Water Analysis: Natural Waters, Wastewater, Seawater. Ed Dunod, Paris, pp. 1475.

Wilcox, L.V. 1948. The quality of water for agricultural use. United States Department of Agriculture Technical Bulletin No. 1962, USDA, Washington DC.

World Bank, 2017. Water Resources Management. https://www.worldbank.org/en/topic/waterresourcesmanagement

Nature Environment and Pollution Technology
An International Quarterly Scientific Journal

p-ISSN: 0972-6268
(Print copies up to 2016)
e-ISSN: 2395-3454

Vol. 23 | No. 1 | pp. 341-354 | 2024

Original Research Paper

https://doi.org/10.46488/NEPT.2024.v23i01.029

Open Access Journal

Farmers' Perception and Adaptation Strategies Towards Climate Change: A Village Level Study in India

Dharma Teja Ratakonda, Ajit Kumar Dash† and Amritkant Mishra
Department of Economics, Birla School of Social Sciences and Humanities, Birla Global University, Bhubaneswar, India
†Corresponding author: Ajit Kumar Dash; ajitkumardash2008@gmail.com

Nat. Env. & Poll. Tech.
Website: www.neptjournal.com

Received: 05-07-2023
Revised: 11-08-2023
Accepted: 23-08-2023

Key Words:
Farmers' perception
Adaptation strategies
Climate change
Sustainable development

ABSTRACT

The present study attempted to observe the perception and adaptation strategies of farmers in the context of climate change. It observes that the majority of the farmers are aware of climate change and understand that they are facing problems due to it. The major problems faced by the farmers are the long duration of dryness due to lack of rainfall, weed pressure, very high temperatures, and crop disease. However, farmers are not very aware of technological adaptation and have changed the cropping time due to changes in the time of monsoon. The study recommends that there is a need for intensive micro and macro policy initiatives in terms of modern green sustainable technology along with awareness and skill development of the farmers. The government should also focus more on policy initiatives for sustainable agricultural practices in line with sustainable development goals.

INTRODUCTION

Around 70% of people in India depend on agriculture. It is the primary sector and is widely known as the largest producer of spices, pulses, rice, and wheat at the world level. The rural economy basically dwells on agriculture bears importance as it provides employment and livelihood to a majority of the population. However, the contribution of the agriculture sector to GDP is only 15%. Today, the greatest threat to agriculture is climate change. The global community is concerned about climate change. Climate change refers to changes in climatic characteristics like temperature and rainfall. Human activities are responsible for environmental degradation, causing pollution resulting in the greenhouse effect and ozone depletion. Agriculture is directly exposed to climate change and suffers from high temperatures, low rainfall, carbon dioxide concentration, etc. Indian agriculture is said to be a gamble of monsoon. Further, climate change is an uncertain factor that affects the cycle of monsoon which changes the water cycle as climate change alters rainfall timing due to changes in holding moisture and evaporation.

Due to high temperatures, water bodies like lakes, rivers, ponds, streams, and other water bodies dry. So, due to climate change, crops take longer time to grow, the product becomes of low quality due to weed pressure, and frequent extreme heat, and ultimately the farmer faces a high level of risk of loss. According to Germanwatch 2020, India is the fifth most vulnerable country to climate change (Eckstein 2021). The rank India was 14th spot in the year 2017 which worsened to 5th in the year 2018. The vulnerability is because of severe rainfall, heavy flooding, and landslides. The Indian states like Kerala, Odisha, Assam, and Bihar suffer from natural calamities like cyclones, floods, and drought. Floods in Kerala in the year November 2018 were realized to be the worst, which killed around 1000 people. According to the Indian Council of Agricultural Research, an increase in temperature by 3-7% cause's decrease in the yields of crops by10-20 % (Agrawal 2009). Likewise, an increase in the incidence of drought and flood increases the possibility of pest attacks and diseases. Similarly, when the sea level rises by one meter, it could submerge 0.18 % of land in Maharashtra, which is a risk for 1.3 million people. It has been observed that production will reduce by 4–5 million tons due rise in temperature by only 1 centigrade.

Therefore, climate change is a major concern for the global community as a whole. The direct sufferers are the farmers in the context of the impact of climate change on life and agricultural income. The fact of the situation is that agriculture is considered to be a long traditional occupation and people have been doing this for a long time. So, it is essential to understand and examine the perception and adaptation strategies towards climate change for effective policy formulation. This study is in this line. The rationale behind this study is to understand the behavior of the farmers

at the grass root level which can be helpful for micro and macroeconomic agricultural policy formulation. The objective of the study is to examine:

- Perception of farmers toward climate change
- Problems faced by farmers due to climate change
- The adaption risk management strategies of farmers towards climate change

PAST STUDIES

Agriculture plays the most important role in any economy. Agriculture not only supplies food but also provides employment. In recent days, food inflation has been a regular phenomenon and has become a major concern in most emerging economies like India (Mishra et al. 2023, Sargani et al. 2023, Mishra & Agrawal 2021). When agricultural productivity determines the food supply the productivity of the agriculture sector depends on good climatic conditions along with other necessary infrastructure. Over time there is a change in the climatic conditions. Agricultural workers, in general, and farmers, in particular, are the contiguous witnesses of the changing behavior of climate. Climate change creates disruptions in their life, the main cause of the struggle for their livelihood. Thus, climate change has received wide attention from academics, policymakers, researchers, and people in general. There is stock of existing literature on climate change and its impact on agriculture. In this section, a few notable recent studies relevant to the present study are reviewed below.

Fosu-Mennash et al. (2012) conducted a study on "Farmers' perception and adaptation to climate change: A case study of Sekyedumase district in Ghana." The study found that climate change has a great impact on rural farmers as their livelihood depends on agriculture. The level of impact largely depends on awareness and the level of adaptation in response to climate change. 92% of farmers feel an increase in temperature, and 87% of farmers perceive a decrease in rainfall. Diversification, planting of short-season varieties, change in crop species, and shift in planting date are the adaptation strategies by the farmers. However, poverty, lack of information, and awareness are the barriers. Another notable study in the context of Ghana (Acquah-de Graft & Onumah 2022) is "Farmers' Perception and Adaptation to Climate Change: An Estimation of Willingness to Pay." This study also observed that the majority of the farmers perceived an increase in temperature and a decrease in rainfall. Still, they found that the level of adaptation is relatively high, with the majority of the farmers who use climate adaptation measures like different crop varieties, soil conservation, changing planting dates, and water harvesting as the major adaptation measures to climate change impacts. According to this study, the barriers to adaptation are lack of information, lack of knowledge on adaptation, insecure property rights, insufficient access to inputs, lack of credits, access to water, and high cost of adaptation. They observed the probability of willingness to pay for climate change mitigation policies increases with age, years of education, and ownership of farmland.

Similarly, Guodaar et al. (2023) found that indigenous adaptation strategies to mitigate severe physical climate risks and disasters, individual farmers implement indigenous like livelihood diversification, construction of hand-dug wells in farms, migration, the building of mounds or ridges, and early marriage of young girls are used in Ghana. The farming communities also do animal sacrifices and spiritual incantations to invoke rains to address prolonged droughts. The study suggests early warning system regarding climate risks and their determinants will be highly helpful in adapting mitigation strategies.

The literature evidence an important study (Akponik et al. 2010) in the context of Sub-Saharan West Africa (SSWA). This study is on "Farmers' perception of climate change and adaptation strategies" The study predicted climate change is to have the main impact on agriculture, the economy, and the livelihood of the populations. The study is based on interviews with 234 farmers in five sub-Saharan West African countries in 78 villages. This study also finds that most of the farmers admit that climate change has an impact, and they depend on geographical area and prevailing climate. The challenge for the farmers is the dryness of their present climate. The rainfall is decreasing, leading to a number of dry spells perceived to have increased. In this region, the farmers are adopting crop management to maintain soil fertility by restricting the use of fertilizer and soil water management to maintain wetness. The ritual ceremonies by rainmakers are also cited to be a core strategy to deal with long dry spells. In the milieu of smallholder farmers' perception, a study (Ayanlade et al. 2017) based on "Comparing smallholder farmers' perception of climate change with meteorological data' in Southwestern Nigeria. The study has used ethnographic analysis, along with Cumulative Departure Index (CDI), Rainfall Anomaly Index (RAI) analysis, and correlation analysis to compare farmers' perceptions with historical meteorological data. The objective is to assess the way farmers' observations mirror the climatic trends. According to their observation, 67% of farmers have felt recent climate changes. The Perceptions of rural farmers towards climate change and variability are consistent with the climatic trend analysis. The impacts of climate change on both crops and livestock appear to be

highly negative rather, it is much more in the case of crops like maize, yam, poultry, and cattle. Another insight from this study is smallholder farmers are particularly vulnerable to climate change as the majority of them do not have enough resources to cope. Farmers' perception and knowledge of climate change and the coping strategies to the related hazards were done by adopting 'Adiha' located in central Tigray of Ethiopia (Mengistu 2011). They found that climate change adversely affects the Ethiopian economy due to the heavy dependence of the agricultural sector on rainfall. Based on focus group discussion on 144 systematically sampled respondents, the study also found that temperature is rising and precipitation is decreasing. Untimely rain and frequent drought are the challenges for crop production leading to livelihood problems vulnerable to health and socio-economic hazards. Lack of modern early warning systems, inflexible cropping calendar, and narrow choice of crop varieties are the basic reasons for vulnerability. So, the study suggests adopting improvements in the forecasting methods and improvements in the dissemination of climate information systems. They also suggest prioritizing irrigation technologies and adjusting planting dates to improve resilience to climate change. A study (Okonya et al. 2013) on farmers' perception and coping strategies towards climate change in Uganda interviewed 192 sweet potato farmer households distributed in six agroecological zones. The objective of this study is to examine perceptions about the effects of climate change and coping strategies. Weather-related events like prolonged dry seasons, floods, storms, mudslides, extreme rainfall, and delayed/early rains are observed to be frequent due to which the rural poor farmers suffer from food insecurity and their livelihood is getting affected. The strategies to cope with the problem are storing food, income diversification, and digging drainage channels. Other strategies include planting trees using high-yielding variety seeds that are early-maturing, drought-tolerant, disease and/or pest-resistant varieties. Similarly, other strategies are planting at the onset of rains and increased pesticide/fungicide application, among others strategies. The study recommends wide awareness relating to changes in rainfall and temperature. In the context of Nepal, a notable study by Manandhar et al. (2010) was regarding the adaptation of cropping systems to cope with climate change. The study is a cross-regional study on farmers' perceptions and practices. It is based on a comparative study performed in two different ecological regions such as Terai (lowland) and Mountain (upland), in the western development region of Nepal. The focus of the study is on perceptions and adaptations to climate change by farmers. It observed that most farmers recognize climate change and respond to it. They believe in their own indigenous knowledge and experiences. The study suggests going beyond the individual level and planning support mechanisms for appropriate technologies and strategies for farmers to cope with climate change. The Ejura-Sekyedumase district of Ghana was considered as a case study (Kemausuor et al. 2011) to examine farmers' perceptions towards climate change. The study has compared farmers' perception of climate variability change with the actual variation on the basis of the climatic data which was recorded from 1993-2009. They conducted interviews with farmers in six out of the nineteen operational areas in the district. The study concluded that the majority of the farmers' temperature is increasing, and rainfall timing has changed, which results in frequent drought. In this line, another notable study (Esham & Garforth 2012) worked on agricultural adaptation to climate change in the case of Sri Lanka. Thus, this study considers the farm-level adaptation strategies for climate change for smallholder farmers. The study revealed that farmers perceive climate change on the basis of their experience. According to this study, there are five groups of adaptation strategies that farmers adopt to cope with climate change. These strategies are crop management, land management, irrigation management, income diversification, and rituals. It is found that non-climatic factors are important strategies to increase farmers' adaption, particularly for resource-constrained smallholder farming. Human cognition and social networks are important determinants of adaptation to climate change. Interestingly, the study observed that social workers also play a significant role in influencing adaptation. Other influencing factors are social barriers, such as cognitive and normative factors, which become economic barriers to adaptation. So, to formulate and implement adaptation strategies, it is necessary to understand the importance of socio-economic, cognitive, and normative aspects of the local groups. Similarly, a study (Alam et al. 2012) on adaptation practices to climatic vulnerabilities in Malaysia. The study has considered paddy farmers as their respondents to understand farmers' perception towards climate variation, vulnerabilities, and techniques they use to adapt to climate change. The study observed that most of the farmers do not have a clear awareness of climatic changes and vulnerabilities. Farmers decide on adaptation strategies mostly based on their common sense. The study suggests that farmers require the necessary training and support from the government. Farmers in the marshlands of South Kivu, Democratic Republic of Congo, adopt adaptation strategies like the use of mulch and manure as per their 'experience and information among fellow farmers, but sustainable practices like crop diversification, drainage, growing low-maintenance crops are advisable (Mushagalusa et al. 2022). Nevertheless, the size of the farm is an important variable in determining the adaptation strategies. It is found by Koirala

et al. (2022) in the case of Nepal that Small-sized farmers tend to adapt much more in response to their climatic perceptions than large-sized farmers. Therefore, agriculture may be losing responsiveness to climate change due to large-sized farmers dominant by holding a majority of land in developing countries.

Studies in the Indian Context

A systematic review of the literature on Climate Change and Indian Agriculture: A Systematic Review of Farmers' Perception, Adaptation, and Transformation by Datta et al. (2022) reveals that Indian farmers have perceived a temperature rise erratic and decreased rainfall. The Indian farmer's changes in land use, resource and labor allocations, occupational patterns, and cropping systems as the adapting strategies to climate change. The influencing factors in deciding the adaptation strategies for Indian farmers are access to sufficient information, adequate credit at the right time, household income, farm size, gender, and resource endowment. Therefore, large-scale investments for the farming sector in general and building farmers' capacity in particular, an adaptation of an integrated approach to understanding the farmer's perception is essential for effective policy modeling. In Banerjee's (2014) study on 'Farmers' perception of climate change, its impact, and adaptation strategies in four semi-arid Indian villages,' it was noted that the region is experiencing limited and unpredictable rainfall. Infertile soils, poor infrastructure, and rapid population affect the socio-economic life of agricultural communities. A study (Shukla et al. 2015) was conducted on Farmers' perception and awareness of climate change considering a case study from Kanchandzonga Biosphere Reserve of India. The study attempted to observe the perception of people on climate change- in five villages. They surveyed 300 households selected randomly. The result of this study is also in line with other studies. It found that the majority of households perceive climate change in the form of increased temperature, uncertain patterns of rainfall, and hot wind. Crop diversification and traditional agroforestry are the adaption strategies followed by people. Correspondingly, another study (Dhanya & Ramachandran 2016) on farmers' perceptions of climate change in a semi-arid region of south India acknowledged climate change as one of the foremost challenges that affect the performance of agriculture and livelihood. Farmers are the worst sufferers due to climatic variations. Farmers perceive climate variability and identify increasing temperatures. Due to delays in rain, the soil dryness increases, which is a critical factor affecting cultivation. Farmers''s perception of drought impacts was in the context of local adaptation and administrative mitigation measures in Maharashtra (Udmale et al. 2014). This study is based on both secondary and primary data collected from a primary survey of 223 farming households. The study reveals that environmental impacts increase in average atmospheric temperature, pasture-forest degradation, deteriorated water quality, damage to fish habitat-wild life, and groundwater depletion are perceived by farmers to a high extent. Though farmers perceive the severe impact of drought and are familiar with various adaptation strategies, they have very little option to adopt this. Though the government provides various mitigation measures, the farmers are not satisfied. Similarly, another study done in Tamil Nadu, India, on the perception of farmers shows that they observed a decrease in the quantity of rainfall over the years, along with the delayed onset of rains. In addition, the farmers felt that the monthly frequency of rains had decreased with increased dry spells (Vardan & Kumar 2014). The key socio-economic variables to influence adaptation strategies are farmer's age, gender, household size, educational level, off-farm income, and farm size influence farmers' adaptation decisions (Jha & Gupta 2021). The study by Sehgal (2023) on crop diversity and farm income found that demographic, farm, and institutional variables play an important for raising farm income. Further, Education level, irrigation, usage of technical information, and possession of the Kisan Credit Card (KCC) facility have a positive impact on agricultural income. Crop diversification helps small farmers to gain more than large farmers. When natural disasters negatively affect farm income, it is suggested that the impact can be mitigated with the help of a higher level of crop diversification. Guodaar et al. (2023) studied the perception of farmers regarding the changing climate, its impact on agriculture, and responsive adaptation strategies of farmers of a major state, i.e., Uttar Pradesh in India. According to their findings, 82% of farmers perceived a temperature rise, 85% believed that the rainfall had altered, and 95% believed that the intensity of rainfall had changed. More than 60% of the farmers agreed that alterations in temperature and precipitation reduce production as well as revenue. The majority of farmers (86-87%) adopt strategies like shifting sowing dates, change of variety, and increase in irrigation. The study also finds interesting observations conservation agriculture or water harvesting are not considered. The most important motivation to opt for such strategies is not the awareness or knowledge but rather monetary benefit.

The above review of the literature shows that most of these studies are either done in the context of foreign countries or the context of other states of India. There are very few studies in the context of Andhra Pradesh. Further, most of the studies have their specific objective and do not give a complete idea about perception and mitigation strategies combined. Our study is in this line.

MATERIALS AND METHODS

The Study Area

Andhra Pradesh is known as a progressive state but farmers' distress is widespread news about this state. An agrarian rural economy predominantly dominates the state. It is the third-largest producer of rice and groundnuts and second in cotton and sunflower flower production in the country. The state has adopted the green revolution and is expected to reap its benefits. The state registers its position in horticulture crops. The National Horticulture Mission (NHM) has identified the state as having the potential to enhance exports of mango, banana, grapes, papaya, guava, brinjal, and cabbage. Diversification is said to be identified as one potential way to enhance growth and ensure stability in agriculture. Andhra Pradesh ranked eighth among the states both in terms of share of agriculture GDP (24.7%) and employment generation (58.55%) as per the 61st round of NSS**.** Of the total geographical area of 27 million ha in the state, 39 percent is net sown area. 4.4 million ha is the net irrigated area, and 6.4 million ha is rain-fed. The average rainfall in the state is 940 mm. 61 percent are marginal farmers, and 22 % are small farmers out of 11.5 million land holdings (Fig. 1).

This field-based study was conducted in two villages, i.e., Ananthasagaram and Bedusupalli, in the Ananthasagaram Mandal in Nellore district located in the coastal Andhra Pradesh state of India. Ananthasagaram Mandal is 79 km away from the district headquarters in Nellor. The study area is located nearer to the Somasila Reservoir, constructed on the river Penna. The distance between the two villages is 3km. According to the 2011 census, the total population of the Ananthasagaram Mandal was 8588, and the total population was 4436 males and 4152 females. The average sex ratio was 936 per 1000 population. The total population of specific two villages was 3100 and there were 812 families. There are a total of 750 acres of land cultivated by 360 families from these villages. The primary occupation is Agriculture, mostly paddy cultivation. Other than agricultural farming, people are engaged in both government and private sectors. Except for rainwater, the main source of water for cultivation in Ananthasagaram Mandal is the MI Tank (Minor Irrigation). 75.2 mm is the average rainfall in this area, but in 2018, it received only 40 mm of rainfall. The mean maximum temperature varies from 39 to 41°C (usually occurring in May), and the mean minimum temperature varies from 19 to 21°C (usually occurring in January). The

Source: Google Maps and Wikipedia.

Fig. 1: The study area.

normal rainfall over the period from June 2014 to May 2019 is 4514.0 mm, but the actual rainfall is 3273.9 mm.

Methodology

Primary and secondary data have been used for this study. Primary data was collected from a survey conducted in two selected villages, i.e., Bedusupalli and Ananthasagaram. Ananthasagaram is the mandala head quarter. First, the villages were selected through a convenience sampling technique, and a random walk sampling technique was adopted in the second stage to choose the households. The secondary data on rainfall and temperature were collected from the District Metrological Department. Primary data was collected with the help of a structured questionnaire. The questionnaire was designed to refer to earlier perception studies by Saylor et al. (2019) with a necessary understanding of the socio-economic scenario of the present study. The questionnaires were administered as a face-to-face interview in the month of February-March 2020. The questionnaire intended to gather information on farmers' basic information like their demographic profile, details of farming, and also subject matter like their awareness, potential problems, and adaption and risk management strategies towards climate change. Finally, 150 data points have been considered collected from 360 families from both villages. From Ananthasagaram, we collected 90 data points, and from Bedusupalli, we collected 80 data points. We rejected 20 questionnaires due to incomplete information. The response rate was almost 100% during a face-to-face interview. For analysis, we have used simple percentage statistics using SPSS 16 software and have presented the results with the help of tables and figures.

RESULTS AND DISCUSSION

Climate Change in the Study Area

Temperature and rainfall are two important parameters to understand the climatic conditions. A rise in temperature and rainfall affects agricultural production negatively. When a rise in temperature affects agricultural production due to an increase in heat stress on crops, a decrease in rainfall is due to an increase in weed and insect pressure. If there is less rainfall, it leads to drought, and if there is heavy rainfall, it leads to floods. Therefore, climate is the most important factor for agriculture in particular and life in general. So, before studying the perception and adaptation strategies of the respondent farmers, we have tried to understand the nature of climate change in the study area.

Rainfall

Fig. 2 presents a comparison between the average annual rainfall in the state and the average rainfall per year in the study area in the last 5 years. The average rainfall in the state (75.2mm) is considered here as normal, and the fluctuation of rainfall in the study area is considered as actual. It can be observed that there is rainfall deficiency in the study area in all the years except in the year 2015-16. In 2014-15, the rainfall was 45.7 mm. In 2015-16, it increased by 90.3 mm, but in 2016-17 there was a fall in rainfall of 66.3 mm, and in 2018-19 again, it decreased by 39.99mm. This indicates that the area is experiencing low rainfall comparatively at the state level.

It is necessary to observe the season-wise rainfall as farming is subject to different seasons. Fig. 3 presents the season-wise rainfall last 5 years. One year is divided into 4 seasons that are Southwest Monsoon (from June to September), Northeast Monsoon (from October to December), winter (from January and February), and summer (from March to May). The graph shows that there is rainfall deficiency in every season except in 2015-16 (Northeast monsoon). Because of rainfall deficiency in the southwest monsoon, they changed their cropping time from southwest monsoon to northeast monsoon.

Temperature

It can be observed that the area is experiencing above

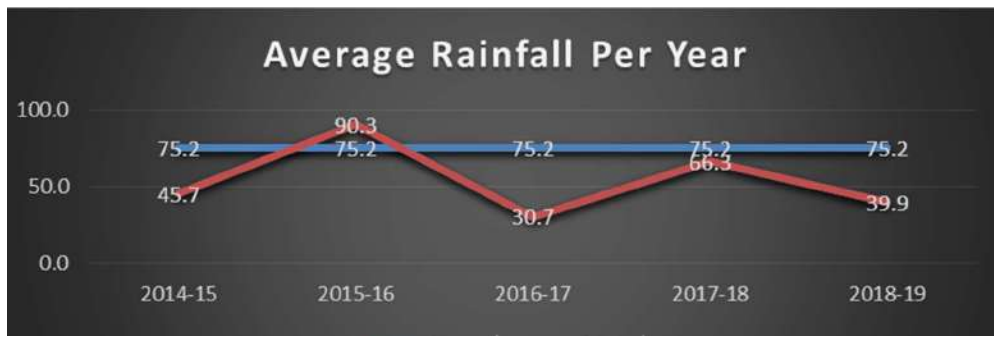

Data Source- IMD District Office, Nellore

Fig. 2: Average annual rainfall (in mm).

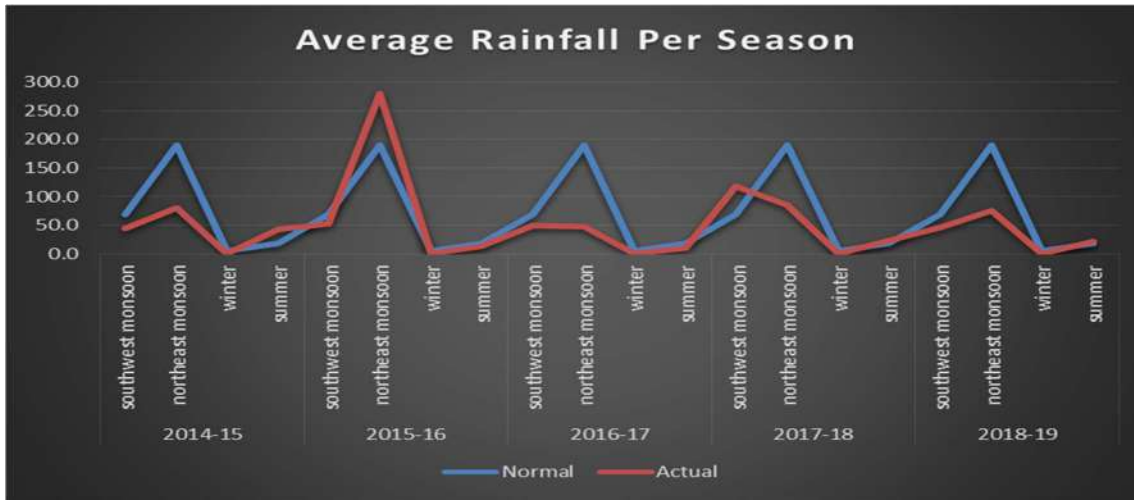

Data Source- IMD District Office, Nellore

Fig. 3: Average Rainfall per Season.

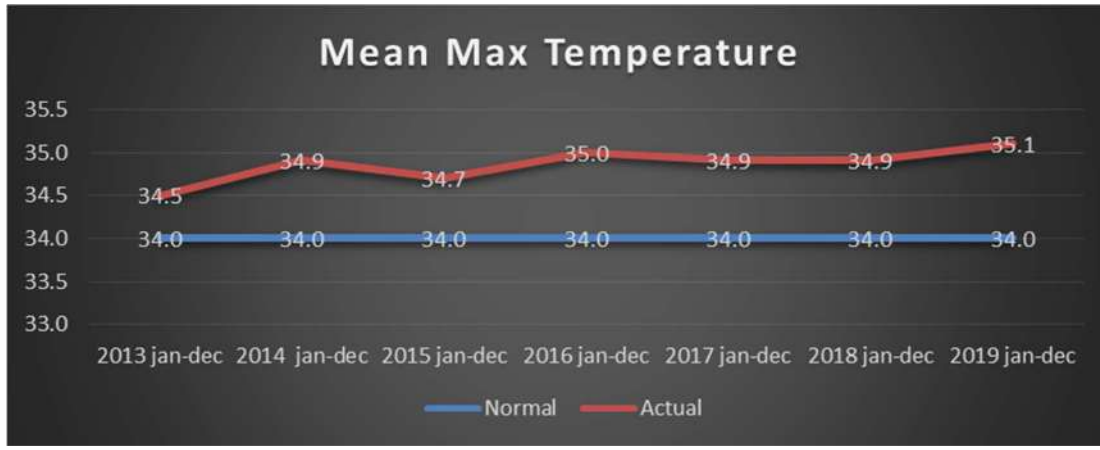

Data Source- IMD District Office, Nellore

Fig. 4: Mean maximum temperature per year.

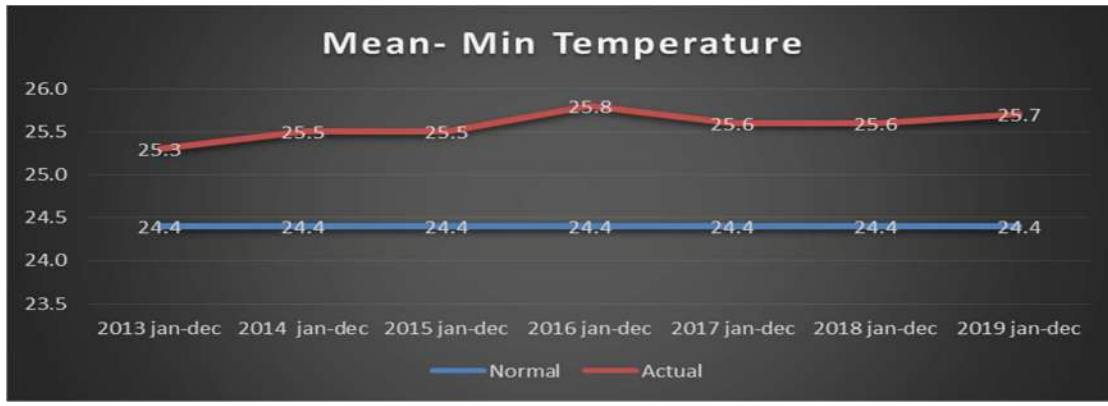

Data Source- IMD District Office, Nellore

Fig. 5: Mean-minimum temperature per year (in Celcius).

the normal temperature. Fig. 4 explains about mean – the maximum temperature of the Nellore district from 2013-2019. The mean maximum temperature is 34.0°C but every year, it has increased around 0.5°C to 1.1°C. So, every year there is above the normal temperature.

Similarly, Fig. 5 explains the mean of the minimum temperature of the Nellore district from 2013-2019. The mean minimum temperature is 24.4°C, but every year, it has increased from 0.9°C to 1.3°C, which indicates that there is an increase in temperature. Fig. 6 explains the mean maximum temperature according to the seasons. By observing the above graph with respect to the variability of temperature in different seasons, it is understood that there is an increase in the average temperature up to 2° Celsius, mostly during the summer season. Fig. 7 presents the mean min- the temperature in different seasons. If we observe the temperature in winter, there is an increase in average temperature up to 2° Celsius.

Field Survey, Data Analysis and Interpretation

Demographic profile: The total data points are 150. Out of that, 3% are female, and the other 97% are male. In the case of age group, 72.7% are above 50 years and 27.3% are 18-50 years. In the case of educational qualification, 4% are illiterate and 94% are less than class 12. Out of the total respondents, 68.7% of people's income is between rupees 20000-60000, and only 5% of farmers' income is above 200000. In the case of financial assistance, 66% of farmers are dependent on bank loans, and 32% are from other sources.

Details of farming: The total cultivated land by respondents is approximately 740 acres. At the same time, the mean of acres of land cultivated is 4.33 acres. More than 10 acres of land are cultivated by only 12.7% of respondents and 51.4% of respondents are cultivating 2 to 4 acres of land each. In the case of farming experience, 66% of farmers have experience

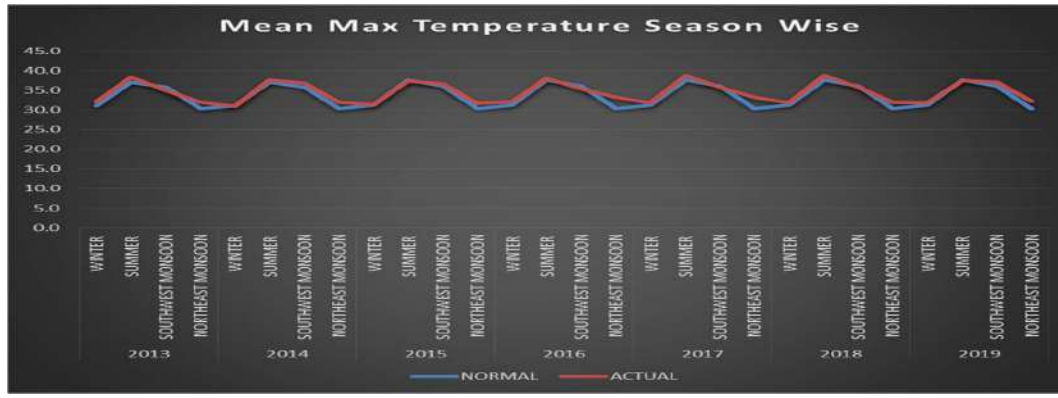

Data Source- IMD District Office, Nellore

Fig. 6: Mean-maximum temperature season-wise (in Celcius).

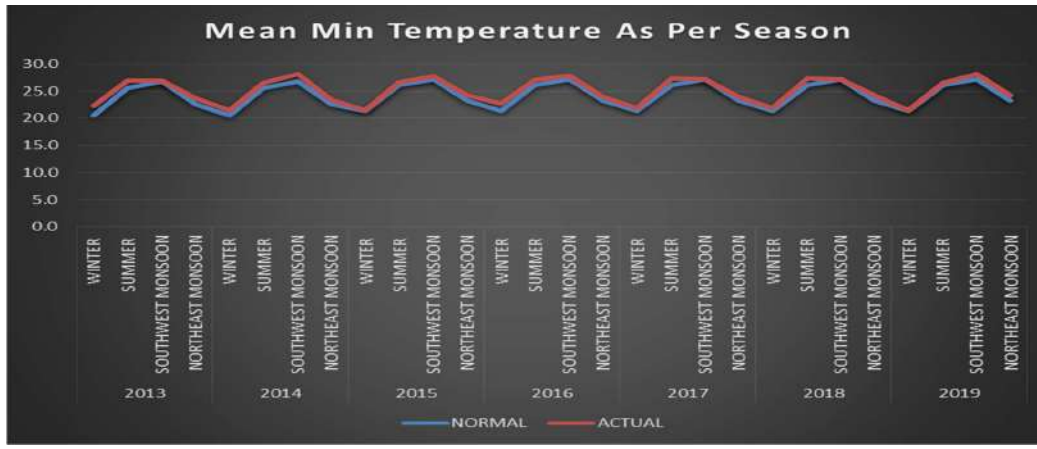

Data Source- IMD District Office, Nellore

Fig. 7: Mean-minimum temperature as per season (in Celsius).

of more than 10 years, and 34% of farmers have experience of less than 10 years. Mainly, they produce paddy and some of the farmers produce Chilli and groundnut as second crop. 16% of respondents are adopting double crops (Rabi and Kharif). In the case of access to irrigation, 66% are using ponds and river water for irrigation.

Farmer's perception of climate change: Out of the total responses, 96.3% of the population is aware of climate change, and 3.3% are not very aware of climate change. Their means of awareness are TV/Radio, their own experience, and the newspaper. 50% of farmers know about climate change from their own experiences. A total of 98% of farmers said that the major climate event experienced is high/extreme temperature. 98% are interested in taking crop insurance as they do not know about crop insurance. Farmers in these two villages are aware of climate change. Their most experienced climate change is high/extreme temperature. Due to the temperature rise, the heat stress on crops is increasing. 68% of farmers are concerned about this and very much concerned about the pressure of heat stress on crops. So, the increase in temperature is having an impact on crop production.

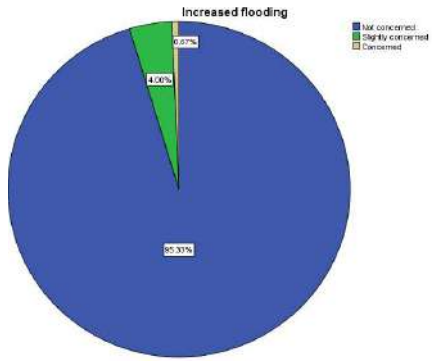

Fig. 8: Increased flooding.

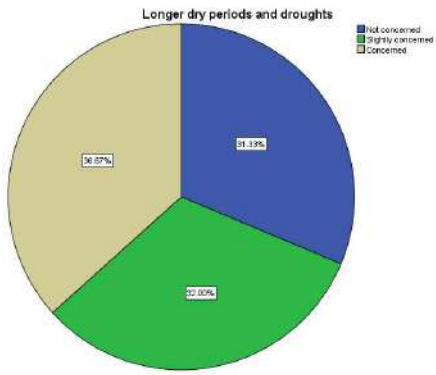

Fig. 9: Longer dry periods and droughts.

Farmers' concern about potential problems in agriculture due to climate change: To collect the views of farmers regarding the degree of their concern about the impact of climate change on crop production, the questionnaire included four options on a Likert scale, i.e., not concerned, slightly concerned, concerned, and very much concerned. Here, if they are not facing that problem, then that is a concern; if they face a very small percentage, then that is a slight concern. If they face that problem frequently, that is a concern, and if the loss is heavy, then that is very much a concern.

Increased flooding: Climate change is responsible for uncertain heavy rain, which causes floods. It is found that 95.33% are not concerned, 4% are slightly concerned and 0.67% of farmers are concerned about this (Fig. 8). The farmers whose farmland is nearer to the canal are facing the problem of flooding, and they are slightly concerned about this. This is due to the problem happening only when a heavy flow of water comes. The heavy flow of water is basically what they experience when the reservoir opens the gates to release extra accumulated water due to heavy rains. The concerned farmers are facing that problem frequently. Flooding only due to heavy rain is not observed to be frequent due to rainfall.

Longer dry periods and droughts: Farming regularly needs water; otherwise, the land becomes dry and disturbs the steps and process of cultivation. This problem occurs when rainfall is deficient or the alternative source of irrigation can provide water. Most farmers depend on rainfall and try to manage with water from irrigation only during shortages or off-season. From the field survey, it is found that a longer dry period is a major concern for the farmer. Fig. 9 shows that 68% of respondents are concerned and slightly concerned about this problem and only 31% revealed that they are not concerned about this problem. The categories of respondents who are not concerned about dryness are having land nearer to the canal or irrigation project.

Increase weeds pressure: The weed pressure damages the crop and results in low productivity and even no output. This creates loss and the farmers' financial management gets affected directly. This problem may occur in different types of seasons. The basic reason behind this problem is irregular and uncertain weather conditions. When the weather condition does not follow their normal feature, the moisture level changes, and the farmers need to withdraw unwanted plants grown with the crop. This further requires care and cost to be incurred. This is one frequent problem faced by the farmers. Fig. 10 shows 83% of respondents are concerned about this problem.

Higher incidence of crop disease: Crop diseases are the most

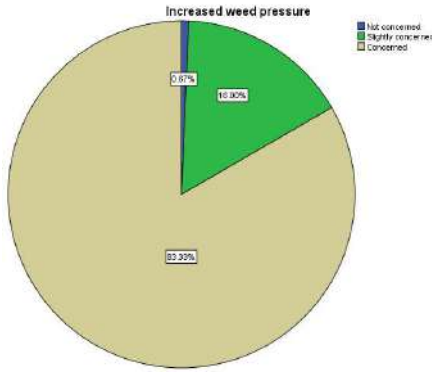

Fig. 10: Increased weed pressure.

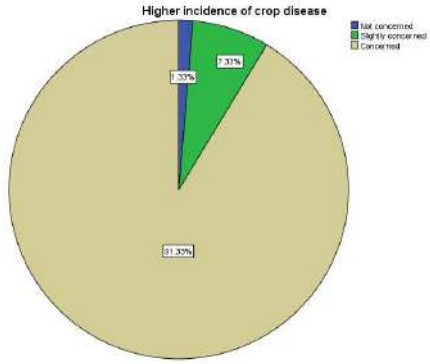

Fig. 11: Higher incidence of crop diseases.

frequent cause of the loss of farmers. The reason behind this problem is uncertain variability in weather causing change in the environment of plants to grow. This is observable due to high moisture in the climate and variability in temperature. In the study area, the cropping time is November; at this time, the temperature comes down crop diseases increase. We can observe from Fig. 11 that 91.33% of farmers are concerned about this, 7% are slightly concerned, and only 2% are not concerned about this.

Most frequent extreme rains: There is a rainfall deficiency in that area., we can say that this is not a problem for them. Approx. 98% of farmers are not concerned about this, and 2% are slightly concerned about this (Fig. 12).

Increase in saturated soils and ponded water: According to the field survey presented in Fig. 13, farmers are not prone to this problem. It occurs in cooler soil temperatures and because of ponded water. The average temperature is increased to 3°Celsius so the farmers are more worried about high temperatures than cold weather. 99% of the respondents have opined that they are not concerned about saturated soil or ponded water.

Increased heat stress on crops: High-temperature level

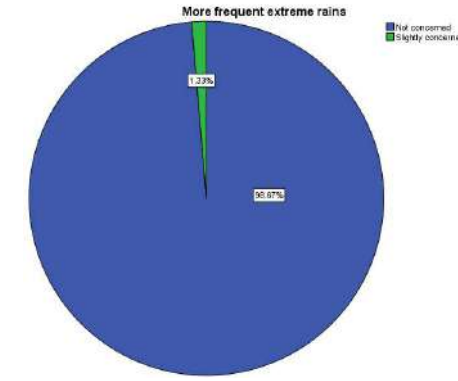

Fig. 12: More frequent extreme rains.

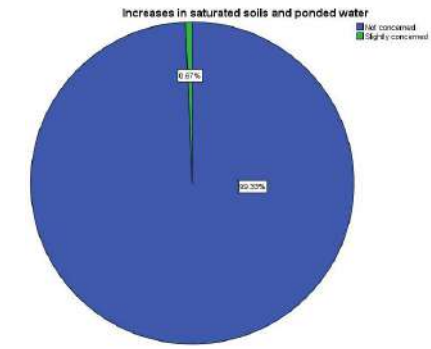

Fig. 13: Increase in saturated soils and ponded water.

creates heat stress on crops which is observed to be a frequent problem in the study area. The sum of the respondents said slightly concerned and very much concerned is 86% (Fig. 14) and only 13% responded they are slightly concerned.

Increased loss of nutrients into waterways: According to farmers, when the flow of water is very high, they need to cut the barricade of the farmland to release the extra water. The problem is when there is uncertain rainfall, and they need to release the extra water. The nutrients given to the crop for better growth also go with the flow of water. This is a loss of nutrients. However, Fig. 15

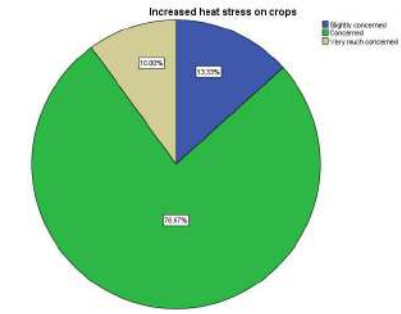

Fig. 14: Increased heat stress on crops.

shows that 98% of farmers are not concerned about this problem.

Increased soil erosion: From Fig. 16 it can be seen that 97% of farmers are not concerned about soil erosion. This is due to low rainfall in the area. Land which is located near the river or canal is prone to this but land which is far away from that is not prone to this. However, the farmers are concerned about a decrease in the fertility of land due to changes in the soil quality.

Adaption and Risk Management Strategies

In the early days, the cropping time was July to January, but due decrease in the variability in rainfall/precipitation, the farmers changed the cropping time from November to April, and due to this, there is a change in harvesting /cutting of crops from January to April. Earlier, the cropping time was spread over 6 months, but currently, the cropping time is spreading over 4 months because of the use of HYV seeds. As the study area is located nearer to the sea and the rainfall from southwest monsoon to the area has decreased in recent days is also a reason for the change in the cropping time. So, farmers are now depending on the northeast monsoon.

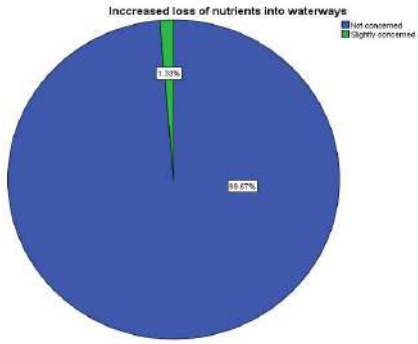

Fig. 15: Increased loss of nutrients into waterways.

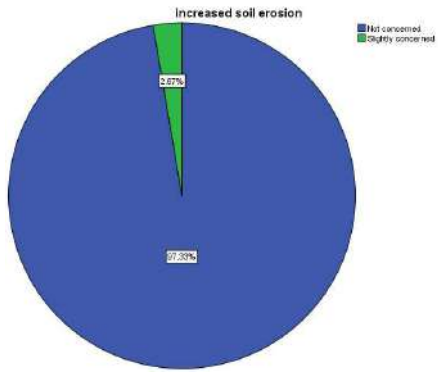

Fig. 16: Increased Soil Erosion.

Different types of adaptation and risk management strategies can be adopted to mitigate climate change. The study assumed few adaptation strategies learning from collected existing literature and attempted to observe whether the farmers in the study area are adopting them or not. The questionnaire included strategies such as adaptation of conservation practices, Purchase of crop insurance, Use of new technologies, Join off-farm jobs to supplement farm income, Restructure expenditure/ income to have less debt, Focusing more on farm production, investing more in inputs, Adopting crop diversification and multiple cropping, Selling or giving a part of the total land for some other purposes, Using a part of the land for some other purposes and finally Thinking/planning to quit farming. To quantify the qualitative response, a Likert scale format has been adopted. The questionnaire includes 3 options in the context of different types of risk and adaptation practices, i.e., doing to manage risk and adopt climate change, not doing now but planning to do, and not doing and not having any plan to do. The objective is to observe the behavior of the farmers toward climate change. The observation is explained below.

Adaptation of conservation practices: Conservation practices include the use of cover crops, the use of green and composted manure, and the gradual reduction of the use of chemical fertilizer. It is observed from Fig. 17 that 42% of farmers are not doing and do not have any plan to do, 36% of farmers are not doing now but to implement, and 22% of farmers are managing risk to adapt to climate change on the use of chemical fertilizers. It is found that though the farmers are not solely following conservation practices as an adaptation categorically they understand that heavy use of chemical fertilizer is changing the composition of soil and reducing the fertility of the land. However, they are using

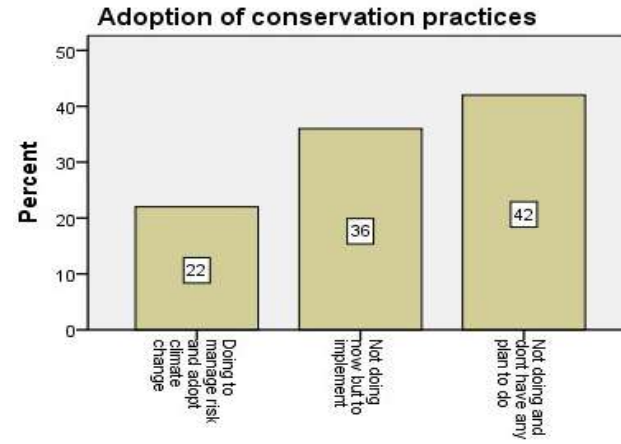

Fig. 17: Adoption of conservation crops.

it because they have to increase productivity. This is not suitable from a long-term productivity point of view, and they are gradually shifting to green and composed manure.

Purchase of crop insurance: To meet the uncertain loss due to climate change, there is a facility for adopting crop insurance. The farmers can purchase crop insurance, but the majority of the farmers do not have crop insurance, or they do not want to go for it. According to the respondent, the main problem in the case of crop insurance is in claiming of insurance amount. The main assumption is they can get a return only when there is damage to the crop in the total area. The total area should be declared as a damaged crop or drought. If the loss happens in individual farmland, then crop insurance does not give any benefit. So, the farmers feel that paying the insurance amount is a net loss. Thus, 98% of farmers are not doing and do not have any plan to take crop insurance as an adoption and risk management strategy.

Use of new technologies: The choice of technology in general and the use of modern agricultural technology is considered to be useful for increasing farm productivity. In the context of modern farm technology, it requires large farmland holding size. Most of the farmers have small farm sizes or do not have the financial capacity to purchase their own. They prefer to hire and use technology like tractors and thresher machines etc., when there is a requirement. Even though loan facility is available they fear taking loans because they fear being defaulter in paying installments to be over debt and financially more stressed. 98% of farmers have opined that they do not consider the use of new technology to be an adaptation strategy.

Join off-farm jobs to supplement farm income: The farmers are engaged in farming during the season and prepare the land during the off-season. They do not join off firm jobs may be due to they do not have the skills for that, or they do not get time for them. Farming is a full-time job and requires regular attention. It is found that 100% of farmers are not interested in joining off-firm jobs.

Restructure expenditure/income to have less debt: Financial management is an important aspect of any production process. When climate change is an influencing factor to production, leading to revenue and expenditure nexus, it is necessary to understand whether farmers are revenue and expenditure to maintain balance. It is observed from the field interaction that they find scope to manage the expenditure rather than having to face the new increase in expenditure due to an increase in input price. They do not have any standard accounting and financial management plan but rather believe in their common sense to manage revenue and expenditure. All the respondents opined that they had not done any restructuring to manage their revenue-expenditure or debt in relation to climate change or change in weather.

Focusing more on farm production, investing more in inputs: Input-out management is another aspect of production. To achieve more productivity, input is managed. To analyze whether the farmers follow any special input management or increase in input to retain production or not, the study had this angle. Conversely, the farmers said that there is no such specific investment. More on the input plan is followed. Whatever expenditure is required, they do. They maintain the soil in whatever possible way.

Adopting crop diversification and multiple cropping: Crop diversification is a scientific way to maintain soil fertility and to have sustainable agriculture. Similarly, multiple cropping is important from a production and income point of view. In the study area, multiple cropping and crop diversification are not observed. The percentage of people who adopt multiple cropping is very low. They basically produce paddy. Their important response is they have changed the month of cropping to face the changing climate.

Selling or giving a part of the total land for some other purposes: Due to the gradual reduction in farm income and increased cost of production, the farmers are facing problems and losing confidence to pursue agricultural farming as their primary occupation. They have debt and are unable to repay to become completely debt-sustainable. Nevertheless, they do not like to sell or show interest in giving a part of their land for some other purposes. Farmers do not consider this is way to face climate change. If there is any emergency, they put the land they own for any mortgage purpose or for some other reason they want to get it back.

Using a part of the land for some other purposes: Most of the farmers are small landholders. They have sufficient land so that a part can be used for some other business purposes. They use a small part of the land for regular use for agriculture-related activities. So, there is no other source of income from the land they own. Totally 100% of farmers are not interested in using a part of the land for some other purposes.

Thinking/planning to quit farming: Weather change due to overall climate change has created a great challenge for farmers. The farmers feel that agriculture is not at all a profitable business, keeping other things like commercialization and the use of modern technology constant. Particularly the small farmers express that agriculture has been a generational occupation for them, and they have to do it. Neither do they have the skills and education to opt for better employment, nor do they have the financial strength to convert their farming to a business model. Though the government is implementing different policies and programs to help them the fact is the prime

variable to influence their farming is climate change in terms of low or uncertain rainfall and increasing temperature. It is observed from the field that 80% of farmers believe that they will not quit farming. They have long years of experience in farming and do not have any other option to opt for.

CONCLUSION

The study focused on three important dimensions such as farmers' perception of climate change, problems faced by farmers in agriculture due to climate change, and farmers' adaption and risk management strategies. It is observed that 97 % of farmers are aware of climate change. 68% of farmers are concerned, and 32% of farmers are not concerned about longer dry periods. 83% of farmers are concerned, and 16 are slightly concerned about weed pressure. 76% are concerned, and the remaining are slightly concerned or not concerned about heat stress on crops. 91.33% of farmers are concerned about crop disease, 7% are slightly concerned, and 2% are not concerned about crop disease. So, climate change is playing a vital role in agriculture. It is affecting farming and farmers' adaptation strategies toward climate change. Due to changes in climate and weather, farmers are changing their cropping time and depending on southwest monsoon to northeast monsoon. Due to changes in cropping time, they are facing problems like an increase in weed pressure and heat stress on crops.

Similarly, due to the lack of rain and increased temperature, a longer dry period is another big problem for them. The major adaptation strategy is changing the period of cropping time and shifting dependency from southwest monsoon to northeast monsoon. However, this has led to problems like increasing weed pressure and heat stress on crops.

The study recommends that the government should focus more on climate change mitigation strategies in one hand and implement effective environmental policies to control factors causing climate change. The findings of the present study are in line with conclusions derived by notable studies like (Banerjee 2014, Guodaar et al. 2023). Farmers must be given priority for skill development in terms of training and awareness programs for suitable agricultural practices. There is a need for the adaptation of sustainable green technology in line with sustainable development goals. Necessary financial assistance schemes should be implemented effectively by the government to encourage farmers to adopt green technology. The study is subject to many limitations, but one of the major limitations is it is based on a specific area, and the conclusion may not be generalized at the global level. However, the study is an important contribution to the literature in the sense that it can be referred to as a case for other regions with similar socio-environmental characteristics. The present study opens a broad perspective of scope in the area of climate change and its impact on agriculture. Further studies can be conducted with an intensive microscopic and ethnographic approach to the behavior of farmers and the changing dimensions of climate.

ACKNOWLEDGMENT

The paper is an outcome of the MA Economics Master Thesis submitted to Birla Global University, Bhubaneswar. An early version of this paper was presented in the first online virtual international conference on sustainable finance, economics, and accounting in the pre and post-pandemic era (30th-31 July 2021) organized by IIM Jammu, India. We are thankful to the participants and the conference chair for their comments and suggestions.

REFERENCES

Acquah-de Graft, H. and Onumah, E. 2022. Farmers' perceptions and adaptations to climate change: An estimation of willingness to pay. Agris, 3(2): 31-39. https://doi.org/10.22004/AG.ECON.120241

Agrawal, P.K. 2009. Vulnerability of Indian Agriculture to Climate Change: Current State of Knowledge. Indian Agriculture Research Institute, New Delhi

Akponikpè, P.B.I., Johnston, P. and Agbossou., E.K. 2010. Farmers' Perception of Climate Change and Adaptation Strategies in Sub-Saharan West Africa. 2nd International Conference: Climate, Sustainability, and Development in Semi-Arid Regions, Fortaleza-Ceará. 2nd International Conference: Climate, Sustainability and Development in Semi-Arid Regions, 16-20 August 2010, Fortaleza-Ceará, Brazil, Springer, NY, pp.1-16.

Alam, M.M., Siwar, C., Molla, R., Talib, B. and Toriman, M.P. 2012. Farmers' adaptation practices to climatic vulnerabilities in Malaysia. Mitig. Adapt. Strateg. Glob. Chang., 17: 415-423

Ayanlade, A., Radeny, M. and Morton, J.F. 2017. Comparing smallholder farmers perception of climate change with meteorological data: A case study from southwestern Nigeria. Weath. Clim. Extre., 15: 24–33. https://doi.org/10.1016/j.wace.2016.12.001

Banerjee, R.R. 2014. Farmers' perception of climate change, impact and adaptation strategies: A case study of four villages in the semi-arid regions of India. Natural Hazards, 75(3): 2829-2845. https://doi.org/10.1007/s11069-014-1466-z

Datta, P., Behera, B. and Rahut, D.B. 2022. Climate change and Indian agriculture: A systematic review of farmers' perception, adaptation, and transformation. Environ. Chall., 8: 543. https://doi.org/10.1016/j.envc.2022.100543.

Dhanya, P. and Ramachandran, M. 2016. Farmers' perceptions of climate change and the proposed agriculture adaptation strategies in a semi-arid region of south India. J. Integr. Environ. Sci., 13(1): 1-18. https://doi.org/10.1080/1943815X.2015.1062031

Eckstein, D. 2021. Global Climate Risk Index 2020. Retrieved from https://germanwatch.org/en/17307 (accessed August 10, 2021)

Esham, M. and Garforth, C. 2012. Agricultural adaptation to climate change: insights from a farming community in Sri Lanka. Mitig. Adapt. Strateg. Glob. Chang., 18(5): 937. https://doi.org/10.1007/s11027-012-9374-6

Fosu-Mensah, B.Y., Vlek, P.L.G., and Maccarthy, D.S. 2012. Farmers' perception and adaptation to climate change: A case study of Sekyedumase district in Ghana. Environ. Dev. Sustain., 14(4): 495-505. https://doi.org/10.1007/s10668-012-9339-7

Guodaar, L., Kabila, A., Afriyie, K., Segbefia, A.Y. and Addai, G. 2023. Farmers' perceptions of severe climate risks and adaptation interventions in indigenous communities in northern Ghana. Int. J. Disas. Risk Reduct., 95: 891. https://doi.org/10.1016/j.ijdrr.2023.103891

Jha, C.K. and Gupta, V. 2021. Farmer's perception and factors determining the adaptation decisions to cope with climate change: Evidence from rural India. Evidence from rural India, Environ. Sustain. Indic., 10: 112. https://doi.org/10.1016/j.indic.2021.100112.

Kemausuor, F., Dwamena, E., Bart-Plange, A. and Kyei-Baffour, N. 2011. Farmers' perception of climate change in the Ejura-Sekyedumase District of Ghana. ARPN J. Agric. Biol. Sci., 6: 26-37.

Koirala, P., Kotani, K. and Managi, S. 2022. How do farm size and perceptions matter for farmers' adaptation responses to climate change in a developing country? Evidence from Nepal. Econ. Anal. Policy, 74: 188-204.

Manandhar, S., Vogt, D.S., Perret, S.R. and Kazama, F. 2010. Adapting cropping systems to climate change in Nepal: A cross-regional study of farmers' perception and practices. Reg. Environ. Chang., 11(2): 335-348. DOI: 10.1007/s10113-010-0137-1

Mengistu, D.K. 2011. Farmers' perception and knowledge on climate change and their coping strategies to the related hazards: A case study from Adiha, central Tigray, Ethiopia. Agric. Sci., 02: 138-145. http://dx.doi.org/10.4236/as.2011.22020

Mishra, A. and Agrawal, A. 2021, Food commodity price volatility and its nexus with monetary factor: an empirical analysis of India. Int. J. Manag. Pract., 14(1): 88-106.

Mishra, A.K., Dash, A.K., and Agrawal. A. 2023. Quest of dynamic linkages between monetary factors and food inflation in India. Theoret. Appl. Econ., 2(635): 199-210.

Mushagalusa, B.A., Munyahali, W., Tshomba Kulumbu, J., Nge Okwe, A., Nkulu Mwine Fyama, J., Kasongo Lenge, E. and Nyumbaiza Tambwe, A. 2022. Understanding farmers' perception of climate change and adaptation practices in the marshlands of South Kivu, Democratic Republic of Congo. Clim. Risk Manag., 15: 236.

Okonya, J.S., Syndikus, K., Kroschel, J. 2013. Farmers' Perception of and Coping Strategies to Climate Change: Evidence from Six Agroecological Zones of Uganda. J. Agric. Sci., 5(8): 252. https://doi.org/10.5539/jas.v5n8p252

Sargani, G.R., Jiang, Y., Joyo, M.A., Liu, Y., Shen, Y. and Chandio, A.A. 2023. No farmer no food, assessing farmers climate change mitigation, and adaptation behaviors in farm production. J. Rural Stud., 100: 3035. https://doi.org/10.1016/j.jrurstud.2023.103035.

Saylor, J.E., Sundell, K.E. and Sharma, G.R. 2019. Characterizing sediment sources by non-negative matrix factorization of detrital geochronological data. Earth. Planet. Sci. Lett., 512: 46-58.

Sehgal, V. 2023. Crop diversity and farm income: Evidence from a large-scale national survey. Indian Growth Devel. Rev., 16(1): 1-17. https://doi.org/10.1108/IGDR-01-2022-0008

Shukla, G., Kumar, A., Pala, N.A. and Chakravarty, S. 2016. Farmers' perception and awareness of climate change: A case study from Kanchandzonga Biosphere Reserve, India. Environ. Dev. Sustain., 18(4): 1167-1176. https://doi.org/10.1007/s10668-015-9694-2

Udmale, P., Ichikawa, Y., Manandhar, S., Ishidaira, H. and Kiem, A.S. 2014. Farmers' perception of drought impacts, local adaptation and administrative mitigation measures in Maharashtra State, India. Int. J. Disas. Risk Red., 10: 250-269. https://doi.org/10.1016/j.ijdrr.2014.09.011

Vardan, R.J. and Kumar, P. 2014. Indigenous knowledge about climate change: validating the perceptions of dryland farmers in Tamil Nadu. Indian J. Trad. Knowl., 13(2): 390-397. https://doi.org/10.1016/j.ijdrr.2014.09.011

Nature Environment and Pollution Technology
An International Quarterly Scientific Journal

p-ISSN: 0972-6268
(Print copies up to 2016)
e-ISSN: 2395-3454

Vol. 23 | No. 1 | pp. 355-363 | 2024

Original Research Paper

https://doi.org/10.46488/NEPT.2024.v23i01.030

Open Access Journal

Feasibility Analysis of Municipal Wastewater Reinjection Technology

Haijie Hu*(**), Huan Zhang*, Lei Han**, Le Zhang****, Tao Yu**(*****)† and Chengtun Qu****

*Shaanxi Zhiyuan Siyuan Environmental Protection Technology Co. Ltd., Xi'an 710065, PR China

**Xi'an Shiyou University, Shaanxi Provincial Key Laboratory for Environmental Pollution Control and Reservoir Protection, Xi'an 710065, PR China

***Weinan Normal University, School of Chemistry and Materials, Weinan 714099, PR China

****Xi'an Aeronautical University, Institute of Energy and Architecture, Xi'an 710077, PR China

*****Yan'an Oil and Gas Field Environmental Pollution, Low-carbon Collaborative Control Technology and Reservoir Protection Key Experiment, Shaanxi Fuquan Environmental Protection Technology Co. Ltd., Yanan 727500, PR China

†Corresponding author: Tao Yu; 569775931@qq.com

Nat. Env. & Poll. Tech.
Website: www.neptjournal.com

Received: 18-07-2023
Revised: 11-09-2023
Accepted: 12-09-2023

Key Words:
Produced water
Municipal sewage
Reinjection technology
Compatibility

ABSTRACT

To study the feasibility of using municipal sewage as a reserve water source for oilfield reinjection, the water sample treated by the municipal sewage treatment plant and the produced water of the Chang 2 reservoir were taken as the research objects. Through the analysis of water quality and compatibility, the optimal ratio of reinjection water samples was determined. At the same time, the clay swelling experiment and reservoir damage experiment were carried out. The experimental results show that the salinity of municipal sewage is low, and the content of scale ions is low. When the ratio of produced water to municipal sewage is 7:3, the scale formation amount can reach 42.5 $mg.L^{-1}$, and when the scale inhibitor is added, the scale formation amount can be reduced to 10.4 $mg.L^{-1}$. The mixed water sample will not cause clay expansion. Meanwhile, Chang 2 reservoir is moderately weak water sensitive and weak acid sensitive. The oil content, suspended solids content, and median particle size of the mixed water sample during reinjection should be controlled at 5 $mg.L^{-1}$, 5 $mg.L^{-1}$, and 5 μm to ensure that the reinjected water sample does not cause damage to the reservoir.

INTRODUCTION

Water injection development in oil fields is an important way to achieve efficient reservoir development. Reliable water sources and stable water quality are the basic requirements for water injection development. However, with the continuous expansion of the water injection scale, the contradiction between the demand for water injection and water supply in oil fields has become increasingly prominent (Ge et al. 2017, Ye et al. 2016). At present, the injected water in most oilfields is mainly produced water, and some water injection stations use circulating water from the boiler in the station and treat domestic sewage in the station as supplementary water sources for reinjection (Xin 2021, Gao et al. 2016). However, in some water injection sites, the amount of water injected is low, resulting in lower formation pressure, which seriously affects the oil recovery. Therefore, it is particularly important to select the appropriate supplementary water source. At present, the national sewage discharge index is increasingly strict, and direct sewage discharge after treatment is also a waste of resources. In 2020, urban sewage discharge in our country reached 57.1 billion m^3 (Zhang et al. 2022). In Northern Shaanxi Province, water resources are especially precious because of drought and less rain. If the treated municipal sewage is used for oilfield reinjection, it can effectively slow down the pressure of oilfield water injection and reduce the cost of oilfield water injection. At the same time, the reuse of municipal sewage is of strategic significance to reduce pollutants, reduce environmental pollution, and alleviate water shortage (Zhang et al. 2020).

Chang 2 reservoir in Yanchang Oilfield is a tight reservoir with low permeability and a small pore throat (Xing 2009, Du et al. 2015, Yang 2002). The treated municipal sewage contains a large number of suspended particles with large particle sizes. The biochemical process is generally used to degrade organic matter in the treatment of municipal sewage, and the bacterial content in the treated water sample exceeds the standard (Liu et al. 2020). If direct injection is made, suspended matter, emulsified oil, dissolved oxygen, bacteria, and other substances injected into the water will block the reservoir, which will seriously decrease the water absorption capacity of the injection well and increase the water injection pressure, thus affecting the liquid output of

the oil well (Wang 2021, Yang 2015, Wu et al. 2012). At the same time, the salinity of produced water is relatively high (Ding et al. 2019). If it is not compatible with municipal sewage, the scale crystals generated will also cause pore throat blockage of the reservoir (Bu et al. 2022). Therefore, the compatibility of reinjection water and reservoir fluids should be considered during reinjection. At the same time, according to the characteristics of reinjection water and the reservoir damage mechanism, the water injection development system and water quality standards in line with the reservoir characteristics should be standardized (Bu et al. 2022, Chang et al. 2017). In this paper, the municipal wastewater and the produced water of Chang 2 reservoir are taken as the research objects, and the water quality analysis, compatibility research, clay swelling experiment, and reservoir damage rate experiment are carried out. The feasibility evaluation of the injected formation of Chang 2 reservoir produced water and municipal wastewater is also carried out, which provides a basis for the injected formation of municipal wastewater and produced water.

MATERIALS AND METHODS

Materials

The municipal sewage used in the experiment was taken from the treated water sample of the Wuqi sewage Treatment plant. The produced water used is the produced water of Chang 2 formation in Wuqi Oil Production Plant. The core used in the experiment was taken from well 10-40 of the resource perimeter in Chang 2 Reservoir.

LDY50-180 multi-functional core flow tester, Nantong Yichuang Experimental Instrument Co., Ltd. Uv-visible spectrophotometer, Shanghai Youke Instrument Co. Ltd.

Analytical Methods

According to the oil and gas industry standards, "Water Quality Index and Analysis Method for Clastic Reservoir Injection" (SY/T 5329-2012), "Oil and gas field water Analysis Method" (SY/T 5523-2016) and "Water and Wastewater Monitoring and Analysis Method" (Fourth edition) for the detection and analysis of total ion content, oil content, suspended matter content, corrosion rate and bacterial content (SY/T 5523-2000, SY/T 5329- 2012).

The produced water from the oil field was mixed with municipal sewage in a certain proportion (9:1-1:9), and the simulated formation temperature was placed at 60°C for 72 h. After the placement, the appearance of the water sample was observed, and the experimental phenomenon was recorded. The compatibility was evaluated by measuring the calcium loss rate and scale amount in the mixed water, and the calcium loss rate was calculated according to the formula:

$$\text{Calcium loss rate} = \frac{C_{\text{before mixing}} - C_{\text{after mixing}}}{C_{\text{before mixing}}} \times 100\%$$

The clay swelling experiment was conducted according to the "Evaluation Method of Clay Stabilizer Performance for Fracturing Acidification and Water Injection in Oil and Gas Fields" (SY/T 5971-2016). 1 g sodium-based bentonite was mixed with a 10 mL water sample, poured into a 10 mL centrifuge tube, and stood at 25°C for 2 h. Then, centrifuged at 1500 r.min^{-1} for 15 min to measure the bentonite volume V_1, and 3%KCl solution was used instead of the reinjection water sample to measure the expansion volume V_2. Calculation formula of relative expansion rate:

$$\text{Relative expansion rate} = \frac{V_1 - V_2}{V_2} \times 100\%$$

Where V_1 represented the expansion volume (mL) of the reinjection sample mixed with clay; V_2 represented the expansion volume of 3% KCl mixed with clay, mL.

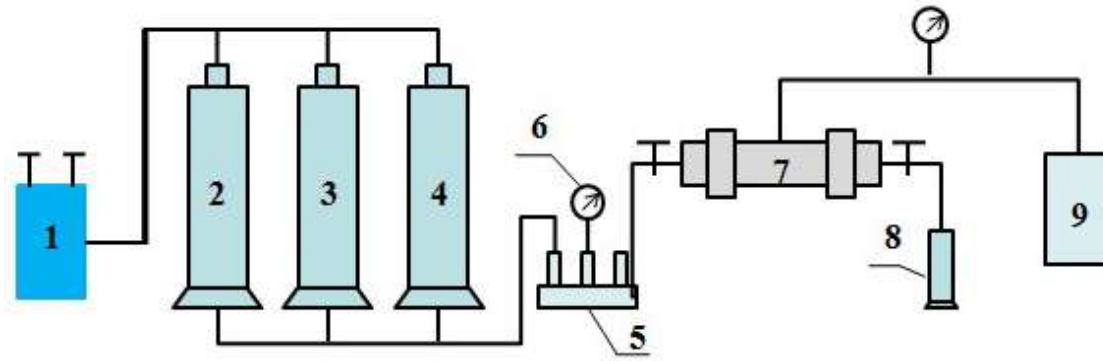

1 - advection pump; 2,3,4 - high pressure tank; 5-6. 6 - pressure gauge; 7 - core gripper; 8 - measuring cylinder; 9 - ring pump
Fig. 1: Flow chart of core damage experiment.

According to the petroleum industry standard SY/T 5358-2010 "Experimental Evaluation Method of Reservoir Sensitivity flow," various sensitivity evaluation experiments were conducted on the Chang 2 reservoir. At the same time, the influencing factors of reservoir damage are analyzed (SY/T53588-2010). The experimental process is shown in Fig. 1.

RESULTS AND DISCUSSION

Water Quality Analysis

Total ion analysis of water quality was carried out on water samples after municipal sewage treatment and oil field-produced water. The experimental results are shown in Table 1.

It can be seen from Table 1 that the scale-forming ions of municipal sewage are relatively low, and the scale-forming ions in the produced water of Chang 2 reservoir are significantly higher than that of municipal sewage. If the two water samples are mixed, scale formation may occur. The dissolved oxygen content in the municipal sewage water sample is significantly higher than that in the produced water, mainly because the municipal sewage treatment process contains aeration. Meanwhile, the dissolved oxygen content in the water will be significantly higher if the municipal sewage is in contact with the atmosphere for a long time (Chi et al. 2021). Therefore, the damage to the reservoir caused by scale formation and suspended matter should be strictly considered when using municipal sewage as a reinjection sample.

Table 1: Water ion composition.

Test items		Produced water	Municipal wastewater
Ca^{2+} [mg·L^{-1}]		669.34	8.42
Mg^{2+} [mg·L^{-1}]		226.08	7.78
Fe^{2+} [mg·L^{-1}]		0.08	0.07
Fe^{3+}[mg·L^{-1}]		0.14	0.08
Cl^{-} [mg·L^{-1})		20893.52	402.54
CO_3^{2-} [mg·L^{-1})		0.00	0.00
HCO_3^{-} [mg·L^{-1}]		280.69	244.08
S^{2-} [mg·L^{-1}]		3.67	0.14
SO_4^{2-} [mg·L^{-1}]		759.76	263.40
K^+ Na^+ [mg·L^{-1}]		1280851	454.49
Salinity [mg·L^{-1}]		35641.79	1381.00
Water type		Calcium chloride	Sodium bicarbonate
pH		6.5	6
Oil content [mg·L^{-1}]		1.25	0
SS [mg·L^{-1}]		3.15	8.76
Median particle size [um]		0.80	1.81
Dissolved oxygen content [mg·L^{-1}]		0.37	3.42
Mean corrosion rate [mm·a^{-1}]		0.0249	0.0527
Bacteria [per cell·mL^{-1}]	SRB	6	0
	FEB	0.6	0.6
	TGB	2.5	6

Mixed Compatibility

The produced water from the oilfield and municipal sewage were mixed. The compatibility of the mixed water sample was analyzed. The experimental results are shown in Fig. 2.

As can be seen from Fig. 2, when the ratio of produced water and municipal sewage is low, the water sample has good compatibility and can reach the reinjection index. The ratio of produced water and municipal sewage is 7:3, the maximum scaling amount reaches 42.5 mg.L^{-1}, and the calcium loss rate reaches 15.90%. After adding a scale inhibitor to the mixed water sample, the scale formation amount of the mixed water sample can be reduced to 10.4 mg.L^{-1}, and the calcium loss rate can be reduced to 4.22%. Therefore, in the later reinjection process, the corresponding scale inhibitor can be added to the mixed water sample to avoid the blockage of the reinjection pipeline, equipment, and reservoir void caused by the scale formation of the mixed water sample, which will affect the reinjection effect (Liu et al. 2015, Wang et al. 2021).

Clay Swelling

When the injected water enters the formation, it will react with the clay material in the formation. Due to the difference in the salinity of the water samples, the clay will produce

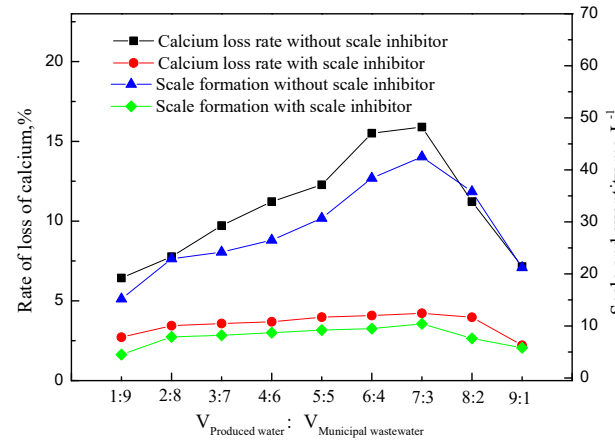

Fig. 2: Experimental analysis of compatibility between municipal sewage and produced water.

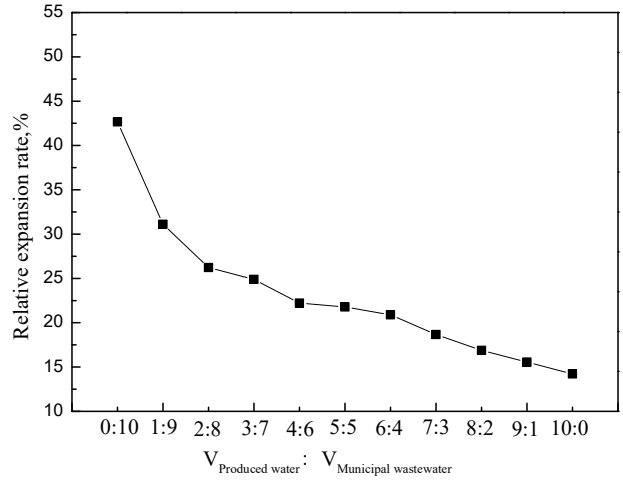

Fig. 3: Effect of reinjection sample on the clay swelling.

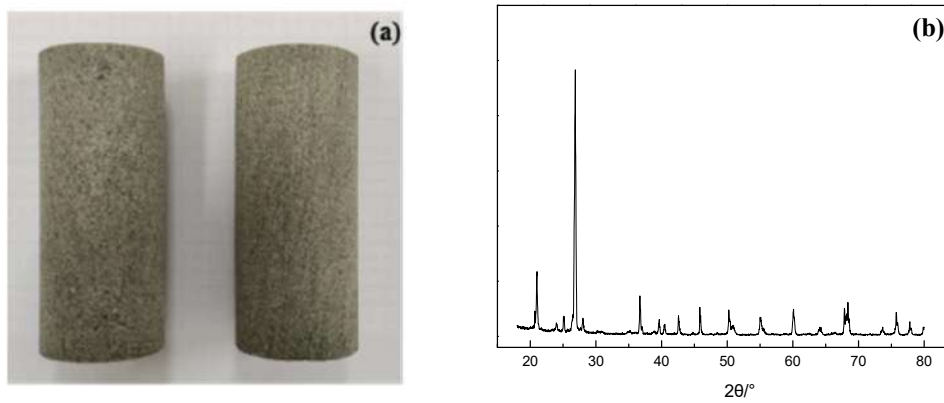

Fig. 4: (a) Core photo of Chang 2 reservoir Group and (b) XRD patterns of Chang 2-layer cores.

hydration expansion and disperse migration. The mixed water samples of produced water and municipal sewage were analyzed by clay swelling experiment. The experimental results are shown in Fig. 3.

It can be seen from Fig. 3 that with the increase in the proportion of produced water in the reinjection sample, the clay swelling rate gradually decreases. The clay swelling rate of produced water is 14.22%, while that of municipal sewage is 42.67%, which is relatively large. The salinity of produced water is relatively high, and divalent ions such as Ca^{2+} and Mg^{2+} in the water sample diffuse to the interlayer of clay, which inhibits the hydration and swelling of clay and makes the mixed water sample with a large proportion of produced water has a relatively low swelling rate (Kang et al. 2019).

Reservoir Damage

Reservoir injury refers to the damage to the natural capacity of the reservoir caused by various human factors during the opening and subsequent development of the reservoir. The causes of reservoir damage mainly include sensitivity factors, clogging factors, and corrosive factors (Ren et al. 2010).

Reservoir Characteristics Analysis

As can be seen from Fig. 4(a), the overall color of the Chang 2 reservoir core in Wuqi Yanchang is light and gray. Its main composition is quartz, kaolinite, chlorite, illite, calcite, feldspar, etc. (Fig. 4(a) and Fig. 4(b)). Based on the analysis of core sample data of Chang 2 reservoir in the study area, Chang 2 reservoir in Yanchang Oilfield is a typical medium-low porosity and ultra-low permeability reservoir. The main distribution range of its porosity is 2.19%~16.4%, and the average porosity is 10.8%. The permeability distribution range was $0.12\sim8.63\times10^{-3}\mu m^2$, and the average permeability was $1.25\times10^{-3}\mu m^2$. Due to the small porosity and low permeability of the Chang 2 reservoir, incompatibility between injection water and formation water

will lead to scaling and precipitation, which will easily block the pore throat, cause reservoir damage, and reduce the water absorption capacity of the injection well. Therefore, it is necessary to conduct research and analysis on injection water compatibility (Yang & Wang 2021).

Reservoir Sensitivity Factors

When the injected water is not compatible with the reservoir rock, the clay in the rock will expand, disperse, and migrate to damage the formation, which usually includes water-sensitive, velocity-sensitive, salt-sensitive, acid-sensitive, and alkali-sensitive (Liu et al. 2020, Hu 2015). The sensitivity test was carried out to analyze and evaluate the core of the Chang 2 reservoir in Yanchang Oilfield, and the experimental results are shown in Fig. 5.

Based on the sensitivity analysis of different cores in the long two layers, it can be seen from Fig. 5(a) that the rate of speed-sensitive damage in the long two layers is 0~25%, which is weak speed-sensitive, and the critical average flow rate is 0.5 mL.min^{-1}. Therefore, the zone is not prone to speed-sensitive damage, and the mining rate can be appropriately increased during water injection and mining. However, due to the shear action of fluid, the clay in the reservoir rock will be dispersed to form particles, which will block the pore throat and cause speed-sensitive damage. As can be seen from Fig. 5(b), the water sensitivity index

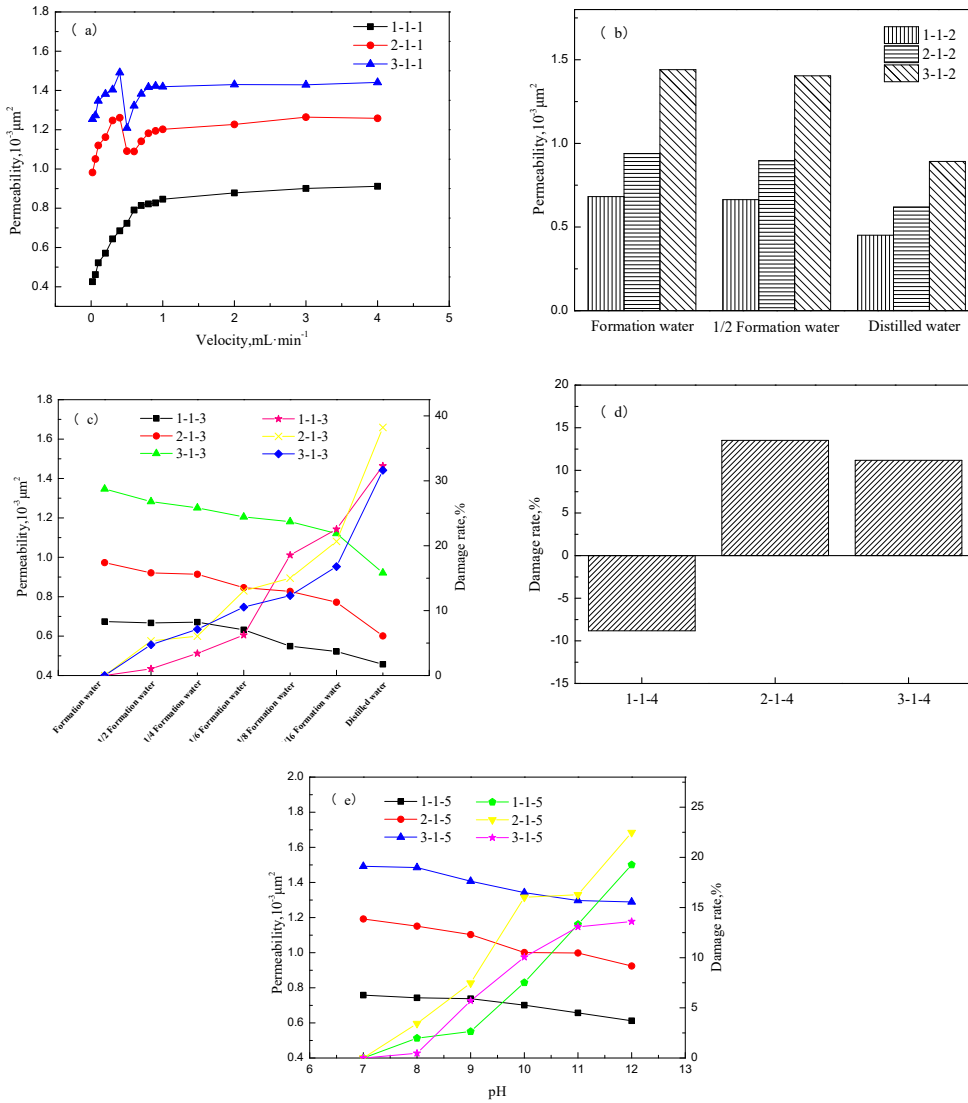

Fig. 5: Results of core velocity sensitivity (a), core water sensitivity (b), core salt sensitivity (c), petrocardiic acid sensitivity (d), and core alkali sensitivity (e).

of the long second layer is 33%-38%, which is moderately weak. The main reason is that there are a large number of clay minerals, such as kaolinite and illite, in the cracks of the Chang 2 reservoir. When the injected water enters the Chang 2 reservoir, the lattice expansion, dispersion, and migration of clay minerals occur, resulting in the blockage of the pore throat, reducing the migration channel of the reservoir, resulting in the reduction of reservoir permeability and water-sensitive damage. As can be seen from Fig. 5(c), when the injected water salinity is 1/16 formation water, the damage rate to the Chang 2 reservoir is greater than 20%. Therefore, the critical salinity of the Chang 2 reservoir is 4455.23~35641.79 mg.L^{-1}. As can be seen from Fig. 5(d), the acid sensitivity index of hydrochloric acid in the Chang 2 reservoir ranges from -8% to 13%, which is moderately weak acid sensitivity. This is because hydrochloric acid solution reacts with acid-sensitive minerals in the core after entering the core, resulting in secondary precipitation or releasing particles to block the pore throat, resulting in a decrease in reservoir permeability. As can be seen from Fig. 5(e), with the increase of pH value of injected water, its damage rate to the reservoir gradually increases. When the pH value is 12, the damage rate to the reservoir is lower than 20%, which is weak alkali sensitive. Therefore, the water-sensitive damage should be considered when the salinity of reinjection water or reinjection water is less than 4455.23 mg.L^{-1}.

Effect of Oil Content

Based on the mixed water sample of municipal sewage and Chang 2 reservoir produced water, injected water with different oil content is prepared to conduct a core damage experiment. Permeability and damage rate of injected water to the reservoir are taken as the investigation objects to determine the maximum oil content of injected water (Zhao 2020). The experimental results are shown in Fig. 6.

As can be seen from Fig. 6(a), with the increase in injection volume, the reservoir permeability will gradually decrease, and the damage rate to the reservoir will gradually increase. With the increase of the oil content in the mixed water sample, the permeability decreases greatly, and the damage rate to the reservoir increases gradually [Fig. 6(a)]. When the oil content is greater than 10 mg/L, and the injection volume increases to 30 PV, the damage rate to the core is greater than 20%, mainly because the crude oil in the water sample will adhere to the pipeline when entering the water injection pipeline. With the increase of the injection volume, the crude oil in the water sample will enter the core, resulting in the blockage of the pore throat of the core and the reduction of core permeability. When the oil content in the water sample is lower than 5 mg.L^{-1}, the permeability of the reservoir gradually decreases, but the damage rate to the reservoir is lower than 20%. This is because, with the increase of injection volume, impurities in the water sample will accumulate and block part of the pore throat, resulting in a slight decrease in core permeability and a low damage rate to the reservoir (Zhang et al. 2001, Cui 2021). Therefore, the oil content in the reinjection water sample should be kept below 5 mg.L^{-1}. However, the oil content in the water sample after mixing municipal sewage and produced water is 0.5 mg.L^{-1}, lower than 3 mg.L^{-1}, and the damage to the reservoir is less than 20%, which can be directly injected back into the Chang 2 reservoir.

Effect of Suspended Matter Content

Based on the mixed water sample of municipal sewage and Chang 2 reservoir produced water, injected water with different suspended solids content was prepared to conduct core damage experiment (Wang et al. 2016, Yang 2012). Permeability and damage rate of injected water to the reservoir were taken as the investigation objects to determine

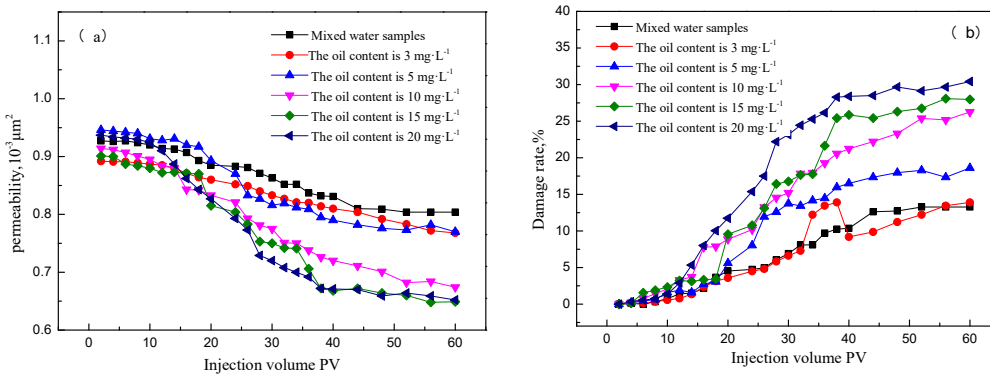

Fig. 6: Effect of oil content on reservoir.

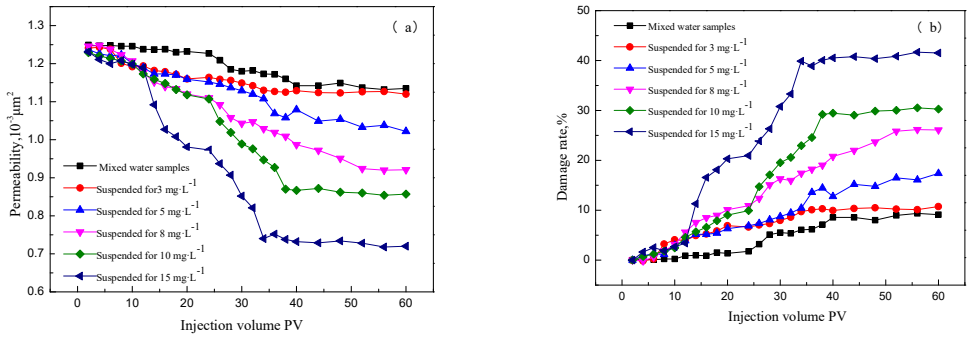

Fig. 7: Influence of suspended matter content on reservoir.

the maximum suspended solids content in injected water. The experimental results are shown in Fig. 7.

As can be seen from Fig. 7(a), with the increase of the content of suspended solids in the reinjection water sample, the permeability of the Chang 2 reservoir gradually decreases with the increase of the injected water volume. The damage rate of injected water to the core gradually increases with the increase of the injected water volume (Fig. 7(b)). When the injected volume is 30 PV, and the content of suspended solids in the water sample is 5 mg.L^{-1}, the damage rate of the core is lower than 10%. When the suspended solids increase to 8 mg/L, the damage rate of injected water to the core is higher than 20%. When the suspended solids content increases to 15 mg.$^{-1}$L, the damage rate of injected water to the core can reach more than 40%. The damage degree to the core is relatively large, so the suspended solids content of injected water can not be higher than 5 mg.L^{-1}. After mixing municipal sewage and produced water, the suspended matter content in the water sample is 1.8 mg.L^{-1}, lower than 5 mg.L^{-1}, and the damage to the reservoir is far less than 20% so that it can be directly injected back into the Chang 2 reservoir.

Effect of Particle Size of Suspended Matter

Based on the mixed water samples of municipal sewage and Chang 2 reservoir produced water, clay with different particle sizes was used to prepare solutions with a suspended solids content of 5 mg.L^{-1}, and core damage experiments were carried out. The maximum particle size of suspended solids in injected water was determined based on the permeability and damage rate of injected water to the reservoir. The experimental results are shown in Fig. 8.

As can be seen from Fig. 8(a), with the increase of the particle size of suspended solids in the reinjection water sample, the permeability of the Chang 2 reservoir gradually decreases with the increase of the injected water volume. The damage rate of injected water to the core gradually increases with the increase of the injected water volume (Fig. 8(b)). When the particle size of a water sample is less than 0.45 μm, with the increase of injection volume, the core has no damage. When the injection volume is 30PV, and the particle size of suspended solids increases from 3 μm to 5 μm, the damage rate of the core increases from %14 to %21. This is because the pore throat of the core will be blocked by the increase of the particle size of suspended solids in the water

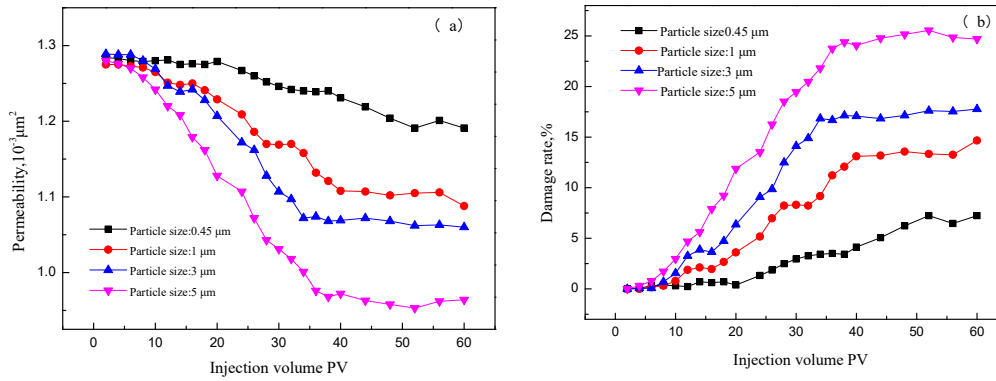

Fig. 8: Influence of particle size of suspended solids on reservoir.

Table 2: Recommended water quality indicators for reinjection.

Project	Recommended indexes
pH	6-9
Oil content [mg.L^{-1}]	≤5
Suspended matter content [mg.L^{-1}]	≤5
Median particle size [μm]	≤5
Corrosion rate [mm.a^{-1}]	≤0.067

sample, resulting in the decrease of reservoir permeability and the increase in damage rate. Therefore, the particle size of suspended solids in injected water is larger than 5 μm, which will cause serious damage to the core. The particle size of suspended solids in reinjected water should be controlled below 5 μm. The particle size of the water sample after mixing municipal sewage and Chang 2 reservoir-produced water is 0.8 μm, so the mixed water sample can be injected directly without harming the reservoir.

Indicators of Reinjection of Water

Through the compatibility test, clay swelling test, and reservoir damage test of municipal sewage and produced water, it can be confirmed that municipal sewage can be used as a reserve water source for oilfield reinjection water. Combined with Recommended Indicators and Analysis Methods for Water Quality of clastic Reservoir Injection (SY/T 5329-2012), the injection standard of mixed water samples of municipal sewage and produced water injected into the Chang 2 reservoir is proposed, and the results are shown in the following table.

CONCLUSION

(1) The water type of municipal sewage is sodium bicarbonate, with a salinity of 1381 mg/L and low-scaling ions. The produced water from the Chang 2 reservoir belongs to the calcium chloride type, with a high content of scaling ions and a mineralization degree of 35641.79 mg.L^{-1}. The static corrosion rate of municipal sewage and produced water is less than 0.076 mm.a^{-1}, which meets the reinjection standard.

(2) When the ratio of produced water to municipal sewage is 7:3, the maximum scaling amount is 42.5 mg.L^{-1}, and the calcium loss rate is 15.90 %. After adding a scale inhibitor, the scaling amount of the mixed water sample is reduced to 10.4 mg.L^{-1}, showing good compatibility. The clay swelling rate of the mixed water sample of produced water and municipal sewage is low, which meets the reinjection effect.

(3) The water sensitivity factor should be considered when the mixed water sample is reinjected into reservoir Chang 2. The contents of oil, suspended solids, and the median particle size of the reinjected water samples should be controlled at 5 mg.L^{-1}, 5 mg.L^{-1}, and 5 μm to avoid the damage of the reinjected water samples to the reservoir when reinjecting mixed water samples.

ACKNOWLEDGMENT

The present work is supported by the Key Project of Shaanxi Provincial Department City Linkage (No. 2022GD-TSLD-69) and the Shaanxi Provincial Department of Education Service Local Special Plan (No. 22JC054).

REFERENCES

Bu, K.Y., Yan, H.B., Cheng, P., Zhang, Y.S., Liu, L.H. and Lin, H. 2022. Study on oilfield-produced water reinjection treatment process. Water Treat. Technol., 13(01): 104-107.

Chang, P., Zhang, Q.Z., Guo, W.Z., Ke, C.Y., Hao, X.P. and Lu, Y. 2017. A study on produced water scaling during reinjection from chang 2 reservoir in Yanchang oilfield. Chem. Eng. Oil Gas, 46(03): 115-120.

Chi, Y.L., Shi, X., Ren, T., Wang, X.C. and Jin, P.K. 2021. Effects of dissolved oxygen on nutrient removal performance and microbial community in low carbon/nitrogen municipal wastewater treatment process. Environ. Sci., 42(09): 4374-4382.

Cui, D.D. 2021. Experimental study on permeability damage of emulsified oil during water injection. J. Sheng. Coll. China Univ. Petrol., 35(04): 41-45.

Ding, P.Y., Dang, W., Wang, L.L. and Liu, J.X. 2019. Current status and prospect of oilfield-produced water reinjection treatment technology. Modern Chem. Ind., 39(03): 21-25.

Du, L.C., Li, F.J., Qu, X.L., Zhang, Y., Hou, J.T. and Su, Y.Y. 2015. Controlling factors of erosion paleogeomorphology oil pool of Chang 2 oil reservoir group in Wuqi area, ordos basin, China. J. Chengdu Univ. Technol., 42(06): 719-725.

Gao, P., Zhou, Y. and Gao, L. 2016. Research on the feasibility of the reinjection of domestic sewage to strata from offshore platforms of Bohai Bay OilfieId. Ind. Water Treat., 36(12): 94-96.

Ge, Z.A., Li, Y.H., Zhang, F.L., Li, R. and Huang, J.X. 2017. Status quo and development prospect of water injection treatment in oilfield production. China Petrochem., (1):5-6.

Hu, S.M. 2015. Study on the damage law of sewage reinjection in Chang 2 reservoir in Yuanmao Well area, Wayaobao. Xi'an Shiyou University, Xi'An, China.

Kang, D.Y., Xue, C., Qu, C.T., Li, Q. and Yu, T. 2019. Reinjection feasibility study of fracturing flow-back fluid. Chem. Eng., 47(07): 5-9.

Liu, M.L., Xiong, H.S., Ma, M., Li, X., Qiu, W.X., Song, X.Q., Zhang, M.M., Leng, Y.L., Chen, Y.H., Yang, Y.F., He, Y.X., Gui, Z.C., Wang, R.N. and Luo, X. 2020. Emission and quantitative microbial risk assessment (QMRA) of bioaerosols in municipal wastewater treatment plant. Water Wastewater Eng., 56: 567-575.

Liu, S.Y., Qu, C.T., Yang, P.H. and Wang, J.D. 2015. Compatibility study of formation and clean water mixed injection in North Shaanxi permeable oil fields. Chem. Eng., 43(06): 6-9.

Liu, X.G., Zhou, Y.Y., Zhang, J.Q. and Xiao, W.L. 2020. Experimental study on properties wastewater reinjection of tight sandstone in Daniudi gas field. Drill. Prod. Technol., 43(06): 100-102.

Ren Z.L., Yang, X.C., Xue, J.M., Lei, L.Q., Wang, M., Kang, L.M. and Shi, Z. 2010. Analysis of the damage factors of the injection water to the reservoirs in the Yanchang oil Region. J. Northwest Univ., 40(04): 667-671.

SY/T 53588-2010, Experimental evaluation method of reservoir sensitivity flow.

SY/T 5329- 2012, Water quality index and analysis method of clastic reservoir.

SY/T 5523-2000, Oil and gas field water analysis method.

SY/T 5971-2016, Performance evaluation method of clay stabilizer for fracturing acidification and water injection in oil and gas fields.

Wang, Q., Hong, Q.L., Cao, J., Zhou, J. and Niu, M. 2016. Study on the damage law of solid particles on the reservoir. Petrochem. Ind. Appl., 35(01): 21-26.

Wang, X.W. 2021. Study on reservoir sensitivity evaluation and key control factors of tight oil reservoirs. Special Oil Gas Reserv., 28(01): 103-110.

Wang, Y.Y., Liu, Q.W., Fan, Z.Z., Wang, B., Guo, H. and Wang, J. 2021. Research progress of common scale inhibitors in the oilfield. Petrochem. Technol., 50(11): 1222-1228.

Wu, X.M., Fu, W., Bai, H.T., Zhou, L. and Ma, Y. 2012. Study on compatibility between formation water and injection water in Jiyuan oilfield. Oilfield Chem., 29(01): 33-37.

Xin, Y.C. 2021. Feasibility study on reinjection into the stratum of domestic sewage. Shandong Chem. Ind., 50(9): 142-144.

Xing, H. 2009. Basis of Petroleum Reservoir Geology. Petroleum Industry Press, Beijing, p. 25.

Yang, H.B. 2015. The adaptability of reinjection reservoir containing poly sewage with research to sea containing poly sewage recycle in certain oilfields as an example. Sci. Technol. Eng., 15(10):180-184.

Yang, J.J. 2002. Tectonic evolution and hydrocarbon distribution in Ordos basin. Petroleum Industry Press, Beijing, p. 16.

Yang, L.Z. 2012. Water Quality Evaluation and Index Optimization of Injected Water In Shaxia Oilfield. Southwest Petroleum University, Beijing.

Yang, Y. and Wang, G.C. 2021. Sedimentary facies of Chang 2 in the Zichang area, ordos basin. Min. Explor., 12(02): 303-309.

Ye, Z.Q., Cui, M.Y., Jiang, W.D. and He, A.L. 2016. Treatment of sulfur-containing produced water for reinjection in Yanchang oilfield. J. Xi'an Shiyou Univ., 31(02): 105-111.

Zhang, G.M., Tang, Z.Y., Yao, H.X. and Fu, H.Y. 2004. Formation damage caused by injection water. Oil Drill. Prod. Technol., (03):46-48.

Zhang, J., Xiao, K., Liang, S. and Huang, X. 2022. Membrane technologies for municipal wastewater treatment and reclamation in China: Application and challenges. Environ. Eng., 40(03): 1-6.

Zhang, Q.Y. and Liu, L.S. 2020. An analysis of the current situation and development trend of rural decentralized domestic sewage based on source separation technology. China Rural Water Hydro., 08: 20-24.

Zhao, P. 2020. Study on Polymer Concentration Effect and Reservoir Damage in Reinjection Wastewater. University of Chemical Technology, Beijing.

Nature Environment and Pollution Technology
An International Quarterly Scientific Journal

p-ISSN: 0972-6268
(Print copies up to 2016)
e-ISSN: 2395-3454

Vol. 23 | No. 1 | pp. 365-379 | 2024

Original Research Paper

https://doi.org/10.46488/NEPT.2024.v23i01.031

Open Access Journal

Mapping and Monitoring of Land Use/Land Cover Transformation Using Geospatial Techniques in Varanasi City Development Region, India

Atul K. Tiwari, Anindita Pal† and Rolee Kanchan

Department of Geography, Faculty of Science, The Maharaja Sayajirao University of Baroda, Vadodara-390002 Gujarat, India

†Corresponding author: Anindita Pal; anindita.geogphd@msubaroda.ac.in

Nat. Env. & Poll. Tech.
Website: www.neptjournal.com

Received: 14-07-2023
Revised: 22-08-2023
Accepted: 21-09-2023

Key Words:
Google Earth Engine
Landsat-9
Machine learning
Random forest classifier
Land use/Land cover

ABSTRACT

Assessing the dynamics and patterns of Land Use and Land Cover (LULC) and its transformation is an important practice of urban planners and environmentalists for a variety of applications, including land management, urban climate modeling, and sustainability of any urban region. Monitoring changes in LULC using geospatial techniques can help to identify areas at risk for indefensible land use, low-grade environment, and especially for sustainable urban planning. This study aims to analyze the changing pattern, dynamics, and alteration of LULC using Google Earth Engine (GEE) and Machine Learning Applications for the years 1991, 2001, 2011, and 2022 in the Varanasi City Development Region (VCDR). The LULC classification was divided into seven classes using random forest classification, and Landsat-5(TM) and 9(OLI-2) satellite data were used. Saga GIS has been utilized for the detection of LULC change during the 1991-2022 period. For validation of classification results, accuracy assessment was estimated using error matrices and through user, producer, and overall accuracy estimation. The Kappa statistics were applied for the reliability of the accuracy assessment result. As a result, the built-up area increased by 507.8 percent, and other classes like agricultural, barren, fallow land, and vegetation cover rapidly declined and altered into concrete areas over the period. Water bodies and river sand classes have been slightly converted into different classes. The finding explains that 114.8 km^2 of fertile agricultural land, 14.81 km^2 barren land, and 12.93 km^2 of vegetation cover transformed into impervious surface, which is unsustainable and causes various problems like food scarcity, environmental degradation, and low quality of urban life. This study can be a useful guide for urban planners, academicians, and policymakers by providing a scientific background for sustainable urban planning and management of VCDR and other cities as well.

INTRODUCTION

The phenomenon of Earth's land cover has changed over the last two centuries, which has been triggered by economic development and population growth (Hu & Hu,2019). Furthermore, it is expected that the pace of these changes will continue to accelerate in the coming years (Geng et al. 2023, Pande 2022, Saravanan & Abijith 2022). The changes that are occurring at a rapid pace are overlaid on top of long-term climate dynamics and scarcity of natural resources (Pandey et al. 2021). The ability of the land to sustain human activities through the provision of multiple ecosystem services is affected by land cover change, and the resultant economic activities cause feedback that affects climate and other facets of global change (Tyagi et al. 2023). Consequently, systematic assessments of Earth's land cover must be conducted at a frequency that allows for the monitoring of both long-term trends and inter-annual or decadal variability (Chandole & Joshi 2023). Moreover, these assessments must be performed at a level of spatial and temporal specificity that permits the examination of human-driven changes (Pal et al. 2023).

Land Use and Land Cover (LULC) refers to all the living and non-living components that are present on the surface of the Earth and are considered to be one of the most critical assets of the Earth system (Chughtai et al. 2021). Its importance stems from three fundamental ways. First of all, land use interacts with the atmosphere, regulating the hydrological cycle and maintaining the energy budget, which is essential for predicting weather and climate. Secondly, it plays a significant role in the carbon cycle, acting as both a source and sink of carbon (Arévalo et al. 2020). Last but not least, land cover reflects the availability of resources such as food, fuel, timber, fiber, and shelter for human beings. It serves as a crucial indicator of other ecosystem services,

such as biodiversity (Osman et al. 2018). The information on land use is vital for many regional (Wagh 2022) and global applications, especially urban land use (Shukla & Jain 2019). To manage and maintain these valuable resources, it is crucial to understand the dynamics of LULC Changes (MohanRajan et al. 2020). With the help of advanced remote sensing technologies, it is now possible to monitor these changes at various scales and provide valuable information for policymakers and academicians (Mishra et al. 2020).

The study of LULC is scholarly important for several reasons, such as sustainable land use practices, protecting ecosystems, mitigating climate change (Sobha & Jose 2023), and promoting the well-being of both humans and the environment of any urban space (Tiware 2014). Hence, the study of patterns and dynamics of LULC in the Varanasi City Development Region (VCDR) is an attractive field of study due to its historical, geographical, and economic importance. The intricate interplay between the forces that shape the utilization and coverage of land is a fascinating phenomenon that requires attention. It is a multifaceted issue that necessitates a subtle comprehension of the factors that influence how land is used and how it evolves over space and time. The objectives of the study are to analyze the trend and pattern of LULC using Google Earth Engine (GEE) and Machine Learning Approach and assess the land transformation during the period in the study area. This study presents a juncture to acquire insights into the complicated pattern of land use and its transformation for the years 1991, 2001, 2011, and 2022.

STUDY AREA

According to Mark Twain, "Benares is older than history, older than tradition, older than legend, and looks twice as old as all of them put together." Varanasi City (Kashi/Benares/Banaras) is one of the oldest settlements in the world and it lies between rivers Varuna and Assi. The Varanasi City Development Region (VCDR) is located between 25º08'01"N to 25º28'35"N and 83º10'17"E to 82º51'04"E. The total geographical area is 67334.22 hectares (Master Plan-2031). The average elevation is 77 m from the mean sea level, but it varies in different parts. The average annual rainfall and temperature are 1067 mm and 33.4ºC respectively. April is the driest and August is the wettest month in the region. The total population of VCDR was around 2.5 million in 2011 and is estimated at 3.36 million in 2021 by the Varanasi Development Authority (VDA). The sex ratio was 887 females/1000 males, and the literacy rate was around 80 percent. The region is one of the fast-growing urban regions of Gangetic Plain due to some major service centers like Shri Kashi Vishwanath Temple, Banaras Hindu University (BHU), Banaras Locomotive Works (BLW), Sarnath Archaeological Sites, Cantonment and Lal Bahadur Shastri International Airport. The planning of the

Table 1: Specification of the Used Satellite Data.

Satellite/Sensor	Landsat-5(TM)	Landsat-9(OLI-2)
Provider	USGS	
Spatial Resolution	30 metre	
Radiometric Resolution	8 bit	12 bit
Spectral Resolution	0.45-2.35(μm)	0.43-12.51
Acquisition Date	21/05/1991; 16&24/05/2001 28/05/2011	18/05/2022
Row/Path	142/042&043	142/042
Period Covered	1991, 2001 & 2011	2022

Source: http://developers.google.com/earth-engine/datasets

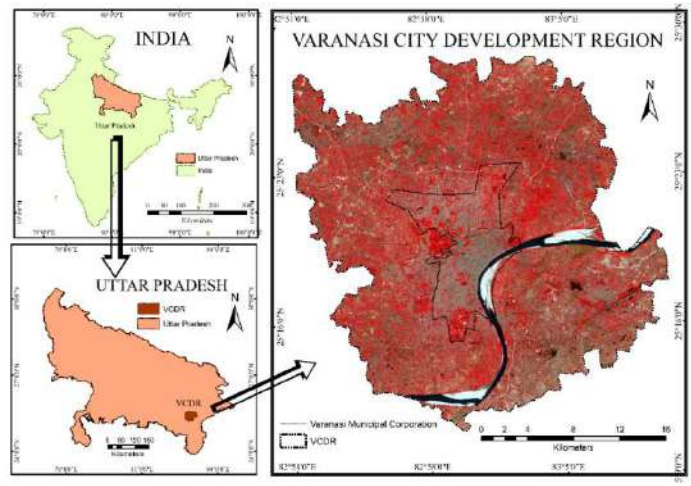

Fig. 1: Study area.

city region is the ideal approach for futuristic and sustainable development. That is the reason for choosing VCDR as the study area (Fig. 1).

MATERIALS AND METHODS

Data Sources and Tools

The LULC classification has been done using secondary data such as satellite images, Google Earth Pro temporal imageries, and prepared LULC maps of different institutions like the National Remote Sensing Centre (NRSC) and Global Land Cover data of the Environmental System Research Institute (ESRI). The primary data was also used for ground truthing and accuracy assessment, such as Global Positioning System (GPS) control points. The Landsat-5 TM and Landsat-9 OLI-2 satellite data of the United States Geological Survey (USGS) have been used for this study (Table 1). All datasets have a 30-meter spatial resolution, but the radiometric and spectral resolutions are different. The satellite data (level-1 and collection-2) was pre-georeferenced to Universal Transverse Mercator (UTM) zone 44 North projection with WGS-84 datum. The entire satellite data was processed and acquired using a custom algorithm and the GEE cloud-based platform. In this study, several tools have been used for image classification, pixel correction, accuracy assessment, finalization of maps, and graph making (Table 2).

Methodology

The significance of the methodology lies in the fact that it ensures that the study is conducted in an organized and exhaustive manner, making the results more reliable, accurate, and simple to replicate. In this study, the task-based methodology has been adopted and applied, which is outlined in Fig. 2.

LULC Classification Using Google Earth Engine

GEE is a cloud-based platform that gives users quick access to massive amounts of geographical data as well as strong analytical capabilities in the spatiotemporal context (Sudmanns et al. 2018). It facilitates scaling computations, time series data analysis, collaborative interaction, and monitoring of environmental fluctuations, etc. (Gomes et al. 2020). It is significant for its data accessibility, scalability, time-series analytic capabilities, collaborative features, conservation and environmental monitoring effect, and promotion of open data and open-source standards (Baig et al. 2022). GEE is also capable of LULC classification and is more convenient in the context of time and data acquisition (Naikoo et al. 2022). In this study, GEE has been used for LULC classification with the following steps with the help of programming in JavaScript.

Initially, the satellite data for Landsat-5 and 9 was acquired for the Area of Interest (AoI). The chosen dataset covers the years 1991, 2001, 2011, and 2022 years. The images were preprocessed using specific plugins available within the Google Earth Engine platform, which effectively eliminated the anomalies present in the satellite imagery, such as cloud cover, shadows, or atmospheric effects, through the application of image processing techniques, specifically cloud masking algorithms. Furthermore, to enhance the quality and consistency of the images, radiometric and atmospheric corrections were initiated. Layer stacking and band composition have been done and converted into a single multiband image for the particular time period. These are important processes that help in the integration of spectral information for achieving more accuracy in the classification and visualization of land features to create the training set process. A set of representative training samples has been created for learning machines to classify each of the seven LULC classes, such as built-up areas, water bodies,

Table 2: Applied Tools and Their Utilisation.

Tool	Version	Utilised For
ArcGIS	10.8	Band composition and final layout of maps
Google Earth Engine	NA	LULC classification
JavaScript	ECMAScript 2020	Programming code generation
Google Earth Pro	Multiple Temporal Images	Accuracy assessment
GPS	Garmin GPS maps 78s	GCPs collection
R-Programme	R-4.3.0	Graph making
Python	Python-3.5.3	
Saga GIS	7.8.2	LULC change detection

Source: Based on the applied tools in the study

Table 3: Description of training sets for classification.

LULC Class	Number of Polygons			
	1991	2001	2021	2022
Built-up land	95	130	129	142
Water Bodies	50	36	43	53
Agricultural land	171	96	126	138
Vegetation Cover	36	65	51	62
River Sand	37	48	19	20
Barren land	55	47	44	39
Fallow Land	54	69	61	52
Total Signatures	498	491	473	506

Source: Based on the Image Classification Process

agricultural land, barren land, fallow land, vegetation cover, and river sand within the study area frame. The training sets were prepared carefully as small polygons, and it was taken using a stratified random sampling technique (Table 3). Additionally, the existing land cover data of ESRI and NRSC were used to test and verify the prepared training samples. The Random Forest Classifier (RFC) algorithm was selected as a classification method to consider the strengths and limitations of the algorithm, such as accuracy, computational efficiency, and sensitivity.

Furthermore, prepared training sets were tested and validated the model using the validation subset to assess its accuracy and make necessary adjustments, such as fine-tuning hyperparameters. The entire stacked images were classified into seven LULC classes using a trained classification model (RFC) and generated the classified raster images (Pande 2022). The prepared raster-classified images have been extracted and post-processed using the ArcGIS 10.8 application.

Accuracy Assessment of Classification

Accuracy assessment is the most significant process for LULC classification. It is an estimation of the reliability of LULC maps. In this work, points have been created using stratified random sampling techniques and a fishnet tool to verify the classified pixels (Singh & Talwar 2013). Three types of accuracy estimation were computed, which are Overall, User, and Producer accuracy using an error matrix. The User Accuracy (UA) has been calculated using the following formula (Eq.1):

$$\alpha = \frac{n}{N} \times 100 \quad \ldots(1)$$

Where 'α' is the UA, 'n' denotes the number of corrected points classified on the image, and 'N' is the number of points verified in the field (Naikoo et al. 2022). The Producer Accuracy (PA) was measured with the help of given formula (Eq.2):

$$\beta = \frac{\sum Dij}{Rj} \quad \ldots(2)$$

Where 'β' is the PA, 'Dij' represents the corrected classified pixels in the row 'i' (diagonal cell), and 'Rj' is the total number of pixels in row 'j' (Smiraglia et al. 2016). The Overall Accuracy (OA) is the most significant accuracy type, which denotes the overall reliability of image classification (Eq.3).

$$\gamma = \frac{\sum Dij}{Cj} \quad \ldots(3)$$

Where 'γ' denotes OA, 'Dij' is the corrected & classified pixels in column j (diagonal cell), and 'Cj' is the total pixels in column 'j'. Kappa statistic is the most broadly used measurement of LULU classification accuracy to establish the relationship between two variables (Eq.4).

$$k = \frac{N\sum_{i-1}^{r} X_{ii} - \sum_{i=1}^{r}(X_{i+} \times X_{+i})}{N^2 - \sum_{i=1}^{r}(X_{i+} \times X_{+i})} \quad \ldots(4)$$

Where 'k' represents the kappa coefficient, 'N' is the total number of observations, 'r' denotes the total number of rows present in the error matrix, X_{ii} is the number of observations present in row and column 'i' respectively, X_{i+} is the total number observations in row 'i' and 'X_{+i} is the total number of observations in column 'i' (Gudex-Cross et al. 2017).

LULC Change Detection Analysis

The analysis of land use change involves assessing LULC data, which were gathered across a number of different periods to identify alterations. The change detection method contributes to an improved understanding of the repercussions of how land is exploited throughout this period (Kim 2016, Baig et al. 2022). Detecting, identifying, and estimating the changes in land use provides insights that could ultimately be used in decision-making and the creation of futuristic plans (Henits et al. 2016). Monitoring land use change through the application of Remote Sensing (RS) and GIS techniques enables an examination of spatial and temporal patterns, which helps in ensuring the oversight of land resources in a sustainable manner (Cao et al. 2022, Mahmoud et al. 2022) and in the resolution of environmental issues (Shi et al. 2021). In the beginning, the prepared classified raster dataset has been converted into a vector file. Through the implementation of the dissolve geoprocessing tool, the dataset has been amalgamated into seven distinct classes as previously outlined. Again, the intersection method was applied to detect the changes during

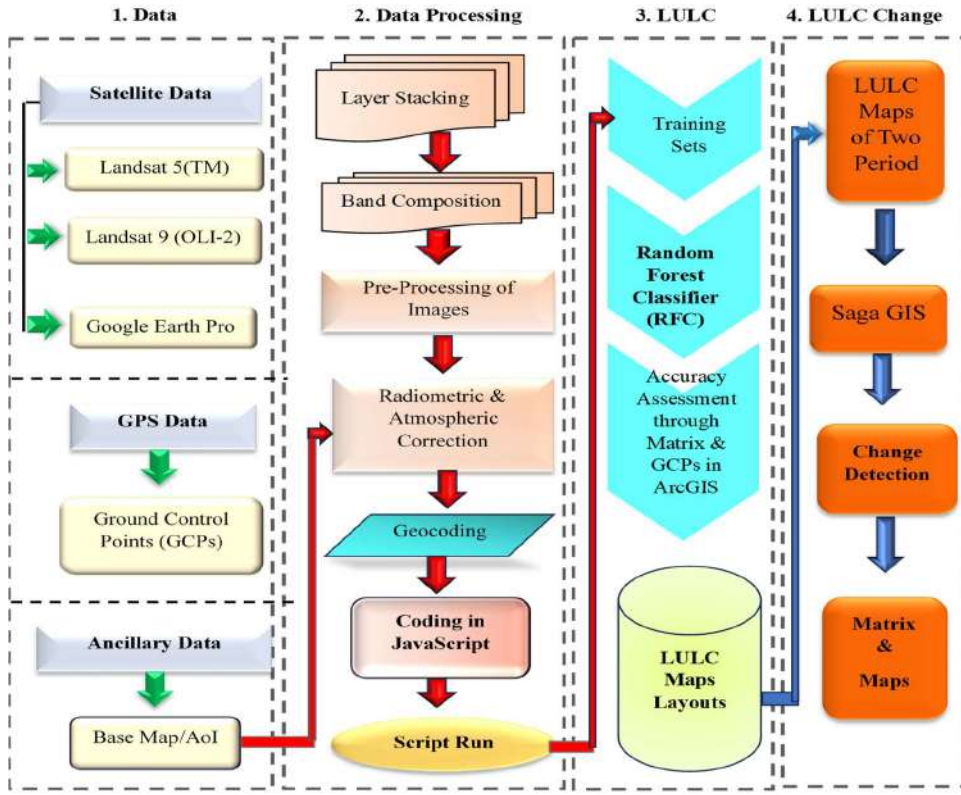

Fig. 2: Picturesque of adopted methodology.

the period classification. The transformation matrix has been exported through the Saga GIS application and plotted using R-programme for making the visual presentation of the statistics of transformed land.

RESULTS

Accuracy Assessment

The accuracy assessment is one of the most significant processes in LULC classification which helps to validate and verify the classification result. In this study, class-wise accuracy has been assessed, and the user, producer, and overall accuracy were also calculated. A total of 735 reference points have been selected through a stratified random sampling method, with 105 points in each LULC class. For estimation of the relationship between user and producer accuracy, the Kappa coefficient has been used. Table 4 presents the range of kappa coefficient values and their strength of covenant.

Accuracy Assessment in 1991

Table 5 presents the accuracy assessment matrix for 1991. Out of 735 reference points, a total of 675 points have been found correctly classified, which describes 91.83 percent of overall accuracy. Overall, above 86 percent user accuracy has been observed for each class, and producer accuracy is above 88 percent for each class. The highest user and producer accuracy were noted in the river sand and water bodies classes, respectively. The Kappa coefficient was 0.9047, which presents the strong agreement between user and producer accuracy variables and also explains the excellent classification results.

Accuracy Assessment in 2001

Table 6 corresponds to the result of the accuracy assessment for the 2001 LULC classification. Out of a total of 735

Table 4: Kappa Coefficient Range and Its Description.

k-value	Strength of Covenant
< 0.20	Strongly Disagree
0.20 - 0.40	Disagree
0.40 - 0.60	Neither Agree Nor Disagree
0.60 - 0.80	Agree
0.80 - 1.00	Strongly Agree

Source: Rwanga and Ndambuki (2017)

Table 5: Error Matrix for Accuracy Assessment of 1991 Classification.

Class	BL	WB	AL	BRL	FL	RS	VC	TU	**UA (%)**
BL	**97**	1	1	3	3	0	0	105	**92.38**
WB	0	**95**	1	0	0	7	2	105	**90.47**
AL	2	0	**94**	2	2	0	5	105	**89.52**
BRL	3	0	2	**91**	5	1	3	105	**86.66**
FL	1	0	1	5	**98**	**0**	0	105	**93.33**
RS	0	1	0	0	0	104	**0**	105	**99.04**
VC	1	0	4	1	3	0	**96**	105	91.42
TP	104	97	103	102	111	112	106	TU=735	**TC=675**
PA (%)	**93.26**	**97.93**	**91.26**	**89.21**	**88.28**	**92.85**	**90.56**		
Overall Accuracy= **91.83%**					Kappa= **0.9047**				

Source: Based on Accuracy Assessment Result of 1991

Table 6: Error Matrix for Accuracy Assessment of 2001 Classification.

Class	**BL**	**WB**	**AL**	**BRL**	**FL**	**RS**	**VC**	**TU**	**UA (%)**
BL	**93**	0	0	6	2	4	0	**105**	**88.57**
WB	0	**105**	0	0	0	0	0	**105**	**100**
AL	1	1	**93**	0	2	0	8	**105**	**88.57**
BRL	10	0	2	**79**	9	3	2	**105**	**75.23**
FL	2	0	14	6	**80**	**2**	1	**105**	**76.19**
RS	0	0	0	0	0	**105**	0	**105**	**100**
VC	1	0	9	1	3	0	**91**	**105**	**86.66**
TP	**107**	**106**	**118**	**92**	**96**	**114**	**102**	**TU=735**	**TC=646**
PA (%)	**86.91**	**99.05**	**78.81**	**85.86**	**83.33**	**92.1**	**89.21**		
Overall Accuracy= **87.89%**					Kappa= **0.8587**				

Source: Based on Accuracy Assessment Result of 2001

reference points, a total of 646 corrected points have been identified, which means the overall accuracy has been 87.89 percent. The user accuracy was 88.57, 100, 88.57, 75.23, 76.19, 100, and 86.66 percent for built-up areas, water bodies, agricultural land, barren land, fallow land, river sand, and vegetation cover, respectively. The highest and lowest producer accuracy were found in water bodies (99.05%) and agricultural land (78.81%) classes, respectively. The kappa coefficient, which was 0.8587, indicated a high level of agreement between the accuracy results of both the user and the producer, with a strong level of precision.

Accuracy Assessment in 2011

Table 7 presents the accuracy assessment result of the image classification of 2011. A total of 638 corrected points were noted, and 97 reference points were found to be incorrectly classified. The producer accuracy was observed to be 85.84, 99.03, 77.58, 86.2, 82.83, 92.1, and 84.31 percent for the built-up area, water bodies, agricultural land, barren land, fallow land, river sand, and vegetation cover, respectively. The result of user accuracy was 92.38, 98.09, 85.71, 71.42, 78.09, 100, and 81.9 percent for the built-up area, water bodies, agricultural land, barren land, fallow land, river sand, and vegetation cover, respectively. The Kappa coefficient was 0.846, which corresponds to the strong agreement between both user and producer accuracy results.

Accuracy Assessment in 2022

Table 8 presents the accuracy assessment matrix for 2022. Out of 735 reference points, a total of 682 points have been found correctly classified, which described 92.79 percent of overall accuracy. Altogether, above 83 percent user accuracy has been noted for each class, and producer accuracy was found to be above 88 percent for each class. The highest user and producer accuracy were established in the river sand and water bodies classes, respectively. The lowest has been noted in fallow land and barren land respectively. The Kappa coefficient was estimated to be 0.9158 which presented a strong covenant between user and producer accuracy variables and also explained the outstanding classification result.

Table 7: Error Matrix for Accuracy Assessment of 2011 Classification.

Class	BL	WB	AL	BRL	FL	RS	VC	TU	UA (%)
BL	**97**	0	0	1	1	6	0	105	**92.38**
WB	0	**103**	0	0	0	2	0	105	**98.09**
AL	0	0	**90**	3	5	0	7	105	**85.71**
BRL	13	1	2	**75**	10	0	4	105	**71.42**
FL	3	0	8	6	**82**	1	5	105	**78.09**
RS	0	0	0	0	0	105	0	105	**100**
VC	0	0	16	2	1	0	86	105	81.9
TP	113	104	116	87	99	114	102	TU=735	TC=638
PA (%)	85.84	99.03	77.58	86.2	82.83	**92.1**	**84.31**		
Overall Accuracy= **86.80%**					Kappa= **0.846**				

Source: Based on Accuracy Assessment Result of 2011

LULC Classification Result

In addition to an assessment of accuracy, the outcome of this study has been partitioned into various categories, including spatial patterns, dynamics, and the detection of changes in LULC. The findings were presented in a manner that corresponds to the LULC classification in chronological order.

Coverage, Trend, and Pattern of LULC

Table 9 presents summary statistics of the LULC results for the years 1991, 2001, 2011, and 2022. As per the overall result, agricultural land was found as the highest LULC class, which was 72.94, 71.36, 69.14, and 59.31 percent in 1991, 2001, 2011, and 2022, respectively. Contrarily, water body class has been observed as 1.56, 1.49, 1.34, and 1.48 percent in 1991, 2001, 2011, and 2022, respectively. The most significant LULC class, which is the built-up area, increased at a faster pace. In 1991, only 4.45 percent area was built-up class and which became 10.01 percent in 2001. In 2011, 16.44 percent area was built up, and it reached 27.05 percent in 2022. The barren land was observed as the second highest class in 1991, and it covered 7.41 percent area of VCDR. It decreased rapidly in the coming periods and was 6.24, 2.83, and 1.45 percent in 2001, 2011, and 2022 respectively. The fallow land occupied 5.19, 4.30, 3.91, and 3.83 percent of the overall geographical expanse in the years 1991, 2001, 2011, and 2022, respectively, indicating a notable decrease in it over the time period. The vegetation cover comes under the most significant LULC class for any urban area, and as a result, 6.53, 4.91, and 4.51 percent of the area was observed under the vegetation cover. It decreased from 1991 to 2011. It increased in 2022 and reached 5.08 percent (Fig. 3).

Spatial Pattern of LULC

Generally, the spatial distribution of land uses in any urban region or umland of metropolitan cities shows a homogeneous character within the city and diversified with

Table 8: Error Matrix for Accuracy Assessment of 2022 Classification.

Class	BL	WB	AL	BRL	FL	RS	VC	TU	UA (%)
BL	**100**	0	0	2	0	3	0	**105**	**95.23**
WB	0	**102**	1	0	0	2	0	**105**	**97.14**
AL	0	0	**97**	1	4	0	3	**105**	**92.38**
BRL	4	0	3	**92**	4	2	0	**105**	**87.61**
FL	1	0	2	9	**88**	0	5	**105**	**83.8**
RS	0	0	0	0	0	**105**	0	**105**	**100**
VC	0	0	6	0	1	0	**98**	**105**	**93.33**
TP	**105**	**102**	**109**	**104**	97	112	106	TU=735	TC=682
PA (%)	95.23	100	88.99	88.46	90.72	93.75	92.45		
Overall Accuracy = **92.79%**					Kappa = **0.9158**				

Source: Based on Accuracy Assessment Result of 2022

Table 9: Summary Statistics of LULC Classification.

LULC Class	1991		2001		2011		2022	
	km^2	%	km^2	%	km^2	%	km^2	%
Built-up Land	29.97	4.45	67.37	10.01	110.75	16.44	182.16	27.05
Water Bodies	10.52	1.56	10.03	1.49	9.07	1.34	10.01	1.48
Agri. Land	491.16	72.94	480.52	71.36	465.59	69.14	399.37	59.31
Barren Land	49.92	7.41	42.04	6.24	19.12	2.83	9.78	1.45
Fallow Land	34.95	5.19	28.98	4.30	26.33	3.91	25.80	3.83
River Sand	12.87	1.91	11.38	1.69	12.07	1.79	12.01	1.78
Veg. Cover	43.94	6.53	33.01	4.91	30.4	4.51	34.20	5.08

Source: Calculated based on the Classification

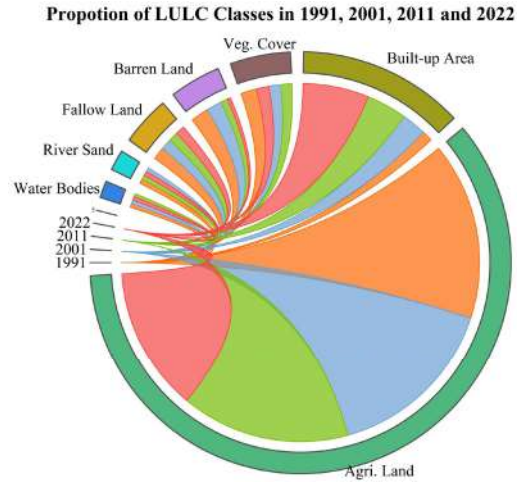

Fig. 3: Proportion of LULC Classes using Chord diagram.

a dynamic nature in the peri-urban region. Partially, the same character of dynamism can be seen in the spatial distribution of land uses in the VCDR from 1991 to 2022.

In 1991, the maximum built-up area was found within the municipal area, and some of it was observed in the southeastern part of the region. The core area and CBD were highly concentrated in the context of impervious surfaces. As a result, most of the area has been noticed under the agricultural land and it was distributed evenly in the outer parts of the city. Although, some patches of agricultural land have been identified within the municipal area. The fallow land was scattered over the region (excluding city parts), and it was more concentrated in the northern and western peripheral portions. The barren land was found in a clustered pattern, which expresses the natural causes behind it to remain barren. The largest patch of barren land was observed in the eastern part of the region and along the River Ganga. Few patches have been identified in the northern parts. Vegetation cover was found scattered, but within the city area, some areas like Banaras Hindu University, Banaras Locomotive Works, and Cantonment had dense vegetation cover.

In 2001**,** the built-up area increased and was spread over the central and southern parts of the municipal area. The leapfrog pattern of built-up land was observed in the northern parts of the city boundary. Similarly, in Pt. Deendayal Upadhyay Nagar (formerly known as Mughal Sarai) few new patches of this land use category have been noted. The extent of vegetation coverage has notably reduced in both the municipal as well as in suburban areas of the city, except for certain areas along the banks of the River Ganga, which exhibit some sporadic patches of vegetation.

In comparison to the previous period, the percentage of barren land decreased in 2001 in totality. A considerable percentage of agricultural land class has been identified. However, there was a slight decline between 1991 and 2001. Conversely, no significant alterations were observed in the remaining LULC categories, such as water bodies, fallow land, river sand, and water bodies.

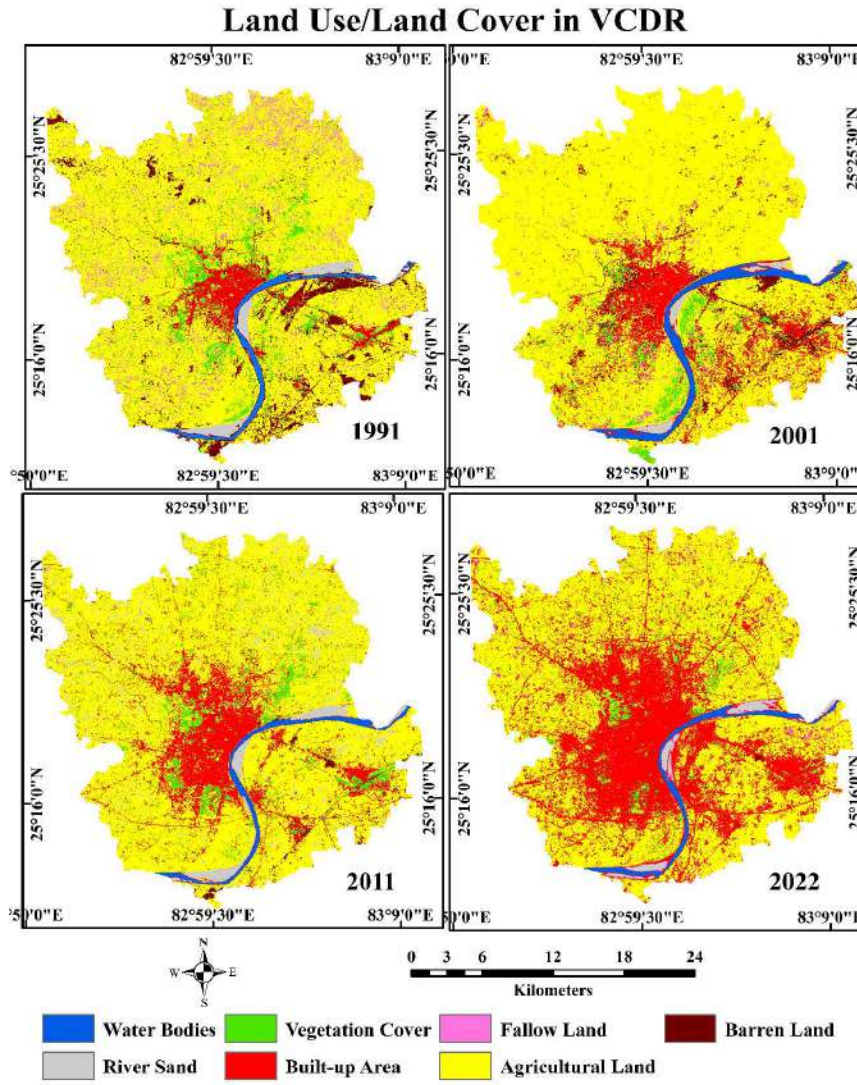

Fig. 4: Spatial distribution of Land Use/Land Cover (1991, 2001, 2011 & 2022).

During the time frame of 2011, there was a noteworthy augmentation in the built-up area along with a simultaneous and rapid escalation in density. Some new highways have been created, and the concentration of built-up areas also increased in the outer villages and towns of the study area. Again, some patches of vegetation cover have been introduced and the concentration of vegetation has increased within the municipal boundary. As a result of previous periods, the fallow, barren, and agricultural land decreased, and more spatial changes have been observed within the municipal boundary and nearer to the city boundary. The fallow and barren land class was transformed into agricultural and built-up land. No significant alterations were observed in the spatial distribution of water bodies and river sand categories.

In 2022, the built-up class has grown in the clustering pattern in the municipal area and an axial pattern in outer parts along the highways, railways, and major roads. Overall, other classes like vegetation cover, fallow, barren, and agricultural land decreased and spatially changed due to the high rate of urbanization. The water bodies and river sand have been distributed as in previous periods (Fig. 4).

Dynamics of LULC

The utilization trend and pattern of land resources can be expressed through the history and current state of a specific type of land, which is also beneficial in understanding the physical and cultural landscape dynamics in a region. In this study, land use was dynamic on a large scale. Some classes, like water bodies, vegetation cover, and river sand,

Table 10: Dynamics of LULC Classes (km^2).

LULC Class	1991-2001		2001-11		2011-22		1991-2022	
	km^2	%	km^2	%	km^2	%	km^2	%
Built-up Land	37.4	124.79	43.38	64.39	71.41	64.47	152.19	507.8
Water Bodies	-0.49	4.65	-0.96	-9.57	0.94	10.36	-0.51	-4.84
Agri. Land	-10.64	-2.16	-14.93	-3.1	-66.22	-14.22	-91.79	-18.68
Barren Land	-7.88	-15.78	-22.92	-54.51	-9.34	-48.84	-40.14	-82.41
Fallow Land	-5.97	-17.08	-2.65	-9.14	-0.53	-2.01	-9.15	-26.18
River Sand	-1.49	-11.57	0.69	-6.06	-0.06	-4.97	-0.86	-6.68
Veg. Cover	-10.93	-24.87	-2.61	-8.99	3.8	12.5	-9.74	-22.16

Sources: Calculated through the LULC classification

Table 11: Change Area Matrix of 1991-2001 (km^2).

LULC Class	Agri. Land	B. Land	Built-up	F. Land	R. Sand	Veg. Cover	W. Bodies
Agri. Land	436.21	4.9	37.21	6.11	0.48	8.46	0.94
B. Land	26.47	5.16	8.15	1.37	0.11	2.74	2.93
Built-up	0	4.36	29.97	0	0	0	0
F. Land	27.78	0.05	0.93	1.38	0.01	0.06	0.01
R. Sand	1.63	0.01	1.89	0.21	4.72	0.01	4.15
Veg. Cover	23.19	7.46	3.34	0.06	0.01	7.07	0.07
W. Bodies	3.2	0.01	0.24	0	0.05	0.04	10.18

Source: Computed through transformation result

remained the same during the time period. While, fertile land, which was either in the form of barren and fallow or agricultural land, decreased and was converted into built-up areas. Table 10 presents the dynamics of LULC for 1991-2001, 2001-11, 2011-2022, and 1991-2022 periods. The built-up area increased by 37.4, 43.38, 71.41, and 152.19 km^2 during the 1991-2001, 2001-11, 2011-2022, and 1991-2022 periods, respectively. It increased by 507.8 percent over the time period. All the other LULC classes have decreased during the study period. 18.68 percent (91.79 km^2) of agricultural land has been lost, which is a major transformation recorded in the city region. The barren and fallow land classes decreased by 82.41 and 26.18 percent, respectively, during the 1991-2022 period. In the same time period, water bodies and river sand classes have decreased by 4.84 and 6.68 percent, respectively. However, vegetation cover decreased by 24.87 and 8.99 percent in the 2001 and 2011 years, respectively. Surprisingly, it increased by 12.5 percent in the 2011 and 2022 period. Whereas, during 1991-2022, it decreased by 22.16 percent.

Change Detection and Transformation of LULC

LULC change detection refers to the process of identifying and analyzing the changes that occur in the use of land over a specific time period. It involves comparing different satellite images at different times to assess the changes in land features, including built-up areas, water bodies, barren land, fallow land, vegetation cover, and agricultural land. In this study, change detection was done to assess the land use transformation between 1991-2001, 2001-11, 2011-22, and 1991-2022.

Land Transformation During 1991-2001

Table 11 corresponds to the LULC transformation matrix for the 1991-2001 period. The most remarkable change was observed in agricultural land to a built-up area by 37.21 km^2, fallow land by 6.11 km^2, barren land by 4.9 km^2, and vegetation cover by 8.46 km^2. 26.47 km^2 of barren land was transformed into agricultural land, built up by 8.15 km^2, fallow land by 3.37 km^2, vegetation cover by 2.74 km^2, and water bodies by 2.93 km^2. The fallow land was converted majorly into agricultural land by 27.78 km^2. Another remarkable land use conversion has been noted in vegetation cover, which has changed 23.19 km^2 in agricultural land, 7.46 km^2 in barren land, and 3.34 km^2 in the built-up area. No changes were observed in agricultural land, barren, built-up, fallow, river sand, vegetation cover, and water bodies by 436.21, 5.16, 29.97, 1.38, 4.72, 7.07, and 10.18 km^2 area respectively (Fig. 5).

Land Transformation During 2001-2011

Table 12 presents the land use transformation during the

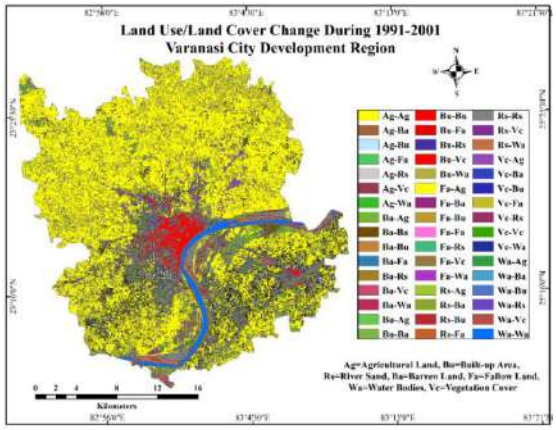

Fig. 5: LULC change detection during1991-2001.

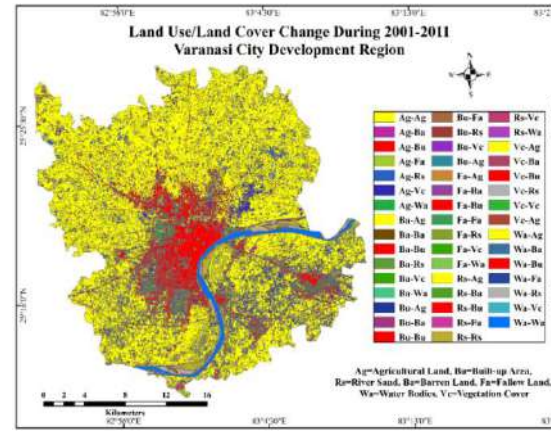

Fig. 6: LULC change Detection during 2001-2011.

2001-11 time period. As per the change detection result, no changes occurred in agricultural land, barren land, built-up area, fallow land, river sand, vegetation cover, and water bodies by 426.76, 2.07, 67.37, 0.01,4.63, 4.06, and 8.13 km^2 respectively. The major conversion was observed in agricultural land, which has transformed into barren land (2.57 km^2), built-up area (46.74 km^2), river sand (2.8 km^2), and vegetation cover (22.58 km^2). Barren land was converted into agricultural land by 12.12 km^2 and built-up area by 8.19 km^2. Whereas the built-up area was only converted into river sand and vegetation cover. Another remarkable conversion has been identified in fallow land, which has changed 8.14 km^2 area into agricultural land and 11.96 km^2 into the built-up area. Negatively, vegetation cover was converted into agricultural land by 14.98 km^2 and built-up area by 8.59 km^2. A total of 7.91 km^2 area of water bodies was transformed into agricultural land, barren land, built-up area, river sand, and vegetation cover (Fig. 6).

Land Transformation During 2011-2022

Table 13 presents the LULC transformation matrix for the 2011-2022 period. It was observed that 114.27 km^2 of agricultural land, 6.18 km^2 of fallow land, and 9.58 km^2 of vegetation cover were converted into built-up areas during the time period. The fallow land (1.01 km^2) was slightly altered into the agricultural land. Another remarkable land use conversion was identified in vegetation cover, in which 12.45 km^2 area changed into agricultural land and 11.48 km^2 into the concreted area. A total of 2.99 and 2.18 km^2 area of barren land were transformed into agricultural and built-up, respectively. The agricultural land, barren, built-up, fallow, river sand, vegetation cover, and water body classes remained by 359.9, 0.31, 110.75, 0.01, 5.98, 10.15, and 8.94 $km^{2,}$ respectively (Fig. 7).

Land Transformation During 1991-2022

During 1991-2022, the land use was drastically altered in VCDR. In these 31 years, 114.8 km^2 of agricultural land has changed into a built-up area, and a total of 152.19 km^2 of built-up area was amplified. It altered into vegetation cover by 11.85 km^2 and fallow land by 6.31 km^2. The barren land was converted into agricultural land and built-up land by 27.5 km^2 and 14.81 $km^{2,}$ respectively (Table 14). A total of 29.37 km^2 of fallow land was converted into agriculture,

Table 12: Change Area Matrix of 2001-11 (km^2).

LULC Class	Agri. Land	B. Land	Built-up	F. Land	R. Sand	Veg. Cover	W. Bodies
Agri. Land	426.76	2.57	46.74	0.01	2.8	22.58	0.25
B. Land	12.12	2.07	8.19	0	0.08	5.26	0.12
Built-up	0	0	67.37	0	2.11	1.95	0
F. Land	8.14	0.03	11.96	0.01	0.82	0.17	1.01
R. Sand	0.65	0.01	0.08	0.02	4.63	0.01	0.01
Veg. Cover	14.98	0.87	8.59	0	0.15	4.06	0.11
W. Bodies	2.2	0.15	1.59	0.04	3.82	0.11	8.13

Source: Computed through transformation result

Table 13: Change Area Matrix of 2011-22 (km^2).

LULC Class	Agri. Land	B. Land	Built-up	F. Land	R. Sand	Veg. Cover	W. Bodies
Agri. Land	359.9	0.02	114.27	6.18	0.34	9.58	0.77
B. Land	2.99	0.31	2.18	0.05	0.01	0.06	0.09
Built-up	0	0	110.75	0	1.18	0	0
F. Land	1.01	0	0.02	0.01	0.01	0	0.01
R. Sand	1.96	0	5.28	2.58	5.98	0.03	1.4
Veg. Cover	12.45	0.01	11.48	0.09	0	10.15	0.08
W. Bodies	0.25	0.01	1.98	0.37	0.52	0.03	8.94

Source: Computed through transformation result

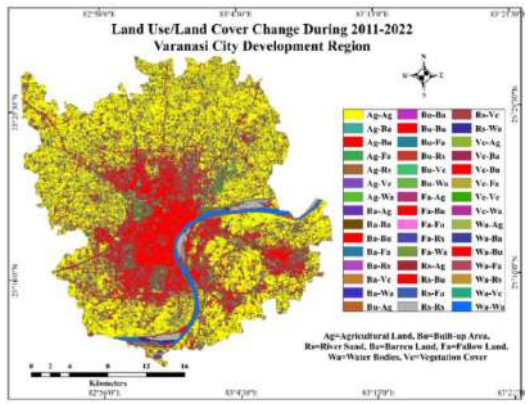

Fig. 7: LULC Change detection during 2011-2022.

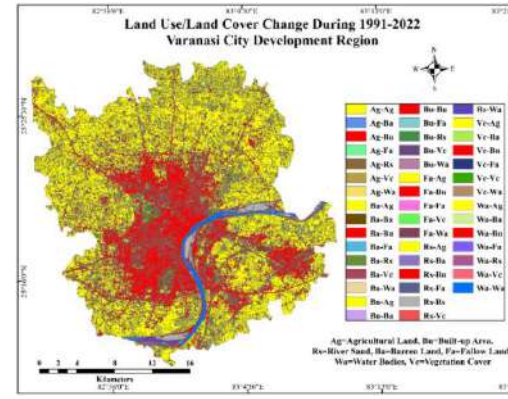

Fig. 8: LULC change detection during 1991-2022.

built-up and vegetation cover, while vegetation cover was transformed into agricultural land (4.41 km^2), barren land (3.02 km^2), and built-up area (12.93 km^2). Whereas, 374.31 km^2 agricultural land and 15.63 km^2 vegetation cover area have not been altered. Similarly, 5.81 km^2 area of river sand and 7.7 km^2 of water bodies were detected as unchanged areas (Fig. 8). Meanwhile, the built-up area class was totally unchanged due to its physical characteristics (Fig. 9).

Spatial Pattern of LULC Transformation During 1991-2022

The LULC transformation results were very interesting, but its spatial distribution was more attention-grabbing for the local governing bodies and policymakers. In the 1991-2001 period, significant changes were noted within and surrounding the municipal area. Pt. Deendayal Upadhyay Nagar town also witnessed the land alteration phenomenon.

Table 14: Change Area Matrix of 1991-2022 (km^2).

LULC Class	Agri. Land	B. Land	Built-up	F. Land	R. Sand	Veg. Cover	W. Bodies bbBBodies
Agri. Land	374.31	0.04	114.8	6.31	0.22	11.85	0.34
B. Land	27.5	0.31	14.81	0.72	0.27	0.82	1.52
Built-up	0	0	29.97	0	0	0	0
F. Land	23.53	0	5.54	0.79	0	0.3	0
R. Sand	1.07	0.01	2.41	1.14	5.81	0.01	1.17
Veg. Cover	4.41	3.02	12.93	0.21	0	15.63	0.83
W. Bodies	0.08	0.19	1.7	0.4	0.65	0.01	7.7

Source: Computed through transformation result

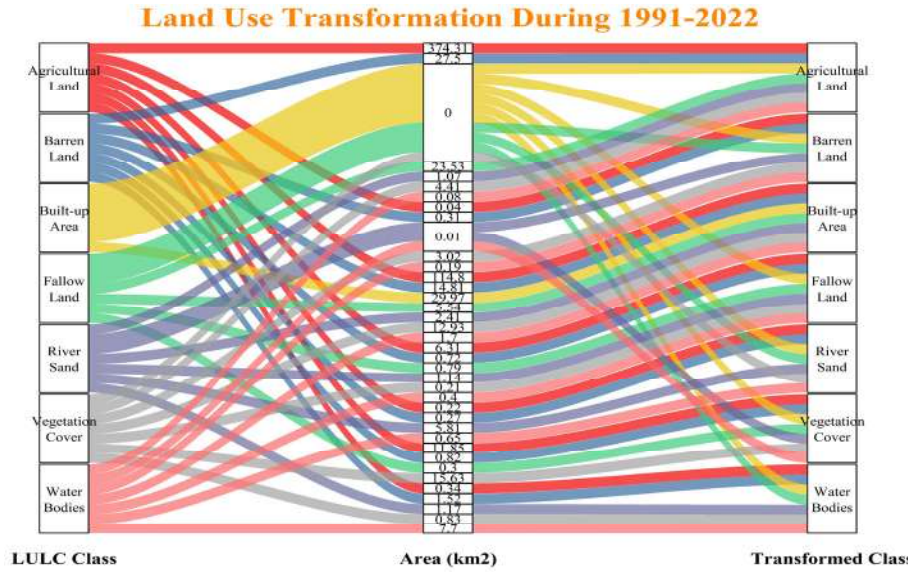

Fig. 9: Land transformation during 1991-2022 using an alluvial diagram (using Tableau and Python).

The built-up area grew at a high rate in the northern and western parts. The localities which are situated at the right bank of Ganga and Ramnagar Town, witnessed the land transformation, especially in the agricultural and barren land use classes. The LULC of peri-urban areas slightly changed into agricultural land, barren land, fallow land, and vegetation cover. In the 2001-2011 period, the axial growth pattern of LULC change was identified, which altered along the major axes like roads, railways, and river banks. The changing pattern of LULC was found towards the periphery of the study area. However, the north-central and eastern areas of the VCDR have been more dynamic than the other outer parts of the city region. In the 2011-2022 period, several urban features like highways, other major roads, railway lines, and built-up setups were constructed. Hence, massive land alteration was observed around these entities. Meanwhile, with the expansion of anthropogenic concretscapes, other land use classes have been transformed simultaneously.

DISCUSSION

According to the USGS's Department of Land Studies, accuracy should be more than 85 percent at micro-level studies, and the result of the accuracy assessment was fine on the standards. It was observed that a faster pace of urbanization is pushing to change the LULC pattern and dynamics in the city region. The agricultural land has shrunk by 18.68 percent during the 1991-2022 time period, which is paving the way for the expansion of the built-up area. This decrease is reducing the rural resources, creating imbalances in the rural economy, food scarcity, ecological degradation, etc. In the study area, the peri-urban region was dominated by agricultural activity, and land resources were converted into impervious surfaces. Although built-up area conversion is one of the indicators of economic development, but ecological imbalances, and food scarcity are great challenges against rapid urbanization. The water bodies decreased by 4.84 percent during the study period due to encroachment by dwellers of the city. However, all shrunk water bodies were located in the municipal area and played an important role in managing the overall environment of the Varanasi city. The barren land decreased by 82.41 percent between 1991 and 2022 because it is the least expensive land for buying and converting into built-up areas for settlements. Fallow land also decreased by 26.18 per cent but it has majorly converted into agricultural land. The vegetation cover shrunk during 1991-2011. The period between 2011 and 2022 witnessed a 12.5 percent increase in inclination toward social forestry, which can be attributed to a major initiative undertaken by the government and the changing perception of people.

Overall, the built-up area noted a high rate of expansion, and it covered 182.16 km^2 in 2022. In the central parts of the city, the horizontal as well as vertical sprawl was observed with dense concreted urban features. High land rent within the municipal area, holy nature, better connectivity, and availability of basic amenities are the main reasons behind the faster pace of urbanization in the VCDR. In consequence, the quality of the environment, urban morphology, and quality of life are declining. In the spatial context, changes in land use have been identified both on the outskirts of the urban region and in proximity to the central business

district. A decrease in the rate of land use transformation was noted on moving away from the CBD and other nuclei of the city. Other parts like Ramnagar town, Pt. Deendayal Upadhyay Nagar and Babatpur developed as satellite towns based on their urban mobility and land use dynamics. The urban expansion of these towns can prove advantageous for the Varanasi city as it has been grappling with the issue of overpopulation for the past few decades and these towns can be new topophila for upcoming migration streams in future time. Varanasi city has grown in the form of multiple axes due to highway expansion and better connectivity to newly established settlements. These facts help to understand the land use pattern and dynamics as well as the cultural and physical morphology of the Varanasi city. Hence, Monitoring land use dynamics through LULC mapping and assessment is one of the most efficient approaches to reducing urban sustainable vulnerability. The geographical information of various LULC classes and their transformation may assist Varanasi City in effective planning and policy to enhance carrying capacity and sustainability by demonstrating where, what, and how changes have happened in the city landscape.

CONCLUSION

The outcome of this study presents that the city is experiencing hyper-urbanization and rapid LULC transformation. Since 1991, the built-up area increased by five times, and other classes like agricultural land, fallow land, and barren land have declined rapidly. The focal points of transformation are within the municipality, nearer to the municipal boundary, and along the roads and railway lines. The fundamental and advanced infrastructural development, like major service centers, geographic location, and religious importance of the city, are the most attractive factors affecting land use alteration. So, proper land use planning for upcoming decades is needed to maintain the optimum land resource utilization, food security, and a healthy physical and social environment. This study has produced an important catalog on the dynamics of LULC and its transformation over the past three decades that can be used as a comprehensive spatial database for planning and policy-making to improve the carrying capacity of the city and bring environmental sustainability to the study area.

ACKNOWLEDGMENT

The authors would like to express their gratitude to USGS and the developers of the GEE web portal. We want to convey our sincere thanks to the University Grant Commission (India) for providing a fellowship as a Senior Research Fellowship. Author Atul K. Tiwari recieves this fellowship (Fellowship ID: 190520639704).

REFERENCES

Arévalo, P., Bullock, E.L., Woodcock, C.E. and Olofsson, P. 2020. A suite of tools for continuous land change monitoring in Google Earth Engine. Front. Clim., 2: 1-19. DOI: 10.3389/fclim.2020.576740

Baig, M.F., Mustafa, M.R.U., Baig, I., Takaijudin, H.B. and Zeshan, M.T. 2022. Assessment of Land Use Land Cover Changes and Future Predictions Using CA-ANN Simulation for Selangor, Malaysia. Water, 14(3): 402. DOI: 10.3390/w14030402

Cao, L.S., Xu, H. and Li, H. 2022. Effect of greening trees on thermal comfort of the pedestrian streets in hot summer and cold winter regions in China. Nat. Environ. Pollut. Technol., 21(4): 1543-1552. DOI: 10.46488/NEPT.2022.v21i04.007

Chandole, V. and Joshi, G.S. 2023. Case study of rainfall and temperature assessment through trend and homogeneity analyses in Vadodara and Chhotaudepur district of Gujarat State, India. Environ. Monit. Assess., 195(5): 561. DOI: 10.1007/s10661-023-11089-w

Chughtai, A.H., Abbasi, H. and Karas, I.R. 2021. A review on change detection method and accuracy assessment for land use land cover. Remote Sens. Appl. Soc. Environ., 22: 100482. DOI: 10.1016/j.rsase.2021.100482

Francis, T. 2012. Land-cover changes: A comparison of change detection techniques. Int. J. Remote Sens., November 2012, 37-41.

Geng, J., Xu, L., Wang, Y. and Tu, L. 2023. Study of land cover change in the city with the fastest economic growth in China (Hefei) from 2000 to 2020 based on Google Earth engine platform. Remote Sens., 15(6): 1604. DOI: 10.3390/rs15061604

Gomes, V.C.F., Queiroz, G.R. and Ferreira, K.R. 2020. An overview of platforms for big earth observation data management and analysis. Remote Sens., 12(8): 1-25. DOI: 10.3390/RS12081253

Gudex-Cross, D., Pontius, J. and Adams, A. 2017. Enhanced forest cover mapping using spectral unmixing and object-based classification of multi-temporal Landsat imagery. Remote Sens. Environ., 196: 193-204. DOI: 10.1016/j.rse.2017.05.006

Henits, L., Jürgens, C. and Mucsi, L. 2016. Seasonal multitemporal land-cover classification and change detection analysis of Bochum, Germany, using multitemporal Landsat TM data. Int. J. Remote Sens., 37(15): 3439-3454. DOI: 10.1080/01431161.2015.1125558

Hu, Y. and Hu, Y. 2019. Land cover changes and their driving mechanisms in Central Asia from 2001 to 2017 supported by Google Earth Engine. Remote Sens., 11(5): 554. DOI: 10.3390/rs11050554

Kim, C. 2016. Land use classification and land use change analysis using satellite images in Lombok Island, Indonesia. For. Sci. Technol., 12(4): 183-191. DOI: 10.1080/21580103.2016.1147498

Lu, Y., Chen, D., Jiang, Y. and Huang, H. rong. 2005. Study of dental caries prevalence in children of Yinchuan in China. West China J. Stomatol., 23(6): 502-504.

Mahmoud, A.S., Mezaal, M.R., Hameed, M.R. and Naje, A.S. 2022. A Framework for Improving Urban Land Cover Using Object and Pixel-Based Techniques via Remotely Sensed Data. Nat. Environ. Pollut. Technol., 21(5): 2189-2200. DOI: 10.46488/NEPT.2022.v21i05.013

Mishra, P.K., Rai, A. and Rai, S.C. 2020. Land use and land cover change detection using geospatial techniques in the Sikkim Himalaya, India. Egypt. J. Remote Sens. Space Sci., 23(2): 133-143. DOI: 10.1016/j.ejrs.2019.02.001

MohanRajan, S.N., Loganathan, A. and Manoharan, P. 2020. Survey on Land Use/Land Cover (LU/LC) change analysis in remote sensing and GIS environment: Techniques and Challenges. Environ. Sci. Pollut. Res., 27(24): 29900-29926. DOI: 10.1007/s11356-020-09091-7

Naikoo, M.W., Rihan, M., Shahfahad, Peer, A.H., Talukdar, S., Mallick, J., Ishtiaq, M. and Rahman, A. 2022. Analysis of peri-urban land use/land cover change and its drivers using geospatial techniques and geographically weighted regression. Environ. Sci. Pollut. Res., 012: 345. DOI: 10.1007/s11356-022-18853-4

Osman, T., Shaw, D. and Kenawy, E. 2018. An integrated land use change model to simulate and predict the future of the greater Cairo metropolitan region. J. Land Use Sci., 13(6): 565-584. DOI: 10.1080/1747423X.2019.1581849

Pal, A., Tiwari, A.K. and Kanchan, R. 2023. Slumscape through the prism of urban geomorphology: A Study of Vadodara City, India. Indian J. Spatial Sci., 14(2): 1-9

Pande, C.B. 2022. Land use/land cover and change detection mapping in Rahuri watershed area (MS), India, using the Google Earth engine and machine learning approach. Geocarto Int., 37(26): 13860-13880. DOI: 10.1080/10106049.2022.2086622

Pandey, P.C., Koutsias, N., Petropoulos, G.P., Srivastava, P.K. and Ben-Dor, E. 2021. Land use/land cover in view of earth observation: Data sources, input dimensions, and classifiers: A review of the state of the art. Geocarto Int., 36(9): 957-988. DOI: 10.1080/10106049.2019.1629647

Rwanga, S.S. and Ndambuki, J.M. 2017. Accuracy assessment of land use/land cover classification using remote sensing and GIS. Int. J. Geosci., 08(04): 611-622. DOI: 10.4236/ijg.2017.84033

Saravanan, S. and Abijith, D. 2022. Flood susceptibility mapping of Northeast coastal districts of Tamil Nadu India using multi-source geospatial data and Machine Learning techniques. Geocarto Int., 1: 1-30. DOI: 10.1080/10106049.2022.2096702

Shi, M., Wu, H., Fan, X., Jia, H., Dong, T., He, P., Baqa, M.F. and Jiang, P. 2021. Trade-offs and synergies of multiple ecosystem services for different land use scenarios in the Yili River Valley, china. Sustainability, 13(3): 1-15. DOI: 10.3390/su13031577

Shukla, A. and Jain, K. 2019. Modeling Urban Growth Trajectories and Spatiotemporal Pattern: A Case Study of Lucknow City, India. J. Indian Soc. Remote Sens., 47(1): 139-152. https://doi.org/10.1007/s12524-018-0880-1

Singh, S. and Talwar, R. 2013. Effects of topographic corrections on MODIS sensor satellite imagery of mountainous region. Sign. Process. Commun., 18: 455-460. https://doi.org/10.1109/ICSPCom.2013.6719833

Smiraglia, D., Ceccarelli, T., Bajocco, S., Salvati, L. and Perini, L. 2016. Linking trajectories of land change, land degradation processes, and ecosystem services. Environ. Res., 147: 590-600. https://doi.org/10.1016/j.envres.2015.11.030

Sobha, P. and Jose, J.P.A. 2023. Investigating the implications of transit-oriented land use development for a potential node in an urban metro for sustainability. Nat. Environ. Pollut. Technol., 22(2): 721-730. https://doi.org/10.46488/NEPT.2022.v21i04.007

Sudmanns, M., Tiede, D., Lang, S. and Baraldi, A. 2018. Semantic and syntactic interoperability in online processing of big Earth observation data. Int. J. Digital Earth, 11(1): 95-112. https://doi.org/10.1080/17538947.2017.1332112

Tiware, A. 2014. Urban sciences, big data, and India. Glob. J. Multidiscip. Stud., 3(12): 14-25.

Tyagi, A., Tiwari, R.K. and James, N. 2023. Mapping the landslide susceptibility considering future land-use land-cover scenario. Landslides, 20(1): 65-76. https://doi.org/10.1007/s10346-022-01968-7

Wagh, N.D. 2022. A review on atmospheric dispersion system for air pollutants integrated with gis in urban environment structures. Nat. Environ. Pollut. Technol., 21(4): 1553-1563. https://doi.org/10.46488/NEPT.2022.v21i04.008

ORCID DETAILS OF THE AUTHORS

Atul K. Tiwari: https://orcid.org/0000-0003-4944-4625
Anindita Pal: https://orcid.org/0000-0001-7839-1855
Rolee Kanchan: https://orcid.org/0000-0001-8773-4362

Nature Environment and Pollution Technology
An International Quarterly Scientific Journal

p-ISSN: 0972-6268
(Print copies up to 2016)
e-ISSN: 2395-3454

Vol. 23 | No. 1 | pp. 381-389 | 2024

Original Research Paper

https://doi.org/10.46488/NEPT.2024.v23i01.032

Open Access Journal

Determinants Influencing the Environmental Impact Assessment Compliance Rate by Industries in Aba City, Southeast, Nigeria

C. Sam-Amobi*, O. J. Ubani†, K. Efobi** and Nathan Ajukwara****

*Department of Architecture, University of Nigeria, Enugu Campus, Enugu State, Nigeria

**Department of Urban and Regional Planning, University of Nigeria, Enugu Campus, Nigeria

†Corresponding author: O. J. Ubani; obinna.ubani@unn.edu.ng

Nat. Env. & Poll. Tech.
Website: www.neptjournal.com

Received: 01-08-2023
Revised: 06-10-2023
Accepted: 10-10-2023

Key Words:
Environmental Impact Assessment
Environmental mitigation
Compliance rate
Principal Component Analysis

ABSTRACT

A United Nations (UN) report on the severity of pollution in cities around the world in 2020 rated Aba City, Nigeria, as the most polluted city in the world. This has become a source of worry and embarrassment for environmental policymakers in the country. The matter of whether industries are efficiently managing their wastes came to the fore, and policymakers questioned the compliance of these industries with environmental laws and Environmental Impact Assessment (EIA) guidelines and the reasons behind the seemingly non-compliance of the industries with these guidelines. The study aimed to investigate the determinants that influence compliance with EIA guidelines by industries in Aba. A survey research method was employed in the study. Questionnaires and interviews were also used to elicit data from industrialists and environmentalists in the study area. 384 industries were sampled in the study. Principal Component Analysis was used to test the hypothesis. The study revealed seven factors that influenced the compliance rate of EIA guidelines by industries, and they include weak public participation (65.5%), ignorance (54.5%), an effective legal system and legislation (42.4%), the cost of compliance (40.5%), weak coordination along the line of departments (town planning officers and consultants) (35.5%), delay in approval (30.5%), and limited scope (28.9%). It was recommended that the government strengthen the legal system as it relates to the implementation of EIA; then, there is a need to involve affected stakeholders in the preparation of EIA documents.

INTRODUCTION

Over the decade, industrialization and urbanization have taken place, thereby giving room to tremendous growth, which in turn has given rise to environmental degradation and depletion. The practice and implementation of environmental impact assessment (EIA) guidelines vary from country to country for many reasons. While developed countries are more effective in the implementation of environmental guidelines, developing countries are less effective in the use of EIA systems.

In 1969, the United States of America promulgated the National Environmental Policy Act (NEPA) as a measure to check the present worldwide desire and efforts to control man's unabating degradation of his environment (Rachael 2017). In Europe, a draft made in 1987, referred to as the Commission of European Communities (CEC), listed the types of projects that must be subjected to an assessment, and this was in response to the US National Environmental Policy Act. In developing countries like Kenya, for instance, the EIA Act was domesticated in 1999 as the Environmental Management and Coordination Act (EMCA) to check the activities of developers of major projects (Kelvin 2016). The issue of environmental impact assessment in developed countries like Europe is in the form of a regional or sub-regional approach, but efforts in other parts of the world have been initiated through measures in the form of legislation and guidelines by individual governments. A good example of such individual countries' initiatives is the Federal Environmental Protection Agency's (FEPA) Decree of 1988 in Nigeria, which was meant to check the development and growth of industrialization and urbanization (Mohammed et al. 2014). However, the Nigerian government in the early 20s created another body, NESERA, to replace FEPA and was saddled with the job of managing the environment. This agency (NESREA), through her consultant, is charged with the onus of carrying out environmental audits within a space of 3 years for industries and reporting such audits to NESREA as specified in the National Guidelines for Environmental Audit in Nigeria. In the law establishing the agency, Section 8(k) of the law charged the body to make laws, one of which is Regulation S.I. No. 29, which

demands industries do environmental audits and submit reports of such audits every 3 years. Various states in Nigeria equally established bodies and agencies that complement the activities of the NESREA in the state; hence, the Abia State Environmental Protection Agency (ASEPA) was saddled with the responsibility of complementing the NESREA effort in enforcing compliance to the extent of environmental regulations in Aba and other cities of Abia State, Nigeria.

There are various developments in Nigeria, particularly in Aba, one of the largest commercial cities in Nigeria. The town is located in Abia State, in the southeast region of the country. These developments span industrial, social, economic, etc., and all these developments have an effect on people and the immediate environment of man. Aba, as one of the commercial nerve centers of Nigeria, has hosted many industries (manufacturing, construction, and production), and efforts have been made by various governments to reduce or mitigate the negative impact of these ever-increasing industrial developments in Aba, especially using the legislative tool called EIA guidelines. Each industry is required by this law to produce guidelines on how development should take place and how to mitigate the anticipated negative effects. However, the level of compliance with this responsibility by various industries has been a concern to policymakers, owing to the fact that there seems to be enormous industrial effluents and pollution in Aba. In Aba, the study area, the nature of the environmental condition is not in any way different from what is obtainable in many other cities in Nigeria. The increase in non-industrial and industrial activities in the urban area, such as plastic manufacturing industries, agricultural processing industries, confectioneries, surgical, and pharmaceutical companies, has necessitated this unhealthful environmental condition. More so, in the recent rating by the UN on the cities that are polluted in the world, Aba was rated the highest among the worst polluted cities (UNEP 2022). This has remained a worry to planners since there has not been any empirical evidence of the compliance rate of industries to development guidelines, let alone ascertain the categories of industrial development and their compliance rate in Aba Urban. It has been speculated that many companies do not comply strictly with the EIA guidelines. It is against this background that environmental compliance with basic environmental guidelines in the industrial and manufacturing sectors is topical. Therefore, the study aimed to empirically investigate the factors that influence the compliance rate of industries with EIA guidelines since such a study has not even been ascertained in Aba, hence the essence of this work. The study hypothesized that the factors that are associated with the compliance rate of industries with EIA guidelines cannot be patterned. The findings of the study will stimulate project proponents, EIA consultants, policymakers, environmental standards, and regulations enforcement agencies to have an empirical understanding and knowledge of the factors responsible for the non-compliance of environmental regulations by industrialists in the city and other Nigerian cities at large, thus evolving policies that will ensure a sustainable, convenient, healthy, and safe environment.

PAST STUDIES

In a study conducted by Hussain et al. (2015) on factors influencing the performance of EIA practices in Pakistan, they posited that ineffective management, centralized decision-making, political setup, bureaucratic structure, and poor control systems are major hindrances to effective compliance with environmental impact assessment guidelines. For Nwafor (2006), the most critical factors affecting compliance with EIA regulations and performance are public participation and a lack of relevant human resources in the implementation of environmental management plans (EMP). Furthermore, Zaelke et al. (2005) did a study on the challenges and status of environmental compliance and audit processes by industries in Kenya. The study posited that most industries carry out audits for compliance purposes only. The study concluded that proponents' concern after initial compliance does not extend to monitoring and effective follow-up; rather, compliance is targeted at obtaining approval from relevant authorities. Also, Wood (1993) researched factors influencing the environmental audit of educational institutions. It was noted from the study that the environmental audit was done primarily to show the areas of weaknesses and strengths, understand the ways that educational institutions follow legislative regulations related to environmental management plans, and know how the audit would help handle environmental problems in the school and its environs, disposal of waste techniques, potential environmental management constraints, and the focus of future audits. The research, however, found that the institutions complied with some environmental laws and legislation but had areas of lapse. And they highlighted these lapses due to a lack of follow-up and monitoring. The finding collaborated with that of Zaelke et al. (2005), who also found a lack of follow-up and monitoring as major factors affecting compliance with EIA guidelines.

Furthermore, Sadler (2011), examining the factors influencing compliance with EIA guidelines in tea factories in an African sub-Saharan country such as Kenya submitted that the primary causes of non-compliance with EIA guidelines in the tea industry were the over-utilization of primary resource bases such as water and forest products, inadequate use of appropriate technologies, insufficient

support for technology change, and weak enforcement of environmental laws.

Morrison et al. (2017), in their study on compliance with environmental safety guidelines in the oil and gas industry, found that compliance with safety environment best practices was weak. This was because stakeholders and staff of the industry were not properly advised and trained by safety professionals; thus, they possess very inadequate skills or competence to enhance compliance. Similarly, Leknes (2001) and Mangogrie (2015) have also identified that legal framework and institutional capacity have a remarkable impact on the performance of EIA practices, including screening, scoping and mitigation, environmental management plans (EMP), and reporting. Also, they found that some countries are more effective in complying with EIA guidelines while others are less effective. They concluded that compliance varies significantly between consultants, the size of the project, and the stage of the EIA process. In contrast to the findings of Leknes (2001) and Mangogrie (2015), Kelvin (2016), in his study on the variables that influence the implementation of EIA recommendations on commercial projects in Kenya, documented poor quality and incomplete Environmental Impact Statements (EIS) often overpopulated with information, inadequate implementation of the proposed mitigation measures, and a lack of meaningful partnership with the concerned public, among others, as factors militating against the implementation of EIA regulations for commercial projects. The findings of his study are in tandem with those of Sadler (2011), who found similar factors responsible for ineffective compliance with EIA guidelines. Salihu et al. (2015) found that the nature of the administrative setup, weak coordination, inadequate screening and scoping, limited scope of EIA review, poor quality of EIA reports, weak public participation, inadequate implementation of mitigation measures and monitoring, effective legal system and legislation, extensive politicization of the EIA process, and availability of baseline data are limitations to EIA guideline compliance. The study corroborates what Leknes (2001), Mangogrie (2015), and Kelvin (2016) posited; they observed that very minimal public participation and involvement are done during the Environmental Impact Assessment process due to the several challenges encountered during the implementation of EIA participation.

In Pakistan, Agwu et al. (2009) attributed poor environmental impact assessment practice to a lack of consultants' experience, proponents' attitudes, inadequate expertise for the review of EIA reports, and inconsistent EIA review criteria. The quality of compliance is normally hard to measure based on the EIA report alone without verification of the project's location and implementation (Kakonge 1998). Again, to further comprehend the factors that influence compliance with EIA guidelines by proponents, Rowan et al. (2016) used a structured questionnaire to measure the variables that explained the reasons proponents fail to comply, and they identified six factors in order of increasing importance that influenced compliance rate: the unclear nature of the EIA system, proponents regard EIA exercise as unnecessary, EIA is too stringent, EIA is too expensive, EIA increases costs, and EIA delays projects. The finding also shows that large projects have a higher level of compliance than smaller projects. He concluded that the implication is that the EIA system is not effectively achieving its intended objectives since strict compliance is necessary to achieve the protection of the environment. As affirmed by Leknes (2001), the factors that affect implementation of EIA compliance are inadequate enforcement of EIA requirements, especially EIA report quality, implementation of mitigation measures and impact monitoring, lack of specialization in EIA, low entry barriers, unethical practices by consultants, and inadequate consultant vetting methods, resulting in EIA services being provided by incompetent consultants even though the competent ones are available, and a lack of up-to-date EIA guidelines to facilitate EIA studies that are scientific and can provide adequate decision-making information. The findings of the researcher agree with those of Rowan et al. (2016), who found lack of specialization in EIA, inadequate consultant vetting methods resulting in EIA services, and unethical practices by consultants as factors affecting compliance with EIA guidelines.

Unfortunately, none of these studies investigated the determinants that influence compliance with Environmental Impact Assessment guidelines by industries in Aba North and South local government areas. Secondly, it was observed that most of the published empirical studies conducted on factors affecting compliance with EIA guidelines did not focus on the three industrial sectors of the economy, manufacturing, construction, and service. Hence, there is a dearth of literature on the factors affecting compliance with EIA guidelines in the manufacturing, construction, and service industrial sectors in Aba. In an attempt to fill the gaps created in the literature, this study investigates the determinants that influence compliance with EIA guidelines by industries in Aba City, southeast Nigeria.

THE STUDY AREA

The study area is the commercial nerve center of Abia State in the southeast region of Nigeria, as seen in Fig. 1. Aba is located between latitudes 5°6' N and 5°7' N and longitudes 7°18' E and 7°22' E and is made up of two local

Fig. 1: Map of Nigeria, showing Abia State, South East of Nigeria.

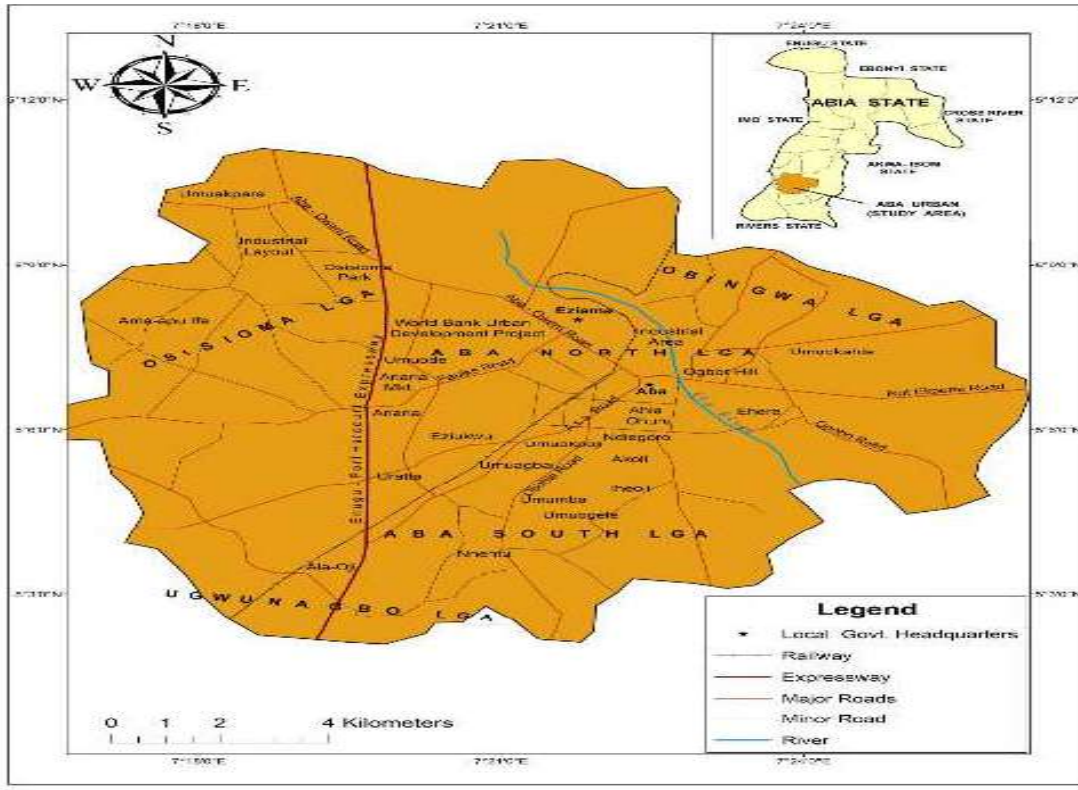

Fig. 2: Abia State map showing the two LGAs under study. Source (Maduko 2016).

governments, Aba North and South (Ofomata 2002), as seen in Fig. 2. The city houses many industrial sectors whose activities impact the environment negatively.

Aba has numerous commercial and industrial activities. Aside from Onitsha, the most pronounced commercial town in the southeast area of Nigeria, the study area is second in its scale of commerce in Nigeria. The body that is responsible for commerce and industry in the study area is the Aba Chamber of Commerce, Industry, Mining, and Agriculture. There are about 2000 industries in Aba, with some of them going moribund and many small-scale industries springing up (ACCIMA 2020). Apart from the large industries, there are also many artisans as well as small and medium-scale industries in the study area. Large-scale industries in the area include 7up Bottling Company Guinness Plc, New Erra Foods, Nigerian Breweries Plc, Clover Paint, Tonimas Oil, and Gas. Medium-scale industries include Nicen Paint, Afro Beverages and Distillers, Starline Nig. Ltd., and Hanonimbiz Foods. Some of the few small-scale industries seen in Aba include John Chuks Metal Ltd., G&C sachet water, Okoson Aluminum, Divine Gate Aluminium Ltd., Aku Plastic, etc.

RESEARCH METHODS

The research adopted a survey research design. The researchers collected data from primary and secondary sources. The list of industries in Aba was sourced from the Aba Chamber of Commerce, Industry, Mines, and Agriculture (ACCIMA) catalog, 2020. The sample population includes the management staff of the various categories of industries/ proponents operating in Aba as well as environmentalists (town planners) from the two local governments of Aba North and South Town Planning Authorities. The sample frame consisted of 384 staff at the management level in the three industrial sectors (production/manufacturing, construction, and services) in the study area. The reason for using only management staff was because they are directly involved in formulating and implementing compliance policies; hence, they possessed the required information regarding how companies comply with EIA guidelines. Cluster and simplified random sampling techniques were employed in this study. Industries were selected using the cluster stratified sampling technique, where the sectors were clustered into three: production/manufacturing, construction, and services. Simple random sampling was then adopted in the selection of the industries in each cluster.

Furthermore, the number of industries in each sector to be included in the sample was determined using proportionate allocation, and each industry had a non-zero probability of being selected. To determine the share of questionnaires to be distributed to each industry, it is calculated as follows:

N_m = total no. of manufacturing industries 1024

N_s = total no. of service industries 722

N_c = total number of construction industries 310

N = total population of the three industries 2056

n = which is the sample size 384

The proportionate allocation method was used to calculate the number of questionnaires that were administered to each sector of the industries and the formula is stated thus:

Therefore $n_h = n \frac{N_h}{N}$ …(1)

Where n = 384

N = 2056

So, $n_m = 384 \frac{1024}{2056}$ = 191 industries

$n_s = 384 \frac{722}{2056}$ = 135 industries

$n_c = 384 \frac{310}{2056}$ = 58 industries

Total = 384 industries

Therefore, 191, 135 and 58 questionnaires were allocated proportionally between the manufacturing, service, and construction industries, respectively, for a total of 384 copies. Out of 384 copies of the questionnaire administered to the three different industrial sectors, 345 were correctly filled out and returned.

Notably, there was no sample selection amongst the town planners or town planning consultants because they were not such a large number. Therefore, 37 copies of the questionnaire were administered to 37 of them (Aba South: 15 town planning officers, Aba North: 13 town planning officers, and 9 planning consultants in the two LGAs). The inferential statistical tool used to test the hypothesis was principal component analysis (PCA)

Selected Variables that Influence Compliance with EIA Guidelines

In Table 1, 13 variables have been identified through literature and questionnaire administration to influence compliance with EIA guidelines, which were later transformed into fewer variables for easier data management. The identified variables are shown in Table 1.

The Principal Component Analysis (PCA) statistical tool was used to compress the 13 identified primary compliance factors into 7 orthogonal dimensions, which then formed the secondary factors. However, for proper evaluation, the 384 responses were transformed by 13 data matrixes, and the varimax rotation was also computed. Thus, their respective

Table 1: Variables have been identified to influence compliance with EIA guidelines.

Variable Identity	Variables
F 1.	Legal system
F 2.	Public participation
F 3.	Cost of compliance
F 4.	Screening and scoping
F 5.	Weak coordination
F 6.	Quality of EIA
F 7.	Limited scope
F 8.	Fear of project change
F9	Ignorant on how to comply
F10	Mitigation measures
F11	Delay in Approval
F12	Meeting requirements
F13	Administration

Eigenvalues were obtained, and the 7 dimensions were selected in their order of importance as presented in their order of importance.

The PCA output shows that seven components (factors) express the bulk of the common variance among the 13 primary variables. These seven factors were referred to in the study as the factors that influenced the compliance rate of the EIA guidelines in the study area. The factor loading for each variable was between ±0.462 and ±0.828, approximately as presented in Table 2. The matching name was used to identify each of the components. Table 3 shows the factor loading of each of the components.

Factor 1: Ineffective legal/ public participation

Factor 2: Cost of compliance

Factor 3: Weak coordination

Factor 4: Limited scope

Factor 5: Mitigation measures

Factor 6: Delay in approval

Factor 7: Meeting requirements

To better understand the output, Table 3 shows the factors and the variables that were the subsets with their factor loading.

The result of the PCA shows that the factors that influence the compliance rate of EIA by industries can be discernibly patterned into seven components. It explained 55.103 percent of the observed variation in compliance with EIA guideline variables. In other words, seven critical factors influence developers' compliance with EIA guidelines

Table 2: The Rotated value of each component in matrix form showing factor loading.

	Component						
	1	2	3	4	5	6	7
Legal system	.746						
Public participation	-.708						
Ignorance							
Cost		-.718					
Screening and scoping		.533					
Cordination			.694				
Quality of EIA			.629				
Fund							
Limited scope				.664			
Change				-.498			
How to comply				.494			.460
Expertise and skills							
Mitigation measures					.828		
Approval						.787	
Meeting requirements							.662
Administration							.462

Extraction Method: Principal Component Analysis.

Rotation Method: Varimax with Kaiser Normalization.

a. Rotation converged in 19 iterations.

Table 3: Component names for the primary compliance variables.

Component Names	Variable Identity	Factor Loadings
FACTOR 1: Ine*ffective legal system/participation*		
Effective legal system	F1	.746
Effective public participation	F2	.708
FACTOR 2:*cost compliance*		
-cost compliance	F3	.718
-screening and scoping	F4	.533
FACTOR 3: Weak coordination		
Weak coordination	F5	.694
Quality of EIA	F6	.629
FACTOR 4: *limited scope of EIA*		
-limited scope	F7	.664
-Fear of change of project	F8	.498
-Ignorant on how to comply	F9	.494
FACTOR 5: *Implementation of mitigation measure*		
Mitigation measures	F10	.828
FACTOR 6: *Delay in approval of EIA reports*	F11	.787
Delay in approval		
FACTOR 7: *poor administrative setup*		
-Administration	F12	462
-Meeting requirements	F13	662

in the study area. These factors were ineffective legal mechanism/public participation (1.760), cost of compliance (1,420), weak coordination (1.251), limited scope (1.201), mitigation measures (1.113), delay in approval (1.038), and administrative (1.034).

DISCUSSION

The study shows that the ineffective legal system and legislation had the strongest influence on the compliance of industries with Environmental Impact Assessment guidelines in Aba. The result of the finding supports what Rachael (2017) proved: a lack of coherent legal framework and guidelines makes for ineffective enforcement of the sections of the EIA guidelines to curb environmental degradation. In the same vein, Rai et al. (2015) found that legal framework and institutional capacity are significantly affecting the performance of Environmental Impact Assessment practices screening, scoping and mitigation, EMP, and reporting. Again, the level of developers' awareness of EIA guidelines strengthens or weakens the legal framework of any environmental endeavor. This assertion, according to Rai et al. (2015), has been validated by the findings of this study in Aba.

In this study, ineffective implementation of mitigation measures and monitoring by lead agencies were found to be influencing the successful implementation of EIA guidelines. This study indicated that there is poor evaluation and monitoring by the staff of the Ministry of Environment, the supervisory body saddled with the responsibility of inspecting the industries to ensure proper management of industrial effluents and waste. This is in sync with the findings of Sadler (2011), who submitted that the monitoring and evaluation of the implementation of EIA guidelines is crucial to preventing environmental degradation and ensuring sustainable development. This proves that adequate evaluation and monitoring have a great impact on the prevention of environmental degradation by industrialists in Aba. The studies of Mahlatse (2015), Kelvin (2016), Maduko (2016), Rachael (2017), and Clarke & Cong (2021) found that the major factor affecting compliance with EIA was the lack of engagement of the affected members of the public during EIA endeavors. This was also seen in this study. It was posited that most of the stakeholders and the public were not consulted during various EIA exercises in the study area. Aba, being one of the commercial nerve centers of the southeast, houses numerous businessmen and women who are always busy with their trading activities and hence devote little or no time to environmental endeavors around them. This is further buttressed by the study, where respondents affirmed that consultation was not done prior to the execution of projects in their area. Furthermore, this finding suggests that there is a very low level of public participation by affected stakeholders prior to development projects in the study area. Nwafor (2006) asserted that though public participation could be time-consuming and may involve huge financial implications, not involving the affected members of the public will have a long-lasting and far-reaching negative effect if the stakeholders revolt through litigation processes. This assertion was supported by Salihu

et al. (2015) in their study in Niger State, which noted that stakeholders were not carried along during the introduction of projects that affected the public. A similar study carried out by Kelvin (2016) in commercial towns and projects in Nakuru Town, Nakuru County, Kenya, found that factors like evaluation and monitoring, budgetary allocation, and public participation had a strong influence on the implementation of EIA recommendations. Lead agencies have tended to overlook the importance of public involvement, either through ignorance or sometimes with the purpose of avoiding sanction by relevant authorities. In this study, it has been proven that poor public involvement by industrialists, lead agencies, and EIA experts has a direct impact on compliance with EIA guidelines in Aba. Stakeholders are therefore very important in the successful implementation of EIA guidelines by industrialists in Aba.

Further, it was posited from the study that delay in project approval does significantly influence compliance with EIA guidelines. In the same vein, Kanyi (2014) reported that delays in approving proponent's proposals by regulatory agencies have caused EIA endeavors to lose integrity and trust among those concerned. Also, Rachael (2017) found that most EIA proposals are not given approval on time and that most times, proponents start and complete their projects even before approval is granted by the relevant agencies.

It was also noted from the study that the government agency's insufficient budgetary allocation for the follow-up of the implementation of EIA guidelines in the study area. These results corroborate Rowan et al.'s (2016) argument that until the benefits of total compliance with EIA guidelines are widely recognized in terms of long-term cost savings and improved environmental management, implementation agencies will continue to under-budget finances for EIA follow-up.

Also, another factor influencing compliance with EIA guidelines in Aba was weak and poor coordination by the supervisory bodies along the lines of departments (EIA consultants). This is substantiated by the respondent's affirmations. Chris (2013) found that coordination among the Federal Ministry of Environment, local financial institutions, EIA proponents and consultants, and the Department of Petroleum Resources is generally poor and weak.

It was observed that the limited scope of the EIA review significantly influences the rate of compliance with Environmental Impact Assessment guidelines by industries in Aba. The EIA review process usually involves third-party participation to ultimately enhance the quality of the EIA study and final report (Kelvin 2016). This third-party involvement in the review can be marked as a salient feature of the EIA process in Nigeria. Although an independent EIA review commission does not exist in Nigeria, more resources are expected to be allocated by the government to transform third-party involvement into formal review bodies. Rowan et al. (2016) found that some anomalies exist in the process due to a lack of technical capacity and subjective review. The study further revealed that 89.8% of the respondents believe that the poor quality of EIA reports does influence compliance with EIA guidelines in the study area. Peter (2016) stated that the standard of the EIA report is a clear reflection of the strength and competence of the EIA review committee members and EIA consultants. The lack of experience of EIA consultants and approval authorities, along with reluctance on the part of the proponents to allocate sufficient resources, are some of the impediments to a better-quality EIA (Shahbaz et al. 2015). The study observed that consultants' role and scope in the study area have been limited to highlighting only the economic gains and benefits of the project, forgetting environmental approval. Unlike what was observed in the study area, Kelvin (2016) reported that 80% of the sampled population in his study were aware of EIA guidelines in Nakuru Town, Kenya. Surprisingly, in Aba, this study found that a significant number (63.7%) were not aware of EIA guidelines in the study area. In the same vein, the findings of this study also contrast with the findings of Muhhamed (2012), who revealed that developers' level of awareness and technical factors influenced compliance with the Environmental Impact Assessment regulation.

CONCLUSIONS

The identified seven factors that affect compliance with EIA guidelines are: ineffective legal system/public participation, cost of compliance, weak coordination along the line of departments (town planning officers and consultants), limited scope of EIA review, inadequate execution of proposed mitigation measures and follow-up, delay in approving of reports by regulatory agencies, and poor administrative set up within the responsible authorities. Furthermore, the developer's level of awareness of EIA guidelines is another identified factor that has a significant influence on the rate of compliance with EIA guidelines. This study is one of the very few that has contributed to the body of existing literature by examining the factors influencing compliance with EIA guidelines in Nigeria. The government should, as a matter of urgency, strengthen the legal and institutional framework to ensure that all issues regarding noncompliance are addressed through a strong legal mechanism and that there should be proper and timely follow-up by regulatory agencies to ensure that the contents of EIA reports as submitted by proponents are complied with as proposed. It is also recommended that NESREA, the body in charge of environmental management

in Nigeria, should, as a matter of policy, strengthen the credibility of its regulatory role through an effective and consistent enforcement mechanism. Also, the government should encourage institutions of higher learning, research organizations, and other private bodies to set up awareness-raising and training programs for industries on environmental management and pollution mitigation.

This study recognized that other variables influence industries' noncompliance with environmental guidelines that were not captured in the work. This therefore presents the essence for further studies, even if situational circumstances are capable of influencing this act. Hence, further research in that regard will be beneficial.

REFERENCES

Aba Chamber of Commerce, Industry, Mining and Agriculture (ACCIMA) 2020. Unpublished Catalogue of Events "3rd International Trade Fair", Umungasi Aba. Abia State, Nigeria.

Agwu, E.I.C., Ezedike, C.E. and Egbu, A.U. 2009. The Concept and Procedure of Environmental Impact Assessment. Oscar Graphics, Owerri Imo State. Nigeria.

Chris, N.O. 2013. Evaluation of environmental impact assessment system in Nigeria. Greener Journal of Environmental Management and Public Safety, 2(1): 022-031.

Clarke, B.D. and Cong, C. V 2021. EIA effectiveness in Vietnam: key stakeholder perceptions. Heliyon, 7: e06157. https://doi.org/10.1016/j.heliyon.2021.e06157.

Hussain, S., Nayyab, H.H., Fareed, Z., Baqir, R., Zulfiqar, B. and Shahzad, F. 2015. An investigation of the factors affecting the performance of environmental impact assessment practices (EIA) in Pakistan. Oeconomics of Knowledge, 7(1): 36.

Kakonge, J.O. 1998. EIA and Good Governance: Issues and Lessons from Africa. Environmental Impact Assessment Review, 48: 289-305.

Kanyi, J. 2014. Factors affecting environmental best practice compliance among retail fuel service stations in Thika East Sub-County-Kenya. Master's thesis submitted to the School of Arts (Environmental Planning and Management), University of Nairobi.

Kelvin, K. K. 2016. Factors influencing the implementation of EIA recommendations on commercial projects, a case of Nakuru town, Nakuru, county Kenya. A thesis report submitted to the Department of Project Planning and Management, Nairobi University.

Leknes, E. 2001. The roles of EIA in the decision-making process. Environmental Impact Assessment Review, 21(4): 309-334.

Maduko, C. E. 2016. Industrial noise levels in Aba urban area, Nigeria. A project report submitted to the School of Postgraduate Studies and the Department of Geography, University of Nigeria, Nsukka.

Mahlatse, J. S. 2015. Comparative analysis of environmental impact assessment compliance by two developers in the Northern Cape Province. A thesis report submitted to the Department of Environmental Management. University of South Africa.

Mangogrie, C. 2015. Methodologies used for determining impact significance and the implications for EIA effectiveness in South Africa. Case Studies from KwaZulu-Natal, University of KwaZulu Natal Westville.

Mohammed, M.U., Musa, I.J. and Jeb, D.N. 2014. GIS-based analysis of the location of filling stations in metropolitan Kano against the physical planning standards. American Journal of Engineering Research, 3:147-158.

Morrison, S. A., Marshal, R. and Arts, K. 2017. EIA Follow-Up International Best Practice Principles, Karachi, Pakistan.

Muhhamed, H.A. 2012. Factors influencing compliance to EIA/Environment Audit Regulation in Kenya, a case of Garissa central division. B.Sc. Project Published on Department of Extra Mural Studies, Kenya. http://ems.uonbi.ac.ke

Nwafor, J.C. 2006. Environmental Impact Assessment for Sustainable Development, the Nigerian Perspective. Published and printed in Nigeria by Environmental And Development Policy Centre for Africa (EDPCA), New Heaven Enugu, Enugu state.

Ofomata, G.E.K. 2002. Relief, Drainage and Landforms: A Survey of Igboland, Onitsha. Africana First Publishers, pp. 83-85.

Peter, K. 2016. Compliance and enforcement of EIA and EMMPs in Asia. Conference Proceedings presented a IAIA Resilience and Sustainability 36th Annual Conference of the International Association for Impact Assessment, 11-14 May 2016, Nagoya Congress Center, Aichi-Nagoya, Japan.

Rachael, K. 2017. Factors influencing compliance to environmental impact assessment (EIA), case of Kitui Central Sub-county. Research Project Report Submitted to the Department of Project Planning and Management. University of Nairobi.

Rai, H. S., Hafiza, N., Zeeshan, F. and Rubina, B. 2015. An Investigation of the factors affecting performance of environmental impact assessment practices (EIA). Pakistan Economics of Knowledge, 7(1): 56-62.

Rowan, K. M., Lakshmanan. G. and James, M. 2016. Compliance with the requirements of the environmental impact assessment guidelines in Zimbabwe: A case study. Journal of Sustainable Development, 9(5): 218-222.

Sadler, B. 2011. Taking stock of SEA. In: Handbook of Strategic Environmental Assessment (Ed.) Sadler, B., pp. 1-18, London: Earthscan.

Salihu, A.C, Nabegu, A.B., Abdulkarim, B. and Mustapha, A. 2015. Environmental Compliance of Facilities in Minna-Niger State, North Central Nigeria. Research Journal of Geography, 2(10): 1-10.

United Nations Environment Programme (UNEP) 2002. Environmental Impact Assessment Training Resource Manual, 2nd ed.; UNEP: Geneva, Switzerland, 2002.

Wood, C., 1993. Environmental impact assessment in Victoria: Australian discretion rules EA. Journal of Environmental Management, 39(4): 281-295.

Zaelke, D., Stilwell, M. and Young, O. 2005. What reason demands: making law work for sustainable development. Making Law Work: Environmental Compliance and Sustainable Development, 1: 29-51.

ORCID DETAILS OF THE AUTHORS

O. J. Ubani: https://orcid.org/0000-0003-0396-254X

Nature Environment and Pollution Technology
An International Quarterly Scientific Journal

p-ISSN: 0972-6268
(Print copies up to 2016)
e-ISSN: 2395-3454

Vol. 23 | No. 1 | pp. 391-399 | 2024

Original Research Paper

https://doi.org/10.46488/NEPT.2024.v23i01.033

Open Access Journal

Hunting Resource Management by Population Size Control by Remote Sensing Using an Unmanned Aerial Vehicle

S. Ivanova*(**)† and A. Prosekov*(****)**

*Department of the Comprehensive Scientific and Technical Program Implementation, Kemerovo State University, Krasnaya Street 6, Kemerovo, 650043, Russia

**Department of General Mathematics and Informatics, Kemerovo State University, Krasnaya Street 6, Kemerovo 650043, Russia

***Laboratory of Biocatalysis, Kemerovo State University, Krasnaya Street 6, Kemerovo, 650043, Russia

****Computer Engineering Center, Kemerovo State University, Krasnaya Street 6, Kemerovo, 650043, Russia

†Corresponding author: Svetlana Ivanova; pavvm2000@mail.ru

Nat. Env. & Poll. Tech.
Website: www.neptjournal.com

Received: 26-10-2021
Revised: 07-01-2022
Accepted: 07-08-2023

Key Words:
Wild animals
Hunting grounds
Biodiversity
Remote sensing
Unmanned aerial vehicle
Management

ABSTRACT

The study was carried out on the territory of the Kemerovo region-Kuzbass (Western Siberia, Russia). The purpose of the study was to obtain information on the species diversity and population of big-game animals. The monitoring was carried out on the forest territories of the region's administrative districts. In the course of remote sensing using an unmanned aerial vehicle, the presence of all types of animals under consideration, except for the bear, was recorded. The deviation of the population number determined using the traditional method of digital technologies varied up to 50%. It was established that environmental measures organized and carried out by the regional administration and hunting farms improved the situation and stabilized the population of the main group of game animals. It was found that when using a sufficiently high sensitivity of the thermal imager (the used thermal imager had a very high sensitivity class ≤ 60 mK at 300 K), long-haired animals, which are characterized by a lower intensity of thermal radiation (for example, wolves) are identified and recognized in the images. The larger the animal and the worse the thermal insulation layer (wool or feathers), the easier it is to identify it in infrared images and the lower the sensitivity requirements of thermal imagers. The ability to recognize and record smaller animals and birds requires additional research on existing technologies. Our research has confirmed the validity of digital remote monitoring methods for managing the wildlife of hunting farms and nature conservation areas of the Siberian Taiga territories.

INTRODUCTION

Conservation of biological diversity is an obligation to future generations. The problem is peculiar to all territories without exception. Siberia has amazing and diverse wildlife. Despite the remoteness of most of the Siberian region from civilization, it has experienced the harmful effects of human presence.

Kemerovo Region is located in the south of Western Siberia and covers an area of 95,725 km^2 (Fig. 1). Coal, chemical industries, and metallurgy are the key economic branches of the Kemerovo region (Prosekov 2021a).

Forest and taiga play a vital role in maintaining the Kuzbass ecosystem. The inhabitants of mountainous areas are directly dependent on forest resources in terms of food, firewood, fodder, and wood. The forest also plays an important role in providing habitat for wildlife. The climate of the Kemerovo region is sharply continental (winter is cold and long, summer is warm and short). Average temperatures in January vary from -17 to -20°C, and in July, from +17 to +18°C. The average annual precipitation ranges from 300 mm on the plains and in the foothill part to 1,000 mm or more in mountainous areas. The frost-free period lasts from 100 days in the north of the region to 120 days in the south of the Kuznetsk Basin.

The game resources of the Kemerovo region-Kuzbass are formed under the influence of sharply differentiated natural conditions of the region, as well as man-made impacts on the natural environment. The natural landscapes of the Kemerovo region-Kuzbass are extremely diverse, and many of them have been greatly changed by human influence. The variety of terrain and climate determines the diversity of vegetation. On the mountain peaks, there are plants of tundra and alpine meadows. The middle and low

Fig. 1: Kemerovo Region-Kuzbass on the map of Russia.

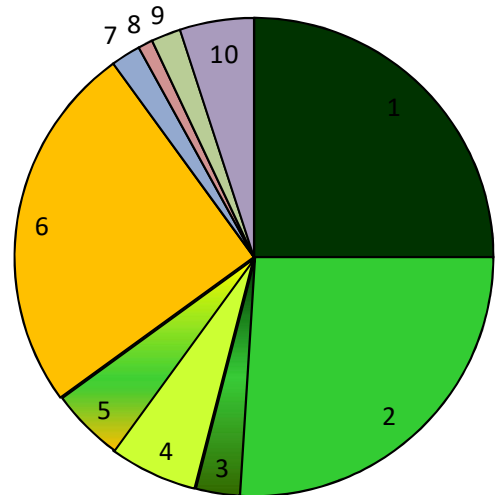

Fig. 2: The structure of the main habitat classes of game animals in the Kemerovo region –Kuzbass: 1 - coniferous forests, 2 - small-leaved forests, 3 - mixed forests, 4 - young forest growth, 5 - meadow-steppe complexes, 6 – farmland, 7 – floodplain complexes, 8 - transformed, damaged areas, 9 - unsuitable for hunting territories, 10 - other (swamps, tundra, etc.).

mountains are overgrown with fir and aspen forests with tall grass and relict plants. The foothills and intermountain basins feature the vegetation of steppes and forest steppes. The diversity of habitats of game animals in the Kemerovo region – Kuzbass is clearly shown by the data in Fig. 2. Coniferous, small-leaved forests, and farmland occupy almost equal shares (about 25%). Small-leaved mixed and meadow-steppe complexes are represented to a lesser extent. All this determines the conditions for the coexistence of forest and steppe flora in the region (Ilyashenko et al. 2019, Skalon et al. 2019).

The publicly accessible hunting grounds (Fig. 3) of the Kemerovo region-Kuzbass amount to 1992.9K hectares (26.2% of the total), including the assigned 5604.2K hectares (73.8%). Almost the entire assigned area (no more than 80% of the lands of the subject of the Federation) in the Kemerovo region – Kuzbass is distributed among hunting providers. There are no public lands in many districts of the region. First of all, these are the territories of the Kuznetsk Basin that are most unfavorable for big-game taiga animals (Leninsk-Kuznetsky, Topkinsky, Promyshlennovsky, Izhmorsky, Chebulinsky municipal districts). In the areas with less anthropogenic load, higher biodiversity, and yield class of hunting grounds, the share of publicly accessible land is higher (for example, in the Tashtagol district, it's more than 90%).

The diversity of climatic and phytocenotic conditions of the Kemerovo region-Kuzbass determines the wildlife diversity. On the territory of the region, there are about 450 species of vertebrates (about 325 species of birds and 75

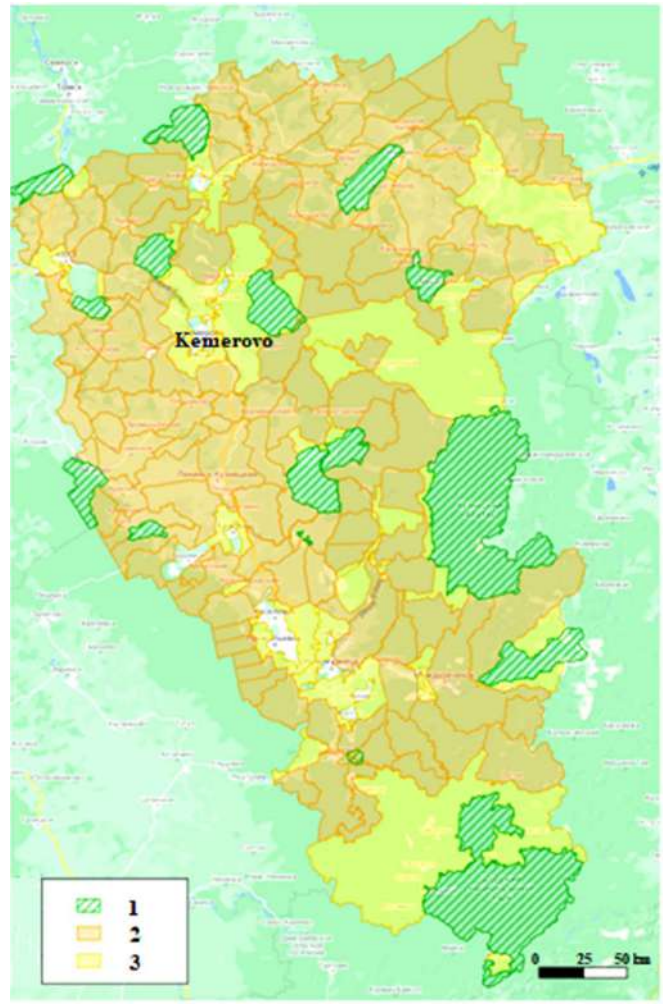

Fig. 3: Boundaries of protected territories and hunting grounds of the Kemerovo region: 1 - specially protected natural territories, 2 - assigned hunting grounds, 3 - publicly accessible hunting grounds.

species of mammals), 70% of which live here permanently. Hunting is in demand almost throughout the region. The most important game mammals are elk, Siberian roe deer, red deer (maral), brown bear, badger, sable, fox, and Arctic hare.

Anthropogenic gradients made the system unsuitable for various wild animals, which led to the loss of both diversity and population size. The population size dynamics are shown in Table 1 (Department NRE of KR 2020, Prosekov 2021b).

A decrease in the population of natural enemies (wolf, lynx), an increase in the area of farmland and the length of power lines, an increase in the area of secondary biotopes, stabilization of the number of maral due to the activities of the Kuznetsky Alatau Nature Reserve and wildlife sanctuaries, the fight against poaching led to fluctuations in the population of animals in both directions.

At the same time, in the Kemerovo region-Kuzbass, the harvest of those species that have practically disappeared or have their population reduced has stopped (Table 2). In particular, Siberian weasel, lynx, wolverine, and wolf, hunting for which is either prohibited or there are no hunting resources, are no longer harvested. Along with this, the harvest of squirrels in the region has almost halved due to a reduction in their population.

The main purpose of the organization of a hunting farm is to determine the position of hunting providers in the general economic system of the projected territory, as well as the choice of the ownership form and its organizational structure. Kemerovo region – Kuzbass has quite considerable hunting potential. The fauna of the region is diverse, but significant anthropogenic impact drastically reduces the yield class of hunting grounds. In general, with a high differentiation of the

Table 1: Dynamics of the population size of game animals in the Kemerovo region – Kuzbass (2001–2019).

Object of the study	Population, specimen					
	2001	2006	2011	2017	2018	2019
Elk	4130	2230	2728	4804	5010	5112
Maral	860	810	410	905	962	985
Siberian roe deer	5020	4740	3848	6858	7086	7436
Wild boar	-	-	228	1096	361	321
Brown bear	2000	2000	2274	3125	3086	3036
Wolf	230	60	6	-	-	7
Red fox	3000	2380	3525	4587	4449	4562
Wolverine	80	80	87	67	71	69
Badger	12500	13000	10292	10786	14370	12046
Sable	7500	9000	7713	14329	14066	12778
Otter	300	300	417	629	689	706
American mink	7300	11000	10006	11067	10850	10778
Siberian weasel	6000	4100	3370	1643	1462	1378
Steppe polecat	1400	940	1047	198	339	193
Stoat	2800	1700	2125	379	377	476
Eurasian beaver	6500	11100	18037	17829	18131	18738
Squirrel	53400	40800	20232	22990	23778	22898
Arctic hare	30800	34700	28129	38108	29653	32275
European hare	900	610	378	352	271	401
Muskrat	28000	30000	28476	17155	17109	16451
Groundhog	3350	4500	3755	4133	4130	4435
Lynx	400	370	242	128	151	111
Capercaillie	13600	7600	7870	13194	11281	6863
Grouse	351000	222300	296213	396436	313471	233116
Black grouse	128000	70500	73856	185509	138957	132452
Waterfowl	64500	83300	74513	49150	50284	52630
Moorfowl	28600	26900	33593	-	-	-

Table 2: Game harvesting dynamics in the Kemerovo region – Kuzbass (2001–2019).

Object of the study	Population, specimen					Harvest,
	2005	2006	2011	2018	2019	%**
Maral	5	3	4	10	15	300.0
Roe deer	115	143	111	207	239	207.8
Elk	–	–	41	96	118	–
Lynx	3	2	2	–	–	–
Wolverine	–	–	–	–	–	–
Sable	928	1256	1612	3142	3163	340.8
Brown bear	59	52	79	219	249	422.0
Wolf	19	12	–	–	–	–
Badger	–	–	155	481	467	–
Wild boar	–	–	5	137	55	–

Table Cont....

Object of the study	Population, specimen					Harvest,
	2005	2006	2011	2018	2019	%**
Squirrel	1108	697	2	827	618	55.8
Beaver	162	163	518	1128	1285	793.2
Fox	674	1245	361	1189	763	113.2
Arctic hare	3699	5570	3700	5565	4594	124.2
Siberian weasel	91	42	–	–	–	–
Grouse	6968	5270	3088	9201	7759	111.4
Black grouse	594	602	829	2602	2312	389.2
Capercaillie	46	40	78	163	204	443.5
Ducks (of all kinds)	618	9085	15855	10176	11029	1784.6

* % of the population size in 2019 compared to 2005.

game animals' habitats in the Kemerovo region-Kuzbass, the habitat conditions improve from the center to the periphery. So, it is important to correctly record the number of animals and birds in lands that differ by quality. It is possible to understand the lands and their yield only in dynamics since they change from year to year due to natural climatic and anthropogenic factors (logging, fires, agricultural activities, etc.) (Albery et al. 2021, Cayuela et al. 2018, Prosekov et al. 2020, Thulin & Rocklinsberg, 2020, van de Walle et al. 2018).

The study aimed to explore the possibility of using digital technologies (remote monitoring with unmanned aerial vehicles) for the control and management of wild game populations.

MATERIALS AND METHODS

Objectives of the Study

The objects of the study were the main game animals of the Kemerovo region – Kuzbass: elk (*Alces Alces*), maral (Cervus elaphus), Siberian roe deer (*Capeiolus pygargus*), wild boar (*Sus scrofa*), brown bear (*Ursus arctos*), wolf (*Canis lupus*), sable (*Martes zibellina*), badger (*Meles Meles*), European beaver (*Castor fiber*), fox (*Vulpes Vulpes*), Arctic hare (*Lepus timidus*).

Area of the Study

The remote monitoring of animals was carried out in the Muryukskoye Hunting Society (I), the Taidonskoye

Fig. 4: Map of Kemerovo region-Kuzbass: 1 - Krapivinsky district, 2 - Chebulinsky district.

hunting farm (II), and the Shestakovskoye hunting farm (III) located in the Chebulinsky and Krapivinsky districts of the Kemerovo region-Kuzbass (Fig. 4) during the winter periods of 2019 and 2020.

Research Methods

To record the wildlife population, the original technology of combined shooting (conventional photo, video, and thermal imaging in the infrared spectrum) was used (Prosekov et al. 2020). When assessing the scale of under-counting errors, there is no fundamental difference between shooting or visual observation using traditional or unmanned aircraft. Thermal imaging is reliable enough to determine the very fact of the presence of an animal by its thermal signature without omissions, provided that there is a significant difference in the temperature of the animal's body and the environment (up to 30-40°C). Still, it does not allow us to distinguish species with similar mass and geometric dimensions (for example, a wolf and a boar).

An unmanned aerial vehicle of the aircraft type "Supercam S250" (LLC "Unmanned Systems," Izhevsk, Russia) with a wingspan of 2.53 m (Fig. 5) was the physical carrier of the shooting and other equipment for the study. The model has the following operational characteristics: flight time – up to 3 h; flight range – up to 180 km; speed – from 65 to 120 km.h^{-1}; permissible distance from the operator (radio line range of action) – 50-70 km; flying height – from 50 to 500 m; permissible wind speed up to 15 m.s^{-1}, air temperature from -50 °C to +45 °C, moderate precipitation (rain, snowfall) is possible. There is a receiver of the global satellite navigation system on board for the most accurate coordinate control.

The specifications of the Sony RX1R II camera (Sony, Japan) and the ATOM500 thermal imager (Sun Creative Zhejiang Technologies Inc, Zhejiang, China) are given in Tables 3 and 4, respectively.

The shooting results were processed using a specialized software product (a PC app in Python), "Thermal Infrared Object Finder" (TIOF), developed at KemSU (Prosekov et al. 2020). The application records "thermal anomalies," i.e., areas in the images that have a higher temperature than the environment, which indicates the presence of an animal. Easy to install and use. The program works with data from any thermal imaging cameras. The program can process different file formats - jpeg, png, avi, mp4. The processing speed depends mainly on the number of streams. Thus, materials

Fig. 5: General view of the UAV used in the study.

Table 3: Key specifications of the camera used.

Specification	Description
Matrix	Exmor R® full-frame CMOS matrix (35.9×24.0 mm), 3:2 screen format; number of effective pixels ~42.4 MP; total number of pixels ~43.6 MP
Lens	ZEISS® Sonnar T*, 8 elements in 7 groups (3 aspherical elements, including advanced AA aspherical elements), focal length f = 35 mm
Camera	Image processor: BIONZ™ X; ISO sensitivity (photography, recommended exposure index): ISO 100–25600 (in 1/3 EV increments) (expandable to ISO 50/64/80/32000/40000/51200/64000/80000/102400), AUTO (ISO 100–102400, with upper/lower limit selection); multi-frame noise reduction: ISO 100-102400 (in 1 EV increments), AUTO (ISO 100–102400, with upper/lower limit selection)

Table 4: Key specifications of the thermal imaging camera used.

Specification	Description
Parameters	Weight without lens 32 g, dimensions without lens 28×28×24 mm
Receiver	Infrared wave receiver on an uncooled microbolometric matrix made of amorphous silicon, resolution 640×480, pixel size 17 microns. Temperature sensitivity ≤ 60 mK at 300 K, 50 Hz. Spectral range 8–14 μm
Image processing	No shutting calibrating technology (NST) Start time less than 5 seconds. Noise reduction through a digital filter. Image resolution 768 × 576/640 × 480 pix. (NTSC resolution and frequency presets). Image frame rate 50 Hz (PAL) and 60 Hz (NTSC). Lens 25 mm.
Image settings	Image color (palette) – shades of gray. Polarity: hot white or hot black. Horizontal and vertical mirror reflection is possible. Digital zoom – x2, x4 and x8. Automatic contrast adjustment.
Power supply system	Power consumption is less than 0.8 watts. Standard supply voltage 3.6 V; possible voltage range 2.5-5.5 V.
Operating conditions	Operating temperature from -40°C to +60°C, storage temperature from -45°C to +65°C. Relative humidity from 5% to 95% (conditions without condensation of moisture). Vibration resistance meets the GJB 150-16 2.3.1 standard; impact resistance meets the GJB 150-8 standard. Resistance to temperature changes up to 5°C.min^{-1}.
Interface	Power connector; RS-232 serial control interface. Analog video output, dual-channel video output support. For navigation and geo-positioning, there is a ground-based geodetic "Javad Triumph 2" GNSS receiver.
Other significant characteristics	Supports geo-positioning in GPS systems,GLONASS, SBAS L1 differential correction systems using the Kalman algorithm to determine the camera location. Data refresh rate 100 Hz. Internal memory 2 GB. Receiver Autonomous Integrity Monitoring, RAIM for correct recording of navigation signals received from the satellite. Lift&Tilt shooting mode with automatic correction of the vertical position. USB connector, Bluetooth and Wi-Fi interface. Antenna, inclinometers (tilt angle meters), compass, lithium-ion batteries.

Table 5: Comparison of the results of winter route census and counting using digital technologies in the "Muryukskoye" hunting society (I), "Taidonskoye" (II) and "Shestakovskoye" (III) hunting farms

Study object	Population, specimen								
	I			II			III		
	1	2		1	2		1	2	
	2019	2019	2020	2019	2019	2020	2019	2019	2020
Maral	3	7	11	2	5	9	85	93	98
Roe deer	48	69	74	25	42	51	220	245	254
Elk	42	57	59	103	99	101	59	57	58
Wild boar	36	42	40	0	0	0	150	172	191
Sable	187	243	260	634	691	734	190	223	256
Badger	36	34	40	131	159	168	140	130	141
Fox	18	22	21	49	41	44	25	21	24
Arctic hare	89	74	69	400	398	395	180	233	225

1 – according to the winter route census data, 2 – according to the data of remote monitoring using UAVs.

from one standard UAV flight with a duration of 100-150 min can be processed in 25-50 s.

RESULTS

The results of remote monitoring of big-game animals (except for brown bears that are not available for registration in winter) using UAVs are presented in Table 5.

The recorded number of animals in the lands is mainly proportional to their share in the area of Chebulinsky (I, III) and Krapivinsky districts (II) (about 10% and 20% of the district area, respectively). At the same time, for most animal species, the ratio of harvesting to population is slightly higher than the regional average, which is due to the dependence of harvesting standards on density, low economic activity, and inaccessibility of hunting grounds.

DISCUSSION

In the studied hunting grounds, the number of most species of game animals was underestimated. In some cases, such deviations reached 30-50% or more (Table 5). Perhaps the reason is the incorrectness of the scaling factors determined at the level of the subject of the Russian Federation in the conditions of small territories or a significant heterogeneity in the density of game populations within the studied hunting

grounds. There was a significant underestimation of ungulate populations (maral, roe deer, and elk) using the winter route census method, which made it possible to identify continuous counting using digital technologies. The large population size of roe deer is explained by its spatial distribution and the difficulty of adequately covering unified routes with the winter route census.

In general, the game population density on the grounds of the Shestakovskoye hunting farm is naturally higher than the average in the Chebulinsky district, which is explained by the breeding and semi-free conditions for a number of species. In particular, the hunting farm has maral, wild boar, and roe deer. The farm did not issue quotas for maral harvesting, due to which the population is steadily increasing. Roe deer population density is quite large. The accuracy of ungulate records in the Shestakovskoye hunting farm is high. At the same time, the ratio of hares and foxes (1:7) is not quite typical for high-yielding lands and may require clarification. As for the wild boar, its population density in the game reserve conditions may be higher.

Differences in the actual number of elk are associated with the movement of the animal to the feeding grounds of hunting farms, during which it isn't easy to differentiate animal tracks by traditional methods. The inflated data on the elk number could be affected by the weather conditions of the corresponding periods, which forced the animals to move more actively (Koetke et al. 2020, Skalon et al. 2019, Jones et al. 2021). Close to the average, the snow cover minimized errors in the counting of wild boars (de Assis Morais et al. 2020, Lemel et al. 2003). In a snowy year, the discrepancies between the winter route census data and the digital survey data would be more significant. The sable population undercount reached almost 30%. The route does not cover part of the taiga zone with a high concentration of sable (Guo et al. 2017, Lavergne et al. 2021 Safronov 2016). The updated fox and hare data allow us to assert that in the lands of the Chebulinsky district, fox exerts strong pressure on the hare population. The predator-prey ratio is even more critical than according to traditional counting methods. Therefore, in the absence of fox hunting, the number of the hare is significantly reduced. In the "Taidonskoe" hunting farm, the number of foxes is lower than the record data, which keeps the hare population stable (Peers et al. 2020, van Beest et al. 2021).

The results of continuous counting using digital technologies for identifying each specimen show that the ungulate and wild boar (bred by the farm) figures have fairly high accuracy. Deviations here do not exceed 15%. In particular, maral and roe deer populations are calculated quite accurately. For species on which the hunting farm does not specialize, the counting accuracy is lower than the actual number.

CONCLUSION

Within the framework of existing approaches, the use of digital technologies for game animal counting usually involves the use of photo cameras. At the same time, the traditional problem of identifying animals in areas with dense vegetation remains. In most cases, when processing photo materials, there will be an undercounting, although somewhat less than with visual observation of animals by a counter. When using infrared imaging, it isn't easy to differentiate animals with similar sizes of the heat-emitting surface. There are also restrictions on the size of the animal. It was found that when using a sufficiently high sensitivity of the thermal imager (the used thermal imager had a very high sensitivity class $\leq$ 60 mK at 300 K), long-haired animals, which are characterized by a lower intensity of thermal radiation (for example, wolves) are identified and recognized in the images. The larger the animal and the worse the thermal insulation layer (wool or feathers), the easier it is to identify it in infrared images and the lower the sensitivity requirements of thermal imagers. For identification by thermal signature, the minimum required length is at least 45-50 cm (hare, sable). Smaller animals and birds are not identified even in an open area and, accordingly, are not recognized during counting. The ability to recognize and record smaller animals and birds requires additional research on existing technologies.

To increase the accuracy of the approach, it is necessary to take into account both the environmental parameters and the operating conditions of the UAV (season, vegetation cover, temperature of various surfaces, time of day, weather conditions, etc.). The influence of most of these factors on the use of digital technologies for recording game animals has not been fully studied. As a rule, such parameters are considered limitations for recording in accordance with the technical characteristics of the equipment used. The significance of the nature and density of vegetation, the presence of snow cover as a contrast for animal recognition also requires study.

The thermal imaging camera reliably detects any large animal, but it is impossible to establish its appearance based on a thermal image. A regular photo is needed for this. The study confirmed the effectiveness of the combined approach (conventional and thermal imaging). However, only the accumulation of the database of animal identifications during remote monitoring will allow us to formulate the conditions of the algorithm that automatically identifies species. The elimination of these features will make it possible to identify the presence of any animal as fully as possible, to carry out data processing automatically, and, therefore, minimize labor costs.

ACKNOWLEDGEMENTS

This research was funded by the Ministry of Science and Higher Education of the Russian Federation, agreement No. 075-15-2021-694.

REFERENCES

Albery, G.F., Turilli, I., Joseph, M.B., Foley, J., Frere, C.H. and Bansal, S. 2021. From flames to inflammation: How wildfires affect patterns of wildlife disease. Fire Ecol., 17(1): 23-23.

Cayuela, H., Rougemont, Q., Prunier, J.G., Moore, J.-S., Clobert, J., Besnard, A. and Bernatchez, L. 2018. Demographic and genetic approaches to study dispersal in wild animal populations: A methodological review. Mol. Ecol., 27(20): 3976-4010.

de Assis Morais, T., da Rosa, C.A., Viana-Junior, A.B., Santos, A.P., Passamani, M. and de Azevedo, C.S. 2020. The influence of population-control methods and seasonality on the activity pattern of wild boars (Sus scrofa) in high-altitude forests. Mamm. Biol., 100(1): 101 -106.

Department NRE of KR. 2020. Report on the State and Environmental Protection of the Kemerovo Region-Kuzbass in 2019. Administration of the Kemerovo region, Department of Natural Resources and Ecology of the Kemerovo Region, pp. 1-219.

Guo, K., Liu, H., Bao, H., Hu, J., Wang, S., Zhang, W., Zhao, Y. and Jiang, G. 2017. Habitat selection and their interspecific interactions for mammal assemblage in the greater Khingan mountains, northeastern China. Wildlife Biol., 27: 00261-00261.

Ilyashenko, V.B., Luchnikova, E.M., Skalon, N.S., Grebentschikov, I.S. and Kovalevsky, A.V. 2019. Long-term dynamics of small-mammal communities in anthropogenically disturbed territories in the South-East of West Siberia. IOP Conf. Ser. Earth Environ. Sci., 224(1): 012055-012055.

Jones, J.D., Proffitt, K.M., Paterson, J.T., Almberg, E.S., Cunningham, J.A. and Loveless, K.M. 2021. Elk responses to management hunting and hazing. J. Wildl. Manage., 85(8): 721- 1738.

Koetke, L.J., Duarte, A. and Weckerly, F.W. 2020. Elk population dynamics when carrying capacities vary within and among herds. Sci. Rep., 10(11): 15956-15956.

Lavergne S.G., Krebs C.J., Kenney A.J., Boutin S., Murray D., Palme R. and Boonstra R. 2021.The impact of variable predation risk on stress in snowshoe hares over the cycle in North America's boreal forest: Adjusting to change. Oecologia, 197(1): 71-88.

Lemel, J., Truvé, J. and Söderberg, B. 2003. Variation in ranging and activity behavior of European wild boar Sus scrofa in Sweden. Wildlife Biol., 9(Suppl. 1): 29-36.

Peers, M.J.L., Majchrzak, Y.N., Menzies, A.K., Studd, E.K., Bastille-Rousseau, G., Boonstra, R., Humphries, M., Jung, T.S., Kenney, A.J., Krebs, C.J., Murray, D.L. and Boutin, S. 2020. Climate change increases predation risk for a keystone species of the boreal forest. Nat. Clim. Chang., 10(12): 1149-1153.

Prosekov, A., Kuznetsov, A., Rada, A. and Ivanova, S. 2020. Methods for monitoring large terrestrial animals in the wild. Forests, 11(8): 808-808.

Prosekov, A.Y. 2021a. Economic entities of the coal mining industry and wildlife resources: problem statement. J. Phys. Conf. Ser., 1749(1): 012009-012009.

Prosekov, A.Y. 2021b. Coal mining is a factor of environmental risk in the development of the hunting sector in Industrial Regions. J. Phys. Conf. Ser., 2021, 1749(1): 012010-012010.

Safronov, V.M. 2016. Climate change and mammals of Yakutia. Biol. Bull. Russ. Acad. Sci., 43(9): 1256-1270.

Skalon, N., Stepanov, P. and Prosekov, A. 2019. Features of seasonal migrations and wintering of epy elks (Alces alces) in the Kuznetsk-Salair mountain region. IOP Conf. Ser. Earth Environ. Sci., 395(1): 012020-012020.

Thulin, C.G. and Röcklinsberg, H. 2020. Ethical considerations for wildlife reintroductions and rewilding. Front. Vet. Sci., 73: 163-163.

van Beest, F.M., Beumer, L.T., Andersen, A.S., Hansson, S.V. and Schmidt, N.M. 2021. Rapid shifts in Arctic tundra species' distributions and inter-specific range overlap under future climate change. Divers. Distrib., 27(9): 1706-1718.

Van De Walle, J., Pigeon, G., Zedrosser, A., Swenson, J.E. and Pelletier, F. 2018. Hunting regulation favors slow life histories in a large carnivore. Nature Commun., 9(11): 1100-1100.

ORCID DETAILS OF THE AUTHORS

S. Ivanova: https://orcid.org/0000-0002-1252-9572
A. Prosekov: https://orcid.org/0000-0002-5630-3196

Nature Environment and Pollution Technology
An International Quarterly Scientific Journal

p-ISSN: 0972-6268
(Print copies up to 2016)
e-ISSN: 2395-3454

Vol. 23 | No. 1 | pp. 401-408 | 2024

Original Research Paper

https://doi.org/10.46488/NEPT.2024.v23i01.034

Open Access Journal

Machine Learning-based Calibration Approach for Low-cost Air Pollution Sensors MQ-7 and MQ-131

L. R. S. D. Rathnayake*, G. B. Sakura*†, N. A. Weerasekara* and P. D. Sandaruwan**
*Civil and Environmental Department, Faculty of Technology, University of Sri Jayewardenepura, Sri Lanka
**Department of Computer Science, University of Ruhuna, Matara, Sri Lanka
†Corresponding author: G.B. Sakura; sakurabogoda@sjp.ac.lk

Nat. Env. & Poll. Tech.
Website: www.neptjournal.com

Received: 24-12-2022
Revised: 21-02-2023
Accepted: 22-02-2023

Key Words:
IoT
MQ-7
MQ-131
ThingSpeak
Machine learning
Neural network

ABSTRACT

Air quality is a vital concern globally, and Sri Lanka, according to WHO statistics, faces challenges in achieving optimal air quality levels. To address this, we introduced an innovative IoT-based Air Pollution Monitoring (APM) Box. This solution incorporates readily available Commercial Off-The-Shelf (COTS) sensors, specifically MQ-7 and MQ-131, for measuring concentrations of Carbon Monoxide (CO) and Ozone (O3) ,Arduino and "ThingSpeak" platform. Yet, those COTS sensors are not factory-calibrated. Therefore, we implemented machine learning algorithms, including linear regression and deep neural network models, to enhance the accuracy of CO and O3 concentration measurements from these non-calibrated sensors. Our findings indicate promising correlations when dealing with MQ-7 and MQ-131 measurements after removing outliers.

INTRODUCTION

Over time, the Earth's atmosphere has undergone changes, influenced by both natural events and human activities. Unfortunately, these alterations have led to an increase in air pollution, impacting humans and plant life negatively. The concerning shift is gradually making the Earth's atmosphere less conducive to the well-being of both humans and other living organisms (Choudhary & Garg, 2013). Addressing these challenges is crucial for a more optimistic environmental future.

As air pollution is a common problem that affects almost all the countries in the world, continuously measuring air pollutants keeps track of the well-being of the public, animals and plants, etc. Usually, economically well-established countries are concerned with measuring air quality to obtain sustainable goals with highly accurate real-time or conventional air quality monitoring systems. In Sri Lanka, air quality is mostly monitored by the Central Environmental Authority (CEA) and the National Building Research Organization (NBRO) using conventional chemical methods and the Mobile Ambient Air Quality Monitoring Lab (MAAQML).

It is possible to reduce air pollution by studying the changes in the composition of different types of gasses in the air and taking appropriate measurements using conventional air quality measuring equipment (Yi et al. 2015). However, due to their high cost, low and middle-income countries tend to use cost-effective sensors to measure air pollution and implement IoT devices (Yi et al. 2015). The air quality of a particular area can be monitored using sensors (gaseous and meteorological) and Arduino/Raspberry Pi (Malleswari & Mohana 2022). In research works carried out by Bathiya et al. (2016), Dhingra et al. (2019), Kennedy et al. (2018), Malhotra et al. (2020), Perumal et al. (2021), and Poonam et al. (2017), The authors presented recently developed systems to monitor air pollution using Arduino and Wireless Sensor Network (WSN) Technology. Here, we try to use the COTS sensors (Karagulian et al. 2019) in the market to measure the composition of the air accurately.

Si et al. (2020), have evaluated and calibrated low-cost particle sensors in ambient conditions using machine learning algorithms. In 2017, machine learning-based calibration methods have been used for COTS temperature sensors. Non-linear calibration models can be used for those non-linear relations shown between the reference instrument and the sensor (Yamamoto et al. 2017). Research works (Chen et al. 2018, Kumar & Sahu 2021, Okafor et al. 2020, Zimmerman et al. 2018) showcase the recently developed ML calibration approaches for COTS sensors for air quality monitoring.

While the most affordable sensors currently available in the market can measure air composition, they often suffer from quality and accuracy issues. As a result, accurate measurements remain challenging without appropriate calibration. Therefore, we tried to calibrate these sensors using machine learning methods, hoping to provide a cost-effective and easily approachable way to use low-cost sensors in air quality measurements.

MATERIALS AND METHODS

APM box was implemented with COTS sensors (MQ-7, MQ-131, DHT11) and controlling components as per the three-level architecture, such as the application layer, control layer (Arduino), and sensor layer (COTS sensors) (Fig. 2). Block diagram of the overall system is in Fig. 4. Components are mounted in a non-transparent plastic box with PVC pipe arms that includes a fan for enabling airflow from inside to outside (Fig. 1). It was designed to provide consistent airflow similar to the outside of the air quality measuring box. A9G Module was used to implement the GPRS connection using AT commands (Bogdanov & Mitrev 2021). The Real-Time Clock (RTC) module was used to record date and time for the best practice of recording data as the A9G module provides the current time obtained from the telecommunication network, and it is not very reliable due to the failures of the mobile network connection and module resets.

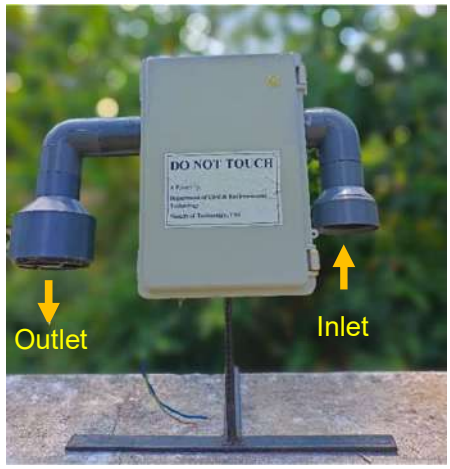

Fig. 1: APM box.

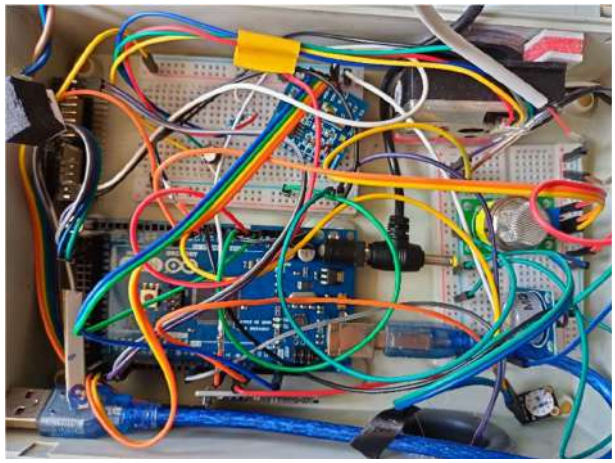

Fig. 2: Prototype of APM box.

Data Acquisition

Data collection was done using an APM box that contains sensors to measure CO, O_3, temperature, and humidity. COTS sensors are MQ-7, MQ-131, and DHT11, respectively. The air quality box was assembled with an Arduino mega microcontroller (Ismailov & Jo`rayev 2022). APM box was co-located with the National Building Research Organizational (NBRO) Automated Mobile Ambient Air Quality Monitoring (MAAQML) System at Colombo Municipal Council (CMC) Sri Lanka in Fig. 3 to record parallel readings. Thus, collected datasets were fed to the machine learning model to calibrate the COTS sensors in the APM box. The data was collected for 3 months approximately.

Data Storing and Transferring

The collected measurements by APM box were uploaded to the "ThingSpeak" (https://thingspeak.com/) databases using a GPRS connection and the IoT device. APM box is utilized to store a backup of the recorded data in case of any emergency, such as communication issues of mobile telecommunication networks.

An Arduino micro SD card module was used to store the backup data. The recorded dataset was sent to

Fig. 3: NBRO MAAQML at Colombo Municipal Council (CMC).

the "ThingSpeak" platform using its Representational State Transfer (REST) based web service using General Packet Radio Service (GPRS) of the (A9G Module) with 5 minutes frequency. This method allowed us to monitor the functionality of the A9G module and also get real-time measurements for the analysis.

Data Visualization and Analysis

"ThingSpeak" provides real-time data visualization using different kinds of graphs and allows users to customize the visualization by supporting plugins with user-defined calculations. It also provides MATLAB support for data analysis. However, we used Google Colaboratory (https://colab.research.google.com/) and conducted the data preprocessing analysis prior to applying ML algorithms.

Data cleaning was performed as the first step to eliminate possible errors once analysis started using Google Co-lab with pandas (https://pandas.pydata.org/) and "NumPy" (https://numpy.org/doc/stable/) library support.

Prediction Methods

Linear regression: Linear regression is a simple machine learning algorithm, and it is important to predict the association of ≥1 independent (predictor) variable with a continuous dependent (outcome) variable (Schober & Vetter 2021).

Simple linear regression: Simple linear regression is performed to determine the association between two quantitative variables. It can be represented as a straight line, as shown in Equation 1.

$$y = mx + c \quad \ldots(1)$$

In this equation, y stands for the outcome variable and x for the predictor. The slope and the interception are denoted by m and c, respectively. In sensor calibration, this method can be used to fit a linear equation to the NBRO measures of the gas and the gas measures of the air quality measuring device that is collected in parallel at the same time.

Multiple linear regression: This regression refers to a regression model that contains multiple independent variables. In sensor calibration, temperature, humidity, and wind flow can be used as multiple predictor variables, as shown in Equation 2.

$$y = m_0\, x_0 + m_1 x_1 + \ldots + m_n x_n + c \quad \ldots(2)$$

Where x_n represents the number of multiple independent variables, and y represents the dependent variable.

In this research work, First, we used the simple linear regression model to identify the correlation between only the NBRO sensor reading and the COTS sensor readings. Next, we used temperature and the COTS sensor readings as independent variables, while the NBRO sensor readings are the dependent variables of a multiple linear regression model.

Feed-forward neural network: A feed-forward neural network is a method of ML that does not have any cycle in the connections between the nodes. As input is only processed in one direction, the feed-forward model is the simplest NN model (Fig. 5). The data may go via a number of hidden nodes, but it always moves forward and never backward.

In this research, first, we designed a feed-forward neural network with an input layer containing one node to represent non-calibrated sensor value. The input layer contained 01 Node and 02 hidden layers, with 64 per layer added next to the input layer. Next, another hidden layer was added with 64 before the output layers that consisted of 01 Node. Each

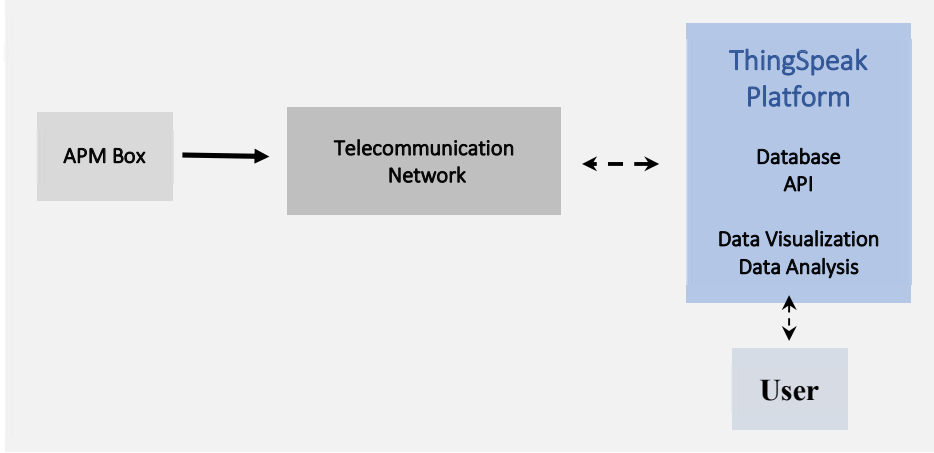

Fig. 4: Block diagram of the system.

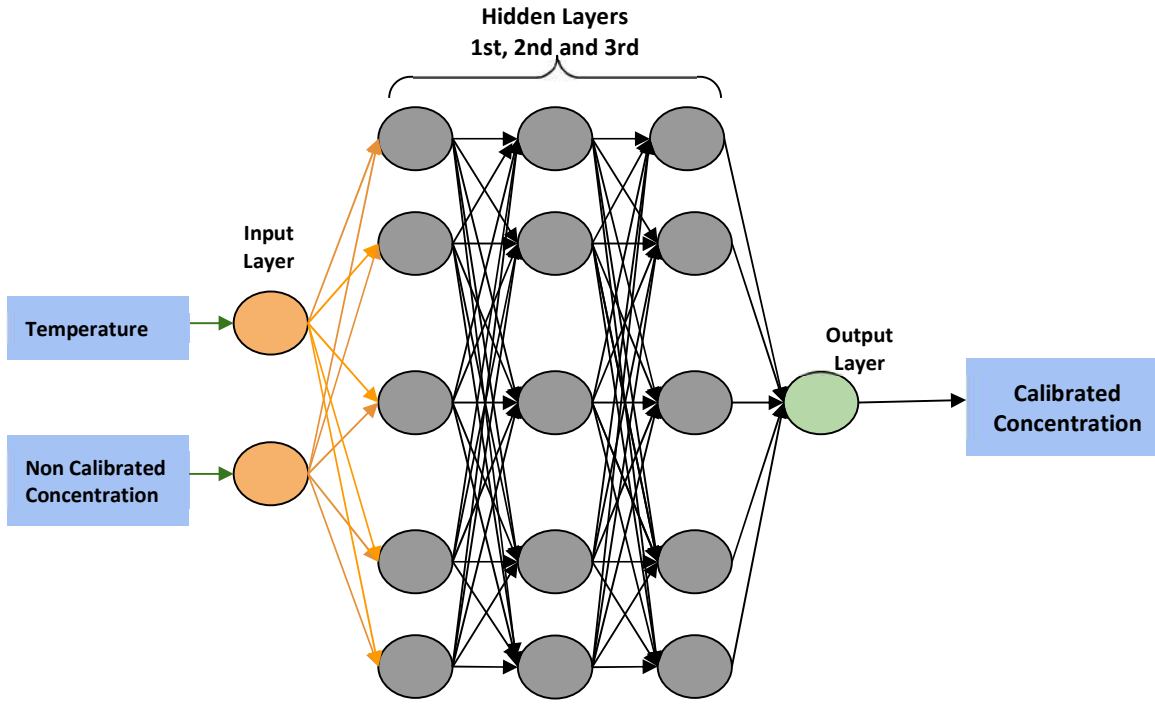

Fig. 5: Illustration of the neural network (NN) layers.

hidden layer has the Rectified Linear Unit ("ReLu") activation as the activation function. Layer weight initializers define the approach for setting the initial random weights of Keras layers. Then, we set the layer initializer as normal to initialize the weights of the hidden layers. Finally, In the output layer, we used the linear function as the activation function, as it needs to get the calibrated concentration as the output value of the NN. There were 8577 total trainable parameters in this model.

As the second approach, we changed the input layer by adding two nodes for the non-calibrated sensor reading and temperature.

RESULTS AND DISCUSSION

The data collection phase was continued for approximately 3 months starting from June 2022, with dynamically parallel to NBRO MAAQML at CMC for CO and O_3 gasses. As these are low-cost, non-factory calibrated COTS sensors, their readings include a higher number of outliers than the amount that can be expected from calibrated higher-accuracy devices. Therefore, we implemented the following procedures before utilizing ML algorithms for readings of the low-cost sensors, specifically the MQ-7 and MQ-131.

First, the measurements were taken at a similar meteorological environment during the same time with all the sensors. Next, we compared the sensor values and selected the sensors that gave the most similar results to build up the APM boxes. This procedure was conducted to identify the malfunctioned sensors before locating them in the field.

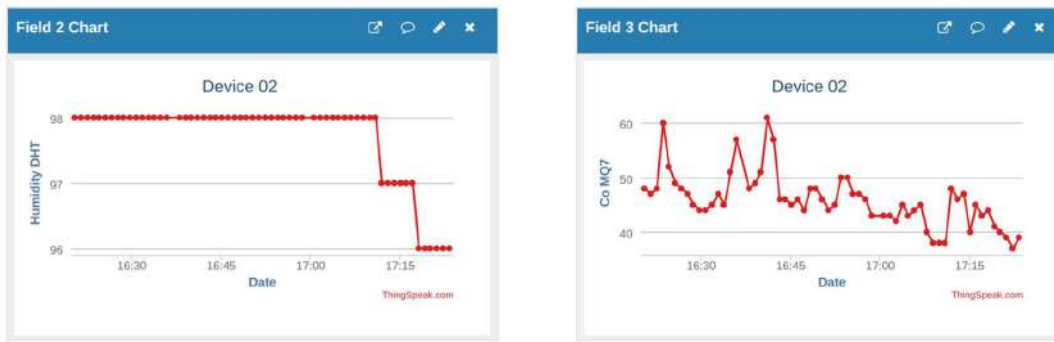

Fig. 6: Real-time data visualization of the "ThingSpeak" platform.

Fig. 6 shows the "ThingSpeak" visualizing the data reading in real time with/without "ThingSpeak" plugins. "ThingSpeak" plugins can be used to set custom functions to visualization that help to compare the analog readings and the values determined by those readings in real-time. After collecting the data, data preprocessing was done, and the datasets were prepared for applying ML algorithms after eliminating the outliers using the IQR method and standard deviation method. The results were evaluated using the Mean Squared Error (MSE) and Coefficient of determination (R-squared value).

MQ Sensors

Usually, low-cost sensors such as MQ-7 and MQ-131 are not accurate enough to use in monitoring pollutant concentrations as they are not factory-calibrated. Here, we have implemented a calibration equation for both MQ-7 and MQ-131 sensors using the direct-taking sensor raw values that had been collected for presenting a calibration method to take accurate CO and O_3 concentrations using ML methods. Fig. 7 shows the generalized circuit for MQ sensors which was used with the Arduino Mega microcontroller.

The following formula, Equation 3 can be used to derive the values of sensor resistance for different gasses using MQ Sensors in modules that use an MOS (Metal Oxide Semiconductor) sensor.

Using V = I x R (Ohm's Law)

$$V_{RL} = [V_C/(R_S + R_L)] \times R_L$$

$$R_S = [(V_C/V_{RL}) - 1] \times R_L \quad \ldots(3)$$

Where, V_C = Circuit Voltage

V_{RL} = Changing Analog Voltage depending on gas Concentration

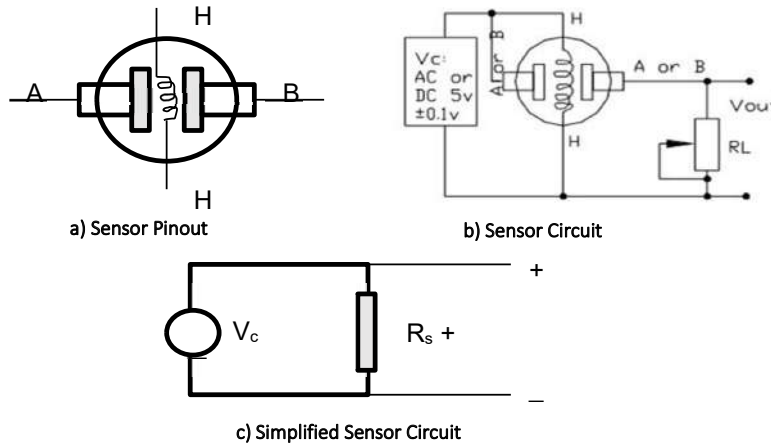

*Rs – resistance of sensor that changes depending on concentration of gas

*R_L – Resistance of sensor at a known concentration without the presence of other gases or fresh air

Fig. 7: Generalized MQ sensor circuit.

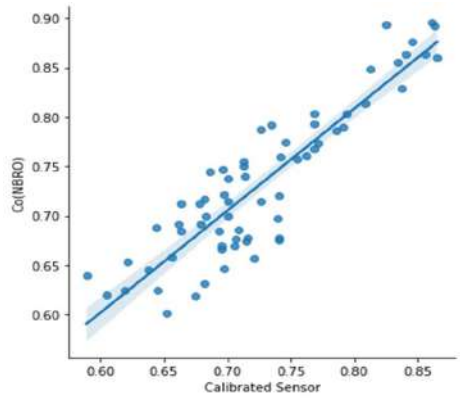

Fig. 8: Simple linear regression model performance-predicted calibrates sensor values Vs NBRO reference data for CO.

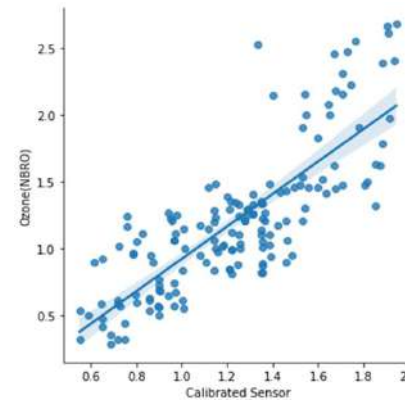

Fig. 9: Multiple linear regression model performance - predicted calibrates sensor values Vs NBRO reference data for CO.

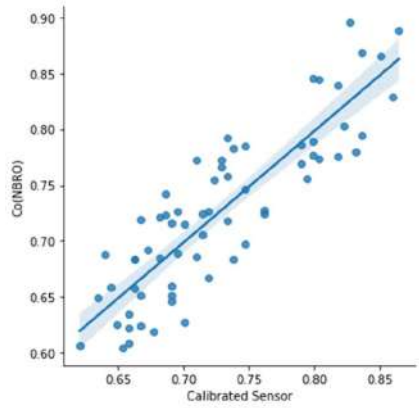

Fig. 10: Simple linear regression model performance - predicted calibrates sensor values Vs NBRO reference data for ozone.

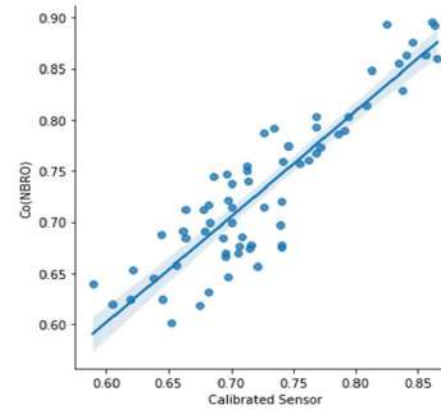

Fig. 11: Multiple linear regression model performance - predicted calibrates sensor values Vs NBRO reference data for ozone.

Gas concentrations and analog voltage generated by sensors are proportionally variate and can be applied to a linear graph to showcase its ideal relation (Karamchandani 2016). Further, it specifies that the analog voltage increases when the gas concentration increases.

Linear Regression on Ozone (O_3) Data

A simple Linear regression method was applied to the Ozone dataset using the "Scikit-Learn" regression functions. The Fig. 8 shows the correlation between the NBRO Ozone data and the MQ-131 sensor data. MSE and R-squared values were 0.105 and 0.59, respectively. Lower MSE shows a lower average squared difference between the MQ-131 readings vs NBRO Ozone sensor data. Mid-level of R-squared shows a considerable correlation between the accurate readings and the low-cost sensor analog reading.

Using the "Scikit-Learn" regression library, a multiple regression model was trained using the particular temperature values along with the non-calibrated sensor readings as independent variables. Fig. 9 shows the result of the test dataset, which provided MSE, MAE, and R-squared values as 0.107, 0.260, and 0.625. Respectively. This shows that a better correlation can be identified when we use independent variables in multiple linear regressions with lower errors.

Linear Regression on Carbon Monoxide (CO) Data

Fig. 10 shows the line obtained from the simple linear regression model using the "Scikit-Learn" library. After fine-tuning the model, the MSE and R-squared values were 0.0012 and 0.80, respectively. This indicates that the average difference between observed and predicted values is much lower and that there is a higher correlation between the MQ-7 readings and the NBRO sensor readings.

Similar to the multiple linear regression model used for Ozone with temperature values, we trained multiple linear regression models for CO readings. As shown in Fig. 11, the model performed well compared to the simple regression model with higher co-relation and fewer errors, as shown in Table 1.

Deep Neural network for both MQ-7 and MQ-131

We trained a deep neural network with an input layer of size 2 for non-calibrated sensor reading and temperature, as deep neural networks can be used for regression problems with multiple input variables. We observed that the deep neural network model performed similarly to the regression models with lower MSE and higher R-squared value, as shown in Table 2 and Fig. 12. We trained to use a lesser number of nodes to avoid the overfitting of the model. After fine-tuning, the trained model was performed on

Table 1: Regression model performance analysis.

Sensor	Independent variables	Coefficients	Intercept	MSE	MAE	R-Squared
MQ-131 (Ozone)	1. Non-Calibrated Sensor value 2. Temperature	1) 0.0356 2) 0.0647	-3.2620	0.1067	0.2596	0.6254
	1. Non-Calibrated Sensor value	1) 0.0393	-1.6626	0.1053	0.2520	0.5895
MQ-7 (Carbon Monoxide)	1. Non-Calibrated Sensor value 2. Temperature	1) 0.0046 2) -0.0019	0.0877	0.0012	0.8010	0.8010
	1. Non-Calibrated Sensor value	1) 0.0047	0.0203	0.0013	0.0314	0.7799

Table 2: Similarities showcased in deep neural network model.

Sensor	The input layer of the model	MSE	MAE	R-Squared
MQ-131 (Ozone)	1. Non-Calibrated Sensor value 2. Temperature	0.1349	0.5265	0.2833
	1. Non-Calibrated Sensor value	0.1493	0.2880	0.4181
MQ-7 (Carbon Monoxide)	1. Non-Calibrated Sensor value 2. Temperature	0.0013	0.0303	0.7858
	1. Non-Calibrated Sensor value	0.0015	0.0321	0.7572

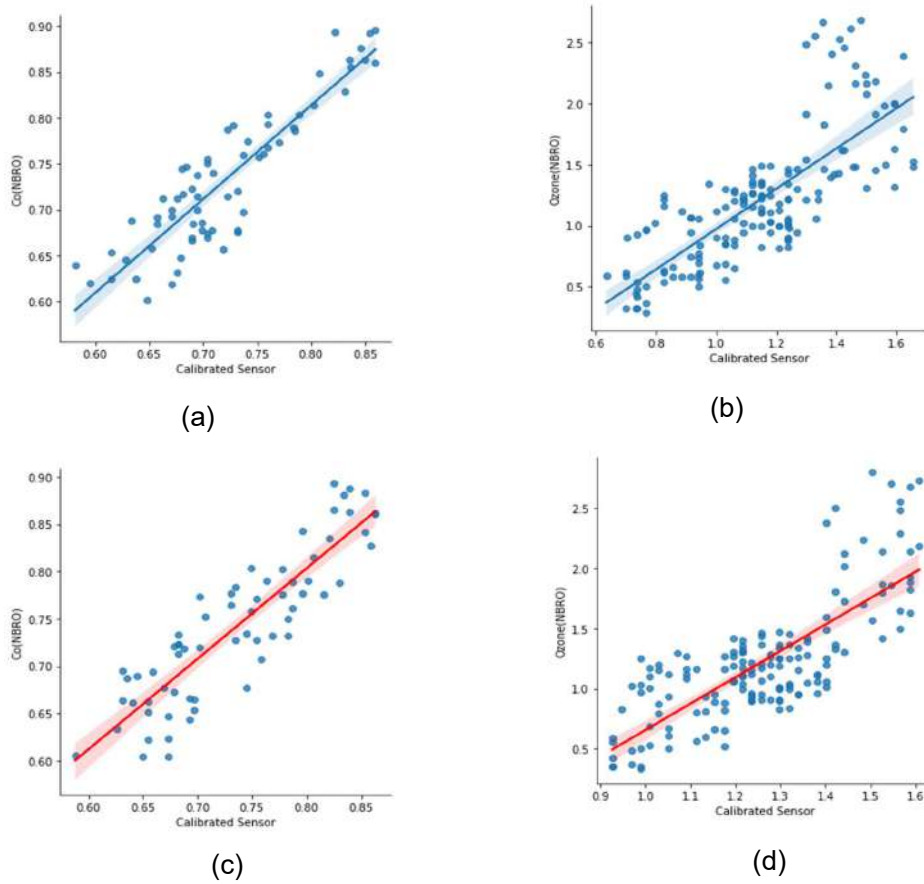

Fig. 12: Neural network (NN) performance analysis.
(a) Calibrated CO sensor values with temperature as inputs vs NBRO reference data.
(b) Calibrated Ozone sensor values with temperature as inputs vs NBRO reference data.
(c) Calibrated CO sensor values Vs NBRO reference data.
(d) Calibrated Ozone sensor values Vs NBRO reference data.

the test datasets of both CO and O_3 datasets separately. The MSE, MAE, and R-squared were calculated by using "Scikit-Learn" library metrics for ML. When there are more input variables, it shows an increase in both ML models.

MQ-7 (CO) sensor readings show a higher correlation between the observed and predicted sensor readings with a lower MSE, indicating a very lower average squared difference of the data. Also, higher R-squared values show the correlation between the sensors.

It is better to have a lesser number of nodes per hidden layer and total trainable parameters with respect to the size of the data set typically (Abiodun et al. 2018). The generalization of this NN is shown as it performed comparatively better for both MQ-7 and MQ-131 senor types with a lesser number of nodes (64) per hidden layer and with lesser total trainable parameters (8577).

CONCLUSION AND FUTURE WORKS

Here, our main goal was to find an ML method for calibrating the low-cost sensors MQ-7 and MQ-131 to monitor air pollution accurately using sensor analog readings. We observed that both simple linear regression and deep neural network models performed better for the calibration. It is more cost-effective than the usual conventional criteria followed using calibration gas. In this research work, we observed that the NN model (64 nodes per layer and 8577 trainable parameters) is more accurate than the linear regression. Also, both ML models performed the calibration better when tested with relevant temperature and sensor analog values. Therefore, this research can be extended using other co-related values such as wind speed, wind direction, and humidity as the input layer variables in the NN model. Also, getting simultaneous readings using a set of similar low-cost non-calibrated sensors in similar environmental conditions instead of getting readings with just one single sensor module is more convenient for monitoring the effects of sensor functionality changes over a longer time period. It would help to increase the reliance and reliability of the ML algorithm for the calibration of that kind of sensor.

ACKNOWLEDGEMENT

This study is supported by the University Research Grant, Faculty of Technology, University of Sri Jayewardenepura, Sri Lanka. (Grant No: ASP/01/RE/FOT/2017/76). And, National Building Research Organization (NBRO), Sri Lanka supported with appropriate certified reference air pollution data.

REFERENCES

Abiodun, O.I., Jantan, A., Omolara, A.E., Dada, K.V., Mohamed, N.A. and Arshad, H. 2018. State-of-the-art in artificial neural network applications: A survey. Heliyon, 4(11): e00938. doi:10.1016/j.heliyon.2018.e00938

Bathiya, B., Srivastava, S. and Mishra, B. 2016. Air Pollution Monitoring Using Wireless Sensor Network. 2016 IEEE International WIE Conference on Electrical and Computer Engineering (WIECON-ECE), 19-21 December 2016, Pune, Maharashtra, India, IEEE, Piscataway, NJ, pp. 1821-1829.

Bogdanov, L. and Mitrev, H. 2021. Flash Programming Microcontrollers Over the GSM Network. 2021 International Conference on Software, Telecommunications, and Computer Networks (SoftCOM), 23-25 September 2021, Hvar, Croatia, IEEE, NJ, pp. 541-551.

Chen, C.C., Kuo, C.T., Chen, S.Y., Lin, H., Chue, J.J., Hsieh, Y.J. and Huang, C.M. 2018. Calibration of Low-Cost Particle Sensors By Using the Machine-Learning Method. IEEE Asia Pacific Conference on Circuits and Systems (APCCAS), 26-30 Oct. 2018, Shangri La, Chengdu, China, IEEE, NJ, pp. 111-114.

Choudhary, D.M. and Garg, V. 2013. Causes, Consequences, and Control of Air Pollution. Springer, Cham.

Dhingra, S., Madda, R.B., Gandomi, A.H., Patan, R. and Daneshmand, M. 2019. Internet of Things mobile–air pollution monitoring system (IoT-Mobair). IEEE Inter. Things J., 6(3): 5577-5584. doi:10.1109/JIOT.2019.2903821

Ismailov, A. and Jo`rayev, Z. 2022. Study of Arduino microcontroller board. Sci. Edu. J., 3(3): 61.

Karagulian, F., Barbiere, M., Kotsev, A., Spinelle, L., Gerboles, M., Lagler, F. and Borowiak, A. 2019. Review of the performance of low-cost sensors for air quality monitoring. Atmosphere, 10(9): 506.

Karamchandani, S. 2016. Pervasive Monitoring of Carbon Monoxide And Methane Using Air Quality Prediction. 2016 3rd International Conference on Computing for Sustainable Global Development (INDIACom), 16-18 March 2016, New Delhi, India, IEEE, NY, pp. 3803-3807.

Kennedy, O., Etinosa, N., Odusami, M., Samuel, J. and Oluga, O. 2018. A smart air pollution monitoring system. Int. J. Civ. Eng. Technol., 9(9): 799-809.

Kumar, V. and Sahu, M. 2021. Evaluation of nine machine learning regression algorithms for calibration of low-cost PM2.5 sensor. J. Aerosol Sci., 157: 105809. doi:https://doi.org/10.1016/j.jaerosci.2021.105809

Malhotra, M., Aulakh, I.K., Kaur, N. and Aulakh, N.S. 2020. Air Pollution Monitoring Through Arduino Uno. ICT Systems and Sustainability, Singapore.

Malleswari, S.M.S.D. and Mohana, T.K. 2022. Air pollution monitoring system using IoT devices: A review. Mater. Today Proceed., 51: 1147-1150. doi:https://doi.org/10.1016/j.matpr.2021.07.114

NBROS. n.d. Strengthen the Air Quality Monitoring Capacity of NBRO with Automated Mobile Ambient Air Quality Monitoring System. National Building Research Organization, Ministry of Defence, Sri Lanka.

Okafor, N.U., Alghorani, Y. and Delaney, D.T. 2020. Improving data quality of low-cost IoT sensors in environmental monitoring networks using data fusion and machine Learn. Appr. ICT Expr., 6(3): 220-228. doi:https://doi.org/10.1016/j.icte.2020.06.004

Perumal, B., Deny, J., Alekhya, K., Maneesha, V. and Vaishnavi, M. 2021. Air Pollution Monitoring System by using Arduino IDE. Paper Presented at the 2021 Second International Conference on Electronics and Sustainable Communication Systems (ICESC), 4-6 August 2021, Coimbatore, Tamil Nadu, Hindustan Institute of Technology, Coimbatore, pp. 797-802.

Poonam, P., Ritik, G., Sanjana, T. and Ashutosh, S. 2017. IoT-based air pollution monitoring system using Arduino. IRJET, 4(10): 515-526.

Schober, P. and Vetter, T.R. 2021. Linear regression in medical research. Anesth Analg., 132(1): 108-109. doi:10.1213/ane.0000000000005206

Si, M., Xiong, Y., Du, S. and Du, K. 2020. Evaluation and calibration of a low-cost particle sensor in ambient conditions using machine-learning methods. Atmos. Meas. Tech., 13(4): 1693-1707. doi:10.5194/amt-13-1693-2020

Yamamoto, K., Togami, T., Yamaguchi, N. and Ninomiya, S. 2017. Machine learning-based calibration of low-cost air temperature sensors using environmental data. Sensors, 17(6): 1290.

Yi, W.Y., Lo, K.M., Mak, T., Leung, K.S., Leung, Y. and Meng, M.L. 2015. A survey of wireless sensor network-based air pollution monitoring systems. Sensors, 15(12): 31392-31427.

Zimmerman, N., Presto, A.A., Kumar, S.P.N., Gu, J., Hauryliuk, A., Robinson, E.S. and Subramanian, R. 2018. A machine learning calibration model using random forests to improve sensor performance for lower-cost air quality monitoring. Atmos. Meas. Tech., 11(1): 291-313. doi:10.5194/amt-11-291-2018.

ORCID DETAILS OF THE AUTHORS

L. R. S. D. Rathnayake: https://orcid.org/0000-0002-7405-7785
G. B. Sakura: https://orcid.org/0000-0003-0533-9380
N. A. Weerasekara: https://orcid.org/0000-0001-6809-8778
P. D. Sandaruwan: https://orcid.org/0009-0007-4819-8684

Nature Environment and Pollution Technology
An International Quarterly Scientific Journal

p-ISSN: 0972-6268
(Print copies up to 2016)
e-ISSN: 2395-3454

Vol. 23 | No. 1 | pp. 409-417 | 2024

Original Research Paper

https://doi.org/10.46488/NEPT.2024.v23i01.035

Open Access Journal

Sustainability Analysis of Landfill Cover System Constructed Using Recycled Waste Materials by Life Cycle Assessment

G. Sanoop, Sobha Cyrus and G. Madhu†
School of Engineering, Cochin University of Science and Technology, Kochi, Kerala, India
†Corresponding author: G. Madhu; profmadhugopal@gmail.com

Nat. Env. & Poll. Tech.
Website: www.neptjournal.com

Received: 17-07-2023
Revised: 06-09-2023
Accepted: 22-09-2023

Key Words:
Life cycle assessment
Landfill cover system
Waste foundry sand
Waste materials

ABSTRACT

The sustainability of using industrial by-products for the construction of landfill cover was determined using Life Cycle Assessment (LCA). LCA was carried out on four materials: sand- bentonite mix, red earth- bentonite mix (amended soil), Waste Foundry Sand (WFS)-Bentonite mix, and WFS- marine clay mix. The former two are commonly used cover soils and the latter two are alternative materials proposed. Environmental impacts based on the extraction of resources, processing, transportation to the site, and site preparation were considered using the 'cradle to site' approach. Analysis was carried out in OpenLCA software using the ReCiPe (H) Midpoint method of impact assessment. Required data for analysis was taken from the Ecoinvent database supplemented with inputs from a field survey. The use of WFS in landfill cover systems was found to be sustainable using LCA studies when compared to conventional materials.

INTRODUCTION

Waste management lags behind the advancements in other fields of technology in developing countries. This, coupled with rapid and unplanned urbanization, consumerism, and industrial production, the pressure mounts on existing systems. In recent times, methods such as incinerating, composting, and recycling have been dominating research space and academia, but landfilling remains the most favored solid waste disposal method globally (Nanda & Berruti 2021, Avarand 2023). An engineered landfill effectively isolates the waste from its surroundings and ensures its safety from failure in the future. The composite-engineered layer employed for this is known as a cover system (Ujaczki et al. 2016).

Although landfill cover is widely discussed as a single unit, it is a complex multi-layered engineering construction, with each sublayer complying with specific requirements in terms of functionality, material composition, and engineering properties (Charles et al. 2019). A typical multi-layered cover system, as shown in Fig. 1, has a gas collection layer, barrier layer, drainage layer, and top soil, with each layer separated by specific geosynthetics. The most important layer in terms of functionality is the barrier layer, which prevents the ingression of fluids from outside the landfill as well as the escape of fluids (gas and liquids) from the landfill (Yamsani et al. 2016). Other layers effectively protect the barrier layer from operational damage and aid the latter in isolating disposed waste and its derivatives. In this investigation barrier layer is considered for sustainability analysis as the other layers remain the same in all the cases considered.

Materials selected for the construction of the barrier layer should satisfy the requirements specified by the Environmental Protection Agency (EPA), the most important of which is that hydraulic conductivity should not exceed 10^{-9} $m.s^{-1}$. Traditionally, sand-bentonite mixtures are commonly used for barrier construction due to their superior performance in terms of hydraulic conductivity and strength. However, the unavailability and high cost of sand inhibit it from being used in landfill construction, but it is still considered a reference material for the barrier layer. Locally available lateritic soil mixed with bentonite clay (to reduce hydraulic conductivity to 10^{-9} $m.s^{-1}$) is a widely used, inexpensive alternative to sand bentonite mix, commonly known as amended soils.

Alternatives to sand bentonite mixture and amended soils using industrial by-products are discussed in this paper. Waste Foundry Sand (WFS) is a by-product of metal casting industries. After several repeated cycles of using and reusing, foundry sand eventually ends up as a waste material with limited use in concrete and pavement construction (Siddique & Singh 2011). With over 60 million tonnes of WFS produced worldwide annually (Sandhu & Siddique

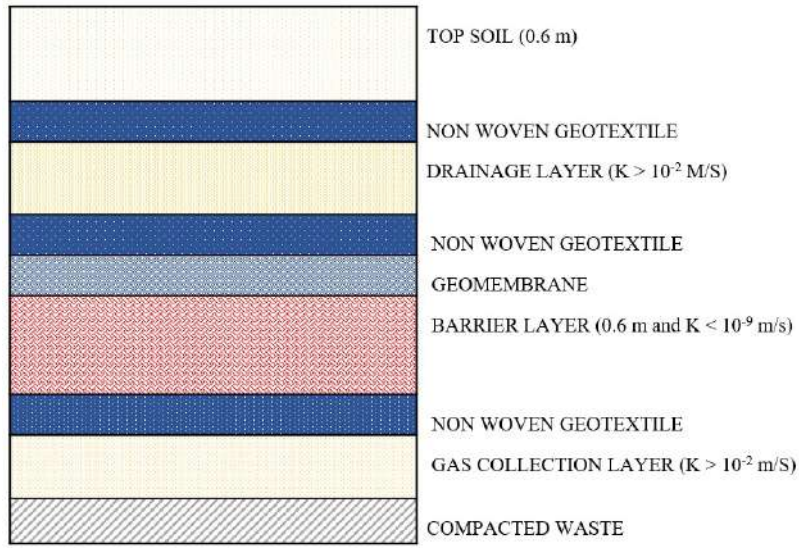

Fig. 1: Typical cross-section of Landfill cover system.

2022), there would be a continuous supply of WFS. WFS does not readily satisfy EPA norms and has to be modified with suitable clay. Bentonite, which is a commonly used clay for barrier soil, and marine clay, which is a naturally occurring clay, is selected for this amendment. Marine clay is a by-product of pile-driving operations in coastal regions. Due to their mineralogical structure, they cannot be used in kilns and hence have limited applications. The use of waste foundry sand and marine clay as landfill cover materials has several benefits, including reducing the need for virgin materials, conserving natural resources, and reducing the amount of waste generated.

Recycling and reusing waste materials for construction purposes promotes resource recovery and thereby contributes to sustainability. However, the allied and dependent processes involved in the same may have greater invisible environmental implications due to the consumption of resources and energy as well as emissions (Cirrincione et al. 2022). Hence, sustainability assessment is very important when a new system or production procedure is proposed. Life Cycle Assessment (LCA) is a method used to qualify, quantify, and evaluate impacts associated with connected processes and product systems. The type and level of impact of each product system can be evaluated, and solutions can be proposed to mitigate negative impacts. The United Nations Organization has stipulated several goals for sustainable development to ensure that the benefits of development are not limited to economic indicators (United Nations 2015).

The broader objective of this study is to ensure sustainability in infrastructure development and waste disposal. The compliance of alternate landfill cover materials with these goals is essential to ascertain the sustainability of the former. The paper aims to assess the sustainability of using WFS and marine clay in the construction of landfill cover systems in comparison with commonly used construction materials for the same.

MATERIALS AND METHODS

Four combinations of soils for barrier construction are considered in this paper, namely sand-bentonite mix, amended soil (red earth-bentonite mix), WFS-bentonite mix, and WFS-marine clay mix. Hence, the basic materials considered for this study were Bentonite, Marine Clay, Red Earth, Waste Foundry Sand, and River Sand. The sand-bentonite mixture is a commonly used reference material for the barrier layer, and the combination used was sand mixed with 20% bentonite, as in available literature (Sivapullaiah et al. 2000, Komine & Ogata 1999).

WFS was collected from the industrial area in Kochi, Kerala, India, and marine clay was collected from a piling site near Kochi coast, from a depth of 8-10 m. Red earth was collected from the locality of Uyogamandal Industrial area, Kochi where an operational engineered landfill exists. Commercially available bentonite was purchased, which was sourced from the North-Western part of India, approximately 1400 km from the site considered. Whereas WFS, red earth, and marine clay were available within a 30 km radius.

Laboratory tests were conducted to check the suitability of using RE- RE-bentonite mix, WFS-bentonite mix, and WFS-marine clay mix as cover materials as per specifications. The test results are shown in Table 1. From these results, the

Table 1: Geotechnical properties of soil mixes used for landfill cover.

Combination	γ_{dmax} [kN.m^{-3}]	OMC [%]	Liquid Limit [%]	Plasticity Index [%]	Corrected Activity Parameter, A_c	Hydraulic Conductivity [m.s^{-1}]	Volumetric Shrinkage [%]	Free Swell Ratio
WFS	17.66	11.70	-	-	-	2.21×10^{-06}	0	1.30
WFS + 5% B	17.80	13.27	41	19	3.29	2.36×10^{-10}	1.31	2.54
WFS + 10% B	17.95	13.68	52	22	2.19	1.08×10^{-11}	2.44	3.88
WFS + 15% B	17.46	14.59	64	30	2.09	3.57×10^{-11}	3.03	4.66
WFS + 20% B	17.01	16.9	67	32	1.72	1.95×10^{-11}	6.11	5.80
RE	17.63	18.00	51	22	1.29	3.24×10^{-08}	1.24	1.11
RE + 3% B	16.69	20.52	55	23	1.20	9.02×10^{-10}	3.07	1.75
RE + 6% B	16.51	21.13	60	26	1.23	8.22×10^{-11}	3.91	1.90
RE + 9% B	15.9	21.86	62	27	1.16	5.61×10^{-11}	6.76	2.12
RE + 12% B	15.49	23.07	67	30	1.18	3.76×10^{-11}	10.90	2.18
WFS + 25% MC	17.83	14.6	19	9	0.65	5.02×10^{-08}	3.97	1.34
WFS + 33% MC	17.46	16.2	23	8	0.45	7.19×10^{-10}	3.93	1.40
WFS + 50% MC	17.17	17.5	29	12	0.46	8.88×10^{-11}	1.93	1.43
MC	14.52	24.00	68	40	0.78	7.00×10^{-11}	16.51	1.50

optimum mixes of soils selected were RE + 6% bentonite, WFS + 10% bentonite, and WFS + 50% marine clay.

Life Cycle Assessment (LCA) method was used for the assessment and comparison of sustainability associated with different materials used in landfill cover construction (ISO 14040 2006, ISO 14044 2006). In simple terms, LCA involves a comparative study based on the functionality of product systems, even though they are made of entirely different materials. Hence, a 'functional unit' is the basic analysis unit (Anh et al. 2022). The sustainability of the Life Cycle Assessment is carried out in a four-stage framework, which includes goal and scope definition, inventory analysis, life cycle impact assessment, and interpretation.

Goal and Scope

The paper covers the utilization of LCA to calculate and analyze the environmental impacts of landfill cover construction using conventional materials and recycled materials with respect to Kochi, India. The functional unit selected for the analysis was 1 acre of landfill cover with a thickness of 0.6 m.

System Boundary

'Cradle to site' approach, which includes material extraction, transportation to site, and site installation, as depicted in Fig. 2. For WFS and marine clay, material extraction was not considered since they are waste materials, and only transportation to site and site installation was considered.

Inventory Analysis

LCA is heavily dependent on the data used for analysis, and it is a laborious process. Ecoinvent database is a global database for materials, energy flows, and emissions and provides data on the environmental impacts of various processes and products. Most data were taken from the Ecoinvent database. Still, some modifications were made

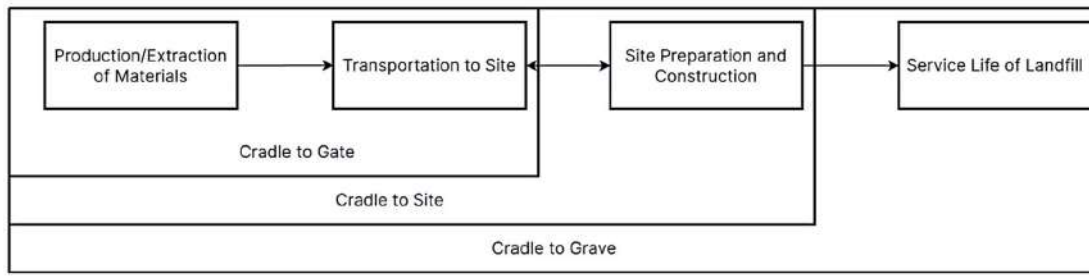

Fig. 2: System Boundary Definition: Cradle to Site.

Table 2: Field data for unit processes (from questionnaire survey).

Unit Process	Rate of Work	Fuel Efficiency
Tipper (Brand – Daimler)	16 m^3 soil per load	2 $km.l^{-1}$ (full load)
Road Roller	2 $km.h^{-1}$	5 $L.h^{-1}$
Excavator	15 $m^3.h^{-1}$	6 $L.h^{-1}$
Soil laying	20 min per tipper load	-
Crusher	150 $t.h^{-1}$	25 $L.h^{-1}$

to suit the data in the Indian context since the database is largely based on data from Europe and the Americas. Table 2 shows the unit processes that were modified based on a questionnaire survey in construction sites. A distance of 30 km was fixed for the transport of materials except bentonite. All vehicles were assumed to be complying with BS-IV emission standards. Also, the emissions rates of modified unit processes were calculated on permitted emissions from diesel vehicles as per BS-IV regulations (The Gazette of India 2015).

Life Cycle Impact Assessment

The calculation of the environmental impacts of the landfill cover system was carried out using an impact assessment method called ReCiPe (H) Midpoint method (also known as the CML 2001 method). The production of bentonite involves the quarrying of clay, refining, packaging, and transportation. River sand production involves the use of dredging equipment, motor boats, and transportation. Red earth is excavated using excavators and transported to the site. The production process of WFS and marine clay was not considered since they are byproducts from another industry. However, transportation of the same using diesel lorries was considered. The results of the assessment are presented as environmental impact categories. The impact categories relevant to the study (with > 1% value) are shown in Table 3.

Table 3: Impact categories relevant to the study.

Impact category	Reference unit
Climate change	kg CO2-Eq
Marine Eutrophication	kg N-Eq
Particulate Matter Formation	kg PM10-Eq
Photochemical Oxidant Formation	kg NMVOC
Terrestrial Acidification	kg SO2-Eq

RESULTS AND DISCUSSION

Fig. 3 shows the values of emissions corresponding to carbon dioxide, carbon monoxide, unburned hydrocarbons, nitrogen oxides, particulate matter, and sulfur dioxide. Here, the sand-bentonite mix is considered as base mix, and the results are presented in comparison with the same. In all parameters evaluated, emissions to the atmosphere and values of impact categories were found to be maximum for sand-bentonite mix, followed by RE-bentonite mix, WFS-bentonite mix, and WFS-marine clay mix, respectively.

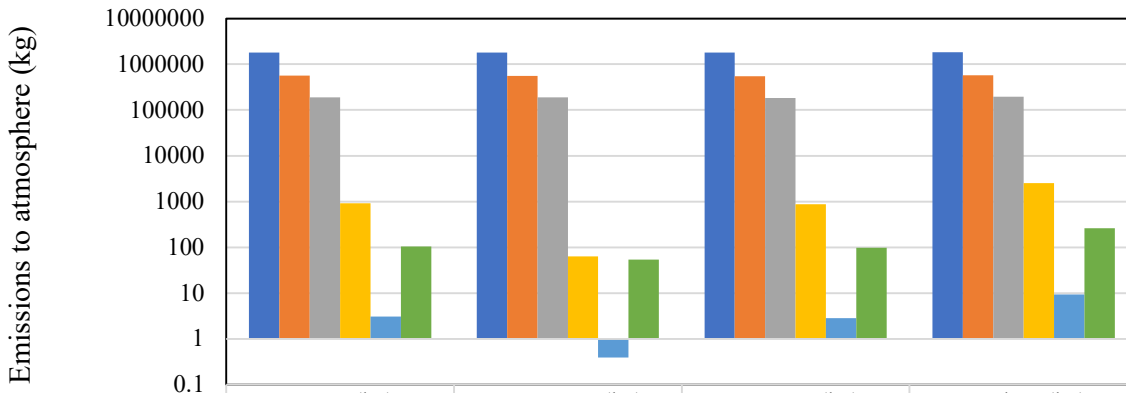

	RE+B (kg)	WFS+MC (kg)	WFS+B (kg)	Sand+B (kg)
Carbon dioxide	1791470	1777537.5	1789678.53	1837506
Carbon monoxide	561807.5	557554.375	550571.35	575481
Hydrocarbons	190744.25	189068.75	185021.9225	195867.6
Nitrogen oxides	922.0736	63.3986	866.749184	2532.7736
Particulates	3.0871	0.3896	2.840132	9.2576
Sulfur dioxide	104.219	53.669	97.96586	264.524

Fig. 3: Emissions from various soil mixes considered during their life cycle.

The life cycle of sand bentonite mix accounts for the production and transportation of sand from the river bed, along with the processes associated with bentonite production and transportation. Hence the maximum values of emission are associated with sand-bondonite mix. Excavation of red earth involves less machinery and fuel compared to sand mining and thus, its emissions are lesser than sand bentonite mix but greater than WFS-bentonite mix. This is due to the fact that the back process of WFS production is not accounted for. WFS-marine clay mix has the least emission values since both WFS and marine clay are byproducts, and the impact of their production was not considered.

Fig. 4 shows the reduction in emissions for RE-bentonite mix, WFS-bentonite mix, and WFS-marine clay mix with respect to sand-bentonite mix. The production of WFS was not considered for assessment since it is a waste product but quarrying operation involving machinery and humans is considered for red earth. RE-bentonite mix and WFS-bentonite mix show a similar range in reduction of emissions even though the impact of transportation of WFS is smaller than that of the multi-stage production and transportation of red earth. This trend indicates the high impact of bentonite in the product system in terms of emissions. It is more evident from the emission values of the WFS- marine clay mix, which has a remarkable 30% less emissions compared to the WFS-marine clay mix. Additionally, the reduction in greenhouse emissions is of lower magnitude compared to NO_x, SO_2, and particulates. This could be attributed to the fact that electricity production in India is predominantly using coal energy (Tiewsoh et al. 2019) and bentonite production consumes a high amount of electricity.

The total energy consumption for each soil mix is shown

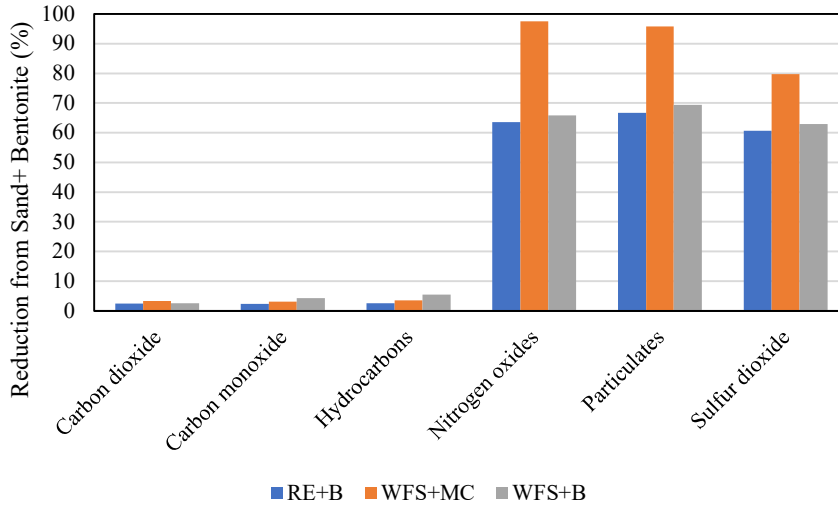

Fig. 4: Reduction in emission values compared to sand-bentonite mix.

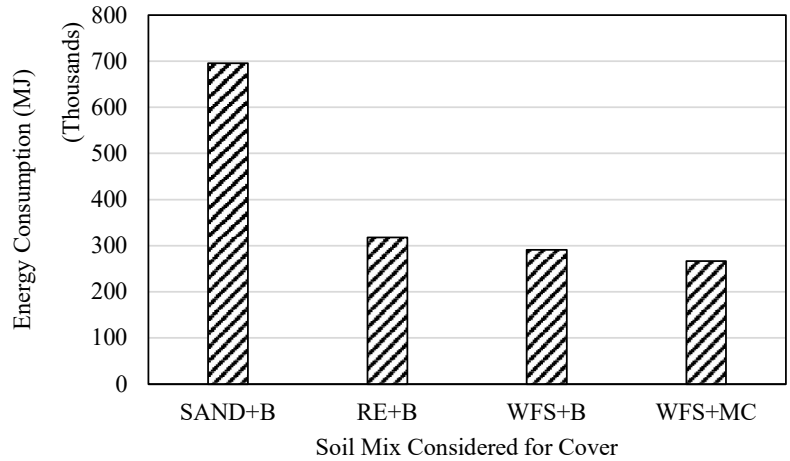

Fig. 5: Energy consumption for soil mixes considered.

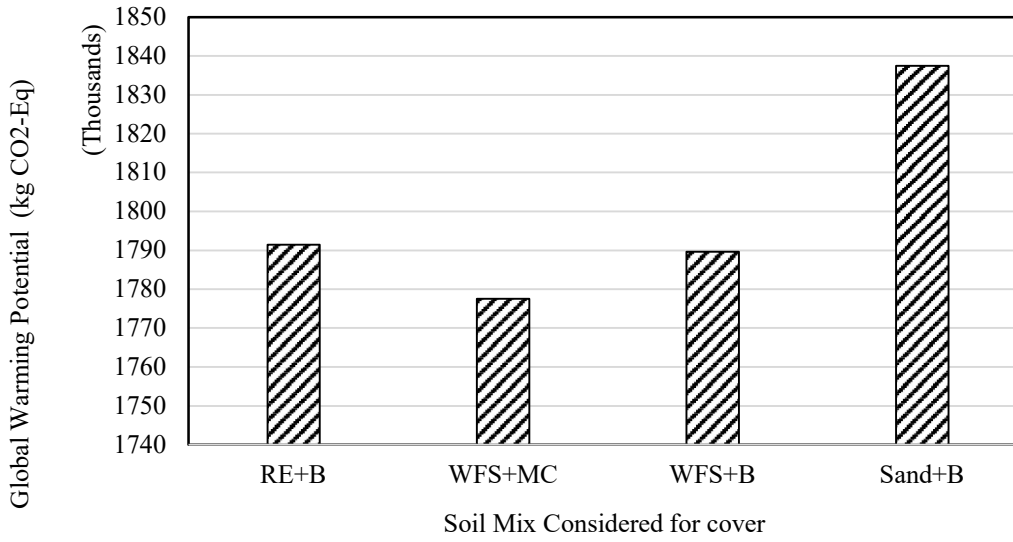

Fig. 6 a: Global warming potential for soil mixes considered.

in Fig. 5. The production of sand-bentonite mix consumes more than two times the energy when compared with all other mixes. River sand mining involves marine equipment and boats which consume higher quantities of fuel and work at a slower pace compared to land types of equipment. This increases the embedded energy associated with river sand considerably. The variation in energy consumption of the other three mixes is in the range of 10%. This modest difference is because diesel consumption for transportation is considerably higher than other energy requirements. Additionally, the WFS+ marine clay mix, which ought to have significantly lower energy consumption, also exhibited only a 10% reduction compared to the WFS+ bentonite mix. The laying of marine clay at the site takes more time compared to other soils, which results in higher fuel consumption.

Figs. 6a to 6e show the variation of impact parameters for soil mixes. Parameters with significant (>1%) contributions are Global Warming Potential (GWP), Marine Eutrophication, Particulate Matter Formation, Photochemical Oxidant Formation, and Terrestrial acidification. Impact parameters are dependent on the indicators represented in Fig. 3. Carbon dioxide and methane in the form of unburned hydrocarbons from diesel exhaust are the prominent greenhouse gases contributing to global warming potential. Among them, methane has 28 times more global warming potential compared to carbon dioxide (Ou et al. 2022). In agreement with the emission values of greenhouse gases and energy consumption, the sand-bentonite mix has the highest contribution to the global warming potential, and the remaining mixes vary by a narrow margin.

Marine eutrophication and photochemical oxidant formation are caused by the release of oxides of Nitrogen (NO_x). Dissolution of NO_x in water bodies may cause eutrophication, which leads to oxygen deficiency in water bodies (Zhou et al. 2019). This leads to the depletion of aquatic life and reduces the self-cleansing capacity of water bodies. Sunlight-sensitive oxides of nitrogen form photochemical oxidants that affect the respiratory system of terrestrial beings and deplete vegetation (Weitekamp et al. 2020). It is evident from Fig. 6b and 6c that reduction in these parameters is remarkably high when substituting sand with WFS and bentonite with marine clay.

Particulate matter or suspended solid particles are released into the atmosphere by diesel exhaust from automobiles and coal-based thermal power plants. Hence, they are directly correlated to the combustion of diesel and coal. River sand mining is found to be the largest contributor to particulate matter formation. Fig. 6d shows that the sand-bentonite mix produces three times the particulate matter compared to the WFS-bentonite mix and RE-bentonite mix.

Terrestrial acidification is caused by SO_2 gas released during the combustion of fossil fuels, which gets dissolved in water to form sulphuric acid. The combustion of coal releases a greater quantity of SO_2 into the atmosphere compared to diesel exhausts (Bhanarkar et al. 2005). It is evident from Fig. 6 e that terrestrial acidification is comparable for all three combinations using bentonite and appreciably less for WFS-marine clay mix, which could be due to the higher electricity consumption associated with bentonite production.

The different impact categories of life cycle assessment show that the WFS- bentonite and WFS- marine clay mixes used for landfill cover construction have an outstandingly low impact with respect to every indicator considered. These mixes also exhibit much lower LCI compared to sand-

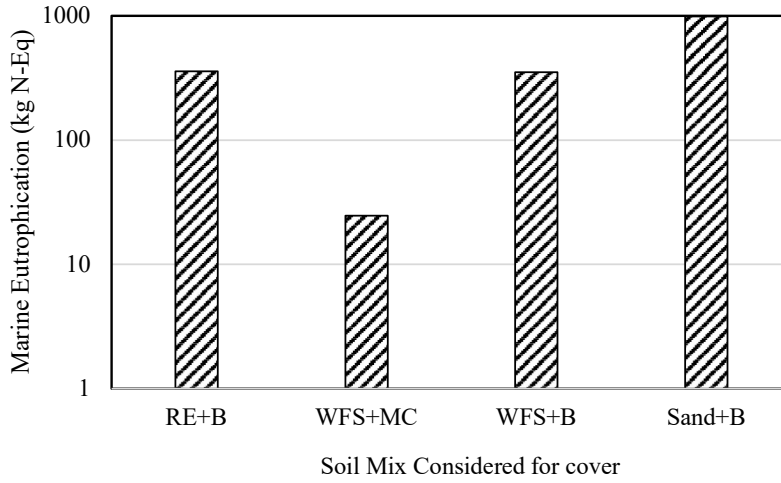

Fig. 6 b: Marine Eutrophication for soil mixes considered.

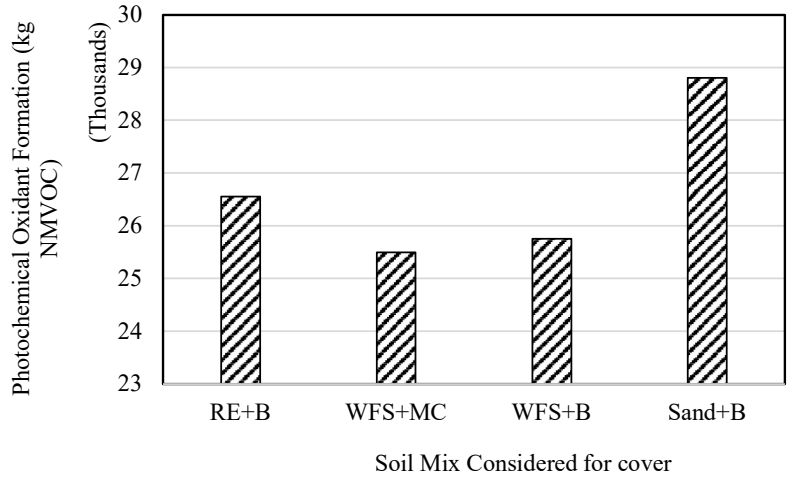

Fig. 6 c: Photochemical oxidant formation for soil mixes considered.

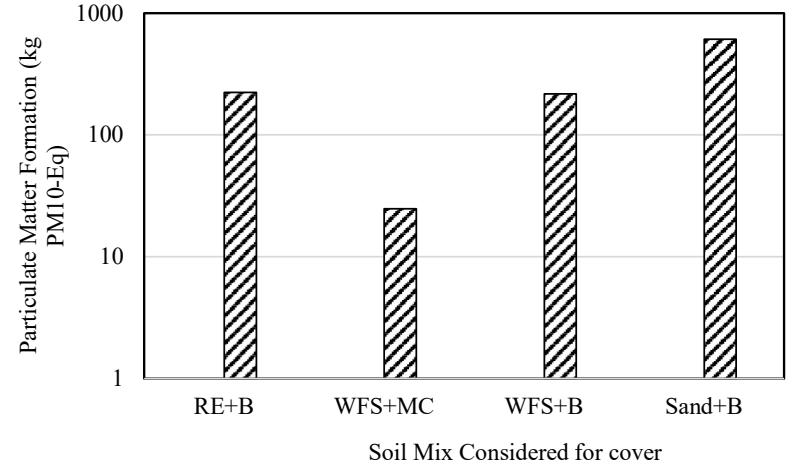

Fig. 6 d: Particulate matter formation for soil mixes considered.

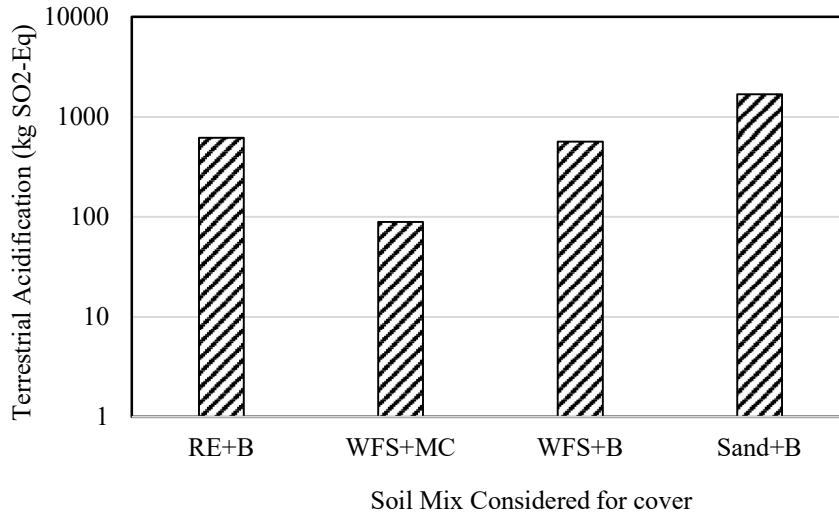

Fig. 6 e: Terrestrial Acidification for soil mixes considered.

bentonite mixes. However, the emission and impact values of WFS-bentonite were similar to those of the red-earth bentonite mix. Hence, both WFS-bentonite and WFS-marine clay mixes may be recommended as sustainable alternatives to landfill cover soil, with the latter proving to be most sustainable with respect to LCA.

The proposed use of industrial by-products like waste foundry sand (WFS) and waste marine clay from the piling industry satisfies criteria SDG-6, SDG-8, SDG-9, SDG-11, SDG-12, SDG-13, SDG-14 and SDG-15 of the UN sustainable development goals. Fulfillment of criteria like clean water and sanitation, climate action, life below water, and life on land was directly attained in the analysis results discussed. Responsible consumption and production are achieved when a waste material is reused as a construction material and further depletion of resources is curtailed. By scaling this concept to industry, innovation and infrastructure development can be achieved. With contribution to waste management and urban growth, possibilities for decent work and economic growth are facilitated and thus lead to sustainable cities and communities.

CONCLUSIONS

The sustainability of replacing sand-bentonite mix and red-earth bentonite mix with industrial by-products such as waste foundry sand and marine clay in landfill cover construction was assessed using Life Cycle Assessment. The following conclusions have been drawn from the study.

- WFS mixed with 10% bentonite and WFS mixed with 50% marine clay were found to be suitable replacements for sand-bentonite and red earth-bentonite mixes.
- WFS- marine clay mix was found to be the most sustainable, with a 60% to 90% reduction in emission values compared to other soil mixes.
- The sustainability of WFS-bentonite was compared to RE- RE-bentonite mix with a 2% to 6% reduction in emission values from the latter. This indicates that bentonite production and transportation are having more impact on the unit processes considered.
- Sand-bentonite mix was found to have 90% more emission compared to WFS-marine clay and 60% compared to WFS-bentonite and RE-bentonite.

REFERENCES

Anh, L.H., Thanh, N.T., Thao, P.T.M. and Schneider, P. 2022. Life cycle assessment of substitutive building materials for landfill capping systems in Vietnam. Appl. Sci., 12(6): 3063. https://doi.org/10.3390/app12063063

Avarand, N., Bora, K.M. and Tavakoli, B. 2023. Life Cycle Assessment of urban waste management in Rasht, Iran. Integr. Environ. Assess. Manag., 11: 475 https://doi.org/10.1002/ieam.4751

Bhanarkar, A.D., Rao, P.S., Gajghate, D.G. and Nema, P. 2005. Inventory of SO2, PM and toxic metals emissions from industrial sources in Greater Mumbai, India. Atmos. Environ., 39(21): 3851-3864. https://doi.org/10.1016/j.atmosenv.2005.02.052

Charles W.W. Ng, R. Chen, J.L. Coo, J. Liu, J.J. Ni, Y.M. Chen, L.T., Zhan, H.W. and Guo, B.W. 2019. A novel vegetated three-layer landfill cover system using recycled construction wastes without geomembrane. Can. Geotech. J., 56(12): 1863-1875. https://doi.org/10.1139/cgj-2017-0728

Cirrincione, L., La Gennusa, M., Peri, G., Rizzo, G. and Scaccianoce, G. 2022. The landfilling of municipal solid waste and the sustainability of the related transportation activities. Sustainability, 14(9): 5272. https://doi.org/10.3390/su14095272

ISO 14040. 2006. Environ. Manage. - Life Cycle Assessment Principles and Framework. Int. Stand. Organ., Geneva.

ISO 14044. 2006. Environ. Manage. - Life Cycle Assessment e Requirements and guidelines. Int. Stand. Organ., Geneva.

Komine, H. and Ogata, N. 1999. Experimental study on swelling characteristics of sand-bentonite mixture for nuclear waste disposal. Soils Found., 39(2): 83-97. https://doi.org/10.3208/sandf.39.2_83

Nanda, S. and Berruti, F. 2021. Municipal solid waste management and landfilling technologies: a review. Environ. Chem. Lett.. 19: 1433–1456. https://doi.org/10.1007/s10311-020-01100-y

Ou, Y., Iyer, G., Fawcett, A., Hultman, N., McJeon, H., Ragnauth, S., Smith, J., Steven, M. and Edmonds, J. 2022. Role of non-CO2 greenhouse gas emissions in limiting global warming. One Earth, 5(12): 1312-1315. https://doi.org/10.1016/j.oneear.2022.11.012

Sandhu, R.K. and Siddique, R. 2022. Durability performance of self compacting concrete made with waste foundry sand. Struct. Concr., 23(2): 722-738. https://doi.org/10.1002/suco.202100164

Siddique, R. and Singh, G. 2011. Utilization of waste foundry sand (WFS) in concrete manufacturing, Resour. Conserv. Recycl., 55(11): 885-892. https://doi.org/10.1016/j.resconrec.2011.05.001

Sivapullaiah, P. ., Sridharan, A. and Stalin, V.K. 2000. Hydraulic conductivity of bentonite-sand mixtures. Canad. Geotech. J., 37(2): 406-413. https://doi.org/10.1139/t99-120

The Gazette of India. 2015. Notification issued for introduction of BS IV compliant four wheel motor vehicles. Government of India - Ministry of Road Transport and Highways.

Tiewsoh, L.S., Jirásek, J. and Sivek, M. 2019. Electricity generation in India: Present state, future outlook and policy implications. Energies, 12(7): 1361. https://doi.org/10.3390/en12071361

Ujaczki, É., Feigl, V., Molnár, M., Vaszita, E., Uzinger, N., Erdélyi, A. and Gruiz, K. 2016. The potential application of red mud and soil mixture as an additive to the surface layer of a landfill cover system. J. Environ. Sci., 44: 189-196. https://doi.org/10.1016/j.jes.2015.12.014

United Nations 2015. The Sustainable Development Goals 2030. Department of Economic and Social Affairs Sustainable Development. https://sdgs.un.org/goals

Weitekamp, C.A., Stevens, T., Stewart, M.J., Bhave, P. and Gilmour, M.I. 2020. Health effects from freshly emitted versus oxidatively or photochemically aged air pollutants. Sci. Tot. Environ., 704: 135772. https://doi.org/10.1016/j.scitotenv.2019.135772

Yamsani, S.K., Sreedeep, S. and Rakesh, R.R. 2016. Frictional and interface frictional characteristics of multi-layer cover system materials and their impact on overall stability. Int. J. Geosynth. Ground Eng., 2: 23. https://doi.org/10.1007/s40891-016-0063-5

Zhou, Y., Xu, X., Han, R., Li, L., Feng, Y., Yeerken, S., Song, K. and Wang, Q. 2019. Suspended particles potentially enhance nitrous oxide (N2O) emissions in the oxic estuarine waters of eutrophic lakes: Field and experimental evidence. Environ. Pollut., 252: 1225-1234. https://doi.org/10.1016/j.envpol.2019.06.076

ORCID DETAILS OF THE AUTHORS

G. Sanoop: https://orcid.org/0000-0001-5847-408X
Sobha Cyrus: https://orcid.org/0000-0003-3271-9661

Nature Environment and Pollution Technology
An International Quarterly Scientific Journal

p-ISSN: 0972-6268
(Print copies up to 2016)
e-ISSN: 2395-3454

Vol. 23 | No. 1 | pp. 419-426 | 2024

Original Research Paper

https://doi.org/10.46488/NEPT.2024.v23i01.036

Open Access Journal

Passivation Effect of Corn Vinasse Biochar on Heavy Metal Lead in Paddy Soil of Pb-Zn Mining Area

M. Xiong*, G. Q. Dai*, R. G. Sun* and Z. Zhao†**

*School of Chemistry and Materials Science, Guizhou Normal University, Guiyang 550025, People's Republic of China

**Guizhou Eco-Environmental Monitoring Centre, Guiyang 550081, China

†Corresponding author: Z. Zhao; 251237969@qq.com

Nat. Env. & Poll. Tech.
Website: www.neptjournal.com

Received: 29-04-2023
Revised: 14-06-2023
Accepted: 17-06-2023

Key Words:
Biochar
Heavy metals
Contaminated soil
Mining areas
Morphological distribution

ABSTRACT

The in-lab incubation experiments were conducted to identify the passivation effect of corn vinasse biochar, which was prepared at different temperatures, on heavy metal Pb in paddy soil of the Pb-Zn mining area. The results showed that after 30 days of biochar amended to the soil, the soil pH and organic carbon content increased by 2.72%-8.47% and 27.79%-65.26%, respectively. The CO_3^{2-} and OH^- contained in corn vinasse biochar could react with Pb and generate carbonate and hydroxide of Pb. In comparison with the treatment control, the bioavailable fractions of Pb were reduced by 26.6%, 23.30%, 26.95%, and 35.33%, respectively, in biochar-amended treatments. Exchangeable fractions of Pb decreased by 21.50%, 21.33%, 22.58%, and 22.58% for the treatment 3% (300°C), 6% (300°C), 3% (600°C), and 6% (300°C) corn vinasse biochar, respectively, compared with the treatment control. As a whole, corn vinasse biochar could effectively promote the transformation of Pb in soil from the exchangeable fractions into the Fe-Mn oxide-bound fractions and residue fractions, with a significant passivation effect for Pb in soil and more effective passivation by high-temperature preparation and increased dosage of biochar.

INTRODUCTION

With the rapid development of China's economy, the problem of heavy metal contamination has become increasingly acute, and the pollution of soil heavy metal has become an environmental issue of worldwide concern. The research has shown that excessive accumulation of heavy metals in soil poses a serious threat to human health, food safety, and soil ecosystems (Wang et al. 2020). According to the "National Soil Pollution Survey Bulletin" issued by the Chinese Government in 2014 (Ministry of Environmental Protection 2014), the exceedance rate of total soil sampling sites was 16.1%. The exceedance rate of soil sampling sites in mining areas accounted for 33.4%, in which heavy metals were the dominant pollutants, with the contamination rate of Pb as high as 1.5% (Chinese Ministry of Environmental Protection and Ministry of Land and Resources 2014). Sun et al. (2021) sampled and analyzed the Pb content in Pb-Zn tailings in Danzhai County, Guizhou Province, and the result showed that the Pb content in the 0-20 cm surface soil was15.2 times higher than the background soil value in Guizhou. Lead (Pb^{2+}) is a typical heavy metal that can be absorbed by plants and animals and then enter the human body through the food chain, causing harm to humans due to its poor biodegradability and easy accumulation (Chen et al. 2020, Edenborn et al. 2017). Due to the undesirable discharge of industrial wastewater containing Pb from mining and ore processing, lead battery manufacturing, printing and dyeing, industrial building materials, and the random piling of waste tailings containing Pb, a large amount of Pb has entered the soil, which has caused soil Pb pollution to become a serious environmental problem (Qin et al. 2010). Therefore, environmentally appropriate management of large quantities of smelting waste, especially safe disposal in combination with sustainable remediation technologies, is a challenge of global importance (Mensah et al. 2021, Antoniadis et al. 2022).

Biochar is an efficient and environmentally friendly material for soil remediation (Kumar et al. 2018, Vamvuka et al. 2019), which mainly immobilizes heavy metals in the soil through physical and chemical adsorption, changing the specific chemical form of heavy metals in soil and inhibiting the biological effectiveness of heavy metals (Komkiene & Baltrenaute 2016, Lu et al. 2014). Biochar has become a frontier and hot spot for in-situ remediation of heavy metal pollution in agricultural fields because of its large specific surface area, the abundance of active functional groups on the surface, and excellent complexation and adsorption properties (Ibrahim et al. 2016, Zhen et al. 2013). Currently,

biochar is mainly derived from plant straw, animal manure, sludge, and household waste, which has strong adsorption and passivation effects on heavy metal ions, and it has been widely used in soil remediation (Liu & Bai 2022). Ahmad et al. (2016) added soybean straw biochar to the soil, which effectively reduced the acid extraction fraction of Pb and Cu; the higher the pyrolysis temperature, the better the effect of passivation. Park et al. (2011) added chicken manure biochar to soil, which has a strong passivation effect on Pb, Cu, and Cd. Khanmohammadi et al. (2017) showed that the addition of sludge biochar not only improved soil fertility but also had a better immobilization effect on Pb, Mn, and Zn. These research results vary depending on the raw materials of biochar. Vinasse is residues produced after brewing that have pH values in the range of 3.5-5, contain large amounts of Na^+ and K^+ ions, and oxygen-containing functional groups (-COOH, -CO-, -OH), which can provide a large number of adsorption sites for the attachment of heavy metals (Petrovic et al. 2016). At present, few studies are focusing on the remediation of Pb-contaminated soil by biochar derived from corn vinasse. Guizhou is a famous liquor industry destination, and with the flourishing of liquor culture, the amount of liquor vinasse produced after liquor production has increased, and new ways of maximizing its resource utilization need to be explored.

Therefore, in this study, the soil of rice fields in the lead-zinc mining area of Danzhai, Guizhou, was used as the research object. The biochar was prepared as raw material derived from corn vinasse at 300°C and 600°C under anaerobic conditions, respectively. We investigated the effects of the application of corn vinasse biochar prepared at different pyrolysis temperatures on the physicochemical properties of soil and the passivation effect of heavy metals Pb in soil by adopting the improved Tessier five-step sequential extraction method and combined with XRD, FTIR, and SEM-EDX characterization methods, which provided a theoretical basis and technical support for the in-situ remediation of Pb-contaminated soil by corn vinasse biochar and also explored new ways for the development and utilization of corn vinasse.

MATERIALS AND METHODS

The corn vinasse was sourced from Renhuai distillery in Guizhou Province, which was washed with deionized water, dried to constant weight at 60°C, crushed to 60 mesh, and put in a dry place. The Pb-contaminated soil was collected from the paddy field soil (107°32'4" N, 26° 10'56" E) in the Pb-Zn mining area of Danzhai County, Qiandongnan Prefecture, Guizhou Province, with a fine gray-brown loam. The soil was collected by the multi-point method, transported to the laboratory, and prepared for use after natural air-drying and removal of plant roots and stone particles. The physical and chemical properties of the soil are shown in Table 1. The soil is weakly acidic, and the content of heavy metal Pb is 4.2 times the risk screening value (100 $mg.kg^{-1}$, $5.5< PH \leq 6.5$) of the soil pollution risk control standard for agricultural land (GB15618-2018).

Table 1: Soil physical and chemical characteristics.

Total soil Pb content/ [$mg.kg^{-1}$]	pH	SOM/[$g.kg^{-1}$]	CEC/[$cmol.kg^{-1}$]
423.67	5.73	4.54	32.917

Preparation of Biochar

The biochar was produced by an oxygen-limited cracking method with the raw material of corn vinasse (Chinese Baijiu Vinasse (CBV)) under the anaerobic environment at a rate of 5°C-min-1 up to 300 and 600°C and constant temperature for 1 h. After natural cool-down to room temperature, the biochar was removed and reserved, marked with CBV300 and CBV600, respectively, and its physicochemical properties are shown in Table 2.

Soil Cultivation Experiment

A total of 5 treatment groups with 3 replicates were set up by adding 3% and 6% of biochar (CBV300 and CBV600) to 3 kg of the trial soils and setting up a blank control group. The group of soil without biochar addition was labeled as KB. The group of soil biochar additions was labeled as T1, T2, T3, and T4, respectively. Its specific design is shown in Table 3. All pots should be placed in a cool, dry place for ventilation and cultivation and weighed and watered every three days to maintain a soil moisture content of about 50%. After 30 days of incubation, the soil was taken out and placed in a cool and ventilated place for air-drying, grinding, passing 200 mesh, and then the physical and chemical properties, Pb content, and morphology were determined.

Measurement Method

The pH electrode determined the PH of soil and biochar,

Table 2: Physicochemical properties of biochar.

Biochar	PH	BET/m^2. g^{-1}	Total hole volume/$mL.g^{-1}$	C/N element ratio %	Content of alkaline groups/$mmol.g^{-1}$
CBV300	8.61±0.0062	2.3263	0.0234	10.14	0.97±0.16
CBV600	10.46±0.0036	9.0693	0.1267	12.03	1.50±0.02

Table 3: Experimental design treatment groups.

KB	Soil
T 1	Soil +3%CBV300
T 2	Soil +6%CBV300
T 3	Soil +3%CBV600
T 4	Soil +6%CBV600

and the organic matter content (SOM) was determined by the potassium dichromate volumetric method. The cation exchange capacity (CEC) was determined by the hexamine cobalt chloride solution-spectrophotometric method (Liu et al. 2020). Analysis of heavy metal fractions according to the modified Tessier five-step graded extraction method (Essier et al. 1979). The heavy metals in the soil were classified into ion exchange fraction (F1), carbonate bound fraction (F2), iron-manganese oxide bound fraction (F3), an organic bound fraction (F4), and residue fraction (F5). The elemental concentrations in the extracts were determined by flame atomic absorption spectrophotometry. The concentrations of the elements in the extracts were determined by flame atomic absorption spectrophotometry.

The surface pore structure was analyzed by vacuum scanning electron microscopy (SEM-EDX), the elemental analyzer determined the C, H, O, and N content of biochar, the acid-base functional groups on the surface of biochar was determined by Bohm titration (Karamanova et al. 2019), the surface functional groups were determined by Fourier infrared spectroscopy (FTIR), and the crystalline substances contained in the biochar before and after action were determined by X-ray diffraction (XRD).

Data Processing and Analysis

Analytical processing was performed using Microsoft Excel 2019 and SPSS 25, with one-way ANOVA analysis of significant differences using LSD, Waller-Duncan and Tukey' s-b tests, and Origin 2021 for plotting.

RESULTS AND DISCUSSION

Effect of Biochar on Soil Physicochemical Properties

Biochar reduces the risk of soil heavy metal contamination by changing the physicochemical properties of soil and then changing the distribution form of heavy metals in the soil (Tang et al. 2022). SOM, pH, and CEC are key factors in the morphological transformation and migration of metals (Li et al. 2022). The value of pH is closely related to the morphology and bioavailability of heavy metals in soil and the process of sorption and desorption of contaminants in soil (Shi et al. 2016). After 30 days of incubation, there was a significant difference in soil pH and SOM but no significant difference in CEC in the biochar remediation treatment as compared to the KB treatment. Compared with KB treatment, all T1-T4 treatments significantly increased the pH value of the soil (Table 4). The application of CBV300 biochar increased the pH value of the soil by 2.66% and 5.54%, respectively. The application of CBV600 was significantly more effective. The value of pH increased by 6.87% and 8.52%, respectively, which was related to the degree of alkalinity of biochar, and biochar CBV600 contained more alkaline functional group content than CBV300 (Table 2). At the same time, CBV600 contains a large number of alkaline substances such as carbonates, strong oxides, and metal oxides that can undergo rapid hydrolysis or adsorption in contact with soil to reduce the exchange level of exchangeable ions such as H^+ and Al^{3+} in the soil, which makes it more effective in raising the PH value of the soil (Houben et al. 2013, Yuan et al. 2011, Novak et al. 2009).

The organic matter can immobilize heavy metals in the soil by adsorption or chelation and, at the same time, has a reduction effect, which reduces the availability of heavy metals in the soil (Li et al. 2017). The organic matter content of biochar-treated soil was significantly enhanced by 27.85-65.18 % compared to KB (Table 4). Due to the rich content of C elements in biochar, the addition of biochar to soil can enhance the soil C/N ratio and increase the organic matter content of the soil (Chan et al. 2007). The application of biochar can effectively reduce the availability of Pb in the soil.

Passivation of Pb on Biochar

The XRD spectra showed that the mineral composition changed before and after the biochar action (Fig. 1), with new $3PbCO_3.2Pb(OH)_2.H_2O$ peaks found in the range of 2θ=20.85° to 30.27° for CBV300 and $Pb_3(CO_3)_2(OH)_2$ in the range of 2θ=24.64° to 34.15° for CBV600, indicating that the reactions of CO_3^{2-} and OH^- in biochar with Pb, where more Pb complexes were observed in CBV600 than in CBV300 biochar. Cao Harris (2010) explored and found

Table 4: Soil pH and SOM content at different treatments group.

Treatments group	pH	SOM/[g.kg $^{-1}$]	CEC/[cmol.kg^{-1}]
KB	6.26 ±0.0le	6.63±0.04c	28.24±0.41a
T1	6.43 ±0.02d	8.47±0.38a	29.36+0.23a
T2	6.61 ±0.00 c	10.94±0.82b	28.14+2.75a
T3	6.69 ±0.02b	9.20±0.17b	30.38+0.65a
T4	6.79 ±0.03a	9.12±0.42b	30.62+1.40a

Note: For the same column, the same lowercase letter indicates no significant difference under the same cycle and different treatments, and different lowercase letters indicate a significant difference, $p < 0.05$, as below.

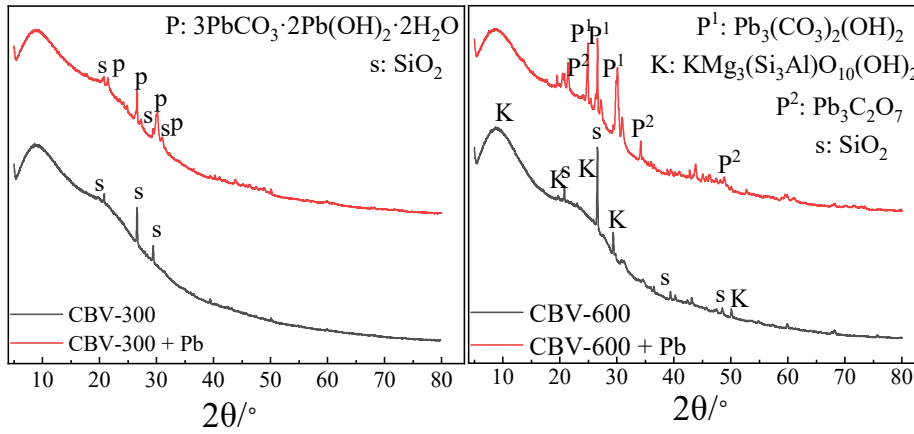

Fig. 1: XRD spectra before and after the action of biochar.

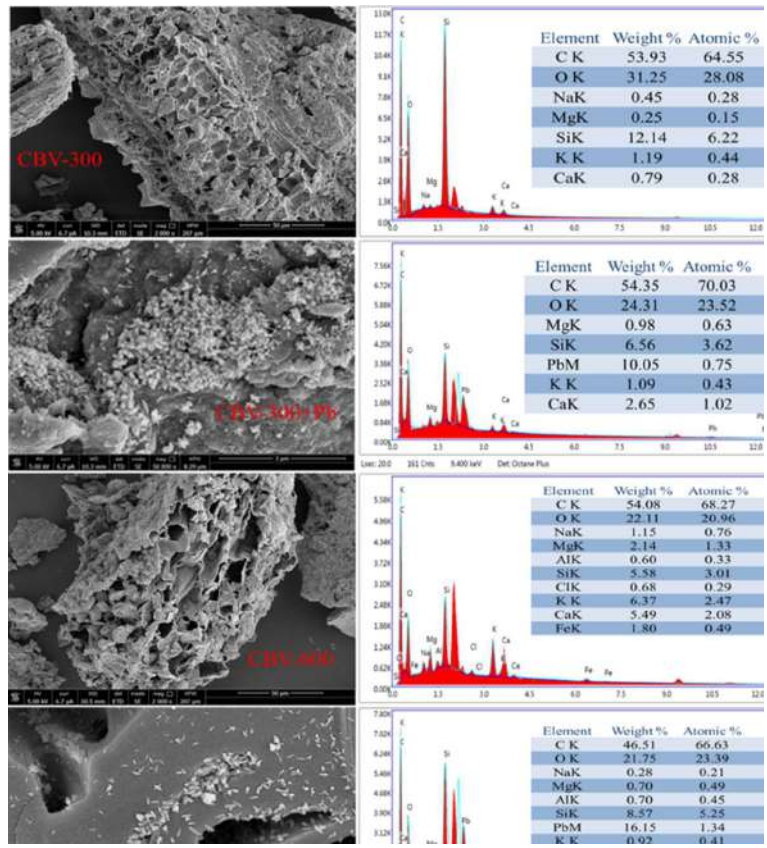

Fig. 2: Scanning electron microscopy spectra (SEM-EDX) of biochar before and after interaction with heavy metals.

that the action of dairy-manure biochar on Pb reacts with Pb to result in precipitates of carbonate and hydroxide. As shown in the SEM electron micrographs (Fig. 2), the size and shape of the particles were different before and after the reaction of biochar, and the surface structure was irregular and contained pore structure, the surface after the action all contained crystalline structure, the results are consistent with the XRD analysis. Combined with the elemental analysis of EDX spectra, it was found that the content and proportion of elements such as Ca, Mg, Na, and K changed, which indicated that ion exchange occurred between Pb and biochar. In addition, the application of biochar increased the soil pH. Pb could combine with OH^- and CO_3^{2-} to form insoluble carbonates and hydroxides, which resulted in reducing the

concentration of bioavailable Pb in the soil. In summary, it can be concluded that the vinasse biochar can effectively consolidate the Pb, and its high-temperature pyrolysis biochar (CBV600) is more effective.

Effect of Biochar on the Morphological Transformation of Pb in Soil and Remediation Effect

Researchers generally evaluate the passivation effect of heavy metals in soils by assessing the mobility and bioavailability of heavy metals in terms of the magnitude of their bioavailable fractions (Song et al. 2015). The application of biochar significantly reduced the bioavailable fraction of Pb in the soil compared to KB (Fig. 3). On the 30th day of incubation, the bioavailable fraction of Pb in the soil was significantly reduced in all treatments. T1-T4 treatment groups decreased by 26.61%, 23.30%, 26.80%, and 35.29%, respectively. With the increase in temperature, the content of the bioavailable state of Pb showed a decreased trend; there was no significant difference in the effect of biochar addition at 300°C. However, at the high temperature of 600°C, the treatment group with 6% biochar content applied had a more significant effect than the 3% treatment group, indicating that 6% CBV600 had a better passivation effect. As high-temperature pyrolysis can increase the pH and Eh values of the biochar itself, which changes the surface activity of the crystalline material in the soil and induces a change in the fugitive form of heavy metal ions in the soil to achieve a reduction in the available fraction of Pb (Zhang et al. 2013). It was evident that the biochar prepared by applying different pyrolysis temperatures reduced the content of Pb in the soil to a certain level, and the high-temperature effect was better.

Compared to KB, the existence form of Pb in the soil was changed after the addition of biochar, with the T1-T4 treatment group mainly existing in the Fe-Mn oxide bound fraction (63%, 64%, 66%, 75%) (Fig. 4). The degree of passivation effect of biochar prepared at different pyrolysis temperatures on Pb varied. After 30 days of incubation, the percentages of F1 in the T1-T4 treatment groups decreased by 21.50%, 21.33%, 22.58%, and 22.58%, respectively. The percentages of the sum of F3 and F4 increased by 21.85%, 23.13%, 24.81%, and 34.80%, respectively, indicating that biochar could promote an exchangeable state of Pb in the soil to the Fe-Mn oxide-binding state and the residue state, the result indicated that biochar played a passivating effect on Pb. The effect of high-temperature pyrolysis biochar was more effective. As high-temperature pyrolysis of biochar contains more inorganic mineral elements and alkaline groups, which can exchange or precipitate with Pb^{2+}, the surface functional groups (-OH, -COOH) and rich pore structure of biochar has a strong affinity for Pb (Wagner & Kaupenjohann 2014). The reactions of heavy metals in soil with functional groups on the surface of biochar are as follows.

$$BC\text{-}OH+Pb^{2+}\rightarrow BC\text{-}OPb^{2+}+H^{+} \quad \ldots (1)$$

$$(BC\text{-}OH)_2+ Pb^{2+}\rightarrow (BC\text{-}O)_2Pb^{+}+H^{+} \quad \ldots (2)$$

$$BC\text{-}COOH+Pb^{2+}\rightarrow BC\text{-}COOPb^{2+}+H^{+} \quad \ldots (3)$$

$$(BC\text{-}COOH)_2+Pb^{2+}\rightarrow (BC\text{-}COO)_2Pb^{+}+H^{+} \quad \ldots (4)$$

The reaction can form a complex of heavy metals on the surface of biochar through intermolecular hydrogen bonds, which have a solidification effect on heavy metals (Gong et al. 2022). According to the infrared spectrum (Fig. 5), -OH vibrated at 3333 cm^{-1}, C=C and C=O in the aromatic ring vibrated at 1627 cm^{-1} and C=O in the carboxyl group vibrated at 1704 cm^{-1}, and aromatic-CH-peak occurred at 860 cm-1 in CBV600, which proved that functional groups such as -OH, -COOH and electron-containing groups in the vinasse biochar could exchange ions, complexation reactions and electron conjugation reactions with Pb, promote the adsorption and

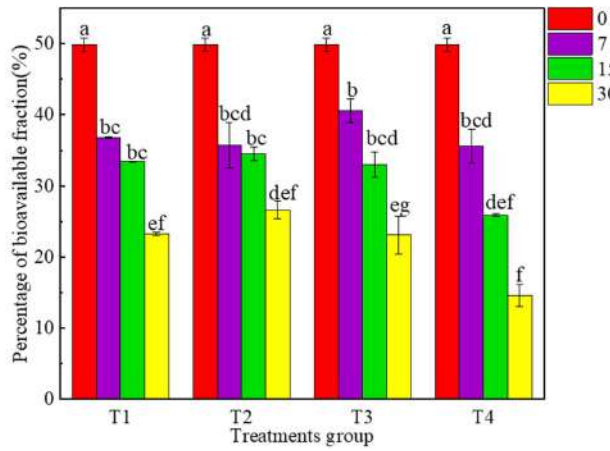

Fig. 3: Effect of biochar on the bioavailable fraction of Pb.

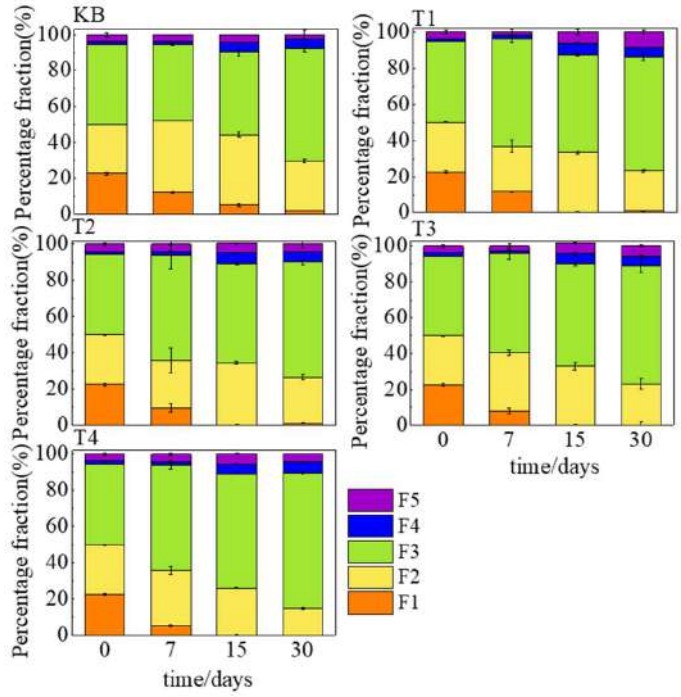

Fig. 4: Effect of biochar on the distribution form of Pb in soil.

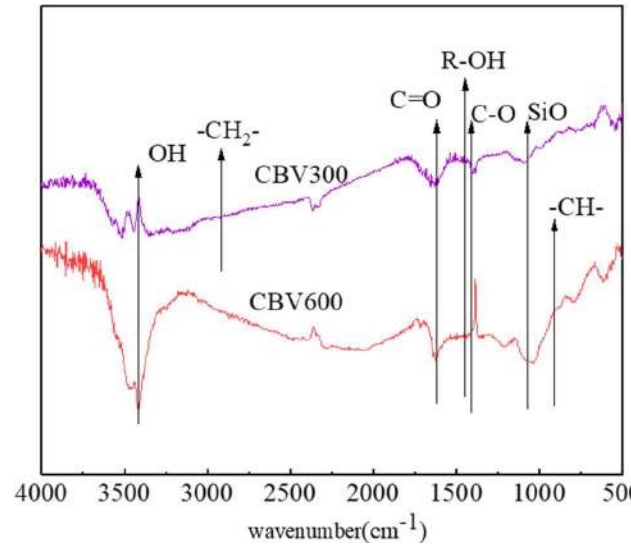

Fig. 5: Infrared spectrum of biochar (FTIR).

precipitation of Pb in soil. In conclusion, corn vinasse biochar has a significant effect on the chemical form of Pb in mine soils. It can promote the transformation of the exchangeable fraction of Pb to the Fe-Mn-oxide bound fraction and residue fraction, significantly reducing the bioavailability of Pb. This process mainly remediates and stabilizes Pb in soils through the occurrence of ion exchange and complexation reactions, and its high-temperature pyrolysis biochar has a better remediation effect.

CONCLUSION

In this study, the application of biochar derived from corn vinasse to Pb-contaminated rice paddy field soil in Pb-Zn

mining area significantly improved the value of pH (2.66%-8.52%) and SOM content (27.85%-65.18%) in Pb-Zn mining area rice paddy field soil. In this study, Pb morphology in soil was analyzed by a modified Tessier five-step extraction method. The results showed that after 30 days of biochar application incubation, the bioavailable state of Pb in the 3% CBV300, 6% CBV300, 3% CBV600, and 6% CBV30 treatment groups decreased by 26.61%, 23.30%, 26.95%, and 35.33%. The soil, the exchangeable state of Pb, was transformed to Fe-Mn oxide-binding and residue states, with the better effect of 6% CBV600. This study combined XRD, SEM-EDX, and FTIR characterization methods and found that functional groups such as -OH, -COOH, and -C=O and electron-containing surface functional groups in the biochar were involved in ion exchange, complexation, and π-electron conjugation reactions with the Pb and the increase of basic groups at high temperatures, which promoted the precipitation of lead ions. In conclusion, the application of corn vinasse biochar could change the exchangeable state of Pb in the soil to the residue state and Fe-Mn oxide-bound state and promote the passivation of Pb in soil, which could reduce the migration and transformation rate of heavy metals in soil. At the same time, high-temperature treatment and increasing the amount of biochar had more significant effects on the passivation of Pb in the soil of the paddy field.

ACKNOWLEDGEMENTS

This work was financially supported by Guizhou Provincial Scientific and Technological Program (Natural Science) (No. Qian ke he ji chu [2020]1Z038) and (Outstanding Young Scientists and Technicians) (No. Qian ke he ping tai ren cai – YQK[2023]027).

REFERENCES

Ahmad, M., Ok, Y.S., Kim, B.Y., Ahn, J.H., Lee, Y.H., Zhang, M., Moon, D.H., Alwabei, M.I. and Lee, S.S. 2016. Impact of soybean Stover- and pine needle-derived biochars on pb and as mobility, microbial community, and carbon stability in a contaminated agricultural soil. J. Environ. Manag., 166: 131.

Chinese Ministry of Environmental Protection and Ministry of Land and Resources. 2014 National Soil Survey.

Chen, Z., Xing, R.Z., Yang, X.G., Zhao, Z.Q., Liao, H.P. and Zhou, S.G. 2020. Enhanced in situ Pb (II) passivation by biotransformation into chloropyromorphite during sludge composting. J. Hazard. Mater., 408: 12497.

Chan, K.Y., Van Z.V.L., Meszaros, I., Downie, A. and Joseph, S. 2007. Agronomic value of green waste biochar as a soil amendment. Geoderma, 45(8): 629.

Cao, X.D. and Harris, W. 2010. Properties of dairy-manure-derived biochar pertinent to its potential use in remediation. Bioresour. Technol., 101(14): 5228.

Edenborn, H.M., Hoeard, B.H., Sams, J.I, Vesper, D.J. and Edenborn, S.L. 2017. Passive detection of Pb in water using rock phosphate agarose beads. J. Hazard. Mater., 336: 240.

Essier, A., Campbeii, P.G.C. and Bissom, M. 1979. Sequential extraction procedure for the speciation of particulate trace metals. Anal. Chem., 51(7): 844.

Gong, H. B., Zhao, L., Rui, X., Hu, J. W. and Zhu, N. W. 2022. A review of pristine and modified biochar immobilizing typical heavy metals in soil: Applications and challenges. J. Hazard. Mater., 432: 128668.

Houben, D., Evvrarad, L. and Sonnrt, P. 2013. Mobility, bioavailability, and PH-dependent leaching of cadmium, zinc, and lead in contaminated soil amended with biochar. Chemosphere, 92: 1450.

Ibrahim, M., Khan, S., Hao, X., Li, G. and Zhu, Y.G. 2016. Biochar effects on metal bioaccumulation and arsenic speciation in alfalfa (Medicago sativa L.) grown in contaminated soil. Int. J. Environ. Sci. Technol., 13: 246.

Kumar, A., Tsechansky, L., Lew, B., Raveh, E, Frenkel, O. and Graber, E. R. 2018. Biochar alleviates phytotoxicity in Ficus elastica grown in Zn-contaminated soil. Sci. Tot. Environ., 618: 188.

Komkiene, J. and Baltrenaute, E. 2016. Biochar as adsorbent for removal of heavy metal ions [Cadmium (II), Copper (II), Lead (II), Zinc (II)] from the aqueous phase. Int. J. Environ. Sci. Technol., 13: 471.

Khanmohammadi, Z., Afyuni, M. and Mosaddeghi, M.R. 2017. Effect of sewage sludge and its biochar on chemical properties of two calcareous soils and maize shoot yield. Ecol. Environ. Sci., 63(2): 198.

Karamanova, B., Stoyanova, A., Schipochka, M., Girginov, C. and Stoyanova, R. 2019. On the cycling stability of biomass-derived carbons as electrodes in supercapacitors. J. Alloys Comp., 803: 882.

Lu, K., Yang, X., Shen, J., Robinson, B., Huang, H.G, Liu, D., Boian, N., Pei, J.C. and Wang, H.L. 2014. Effect of bamboo and rice straw biochars on the bioavailability of Cd, Cu, Pb, and Zn to Sedum plumbizincicola. Agric. Ecosyst. Environ., 191: 124.

Liu, Q.S. and Bai, G.M. 2022. Research progress of biochar and its modification technology for remediation of soil heavy metal pollution. Appl. Chem. Ind., 51(11): 3285.

Liu, R., Deng, M., Li, Y.Y., Wang, X.Y., Xiao, Y.P., Huang, X.R., Zhou, W.Q. and Zhang, Y.J. 2020. Optimization for the determination of cation exchange capacity in soils with different acidity and alkalinity. Environ. Monit. China, 36(1): 125.

Li, Q., Wang, Y.H., Li, Y.C., Li, L.F., Tang, M.D., Hu, W.F., Chen, L. and Ai, S.Y. 2022. Speciation of heavy metals in soils and their immobilization at micro-scale interfaces among diverse soil components. Sci. Total Environ., 825: 153862.

Li, Z., Liang, D.L., Peng, Q., Cui, Z.W., Huang, J. and Lin, Z. Q. 2017. Interaction between selenium and soil organic matter and its impact on soil selenium bioavailability: A review. Guiy. Guizh. Normal Univ., 295: 69.

Mensah, A.K., Marschner, B., Antoniadis, V., Stemn, E., Shaheen, S. M. and Rinklebe, J. 2021. Human health risk via soil ingestion of potentially toxic elements and remediation potential of native plants near an abandoned mine spoil in Ghana. Sci. Tot. Environ., 798: 149272.

Novak, J.M., Frederick, J.R., Baure, P.J. and Watts, D.W. 2009. Rebuilding organic carbon contents in coastal plain soils using conservation tillage systems. Soil Sci. Soc. Am. J., 73(2): 622.

National Soil Pollution Survey Bulletin of China. 2014. Ministry of Environmental Protection, http://www.gov.cn/foot/site1/20140417/782bcb88840814ba158d01. Pdf.

Petrovic, J.T., Stojanovic, M.D., Milojkovic, J.V., Petrovic, M.S., Sostaric, T.D., Lausevic, M.D. and Mihajlovic, M.L. 2016. Alkali modified hydrochar of grape pomace as a perspective adsorbent of Pb^{2+} from aqueous solution. J. Environ. Manag., 182: 292.

Park, J.H., Choppala, G.K., Bolan, S.T., Chuang, J.W. and Chuasavathht, T. 2011. Characteristics of chicken manure biochars and its effect on Cd and Pb remediation in water and soil. Trans. Chin. Soc. Agric. Eng., 348: 439.

Qin, J.F., Li, Z.X. and Lou, M.T. 2010. Status, sources of pollution and

control measures of Chinese children lead poisoning. Guang. Trace Elements Sci., 17(1): 1.

Shi, R.Y., Li, J.Y., Xu, R.K. and Qian, W. 2016. Ameliorating effects of individual and combined application of biomass ash, bone meal, and alkaline slag on acid soils. Soil Till. Res., 162: 41.

Song, W.E., Chen, S.B., Liu, J.F., Chen, L., Song, N.N. and Liu, B. 2015. Variation of cd concentration in various rice cultivars and derivation of cadmium toxicity thresholds for paddy soil by species-sensitivity distribution. J. Integr. Agric., 14(9): 1845.

Sun, R.G., Gao, Y. and Yang, Y. 2021. Leaching of heavy metals from lead-zinc mine tailings and the subsequent migration and transformation characteristics in paddy soil. Chemosphere, 291(1): 132792.

Tang, B., Xu, H.P., Song, F.M., Ge, H.G., Chen, L., Yue, S.Y. and Yang, W.Y. 2022. Effect of biochar on immobilization remediation of Cd contaminated soil and environmental quality. Environ. Res., 204: 111840.

Vamvuka, D., Sfakiotakis, S. and Pantelaki, O. 2019. Evaluation of gaseous and solid products from the pyrolysis of waste biomass blends for energetic and environmental applications. Fuel, 236: 574.

Wagner, A. and Kaupenjohann, M. 2014. Suitability of biochars (pyro- and hydrocars) for metal immobilization on former sewage-field soils. Europ. J. Soil Sci., 65(1): 139.

Wang, X., Cui, Y.X., Zhang, X.C., Ju, W.L., Duan, C.J., Wang, Y.Q. and Fang, L.C. 2020. A novel extracellular enzyme stoichiometry method to evaluate soil heavy metal contamination: evidence derived from microbial metabolic limitation. Sci. Tot. Environ., 738: 139709.

Yuan, J.H., Xu, R.K. and Zhang, H. 2011. The forms of alkalis in the biochar are produced from crop residues at different temperatures. Bioresour. Technol., 102(3): 3488.

Zhen, R.L., Chen, Z., Chao C., Wang, X. H., Huang, Y. Z., Xiao, B. and Sun, G.X. 2013. Effect of biochar from rice husk, bran, and straw on heavy metal uptake by pot-grown wheat seedling in a historically contaminated soil. Bioresources, 8(4): 5965.

Zhang, X.K., Wang, H.L., He, L.Z., Lu, K.P., Sarmah, A., Li, J.W., Bolan, N.S., Pei, J.C. and Huang, H.G. 2013. Using biochar for remediation of soils contaminated with heavy metals and organic pollutants. Environ. Sci. Pollut. Res., 20(12): 8472.

Nature Environment and Pollution Technology
An International Quarterly Scientific Journal

p-ISSN: 0972-6268
(Print copies up to 2016)
e-ISSN: 2395-3454

Vol. 23 | No. 1 | pp. 427-434 | 2024

Original Research Paper

https://doi.org/10.46488/NEPT.2024.v23i01.037

Open Access Journal

Enhancing Enzymatic Hydrolysis and Delignification of Sugarcane Bagasse Using Different Concentrations of Sodium Alkaline Pretreatment

Arti Yadav†, Pushpa Rani, Deepak Kumar Yadav, Nisha Bhardwaj, Asha Gupta and Narsi Ram Bishnoi
Department of Environmental Science and Engineering, Guru Jambheshwar University of Science & Technology, Hisar-125001, Haryana, India
†Corresponding author: Arti Yadav; artiyadav0717@gmail.com

Nat. Env. & Poll. Tech.
Website: www.neptjournal.com

Received: 07-08-2023
Revised: 13-09-2023
Accepted: 22-09-2023

Key Words:
Sugarcane bagasse
Enzymatic hydrolysis
Pretreatment
Delignification
Cellic CTec2

ABSTRACT

Lignin, being highly resistant, needs to be eliminated in the process of extraction of soluble reducing sugar and bioethanol production from lignocellulosic biomass. In the present work, pretreatment of sugarcane bagasse (SCB) was performed using NaOH of various concentrations (1-5%) to facilitate delignification. The hydrolysis efficiency of pretreated SCB was evaluated at different reaction times by the production of reducing sugar using the Cellic CTec2 enzyme. The maximum cellulose content of 57.6% and lignin removal of 62.04% were observed with 2% sodium hydroxide at 121°C autoclaved for 60 min. The hemicellulose content decreased with increasing NaOH concentration with the maximum decrease of 13.6% from native bagasse having 26.5% xylan content. The microstructure, morphology, and chemical composition of SCB were analyzed using Field Emission Scanning Electron Microscopy (FESEM), Fourier Transform InfraRed (FTIR), and XRD. The hydrolysis with 10 FPU.g^{-1} of enzyme at 48 h of reaction time shows a maximum yield of 12.34 g.L^{-1} corresponding to 55.53 ± 0.45% at 2% NaOH pretreated SCB. This study claims that lignin components exhibited the highest susceptibility to NaOH pretreatment, which directly affects enzymatic hydrolysis.

INTRODUCTION

While first-generation ethanol production from starchy edible grain materials has advanced well, second-generation ethanol production from lignocellulosic biomass is still considering its economic viability. The potential sources of bioethanol production include agricultural and wood processing waste. Lignocellulose feedstock is a complex matrix that is degradation-resistant and provides hydrolytic stabilization and compositional robustness. This is mainly because cellulose, hemicellulose polysaccharides, and lignin are linked together through ester and ether bonds (Sharma et al. 2022, Madadi et al. 2023).

Lignin is present in wood plant tissue as deposited cell walls around cellulose and hemicellulose. It might include 15-20% of the dry matter in the entire feedstock. Lignin is a complex polymer and aromatic matrix containing phenolic compounds along with different types of functional groups like carbonyl, hydroxyl, and methoxyl (Wunna et al. 2017). Lignin's recalcitrant nature became one of the key obstacles to the manufacture of bioethanol economically. It must be removed so that a larger amount of sugar can be extracted from lignocellulosic feedstock, or bioethanol can be produced from them. Sugarcane is the main bioenergy crop with higher production. Brazil ranked first, which has been successfully exploited to make bioethanol. Sugarcane bagasse contains 36-46% of cellulose as the most abundant component, hemicellulose as the second highest with an amount between 15.91-28.7%, lignin composition is between 9.8-26.2%, and a slight amount of pectin (Wunna et al. 2021, Periyasamy et al. 2022).

Several pretreatment strategies can be used depending on the high yield of sugar and fermentable ethanol production through hydrolysis and fermentation procedures. Pretreatment can reduce the level of polymerization and polysaccharide crystallinity, as well as modify the molecular structure of biomass feedstock to increase its accessibility for enzymes. These techniques can be divided into biological, physical, chemical (involving acid and alkaline methods), and physicochemical methods of pretreatment. Compared to different pretreatment techniques, alkali pretreatment is used extensively during biomass pretreatment and is considered efficacious (Kininge & Gogate 2022). It increases the lignin removal percentage and enhances the cellulose yield in pretreated solid residue, which leads to easier saccharification to obtain a greater quantity of

glucose. Alkali pretreatment is preferred over the acidic pretreatment method because it can be performed under milder conditions. This method does not necessitate the need for expensive materials and specific designs to cope with harsh reactions and corrosion conditions. The alkali pretreatment reaction process involves the breakdown of intermolecular ester linkages and lignin, hemicellulose dissolution to break the rigid cell wall structure to facilitate the cellulose hydrolysis by increasing the accessibility for the hydrolytic enzyme (Nasution et al. 2022). Alkali reagents like NaOH, KOH, lime, or NH_4OH are typically used for alkali pretreatments. Sodium hydroxide is thought to be the most efficient chemical due to its greater solubility, lower cost, and more potent alkalinity (Wunna et al. 2021, Wang et al. 2020).

The current study concentrated on the pretreatment of SCB with different concentrations of sodium hydroxide for removing lignin significantly and to improve the amount of glucan in SCB for its application in the hydrolysis of cellulose and hemicellulose to reduce sugar. In this pretreatment experiment, NaOH concentrations were varied at constant temperature (121°C) to evaluate their effect on the lignin removal and hydrolysis yield (%) of SCB. Enzymatic hydrolysis was performed on 1-5% NaOH pretreated SCB using Cellic CTec 2 enzyme, which is a cocktail of cellulase, hemicellulase, and -glucosidase enzymes for the application of degrading cellulose to fermentable sugars. The impact of alkali pretreatment on the modification of lignin monomeric units and its subsequent effects on enzymatic hydrolysis must be thoroughly investigated to maximize the utilization of SCB biomass.

MATERIALS AND METHODS

Sample Collection, Preparation, and Characterization

Sugarcane bagasse (SCB) raw samples were collected from juice vendors in Hisar district, Haryana (India). The substrate was sun-dried and washed thoroughly with running tap water to get rid of debris and then dried in a hot air oven to ensure complete dryness. After this, these 1-2 cm long substrates were then grounded to 0.2 mm size. The sample was then characterized for compositional (Moisture, Cellulose, hemicellulose, and lignin) and proximate properties (ash content, total organic carbon). Organic carbon was estimated by using the dry combustion method (Nelson & Sommers 1983), and ash content was determined using the method given by (Han & Rowell1997). The Goering & Van Soest (1970) approach was used to determine the contents of lignin, cellulose, and hemicellulose by using an acid detergent and neutral detergent solution.

$$\text{Cellulose (\%)} = \frac{\text{Weight of crucible after}\left(\text{reflux}\right) - \left(\text{KMnO}_4\text{treatment}\right)}{\text{Initial sample weight}} \times 100$$

Hemicellulose (%) = NDF (%) – ADF (%)

Lignin (%) = ADF (%) – $KMnO_4$ fiber (%)

[ADF- Acid detergent fiber, NDF- Neutral detergent fiber]

Alkaline Pretreatment of SCB

Alkali pretreatment was performed using NaOH, which was prepared at different concentrations (1-5 wt%). The solution was then added to a substrate at a solid loading of 10% w/v, and the mixture was subjected to pretreatment in an autoclave at 12°C and 15 psi for 60 min. After heating, the sample was allowed to cool by resting it to room temperature and then the pretreated solid residues were separated from liquid hydrolysate by filtration with muslin cloth. The obtained solid residue was then neutralized by washing them thoroughly with distilled H_2O and was dried at 50°C for further analysis of cellulose, hemicellulose, and lignin components, as mentioned earlier. All experimental runs were performed in triplicates.

Enzymatic Saccharification of Pretreated SCB

Saccharification of alkali pretreated SCB (1-5% NaOH) was carried out in a 250 mL Erlenmeyer flask by adding 1g of substrate to 50 mL of citrate buffer having pH 5.0 enclosed with rubber septum and an aluminum cap and placed in a shaker incubator set at 100 rpm, 50°C for a different time interval (12-48 h) (Nosratpour et al. 2018). Then, a 10 $FPU.g^{-1}$ dose of Cellic CTec2 (procured from Sigma Aldrich, USA) was added to a flask having enzyme activity of 127 $FPU.mL^{-1}$ as determined by the Ghose (1987) method. Additionally, sodium azide had been added at a dosage of 0.005% to prevent any growth of microbes during hydrolysis. Samples of hydrolysate were extracted at various time intervals during the hydrolysis process and subjected to analysis for the quantification of total reducing sugar using the dinitro salicylic acid (DNS) method and analyzed by High-performance liquid chromatography (HPLC) using an Agilent system with a refractive index detector (RID) utilizing NH_2 column with a flow rate of $1mL.min^{-1}$. At a temperature of 50°C (Miller 1959). The percentage of saccharification was determined using the equation proposed by Mandels and Sternberg (1976) as follows:

$$\text{Saccharification}(\%) = \frac{\text{Reducing sugars}\left(\text{g/L}\right) \times 0.9}{\text{Initial concentration (g/L)}} \times 100$$

Sugarcane Bagasse Characterization

Morphological and structural characterization of untreated raw bagasse and pretreated SCB has been examined. Characterization of functional groups and change in biomass vibrational frequency has been predicted by Fourier Transform InfraRed (FTIR) spectrophotometer (Perkin Elmer model) within a wavelength range of 400-4000 cm^{-1} using pre-dried KBr powder. To investigate the alterations in biomass surface following pretreatment, the morphological features of both the untreated SCB and the solid residue obtained after pretreatment were examined. Prior to image analysis, which was performed using a high-resolution field emission scanning electron microscope (FESEM) (7610F Plus/JEOL), dried fine powdered samples of SCB were placed on the aluminum stubs and coated with a layer of gold. This gold coating ensures better conductivity and enhances the image quality obtained during the subsequent image analysis process. The X-ray diffraction analysis was performed on untreated and alkali-treated SCB substrate using a monochromatic CuK energy basis X-ray diffractometer. The analysis was conducted in the 2 range value scanned from 10-50º with a phase of 0.04 and a scanning time of 5 min. The Crystallinity Index (CrI) can be calculated using the following equation:

$$\mathrm{CrI}(\%) = I_{002} - \frac{I_{am}}{I_{002}} \times 100$$

where,

I_{002}, the intensity of the crystalline part of the biomass with a peak around 22° (e.g., cellulose)

I_{am} the intensity of the amorphous part of the biomass.

Statistical Analysis

The given experiments were conducted independently in triplicates, and the findings are expressed as the mean value with its corresponding standard deviation.

RESULTS AND DISCUSSION

The raw SCB used in this study has a composition of 43.02% cellulose, 26.5% hemicellulose, and 16.6% lignin content. In addition to these compositional components, lignocellulosic biomass also contains other components such as ash, organic carbon, moisture, nitrogen, and various trace elements. Table 1 presents the proximate and compositional properties of the raw untreated sugarcane bagasse. It is important to consider the complete composition of lignocellulosic biomass, including these additional components, as they can have implications for the bioconversion processes, such as bioethanol production, and may influence the overall efficiency and yield of the process. In the study mentioned, the composition of the sugarcane bagasse (SCB) used is within the reported ranges for cellulose, hemicellulose, and lignin content in other research studies. The hemicellulose and lignin content of the SCB was reported as 26.5% and 16.6%, respectively, which falls within the reported range of 28-47% and 14-22% mentioned in other studies (Hernandez et al. 2019, Melesse et al. 2022, Alarcón et al. 2022).

Pretreatment Effect on Compositional Properties of SCB

The objective of the pretreatment is to enhance lignin removal and glucan content in the SCB, which is important for bioethanol production. The given text describes the results of the alkali (NaOH) pretreatment of SCB, which was employed for enhancing the hydrolysis of lignocellulosic, which further results in bioethanol production. Generally, pretreatment with NaOH is known to cause hemicellulose solubilization and removal from the biomass. The alkali pretreatment using NaOH induces delignification by extensively breaking the cross-ester bonding between complex lignin and hemicellulose carbohydrates like arabinoxylan (Jung et al. 2020). In this study, different concentrations of NaOH (1-5%) were utilized for pretreatment to analyze their effect on bagasse composition. Enhancing the alkali concentration per gram of biomass or extending the pretreatment duration can lead to the significant cleavage of ester-linking in the biomass. In their study, the researchers noted a substantial increase in the extraction of guaiacyl lignin (G type) through NaOH pretreatment in comparison to syringyl (S) and hydroxy phenyl (H) lignins (Laskar et al. 2013).

As shown in Fig. 1, as a result of alkali pretreatment, the cellulose content of SCB increased while hemicellulose and lignin decreased. The cellulose content showed a maximum increase of 57.6% at 2% NaOH concentration. When NaOH concentration was further increased, the cellulose content decreased, indicating that some of the glucan may have been partially decomposed. The obliteration of hemicellulose and lignin components exposes the cellulose fraction, making it

Table 1: Composition of raw SCB [ADL- Acid detergent lignin, AIA= Acid insoluble ash].

Properties	Components	Sugarcane bagasse
Compositional properties	Moisture [%]	6.4±0.2
	Cellulose (ADF-ADL) [%]	43.02±07
	Hemicellulose (NDF-ADF) [%]	26.5±0.6
	Lignin (ADL-AIA) [%]	16.6±0.9
Proximate properties	Ash [%]	4.27±0.4
	Total Organic Carbon [%]	46.6±1.2

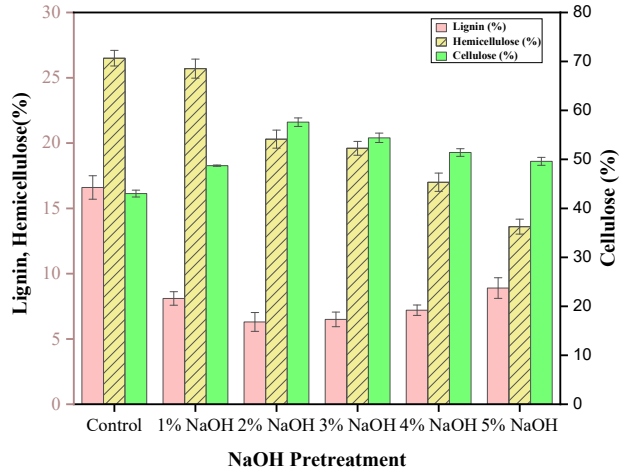

Fig. 1: Variation in composition of raw and NaOH treated (1-5%) sugarcane bagasse.

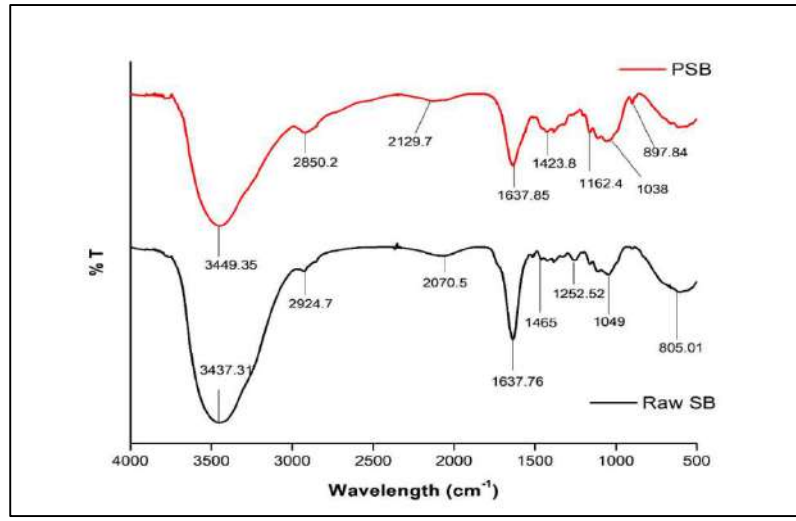

Fig. 2: FTIR spectrum of raw and 2% NaOH pretreated SCB.

more accessible to subsequent enzymatic hydrolysis or other conversion processes.

At lower NaOH concentrations (1-2%), the effect on hemicellulose content may be relatively moderate. At 2% NaOH concentration, the hemicellulose content decreased to 20.3%. These concentrations of NaOH can partially break down hemicellulose, leading to some degree of removal of hemicellulose from the sugarcane bagasse. However, a significant portion of hemicellulose may still remain in the pretreated biomass. As the concentration of NaOH was increased (3-5%), the effect on hemicellulose content became more pronounced. It decreased up to 13.6%. Higher concentrations of NaOH can lead to greater solubilization and removal of hemicellulose from the sugarcane bagasse. The results obtained in this study are consistent with the previous research conducted by Melesse et al. (2022) and Saad et al. (2023), which also displayed a decrease in hemicellulose content with an increased concentration of NaOH.

The lignin content of the SCB was significantly decreased with increased concentration of NaOH. At 2% and 3%, maximum removal of lignin, 62.04% and 60.8% were obtained, respectively. The decrease in lignin content varied from 46-56%, with an increase in NaOH concentration up to 5%. The loss of cellulose was considered while calculating hydrolysis yield efficiency. The present study compositional analysis showed that when NaOH concentrations above 2% were used it did not lead to significant removal of hemicellulose and lignin or enrichment of cellulose in the sample. Excessively high concentrations or prolonged exposure to NaOH can also lead to the degradation of

cellulose and lignin, impacting the overall composition and structural integrity of the biomass (Jin et al. 2020).

Characterization of Raw and Alkali Pretreated SCB

FTIR characterization: The spectra analysis of fresh (untreated) bagasse and bagasse after NaOH pretreatment revealed significant differences, indicating structural changes due to alkaline treatment, as shown in Fig.2. Between 3500 and 600 cm^{-1}, the unaltered fresh SCB and pretreated bagasse spectra showed the most noticeable differences in this range. The raw sugarcane bagasse showed a broad peak at 3400 to 3500 $cm^{-1,}$ which suggests the presence of the functional group -OH. The presence of $-CH_2$ groups was indicated by a stretching vibration of CH bonds at a 2924 cm^{-1} absorbance peak. The absorption at 1049 cm^{-1} represents the C-O-C stretching of the glycoside bond β-(1-4), indicating the presence of cellulose. In the bagasse spectrum, the O-H bending of the adsorbed water produces absorbance maxima at about 1637 $cm^{-1,}$ and similar results were reported by Wang et al. (2020).

The increased peak intensity between 900-1150 cm^{-1} indicates elevated levels of cellulose, suggesting an increase in cellulose content after delignification as presented in Fig. 2b. The absorbances around 1423.8, 1162 cm^{-1} were linked with the typical value of cellulose. The peak observed at 2924 cm^{-1} wavelength was contributed by the $-CH_2$ function group stretching in raw SCB, but after pretreatment of bagasse, the peak absorption shifted to 2850.2 cm^{-1}. After delignification, the NaOH peak at 1252.52 cm^{-1} diminished completely, indicating the effective removal of acetyl groups from hemicellulose. The absorbance at 1038 cm^{-1} contributes to the C-O stretching functional group at C-6, which is attributed to cellulose. The NaOH extracted bagasse spectrum showed an absorption peak at 1162 $cm^{-1,}$ which is related to the asymmetric stretching vibration of cellulose/hemicellulose C-O-C pyranose ring. The absorption frequency signals become very weak after NaOH pretreatment, indicating the breakage of linkages. Similar FTIR spectral results of raw and pretreated SCB were shown in previous studies conducted by Zhu et al. (2016), da Costa et al. (2023), and Saad et al. (2023).

Overall, the spectral analysis provides evidence of structural changes in the bagasse after delignification with NaOH. It suggests a decrease in lignin content, removal of acetyl groups from hemicellulose, and an increase in cellulose content, which are desirable changes for various applications of bagasse biomass.

FESEM morphological analysis: The use of FESEM allowed for the observation of changes in the morphology of biomass throughout the pretreatment process. Alkali-based pretreatments, such as alkaline peroxide or sodium hydroxide, can cause lignin swelling and redistribution, resulting in the exposure of cellulose-rich regions (Thite et al. 2019). The surface of the raw untreated biomass initially appeared to be smooth, compact, rigid, and tightly woven undamaged fibers, as presented in Fig. 3(a,b).

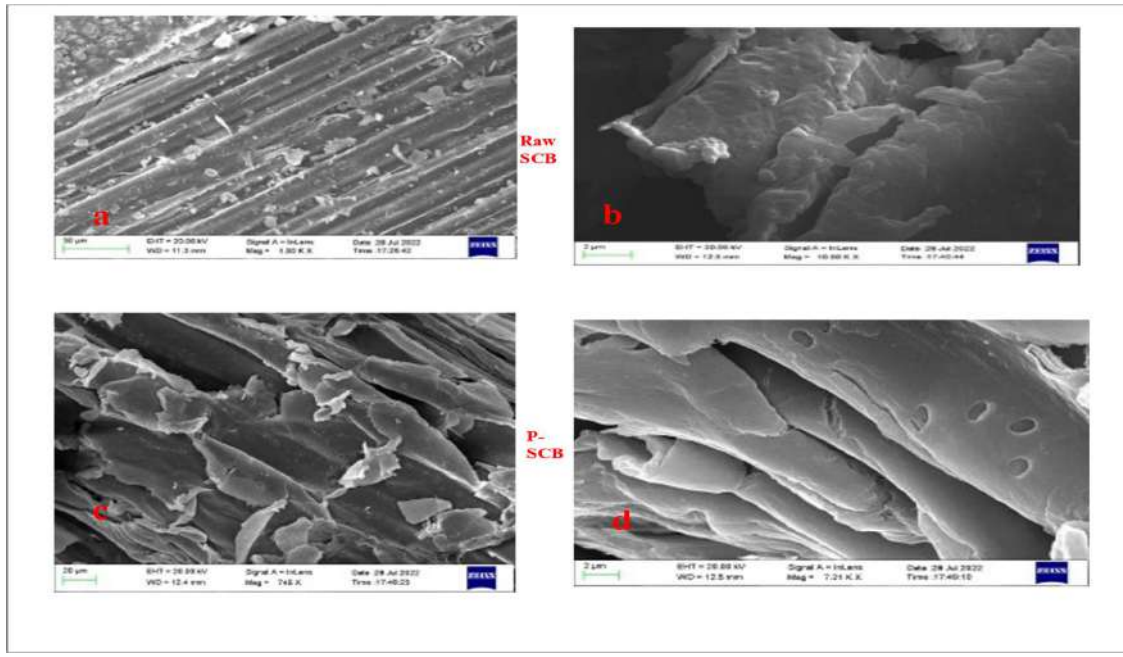

Fig. 3: FESEM images of raw SCB fragments (a,b) and 2% NaOH treated micrograph (c,d).

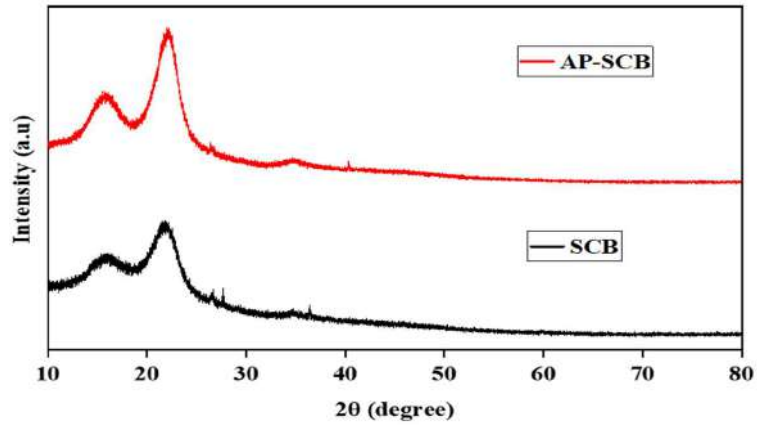

Fig. 4: XRD analysis of raw and alkali-pretreated sugarcane bagasse samples.

However, after alkali pretreatment, the biomass exhibited a disorganized or distorted appearance and also resulted in the formation of pores or holes. Increased porosity and a larger surface area that is accessible to enzymes resulted from the separation and full exposure of the microfibrils inside the biomass. The mild alkaline conditions (>1%) facilitate the breakdown of lignin and detach it from the fibers. As a result, the bundles of bagasse fibers start to dismantle. At higher concentrations of NaOH (2-3%), the bundles of bagasse fibers become more unstructured, resulting in complete detachment, as shown in Fig. 3(c,d). The enhanced porosity and increased enzyme-accessible surface area facilitated the enzymatic hydrolysis of the biomass. As a result of this hydrolysis process, the biomass underwent further degradation. Similar SCB morphological appearances from FESEM analysis have also been reported by Kumari et al. (2015) and Prajapati et al. (2020) after alkali delignification.

X-ray diffraction crystallinity analysis (XRD): The degree of crystallinity in alkali-treated SCB indicates the proportion of amorphous and crystalline cellulose components. The diffraction patterns consistently display peaks at approximately 2θ angles of 16.3 and 22.5° as observed in Fig. 4. These particular peaks correspond to the characteristic (100) and (002) planes of cellulose I. The SCB that was pretreated with sodium hydroxide showed a higher elevated peak compared to the untreated SCB biomass. After undergoing pretreatment, the structure and crystallinity of cellulose in the biomass may change due to the disruption of inter and intra-chain H-bonding of cellulosic fibrils. The cellulose is considered crystalline, while lignin and hemicellulose are amorphous, impacting the crystalline index (CrI) of complex biomass. The Segal method was employed to determine the CrI for the examined SCB samples (Kundu et al. 2023, Sharma et al. 2023). The raw SCB had a CrI value of 38.8%. In contrast, alkaline pretreatment resulted in CrI values of 53.64%. The reported observation underscores that crystallinity plays a pivotal role in enzymatic hydrolysis efficiency. This is attributed to the substantial crystalline structure of cellulose, which renders the biomass less accessible to enzymatic degradation. The pretreatment using dilute sodium hydroxide removed amorphous lignin and hemicellulose components (Alokika & Singh 2020). After pretreatment, the crystallinity index may increase due to the hydrolysis of glycosidic bonds in the exposed cellulose area. These findings align with various studies that have noted an uptick in this index value following biomass pretreatment (da Costa et al. 2023, Kininge & Gogate 2022, Melesse et al. 2022, Sharma et al. 2023).

Enzymatic Hydrolysis of Pretreated SCB

Enzymatic saccharification was conducted on SCB pretreated with different concentrations of sodium hydroxide using the Cellic ctec2 cocktail enzyme. Alkaline pretreatment is attributed to the substantial release of glucose and xylose during enzymatic hydrolysis due to the effective delignification process in biomass, cleaving bonds between complex structures of lignin and carbohydrates (Hans et al. 2021). The glucose yield (%) of delignified SCB at different time intervals is represented in Fig. 4. The hydrolysis of pretreated SCB is influenced by the enzymatic reaction time. The given result showed that with a longer reaction time, there was an increase in the concentration of released soluble reducing sugars. The bagasse that had been processed with 2% NaOH exhibited the highest concentration of glucose, measuring 12.34 ± 0.53 $g.L^{-1}$ at 48 h hydrolysis reaction time. Among the three different enzymatic reaction times applied, hydrolysis yields (%) of the 1% NaOH pretreated samples hydrolyzed at 24 h were found to be the lowest. The hydrolysis yields varied between 14.24 and 55.53% for different concentrations of alkali (NaOH) pretreatment

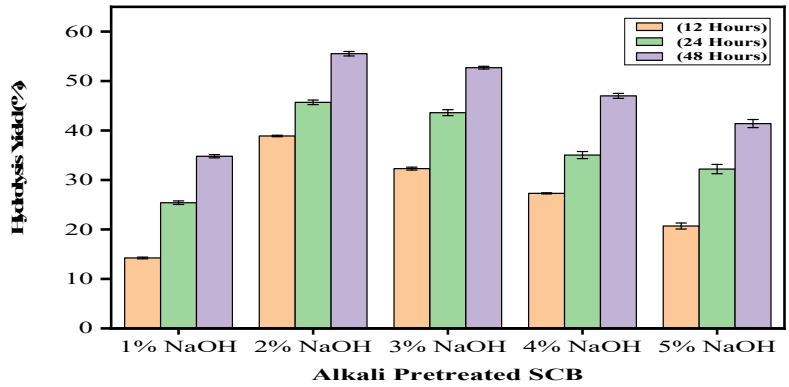

Fig. 5: Hydrolysis yield of pretreated (1-5%) SCB at 12, 24 and 48 hours.

(Fig. 5). Nosratpour et al. (2018) observed that pretreatment of sugarcane with 0.25 M sodium sulfite solution at 180°C provided 12.87g.L^{-1} of glucose when hydrolyzed with 10 FPU.g^{-1} of Cellic CTec2. Throughout the enzymatic hydrolysis process, the saccharified hydrolysates from various pretreated batches exhibited glucose as the primary reducing sugar, with significant amounts of xylose and minor quantities of cellobiose present. Tiwari et al. (2020) observed similar results with 5% and 10% NaOH pretreated sugarcane bagasse when hydrolyzed by Cellulase and xylanase enzymes, which were produced by a bacterial strain of *Pseudomonas sp*. *CVB-10* and *Bacillus paramycoides T4*. The maximum cellulose saccharification was obtained at 30 h of hydrolysis reaction time at a substrate concentration of 2%. The results showed that reducing sugar concentration increased with increasing reaction time. Sakuragi et al. (2018) conducted ammonia pretreatment on hardwood birch, which further resulted in glucose and xylose yields of 53.3% and 64.8%, respectively, after subjecting to 48 h of enzymatic hydrolysis employing a mixture of Cellic CTec2 and Cellic HTec2 enzymes (in a ratio of 1:1) at 4% v/v loading and 1% w/v solid concentrations at 37°C.

CONCLUSION

Among the potential feedstocks for 2nd generation bioethanol production, sugarcane bagasse stands out as a highly promising option. 2% NaOH was found to be an optimum concentration for sugarcane bagasse pretreatment. At this concentration, the maximum amount of delignification and cellulose extraction from biomass occurred. The raw sugarcane bagasse biomass had 16.6% lignin, which was reduced to 6.3%, and cellulose content increased to 57.6% from untreated 43.6%. Hydrolysis of pretreated solid residue was performed by an enzyme cocktail of Cellic CTec2, which is a complex of both cellulase and hemicellulase enzymes. The 12.34 g.L^{-1} of total reducing sugar was produced at 48 h of enzymatic reaction time which showed that saccharification efficiency improved as reaction time was increased from 12 to 48 h. Scanning electron micrograph of 2% NaOH pretreated bagasse showed the increase in porosity and disorderly appearance of biomass fiber fragments compared to the compact structure of untreated biomass. While FTIR results showed enrichment of cellulose content in pretreated SCB. The SCB's crystallinity increased based on the X-ray diffraction graph after treatment. This pretreatment process showed a promising positive effect in reducing biomass recalcitrance and higher glucan content, which can greatly facilitate catalytic hydrolysis and make saccharification easier. This, in turn, enables the production of high sugar concentrations and high ethanol concentrations during the fermentation process.

ACKNOWLEDGEMENT

The authors would like to extend their heartfelt appreciation to the Department of Environmental Science & Engineering and the Central Instrumentation Laboratory at Guru Jambeshwar University of Science & Technology, Hisar, for their valuable support and contribution to this study.

REFERENCES

Alarcón, E., Hernández, C., García, G., Ziarelli, F., Gutiérrez-Rivera, B., Musule, R. and Gardner, T.G. 2022. Changes in the chemical and structural composition of sugarcane bagasse caused by alkaline pretreatments [$Ca(OH)_2$ and NaOH] modify the amount of endoglucanase and β-glucosidase produced by Aspergillus niger in solid-state fermentation. Chem. Engg. Commun., 209(5): 594-606.

Alokika, M. and Singh, B. 2020. Enhanced production of bacterial xylanase and its utility in saccharification of sugarcane bagasse. Bioprocess Biosyst. Eng., 43: 1081-1091.

da Costa, R.A.M., Rubio-Ribeaux, D., Carneiro, B.C., Franco, P.M., de Azevedo Mendes, G., da Silva, I.L. and da Silva, S.S. 2023. Sugarcane bagasse pretreated by different technologies is used as a support and carbon source in solid-state fermentation by Aureobasidium pullulans LB83 to produce a bioemulsifier. Biomass Convers. Biorefin., 16: 1-14.

Ghose, T.K. 1987. Measurement of cellulase activities. Pure Appl. Chem., 59(2): 257-268.

Goering, H.K. and Van Soest, P.J. 1970. Forage Fiber Analyses (Apparatus, Reagents, Procedures, And Some Applications). Technical Report No. 379. US Agricultural Research Service, Washington DC.

Han, J. and Rowell, J. 1997. Chemical composition of agro-based fibers. Pap. Comp. Agro. Resour., 81:134.

Hans, M., Garg, S., Pellegrini, V.O., Filgueiras, J.G., de Azevedo, E.R., Guimaraes, F.E. and Kumar, S. 2021. Liquid ammonia pretreatment optimization for improved release of fermentable sugars from sugarcane bagasse. J. Clean. Prod., 281: 123922.

Jin, X., Song, J. and Liu, G.Q. 2020. Bioethanol production from rice straw through an enzymatic route mediated by enzymes developed in-house from *Aspergillus fumigatus*. Energy, 190: 116395.

Jung, W., Savithri, D., Sharma-Shivappa, R. and Kolar, P. 2020. Effect of sodium hydroxide pretreatment on lignin monomeric components of *Miscanthus giganteus* and enzymatic hydrolysis. Waste Biomass Valor., 11: 5891-5900.

Kininge, M.M. and Gogate, P.R. 2022. Intensification of alkaline delignification of sugarcane bagasse using ultrasound-assisted approach. Ultrason. Sonochem., 82: 105870.

Kumari, S. and Das, D. 2015. Improvement of gaseous energy recovery from sugarcane bagasse by dark fermentation followed by methanation process. Bioresour. Technol., 194: 354-363.

Kundu, S., Mitra, D. and Das, M. 2023. Influence of chlorite treatment on the fine structure of alkali pretreated sugarcane bagasse. Biomass Convers. Biorefin., 41: 1-15.

Laskar, D.D., Zeng, J., Yan, L., Chen, S. and Yang, B. 2013. Characterization of lignin derived from water-only flowthrough pretreatment of *Miscanthus*. Ind. Crops Prod., 50: 391-399.

Madadi, M., Nazar, M., Shah, S.W.A., Li, N., Imtiaz, M., Zhong, Z. and Zhu, D. 2023. Green alkaline fractionation of sugarcane bagasse at cold temperatures improves digestibility and delignification without the washing processes and release of hazardous waste. Ind. Crops Prod., 200: 116815.

Mandels, M. and Sternberg, D.J.J.F.T. 1976. Recent advances in cellulase technology. Hakko Kogaku Zasshi, 54(4): 1154.

Melesse, G.T., Hone, F.G. and Mekonnen, M.A. 2022. Extraction of cellulose from sugarcane bagasse optimization and characterization. Adv. Mater. Sci. Eng., 11: 121-136.

Miller, G.L. 1959. Use of dinitrosalicylic acid reagent for determination of reducing sugar. Anal. Chem., 31(3): 426-428.

Nasution, M.H., Lelinasari, S. and Kelana, M.G.S. 2022. A review of sugarcane bagasse pretreatment for bioethanol production. IOP Conf. Ser. Earth Environ. Sci., 963(1): 012014.

Nelson, D.A. and Sommers, L. 1983. Total carbon, organic carbon, and organic matter. Chem. Microbiol. Prop., 9: 539-579.

Nosratpour, M.J., Karimi, K. and Sadeghi, M. 2018. Improvement of ethanol and biogas production from sugarcane bagasse using sodium alkaline pretreatments. J. Environ. Manag., 226: 329-339.

Periyasamy, S., Karthik, V., Senthil Kumar, P., Isabel, J.B., Temesgen, T., Hunegnaw, B. and Nguyen, V.D.V. 2022. Growth of agricultural waste, its disposal, and related environmental issues: A review. Environ. Chem. Lett., 20(2): 1129-1152.

Prajapati, B.P., Jana, U.K., Suryawanshi, R.K. and Kango, N. 2020. Sugarcane bagasse saccharification using *Aspergillus tubingensis* enzymatic cocktail for 2G bio-ethanol production. Renew. Energy, 152: 653-663.

Saad, A.A., Ahmed, H.S., Megally, I.A.N., Ahmed, M., Ibraheem, M.T., Farouk, S.M. and Khalaf, E.S.A. 2022. Optimization and characterization of cellulose extracted from sugarcane bagasse. Int. Undergrad. Rese. Conf., 6: 1-9.

Sakuragi, K., Igarashi, K. and Samejima, M. 2018. Application of ammonia pretreatment to enable enzymatic hydrolysis of hardwood biomass. Polym. Degrad. Stab., 148: 19-25.

Sharma, S., Tsai, M.L., Sharma, V., Sun, P.P., Nargotra, P., Bajaj, B.K. and Dong, C.D. 2022. Environment-friendly pretreatment approaches for the bioconversion of lignocellulosic biomass into biofuels and value-added products. Environment,10(1): 6.

Sharma, V., Nargotra, P., Sharma, S., Sawhney, D., Vaid, S., Bangotra, R. and Bajaj, B.K. 2023. Microwave irradiation-assisted ionic liquid or deep eutectic solvent pretreatment for effective bioconversion of sugarcane bagasse to bioethanol. Energy Ecol. Environ., 8(2): 141-156.

Thite, V.S. and Nerurkar, A.S. 2019. Valorization of sugarcane bagasse by chemical pretreatment and enzyme-mediated deconstruction. Sci. Rep., 9(1): 15904.

Tiwari, S., Yadav, J., Gaur, R. and Yadav, J.S. 2020. Evaluation of pretreatment methods (acid and alkali) in improving the enzymatic saccharification of sugarcane bagasse: Structural and chemical analysis. Res. Sq., 14: 1-27

Wang, W., Wang X., Zhang, Y., Yu, Q., Tan, X., Zhuang, X. and Yuan, Z. 2020. Effect of sodium hydroxide pretreatment on physicochemical changes and enzymatic hydrolysis of herbaceous and woody lignocellulose. Ind. Crops Prod., 145: 112145.

Wunna, K., Nakasaki, K., Auresenia, J., Abella, L. and Gaspilo, P.A. 2021. Enhancement of Delignification and Glucan Content of Sugarcane Bagasse by Alkali Pretreatment for Bioethanol Production. Asean J. Chem. Eng., 21(2): 133-142.

Zhu, Z., Rezende, C.A., Simister, R., McQueen-Mason, S.J., Macquarrie, D.J., Polikarpov, I. and Gomez, L.D. 2016. Efficient sugar production from sugarcane bagasse by microwave-assisted acid and alkali pretreatment. Biomass Bioenergy, 93: 269-278.

Nature Environment and Pollution Technology
An International Quarterly Scientific Journal

p-ISSN: 0972-6268
(Print copies up to 2016)
e-ISSN: 2395-3454

Vol. 23 | No. 1 | pp. 435-442 | 2024

Original Research Paper

https://doi.org/10.46488/NEPT.2024.v23i01.038

Open Access Journal

Threshold Effect of Trade on Climate Change in South Africa

Teboho J. Mosikari*† and Kesaobaka Mmelesi**
*Department of Economics, North-West University, South Africa
**School of Economics, University of Johannesburg (UJ), South Africa
†Corresponding author: Teboho J. Mosikari; tebohomosikari@gmail.com

Nat. Env. & Poll. Tech.
Website: www.neptjournal.com

Received: 20-05-2023
Revised: 05-07-2023
Accepted: 07-07-2023

Key Words:
Trade
Climate change
South Africa
Threshold regression

ABSTRACT

The relationship between trade and climate change is not a simple linear relationship. In this paper, using the threshold regression model, we estimated the effect of trade on climate change in South Africa. The paper applied the LM test to examine the nonlinear inference approach to test whether nonlinearity existed and if the threshold model was relevant to the study. The results show that when energy use is set as the threshold variable, the relationship between trade and climate change measured as methane is U-shaped. Also, in other models of GHG as climate change indicators, the results show that the effect of trade on climate change is not dynamic. This result supports the idea that high and low trade effects may have different impacts on climate change indicators. It is, therefore, recommended that all exporters in South Africa resort to more innovative environmental mechanisms to reduce the contribution to climate. The suggestion for future studies is to consider exports of different sectors to climate change. This approach will avoid the generalization of exporting firms as the worst emitters.

INTRODUCTION

Climate change is presently being recognized as a dominant problem in humankind leading to wide research that roots and affects the environmental degradation of the climate (Khan et al. 2022). However, not a shock that Beeson (2010) has described the atmosphere as a vital public policy issue. Around the world, several public sectors have embraced an environmental protection policy. For instance, France mandated that every registered company submit a report on how their operations may benefit or harm the environment. In most worldwide solutions to climate change, the significance of the environmental issue and the urgency of lowering greenhouse gas emissions are frequently highlighted.

Despite this, the "United Nations Framework Convention" on Climate Change 1992, the "Kyoto Protocol" 1997, the "Doha Agreement" 2012, and the "Paris Agreement" 2016 established the objectives and commitments from both developed and developing countries to reduce GHG emissions by producing and consuming less carbon. Carbon emissions are known to be the primary cause of global warming (Balogh & Jambor 2017, Friedl & Getzner 2003), while anthropogenic greenhouse gas emissions are known to be the primary cause of climate change (Appiah et al. 2019, Tang & Tan 2015).

Trade openness includes nations that purchase specific goods they are unable to produce from other nations and export goods that profit from their lower opportunity costs. Then, as part of the international exchange process, items are moved from one economy to another during manufacturing to the final point of consumption. However, increases in trade openness could lead to an increase in transport services in both countries, for instance, when importing and exporting from different nations. The correlation between trade and climate change has drawn the attention of many economists, policymakers, and members of society today. In recent literature, it is presumed that trade has profound effects on climate change. The scale impact predicts that more trade will result in increased energy consumption, which would, therefore, result in increased environmental deterioration. Free trade may have negative or positive environmental effects depending on "size, technique, and content," according to Antweiler et al. (2001).

Furthermore, economic growth brought on by commerce may have an impact on the environment. Economic expansion initially has a detrimental influence on the environment because of the extensive consequences of increased energy use. Nevertheless, in the long run, it might benefit the ecology.

African region contributed 2.5% to the international anthropogenic carbon dioxide emissions from 1980–2005 (Canadell et al. 2009). Even though "sub-Saharan Africa's" (SSA) emissions are the slightest internationally, this has

been rising in the previous era. Since the significance of this hasty population upsurges in "carbon emissions" related to the contrary impacts, they are more worrying. Despite housing 14% of the world's population, the SSA has one of the fastest rates of population increase in the world and emits 7.1% of all GHGs (The Economist 2018).

A developing country, such as South Africa, is one of the major emitters of carbon emissions, accounting for 1.09% of global emissions (World Bank 2021). South Africa is currently ranked fifteenth in terms of annual carbon dioxide emissions. The country is primarily reliant on the energy sector, as coal is the main fuel used. This makes South Africa an even more intriguing place for this study. Even with South Africa's trade policy revisions, its conservation impact is being established as one that receives less attention (World Bank 2021). The issue of how this trade is affecting the environment or carbon dioxide emissions is now on the rise. This is the central question of this paper is to understand the effect of trade on climate change in South Africa.

Firstly, our paper contributes to the existing literature by applying the novel threshold regression by Bruce & Hansen (2000). This method provides an advantage over traditional regression in the sense that the method models the phenomena depending on change points or thresholds. Threshold regression provides a simple but elegant and interpretable way to model certain kinds of nonlinear relationships between the outcome (climate change) and a predictor (trade). *Secondly*, our paper contributes by exploring the use of three measures for climate change which are methane, nitrous oxide, and greenhouse gas emissions. This approach is very critical in the sense that it will provide a more inclusive view on measures of environmental quality, and this may avoid misleading policymaking by only using one measure of climate change.

The study Is organized as follows for the remaining portions. The literature is examined in Section 2. Section 3 presents the research method. While Section 4 provides results and discussion. Section 5 presents the conclusions of the study.

PAST STUDIES

The first to offer a theoretical framework for the environmental consequences of economic openness were Grossman & Krueger (1995) and Copeland & Taylor (1994). Multiple elements influencing carbon emissions and the ways that trade can have an impact on the environment are highlighted by Antweiler et al. (2001), who further expanded on it. To classify the environmental influences, the study divides them into effects of composition, method, and scale. The degree of environmental deterioration is influenced by the structural nature of an industrialized country's output. This structural composition, therefore, has an environmental influence, which is captured by the composition effect. Because people like a clean environment and stricter environmental rules are implemented as income levels rise, the technique effect leads to greater environmental quality (Kebede 2017). While less developed countries with loose and compromised environmental standards constantly prioritize producing more products with a high pollution footprint, industrialized nations with stringent environmental controls often manufacture fewer products with a significant carbon footprint.

Numerous studies in empirical literature have investigated the relationship between trade and climate change. However, across a range of methodological frameworks and countries under examination, the outcomes of these studies are generally unclear and conflicting. The empirical study by Ibrahim & Ajide (2021a) found that trade openness raises CO_2 emissions in the G-7. Similar results were provided by Van Tran (2020), who showed that, between 1971 and 2017, 66 developing economies' environmental conditions deteriorated because of trade. In contrary Dogan and Turkekul (2016) conducted an analogous analysis in the USA to determine the relationships between carbon emissions, urbanization, economic development, trade, energy depletion, and financial expansion. The findings demonstrated that more trade helps the US environment. Furthermore, Ibrahim & Ajide (2021b) found that trade openness slows down environmental deterioration in the setting of G-20 countries using the common correlated effect mean group (CCEMG) and mean group (MG).

The literature further demonstrates in developing economies, trade facilitation (TF) as a measure of trade openness for 48 Sub-Saharan African countries from 2005 to 2014. Ibrahim and Ajide (2022) conclude that TF is environmentally friendly and raises environmental quality in the area. The work of Adams and Osei-Opoku (2020) employed a time series from 1995 to 2014 and focused on 22 Sub-Saharan African countries. The paper examined the relationship between two carbon emissions indicators and trade performance (split into imports, exports, and total commerce) as well as figures on territory-based carbon emissions. It was found that trading generally lowers emissions using the system's generalized method of moments. Appiah et al. (2022) used the Driscoll-Kraay error's regression in pooled OLS to determine the long-run coefficients. The results show that increased exports and urbanization are reported to benefit the environment of emerging countries, albeit this gain is not statistically

significant. Khan & Ozturk (2021), by using the difference and system generalized method of moment models, discovered that between 2000 and 2014, 88 developing nations' CO_2 emissions increased because of trade. Similar findings were made by Ali et al. (2020), who discovered that the Organization of Islamic Cooperation countries' exposure to the global commodities market results in a significant deterioration of those countries' environmental circumstances.

The literature further shows that for developing single countries, the study by Khan et al. (2022) found that Pakista's openness to trade makes the environment's condition worse. Furthermore, the paper by Halicioglu (2009) examined the relationship between foreign trade, energy use, income, and carbon emissions in Turkey. The paper found a long-term connection between global trade and pollution emissions. Antweiler et al. (2001) investigated how pollutant concentrations are impacted by global trade in products. Findings showed that when the overall composition of national production is changed, foreign trade causes a minor marginal shift in environmental degradation. There are also empirical papers in China regarding trade and climate change. The paper by Weber et al. (2008) on trend analysis suggests that the main reason for the rise in China's CO_2 emissions is an increase in exports.

Furthermore, Chinese researchers examined the relationship between trade exports and carbon emissions (Xuemin 2009). The analysis revealed a two-way causal relationship between trade exports and CO_2 emissions, leading to the conclusion that exports had a significant impact on China's emissions level. Toda and Yamamot's causality test and the vector autoregression approach were both used by Michieka et al. (2013) to investigate the relationship between CO_2 emission, coal use, and export commerce in China for the period 1970 to 2010. The findings revealed that there is a cointegration between exports and carbon emissions. Jalil & Mahmud (2009) have established the long-term connections between environmental degradation, energy consumption, income, and international commerce in China. The paper used time series data for the years 1975 to 2005. Their research paper shows that trade opening has been beneficial but is classed as having a statistically modest effect. The analysis demonstrates that trade liberalization has improved China's environment, yet it is deemed to have a statistically minor impact. In the South African context, an empirical study by Udeagha & Ngepah (2019, 2022) demonstrates that access to global markets for goods causes the environment to deteriorate over time in South Africa. The author'' analysis also reveals a strong link between CO_2 emissions and trade openness.

According to the literature above, numerous empirical studies have been conducted to examine trade and climate change in industrialized and developing countries. There have been inconsistent results from earlier empirical studies on the relationship between trade and climate change, ranging from the assertion that rising trade leads to rising concerns about climate change. Empirical research has produced uneven and typically mixed results. All these earlier studies, such as Jalil & Mahmud (2009), Xuemin (2009), and Udeagha & Ngepah (2019), only used one measure of climate change as opposed to different measures analytically and for policy. Our paper gives estimation results for both, which also aids in testing the reliability of our findings. Different from these previous studies, this study investigates trade and climate change in South Africa.

MATERIALS AND METHODS

The study adopts and modifies the model used by Michieka et al. (2013) to explore the impact of trade on climate change in South Africa. The econometric model takes on the following form:

$$CC_t = \alpha_0 + \alpha_1 URP_t + \alpha_2 EPT_t + \theta_t \quad \ldots(1)$$

Where CC_t accounts for climate change, in which for this study is measured using various indicators such as Met_t which is the methane, Nit_t to describe nitrous oxide and Nit_t greenhouse gas emissions. These indicators serve as the dependent variables for each variation of equations to be considered. The independent variables to be considered are EU energy use, URP, which is the urban population, and EPT is the export of goods to measure the trade component of the study. The empirical literature is widely suggesting that there may be a non-linear relationship between trade and climate change. Hence, according to Bruce & Hansen (2000), the current study develops an econometric model with a single threshold model and is as follows:

$$CC_t = \alpha_0^1 + \alpha_1^1 URP_t + \alpha_2^1 EPT_t + \theta_t, \ \ if \ q_t \leq \gamma > \alpha_0^2 + \alpha_1^2 URP_t + \alpha_2^2 EPT_t + \theta_t, \ \ if \ q_t > \gamma \quad \ldots(2)$$

Where q_t is the threshold variable used to split the sample into regimes, for the current study, is EU_t energy use and the parameter value is unknown. This type of estimation strategy allows the role of nuclear energy to differ depending on whether the carbon emissions are below or above some unknown level of gamma. In this model, GDP acts as a sample-splitting or threshold variable. The effect of nuclear energy on carbon emissions is designated β_1^1 and β_2^1 for low carbon emissions or β_1^2 and β_2^2 for high carbon

Table 1: Data source and description.

Abbreviation	Variable description	Data source
met	Methane emissions (kt of CO_2 equivalent)	United Nations Framework Convention on Climate Change.
Nit	Nitro oxide	IEA Statistics OECD/ IEA 2014
GHG	GHG net emissions/ removals by LUCF (Mt of CO_2 equivalent)	Climate Watch. 2020. GHG Emissions. Washington, DC: World Resources Institute
URP	Urban population	World Bank
EU	Energy use (kg of oil equivalent per capita)	IEA Statistics OECD/ IEA 2014
EXP	Exports of goods and services (% of GDP)	World Bank

emissions. On the other hand, under the hypothesis $\beta_1 = \beta_2$ the model becomes linear and reduces to (1).

This paper employs a time series of data from 1990 to 2020 for South Africa. Depending on data availability, data for the period 1990 to 2020 is adequate for maximizing the number of collected observations to investigate the effects of trade on climate change. Table 1 depicts the list of the variables used in the study.

RESULTS AND DISCUSSION

Graphical and descriptive statistics are used to describe the basic characteristics of the data that are employed in the study. In a preliminary analysis, the study examined each variable at levels and first differences. The study explored the time series plots of variables in levels. Fig. 1, therefore, presents all the variables. It shows that Methane (Met), nitrous-oxide (Nit), greenhouse gases (GHG), exports of goods (EXP), and energy use (EU) have a random walk, whereas the urban population (URP) has an upward trend.

The descriptive statistics of the variables of the study are presented in Table 2. In South Africa, the average export of goods was around 3.21% from 1990 to 2022, whereas for the urban population, it was 17.17, and for energy use, it was 7.86. and for climate change indicators, for methane was 11.18, for Nitrogen was 2.97, and for greenhouse gases was 2.23. South Africa had a maximum greenhouse gas at 2.37%, where methane was 11.29 and 3.04 for nitrous oxide.

As the basis approach to empirical analysis, in the current paper, we primarily estimated the linear model given in equation (1). Estimation results are presented in Table 3. The table shows 3 variations of regression results, where the dependent variable climate change is measured in terms as Met_t which is the methane, Nit_t to describe nitrous oxide and Nit_t greenhouse gas emissions.

The linear model shows that the effect of trade on climate change has different effects on different measures. Specifically, results show that trade has a positive effect on climate change when it is measured as nitrous oxide and greenhouse gas emissions. Whereas trade on climate change measured as methane it shows a negative effect, but it is not statistically significant. For the control variable, urban population, the results show that when climate change is measured as methane and greenhouse gases, their trade has a positive effect, and the parameters are statistically significant. As the literature indicated, the relationship between trade on climate change can also be non-linear in nature; therefore, the current paper explores such a relationship.

Bruce & Hansen's (2000) procedure also must test whether the true relation given in equation (1) is linear or not. The LM-test statistic was applied to test the linearity of data as the null hypothesis. From the three models, it is evidenced that the models Met and GHG are significant. The LM-test statistics are calculated as 8.664 (with p-value = 0.048) and 16.593 (0.00), respectively (Table 4). Therefore, those models imply that nonlinearity was quite acceptable. For Nit as the climate change indicator, the results failed the test on non-linearity.

In detecting nonlinearity, the paper applied the LM test proposed by Bruce & Hansen (2000), which allowed the study to understand if a threshold effect existed for each of the explanatory variables. Table 5 presents test results for the threshold effects of trade on climate change with a control variable as the urban population. The table reports the three models measuring climate change as methane, Nitrogen,

Table 2: Descriptive statistics of variables.

Variable	Obs	Mean	Std. Dev.	Min	Max
Met	32	11.187	.087	11.054	11.291
Nit	32	2.97	.034	2.89	3.043
GHG	32	2.239	.076	2.118	2.37
Urp	32	17.172	.221	16.768	17.523
Eu	32	7.862	.058	7.737	7.99
Exp	32	3.213	.147	2.942	3.474

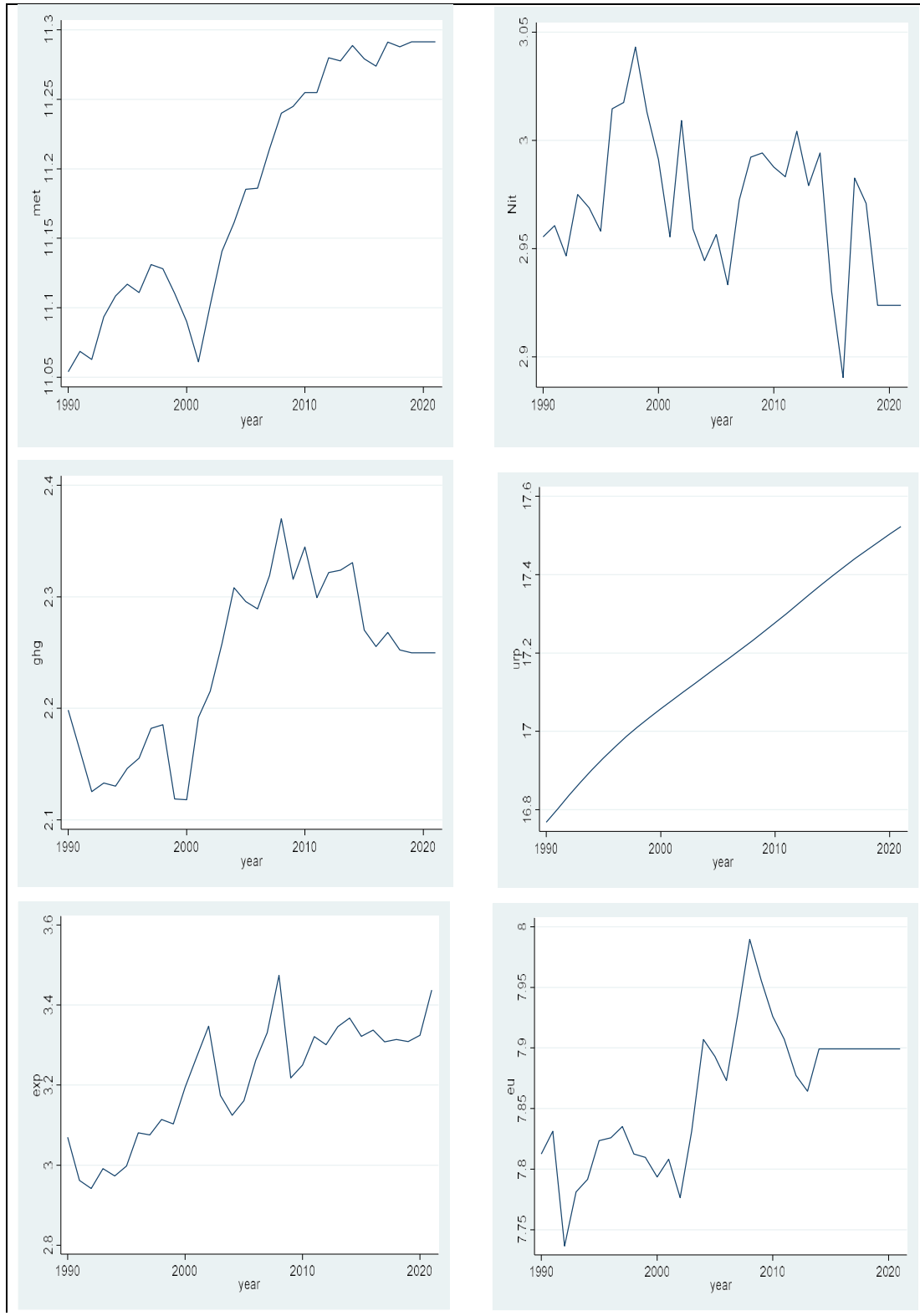

Fig 1: Line graphs for all variables of the study.

Table 3: OLS Estimation without threshold.

	Met	Nit	GHG
Intercept	4.305	4.459	0.205
	(5.732)***	(7.544)***	(0.205)
URP	0.415	-0.105	0.062
	(6.792)***	(2.560)***	(0.794)
EXP	-0.080	0.102	0.298
	(0.816)	(2.138)***	(2.504)***
R-squared	0.895	0.152	0.550

Table 4: Results of the threshold test.

	Met	Nit	GHG
LM-test for no threshold:	8.664	4.630	16.593
Bootstrap P-Value:	0.048**	0.611	0.000***

and greenhouse gases. It is important to mention that the nitrogen model is not significant for threshold analysis but is just presented for observation purposes.

From the model of Met, the results show that when energy use is set as the threshold variable, the relationship between trade and climate change measured as methane is U-shaped. It shows that when energy use is above 7.83, trade has a positive effect on climate change. This implies that a 1% increase in trade will result from a positive effect on climate change (methane) with a 0.208% change. Also, the results show that when energy use is below 7.83, trade has a negative effect on climate change, measured as methane.

This implies a 1% increase in trade, which will result negative effect on climate change with 0.104% change. For the control variable, urban population, it shows that in both regimes, urban population has a positive effect on climate change, and the effect is statistically significant. For the GHG model, the results show that trade has a positive effect on climate change in both regimes. It shows that when energy use is below 7.83, trade has a positive effect on climate change measured as greenhouse gases. This implies that a 1% increase in trade will result from a positive effect on climate change (greenhouse gases) with a 0.231% change. Also, the results show that when energy use is above 7.83, trade has a positive effect on climate change measured as greenhouse gases. This implies a 1% increase in trade, which will result from a positive effect on climate change with a 0.224% change. For the GHG model, it can be concluded that the effect of trade on climate change is not dynamic.

Fig. 2 presents the normalized likelihood value using the likelihood ratio sequence for all the models estimated in this paper. The Likelihood Sequence (LS) parameter of is the value that minimizes these graphs at 7.83%. The 95% critical value line is plotted with a confidence interval of asymptotic

Table 5: Threshold regression results.

	Met	Nit	GHG
Threshold	7.835	7.835	7.835
Intercept_0	6.502	-0.364	2.475
	(8.993)***	(-0.342)	(0.942)
URP_0	0.308	0.206	-0.060
	(6.039)***	(0.287)	(-0.348)
EXP_0	-0.208	-0.051	0.231
	(-3.250)***	(-0.698)	(2.242)***
Intercept_1	6.080	5.186	6.553
	(17.421)***	(7.113)***	(11.125)***
URP_1	0.278	-0.145	-0.288
	(13.900)***	(-3.222)***	(-8.470)***
EXP_1	0.104	0.087	0.224
	(3.058)***	(0.165)	(5.209)***

95%, which crosses the dotted line. These findings suggest that there is support for two regime sampling for Met and GHG models only.

CONCLUSION

The climate change influence from trade has been strongly argued over the recent years. This paper aimed to investigate the threshold impact of trade on climate change for the period 1990 to 2022. Our paper used the methodology developed by Bruce & Hansen (2000), which allows the data to endogenously split the sample into two regimes. The current paper made an argument that it is best to measure climate change in different ways to avoid misspecification. The study applied different measures such as methane (Met), nitrous oxide (Nit), and greenhouse gases (GHG) as indicators of climate change in South Africa. The paper used energy use as the threshold variable. Therefore, three models were estimated, and climate change was proxied as Met, Nit, and GHG as the dependent variables.

The paper tested in all models of climate change indicators whether nonlinearity exists and if the threshold model is appropriate in each case. It was found that only two models passed the test of non-linearity which is the Met model and GHG model. The results show that when energy use is set as the threshold variable, the relationship between trade and climate change measured as methane is U-shaped. Also, in other models of GHG as climate change indicators, the results show that the effect of trade on climate change is positive in all regimes. This result supports the idea that high and low trade effects may have different impacts on climate change indicators, especially when climate change is measured as Methane.

Policy implication from this study is the importance of policymakers' approach to the idea of climate change. Policy design must be specific to a particular indicator in the fight

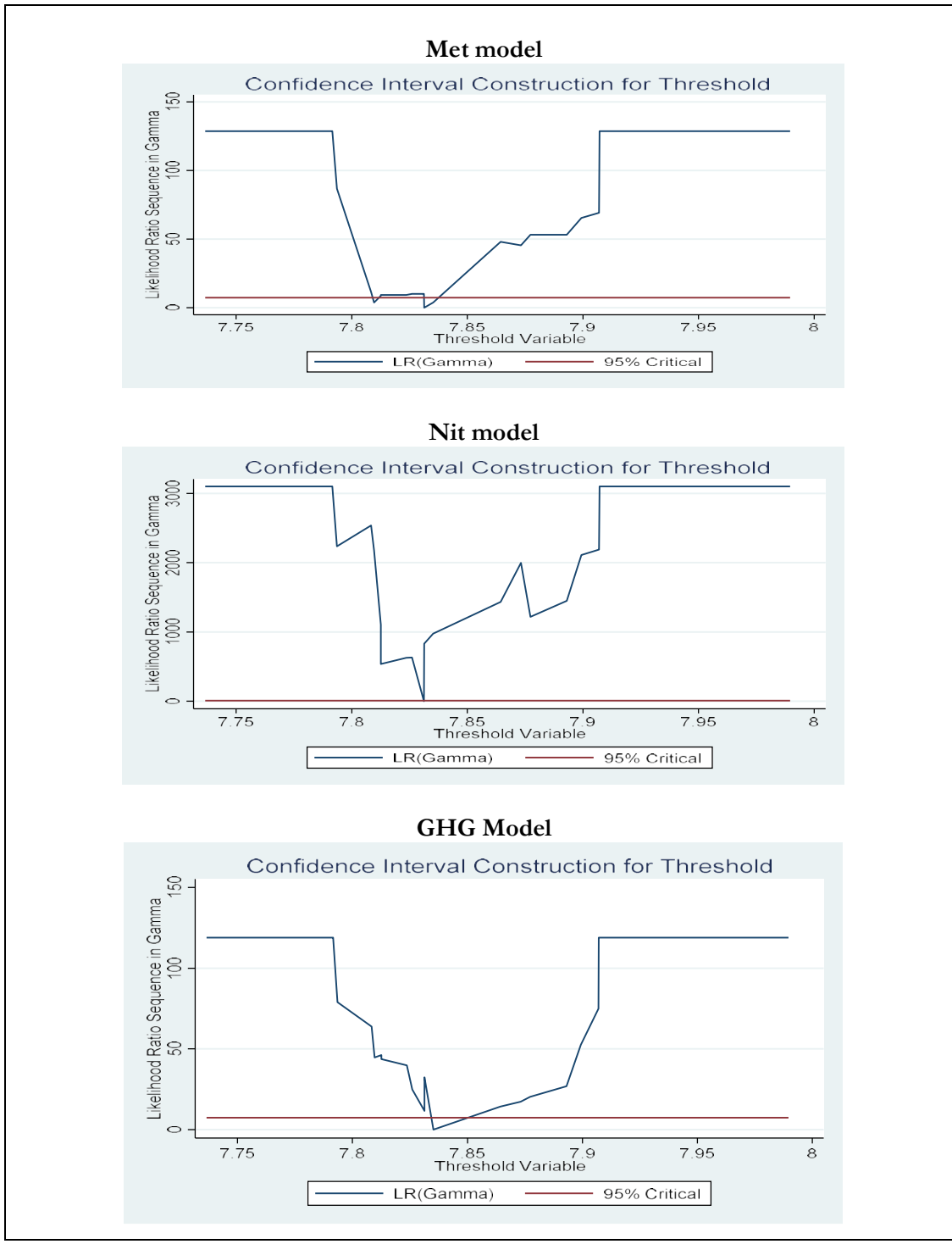

Fig. 2: Confidence interval construction for the threshold levels.

to mitigate climate change. Also, the result of this study implies that after a certain level (threshold) of energy use, exports seem to deteriorate the environment. It is, therefore, recommended that all exporters in South Africa resort to more innovative environmental mechanisms to reduce the contribution to climate. The suggestion for future studies is

to consider exports of different sectors to climate change, and this approach will avoid the generalization of exporting firms as the worst emitters.

REFERENCES

Adams, S. and Osei-Opoku, E.E. 2020. Trade and environmental pollution in Africa: Accounting for consumption and territorial-based emissions. Environ. Sci. Pollut. Res., 27: 44230-44239 https://doi.org/10.1007/s11356-020-10328-8.

Ali, S., Yusop, Z., Kaliappan, S.R. and Chin, L. 2020. Dynamic common correlated effects of trade openness, FDI, and institutional performance on environmental quality: evidence from OIC countries. Environ. Sci. Pollut. Res. Int., 27(11): 11671-11682. https://doi.org/10.1007/s11356-020-07768-7.

Antweiler, W., Copeland, B.R. and Taylor, M.S. 2001. Is free trade good for the environment? Am. Econ. Rev., 91(4): 877-908.

Appiah, K., Du, J., Yeboah, M. and Appiah, R. 2019. The causal relationship between industrialization, energy intensity, economic growth, and carbon dioxide emissions: Recent evidence from Uganda. Int. J. Energy Econ. Policy, 9(2): 237-245.

Appiah, K., Worae T.A., Yeboah B. and Yeboah M. 2022. The causal nexus between trade openness and environmental pollution in selected emerging economies. Ecol. Indic., 138: 108872.

Balogh, J.M. and Jambor, A. 2017. Determinants of CO_2 emission: A global evidence. Int. J. Energy Econ. Policy, 7(5): 217-226.

Beeson, M. 2010. The coming of environmental authoritarianism. Environ. Politics, 19(2): 276-294. DOI: https://doi.org/10.1080/09644010903576918.

Bruce, E. and Hansen, B.E. 2000. Sample splitting and threshold estimation. Econometrica, 68(3): 575-604.

Canadell, J.G., Raupach, M.R. and Houghton, R.A. 2009. Anthropogenic CO_2 emissions in Africa. Biogeosci., 6: 463-468. DOI https://doi.org/10.5194/bg-6-463-2009.

Copeland, B.R. and Taylor, M.S. 1994. North-South trade and the environment. J. Econ., 109(3): 755-787. https://doi.org/10.2307/2118421.

Dogan, E. and Turkekul, B. 2016. CO_2 emissions, real output, energy consumption, trade, urbanization, and financial development: testing the EKC hypothesis for the USA. Environ. Sci. Pollut. Res., 23(2): 1203-1213.

Friedl, B.B. and Getzner, M. 2003. Determinants of CO_2 emissions in a small open economy. Ecol. Econ., 45(1): 133-148.

Grossman, G. and Krueger, A. 1995. Economic growth and the environment. J. Econ., 110(2): 353-377. https://doi.org/10.2307/2118443.

Halicioglu, F. 2009. An econometric study of CO_2 emissions, energy consumption, income and foreign trade in Turkey. Energy Policy, 37(3): 1156-1164.

Ibrahim, R.L. and Ajide, K.B. 2021a. Non-renewable and renewable energy consumption, trade openness, and environmental quality in G-7 countries: the conditional role of technological progress. Environ. Sci. Pollut. Res., 28: 45212-45229.

Ibrahim, R.L. and Ajide, K.B. 2021b. Disaggregated environmental impacts of non-renewable energy and trade openness in selected G-20 countries: the conditioning role of technological innovation. Environ. Sci. Pollut. Res., 28: 67496-67510.

Ibrahim, R.L. and Ajide, K.B. 2022. Trade facilitation and environmental quality: empirical evidence from some selected African countries. Environ. Dev. Sustain., 24(1): 1282-1312.

Jalil, A. and Mahmud, S.F. 2009. Environment Kuznets curve for CO_2 emissions: A cointegration analysis for China. Energy Policy, 37(12): 5167-5172.

Kebede, S. 2017. Modeling energy consumption, CO_2 emissions and economic growth nexus in Ethiopia: evidence from ARDL approach to cointegration and causality analysis. Munich Personal RePEc Archive (MPRA) Paper No. 83214.

Khan, A., Safdar, S. and Nadeem, H. 2022. Decomposing the effect of trade on the environment: a case study of Pakistan. Environ. Sci. Pollut. Res., 30: 3817-3834. https://doi.org/10.1007/s11356-022-21705-w

Khan, M. and Ozturk, I. 2021. Examining the direct and indirect effects of financial development on CO_2 emissions for 88 developing countries. J. Environ. Manage., 293: 112812. https://doi.org/10.1016/j.jenvman.2021.112812.

Michieka, N.M., Fletcher, J. and Burnett, W. 2013. An empirical analysis of the role of China's exports on CO_2 emissions. Appl. Energy, 104(C): 258-267.

Tang, C.F. and Tan, B.W. 2015. The impact of energy consumption, income, and foreign direct investment on carbon dioxide emissions in Vietnam. Energy, 79(C): 447-454. doi: 10.1016/j.energy.2014.11.033.

The Economist. 2018. A burning issue in Africa: Africa's big carbon emitters admit they have a problem. https://www.economist.com/middle-east-and-africa/2018/04/21/africas-big-carbon-emittersadmit-they-have-a-problem.

Udeagha, M.C. and Ngepah, N. 2019. Revisiting trade and environment nexus in South Africa: Fresh evidence from new measure. Environ. Sci. Pollut. Res., 26(28): 29283-29306. https://doi.org/10.1007/s11356-019-05944-y.

Udeagha, M.C. and Ngepah, N. 2022. Does trade openness mitigate the environmental degradation in South Africa? Environ. Sci. Pollut. Res., 29(13): 19352-19377. https://doi.org/10.1007/s11356-021-17193-z.

Weber, C.L., Peters, G.P., Guan, D. and Hubacek, K. 2008. The contribution of Chinese exports to climate change. Energy Policy, 36(9): 3572-3577.

World Bank. 2021. World development indicators. http://www. World bank. org (Accessed 15 Oct 2021).

Xuemin, N. 2009. A Survey on Interrelationship between Carbon Emission and Exports in China. Ecol. Econ., 11: 1873-6106.

Nature Environment and Pollution Technology
An International Quarterly Scientific Journal

p-ISSN: 0972-6268
(Print copies up to 2016)
e-ISSN: 2395-3454

Vol. 23 | No. 1 | pp. 443-450 | 2024

Original Research Paper

https://doi.org/10.46488/NEPT.2024.v23i01.039

Open Access Journal

An Investigation in Temperature Data Analysis of Middle Atmospheric Variation from SABER Satellite

E. Raghavendrakumar*†, V. Kamalakar* and K. Sunil Kumar**

*Department of Physics, Veltech Rangarajan Sagunthala R&D Institute of Science and Technology, Avadi-600 062, Tamil Nadu, India

**Department of Mechanical Engineering, Mohamed Sathak A.J. College of Engineering, IT park, Siruseri, Chennai, 603103, India

†Corresponding author: E. Raghavendrakumar; raghavanaidu212@gmail.com

Nat. Env. & Poll. Tech.
Website: www.neptjournal.com

Received: 06-06-2023
Revised: 05-07-2023
Accepted: 14-07-2023

Key Words:
Saber Satellite
Temperature deviation
Ozone deviation
Middle atmosphere

ABSTRACT

This paper focuses on significant data analysis for middle atmospheric variations of height of 0 km 100 km. This data was downloaded from the SABER satellite NASA and analyzed with the help of MATLAB. The analysis includes the determination of propagation of wavelengths and oscillations for the semi-annual oscillation (SAO), Annual oscillations (AO), quasi-annual oscillations (QBO), EINIO southern oscillation (ENSO) from the period of Jan 2002 to Dec 2022 past twenty years data. The monthly mean Temperatures, monthly ozone deviations, and overall mean temperatures with standard deviations are estimated for the following altitude regions concerning troposphere (0-20km), stratospheric (21-50 km), mesospheric (51-90 km), and thermospheric regions (91-105 km). However, the results proved that the maximum temperature variations would affect the ozone depletion for the areas concerning the altitude height of 15-40 km region between troposphere and stratospheric in the temperature range of 260K, and average deviations are found in the order of 0.000010 μm for the troposphere region. The presence of harmful gases such as CO, CO_2, NOx, H, and CH_4 released from the automobile and powerplant industry may deplete the ozone layer and cause adverse effects.

INTRODUCTION

The region is subdivided into three categories: 0-10 N, 10-20 N, and 20-30 N. It is necessary to predict the ozone layer variations that occur due to the evolution of various gases and high temperature-based air from different sources like automobiles and power plant-based industries, resulting in higher temperature variations that affect the ozone layer and form global warming (Hansen et al. 2016). The major constituents present in the exhaust gases, such as NO_X, CO, CO_2, H, and S, will affect the atmosphere and may cause serious adverse effects on humans and other living organisms (Samad & Shah 2017). The movement of gases from lower attitudes to higher attitudes by the impact of higher densities in the form of turbulent motion causes the change in atmospheric variation levels. It is noted that at lower altitudes, the transfer of heat is significantly less due to lower temperature regions, and air velocities were very low compared to higher attitudes (Huang et al. 2017). Various research proves that the density of the gases or air increased at higher altitudes in the range of above 40 km will affect the atmospheric change in variations like an increase in temperatures and an increase in air velocities (Kumar et al. 2016a). Various researchers proved the second important factor that affects the change in atmospheric variations. From the various literature, it was observed that the temperature variations depend upon the turbulence effects, atmospheric effects, and wind velocities (Williams 2017). According to Zareie et al. (2016), an increase in the earth's surface temperatures causes a change in climatic conditions and a change in regions. Although various researchers have scientifically proven that 70% of the change in atmospheric variations occurred during the summer seasons due to the availability of a gradual increase in surface temperatures of the earth (Prats et al. 2018). According to Srimanickam and Kumar (2021), the maximum surface temperature of the earth due to this turbulence effect was raised from 27°C to 56°C. The work comprises low latitudes ranging from 0-10N, 10-20N, and 20-30 N at attitude heights of 25 km to 100 km for specifically finding the change in middle atmospheric variations to find the oscillations such as SAO, AO, QBO, and ENSO. This analysis is used to forecast the central atmospheric dynamics that allow various researchers to minimize the constituents present in the air

that prevent ozone layer depletion and global warming. The objective of this research is to determine the thermal performance over the international atmosphere for different altitudes: troposphere (0-20 km), stratospheric (21-50 km), mesospheric (51-90 km), and thermospheric regions (91-105 km). This analysis will be helpful to the young researchers for the maximum temperatures emitted from various automobiles and powerplants and the importance of emissions that will affect the atmospheric regions. Hence, each young researcher must focus on exhaust gas emission reduction by implementing multiple alternative sources of energy that emit fewer pollutants in the replacement of diesel engines and the replacement of fuels in power stations. The various technologies replacing automobiles and emissions sources must be controlled with adaptive sensor technology for building less harmful effects and more conventional time.

MATERIALS AND METHODS

Fig. 1. indicates the methodology process involved in this analysis. The data from Jan 2002 to Dec 2022 was downloaded from the website link of NASA source as Saber satellite and analyzed in Matlab to measure the thermal behavior of gases and air in the ozone layer. This range selection was considered from Lattitude 0-30 N and Longitude 74-84 E. The temperature data is a source for measuring the mean deviations. Wavelet and amplitude analyses were carried out. The properties, such as standard deviation, were analyzed monthly, and this analysis was based on daytime layer O_3-96. The measurement of gases and airflow rate by FFT per amplitude for oscillations was also carried out to determine the wavelength range with respect to temperatures (Karthickeyan et al. 2017)

Experimental Procedure

Fig. 2. represents the experimental procedure involved in this analysis. The central theme of this analysis is to analyze the temperatures from the low latitudes in the range of 0-30 N and longitudes 60-90 E. The periodic time for this analysis is taken as JAN 2002 to DEC 2022. Twenty years of data are recorded in a data logger (Arun et al. 2017, Rupesh et al. 2022). The satellite receives the data and stores it in the data logger. The recorded data was downloaded, and the amplitude variations and wavelet variations in the ozone layer were analyzed to predict the temperature trends that will affect the ozone layer (Li et al.2019, Bishnoi 2023). The analysis is conducted in the altitude range of 25 km to 100 km to determine the mean deviations and oscillations and estimate the trends between the ozone layer. This analysis gives a brief idea about the ozone layer depletion caused due to severe temperatures due to greenhouse gases. The majority of the gas, such as nitrogen dioxide, is released from

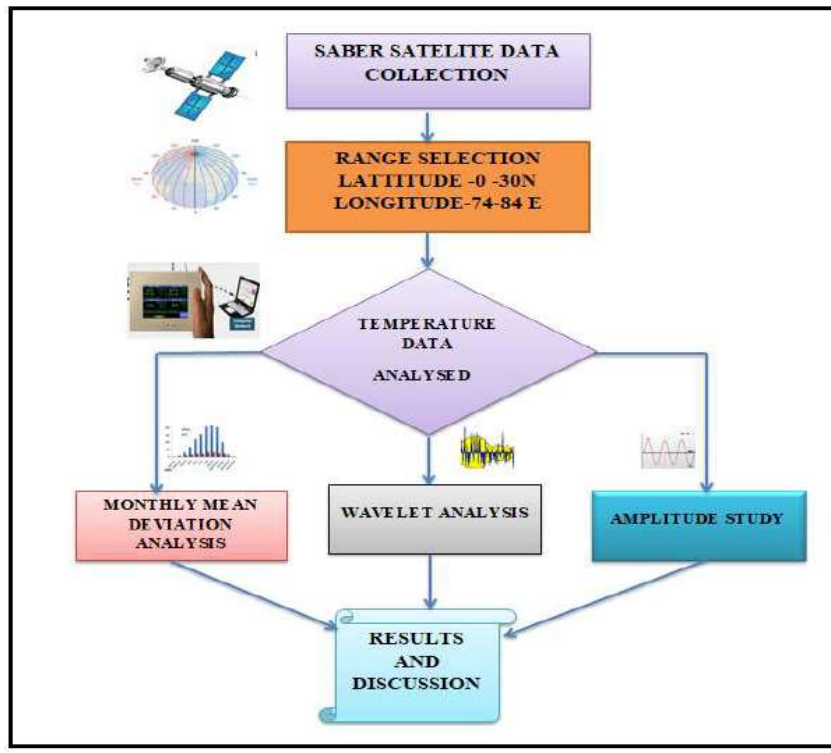

Fig. 1: Methodology.

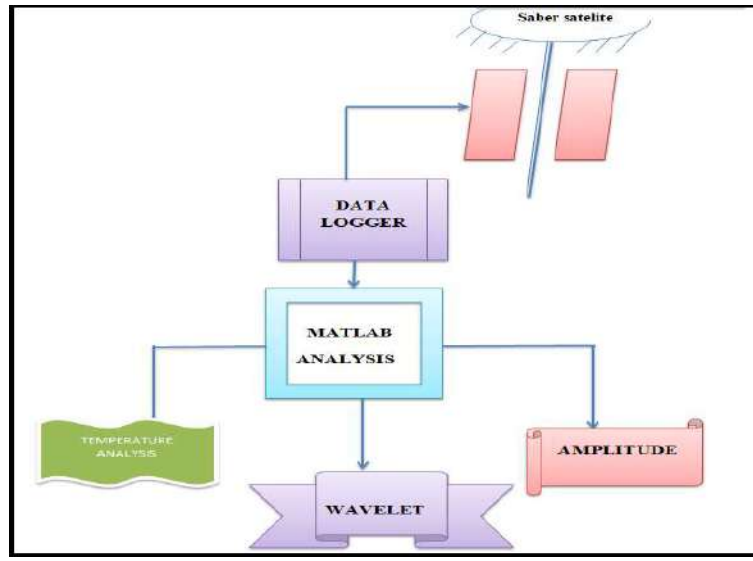

Fig. 2: Experimental procedure.

Table 1: Average temperature data for the period of Jan 2002 to Dec 2022.

S. No.	Altitude in km	Temperature in K	Temp-Standard deviation in K	Ozone-O_3 in mol mol^{-1}	O_3-Standard deviation in mol mol^{-1}
1.	20-25	221.9426	2.34645	$6.75909E^{-06}$	$1.0918E^{-06}$
2.	25-30	230.7924	2.528651	$9.97117E^{-06}$	$6.35033E^{-07}$
3.	30-35	239.9935	2.849822	$9.3162E^{-06}$	$4.57383E^{-07}$
4.	35-40	251.7469	3.082096	$7.07007E^{-06}$	$4.33035E^{-07}$
5.	40-45	260.1246	2.75563	$4.68518E^{-06}$	$3.1743E^{-07}$
6.	45-50	259.084	3.214266	$2.98101E^{-06}$	$2.02864E^{-07}$
7.	50-55	250.1491	3.720108	$1.9012E^{-06}$	$1.44102E^{-07}$
8.	55-60	236.2632	3.951742	$1.17573E^{-06}$	$1.1067E^{-07}$
9.	60-65	221.2786	4.232187	$6.82337E^{-07}$	$1.00247E^{-07}$
10.	65-70	211.351	4.863111	$4.1822E^{-07}$	$7.88635E^{-08}$
11.	70-75	199.2492	5.657504	$2.08599E^{-07}$	$6.08634E^{-08}$
12.	75-80	193.6458	6.358009	$2.82699E^{-07}$	$1.28711E^{-07}$
13.	80-85	193.1838	6.582142	$6.55015E^{-07}$	$2.36238E^{-07}$
14.	85-90	188.3699	5.625287	$1.26276E^{-06}$	$4.18805E^{-07}$
15.	90-95	178.9586	5.649485	$1.21886E^{-06}$	$4.809E^{-07}$
16.	95-100	176.7688	7.651902	$7.22041E^{-07}$	$4.06443E^{-07}$

the power industry and the automobile sector, causing the harsh effect of ozone layer depletion (Gholami et al. 2020). Table 1 represents the average temperature data for the period of January 2002 to 2022.

RESULTS AND DISCUSSION

Monthly Mean Temperatures

It is essential to monitor the temperature distribution in the layers concerning various altitudes for the troposphere (0-20 km), stratospheric (21-50 km), mesospheric (51-90 km), and thermospheric regions (91-105 km). This graphical data gives a brief idea of harmful effects in various areas and causes at multiple altitudes (Ma et al. 2020a). From Fig. 3, it is keenly observed that for maximum temperatures of 260 K, there is a formation of ozone depletion. Beyond this temperature, it is essentially noted that there are no variations formed, and while exceeding and reaching this

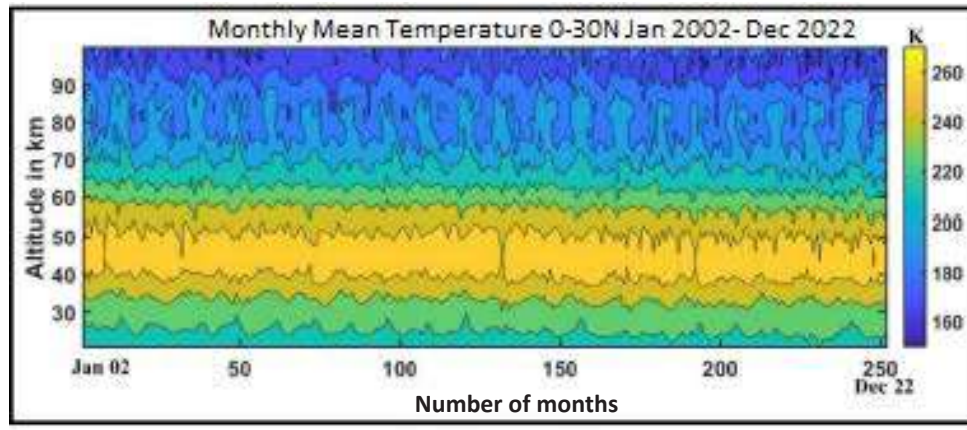

Fig. 3: Monthly Mean temperature variations.

temperature, it causes ozone depletion (Hilton & West 2020). The main constituents such as CO, CO_2, NOx, H, and CH_4 in the summer season released from various automobiles and power plants may cause the highest deviations for the troposphere and stratospheric region (Kumar et al. 2017, Tamura et al. 2020). The highest temperature difference of 260 K is attained in the summer seasons due to an increase in marginal temperatures caused by green gases. This will affect the performance of the ozone layer to deplete the layer.

Monthly Ozone Deviations

Fig. 4. represents the ozone deviations subjected to different attitudes in the range of 25-100 km attitudes. The measurement of ozone depletion is necessary to predict the difference in ozone layer depletion due to temperature differences caused by various green gases (Ma et al. 2020b). The greenhouse gases such as CO, CO_2, NO_x, H, and CH_4 huge green gas have enormous releases that will affect the ozone layer depletions in the altitude range of 10-100 km. It is observed from Fig. 4 that High ozone depletion occurs in the range of 15 km to 35 km. This is due to the concern of high-temperature dissipation of nitrogen gases released from automobiles in the range of 43.5% and sulfur gases in the range of 22% from various power plants (Sunil Kumar et al. 2022). Another reason behind the increase in high ozone variability in the attitudes of 15- 35 km is the dissipation of heat is very low, always in the troposphere region due to the rise in surface temperatures. 70% of heat can be dissipated, and 30% causes the stratosphere to form ozone layer depletion. It is also observed from Fig. 3 that medium ozone variability occurs in the range of 40 to 60 km attitude. Heat dissipation is very low compared to 15 km to 35 km (Tyson & Kennedy 2020). This is due to the lower convective phenomenon occurring in this region due to lower

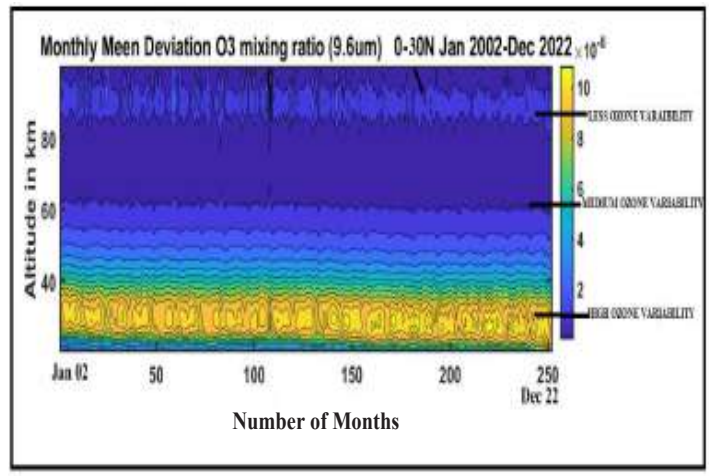

Fig. 4: Ozone deviations.

thermal heat dissipation caused in these regions. Almost 80% of heat dissipation is completed in the area of 15 km to 35 km altitude (Yu et al. 2021). The minimal percentage of 2% heat dissipation doesn't affect the ozone, and there are fewer amplitude variations compared to the troposphere. Very few thermal deviations occurred in the mesosphere region in the range of 60 km to 80 km (mesosphere) and 80 km to 100 km (thermosphere). This is due to the decrease in substantial temperature dissipation concerning the significantly less heat transfer and significantly less convective phenomenal medium of green gases (Mlynczak et al. 2022). An important marginal difference of 2% is happening for the mesosphere region and 1.3% for the thermosphere region compared to the troposphere.

Estimation of Overall Mean Temperatures

It is essential to monitor and measure the overall mean temperatures to estimate the overall thermal performance and heat dissipations for each layer, starting from the troposphere, stratosphere, mesosphere, and thermospheric conditions (Davis et al. 2020). The mean temperature data significantly represents the temperature difference caused at each layer due to the thermodynamic behavior of the green gases evolved in various regions (Meng et al. 2017). Fig.5 depicts the overall thermal temperatures with average standard deviations. From Fig. 5., It is keenly observed that the mean temperature is high at the altitude height of 0 - 45 km in the range of 260 K. This is due to the reason that increases in marginal growth of high-temperature gases were released in this layer 0-20 km (tropospherical region) and 21-45 km (stratospherical part). The heat dissipation occurs by the phenomenon of centrifugal and turbulence effects caused by forced convection phenomenon for the layer 0-20 km (tropospheric area), inductive convection medium occurred at the area 21- 45 km (stratospheric area). The combination of convective and inductive at various wind velocities in the range of 20m/s to 50m/s in the temperature zone of 260 K causes ozone layer depletion (Richardson et al. 2018). Hence, it is required to minimize the usage of greenhouse gases by alternative fuels in the automobile and power industry. For the regions mesosphere and thermosphere at the altitudes height of 50-80 km and 80 -110 km, the overall mean temperature difference is meager in the fields of 180 K and 140 K. A substantial decrease in

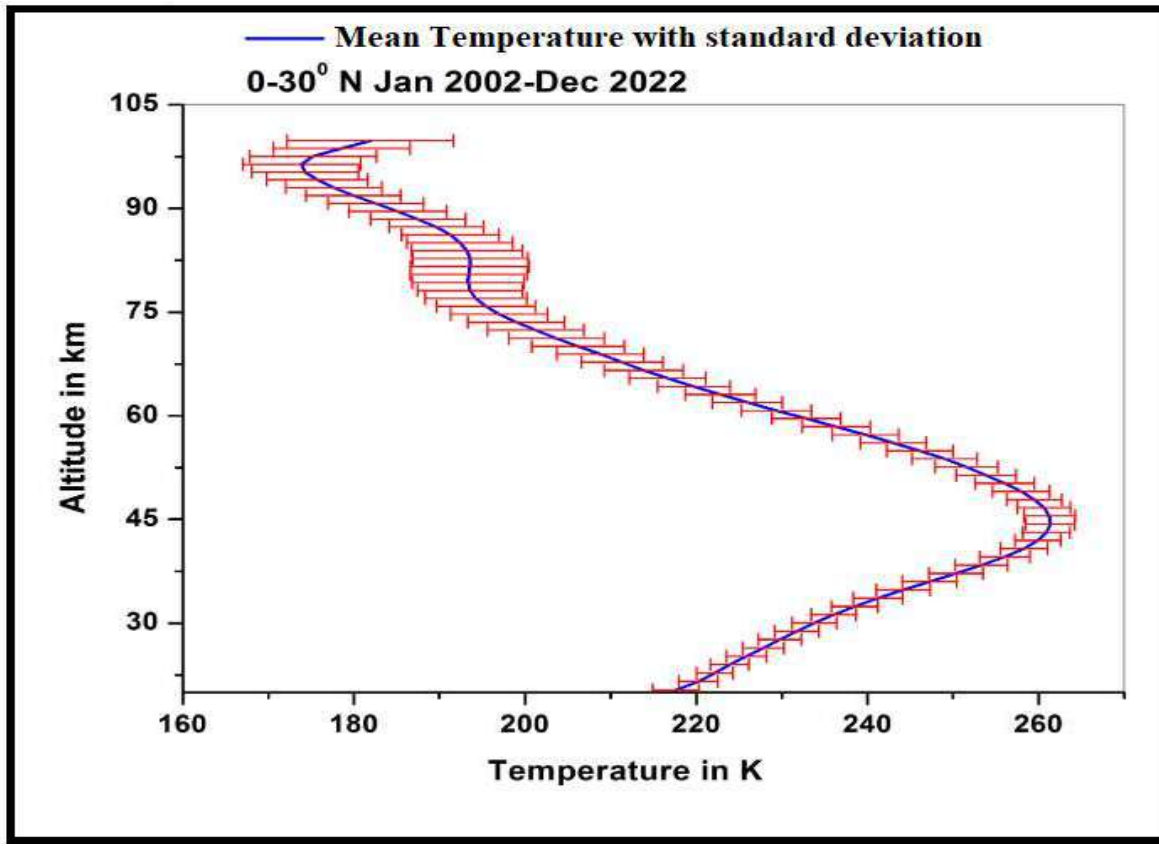

Fig. 5: Overall mean temperatures with standard deviations.

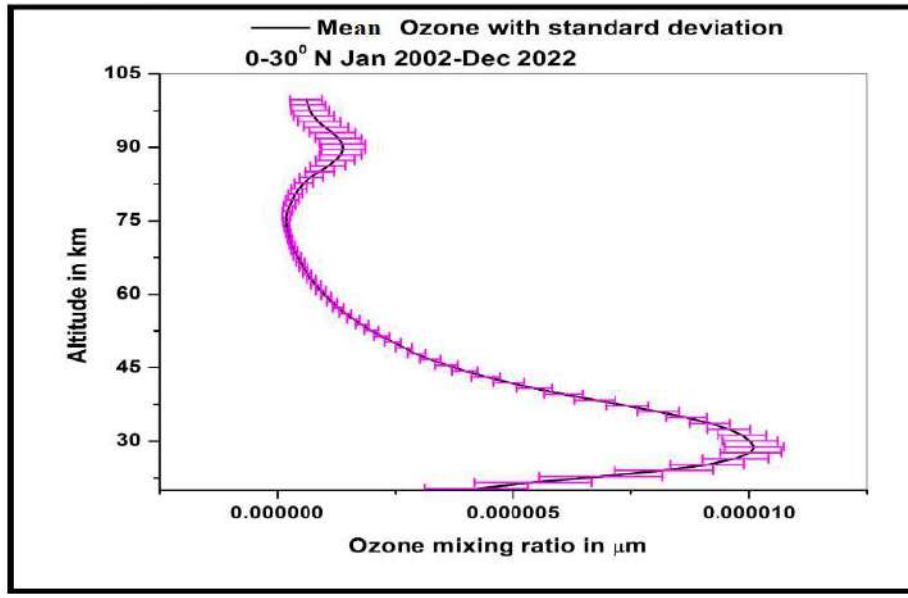

Fig. 6: Overall deviations in ozone.

temperatures is found in the range of 35% for the mesosphere compared to the stratospheric region and a 42% decrease in mean temperatures for the region troposphere compared to the stratospheric region (Vivekananthan et al. 2023). This is due to the absence of convective and inductive forces in this region, which might reduce the turbulence effects and the temperatures compared to the troposphere and stratosphere (Kumar et al. 2016b, Cai et al. 2022).

Estimation of Overall Deviations in Ozone

It is essential to measure the performance by assessing ozone deviations concerning the gases. The ozone mixing depends upon the intensity of the gases released from various sources such as automobiles and power plants. The combined effects of convective and radiative medium with centrifugal and turbulence effects rapidly deplete the ozone layer (Ansmann et al. 2022). Fig. 6. depicts the mixing ratio of ozone due to highly harmful gases released from various sources. From Fig. 6, it is observed that at the tropospheric region, the average deviation is found in the order of 0.000010 μm for the altitude (0-40 km). This is the maximum average standard deviation recorded for the entire period from Jan 2002 to Dec 2022. The rapid extrusion due to the combination of all turbulence effects may propagate the maximum deviations compared to other regions (Muniamuthu et al. 2022). For the regions mesosphere and thermosphere at the altitudes height of 50 -80 km and 80 -110 km, the overall average ozone deviations are very low in the range of 0.00015 μm and 0.0005 μm. This is due to the phenomenon of less corrugated forces and less intensity of radiations in this region due to the formation of fewer temperature distributions at night time compared to the troposphere and stratosphere (Zidan et al. 2022, Kumar et al. 2023).

CONCLUSION

The temperature data from Jan 2002 to Dec 2022 has been downloaded from Saber satellite using the latest data logger. The analysis, such as temperature concerning monthly data and overall year data, is analyzed with the help of Matlab software. The total variations for the entire period are explored, ranging from 0 to 100 km, concerning all the regions troposphere (0-20 km), stratospheric (21-50 km), mesospheric (51-90 km) and thermospheric regions (91-105 km). The effect of ozone layer depletion for the above periods is discussed, and the following results were observed from the analyses. The temperature data is a source for measuring the mean deviations, and wavelet and amplitude analyses were carried out. The main constituents such as CO, CO_2, NOx, H, and CH_4 in the summer season released from various automobiles and power plants may cause the highest deviations for the troposphere and stratospheric regions. High ozone depletion occurs in the range of 15 km to 35 km. This is due to the concern of high-temperature dissipation of nitrogen gases released from automobiles in the field of 43.5% and sulfur gases in the range of 22% from various power plants. The combination of convective and inductive at multiple wind velocities in the field of 20m/s to 50m/s in the temperature zone of 260K causes ozone layer depletion and greenhouse effects. Very few thermal deviations occurred in the mesosphere region in the range of 60 km to 80 km

(mesosphere) and 80 km to 100 km (thermosphere). This is due to the decrease in substantial temperature dissipation concerning the less heat transfer and significantly less convective phenomenal medium of green gases. Hence, this study will give a brief idea to young researchers working in the field of NASA to evolute and minimize the harmful gases released to the atmosphere with the help of other conventional energy sources.

ACKNOWLEDGEMENT

The authors would like to thank NASA, a Saber satellite located in the United States of America, for providing valuable information and data for analyzing this research. The authors would like to thankful to Dr. Aloktaori, scientist NRSI, Hyderabad, for support in carrying out this analysis.

REFERENCES

Ansmann, A., Ohneiser, K., Chudnovsky, A., Knopf, D.A., Eloranta, E.W., Villanueva, D., Seifert, P., Radenz, M., Barja, B., Zamorano, F. and Jimenez, C. 2022. Ozone depletion in the Arctic and Antarctic stratosphere induced by wildfire smoke. Atmos. Chem. Phys., 22(17): 11701-11726.

Arun, S., Nagoorvali, S.K., Kumar, K.S. and Mohan, G.S. 2017. Automation of main bearing bolt and cap loosening machine for automobile crankshaft. Int. J. Mech. Eng. Technol., 2(8): 141.

Bishnoi, D. 2023. Pressure exertion and heat dissipation analysis on uncoated and ceramic (Al2O3, TiO2, and ZrO2) coated braking pads. Mater. Today Proceed., 74: 774-787.

Cai, X., Wang, W., Burns, A., Qian, L. and Eastes, R.W. 2022. The effects of IMF By on the middle thermosphere during a geomagnetically "quiet" period at solar minimum. J. Geophys. Res. Space Phys., 127(5): e2021.

Davis, N.A., Davis, S.M., Portmann, R.W., Ray, E., Rosenlof, K.H. and Yu, P. 2020. A comprehensive assessment of tropical stratospheric upwelling in the specified dynamics Community Earth System Model 1.2. 2–Whole Atmosphere Community Climate Model (CESM (WACCM)). Geosci. Model Develop., 2(13): 717-734.

Gholami, F., Tomas, M., Gholami, Z. and Vakili, M. 2020. Technologies for the nitrogen oxides reduction from flue gas: A review. Sci. Total Environ., 714: 136712.

Hansen, J., Sato, M., Hearty, P., Ruedy, R., Kelley, M., Masson-Delmotte, V., Russell, G., Tselioudis, G., Cao, J., Rignot, E. and Velicogna, I. 2016. Ice melt, sea level rise, and superstorms: evidence from paleoclimate data, climate modeling, and modern observations that 2 C global warming could be dangerous. Atmos. Chem. Phys., 16(6): 3761-3812.

Hilton, R.G. and West, A.J. 2020. Mountains, erosion, and the carbon cycle. Nature Rev. Earth Environ., 6)1): 284-299.

Huang, J., Yu, H., Dai, A., Wei, Y. and Kang, L. 2017. Drylands face potential threat under 2 C global warming target. Nature Clim. Change, 7(6): 417-422.

Karthickeyan, N.K., Arun, S., Mohan, G.S. and Kumar, S. 2017. Structural analysis of exhaust manifold for 1500 Hp engine. Int. J. Mech. Eng. Technol., 3(8): 379-387.

Kumar, K.S., Babu, J.M., Prakash, P.J. and Nagappan, M. 2023, May. Modal analysis of natural rubber-enhanced suspension system for vibration reduction. AIP Conf. Proceed., 2715: 114123.

Kumar, K.S., Muniamuthu, D.S., Arun, S. and Mohan, A. 2016a. Identification experimental analysis of noise and vibration reduction in windmill gearbox for 5MW wind turbine. Int. J. Mech. Eng. Technol., 6(7): 76-85.

Kumar, K.S., Palanisamy, R., Aravindh, S. and Mohan, G.S. 2017. Design and analysis of windmill blades for domestic applications. Int. J. Mech. Eng. Technol., 1(8): 25-36.

Kumar, K.S., Raju, D.B.N., Arulmani, J. and Amirthalingam, P. 2016b. Design and structural analysis of liquified cryogenic tank under seismic and operating loading. Int. J. Mech. Eng. Technol., 7(6): 345-366

Li, X., Tong, F.L., Yu, C.P. and Li, X.L. 2019. Statistical analysis of temperature distribution on vortex surfaces in a hypersonic turbulent boundary layer. Phys. Fluids, 31(10): 106101.

Ma, S., Xiong, J., Cui, R., Sun, X., Han, L., Xu, Y., Kan, Z., Gong, X. and Huang, G. 2020a. Effects of intermittent aeration on greenhouse gas emissions and bacterial community succession during large-scale membrane-covered aerobic composting. J. Clean. Prod., 266: 121551.

Ma, Z., Gong, Y., Zhang, S., Luo, J., Zhou, Q., Huang, C. and Huang, K. 2020b. Comparison of stratospheric evolution during the major sudden stratospheric warming events in 2018 and 2019. Earth Planet. Phys., 5(4): 493-503.

Meng, J., Yao, Z., Du, H. and Lv, M. 2017. Thermal protection method of the solar array for stratospheric airships. Appl. Thermal Eng., 111: 802-810.

Mlynczak, M.G., Hunt, L.A., Garcia, R.R., Harvey, V.L., Marshall, B.T., Yue, J., Mertens, C.J. and Russell III, J.M. 2022. Cooling and contraction of the mesosphere and lower thermosphere from 2002 to 2021. J. Geophys. Res. Atmos., 22(127): e2022.

Muniamuthu, S., Kumar, K.S., Raja, K. and Rupesh, P.L. 2022. Dynamic characterization of hybrid composite based on flax/E-glass epoxy composite plates. Mater. Today Proceed., 59: 1786-1791.

Prats, J., Reynaud, N., Rebière, D., Peroux, T., Tormos, T. and Danis, P.A. 2018. LakeSST: Lake skin surface temperature in French inland water bodies for 1999–2016 from Landsat archives. Earth Syst. Sci. Data, 10(2): 727-743.

Richardson, P.L., Wakefield, E.D. and Phillips, R.A. 2018. Flight speed and performance of the wandering albatross with respect to wind. Move. Ecol., 6(1): 1-15.

Rupesh, P.L., Raja, K., Kumar, K.S., Vijaydharan, S., Reddy, A.M.M. and Kumar, P.D. 2022. Experimental evaluation of thermal stress on the surface of butterfly specimen through the irreversible color change of thermal paint. Mater. Today Proceed., 59: 1768-1775.

Samad, S. and Shah, A. 2017. Role of binary cement, including Supplementary Cementitious Material (SCM), in production of environmentally sustainable concrete: A critical review. Int. J. Sustain Built Environ., 2(6): 663-674.

Srimanickam, B. and Kumar, S. 2021. Drying investigation of coriander seeds in a photovoltaic thermal collector with solar dryer. Int. J. Mech. Eng. Technol., 14: 659-668

Sunil Kumar, K., Babu, J.M. and Venu, H. 2022. Performance, combustion, and emission characteristics of a single-cylinder DI diesel engine fuelled with lotus biodiesel-diesel-n-butanol blends. Int. J. Amb. Energy, 43(1): 7941-7951.

Tamura, M., Gotou, T., Ishii, H. and Riechelmann, D. 2020. Experimental investigation of ammonia combustion in a bench scale 1.2 MW-thermal pulverized coal firing furnace. Appl. Energy, 277: 115580.

Tyson, A. and Kennedy, B. 2020. Two-thirds of Americans think government should do more on climate. Pew Research Center.1-39

Vivekananthan, V., Vignesh, R., Vasanthaseelan, S., Joel, E. and Kumar, K.S. 2023. Concrete bridge crack detection by image processing technique by using the improved OTSU method. Mater. Today Proceed., 74: 1002-1007.

Williams, P.D. 2017. Increased light, moderate, and severe clear-air turbulence in response to climate change. Adv. Atmos. Sci., 34(5): 576-586.

Yu, T., Wang, W., Ren, Z., Cai, X., Yue, X. and He, M. 2021. The response of middle thermosphere (~ 160 km) composition to the November 20 and 21, 2003 superstorm. J. Geophys. Res. Space Phys., 10(126): e2021.

Zareie, S., Khosravi, H., Nasiri, A. and Dastorani, M. 2016. Using Landsat Thematic Mapper (TM) sensor to detect a change in land surface temperature in relation to land use change in Yazd, Iran. Solid Earth, 7(6): 1551-1564.

Zidan, A.M., Nayak, M.K., Karimi, N., Dogonchi, A.S., Chamkha, A.J., Hamida, M.B.B. and Galal, A.M. 2022. Thermal management and natural convection flow of nano encapsulated phase change material (NEPCM)-water suspension in a reverse T-shaped porous cavity enshrining two hot corrugated baffles: A boost to renewable energy storage. J. Build Eng., 53: 104550.

ORCID DETAILS OF THE AUTHORS

E. Raghavendrakumar: https://orcid.org/0009-0007-0198-547X
V. Kamalakar: https://orcid.org/0000-0002-7747-674X
K. Sunil Kumar: https://orcid.org/0000-0002-5093-7307

Nature Environment and Pollution Technology
An International Quarterly Scientific Journal

p-ISSN: 0972-6268
(Print copies up to 2016)
e-ISSN: 2395-3454

Vol. 23 | No. 1 | pp. 451-458 | 2024

Original Research Paper

https://doi.org/10.46488/NEPT.2024.v23i01.040

Open Access Journal

Effect of Humic Acid Fertilizer on Mercury Release from Greenhouse Soils

Z. Zhao*, L. Y. Long, H. Gu** and R. G. Sun**†**

*Guizhou Eco-Environmental Monitoring Centre, Guiyang 550081, China

**School of Chemistry and Material, Guizhou Normal University, Guiyang 550025, China

†Corresponding author: Rongguo Sun; srg@gznu.edu.cn

Nat. Env. & Poll. Tech.
Website: www.neptjournal.com

Received: 16-05-2023
Revised: 05-07-2023
Accepted: 07-07-2023

Key Words:
Soil mercury release
Humic acid fertilizer
Greenhouse
Hg-contaminated soil

ABSTRACT

The elemental mercury (Hg^0) release characteristics from the Hg-contaminated soil applied with Humic acid fertilizer (HAF) in the greenhouse were identified. The adsorption features of mercuric ion (Hg^{2+}) on HAF under different reaction times and pH were investigated to elucidate the influencing mechanism of HAF on soil Hg^0 release. Besides, the microstructure of HAF loading with Hg^{2+} was characterized by using Fourier transform infrared spectroscopy (FTIR) and scanning electron micrograph-energy dispersive spectrometry–EDS). The results showed that with the increasing HAF dosage, soil oxidation-reduction potential (Eh), and organic matter (SOM) content, as well as the decreasing soil pH, the soil Hg^0 release fluxes showed a decreasing tendency. The soil pH, Eh, SOM, and total Hg content are the key factors that can affect the soil Hg^0 release fluxes. The interior air temperature, light intensity, soil moisture, and soil temperature have little impact on soil Hg^0 release fluxes when the greenhouse soil is applied with HAF. The HAF can immobilize Hg^{2+} and reduce its activity by surface precipitation and specific adsorption, then affecting the soil Hg^0 release fluxes. The results of this study provide a basis for the application of HAF to reduce soil Hg^0 release fluxes in the greenhouse of Hg-contaminated areas.

INTRODUCTION

The mercury (Hg) is a highly toxic element to the environment and has caused many public health hazards. It is one of the world's most recognized environmental pollutants and can damage the human nervous, urinary, digestive, and respiratory systems, causing mental and motor functional disorders (Mario et al. 2020, Baragano et al. 2022). Tongren Hg mining area is the largest Hg mining area in China. Long-term mining of Hg has not only caused serious terrain damage and Hg pollution to the surrounding areas but also led to the depletion of the Hg mine's resources. Therefore, the government planted to rehabilitate the mining and surrounding areas, and a large number of vegetable greenhouses were constructed to achieve regional resource transformation. The Hg concentrations of most crops grown in the farmlands of Wanshan Hg mine areas were higher than the governmental reference values (10 or 20 $\mu g \cdot kg^{-1}$) (Xia et al. 2020). As a result, the exposure risk of Hg to residents was high.

Previous studies had found that the light intensity, atmospheric Hg concentration, and land use type were the dominant factors involved in soil Hg release fluxes in Wanshan Hg mining areas (Wang et al. 2021, Zhao et al. 2022, Federico et al. 2023). The greenhouse is in a relatively confined environment where soil Hg release fluxes are generally higher than that of the external bare ground due to the greenhouse effect. The soil Hg release is the main source of interior atmospheric Hg in the greenhouse, which the leafy part of vegetables will assimilate (Liu et al. 2022). Fertilizer application can change the soil physicochemical properties around plant roots, which in turn affects the transport and accumulation of Hg in the soil-plant system (Geng et al. 2023). Humic acid fertilizer (HAF) is a brown or black amorphous polymeric colloidal complex that is the main component of soil organic matter (SOM), and HAF shows great affinity for Hg in soil (Boguta et al. 2019). HAF has a variety of reactive groups, including carboxyl, phenolic hydroxyl, alcohol hydroxyl, amino, and carbonyl groups, which can adsorb and complex with Hg in soil (Zhang et al. 2009).

By changing the amount of HAF in the soil, the adsorption and complexation of Hg with HAF will increase in the soil environment, then the reactivities of mercuric ion (Hg^{2+}) will decrease. As a result, the production of Hg^0 decreases, causing the soil Hg^0 release fluxes to reduce. Ultimately, the contamination of atmospheric Hg caused by soil Hg^0 release may be controlled.

Therefore, the soil Hg^0 release characteristics from greenhouse soil applied with HAF were identified by the

simulated greenhouse. The adsorption features of Hg^{2+} in soil and HAF system were investigated to elucidate the influencing mechanism of HAF on the soil Hg release process. The purpose of this study is to verify whether the HAF can be used in controlling soil Hg^0 release from the Hg-contaminated soil in a greenhouse, which will provide a new direction and theoretical basis for remediating Hg-contaminated soil.

MATERIALS AND METHODS

Incubation Experiment

The Hg^0 release characteristics from the greenhouse soil applied with HAF were identified by using an incubation experiment. The test soil was collected from a vegetable field (106.64°E, 26.40°N) in Guiyang, Guizhou Province, China. After the weeds and debris were removed, the soil was dried at room temperature, crushed, and mixed homogeneously. Then, the soil was spiked with $Hg(NO_3)_2$ solution to make the final soil Hg content to be ~40 $mg.kg^{-1}$ (Yan et al. 2019). The soil was mixed thoroughly again and left to equilibrium for 6 months. Then 18 kg of Hg-contaminated soil was placed into each greenhouse (length 80 cm, width 60 cm, and height 50 cm) with a height of ~20 cm. The 0 (CK), 180 (1%), 540 (3%), and 900 (5%) g of HAF (Plant Source Ecological Technology, Co. Lid., Tianjin, China) were amended to each greenhouse soil. Both the physical and chemical properties of test soil and HAF are shown in Table 1. The greenhouse film was made of polyethylene, whose transmittance of visible light is 85%. On 0 (just after the HAF was amended to soil), 5, 15, 30, and 60 d, the soil redox potential (Eh), soil temperature, air temperature, light intensity, and soil moisture content were monitored, simultaneously, the greenhouse soils were sampled to detect the total Hg (THg) content, pH, and organic matter (SOM) concentration.

Adsorption Experiment

The adsorption of Hg^{2+} on soil can affect the reactivities of soil Hg, then influencing the generation of soil Hg^0 via reduction reaction. As a result, the soil Hg^0 release fluxes were affected by adsorption. The amendment of HAF could change the physical and chemical properties of the soil environment, resulting in the adsorption characteristics of Hg^{2+} on soil changing simultaneously. Therefore, the adsorption characteristics of Hg^{2+} on the soil amended with HAF need to be identified. According to Table 2, a certain amount of HAF and/or soil was added to a centrifuge tube (50 mL). Then 20 mL Hg solution (50 $mg.L^{-1}$) was added, and the solution pH was adjusted by using NaOH (1 $mol.L^{-1}$) and HNO_3 (1 $mol.L^{-1}$). After that, the centrifuge tube was sealed with a cap and shaken at 120 $r.min^{-1}$ for a certain time (Table 2) under 25°C. The reaction solution was centrifuged at 4500 $r.min^{-1}$ for 5 min to collect the supernatant, which was used for Hg content detection. The precipitate was collected to characterize the microstructure. The microstructure and surface morphology of HAF were observed by scanning electron microscopy (SEM) (FEI Versa3D, USA), the surface elements of HAF were analyzed by applying EDS energy spectroscopy (point sweep), and Fourier analyzed the groups of HAF transform infrared spectroscopy (FTIR, Nicolet iS5, Thermo Scientific, USA).

Table 1: The physical and chemical properties of tested soil and HAF.

Parameters	HAF	Soil
Hg concentration [$mg{\cdot}kg^{-1}$]	0.13	0.28
Organic matter [$g{\cdot}kg^{-1}$]	266.45	34.66
Eh [mV]	673.34	569
pH	5.8	6.7

The experimental data was simulated and fitted using pseudo-first-order (eq.(1)) and pseudo-second-order (eq.(2)) kinetic model equations.

$$ln(q_e - q_t) = ln\, q_e - k_1 t \quad \ldots(1)$$

$$\frac{t}{q_t} = \frac{1}{k_2 \times q_e^2} + \frac{t}{q_t} \quad \ldots(2)$$

where, q_e and q_t ($mg{\cdot}g^{-1}$) are the adsorption capacities of of Hg^{2+} on HAF at equilibrium and time t (min), respectively, k_1 (min^{-1}) and k^2 ($g{\cdot}mg^{-1}{\cdot}min^{-1}$) are the adsorption rate constants for pseudo-first-order and pseudo-second-order kinetic model equations, respectively.

Measurement Methods

The soil Hg release fluxes were measured using the kinetic fluxes box method, as described in the literature (Liu et al. 2022). The soil THg content was determined with a cold atomic absorption Hg detector (Model III, Brooks Rand, USA) after digestion using aqua regia (50%) (Li et al. 2020).

Table 2: The design of the adsorption experiment.

Treatment	HAF dosages [g]	Soil dosages [g]	pH	$t.min^{-1}$
CK	0	0	3, 4, 5, 6, 7, and 8	1440
Soil	0	0.1		
HAF	0.03	0		
Soil+HAF	0.03	0.1		
CK	0	0	6	5, 15, 30, 60, 120, 240, 480, 720, and 1440
Soil	0	0.25		
HAF	0.075	0		
Soil+HAF	0.075	0.25		

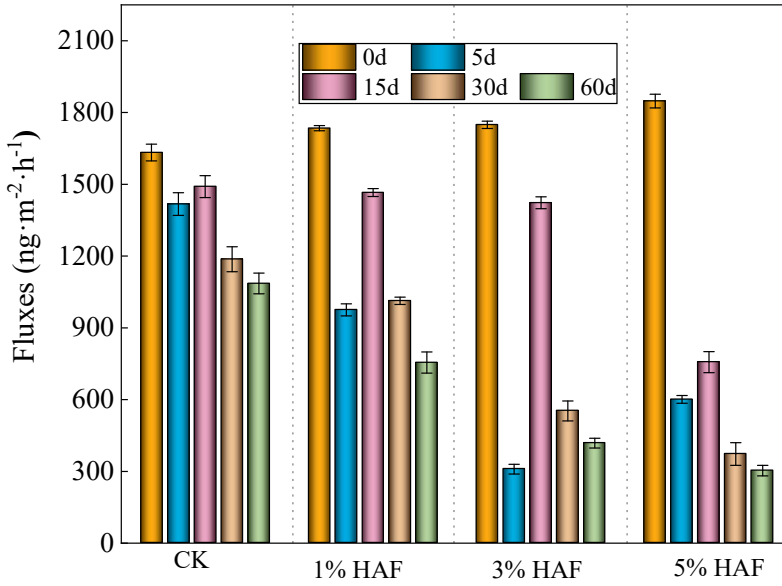

Fig. 1: The soil Hg^0 release fluxes in the greenhouse with the application of HAF.

The air-dried soil (particle size 2 mm) was dissolved in deionized water (solid to liquid ratio 1:2.5), stirred for 1 min, rested for 30 min, and determined by a pH meter (PHS-3C, INESA instrument, Shanghai, China). The SOM content was determined by the potassium dichromate oxidation method (Yao et al. 2022). The Soil oxidation-reduction potential (Eh) was determined by an ORP meter (TR-901, Remagnet Shanghai, China). The soil temperature and soil moisture content were determined by a soil temperature and humidity meter (TR-6D, Tianjin, China). The light intensity and air temperature in the greenhouse were measured with an illuminance meter (Digital Lux Mater GM1020, Beijing, China).

RESULTS AND DISCUSSION

Soil Hg^0 Release Characteristics

Generally, the soil Hg^0 release fluxes decreased with the increasing incubation time and HAF dose (Fig. 1). For all treatments, the soil Hg^0 release fluxes were highest at the initial stage (0 d). On 0 d, for the treatment CK, 1%, 3%, and 5% HAF, the soil Hg^0 release fluxes were measured to be 1633.00, 1734.70, 1748.44, and 1847.65 $ng \cdot m^{-2} \cdot h^{-1}$, respectively. Compared to 0 d, on 5 d, the soil Hg^0 release fluxes respectively decreased by 13.2%, 43.79%, 82.21% and 67.48%. On 15 d, although the soil Hg^0 release fluxes were significantly higher than that on 5 d, 30 d, and 60 d, it still showed a tendency that decrease with increasing HAF dose. The smallest soil Hg^0 release fluxes were found on 60 d. On 60 d, the soil Hg^0 release fluxes respectively decreased by 33.54%, 56.78%, 79.09%, and 83.59% compared with 0 d. At the initial stage (0 d), the soil needed to be turned over to ensure that the HAF could be mixed uniformly with the soil, causing the originally attached Hg^0 of the soil particles surface to migrate rapidly to the atmosphere (O'Connor et al. 2019). Therefore, the soil Hg^0 release fluxes were high on 0 d. With increasing time and the impact of watering (to maintain soil moisture at ~50%), the soil surface gradually becomes dense, and the exposed area to air decreases; thereby, the soil Hg^0 release fluxes decrease simultaneously (O'Connor et al. 2019). The application of HAF can significantly reduce the soil Hg release fluxes, which can be attributed to the fact that the HAF will adsorb and immobilize Hg ions in the soil, reducing the reactive activity of Hg. The generation of Hg^0 is inhibited (Yan et al. 2019).

The Influence of Soil Physical and Chemical Properties and Environmental Conditions on Soil Hg^0 Release Fluxes

Previous studies have found that the soil THg content (Moore & Carpi 2005), pH (Zhang & Lindberg 1999), Eh (Martyniuk & Ckowska 2003), SOM (Wang et al. 2005), light intensity, soil moisture, and temperature (Nascimento & Masini, 2014) are the key factors that can determine the soil Hg^0 release fluxes. Generally, the soil Hg^0 release fluxes are elevated when the soil THg concentrations height (Wang et al. 2007). For all treatments, the soil THg concentrations decreased with the increasing incubation time (Fig. 2a). On 60 d, for the treatments CK, 1%, 3%, and 5% HAF, the soil THg concentrations reduced by 6.99, 7.74, 8.17, and 6.84 mg kg, respectively, compared with 0 d. The correlation

analysis found that the coefficient between soil Hg^0 release fluxes and soil THg concentrations for the HAF addition treatments ($R^2 = 0.31$) was significantly lower than that for the CK treatment ($R^2 = 0.62$, Fig 3e). This indicates that soil Hg concentration is an important factor that can affect the soil Hg release fluxes when HAF is not applied. However, when the soil was amended with HAF, it would hide the influence of soil THg on Hg^0 release fluxes.

In the soil environment, the rate of reduction of Hg^{2+} to Hg^0 decreased, and soil Hg^0 release fluxes decreased under low soil pH conditions (Yang et al. 2007). When the soil pH increases, Hg^{2+} will combine with OH- in the liquid phase of the soil, reducing the surface adsorption of Hg^{2+} on soil minerals and facilitating Hg^0 release (Xin & Gustin 2007). In the present study, we did not find significant fluctuation of soil pH for the treatment CK. However, for the HAF treatments, the soil pH decreased gradually with the increase of incubation time. Compared to 0 d, the soil pH of 1%, 3%, and 5% HAF treatments decreased by 2.79%, 4.48%, and 9.85% on 60 d (Fig. 2b). This suggests that the application of HAF can reduce soil pH, which the degradation of HAF may cause to generate humic acid (HA), xanthic acid (FA) and humic acid (HU) (Moore & Castro 2012, Peng et al. 2022). The correlation analysis found that the soil Hg^0 is positively related to soil pH ($R^2 = 0.35$). Even so, we think that the soil pH may not be the predominant factor involved in the Hg^0 release process because the coordination of HAF with Hg may be the key influencing factor.

The soil Eh of CK, 1%, 3%, and 5% HAF treatments were 485, 487, 508, and 495 mV on 0 d, respectively. Then, it was found that the soil Eh showed slightly increasing tendencies with incubation time for the HAF treatments. On 60 d, the respective soil Eh of 1%, 3%, and 5% HAF treatments increased by 69, 65, and 92 mV, respectively (Fig. 2c). This suggested that the application of HAF could elevate the soil Eh, resulting in that the soil environment would be more oxidative. Therefore, the soil Hg might undergo an oxidation process to generate Hg^{2+} and/or Hg^+, then the soil Hg^0 release fluxes decreased (Wang et al. 2005). There is a negative correlation between soil Hg^0 release fluxes and Eh ($R^2 = 0.46$), which also suggests that soil Eh is an important factor involved in the Hg^0 release process.

The SOM can sorb and immobilize Hg ions in the soil, causing the reactivity of soil Hg to decrease, which in turn affects the soil Hg release process (Wang et al. 2005). With the extension of incubation time, the SOM content of CK treatment did not fluctuate significantly. Still, a significant increase of SOM content was found in HAF treatment (Fig. 2d). This could be attributed to the that there was a large amount of organic matter contained in HAF, which was introduced to the soil environment. Correlation analysis revealed that the soil Hg^0 release fluxes significantly negatively correlated with SOM content after amending with HAF (R^2 = 0.75, Fig. 2d). This suggested that the application of HAF could affect the soil's physical and chemical properties, then influencing the Hg^0 release fluxes.

The correlation analysis showed that the linear regression coefficients between the soil Hg^0 release fluxes and soil moisture, greenhouse air temperature, light intensity, or soil temperature were all low (Fig. 3). This suggested that the other parameters, except for soil temperature, were not the key factors that can affect soil Hg^0 release fluxes. The soil temperature was as high as 35.9°C on 15 d, which was significantly higher than the soil temperature at other periods. Then the thermal movement of Hg molecules increased, and the adsorption capacity of Hg^0 on the soil surface decreased,

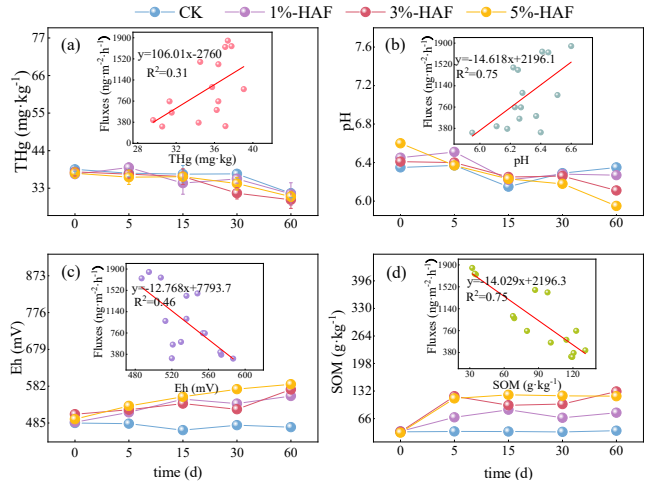

Fig. 2: The fluctuation of soil THg (a), pH (b), Eh (c), and SOM (d).

promoting the soil Hg^0 entering the pores. As a result, the soil Hg^0 release fluxes elevated with high soil temperature (Moore & Carpi 2005). This may be the key reason for the significant increase in soil Hg release fluxes at 15 d.

It can be seen that soil pH, Eh, SOM, and THg are the key factors that can affect soil Hg^0 release fluxes in a greenhouse under fertilization conditions, while greenhouse air temperature, light intensity, soil moisture content, and soil temperature have less effect on soil Hg^0 release fluxes. This result is somewhat different from the conclusion of previous studies that light intensity, temperature, and soil water content are the important factors involved in soil Hg^0 release (Carpi & Lindberg 1997, Zhang & Lindberg 1999, Hamush et al. 2012, Shen et al. 2019). This is mainly due to the relatively closed environment of the greenhouse, low air mobility, and high temperature of the greenhouse. Besides, the light intensity is weakened by the greenhouse membrane, resulting in temperature, and light intensity is no longer the main influencing factor. In addition, the soil moisture content is maintained at ~20%, so it is not a key influencing factor.

Adsorption Characteristics of Hg^{2+} on Soil and HAF Mixed Systems

The main component of HAF is organic matter, which contains functional groups such as -COOH, -SH, -OH, etc. These functional groups have a strong adsorption effect for Hg ions in soil, which affects the reactivity of Hg in soil and then affects the production and release of Hg^0. Therefore, it is necessary to investigate the effect of HAF on the adsorption of Hg^{2+} in soil. It was found that the soil, HAF, and soil+HAF treatments showed rapid adsorption of Hg^{2+}, basically reaching equilibrium within 5 min (Fig. 4a). The concentrations of Hg^{2+} in the solutions of the soil treatment (3.58-11.93 $mg{\cdot}L^{-1}$) were higher than those of HAF treatment (2.130-7.821 $mg{\cdot}L^{-1}$) under different pH conditions. The application of HAF could further reduce the concentrations of Hg in the solutions, indicating that HAF promoted the adsorption of Hg^{2+} by the soil (Fig. 4b). The kinetic model equations found (Table 3) that although the pseudo-first-order order kinetic model could well describe the adsorption of Hg^{2+} on HAF, soil + HAF, and soil, the fitted theoretical adsorption capacity(q_{e1}) differed significantly from the experimental results. The fitting coefficients (R_2^2) of the pseudo-second-order equation were higher than that of the pseudo-first-order order kinetic model. Additionally, there was no difference between the theoretical adsorption capacity (q_{e2}) and the experimental results. This indicated that the pseudo-second-order kinetic model can better describe the adsorption of Hg^{2+} by HAF. The adsorption process is dominated by chemisorption, which may include surface precipitation as well as specific adsorption (Martyniuk & Ckowska 2003).

FTIR characterization revealed that before the HAF adsorbing Hg^{2+}, the peaks at 3305-3500 cm^{-1} were the stretching vibration of -OH and -NH_2, the peaks at 1557 cm^{-1} were C=C and C=O, the peaks at 1378 cm^{-1}, 1005 cm^{-1}, and 912 cm^{-1} were telescopic vibration peaks of phenolic hydroxyl, C-O and Si-O (Nascimento & Masini 2014, Perla et al. 2023). After the HAF loading with Hg^{2+}, the characteristic peaks of carboxyl, amino, and phenolic groups were shifted to the right, and the intensity of the peaks was significantly weakened, which indicated that carboxyl,

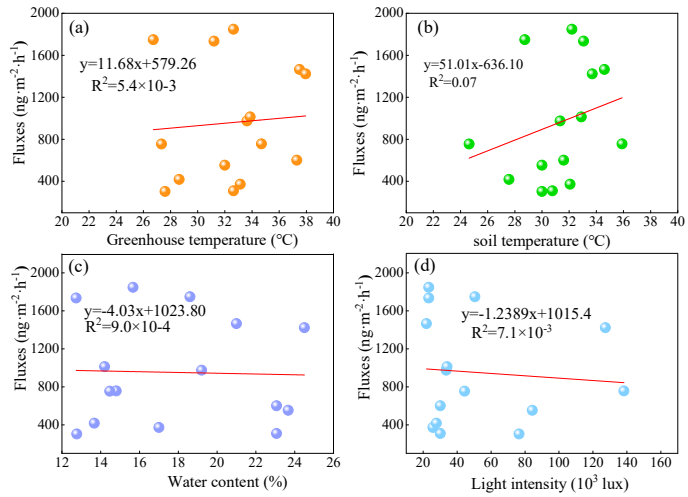

Fig. 3: The relationship between the soil Hg^0 release fluxes and the light intensity (a), soil moisture (b), soil temperature (c), and greenhouse air temperature (d).

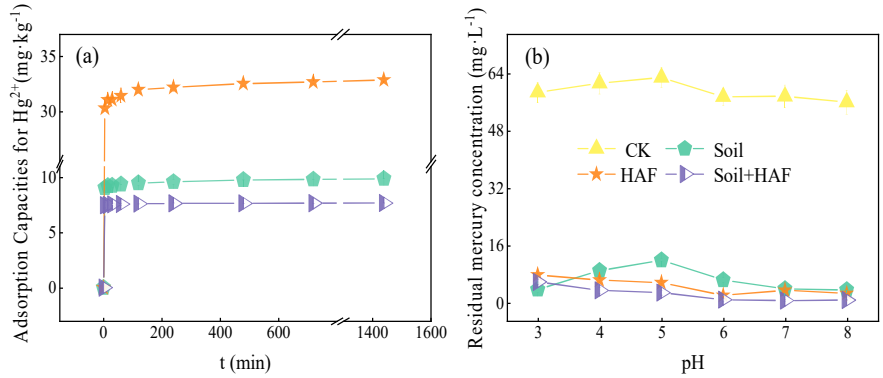

Fig. 4: The adsorption capacity (a) with time and residual Hg concentration (b) with pH for each treatment.

Table 3: The fitting results of pseudo-first-order and pseudo-second-order kinetic model.

Data of this experiment		pseudo-first-order order kinetic model			pseudo-second-order kinetic model		
Type	q_e [$mg \cdot g^1$]	q_{e1} [$mg \cdot g^{-1}$]	k_1[min^{-1}]	R_1^2	q_{e2} [$mg.g^{-1}$]	K_2[$g \cdot mg^{-1} \cdot min^{-1}$]	R_2^2
HAF	32.87	1.83	0.0055	0.9673	32.89	0.0111	1
Soil+HAF	7.65	0.14	0.0069	0.9385	7.67	0.1702	1
Siol	9.87	0.69	0.0053	0.9877	9.88	0.0289	1

amino, and phenolic groups could be coordinated with Hg^{2+} to form complexes (Fig. 5).

Before the Hg^{2+} was adsorbed on HAF, whose surface structure was arranged orderly after the HAF adsorbed Hg^{2+}, the pore structure of HAF would collapse. Fragments would exist in the pores (Fig. 6). This could be attributed to the complexation between Hg^{2+} and carboxyl groups, hydrogen bonds, and other functional groups of HAF, then generating cations, which in turn form aggregates (Liu et al. 2016).

EDS spectra showed that the main elements in HAF were C, O, Si, S, K, Ca, Al, and Fe (Fig. 7). The Hg elemental was observed in the range of 2-2.5 and 9.1-11.7 keV before HAF adsorbed Hg^{2+}. After the adsorption of Hg^{2+}, the characteristic intensity of Hg increased slightly, and the weight percentage of elemental Hg increased from 1.3 to 23.91, indicating that a large amount of Hg is attached to the surface of HAF. The characteristic intensity of O and S elements becomes relatively weaker, and their weight

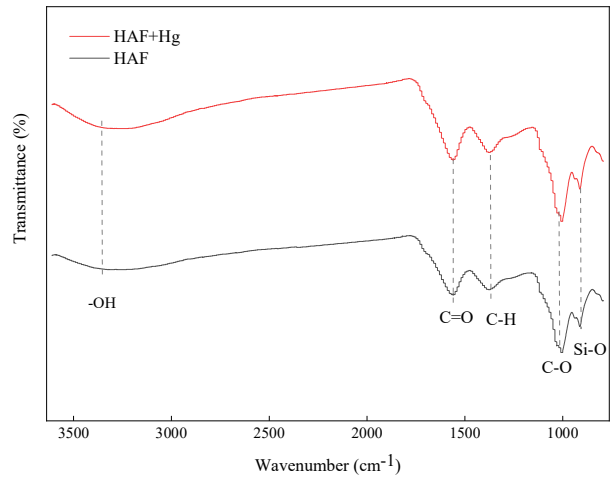

Fig. 5: The FTIR spectra before and after HAF adsorbing Hg^{2+}.

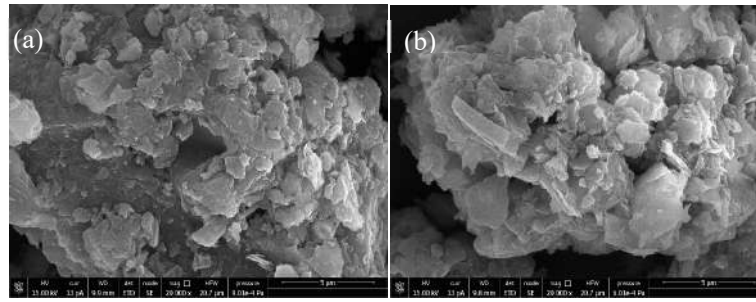

Fig. 6: The SEM images of HAF before and after adsorbing Hg^{2+}.

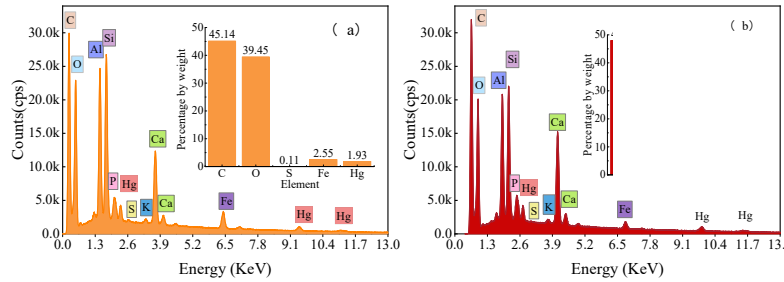

Fig. 7: EDS spectrum before (a) and after the HAF adsorbed Hg^{2+}.

percentage decreases. The changes in the intensity of characteristic peaks may be due to the complexation of Hg^{2+} with O and S elements to form aggregates.

Based on the results of SEM, FTIR, and EDS elemental analysis, combined with previous research results (Zhang et al. 2020), it was hypothesized that the mechanism of HAF adsorption of Hg^{2+} might be:

$$\text{-COOH+Hg}^{2+} \rightarrow \text{-COO-Hg}^{+}\text{+H}^{+} \quad (3)$$

$$\text{-OH+Hg}^{2+} \rightarrow \text{-O-Hg}^{+}\text{+H}^{+} \quad (4)$$

$$\text{-NH}_2\text{+Hg}^{2+} \rightarrow \text{-NH-Hg}^{+}\text{+H}^{+} \quad \cdots(5)$$

$$\text{-SH+Hg}^{2+} \rightarrow \text{-SHg}^{+}\text{+H}^{+} \quad \ldots(6)$$

$$\text{-S-+Hg}^{2+} \rightarrow \text{-S(Hg)-} \quad \ldots(7)$$

The strong adsorption of functional groups contained in HAF may lead to a decrease in the reactivity of Hg in the soil environment, which inhibits the conversion of Hg^{2+} to Hg^0 and then affects the soil Hg release process in the greenhouse.

CONCLUSION

Temperature, light intensity, soil moisture content, and soil temperature have little effect on soil Hg^0 release fluxes. This is different from previous studies and may be related to the stable and controllable environmental conditions of the greenhouse versus variable and uncontrollable environmental factors in the natural state. The soil pH, Eh, SOM, and THg have a strong influence on the soil Hg^0 release fluxes when the greenhouse soil is amended with HAF. The addition of HAF changed the soil pH, Eh, and SOM, then decreased the soil Hg^0 release fluxes. The main effects were as follows: (1) Enhancing the soil acidity in the greenhouse caused a decrease in the rate of reduction of Hg^{2+} to Hg^0, which in turn reduces the soil Hg^0 release fluxes. (2) Alteration of the soil Eh, which enhanced soil oxidation states and induced a shift of Hg^0 to a stable higher valence state, thereby reducing the soil Hg^0 release fluxes. (3) Increased the soil SOM content in the greenhouse, the strong adsorption of functional groups in SOM will adsorb and fix the Hg ions in the soil, reducing the reaction activity of Hg and, thus, the production of Hg^0 decreased, which in turn reduced the soil Hg^0 release fluxes. The soil Hg^0 release fluxes of greenhouse decreased with the increase of incubation time and decreased with the increasing dosage of HAF. The adsorption kinetic characteristics are in accordance with the pseudo-second-order kinetic model, and the adsorption process is dominated by chemisorption, which may include surface precipitation as well as specific adsorption.

ACKNOWLEDGMENTS

This work was financially supported by Guizhou Provincial Scientific and Technological Program (Natural Science) (No. Qian ke he ji chu [2020]1Z038) and (Outstanding Young Scientists and Technicians) (No. Qian ke he ping tai ren cai – YQK[2023]027), and Anshun College

Graduate Student Innovation Special Program Project (No. asxyyjscx(20220).

REFERENCES

Baragano, D., Forjana, R., Alvarez N., Gallego, J.R. and Gonzalez, A. 2022. Zero valent iron nanoparticles and organic fertilizer assisted phytoremediation in a mining soil: Arsenic and Hg accumulation and effects on the antioxidative system of Medicago sativa. J. Hazard. Mater., 433: 128748.

Boguta, P., D'orazio, V., Senesi, N., Sokolowska, Z. and Katarzyna, S.K. 2019. Insight into the interaction mechanism of iron ions with soil humic acids: The effect of the pH and chemical properties of humic acids. J. Environ. Manage., 245: 363-374.

Carpi, A. and Lindberg, S. 1997. Sunlight-mediated emission of elemental hg from soil amended with municipal sewage sludge. Environ. Sci. Technol., 31: 2085-2091.

Federico, F., Valeria, Z., Jadran, F. and Stefano, C. 2023. Gaseous Hg evasion from bare and grass-covered soils contaminated by mining and ore roasting (Isonzo River alluvial plain, Northeastern Italy). Environ. Pollut., 318: 120921.

Geng, H.T., Wang, X.D., Shi, S.B., Ye, Z.Q. and Zhou, W.J. 2023. Fertilization makes strong associations between organic carbon composition and microbial properties in paddy soil. J. Environ. Manage., 325: 116605.

Hamush, C.H., Waltwes, N.E. and Heyst, B.J.V. 2012. Evaluating the effects of sub-zero temperature cycling on Hg Fluxes from soils. Atmos. Environ., 63: 102-108.

Li, Q.H., Tang, L., Qiu, G.L. and Liu, C.H. 2020. Total Hg and methylHg in the soil and vegetation of a riparian zone along a Hg-impacted reservoir. Sci. Total Environ., 738: 139794.

Liu, C.S., Long, L.Y., Yang, Y., Zhang, Y.T., Wang, J. and Sun, R.G. 2022. Sci. The mechanisms of iron-modified montmorillonite in controlling Hg release across Hg-contaminated soil-air interface in the greenhouse. Total Environ., 812: 152432.

Liu, P., Ptacek, C.J., Blowes, D.W. and Landis, R.C. 2016. Mechanisms of Hg removal by biochars produced from different feedstocks determined using X-ray absorption spectroscopy. J. Hazard. Mater., 308: 233-242.

Mario, E.D.A., Liu, C., Ezugwuc, C.I., Mao, S.J., Jia, F.F. and Song, S.X. 2020. Molybdenum disulfide/montmorillonite composite as a highly efficient adsorbent for Hg removal from wastewater. Appl. Clay Sci., 184: 150370.

Martyniuk, H. and Ckowska, J.W. 2003. Adsorption of metal ions on humic acids extracted from brown coals. Fuel Process. Technol., 84: 23-36.

Moore, C. and Carpi, A. 2005. Mechanisms of the emission of Hg from soil: Role of UV radiation. J. Geophys. Res., 110: D24302-1-D24302-9.

Moore, C.W. and Castro, M.S. 2012. Investigation of factors affecting gaseous Hg concentrations in soils. Sci. Total Environ., 419: 136-143.

Nascimento, F.H.D. and Masini, J.C. 2014. Influence of humic acid on adsorption of Hg(II) by vermiculite. J. Environ. Manage., 143: 1-7.

O'Connor, D., Houa. D.Y., Ok, Y.S., Mulder, J., Duan, L., Wu, Q.W., Wang, S.X., Tanck, F.M.G. and Rinkled, J. 2019. Hg speciation, transformation, and transportation in soils, atmospheric Fluxes, and implications for risk management: A critical review. Environ. Int., 126: 747-761.

Peng, X.X., Gai, S, Cheng, K. and Yang, F. 2022. Roles of humic substances redox activity on environmental remediation. J. Hazard. Mater., 435: 129070.

Perla, G.G., Luis, M.T., Josefa, B.B., Fanusto, C. and Octavio, M. 2023. Study of the cholesterol adsorption and characterization of montmorillonite and bentonite clay Mater. Today Commun., 35: 105604.

Shen, C., Zhao, Y.Q., Li, W.X., Ya, Y., Liu, R.B. and Morgen, D. 2019. The global profile of heavy metals and semimetals adsorption using drinking water treatment residual. Chem. Eng. J., 372: 1019-1027.

Wang, C.J., Wang, Z.W., Gao,Y. and Zhang, X.S. 2021. Planular-vertical distribution and pollution characteristics of cropland soil Hg and the estimated soil–air exchange Fluxes of gaseous Hg over croplands in northern China. Environ. Res., 195: 110810.

Wang, S.F., Feng, X.B., Qiu, G.G., Wei, Z.Q. and Xiao, T.F. 2005. Hg emission to the atmosphere from Lanmuchang Hg-Tl mining area, Southwestern Guizhou. Atmos. Environ., 39: 7459-7473.

Wang, S.F., Feng, X.B., Qiu, G.L. and Wang, C.J. 2007. Characteristics of Hg exchange Fluxes between soil and air in the heavily air-polluted area, eastern Guizhou, China. Atmos. Environ., 41: 5584-5594.

Xia, J.C., Wang, J.X., Zhang, L.M., Anderson, C.W.N., Wang, X., Zhang, H., Dai, Z.H. and Feng X.B. 2020. Screening of native low Hg accumulation crops in a Hg-polluted mining region: Agricultural planning to manage Hg risk in farming communities. J. Cleaner Prod., 262: 121324

Xin, M., Gustin M.S. 2007. Gaseous elemental Hg exchange with low Hg-containing soils: Investigation of controlling factors. Appl. Geochem., 22: 1451-1456.

Yan, J.Y., Wang, C., Wang, Z.H., Yang, S.C. and Lia, P. 2019. Hg concentration and speciation in mine wastes in Tongren Hg mining area, southwest China and environmental effects. Appl. Geochem., 106: 112-119.

Yang, Y.K, Zhang, C, Shi, X.J., Lin, T. and Wang, D.Y. 2007. Effect of organic matter and pH on Hg release from soils. J. Environ. Sci., 19: 1349-1351.

Yao, B.M., Wang, S.Q., Xi, S.T., Li, Q. and Sun, G.X. 2022. Optimal soil Eh, pH for simultaneous decrease of bioavailable Cd, As in co-contaminated paddy soil under water management strategies. Sci. Total Environ., 806: 151342.

Zhang, H. and Lindberg, S.E. 1999. J. Processes influencing the emission of Hg from soils: A conceptual model. Geophys. Res., 104: 21889-21896.

Zhang, J., Dai, J.L., Wang, R.Q., Li, F.S. and Wang, W.X. 2009. Adsorption and desorption of divalent Hg (Hg2+) on humic acids and fulvic acids extracted from typical soils in China. Colloids Surf. A Physicochem. Eng. Aspects, 335: 194-201.

Zhang, S.S., Song, J.P., Du, Q., Cheng, K. and Yang, F. 2020. Analog synthesis of artificial humic substances for efficient removal of Hg. Significance of soil moisture on the temperature dependence of Hg emission. Chemosphere, 250: 126606.

Zhao, S., Terada, A., Nakamura, K., Nakashim, M., Komai, T., Riya, S., Hosomi, M. and Hou, H. 2022. Significance of soil moisture on the temperature dependence of Hg emission. J. Environ. Manage., 305: 114308.

Nature Environment and Pollution Technology
An International Quarterly Scientific Journal

p-ISSN: 0972-6268
(Print copies up to 2016)
e-ISSN: 2395-3454

Vol. 23 | No. 1 | pp. 459-465 | 2024

Original Research Paper

https://doi.org/10.46488/NEPT.2024.v23i01.041

Open Access Journal

Impact of Cadmium-Induced Stress on Physiological Traits with Induced Osmolyte and Catalase-Mediated Antioxidative Defense in Rice (*Oryza sativa* L.)

J. Yomso and A. Siddique†

Department of Agronomy, School of Agriculture, Lovely Professional University, Phagwara-144411, Punjab, India

†Corresponding author: anaytullahsiddique@gmail.com

Nat. Env. & Poll. Tech.
Website: www.neptjournal.com

Received: 07-06-2023
Revised: 12-07-2023
Accepted: 15-07-2023

Key Words:
Catalase
Cadmium
Membrane stability index
Proline
Relative water content

ABSTRACT

Cadmium is one of the most carcinogenic and hazardous heavy metals on the earth for causes many serious diseases and disorders in the plant body. The presence of Cd in the soil is equally harmful to the production of rice crops and human beings. A pot experiment was conducted to analyze the consequences of cadmium-induced stress on the antioxidative defense system in rice plants. The assessment of antioxidative defense mechanism based on the cadmium-induced stress in the range of 100 to 300 ppm while the parameters, Chlorophyll Content Index (SPAD), nitrogen (%), relative water content (%), membrane stability index (%), proline content (μg.g^{-1}), and catalase activity (nm H_2O_2 mg^{-1}.min^{-1}) were used. The highest reduction in the Chlorophyll Content Index (CCI), nitrogen (%), RWC (%), and MSI (%) was recorded at the highest concentrations of Cd Cl_2 (300 ppm). However, at the same time, an increase in proline content (μg.g^{-1}) and catalase activity (nm H_2O_2 mg^{-1}.min^{-1}) were also detected at all the intervals of the study. The activity of CCI, amino acid, and enzyme were presented in % increase/decrease over the control of Cd-induced stress in rice plants. The reduction (%) in CCI (SPAD) and RWC (%) was recorded maximum at 75 Days after transplanting (DAT), while nitrogen (%) and MSI (%) were recorded at 50 DAT. However, the increase (%) in proline and Catalase activity was maximum at 75 and 50 DAT.

INTRODUCTION

Heavy metals are serious threats to the health of human beings as well as crop production. The heavy metal cadmium (Cd) is one of them. There are several sources of Cd in the soil in which chemical fertilizers, the use of wastewater as a source of irrigation, sewage sludge, and weathering of rocks are the major sources (Aebi 1984, Ahmad et al. 2015, Ali et al. 2014, Anjum et al. 2015). Being a non-degradable compound, its presence in soil is always considered an alarm situation for soil health and crop production, while its easily absorbing nature makes it more dangerous compared to other heavy metals. Cadmium-infected plant affects several physicochemical processes of the plant during the entire growth period. It reacts directly or indirectly with plant cells, resulting in lipid peroxidation, and consequently produces several kinds of reactive oxygen species (ROS) like O_2^-, OH^* and H_2O_2 (Saidi et al. 2013, Zhang et al. 2014, Howladar 2014).

Moreover, the presence of cadmium in plants shows negative effects in many ways. It can damage the photosystem, especially the thylakoid membrane, affect the uptake and distribution of nutrients throughout the plant body, and alter the activity of antioxidative enzymes (Asgher et al. 2014, Ali et al. 2014, Khan et al. 2015). During heavy stress, anti-oxidative compounds are also present in the plant body, like Superoxide dismutase (SOD), Catalase (CAT), Ascorbate peroxidase (APX), and Proline. All these compounds help in the safe dissipation of ROS from the plant body while it depends on many other complex processes (Balestri et al. 2014, Siddique et al. 2018).

MATERIALS AND METHODS

Experimental Details

The present piece of work was undertaken to evaluate the consequences of $CdCl_2$-induced stress in the rice plant (*Oryza sativa* L.) over the research farm of Lovely Professional University while the variety of rice (Pusa Basmati 1121) was procured from Punjab Agriculture University, Ludhiana, Punjab. 21 days old seedlings were placed in $CdCl_2$ treated pot (diameter is 46 cm) wherein clay 8 and 2 kg of clay loam soil and FYM was used in each pot while the pots were arranged in a Completely Randomized Design comprises of five replications. To evaluate the effect of externally imposed $CdCl_2$ stress, five different concentrations ranging

from 100 to 300 ppm were used, while a set of pots was used as a control. The recommended Agronomic practices were followed to grow the rice crop. At the same time, the observations of all the physiological and biochemical observations were carried out at regular intervals of 25 days up to 75 DAT.

Chlorophyll Content Index CCI and Nitrogen

The observation regarding the CCI was recorded through the SPAD meter Model No. 502 in terms of the SPAD unit, while the estimation of total nitrogen was carried out in flag leaf through KEL PLUS.

Relative Water Content

Estimation of RWC% was carried out according to (Weatherly 1962). 0.2 g leaf sample was cleaned properly and recorded fresh weight before being saturated in 100 mL of distilled water for 2 h and recorded turgid weight. Samples were placed in a hot air oven at 80°C for 48 h to record dry weight, while the following formula was used to calculate RWC%.

$$\text{RWC}\ (\%) = \frac{\text{FW of the sample} - \text{DW of the sample}}{\text{TW of the sample} - \text{DW of the sample}} \times 100$$

Membrane Stability Index

MSI% was calculated using the method described by (Sairam et al. 1990), in which 0.5 g of uniformly sized leaf strips were placed in two separate test tubes, each containing 10 mL of distilled water. The test tubes in one set were placed in a water bath at 40°C for 30 min to measure their electrical conductivity (C_1), while the test tubes in the second set were placed in a water bath at 100°C for 15 min. to measure their electrical conductivity [C_2]. The following formula was used to express the amount of MSI %.

$$\text{MSI \%} = [-1\ C_1/C_2]$$

Estimation of Proline Content (µg.g^{-1})

The estimation of proline content was carried out according to (Bates et al. 1973), wherein 0.5 g of fresh leaf sample was homogenized in 5 mL of 3% sulphosalicylic acid using a mortar and pestle followed by a centrifugation process at 3000 rpm for 10 min. Two mL of each extracted sample, glacial acetic acid, and ninhydrin reagent were pipette out in a separate test tube and placed in a water bath at 100°C for 30 min. After that, the proline was separated with the help of 6 mL toluene in a separating funnel. The OD of proline present in the samples was measured at 520 nm, and the final calculation was done with the help of the proline standard curve.

Catalase Activity

Catalase activity was determined using (Aebi 1984), in which 0.1 g of leaf sample was pulverized in 5 mL of phosphate buffer (0.1M) and centrifuged at 10000 rpm for 20 min. The enzyme activity was determined by adding 2.6 mL of phosphate buffer, 0.1 mL of enzyme extract, and 0.1 mL of H_2O (1%) to the reaction mixture, while a blank sample was prepared by adding phosphate buffer instead of enzyme extract to the reaction mixture. The OD was measured at 240 nm at 15-second intervals up to 2 min. The unit of CAT activity was calculated as nmol H_2O_2 min^{-1} (extinction coefficient 36 mM.cm^{-1}).

The statistical analysis of results collected from the experimental trial was analyzed through SPSS software (21st Version), whereas the mean comparisons were carried out by using DMRT at 5% probability.

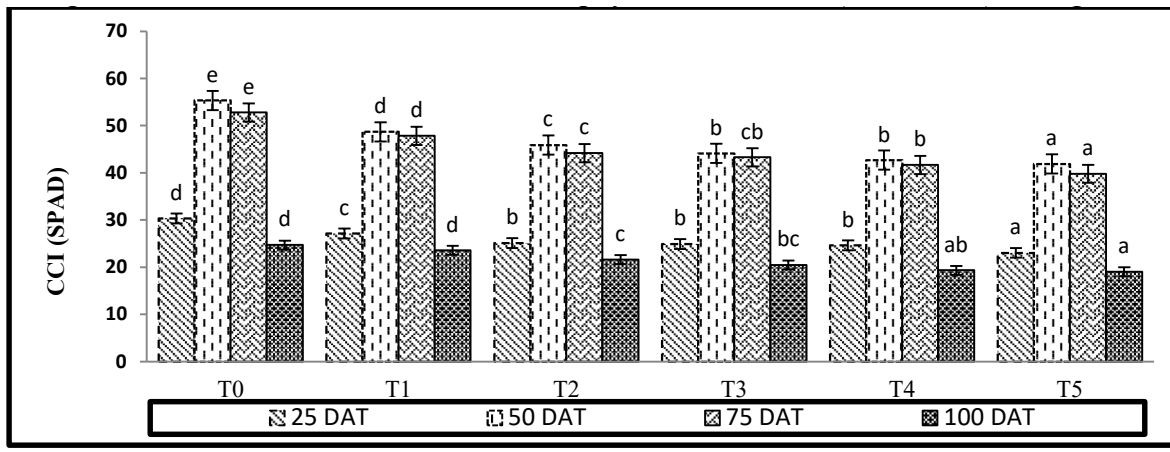

Fig. 1: Effect of $CdCl_2$ treatment on chlorophyll content index (SPAD unit) in flag leaf.

Table 1: Effect of cadmium chloride-induced stress on % increase/decrease in rice plant.

Days After Transplanting Percentage Increase/decrease between Control to HLCT	25 DAT	50 DAT	75 DAT
CCI (SPAD)	-24.06	-24.30	-24.60
Nitrogen (%)	-31.09	-35.67	-24.44
RWC (%)	-28.04	-29.07	-38.28
MSI (%)	-13.19	-37.77	-35.81
Proline content (μg g^{-1})	+46.23	+38.10	+38.34
Catalase activity (nm H_2O_2 mg^{-1} min^{-1})	NA	+77.91	+77.76

*HLCT= Highest level of cadmium toxicity, NA= not analyzed

RESULTS AND DISCUSSION

The present study was executed to evaluate the consequences of $CdCl_2$-induced stress in rice plants. The data depicted in Fig. 1 indicated that the maximum CCI reading was recorded at 50 DAT in all the sets of treatments compared to the remaining DATs, *i.e*., 25, 75 and 100 DAT, while the significant detrimental effect of $CdCl_2$-induced stress among the treatments was recorded at maximum in T_5 at all the time of observations (23.01, 41.91, 39.81 and 19.06) contains the highest concentration of $CdCl_2$ (300 ppm) compared to a control set T_0 (30.38, 55.36, 52.80 and 24.71). The data regarding the increase/decrease (%) over the control Table 1 also showed the highest reduction of CCI (SPAD) reading in T_5 (24.06, 24.30 and 24.60%).

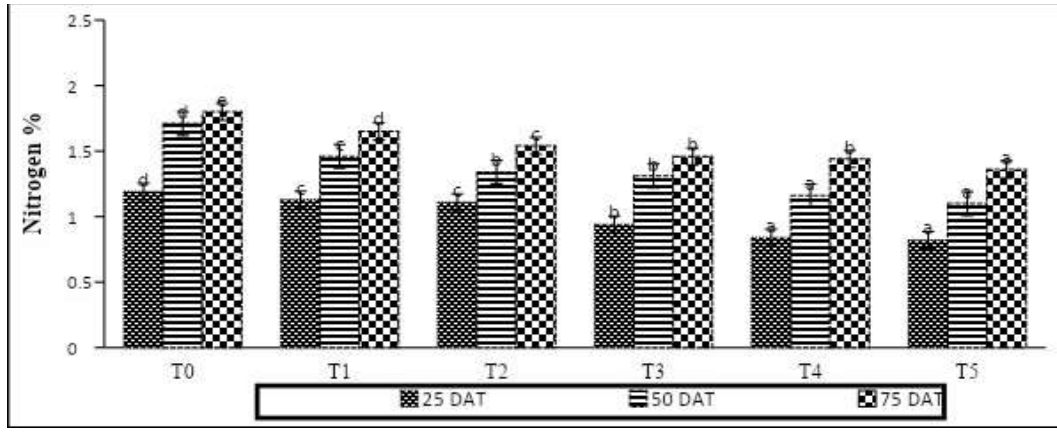

Fig. 2: Effect of $CdCl_2$ treatment on Nitrogen content (%) in dry flag leaf.

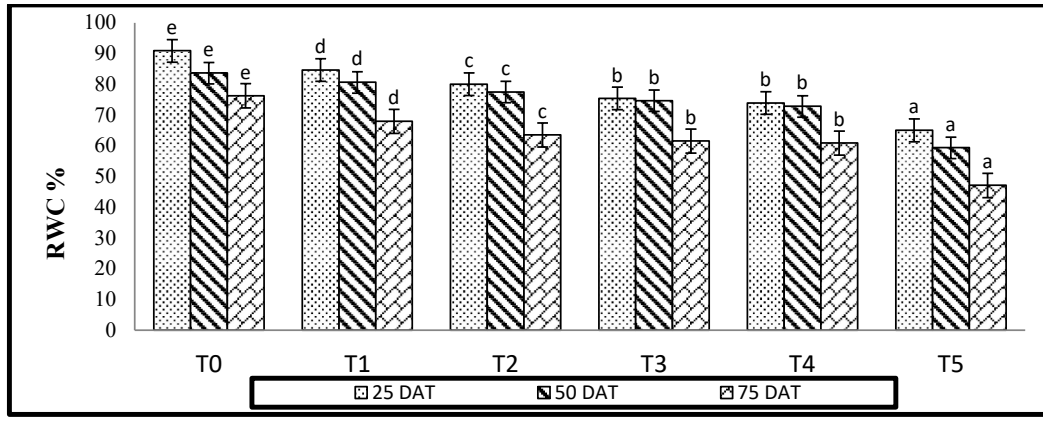

Fig. 3: Effect of $CdCl_2$ treatment on RWC (%) in flag leaf.

Data presented in Fig. 2 indicate that the nitrogen content present in the leaf gradually increased along with the age of the plant up to 75 DAT in all the sets of treatments, including control, while it decreased simultaneously with the elevation of $CdCl_2$ concentration from 100 to 300 ppm. The maximum reduction in nitrogen content was found in T_5 (0.82, 1.10, and 1.36%) compared to control one (1.19, 1.71, and 1.80%), which was followed by T_4> T_3> T_2> and T_1. Data presented in Table 1 also showed that the % reduction of nitrogen content was recorded maximum in T_5 at 50 DAT (35.67%) followed by 25 and 75 DAT (31.09 and 24.44 %). Data pertaining in Fig. 3 and 4 represented the effect of externally imposed $CdCl_2$ stress on RWC (%) and proline content (µg.g^{-1}) was recorded at regular intervals of 25, 50, and 75 DAT in rice and found that the amount of RWC % was decreased while the amount of proline increased gradually along with the advancement of growth phases of rice plant from 25 to 75 DAT. A similar trend was also observed concerning $CdCl_2$ treatment from 100 to 300ppm concentrations whereas the close analysis of both the data indicated that RWC% and proline content have a negative relationship among them Fig. 5. The data of increase/ decrease (%) over the control for the proline content and RWC % was found in T_5 (46.23) at 25 DAT and (38.28) at 75 DAT (Table 1). while a reduction (%) for RWC% was recorded at 25 DAT and 75 DAT (46.23 and 38.28) over the range of externally induced $CdCl_2$ stress Table 1.

The data regarding the membrane stability index (MSI%) presented in Fig. 6 reveals that the minimum stability of the membrane due to the elevated levels of $CdCl_2$ was found in T_5 (13.9, 21.32, and 25.50%) at all the DAT compared to the rest of the treatments including control (18.19, 34.41 and 39.65%). In comparison, the correlation studies among the MSI % and Proline content (µg.g^{-1}) show a negative

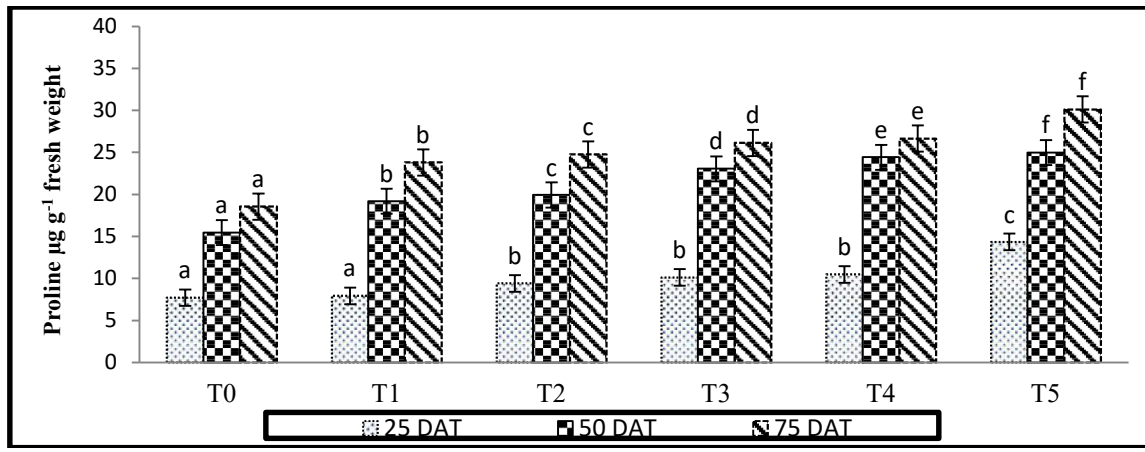

Fig. 4: Effect of $CdCl_2$ treatment on Proline content (µg g^{-1} Fresh weight) in flag leaf.

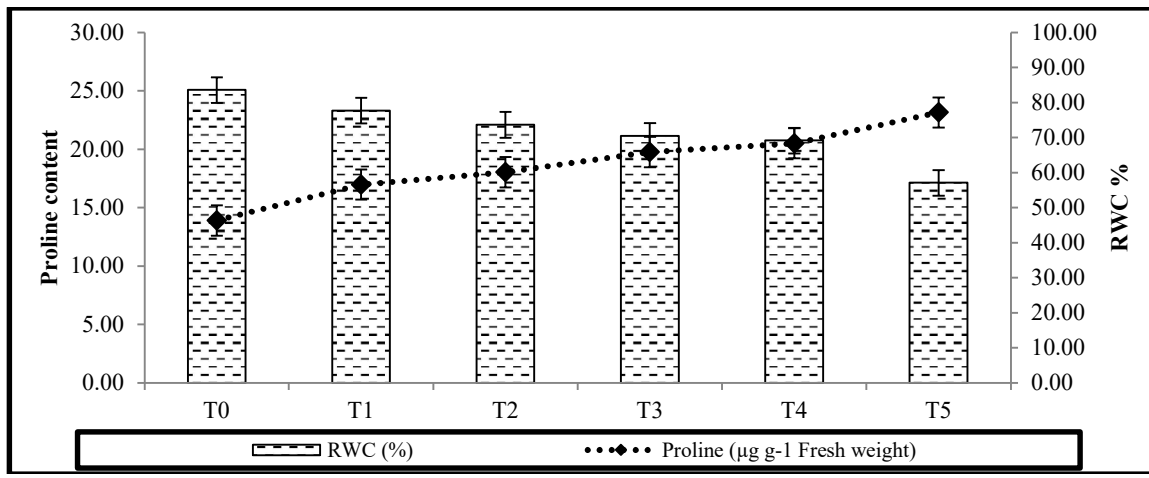

Fig. 5: Effect of different concentrations of cadmium chloride ($CdCl_2$) treatment on Proline content and RWC.

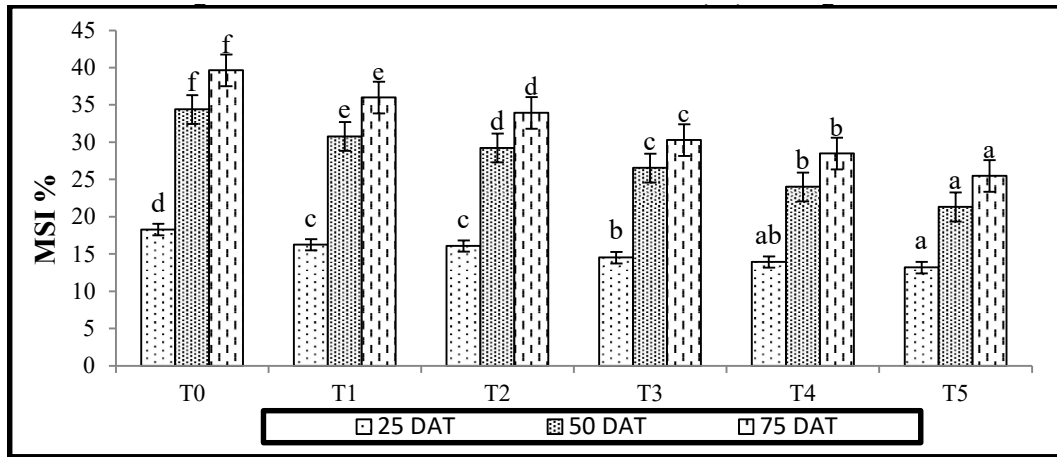

Fig. 6: Effect of $CdCl_2$ treatment on MSI (%) in flag leaf.

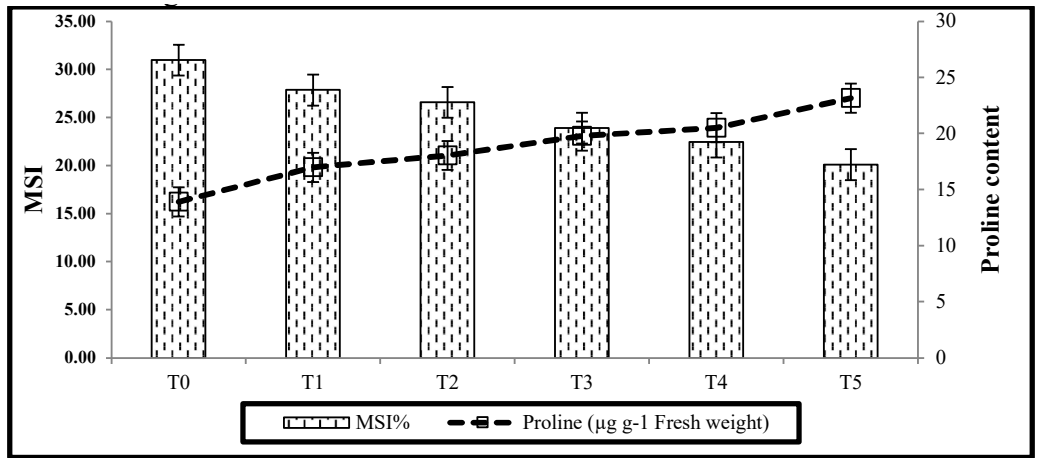

Fig. 7: Effect of $CdCl_2$ treatment on MSI and Proline content.

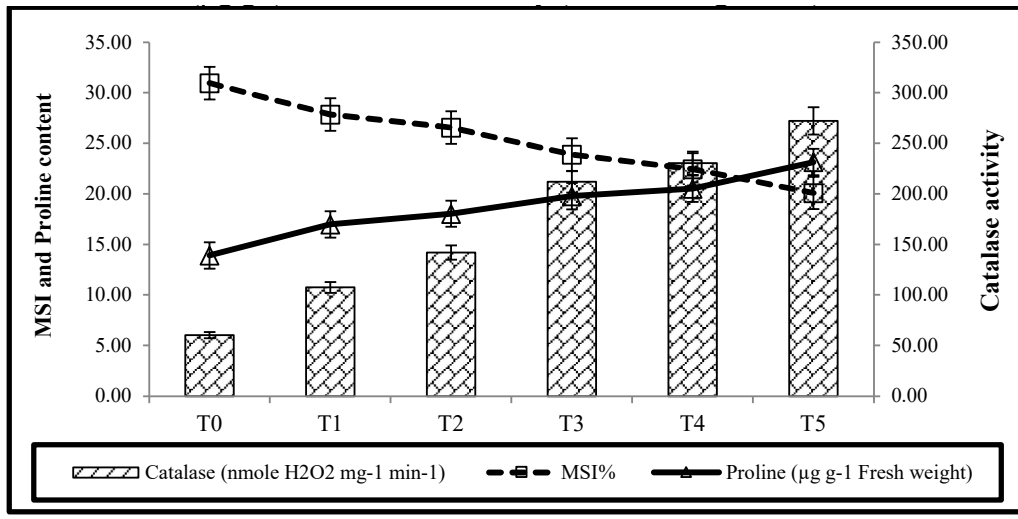

Fig. 8: Effect of $CdCl_2$ treatment on relationship between MSI %, Proline content (µg g^{-1}) and Catalase activity (nm H_2O_2 $mg^{-1}min^{-1}$).

relationship. In contrast, the MSI % was gradually decreased while the proline was increased Fig. 7. The maximum % reduction of MSI was recorded in T_5 at 50 DAT (37.77%) over the range of externally induced $CdCl_2$ stress Table 1.

Data depicted in Fig. 8 shows a relationship among MSI%, proline content ($\mu g.g^{-1}$), and catalase activity (nm H_2O_2 $mg^{-1}.min^{-1}$), where it was observed that proline content and catalase activity were increased significantly along with the elevation of $CdCl_2$ treatments while a negative relationship of MSI % was observed compared to proline and catalase activity.

The present study was executed to know the consequences of an antioxidative defense system in rice under the elevated conditions of $CdCl_2$ stress, whereas the entire sets of $CdCl_2$-treated plants showed a gradual change in the leaf color from green to yellow and a reduction in nitrogen content Fig. 1 and 2. The greenness of leaves was measured through a SPAD meter, and it found that T_5 which was represented the highest concentration of $CdCl_2$. Enough evidence is available to understand the reason behind chlorosis in such types of treated plants, consequently reducing the rate of photosynthesis. The absorption of Cd by the roots and its translocation towards the leaf has a detrimental effect on the biosynthesis of chlorophyll because it inhibits the synthesis of the most important enzymes, amino levulinic acid (ALA) and δ-amino levulinic dehydrogenase (ALDA) in which ALA is substantial than ALDA (Zhao et al. 2021, Morsch et al. 2002) The results of the present work was positively related with the finding of (Pireh et al. 2017) who reported that elevated levels of cadmium toxicity not only inhibit the biosynthesis of chlorophyll but also affect the key enzymes of nitrogen assimilation in the plant that impaired rate of photosynthesis followed by growth and development (Djebali et al. 2005, Zhang et al. 2020, Gratao et al. 2019). It seems from the data depicted in Fig. 3 that the relative water content (RWC %) decreased when the concentrations of externally imposed $CdCl_2$ were increased, while the parallel increase in proline content Fig. 4 and MSI% Fig. 6 was also detected in rice plants.

Moreover, the relation between the RWC% versus proline content Fig. 5 and MSI % versus proline endorse a negative relationship among them. The results are according to the findings of (Rahman et al. 2016), who reported that the presence of Cd in the soil alters the relationship of soil plant water relation that impairs the cell structure and its membrane; hence, RWC % decreased in the plant (Ahmad et al. 2015), a remarkable reduction in membrane stability % (Janmohammadi 2010, Anjum et al. 2015). It was observed from the data that the synthesis of proline and catalase activity increased due to the externally imposed $CdCl_2$ Fig. 4 and 6. The findings are consistent with those of (Siddique et al. 2018), who found that higher concentrations of Cd in the plant cell caused oxidative stress, which increased the production of ROS (O_2^-, OH*, and H_2O_2). ROS overproduction interferes with ETC and mineral uptake (Hasanuzzaman et al. 2012, Ajum et al. 2015, Siddique et al. 2018). However, a natural defense mechanism already exists in the plant body that aids in detoxification because proline is an osmoregulatory compound that maintains water balance and osmotic homeostasis. The enzyme catalase facilitates the scavenging process of overproduced ROS (Qadir et al. 2004, Hasanuzzaman et al. 2012).

CONCLUSION

The present study was conducted to know the consequences of externally induced $CdCl_2$ stress on the antioxidative defense mechanism. Externally induced $CdCl_2$ stress negatively affected the biosynthesis of chlorophyll, nitrogen assimilation, RWC%, and MSI% during the crop growth period. However, at the same time, an upregulation of proline biosynthesis synthesis and activity of catalase enzyme (CAT) was recorded. The defensive role of the compound proline and catalase activity is well known for the antioxidative process that coordinates in balancing soil plant water relationship and scavenging overproduced ROS in rice plants. To overcome the damage that occurs due to the high concentration of $CdCl_2$, further studies are required to find out the substantial treatments that protect the plant in prevailing situations rather than the naturally available antioxidative defense system.

ACKNOWLEDGMENTS

The authors are highly thankful to Lovely Professional University for providing a well-developed research farm and well-equipped research laboratory to conduct the trial and analyze the biochemical parameters needed in the present study. The authors are also thankful to Mr. Robin Paul for coordinating and providing the necessary chemicals for the biochemical analysis.

REFERENCES

Aebi, H. 1984. Catalase in vitro. Methods Enzymol., 105: 121-126.

Ahmad, P., Sarwat, M., Bhat, N.A., Wani, M.R. Kazi, A.G. and Tran, L.S.P. 2015. Alleviation of cadmium toxicity in *Brassica juncea* L. (Czern. & Coss.) by calcium application involves various physiological and biochemical strategies. PloS one, 10: e0114571.

Ali, B., Gill, R.A., Yang, S., Gill, M.B., Ali, S., Rafiq, M.T. and Zhou, W. 2014. Hydrogen sulfide alleviates cadmium-induced morpho-physiological and ultra-structural changes in *Brassica napus*. Ecotoxicol. Environ. Safety, 110: 197-207.

Anjum, S.A., Tanveer, M., Hussain, S., Bao, M., Wang, L., Khan, I. and Shahzad, B. 2015. Cadmium toxicity in Maize (*Zea mays* L.): consequences on antioxidative systems, reactive oxygen species, and cadmium accumulation. Environ. Sci. Pollut. Res., 22: 17022-17030.

Asgher, M., Khan, N.A., Khan, M.I.R., Fatma, M. and Masood, A. 2014. Ethylene production is associated with the alleviation of cadmium-induced oxidative stress by sulfur in mustard types differing in ethylene sensitivity. Ecotoxicol. Environ. Safety, 106: 54-61.

Balestri, M., Bottega, S. and Spano, C. 2014. Response of *Pteris vittata* to different cadmium treatments. Acta Physiol. Plant., 36: 767-775.

Bates, L., Waldren, R.P. and Teare, I.D. 1973. Rapid determination of free proline for water-stress studies. Plant Soil, 39: 205-207.

Bose, B., Kumari, S., Anaytullah, M., Srivastava, A.K., Kuril, S.K. and Singh, P.K. 2008. Effect of mercuric chloride on seed germination, seedling growth, and enzyme activities in maize (*Zea mays* L.). Indian J. Plant Physiol., 290-284 :13.

Briffa, J., Sinagra, E. and Blundell, R. 2020. Heavy metal pollution in the environment and their toxicological effects on humans. Heliyon, 6: e04691.

Djebali, W., Zarrouk, M., Brouquisse, R., El Kahoui, S., Limam, F., Ghorbel, M.H. and Chaïbi, W. 2005. Ultrastructure and lipid alterations induced by cadmium in tomato (*Lycopersicon esculentum*) chloroplast membranes. Plant Biol., *7*(04): 358-368.

Elloumi, N., Zouari, M., Chaari, L., Jomni, C., Rouina, B.B. and Abdallah, F.B. 2014. Ecophysiological responses of almond (*Prunus dulcis*) seedlings to cadmium stress. Biologia, 69: 604-609.

Gratão, P.L., Alves, L.R. and Lima, L.W. 2019. Heavy metal toxicity and plant productivity: role of metal scavengers. In: Srivastava S., Srivastava A., Suprasanna P. (eds), Plant-Metal Interactions, Springer, Cham, pp. 49-60.

Hasanuzzaman, M., Hossain, M.A., da Silva, J.A.T. and Fujita, M. 2012. Plant Response and Tolerance to Abiotic Oxidative Stress: Antioxidant Defense is a Key Factor. In Venkateswaralu, B., Shanker, A.K., Shanker, C. and Maheswari, M. (eds), Crop Stress and Its Management: Perspectives and Strategies, Springer, Dordrecht, pp. 261-315.

Hédiji, H., Djebali, W., Belkadhi, A., Cabasson, C., Moing, A., Rolin, D. and Chaïbi, W. 2015. Impact of long-term cadmium exposure on the mineral content of *Solanum lycopersicum* plants: consequences on fruit production. South Afr. J. Bot., 97: 176-181.

Howladar, S.M. 2014. A novel *Moringa oleifera* leaf extract can mitigate the stress effects of salinity and cadmium in bean (*Phaseolus vulgaris* L.) plants. Ecotoxicol. Environ. Safety**,** 100: 69-75.

Janmohammadi, M. 2010. Alleviation of the adverse effect of cadmium on seedling growth of greater burdock (*Aractium lappa* L.) through pre-sowing treatments. Poljop. Sumar. Titogr., 56(1-4): 5570.

Khan, M.I.R., Nazir, F., Asgher, M., Per, T.S. and Khan, N.A. 2015. Selenium and sulfur influence ethylene formation and alleviate cadmium-induced oxidative stress by improving proline and glutathione production in wheat. J. Plant Physiol., 18-9 :173.

Morsch, V.M., Schetinger, M.R.C., Martins, A.F. and Rocha, J.B.T. 2002. Effects of cadmium, lead, mercury, and zinc on-aminolevulinic acid dehydratase activity from radish leaves. Biol. Plant., 89-85 :45.

Pireh, P., Yadavi, A. and Balouchi, H. 2017. Effect of cadmium chloride on soybean in the presence of arbuscular mycorrhiza and vermicompost. Legume Research, 40: 63-68.

Qadir, S., Qureshi, M.I., Javed, S. and Abdin, M.Z. 2004. Genotypic variation in phytoremediation potential of *Brassica juncea* cultivars exposed to Cd stress. Plant Sci., 1181-1171 :167.

Rahman, A., Nahar, K., Hasanuzzaman, M. and Fujita, M. 2016. Manganese-induced cadmium stress tolerance in rice seedlings: Coordinated action of antioxidant defense, glyoxalase system, and nutrient homeostasis. Compt. Rend. Biol., 474-462 :339.

Saidi, I., Ayouni, M., Dhieb, A., Chtourou, Y., Chaibi, W. and Djebali, W. 2013. Oxidative damages induced by short-term exposure to cadmium in bean plants: protective role of salicylic acid. South Afr. J. Bot., 85: 32-38.

Sairam, R.K., Deshmukh, P.S., Shukla, D.S. and Ram, S. 1990. Metabolic activity and grain yield under moisture stress in wheat genotypes. Indian J. Plant Physiol., 33: 266-231.

Siddique, A., Kandpal, G. and Kumar, P. 2018. Proline accumulation and its defensive role under diverse stress conditions in plants: An overview. J. Pure Appl. Microbiol., 1659-1655 :12.

Siddique, A., Dubey, A.P. and Kumar, P. 2018. Cadmium-induced physio-chemical changes in roots of wheat. Vegetos, 31(3): 113-118.

Weatherly, P.E. 1950. Studies in water relation of cotton plant.1. The field measurement of water deficit in leaves. New Phytol., 49: 81-87.

Zhang, X., Gao, B. and Xi, H. 2014. Effect of cadmium on growth, photosynthesis, mineral nutrition, and metal accumulation of bana grass and vetiver grass. Ecotoxicol. Environ. Safety, 106**:**102-108.

Zhang, H., Xu, Z., Guo, K., Huo, Y., He, G., Sun, H. and Sun, G. 2020. Toxic effects of heavy metal Cd and Zn on chlorophyll, carotenoid metabolism, and photosynthetic function in tobacco leaves revealed by physiological and proteomics analysis. Ecotoxicol. Environ. Safety, 110856 :202.

Zhao, H., Guan, J., Liang, Q., Zhang, X., Hu, H. and Zhang, J. 2021. Effects of cadmium stress on growth and physiological characteristics of sassafras seedlings. Sci. Rep., 9913 :(1)11.

ORCID DETAILS OF THE AUTHORS

A. Siddique: https://orcid.org/0000-0001-6349-4472

Nature Environment and Pollution Technology
An International Quarterly Scientific Journal

p-ISSN: 0972-6268
(Print copies up to 2016)
e-ISSN: 2395-3454

Vol. 23 | No. 1 | pp. 467-473 | 2024

Original Research Paper

https://doi.org/10.46488/NEPT.2024.v23i01.042

Open Access Journal

Why Renewable Energy Gained Attention and Demand Globally?

S. As'ad†
Department of Renewable Energy Engineering, Middle East University, Amman 11831, Jordan
†Corresponding author: S. As'ad; sasad@meu.edu.jo

Nat. Env. & Poll. Tech.
Website: www.neptjournal.com

Received: 30-06-2023
Revised: 11-08-2023
Accepted: 20-08-2023

Key Words:
Renewable energy
Fossil fuels
Energy security
Environmental issues
Sustainability
Climate change

ABSTRACT

Energy security and stable supply are the most important aspects for any nation. The rising need for energy, caused by both population growth and economic activity, is a problem for many nations throughout the world. Consequently, they have to find a way to meet energy demand while also making sure it is inexpensive and sustainable. The use of renewable energy has gradually become one that is being given a lot of attention since it does not cause any harm to the environment. On the other hand, renewable energy is gaining popularity for a variety of different reasons. A paradigm shift toward renewable resources is relevant, as they have the ability to lessen reliance on fossil fuels and decrease environmental consequences; this article will provide several reasons why renewable energy is attracting attention on a global scale. Indeed, renewable energy is plentiful, clean, and might one day provide all of our energy needs. A country's carbon footprint and reliance on fossil fuels may be reduced by investing in renewable energy sources. In addition, there are several health and environmental problems associated with air and water pollution; nevertheless, renewable energy may assist decrease these problems.

INTRODUCTION

Energy may be thought of as the power that drives the planet. It allows for the creation of new technologies, provision of communication, powering of industries, transportation, and essential community services, as well as fueling the heating of buildings. Resources such as solar, wind, hydropower and geothermal are examples of renewable energy. These types of energy sources are replenished naturally, yet they do not run out of energy when they are consumed. Renewable energy is capable of delivering a substantial quantity of energy to generate heat and to provide cooling for both residential and industrial sectors. The use of renewable energy technology is becoming more widespread in a variety of nations all over the globe.

Renewable energy is now in the interest of different countries for various reasons, it is considered a vital instrument for fighting the global warming phenomenon and mitigating CO_2 emissions. It is also considered as an opportunity to diversify the economy and lessen reliance on costly foreign fuels. Additionally, renewable energy is often cheaper than fossil fuels in the long run and can provide reliable power during times of crisis. In contrast, nonrenewable energy is energy derived from resources that are not naturally replenished on a human timescale, such as oil, natural gas, and coal. These resources are finite, meaning that they will eventually be depleted. Nonrenewable energy has traditionally been the dominant source of energy production in many countries, but its use is becoming more contentious due to environmental impacts.

It is worth mentioning that the oil embargo that took place in 1973 triggered widespread interest in alternative energies, which stimulated several approaches to extracting power from renewable sources (Berasaluce & Mendoza-Palacios 2022). It was a major impetus behind the development of renewable energy and increased investment in energy efficiency. Among them, photovoltaic panels began to be regarded as a practical choice for usage in commercial settings. The purpose of this paper is to underscore the significance of making a paradigm shift to renewable resources and to explain why renewable energy is gaining traction on a worldwide scale by offering various explanations.

FOSSIL FUELS ARE FINITE RESOURCES

Oil, in particular, is a finite resource. This means that it is not renewable and will eventually run out. The amount of oil left in the world is decreasing as it is used up, and when it is gone, it will not be available again. The world has proven reserves equivalent to 46.6 times its annual consumption levels. This means that it has about 47 years of oil left (at current consumption levels and excluding unproven reserves) (WorldoMeters 2016). However, it's worth mentioning

that some countries that produce oil have strategic plans to increase their production of oil in the near future.

Furthermore, it is anticipated that the oil demand will rise from almost 97 million barrels a day ($mb.d^{-1}$) in 2021 to over 110 $mb.d^{-1}$ in 2045. As a result, oil is expected to retain the largest share in the energy mix throughout the outlook period, with almost a 29% share in 2045 (OPEC 2022). Accordingly, the period of 47 years will shrink and get shorter.

FLUCTUATION OF OIL PRICES

In regards to global energy supplied by the source, oil supplied 9% of new demand in 1900-20, accelerating to 17% in 1920-40, 29% in 1940-80 (Fattouh et al. 2019), and it reached 34% in 2019 (Haider 2020). However, Oil prices are subjected to unpredictable fluctuations due to a variety of factors. These include shifts in the global economic conditions, supply and demand, geopolitical tensions, speculation, and trading. In addition, weather patterns, technological advances, and the discovery of new oil reserves can also impact oil prices.

The forces of supply and demand determine oil prices in the global oil market. Supply is determined by how much oil is produced by the Organization of the Petroleum Exporting Countries (OPEC), non-OPEC producers, and how much is in inventory. Demand is determined by the amount of oil that is consumed globally. When the demand for oil increases, the price of oil rises. When the demand for oil decreases, the price of oil falls. There is no way to accurately predict the future price of oil, so it is important to be prepared for the possibility of price volatility in the market.

Consequently, this fluctuation in the price of oil can have a significant impact on the government budget and can have a negative impact on Gross Domestic Product (GDP). In extreme cases, price volatility can cause economic hardship and even the collapse of governments. However, this can be offset by investing in renewable energy sources, which will help to stabilize government budgets and create economic growth. Fig. 1 illustrates the price of oil in the past decades. Fig. 1 reveals that there have been several falls and rises in the oil price from 1998 to the beginning of 2023 (Lin & Bai 2021).

FUTURE ENERGY DEMAND

According to the United Nations, the world population is currently estimated to be 7.7 billion people, and the global energy demand is estimated to grow by 28% from 2017 to 2040 (World Energy Outlook 2018). This represents an average annual growth rate of 1.3 percent. The International Energy Agency (IEA) states that the growth in energy demand will be driven mainly by increases in population and economic activity. In particular, emerging economies will be the main drivers of energy demand growth, accounting for 70% of the total increase in global energy use by 2040. The growing demand for electricity and transportation fuels will drive the increase in energy demand.

However, approximately 1.2 billion people, or 17% of the world's population, living in rural areas do not have

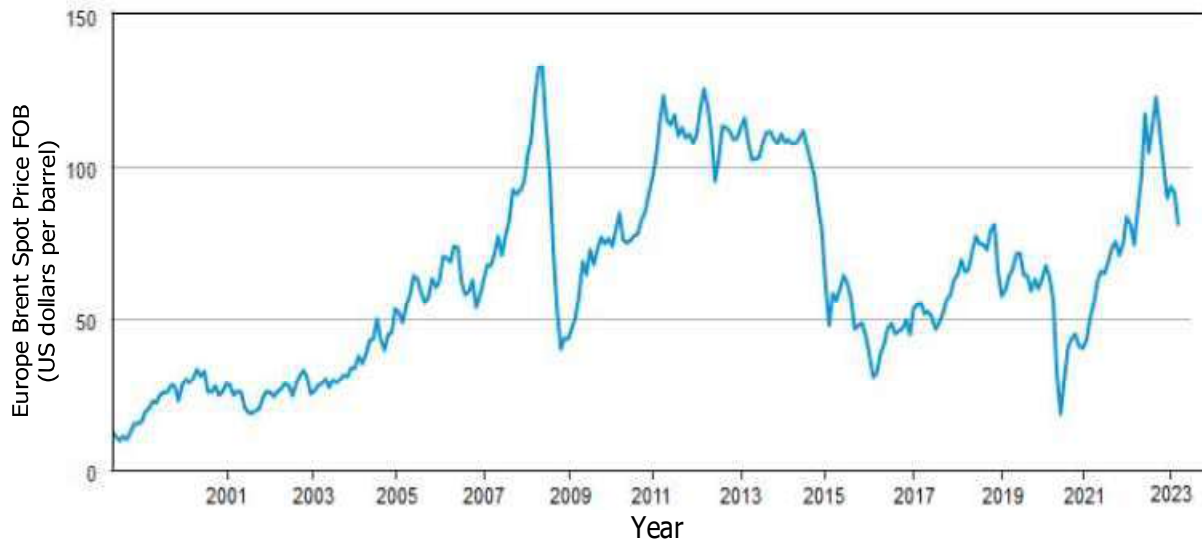

Fig. 1: Dynamic change trend of Brent crude oil price from 2000 to 2023 (US Energy Information Administration. 2023). (FOB free on board)

access to electricity (World Bank). Developing an electrical infrastructure in such areas is usually not feasible due to the extreme distance from existing electric grids. Further, building new power plants in remote areas is not cost-effective due to the relatively low electricity consumption. In these cases, alternative solutions must be sought to provide electricity to these remote areas. One potential solution is to utilize renewable energy sources, such as solar, wind, or hydropower. By using these renewable sources, electricity can be generated and supplied to such areas, as well as providing hot water and energy for cooking without the need for costly infrastructure investments or upgrades.

ENERGY SECURITY

Energy is the essence of any production process, and it must be secured for the economic growth of the nations (Gökgöz & Güvercin 2018). Energy security concerns raise global awareness of renewable energy. High and volatile fossil fuel prices in the wake of Russia's invasion of Ukraine highlight the risks inherent in today's energy system as well as the significance of energy security to the economies and daily lives (World Energy Outlook 2022). In the current energy scenario, energy security is a big issue.

Energy transitions present an opportunity to construct a more secure, long-term energy infrastructure that lessens reliance on volatile fuel prices and lowers monthly utility bills. Renewable energy has been shown to enhance energy security in many ways. It can reduce reliance on imported fuels, which are increasingly expensive and insecure due to geopolitical instability, help stabilize energy prices, and support local economic development. As the world transitions away from the use of fossil fuels, renewable energy sources will play an increasingly important role in ensuring a stable energy supply for the future.

Norway is a leader in energy security due to its abundant natural resources and its commitment to renewable energy production. Norway is one of the world's top oil and natural gas producers. However, the country has invested heavily in renewable energy sources through setting ambitious goals to reduce its emissions and has committed to achieving carbon neutrality by 2050. Additionally, the government has instituted a number of programs, including subsidies, tax incentives, and public investments to boost the proportion of renewable energy sources in the overall energy mix. It should be noted that around 98% Norway's electrical generation comes from renewable sources (Razmjoo et al. 2022).

RENEWABLE ENERGY IS COST COMPETITIVE

The oil shortages that occurred in the 1970s played a role in promoting the need to come up with alternative energy sources and increasing investment in energy conservation. Ongoing research and development efforts to enhance energy scalability and improve efficiency have the potential to make renewable energy more affordable in the future. (Timilsina & Shah 2022).

The price of energy has been decreasing over the past few years due to the evolution of technology in this sector

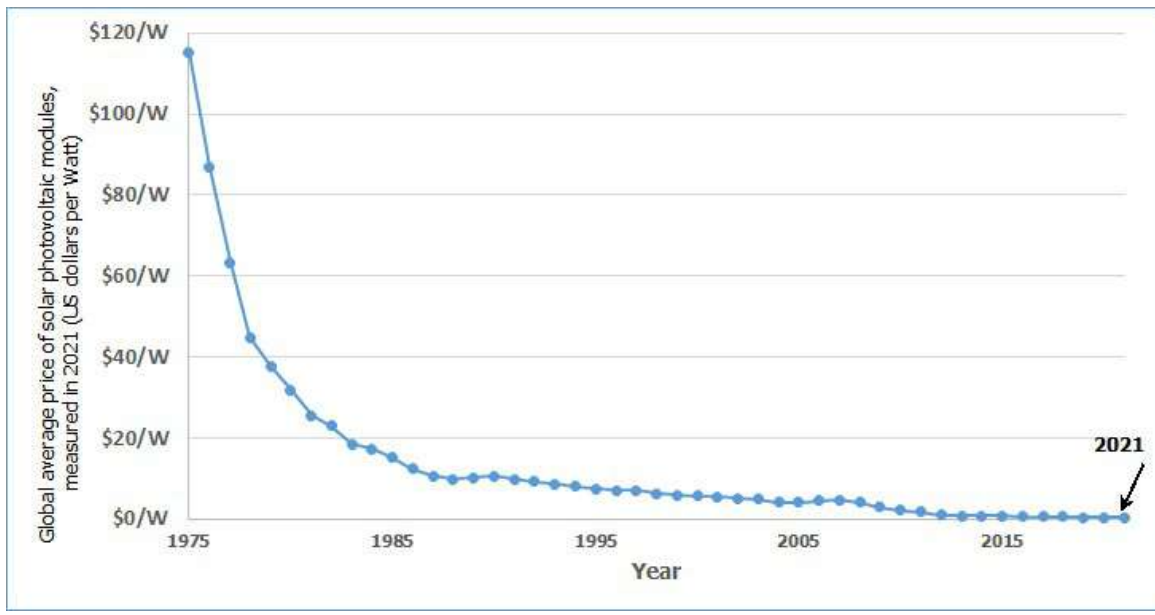

Fig. 2: Global average price of photovoltaics - US$ per Watt.

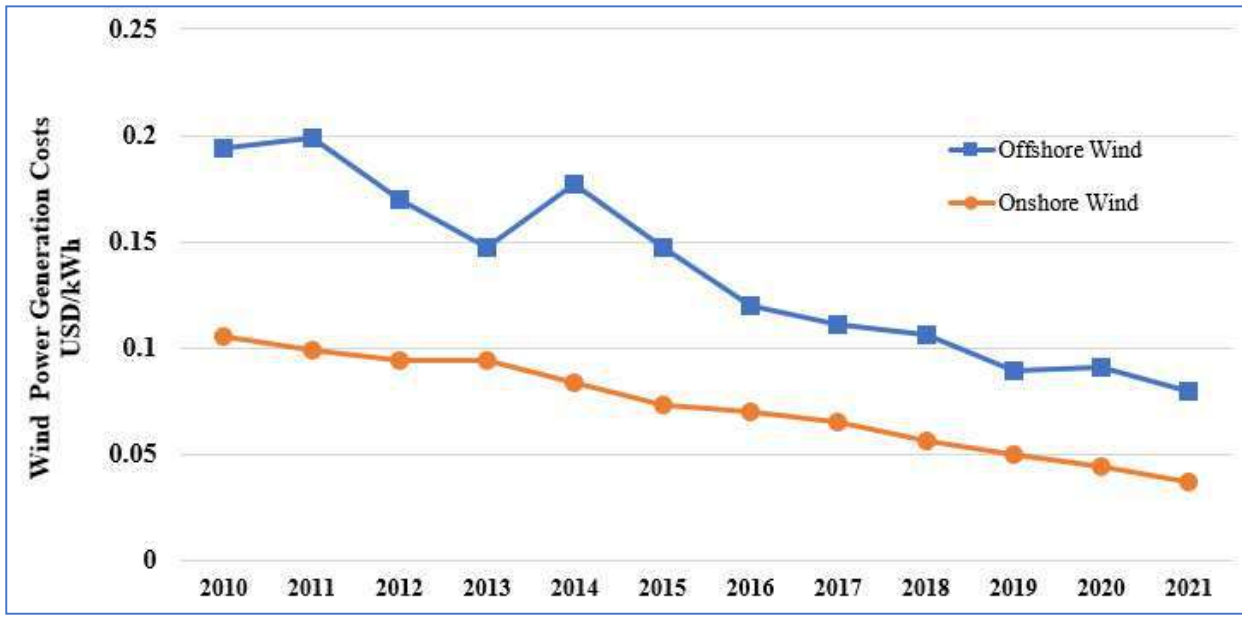

Fig. 3: Costs of onshore and offshore utility-scale - US$ per kWh.

and market competition. For instance, during the period from 2010 to 2018, electricity from utility-scale photovoltaic and wind sources dropped by 77% and 35%, respectively (He et al. 2020). This trend is expected to continue in the new era as more renewable energy sources are brought online and more efficient technologies are developed against traditional sources of electricity. In addition, renewable energy is more cost-competitive when compared to traditional sources of energy on a life-cycle basis. While the upfront costs of renewable energy may be higher than those of traditional sources, the long-term costs are lower because these sources of energy produce zero emissions and require little or no maintenance.

Fig. 2 shows the average price of photovoltaic modules from 1976 to 2021. It is important to note that in 1976, the price was 115.28 US$/W, but in 2021, the price was only 0.27 US$/W (Hannah et al. 2022). Similarly, from 2010 to 2021, utility-scale onshore wind power costs dropped 68%, and offshore wind power dropped 60%. With electricity savings from various renewable energy sources, IRENA estimates that people around the world could save $55 billion in 2022 (IRENA 2022). Fig. 3 illustrates the falling cost of both onshore and offshore wind power.

HUMAN DEVELOPMENT INDEX

The index that is used to measure the human development level of a country in regards with UN Charter as outlined under HDI or Human Development Index. This is an index that includes other indicators such as life expectancy or health, education, and per capita income. It is a classical indicator of welfare, and it equals to the three-dimensional indicators' arithmetic average, thus ranging between 0 and 1. HDI is a very useful indicator since it can be used in comparing development levels between countries and overtime for measuring improvement. Those countries having an HDI rate of 0.8 or above are said to belong under the classification of developed countries, and other counterparts with a below amounting up to only about 0.5 magnitude will generally be designated as developing countries.

Electricity consumption and economic growth, as measured by monetary metrics like Gross National Product (GNP) and GDP, have been subjected to several studies for numerous nations around the world. The studies have shown a causal relationship and long-run co-integration between national economic performance and electricity use. (Lu 2016, Aviral et al. 2021, Eras et al. 2022, Hassan et al. 2022).

Fig. 4 depicts the positive correlation between the HDI and the annual per capita consumption of electricity because a higher HDI indicates a higher standard of living, which is associated with increased access to electricity. Consequently, economic growth in a country might be enhanced with social welfare and broader access to electricity and other services, and this can be attained through utilizing low-cost energy resources, renewable energy in particular.

RENEWABLE ENERGY IS CREATING UNIQUE JOBS

The shift to renewable energy is creating a wide range of

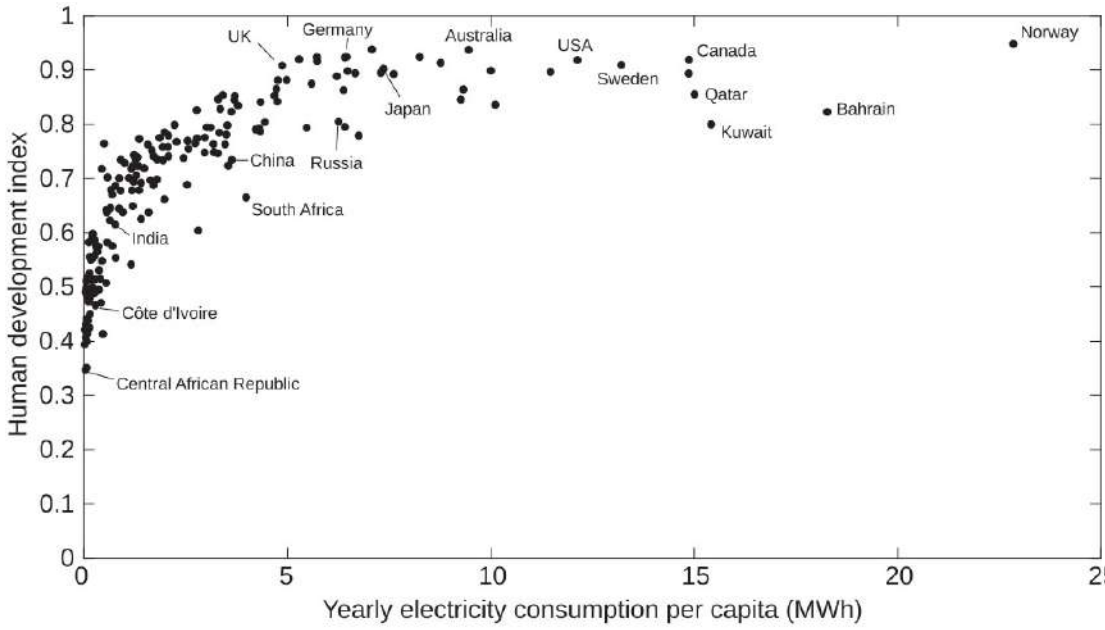

Fig. 4: HDI vs. Electricity consumption (Jahan 2016).

new jobs, from research and development to engineering and manufacturing. For instance, solar photovoltaic installers, wind turbine engineers, and energy storage technicians are some of the most in-demand jobs in the renewable energy sector. Other areas of job growth include energy efficiency advisors, environmental advocacy, and policy analysis. Renewable energy is also creating jobs in finance, legal services, marketing, and communications. Many of these jobs are new and unique to the renewable energy field.

Electricity generated by Renewable Energy generally creates many times more direct work opportunities in the Developing World than fossil or nuclear energies. For example, solar thermal (10.4 jobs.GWh^{-1}) creates 35 times more than current coal (0.3 jobs.GWh^{-1}). When nuclear energy and gas are compared with PV, 620 times more direct jobs will be created. This excludes significant numbers of indirect and induced jobs (Detlef & Scherer 2013). According to a report from the International Renewable Energy Agency, renewable energy sources such as solar and wind created more than 10 times more direct jobs in 2015 than fossil fuels. This is because renewable energy sources require more specialized skills, hands-on maintenance, and installation than fossil fuels. Moreover, an analytical job creation assessment for the global power sector from 2015 to 2050 on a regional basis has shown that the number of direct jobs in electricity would grow from over 21 million to nearly 35 million. The primary technologies that will create new jobs are solar photovoltaic, batteries, and wind power (Ram et al. 2020)

SEVERE HEALTH AND ENVIRONMENTAL PROBLEMS

Fossil fuels pose a huge threat to environmental balance and are a cause of a wide variety of ecological hazards (Shahzad 2012). Emissions released into the atmosphere include carbon dioxide, nitrogen oxides as well sulfur dioxide. Such undesired pollutants of the air contribute highly to environmental pollution, in that they can cause some sicknesses including asthmatic attack and bronchitis as well as other forms of respiratory related ailments. In addition, mining of these sources can cause heavy metals to be released into the environment and contaminate waterways, while the burning of these sources can release toxic chemicals into the air, which can then fall back to the earth in the form of acid rain, causing land and water pollution. Consequently, these factors would strain the environment.

Countries are required to mitigate CO_2 emissions by implementing strict measures. The most important step the world is currently emphasizing is to shift the industrial structure to renewable energies. To serve this purpose, renewable energy is seen as a key investment opportunity for countries looking to break into the global low-carbon economy (Chen et al. 2022).

CLIMATE CHANGE

The Intergovernmental Panel on Climate Change (IPCC) and other international groups are demanding drastic cuts in greenhouse gas (GHG) emissions due to the severity of

human-caused climate change (Metz et al. 2007). By 2050, global GHG emissions should be roughly cut to 50% of the emission level of the year 2000 (Hohmeyer & Bohm 2015). As mentioned before, burning fossil fuels releases large amounts of carbon dioxide, methane, and other greenhouse gases into the atmosphere. These gases absorb and trap heat in the atmosphere, causing temperatures to rise. This process is called the greenhouse effect, and it contributes a major part of Global warming. There is a change in climate patterns as temperatures rise, which escalates to more droughts, floods, hurricanes, and many other extreme weather events. Such occurrences cause destruction to ecosystems, human health and cripple the economy.

Considering that the majority of electricity is derived from nonrenewable resources, the reduction of environmental impact could be accomplished through renewable energy technology (Biekša et al. 2021). There are also other environmental problems related to fossil fuels like air pollution, water contamination, and land degradation. Switching to renewable energy and reduced reliance on fossil fuels would mitigate all these negative effects. In other words, encouraging renewable energy sources' development has been a critical strategy of energy strategy for most governments across the globe in order to combat climate change effects (Zhao et al. 2022).

RENEWABLE ENERGY IS SUSTAINABLE

As the world moves towards a low carbon future, renewable energy sources are gaining in importance and viewed as central to sustainable development. The United Nations in 2015 releases a number of Sustainable Development Goals (SDGs) to address the major global issues by 2030 that include poverty, climate change impact, inequalities and economic problems. The sustainable energy is the centerpiece of these SDG's (UN DESA 2017).

However, it is crucial to note that the global evaluation of sustainability effects within countries as a result of renewable energy was used globally from 1990 through 2014. It was determined that the most important factor to have a positive influence on sustainability, regardless of whether it is measured from economic prosperity or environmental protection viewpoint would be share of renewable energy in total domestic energy consumption. This also shows that renewable energy has made a substantial positive impact on improving world sustainability (Sueyoshi et al. 2022).

CONCLUSIONS

In conclusion, renewable energy has become a major talking point in recent years, as many countries around the world are considering it in their energy strategy to make a push to transition away from fossil fuels and towards a greener energy source. It's an eco-friendly and long-term solution to many energy generation problems. Solar and wind energies are just a few examples of renewable energy that have the potential to meet the growing electricity demand. Reflecting this trend, the majority of success in raising the percentage of renewables in the energy supply has been made in the power sector, with renewable energy supplying almost 30% (with solar and wind power accounting for 12.1%) of global electricity generation in 2022, compared to 21.3% (with solar and wind power accounting for 2.8%) in 2012.

This means that the renewable share of global electricity generation increased by almost 9 percentage points in the past decade. In addition to being cost-competitive, renewable energy also provides other economic benefits. For example, it can help reduce the need for expensive infrastructure upgrades and maintenance, such as the modernization of power plants, which can be costly. It can also create new jobs and stimulate economic growth in communities that adopt renewable energy technologies. Governments should offer tax breaks, subsidies, and grants for research and development to encourage people and businesses to use renewable energy sources since it would be a great option for the new generation.

They can also help reduce our dependence on foreign sources of energy, making us more secure and self-sufficient. Overall, this article demonstrates that renewable energy is a win-win situation and emphasizes the need for a paradigm change from traditional to renewable resources for the reasons stated. If the proper laws and policies are put in place, renewable energy can indeed contribute to the development of a better and more sustainable future.

ACKNOWLEDGEMENTS

The author is grateful to the Middle East University, Amman, Jordan, for the financial support granted to cover the publication fees of this research article.

REFERENCES

Aviral, T., Eapen, L. and Nair, S. 2021. Electricity consumption and economic growth at the state and sectoral level in India: Evidence using heterogeneous panel data methods. Energy Econ., 94: 105064.

Berasaluce, J. and Mendoza-Palacios, S. 2022. Using total variation distance to study technological transitions: The case of renewable energy generation. SSRN, 1: 74.

Biekša, K., Zonienė, A. and Valiulė, V. 2021. Sustainable investment: A solution to reduce environmental footprint. Energies, 14(11): 3104.

Chen, H., Shi, Y. and Zhao, X. 2022. Investment in renewable energy resources, sustainable financial inclusion, and energy efficiency: A case of US economy. Resour. Policy, 77: 102680.

Detlef, S. and Scherer, V. 2013. Transition to Renewable Energy Systems. Wiley-VCH Verlag GmbH & Co. KGaA, NY.

Eras, J.J.C., Fandiño, J.M.M., Gutiérrez, A.S. and Bayona, J.R. 2022. Assessing the causality relationship and time series model for electricity consumption per capita and human development in Colombia. Energy Rep., 8: 10464-10477.

Fattouh, B., Poudineh, R. and West, R. 2019. The rise of renewables and energy transition: what adaptation strategy exists for oil companies and oil-exporting countries? Energy Trans., 3(1-2): 45-58.

Gökgöz, F. and Güvercin, M.T. 2018. Energy security and renewable energy efficiency in EU. Renew. Sustain. Energy Rev., 96: 226-239.

Haider, W. 2020. Estimates of total oil & gas reserves in the world, future of oil and gas companies, and SMART investments by E & P companies in renewable energy sources for future energy needs. Int. Petrol. Technol. Conf., 16: 45-56.

Hannah, R., Max, R. and Pablo, R. 2022. Energy Our World in Data. https://ourworldindata.org/energy.

Hassan, M.S., Mahmood, H. and Javaid, A. 2022. The impact of electric power consumption on economic growth: A case study of Portugal, France, and Finland. Environ. Sci. Pollut. Res., 6: 1-17.

He, G., Lin, J., Sifuentes, F., Liu, X., Abhyankar, N. and Phadke, A. 2020. Rapid cost decrease of renewables and storage accelerates the decarbonization of China's power system. Nat. Commun., 11(1): 2486

Hohmeyer, O.H. and Bohm, S. 2015. Trends toward 100% renewable electricity supply in Germany and Europe: A paradigm shift in energy policies. Energy Environ., 4(1): 74-97.

International Renewable Energy Agency (IRENA). 2022. Renewable Power Generation Costs in 2021. https://www.irena.org/publications /2022/Jul/Renewable-Power-Generation-Costs-in-2021.

Jahan, S. 2016. Human Development Report 2016: Human Development for Everyone. Technical Report. United Nations Development Program, New York, USA.

Lin, B. and Bai, R. 2021. Oil prices and economic policy uncertainty: Evidence from global, oil importers, and exporters' perspective. Res. Int. Bus. Fin., 56: 65-70.

Lu, W.C. 2016. Electricity consumption and economic growth: Evidence from 17 Taiwanese industries. Sustainability, 9(1): 56-63.

Metz, B., Davidson, O.R., Bosch, P.R., Dave, R. and Meyer, L.A. (eds). 2007. IPCC, Climate Change: Mitigation. Contribution of Working Group III to the Fourth Assessment Report of the Intergovernmental Panel on Climate Change. Cambridge University Press, Cambridge.

OPEC. 2022. OPEC World Oil Outlook (WOO). International Petroleum Exhibition and Conference.

Ram, M., Aghahosseini, A. and Breyer, C. 2020. Job creation during the global energy transition towards a 100% renewable power system by 2050. Technol. Forecast. Soc. Change, 151: 119682.

Razmjoo, A., Mirjalili, S., Aliehyaei, M., Østergaard, P.A., Ahmadi, A. and Nezhad, M.M. 2022. Development of smart energy systems for communities: Technologies, policies, and applications. Energy, 248: 123540

Shahzad, U. 2012. The need for renewable energy sources. Int. J. Inform. Technol. Electr. Eng., 5: 16-18.

Sueyoshi, T., Mo, F. and Wang, D.D. 2022. Sustainable development of countries all over the world and the impact of renewable energy. Renew. Energy, 184: 320-331.

Timilsina, G.R. and Shah. K.U. 2022. Economics of Renewable Energy: A Comparison of Electricity Production Costs Across Technologies. Oxford Research Encyclopedia of Environmental Science.

United Nations Department of Economic and Social Affairs (UN DESA). 2017. Sustainable development goal 7: ensure access to affordable, reliable, sustainable, and modern energy for all UN DESA. New York, NY. https://sustainabledevelopment.un.org/sdg7.

US Energy Information Administration. 2023. Europe Brent Spot Price FOB. Spot Prices for Crude Oil and Petroleum Products

World Energy Outlook. 2018. International Energy Agency. https://www.iea.org/reports/world-energy-outlook-2018

World Energy Outlook. 2022. International Energy Agency. https://www.iea.org/reports/world-energy-outlook-2022

WorldoMeters 2016. World Oil Reserves. https://www.worldometers.info/oil/

ORCID DETAILS OF THE AUTHORS

S. As'ad: https://orcid.org/0000-0003-4127-3286

Nature Environment and Pollution Technology
An International Quarterly Scientific Journal

p-ISSN: 0972-6268
(Print copies up to 2016)
e-ISSN: 2395-3454

Vol. 23 | No. 1 | pp. 475-483 | 2024

Original Research Paper

https://doi.org/10.46488/NEPT.2024.v23i01.043

Open Access Journal

Extraction of Environment-Friendly Biodegradable Poly-Hydroxy Butyrate Using Novel Hydrodynamic Cavitation Method

A. A. Lad*, V. D. Gaikwad*†, S. V. Gaikwad, A. D. Kulkarni* and S. P. Kanekar***

*Department of Chemical Engineering and Bioengineering, Dr. Vishwanath Karad MIT World Peace University, Pune-411038, Maharashtra, India

**Department of Biosciences and Technology, Dr. Vishwanath Karad MIT World Peace University, Pune-411038, Maharashtra, India

†Corresponding author: V. D. Gaikwad; vikrant.gaikwad@mitwpu.edu.in

Nat. Env. & Poll. Tech.
Website: www.neptjournal.com

Received: 16-06-2023
Revised: 23-07-2023
Accepted: 17-11-2023

Key Words:
Polyhydroxy butyrate
Hydrodynamic cavitation
Haloarchaea
Biopolymers

ABSTRACT

Polyhydroxy butyrate (PHB) is one of the best environment-friendly bioplastic alternatives for petroleum-based plastic due to its biodegradability. However, it has less commercial popularity owing to the high cost of downstream processing that involves repeated centrifugation and the use of costly harmful solvents, as well as a labor-intensive process. Hydrodynamic Cavitation (HC) offers easy and simple mechanisms for downstream processing. Also, biopolymer extracted for haloarchea show an advantage of least contamination under the halophilic condition on an industrial level. In this paper, a haloarchaeal consortium producing biopolymer isolated from commercial rock salt has been subjected to HC as well as distilled water lysis. A maximum of 23 $g.L^{-1}$ PHB was extracted in 40 min run with 50 passes and 0.10 cavitation number at 3.9 bar pressure. The extracted biopolymer was characterized and was found to be PHB. Comparative analysis shows that HC results in a substantial reduction in the downstream processing time. Moreover, it has double the efficiency of PHB extraction as compared to the distilled water lysis method. This paper reports the HC process as a techno-commercial alternative to industrial PHB extraction.

INTRODUCTION

The management of solid waste, especially when it consists of non-biodegradable plastic, is a major cause of environmental pollution. The accumulation of plastic waste has led to overflowing landfills, clogged waterways, health hazards to human life, and endangered terrestrial as well as marine habitats. A cost-effective alternative to petroleum plastic production is the need of the hour. Therefore, accelerating the development of biodegradable polymers needs utmost attention. Polyhydroxy butyrate (PHB), under the class of polyhydroxy alkanoates (PHA), is one such example of a biodegradable polymer with multiple applications (Niti Aayog 2022).

Under nutrient-deficient situations, several types of bacteria accumulate PHAs intracellularly as carbon and energy reserves (Kanekar et al. 2014). Amongst them, haloarchaea are one of the abundantly available species known to produce PHB (Simó-Cabrera et al. 2021). These haloarchaea can be isolated from rock salt available in different regions of the world (Jaakkola et al. 2014, Kondo 2015).

Extraction of PHB from these cells is popularly done with the help of organic solvents such as acetone, chloroform, methylene chloride, and methanol. However, these solvents are both expensive and harmful to the environment. The typical solvent extraction technique necessitates the storage, management, transportation, and recovery of the solvent. It necessitates substantial capital expenditures for the equipment as well as substantial running expenditures throughout the process. Additionally, trash disposal requires treatment. Moreover, obstacles such as poor substrate availability, cost of the carbon sources, low yield, microbe instability under changing circumstances, and greater energy requirements of downstream processing leading to high production costs have restricted the large-scale production of PHB ((Niti Aayog 2022, BIRAC 2021).

One way to reduce the downstream processing cost is using hydrodynamic cavitation. Hydrodynamic cavitation (HC) is an environmentally friendly process in which a great deal of energy is discharged in a flowing liquid as a result of the disintegration of a bubble caused by a decrease and concurrent increase in local pressure. The process consists of passing the liquid through a constriction like an aperture

or venturi or by rotating an item in a liquid (Chen et al. 2023). This method has been used for wastewater treatment, synthesis of chemicals using various reactions like oxidation reactions, emulsion generation, sludge treatment, biodiesel synthesis, degradation of residues from pharmaceutical or dye industries, food processing, and component extraction (Chen et al. 2023, Patil et al. 2021a, Zheng et al. 2022, Wang et al. 2021, Sun et al. 2022, Randhavane & Khambete 2017). Wang et al. (2021) reviewed the advantages of cavitation-based processes, such as cost-effectiveness in operation, higher energy efficiencies, and large-scale operation for treating industrial effluents (Wang et al. 2021). Because of its great energy efficiency, cost-effective operation, ability to generate chemical reactions and scale-up capabilities, HC has been regarded as a viable technology for process intensification (Zheng et al. 2022, Wang et al. 2021).

On similar lines, this approach can be utilized efficiently for industrial cell disruption to extract PHB on an industrial scale. This method will reduce all these expenses, rendering the method cost-effective. Several workers have studied the use of hydrodynamic cavitation for the extraction of metabolites and enzymes. Recent research by Wu et al. (2019) examined the extraction of bioactive chemicals from plants, lipids from algal biomass, and the delignification of lignocellulosic biomass via hydrodynamic cavitation (Wu et al. 2019). Verdini and co-workers evaluated the effectiveness of cavitation as a pretreatment strategy for cellulose recovery by disrupting the resistant lignocellulosic matrix (Verdini et al. 2021). This was accomplished in temperatures as low as 35 to 50°C. Setyawan et al. (2018) extracted the lipids from the microalgae *Nannochloropsis* sp. Using a hydrodynamic cavitation setup of the venturi type and compared it to traditional solvent extraction. Based on the volumetric mass transfer coefficient data, it was determined that hydrodynamic cavitation is more effective than its counterpart (Setyawan et al. 2018). Thus, the utilization of hydrodynamic cavitation for cell disruption on a wide scale with high energy efficiency possesses enormous promise.

Using the concept of location factor, Balasundaram & Pandit (2001b) measured the dependence of enzyme release on their position within the cell. The location factor was defined as the rate of enzyme released to the rate of total protein released. Typically, the location factor for periplasmic enzymes was more than 1, whereas it was less than 1 for cytoplasmic enzymes (Balasundaram & Pandit 2001b). Due to the importance of the enzyme's cellular location, pretreatment techniques can be used to modify the enzyme's cellular location prior to the actual cell disruption procedure. By pretreatment, the translocation of enzymes from the cytoplasm to the periplasm can be used to improve the efficacy of cell disruption and reduce energy needs (Balasundaram & Pandit 2001a). Literature reports that heat stress, period of culture in the fermentation process (Balasundaram & Harrison 2006), variable pH operation, and chemical pre-treatment (Anand et al. 2007) are among the approaches employed for translocation. Compared to the standard solvent extraction approach, this process has been found to be economical, energy efficient, and environmentally friendly (Wu et al. 2019, Gaikwad et al. 2016, Patil et al. 2021a, Patil et al. 2021b).

The purpose of this paper is to investigate the efficacy of the hydrodynamic cavitation method for the extraction of PHB with respect to the osmotic pressure method using distilled water, which further involves the use of solvents.

MATERIALS AND METHODS

Source of Haloarchaea

The haloarchaeal consortium was developed using commercial rock salt procured from the local market in Pune, Maharashtra, India. The haloarchaea were enriched in a modified Sehgal-Gibbons (SG) medium with 20 g% NaCl (Sehgal & Gibbons 1960) and were further grown in PHB Accumulation Medium (PAM) (Kanekar 2014).

Qualitative Characterization of Poly Hydroxy Butyrate (PHB) Producing Haloarchaea Using Sudan Black B Staining

The haloarchaea were grown in PHB Accumulation Medium (PAM), and after 96 hours, Sudan Black B staining was done according to standard protocol (Sheehan & Story 1977).

PHB Production by Haloarchaea

The haloarchaea were inoculated (10% v/v) in PAM with glucose (1%) as a carbon source and 20 g% NaCl in open 3 L in a conical flask. Aeration was provided with the help of an aerator, and the flask was incubated at 37°C in the incubator.

Extraction of PHB Using Hydrodynamic Cavitation Setup

The hydrodynamic cavitation experimentation setup was procured from Vivira Process Technologies, Pune. The schematic in Fig. 1 represents the actual setup. The working volume of the holding tank was 3 L. The line size was 0.25 inches, and a pump of 1.5 hp was used. The valve V1 was provided to regulate the flow rate. A bypass valve (V2) was provided, which was used to vary the pressure from 0 to 4 bar. The culture medium was passed through the cavitation device for cell lysis and collected in the holding tank. This

was recirculated through the device for several runs, which were conducted for up to 30-60 min and translated to 50 passes. The cavitation number was found to be 0.1, as per the methodology described by Marjadi & Dharaiya (2014). The flow rate was between 320-430 $L.h^{-1}$. Inoculum density was monitored and maintained by taking absorbance at 600 nm and CFU (Colony Forming Unit)/mL. Samples were collected at intervals of every 10 min and analyzed for temperature, density, and pH. The experiment was done in duplicate and analyzed for variance. These samples were used further for the extraction of PHB.

The liquid media obtained after hydrodynamic cavitation was subjected to centrifugation for 20 min at a speed of 8000 rpm. The white-colored PHB pellet was dissolved in chloroform and weighed after drying at ambient temperature (37±2°C). PHB dissolved in chloroform was cast in a petri dish and was allowed to dry at 65°C in the oven. After complete drying, PHB film was subjected to characterization by various methods. PHB film was precipitated using methanol, and a methanol precipitate of PHB was obtained.

Extraction Using Distilled Water Lysis

For comparison, liquid growth was subjected to centrifugation for 20 min at 8000 rpm, and the product was resuspended in distilled water. The suspension was allowed to stand for 30 min at ambient temperature to ensure proper lysis. The suspension was centrifuged at 2500 rpm repetitively till the red-orange color of the cells disappeared, and the white PHB pellet remained. The white PHB pellet was dissolved in chloroform and weighed after drying at ambient temperature (37±2°C). The dry cell weight of PHB by HC and distilled water lysis was compared.

Characterization of Biopolymer Using Spectrophotometric Analysis, FTIR

The confirmation and characterization of the PHB were characterized by crotonic acid assay, spectrophotometric analysis, and FTIR.

Estimation of PHB by Crotonic Acid Assay

The amount of PHBs in a sample taken was determined by spectrophotometric assay (Selvakumar et al. 2011). This assay was aided by the transformation of PHBs to crotonic acid via sulfuric acid treatment. Crotonic acid standard solutions of increasing concentrations (10 to 40 g) were developed. Crotonic acid absorbance was determined at 230 nm, and a standard curve was generated. The sample was then placed in a clean test tube containing 5 to 50 g of polymer in chloroform, and the solvent was evaporated by heating in a boiling water bath. The tube was then filled with 10 mL of concentrated H_2SO_4 and heated in a water bath for 10 min at 100°C. After that, the solution was chilled and well mixed. After that, the sample was transferred to a quartz cuvette, and the absorbance at 230 nm was measured against a sulfuric acid blank. A graph was then plotted to calculate the amount of crotonic acid.

UV-Vis Spectroscopic Analysis of PHB

The principle of this assay is to dissolve the samples isolated

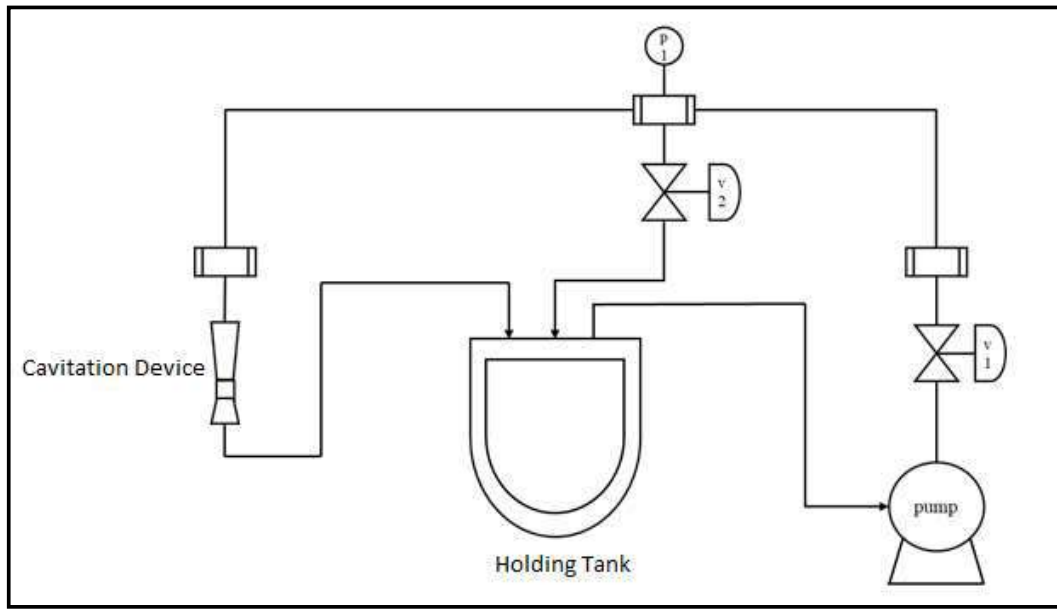

Fig. 1: Schematic representation of hydrodynamic cavitation setup.

from haloarchaeal culture in a suitable solvent and subject them to scanning in a UV-Vis spectrophotometer under a prescribed wavelength range (Selvakumar et al. 2011). The spectrum was then analyzed after the PHB compound was dissolved in chloroform and scanned with a UV-Vis spectrophotometer (Shimadzu) in the range of 800-200 nm against a chloroform blank.

Analysis of PHB Using FTIR (Fourier Transform Infra-Red) Spectrophotometer

A PHB extract sample weighing around 1 mg was dissolved in 5 cubic cm (cc) of chloroform. After the addition of KBr produced a pellet, spectra were captured using the Spectrum 65 FTIR (PerkinElmer) in the 4000-400 cm^{-1} range. The extracted PHB was dissolved in chloroform and scanned in the range of 200–320 nm (UV/Vis spectrophotometer RS-290) against chloroform blank, and the spectrum was analyzed for a sharp peak at 240 nm (Selvakumar et al. 2011).

RESULTS AND DISCUSSION

Source of Haloarchaea

The haloarchaeal consortium was red-orange colored when grown in SG liquid medium and required an optimum 22 g% NaCl for growth. The well-grown haloarchaeal consortium was further grown in nutrient-deficient (C: N – 10:1) PHB Accumulation Medium (PAM) for the production of PHB. Haloarchaea has been isolated from different rock salt samples from different regions of the world (Jaakkola et al. 2014, Kondo 2015). Still, there has not been a study about the extraction of PHB from haloarchaea isolated from rock salt.

Qualitative Characterization of PHB-Producing Haloarchaea Using Sudan Black B Staining

Culture from PHB accumulation medium, when stained with Sudan Black B, black-colored cells, indicate accumulation of PHB inside the cells while pink-colored cells indicate non-PHB producing cells (Fig. 2). This indicates that in PHB accumulation medium, PHB is produced inside the haloarchaeal cells and can be qualitatively confirmed using the method of staining by Sudan Black B (Selvakumar et al. 2011). Marjadi and Dharaiya (2014) stained the haloarchaeal cells of *H. marismurti* with Sudan Black B and have been found to produce PHB intracellularly, in agreement with our findings (Marjadi & Dharaiya 2014).

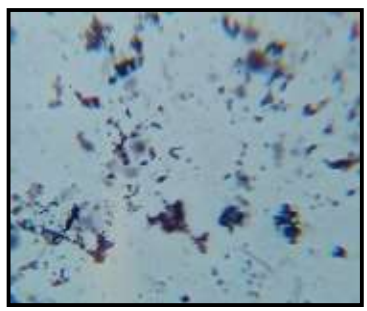

Fig. 2: Sudan Black B staining of PHB producing haloarchaeal culture.

PHB Production by Haloarchaea

As the haloarchaea could grow at a high salt concentration of 20 g%, contamination from other microorganisms was minimized. The culture could grow in an open 3 L flask and was used further for the HC experiment. This proved to be a major advantage of haloarchaea over other microorganisms on a scale-up level (Sheehan & Story 1977). 10% inoculum from haloarchaeal consortium grown in SG medium was used in PAM for scale-up studies.

Extraction of PHB Using Hydrodynamic Cavitation Setup

The growth of the culture was monitored at 600 nm, and in the late log phase or early stationary phase, the liquid culture was subjected to HC. This was the best phase when the organism produced maximum PHB, and thus, maximum PHB from cells could be harvested. In HC experiments, the pressure was varied from 2.5 to 3.9 bar, and the yield of PHB in $g.L^{-1}$ was calculated from the samples taken at 10-minute intervals. Table 1 gives the values of various parameters obtained for the different experimental runs. The results are analyzed in Fig. 3. The graph (Fig. 3) shows time in min on the X-axis and PHB $g.L^{-1}$ on the Y-axis. It can be seen that in the first run, at 2.5 bar pressure, 2.9 $g.L^{-1}$ PHB was extracted after 30 min of HC. In the second run, around 6.6 $g.L^{-1}$ PHB was extracted after 30 min at 3.2 bar pressure. In the third run, 3.9 bar pressure was applied, around 9 $g.L^{-1}$ PHB was extracted at 30 min, and a maximum of 27.097 $g.L^{-1}$ PHB was obtained at 40 min. This was the maximum PHB $g.L^{-1}$ obtained from the haloarchaeal consortium from rock salt.

The results indicate that at higher cell density, more cells produce PHB inside their cells, and thus, maximum PHB production can be achieved. In the third run, it was also seen that as pressure increased from 2.5 to 3.9 bar, the increase in PHB extraction increased proportionately. As the pressure increased, density changed too. This was due to an increase in density of the cellular component after the breakage of cells. Initial cell count (Colony Forming Unit – $CFU.mL^{-1}$)

Table 1: Comparative PHB dry cell weight.

HC run	Absorbance 600 nm	Flow rate, $l.h^{-1}$	Pressure, Bar	Time, min	pH	Density	*CFU.mL^{-1}	Max Temp, °C	PHB, $g.L^{-1}$ dry cell weight	Std. Dev.
1	0.89	321.9	2.5	0	6.5-7	1.206	7.5×10^7	30	1.3	0.065
			2.5	10	6.5-7	1.159		38	2.6	0.13
			2.5	20	6.5-7	1.152		36	1.6	0.08
			2.5	30	6.5-7	1.156		38	2.9	0.145
2	1.0	360.6	3.2	0	7.20	1.111	8.4×10^8	35	1.599	0.0799
			3.2	10	7.27	1.090		39	4.399	0.219
			3.2	20	7.23	1.208		44	7.899	0.394
			3.2	30	7.27	1.182		47	6.599	0.329
3	1.8	427.1	3.9	0	7	1.133	1.5×10^{12}	34	0.199	0.009
			3.9	10	7	1.134		38	8.283	0.414
			3.9	20	7	1.151		41	4.732	0.236
			3.9	30	7	1.165		46	9.032	0.451
			3.9	40	7	1.139		50	27.097	1.354
			3.9	50	7	1.169		53	10.965	0.548
			3.9	60	7	1.149		55	3.033	0.151
**D/W lysis									11.0	0.55

*CFU – Colony Forming Unit

**D/W – Distilled Water

also increased as the optical density increased. This means to get maximum PHB production, more initial number of PHB-producing cells is necessary. The results of the third run at 40 min at 3.9 bar pressure seem to be promising but will need further evaluation and analysis. HC method has been useful in synthesis of chemicals using oxidation reactions (Zheng et al. 2022), sludge and wastewater treatment (Chen et al. 2023, Patil et al. 2021a, Randhavane & Khambete 2017), synthesis of petrochemical products like biodiesel, degradation of pharmaceutical or dye industries residue, extraction of food processing products and cellular component extraction like enzymes, lipids (Wang et al. 2021, Wu et al. 2019, Sun et al. 2022). However, there is no report regarding PHB extraction using HC.

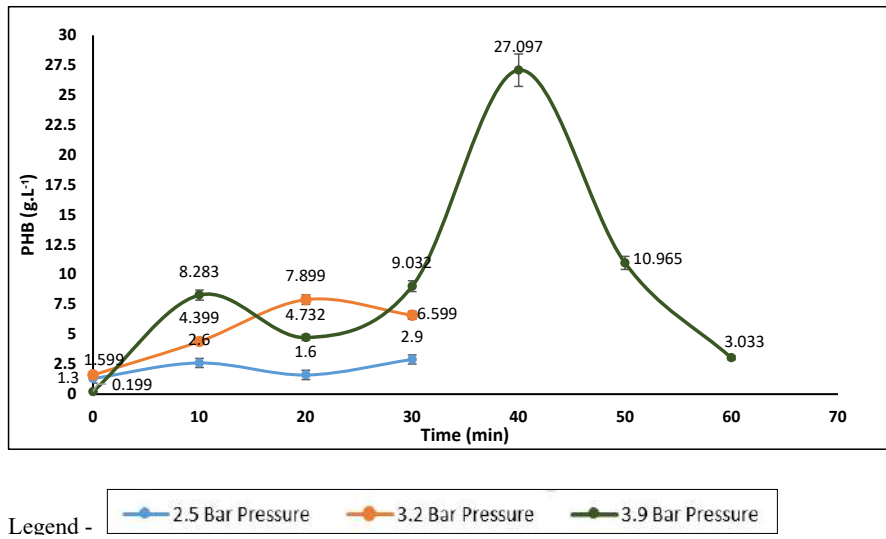

Fig. 3: Graphical representation of HC run for PHB extraction.

Fig. 4a: Casting of PHB film.

Fig. 4b: Methanol precipitate of PHB film.

Table 1 shows that as the initial cell count and pressure increased, PHB extraction increased proportionately. The comparative method of distilled water analysis showed PHB production of 11 $g.L^{-1}$, which is comparable to all the runs at 30 min. In the third run, as the time was increased further to 40 min, PHB extraction doubled, reaching a maximum of 27 $g.L^{-1}$. This indicated further optimization and analysis should be done considering 3.9 bar pressure and 60 60 min run to maximize PHB production.

The PHB film was cast using chloroform and dried in an oven at 65°C (Fig. 4a). This film was milky white and translucent. The film was precipitated using methanol, and a methanol precipitate of PHB film was done (Fig. 4b). It was found to be brittle. Selvakumar et al. (2011) extracted PHB from *Haloarcula marismurti* using the same distilled water lysis method, similar to our results (Selvakumar et al. 2011).

Extraction Using Distilled Water Lysis

For comparison, extraction of PHB using distilled water lysis was done, and it was found that 11 $g.L^{-1}$ PHB could be extracted. As compared to HC, this result is comparable with 30 min of HC at 3.9 bar pressure (9.032 PHB $g.L^{-1}$) but is half when compared to 40 min of HC at 3.9 bar pressure. This supports that HC could be a better alternative for the extraction of haloarchaeal PHB than the distilled water lysis method on an industrial level.

Characterization of PHB Using Crotonic Acid Assay, Spectrophotometric Analysis, and FTIR

Estimation of PHB by crotonic acid assay: For standard crotonic acid assay, 10 to 40 $\mu g.mL^{-1}$ of standard crotonic acid was subjected to H_2SO_4 acid treatment. The peaks of the same standard crotonic acid can be seen in the graph (Fig. 5). The PHB extracted after 30 min of HC was purified and dried.

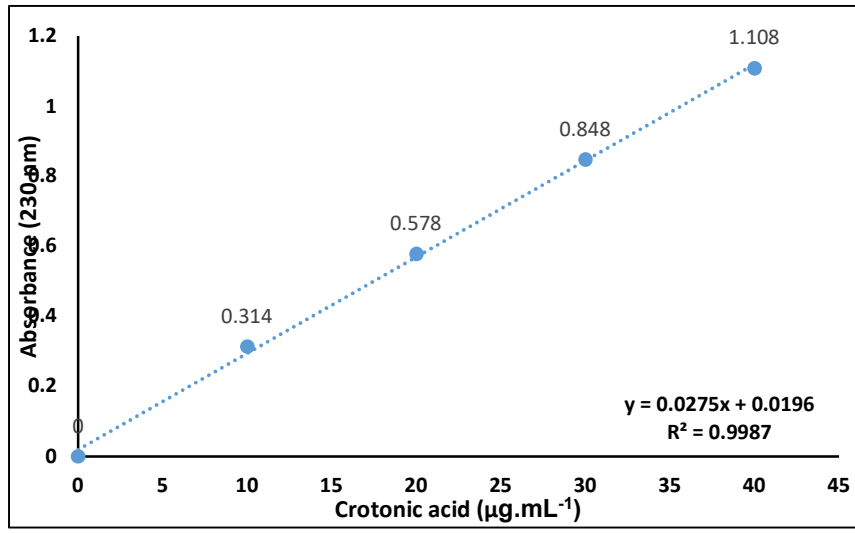

Fig. 5: Standard crotonic acid assay.

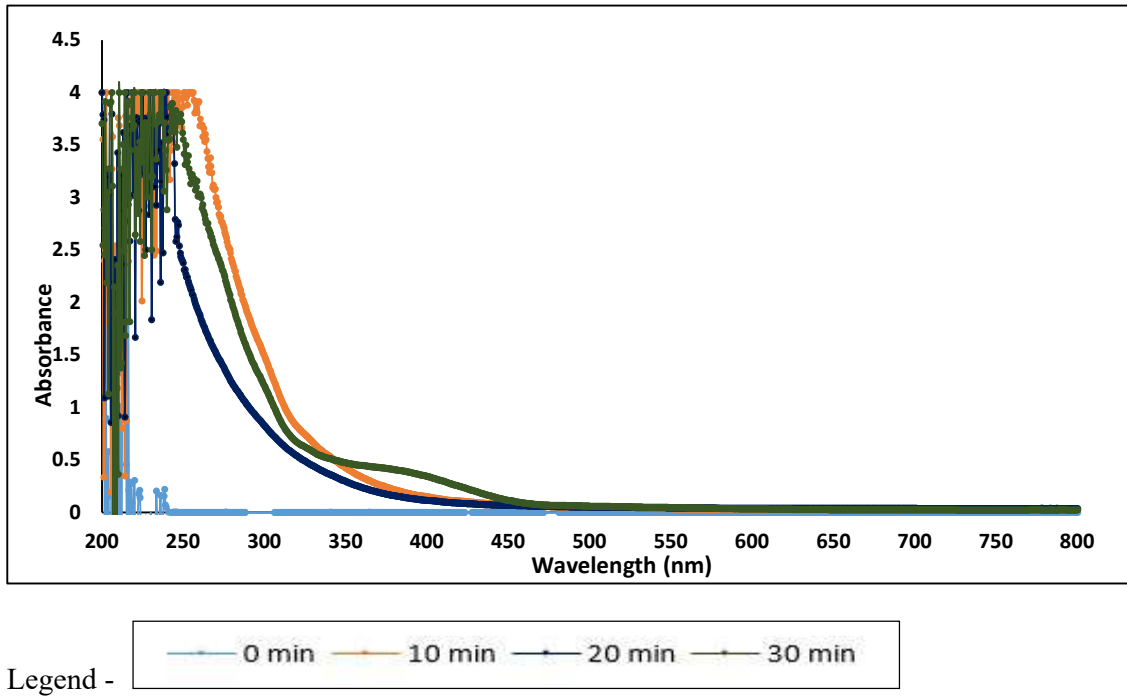

Fig. 6: UV spectrum analysis graph of PHB.

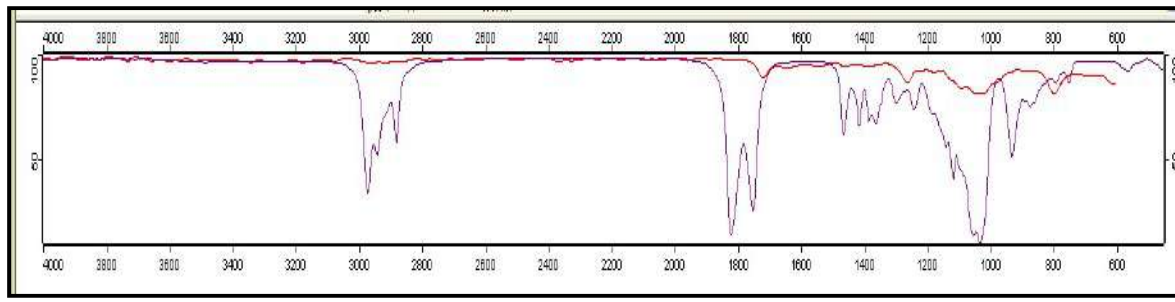

Legend – PHB Test sample (Red line), PHB standard sample (– Purple line)
Fig. 7: FTIR analysis of PHB sample after HC extraction.

This PHB was subjected to acid treatment as previously and was analyzed at 230 nm. The PHB sample showed a peak at 230 nm with more Area Under Curve at 40 $\mu g.mL^{-1}$ crotonic acid, and it was calculated that the PHB content in the sample after 30 min was found to be 51.19 $\mu g.mL^{-1}$. Selvakumar et al. have used Crotonic acid assay to detect PHB and have got similar results (Selvakumar et al. 2011).

UV-Vis spectroscopic analysis of PHB: Samples from the HC experiments at time intervals of 0, 10, 20, and 30 min were dissolved in chloroform and subjected to UV-Vis spectroscopy over the wavelength range of 200-800 nm. The outcome achieved thus far has revealed a prominent peak and absorbance at 240 nm (Fig. 6). In contrast, there was no similar absorption at 240 nm in the control solvent (chloroform). The peak at 240 nm was present in all samples, amply demonstrating the existence of PHB in the extracted material. A similar study by Selvakumar et al. (2011) showed a UV spectrum peak at 240 nm of PHB extracted from *H. marismurti* (Selvakumar et al. 2011).

FTIR spectrophotometer analysis of PHB: It was observed that the FTIR spectrum of the standard and test samples of PHB showed overlapping peaks. The PHB sample (red line) after HC extraction showed a peak overlapping the peaks of PHB (poly-hydroxy butyrate) (butyric anhydride-Purple line) (Fig. 7). This confirms the presence of butyric acid in the test sample.

The spectrum obtained was compared with the spectrum obtained by Marjadi and Dharaiya (2014), as shown in

Table 2: FTIR spectrum of haloarchaeal PHB sample and standard PHB.

Sample	Peak region	Comment
PHB Sample	1650	Carbonyl group (C=O)
	2963	Methine groups (CH)
	1092	Ester group (C-O)
	3578.55	Intramolecular H bond
	3415.06	H bond
PHB (Sigma Aldrich Company)	1673	Carbonyl group (C=O)
	2928	Methine groups (CH)
	1076	Ester group (C-O)
	3330.13	Intramolecular H bond
	3417.70	H bond

Table 2. In that work, the FTIR spectrum of the compounds was recorded in the range of 800-4000 cm^{-1} and showed characteristic bands for the groups CH, C=O, and C-O. Strong bands in the ranges of 1325.99-1439.32 and 2945.23-3038.73 were produced by the methine groups (CH). Due to polymerization, these frequency values were higher than the typical values. The carbonyl group (C=O) produced a noticeable band between 1610.74 and 1670.24. Due to polymerization, these frequency values were lower than the expected value. The (C-O) group demonstrated robust and widespread absorption in the 1048.32–1100.74 range.

Compared to the literature, our results of PHB extraction indicate that HC could be used efficiently for downstream processing for PHB extraction in the near future. To the authors' best knowledge, HC has not been used for PHB extraction to date. Thus, this could be the first report on the use of HC for PHB extraction.

CONCLUSIONS

The present paper describes hydrodynamic cavitation as one of the best alternatives for biopolymer extraction (PHB). HC has been used in wastewater treatment and enzyme extraction successfully, but there is no research related to biopolymer extraction. This paper significantly describes the optimization of parameters related to HC for biopolymer extraction. The results showed that the haloarchaeal consortium showed the presence of PHB inside the cells using Sudan Black B staining. The culture was scaled up to 3 liters in a PHB accumulation medium, and PHB was extracted using HC. The pressure was varied from 2.5 to 3.9 bar in three runs, and it was found that maximum PHB production was found in the third run with a 3.9 bar run after 40 min. This PHB production was approximately twice as compared to distilled water lysis PHB extraction. UV spectrum analysis, Crotonic acid assay, and FTIR confirmed the presence of PHB.

Individual isolates have been used for PHB production and have been reported, but a haloarchaeal consortium from rock salt for PHB production has not been reported. Furthermore, HC has been used for a variety of intracellular and periplasmic enzymes but has not been used for PHB extraction yet. Compared to other methods of PHB extraction, HC thus offers an advantage of large-scale downstream processing in reduced time. Further standardization of parameters for PHB extraction described in this paper can help in future research related to PHB extraction using hydrodynamic cavitation.

ACKNOWLEDGEMENTS

The authors wish to acknowledge Vivira Process Technologies and the staff of Dr. Vishwanath Karad, MIT World Peace University, for their support in this research project.

REFERENCES

Anand, H., Balasundaram, B., Pandit, A.B. and Harrison, S.T L. 2007. The effect of chemical pretreatment combined with mechanical disruption on the extent of disruption and release of intracellular protein from *E. coli*. Biochem. Eng. J., 35(2): 166-173. https://doi.org/10.1016/j.bej.2007.01.011

Balasundaram, B. and Harrison, S.T.L. 2006. Disruption of Brewers' yeast by hydrodynamic cavitation: Process variables and their influence on selective release. Biotechnol. Bioeng., 94(2): 303-311. https://doi.org/10.1002/bit.20878

Balasundaram, B. and Pandit, A.B. 2001a. Selective release of invertase by hydrodynamic cavitation. Biochem. Eng. J., 8(3): 251-256. https://doi.org/10.1016/S1369-703X(01)00114-0

Balasundaram, B. and Pandit, A.B. 2001b. Significance of location of enzymes on their release during microbial cell disruption. Biotechnol. Bioeng., 75(5): 607-614. https://doi.org/10.1002/bit.10072

BIRAC. 2021. India Bioeconomy Report. https://birac.nic.in/webcontent/1658318307_India_Bioeconomy_Report_2022.pdf

Chen, Y., Yin, C. and Song, Y. 2023. Application of hydrodynamic cavitation in the field of water treatment. Chem. Pap., 77: 3521-3546. https:// doi.org/ 10.1007 /s11696 -023-02754-y

Gaikwad, V.V., Gaikwad, S.V. and Ranade, V.V. 2016. Effect of orifice shape on water disinfection efficacy. Poll. Res., 35(4): 765-771.

Jaakkola, S. T., Zerulla, K., Guo, Q., Liu, Y., Ma, H., Yang, C., Bamford, D. H., Chen, X., Soppa, J. and Oksanen, H. M. 2014. Halophilic archaea cultivated from surface sterilized middle-late eocene rock salt are polyploid. PloS One, 9(10): e110533. https://doi.org/10.1371/journal.pone.0110533

Kanekar, P.P., Kulkarni, S.O, Nilegaonkar, S.S., Sarnaik, S.S., Kshirsagar, P.R., Ponraj, M. and Kanekar, S.P. 2014. Environmental friendly microbial polymers, polyhydroxyalkanoates (PHAs) for packaging and biomedical applications. In: Alavi, S.Y.S., Sabu, T., Sandeep, K.P., Kalarikkal, N. and Varghese J. (eds), Polymers for Packaging Applications, Apple Academic Press. Toronto, Canada, pp. 197-226.

Kanekar, S.P. 2014. Biodiversity and Biotechnological Exploration of Halophiles from the Andaman Islands and Lonar Lake, India. Doctoral Thesis. Department of Microbiology, Savitribai Phule Pune University, Pune, Maharashtra, India.

Kondo, Y., Minegishi, H., Echigo, A., Shimane, Y., Kamekura, M., Itoh, T., Ohkuma, M., Takahashi-Ando, N., Fukushima, Y., Yoshida, Y. and Usami, R. 2015. *Halorubrum gandharaense* sp. Nov., an alkaliphilic

haloarchaeon from commercial rock salt. Int. J. Syst. Evol. Microbiol., 65: 2345-2350. https://doi.org/10.1099/ijs.0.000261

Marjadi, D. and Dharaiya, N. 2014. Recovery and characterization of poly (3-Hydroxybutyric acid) synthesized in *Staphylococcus epidermidis*. Afr. J. Environ. Sci. Technol., 8(6): 319-329. https://doi.org/10.5897/AJEST2014.1645

Niti Aayog 2022. Report on Alternative Products and Technologies to Plastics and Their Applications. http://www.indiaenvironmentportal.org.in

Patil, P.B., Bhandari, V.M. and Ranade, V.V. 2021a. Wastewater treatment and process intensification for degradation of solvents using hydrodynamic cavitation. Chem. Eng. Process. Intensif., 166:108485. https://doi.org/10.1016/j.cep.2021.108485.

Patil, P.B., Bhandari, V.M. and Ranade, V.V. 2021b. Improving efficiency for removal of ammoniacal nitrogen from wastewaters using hydrodynamic cavitation. Ultrasonics Sonochem., 70: 105306. https://doi.org/10.1016/j.ultsonch.2020.105306.

Ranade, V.V. 2022. Modeling of hydrodynamic cavitation reactors: Reflections on the present status and path forward. ACS Eng., 2(6): 461-476. https://doi.org/10.1021/acsengineeringau.2c00025

Randhavane, S.B. and Khambete, A.K. 2017. Hydrodynamic cavitation: A novel treatment approach. Mater. Today Proceed., 4: 9680–9684. https://doi.org/10.1016/j.matpr.2017.06.246

Sehgal, S.N. and Gibbons, N.E. 1960. Effect of some metal ions on the growth of *Halobacterium cutirubrum*. Can. J. Microbiol., 6: 165-169. https://doi.org/10.1139/m60-018

Selvakumar, K., Srinivasan, G., Baskar, V. and Madhan, R. 2011. Production and isolation of polyhydroxy alkanoates from *Haloarcula marismortui* MTCC1596 using cost-effective osmotic lysis methodology. Europ. J. Exper. Biol., 1(3):180-187.

Setyawan, M., Budiman, A., Mulyono, P. and Sutijan. 2018. Optimum extraction of algae-oil from microalgae using hydrodynamic cavitation. Int. J. Renew Energy Res., 8(1): 451-58. https://doi.org/10.20508/ijrer.v8i1.6887.g7320

Sheehan, H.L. and Story, G.W. 1977. Sudan black B stain: Stability. J. Path. Bacter., 59: 336.

Simó-Cabrera, L., García-Chumillas, S., Hagagy, N., Saddiq, A., Tag, H., Selim, S., AbdElgawad, H., Agüero, A.A., Monzó Sánchez, F., Cánovas, V., Pire, C. and Martínez-Espinosa, R.M. 2021. Haloarchaea as cell factories to produce bioplastics. Marine Drugs, 19(3): 159. https://doi.org/ 10.3390/ md19030159

Sun, X., You, W., Wu, Y., Tao, Y., Yoon, J.Y., Zhang, X. and Xuan, X. 2022. Hydrodynamic cavitation: A novel non-thermal liquid food processing technology. Front. Nutr., 9: 843808. https://doi.org/10.3389/fnut.2022.843808

Verdini, F., Gaudino, E.C., Grillo, G., Tabasso, S. and Cravotto, G. 2021. Cellulose recovery from agri-food residues by effective cavitational treatments. Appl. Sci., 11(10): 4693. https://doi.org/10.3390/app11104693

Wang, B., Su, H. and Zhang, B. 2021. Hydrodynamic cavitation as a promising route for wastewater treatment: A review. Chem. Eng. J., 412:128685. https://doi.org/10.1016/j.cej.2021.128685

Wu, Z., Ferreira, D.F., Crudo, D., Bosco, V., Stevanato, L., Costale, A. and Cravotto, G. 2019. Plant and biomass extraction and valorisation under hydrodynamic cavitation. Processes, 7(12): 965. https://doi.org/10.3390/pr7120965

Zheng, H., Zheng, Y. and Zhu, J. 2022. Recent developments in hydrodynamic cavitation reactors: cavitation mechanism, reactor design, and applications. Engineering, 19: 180-198. https:/ /doi.org/10.1016/j.eng.2022.04.027

ORCID DETAILS OF THE AUTHORS

V. D. Gaikwad: https://orcid.org/0000-0002-8363-031X
S. V. Gaikwad: https://orcid.org/0000-0003-2426-4978
A. D. Kulkarni: https://orcid.org/0000-0003-4704-381X
S. P. Kanekar: https://orcid.org/0000-0002-6285-4920

Nature Environment and Pollution Technology
An International Quarterly Scientific Journal

p-ISSN: 0972-6268
(Print copies up to 2016)
e-ISSN: 2395-3454

Vol. 23 | No. 1 | pp. 485-490 | 2024

Original Research Paper

https://doi.org/10.46488/NEPT.2024.v23i01.044

Open Access Journal

Knowledge, Attitude, and Practices on Climate Change Among Rice Farmers in Central Luzon, Philippines

E. N. Farin†, R. R. Sazon, R. A. Sazon, D. V. Rogayan Jr., K. B. Manglicmot, S. G. Mendoza and E. M. Cabal

President Ramon Magsaysay State University, Iba, Zambales, Philippines

†Corresponding author: E.N. Farin; Elizabeth_farin@yahoo.com

Nat. Env. & Poll. Tech.
Website: www.neptjournal.com

Received: 24-05-2023
Revised: 05-07-2023
Accepted: 06-07-2023

Key Words:
Disaster risks
Rice farmers
Knowledge
Attitude
Climate change

ABSTRACT

The Philippines has been listed as the topmost affected country by climate change. One of the sectors affected by this climatic change is the agricultural sector. This study aimed to document the knowledge, attitude, and practices (KAPs) on climate change among rice farmers as a baseline study in disseminating the practices on disaster risk reduction management to rice farmers in Central Luzon to reduce risks and improve the rice yield and income of rice farmers. A total of 969 respondents were randomly sampled from the seven provinces of Central Luzon. A survey questionnaire and an unstructured questionnaire were used as instruments in gathering the needed data. Descriptive and thematic analysis were used in analyzing the data. Results revealed that rice farmers are knowledgeable and have favorable attitudes toward the impact of climate change on farming. They sometimes practice climate-smart agricultural practices. Generally, the farmers are affected by weather and climatic conditions as well as the hazards that cause a reduction in rice yield. Climate change has affected farmers in their social well-being, economic aspect, and rice production. In terms of climate change disaster adaptation measures, the farmers sometimes adopt measures in terms of flood and drought and seldom adopt measures in typhoons, erosion, and volcanic eruptions. The study recommends the conduct of capability training on disaster risk reduction in rice production (such as early planting and planting of high-yielding varieties) based on the specific needs of each province.

INTRODUCTION

The Global Climate Risk Index 2020 listed the Philippines as the topmost affected country by climate change, using 2018 data. Since the Philippines is an archipelago lying in the western Pacific Ocean, it is surrounded by naturally warm waters that will likely get even warmer as the average sea surface temperatures continue to rise. Jabines & Inventor (2007) likewise considered the country as one of the climate hotspots due to its geographical location and low level of economic development, further aggravated by its people's poor access to resources.

Climate change and, in particular, increasing surface temperature, rising sea levels, and increased precipitation will cause significant changes in the lives of people in the forthcoming years (Celik 2020, Ebi & Hess 2020, Griggs & Reguero 2021). Drastic changes in temperature and rainfall levels are predicted. Droughts will be more intense and frequent, as well as typhoons and, consequently, flooding and landslides. The country has experienced the world's strongest storm to make landfall in Philippine history, typhoon Yolanda or Haiyan. The devastation from that typhoon propelled the country to the top of the list of the most vulnerable countries to climate change based on the annual Global Climate Risk Index of Germanwatch (Ranada 2015). Central Luzon and Bicol Regions are two of the most disaster-prone areas in the country due to their geophysical location. The natural hazards in Central Luzon, mainly storms and floods, put the lives of vulnerable households at risk. Four of the 7 provinces of Central Luzon – Pampanga, Tarlac, Nueva Ecija, and Bulacan are among the top 10 provinces which are highly susceptible to flooding (Mines & Geosciences Bureau 2015).

Agriculture played a very important role in providing about 30% of employment and 10% of the country's gross domestic product (GDP) in 2013. Natural calamities and the changing climate have affected crop and livestock production in the country, causing economic loss and food insecurity (Hidrobo et al. 2014). Flora (2018) reported that "agriculture is the most affected sector in the country in terms of the effects of climate change, according to Chief Legal Counsel of the Climate Change Commission Efren Basco. The

country faced the biggest challenge in the agriculture sector when typhoon Haiyan (locally known as Super Typhoon *Yolanda*) devastated the country in 2013, destroying around P17,321,150,996.38, which is considered the biggest in the country's history.

Central Luzon, the rice granary of the Philippines, is not spared from the damage brought about by typhoons. Central Luzon accounts for 14-15% of the total rice production in the country (Flora 2018). According to Suarez (2013), Central Luzon rice production areas were damaged by several typhoons. In 2015, the total damaged rice production area due to several typhoons, including the most destructive Lando, was 51,398.6 hectares, and the province of Pampanga was the worst hit with 26,514 hectares. In 2015, Typhoon Lando damaged at least P5 billion worth of crops in Central Luzon. In 2016, the total recorded damage was 7,081.54 hectares. Pampanga had the highest damage in terms of production areas. In 2018, a total of 174,468 hectares were damaged by 6 typhoons, Ompong was the most damaging, and Nueva Ecija was the most affected, with more than 93,000 hectares of rice affected. However, the region recorded a damage of at least P5B worth of crops in 2015 due to typhoon Lando, and this was compounded by the damage in rice crops due to flooding brought by typhoon Nona before the end of 2015 and by typhoon Nina in 2016, wherein Nueva Ecija is the hardest hit. In the province of Zambales, the onslaught of typhoon Lando in Sta. Cruz alone caused P500 M losses in food, rice, mango, and fish production. Aside from typhoons, drought also affected rice production. In 2016, 10 441.48 hectares were damaged, with a total loss of more than Php589M in rice production.

Since the state of the farmers is mostly affected by changing climate, particularly the rising temperature and fluctuations in precipitation (changing intensity and duration of rainfall) resulting in hazards, the promotion of disaster risk reduction management to the rice farmers in Central Luzon is deemed necessary.

The findings of this study will be used as benchmark information for the identification of priority areas for action and as a guide for the development of a regional adaptation program. This could also pave the way to the development of a strong institutional mechanism with enabling policies to ensure that the rice farming communities and their practices are resilient and sustainable so as to cope with the impacts of the changing climate.

OBJECTIVES OF THE STUDY

Generally, this research aimed to ascertain the rice farmers' knowledge, attitude, and practices (KAPs) on climate change as a basis for promoting disaster risk reduction management to rice farmers in Central Luzon to reduce risks and improve the rice yield and income of rice farmers. The study specifically identified the impact of natural disasters on the socio-cultural and economic conditions of the rice farming community and the farmers' coping mechanisms and adaptive practices.

MATERIALS AND METHODS

Study Design

The descriptive method of research was employed in the study. Descriptive research is characterized by the objective description and systematic analysis of phenomena without manipulating variables. It aims to provide a comprehensive and accurate portrayal of the characteristics, behaviors, or conditions under investigation.

Study Population Size and Location

Table 1 presents the distribution of the respondents by province.

As gleaned from the table, most of the respondents came from Tarlac (26.21%), followed by Zambales (19.20%) and Aurora (15.58%). Other respondents came from Pampanga, Bulacan, Nueva Ecija, and Bataan. A total of 969 rice farmers took part in the study.

The data was collected in the seven provinces of Central Luzon through random sampling. Random sampling involves selecting participants from the population in such a way that each individual has an equal chance of being chosen. Central Luzon is the highest rice-producing region in the Philippines. Fig. 1 shows the location of the study where data were collected.

Data Collection Method

The triangulation method was used in which the information was generated through Focus Group Discussion (FGD)/ Key Informant Interview (KII), Face-to-face interview, and the use of secondary data. The unstructured questionnaire

Table 1: Frequency distribution of the respondents.

Provinces	F	%
Aurora	151	15.58
Bataan	94	9.70
Bulacan	68	7.02
Nueva Ecija	86	8.88
Pampanga	130	13.42
Tarlac	254	26.21
Zambales	186	19.20
Total	969	100.0

Fig. 1. Map of the study area.

was used for FGD and KII, while an Interview Schedule (structured questionnaire) was formulated for interviewing the randomly selected respondents. Participatory Rural Appraisal (PRA) was utilized in this undertaking.

Data Analysis and Presentation

The data collected was organized, tallied, and tabulated in an Excel spreadsheet. Statistical tools like Percentage, Arithmetic Weighted Mean, and Pearson-r were used. The Likert Scale was used in the interpretation of the generated data.

RESULTS AND DISCUSSION

Knowledge, Attitude, and Practices of Rice Farmers on Climate Change and Farming

Table 2 shows the knowledge of rice farmers on climate change and farming.

As given in the table, the rice farmers are moderately knowledgeable about climate change, as shown by the overall mean of 3.28 (SD=0.57). They moderately understand what climate change is (M=3.40, SD=0.83) and are moderately

Table 2: Knowledge of rice farmers on climate change and farming.

Knowledge	M	SD	QI
1. I understand what climate change is	3.40	0.83	M
2. The climate change is changing and becoming more unpredictable	3.36	0.79	M
3. Climate change can negatively affect rice production	3.39	0.80	M
4. Frequent and stronger typhoons can be a result of climate change	3.36	0.85	M
5. The temperature is increasing, and it may increase more in the coming years	3.29	0.89	M
6. I am aware that the sea level is rising	3.04	0.98	M
7. Peoples activities like the operation of power plants and tree logging can contribute to a change in climate	3.27	0.93	M
8. Drought can also be a result of climate change	3.36	0.82	M
9. Aerosols, refrigerants, and other chemicals can contribute to a change in climate	3.16	0.91	M
10. Flooding is also a possible result of climate change	3.29	0.84	M
11. I understand what crop insurance is.	3.31	0.96	M
Overall Mean	3.28	0.57	M

Legends: H-Highly Knowledgeable (3.50-4.00); M-Moderately Knowledgeable (2.50-3.49); Slightly Knowledgeable (1.50-2.49); N-Not Knowledgeable (1.00-1.49); M-Mean; SD-Standard Deviation; QI-Qualitative Interpretation

knowledgeable that climate change can negatively affect rice production (M=3.39, SD=0.80). They moderately know that drought can also be a result of climate change (M=3.36, SD=0.82) and that frequent and stronger typhoons can be a result of climate change (M=3.36, SD=0.85). According to Mandal & Singh (2020), 75- 80% of farmers in Nepal feel that temperature increases, rainfall duration and frequency decrease due to global warming. About 33.33% of farmers experience an increase in flooding hazard due to an increase in rainfall intensity during the rainy season in Siraha and its vicinity. The majority of respondents perceived an increase in weed and pest (65%) and new weed (30%) and new pest (26.7%) infestation due to climate change. About 18% of respondents had a clear knowledge of climate change.

The lowest means were obtained in the following indicators: I am aware that the sea level is rising (M=3.04, SD=0.98), Aerosols, refrigerants, and other chemicals can contribute to a change in climate (M=3.16, SD=0,91), and peoples activities like the operation of power plants and tree logging can contribute to a change in climate (M=3.27, SD=0.93).

The results imply that the rice farmers have a moderate level of knowledge about climate change and its effects on rice farming. Information dissemination driven through training may further improve their level of knowledge about the phenomenon. Similar findings were found by Islam et al. (2019) that an overwhelming majority (78.8%) of the respondents had medium to high knowledge of climate change effects on agriculture. On the other hand, the findings of Grace et al. (2015) show that the farmers are generally aware of direct and observable causes of climate change and the main impacts of climate change on agriculture but are not clear about the interconnections between the natural environment and farm management activities that result in climate change. Table 3 presents the attitude of rice farmers on climate change and farming.

As presented in the table, the rice farmers agree about the different attitude indicators, as shown by the overall mean of 3.12 (SD=0.56). This suggests that rice farmers have a favorable attitude toward climate change. Most farmers in Central Luzon were willing to invest in crop insurance as their way to address climate change effects, having a mean of 3.44 (SD=0.87). However, in the study of Holloway & Ilberry (1996), the farmers indicated a combination of positive and negative impacts from global warming, but most think that changes will enable them to adapt to climate change, and most would also consider the possibility of introducing new crops such as navy beans. The willingness of the farmers to use new technologies in addressing climate change to minimize losses got a favorable attitude for the farmers, with a mean of 3.42 (SD=0.85). In Pakistan, the adoption of such varieties has not been widely adopted due to high prices and a lack of availability. The absence of government subsidies holds back productivity gains, a shortage of credit facilities, a lack of awareness, poor infrastructure, rising costs of fertilizers, and a shortage of irrigation water (Stone & Nicholas 1995). Table 4 shows the practices of rice farmers on climate change and farming.

Table 4 shows the practices of farmers to address climate change. The farmers indicated that the most important practice for them to address climate change is being updated on the weather forecast of Pag-asa with a Mean of 3.59 (SD =0.79). This will determine whether they can plant rice already, especially for the upland areas. The occurrence of typhoons is also being monitored, whether to harvest early or later the mature play. The use of hybrid seeds that are

Table 3: Attitude of rice farmers on climate change and farming.

Attitude	M	SD	QI
1. I am willing to use hybrid rice/climate-smart rice in order to increase my harvest	3.35	0.93	A
2. I am willing to use the new technologies being offered by the concerned agencies to minimize crop losses	3.42	0.85	A
3. I believe that climate change will inevitably affect my crop yield	3.24	0.94	A
4. I am willing to invest and apply for crop insurance in order to minimize crop losses brought about by climatic hazards	3.44	0.87	A
5. I believe that organic farming can help reduce the impacts of climate change on rice farming	3.14	0.97	A
6. I am convinced that I can avoid the impacts of changing climate on my farming activities by adjusting to the existing climatic conditions	3.21	0.93	A
7. I do not believe in climate change*	2.84	1.21	A
8. Rice farmers should not worry about climate change. It is a natural event.*	2.33	1.20	D
Overall Mean	3.12	0.56	A

Legends: SA-Strongly Agree (3.50-4.00); A-Agree (2.50-3.49); D-Disagree (1.50-2.49); SD-Strongly Disagree (1.00-1.49); M-Mean; SD-Standard Deviation; QI-Qualitative Interpretation

Table 4: Practices of rice farmers on climate change.

Practice	M	SD	QI
I shifted my planting and harvesting schedule based on the existing climatic conditions.	3.24	0.93	S
I am using hybrid seeds that are adapted to drought or flooding conditions	2.93	1.25	S
I am using the new technologies being promoted by the Department of Agriculture and other agencies to minimize my crop losses due to climatic hazards.	3.34	0.92	S
I am practicing organic rice farming.	2.83	1.10	S
I keep myself updated on the weather forecast of PAGASA.	3.59	0.79	AL
I increase my agricultural inputs to increase my harvest.	3.29	0.98	S
I am practicing crop and animal diversification	2.92	1.14	S
Overall Mean	3.16	0.65	S

Legends: AL-Always (3.50-4.00); S-Sometimes (2.50-3.49); R-Rarely (1.50-2.49); N-Never (1.00-1.49); M-Mean; SD-Standard Deviation; QI-Qualitative Interpretation

adapted to drought and flooding conditions was sometimes practiced by farmers with a Mean of 2.93 (SD=1.25). Mandal & Singh (2019) indicate that a majority (76.67%) of the respondents in their study in Nepal used the improved rice variety Sonamansuli, followed by Lalka basmati 20%. The study found an increase in disease, pest, and weed infestation in the present context as compared to the past ten years. Farmers of the study area just started adopting different drought-resistant flood-resistant rice varieties to cope with the climate change adversities. About 17% of respondents have used green manuring in their field, and 15% have used the DSR cultivation method. The study explored that only 63.33% of respondents acknowledged crop insurance, but none of them brought in actual practices of crop insurance for any crop or livestock, as shown. Rought and flood. In response to the rising trend of extreme weather events, farmers may take various physical and non-physical measures. Physical measures include investments in and maintenance of irrigation facilities such as canals, tube wells, cisterns, ponds, and pump equipment; non-physical measures include farm management, crop insurance, and other measures that do not require large investments (Wang et al. 2014). This study specifically focuses on non-physical measures such as farm management, which are usually the most convenient type that farmers can implement during crop growing season. Based on field surveys, the most common farm management measures used by farmers related to drought and flood are reseeding, fixing, and cleaning seedlings.

Falco et al. (2014) found that (i) demand for insurance products is likely to increase in response to climatic conditions, and (ii) the use of insurance reduces the extent of risk exposure. We also find that farms growing more crops are less likely to adopt the insurance scheme. This confirms what is found in the theoretical literature. Crop diversification can be a substitute for financial insurance in hedging against the impact of risk exposure on welfare.

Relationship Among the KAPs of Rice Farmers on Climate Change

Table 5 shows the correlation among the knowledge, attitude, and practices of rice farmers on climate change.

Table 5: Correlation among the knowledge, attitude, and practices of rice farmers on climate change.

		Knowledge	Attitude	Practices
Knowledge	Pearson Correlation	1		
	Sig. (2-tailed)			
	N	948		
Attitude	Pearson Correlation	**0.568****	1	
	Sig. (2-tailed)	0.000		
	N	946	961	
Practices	Pearson Correlation	**0.504****	**0.658****	1
	Sig. (2-tailed)	0.000	0.000	
	N	937	951	954

**.Correlation is significant at the 0.01 level (2-tailed).

As shown in the table, the knowledge and attitude of the rice farmers on climate change had a significant positive moderate correlation (r=0.568, p<0.01). Their knowledge and practices also obtained a significant positive moderate correlation (r=0.504, p<0.01), and their attitude and practices likewise had a significant positive moderate correlation (r=0.658, p<0.01). The findings conform to several researches that found significant correlations in the farmers' KAPs towards climate change (Akhtar et al. 2020, Ojo & Baiyegunhi 2021).

CONCLUSION AND RECOMMENDATIONS

The farmers are knowledgeable and have favorable attitudes toward the impact of climate change on farming. They sometimes practice climate-smart agricultural practices. Generally, the farmers are affected by weather and climatic conditions as well as the hazards that cause a reduction in rice yield. Climate change has affected farmers in their social well-being, economic aspect, and rice production.

The government may conduct capability training on disaster risk reduction in rice production (such as early planting and planting of high-yielding varieties) based on the specific needs of each province. It may spearhead training to promote integrated farming systems and crop diversification to build the resilience of agricultural communities to disaster impacts. Seminars on how to reduce the adverse impacts of chemical fertilizers and pesticides in agriculture from the national to the local level in rice production may be conducted. IEC materials based on the baseline data gathered from this study to promote DRRM practices among rice farmers may be developed.

ACKNOWLEDGMENT

The project was funded by the Department of Agriculture-Region 3.

REFERENCES

Akhtar, R., Afroz, R., Masud, M.M., Rahman, M., Khalid, H. and Duasa, J.B. 2020. Farmers' perceptions, awareness, attitudes and adaption behaviour towards climate change. In: Climate Change Mitigation and Sustainable Development. Routledge, 60-76.

Celik, S. 2020. The effects of climate change on human behaviors. Environ. Clim. Plant Veg. Growth, 577-589.

Ebi, K. L. and Hess, J. J. 2020. Health risks due to climate change: Inequity in causes and consequences: Study examines health risks due to climate change. Health Aff., 39(12): 2056-2062.

Falco, S. D., Adinolfi, F., Bozzola, M. and Capitanio, F. 2014. Crop insurance as a strategy for adapting to climate change. J. Agri. Econ., 65(2): 485-504.

Flora, I.O. 2018. The Agriculture Sector Faces the Greatest Impact of Climate Change. Retrieved from https://www.sunstar.com.ph/article/426910 (accessed December 11, 2018).

Grace, W. K., Genixng, P., Stephen, J., Liu, X., Zheng, J., Xuhui, Z. and Lianqing, L. 2015. More than two decades of climate change alarm: Farmers knowledge, attitudes and perceptions. Afr. J. Agri. Res., 10(27): 2617-2625.

Griggs, G. and Reguero, B. G. 2021. Coastal adaptation to climate change and sea-level rise. Water, 13(16): 2151.

Hidrobo, M., Hoddinott, J., Kumar, N. and Olivier, M. 2014. Social protection and food security. Paper prepared by the International Food Policy Research Institute.

Holloway, L. and Ilbery, B. 1996. Farmers' attitudes towards environmental change, particularly global warming, and the adjustment of crop mix and farm management. Appl. Geogr., 16(2): 159-171.

Islam, S., Kabir, M., Ali, S., Sultana, S. and Mahasin, M. 2019. Farmers' knowledge on climate change effects in agriculture. Agric. Sci., 10(3): 45.

Jabines, M., Abigail, P. and Inventor, J. 2007. The Philippines: A Climate Hotspot. Climate Change Impacts and the Philippines. Greenpeace Southeast Asia, Climate and Energy Campaign. Retrieved from http://www.greenpeace.org/raw/content/seasia/en/press/reports/the-philippines-aclimate-hot.pdf. (accessed February 26, 2018).

Mandal, A. C. and Singh, O. P. 2020. Climate Change and Practices of Farmers' to maintain rice yield: A case study. Int. J. Biol. Innov., 2(1): 42-51.

Mines and Geosciences Bureau 2015. Top 10 provinces highly susceptible to flooding. Retrieved from https://www.denr.gov.ph/priority-programs/geo-hazard-mapping-and-assessment-program.html (accessed February 26, 2018).

Ojo, T.O, and Baiyegunhi, L.J.S. 2021. Climate change perception and its impact on net farm income of smallholder rice farmers in South-West, Nigeria. J. Clean. Prod., 310: 127373.

Ranada, P. 2015. PH named top 4th country affected by climate change in 2014. Rappler. Retrieved from https://www.rappler.com/environment/114829-philippines-global-climate-risk-index-2016/ (accessed February 26, 2018).

Stone, P. and Nicolas, M. 1995. Effect of timing of heat stress during grain filling on two wheat varieties differing in heat tolerance. Funct. Plant Biol., 22(6): 927-934.

Suarez, K. 2013. Typhoon Labuyo: 4 dead; P69-M Houses, P438-M crops damaged. Rappler. Retrieved from http://www.rappler.com/nation/36288-20130813-labuyo-casualties-damage (accessed February 26, 2018).

Tiet. T., To-The. N. and Nguyen-Anh. T. 2022. Farmers' behaviors and attitudes toward climate change adaptation: evidence from Vietnamese smallholder farmers. Environ. Dev. Sustain., 1-26.

Wang, Y. J., Huang, J. K. and Wang, J. X. 2014. Household and community assets and farmers' adaptation to extreme weather event: the case of drought in China. J. Integr. Agric., 13(4): 687-697.

ORCID DETAILS OF THE AUTHORS

E.N. Farin: https://orcid.org/0000-0001-7773-4369
R.R. Sazon: https://orcid.org/0000-0001-5158-4091
R.A. Sazon: https://orcid.org/0000-0002-7096-2454
D.V. Rogayan Jr: https://orcid.org/0000-0002-8597-7202
K.B. Manglicmot: https://orcid.org/0000-0003-3216-3800
S.G. Mendoza: https://orcid.org/0000-0002-8576-1989
E.M. Cabal: https://orcid.org/0000-0002-6026-7335

Nature Environment and Pollution Technology
An International Quarterly Scientific Journal

p-ISSN: 0972-6268
(Print copies up to 2016)
e-ISSN: 2395-3454

Vol. 23 | No. 1 | pp. 491-497 | 2024

Original Research Paper

https://doi.org/10.46488/NEPT.2024.v23i01.045

Open Access Journal

Analysis of the Phytochemical Composition of Leaves of Six Superior Salt-Tolerant Mulberry Germplasm Grown Under Coastal Saline Soils of South 24 Parganas District of West Bengal, India

Ritwik Acharya*, Debnirmalya Gangopadhyay*, S. Rehan Ahmad† and Phalguni Bhattacharyya*****

*Department of Sericulture, Raiganj University, Raiganj 733134, West Bengal, India

**Department of Zoology, Hiralal Mazumdar Memorial College for Women, Kolkata 700035, West Bengal, India

***Department of Botany, Shibpur Dinobundhoo Institution (College), Howrah 711102, West Bengal, India

†Corresponding author: S. Rehan Ahmad; prof.rehaan@gmail.com

Nat. Env. & Poll. Tech.
Website: www.neptjournal.com

Received: 18-06-2023
Revised: 26-07-2023
Accepted: 28-07-2023

Key Words:
Sericulture
Mulberry germplasm
Saline area
Anti-oxidant
Scarce land

ABSTRACT

The nutritive value of mulberry leaves makes it the only food of silkworms (*Bombyx mori* L.). It is recorded that 6.73 million hectares of area are affected by salinity and sodicity stresses covering various states of the country, which is becoming one of the major threats to popularizing sericulture in India. In the present study, chlorophyll, protein, catalase, peroxidase, and superoxide dismutase content of leaves of six mulberry germplasm viz., English Black, Kolitha-3, C776, Rotundiloba, $BC_2$59, and S1 grown under coastal saline soils of South 24 Parganas district of West Bengal, India was investigated. Results demonstrated a sharp decrease in the chlorophyll (2.35 to1.19 mg.g FW^{-1}) and protein (30.10 to 15.20 mg.g FW^{-1}) contents of leaves of all the mulberry germplasm with increasing soil salinity (1.60 to 22.70 $dS.m^{-1}$). On the contrary, the number of stress-related antioxidant enzymes like catalase, peroxidases, and superoxide dismutase increased from 1.15 to 5.43, 1.43 to 4.76, and 8.65 to 25.15 g^{-1} $FW.min^{-1,}$ respectively. Overall, the field study indicated the superiority of Kolitha-3 and C776 grown in Canning (Canning I and II), Basanti, Namkhana, Kakdwip, and Sagar blocks of coastal regions of South 24 Parganas. The study deals with issues of the utilization of scarce land promoting income-generating avenues like sericulture in saline areas.

INTRODUCTION

The current state of competition for rapid urbanization and industrialization adversely brings an alarming rate of natural resource degradation along with biodiversity loss (Singh & Singh 2017), which has necessitated a paradigm of conversion of the conventional ways and means of agricultural production. The continued land degradation due to increased incidences of soil salinity becomes one of the major threats to agricultural sustainability (Sharma & Singh 2015). For instance, it is estimated that there is around 1128 m ha area in the world which is affected by salinity and sodicity stresses (Wicke et al. 2011). The rise in the sea level, the consequent increase in salt intrusion, and the increased frequency of cyclonic storms negatively impacted the productivity of coastal agroecosystems (Yeo 1998). In the coastal or deltaic regions, the salinity of soils occurs mainly by salts that contaminate the freshwater supply through the intrusion of seawater. Coastal agriculture may also be affected by saline aerosols, which are produced by violent wave activity during storms or heavy winds on the sea surface. These salts can also move inland up to a significant distance, but the most harmful effects occur on vegetation or crops grown near shore (Grieve et al. 2012). The state of West Bengal has the highest proportion of areas susceptible to salinity (0.82 million hectares) under coastal saline lands, with more than 50% of the coastal stretch of the state West Bengal confined primarily to the districts of South 24 Parganas (Bhowmick et al. 2020). Therefore, it is crucial to consider a wider perspective to address the concerns of optimal use of limited land resources while encouraging more avenues of income for those who live in salinity-prone areas.

The resilient, deeply rooted, and perennial mulberry tree is used to produce raw silk. Its leaves are fed to the monophagous silkworm *Bombyx mori* L. The sericultural flora and fauna of India are very diverse. The national repository has 1317 different types of mulberry germplasm (CSGRC Annual Report). Despite the immense potential for sericulture to be explored for economic growth, India has not

used its full potential to meet the rising local demand for the silk industry during the past few decades. Alongside that, the exploitation of mulberry in the food and pharmaceutical industries is also mere in our country, though there are a plethora of opportunities. The main challenge to the spread of moriculture in India is the degradation of land caused by soil salinity.

Salinity-induced stress results in many physiological and biochemical impairments in plants, such as the reduced amount of photosynthate, ionic imbalance, and oxidative injury to proteins (enzymes) (Zhu 2001, Xiong & Zhu 2002, Muchate et al. 2016). Salinity also affects mulberry plants in various ways. The first visible symptom of salt injury in mulberry is the appearance of yellow patches (Vijayan et al. 2008), which occur due to chlorophyll depletion by increasing the activity of the chlorophyllase enzyme (Singh & Singh 1999). Protein concentrations in the leaves of mulberry grown under salinity decline significantly (Vijayan et al. 2008) due to the breakage of electrostatic bonds and an increase in hydrophobic interactions (Melander & Horvath 1977). The adverse effect of salinity on the rate of photosynthesis is also found in mulberry plants like other woody plants (Kumar et al. 2003, Vijayan et al. 2008). Simultaneously, to defend themselves against oxidants, mulberry has developed specialized defense mechanisms that involve enzymes and antioxidant molecules (Sudhakar et al. 2001).

In woody plant species such as Thai neem (Cha-um et al. 2004), olive (Marin et al.1995), pine (Khasa et al. 2002), and mulberry (Hossain et al. 1991, Tewary et al. 2000, Vijayan et al. 2003, 2008, Jhansilakshmi et al. 2016), screening for salt tolerance has been studied. The biochemical traits have been investigated in different salt-tolerant and salt-susceptible mulberry germplasm to study the mechanism of salinity tolerance at an early stage of growth (Vijayan et al. 2008). It has been shown that an increase in the electrical conductivity (EC) of an experimental soil substrate led to a detrimental effect on the productivity of mulberry, including reduced leaf protein content, chlorophyll fluorescence, and an extremely elevated level of antioxidants (Vijayan et al. 2008, Sudhakar et al. 2001).

In the recent past, the effectiveness of mulberry germplasm against salinity has been realized, and a few salinity-resistant and high-yielding mulberry germplasm have been identified (Tewary et al. 2000, Vijayan et al. 2003, 2008, Jhansilakshmi et al. 2016). The purpose of this study is to comprehend how the physicochemical characteristics of six different salt-tolerant mulberry germplasm in the soil of coastal blocks of the South 24 Parganas district respond. The study's findings are anticipated to assist the dual purposes of wasteland management and sericultural farm output while debilitating the impacts of increasing soil salinity, particularly in coastal areas.

MATERIALS AND METHODS

Study Area

The study was conducted along the coastal regions of South 24 Parganas district (located between latitudes 21°88′ N and 22°16′ N and longitudes 88°11′ E and 88°82′ E) in West Bengal, India. Separate field tests with salinity stresses ranging from 18 to 23 $dS.m^{-1}$ were carried out in the five experimental farms of Canning I and II, Basanti, Namkhana, Kakdwip, and Sagar. A brief profile of the study area is given in Table 1.

Plant Materials and Experimental Setup

For field testing, the salt-tolerant mulberry germplasms English Black, Kolitha-3, C776, Rotundiloba, $BC_2$59, and S1 were chosen (collected from the Central Sericultural Research and Training Institute, Berhampore, West Bengal, India). Details of the exploited germplasm are given in Table 2. Three replications of the trials were used and compared to plants grown in non-saline conditions (EC between 1.60 $dS.m^{-1}$) using a randomized complete block design (RCBD). The size of each plot was 4 m × 4 m, while the distance between plants was maintained at 0.9 m. The plantation was done through stem cuttings in March, whereas the performance of the crop was evaluated after the 60^{th} day of pruning in the first week of May. Recommended agronomical practices were followed throughout the growth period (Datta 2000).

Table 1: Brief profile of the study area. Data collected from Department of Planning and Statistics, Govt. of West Bengal. http://www.wbpspm.gov.in/SiteFiles/Publications/13_21062017112440.pdf/(accessed 16 June 2023).

Blocks	Total area [sq. km]	Net area under cultivation [ha]	Saline Area [%]	Salinity (EC) [$dS.m^{-1}$]	Agricultural workers [%]
Canning I and II	402.80	31610	18	18.04	55.53
Basanti	404.21	26151	19	19.54	74.02
Namkhana	370.61	16910	21	20.69	63.81
Kakdwip	252.74	15973	20	21.08	53.26
Sagar	282.11	17436	23	22.70	73.95

The Physiological Study

For all biochemical studies, leaf samples were collected on the 60th day of the pruning. The 5th leaf from the top of each twig was used for the study (Vijayan et al. 2003).

Leaf Chlorophyll Content Assay

Leaf tissues of 100 mg were suspended in 10 mL of 80% acetone, mixed well, and kept at 4°C overnight in the dark. The supernatant was withdrawn after centrifugation at 5000 rpm (Remi PR-24), and absorbance was recorded at 663 and 645 nm in a spectrophotometer (Shimadzu, UV-1700). The amount of chlorophyll was calculated according to the equation given below, as mentioned by Arnon (1949).

Chlorophyll a [$\mu g.mL^{-1}$] = 12.7 (A_{663}) – 2.69 (A_{645})

Chlorophyll b [$\mu g.mL^{-1}$] = 22.9 (A_{645}) – 4.68 (A_{663})

Total chlorophyll [$\mu g.mL^{-1}$] = 20.2 (A_{645}) + 8.02 (A_{663})

Leaf Protein Assay

For estimating the total soluble proteins, the Lowry et al. (1951) method has been adopted. A 100-mg leaf sample was ground in 10% trichloroacetic acid. The TCA solution was removed by centrifugation (Remi PR-24), and 1N NaOH solution was added to the precipitated proteins. After thorough mixing, it was boiled at 65°C for 10 minutes in a water bath and then centrifuged. The supernatant liquid was taken for protein estimation. The assay mixture, containing 1 mL of protein solution and 3 mL of alkaline solution (50 mL of solution containing 2% sodium carbonate in 0.1 N NaOH and 2 mL of 1% $CuSO_4.5H_2O$ in 1% sodium potassium tartrate), was allowed to stand for 10 min. Finally, 0.7 mL of folin-phenol reagent was added rapidly. The reaction was allowed to take place for a period of 30 min, and the blue color developed in the assay mixture was measured at 660 nm in a spectrophotometer (Shimadzu, UV-1700) against a blank containing sodium hydroxide instead of protein solution. The protein was estimated by using the standard curve, which was prepared by plotting the percentage transmittance against the standard protein concentration of bovine serum albumin.

Study of the Antioxidant Enzymes from Leaves

Catalase and Peroxidase: The leaf tissues, weighing about 200 mg, were homogenized with 10 mL of phosphate buffer pH 6.8 (0.1 M) and then centrifuged at 4°C for 15 min at 5000 rpm in a cold centrifuge (Remi CM-12 Plus). The clear supernatant was taken as the enzyme source. The activity of catalase, as well as peroxidase, has been assayed following the method of Chance and Maehly (1955). Three milliliters of the assay mixture for the catalase activity comprised 1 mL of 0.1% H_2O_2 and 2 mL of the enzyme extract. After incubation at 25°C for 15 min, the reaction was stopped by adding 3 mL of 5% (v/v) H_2SO_4, and the residual H_2O_2 was titrated against 0.01 N $KMnO_4$ until a faint purple color persisted for at least 15 sec. A control was run at the same time in which the enzyme activity was stopped at "zero" time. One unit of catalase activity is defined as the amount of enzyme that breaks down 1 g of tissue per minute.

Five milliliters of the assay mixture for the peroxidase activity comprised 125 µmoles of phosphate buffer, pH 6.8, 50 mmoles of pyrogallol, 50 µmoles of H_2O_2, and 1 mL of the 20 times-diluted enzyme extract. This was incubated for

Table 2: A detailed list of mulberry germplasm utilized in the study.

Sl. No.	Germplasm	Accession No.	Species	Origin	Salient feature
1.	English Black	ME-0004	*Morus latifolia* Poir.	Exogenous (France)	Branching semi-erect; homophyllous, deeply green, ovate-shaped leaves with a dentate edge.
2.	Kolitha-3	MI-0108	*Morus alba* L.	Indigenous	Semi-erect, straight-branched with heterophyllous, deep-ovate leaves and serrated margins.
3.	C776	MI-0158	*Morus indica* L.	English Black × *M. multicaulis*	Erect branching with straight branches, mature; homophyllous leaves are green in color, ovate in shape, and have a serrated margin.
4.	Rotundiloba	ME-0095	*Morus rotundiloba* Koidz.	Exogenous	Semi-erect branching, branches are slightly curved; leaves are green and homophyllous, ovate in shape with a serrated margin and slightly rough surface having free lateral, caducous stipule.
5.	$BC_2$59	MI-0080	*Morus latifolia* Poir.	*M. indica var.* Matigara Local X Kosen	Branching erect, leaves are homophyllous green in color with dentate margin and smooth surface.
6.	S-1	ME-0065	*Morus indica* L.	Clonal selection from Mandalaya	Wide branching; branches are slightly curved; leaves are homophyllous, deep green, ovate with dentate margin and smooth surface.

Source: Compiled by the authors

5 min at 25°C, after which the reaction was stopped by adding 0.5 mL of 5% (v/v) H_2SO_4. The amount of purpurogallin formed was determined by measuring the absorbency at 420 nm with a spectrophotometer (Shimadzu, UV-1700).

Superoxide dismutase: SOD was determined as described by Beauchamp and Fridovich (1971). Measured by the inhibition in the photochemical reduction of nitroblue tetrazolium. In the spectrophotometric assay, 1 mL reaction mixture contained 50 mM phosphate buffer (pH 7.8), 0.1 m M EDTA, 13 mM methionine, 75 µM nitroblue tetrazolium (NTB), 2 µM riboflavin, and 100 µL of the supernatant (prepared from leaf extract after centrifugation at 5000 rpm in Remi PR-24 centrifuge). Riboflavin was added at last, and the reaction was initiated by placing the tubes under two 15-W fluorescent lamps. The reaction was terminated after 10 min by removal from the light source. Non-illuminated and illuminated reactions without supernatant served as calibration standards. The reaction product was measured at 560 nm by spectrophotometer (Shimadzu, UV-1700). One unit of superoxide dismutase activity (expressed as unit.g^{-1} FW.min^{-1}) is defined as the amount of enzyme required to cause 50% inhibition of nitroblue tetrazolium reduction, which was monitored at 560 nm.

Statistical Analysis

The data is presented as means ± standard deviation (SD). The data were subjected to analysis of variance (ANOVA) following Tukey's honestly significant difference (HSD ($p \leq 0.05$) using GraphPad Prism version 9.4.0. Tukey's HSD test was used to compare pairwise significant differences between the groups.

RESULTS AND DISCUSSION

The experimental trials of mulberry germplasm at relatively lower salinity levels showed superior performance than the trials at higher soil salinity stresses. All the mulberry germplasm propagated at soil salinity levels of 18 to 20 dS.m^{-1} (Canning I & II and Basanti), while no survivability was recorded in Rotundiloba, $BC_2$59, and S1 at salinity levels of 21 to 23 dS.m^{-1} (Namkhana, Kakdwip, and Sagar).

Physiological Study

Leaf Chlorophyll Content Assay: Leaf chlorophyll concentration of the mulberry germplasm decreased in the soil of the all-salinity-prone blocks (Table 3). In Canning and Basanti, the percentage of decrease is on the lower side, whereas it is comparatively on the higher side in Namkhana, Kakdwip, and Sagar. In the most salinity-prone soils, superior performers like English Black, Kolitha-3, and C776 have a percentage decrease in chlorophyll content of 32.44%, 42.13%, and 21.54%, respectively. Salinity stress significantly lowered the amount of chlorophyll in the leaf, which may have been brought on by a high rate of chlorophyll breakdown or a reduction in pigment synthesis (Yeo & Flowers 1983). Vijayan et al. (2008) observed an initial increase in chlorophyll content when they performed an *ex vitro* experiment in NaCl-induced salinity-prone soil. Still, the amount of initial salinity in terms of EC observed there was comparatively on the lower side than the present experimental soils of the coastal blocks. In salt-tolerant germplasm, lesser depletion of the chlorophyll content may be considered as a preliminary selection criterion in mulberry for salinity stress (Jimenez et al. 1997).

Leaf Protein Assay: The protein content of almost all germplasm declined sharply at all the salinity-prone blocks (Table 4). The percentage of decrease in the protein content in Kolitha-3 is 41.10%, followed by English Black 27.39% at the most salinity-prone block, Sagar. However, in C776, protein concentration was greater in all salinity-prone blocks compared to other germplasm, which appeared similar to the observation of Vijayan et al. (2008). For many Lepidopteron larvae, leaf protein is a key nutrient quality indicator. It is well known that fibroin and sericin, which make up nearly 69% of the protein content of raw silk, are

Table 3: Chlorophyll Content (mg.g FW^{-1}).

		Community Development Blocks of South 24 Parganas				
Germplasm	Control	Canning I and II	Basanti	Namkhana	Kakdwip	Sagar
English Black	2.25±0.25^a	1.89±0.17^a	1.76±0.25^a	1.66±0.25^a	1.62±0.14^a	1.52±0.21^a
Kolitha-3	2.16±0.04^a	1.78±0.11^a	1.68±0.19^a	1.46±0.10^a	1.48±0.21^a	1.25±0.11^b
C776	1.81±0.22^b	1.72±0.21^a	1.74±0.18^a	1.54±0.17^a	1.59±0.15^a	1.42±0.10^a
Rotundiloba	2.35±0.30^a	2.29±0.08^b	2.18±0.05^b	-	-	-
$BC_2$59	1.68±0.27^b	1.36±0.20^c	1.19±0.13^c	-	-	-
S1	1.52±0.18^b	1.56±0.16^c	1.75±0.27^a	-		-

Values are means (± SD) of three replications. Different superscript letters in the same column are significantly different ($p \leq 0.05$, ANOVA, Tukey-HSD).

Table 4: Protein content (mg.g FW^{-1}).

		Community Development Blocks of South 24 Parganas				
Germplasm	Control	Canning I and II	Basanti	Namkhana	Kakdwip	Sagar
English Black	24.10±2.36[a]	26.70±2.25[a]	24.40±1.32[a]	21.60±2.01[a]	19.70±1.99[a]	17.50±2.08[a]
Kolitha-3	25.80±0.49[a]	24.20±1.66[a]	24.10±1.77[a]	20.50±1.93[a]	18.20±2.40[a]	15.20±2.02[a]
C776	23.60±1.07[a]	27.90±1.73[a]	26.60±1.31[b]	24.10±1.87[b]	23.10±0.26[b]	21.20±0.80[b]
Rotundiloba	29.60±2.16[b]	26.40±1.02[a]	26.80±2.10[b]	-	-	-
$BC_2$59	28.50±2.63[b]	27.30±2.23[a]	26.30±0.99[b]	-	-	-
S1	30.1±0.45[b]	28.8±0.31[a]	25.9±0.15[b]	-	-	-

Values are means (± SD) of three replications. Different superscript letters in the same column are significantly different ($p \leq 0.05$, ANOVA, Tukey's-HSD).

directly biosynthesized from mulberry leaf protein, with the remaining 31% coming from silkworm body tissue and hemolymph protein (Bose & Bindroo 2001). Different mulberry germplasm's protein contents had a direct impact on larval development, particularly on the development of silk glands and the features of silkworm cocoons.

Study of the Antioxidant Enzymes from Leaves

Catalase: The catalase activity was significantly elevated in the leaves of all the germplasm, along with the increasing salinity stress levels in the coastal blocks (Table 5). The rate of increase in the enzyme activities was dependent on the severity of the salinity stress level. In comparison to the control, the catalase activity in Kolitha-3 and C776 increased almost 3.6 and 4.1 times, respectively. Catalase is mostly present in peroxisomes and glyoxysomes in plants, where it works to eliminate H_2O_2 produced during photorespiration or the oxidation of fatty acids in glyoxisomes. By lowering the harmful amounts of hydrogen peroxide generated during cell metabolism, an increase in catalase activity is thought to be an adaptive feature that may aid in overcoming the damage to tissue metabolism (Rasheed & Mukherji 1991). In the present study, the greater increase in catalase activity of C776 than other germplasm may suggest its effective scavenging mechanism to remove H_2O_2.

Peroxidase: The increased rate of peroxidase activity in C776 is almost 3.9 times, followed by Kolitha-3 and English Black almost 2.6 and 2.3 times, respectively (Table 6). The ability of plants to tolerate salt has been linked to enhanced antioxidant levels (Gossett et al. 1994; Hernandez et al. 1995). POD activity was shown to be higher in tolerant plant species, allowing the plants to defend themselves against oxidative stress, while this high activity was not seen in sensitive plant species (Sudhakar et al. 2001). Similarly, in the current study, in all three germplasm, peroxidase activity increased significantly.

Superoxide dismutase: Superoxide dismutase activity was significantly elevated in the stressed plants over control plants for all germplasm at all stress regimes (Table 7). In the salinity stress level of Sagar block, there was a significant increase in enzyme activity in English Black, Kolitha-3, and C776. Nevertheless, the increase in enzyme activity was higher in Kolitha-3 (2.6 times), followed by C776 (2.3 times) and English Black (2.2 times). Reportedly, SOD plays an important role in cellular defense against oxidative stress because its activity can directly modulate the amount of O_2^- and H_2O_2, the two Haber-Weiss reaction substrates (Sudhakar et al. 2001). Salinity caused a significant increase in SOD activity in all the germplasm. The rate of increase was higher in Kolitha-3 than in other germplasm. The observed

Table 5: Catalase (g^{-1} FW.min^{-1}).

		Community Development Blocks of South 24 Parganas				
Germplasm	Control	Canning I and II	Basanti	Namkhana	Kakdwip	Sagar
English Black	1.43±0.26[a]	2.83±0.23[a]	2.90±0.29[a]	3.40±0.16[a]	3.46±0.17[a]	4.80±0.29[a]
Kolitha-3	1.50±0.22[a]	2.90±0.22[a]	3.10±0.22[a]	4.47±0.46[b]	4.57±0.46[b]	5.43±0.62[b]
C776	1.27±0.19[a]	2.67±0.33[a]	3.10±0.14[a]	3.20±0.14[c]	3.27±0.05[c]	5.17±0.12[b]
Rotundiloba	1.15±0.04[b]	2.85±0.37[a]	3.20±0.24[a]	-	-	-
$BC_2$59	1.33±0.05[a]	2.80±0.16[a]	3.10±0.08[a]	-	-	-
S1	1.33±0.09[a]	2.56±0.25[b]	3.43±0.20[b]	-	-	-

Values are means (± SD) of three replications. Different superscript letters in the same column are significantly different ($p \leq 0.05$, ANOVA, Tukey's-HSD).

Table 6: Peroxidase (g^{-1} FW.min^{-1}).

		Community Development Blocks of South 24 Parganas				
Germplasm	Control	Canning I and II	Basanti	Namkhana	Kakdwip	Sagar
English Black	1.70±0.22[a]	3.10±0.14[a]	3.13±0.09[a]	3.46±0.09[a]	3.50±0.14[a]	3.93±0.54[a]
Kolitha-3	1.80±0.08[a]	3.16±0.09[a]	3.23±0.05[b]	3.93±0.05[b]	4.13±0.12[b]	4.60±0.09[b]
C776	1.67±0.05[a]	3.20±0.08[a]	3.26±0.12[b]	4.23±0.16[c]	4.20±0.08[b]	4.76±0.09[c]
Rotundiloba	1.73±0.12[a]	3.13±0.09[a]	3.30±0.16[b]	-	-	-
$BC_2$59	1.80±0.14[a]	2.93±0.05[b]	3.13±0.05[a]	-	-	-
S1	1.43±0.18[b]	3.00±0.16[a]	3.33±0.12[b]	-	-	-

Values are means (± SD) of three replications. Different superscript letters in the same column are significantly different ($p \leq 0.05$, ANOVA, Tukey's-HSD).

Table 7: Superoxide dismutase (g^{-1} FW.min^{-1}).

		Community Development Blocks of South 24 Parganas				
Germplasm	Control	Canning I and II	Basanti	Namkhana	Kakdwip	Sagar
English Black	9.15 ± 0.04	12.65 ± 0.10	12.79 ± 0.17	14.65 ± 0.11	14.95 ± 0.02	20.30 ± 0.17
Kolitha-3	9.83 ± 0.03	12.15 ± 0.04	12.45 ± 0.06	18.25 ± 0.05	19.05 ± 0.28	25.15 ± 0.07
C776	8.65 ± 0.07	11.67 ± 0.05	12.12 ± 0.07	15.15 ± 0.07	15.28 ± 0.08	19.19 ± 0.09
Rotundiloba	9.95 ± 0.04	12.45 ± 0.07	12.85 ± 0.10	-	-	-
$BC_2$59	10.14 ± 0.43	12.85 ± 0.09	12.95 ± 0.03	-	-	-
S1	9.57 ± 0.29	12.56 ± 0.12	12.78 ± 0.09	-	-	-

Values are means (± SD) of three replications. Different superscript letters in the same column are significantly different ($p \leq 0.05$, ANOVA, Tukey's-HSD).

increase in SOD activity could increase the ability of the leaves to scavenge O_2^- radicals, which on the other hand, can also lead to severe membrane damage.

CONCLUSIONS

In conclusion, mulberry is generally moderately tolerant to salinity, but significant varietal differences exist in salt tolerance. Mulberry germplasm in the soil of the coastal South 24 Parganas district showed varied physiological and biochemical responses. Overall, the experiment revealed that mulberry germplasm C776, Kolitha-3, and English Black established its nutritional and salinity tolerance superiority with respect to total proteins and total chlorophyll contents alongside the antioxidant responses. From the observations, it is also clear that the mulberry germplasm, particularly C776, and Kolitha-3, turned out to be superior in leaf biochemical analysis compared to other germplasm studied under the same agro-climatic conditions. It may be recommended for silkworm rearing experimentation at the field level to test the cocoon parameters to confirm the possibilities of the establishment of sericultural farms in the socio-economically backward coastal regions of South 24 Parganas district of West Bengal. This establishment is important from both the socio-economic perspective and the effective utilization of the salinity-prone barren lands.

ACKNOWLEDGMENTS

The authors are grateful to the Hon'ble Vice Chancellor of Raiganj University and Hon'ble Principal of Hiralal Mazumdar Memorial College for Women, India, for providing the necessary infrastructural facilities in carrying out the experimentation. The research is part of the doctoral research work of the first author.

REFERENCES

Arnon, D.I. 1949. Copper enzymes in isolated chloroplasts: Polyphenoloxidase in Beta vulgaris. Plant Physiol., 1)24): 1.

Beauchamp, C. and Fridovich, I. 1971. Superoxide dismutase: improved assays and an assay applicable to acrylamide gels. Anal. Biochem., 1)44): 276-287.

Bhowmick, M.K., Srivastava, A.K., Singh, S., Dhara, M.C., Aich, S.S., Patra, S.R. and Ismail, A.M. 2020. Realizing the potential of coastal flood-prone areas for rice production in West Bengal: prospects and challenges. New Front. Stress Manag. Agric., 16: 543-577.

Bose, P.C. and Bindroo, B.B. 2001. A comparative biochemical study of seven promising mulberry (Morus alba L.) varieties under rainfed conditions of subtropical region. Indian J. Seric., 40: 171-173.

Chance, B. and Maehly, A. C. 1955. Assay of catalases and peroxidases. Meth. Biochem. Anal., 1: 357-424

Cha-Um, X., Suriyan, K. and Kirdmanee, C. 2008. Assessment of salt tolerance in eucalyptus, rain tree, and Thai neem under laboratory and field conditions. Pak. J. Bot., 40(5): 2041-2051.

CSGRC Annual Report. 2020-21 Annual Report of CSGRC, Central Silk Board, Ministry of Textiles, Govt. of India. Retrieved from http://csgrc.res.in/downloads/csgrc_ar_2020_21.pdf/ (Accessed 28 July 2022).

Datta R.K. 2000. Mulberry Cultivation and Utilization in India. Proceedings of the FAO Electronic Conference on Mulberry for Animal Production (*Morus* L.), Rome, Italy, 2000, pp. 45-62.

Gossett, D.R., Millhollon, E.P. and Lucas, M.C. 1994. Antioxidant response to NaCl stress in salt-tolerant and salt-sensitive cultivars of cotton. Crop Sci., 34(3): 706-714.

Grieve, C.M., Grattan, S.R. and Maas, E.V. 2012. Plant salt tolerance. ASCE Manual Rep. Eng. Prac., 71: 405-459.

Hernandez, J.A., Olmos, E., Corpas, F.J., Sevilla, F. and Del Rio, L.A. 1995. Salt-induced oxidative stress in chloroplasts of pea plants. Plant Science, 105(2): 151-167.

Hossain, M., Rahaman, S.M. and Joarder O.I. 1991. Isolation of sodium chloride-resistant genotypes in some mulberry cultivars. Bull. Seric. Res., 2: 67-73.

Jhansilakshmi, K., Borpuzari, M.M., Rao, A.A. and Mishra, P.K. 2016. Differential response of mulberry (Morus spp.) accessions for salinity stress. J. Appl. Biosci., 42(1): 30-35.

Jimenez, M.S., Gonzalez-Rodriguez, A.M., Morales, D., Cid, M.C., Socorro, A.R. and Caballero, M. 1997. Evaluation of chlorophyll fluorescence as a tool for salt stress detection in roses. Photosynthetica, 33: 291-301.

Khasa, P.D., Hambling, B., Kernaghan, G., Fung, M. and Ngimbi, E. 2002. Genetic variability in salt tolerance of selected boreal woody seedlings. Forest Ecol. Manag., 257-269: (3-1)165.

Kumar, S.G., Reddy, A.M. and Sudhakar, C. 2003. NaCl effects on proline metabolism in two high-yielding genotypes of mulberry (*Morus alba* L.) with contrasting salt tolerance. Plant Sci., 6)165): 1245-1251.

Lowry, H., Rosebrough, N.J., Farr, A.L. and Randall, R.J. 1951.Protein measurement with the Folin phenol reagent. J. Biol. Chem., 193: 265-275.

Marin, L., Benlloch, M. and Fernández-Escobar, R. 1995. Screening of olive cultivars for salt tolerance. Sci. Horti., 113-116 :(2-1)64.

Melander, W. and Horváth, C. 1977. Salt effects on hydrophobic interactions in precipitation and chromatography of proteins: an interpretation of the lyotropic series. Arch. Biochem. Biophys., 1)183): 200-215.

Muchate, N.S., Nikalje, G.C., Rajurkar, N.S., Suprasanna, P. and Nikam, T.D. 2016. Plant salt stress: Adaptive responses, tolerance mechanism and bioengineering for salt tolerance. Bot. Rev., 82: 371-406.

Rasheed, P. and Mukerji. S. 1991. Changes in catalase and ascorbic acid oxidase activities in response to lead nitrate treatments in mung bean, Indian J. Plant Physiol., 34: 143-146.

Sharma, D.K. and Singh, A. 2015. Salinity Research in India: Achievements, Challenges and Future Prospects. Springer, Singapore

Singh, A.K. and Singh, R.A. 1999. Effect of salinity of photosynthetic pigments in chickpea (Cicer arietinum L.) leaves. Indian J. Plant Physiol., 4: 49-51.

Singh, R.L. and Singh, P.K. 2017. Global environmental problems. Principles and applications of environmental biotechnology for a sustainable future. Indian J. Plant Physiol., 4: 13-41.

Sudhakar, C., Lakshmi, A. and Giridarakumar, S. 2001. Changes in the antioxidant enzyme efficacy in two high-yielding genotypes of mulberry (Morus alba L.) under NaCl salinity. Plant Sci., 3)161): 613-619.

Tewary, P.K., Sharma, A., Raghunath, M.K. and Sarkar, A. 2000. In vitro response of promising mulberry (Morus sp.) genotypes for tolerance to salt and osmotic stresses. Plant Grow. Reg., 1)30): 17-21.

Vijayan, K., Chakraborti, S.P. and Ghosh, P.D. 2003. In vitro screening of mulberry (Morus spp.) for salinity tolerance. Plant Cell Rep., 22: 350-357.

Vijayan, K., Chakraborti, S.P., Ercisli, S. and Ghosh, P.D. 2008. NaCl induced morpho-biochemical and anatomical changes in mulberry (Morus spp.). Plant Grow. Reg., 56: 61-69.

Wicke, B., Smeets, E., Dornburg, V., Vashev, B., Gaiser, T., Turkenburg, W. and Faaij, A. 2011. The global technical and economic potential of bioenergy from salt-affected soils. Energy Environ. Sci., 8)4): 2669-2681.

Xiong, L. and Zhu, J. K. 2002. Molecular and genetic aspects of plant responses to osmotic stress. Plant Cell Environ., 2)25): 131-139.

Yeo, A. 1998. Molecular biology of salt tolerance in the context of whole-plant physiology. J. Exp. Bot., 323)49): 915-929.

Yeo, A.R. and Flowers, T.J. 1983. Varietal differences in the toxicity of sodium ions in rice leaves. Physiol. Plant., 2)59): 189-195.

Zhu, J.K. 2001. Plant salt tolerance. Trends Plant Sci., 2)6): 66-71.

ORCID DETAILS OF THE AUTHORS

S. Rehan Ahmad: https://orcid.org/0000-0003-0796-5238

Nature Environment and Pollution Technology
An International Quarterly Scientific Journal

p-ISSN: 0972-6268
(Print copies up to 2016)
e-ISSN: 2395-3454

Vol. 23 | No. 1 | pp. 499-504 | 2024

Original Research Paper

https://doi.org/10.46488/NEPT.2024.v23i01.046

Open Access Journal

Impact of Small Anaerobic Digester on Household Economy of Bangladeshi Livestock Farmers

N. Sultana*, J. S. Khanam*†, K. S. Huque*, B. K. Roy*, N. Huda and M. K. Alam***

*Animal Production Research Division, Bangladesh Livestock Research Institute, Savar, Dhaka-1341, Bangladesh

**University of Reading, United Kingdom

†Corresponding author: J. S. Khanam; shovnajobaida07@gmail.com

Nat. Env. & Poll. Tech.
Website: www.neptjournal.com

Received: 13-07-2023
Revised: 10-08-2023
Accepted: 22-08-2023

Key Words:
Manure
Bio-digester
CH_4-emission
Power generation
Household economy

ABSTRACT

An extensive survey was performed covering all the regions of the country to find out the overall impacts of bio-digester on the economy of livestock farmers. Five districts were selected; ten farmers with having bio-digester of 3.2 m^3 on average and ten farmers who have no bio-digester were selected from each district. Through direct interviewing and farm monitoring, all farm characteristics, i.e., diurnal biogas production, power generation, cooking time, income and expenditures, farmer's gross earnings, and manure management practices data were collected accordingly. Descriptive statistics and student t-test was made to express the comparison response of the farms by using XL and SPSS software. It was observed that the owners of anaerobic digesters earned significantly ($p < 0.001$) more than the traditional farmers by selling animals and biogas (1715 & 306; 1146 & 0.00 USD, respectively). Not only that, by selling milk and fresh manure, the owners of bio-digester harvested more ($p < 0.05$) annual income than non-bio-digester farmers (4162, 3408 & 60.91, 44.63 USD, respectively). Though the expenditure of farmers having digester was high, but in a single fiscal year, they earned more ($p < 0.05$) profit than the conventional farmers (USD 4329 & 2842, respectively). However, owners of bio-digester used 67.2 % of their produced manure for gas production. Regarding storing manure as biomass and using it for cooking purposes significant difference ($p < 0.001$) was observed that was also reflected in the total manure management system of a farm. The farmers having no bio-digester stored 71.95% of their total manure in solid form, whereas the farmers who had bio-digester only stored 20.4% of their manure, which made a significant ($p < 0.001$) difference. From the biogas chamber, in an average one farmer used a gas stove for 4-5 hours and a gas lamp for 6-8 hours, which saved at least the expenditure of 18 USD per month/household. The notable thing was that the bio-digester alone contributed 7% to those farmers' gross economy by producing gas. It can be recommended that the rural householders could generate power by installing bio-digester and turn a small bio-digester as a beneficial avenue of their household economy.

INTRODUCTION

Bangladesh has not had enough base energy to bloom its economy for a long time. Global energy demands, the price of energy, and its related politics are growing up day by day. Biogas production through recycling waste is the least cost-effective and justified technology for the rural ecological condition of Bangladesh. Fifty years ago, in 1972, biogas technology began its journey in Bangladesh. At present, more than 100,000 small households have anaerobic bio-digester in their premises, which accounts for 0.4 percent of total rural households in Bangladesh. Rural households, over 90 percent of the total, still depend on conventional biomass for their cooking, and surprisingly, this biomass is about half of the total supplied energy of Bangladesh (IDCOL Final Report 2018). In Bangladesh, home cooking mostly depends on solid fuels, and the direct combustion of wood hampered the environment.

Manure can be used for cooking purposes, and in this way, forests can save from loss, resulting in keeping the environment green along lowering greenhouse gas emissions at a significant level (Cuellar & Webber 2008). The energy derived from bio-digester replaces fossil fuels and substitutes biogas, which surely reduces cooking time and greenhouse gas emissions too (Axaopoulos & Panagakis 2003). Biogas energy brought factual benefits to those women who suffered the most by using fossil fuel, and at the same time, it ensured more economic returns in terms of money (Kohlin et al. 2011). Not only for cooking means but also for electricity generation, biogas is now considered as a cheap source of energy. Because of the worldwide renewable energy

production demand and the shortage of harnesses on the natural gas reserve, the anaerobic digester is recognized as a promising technology nowadays. It needs rather a lowest investment to produce energy comparison to others. This potential source of power can secure electrification in rural areas. In case of shortfalls, it also can ensure the uninterrupted electricity supply in the urban and peri-urban areas. Biogas energy can also facilitate the irrigation of agricultural land (Hamid et al. 2013). The sustainability and secured growth of economics are closely interlinked with the uninterrupted energy supply that is truly vital for a nation, particularly for Bangladesh (Hasan & Ammenberg 2019). However, on the other hand, in the case of global warming, livetock is responsible for emissions of anthropogenic CH4 at a rate of 33% of total global emissions. Enteric methane emission from ruminants engulfs most of this portion (90%), and the manure produces the rest of the amounts. Though it looks negligible, it has huge impacts on agriculture and influences the climate. Substantial management practices of manure management are deleterious, and they exist only because of the lack of knowledge of farmers about the value of livestock manure and its integrated multiple management (Teenstra et al. 2014). On the basis of a study of 2016 in Bangladesh, Rahman et al. (2019) cited that around 102.6 million tons of cow dung and 12.9 million tons of poultry litter are being wasted in a year. Integrated or advanced practices like the adoption of an anaerobic digester can change the manure management scenario, and opportunities can be created to develop the economy of farmers. It is believed that an advanced system along with integrated infrastructure is required to develop for versatile and efficient use of biogas. It is assumed that as green fuel, biogas can bring synergy to a sustainable economy. Therefore, it is essential to identify whether the farmers who are adopting advanced technology like bio-digesters are being benefited and, if so, how. This experiment was conducted to figure out the beneficial opportunity of biogas digester and its related avenue of how it can impact the economy of rural households.

MATERIALS AND METHODS

The work was conducted by the Bangladesh Livestock Research Institute (BLRI) in collaboration with the Stockholm Environment Institute of Asia-Centre, Bangkok. The survey was operated through a random selection of dairy farmers from different districts of Bangladesh representing different dairy production areas. Having ten cows on an average number in their farms also was the selection criteria. The selected district was namely Dhaka, Chittagong, Mouluvibazar, Rangpur, and Mymensingh. From each region, ten farms having bio-digester and ten farms that have no bio-digester were selected for data collection. The average size of the bio-digester of all farmers was 3.2 m^3 installed by IDCOL/BCSIR. A questionnaire pertaining to farmers' responses on farming status, annual income and expenditures of farms, farming characteristics including cost efficiency, the contribution of bio-digester on farmer's gross earnings, and changing pattern of manure management for bio-digester was developed and surveyed accordingly. Prior to the survey, the questionnaire was tested among the farmers of the Dhaka district and updated with necessary revisions to make the questionnaire ready for use. A comparative study was conducted comprising a total of 100 dairy farms where 50 farms had bio-digester, and 50 farms had no bio-digester. The researchers visited each farm, and data were collected after an initial briefing on the purpose of the work through face-to-face information sharing. An in-depth interview, along with personal observations, was made with each farmer to collect authentic data from the respondent farmers. Average data on daily milk yield, use of feed, and manure production were collected. At the same time, the daily cost of feed, medical, maintenance, and all related expenditures were collected. Regarding bio-digester, information about biogas production, water and power use, cooking time, etc., was also collected daily, and in the case of any necessity to ensure the actual data, the help of family members was taken.

Additionally, farmers' stock books were used where available. Numerical collected data of the variables were inserted into Excel spreadsheets. Descriptive statistics was used to present the characteristics of all farms having a bio-digester and no bio-digester. A comparison of the response differences between the two types of farms was expressed using the Student t-test. All the analyses were done using the SPSS 20 software.

RESULTS

Economic Evaluation

Through the survey, it is revealed that farmers who installed bio-digesters in their homesteads were benefited. Considering the earnings from animal selling and biogas consuming farmers having bio-digester got more significant ($p < 0.001$) income (1715 & 306 USD, respectively) than the traditional farmers (1146 & 0.00 USD, respectively). By selling milk and fresh manure, the farmers having bio-digester earned more ($p < 0.05$) annual income (4162 & 60.91 USD, respectively) than the farmers who have no bio-digester (3408 & 44.63 USD, respectively). In total, on the basis of these income sources, the annual income of the first group of farmers (6245 USD) was significantly higher ($p=0.002$) than the later group of farmers (4599 USD). In the case of expenditure, it is observed that only the maintenance cost of two groups of farmers varied significantly ($p < 0.05$), and more money was

spent by the farmers who have bio-digesters (1186 & 1015 USD, respectively). Though the feed costs, veterinary, and AI costs were not significantly varied between the groups, cumulatively, owners of bio-digester spent more money (1915 USD) at a 5% level of significance than the traditional farmers (1756 USD) to run their farms. At the end of the business year, it is calculated that farmers having bio-digester gained profit (4329 USD) at a significantly higher rate ($p = 0.004$) than the farmers who have no bio-digester (2842 USD) from their farms, shown in Table 1.

How livestock and associated bio-digester had contributed to the farmer's gross economy was also evaluated. It was recognized that the contribution that comes from livestock was higher for farmers having bio-digesters than the conventional farmers (36% and 32%, respectively). The most important thing was that the bio-digester, by producing gas, contributed on gross economy of farmers by 7 % alone. So, livestock part with gas contributed almost half (43%) of the economy of those farmers who had bio-digester. This consequence revealed that the farmers who had digester were much more benefited from livestock in comparison with the farmers who had no bio-digester. It is also found that the farmers of non-bio-digesters earned almost one-third of their whole income (29%) from otherwise businesses, whereas the farmers having bio-digesters earned only 16% from other businesses (Fig. 1). So, it can be said that the bio-digester contributed as a factor to change the gross economy of farmers to some extent.

Besides the farm economy, it was found that the bio-digester had multidimensional effects on the manure

Table 1: Farmers annual income and expenditure from livestock farms (USD).

Parameter	Farmer category		*P* value	Significance
	Digester	Non-digester		
Income				
Animal Selling	1715.44 ± 29.34	1146.16 ± 32.36	0.000	***
Milk Selling	4162 ± 53.05	3408 ± 194.4	0.02	*
Biogas Consumption	306.41	0.00	0.000	***
Fresh manure selling	60.91 ± 3.20	44.63 ± 0.93	0.006	**
Total (USD/Year)	6245.46 ± 26.76	4599.08 ± 218.70	0.002	**
Expenditure				
Feed	495 ± 3.01	512 ± 7.89	0.116	NS
Maintenance	1186 ± 10.63	1015 ± 47.57	0.025	*
Veterinary and AI	232 ± 12.69	228 ± 4.07	0.760	NS
Total (USD/Year)	1915.54 ± 7.90	1756.93 ± 40.84	0.019	*
Profit	4329 ± 31.97	2842 ± 245	0.004	**

AI = Artificial insemination, * = P < 0.05; ** = P < 0.01; *** = P < 0.001; NS = non-significant

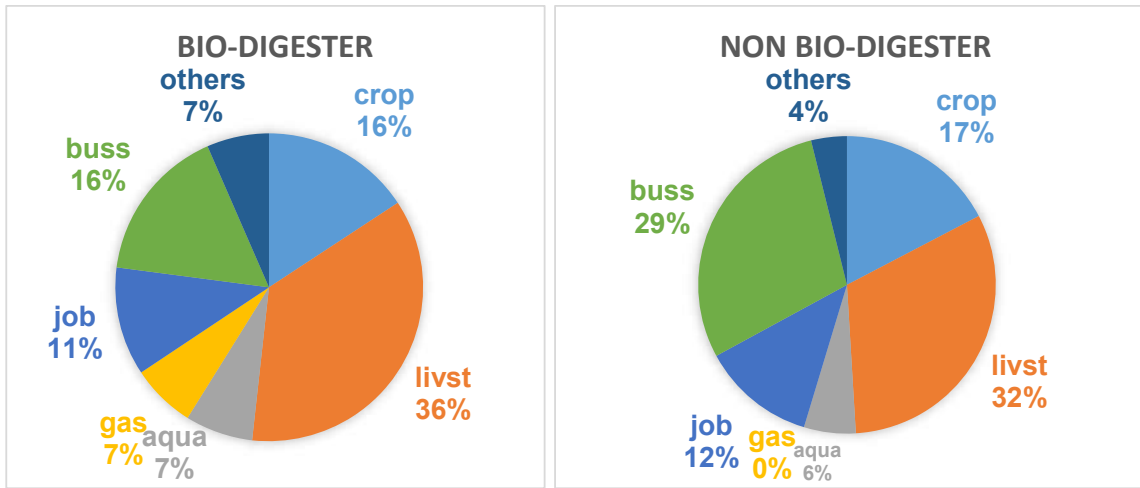

Fig. 1: Contribution of bio-digester on farmers' gross earnings.

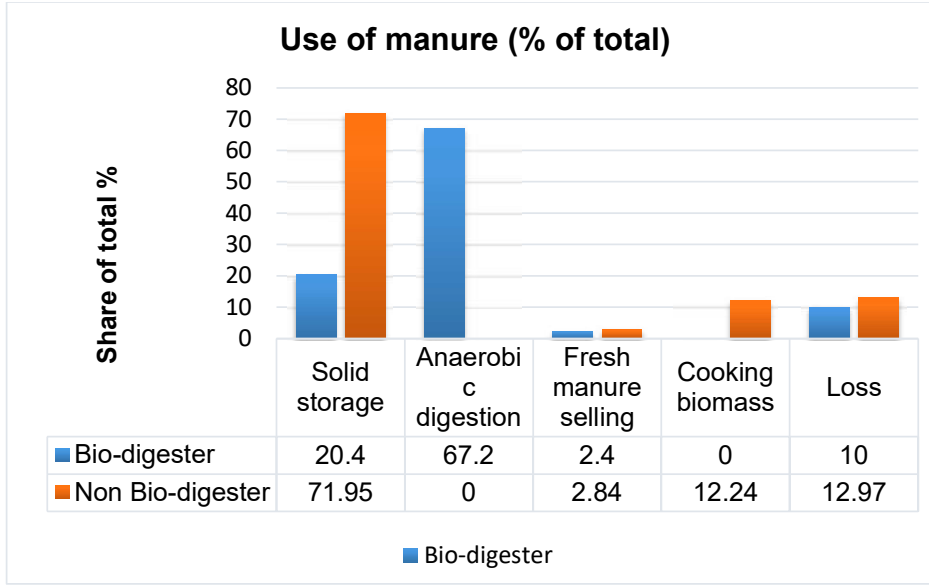

Fig. 2: Effect of bio-digester on changing manure management systems.

management system. The conventional farmers stored 71.95% of their total manure in solid form, whereas the farmers having bio-digesters only stored 20.4% of their total manure. The difference between the systems was significantly large ($p < 0.001$). Because of having a bio-digester, the farmer used manure for gas production at 67.2% of the total amount. As the conventional farmers had no bio-digester, the parameter of anaerobic digestion represented zero value. Vice versa, as those who had bio-digesters, they did not used biomass for cooking. In this regard, the conventional farmers used 12.24% of their total manure for cooking purposes. In the case of wasting manure, there was no significant difference between the two groups (Fig. 2). The farmers, having bio-digesters or not, waste 10% and 12.97% of their total manure, respectively.

From these findings, it can be said that the bio-digesters may play a significant role in changing the pattern of manure management very widely.

Collateral Efficacy of Bio-digester

The gas produced from anaerobic digester is used for cocking purposes. The gas was also used to enlighten the household. According to the data obtained from different households, it was found that they used gas stoves for 4-5 hours and were able to illuminate gas lamps for 6-8 hours. In this way, the farmers having anaerobic digester saved at least 14 and 5 USD monthly from firewood and electricity expenditures, respectively. As the conventional farmer store most of their manure, a huge amount of methane is emitted from stored manure. In this context, it can be assumed that biogas plants controlled the methane emission at a large rate. Besides this, it was identified through the statement of farmers that both the respondent groups used cow dung or slurry as fertilizer in their crop fields directly or by sun drying, respectively.

Prospects of Small Household Bio-digester in Bangladesh

From this study, along with different survey results, it was estimated that at present, in Bangladesh, 100,000 small household anaerobic digesters are functioning. The average size of their bio-digester is 3.1 m^3 and each of them produce 2920 liters of gas individually daily. The owners of the digesters are capable to support their household with one burner and three gas lamps for at least four hours. From these pieces of information, it can be assumed that an annual gas production of 113.15 million m^3 is possible following this approach. Furthermore, 87,038 MW of electricity can be produced from this source, and it can be added to the national grid. These estimated data could be used for policymaking to targeting the betterment of rural people of the nation (Table 2).

DISCUSSION

Figuring the overall income and expenditure of this study, the profitability of biogas farmers showed a significantly higher rate than the conventional farmers. This finding was fully agreeable with the study of Moli et al. (2021); they also found significantly higher income of biogas adopters than

Table 2: The prospects of small household bio-digester in Bangladesh.

Indicators	Status	Supporting References
Total Biogas plant (Small household)	100,000	IDCOL Final Report (2018)
The average size of installed plant	3.1 m^3	Hamid et al. (2013)
One household burner and three gas lamps (60 W bulb) can run four hours by	2920 L of Gas (can produce from 3 m^3)	Vogeli et al. (2014)
Annual gas production	113.15 million m^3	Zareei (2018)
Electricity can produce at least (~ 1300 m^3= 1 MW)	87,038	Osei-Marfo et al. (2018)

All these estimated values generated based on the supporting references

that of those farmers who had no biogas chamber. Not only that, but they also stated that raising the number of cattle on farms and expenditure on fuel are positively interlinked with the anaerobic digester. The present study also observed a similar trend in the case of selling animals from farms. Selling milk from farms is the primary source of income; it is recognized for any dairy farm. Like animal selling, farmers having bio-digesters got more profit by milk selling than the non-bio-digester farmers, as observed from the present survey. Pochwatka et al. (2020) gave a supportive statement with this finding. Additionally, many scientists around the world referred to the biogas digester as a substantial income source for rural people. Garcia et al. (2019) and Zemo et al. (2019) stated that the production of biogas helps farmers in rural areas to develop their economies. In society, it promotes the circular economy as well. In this context, Kabir et al. (2012) very much appropriately stated that raw materials used in digesters came from animals or feed waste of farms and returned a valuable product as gas, additionally energy as a bonus. It can be said that this is how the economy of farmers having bio-digesters under this study was improved. This study revealed that the farmer's gross economy concentrated through the adoption of the digester. This statement is agreed with the findings of Chakrabarty et al. (2013). They said that when biogas plants generated income for rural farmers by creating green employment, others were influenced to adopt this. It can be said that this feature influenced the biogas farmers of this study to give more emphasis on the biogas business rather than engage with other businesses. In this study, those who have no bio-digester were engaged higher in number with other businesses. This finding was in line with the observations of Hafeez et al. (2017); they found 44% engagement of biogas farmers compared with 70% engagement of conventional farmers in other businesses. In this study, it is found that conventional farmers stored most of their farm manure (71.95%) in solid form. On the other hand, farmers having anaerobic digesters store 20.4% of their total farm manure because of using manure as substrate, resulting in impacts on keeping the environment clean and green. Using manure in a bio-digester was recognized as a profitable solution by scientists (Achinas & Euverink 2020), and a scientist in another study recommended that this approach has a huge impact on keeping the environment clean (Zareei 2018). Not only the economic or environmental aspects but also the human health aspect, the use of manure in biogas plants rather than stored in solid form has an additional benefit. It is proven that through anaerobic digestion, the antibiotics of manure are destroyed (Taleghani et al. 2020). In another study, Thu et al. (2012) stated that an anaerobic digester has several effects on the manure management of respective farms that are in line with the statement of this study. It was found through this study that conventional farmers used manure (12.24% of the total) for cooking purposes. Kelebe (2018) claimed this is dirty fuel, and he identified that women are the main victims of this practice. But, through this study, no biogas farms were seen using raw manure as fuel. Regarding the size of the installed biogas plant, it was found that the diameter was as it is according to the statement of IDCOL report 2018 and Hamid et al. (2013). The observation of cooking and lighting was in line with the findings of Vogeli et al. (2014). Farmer's monthly savings from firewood and electricity expenditure were roughly evaluated in-country context, which was justified by the statement of Rahman et al. (2019). In this context, Kelebe (2018) stated that farmers having anaerobic digesters can save 20–36% of their monthly expenditure than conventional farmers. Amigun et al. (2012) also support this statement of saving money, and additionally, they stated that it ensures the use of clean cooking fuel alongside motivating others to adopt the digester. The secondary data on annual gas production estimated through this study was based on the observations of Zareei (2018), who stated that Iran can produce 2740 million m^3 of methane gas each year using the anaerobic digester. Besides this, the findings of electricity generation of this study were produced following the results of the study of Osei-Marfo et al. (2018). In Ghana, through combined heat and power, they converted 2,800 m3 of gas into 2.2 MW of electricity. On the contrary, Pochwatka et al. (2020) calculated 1770 MWh of electricity production from 443,000 m^3, which showed much more volume than

the previous one. However, they discussed that it may vary for the capacity of the plant and its installation technique for producing electricity.

CONCLUSION

Based on all the findings, it can be said that owners of anaerobic digesters had various avenues to gain profit. Biogas chambers played a significant effect in changing farmers' gross economy and the manure management pattern of farms. The anaerobic digester has a huge prospect for gas production and power generation. Most importantly, it mitigates the emission of methane gas from farm premises.

ACKNOWLEDGMENT

This research has been conducted with the support of the Bangladesh Livestock Research Institute and supervised by the Animal Production Research Division of the same institute.

REFERENCES

Achinas, S. and Euverink, G.J.W. 2020. Rambling facets of manure-based biogas production in Europe: A briefing. Renew. Sustain. Energy. Rev., 119: 109566.

Amigun, B., Musango, J.K. and Stafford, W. 2012. Biofuels and sustainability in Africa. Renew. Sust. Energ., 15(2): 1360-1372.

Axaopoulos, P. and Panagakis, P. 2003. Energy and economic analysis of biogas heated livestock buildings. Biomass Bioenergy, 24 : 239-248.

Chakrabarty, F.I.M.S., Boksh, M. and Chakraborty, A. 2013. The economic viability of biogas and green self-employment opportunities. Renew. Sust. Energ., 28: 757-766.

Cuellar, A.D. and Webber, M.E. 2008. Cow power: The energy and emissions benefits of converting manure to biogas. Environ. Res. Lett., 3: 034002

Garcia, N.H., Mattioli, A., Gil, A., Frison, N., Battista, F. and Bolzonella, D. 2019. Evaluation of the methane potential of different agricultural and food processing substrates for improved biogas production in rural areas. Renew. Sustain. Energy. Rev., 112: 1-10.

Hafeez, G.A.S.M., Roy, D.R., Majumder, S. and Mitra, S. 2017. Adoption of Biogas for Household Energy and Factors Affecting the Livelihood of Users in Rural Bangladesh. The 9th ASAE International Conference: Transformation in agricultural and food economy in Asia, 11-13 January 2017, Bangkok, Thailand, pp. 1642-1661.

Hamid, M.R., Haque, M.N., Rouf, M.A. and Islam, M.S. 2013. Dissemination of domestic biogas plants in Bangladesh - current state, problems faced, and barriers. Int. J. Sci. Eng. Res., 4(3): 1-4.

Hasan, M. and Ammenberg, J. 2019. Biogas potential from municipal and agricultural residual biomass for power generation in Hazaribagh, Bangladesh- A strategy to improve the energy system. Renew. Energy. Focus., 29: 14-23.

IDCOL Final Report. 2018. Research and Development on Biogas Production Efficiency in Domestic Biogas Digesters Suitable for Bangladesh Package. Infrastructure Development Company Limited (IDCOL), Bangladesh. No. S-32 under REREDPII Ref No.: IDCOL/REREDPII/S-32/2015/03. Dhaka, Bangladesh, pp. 1-91.

Kabir, H., Palash, M.S. and Bauer, S. 2012. Appraisal of domestic biogas plants in Bangladesh. Bangla J. Agric. Econ., 35(1&2): 71-89.

Kelebe, H.E. 2018. Returns, setbacks, and prospects of bio-energy promotion in northern Ethiopia: the case of family-sized biogas energy. Energy Sustain. Soc., 8(30): 1-14.

Kohlin, G., Sills, E.O., Pattanayak, S.K. and Wilfong, C. 2011. Energy, Gender, and Development: What Are the Linkages? Where Is the Evidence? Policy Research Working Paper Series 5800, The World Bank, Washington DC.

Moli, D.R.B., Hafeez, A.S.M.G., Majumder, S., Mitra, S. and Hasan, M. 2021. Does biogas technology adoption improve the livelihood and income level of rural people? Int. J. Green Energy, 18(10): 1081-1090.

Osei-Marfo, M., Awuah, E. and de Vries, N.K. 2018. Biogas technology diffusion and shortfalls in the central and greater Accra regions of Ghana. Water Prac. Technol., 13 (4): 932-946.

Pochwatka, P., Kowalczyk-Juśko, A., Mazur, A., Janczak, D., Pulka, J., Dach, J. and Mazurkiewicz, J. 2020. Energetic and economic aspects of biogas plants feed with agriculture biomass. Proc. Int. Conf. Green Energy, 15: 130-133.

Rahman, K.M., Melville, L., Edwards, D.J., Fulford, D. and Thwala, W.D. 2019. Determination of the potential impact of domestic anaerobic digester systems: A community-based research initiative in rural Bangladesh. Processes, 7: 512.

Taleghani, A.H., Lim, T.T., Lin, C.H., Ericsson, A.C. and Vo, P.H. 2020. Degradation of veterinary antibiotics in swine manure via anaerobic digestion. Bioengineering, 7: 123.

Teenstra, E., Vellinga, T., Aektasaeng, N., Amatayakul, W., Ndambi, A., Pelster, D., Germer, L., Jenet, A., Opio, C. and Andeweg, K. 2014. Global Assessment of Manure Management Policies and Practices. Livestock Research Report 844. Wageningen UR (University & Research Center) Livestock Research, Wageningen.

Thu, C.T.T., Cuong, P.H., Hang, L.T., Chao, N.V., Anh, L.X., Trach, N.X. and Sommer, S.G. 2012. Manure management practices on biogas and non-biogas pig farms in developing countries - using livestock farms in Vietnam as an example. J. Clean. Prod., 27: 64-71.

Vogeli, Y., Lohri C.R., Gallardo, A., Diener, S. and Zurbrügg, C. 2014. Anaerobic Digestion of Biowaste in Developing Countries: Practical Information and Case Studies. Swiss Federal Institute of Aquatic Science and Technology (Eawag), Dübendorf, Switzerland.

Zareei, S. 2018. Evaluation of biogas potential from livestock manures and rural wastes using GIS in Iran. Renew. Energy, 118: 351-356.

Zemo, K.H., Panduro, T.E. and Termansen, M. 2019. Impact of biogas plants on rural residential property values and implications for local acceptance. Energy Policy, 129: 1121-1131.

ORCID DETAILS OF THE AUTHORS

J. S. Khanam: https://orcid.org/0000-0002-4390-3344
B. K. Roy: https://orcid.org/0000-0003-0559-4488
N. Huda: https://orcid.org/0000-0001-6570-1703

Nature Environment and Pollution Technology
An International Quarterly Scientific Journal

p-ISSN: 0972-6268
(Print copies up to 2016)
e-ISSN: 2395-3454

Vol. 23 | No. 1 | pp. 505-515 | 2024

Original Research Paper

https://doi.org/10.46488/NEPT.2024.v23i01.047

Open Access Journal

Removal of Nickel from Industrial Wastewater by an Agro-based Composite Adsorbent

R. M. Bhagat† and **S. R. Khandeshwar**
Department of Civil Engineering, Yeshwantrao Chavan College of Engineering, Nagpur-441110, Maharashtra, India
†Corresponding author: R. M. Bhagat; rajeysh7bhagat@gmail.com

Nat. Env. & Poll. Tech.
Website: www.neptjournal.com

Received: 20-06-2023
Revised: 22-08-2023
Accepted: 17-11-2023

Key Words:
Agricultural waste material
Activated carbon
Adsorption
Composite adsorbent
Nickel
Column experimentation

ABSTRACT

For many years, especially in emerging nations like India, the environment has been threatened by the increased output of industrial wastes and heavy metal toxicity. The usage of inexpensive adsorbents has recently attracted a lot of attention in studies on the removal of heavy metals like nickel from industrial wastewater. The use of agro-based adsorbent is an alternative to conventionally used activated charcoal. In this research, adsorption experiments were carried out using agro-based adsorbent prepared from rice husk, wheat husk, and soybean husk to reduce nickel from industrial wastewater. The adsorption process is simple, economical, and effective is the most preferred method used for the removal of toxic metals like nickel from industrial wastewater. Adsorbents prepared from these husks can be effectively used for adsorption due to low cost & high availability. Characterization of agricultural material by various tests like XRF, proximate analysis, bulk density, and iodine number was conducted on agro-based adsorbents to know the co-relation between removal efficiency and adsorption capacity. The effect of turbidity and pH parameters on Ni removal efficiency is also studied. Results indicated that wheat husk adsorbent appeared to be the most effective for the adsorption of Ni from wastewater as compared to soybean husk and rice husk adsorbent. Wheat husk, soybean husk, and rice husk have removal efficiency in the range of 62.50 to 73.33. Composite absorbents CA-2 with the proportion of 50% wheat husk, 33% soybean husk, and 17% rice husk have 82.50% efficiency, and CA-3 has 80.83% efficiency in removing Nickel. Wheat husk adsorbent, CA-2, and CA-3 are more effectively and sustainably used for the treatment of industrial wastewater to remove heavy metals.

INTRODUCTION

In response to global urbanization and increased industry, toxic effluents are routinely released, and many industrial processes produce wastes that contain metals, including Cu, Ni, Cr, and Pb (Perumal et al. 2014). They enter the biological cycle through the consumption of food, water, and air. Because they bioaccumulate, heavy metals are hazardous (Febrianto et al. 2009, Ngah & Hanafiah 2008). Industries like metal plating, mining, battery production, PCB manufacture, etc., discharge heavy metals into the environment. Wastewater contains the hazardous heavy metal ion nickel, which is non-biodegradable. Mammals are teratogenic and carcinogenic to metallic nickel. There is an urgent need for a method that can effectively remove heavy metals from aqueous effluents without incurring high costs due to drawbacks such as incomplete removal, high reagent costs and energy requirements, and the production of toxic sludge that needs to be disposed of carefully. Adsorption is a process in which specific adsorptives are transferred arbitrarily from the fluid phase to the surface of suspended particles. Adsorption has advantages over other technologies due to its straightforward design, sludge-free environment, and potential for inexpensive initial investment, as well as land requirements. One of the many readily available lignocellulose materials in the globe is rice straw. The third-largest grain crop in the world by overall production is rice. The cellulose, hemicelluloses, and lignin are found in rice straws. Both natural and wheat husk fibers are three-dimensional polymeric composites that are predominantly composed of cellulose, hemicelluloses, and lignin, with a very tiny amount of protein, starch, fat, and ash. Soybean husk has several qualities that make it a possible adsorbent with binding sites capable of extracting metals from an aqueous solution. The wheat husk is easily accessible in large quantities, and the treatment method of bio-sorbent appears to be cost-effective (Said et al. 2018). Using agricultural leftovers, such as rice straw, has several benefits, including ease of regeneration, low cost, little processing needed, strong adsorption capacity, and simple technique (Asif & Chen 2017). A study was carried out on the removal of nickel

from wastewater and found that the removal of nickel from wastewater is effectively possible by different technologies. Different technologies to remove nickel are studied with their effectiveness, and the findings are discussed (Bhagat & Khandeshwar 2019). With a percentage removal of up to 99%, adsorption employing a variety of inexpensive adsorbents was found to be a very effective method (Dhokpande et al. 2013). Biological methods were also effective and produced encouraging results. The injection of nickel at a higher percentage through water results in serious health issues such as damage to the lungs, kidneys, and gastrointestinal tract. It has also been linked to cancer. Therefore, it is essential to create efficient and affordable technologies to extract and/or recover nickel (Arunkumar et al. 2015). Using an agricultural adsorbent to remove the nickel from wastewater is possible to treat chemical wastes by turning agricultural solid wastes into adsorption media—a practice known as waste-to-waste treatment. By treating wastewater containing nickel and other

A. Procurement and drying of husk.

B. Chemical treatment of husk.

C. Husk before thermal treatment.

D. Husk after thermal treatment.

E. Husk before thermal treatment.

F. Husk after thermal treatment.

Fig. 1: Preparation of adsorbents from agricultural husk.

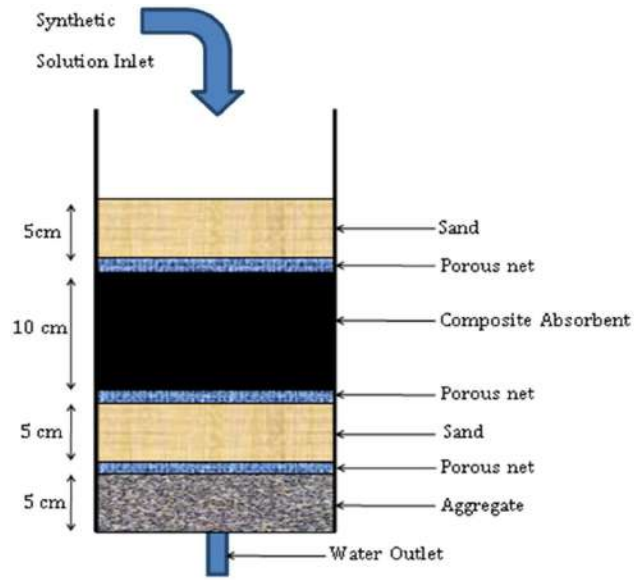

Fig. 2: Filter model with adsorbent, net, sand, and aggregates.

heavy metal ions, pine sawdust's ability to adsorb nickel and other heavy metal ions was examined in this work. To ascertain the interactive effects of the various components on the adsorption capacity, the results were analyzed using response surface methods and a factorial design. The utilization of pine sawdust may offer a potential method for removing nickel ions from multi-component aqueous solutions, according to the study's findings (Moodley et al. 2011). Removal of heavy metals utilizing various fruit peels, vegetable peels, and organic waste is effectively used. Researchers discovered that it is feasible to remove and recover Ni from electroplating wastewater using orange peel. The recovery of Ni by column operation is found to be higher than by batch method. This study demonstrated the fundamental effects of several parameters over the banana peel, including pH agitation, speed, and contact time, with the best results at pH 7,100 rpm and 90 minutes of contact time. The study investigated the carbon bio-sorbent made from pomegranate peels for removing iron from aqueous solutions (Abdulfatai et al. 2013, Darge & Mane 2015). Studies concluded that the sustainable methods for converting waste materials into valuable low-cost adsorbents utilized are quite successful at either treating or removing heavy metals from the environment (Khalili et al. 2000, Jain 2015)

MATERIALS AND METHODS

Materials and reagents are required for physical, chemical treatment, and thermal treatment to obtain adsorbent: rice husk, wheat husk, soybean husk, phosphoric acid, distilled water, and nickel powder.

Instrumentation required: Muffle furnace, oven, weighing machine, pH meter, UV spectro-photometer, sieve shaker, XRF machine, SEM, and XRD.

Every year, a large amount of rice husk (RH), Wheat Husk (WH), and Soybean Husk (SH) are generated in agricultural areas as bi-products and considered agricultural waste. To get rid of dirt and other soluble contaminants, these full husks were repeatedly washed in double-distilled water. Then, they were dried for 24 h at 105°C. The desired adsorbent size of 1 mm was obtained by sieving it through meshes, and it was then kept in an airtight container. To ensure that the reagents were completely adsorbed onto the raw material, these 500 g of husks were combined and steeped in a 1 M H_3PO_4 solution for 24 h at room temperature in 500 mL with 150 rpm of stirring. Following this procedure, the chemically treated husks were repeatedly washed in distilled water to maintain a steady pH level. This adsorbent was later oven-dried for 4 h at 110°C. After this, thermal treatment in a muffle furnace is given in the absence of oxygen at a temperature of 320°C to obtain the agro-based adsorbent (Fig. 1).

Similarly, all husks (WH, SH & RH) are treated, and adsorbents are prepared to carry out the adsorption process. A synthetic solution containing nickel is prepared concentration of 6 $mg.L^{-1}$ from standard nickel solution (1000 $mg.L^{-1}$ Ni in diluted HNO_3) with distilled water (Zhang et al. 2014). A filter unit was prepared for the treatment of water. It is a circular acrylic pipe consisting of coarse aggregate, fine aggregate, adsorbent material, and sand placed bottom to top in order of decreasing grain size (Fig. 2, Table 1). Each layer was separated by a net so that the materials did not get

Table 1: Filter components with dimension.

S.N.	Component	Dimension
1.	Filter unit	Diameter = 10 cm & Height = 60 cm
2.	Aggregate	Size = 20 mm & Height = 05 cm
3.	Porous Net	Micro-net 600 micron
4.	Sand	Size = 150-600 micron & Height = 5 cm
5.	Adsorbent material	Height = 10 cm

mixed, and there was continuous passage of water through the filter (Ratnoji & Singh 2014).

The specifications of the filter unit are as follows:

A synthetic solution of Ni concentration 6 $mg.L^{-1}$ is prepared and passed through the designed filter, where an adsorbent layer is sandwiched between sand layers. The aggregate layer also supports the bottom sand layer. A porous net separates every layer to avoid disturbance of layers in the filter unit.

Various tests are performed on husk to co-relate the adsorption process and the Ni removal efficiency:

1) Proximate analysis: Proximate analysis is the process of using established techniques to estimate the contents of moisture, volatile matter, fixed carbon, and ash.
   a. A sample's moisture content is determined by dividing the mass of its solids by the mass of its water, represented as a percentage.
   b. Ash content: The amount of any organic material that is left over after being burned at extremely high temperatures is known as the ash or mineral content.
   c. The amount of volatile matter in a sample is calculated as the mass loss following a 7-minute heating process at 900 degrees Celsius, with less moisture loss.
   d. Fixed carbon is the solid, combustible residue that is left behind when a particle is heated, and the volatile stuff is evacuated.
2) Bulk Density: Bulk density is the weight of a material per unit volume. It is typically used for material powders.

Table 2: Proximate analysis of agricultural husk.

S.N.	Proximate Analysis Parameter	Wheat Husk	Soybean Husk	Rice Husk
1.	Moisture Content, %	8	10	6
2.	Volatile Matter, %	51	54	59
3.	Ash Content, %	15	15	16
4.	Fixed Carbon, %	26	21	19

3) Iodine number: The amount of iodine that one gram of activated carbon may adsorb from a typical 0.1N iodine solution when the equilibrium iodine concentration is precisely 0.02N is known as the iodine number. The iodine number determines the amount of micro-pores in the activated carbon.
4) X-ray fluorescence (XRF) is a non-destructive analytical method for figuring out the elemental makeup of materials. An approach for gauging coating thickness and for studying materials is X-ray fluorescence Analysis (ED-XRFA).

Effects of pH and turbidity are also studied. pH is a measure of hydrogen ion concentration, a way to quantify a solution's acidity or alkalinity. Like smoke in the air, turbidity is the cloudiness or haziness that results from a vast number of tiny particles that are often imperceptible to the unaided eye. By measuring the intensity of light as a beam of light travels through a sample solution, a technique called spectrophotometry can determine how much light a chemical component absorbs. Every substance either absorbs or transmits light across a specific spectrum of wavelengths, according to the fundamental tenet. The spectrophotometer measures Ni removal. The study of characterization provides valuable insights into the effects of modifications on the adsorption behavior of activated carbon, which is the main cause of adsorption processes (Ahmadpour 1996).

RESULTS AND DISCUSSION

Characterization of agricultural waste material is done in various ways and starts with proximate analysis, where fixed carbon content is measured by following the formula.

Table 3: Developed Composite Adsorbent (CA) and their combination.

SN	Combinations			Composite Adsorbent	
1.	Rice Husk (17%)	Wheat Husk (33%)	Soybean Husk (50%)	CA-1	RH:WH:SH (17:33:50)
2.	Rice Husk (17%)	Wheat Husk (50%)	Soybean Husk (33%)	CA-2	RH:WH:SH (17:50:33)
3.	Rice Husk (33%)	Wheat Husk (50%)	Soybean Husk (17%)	CA-3	RH:WH:SH (33:50:17)
4.	Rice Husk (33%)	Wheat Husk (17%)	Soybean Husk (50%)	CA-4	RH:WH:SH (33:17:50)
5.	Rice Husk (50%)	Wheat Husk (33%)	Soybean Husk (17%)	CA-5	RH:WH:SH (50:33:17)
6.	Rice Husk (50%)	Wheat Husk (17%)	Soybean Husk (33%)	CA-6	RH:WH:SH (50:17:33)

Table 4: Proximate analysis of composite adsorbents.

S.N.	Proximate Analysis Parameter	CA-1	CA-2	CA-3	CA-4	CA-5	CA-6
1.	% Moisture Content	8	10	9	7	7	6
2.	% Volatile Matter	52	48	49	55	54	56
3.	% Ash Content	17	13	15	17	17	18
4.	% Fixed Carbon	23	29	27	21	22	20

Fixed carbon FC = 100 – (% Moisture content + % Volatile matter content + %Ash content)

The fixed carbon content for wheat husk is 26%, soybean husk is 21%, and rice husk is 19%, which is good for the adsorption process (Table 2). Proximate analysis indicates that all three waste materials have good potential to be good adsorbent. Proximate analysis of composite adsorbent is also carried out for the same above-mentioned reason.

Six different types of agro-based composite adsorbents (CA-1, CA-2, CA-3, CA-4, CA-5 & CA-6) are developed from agricultural waste (Table 3). These six developed composite adsorbents are used in the filter unit as one of the layers for heavy metal removal, and the results of individually used adsorbents with composite adsorbents are compared.

Fixed carbon content for CA-1 is 23%, CA-2 is 29%, CA-3 is 27%, CA-4 is 21% CA-5 is 22% and CA-6 is 20%. CA-2 and CA-3 have a little bit more fixed carbon content, and the remaining CA has a fixed carbon content in the range of 20% to 23%, which is good for the adsorption process. Proximate analysis indicates that all six CA have good potential to be good adsorbents (Table 4, Fig. 3).

The bulk density of a material is directly proportional to the adsorption capacity of that material. The more bulk density, the better the adsorption will be carried out. As per calculation, the bulk density of WH, SH, CA-2, and CA-3 were found to be maximum as compared to others (Table 5). A graphical representation of bulk density is shown in Fig. 4.

Iodine adsorption is a simple and quick technique to determine the adsorptive capacity of adsorbent, also known as iodine number. As per the results, the Iodine number of WH, CA-2, and CA-3 are found to be maximum (Table 6). Overall, all the adsorbents have a good iodine number. It suggests that WH adsorbent and composite adsorbents like CA-2 and CA-3 have good adsorption capacity (Fig. 5).

The XRF analysis reveals the SiO_2 content of the rice husk, wheat husk, and soybean husk (Table 7,

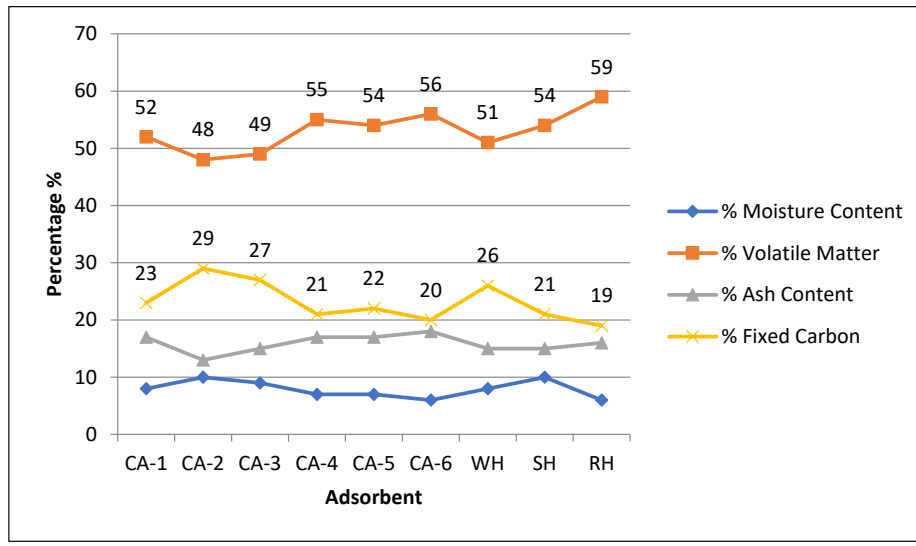

Fig. 3: Fixed carbon content by proximate analysis.

Table 5: Bulk density of husk and composite.

Adsorbent Material	RH	WH	SH	CA-1	CA-2	CA-3	CA-4	CA-5	CA-6
Bulk Density, $g.cc^{-1}$	0.65	0.90	0.78	0.80	0.89	0.88	0.70	0.75	0.69

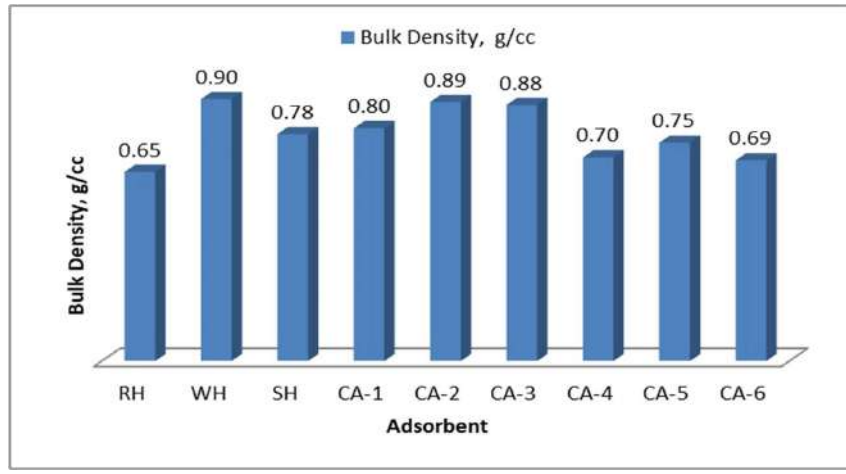

Fig. 4: Bulk density of husk and composite.

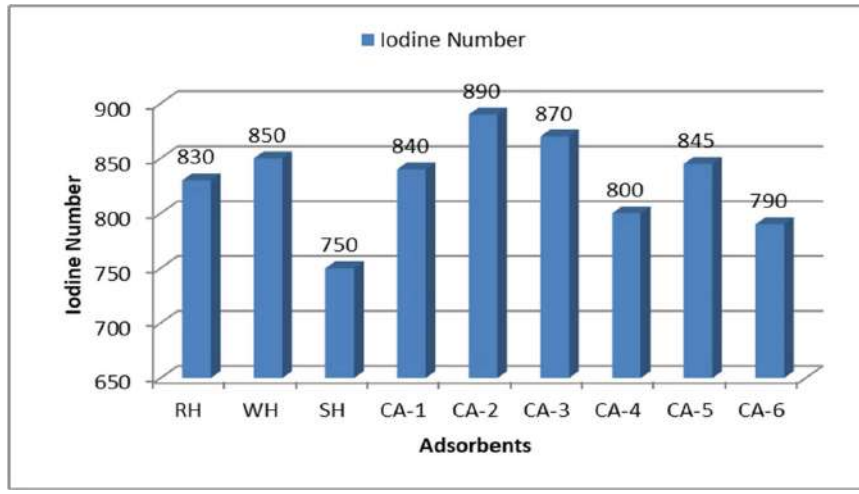

Fig. 5: Iodine number of adsorbents.

Table 6: Iodine number of adsorbent.

Adsorbent	RH	WH	SH	CA-1	CA-2	CA-3	CA-4	CA-5	CA-6
Iodine Number, $mg.g^{-1}$	830	850	750	840	890	870	800	845	790

Table 7: Elemental composition by XRF.

S.N.	Constituents	Wheat Husk [%wt.]	Rice Husk [%wt.]	Soybean Husk [% wt.]
1.	SiO_2	70.8	38.6	44.4
2.	CaO	0.21	8.01	7.44
3.	MgO	0.097	0.3	0.25
4.	Al_2O_3	6.01	25.879	24.7
5.	Fe_2O_3	3.105	11.3	10.7
6.	TiO_2	0.03	1.46	1.35
7.	S	1.24	9.02	8.5
8.	P	18.5	2.38	1.84

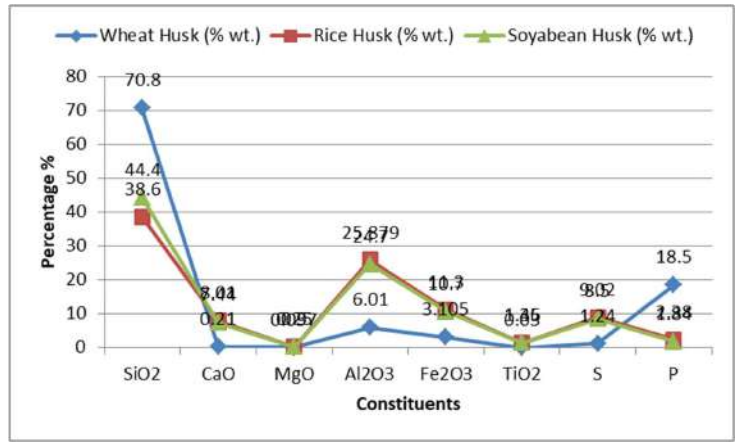

Fig. 6: Constituents (SiO_2) by XRF.

Table 8: Changes in pH after circulation through filter unit.

S.N.	Adsorbent	Initial pH	pH after 1st circulation	pH after 2nd circulation	pH after 3rd circulation	pH after 4th circulation	pH after 5th circulation
1.	Wheat Husk	2.60	5.45	5.80	6.55	6.80	6.75
2.	Soybean Husk	2.60	5.05	5.55	6.10	6.05	6.10
3.	Rice Husk	2.60	5.00	5.40	5.85	6.10	6.05
4.	CA-1 R17:W33:S50	2.60	5.40	5.75	6.10	6.40	6.45
5.	CA-2 R17:W50:S33	2.60	5.50	5.95	6.55	6.85	6.95
6.	CA-3 R33:W50:S17	2.60	5.45	5.90	6.50	6.80	6.75
7.	CA-4 R33:W17:S50	2.60	5.40	6.05	6.30	6.40	6.50
8.	CA-5 R50:W33:S17	2.60	5.35	5.60	6.00	6.10	6.10
9.	CA-6 R50:W17:S33	2.60	5.00	5.25	5.90	6.00	6.05

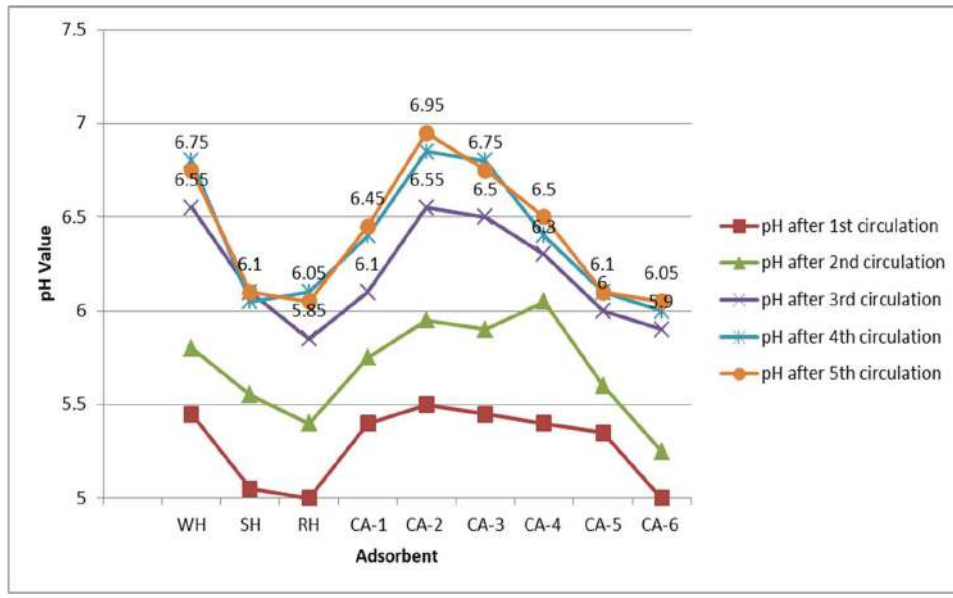

Fig. 7: Changes in pH after passing through filter unit.

Table 9: Changes in turbidity

S.N.	Adsorbent	Initial turbidity (NTU)	Turbidity after 1st circulation	Turbidity after 2nd circulation	Turbidity after 3rd circulation	Turbidity after 4th circulation	Turbidity after 5th circulation
1.	Wheat Husk	0	0.30	0.35	0.40	0.50	0.70
2.	Soybean Husk	0	0.10	0.20	0.20	0.35	0.55
3.	Rice Husk	0	0.20	0.25	0.30	0.35	0.45
4.	CA-1 R17:W33:S50	0	0.05	0.15	0.25	0.40	0.55
5.	CA-2 R17:W50:S33	0	0.25	0.30	0.30	0.45	0.65
6.	CA-3 R33:W50:S17	0	0.15	0.20	0.25	0.30	0.50
7.	CA-4 R33:W17:S50	0	0.05	0.05	0.15	0.20	0.40
8.	CA-5 R50:W33:S17	0	0.05	0.10	0.15	0.35	0.55
9.	CA-6 R50:W17:S33	0	0.10	0.15	0.20	0.30	0.40

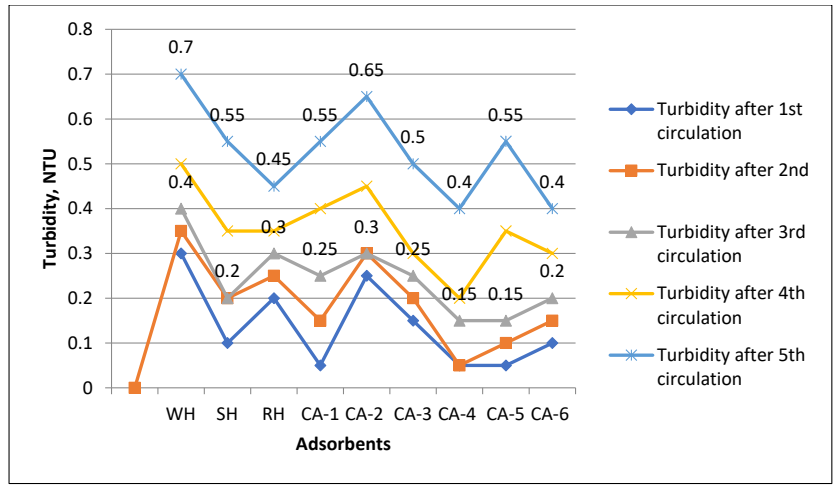

Fig. 8: Changes in turbidity after circulations.

Table 10: Nickel removal by developed adsorbent.

S.N.	Adsorbent	Initial Ni concentration [mg.L^{-1}]	Ni after 1st circulation [mg.L^{-1}]	Ni after 2nd circulation [mg.L^{-1}]	Ni after 3rd circulation [mg.L^{-1}]	Ni after 4th circulation [mg.L^{-1}]	Ni after 5th circulation [mg.L^{-1}]	Ni Removal %
1.	Wheat Husk	6	4.7	3.35	1.6	1.55	1.45	73.33
2.	Soybean Husk	6	4.8	3.75	1.7	1.6	1.55	71.67
3.	Rice Husk	6	4.85	3.85	2.25	2.1	1.8	62.50
4.	CA-1 R17:W33:S50	6	4.75	3.55	2.2	2.1	2.05	63.33
5.	CA-2 R17:W50:S33	6	4.35	2.95	1.05	1	0.95	82.50
6.	CA-3 R33:W50:S17	6	4.55	3.2	1.15	1.05	1	80.83
7.	CA-4 R33:W17:S50	6	4.65	3.7	1.55	1.45	1.4	74.17
8.	CA-5 R50:W33:S17	6	4.65	3.3	1.65	1.55	1.5	72.50
9.	CA-6 R50:W17:S33	6	4.8	3.75	1.95	1.9	1.8	67.50

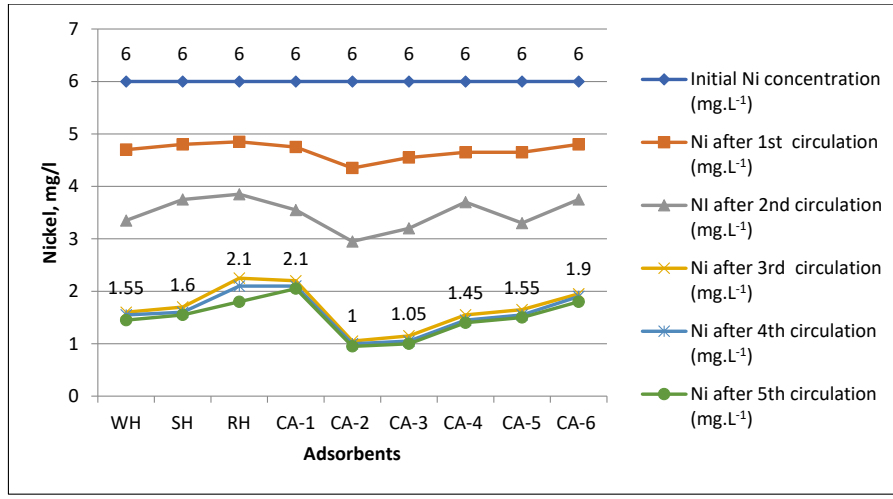

Fig. 9: Changes in Nickel concentration after passing through filter unit.

Fig. 6). Since the SiO_2 content is higher in the wheat husk, the capacity to absorb the adsorbates will be greater.

Variation in pH Value

Initially, the pH of the synthetic solution was the same as we have only one type of solution. On passing the synthetic solution through the filter, it did not give much changes in pH, but it had a change in pH as the number of circulations increased. Wheat husk adsorbent has the maximum impact on pH value and gives a pH value of 6.20. CA-2 and CA-3 are good in bringing pH value to neutral. The changes in pH were recorded in the removal of nickel from the industrial wastewater by adsorption (Table 8, Fig. 7).

WH adsorbent, CA-2, and CA-3 bring pH greater than 6.5 after the third circulation, and that shows great potential to neutralize the acidic wastewater.

Turbidity Variation

A synthetic solution prepared from distilled water and nickel consists of no turbidity initially. However, as a synthetic solution comes in contact with an adsorbent little bite, turbidity increases, which is negligible, and it can be removed by other options in combination.

There was a general increase in turbidity after each circulation from the filter unit (Fig. 8). This is because of the use of adsorbent. From Table 9, it is evident that the turbidity of CA-4 and CA-6 was found to be minimal.

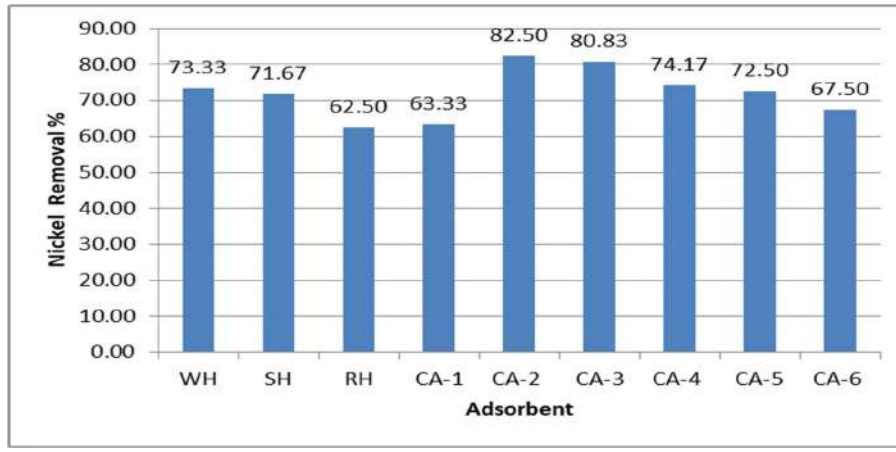

Fig. 10: Nickel removal % after 3rd circulation.

Removal of Nickel by Filter Unit Containing Adsorbent

As shown in Fig. 2, filter units containing adsorbents are used to remove nickel by passing the synthetic solution through a layer of adsorbent, and the results observed are presented in Table 10.

The initial nickel concentration in the synthetic solution was 6 $mg.L^{-1}$. After every circulation of the solution from the filter, the nickel concentration was found to be reduced. Nickel reduction by wheat husk is 1.60 $mg.L^{-1}$, which is more as compared to rice husk and soybean husk adsorbent (Fig. 9). Maximum reduction of nickel by CA-2 and CA-3 as compared to CA-1, CA-4, CA-5, and CA-6.

Though all the materials show a reduction of nickel in the range of 1.60 to 2.25 after 3rd circulation and 3 $mg.L^{-1}$ is the permissible value as per WHO standards for industrial wastewater effluent, therefore after 3rd circulation, all adsorbents reduce the concentration of nickel below 3 $mg.L^{-1}$. Hence, all developed agro-based adsorbents are efficient for treatment, and only three circulations through filter units are needed.

Wheat husk adsorbent has a 73.33% nickel removal efficiency, which is the highest in comparison with rice husk and soybean husk adsorbent. CA-2 has the 82.50% nickel removal efficiency which is the highest as compared to CA-1, CA-4, CA-5, and CA-6 (Fig. 10).

CONCLUSION

In this work, three agro-based adsorbents from WH, SH, and RH were developed, and six different combinations above three husks were used to develop six composite adsorbents. After testing samples for characterization of material by proximate analysis, bulk density, iodine number, and XRF, it is concluded from testing results that wheat husk has more potential to carry out the adsorption process and remove more heavy metals like nickel from wastewater. In proximate analysis, the fixed carbon content in the wheat husk is 26%, the soybean husk is 21%, and the rice husk is 19%. Bulk density for all husk material is found in the range of 0.65 to 0.90 $g.cc^{-1}$, which indicates good potential to carry out the adsorption. The iodine number indicate the adsorption potential, and all developed adsorbent has the iodine number in the range from 750 to 890 $mg.g^{-1}$. Wheat husk has the iodine number 850 $mg.g^{-1}$, and rice husk has the 750 $mg.g^{-1}$, which is the lowest as compared to other developed adsorbents. CA-2 has the highest adsorbent number, 890 $mg.g^{-1}$. Iodine number 890 $mg.g^{-1}$ indicates great potential to carry out the adsorption process. We also tested the material by XRF to know the various constituents present in the material. As per the XRF result, the SiO2 percentage is more than other constituents. In wheat husk, the SiO2 percentage is 70.80%, which is favorable for adsorption. WH adsorbent, CA-2, and CA-3 bring pH greater than 6.5 after the third circulation, and that shows great potential to neutralize the acidic wastewater. Nickel concentration in industrial wastewater is 6 $mg.L^{-1}$; therefore synthetic solution of the same concentration of 6 $mg.L^{-1}$ is prepared. With the help of a filter containing adsorbent nickel is removed. After every circulation of the solution from the filter, the nickel concentration was found to be reduced. Nickel reduction by wheat husk is 1.60 $mg.L^{-1}$, which is more as compared to rice husk and soybean husk adsorbent. Maximum reduction of nickel by CA-2 and CA-3 as compared to CA-1, CA-4, CA-5, and CA-6. All the used adsorbent materials show a reduction of nickel in the range of 1.60 to 2.25 after 3rd circulation, and 3 $mg.L^{-1}$ is the permissible value as per WHO standards for industrial wastewater effluent; therefore, after 3rd circulation, all adsorbents reduce the concentration of nickel bellow 3 $mg.L^{-1}$.

All developed agro-based adsorbents are efficient for treatment, and only three circulations through filter units are needed. Wheat husk adsorbent has a 73.33% nickel removal efficiency, which is the highest in comparison with rice husk and soybean husk adsorbent. CA-2 has the 82.50% nickel removal efficiency, which is the highest as compared to CA-1, CA-4, CA-5, and CA-6. Fixed carbon content, iodine number, bulk density, and SiO2 constituents were found in the required proportion, which supports our experimental work's results of nickel removal.

ACKNOWLEDGMENTS

The authors would like to thank my research place, Yeshwatrao Chavan College of Engineering, for providing funds for experimental setup and material testing. They also thank Dr. J. M. Raut, Dr. M. S. Bhagat, Dr. A. R. Gajbhiye, Dr. P. T. Dhorabe, Prof. A. S. Kurzekar, and Prof. Y. P. Kherde for continuous guidance, support and help during all phases of research work.

REFERENCES

Abdulfatai, J., Saka, A.A., Afolabi, A.S. and Micheal, O. 2013. Development of adsorbent from banana peel for wastewater treatment. Appl. Mech. Mater. Trans. Tech. Publi., 248: 310-315.

Ahmadpour, M. 1996. Characterization of modified activated carbons: Equilibra and dynamic studies. Fuel Energy Abst., 37(3): 184-189.

Asif, Z. and Chen, C. 2017. Removal of arsenic from drinking water using rice husk. Appl. Water Sci., 7: 1449-1458

Bhagat, R.M. and Khandeshwar, S.R. 2019. A synoptic review on composite adsorbents to remove heavy metals from industrial wastewater. Int. J. Innov. Eng. Sci., 4(8): 185-189.

Darge, A. and Mane, S. J., 2015. Treatment of wastewater removal by using

banana peels and fish scales. Int. J. Sci. Res., 4(7): 600-604.
Dhokpande. S.R., Kaware, J.P. and Kulkarni, S.J. 2013. Activated sludge process for heavy metal removal with emphasis on nickel: a summary of research and studies. Int. J. Innov. Res. Sic. Eng., 4(6): 105-109.
Febrianto, J., Kosasih, A.N., Sunarso, J., Ju, H., Indraswati, N. and Ismadji, S. 2009. Equilibrium and kinetic studies in adsorption of heavy metals using bio-sorbent: A summary of recent studies. Journal of Hazardous Materials., (162)2: 616-645.
Jain, N. 2015. Removal of heavy metals by using different fruit peels, vegetable peels, and organic waste. Int. J. Adv. Res., 16: 45-63
Khalili, N.R., Campbell, M., Sandi, G. and Golas, J. 2000. Production of micro and mesoporous activated carbon from paper mill sludge and effect of zinc chloride activation. Carbon, 8(14): 1905-1915.
Moodley, K., Singh. S., Musapatika, E.T., Onyango, M.S. and Ochieng, A. 2011. Removal of nickel from wastewater using an agricultural adsorbent. Water Res. Comm. Water SA, 37(1): 612.
Ngah, W.S.W. and Hanafiah, M.A.K.M. 2008. Removal of heavy metal ions from wastewater by chemically modified plant wastes as adsorbents: A review. Bioresour. Technol., 99(10): 3935-3948.
Perumal, A.C., Perumal, R., Lakshmi, N.S. and Arunkumar J. 2014. Use of corn cob as a low-cost adsorbent for the removal of Nickel (II) from aqueous solution. Int. J. Adv. Biotechnol. Res., 5(3): 325-333.
Ratnoji, S.S. and Singh, N. 2014. A study of coconut shell-activated carbon for filtration and its comparison with sand filtration. International Journal of Renewable Energy and Environmental Engineering, 2(3).
Said, E., Badawy, A.G. and Garamon, S.E. 2018. Adsorption of heavy metal ions from aqueous solutions onto rice husk ash low-cost adsorbent. J. Environ. Anal. Toxicol., 21: 0525.
Zhang, Y., Zheng, R., Zhao, J., Ma, F., Zhang, Y. and Meng, Q. 2014. Characterization of H3PO4 treated rice husk adsorbent and adsorption of copper(II) from aqueous solution. Bio-Med Res. Int., 201: 496878

ORCID DETAILS OF THE AUTHORS

R. M. Bhagat: https://orcid.org/0000-0001-7672-0133

Nature Environment and Pollution Technology
An International Quarterly Scientific Journal

p-ISSN: 0972-6268
(Print copies up to 2016)
e-ISSN: 2395-3454

Vol. 23 | No. 1 | pp. 517-523 | 2024

Original Research Paper

https://doi.org/10.46488/NEPT.2024.v23i01.048

Open Access Journal

A Projection Study of Gaseous Pollutants Formed, Potential Health Effects and Clinical Codification in Piyungan Landfill

E. Fikri*(**)†, Y. W. Firmansyah*(****) A. S. Afifah***** and R. K. Dewi******

*Department of Environmental Sanitation, Bandung Health Polytechnic, Bandung City, 40171, Indonesia
**Center of Excellence on Utilization of Local Material for Health Improvement, Bandung Health Polytechnic, Bandung, 40171, Indonesia
***Department of Health Information and Medical Record, Vocational Faculty of Santo Borromeus University, West Bandung Regency, 40553, Indonesia
****Environmental Science Doctoral Program, Graduate School of Sebelas Maret University, Surakarta City, 57126, Indonesia
*****Department of Furniture Production Engineering, Polytechnic of Furniture and Wood Processing Industry, Kendal Regency, 51371, Indonesia
******Department of Health Information Management, Health and Science Faculty of Nasional Karangturi University, Semarang City, 50227, Indonesia
†Corresponding author: E. Fikri; elanda.fikri@gmail.com

Nat. Env. & Poll. Tech.
Website: www.neptjournal.com

Received: 10-08-2023
Revised: 02-10-2023
Accepted: 13-10-2023

Key Words:
Carbon dioxide
LandGEM
Methane gas
Municipal solid waste
Non-methane organic compounds
Landfill gas

ABSTRACT

The world is currently facing significant environmental challenges due to increasing urbanization and globalization. Human activities can produce greenhouse gases (GHGs) such as CO_2 and CH_4. One of the contributors to GHG generation is the open dumping of Municipal Solid Waste (MSW), particularly because much of the waste is organic. It undergoes anaerobic decomposition, leading to the formation of GHGs, particularly methane. However, CH_4 has a high potential for energy generation, and if harnessed properly, it can be highly beneficial. This study aims to assess the total air pollutants emitted from the landfill gas (LFG), including methane (CH_4), carbon dioxide (CO_2), and nonmethane organic compounds (NMOC) at the Regional Piyungan landfill in D.I. Yogyakarta province. The study also projected the year when the production of these gaseous pollutants would peak and when they are expected to be exhausted. Additionally, the study aimed to identify the potential health problems and clinical codification caused by these gaseous pollutants. To achieve these objectives, the LandGEM 3.03 version of the model developed by USEPA was used for the period 2023-2071. Clinical coding used the 2019 version of the ICD-10 reference. The estimated values for total LFG were 1.648E+04 (2024) and 1.584E+04 (2025) Mg/year, while CH_4 was estimated at 4.403E+03 (2024) and 4.230E+03 (2025) Mg/year. CO_2 was estimated to be 1,208E+04 (2024) and 1,161E+04 (2025) Mg/year, and NMOC was projected at 2,839E+01 (2024) and 2,727E+01 (2025) Mg/year. Some of the toxic effects that can occur cause respiratory, visual, and mental disorders with a variety of clinical codes.

INTRODUCTION

The Piyungan landfill is one of the overloaded landfills in Indonesia that will soon be closed. It is located in the Piyungan sub-district, Bantul Regency, and serves as a zoning site for waste collection from three cities: Sleman, Bantul, and Yogyakarta. The D.I. Yogyakarta government announced in a Circular Letter of the Regional Secretary of D.I. Yogyakarta number 658/8312 year 2023 that the Piyungan Regional landfill will no longer be able to accept waste from July 23, 2023, until September 5, 2023. This decision comes as a result of the daily incoming waste generation reaching an average of 450 tons. In 2022, the waste entering the Piyungan Regional landfill reached 97,086 $t.y^{-1}$ (Pemda Kabupaten Bantul 2022), while the landfill's total area is only 12.5 hectares. Out of this, 10 hectares are already used as landfills, and the remaining 2.5 hectares function as supporting facilities, including offices, workshops, weighbridges, and buffers (Ariyani et al. 2019). In addition, the waste managed at the Piyungan Regional landfill is only 4,951 tons per year, primarily through scavenger recovery. However, the waste management at the Piyungan Regional landfill is not optimal due to the damaged and poorly maintained leachate treatment plant (KLH 2023).

The quality of waste services in landfills is directly proportional to the existing infrastructure and the management of waste. When waste is left unmanaged in landfills, it can lead to various problems, one of which is the presence of hazardous landfill gas (LFG) pollutants. Methane gas (CH_4) and carbon dioxide (CO_2) are two groups of gases that can be found in landfills. It is estimated that municipal solid waste can produce approximately 50-60% CH_4 gas and 40-50% CO_2, respectively (Amini et al. 2012, Gasbarra et al. 2019). Gas production in landfills can occur due to anaerobic decomposition, evaporation, and chemical reactions from other processes (ASTDR 2023, Sonibare et al. 2019, USEPA 2023a, 2023b). Recent studies of landfills conducted in European countries revealed that about 20% of CH_4 from anthropogenic activities is attributed to municipal solid waste (MSW) undergoing processing in landfills (Delgado et al. 2023). Similarly, a recent report submitted by the USEPA observed that CH_4 from landfills in the US accounted for 17% of the total CH_4 generated (USEPA 2023a, 2023b). Studies in 2000 have projected that developing countries are responsible for 29% of total GHG, which is expected to increase to 64 and 76% by 2030 and 2050, respectively (Rafiq et al. 2018).

The Landfill Gas Emission Model (LandGEM) is a numerical model developed by the USEPA to project CH_4 at United States landfill sites. The use of the model has been used globally to assess CH_4 from various landfills after considering input values to represent appropriate site conditions. A study conducted at the rehabilitated La Gabarre waste dome estimated a total CH_4 of no less than 1.80×108 m^3 during the study period of 1995-2135 (Plocoste & Jacoby Koaly 2016). The study in Tirupati estimated a CH_4 concentration of 1.66×107 $m^3.y^{-1}$ in 2042 using the LandGEM model (Ramprasad et al. 2022). Studies at Benowo and Antang landfills showed that CH_4 at Benowo landfill in 2032 reached the highest value of 24,190 $Mg.y^{-1}$, and in 2030, at the Antang landfill, it was 123,900 $Mg.y^{-1}$ (Mahful & Managi 2018). The LandGEM model was also used to predict CH_4 in Sarimukti, West Java landfill. The highest result was in 2025 at 14,810.41 $Mg.y^{-1}$ (Wijaya et al. 2021). The study conducted between 2018 and 2047 in Muara Fajar Landfill 2 Pekanbaru City showed that the highest CH_4 emissions in 2047 amounted to 21,290 $Mg.y^{-1}$ (Betharia & Aryo Sasmita 2021). The accuracy of the predicted values in the model is highly dependent on the input parameters. Based on these considerations, some limited research has considered analyzing the uncertainty in CH_4 caused by the accuracy of input parameters (Ghosh et al. 2019, Srivastava & Chakma 2020). This study is conducted at the Regional Piyungan landfill. Considering the urgent problem of the landfill facing the closure of waste services, the study aims to achieve the following objectives: (a) Estimate the total air pollutants emitted from the LFG, CH_4, carbon dioxide, and nonmethane organic compounds (NMOC). (b) Project the year when the production of these gaseous pollutants reaches its peak and is expected to be exhausted. (c) Knowing potential health problems and clinical codification caused by these gaseous pollutants. This study will contribute to the projection of gaseous pollutants that could arise in the Piyungan Regional Landfill until 2071.

MATERIALS AND METHODS

Type and Design of Research

The research conducted in this study adopts an inquiry mode-quantitative approach to explore and quantify the concentration of LFG, CH_4, CO_2, and NMOC pollutants at the Piyungan Regional landfill for the upcoming year. Meanwhile, the study design utilized is reference period-prospective, aimed to estimate and project gas pollutants until the year 2071 using the LandGEM modeling approach. The data source for this study consists of secondary data obtained from various sources, including the National Waste Management Information System (SIPSN) of the Ministry of Environment and Forestry of the Republic of Indonesia, the Provincial Environment Office of D.I. Yogyakarta; World Health Organization (WHO)for clinical coding data; and database journals and government to determine the potential health risks that occured. The quantitative data used in this study pertains to the incoming waste for the years 2021, which was 98,436 $t.y^{-1}$, and 2022, which was 97,086 $t.y^{-1}$ (KLH 2023). To estimate the average incoming waste for the Piyungan Regional landfill, an assumption is made, and the average incoming waste is considered to be 97,761 $t.y^{-1}$. Additionally, the study utilizes rainfall data for D.I. Yogyakarta province, which indicates an average below 500 $mm.y^{-1}$ for the years 2018 and 2021, according to conventional classification (Buwono 2021, DLH Kota Yogyakarta 2018).

Data Analysis

This study employs mathematical modeling using the LandGEM software. The LandGEM modeling tool was developed by the United States Environmental Protection Agency (USEPA) to estimate landfill gas for sites located in the United States (Mou et al. 2015). The model was designed to predict uncontrolled occurrences at landfill sites and can project the resulting LFG over several years (Ramprasad et al. 2022). The advantage of this model is its flexibility in used inputs, making it a suitable choice for predicted LFG (Anh et al. 2022). LandGEM is one of the instruments that can be used to predict LFG from MSW at a study site. The

instrument can be used to see the amount and composition of gases from organic matter degradation processes (Kale & Gökçek 2020, Sughosh et al. 2019). The equations used in the LandGEM (v3.03) model are shown in the following equations (Equation 1),

$$QCH4 = \sum_{i=1}^{n} \sum_{j=0.1}^{1} kL0 \left(\frac{Mi}{10}\right) e^{-ktij}$$

Equation 1. The Mathematical Modeling of LandGEM (v3.03)

Where,

QCH_4 = annual methane generation in the year of the calculation ($m^3.y^{-1}$)

i = 1-year time increment

n = (year of the calculation) - (initial year of waste acceptance)

j = 0.1-year time increment

k = methane generation rate (year-1)

L_0 = potential methane generation capacity ($m^3.Mg^{-1}$)

M_i = mass of the waste accepted in the i^{th} year (Mg)

t_{ij} = age of the j^{th} section of waste mass M_i accepted in the i^{th} year (decimal years)

The accuracy of the LFG prediction value depends on the input parameters. However, determining various input parameters related to municipal solid waste (MSW) characteristics is often complex, and in many cases, suggested or default values are preferred. For instance, parameters like MSW_F, L_0, and K may be assigned specific values (Srivastava & Chakma 2020), where K varies between 0.04 and 0.06, and MSWF varies between 70% and 90%, with 80% being the default value (Ghosh et al. 2019, Srivastava & Chakma 2020). Using these suggested or default values can introduce uncertainties in CH_4 estimation, which require careful assessment.

RESULTS AND DISCUSSION

The SIPSN declared in 2021, the Piyungan Regional Landfill received incoming waste of 98,436 $t.y^{-1}$, and in 2022, it received 97,086 $t.y^{-1}$. Due to incomplete data on incoming waste from the establishment of the landfill in 1996, we used the last two years of data as an assumption of the average 97,761 $t.y^{-1}$ of incoming waste at the Regional Piyungan landfill (KLH 2023). The study projected the concentration of LFG from 2023 to 2071. Here are the results,

Table 1: The Projection Results of total LFG, CH_4, CO_2, NMOC Pollutants at Piyungan Regional Landfill 2023 to 2071

Year	Total Landfill Gas [$Mg.y^{-1}$]	Methane [$Mg.y^{-1}$]	Carbon Dioxide [$Mg.y^{-1}$]	NMOC [$Mg.y^{-1}$]
2023	1,616E+04	4,316E+03	1,184E+04	2,783E+01
2024	1,648E+04	4,403E+03	1,208E+04	2,839E+01
2025	1,584E+04	4,230E+03	1,161E+04	2,727E+01
2026	1,522E+04	4,064E+03	1,115E+04	2,620E+01
2027	1,462E+04	3,905E+03	1,071E+04	2,518E+01
2028	1,405E+04	3,752E+03	1,029E+04	2,419E+01
2029	1,350E+04	3,605E+03	9,891E+03	2,324E+01
2030	1,297E+04	3,463E+03	9,503E+03	2,233E+01
2031	1,246E+04	3,328E+03	9,130E+03	2,145E+01
2032	1,197E+04	3,197E+03	8,772E+03	2,061E+01
2033	1,150E+04	3,072E+03	8,428E+03	1,980E+01
2034	1,105E+04	2,951E+03	8,098E+03	1,903E+01
2035	1,062E+04	2,836E+03	7,780E+03	1,828E+01
2036	1,020E+04	2,724E+03	7,475E+03	1,757E+01
2037	9,800E+03	2,618E+03	7,182E+03	1,688E+01
2038	9,415E+03	2,515E+03	6,900E+03	1,621E+01
2039	9,046E+03	2,416E+03	6,630E+03	1,558E+01
2040	8,692E+03	2,322E+03	6,370E+03	1,497E+01
2041	8,351E+03	2,231E+03	6,120E+03	1,438E+01
2042	8,023E+03	2,143E+03	5,880E+03	1,382E+01
2043	7,709E+03	2,059E+03	5,650E+03	1,328E+01
2044	7,406E+03	1,978E+03	5,428E+03	1,276E+01
2045	7,116E+03	1,901E+03	5,215E+03	1,225E+01
2046	6,837E+03	1,826E+03	5,011E+03	1,177E+01
2047	6,569E+03	1,755E+03	4,814E+03	1,131E+01
2048	6,311E+03	1,686E+03	4,626E+03	1,087E+01
2049	6,064E+03	1,620E+03	4,444E+03	1,044E+01
2050	5,826E+03	1,556E+03	4,270E+03	1,003E+01
2051	5,598E+03	1,495E+03	4,102E+03	9,640E+00
2052	5,378E+03	1,437E+03	3,942E+03	9,262E+00
2053	5,167E+03	1,380E+03	3,787E+03	8,899E+00
2054	4,965E+03	1,326E+03	3,639E+03	8,550E+00
2055	4,770E+03	1,274E+03	3,496E+03	8,215E+00
2056	4,583E+03	1,224E+03	3,359E+03	7,893E+00
2057	4,403E+03	1,176E+03	3,227E+03	7,583E+00
2058	4,231E+03	1,130E+03	3,101E+03	7,286E+00
2059	4,065E+03	1,086E+03	2,979E+03	7,000E+00
2060	3,905E+03	1,043E+03	2,862E+03	6,726E+00
2061	3,752E+03	1,002E+03	2,750E+03	6,462E+00
2062	3,605E+03	9,630E+02	2,642E+03	6,209E+00
2063	3,464E+03	9,252E+02	2,539E+03	5,965E+00
2064	3,328E+03	8,889E+02	2,439E+03	5,731E+00
2065	3,197E+03	8,541E+02	2,343E+03	5,507E+00
2066	3,072E+03	8,206E+02	2,251E+03	5,291E+00
2067	2,952E+03	7,884E+02	2,163E+03	5,083E+00
2068	2,836E+03	7,575E+02	2,078E+03	4,884E+00
2069	2,725E+03	7,278E+02	1,997E+03	4,692E+00
2070	2,618E+03	6,993E+02	1,919E+03	4,508E+00
2071	2,515E+03	6,718E+02	1,843E+03	4,332E+00

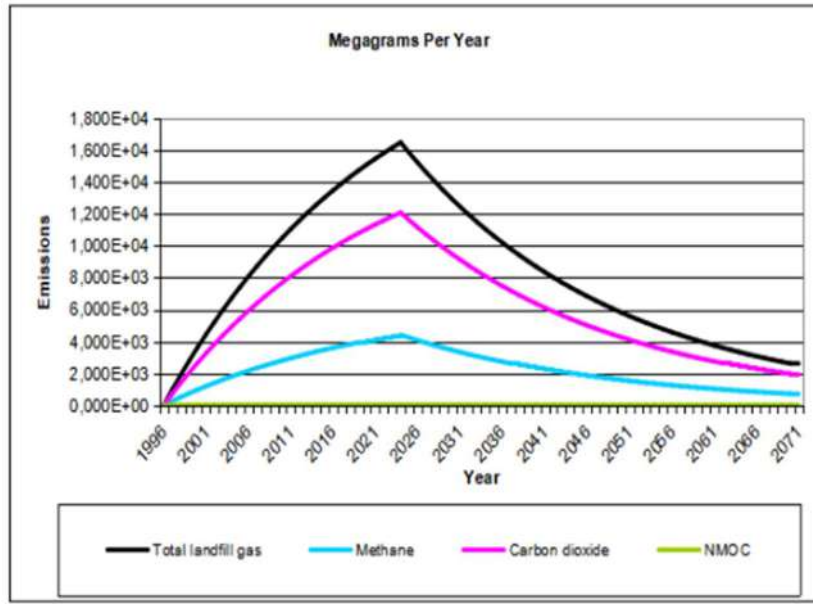

Fig. 1: The Estimation of gas existence in regional Piyungan landfill 1996 to 2071.

Previous assessments conducted for LFG estimation have published that, of the total LFG radiated, approximately 50% is CH_4, 45-50% is CO_2, and there are trace concentrations of NMOC (Aydi 2012, Saral et al. 2009). In the LandGEM (v3.03) assessment Table 1, there was no gas production recorded at the Regional Piyungan landfill in 1996 (DLH DI Yogyakarta, 2020). These gaseous pollutants reach their optimal production process in 2024. These gaseous pollutants will experience an optimal increase process from 2024 to 2025 and experience a trend of decreasing concentrations after 2026 (Fig. 1).

Based on the projection results, with the assumption that the Piyungan Regional Landfill experienced a temporary closure from July 23 to September 5, 2023, the estimated CH_4 generation rate was 0.04 year-1. The value of L_0 (potential methane generation capacity) is 100 $m^3.mg^{-1}$, while NMOC is estimated at 600 ppm as hexane, with a CH_4 content of 50% by volume. It is essential to note that these values come with a level of uncertainty, as they depend on factors such as the amount of incoming waste (MSW_f) and rainfall (k and L_0), with D.I. Yogyakarta Province classified as inventory conventional (k = 0.04). A parallel study conducted in Kapur City, India, found that uncertainties in the value of K (ranging from 0.04 to 0.06) resulted in variations in CH_4, around 233.44 to 350.16 in total LFG; 116.75-175.13 in CH_4 and CO_2; and 0.93-1.395 $Mm^3.y^{-1}$ in NMOC generation (Chandra & Ganguly 2023). Similarly, a study at a landfill site in Delhi, India, also revealed large variations in CH_4 due to uncertain values of MSW_F and k in LFG (Srivastava & Chakma 2020). These uncertainties emphasize the importance of accurately determining input parameters to improve the reliability of CH_4 estimations from landfills.

The active zone in the Piyungan Regional Landfill is not entirely closed, leading to the decomposition of organic waste by microorganisms and the production of gaseous pollutants (Rajesh et al. 2020). Additionally, the non-functional leachate treatment plant results in the generation of leachate from landfill activities, primarily influenced by rainfall, surface water from the surrounding environment, and the decomposition of waste in the landfill. As leachate filters through the waste, it leaches out certain chemicals from the waste pile, leading to concerns about rising odor levels, groundwater contamination, and insect breeding grounds (Teng et al. 2021). Studies have shown that leachate generated from open dumpsites can cause groundwater to exceed permissible limits for physicochemical parameters and heavy metals, with water quality improving further downstream from the dumpsite (Sharma et al. 2020). Landfill operations generate a lot of toxic gaseous pollutants that have the potential to harm public health (Njoku et al. 2019). The presence of trash, dust, rodents, and the potential for unexpected fires are other risk factors present in landfills (Manheim et al. 2021). LFG can kineticize to the subsurface. Then, the gas builds up through the groundwater and soil. They eventually kineticize to the top surface. Fractures or other pathways in the subsurface can be a contributing factor to gas formation (Fay et al. 2011).

Total LFG, CH_4, CO_2, and NMOC have toxic effects that can cause health problems. We have collected data on

the health risks that can occur due to these gases from the websites of health departments of several countries and journals. The data is presented in Table 2 using ICD 10 version 2019.

The toxic effects of CH_4 in Table 2 may occur because the presence of CH_4 in the air is greater than the availability of oxygen. The toxic effects of CH_4 in Table 2 may occur because the presence of CH_4 in the air is greater than the availability of oxygen. Methane gas, when concentrated in high amounts, can displace oxygen in the air. As a result, exposed people may experience oxygen deprivation or hypoxia. This hypoxia can cause cells in various parts of the body, including cells in the lungs, to not get enough oxygen to perform their normal functions (Hsieh & Chiou 2014). Methane is an irritant to the respiratory tract. Exposure to this gas can irritate the mucous membranes of the bronchi and bronchioles, which can stimulate an inflammatory response and produce mucus (Chien et al. 2017, Zhang et al. 2019). This can result in symptoms such as coughing, breathlessness, and increased mucus production. High methane exposure can cause inflammation of the lung tissue. This inflammatory process can affect the normal functioning of the lungs and cause symptoms such as chest pain, coughing, and difficulty breathing (Guo et al. 2012, Mo et al. 2017). High methane exposure can lead to a build-up of gas in the lung spaces, which can obstruct airflow and cause airway blockage. This can lead to symptoms such as significant breathlessness. Due to the lack of oxygen, the body may respond by increasing the rate of breathing (hyperpnoea) to try to increase oxygen uptake. This can lead to respiratory fatigue and increased workload on the respiratory system. Exposure to methane gas can also trigger oxidative processes in lung cells, which can damage cells and cause oxidative stress (Lin et al. 2013, Zhang et al. 2018). This damage can exacerbate inflammation and be detrimental to lung function. Poor respiratory conditions, such as prolonged oxygen deprivation, can have systemic effects on other organs in the body. This can lead to serious health complications, including disorders of the cardiovascular and nervous systems (Chen et al. 2013, Wellenius 2012).

While CO_2 comprises 40-60% of landfills, the denser-than-air nature of CO_2 will cause the gas to collect in confined spaces such as leachate impoundments. People in communities near the landfill are often concerned about the odor emitted from the landfill. They say that these odors are the source of undesirable health effects or symptoms, such as headaches and nausea (Henrotin et al. 2010). At low-level concentrations - usually associated with landfill gas - it is unclear whether it is the concentration itself or the odor that triggers the response (Miller et al. 2007). Typically, these effects diminish when the odor is no longer detectable. Bacterial or chemical processes produce landfill gas odors and can come from active or closed landfills.

These odors can migrate to surrounding communities. Potential sources of landfill odors are NMOCs (vinyl chloride and hydrocarbons) if present at high enough concentrations. Many NMOCs have irritant properties to the respiratory tract. High exposure may irritate the mucous membranes in the respiratory tract, which may result in symptoms such as coughing, shortness of breath, and chest discomfort (Ferguson et al. 2017, Yorifuji et al. 2013). Some NMOCs can have direct toxic effects on lung cells. This can cause inflammation and cell damage, resulting in impaired lung function and leading to more serious respiratory symptoms (Chung et al. 2017, Lee et al. 2014). The disposal of certain types of waste, such as manure and fermented grains, can also generate landfill odors.

Table 2: Possible health risks and clinical codifications that may result from exposure to total LFG, CH_4, CO_2, and NMOCs in Landfills.

Pollutants	Possible Health Risks	Possible Clinical Codifications
CH_4	CH_4 is a precursor of ozone (O_3). CH_4 does not enter directly but through exposure to ozone. Exposure to ozone can cause chronic obstructive pulmonary disease (COPD), impaired lung function, and asthma.	1. Sub-category J44 other chronic obstructive pulmonary disease and its derivatives 2. Sub-category J06 (acute respiratory infection) and J18 (pneumonia) 3. Sub-category J45 asthma and its derivatives (Forouzanfar et al. 2015, Turner et al. 2016, Van Dingenen et al. 2018, Zhang et al. 2019)
CO_2	CO_2 concentrations of 10% or more can cause unconsciousness and death. Meanwhile, lower concentrations can cause sweating, headache, tremors, headache, rapid breathing, increased heart rate, shortness of breath, mental depression, dizziness, and visual disturbances.	R51 headache and its derivatives R25.1 tremor unspecified and its derivatives F32.9 depressive disorder H53-H54 visual disturbance and its derivatives (ATSDR 2001)
NMOC	NMOCs such as vinyl chloride and hydrocarbons are included in odors that can disrupt sleep and frustrate stress.	Sub-category T59 (toxic effect of other gases, fumes, and vapors) complicated by biochemical evidence of fetal stress (ATSDR 2001)

One of the main limitations of this study is the use of assumptions regarding the incoming waste at the Regional Piyungan landfill in 2021 and 2022, obtained through the SIPSN. The incoming waste data may be complete from 1996 to 2022, allowing for a more accurate projection of outgassing results using this refined value in the LandGEM model. Furthermore, the determination of conventional inventory rainfall categories (k and L0) relies on a study conducted by the Environmental Agency of D.I. Yogyakarta province in 2018 and 2021 due to limited access to rainfall data, which ideally should use justifications from the last 5 to 10 years to ensure better accuracy.

CONCLUSION

The landfill gas generation at the Regional Piyungan landfill in D.I. Yogyakarta province was estimated using the LandGEM model version 3.03. The study shows that these gaseous pollutants will experience an optimal increase process from 2024 to 2025 and will subsequently exhibit a trend of decreasing concentrations after 2026. The estimated values for total landfill gas are 1.648E+04 and 1.584E+04 $Mg.y^{-1}$ for the respective years, while CH_4 gas is estimated at 4.403E+03 and 4.230E+03 $Mg.y^{-1}$. Carbon dioxide is estimated to be 1.208E+04 and 1.161E+04 $Mg.y^{-1}$, and NMOC is projected at 2.839E+01 and 2.727E+01 $Mg.y^{-1}$. These findings suggest that high LFG, particularly CH_4, significantly impacts the ambient air quality of D.I. Yogyakarta province. The gas has varied toxicity and clinical codification, with possible health problems such as respiratory system disorders, vision, and mental disorders. The study also underscores the importance of accurately determining input parameters for predicting CH_4, as even small variations can result in significant uncertainties. Furthermore, the study highlights the potential for energy recovery from the CH_4 generated in landfills. By harnessing the energy generated from MSW in D.I. Yogyakarta province, CH_4 can be significantly reduced while simultaneously serving as a valuable local energy source.

ACKNOWLEDGEMENT

This study was supported by The Bandung Health Polytechnic, Ministry of Health Indonesia; Santo Borromeus University; Sebelas Maret University; Polytechnic of Furniture and Wood Processing Industry; Nasional Karangturi University, Indonesia. The authors would like to thank Adi Anggoro Parulian as the clinical codifier of Santo Borromeus University.

REFERENCES

Agency for Toxic Substance and Disease Registry (ASTDR). 2023. Landfill Gas Primer: An Overview for Environmental Health Professionals. Retrieved from https://www.atsdr.cdc.gov/hac/landfill/html/ch2.html

Amini, H.R., Reinhart, D.R. and Mackie, K.R. 2012. Determination of first-order landfill gas modeling parameters and uncertainties. Waste Manag., 32(2): 305-316.

Anh, L.H., Thanh Truc, N.T., Tuyen, N.T.K., Bang, H.Q., Son, N.P., Schneider, P. and Moustakas, K. 2022. Site-specific determination of methane generation potential and estimation of landfill gas emissions from municipal solid waste landfill: a case study in Nam Binh Duong, Vietnam. Biomass Conv. Bioref., 12(8): 3491-3502.

Ariyani, S.F., Putra, H.P., Kasam, D.E. and Sembiring, E. 2019. Evaluation of waste management in Piyungan landfill, Bantul Regency, Yogyakarta, Indonesia. MATEC Web Conf., 280: 05018.

Agency for Toxic Substance and Disease Registry (ATSDR). 2001. Landfill Gas Primer - An Overview for Environmental Health Professionals: Landfill Gas Safety and Health Issues_. Retrieved from https://www.atsdr.cdc.gov/hac/landfill/html/ch3.html

Aydi, A. 2012. Energy recovery from a municipal solid waste (MSW) landfill gas: A Tunisian case study. J. Waste Water Treat. Anal., 03(04): 1-10.

Betharia, N. and Aryo Sasmita, J.A. 2021. Analysis of CO_2 emission levels and electrical energy potential from Muara Fajar TPA 2 gas landfill, Pekanbaru City, using Landgem version 3.02 modeling. Jom FTEKNIK, 8(2): 1-8.

Buwono, H. 2021. Yogyakarta Special Region Province Regional Environmental Management Performance Information Document for 2021. Retrieved from https://dlhk.jogjaprov.go.id/storage/files/1_Laporan Utama DIKPLHD DIY 2022_ok upload website dlhk.pdf

Chandra, S. and Ganguly, R. 2023. Assessment of landfill gases by LandGEM and energy recovery potential from municipal solid waste of Kanpur city, India. Heliyon, 9(4): e15187.

Chen, R., Zhang, Y., Yang, C., Zhao, Z., Xu, X. and Kan, H. 2013. Acute effect of ambient air pollution on stroke mortality in the China air pollution and health effects study. Stroke, 44(4): 954-960.

Chien, T.Y., Ting, H.W., Chan, C.L., Yang, N.P., Pan, R.H., Lai, K. and Hung, S.I. 2017. Does the short-term effect of air pollution influence the incidence of spontaneous intracerebral hemorrhage in different patient groups? Big data analysis in Taiwan. Int. J. Environ. Res. Public Health, 14(12): 1547.

Chung, J.W., Bang, O.Y., Ahn, K., Park, S.S., Park, T.H., Kim, J.G. and Bae, H.J. 2017. Air pollution is associated with ischemic stroke via cardiogenic embolism. Stroke, 48(1): 17-23.

Delgado, M., López, A., Esteban-García, A.L. and Lobo, A. 2023. The importance of particularising the model to estimate landfill GHG emissions. J. Environ. Manage., 325: 116600.

DLH IN Yogyakarta. 2020. Information at a glance at Piyungan TPST. Retrieved from https://dlhk.jogjaprov.go.id/sekilas-info-tpst-piyungan#:~:text=Piyungan TPA or Disposal Site, based on Governor's Decree No. 18.

DLH Yogyakarta City. 2018. Main Report Information Document on Regional Environmental Management Performance of Yogyakarta City in 2018. Retrieved from http://perpustakaan.menlhk.go.id/pustaka/images/docs/Laporan IKPLHD Yogyakarta City 2018_Full.pdf

Fay, C., Doherty, A.R., Beirne, S., Collins, F., Foley, C., Healy, J. and Diamond, D. 2011. Remote real-time monitoring of subsurface landfill gas migration. Sensors, 11(7): 6603-6628.

Ferguson, K.K., McElrath, T.F., Pace, G.G., Weller, D., Zeng, L., Pennathur, S. and Meeker, J.D. 2017. Urinary polycyclic aromatic hydrocarbon metabolite associations with biomarkers of inflammation, angiogenesis, and oxidative stress in pregnant women. Environ. Sci. Technol., 51(8): 4652-4660.

Forouzanfar, M.H., Alexander, L., Anderson, H.R., Bachman, V.F., Biryukov, S., Brauer, M. and Murray, C.J. 2015. Global, regional, and national comparative risk assessment of 79 behavioral, environmental and occupational, and metabolic risks or clusters of risks in 188

countries, 1990–2013: A systematic analysis for the global burden of disease study 2013. Lancet, 386(10010); 2287-2323.

Gasbarra, D., Toscano, P., Famulari, D., Finardi, S., Di Tommasi, P., Zaldei, A. and Gioli, B. 2019. Locating and quantifying multiple landfill methane emissions using aircraft data. Environ. Pollut., 254: 112987.

Ghosh, P., Shah, G., Chandra, R., Sahota, S., Kumar, H., Vijay, V.K. and Thakur, I.S. 2019. Assessment of methane emissions and energy recovery potential from the municipal solid waste landfills of Delhi, India. Bioresour. Technol., 272: 611-615.

Guo, S., Yang, F., Tan, J. and Duan, J. 2012. Nonmethane Hydrocarbons in Ambient Air of Hazy and Normal Days in Foshan, South China. Environ. Eng. Sci., 29(4): 262-269.

Henrotin, J.B., Zeller, M., Lorgis, L., Cottin, Y., Giroud, M. and Bejot, Y. 2010. Evidence of the role of short-term exposure to ozone on ischaemic cerebral and cardiac events: The Dijon Vascular Project (DIVA). Heart, 96(24): 1990-1996.

Hsieh, F.I. and Chiou, H.Y. 2014. Stroke: Morbidity, Risk Factors, and Care in Taiwan. J. Stroke, 16(2), 59.

Kale, C. and Gökçek, M. 2020. A techno-economic assessment of landfill gas emissions and energy recovery potential of different landfill areas in Turkey. J. Clean. Prod., 275: 122946.

KLH. 2023. Data on Waste Generation (Provincial) in Indonesia. Retrieved from https://sipsn.menlhk.go.id/sipsn/public/home/fasilitas/tpa-tpst

Lee, J.T., Chung, W.T., Lin, J.D., Peng, G.-S., Muo, C.H., Lin, C.C. and Hsu, C. Y. 2014. Increased risk of stroke after septicaemia: A population-based longitudinal study in Taiwan. PLoS ONE, 9(2): e89386.

Lin, Y.K., Chang, C.K., Wang, Y.C. and Ho, T.J. 2013. Acute and prolonged adverse effects of temperature on mortality from cardiovascular diseases. PLoS ONE, 8(12): e82678.

Mahful, R. and Managi, S. 2018. Estimating methane emission from solid waste landfills using various different methods. IOP Conf. Ser. Mater. Sci. Eng., 403(1): 012005.

Manheim, D.C., Yeşiller, N. and Hanson, J. L. 2021. Gas emissions from municipal solid waste landfills: A comprehensive review and analysis of global data. J. Indian Inst. Sci., 101(4): 625-657.

Miller, K.A., Siscovick, D.S., Sheppard, L., Shepherd, K., Sullivan, J.H., Anderson, G.L. and Kaufman, J.D. 2007. Long-term exposure to air pollution and incidence of cardiovascular events in women. N. Engl. J. Med., 356(5): 447-458.

Mo, Z., Shao, M., Lu, S., Niu, H., Zhou, M. and Sun, J. 2017. Characterization of non-methane hydrocarbons and their sources in an industrialized coastal city, Yangtze River Delta, China. Sci. Total Environ., 593-594: 641-653.

Mou, Z., Scheutz, C. and Kjeldsen, P. 2015. Evaluation and application of site-specific data to revise the first-order decay model for estimating landfill gas generation and emissions at Danish landfills. J. Air Waste Manag. Assoc., 65(6): 686-698.

Njoku, P.O., Edokpayi, J.N. and Odiyo, J.O. 2019. Health and environmental risks of residents living close to a landfill: A case study of Thohoyandou Landfill, Limpopo Province, South Africa. Int. J. Environ. Res. Public Health, 16(12): 2125.

Pemda Kabupaten Bantul 2022. Emergency! Illegal Waste Dumpers Are Increasingly Mushrooming! Retrieved from https://dlh.bantulkab.go.id/news/darurat-pelaku-pembuangan-sampah-liar-semakin-menjamur

Plocoste, T. and Jacoby Koaly, S. 2016. Estimation of methane emission from a waste dome in a tropical insular area. Int. J. Waste Resour., 6(2): 54-68.

Rafiq, A., Rasheed, A., Arslan, C., Tallat, U. and Siddique, M. 2018. Estimation of greenhouse gas emissions from Muhammad Wala open dumping site of Faisalabad, Pakistan. Geol. Ecol. Landsc., 2(1): 45-50.

Rajesh, S., Roy, S. and Khan, V. 2020. Methane Emission from Municipal Solid Waste Landfill. In Gupta, T., Singh, S.P., Rajput, P. and Agarwal, A.K. (eds), Estimation and Control BT - Measurement, Analysis, and Remediation of Environmental Pollutants, Springer, Singapore, pp. 375-395.

Ramprasad, C., Teja, H.C., Gowtham, V. and Vikas, V. 2022. Quantification of landfill gas emissions and energy production potential in Tirupati municipal solid waste disposal site by LandGEM mathematical model. MethodsX, 9: 101869.

Saral, A., Demir, S. and Yıldız, Ş. 2009. Assessment of odorous VOCs released from a main MSW landfill site in Istanbul-Turkey via a modeling approach. J. Hazard. Mater., 168(1): 338-345.

Sharma, A., Ganguly, R. and Kumar Gupta, A. 2020. Impact assessment of leachate pollution potential on groundwater: An indexing method. J.Environ.Eng., 146(3):

Sonibare, O.O., Adeniran, J.A. and Bello, I.S. 2019. Landfill air and odor emissions from an integrated waste management facility. J. Environ. Health Sci. Eng., 17(1): 13-28.

Srivastava, A.N. and Chakma, S. 2020. Quantification of landfill gas generation and energy recovery estimation from the municipal solid waste landfill sites of Delhi, India. Energy Sour. Part A Recov. Utiliz. Environ. Effects, 61: 1-14.

Sughosh, P., Anusree, N., Prathima, B. and Babu, G.L.S. 2019. Estimation of Landfill Gas Emissions and Energy Recovery Potential from Landfills of Bangalore and Mysore: A Case Study. American Society of Civil Engineers, Reston, pp. 432-439.

Teng, C., Zhou, K., Peng, C. and Chen, W. 2021. Characterization and treatment of landfill leachate: A review. Water Res., 203: 117525.

Turner, M.C., Jerrett, M., Pope, C.A., Krewski, D., Gapstur, S.M., Diver, W.R. and Burnett, R.T. 2016. Long-term ozone exposure and mortality in a large prospective study. American J. Resp. Crit. Care Med., 193(10): 1134-1142.

USEPA 2023a. Greenhouse Gas Emissions and Sinks: 1990-2020. United States Environmental Protection Agency. Retrieved from https://www.epa.gov/ghgemissions/inventory-us-greenhouse-gas-emissions-and-sinks

USEPA 2023b. Basic Information about Landfill Gas. United States Environmental Protection Agency. Retrieved from https://www.epa.gov/lmop/basic-information-about-landfill-gas

Van Dingenen, R., Crippa, M.J., Anssens-Maenhout, G., Guizzardi, D. and Dentener, F. 2018. Global trends of methane emissions and their impacts on ozone concentrations. JRC Sci. Pol. Rep., 29: 349

Wellenius, G.A. 2012. Ambient air pollution and the risk of acute ischemic stroke. Arch. Int. Med., 172(3): 229.

Wijaya, S.P., Ainun, S. and Permadi, D.A. 2021. Methane Emission Estimation and Dispersion Modeling for a Landfill in West Java, Indonesia. J. Civ. Eng. Forum, 7(3): 239.

Yorifuji, T., Kashima, S., Tsuda, T., Ishikawa-Takata, K., Ohta, T., Tsuruta, K. and Doi, H. 2013. Long-term exposure to traffic-related air pollution and the risk of death from hemorrhagic stroke and lung cancer in Shizuoka, Japan. Sci. Tot. Environ., 443: 397-402.

Zhang, H.W., Kok, V.C., Chuang, S.C., Tseng, C.H., Lin, C.T., Li, T.C. and Hsu, C.Y. 2019. Long-term ambient hydrocarbon exposure and incidence of ischemic stroke. Plos One, 14(12): e0225363.

Zhang, J., Wei, Y. and Fang, Z. 2019. Ozone pollution: A major health hazard worldwide. Front. Immunol., 10: 615.

Zhang, R., Liu, G., Jiang, Y., Li, G., Pan, Y., Wang, Y. and Wang, Y. 2018. Acute effects of particulate air pollution on ischemic stroke and hemorrhagic stroke mortality. Front. Neurol., 12: 9.

Nature Environment and Pollution Technology
An International Quarterly Scientific Journal

p-ISSN: 0972-6268
(Print copies up to 2016)
e-ISSN: 2395-3454

Vol. 23 | No. 1 | pp. 525-535 | 2024

Original Research Paper

https://doi.org/10.46488/NEPT.2024.v23i01.049

Open Access Journal

A Short-Term Autoregressive Model for the Prediction of Daily Average NO_2 Concentration in Nagercoil, Tamil Nadu, India

P. Muthukrishnan* and R. Krishna Sharma†**

*Department of Chemistry, ST Hindu College, Nagercoil-629002, Tamilnadu, India

**Department of Physics, ST Hindu College, Nagercoil-629002, Tamilnadu, India

†Corresponding author: R. Krishna Sharma; krishsharma5555@gmail.com

Nat. Env. & Poll. Tech.
Website: www.neptjournal.com

Received: 04-07-2023
Revised: 12-08-2023
Accepted: 21-08-2023

Key Words:
Akaike information criterion
Autoregressive model
Diurnal changes
Jarque-Bera test
NO_2

ABSTRACT

Nitrogen dioxide (NO_2) is one of the pollutants that can cause potential damage to the ecosystem. NO_2 emitted from vehicles forms the primary precursor for ground-level ozone. In this study, an analysis of the daily average of NO_2 concentration with meteorology measured for two years 2021 and 2022 is being carried out. It is evident from the analysis that NO_2 concentration followed an apparent diurnal pattern with a maximum value in the morning hours and a minimum during the afternoon hours. Summer months recorded the highest, and North East Monsoon (NEM) recorded the lowest values of NO_2. A statistically significant positive correlation was found between NO_2 and Temperature. An autoregressive model was formulated to forecast the daily average values of NO_2 concentration. Unit root test was performed to check the stationarity of the data points, which is important in determining trends and seasonal changes. From the model procedure, the order that best fits the data was identified as AR (4), in which the process has the current value based on the previous three values. The Akaike Information Criterion (AIC) and Schwartz Criterion (SC), which are estimators of prediction error for AR (4), are low. The Jarque confirmed the normal distribution-Bera test, which again approves the satisfactoriness of the model..

INTRODUCTION

Nitrogen Dioxide (NO_2) is a prominent potential pollutant and is formed in the atmosphere through the oxidation of nitric oxide (NO). NOx is the broader term that comprises the other oxides of nitrogen. NO_2 is a very reactive and significant species in the atmosphere, and vehicle transport plays a major role in increasing NO_2 concentrations (Lawrence et al. 2015). It plays a significant part in the formation of tropospheric ozone, as an aerosol-producing agent, and in the production of acidic species (Logan 1983, Pitts & Pitts 1986). Nitrogen dioxide (NO_2) is mainly affected by local emissions and meteorology rather than long-range transport (Yin et al. 2022). Ambient sources of NOx can be categorized into anthropogenic and natural sources, but the major contribution is from anthropogenic sources. It is to be noted that the majority of the countries consider NO2 concentration as an important indicator of air quality (Xue et al. 2020). Estimates of lightning-based NOx emissions for North America range from 1.2 to 1.7 $Tg.y^{-1}$ of NO_2 (Placet et al. 1990). Crutzen & Schmailz (1983) estimated global NOx emissions from stratospheric injection to be 0.5 $Tg.y^{-1}$. Numerous studies are showing a steady relationship between NO_2 exposure with reduced lung activity and increased respiratory symptoms (Ackermann-Liebrich 1997, Schindler 1998, Smith 2000). NO_2 causes bronchiolitis obliterans, a serious condition within a couple of weeks after exposure to around 150 ppm. NO_2 exposure of 500 ppm causes terminal illness (Gauderman et al. 2000). Chiusolo et al. (2011) found that there is a strong relationship between the rise in NO_2 and the mortality rate. Gurjar et al. (2010) estimated that elevated levels of NO_2 and SO_2 resulted in more number of deaths in Mumbai and Delhi. There exists a high correlation between NO_2 concentration and other pollutants that are formed through some chemical reactions (Burnett et al. 2007). NO_2 is an efficient absorber of visible radiation, and it has been projected as a plausible source of additional climatic influences (Wuebbles et al. 1989). Several mathematical models have been developed for forecasting pollutants in the atmosphere. The effects of elevated levels of NOx in China were investigated by Liu et al. (2003) using a three-dimensional chemical model. Multilayer Perceptron models were used in the prediction of NOx and NO_2 levels (Gardner & Dorling 1998). Lengyel et al. (2004) proposed a principal component analysis for analyzing NO_2. Many air-quality studies use PCA to develop statistically independent basic components (Maenhaut et al. 1989). Statheropoulos et al. (1998) and Vaidya et al. (2000) examined the pollutant

concentration with the use of component analysis. Recently, predictions for Fuzzy time series were performed using a multivariate heuristic model (Huarang et al. 2007), and a new method using Fuzzy relation based on a neural network algorithm was suggested for high-dimensional time series data (Egrioglu et al. 2009). These models must gratify many conditions and constraints (Isufi et al. 2019). This work aims to examine the variation of nitrogen dioxide concentration and forecast the daily average concentration of NO_2 for a short term using Autoregressive Integrated Moving Average (ARIMA) time series model.

MATERIALS AND METHODS

Study Area and Data Collection

Nagercoil (8.1833 N 77.4119 E) is one of the busy traffic-prone towns of south Tamil Nadu. Also, there are many brick kiln industries in and around that emit NOx into the atmosphere. To analyze the lifetimes, accumulation, and impacts, it is vital to know the interactions among various trace gases in the atmosphere. Studies suggest that NO_2 in traffic or on throughways can be two times as high as levels observed in residential areas. Fig.1 shows the study area and NO_2 monitor.

There are various mathematical models available for predicting the pollutants. Generally autoregressive (AR) model is a representation to study some time-varying processes in the environment. In particular, an ARIMA model was formulated for predicting the daily average values of NO_2 concentration.

Analysis

To carry out the optimization of various variables, including the number of parameters, criteria like Akaike's Information Criteria (AIC) and Bayesian Information Criteria (BIC), accuracy, and easiness of implementation, an autoregressive model was chosen. The estimation of the coefficients was carried out using "Eviews" software. In time series analysis, Auto Regressive Moving Average (ARMA) or Auto-Regressive Integrated Moving Average (ARIMA) models are generally proposed for better futuristic prediction (Adejumo & Momo 2013, Chattha 2021). This approach essentially has the following stages.

Stationarity test: In ARIMA modeling, it is noted that the data has to be changed to stationary form before doing analysis. It is easy to model when the data on a time series is stationary. Statistical modeling requires the data to be stationary for the effective forecast. If the data

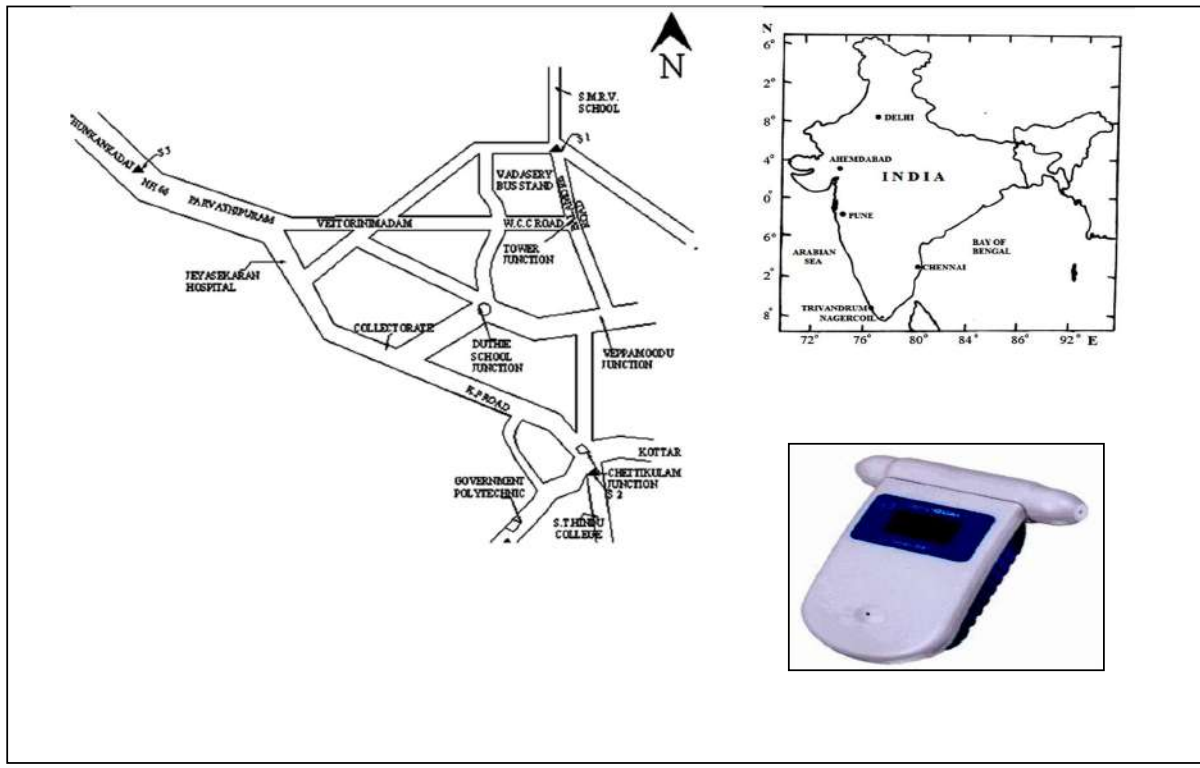

Fig. 1: Study area and monitor.

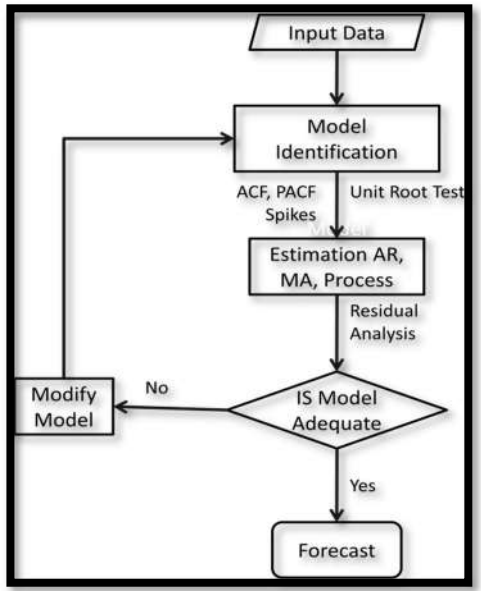

Fig. 2: Steps to be followed in modeling.

shows some trend, removal of the trend is vital. First, differencing is suitable for detrending the data points. Unit root tests (Dickey-Fuller tests) help to decide whether data should be first differenced or regressed. A stationary time series is significant in forecasting if the series is non-stationary.

Consider a time series equation, Z (t), such that

$$\{Z(t), t=1,\ldots\ldots \infty\}.$$

Suppose the AR term of p^{th} order is written as

$$Z_t = a_1 y_{t-1} + a_2 y_{t-2} + \ldots\ldots apyt_{-p} + £_t \quad \ldots(1)$$

The error term $£_t$ should have constant variance and must not be serially uncorrelated. If any one of the roots of equation (1) is equal to unity, then it has a unit root. This shows the non-stationarity of the series. The successive differencing methods reduce the trend effects and give the stationary series.

Autocorrelation plots: The autocorrelation function (ACF) and partial autocorrelation function (PACF) plots are useful for determining the number of values that are statistically significant over the different lagged periods. The significant spikes of PACF are used for determining the order of the autoregressive model and vice versa. The parameters of the ARMA model are characterized by the orders of both auto-regressive and moving average series. The primary step is to determine the suitable models using the functions ACF and PACF (Sharma et al. 2009). The process of identification is the most vital and also the most challenging step (Dobre & Alexandru 2008).

Diagnostic Check and Forecast

Diagnostic Check has turned out to be a regular tool for the identification of models before predicting the data. This check is applied to assess the residuals from the model when a model is estimated and also serves as the test of model adequacy. In specific, the residuals must not be dependent on one another and should be invariant in mean and deviation (Adejumo & Momo 2013). Suppose the residuals are not correlated, and the histogram follows a Gaussian distribution with mean zero and constant variance. In that case, the model is considered to be correct, and the data can be forecasted. In this work, we have used various kinds of software like Microsoft Excel (MS Excel) and Eviews 7 for creating the ARIMA model. Fig. 2 shows the various steps involved in modeling.

RESULTS AND DISCUSSION

Diurnal Variation

The distribution of the daily average of NO_2 and meteorological parameters is depicted in Fig. 3. The overall averaged diurnal variation is represented in Fig. 4. The minimum value of averaged diurnal NO_2 concentration was found to be 1.86 ppb, and the maximum value was 6.49 ppb. The diurnal cycle showed two characteristic peaks in a day. The appearance of the first peak was at 08:30 H, and the next peak was around 23:30 H. The maximum value was recorded during nighttime. The gradual increase in NO_2 concentration from early morning to 0830 H was mainly due to the increase in vehicular flow. This is also related to the features of nighttime boundary layer height (Teixeira et al. 2009). A minimum value was noticed at noon time, around 1430 H. Since NO_2 gets converted to ozone in the presence of sunlight, the drop in NO_2 was mainly due to this conversion in the selected site. The photochemical reaction stops after sunset, and hence, the conversion rate decreases, resulting in the build-up of NO_2 concentration.

Variation of NO_2 with Meteorology

The overall variation of daily average NO_2 concentration for two years is given in Fig. 5. The daily average recorded a minimum of 3.16 ppb and a maximum of 6.88 ppb. The matrix plot of NO_2 and meteorological parameters such as temperature, RH, and wind speed is depicted in Fig. 6. The analysis showed a positive correlation of 0.473 ($p<0.05$) between NO_2 and temperature, whereas for NO_2 and RH was significantly negative with a coefficient of -0.237. A weak correlation between NO_2 and wind speed was noted with a coefficient value of 0.192.

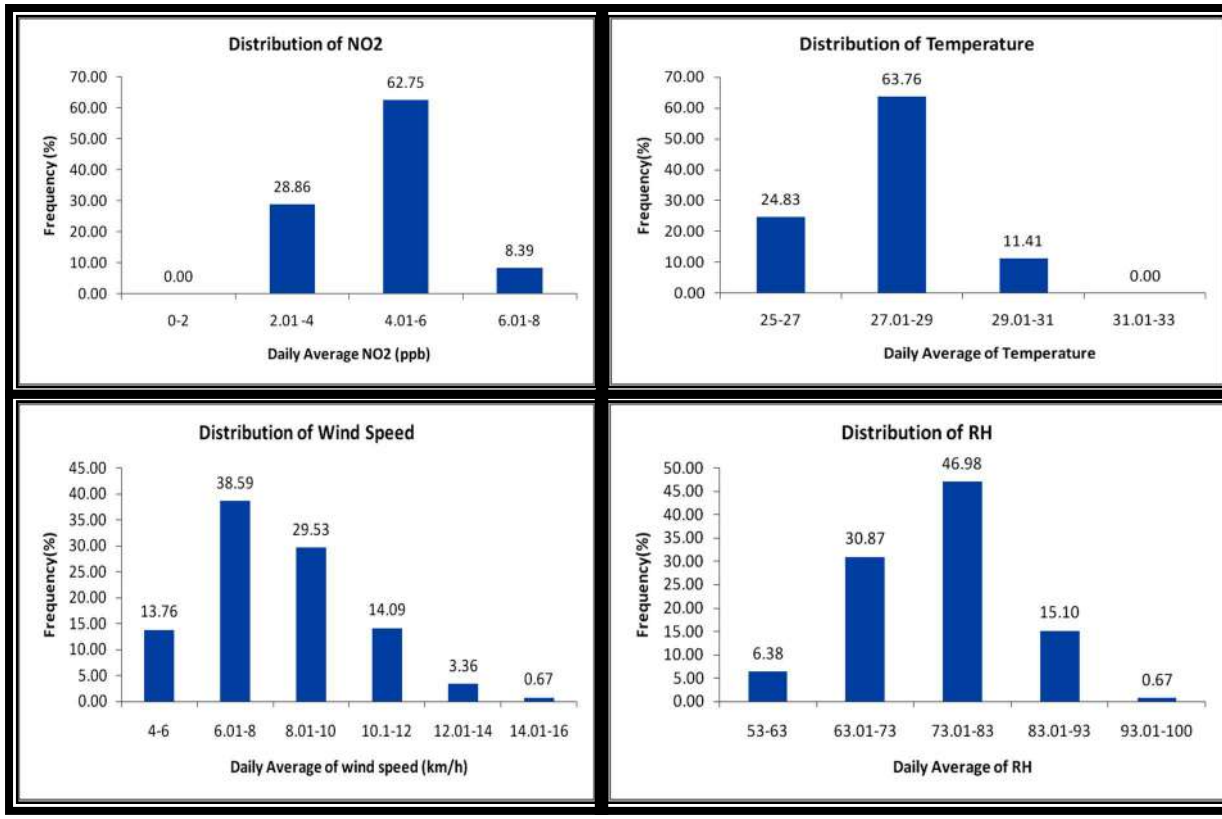

Fig. 3: Frequency distribution.

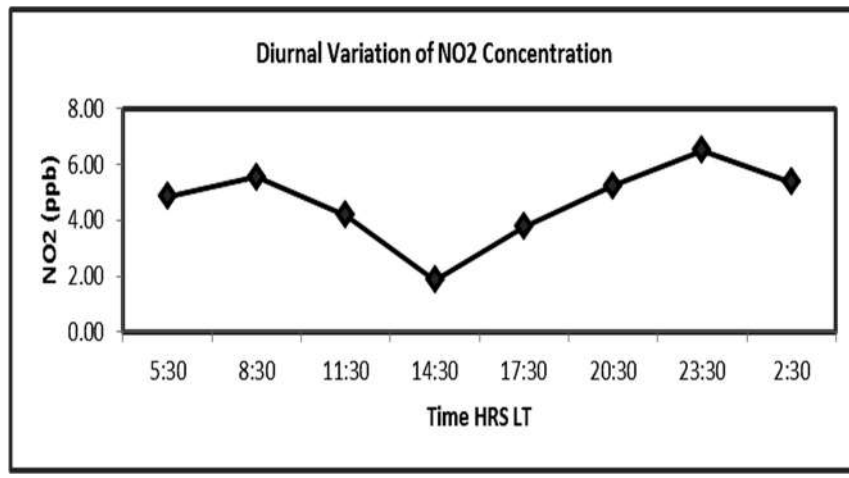

Fig. 4: Diurnal variation of NO_2.

Seasonal Variation

The seasonal division of Nagercoil City is in accordance with the meteorological standard of the Indian Meteorological Department (IMD). Summer is from March to May, and South West Monsoon (SWM) extends from June to September. North East Monsoon (NEM) starts in October and ends in December. January and February are winter months. The seasonal variation of NO_2 and meteorological parameters is depicted in Fig. 7. For both years, the summer season recorded the highest daily average concentration of NO_2, followed by SWM. This may be because of the high

oxidation rate of Nitric oxide (NO) to NO_2 and also due to conversion by ozone. Lowest values of NO_2 were recorded in NEM for both years owing to the pollutant washout due to monsoon rain. There is an increase in the daily average NO_2 concentration moving from NEM to winter. The high values of NO_2 in winter are attributed to relatively low temperatures and the accumulation of the pollutant. This is inconsistent with the study reported by Wang et al. (2019).

ARIMA (Box-Jenkinson) Model

Box-Jenkins Analysis discusses an orderly way of recognizing, fitting, and testing, uses moving average time series models, and is suitable for time series of moderate intervals. This work mainly aims to forecast daily averaged nitrogen dioxide concentration. The first step is to trace out the presence of seasonality in the data set and to

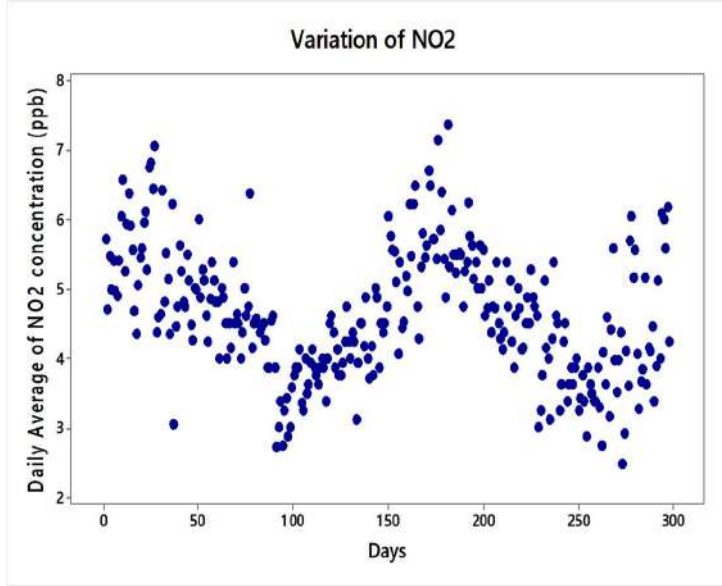

Fig. 5: Overall variation of NO_2.

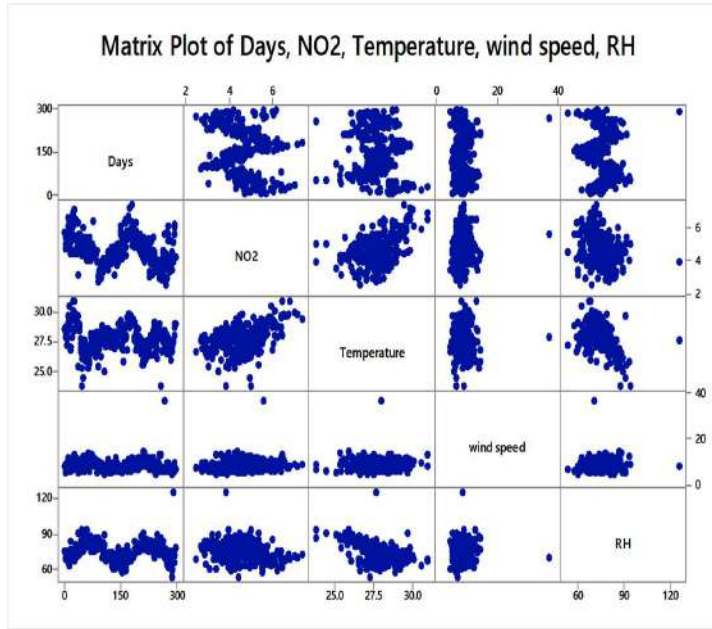

Fig. 6: Matrix plot of NO_2 and meteorology.

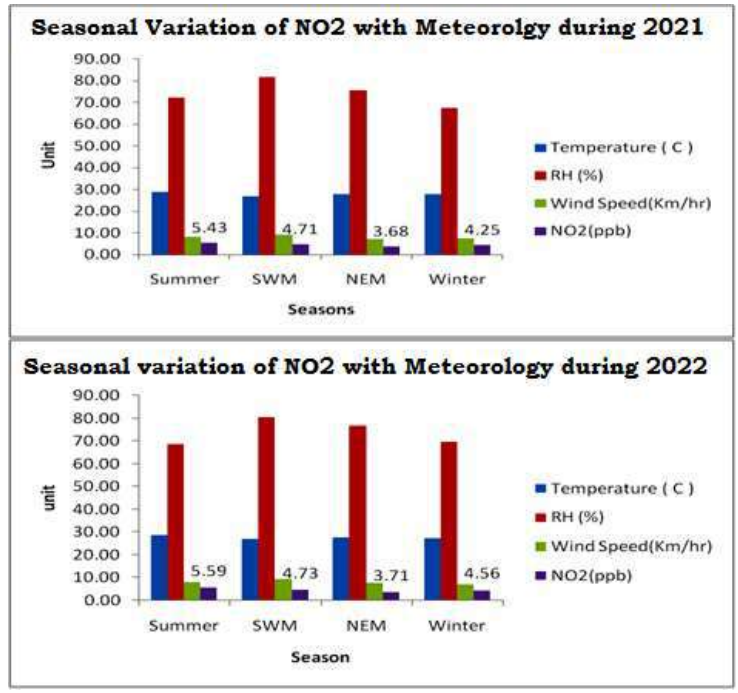

Fig. 7: Seasonal variation of NO_2.

deseasonalize the data. Unit root analysis was performed with the Augmented Dickey-Fuller test for 40 lags to elucidate the seasonality. Fig. 8 depicts the raw data with seasonal patterns. The data points were deseasonalized after performing the first difference, and the probability value became zero, which is given in Fig. 9. The test results display that statistics Dickey-Fuller (-10.86681) is smaller than the threshold values (-3.500669, 2.892200, and -2.583192) relating to critical thresholds of one percent, five percent, and ten percent, respectively. Thus, it is concluded that the series does not have a unit root and is stationary. The correlogram of the data series after removing seasonality is given in Fig. 10.

The next step is to identify the relevant ARMA (p, q) process. This is done by examining the ACF and PACF of the data for selecting the most favorable autoregressive and moving average terms of the model to be selected. From the plot, it can be noted that the simple function of autocorrelation exhibits a minor peak at shift 1, whereas the partial autocorrelation function has peaks up to shift 4. Therefore, it is reasonable to suspect that a moving average of the first order and autoregressive term of the fourth order would be a suitable estimate. Thus, the models AR (1), MA (1), AR (1 2 3 4), and ARMA (4 1) are identified. The performance of the identified models was verified based on

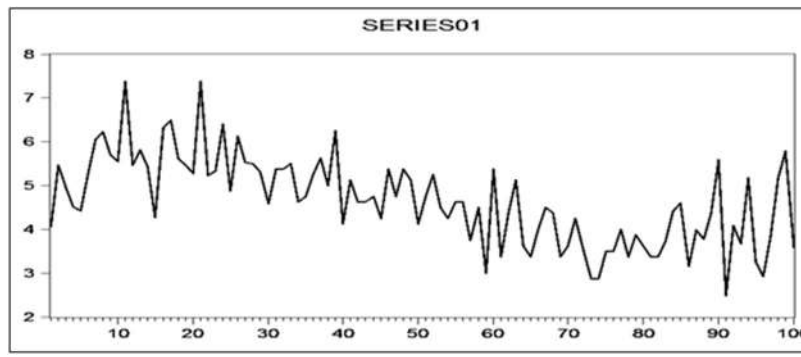

Fig. 8: Raw data with seasonality.

Null Hypothesis: D(SERIES01) has a unit root
Exogenous: Constant
Lag Length: 3 (Automatic - based on SIC, maxlag=40)

		t-Statistic	Prob.*
Augmented Dickey-Fuller test statistic		-10.86681	0.0000
Test critical values:	1% level	-3.500669	
	5% level	-2.892200	
	10% level	-2.583192	

*MacKinnon (1996) one-sided p-values.

Augmented Dickey-Fuller Test Equation
Dependent Variable: D(SERIES01,2)
Method: Least Squares
Date: 11/09/16 Time: 17:01
Sample (adjusted): 6 100
Included observations: 95 after adjustments

Variable	Coefficient	Std. Error	t-Statistic	Prob.
D(SERIES01(-1))	-3.874626	0.356556	-10.86681	0.0000
D(SERIES01(-1),2)	1.946170	0.296759	6.558090	0.0000
D(SERIES01(-2),2)	1.137050	0.205217	5.540727	0.0000
D(SERIES01(-3),2)	0.444364	0.100436	4.424326	0.0000
C	-0.011767	0.074141	-0.158716	0.8742

R-squared	0.837246	Mean dependent var	-0.022247
Adjusted R-squared	0.830012	S.D. dependent var	1.751567
S.E. of regression	0.722163	Akaike info criterion	2.238064
Sum squared resid	46.93675	Schwarz criterion	2.372479
Log likelihood	-101.3080	Hannan-Quinn criter.	2.292378
F-statistic	115.7454	Durbin-Watson stat	1.920820
Prob(F-statistic)	0.000000		

Fig. 9: Output of unit root test after removing seasonality.

Sample: 1 100
Included observations: 99

Autocorrelation	Partial Correlation		AC	PAC	Q-Stat	Prob
		1	-0.493	-0.493	24.788	0.000
		2	0.006	-0.313	24.791	0.000
		3	-0.059	-0.308	25.156	0.000
		4	-0.051	-0.394	25.428	0.000
		5	0.319	0.080	36.232	0.000
		6	-0.239	0.004	42.365	0.000
		7	0.001	-0.060	42.365	0.000
		8	0.000	-0.043	42.365	0.000
		9	0.012	-0.051	42.382	0.000
		10	0.129	0.028	44.246	0.000
		11	-0.090	0.117	45.171	0.000
		12	-0.053	0.046	45.492	0.000
		13	0.017	0.001	45.524	0.000
		14	-0.023	-0.102	45.585	0.000
		15	0.148	0.026	48.194	0.000
		16	-0.116	0.004	49.805	0.000
		17	0.040	0.116	50.001	0.000
		18	-0.067	0.028	50.560	0.000
		19	0.093	0.116	51.632	0.000
		20	-0.080	-0.114	52.434	0.000
		21	-0.003	-0.136	52.435	0.000
		22	0.077	-0.001	53.210	0.000
		23	-0.024	0.116	53.287	0.000
		24	-0.052	-0.045	53.648	0.000
		25	0.056	0.067	54.079	0.001
		26	-0.111	-0.179	55.756	0.001
		27	0.121	-0.146	57.800	0.001
		28	-0.026	-0.040	57.893	0.001
		29	-0.081	-0.040	58.838	0.001
		30	0.081	-0.035	59.789	0.001
		31	-0.026	0.081	59.889	0.001
		32	0.140	0.177	62.828	0.001
		33	-0.226	-0.091	70.542	0.000
		34	0.101	0.012	72.121	0.000
		35	-0.046	-0.012	72.455	0.000

Fig. 10: Correlogram of the data after removing seasonality.

Dependent Variable: D(SERIES01)
Method: Least Squares
Date: 11/09/16 Time: 17:06
Sample (adjusted): 6 100
Included observations: 95 after adjustments
Convergence achieved after 3 iterations

Variable	Coefficient	Std. Error	t-Statistic	Prob.
C	-0.003037	0.019131	-0.158750	0.8742
AR(1)	-0.928456	0.095856	-9.685952	0.0000
AR(2)	-0.809120	0.120348	-6.723156	0.0000
AR(3)	-0.692686	0.124394	-5.568474	0.0000
AR(4)	-0.444364	0.100436	-4.424326	0.0000

R-squared	0.519611	Mean dependent var	-0.008821
Adjusted R-squared	0.498261	S.D. dependent var	1.019521
S.E. of regression	0.722163	Akaike info criterion	2.238064
Sum squared resid	46.93675	Schwarz criterion	2.372479
Log likelihood	-101.3080	Hannan-Quinn criter.	2.292378
F-statistic	24.33707	Durbin-Watson stat	1.920820
Prob(F-statistic)	0.000000		

Inverted AR Roots	.20+.82i	.20-.82i	-.66-.43i	-.66+.43i

Fig. 11: Output of the estimated model.

Akaike Information Criterion (AIC), Schwartz Criterion (SC), Histogram Normality test, and residuals check. The output obtained after estimating the equation for the AR (4) model is given in Fig. 11. From the table, it is evident that the probability values tend to be zero, and the AIC and SC values are getting lowered. In statistics, the Schwarz criterion is a condition for model selection among a limited set of models. The model with the least BIC is preferred.

Two criteria normally used are the Akaike Information Criterion (AIC) and the Schwarz Criterion (SC; also known as the Bayesian information criterion or BIC).

Table 1 gives the estimated output of the various identified models. From the table, it is confirmed that the model AR (1 2 3 4) has the least value for AIC and SC. The right model can be chosen for that which reduces the Akaike Information Criterion (AIC) and the Schwarz Criterion (SC) values. To confirm the adequacy of the selected model, it is important to test residuals. The analysis involves checking whether the residuals are inside the upper limit. Hence, the sample ACF and PACF of the residuals were tested to check whether they do not follow any pattern and are strongly significant. The correlogram of the residuals is shown in the Fig. 12.

The histogram–normality distribution of the selected model is given in Fig. 13. The Jarque-Bera test allows us to assess the residual normality. The null hypothesis is that the residuals follow the Gaussian distribution. From Fig. 13, the normal distribution of the data is evident. If the Jarque-Bera value is higher than the chi-square critical value with two degrees of freedom, the alternate hypothesis must be accepted. The Jarque-Bera test statistic of 1.219970 is less than the chi-square critical value of 5.99 at the five

Table 1: Comparison of AIC & SC for identified models.

Identified models	AIC	SC	P-value
AR(1)	2.6360	2.659	0.000
MA(1)	2.3302	2.3535	0.000
ARMA(4 1)	2.2768	2.4200	0.889
AR(4)	2.2380	2.3724	0.000

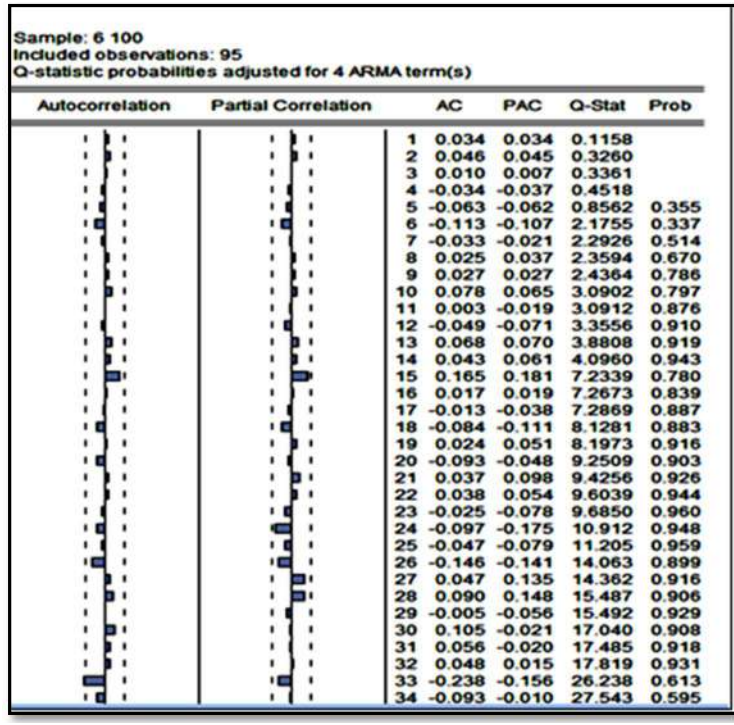
Sample: 6 100
Included observations: 95
Q-statistic probabilities adjusted for 4 ARMA term(s)

Autocorrelation	Partial Correlation		AC	PAC	Q-Stat	Prob
		1	0.034	0.034	0.1158	
		2	0.046	0.045	0.3260	
		3	0.010	0.007	0.3361	
		4	-0.034	-0.037	0.4518	
		5	-0.063	-0.062	0.8562	0.355
		6	-0.113	-0.107	2.1755	0.337
		7	-0.033	-0.021	2.2926	0.514
		8	0.025	0.037	2.3594	0.670
		9	0.027	0.027	2.4364	0.786
		10	0.078	0.065	3.0902	0.797
		11	0.003	-0.019	3.0912	0.876
		12	-0.049	-0.071	3.3556	0.910
		13	0.068	0.070	3.8808	0.919
		14	0.043	0.061	4.0960	0.943
		15	0.165	0.181	7.2339	0.780
		16	0.017	0.019	7.2673	0.839
		17	-0.013	-0.038	7.2869	0.887
		18	-0.084	-0.111	8.1281	0.883
		19	0.024	0.051	8.1973	0.916
		20	-0.093	-0.048	9.2509	0.903
		21	0.037	0.098	9.4256	0.926
		22	0.038	0.054	9.6039	0.944
		23	-0.025	-0.078	9.6850	0.960
		24	-0.097	-0.175	10.912	0.948
		25	-0.047	-0.079	11.205	0.959
		26	-0.146	-0.141	14.063	0.899
		27	0.047	0.135	14.362	0.916
		28	0.090	0.148	15.487	0.906
		29	-0.005	-0.056	15.492	0.929
		30	0.105	-0.021	17.040	0.908
		31	0.056	-0.020	17.485	0.918
		32	0.048	0.015	17.819	0.931
		33	-0.238	-0.156	26.238	0.613
		34	-0.093	-0.010	27.543	0.595

Fig. 12: Correlogram of residuals.

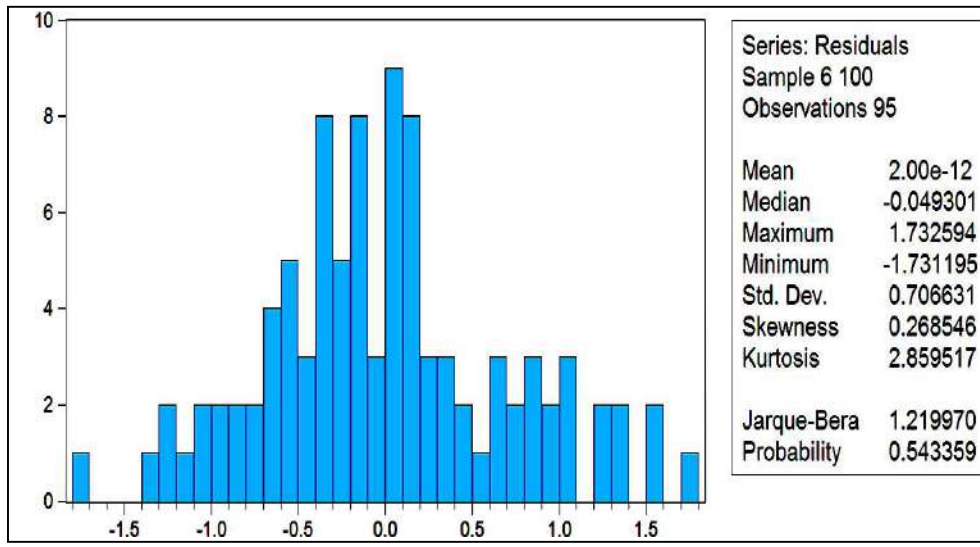

Fig. 13: Normality test histogram.

percentage level of significance. Thus, the null hypothesis is accepted as that the residuals follow a normal distribution. The mean value is also very close to zero. Hence, the identified AR (4) model is very much suitable for forecast.

Forecast

NO_2 concentration has been increasing day by day because of increased vehicular activities. Hence, it is vital to measure the concentration of pollutants in order to mitigate them. Forecasting plays an outstanding role in developing strategies and policies to reduce the amount of primary and secondary pollutants. In this study, we have carried out a short-term static forecast to test the capability of the model. Table 2 displays the results of the forecast.

Table 2: Measured and forecasted values.

S.No	Actual value	Forecasted Value	Residuals
1.	3.72655	3.661018	-0.06553
2.	3.385	4.177981	0.792981
3.	6.4145	4.790519	-1.62398
4.	5.1275	5.063513	-0.06399
5.	3.625	4.184011	0.559011
6.	4.115086	3.93136	-0.18373
7.	3.98877	4.258823	0.270053
8.	5.57635	5.380297	-0.19605
9.	5.578752	4.713327	-0.86543
10.	4.371929	4.285547	-0.08638
11.	4.230024	4.372855	0.142831
12.	4.573359	4.489647	-0.08371
13.	4.941783	5.220355	0.278572
14.	5.411842	5.05643	-0.35541
15.	6.039253	4.589683	-1.44957
16.	5.787678	4.764763	-1.02292
17.	5.899204	5.058178	-0.84103
18.	5.156884	5.348773	0.191889
19.	4.230024	5.587653	1.357629
20.	4.573359	5.60446	1.031101
	Average forecasted error		-0.11068
	Average Absolute error		0.573089

From Table 2, it is evident that the residuals are very small, and they are within ±1.8 deviations. The average forecast error is nearer to zero, which again confirms that the model is satisfactory. The Annual variation of NO_2 concentration shows an increasing trend from the year 2021 to 2022 and is depicted in Fig. 14.

CONCLUSION

An autoregressive model was employed to predict a short-term variation of the daily average NO_2 concentration measured at Nagercoil, India. Out of various models identified from the correlogram plots, the AR (4) model was chosen because of minimum AIC and SC values.NO_2 concentration showed a clear diurnal pattern with two peaks and a minimum value during afternoon hours. The residuals were within the critical limit and were white noise. The Jarque-Bera test followed a normal distribution, and the mean value was very close to zero (2.0e12). Prior to the results obtained from the tests, the AR (4) model was used to forecast the NO_2 concentration. The residuals between forecasted with measured values are very small, and they are within ±1.8 deviations. Also, the average forecast error is nearer to zero, which again confirms that the selected model is very suitable for this study.

REFERENCES

Ackermann-Liebrich, U. 1997. Lung function and long-term exposure to air pollutants in Switzerland: Study on air pollution and lung diseases in adults (SAPALDIA) team. Am. J. Respir. Crit. Care Med.,155: 122-129.

Adejumo, A.O. and Momo, A.A. 2013. Modeling Box-Jenkins methodology on retail prices of rice in Nigeria. Int. J. Eng. Sci., 2: 75-83.

Burnett, R.T., Dann, T.F., Cakmak, S., Goldberg, M.S., Fan, X. and Wheeler, A.J. 2007. Further interpretation of the acute effect of nitrogen dioxide observed in Canadian time series studies. J. Expos. Sci. Environ. Epidemiol., 17: 36-44.

Chattha, M.A. 2021. Deep LSF: Fusing knowledge and data for time series forecasting. Techrxiv, 1: 744.

Chiusolo, M., Ennio, C., Massimo, S., Galassi, C., Berti, G. and Annunziata, F. 2011. Short-term effects of nitrogen dioxide on mortality and susceptibility factors in ten Italian cities: The epic air study. Environ. Health Perspect., 119: 1233-1238.

Crutzen, P.J. and Schmailz, U. 1983. Chemical budgets of the stratosphere. Plant Space Sci., 31: 1009-1032.

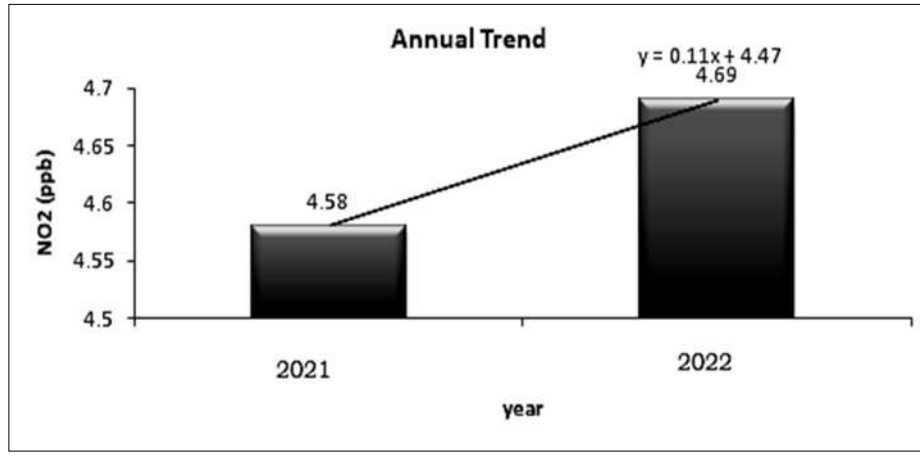

Fig. 14: Annual variation.

Dobre, I. and Alexandru, A.A. 2008. Modeling unemployment rate using Box-Jenkins procedure. J. Appl. Quant. Methods, 3: 156-166.

Egrioglu, E., Aladag, C.H., Yolcu, U., Uslu, V.R. and Basaran, M.A. 2009. A new approach based on artificial neural networks for high-order multivariate fuzzy time series. Expert Syst. Appl., 36: 10589-10594.

Gardner, M.W. and Dorling, S.R. 1998. Artificial neural network (the multilayer perceptron) – A review of applications in the atmospheric sciences. Atmos. Environ., 32: 2627-2636.

Gauderman, W.J., McConnell, R., Gilliland, F., London, S., Thomas, D. and Avol, E. 2000. Association between air pollution and lung function growth in southern California children. Am. J. Respir. Crit. Care Med., 162(4):1383-1390.

Gurjar, B.R., Jain, A., Sharma, A., Agarwal, A., Gupta, P., Nagpure, A.S. and Lelieveld, J. 2010. Human health risks in megacities due to air pollution. Atmos. Environ., 44 (36): 4606-4613.

Huarang, K.H., Yu, T.H.K. and Hsu, Y.W. 2007. A multivariate heuristic model for fuzzy time-series forecasting. IEEE Trans. Syst. Man Cybern. Part B, 37: 836-846.

Isufi, E., Loukas, A., Perraudin, N. and Leus, G. 2019. Forecasting time series with Varma recursions on graphs. IEEE Trans. Signal Process, 67: 4870-4885.

Lawrence, J.P., Anand, J.S., Vande Hey, J.D., White, J., Leigh, R.R., Monks, P.S. and Leigh, R .J. 2015. High–resolution measurements from the airborne atmospheric nitrogen dioxide imager (ANDI). Atmos. Meas. Tech., 8: 4735-4754.

Lengyel, A., Héberger, K., Paksy, L., Bánhidi, O. and Rajkó, R. 2004. Prediction of ozone concentration in ambient air using multivariate methods. Chemosphere, 57: 889-896.

Liu, Y., Isaksen, I.S.A. and Sundet, J.K. 2003. NO_x change over China and its influences. Adv. Atmos. Sci., 21:132-140.

Logan, J.A. 1983. Nitrogen oxides in the troposphere: global and regional budgets. J. Geogr. Res., 88: 10785-10807.

Maenhaut, W., Cornille, P., Pacyna, J. and Vitols, V. 1989. Trace element composition and origin of the atmospheric aerosol in the Norwegian Arctic. Atmos. Environ., 23: 2551-2569.

Pitts, F.C. and Pitts, J.N. 1986. Atmospheric Chemistry: Fundamentals and Experimental Techniques. John Wiley, Hoboken, p. 63.

Placet, M., Battye, R.E., Fehsenfeld, F.C. and Bassett, G.W. 1990. Emissions are Involved in Acidic Deposition Processes. State-of-Science/ Technology Report. The US National Acid Precipitation Assessment Program (NAPAP) US Government Printing Office, Washington DC.

Schindler, C. 1998. Associations between lung function and estimated average exposure to NO_2 in eight areas of Switzerland: Swiss study of air pollution and lung diseases in adults. Epidemiology, 9: 405-411.

Sharma, P., Avinash Chandra, S. and Kaushik, C. 2009. Forecasts using Box-Jenkins models for the ambient air quality data of Delhi City. Environ. Monit. Assess., 157: 105-112.

Smith, B.J. 2000. Health effects of daily indoor nitrogen dioxide exposure in people with asthma. Eur. Respir. J., 16: 879- 885.

Statheropoulos, M., Vassiliadis, N. and Pappa, A. 1998. Principal component and canonical correlation analysis for examining air pollution and meteorological data. Atmos. Environ., 32: 1087-1095.

Teixeira, E.C., Eduardo, R.S., Flavio, W. and Jandyra, F. 2009. Measurement of surface ozone and its precursors in an urban area in South Brazil. Atmos. Environ., 43: 2213-2220.

Vaidya, O.C., Howell, G.D. and Leger, D.A. 2000. Evaluation of the distribution of mercury in lakes in Nova Scotia and Newfoundland. Water Air Soil Pollut., 117: 353-369.

Wuebbles, D.J., Grant, K.E., Connell, P.S. and Penner, J.E. 1989. The role of atmospheric chemistry in climate change. J. Air Pollut. Contr. Assoc., 39: 22-28.

Xue, R., Wang, S., Li, D., Zou, Z., Chan, K.L., Valks, P., Saiz-Lopez, A. and Zhou, B. 2020. Spatio-temporal 915 variations in NO2 and SO2 over Shanghai and Chongming Eco-Island were measured by the ozone 916 monitoring instrument (OMI) from 2008–2017. J. Clean Prod., 258: 917-926.

Yin, H., Sun, Y., Notholt, J., Palm, M. and Liu, C. 2022. Spaceborne tropospheric nitrogen dioxide (NO_2) observations from 2005-2020 over the Yangtze River Delta (YRD), China: variabilities, implications, and drivers, Atmospheric Chemistry and Physics, 1-32. https://doi.org/10.5194/acp-2021-1089.

ORCID DETAILS OF THE AUTHORS

R. Krishna Sharma: https://orcid.org/0000-0002-8469-1106

Nature Environment and Pollution Technology
An International Quarterly Scientific Journal

p-ISSN: 0972-6268
(Print copies up to 2016)
e-ISSN: 2395-3454

Vol. 23 | No. 1 | pp. 537-544 | 2024

Original Research Paper

https://doi.org/10.46488/NEPT.2024.v23i01.050

Open Access Journal

Effects of Addition of Humic and Fulvic Acids on Soil Properties and Germination Percentage of Cucurbit Plants (Zucchini and Cucumber)

A. O. Khashroum†*, Y. Kh. Fawadleh, H. J. Hamad*** , Sh. A. Saewan****, I. Almashagbeh***** , M. O. Alalawneh****** S. M. Daradkeh******* and Abeer Saqr********

*Department of Plant Production and Protection, Faculty of Agriculture, Jerash University, Jordan
**Al Dhaleel Comprehensive Secondary School, Ministry of Education, Zarqa, Jordan
***Department of Clinical Nutrition and Dietetics, Faculty of Allied Medical Sciences, Philadelphia University, Jordan
**** Department of Food Science and Nutrition, Faculty of Agriculture, Jerash University, Jerash 26110, Jordan
*****Water Analysis Department, Ministry of Water and Irrigation, Mafraq Municipality, Jordan
******Curriculum Specialist, Ministry of Education, United Arab Emirates (UAE)
*******Ministry of Local Administration, Jordan
********Head of Extension Programs, Ministry of Agriculture, Jordan
†Corresponding author: A.O. Khashroum; askshb@yahoo.com

Nat. Env. & Poll. Tech.
Website: www.neptjournal.com

Received: 12-07-2023
Revised: 11-09-2023
Accepted: 12-09-2023

Key Words:
Humic acid
Fulvic acids,
Soil properties, Germination,
Cucurbit plants

ABSTRACT

This research was conducted to study the effect of adding humic and fulvic acids to the irrigation water on soil properties and germination percentage of two cucurbit plants: zucchini and cucumber. The study was conducted in an open field in Sokhna District in the governorate of Zarqa (Jordan). The field soil was transported to calcareous sandy soil. In the beginning, the weeds and stones were removed, and the land was smoothed and plowed. Effort was made to control weeds and insects at all stages of plant growth. Then, an irrigation network was installed. The fulvic acid-humic acid (FA-HA) biostimulant mixture was incorporated with the irrigation water, and irrigation was practiced three days per week for four weeks. During this period, every irrigation round lasted for two to three hours. A mixture of humic acid (8.0%) and fulvic acid (8.0%) was added to the irrigation water. Three treatments were considered, corresponding to three acid mixture concentrations: 0.50 $mL.L^{-1}$, 1.00 $mL.L^{-1}$, and 1.50 $mL.L^{-1}$. The acid mixtures were added continuously at all stages of plant growth until plant maturity and harvest. Four replicates of the experiment were made. The plant growth variables of interest were germination percentage, number of leaves, date of fruition, size of fruit, and overall mass of fruits. Meanwhile, the soil parameters of interest were soil pH and soil salinity (electric conductivity (EC)) before and after adding the FA-HA mixture. The study found that the 0.5 $mL.L^{-1}$ acid mixture treatment led to the early growth of the zucchini plant seeds and that fruition took place 12 days after planting. In addition, the results showed an increase in plant germination under the 0.5 $mL.L^{-1}$ acid mixture treatment in light of the increase in the number of male and female plant flowers, with fruiting taking place on time. In conclusion, the relationship between zucchini growth and yield with FA-HA mixture concentration is non-linear. It is also concluded that the optimum acid mixture concentration and application rate are crop-specific. Hence, for each crop, the most appropriate acid mixture concentration should be determined first before the broad-scale application of amendments to the soil to ensure the contribution of this environmentally friendly practice to sustainable agriculture.

INTRODUCTION

Humic substances (e.g., humic acids (HAs) and fulvic acids (FAs)) are ubiquitous compounds that occur naturally in soils and waters. These complex superstructures are derived from the decomposition of dead plant and animal matter, and they are vital to soil health. They are heterogeneous in composition, which is specific to their site of origin, and they consist of weakly bound aggregates of small organic compounds that can sequester minerals and make them available for plants. As such, they may have nutritional value for humans. Extracts of fulvic and humic acids can be produced that can be suitable for such purposes (Murbach et al. 2020). In other respects, the HAs and FAs influence the fates and transport of various compounds in the soil (Makrigianni et al. 2022).

Canellasa et al. (2015) reviewed the use of humic substances as biostimulants in horticulture, with emphasis on (i) their effects on nutrient uptake and plant metabolism, (ii) the relationships between the chemical properties of humified matter and its bioactivity, with specific reference to the promotion of lateral root growth; and (iii) evaluation of the experimental data related to the overall effects of humic substances applied to horticultural crops.

Humic substances (HSs), which are friendly organic ligands, are vicariously introduced because they have positive effects on soil redox condition, plant properties, and metal speciation in soil. They are ubiquitously distributed in nature, and they mainly consist of HA, FA, and humus. The structures and characteristics of HA and FA vary broadly from one location to another, depending on many factors like their origin, environmental conditions, and age (Gao et al. 2022).

Murbach et al. (2020) clarified that "Historically, humic acids (HA; CAS no. 1415-93-6) have been defined as precipitates that form when basic extracts of humic matter are acidified while fulvic acids (FA; CAS no. 479-66-3) are those that remain in solution following this process." They further explained that HAs are soluble at alkaline pH while FAs exhibit pH-independent solubility. The solubility of FAs is imparted by hydrophilicity within the associations of small molecules due to an abundance of acidic functional groups, whereas the associations of molecules in the HAs are hydrophobic, which is a property that results in their stabilization at neutral pH and clumping at acidic pH (Murbach et al. 2020).

Recently, attention has grown to the use of HAs and FAs in agricultural production. For example, Bayat et al. (2021) investigated the comparative effects of HA and FA on growth, antioxidant activity, and nutrient content of the Eurasian plant (yarrow). The experimental treatments corresponded to additions of HA and FA to soil at concentrations of 5, 10, 15, and 20 $kg.ha^{-1}$. The results showed that the application of HA and FA to soil improved the growth of yarrow and the amounts of photosynthetic pigments and antioxidants in it. The results also indicated that the highest shoot dry weight in the field-grown plants was associated with the 15 $kg.ha^{-1}$ addition of HA, while in the greenhouse experiment, the highest shoot dry weight was concomitant to the 20 $kg.ha^{-1}$ FA treatment. These researchers, accordingly, concluded that the application of HA or FA to soil has positive effects on the growth and antioxidant activity of yarrow, especially under field conditions.

Ran et al. (2022) conducted pot experiments to investigate the influence of extracts of FA and HA on methylation and bioaccumulation of mercury (Hg) in paddy soil. They found that the FA and HA extracts largely increased the abundance of Hg-methylating microbes and low molecular weight organic matter (e.g., cysteine) in the paddy soil. Furthermore, the results showed that all the FA treatments increased the mobility and methylation of Hg in the soil and its absorption by plant roots.

Gao et al. (2022) studied the mechanism of heavy metal activation or passivation and the plant response that is triggered by FA and HA addition to soil. They examined the Cd activation effect of FAs and HAs derived from pig, goat, and duck manure composts, straw compost, and commercial materials (i.e., PC, GC, DC, SC, and CM). Moreover, they looked into the roles of these materials in plant growth promotion and Cd uptake. The results pointed out that due to the reduction of soil pH by FA and HA and the multiple functional groups of the various FA-and HA-containing materials that were added to soil, the concentration of available Cd increased by 4.3–4.8% and 3.6–6.3% when FA and HA from the various sources, respectively, were applied to soil for 30 days. Slight inhibitory effects of plant growth and Cd uptake were observed, which led to a reduction of Cd accumulation with DHA, SHA, and CHA treatments. The corresponding soil Cd removal efficiencies of PFA and PHA were 43.5% and 34.6%, respectively, which have abundant O- and N-containing functional groups.

In Jordan, there is a lack of studies on the impacts of the addition of FA and HA to soil on its properties and plant germination and growth parameters of both the cucurbit plants and other plants. This research addresses this knowledge gap. It examines the effects of FA and HA addition to soil on its properties and on the germination and growth of two cucurbit plants: zucchini and cucumber.

MATERIALS AND METHODS

This research was conducted in an open field in Sokhna District in the governorate of Zarqa, Jordan. The field soil was transported to calcareous sandy soil. In the beginning, the weeds and stones were removed from the field. Then, the land was smoothed and plowed. After that, an irrigation network was installed and tested. After that, the two cucurbit plants under study, namely, zucchini and cucumber, were planted in furrows with suitable distances between plants and rows. Rows were separated from one another by a distance of 120 cm. In the meantime, the distances between plants were 40 cm in the case of cucumber and 80 cm in the case of zucchini. Plant irrigation was performed using a drip irrigation system with an FA-HA mixture added to the irrigation water at a concentration of 8.0% each. Drip irrigation was practiced three days per week for four weeks, and each irrigation round lasted from two to three hours. Effort was made to control

weeds and insects at all stages of plant growth. For example, insect traps were employed to control the whiteflies.

An aqueous mixture of 8.0% HA and 8.0% FA (Humilic 8-8 (JISA, Jordan)) was added to the irrigation water. The acids were added simultaneously and continuously at all stages of plant growth until plant maturity and harvest. Three treatments were considered, corresponding to the acid mixture concentrations of 0.50 $mL.L^{-1}$, 1.00 $mL.L^{-1}$, and 1.50 $mL.L^{-1}$. Accordingly, the experiment had a completely randomized experimental design with three treatments and four replicates. As such, besides the control block (T_0), the experiment included three treatment blocks: T_1 (acid mixture application at a concentration of 0.50 $mL.L^{-1}$), T_2 (acid mixture application at a concentration of 1.00 $mL.L^{-1}$), and T_3 (acid mixture concentration at a rate of 1.50 $mL.L^{-1}$).

The irrigation water parameters of concern were pH and electric conductivity (EC), while the soil parameters of interest were soil pH and soil salinity in terms of EC. Meanwhile, the plant growth variables of interest were germination percentage, number of leaves, date of fruition, size of fruit, and overall mass of fruits.

The field and laboratory data were compiled and analyzed statistically. Comparisons were held between the control group and the treatment groups, as well as between the treatment groups, in the study variables using One-Way Analysis of Variance (ANOVA). When this test revealed significant differences between the compared groups, pairwise comparisons were made between the groups using Fisher's Least-Significant Difference (LSD) *post hoc* test to identify the similar groups. All statistical tests were performed in XLSTAT (v. 2019.2.2.59614) at the 0.05 level of statistical significance (α).

RESULTS AND DISCUSSION

Effect of Acid Mixture Addition on Irrigation Water

This study examined the effect of the addition of FA and HA to irrigation water on its pH and salinity in terms of electric conductivity (EC). The mean water pH values of the various treatments and four replicates are listed in Table 1. It is seen that the original irrigation water had a pH value of 9.00. The addition of the 1:1 FA-HA mixture increased the water pH. The new pH values associated with the 0.5, 1.0, and 1.50 mL.L acid mixture concentrations were 9.90, 9.50, and 10.70, respectively. It is found that the higher the concentration of the acid mixture, the higher the increase in the pH value of the irrigation water.

One-Way Analysis of Variance (ANOVA) unclosed significant differences in the pH values between the treated water and the blank water. Fisher's LSD *post hoc* test unveiled that the irrigation water treated with FA-HA mixture at the concentration of 1.50 $mL.L^{-1}$ had a significantly higher pH value than the control water and the other two treatments. Meanwhile, the differences in mean pH values between the control water and the water treated with 0.50 $mL.L^{-1}$ and 1.0 $mL.L^{-1}$ acid mixture are statistically insignificant. The 1.50 $mL.L^{-1}$ acid mixture treatment increased the water pH value to significantly higher values than those of the blank and the other treatments (0.5 and 1.0 $mL.L^{-1}$).

The mean electric conductivity (EC) values of the irrigation water before FA-HA mixture addition and under the different treatments are provided in Table 2. The initial or original irrigation water is non-saline (freshwater). It had an EC value of 592.0 $\mu S.cm^{-1}$. The results demonstrate that the 0.50 $mL.L^{-1}$ treatment reduced the EC of the irrigation

Table 1: Effect of addition of fulvic acid-humic acid mixture to irrigation water on its pH.

Plant	Week	pH			
		Acid Concentration			
		Blank	0.5 $mL.L^{-1}$	1.0 $mL.L^{-1}$	1.5 $mL.L^{-1}$
Zucchini	1	9.00^{b}	9.50^{b}	9.90^{ab}	10.70^{a}
	2	9.00^{b}	9.50^{b}	9.90^{ab}	10.70^{a}
	3	9.00^{b}	9.50^{b}	9.90^{ab}	10.70^{a}
	4	9.00^{b}	9.50^{b}	9.90^{ab}	10.70^{a}
	5	9.00^{b}	9.50^{b}	9.90^{ab}	10.70^{a}
Cucumber	1	9.00^{b}	9.50^{b}	9.90^{ab}	10.70^{a}
	2	8.80^{b}	9.50^{b}	9.90^{ab}	10.70^{a}
	3	9.00^{b}	9.50^{b}	9.90^{ab}	10.70^{a}
	4	9.00^{b}	9.50^{b}	9.90^{ab}	10.70^{a}
	5	9.00^{b}	9.50^{b}	9.90^{ab}	10.70^{a}

Table 2: Effect of addition of fulvic acid-humic acid mixture to irrigation water on its electric conductivity.

Plant	Week	Electric Conductivity (EC [μS.cm^{-1}])			
		Acid Concentration			
		Blank	0.5 mL.L^{-1}	1.0 mL.L^{-1}	1.5 mL.L^{-1}
Zucchini	1	592.00 ^{a}	405.00 ^{a}	422.00 ^{a}	448.00 ^{a}
	2	592.00 ^{a}	405.00 ^{a}	422.00 ^{a}	448.00 ^{a}
	3	592.00 ^{a}	405.00 ^{a}	555.33 ^{a}	448.00 ^{a}
	4	592.00 ^{a}	405.67 ^{a}	422.00 ^{a}	431.33 ^{a}
	5	592.00 ^{a}	405.00 ^{a}	422.00 ^{a}	448.00 ^{a}
Cucumber	1	592.00 ^{a}	405.00 ^{b}	422.00 ^{b}	448.00 ^{ab}
	2	592.00 ^{a}	405.00 ^{b}	422.00 ^{b}	448.00 ^{ab}
	3	592.00 ^{a}	405.00 ^{b}	422.00 ^{b}	448.00 ^{ab}
	4	592.67 ^{a}	405.33 ^{b}	422.00 ^{b}	448.00 ^{ab}
	5	592.67 ^{a}	438.33 ^{b}	422.00 ^{b}	448.00 ^{ab}

Table 3: Effect of addition of fulvic acid-humic acid mixture to irrigation water on soil solution pH.

Plant	Week	pH			
		Acid Concentration			
		Control	0.5 mL.L^{-1}	1.0 mL.L^{-1}	1.5 mL.L^{-1}
Zucchini	1	8.50^{a}	8.70^{a}	8.30^{a}	8.50^{a}
	2	8.50^{a}	9.30^{a}	9.20^{a}	9.20^{a}
	3	8.50^{a}	8.80^{a}	9.10^{a}	8.60^{a}
	4	8.50^{a}	8.80^{a}	9.10^{a}	8.60^{a}
	5	8.50^{a}	8.80^{a}	9.00^{a}	8.50^{a}
Cucumber	1	8.40 ^{a}	8.70 ^{a}	8.30 ^{a}	8.70 ^{a}
	2	8.50 ^{a}	9.30 ^{a}	9.20 ^{a}	9.20 ^{a}
	3	8.50 ^{a}	8.80 ^{a}	9.10 ^{a}	8.60 ^{a}
	4	8.50 ^{a}	8.80 ^{a}	9.10 ^{a}	8.60 ^{a}
	5	8.40 ^{a}	8.80 ^{a}	9.00 ^{a}	8.50 ^{a}

water from 592.0 μS.cm^{-1} to 405.0 μS.cm^{-1}. The other two acid mixture treatments also reduced the EC of the irrigation water, however, to somewhat lower extents. Specifically, the 1.0 mL.L^{-1} treatment decreased the mean EC of the irrigation water from 592.0 μS.cm^{-1} to 422.0 μS.cm$^{-1,}$ while the 1.5 mL.L^{-1} treatment reduced it to 448.0 μS.cm^{-1}. So, the highest decrease in salinity of the irrigation water was associated with the lowest acid mixture concentration (0.50 mL.L^{-1} (Table 2)). This indicates that the higher the FA-HA mixture concentration, the lower the reduction in irrigation water EC.

One-way analysis of Variance (ANOVA) brought to notice that the differences in the mean EC values between the treated water and the blank water are statistically significant, while differences between the mean EC values of the treated water are statistically insignificant. In other words, analysis supports that there are no statistically significant differences in the mean EC values between the three irrigation water treatments (405.0-448.0 μS.cm^{-1}). However, the mean EC values of the treated water are significantly lower than the mean EC of the control (original) water. Thereupon, it is concluded that FA-HA mixture treatment of the irrigation water reduces its salinity noticeably.

Effect of Acid Addition on Soil

This study investigated the impact of the addition of FA-HA biostimulant mixture to irrigation water on the pH and EC of the soil solution. The results (Table 3) point out that the control soil had alkaline pH, ranging from 8.40 to 8.50. In general, the addition of the FA-HA mixture to the soil via the irrigation water increased the soil solution pH. However, the changes in soil pH varied with treatment. For example, under the 0.50 mL.L^{-1} acid mixture treatment, the mean soil pH increased slightly in the first week from 8.50 to 8.70, then it jumped to 9.30 in the second week and stabilized later to 8.80 (Table 3). Comparable results were recorded under the 1.5 mL.L^{-1} acid mixture treatment. In the case of

the 1.0 mL.L^{-1} acid mixture treatment, however, the mean soil pH dropped slightly in the first week from 8.50 to 8.30. It increased to 9.20 in the second week and almost stabilized at 9.10 afterward. So, the soil solution pH keeps changing during the first three weeks of the acid mixture addition and stabilizes at a higher than the original pH value afterward.

One-way analysis of Variance (ANOVA) revealed that the reported differences in the mean soil solution pH values between the control and the treated soils are statistically insignificant. So are the differences between the three treated soils. Stated otherwise, statistical testing supports that there are no statistically significant differences in the mean pH values between the control soil and the treated soils or between the three soils under the different FA-HA mixture treatments during the study period. Generally, the increases in mean soil solution pH by the effect of the acid mixture treatment were the highest during the second week of the growing season. In view of the study results (Table 3), the researchers conclude that, in general, FA-HA treatment of the soil leads to an increase in soil solution pH, however, insignificantly. In this respect, it should be recalled that the addition of acids, even if weak and at low concentrations, to alkaline soil reduces its pH.

The influence of FA-HA mixture addition to the soil via the irrigation water on the EC of the soil solution was analyzed in the present study. Table 4 presents the weakly mean soil solution EC values during the growing season pooled over replicates. The measurements spotlight that the field soil originally had a mean EC value of 349.0 μS.cm^{-1} and that EC generally increased from one week to another in the growing season. The highest increase in the mean EC was 296 μS.cm^{-1}, an increase from 349 to 745 μS.cm^{-1}. It was reported in the second week of the growing season (Table 4). After that, the soil solution EC dropped profoundly but remained still higher than the original, or starting, EC (349 μS.cm^{-1}). In all cases, a slight drop in EC took place in the fifth week of the growing season.

Table 4 shows that the mean weak EC values of the soils planted with Zucchini were about the same as those planted with cucumber. Further, the study results disclose that the FA-HA mixture treatments affected soil solution EC by increasing them in the first growing week and reducing them in the subsequent weeks (Table 4).

Statistically significant differences in soil solution EC were detected. However, the differences varied from growing week to another. As an example, in the first growing week, the treated soils had significantly higher mean EC values (619.0-671.0 μS.cm^{-1}) than the control soil (349.0 μS.cm^{-1}), and there were no statistically significant differences in EC values between the soils under the three treatments (Table 4). In the second growing week, the treated soils had significantly lower EC values than the control soil. There were no significant differences in EC values between the soils under the three treatments, both those planted with Zucchini and those planted with cucumber, except in the first week in the case of cucumber, in which the 1.50 mL.L^{-1} acid mixture treatment resulted in an EC value comparable to that of the control soil, which is significantly lower than the mean EC values associated with the other treatments (Table 4).

During the third, fourth, and fifth growing weeks, the treated soils had significantly lower EC values than the control soil. Additionally, the soil treated with 1.50 mL.L^{-1} FA-HA mixture generally had a significantly lower EC value than that treated with 1.0 mL.L^{-1} acid mixture. Also, the soils treated with 0.50 mL.L^{-1} acid mixture had significantly higher EC values than the soils receiving the aforementioned two treatments. These general trends were nearly the same in the soils, irrespective of whether they were planted with

Table 4: Effect of addition of fulvic acid-humic acid mixture to irrigation water on the soil solution electric conductivity.

Plant	Week	Electric Conductivity (EC [μS.cm^{-1}])			
		Acid Concentration			
		Control	0.5 mL.L^{-1}	1.0 mL.L^{-1}	1.5 mL.L^{-1}
Zucchini	1	349.00 ^{e}	654.00 ^{ab}	671.00 ^{ab}	619.00 ^{ab}
	2	745.00 ^{a}	376.00 ^{e}	335.00 ^{e}	384.00 ^{e}
	3	678.00 ^{ab}	584.00 ^{abc}	422.00 ^{cde}	386.00 ^{e}
	4	687.00 ^{ab}	584.00 ^{abc}	422.00 ^{cde}	386.00 ^{e}
	5	675.00 ^{ab}	580.00 ^{bcd}	420.00 ^{de}	376.00 ^{e}
Cucumber	1	348.00 ^{d}	694.00 ^{ab}	678.00 ^{ab}	269.00 ^{d}
	2	749.00 ^{a}	379.00 ^{d}	338.00 ^{d}	384.00 ^{d}
	3	678.00 ^{ab}	585.00 ^{bc}	428.00 ^{cd}	396.00 ^{d}
	4	659.00 ^{ab}	594.00 ^{ab}	428.00 ^{cd}	398.00 ^{d}
	5	680.00 ^{ab}	575.00 ^{bc}	427.00 ^{cd}	367.00 ^{d}

Zucchini or cucumber. Accordingly, it may be stated that, in general, the highest reduction in the soil EC is concomitant to the 1.50 mL.L^{-1} acid mixture treatment. In other words, the higher the FA-HA mixture, the lower the soil solution EC.

A review of the literature shows that few studies examined the impacts of the application of HA and/or FA to soil on its physico-chemical characteristics. In one of these studies, Khalil et al. (2011) reported that separate applications of FA and HA to soil at the concentrations of 5, 10, 15, and 20 L.acre^{-1}, each decreased soil pH and EC and that these acids resulted in almost equal reductions in soil pH and EC that increase with acid concentration. Stated otherwise, the higher the concentration of the acid added to the soil, the relatively higher the drop in soil pH and EC. Though the acids were added separately to the soil, nearly the same changes (reductions) in soil pH and EC were induced by the similar concentrations of the two acids. Gao et al. (2022) also reported that FA and HA addition to soil reduced its pH.

Effect of Acid Addition on Cucurbit Plants

Effects of the addition of FA-HA mixture to irrigation water on cucumber and zucchini germination and growth were investigated. The investigation encompassed the germination percentage, number of leaves, fruit size, and overall fruit mass. The main findings are given and discussed in the following two sub-sections.

Zucchini (*Cucurbita pepo*)

Zucchini had higher mean germination percentages, in general, than cucumber. Table 5 spotlights that the mean germination percentage of Zucchini was 99.67% in the control plot. The addition of the FA-HA mixture at the concentration of 0.50 mL.L^{-1} resulted in 100.0% germination. Meanwhile, the FA-HA mixture concentration of 1.0 mL.L^{-1} did not produce a change in the average germination percentage, which was equivalent to that of the control plants (99.67% (Table 5)). The acid mixture concentration of 1.50 mL.L^{-1} led to 100.0% germination of Zucchini. In addition, the ANOVA uncovers that the differences between the control and the treatments, as well as between the treatments themselves, in the mean germination percentage are not significant statistically (Table 5).

As to the mean number of leaves, the study results (Table 5) demonstrate that they were almost the same, both in the control plot and under the different acid-mixture treatments; they ranged from 9 to 11 leaves. Statistical testing revealed that there are no statistically significant differences in these numbers between the control and treatments or among treatments. So, differences in the average numbers of zucchini leaves between the control and treatments, as well as between the treatments, are statistically insignificant.

Comparison of the findings of this study with those of previous studies indicates similarities and differences. For example, El-Masry et al. (2012) reported that the application of HA to soil significantly increased the vegetative growth of squash (*Cucurbita pepo* L.), including the stem length, the number of leaves per plant, the leaf area, the total leaf area per plant, and the dry weights of stems and leaves. Meantime, the average fruit weight increased only slightly. Omar et al. (2020) obtained some similar results. They found that foliar application of potassium fulvate (6, 9, and 12 kg.acre^{-1}) to squash (*Curcurbita pepo* L.) resulted in improved growth and yield. Potassium fulvate application produced profound increases in plant length, leaf fresh weight, leaf dry weight, total leaf area per plant, fruit length, fruit diameter, fruit mass, and total yield. However, the best growth results were produced by the 6.0 kg.acre^{-1} treatment after the first 40 days of planting and by the 9.0 kg.acre^{-1} after 70 days of planting. This suggests that the relationship between squash growth and yield with concentration of potassium fulvate is not linear and that it is time-dependent; higher concentrations of this biostimulant are needed with time within the same growing season. Consequently, the best yield parameters were associated with the 9.0 kg.acre^{-1} treatment.

Table 5: Effect of addition of fulvic acid-humic acid mixture to irrigation water on plant germination and growth.

Plant	Acid Mixture Concentration	Germination Percentage	No. of Leaves	Fruit Shape	Fruit Mass
Zucchini	0	99.67 ^{a}	10.00 ^{a}	0.00 ^{b}	0.00 ^{b}
	0.5	100.00 ^{a}	11.00 ^{a}	4.76 ^{a}	1383.33 ^{a}
	1.0	99.67 ^{a}	10.33 ^{a}	0.00 ^{b}	0.00 ^{b}
	1.50	100.00 ^{a}	9.00 ^{a}	0.00 ^{b}	0.00 ^{b}
Cucumber	0	70.00 ^{c}	4.00 ^{b}	0.00 ^{b}	0.00 ^{b}
	0.5	90.00 ^{a}	7.00 ^{a}	2.00 ^{a}	250.00 ^{a}
	1.0	80.00 ^{b}	5.00 ^{b}	0.00 ^{b}	0.00 ^{b}
	1.50	90.00 ^{a}	4.00 ^{b}	0.00 ^{b}	0.00 ^{b}

Cucumber (*Cucumis sativus*)

Cucumber plants that received FA-HA mixture treatment generally had higher mean germination percentages than the control plants. Table 5 shows that the mean germination percentage of cucumber was 70.0% in the control plot. The FA-HA mixture concentrations of 0.50 $mL.L^{-1}$ and 1.50 $mL.L^{-1}$ did, each increased this percentage to 90.0%. Meanwhile, the FA-HA mixture concentrations of 1.0 $mL.L^{-1}$ increased the average germination percentage to 80.0%. This means that the concentrations of 0.50 $mL.L^{-1}$ and 1.50 $mL.L^{-1}$ have better effects on cucumber germination than the 1.0 $mL.L^{-1}$ concentration. These differences are statistically significant. That is treatment results in significantly higher germination percentages (80.0-90.0%) than the percentages obtained with no FA-HA mixture treatment (70.0%). In addition, the results (Table 5) indicate that the FA-HA mixture treatments have higher positive germination effects on Zucchini (99.67-100.0%) than on cucumber (80.0-90.0%).

Regarding the mean number of leaves of cucumber, the experimental results (Table 5) demonstrate that the mean numbers of leaves were very close in the control plot and under the 1.0 $mL.L^{-1}$ and 1.50 $mL.L^{-1}$ acid mixture concentration treatments. The mean number of leaves under the treatment of 0.50 $mL.L^{-1}$ acid mixture concentration was significantly higher (7) than the mean numbers of leaves of cucumber in the control plot (4) and under the other two treatments (5 and 4).

The foregoing findings were compared with the findings of previous studies. Hamail et al. (2014) found that foliar application of HA (20 $mL.L^{-1}$) to cucumber plants resulted in early fruit setting, reduced number of male flowers, an increased number of female flowers and fruits per plant, and a higher total yield. Foliar application of FA (20 $mL.L^{-1}$) gave comparable results. However, in comparison with HA, it led to earlier fruit setting, a higher reduction in the number of male flowers, higher increases in the numbers of female flowers and fruits per plant, and a higher total yield.

These results have some similarities with the results of previous studies. For example, El-Nemr et al. (2012) found that all growth parameters of cucumber (*Cucumis sativus* L.) increased by foliar application of HA (1.0, 2.0, and 3.0 $g.L^{-1}$) to this plant and that the higher the employed acid concentration, the higher the positive effects. The parameters included plant height, number of stems per plant, number of leaves per plant, fresh weights of leaves, number of fruits per plant, fruit mass, and plant yield. In addition, all treatments resulted in an earlier-than-usual fruit setting. Identical results were reported by Shafeek et al. (2016). However, the HA treatments in Shafeek et al. (2016) work corresponded to the application of acid solutions to the soil at concentrations of 3.0, 6.0, and 9.0 $L.acre^{-1}$. However, responses of all the aforementioned growth and yield parameters to the HA applications were identical in El-Nemr et al. (2012) and Shafeek et al. (2016) work, despite differences in the acid concentrations applied and the application methods.

CONCLUSIONS

Conclusions were drawn from the research results. One of these conclusions is that aqueous solutions of FA-HA mixture can be promising soil amendment and plant growth biostimulant that increases plant growth and yield and reduces plant stress. Another conclusion is that the addition of this acid mixture to water has noticeable effects on its pH and EC, as well as on those of the receiving soil. A conclusion, too, is that the FA-HA mixture treatments have higher positive effects on germination and growth (e.g., number of leaves) of zucchini than on cucumber. This suggests that zucchini responds better to the FA-HA mixture additions than cucumber. In other words, applying this acid mixture treatment to zucchini is more cost-effective than applying it to cucumber, which may need higher concentrations of this acid mixture or different combinations of the two acids to produce similar germination and growth to those of zucchini.

The researchers also conclude that FA-HA mixture application to soil has positive effects on plant growth until a certain concentration (0.50 $mL.L^{-1}$ in the present study), above which deleterious effects on plant growth are observed. This leads to the conclusion that the relationship between zucchini growth and yield with FA-HA mixture concentration is non-linear. The same applies to cucumber. It is also concluded that the optimum acid mixture concentration and application rate are crop-specific. Hence, for each crop, the most appropriate acid mixture concentration should be determined first before the broad-scale application of amendments to the soil to ensure the contribution of this environmentally friendly practice to sustainable agriculture.

REFERENCES

Bayat, H., Shafie, F., Aminifard, M.A. and Daghighi, S. 2021. Comparative effects of humic and fulvic acids as biostimulants on growth, antioxidant activity, and nutrient content of yarrow (Achillea millefolium L.) Sci. Hort., 279: 109912.

Canellasa, L.P., Olivaresa, F.L., Aguiara, N.O., Jonesb, D.L., Nebbiosoc, A., Mazzeic, P. and Piccolo, A. 2015. Humic and fulvic acids as biostimulants in horticulture. Sci. Hortic., 196: 15-27.

El-Masry, T.A., Osman, A.S., Tolba, M.S. and Abd El-Mohsen, Y.H. 2014. Increasing nitrogen efficiency by humic acid soil application to squash plants (Cucurbita pepo L.) grown in newly reclaimed saline. Soil Egypt. J. Hort., 41: 17-38.

El-Nemr, M.A., El-Desuki, M., El-Bassiony, A.M. and Fawzy, Z.F. 2012. Response of growth and yield of cucumber plants (Cucumis sativus L.) to different foliar applications of humic acid and bio-stimulators. Aust. J. Basic Appl. Sci., 6: 630-637

Gao, M., Tang, F., Wang, K., Zeng, F., Wang, Y. and Tian, G. 2022. The heterogeneity of humic/fulvic acids derived from composts explains the differences in accelerating soil Cd-hyperaccumulation by Sedum Alfredii. J. Environ. Manag., 301:113837.

Hamail, A.F., Hamada, M.S., Tartoura, E.A. and Abd El-Hady, M.A. 2014. Effect of N-forms and bio-stimulants on the productivity of cucumber: 2-flowering characters, yield and its components. J. Plant Prod., 5: 573-583.

Khalil, H.M., Laila, K.M.A. and Mahmoud, A.A. 2011. Impact of applied humic and fulvic acids on the soil physic-chemical properties and cucumber productivity under protected cultivation conditions. J. Soil Sci. Agric. Eng., 2: 183-201

Makrigianni, E.A., Papadaki, E.S., Chatzimitakos, T., Athanasiadis, V., Bozinou, E. and Lalas, S.I. 2022. Application of humic and fulvic acids as an alternative method of cleaning water from plant protection product residues. Separations, 9: 313.

Murbach, T.S., Glávits, R., Endres, J.R., Clewell, A.E., Hirka, A., Vértesi, A., Béres, E. and Szakonyiné, I.P. 2020. A toxicological evaluation of a fulvic and humic acids preparation. Toxicol. Rep., 7: 1242-1254.

Omar, M.M., Taha, A.A. and Shokir, S.A. 2020. Effect of applying potassium phosphite with potassium fulvate on plant growth. J. Soil Sci. Agric. Eng., 11: 255-263.

Ran, S., He, T., Zhou, X. and Yin, D. 2022. Effects of fulvic acid and humic acid from different sources on Hg methylation in soil and accumulation in rice. J. Environ. Sci., 119:93-105.

Shafeek, M.R., Helmy, Y.I. and Omar, N.M. 2016. Effect of spraying or ground drench from humic acid on growth, total output, and fruits nutritional values of cucumber (Cucumis sativus L.) grown under plastic house conditions. Int. J. PharmTech Res., 9: 52-57.

Nature Environment and Pollution Technology
An International Quarterly Scientific Journal

p-ISSN: 0972-6268
(Print copies up to 2016)
e-ISSN: 2395-3454

Vol. 23 | No. 1 | pp. 545-552 | 2024

Original Research Paper

https://doi.org/10.46488/NEPT.2024.v23i01.051

Open Access Journal

The Global Clothing Oversupply: An Emerging Environmental Crisis

M. S. Neethu and R. Bhuvaneswari†
School of Social Sciences and Languages, Vellore Institute of Technology, Vandalur-Kelambakkam Road, Chennai-600127, Tamil Nadu, India
†Corresponding author: R. Bhuvaneswari; bhuvanadoss@yahoo.co.in

Nat. Env. & Poll. Tech.
Website: www.neptjournal.com

Received: 07-07-2023
Revised: 08-08-2023
Accepted: 21-08-2023

Key Words:
Fast fashion
Nature
Ecology
Ecological sustainability
Green economy
Sustaincentrism
Pollution

ABSTRACT

Fashion is a potent visual indicator of our times, almost a language that speaks for us and something popular or in style, a zeitgeist. Fashion, specifically fast fashion, has gained prominence in discussions about fashion, sustainability, and environmental awareness. The speed of the hedonic treadmills continues to increase exponentially, and the so-called fast fashion has won legions of young fans who can snap up relatively cheap clothes online, but the trend masks darker environmental problems. Concerns about the fashion industry's environmental impact have increased in recent years. This realization was prompted by accumulated evidence of a rise in clothing consumption due to greater availability and affordability. This shift has fostered not only heedless and hasty clothing consumption but also heedless and hasty clothing disposal. This article attempts to elucidate the relationship between humans and the environment. It also tries to incorporate the concepts of sustaincentrism and traceability to pave the way for sustainable development. This study employs an experimental survey method to ascertain consumers' perceptions of sustainable fashion and to assess the implications of their current purchasing behavior. The SPSS software is used to analyze the data's reliability, and regression analysis was employed to determine the fashion industry's environmental impact. The survey results indicate optimism for a rise in ethical business strategies and the adoption of sustainable approaches within the fashion industry, thereby establishing a green economy.

INTRODUCTION

In recent years, the fashion industry has received severe criticism for its lack of concern for social and environmental problems, which has heightened the issue of fashion's non-economic consequences to the forefront of public consciousness. Fashion, nested in a broader system, has been at odds with sustainability. Consciously or unconsciously, industrialization has intensified its octopus-like stranglehold on nature for human purposes. Gadamer postulates, "If we continue to pursue industrialization, to think of work only in terms of profit, and to turn our earth into one vast factory as we are doing at the moment, then we threaten the conditions of human life in both the biological sense and in the sense of specific human ideals [love, justice, charity, peace] even to the extremes of self-destruction" (Gadamer 2013).

Fashion is no longer a privileged realm accessible only to the wealthy. Today, 'fast fashion' is widely available, rapidly produced, globally promoted, and universally embraced. This brand-new fashion reality is centered on affordability, made possible by using inexpensive fabrics. The underpinning of the fashion market hinges on deception. It was fuelled by the fallacy that consumers demand fashion, whose fickle preferences force clothing manufacturers to respond swiftly to these changes. Once upon a time, worn-out, repaired, and mended garments were repurposed as dishcloths and oil rags. In nations with a high standard of living, it is increasingly common to purchase, discard, and replace upholstered furniture, footwear, and clothing with the most recent fashions.

We are currently clamoring to combat climate change and pondering sustainable fashion. Sustainable fashion emphasizes a holistic approach that encompasses the entire lifecycle of fashion products, from design and production to use and disposal, to minimize harm and maximize positive social and environmental results. Therefore, sustainable fashion is fashion that is produced, used, and consumed in a responsible, socially ethical, and economically viable manner.

When analyzing The Indian textile industry has a long history of textile production embarking antiquity. India is one of the largest garment producers in the globe. The clothing industry significantly contributes to the Indian economy and employs millions. Since 2000, the fast fashion industry has been rooted in the Indian textile industry. Until then,

the Indian mindset was characterized by few purchasing excursions. In the 2000s, global fashion firms devised a business strategy that created 52 'micro seasons' per year, meaning a new collection is instigated weekly. Since then, the term 'fast fashion' has been used, especially for these global brands, to refer to the quick pace of fashion consumption spurred by the volume of new garments introduced to the market. According to the Indian Textile Journal, "In India, more than 1 million tonnes of textiles are thrown away every year, most of this coming from household sources. Textiles make up about 3% of the weight of a household bin. Textile waste is also the third largest source of municipal solid waste in India." (quoted in Lopes 2021)

The fashion industry thus contributes to environmental devastation to a certain extent; therefore, it is essential to investigate the fashion industry's problems and possible solutions. This article attempts to elaborate on the entanglements between humans and the environment and presents two opposing concepts: greenwashing and green economy. The article further investigates the viability of the term's traceability and sustaincentric in accelerating sustainable development. There is no getting away from dressing up because it has become a necessary element of daily life and is seen as an expression of one's personality.

The Glut of Fast Fashion: An Overview

The fashion industry has existed for centuries, fostering individuality and allowing people to express themselves and convey cultural stories through their attire. However, the industry, particularly fast fashion, contributes to numerous environmental, social, and economic issues. Due to its production and marketing strategies, it has been accused of not taking sufficient responsibility for its actions toward resolving environmental problems and issues of overconsumption of natural resources. A great deal of evidence has accumulated over the years to demonstrate the industry's catastrophic effects on the environment. There have been discussions in the fashion community about adopting new materials and economic models to reduce the environmental impact of fashion production, operations, utilization, and disposal (Brooks et al. 2017).

According to Rosenthal (2007), clothing can be distinctly divided into low-end, mass-market, and high-end items based on price, brand, and quality; however, the distinction between a skirt that costs $10 and one that costs $200 is now nearly indistinguishable. Items that appear upscale in design, brand, and quality can be purchased for less than the cost of a sandwich. As a result, in many locations, inexpensive, readily disposable clothing has replaced hand-me-downs and more durable garments as the primary source of clothing. Fashion traders are enticing customers to visit their stores frequently by marketing the idea of limited goods collections by nurturing the idea of "Here Today, Gone Tomorrow." This indicates a shortened life cycle and higher profit margins from the sale of merchandise that sells quickly, avoiding the markdown process (Sydney 2008).

In the article titled "Environmental Prospects for Mixed Textile Recycling in Sweden," global per capita apparel production increased from 5.9 kg to 13 kg per year between 1975 and 2018. Similarly, the estimated annual global consumption of apparel has increased to 62 million tonnes and is expected to reach 102 million tonnes by 2030. As a result, fashion firms now generate about twice as many clothes as they did before the year 2000 (Peters et al. 2019). Fast fashion is a business strategy based on giving consumers frequent novelty in the form of reasonably priced, trend-driven products. It has emerged as a result of the drastically rising textile production and fashion consumption. Instilling a sense of urgency when purchasing, fast fashion relies on frequent buying and impulsive purchases. Due to its consistent growth, higher profits than more conventional fashion retail, and the arrival of novel competitors like internet retailers, who can provide better agility and more regular delivery of new products, this business model has proven to be incredibly successful. (Anguelov 2015). The fast-fashion model is facilitated by the phenomenon of purchasing more items and donning them less frequently, which is exacerbated by low prices. The average American consumer purchases a new set of apparel every 5.5 days (MacArthur 2019).

According to Weinzettel and Pfister, cotton cultivation accounts for 87% and 93% of the total water consumption in the production of a T-shirt and a pair of jeans, respectively. Of all the fashion fibers, cotton has the biggest water footprint. Since 44% of cotton is cultivated for export, Cotton cultivation has an impact on local water use that is fuelled in part by worldwide demand. Using trade relations as a mirage, the EU consumes water from the Aral Sea for cotton production, which results in 20% water loss (Weinzettel & Pfister 2019)

When viewed in the context of the Indian fashion industry, the situation is strikingly similar. In India, 7800 kilotons of textile waste are accumulated annually. The majority of India's textile waste, approximately 51%, comes from Indian consumers - post-consumer waste - followed by factory waste and offcuts - pre-consumer waste - and imported waste, which contributes the remaining 7%. India's textile waste accounts for 8.5% of the global whole; only 59% of India's textile waste is reintroduced into the garment industry through reuse and recycling, and only a small portion returns to the global supply chain (Quest Impact Design Studio 2022).

MATERIALS AND METHODS

This article employs both Descriptive Research Design and Experimental Survey Research. The survey uses a snowball sampling technique. The reliability of the data is analyzed using Statistical Package of Social Sciences (SPSS) version 20. In SPSS, correlation and regression are two of the most frequently employed tests for data analysis. This article analyzed data using a regression test to find the relationship between fast fashion and its repercussions on the environment. The primary objective is to collect voluminous survey data to characterise how a representative sample of individuals perceive and interact with the fashion industry and determine what promotes sustainability in the industry. To pave the way for sustainable development, the research attempts to incorporate the concepts of sustaincentrism and traceability. This paper also attempts to argue that negative externalities at each stage of the fast fashion supply chain have imposed enormous ecological stress and created a global environmental justice dilemma. As we stand at the crossroads of ecocide, this paper also aims to revitalize the fashion surplus through the lens of ecological sustainability and rekindle the concept of a green economy.

Fashion and Environment

Fashion is a powerful visual indicator of our times, almost a language that speaks for us, or something popular or in style, a zeitgeist. Style is distinct from fashion in that what is prevalent today may no longer be so tomorrow. When a critical mass of the market reflects on what is fashionable and current in a time-sensitive manner, that product becomes fashionable. Everything depends on differing preferences. However, consumers do not change their initial opinions regarding what is fashionable. The fashion trendsetters, who have always been industry insiders, sustain the changing cycle. The fashion industry, not its consumers, determines the prevailing style. Therefore, fashion sales are driven by retailers rather than by consumers. Fast fashion has been a popular market segment with enviable growth. Fast fashion refers to "cheaply produced and priced garments that copy the latest catwalk styles and get pumped quickly through stores to maximize on current trends" (Maiti 2022). The COVID-19 pandemic completely halted the fashion industry. Now that the world is expanding, we want to dress up again for socializing and traveling. However, now is an excellent time to consider the repercussions of our apparel decisions, having lived a constrained and simpler lifestyle during COVID-19.

Today, 80 billion apparel items are produced annually, nearly 400% more than twenty years ago. The speed of hedonic treadmills continues to increase exponentially, and so-called fast fashion has gained legions of young fans who can purchase inexpensive clothing online. However, the trend conceals deeper environmental issues. According to the State fashion report, one in three young women considers once-or-twice-worn apparel outdated. In addition to the logistical issue of ineffective environmental practices regarding land use, water contamination, and carbon ejections, there is a genuine systemic attitude of 'want' to be reflected in consumer markets. This may result in a decline in the perceived value of clothing in the eyes of consumers, as affordable clothing and new fashion trends entice and persuade consumers to seek out more. The standard practice of fast fashion retailers is to adopt celebrity fashion trends to mass-produce and sell significantly less expensive fast fashion clothing, which is produced at unprecedented speed to meet consumer demand. This type of embezzlement occurs frequently among independent designers.

Today's fashion market is highly competitive, and the constant need to 'refresh' product ranges means that there is an inevitable move by many retailers to extend the number of 'seasons,' that is, the frequency with which the entire merchandise within the store is changed. With the emergence of small collections of merchandise, fashion retailers are encouraging consumers to visit their stores more frequently with the idea of 'Here Today, Gone Tomorrow.' This indicates a shorter life cycle and higher profit margins from the sale of fast-selling merchandise, skipping the markdown process altogether (Sydney 2008).

Environmental Impacts

To assess the environmental effects of fast fashion, a survey was conducted as part of the research. The sample considered for participation in this survey comprised 205 respondents between the ages of 18 and 65, with samples selected based on convenience. The geographic scope of the investigation is limited to customers and brands in South India. An infinite population was drawn from the population pool for a basic random cross-sectional sample. The responses were collected regardless of gender or profession. To make the survey more compatible, it was conducted via Google Forms. The respondents include college students, researchers, and professionals from various fields.

The graph below (Fig. 1) depicts the purchasing frequency of consumers throughout the year. Reviewing the pie chart reveals that more than 50% of individuals typically purchase apparel within a six-month window, and more than 40% do so within a three-month window. This statistic also demonstrates the frequency with which we engage in compulsive purchasing, and this behavior causes environmental damage.

To determine whether respondents favor eco-friendly clothing brands, we received various responses indicating

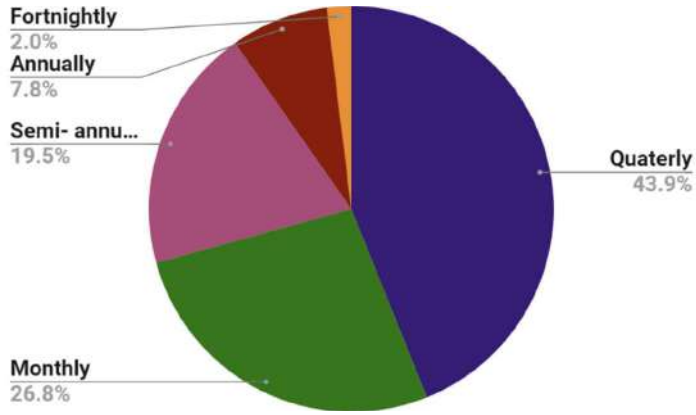

Source: Author

Fig. 1: Frequency of buying clothes.

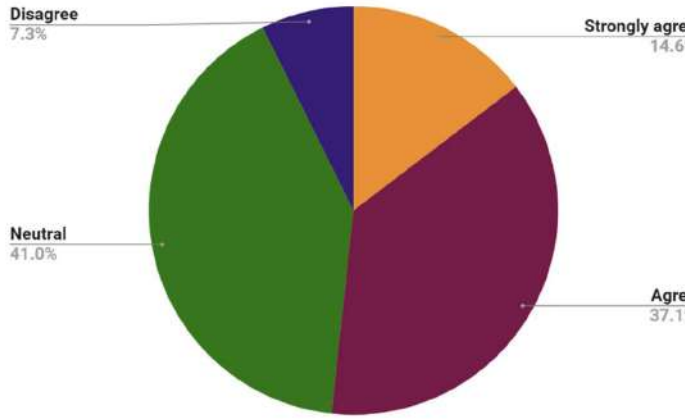

Source: Author

Fig. 2: Preference for eco-friendly clothing brands.

that over 51% of respondents prefer eco-friendly clothing brands. The other half of the population is entirely apathetic toward eco-friendly brands (Fig. 2).

While throwing light on the repercussions of fast fashion on our nature the most perennial among them was its reverberations in polluting the water sources. The garment industry is the second-largest consumer of water and polluter of water globally. "It consumes one-tenth of the water used industrially to run factories and clean products. It takes 10,000 liters of water to produce 1 kg of cotton or approximately 3,000 liters of water for one cotton shirt" (Le 2020).

This procedure generates approximately 20% of the wastewater, ultimately ending up in our oceans. Unfortunately, this untreated wastewater is exceptionally hazardous, and in many cases, it cannot be made secure. In addition to exacerbating water scarcity, the garment industry affects local water supplies by generating effluents. As some industrial chemicals are toxic, improperly treated wastewater penetrating the local groundwater may deteriorate the ecosystem. While taking into account Cambodia's case, "the fashion industry, which is responsible for 88% of all industrial manufacturing (as of 2008), has caused an estimated 60% of water pollution and 34% of chemical pollution" (Anguelov 2015).

Synthetic materials are the primary culprits that cause plastic microfibers to enter our oceans. To be exact, approximately 35% of all microplastics are from these synthetic materials. To further lower the price, producers turn to materials that may be of low quality. For example, many of the fibers are made of polyester, consisting of plastic, and tend to release far more carbon emissions than cotton (Le 2020).

As we consider, the introduction of viscose rayon as an alternative to cotton production in the 1890s accelerated carbon emissions and the use of chemicals in its production.

The high carbon footprint of the fashion industry results from its high energy consumption, which is affected by the energy source. For instance, "in China, textile manufacturing depends on coal-based energy and, as a result, 40% more carbon footprint than textiles made in Turkey or Europe. High energy demands and CO_2 emissions are associated with textile manufacturing and consumer use (namely, laundering), as well as shipping when air freight is used" (Peters et al. 2019). "However, in the garment life cycle, energy use and CO_2 emission are highest during initial fiber extraction, especially for synthetic fibers, such as acrylics, as they originate from fossil fuels" (Munasinghe et al. 2016). As there is a consumer temperament that well-known apparels are produced in foreign countries. As a result of the processing and transportation of raw materials from one country to another using various methods, more non-recyclable plastics and cardboard boxes are produced.

While contemplating ecological sustainability in the fashion industry, we must identify the circumstances that impede sustainable development. To promote sustainable development in the fashion industry, we must consider second-hand stores or thrift shops in our current environment. The opinion of consumers regarding thrift stores is displayed in Table 1.

The table illustrates the association between the preference for thrift stores and other independent variables. This table makes it abundantly evident that the values are statistically significant (<0.05) or that the dependent variable is related to the independent variables. The significance of the values demonstrates that current fashion trends and celebrity models influence consumers to purchase a more significant proportion of novel products and are hesitant to purchase used clothing.

According to the data in Table 2, celebrity fashion and the newest fashion industry trends prompted consumers to make more purchases without considering the environmental impact. According to them, fast fashion is environmentally damaging. Ironically, more than half of consumers are unconcerned about the environmental impact of the apparel they purchase despite being aware that it hurts the environment.

The effects of fast fashion on the environment are illustrated in Table 3. As demonstrated, a value of less than 0.05 indicates that one's attire influences how others perceive them and contributes to environmental degradation. The way we dress and the variety we add to our wardrobes to appear fashionable and alluring to others contribute to environmental degradation.

In recent decades, there has been a meteoric rise in textile consumption. Even though it may benefit the economy, more waste is being disposed of in landfills. As low-quality clothing deteriorates after just a few launderings, the demand for new clothing increases. According to Frost, the globe consumes approximately 80 quadrillion new apparel items annually, fourfold the amount consumed just two decades ago (Frost 2019). This indicates that humans are producing

Table 1: Regression variable for DV1 and IVs

Model	Unstandardized Coefficients		Standardized Coefficients	T	Sig.
	B	Std. Error	Beta		
(Constant)	1.556	0.536		2.902	0.004
What is your preferred shopping mode for clothing?	0.304	0.135	0.176	2.252	0.026
I keep up with the latest fashion trends in clothing	0.270	0.118	0.198	2.287	0.024
Celebrities' and models' fashion sense influences your choice of apparel.	0.232	0.101	0.208	2.301	0.023

a. Dependent Variable: I prefer thrift stores for clothing (Second-hand clothing).

Table 2: Regression variable for DV2 and IVs.

Model	Unstandardized Coefficients		Standardized Coefficients	t	Sig.
	B	Std. Error	Beta		
(Constant)	2.201	0.530		4.154	0.000
I keep up with the latest fashion trends in clothing.	0.212	0.117	0.164	1.814	0.072
Celebrities' and models' fashion sense influences your choice of apparel.	0.136	0.100	0.130	1.368	0.174

a. Dependent Variable: When you shop, do you contemplate the effects of your actions on the environment?

Table 3: Regression variable for DV3 and IVs.

`	Unstandardized Coefficients		Standardized Coefficients	t	Sig.
	B	Std. Error	Beta		
(Constant)	1.731	.410		4.224	0.000
The way you dress influences how other people perceive you	0.108	0.077	0.125	1.403	0.163

a. Dependent Variable: Fast fashion affects the environment.

more textile debris than ever before. Savannah Rags, one of the recycling industries in Nottingham, England, noted that only 25% of the garments brought to the facility are recycled.

In comparison, the remaining 75% are sent to landfills in Africa, Finland, and other developing nations. When we travel through third-world countries, particularly Africa, the industrialized West, which has garnered the benefits of modernization, is compelled to pause or reflect. Every year, developed countries dump 300,000 tonnes of post-consumer waste in these nations, leading to landfills and making it the fastest-growing waste category worldwide. It is appraised that by 2050, global clothing will end up more than triple.

In addition to producing waste, the fashion industry also misleads consumers through greenwashing. Greenwashing has increased green skepticism and would mislead consumers about the environmental strategies followed by a company or the environmental benefits of a product or service. Greenwashing convinces consumers that a company's products are environmentally friendly and deceives customers who favor sustainable fashion brands into purchasing the company's products. The most prevalent form of greenwashing is the use of environmental imagery, deceptive labels, language, and concealed trade-offs, in which a company emphasizes any one sustainable aspect of a product while engaging in environmentally destructive actions.

Sustainability and Fast Fashion

Sustainability, as defined by the Brundtland World Commission on Environment and Development (UN 1987), is a development that "(meets) the needs of the present without compromising the ability of future generations to meet their own needs" (Sustainability). According to the 'Triple Bottom Line (TBL)' of sustainability, sustainable practices are evaluated from three perspectives, namely environmental, economic, and social. According to Gladwin's technocentric perspective, as mentioned in the article "Shifting paradigms for sustainable development: Implications for management theory and research," the economy is a confined, nature-isolated system in which only industrial and familial exchanges of value occur. Human desires are limitless, and as a result, the ideal of a happy existence is prevalent. As anticipated by the optimal economic framework of laissez-faire capitalism, individuals, therefore, act to maximize their utility. According to the ethics of ethnocentrism, more growth is not merely desirable but the ideal of all conceivable worlds. Sustaincentrism emphasizes the coexistence of humans and nature, the importance of satisfying non-material demands through non-material means, and a reduction in materialistic attitudes. In sustaincentrism, where ethics, economics, and ecology are all intertwined, ecological and social externalities are internalized. Sustaincentrism, which combines ecocentrism with practical socio-economic considerations, emphasizes the interconnectedness of cause and effect and holds that all human values are contingent on a sustainable ecological, economic, and social environment (Gladwin et al. 1995).

In recent years, consumer ethics has played a substantial role in addressing the "throwaway culture." Ethical consumers take into account the effects of a product's consumption on the environment, humans, and animals (Barnett et al. 2005). Although ethical customers are concerned with environmentally friendly products and practices, many customers have yet to execute these methods for certain commodities, according to research (Harrison et al. 2005, Carrigan & Attalla 2005). Herein arose the need for a new set of problem-solving strategies, one of which is sustaincentrism. In the fashion industry, we analyze fast and slow fashion through their respective conceptual frameworks and outline the key elements of a sustaincentric perspective. According to an anthropocentric hierarchy with human beings at the apex, humans believe in the right to subjugate nature for their own needs. This viewpoint assumes that there is no need to concern future generations and resource availability and that nature is only an instrumental and economically quantifiable one —a resource to be exploited. Green production is another concept that aligns with the sustaincentrism philosophy. Vachon & Klassen (2008) noted that green production exercises can assist businesses in achieving the economic benefits of a more extensive consumer base and gaining a competitive advantage.

Traceability is an equally important concept in the fashion industry alongside sustainability. In reference to the fashion industry, traceability facilitates transparency. In the 1980s,

the food industry witnessed the introduction of traceability. This technique can also be applied to the textile industry to create a greener environment and a more sustainable future. Traceability in relation to the fashion industry paves the way for transparency, which informs customers about the environmental ramifications of clothing and manufacturing as well as the working conditions in various units of garment industries. The entire clothing production process needs to be traceable by the public for better clarity, which could increase demand for ethically produced goods while diminishing the appeal of those produced under questionable conditions.

From the perspective of Indian fashion, there is a clear connection between natural fibers and ethical, ecological textile production. Natural fibers are prevalent in India and were regarded as the foundation of the Indian textile industry despite competition from synthetic alternatives. Natural fiber composites have numerous applications in the building, construction, packaging, textile, and furniture industries. Cotton, silk, jute, wool, and linen are among the numerous natural fibers that hold enormous potential for Indian agriculture.

In recent years, the terms 'sustainable' and 'organic' have gained popularity in India's fashion industry. Consequently, many companies have pledged to be entirely organic and use only natural fibers. Growing environmental concerns, which India's increasingly dangerous COVID-19 outbreak has aggravated, are encouraging veteran Indian designers like Rohit Bal, Rajesh Prasad Singh, and Ritu Kumar to revive forgotten regional weaves, support artisan communities, and utilize eco-friendly materials. The natural hand-spun fabrics used by Delhi-based designer Gautam Gupta are made from bananas, bamboo, coffee beans, and natural silks. Pero Recycle and Pero Upcycle, two new labels by the designer Aneeth Arora, are devoted to environmental protection. In addition to the Handloom and Handicrafts Development Programme and the Sustainable Fashion and Indian Textiles (SUIT) initiative, the Indian government has devised several programs to promote sustainable fashion. These programs aim to promote the production of eco-friendly textiles and the development of sustainable fashion enterprises. By embracing natural fibers, India's fashion is progressively becoming more egalitarian and environmentally responsible. These novel ideas unwrap the idea of a green economy, which endeavors to mitigate environmental risks and ecological scarcities. UNEP has defined the green economy as "one that improves human well-being and social equity while significantly reducing environmental risks and ecological scarcities. It is low carbon, resource efficient, and socially inclusive" (UNEP 2011).

Also, at the consumer level, we can prevent infringement by altering our perception of overproduced clothing and clothing brands. If you can afford to go on frequent shopping sprees, rather than purchasing large quantities of clothing from fashion brands, purchase your clothing from reputable retailers. Sewing is another way to combat fast fashion. Sewing was an ordinary skill our generation no longer seems to possess. Our ancestors sewed holes and buttons rather than discarding their clothing, which is not a novel concept. There are viable alternatives to viscose, such as cellulosic fibers, that are more environmentally friendly. In Finland, a company known as Spinnova has converted fibers from wood into recyclable fibers without involving chemical components such as caustic soda, carbon disulfide, and sodium hydroxide, which are typically detected in viscose (Le 2020). Spiders' web weaving inspired the application of this technique to wood fiber material. It consumes relatively little amount of water compared to the production of cotton fabrics. This strategy would ensure non-toxic because it employs reusable fibers and provides evidence that procuring sustainability is feasible for many other businesses. A second option for this is a second-hand store. There are second-hand retailers all over the world. Many websites and apps also offer a vast selection of pre-owned apparel, ranging from inexpensive to branded items.

CONCLUSION

The fashion industry has a long way to go regarding sustainable fashion. However, it progresses as more businesses and consumers adopt environmentally responsible products and purchasing practices. Numerous new strategies are being presented, and support is being provided for sustainable fashion, ranging from small fair-trade businesses to industry leaders. The collected data indicate optimism for a rise in ethical business strategies and the adoption of sustainable approaches and practices in the industry, as indicated by the results of the survey. It is possible to discern a company's direction and priorities by investigating where and how sustainability fits into the larger corporate structure. It is essential to remember that there is no one-size-fits-all structure; each company must tailor its strategies to what makes the most sense given its business model, organizational structure, available resources, and level of sustainability integration.

The most effective method for combating fast fashion is discouraging these fashion companies from overproducing. For this reason, consumers must reconsider the impact of their growing clothing demand. Therefore, we cannot merely blame the fashion industry for its disregard for the environment; it is also the customers' responsibility to promote sustainability and protect the environment. Customers must view fashion as a utilitarian product

rather than an amusement, and they must be willing to pay higher costs that reflect the environmental reverberation of fashion. As with this soiled linen, we may not immediately observe the effects, but they will eventually suffocate us. By emphasizing a greener wardrobe and purchasing fewer, more cost-effective classics that endure the test of time and fashion, it is possible to impact society significantly. As our planet continues to deteriorate, we are learning to purchase, use, and discard items with greater care merely because Planet B does not exist. We must consider the diversity of our wardrobes, and our instant gratification is at the expense of the environment. A sustainable lifestyle is not an option; it is a requirement.

REFERENCES

Anguelov, N. 2015. The Dirty Side of the Garment Industry: Fast Fashion and Its Negative Impact on Environment and Society. CRC Press, Florida.

Barnett, C., Cloke, P., Clarke, N. and Malpass, A. 2005. Consuming ethics: Articulating the subjects and spaces of ethical consumption. Antipode, 37(1): 23-45. https://doi.org/10.1111/j.0066-4812.2005.00472.x

Brooks, A., Fletcher, K., Francis, R.A., Rigby, E.D. and Roberts, T. 2017. Fashion, sustainability, and the Anthropocene. Utop. Stud., 28(3): 482-504. https://doi.org/10.5325/utopianstudies.28.3.0482

Carrigan, M. and Attalla, A. 2001. The myth of the ethical consumer – do ethics matter in purchase behavior? J. Consum. Market., 18(7): 560-578. https://doi.org/10.1108/07363760110410263

Frost. 2019. Vogue features Zara's sustainability pledge, but is it greenwashing? Retrieved from https://www.euronews.com/green/2019/07/17/vogue-feature-zara-s-sustainability-pledge-but-is-it-greenwashing (accessed May 12, 2023)

Gadamer, H. 2013. Truth and Method. Bloomsbury Publishing, London.

Gladwin, T.N., Kennelly, J.J. and Krause, T. 1995. Shifting paradigms for sustainable development: Implications for management theory and research. Acad. Manag. Rev., 20(4): 874-907. https://doi.org/10.5465/amr.1995.9512280024

Harrison, R., Newholm, T. and Shaw, D. 2005. The Ethical Consumer. SAGE Publications Ltd, NJ. https://doi.org/10.4135/9781446211991

Le, 2020. The Impact of Fast Fashion on the Environment. Retrieved from https://psci.princeton.edu/tips/2020/7/20/the-impact-of-fast-fashion-on-the-environment. (accessed date June 7, 2023)

Lopes, F. 2021. Climate change: How fast fashion hurts the environment. IndiaSpend: Data journalism, analysis on Indian economy, education, healthcare, agriculture, politics. Retrieved from https://www.indiaspend.com/earthcheck/climate-change-how-fast-fashion-hurts-the-environment-793662 (accessed date May 25, 2023)

MacArthur. 2017. Circular Economy. How to Build a Circular Economy | Ellen MacArthur Foundation. Retrieved from https://www.ellenmacarthurfoundation.org (accessed date May 27, 2023)

Maiti, R. 2022. Fast fashion: Its detrimental effect on the environment. Earth. Org. Retrieved from https://earth.org/fast-fashions-detrimental-effect-on-the-environment/ (accessed date May 25, 2023).

Munasinghe, M., Jayasinghe, P., Ralapanawe, V. and Gajanayake, A. 2016. Supply/value chain analysis of carbon and energy footprint of garment manufacturing in Sri Lanka. Sustain. Prod. Consump., 5: 51-64. https://doi.org/10.1016/j.spc.2015.12.001

Peters, G.M., Sandin, G. and Spak, B. 2019. Environmental prospects for mixed textile recycling in Sweden. ACS Sustain. Chem. Eng., 7(13): 11682-11690. https://doi.org/10.1021/acssuschemeng.9b01742

Quest Impact Design Studio. 2022. Wealth in Waste: India's Potential to Lead Circular Textile Sourcing. Fashion for Good. Retrieved from https://fashionforgood.com/our_news/wealth-in-waste-indias-potential-to-lead-circular-textile-sourcing/ (accessed date June 15, 2023).

Rosenthal, M. 2007. Can Polyester Save the World? New York Times. Retrieved from https://www.nytimes.com/2007/01/25/fashion/25pollute.html (accessed date May 25, 2023).

Sydney. 2008. Fast fashion is not a trend. https://www.sydneylovesfashion.com/2008/12/fast-fashion-is-trend.html

United Nations (UN). 1987. Sustainability. Retrieved from https://www.un.org/en/academic-impact/sustainability (accessed date May 21, 2023).

United Nations Environment Programme (UNEP). 2011. Green Economy. Retrieved from https://sustainabledevelopment.un.org/index.php? (accessed date May 23, 2023).

Vachon, S. and Klassen, R.D. 2008. Environmental management and manufacturing performance: The role of collaboration in the supply chain. International Journal of Production Economics, 111(2), 299-315. https://doi.org/10.1016/j.ijpe.2006.11.030

Weinzettel, J. and Pfister, S. 2019. International trade of global scarce water use in agriculture: Modeling on a watershed level with monthly resolution. Ecol. Econ., 59: 301-311. https://doi.org/10.1016/j.ecolecon.2019.01.032

ORCID DETAILS OF THE AUTHORS

M. S. Neethu: https://orcid.org/0000-0003-2072-8296
R. Bhuvaneswari: https://orcid.org/0000-0003-4660-7118

Nature Environment and Pollution Technology
An International Quarterly Scientific Journal

p-ISSN: 0972-6268
(Print copies up to 2016)
e-ISSN: 2395-3454

Vol. 23 | No. 1 | pp. 553-557 | 2024

Original Research Paper

https://doi.org/10.46488/NEPT.2024.v23i01.052

Open Access Journal

The Association Between CO_2 Emission and Temperature in Thailand

Piyavadee Srivichai†
Program in Environmental Health, School of Public Health, University of Phayao, Phayao 56000, Thailand
†Corresponding author: Piyavadee Srivichai; piyavadee.sr@up.ac.th

Nat. Env. & Poll. Tech.
Website: www.neptjournal.com

Received: 20-07-2023
Revised: 08-09-2023
Accepted: 10-09-2023

Key Words:
Carbon dioxide
Climate change
Temperature
Emission
Energy

ABSTRACT

The important source of carbon dioxide (CO_2) emission is identified to be energy usage, which the demand is gradually increasing. Currently, many people are exposed to increasing temperatures, which affects to health, environment, and quality of life. Moreover, there are many worries about its continuously increasing trend. This work is interested in studying the association between the annual CO_2 emission and the annual mean temperature in Thailand. At a confidence interval of 90%, a statistically significant association between the annual CO_2 emission and the annual mean temperature was observed. The appropriate predictive equation represented that the CO_2 emission at 0.481 M ton increased the annual mean temperature by about 1°C. The results are useful for planning the reduction of CO_2 emissions in Thailand. Fascinatingly, the largest source comes from electricity production, and the most significant energy type is finished oil. Therefore, they should be controlled as the priority. Integrated methods are considered as more efficient strategies for the CO_2 crisis.

INTRODUCTION

Awareness raising about carbon dioxide (CO_2) emission occurs in many countries around the world. Especially the 192 countries joined the Kyoto Protocol in 2005. These are committing industrialized and transitive economic countries that can afford to decrease greenhouse gas (GHG) emissions according to accepted individual targets (United Nations Climate Change 2023). CO_2 is a major greenhouse gas as the cause of far-ranging adverse health and environmental effects (U.S. Environmental Protection Agency 2023).

Thailand is a large CO_2 emission source, releasing up to 263 Mton in 2018, most of it was from fuel combustion (Energy Policy and Planning office 2023). Presently, the Thai government has a long-term target to decrease greenhouse gas emissions by 20% by 2030, as compared with 2005. This was submitted in October 2021 under the Paris Agreement (Ministry of Energy 2011). The amount of CO_2 is related to climate change by trapping heat in the atmosphere (Picano et al. 2022). There are many potential health risks of CO_2 exposure, such as inflammation, bone demineralization, kidney calcification, decrease in more-level cognitive abilities, endothelial disorder, and oxidative stress (Tyler et al. 2019, Breeze Technologies 2020). As well known that multiple advantages will be obtained from the reduction of CO_2 emissions, such as saving the environment and protecting people's health. Moreover, large and immediate economic co-benefits are obtained, which can help to reduce a lot of costs for mitigating air pollution and environmental crisis (Grantham Research Institute 2017).

This research aims to study the association between the annual CO_2 emission and the annual mean temperature in Thailand. In addition, quantifies the main economic sections and energy types related to CO_2 emission. Their applications need to be considered, planned, and managed properly.

MATERIALS AND METHODS

The secondary data consisting of the annual mean temperature, the total energy usage, and the emission of CO_2 were obtained from the Energy Policy and Planning Office (EPPO), Ministry of Energy, Thailand. The year 2009-2022 were selected as the study period. After that, a single linear regression analysis was used to assess the association between the annual CO_2 emission and the annual mean temperature in Thailand with the enter method. Lastly, the proper predictive equation was developed to predict the annual mean temperature from the CO_2 emission volume in Thailand.

RESULTS AND DISCUSSION

Thailand Overview Situation

Thailand's temperature trend: It is noteworthy that the annual mean temperature trend fluctuated strongly all the time (Fig. 1). Thailand's average temperature is now

around 27.2°C warmer than its temperature in 2009 equals 27.4°C. It has continuously increased by about 0.2°C in this study period, which will result in people being exposed to dangerous heat. There are warnings that every 1°C of warming higher than normal level will affect area drought and labor productivity, including a reduction of economic growth by approximately 1.3% per year (Duan et al. 2022). It is predicted that the Thai temperature will reach up to 1 degree Celsius in 2092, approximately 70 years later. Anxiously, unawareness of the CO_2 emissions will lead Thailand to approach many serious problems shortly.

Trends in Thailand's energy usage and CO_2 emission: The energy usage and the total CO_2 emission have the same trend as presented in Fig. 2. It indicates that the energy usage is related directly to the CO_2 emission. Excluding 2020, they were reduced a bit, which resulted from The Thailand Energy Efficiency Plan 2018 - 2037 (EEP 2018). The EEP 2018 has many mitigation measures to reduce energy usage (Department of Alternative Energy Development and Efficiency 2015).

The calculation of CO_2 emissions per capita is around 3.75 tons per capita in Thailand in 2022 (based on the number of populations at 66,090,475 persons. (National Statistical Office 2022). As compared with the top thirty countries in 2011 stayed in the range of 32.47 – 7.51 tons per capita, and the low-middle-income country was average at 1.77 tons per capita. This pointed out that Thai people release a higher CO_2 level than the typical middle-income country, up to

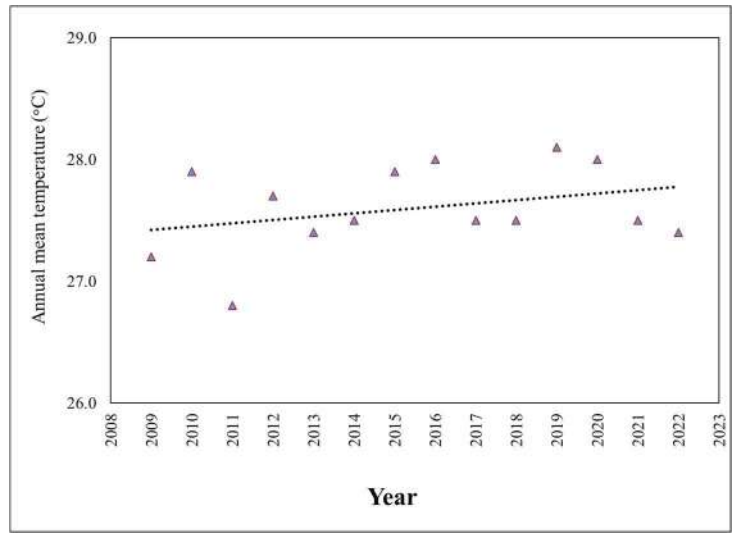

Fig. 1: The annual mean temperature of Thailand between 2009 and 2022.

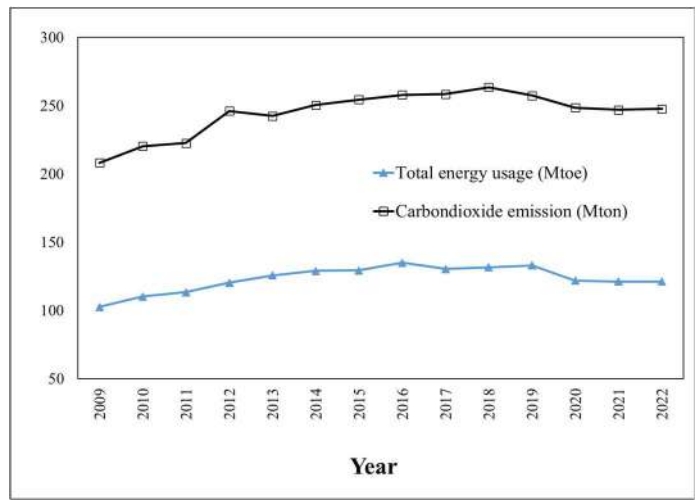

Fig. 2: The total energy usage and the CO_2 emission in Thailand.

2.12 times, which the Thai government should be aware of limiting CO_2 emissions (Amin 2011).

The Association Between the CO_2 Emission and the Mean Temperature

The simple linear regression result: Analysis of variance (ANOVA) was used to illustrate the association between the CO_2 emission and the mean temperature (Table 1). The P value less than 0.10 means that there is a significant association at 90% confidence intervals. Nevertheless, it shows a low R square value because it may have even noisy or high variable data. Therefore, the application of the obtained equation to predict the future annual mean temperature should be careful.

The predictive equation model of the annual mean temperature from the CO_2 emission in Thailand was represented using Eq.1 as follows:

The annual mean temperature (°C) = 0.481 The total CO_2 emission (M ton) …(1)

Particularly, the CO_2 emission rising around 0.481 Mton led to the increase in annual mean temperature by 1°C (Tables 2 & 3).

The results pointed out that Thailand would require the reduction of CO_2 emissions. According to the Paris Agreement of 2015 committed to trying to decrease GHG enough to limit warming to lower than 2 degrees by 2100 (Wike 2019). Nordhaus (2017) found that the social cost of carbon management was about 31 dollars per ton of CO_2 in 2010. It is estimated the huge boundary costs for managing and mitigating carbon in Thailand that is the end-of-pipe (EOP) method. Moreover, a lot of hidden costs are spent and lost, such as images of tourists, quality of life, etc. Thus, preventive measures are more appropriate, such as CO_2 source reduction, emission minimization, etc. Additionally, there was a study about the advantages and disadvantages of a carbon tax for reducing and managing CO_2 emissions (Prasad 2022).

Table 1: The ANOVA results.

Parameter	Sum of squares	Df	Mean Square	F value	P value
Regression	0.388	1	0.388	3.602	0.082
Residual	1.292	12	0.108		
Total	1.680	13			

Table 2: The appropriate analysis of the predictive equation.

R	R square	Adjusted R square	Standard error of the estimate
0.481	0.231	0.167	0.328

Table 3: The coefficients of the predictive equation.

Parameter	Unstandardized coefficients		Standardized coefficients	t value	P value
	B	Standard error	Beta		
Constant	25.008	1.368		18.275	0.000
Total CO_2 emission	0.011	0.006	0.481	1.898	0.082

The Emission of CO_2 Divided by Economic Sections and Energy Types

Following the result, the largest CO_2 portion released from electricity production rose to the maximum record at 99 Mton in 2016. In 2023, the total annual Thai electricity net production by all-scale electric power plants of approximately 16,003 GWh from various energy sources consisting of natural gas (51%), coal (16%), renewable energy (14%), water energy (4%), and oil (1.4%) (Ministry of Energy 2023).

Both the transportation and industry sections are quite in the same values (Fig. 3). Interestingly, the decrease in CO_2 emission of the industry section was in 2022 because of the COVID-19 delay. In contrast, the transportation section had an increasing CO_2 emission level.

Nowadays, the governor encourages increasing renewable and alternative energy (waste to energy, heat, wind, biogas, biomass, solar energy) by 20% instead of fossil energy by 2030 (International Renewable Energy Agency 2017). This policy may benefit the country by providing the following effective and practical measures for the reduction of CO_2 emissions.

Consideringly, CO_2 emissions are categorized by energy types (Fig. 4). Most CO_2 emissions were from the use of finished oil by about 36.62-41.91%. In the present day, the finished oil is used for various purposes in Thailand, such as electricity production, transportation, and several industries. Unsurprisingly, it is the largest source of CO_2 emission. Additionally, there was a rising trend from 2009 until the present, which had a temporary decrease only in 2020 and 2021 during the Covid crisis.

It is followed by natural gas and coal, respectively. Markedly, there is a bit of difference between both. Mostly, the use of coal released CO_2 lower than the use of natural gas, except for 2021. This is the consequence of the increase in electricity consumption and the start of economic recovery after the Covid crisis. At the end of the graph (2015 - 2022), the CO_2 emission from natural gas had a small reduction. On the other hand, the distribution from coal depicted the high fluctuated values. This is because of uncertain occurrences

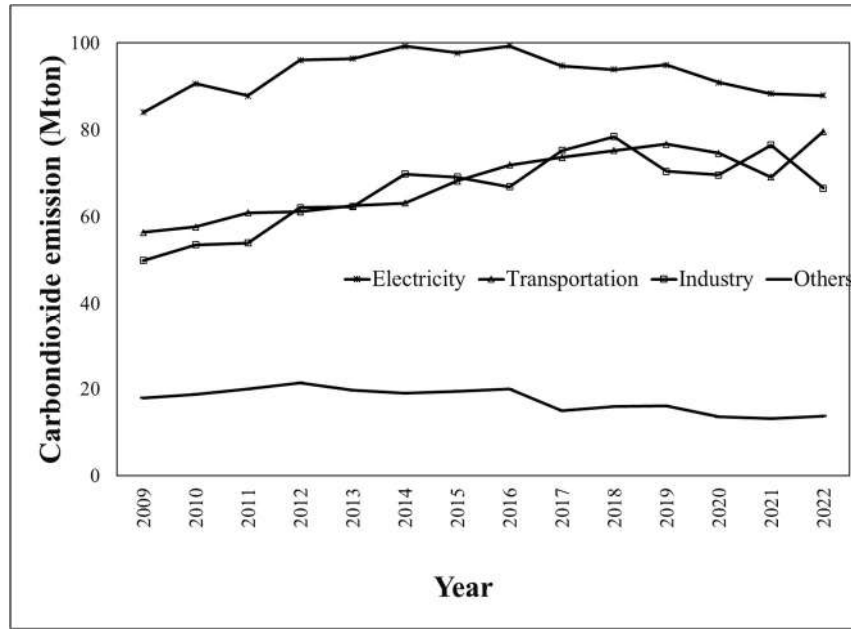

Fig. 3: The annual CO_2 emission divided by economic sections.

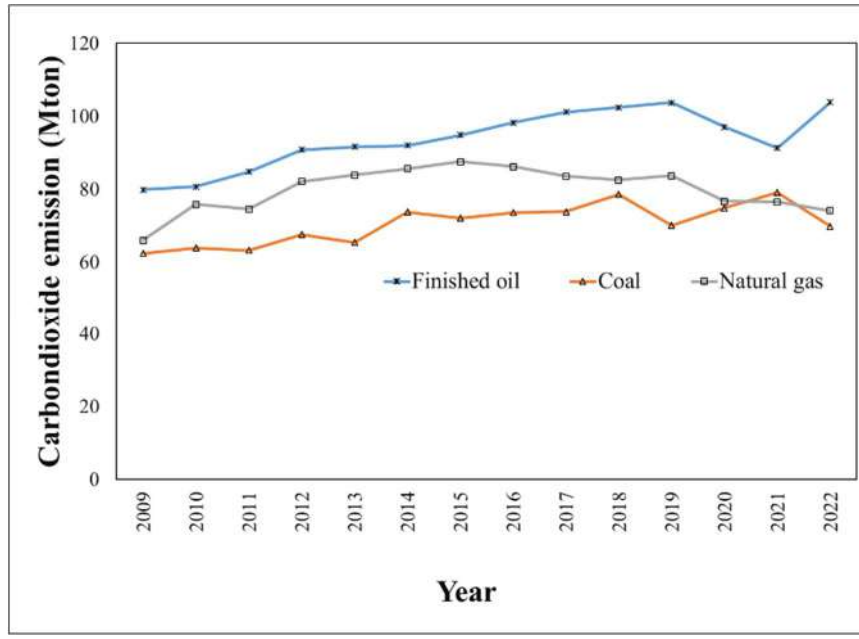

Fig. 4: The annual CO_2 emission divided by types of energy.

such as the Covid crisis, the Russia-Ukraine war, the energy crisis, etc.

CONCLUSION

The trend of annual mean temperature was presented to continuously increase between 2009 and 2022 in Thailand. The CO_2 emission is related directly to energy usage. Also, the statistical result indicated that the volume of CO_2 emission has a significant association with the annual mean temperature. The CO_2 emission at 0.481 M ton led to the rise of annual mean temperature by 1°C. In addition, the highest quantity of CO_2 was generated from the electricity production process. In the future, it will require a continuous

increase to a higher level. Interestingly, finished oil is the most important energy type of CO_2 emission, approximately 36.62-41.91%. Thus, the use of finished oil should be reduced and used properly.

REFERENCES

Amin, M.C. 2011. The Target of Limiting Global Warming to Less Than 1.5 Degrees Is Practically Dead. Why Do Emissions Per Capita Matter? Retrieved from https://www.atlanticcouncil.org/blogs/econographics/the-target-of-limiting-global-warming-to-less-than-1-5-degrees-is-practically-why-do-emissions-per-capita (accessed date June 9, 2023)

Breeze Technologies. 2020. The Health Impact of Specific Air Pollutants. Retrieved from https://www.breeze-technologies.de/blog/health-impact-of-specific-air-pollutants (accessed date June 13, 2023)

Department of Alternative Energy Development and Efficiency. 2015. Energy Efficiency Plan 2015-2036 (EEP 2015). Retrieved from https://www.eppo.go.th/images/POLICY/ENG/AEDP2015ENG.pdf (accessed date)

Duan, H., Yuan, D., Cai, Z. and Wang, S. 2022. Valuing the impact of climate change on China's economic growth. Econ. Anal. Poli., 74: 155-174.

Energy Policy and Planning Office. 2023. Economic Data and Analysis. Retrieved from https://www.eppo.go.th/index.php/en/en-energystatistics/energy-economy-static (accessed date June 10, 2023)

Grantham Research Institute. 2017. Economic co-benefits of reducing CO_2 emissions outweigh the cost of mitigation for most big emitters. Retrieved from https://www.lse.ac.uk/granthaminstitute/news/economic-co-benefits-of-reducing-co2-emissions-outweigh-the-cost-of-mitigation-for-most-big-emitters/ (accessed date June 13, 2023)

International Renewable Energy Agency. 2017. Renewable Energy Outlook: Thailand, International Renewable Energy Agency, Abu Dhabi. Retrieved from https://www.irena.org/publications/2017/Nov/Renewable-Energy-Outlook-Thailand (accessed date June 13, 2023)

Ministry of Energy. 2011. Thailand 20-Year Energy Efficiency Development Plan (2011 - 2030). Minister of Energy Thailand. Retrieved from https://www.eppo.go.th/images/POLICY/ENG/EEDP_Eng.pdf (accessed date June 9, 2023)

Ministry of Energy. 2023. The Overview of Energy January 2023. Retrieved from https://www.eppo.go.th/images/Energystatistics/energyinformation/Energy_Statistics/00All.pdf (accessed date June 13, 2023)

National Statistical Office. 2022. Demography Population and Housing Branch. Retrieved from http://statbbi.nso.go.th/staticreport/page/sector/en/01.aspx (accessed date June 9, 2023)

Nordhaus, W.D. 2017. Revisiting the social cost of carbon. PNAS., 114(7): 1518-1523.

Picano, E., Mangia, C. and D'Andra, A. 2022. Climate change, carbon dioxide emission, and medical imaging contribution. J. Clin. Med., 20(12): 1-9.

Prasad, M. 2022. Hidden benefits and dangers of carbon tax. PLOS. Clim., 1(7): 1-10.

Tyler, A.J., Jasdeep, S.K., Michael, T.H., Rudolf, K.B., Keith, C.M. and William, E.F. 2019. Direct human health risks of increased atmospheric carbon dioxide. Nat. Sustain., 2: 691-701.

U.S. Environmental Protection Agency. 2023. Overview of greenhouse gases. Retrieved June 12, 2023, from https://www.epa.gov/ghgemissions/overview-greenhouse-gases

United Nations Climate Change. 2023. What is the Kyoto Protocol? Retrieved from https://unfccc.int/kyoto protocol (accessed date June 12, 2023)

Wike, C. 2019. CO_2 Emissions Are on Track to Take Us Beyond 1.5 Degrees of Global Warming. Retrieved from https://www.sciencenews.org/article/co2-emissions-global-warming (accessed date June 13, 2023)

ORCID DETAILS OF THE AUTHORS

Piyavadee Srivichai: https://orcid.org/0000-0002-6762-5465

Nature Environment and Pollution Technology
An International Quarterly Scientific Journal

p-ISSN: 0972-6268
(Print copies up to 2016)
e-ISSN: 2395-3454

Vol. 23 | No. 1 | pp. 559-568 | 2024

Original Research Paper

https://doi.org/10.46488/NEPT.2024.v23i01.053

Open Access Journal

Energy Requirement of Wastewater Treatment Plants: Unleashing the Potential of Microalgae, Biogas and Solar Power for Sustainable Development

Urvashi Gupta*, Abhishek Chauhan*†, Hardeep Singh Tuli, Seema Ramniwas***, Moyad Shahwan****(*****) and Tanu Jindal***

*Amity Institute of Environmental Toxicology, Safety and Management, Amity University, Noida, India
**Department of Biotechnology, Maharishi Markandeshwar (Deemed to be University), Mullana, Ambala, Haryana, India
***University Centre for Research & Development, University Institute of Pharmaceutical Sciences, Chandigarh University, Gharuan, Mohali, Punjab, India
****Department of Clinical Sciences, College of Pharmacy and Health Sciences, Ajman University, Ajman 346, United Arab Emirates
*****Centre of Medical and Bio-Allied Health Sciences Research, Ajman University, Ajman 346, United Arab Emirates
†Corresponding author: Abhishek Chauhan; akchauhan@amity.edu

Nat. Env. & Poll. Tech.
Website: www.neptjournal.com

Received: 07-07-2023
Revised: 11-09-2023
Accepted: 21-09-2023

Key Words:
Wastewater
Sewage treatment plant
Biofuel
Solar energy

ABSTRACT

Sustainable energy legislation in the modern world is the primary strategy that has raised the benchmark for energy and environmental security globally. The rapid growth in the human population has led to rising energy needs, which are predicted to increase by at least 50% by 2030. Waste management and environmental pollution present the biggest challenge to developing countries. The improvement of energy efficiency while ensuring higher nutritional evacuation wastewater treatment plants (WWTPs) is a significant problem for many wastewater treatment plants. Some treatment techniques require high energy input, which makes them expensive to remediate water use. Pollutants like chemical pesticides, hydrocarbons, colorants (dyes), surfactants, and aromatic compounds are present in wastewater and are contributing to other problems. Israel consumes 10% of the global energy supply, significantly more than other countries. The lagoon and trickling filters are the most widely used technologies in South African WWTPs, where the electricity intensity ranges from 0.079 to 0.41 $kWh.m^{-3}$ (Wang et al. 2016). Korea and India use almost the same energy (0.24 $kWh.m^{-3}$). An estimated one-fifth of the energy used in a municipality's WWTPs is used for overall public utilities, and this percentage is anticipated to rise by 20% over the next 15 years owing to expanding consumption of water and higher standards. In this review paper, we examined the potential for creating energy-self-sufficient WWTPs and discussed how much energy is currently consumed by WWTPs. The desirable qualities of microalgae, their production on a global level, technologies for treating wastewater with biogas and solar power, its developments, and issues for sustainable development are highlighted. The scientific elaboration of the mechanisms used for pollutant degradation using solar energy, as well as their viability, are the key issues that have been addressed.

INTRODUCTION

The primary strategy that has raised the standard of energy and environmental security globally is sustainable energy legislation in the present world. The enhancement of the energy effectiveness of the current facilities is one of its pillars. The infrastructure for water and sewage systems in cities is the biggest consumer of electricity, accounting for as much as %40 of total consumption. The whole water management industry accounts for %4 of the power usage in the globe. The actions intended to improve resource efficiency in the industry are needed because of the rising wastewater production and water demand. Global nutrient requirements, as well as water and energy restoration from wastewater, are currently the main forces driving the development of the wastewater industry. Due to the inclusion of energy generation and resource rehabilitation during the manufacture of safe and clean water, urban wastewater treatment plants can be a significant component of circular sustainability.

It is significant to note that electricity accounts for 20% of the expenditures associated with the supply and treatment of water supply and sometimes even up to 40% of the operating budget of water business units (Di Fraia

et al. 2018). Furthermore, it is anticipated that municipal water supply mechanisms will use an additional 60–100% more energy in the coming 15 years (Masłoń et al. 2018). Global nutrient requirements, as well as water and energy restoration from wastewater, are currently the main forces driving the development of the wastewater industry (Neczaj & Grosser 2018). The near future will see the development of "ecologically sustainable" technological systems for WWTPs. However, over the past 25 years, many significant forces have highlighted the necessity of recovering the resources present in wastewater.

Rising energy needs are a result of the quick increase in the human population, and by 2030 those needs are expected to rise by at least 50%. Natural petroleum is unable to keep up with the current rate of consumption, which is already 105 times faster than what nature can produce. Additionally, the use of fossil fuels harms our environment by emitting greenhouse gases, which contribute to global warming. Thus, finding "clean" energy has become one of the most difficult tasks. Several alternatives are being researched and used right now. Biofuels, or fuels derived from living organisms, are advantageous for the environment because they reduce harmful CO_2 and hydrocarbon emissions and eliminate SOx emissions, which reduces the greenhouse effects.

The primary obstacle to developing nations comes from the management of waste and environmental contamination. A major issue for numerous wastewater treatment plants is the advancement of energy efficiency while ensuring higher nutritional evacuation (WWTPs). Water bodies are disturbed, and surface and groundwater are contaminated as a consequence of poor treatment and the release of industrial contaminants into the environment. According to estimates from the World Health Organization (WHO), 1.8 billion people do not have adequate drinking water that is safe to consume. The amount of drinkable water that is readily available for direct utilization is less than 1% of the total water capacity. According to the United Nations and other nations, having access to safe, clean water is a human right of fundamental importance (Pandey et al. 2021).

Energy from the sun's interfacial evaporation is a process used in desalinated water, treatment of wastewater, generation of electricity, and residential water heating systems as a reliable way to capture solar energy and remove the soluble pollutants in water (Gao et al. 2019, Geng et al. 2019). Interfacial evaporation of solar energy occurs when sunlight's thermal energy is transferred to water molecules at the air-water interface, where it continuously evaporates into steam (Tao et al. 2018, Li et al. 2019). The Electricity Regulatory Commission Act of 1998 developed the Regulatory Commissions to promote innovation in the electricity sector by fostering competitive pressure, boosting efficiency, and promoting economic growth in the electricity industry. India is also at the forefront of economic growth by focusing on the change in the power sector (Sharma et al. 2012). Our attention has been focused on using renewable energy as a source of energy that is environmentally friendly due to the alarming challenge of a growing population and depleting natural resources. The addition of renewable energy to the energy mix would reduce the system's reliance on the grid connection, increase system reliability in terms of efficiency, and reduce carbon emissions (Singh 2016).

There has been a lot of interest in photothermal materials with high energy conversion and broad solar absorption nowadays. They are quickly expanding as a research area of interest in the generation of clean water by solar-driven vaporization. The eco-sustainable water vaporization technology powered by solar energy has attracted interest as a long-term remedy for the shortage of water (Gao et al. 2019). In this review paper, we investigated the possibility of developing energy-self-sufficient WWTPs and talked about the energy consumption of WWTPs today. The advantages of microalgae, their production on a global scale, biogas and solar energy technologies for wastewater treatment, as well as their advancements and concerns for sustainable development, are highlighted. The key issues have been addressed, including the scientific development of the processes used for the degradation of pollutants using solar energy and their viability.

WASTEWATER TREATMENT PLANTS (WWTPS)

Wastewater treatment plants (WWTPs) are a necessary component of a local government framework. To transport wastewater, carry out technological processes, and run office equipment, these facilities need to be supplied with a sizable amount of electricity (Di Fraia et al. 2018). An important portion of an object's operational costs, in particular, go towards ensuring the continued viability of industrial applications (Roots et al. 2020). Consequently, there continues to be a demand for solutions to increase the efficacy of both thermal and electrical energy production and recovery at WWTPs. Because of this, cutting-edge technologies for wastewater treatment that rely on embedded methods, such as the Anammox process (Wang et al. 2019) or agglomerated activated sludge (Czarnota et al. 2020) for nitrogen extraction, are being developed. The water resource has been heavily polluted by inorganic compounds, organic, as well as other harmful emissions as a result of rapid industrialization. When compared to more traditional alternative technologies, these systems are distinguished by their lower energy consumption. Additionally, different

Fig. 1: Wastewater system (Neczaj & Grosser 2018).

aeration system operational and control strategies are used, as well as energy consumption optimization using a sophisticated, fully automated system for collecting data, simulation, and prediction (Drewnowsk 2019, Szeląg 2020).

WWTPs are gradually becoming a key hub for SMART cities. Fig. 1 depicts the idea of an intelligent wastewater system in which WWTPs produce energy and fertilizer in addition to treating wastewater effectively enough to allow for effluent reuse. Around the world, more and more cities are putting SMART ideas into practice. The City of Bors in Sweden, for instance, has developed a project in which the local power plant and the WWTP will coexist, and the WWTP will provide renewable fuel for the city power plant (Swedish Utility Selects Veolia for Wastewater to Energy Project (Metering 2018).

The demand for freshwater at this time has exponentially increased. In India, Pakistan, and other parts of the world, there is a critical need for fresh water. The amount of water used in manufacturing has greatly increased over the past few years. Water shortages are a result of corporate water use (Sharshir et al. 2020). This phenomenon aims to treat regenerative/non-biodegradable wastewater that cannot be adequately treated using industrially common biological and medicinal processes. To enhance the efficacy of contaminant oxidation that exists in wastewater and maintain economic growth, untreated pharmaceutical industry effluent was oxidized using a heterogeneous photo-catalytic method (Haddeland et al. 2014).

Freshwater availability is now the main concern for contemporary society. The process of treating wastewater that has been adulterated by business and manufacturing operations requires a lot of energy and relies on traditional energy sources. There is growing interest in solar energy as a potential solution for water treatment. The level of sophistication in solar-powered treatment of wastewater can range from basic Solar stills and Solar Water Disinfection (SODIS) to advanced Membrane distillation (MD), Multi-Stage Flash (MSF), and Reverse-osmosis (RO). The choice of these technologies depends greatly on the site. Solar still and SODIS are appropriate for tropical nations with plenty of solar energy but lacking resources and skilled labor (Sansaniwal 2022).

An organic semiconductor material called a photocatalyst possesses an established activity-level framework according to sound quantum theory (Bahnemann 2004).

The global issue of long-term energy and the decrease of freshwater can be resolved using solar energy, which is plentiful and accessible in many places. Researchers try their best to find various solutions to this issue. Since solar energy is a source of fresh water, numerous studies have been done to increase the effectiveness of solar desalination, evaporation, and wastewater treatment (Sharshir et al. 2020).

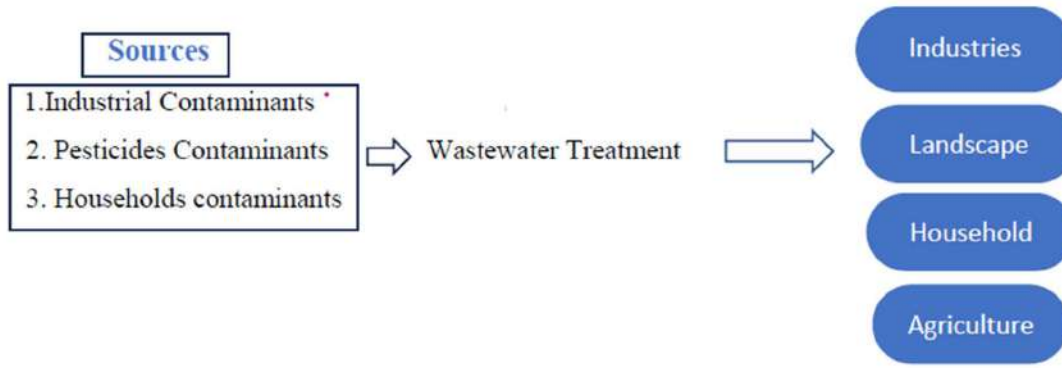

(Source: Pandey et al. 2021).

Fig. 2: Usage of solar energy in wastewater treatment.

POLLUTANTS PRESENT IN WASTEWATER

Drinking water demand is rising quickly, along with population growth. The primary source of drinking water is increasingly being harmed by pollution discharge from the industrial sector as well as the agricultural sector (Agalit et al. 2020). These contaminants, even in small quantities, pose a serious threat to the ecosystem and public health. Therefore, before being discharged or put to other uses, the human pollutant needs to be effectively differentiated from water and wastewater. In addition to organic pollutants, synthetic pesticides, and industrial effluents are now significant contributors to wastewater contamination. Despite being discharged in small amounts, these effluents pose a serious threat to freshwater and marine species, seriously disrupting the ecological system.

The existence of pharmaceutical substances in aquatic environments may have an impact on equal biota as well as the health of humans because these micropollutants can change the metabolism and reproductive capabilities of the aquatic ecosystem's live organisms. These pollutants primarily enter the aquatic environment through the effluents of wastewater treatment plants (WWTPs). Diclofenac (DCF) and carbamazepine (CBZ) are two examples of substances that endure treatment with little to no degradation (Casierra-Martinez 2020).

Dye is a crucial chemical in many sectors, including manufacturing, food, furniture, and agriculture. In actuality, dumping dye pollutants into water has seriously harmed the environment and human health. Many researchers around the world are urged to create standard techniques for effectively treating dye wastewater employing solar energy (Haddeland et al. 2014). Traditional methods, such as microbial breakdown, coagulation, flocculation, adsorption on active carbon, adsorption filtration, and sewage, have been used to treat dye-polluted water. Endocrine disruptors, pesticides, industrial dyes, and other contaminants of the utmost importance are found in the environment.

Waste from domestic sources that consists of toxic materials is considered a household pollutant. Due to rising levels of pollution from municipal solid waste, household garbage is currently attracting more attention. It can be determined whether a household pollutant will have an adverse effect on the natural environment or human health by understanding how it gets from a home to a disposal facility. Waste from domestic sources that contain hazardous substances is considered a household pollutant. Due to rising levels of pollution from municipal solid waste, household waste has recently received more attention. Knowing how household pollutants are transported to disposal sites can help determine whether they have the potential to harm the environment or the health of humans (Pandey et al. 2021). A significant contributor to environmental pollution is the leather industry. Even after treatment at a Common Effluent Treatment Plant (CETP), the wastewater produced by the leather manufacturing sector has extremely high pollution-related parameters because of its containment of an intricate combination of inorganic and organic contaminants, which interferes with the ecological ecosystem (Yadav 2019).

Wastewater treatment plants should strive to maximize their energy efficiency. Rising energy prices emphasize the demand for energy self-sufficiency in WWTPs and worries about climate change. Studies on energy-self-sufficient WWTPs have been conducted to lower operating expenses, minimize energy use, and attain balancing of carbon.

ENERGY-SELF-SUFFICIENT WASTEWATER TREATMENT PLANTS

Wastewater treatment plants should strive to maximize their energy efficiency. Rising energy prices emphasize the demand for energy self-sufficiency in WWTPs and worries about climate change. Studies on energy-self-sufficient WWTPs have been conducted to lower operating expenses, minimize energy use, and attain balancing of carbon (Gu et al. 2017).

Wastewater treatment plants (WWTPs) must become energy self-sufficient if they are to sustainably meet the environmental regulatory requirements that are changing quickly. Only a small portion of WWTPs worldwide currently generate energy for useful purposes, and only a few of these facilities are energy-independent (Sarpong & Gude 2020).

There are typically three phases in a traditional municipal WWTP: primary, secondary, as well as advanced. The energy expenditure for collecting and pumping raw wastewater for primary treatment varies from 0.02 to 0.10 $kWh.m^{-3}$ in Canada, 0.04 to 0.14 $kWh.m^{-3}$ in Hungary, and 0.01 to 0.37 $kWh.m^{-3}$ in Australia (Pitas et al. 2010). According to reports, the average energy input for conventional activated sludge (CAS) treatment processes is 0.46 $kWh.m^{-3}$ in Australia, 0.26 $kWh.m^{-3}$ in China, 0.33 $kWh.m^{-3}$ to 0.60 $kWh.m^{-3}$ in the USA, and 0.30 $kWh.m^{-3}$ to 1.89 $kWh.m^{-3}$ in Japan (Bodik & Kubaska (2013)). The part of the wastewater treatment technology with the highest energy consumption is the aeration process in secondary treatment (Liu 2012). Most medium-sized and large WWTPs with CAS systems use between 50 and 60 percent of their total electricity for aeration, 15 to 25 percent for sludge treatment, and 15 percent for secondary sedimentation involving recirculation pumping systems (Mamais 2015). The reported average

Table 1: Depicts energy distribution in standard activated sludge setups (Gu et al. 2017).

Conventional activated sludge system	Percentage Energy distribution
Chlorination, Return Sludge Pumping, and Thickening	1%
Clarifiers and Belt Press	3%
Lighting and buildings	6%
Anaerobic digestion	11%
Wastewater Pumping	12%
Aeration	60%

energy intensity in India was reported to be lower than that in the UK (0.46 kWh.m^{-3}) as a result of the support of low-energy technologies that utilize up-flow anaerobic sludge blanket (UASB) reactors or employ sunlight to generate heat for sludge drying in India. (Lee et al. 2017).

Table 1 and Fig. 3 display the outcomes of the overall distribution of energy in CAS systems. Because of the longer duration of hydraulic retention time (HRT) and greater consumption of electricity for a higher specific demand for oxygen, the oxidation ditch (OD) has a greater amount of energy demand compared to the CAS system of 0.5-1.0 kWh.m^{-3} (Australia), 0.302 kWh.m^{-3} (China), or 0.43-2.07 kWh.m^{-3} (Japan) (Yang et al. 2010).

USAGE OF ENERGY OF WWTPS IN DIFFERENT LOCATIONS

Comparing the amount of energy used in WWTPs across the world is interesting and crucial. Table 1 displays the energy intensity proportion and national-level consumption of energy in WWTPs for various nations. With an average unit electrical use for WWTPs of 0.52 kWh.m^{-3}, the USA is a standard established nation. According to estimates, the USA's annual electricity consumption for wastewater treatment in 2008 made up 0.6% of the total (Wang et al. 2016). Asian nations exhibit a lesser energy strength for the treatment of wastewater in comparison to the USA. (China 0.31 kWh.m^{-3}, Japan 0.304 kWh.m^{-3}, in addition to Korea 0.243 kWh.m^{-3}) (Wang et al. 2016, Chae et al. 2013).

Energy is mainly regarded as a cost factor in wastewater design in India. The preparation for the supply of water and energy is not yet being done in a systematic, integrated manner. Saving energy in WWTPs is becoming more popular, especially for wastewater plants that have not yet been built. In Delhi, it is required of the electricity provider to maintain a steady supply to WWTPs, minimizing power outages. Newly constructed WWTPs must generate up to 60% of their electricity, typically through the production of combined heat and power biogas. Although Delhi has implemented a national feed-in tariff for biogas, none of

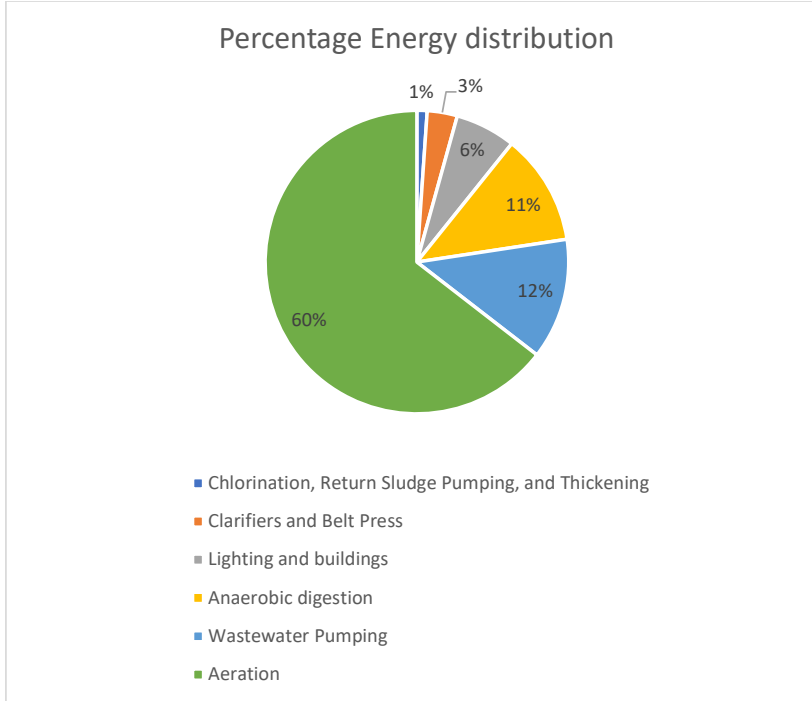

Fig. 3: Percentage of energy distribution in typical activated sludge systems.

Table 2: National-level intensity of energy proportion and consumption in WWTPs in 44 countries.

Countries	Process and WWTPs	Energy intensity [kWh.m^{-3}]	Reference
Korea	Municipal WWTPs	0.243	Chae and Kang (2013)
India	Conventional Activated Sludge in Delhi	0.24	Never and Stepping (2018)
Germany	Average of 10,200 WWTPs	0.40-0.43	Wang et al. (2016)
Brazil	Conventional activated sludge system	0.24	Never and Stepping (2018)
Japan	Municipal WWTPs	0.304	Yang et al. (2010), Soares et al. (2017)
Sweden	Municipal WWTPs	0.42	Olsson (2012), Soares et al. (2017)
China	i) Humic filter ii) Aeration trench or anoxide-oxide system or rapid infiltration	0.31 0.4 – 0.5	Wang et al. 2016 Soares et al. 2017
South Africa	i) Lagoon treatment technology ii) Activated sludge	0.079-0.41 0.33–0.61	Wang et al. (2016
USA	i) Encina Water WPCF, CA ii) With chlorine disinfection in NYCDEP Owls Head WWTP, NY	0.52 0.29	Wang et al. (2016)
Israel	NA	NA	Olsson (2012)
Greece	Activated Sludge Wastewater Treatment Plants	0.12, and 2.19	Siatou et al. (2020)

the WWTPs are currently producing excess biogas for transmitting electricity back to the grid. Table 2 displays the national-level intensity of energy proportion and consumption in WWTPs for various nations.

Israel uses 10% of the energy in the world, which seems like a lot more than other nations. The severe water shortage issue in Israel may have played a role in this. The most popular technologies for the lagoon and trickling filters are used in South African WWTPs, where the electricity intensity ranges from 0.079 to 0.41 kWh.m^{-3} (Wang et al. 2016). The energy intensity of India and Korea utilizes almost the same 0.24 kWh.m^{-3}. According to estimates, a municipality's total energy use for public utilities accounts for about one-fifth of the energy used in its WWTPs, and due to rising water consumption and stricter regulations, this percentage is expected to increase by 20% over the next 15 years. Therefore, it is essential to optimize the WWTP's energy utilization efficiency.

BIOFUELS AS A PROMISING ALTERNATIVE AND RENEWABLE ENERGY

Biofuels are fuels that have energy from living organisms that have recently fixed carbon in the earth's atmosphere. Starch, vegetable oils, animal fats, waste biomass, or algal biomasses—all of which are non-toxic, biodegradable, and renewable—can be used to make biofuels (Song 2008). Biofuels are divided into first, second, third, and fourth-generation biofuels based on the types of feedstocks used and their current and future availability (UNEP 2009). They benefit the environment because when used, harmful emissions like those of CO_2, hydrocarbons, and particulate matter are reduced, and Sox emissions are eliminated, which reduces the impact of greenhouse gases. In actuality, burning biofuels releases less carbon into the atmosphere than burning fossil fuels because the carbon released is already present in the current carbon cycle (Popp 2014).

The generation of biogas in WWTPs can be increased in several ways. The use of a process for anaerobic co-digestion (AcoD) is among the most promising. To increase the efficiency and stability of the anaerobic digestion (AD) process, a suitable, carefully chosen substance is added to the primary substrate. Several applications of the AD process have been reported thus far (Rabii 2019).

Microalgae: A Versatile Option for Sustainable Energy

Microalgae have long been regarded as a promising replacement for renewable feedstock in the manufacture of biofuels. This study evaluated the probable suitability of two different species, *Chlorella minutissima* along *Nannochloropsis gaditana*, to be assessed as essential components for ethyl esters that produce biodiesel value considering the presence of the numerous oleaginous strains of microalgae (Zorn 2022). Microalgae have received a lot of attention recently due to their potential as energy crops, the worth of the natural products they produce, and their capacity to clean up effluents. Algal fuel, also known as oilgae or third-generation biofuel, is a biofuel made from algae. This is the best course of action for the production

of biofuels because algae have enormous possibilities for renewable energy functions (like a low-input, high-yield prospect) (Satyanarayana 2011). As a result, this potential may make it possible to completely replace transport fuels made from petroleum without resorting to the contentious "food for fuel" argument. Microalgal biofuels are receiving more attention these days as a result of growing issues over fossil fuels, availability of energy, greenhouse gas emissions, and the claim that other biofuels can be used as "food for fuel" (Pienkos 2009).

The global energy crisis and rising greenhouse gas emissions have sparked the need for new, renewable energy sources that are environmentally friendly. Microalgae biofuel has the potential to displace fossil-based fuels and is one of the primary forms of renewable energy for sustainable growth, according to life cycle analysis. The main drawbacks of oil crops and lignocellulose-based biofuels were not present in microalgae biofuel. Algae-based biofuels are technically, economically, and cost-competitively viable. They don't need any new lands, use a lot less water, and reduce Iic CO_2. However, because of the low concentration of biomass and expensive downstream processes, the commercial manufacture of microalgae biodiesel is still not practical (Medipally 2015).

Designing sophisticated photobioreactors and creating low-cost methods for harvesting, drying, and oil extraction from biomass will enable the viability of microalgae-based biodiesel production. In order to control environmental stress conditions and engineer metabolic pathways for high lipid production, commercial production can also be achieved by enhancing genetic engineering techniques. Algal-bacterial interactions for enhancing microalgal growth and lipid production are among the new emerging technologies that are being investigated. This review primarily focuses on the issues that arise during the commercial generation of microalgae biofuels as well as potential solutions (Udayan 2022).

SOLAR-POWERED AND BIOGAS WASTEWATER TREATMENT TECHNOLOGIES: ADVANCEMENTS AND CHALLENGES FOR SUSTAINABLE DEVELOPMENT

Water treatment systems that are economical and sustainable are essential for developing countries. The availability of water is failing to keep up with the growth in the human population in India. Based on tested theory and technology, a flexible, affordable, and environmentally friendly wind/solar-powered wastewater treatment system is suggested. The proposed system is used to demonstrate how it functions in a household in India where wastewater is recycled utilizing an innovative combination of water purification devices driven by solar/wind energy. The system that is being used in this demonstration is specifically made for small-scale applications, such as for a single household.

Access to clean water is now the main concern for contemporary society. The process of treating wastewater that commercial and industrial operations have contaminated requires a lot of energy and relies on traditional energy sources. There is growing interest in solar energy as a potential solution for water treatment. Simpler systems like solar stills and SODIS and more sophisticated ones like MD, MSF, and RO can all be used to treat wastewater using solar power. The choice of these technologies depends greatly on the site. For tropical countries with plenty of solar energy but little investment or skilled labor, solar still and SODIS are suitable. Compared to solar MSF and solar MD, solar MED is more economically and technologically competitive. Although prohibitively costly, the PV-RO system is feasible. Modern market opportunities could result from these technologies being upgraded (Sansaniwal 2022).

All types of waste management demand a lot of energy, which is hard to come by during the global energy crisis. Both types of waste, i.e., solid and liquid, are actively treated using a lot of solar energy. According to Ugwuishiwu et al. (2016), methods including solar desalination, solar pathogenic organic destruction, solar photocatalytic degradation, along solar distillation are implemented to treat liquid waste. The challenges of cleaning up wastewater using solar energy are highlighted in the following section and are illustrated in Fig. 4 despite the advantages of each technique for water treatment (Pandey 2021).

Wastewater is regarded as an alternative way to generate energy (Frijns 2013). The biogas formed in the digester is the major source of energy in a WWTP. In comparison to a WWTP without sludge digestion, one with pre-settling and sludge digestion uses 40% less net energy on average. Some WWTPs, including Strass (Austria) (Schaubroeck 2015), Steinhof (Germany) (Remy CaL 2015), Sheboygan (America) (Sheboygan 2015), and others have adopted sludge anaerobic digestion with Combined Heat and Power (CHP). Sludge digestion is already widespread practice in the Netherlands, where many WWTPs produced 95 million Nm^3 of biogas in 2006, which was then converted to electricity (143 MWh) and heat (used to heat the digestion reactor) by a CHP mechanism (Frijns 2013). Several WWTPs integrate kitchen wastes with sludge for anaerobic co-processing to stabilize kitchen waste materials. This aids in substrate modification, improves organic loads, biogas yields, and the generation of energy, as well as increases equipment capacity factor, and lowers investment (Kai 2005). Although it still needs a lot of development before it can be used in practice,

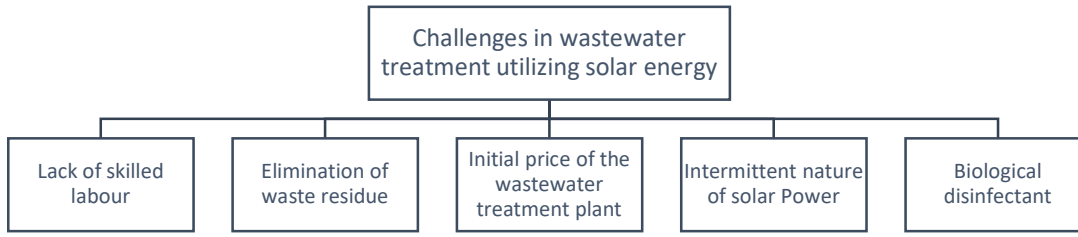

Fig. 4: Challenges in WWTPs using solar energy.

microbiological fuel cell (MFC) technology can generate electric power from wastewater (Li 2015).

A significant source of renewable energy is the thermal energy found in wastewater. Thermal energy generated from wastewater can be used to heat nearby homes or be transmitted to the district heating system by using heat exchangers and heating pumps. Using China as an example, it is entirely feasible to offset the energy deficit caused by insufficient energy conversion from excess sludge by recovering at least 50% of the energy consumed by a WWTP from thermal energy (Hao 2015). The amount of heat generated during treatment processes exceeds the amount of energy required for plant heating. Changing the heat source of heat pumps for district heating from wastewater to cooling water regeneration is another way to provide heat and save money at the same time.

Rising energy needs are a result of the quick increase in the human population, and by 2030, those needs are expected to rise by at least 50%. The current rate of consumption, which is reportedly 105 times faster than what nature can produce, cannot be met by natural petroleum (Maness 2009). Furthermore, the combustion of fossil fuels harms our environment by emitting greenhouse gases, which causes global warming. Thus, finding "clean" energy has become one of the most difficult tasks. Various alternatives are currently being researched and put into practice. Biofuels, or fuels derived from living organisms, are advantageous for the environment because they reduce harmful CO_2 and hydrocarbon emissions and eliminate SOx emissions, which reduces the greenhouse effects. Scenedesmus obliquus is highlighted as one of the micro-algal species that have so far been found to be suitable for the production of biofuel. The most recent initiatives and successes in enhancing production economies by genetic as well as metabolic engineering of microalgal strains are also covered. Other potential uses for biofuel production are described, including CO_2 mitigation and wastewater treatment. The biofuel industry's promises and obstacles related to algae are finally revealed (Shubha 2018). Rittmann (Medipally 2015) outlined three risks associated with relying on fossil fuels: diminishing fossil fuel reserves, the geopolitical conflict caused by resource scarcity, and climate change brought on by rising atmospheric CO_2 concentrations. As a result, finding "clean" energy has emerged as one of the most difficult problems.

CONCLUSION

The purpose of the current review work is to address specific queries that will aid in a better understanding of how solar power can be used to treat domestic and commercial wastewater. A detailed review is done on the main issues, such as the pollutants found in domestic and industrial wastewater, wastewater treatment methods, and the environmental advantages of treating wastewater. In this review paper, we discussed how much energy is currently used by WWTPs and browsed into the potential of developing energy-self-sufficient WWTPs. Recent attention has been focused on research initiatives on microalgae and their production on a global scale due to these desirable characteristics of microalgae. Even though current technology only makes up a very small portion of total energy consumption, solar thermal system research has been steadily progressing for decades.

It is expensive to remediate water using some treatment methods because they involve high energy input. The presence of pollutants in the wastewater, such as chemical pesticides, hydrocarbons, colorants (dyes), surfactants, as well as aromatic compounds, is causing additional problems. The hazardous substances cannot be eliminated by one method of treatment. The degradation of a variety of contaminants using innovative and alternative greener technology is, therefore, the focus of research. Utilizing solar energy for wastewater treatment reduces the need for conventional power, which lowers GHG emissions. Although pollution can be completely reduced by solar photocatalysis or solar thermal electrochemistry, the removal of waste sediment following wastewater treatment with solar desalination requires additional steps.

FUTURE PROSPECTS

Many scientists and government officials from various nations have given the issue a lot of thought. Researchers spend a lot of time studying microalgae, and many

governments contribute a sizable sum of money to microalgae-related projects. Despite the numerous obstacles to the production of microalgal biodiesel, more and more innovators are persuaded that the benefits will eventually outweigh the risks, and, to date, microalgae investments have exceeded $900 million globally. To examine future development opportunities, it is necessary to discuss the research gaps, market opportunities, and future advancement directions of solar energy in wastewater plant systems. Even though the construction of energy-self-sufficient WWTPs is undoubtedly feasible, there are still numerous obstacles to overcome, especially in developing nations. Additional work is required in technological advances, expenditures, and safeguarding the environment.

ACKNOWLEDGMENTS

I am thankful to Amity Institute for Environmental Toxicology, Safety and Management Amity Institute, Noida Campus, for suggesting the topic, which is an important concern nowadays to review.

REFERENCES

Agalit, H., Zari, N. and Maaroufi, M. 2020. Suitability of industrial wastes for application as high-temperature thermal energy storage (TES) materials in solar tower power plants–A comprehensive review. Solar Energy, 208: 1151-1165.

Bahnemann, D. 2004. Photocatalytic water treatment: solar energy applications. Solar Energy, 77(5), 445-459.

Bodik, I. and Kubaska, M. 2013. Energy and sustainability of operation of a wastewater treatment plant. Environ. Prot. Eng., 39(2): 15-24.

Casierra-Martinez, H.A., Madera-Parra, C.A., Vargas-Ramírez, X.M., Caselles-Osorio, A. and Torres-López, W.A. 2020. Diclofenac and carbamazepine removal from domestic wastewater using a constructed wetland-solar photo-fenton coupled system. Ecol. Eng., 153: 105699.

Czarnota, J., Masłoń, A., Zdeb, M. and Łagód, G. 2020. The impact of different powdered mineral materials on selected properties of aerobic granular sludge. Molecules, 25(2): 386.

Di Fraia, S., Massarotti, N. and Vanoli, L. 2018. A novel energy assessment of urban wastewater treatment plants. Energy Convers. Manag., 163: 304-313.

Drewnowski, J., Remiszewska-Skwarek, A., Duda, S. and Łagód, G. 2019. Aeration process in bioreactors as the main energy consumer in a wastewater treatment plant. Review of solutions and methods of process optimization. Processes, 7(5): 311.

Frijns, J., Hofman, J. and Nederlof, M. 2013. The potential of (waste) water as energy carrier. Energy Convers. Manage., 65: 357-363.

Gao, M., Zhu, L., Peh, C.K. and Ho, G. W. 2019. Solar absorber material and system designs for photothermal water vaporization towards clean water and energy production. Energy Environ. Sci., 12(3): 841-864.

Gu, Y., Li, Y., Li, X., Luo, P., Wang, H., Wang, X. and Li, F. 2017. Energy self-sufficient wastewater treatment plants: feasibilities and challenges. Energy Procedia, 105: 3741-3751.

Geng, Y., Zhang, K., Yang, K., Ying, P., Hu, L., Ding, J. and Li, M. 2019. Constructing hierarchical carbon framework and quantifying water transfer for novel solar evaporation configuration. Carbon, 155: 25-33.

Haddeland, I., Heinke, J., Biemans, H., Eisner, S., Flörke, M., Hanasaki, N. and Wisser, D. 2014. Global water resources are affected by human interventions and climate change. Proc. Natl. Acad. Sci. U.S.A., 111(9): 3251-3256.

Hao, X., Liu, R. and Huang, X. 2015. Evaluation of the potential for operating carbon-neutral WWTPs in China. Water Res., 87: 424-431.

Kai, K. 2005. Study of Anaerobic Co-Digestion of Sludge in Sewage Mixed with Organic Wastes. Shanghai Construction Science & Technology, China.

Lee, M., Keller, A. A., Den, W. and Wang, H. 2017. Water-energy nexus for urban water systems: A comparative review on energy intensity and environmental impacts in relation to global water risks. Appl. Energy, 15: 589-601.

Li, X., Zhu, B. and Zhu, J. 2019. Graphene oxide-based materials for desalination. Carbon, 146: 320-328.

Li, Y., Liu, L., Yang, F. and Ren, N. 2015. Performance of carbon fiber cathode membrane with C–Mn–Fe–O catalyst in MBR–MFC for wastewater treatment. J. Membrane Sci., 484: 27-34.

Liu, F., Ouedraogo, A., Manghee, S. and Danilenko, A. 2012. A primer on energy efficiency for municipal water and wastewater utilities. openknowledge.worldbank.org.

Mamais, D., Noutsopoulos, C., Dimopoulou, A., Stasinakis, A. and Lekkas, T. D. 2015. Wastewater treatment process impact on energy savings and greenhouse gas emissions. Water Sci. Technol., 71(2): 303-308

Maness, P. C., Yu, J., Eckert, C. and Ghirardi, M. L. 2009. Photobiological hydrogen production-prospects and challenges. Microbe, 4(6): 659-667.

Masłoń, A., Czarnota, J., Szaja, A., Szulżyk-Cieplak, J. and Łagód, G. 2020. The enhancement of energy efficiency in a wastewater treatment plant through sustainable biogas use: A case study from Poland. Energies, 13(22): 6056.

Masłoń, A., Wójcik, M. and Chmielowski, K. 2018. Efficient use of energy in wastewater treatment plants. Energy Policy Stud., 1(2): 12-26.

Medipally, S. R., Yusoff, F. M., Banerjee, S. and Shariff, M. 2015. Microalgae as sustainable renewable energy feedstock for biofuel production. BioMed Res. Int., 54: 415-422.

Metering. 2018. Swedish Utility Selects Veolia for Wastewater to Energy Project. Available online: https://www.metering.com/news/swedish-utility-selects-veolia-for-rollout-of-wastewater-project/ (accessed 11 October 2018).

Neczaj, E. and Grosser, A. 2018. Circular economy in wastewater treatment plant–challenges and barriers. Proceedings, 2(11): 614.

Never, B. and Stepping, K. 2018. Comparing urban wastewater systems in India and Brazil: options for energy efficiency and wastewater reuse. Water Policy, 20(6): 1129-1144.

Obotey Ezugbe, E. and Rathilal, S. 2020. Membrane technologies in wastewater treatment: A review. Membranes, 10(5): 89.

Olsson, G. 2012. Water and Energy Nexus. Lund University, Sweden, pp. 137-164.

Pandey, A.K., Kumar, R.R., Kalidasan, B., Laghari, I.A., Samykano, M., Kothari, R. and Tyagi, V.V. 2021. Utilization of solar energy for wastewater treatment: Challenges and progressive research trends. J. Environ. Manage. 297: 113300.

Papa, M., Foladori, P., Guglielmi, L. and Bertanza, G. 2017. How far are we from closing the loop of sewage resource recovery? A real picture of municipal wastewater treatment plants in Italy. J. Environ. Manage., 198: 9-15.

Pienkos, P.T. and Darzins, A.L. 2009. The promise and challenges of microalgal-derived biofuels. Biofuels, Bioprod. Bioref., 3(4): 431-440.

Pitas, V., Fazekas, B., Banyai, Z. and Karpati, A. 2010. Energy efficiency of municipal wastewater treatment. J. Biotechnol., 150: 163-164.

Popp, J., Lakner, Z., Harangi-Rákos, M. and Fari, M. 2014. The effect of bioenergy expansion: Food, energy, and environment. Renew. Sustain. Energy Rev., 32: 559-578.

Rabii, A., Aldin, S., Dahman, Y. and Elbeshbishy, E. 2019. A review of anaerobic co-digestion with a focus on the microbial populations and the effect of multi-stage digester configuration. Energies, 12(6): 1106.

Remy CaL, B. 2015. Optimization of energy and nutrient recovery in wastewater treatment schemes. http://www.kompetenzwasser.de/fileadmin/user_upload/pdf/forschung/CoDiGreen/CoDiGreen_Executive_Summaryfinal_01.pdf. (Accessed on 28/01/2015).

Roots, P., Sabba, F., Rosenthal, A.F., Wang, Y., Yuan, Q., Rieger, L. and Wells, G.F. 2020. Integrated shortcut nitrogen and biological phosphorus removal from mainstream wastewater: process operation and modeling. Environ. Sci. Water Res. Technol., 6(3): 566-580.

Sansaniwal, S.K. 2022. Advances and challenges in solar-powered wastewater treatment technologies for sustainable development: A comprehensive review. Int. J. Ambient Energy, 43(1): 958-991.

Sarpong, G. and Gude, V.G. 2020. Near future energy self-sufficient wastewater treatment schemes. Int. J. Environ. Res., 14(4): 479-488.

Satyanarayana, K.G., Mariano, A.B. and Vargas, J.V.C. 2011. A review on microalgae, a versatile source for sustainable energy and materials. Int. J. Energy Res., 35(4): 291-311.

Schaubroeck, T., De Clippeleir, H., Weissenbacher, N., Dewulf, J., Boeckx, P., Vlaeminck, S.E. and Wett, B. 2015. Environmental sustainability of an energy self-sufficient sewage treatment plant: improvements through DEMON and co-digestion. Water Res., 74: 166-179.

Scott, C.A., Pierce, S.A., Pasqualetti, M.J., Jones, A.L., Montz, B.E. and Hoover, J.H. 2011. Policy and institutional dimensions of the water-energy nexus. Energy Policy, 39(10): 6622-6630.

Sharma, N.K., Tiwari, P.K. and Sood, Y.R. 2012. Solar energy in India: Strategies, policies, perspectives, and future potential. Renew. Sustain. Energy Rev., 16(1): 933-941.

Sharshir, S.W., Algazzar, A.M., Elmaadawy, K.A., Kandeal, A.W., Elkadeem, M.R., Arunkumar, T. and Yang, N. 2020. New hydrogel materials for improving solar water evaporation, desalination, and wastewater treatment: A review. Desalination, 491: 114564.

Sheboygan 2015. Sheboygan Regional Wastewater Treatment Facility. http://www.sheboyganwwtp.com/index.php.

Shuba, E.S. and Kifle, D. 2018. Microalgae to biofuels: Promising alternative and renewable energy, review. Renew. Sustain. Energy Rev., 81: 743-755.

Siatou, A., Manali, A. and Gikas, P. 2020. Energy consumption and internal distribution in activated sludge wastewater treatment plants of Greece. Water, 12(4): 1204.

Singh, P. 2016. The energy demand of decentralized STPs and application of solar PV modules. J. Adv. Res. Sci. Eng., 5(1): 816-822.

Soares, R.B., Memelli, M.S., Roque, R.P. and Gonçalves, R.F. 2017. Comparative analysis of the energy consumption of different wastewater treatment plants. Int. J. Archit. Arts Appl., 3(6): 79-86.

Song, D., Fu, J. and Shi, D. 2008. Exploitation of oil-bearing microalgae for biodiesel. Chin. J. Biotechnol. 24(3): 341-348.

Szeląg, B., Drewnowski, J., Łagód, G., Majerek, D., Dacewicz, E. and Fatone, F. 2020. Soft sensor application in identification of the activated sludge bulking considering the technological and economical aspects of smart systems functioning. Sensors, 20(7): 1941.

Tao, P., Ni, G., Song, C., Shang, W., Wu, J., Zhu, J. and Deng, T. 2018. Solar-driven interfacial evaporation. Nat. Energy, 3(12): 1031-1041.

Udayan, A., Pandey, A.K., Sirohi, R., Sreekumar, N., Sang, B.I., Sim, S.J. and Pandey, A. 2022. Production of microalgae with high lipid content and their potential as sources of nutraceuticals. Phytochem. Rev., 1-28.

Ugwuishiwu, B.O., Owoh, I.P. and Udom, I.J. 2016. Solar energy application in waste treatment-a review. Niger. J. Technol., 35(2): 432-440.

UNEP 2009. Towards Sustainable Production and Use of Resources: Assessing Biofuels. United Nations Environment Programme. Biofuels Working Group, & United Nations Environment Programme. International Panel for Sustainable Resource Management. UNEP/Earthprint.

Wang, B., Guo, Y., Zhao, M., Li, B. and Peng, Y. 2019. Achieving energy-efficient nitrogen removal and excess sludge reutilization by partial nitritation and simultaneous anammox denitrification and sludge fermentation process. Chemosphere, 218: 705-714.

Wang, H., Yang, Y., Keller, A.A., Li, X., Feng, S., Dong, Y.N. and Li, F. 2016. Comparative analysis of energy intensity and carbon emissions in wastewater treatment in USA, Germany, China and South Africa. Appl. Energy, 184: 873-881.

Yadav, A., Raj, A., Purchase, D., Ferreira, L.F.R., Saratale, G.D. and Bharagava, R.N. 2019. Phytotoxicity, cytotoxicity, and genotoxicity evaluation of organic and inorganic pollutants rich tannery wastewater from a Common Effluent Treatment Plant (CETP) in Unnao district, India using Vigna radiata and Allium cepa. Chemosphere, 224: 324-332.

Yang, L., Zeng, S., Chen, J., He, M. and Yang, W. 2010. Operational energy performance assessment system of municipal wastewater treatment plants. Water Sci. Technol., 62(6): 1361-1370.

Zorn, S.M., Reis, C.E., Bento, H.B., de Carvalho, A.K.F., Silva, M.B. and De Castro, H.F. 2020. In situ transesterification of marine microalgae biomass via heterogeneous acid catalysis. BioEnergy Res., 13(4): 1260-1268.

Nature Environment and Pollution Technology
An International Quarterly Scientific Journal

p-ISSN: 0972-6268
(Print copies up to 2016)
e-ISSN: 2395-3454

Vol. 23 | No. 1 | pp. 569-575 | 2024

Original Research Paper

https://doi.org/10.46488/NEPT.2024.v23i01.054

Open Access Journal

System of Wheat Intensification: An Innovative and Futuristic Approach to Augment Yield of Wheat Crop

Maninder Singh*, Arshdeep Singh*, Anita Jaswal* and Shimpy Sarkar**

*Department of Agronomy, School of Agriculture, Lovely Professional University, Phagwara-144411, Punjab, India

**Department of Entomology, School of Agriculture, Lovely Professional University, Phagwara-144411, Punjab, India

†Corresponding author: Maninder Singh; maninder.27452@lpu.co.in, ms23049@gmail.com

Nat. Env. & Poll. Tech.
Website: www.neptjournal.com

Received: 20-07-2023
Revised: 06-09-2023
Accepted: 22-09-2023

Key Words:
Food security
Sustainability
Wheat intensification
Yield

ABSTRACT

There is a new method of wheat production called the System of Wheat Intensification (SWI) that manages seed treatment, seed rate, spacing, weeding, and watering. The SWI and traditional methods of wheat sowing differ from each other in terms of potential yield. In comparison to the traditional method of wheat sowing, SWI allows seed treatment, which increases the number of tillers, the number of grains in spike, and the weight of the grain. Wheat seeding in the traditional approach is done at a much closer distance than in the SWI method, which results in faulty germination as a result of increased competition between the plants. In SWI, proper root formation in the early stages of crop growth can be encouraged by increasing the space between plants and rows, as well as increasing the density of plants. For small and medium-sized farmers, it is a great way to boost productivity and income while reducing food poverty at the same time. Using organic manure instead of chemical fertilizer is a new strategy that helps support sustainable agriculture. To help the poorest farmers and enhance their productivity and profit, SWI should be recommended.

INTRODUCTION

Wheat (*Triticum aestivum* L.) is one of the most significant cereal food crops, ranking first in India in terms of area and production of grain crops and second in the world in terms of production after China. It may be grown from below sea level to 5000 m altitude and in regions with 300-1130 mm of annual precipitation. The subtropical region of India is mostly responsible for the country's wheat production. Winters that are cool and sunny are ideal for wheat crop growth. Wheat comprises around 32 percent of the world's cereal-growing acreage. Wheat is cultivated throughout the year in many regions of the globe. China, India, the United States of America, Russia, France, Canada, Germany, Turkey, Australia, and Ukraine are the leading wheat-producing nations.

In India during 2020-2021, the area under wheat cultivation was 31.61 million hectares with production of 109.52 million tones and a yield of 34.64 quintals per hectare. Punjab now occupies the third position in terms of area, after Uttar Pradesh and Madhya Pradesh. In Punjab, the area was 3.53 million hectares, which was 11.15 percent of India's total area, and production was 17.14 million tonnes (Agricultural Statistics at a Glance 2021).

The system of wheat intensification (SWI) method can significantly increase wheat productivity and yield. It provides favorable growing conditions by modifying soil, water, sowing methods, and fertilizer management. SWI gives a 54 percent greater yield than the best available conventional sowing techniques (Uphoff et al. 2011, Bhargava et al. 2016, Raghavendra et al. 2019, Adhikari 2013**),** which can, in turn, give a higher financial return (Raol 2012). This is a new method of wheat cultivation in which seeds are sown with a plant-to-plant and row-to-row distance of 25 centimeters. This type of sowing with proper spacing allows for sufficient aeration, moisture, and nutrient availability, resulting in proper and healthy root development from the early stages of crop growth till harvesting. SWI is the application of intensive care at every stage of plant development and the modification of agronomic practices, such as a lower seed rate, seed treatment, and effective management of water and inter-cultivation practices, which results in a greater number of tillers to parental seedlings, a greater number of effective tillers per hill, an increase in panicle length and bolder grains and ultimately an increase in wheat yield. In the conventional approach, farmers use approximately 100-140 $kg.ha^{-1}$ of seed, but the SWI method requires only 5%-7.5% of this quantity (Styger & Ibrahim 2009). An optimal ratio of organic to inorganic nutrient inputs is required for productive agriculture (Reganold et al. 1990). The crop requires moderate temperatures during the

maturation stage, but in certain regions, terminal heat stress affects the duration of grain growth and, consequently, grain production (Mukherjee 2012).

The use of this technique has resulted in a doubling of wheat's maximum grain production compared to its prior maximum output. Appropriate spacing, usage of organic manure, and organic seed treatment all contribute to a greater yield. A sufficient distance between plants and the seeding of two germinated seeds at a single location facilitates the appropriate moisture, aeration, nutrition, and illumination of the crop roots. This promotes faster plant development. Only two to three cycles of watering and weeding using a hand wheel hoe save time and money on labor.

WHEAT INTENSIFICATION SYSTEM IN RELATION TO CONVENTIONAL WHEAT SOWING METHOD

Approximately 10 million hectares of land are covered by the Rice-Wheat cropping system in northern India if we consider the current status of this system. It is only achievable via the use of rigorous inputs such as robust seeds, inorganic fertilizers, weedicides, insecticides, and pesticides. If these inputs are not used properly, and in balance, they may have a negative impact on the environment, soil rhizosphere, as well as on the output and productivity of the land.

The system of wheat intensification is based on the system of rice intensification. SWI is an excellent strategy for intensifying wheat production and productivity in the current situation. The system of wheat intensification has a high likelihood of contributing to an increase in wheat output per unit of water and kilogram of agricultural resources such as seeds, inorganic fertilizer, and organic fertilizer. Also, it adheres to the SRI technology of rice cultivation (Dhar et al. 2014). Uphoff et al. (2011) and Adhikari (2012) found that SWI and some modified SWI implementation activities may result in a 54 percent increase in yield compared to the best accessible conventional sowing approaches and may have economic advantages (Styger 2009). Widespread wheat cultivation requires more inorganic fertilizers along with a seed rate between 100 and 140 kg of seed per acre as indicated in Table 1. In contrast, SWI utilizes just 25-30 kg of modified seeds per hectare having row-to-row and plant-to-plant spacing of 25 cm (Raol 2012). One of the other reasons for potential yield under the SWI system is resistance to abiotic stress, a decrease in input requirement rate, and an increase in financial possibilities (Satyanarayana et al. 2007).

SWI saves 30 percent more water than the typical way of sowing, according to farmers' field reports (Uphoff 2012). The height of the plant, number of tillers per hill, number of effective tillers, panicle length, and yield were determined to be higher using the SWI approach. In SWI, line sown, and broadcast methods, the wheat variety (Bhirkuti) yielded 2,6, 2,4, and 2,3 $kg.m^{-2,}$ respectively. Chopra and Sen (2013) showed a similar correlation between wheat grain production and the broadcast technique of planting. The results of the trial indicate that the SWI approach produces a higher yield than the conventional method as presented in Table 2.

Bhargava et al. (2016) claimed that the implementation of the SWI technique by maintaining adequate plant spacing and nutrient management might significantly increase wheat yield, particularly in all regions of Madhya Pradesh. Bhargwa himself also recommends the use of the SWI method. The SWI technique of wheat cultivation is preferably more beneficial to farmers as compared to the conventional method. Abraham et al. (2014) observed a rise of 18-67 percent in grain production and a 9-27 percent in straw yield of wheat at the farmer's field in SWI compared to the broadcast technique. The results of several observations indicate that this method was effective.

NECESSITY OF SWI IN THE PRESENT SCENARIO

SWI is required primarily to provide high wheat yield per unit of inputs/resources. SWI is important in light of the need for a retooling of food grain production, particularly wheat, to fulfill the growing population's needs. The continuous, excessive, and unprofessional use of synthetic agrochemicals results in soil and environmental damage. Additionally, there is a steady reduction in crop responsiveness to inputs,

Table 1: System of wheat intensification at a glance.

Serial number	Modified practices	Expected outcome
1.	Lowering seed rate	The tillers and mother seedling ratio is higher as compared to normal
2.	Treatment of seeds using fungicide	The number of effective tillers/hills improved
3.	Sowing of seed at a broad spacing	The length of the panicle is increased, and healthy grains
4.	Management of water in a precise manner	Yield per hectare is increased
5.	Performing intercultural operations like hoeing and weeding using Conoweeders	The conflict between weed and crop is controlled efficiently.

Source: Sheehy et al. (2004)

Table 2: Comparative studies between conventional wheat cultivation and SWI.

S.No.	Conventional cultivation	SWI Method
1.	The seed requirement is 100-125 kg/ha	The seed requirement is only 20-30kg/ha
2.	The seed treatment is usually not done	Seed treatment is done with fungicides, Cow urine, and Jaggaery (GUR)
3.	The method of sowing is broadcasting	Generally, line sowing should be done with broader spacing
4.	No plant-to-plant spacing is maintained	Spacing of 20cm X20cm to 50cm X20 cm is maintained
5.	No intercultural operation is done to uproot the weeds	Weeding/hoeing should be done with Conoweeders
6.	The length of the panicle should be 10-11 cm	The length of the panicle should be 15 cm
7.	The number of grains per panicle ranges between 18-50	The number of grains per panicle ranges between 60-120
8.	The number of spikes per hill is 1-2 in normal stand and 2-4 in good stand	The number of spikes per hill is 20-45
9.	The time of emergence is generally one week after sowing	The time of emergence is generally 2-3 days after sowing
10.	Leaf width is thin with a lesser leaf area index	Leaf width is broad with more leaf area index
11.	The width of the stem is thin	The width of the stem is thick
12.	The depth of the root is shallow	The depth of the root is deeper (8-10inches)
13.	The number of irrigations is 2-4	The number of irrigations is 4-5
14.	The yield is 1-2 tonnes per hectare	The yield is 3-4 tonnes per hectare

Source: ATMA (2008), PRADAN (2012)

especially in the setting of climate change. Intensive tillage, crop residue burning, loss of soil organic matter, degradation of soil fertility, loss of soil health, lack of high-quality and adequate irrigation water, salinity difficulties, arsenic concerns, etc., are additional significant problems linked with chemical agriculture. All of these factors result in stagnant wheat output levels. Under such conditions, SWI has promising potential, as it strives to increase wheat yield with minimal input costs and without compromising soil and environmental quality. In addition, it may be a viable solution for increasing wheat output in Eastern India's less productive regions. As SWI employs a method of alternating soaking and drying, it also has a promising future in arid regions Biswas and Das (2021).

MAJOR AGRICULTURAL CHALLENGES ADDRESSED BY SWI

Lack of high-quality irrigation water: Integrated water management is the foundational principle for water management practices, which rely on the careful use of high-quality water and the uniform application of water; to remedy this situation, SWI can be implemented with greater water use efficiency.

The imperative of mitigating the effects of climate change: The steadily increasing temperature is the primary cause of the declining wheat yield, which is expected due to the shortened growing season. Due to the doubling of CO_2 and a 3°C increase in India's diffusive temperature, it is expected that both the area and yield of wheat would continue to decline. (FAO 2012). For overcoming the effects of climate change, SWI may assist in determining the optimal sowing time, seedling operations, surface debris retention for temperature control, and water sustenance.

Focusing on low-productivity regions: Compared to other parts of India, the Eastern region of India has the lowest wheat output. Based on statistical data, the yield of wheat in the eastern portion of India ranges from 1.30 to 2.78 $t.ha^{-1}$, as compared to the yield of major wheat-producing states such as Punjab (4.72 $t.ha^{-1}$) and Haryana (4.45 $t.ha^{-1}$). Based on statistics, the output of wheat in eastern India may be boosted by utilizing the SWI technique instead of the traditional way of wheat farming.

Production methods for arid regions: When discussing dry land farming, it is important to note that rainfed agriculture accounts for around 55% of the total planted area in India, which is 78 million hectares (NRAA 2012), and 40% of the overall food output (Ravindra Chary et al. 2012). Dry land agriculture cultivation is affected by atypical weather conditions, soil deterioration, small farmers, farmers with limited assets, etc., and the interdependence of these elements (Ravindra Chary et al. 2012). This constraint should be the focus of organized and productive uses of scarce resources that are available under these conditions for the development of more efficient and effective dry land technology.

FUNDAMENTALS OF SWI

SWI is essentially founded on two crop production principles:

1. The fundamentals of root development
2. Fundamentals of intensive care

The Fundamentals of Root Development

For a plant's optimal growth, its root system should be well. Root development is the initial phase in a plant's proper growth and development. It demands enough nutrition and adequate space surrounding the plant, which is essential for crop growth and development.

The Fundamentals of Intensive Care

Increased frequency does not refer to a high number of plants per unit of area rather, it is the preservation of the space and noticeable care to the plants. To increase yield, intense care is required at every stage of plant growth, particularly weed, pest, disease, organic fertilizers, and irrigation management.

AGRONOMICAL/CULTURAL PRACTICES ADOPTED IN SWI

Modifications in sowing geometry, weed management, and an emphasis on organic manuring provide a favorable environment for crop growth in SWI (Fig. 1). Yet, the core principles of wheat agriculture remain relatively unchanged. It tries to boost agricultural yields while increasing the land's inherent productivity with little external inputs. SWI needs a number of stages for effective improvement in grain and straw production, including site assessment and anticipation, selection, and treatment of seeds, sowing, weed management, application of manure, and adequate water management. These procedures are briefly described below.

Site assessment and anticipation: Well-drained, loamy, rich soil with a pH between 6.0 and 8.5 is good for wheat growing. Resist saturated soils and choose land with a good drainage system capable of eliminating surplus water. Three ploughings are necessary to achieve a suitable tilth for wheat planting in SWI. The initial plowing is performed to remove the roots of previous crops grown in the area. After one to one and a half months, compost is added, and the soil is tilled again. The last tillage is performed before sowing wheat seeds.

Selection and treatment of seeds: Putting 20-25 $kg.ha^{-1}$ seeds in a 20 percent salt-to-water solution and removing the floating seeds yields robust and vigorous wheat seeds. Thus, for seed treatment, make a combination of 10 liters of hot water (60°C), 2 kilograms of well-decomposed compost or vermicompost, 3 liters of cow urine, and 2 kg of jaggery in a clay pot. After adequate mixing, 5 kg of seeds were dipped in the mixture and allowed for 6 to 8 h. With the same proportion of the aforementioned ingredients, a larger quantity of seed can be treated with the combination. The next step is to remove the seeds from the mixture using a filter and clean water. By the time treated seeds have been maintained in the shade for 10-12 h, they have fully sprouted.

Sowing: The sprouting seeds will be sown in the field using a dibble method with two seeds per hill. According to the moisture content, different row-to-row and plant-to-plant spacing (15 cm×15 cm or 20 cm×20 cm) can be utilized. For sowing, a manual or powered seed drill can be employed. If a seed drill is unavailable, the fields are marked at 15/20 cm intervals using rope or thread. Using a dibbler or pegs,

Fig. 1: Agronomical practices followed in the system of wheat intensification.

seeds will be planted at a depth of 2.5-3 cm. When sowing germinated seed, the soil must contain an adequate amount of moisture. Within 10 days of seeding, gaps were filled with germinated seeds wherever seeds failed to germinate or were eliminated. To limit competition, extra seeds grown on a hill have been removed.

Weed management: Hoeing is a crucial component of sustainable agriculture because it destroys weeds that compete with crops for space, light, and water. Hoeing of weeds softens the soil and efficiently oxygenates the roots, permitting exploration of the soil that leads to improved nutrient and water uptake from bottom soil. The incorporation of weeds into the soil increases the soil's water-holding capacity and nutritional status. In SWI, weeding is typically performed thrice, beginning 20 to 25 days after sowing (DAS). The successive weedings are performed 10 days apart.

Application of manure: A healthy wheat crop requires the right proportions of nitrogen, phosphorus, and potassium, i.e., 80-125:40-60:30-40 kg.ha^{-1}. To maintain a balance of vital nutrients, soil test-based nutrient recommendations are followed by the application of organic manures such as farm yard manure, vermicompost, NADEP (Narayan Deotao Pandharipande) compost, liquid manure like Panchagavya, Amritghol and Matkakhad (PAM) and other manures (such as agricultural residues and animal wastes are commonly used in practice).

Water management: In SWI, the soil is frequently made wet and dry, and 3-5 irrigations are provided based on soil moisture state. The initial irrigation is applied at 15 DAS before the crown root initiation (CRI) stage. After 40 DAS, a second watering will be done if the soil develops fine cracks. Irrigation is performed prior to weeding in the early stages of crop development. At 75 DAS, a third irrigation was provided. The fourth irrigation was administered during the blooming stage, while the fifth irrigation was administered during the grain-filling stage.

Pest and disease management: Varieties that are resistant to pests and diseases are chosen, and seed treatment can be performed before planting to reduce crop damage inflicted by biotic stress. SWI promotes the use of biological pest management methods, such as biological agents and organic pesticides.

Harvesting: Productive tillers/hills are the result of enough sunlight, water, and air circulation. With the appropriate implementation of the SWI package and practices, the crop develops on time and is reaped whenever the wheat grain's moisture content is between 20 and 25 percent as indicated in Table 3.

IMPLEMENTATION OF SWI IN THE WORLD

Since 2006, the Institute of Yanjiang Agricultural Sciences in Jiangsu has collaborated with the Centre of Agro-ecology and Farming Systems of the China Academy of Agricultural Sciences on SWI, recommending that the SRI Principle be implemented in wheat-rice cropping systems. China and the Indo-Gangetic Plains of South Asia have adopted this recommendation.

Since 2010, SWI has also tested in the western districts of Doti, Dadeldhura, Baitadiand, and Kailali with the assistance of two NGOs, namely Mercy Corps Nepal and FAYA-Nepal. Based on this trial, it has been shown that SWI produces 91 to 100 percent higher yield than traditional wheat farming.

Since 2011-12, SWI has also been exhibited in the Sindhuli area of Nepal on farmer fields with updated technology. Which increases output and economic return, and it was noticed that under the same conditions of farm inputs such as water management, fertilizer availability, etc., the Bhirkuti type of wheat utilized for demonstration yielded 54 percent higher than conventional planting. Based on the demonstration, SWI yielded 6.5 tons.ha^{-1}, greater than broadcasting and line sowing, which produced 3.7 tons.ha^{-1} and 5 tons.ha^{-1}, respectively.

IMPLEMENTATION OF SWI IN INDIA

SWI was originally tested in India in 2006 by PSI (People

Table 3: Yield characters of wheat sown under SWI and conventional method.

Parameters	2013- 2014		2014-2015		2015-2016	
	Conventional	SWI	Conventional	SWI	Conventional	SWI
Number of tillers	6	27	5	25	7	32
Grains per spike	24.6	49.8	22.4	46.8	50.3	73.5
Number of spikes /m^2	315	426	307	403	407	462
1000 - grain weight [gm]	53	68	50	61	54	76
Grain yield [q.ha^{-1}]	31.9	57.3	30.6	54.8	32.8	61.3
Straw yield [q.ha^{-1}]	5.4	7.4	5	6.9	5.9	8.12

Source: Bhargava et al. (2016)

Table 4: Comparison of Cost of cultivation under conventional method of wheat cultivation and system of wheat intensification (SWI).

Particulars	Conventional	System of Wheat Intensification
A) Operations		
Ploughing	3000	3000
Seed	650	300
Weeding	0	1800
Irrigation	300	500
Fertilizers and plant protection chemicals	200	400
Harvesting and threshing	2000	2000
Total	6150	8000
B) Yield and income		
Grain yield (quintal/hectare)	6	10
Gross income @1100 per quintal	6600	11000
Straw yield (quintal/hectare)	10	16
Straw income@200 per quintal	2000	3200
Total gross income	8600	14200
Net income (Rs)	2450	6200

Source: Relkar (2011)

Science Institute) in North India using forty farmers in twenty-five villages, achieving a 66 percent increase in production above conventional approaches. Throughout 3 years, approximately 12,000 farmers in Himachal Pradesh and Uttarakhand adopted these new techniques. In Bihar, where 415 farmers, largely women, tested SWI techniques in 2008-09, a yield up to 3.6 $t.ha^{-1}$ was achieved in comparison to 1.6 $t.ha^{-1}$ using conventional procedures. In 2009-10, 15,808 farmers adopted SWI, yielding an average of 4.6 $t.ha^{-1}$. The SWI area in Bihar was reported to be 183,063 ha in 2011/12, with a yield potential of 4.5 $t.ha^{-1}$ as presented in Table 4.

Some community workers in India launched the SWI approach in 2006 on the fields of small and marginal farmers, and their good results paved the way for systematic research among farmers (Kumar et al. 2015). SWI has been evaluated as an innovative method for boosting production and is being implemented in Chhindwara, Madhya Pradesh (MP). SWI is evolving and is being evaluated in many other locations in MP. The development of SWI has yielded excellent benefits in reducing hunger among marginalized and small-scale farmers. These technologies are expected to reduce farmer's dependence on multinational corporations for seeds, fertilizers, and their livelihoods (Rout et al. 2010).

PROS AND CONS OF USING SWI

In SWI, the seed requirement is less (Only 20 to 25 $kg.ha^{-1}$), and it helps in seed saving up to (Seventy-five to eighty percent). It increases the number of efficient tillers in the wheat crop. Due to the modification of cultural/agronomical practices, crops should not suffer from lodging, which results in higher productivity. By adopting SWI, flowering and crop maturation are earlier. It results in excellent grain quality, and grains are long and lustrous. It produces a good amount of straw and makes the availability of more feed for livestock. There are fewer instances of pathogen and pest infestation. Weeding by conoweeder promotes healthy root aeration and significantly less water requirement, i.e., 20-30 percent. Improved germination percentage leads to more plant stands in the field is another benefit of SWI. SWI enriches soil fertility and helps in achieving sustainability. There are some major constraints to using SWI. For adopting the SWI technique, appropriate sowing tools are required.

Along with this, rigorous scientific study is required at all the research centers for the success of SWI. Cono-weeding is challenging on abrasive soil and is confined to male farmers only. In many locations, the supply of organic manures is occasionally limited, which 0is the other major challenge to adopt. Small-scale farmers cannot afford it sometimes, and there are insufficient extension services that can promote the SWI along with farmers.

CONCLUSIONS

SWI is a new aspect for increasing wheat output that can immediately enhance farmers' revenue and decrease their food shortages. It may help the crop to tolerate biotic and abiotic challenges that are intensifying as a result of climate

change. By conserving agricultural inputs, the implementation of SWI can raise the productivity and profit of their source impoverished farmers. Wheat Intensification System, when compared to the conventional approach, showed a good response on all examined growth parameters, yield characteristics, and yield output. It has a favorable response to seed treatment and wider-area seeding. According to the findings of many researchers, SWI increases wheat grain production by 18-67 percent and straw output by 9-27 percent compared to the broadcast approach. Due to larger spacing, SWI prefers a lower seed rate compared to conventional wheat cultivation methods. Due to the reduced seed rate, it is more cost-effective for farmers. It reduces the cost of cultivation by using, for instance, a conoweeder to manage weeds instead of human hand weeding. Conoweeders are cost-effective, simple to use, and widely utilized in India today. SWI is highly trustworthy and economically beneficial for small-holding farmers.

REFERENCES

Abraham, B., Araya, H., Berhe, T., Edwards, S., Gujja, B., Khadka, R.B. and Verma, A. 2014. The system of crop intensification: reports from the field on improving agricultural production, food security, and resilience to climate change for multiple crops. Agric. Food Secur., 3(1): 1-12.

Adhikari, D. 2013. System of wheat intensification in farmers' field of Sindhuli, Nepal. Agron. J. Nepal, 3: 168-171.

Agricultural Statistics at a Glance. 2021. Directorate of Economics and Statistics, Ministry of Agriculture, Govt. of India (Website: http://www.dacnet.nic.in/eands)

Bhargava, C., Deshmukh, G., Sawarkar, S.D., Alawa S.L. and Ahirwar, J. 2016. The system of wheat intensification, in comparison with the conventional method of wheat line sowing, increases wheat yield with low input cost. Plant Arch., 16(2): 801-804.

Biswas, S. and Das, R. 2021. System of wheat intensification (SWI). Agric. Food. Newslett., 3(5): 175-178.

Chopra, R. and Sen, D. 2013. Golden wheat becomes more Golden - Extending SRI to wheat. LEISA India, 15: 30-32.

Dhar, S., Barah, B.C. and Vyas, A.K. 2014. Comparative Performance of System of Wheat Intensification (SWI) and Other Methods of Wheat Cultivation in North Western Plain Zone of India. Indian Agricultural Research Institute, New Delhi.

Food Agriculture Organization (FAO). 2012. FAO Statistical Yearbook 2012: World Food and Agriculture. Retrieved from http://www.fao.org (accessed 12th April 2015).

Kumar, A., Kumar, N., Baredar, P. and Shukla, A. 2015. A review on biomass energy resources, potential, conversion and policy in India. Renewable and Sustainable Energy Reviews, 45: 530-539.

Mukherjee, D. 2012. Effect of different sowing dates on growth and yield of wheat (Triticum aestivum) cultivars under the mid-hill situation of West Bengal. Indian J. Agron., 57: 152-156.

NRAA. 2012. Prioritization of rainfed areas in India (Study Report 4). National Rainfed Agriculture Authority (NRAA) Publication, New Delhi.

PRADAN. 2012. Cultivating Wheat with SRI Principle: A Training Manual. Bihar Rural Livelihood Promotion Society (BRLPS), the Agricultural Technology Management Agency (ATMA), and the NGO PRADAN, Nalanda, Gaya

Raghavendra, M., Singh, Y.V., Verma, R.K., Halli, H.M. and Goud, B.R. 2019. System of wheat intensification: An innovative approach. Indian Farm., 69(4): 456-472.

Raol, R.K. 2012. SWI Experience in Bihar. Aga Khan Rural Support Programme-India, New Delhi.

Ravindra Chary, G., Venkateswarlu, B., Sharma, S.K., Mishra, J.S., Rana, D.S. and Kute, G. 2012. Agronomic research in dryland farming in India: An overview. Indian J. Agron. 3rd IAC Special Issue, pp. 157-167.

Reganold, J.P., Robert, L.P. and Parr, J.F. 1990. Sustainability agriculture in the United States. In overview sustainable agriculture issues perspective and prospects in semi arid tropics. Int. J. Trop. Agric., 8: 203-208.

Relkar, P.M. 2011. System of wheat intensification (SWI). Tech. Dig., 13: 11-15.

Rout, N., B.S. Kumar, R.M. and Bajarachayra, M. 2010. Agricultural intensification: Linking livelihood improvement and environmental degradation in the mid-hills of Nepal. J. Agric. Environ., 11: 209-211.

Satyanarayana, A., Thiyagarajan, T.M. and Uphoff, N. 2007. Opportunities for water saving with higher yield from the system of rice intensification. Irrig. Sci., 25: 99-115.

Sheehy, J.E., Peng, S., Dobermann, A., Mitchell, P.L., Ferrer, A., Yang, J., Zou, Y., Zhong, X. and Huang, J. (2004). Fantastic yields in the system of rice intensification: the fact of fallacy? Field Crops Res., 88: 1-8.

Styger, E. and Ibrahim, H. 2009. The System of Wheat Intensification (SWI): Initial Test by Farmers in Goun-dam and Dire, Timbuktu, Mali, Africare, Mali, Bamako. Available at URL: http://ciifad.cornell.edu/sri/countries/mali/MaliSWIrpt071309.pdf (Accessed 23rd January 2015).

Styger, E. 2009. Sixty farmers evaluate the system of Rice Intensification in Timuktu. Available at URL: http//www.erikastyger.com/SRI_Timbuktu_Blog/SRI_Timbuktu_Blog. html. (Accessed 23rd January, 2015).

Uphoff, N., Kassam, A. and Harwood, R. 2011. SRI as a methodology for raising crop and water productivity: productive adaptations in rice agronomy and irrigation water management. Paddy Water Environ., 9: 3-11

Uphoff, N. 2012. Supporting food security in 21st century through resource conserving increases in Agriculture production. Agric. Food Sec., 1 : 18.

Nature Environment and Pollution Technology
An International Quarterly Scientific Journal

p-ISSN: 0972-6268
(Print copies up to 2016)
e-ISSN: 2395-3454

Vol. 23 | No. 1 | pp. 577-582 | 2024

Original Research Paper

https://doi.org/10.46488/NEPT.2024.v23i01.055

Open Access Journal

Experimental Investigations on the Effect of Pretreatment in Anaerobic Digestion of Coir Pith Agro Waste

Smitha Krishna Warrier*† and **P. Sindhu****

*Department of Engineering, University of Technology and Applied Sciences, Al Mussanah, Sultanate of Oman

**Department of Civil Engineering, College of Engineering, Trivandrum, Kerala, India

†Corresponding author: Smitha Krishna Warrier; smitha@act.edu.om

Nat. Env. & Poll. Tech.
Website: www.neptjournal.com

Received: 10-07-2023
Revised: 23-08-2023
Accepted: 21-09-2023

Key Words:
Anaerobic digestion
Biogas
Coir pith
Fungal culture
Pleurotus
Trichoderma

ABSTRACT

The coir industry in India's southern coastal regions, especially in the state of Kerala, is becoming increasingly concerned about the environmental impact of the accumulation and incremental increase of coir pith each year. The objective of this study was to assess the effect of pretreatment on the anaerobic digestion of coir pith. The characterization study of coir pith shows high organic content, which can be anaerobically digested to produce biogas. But, the high lignin content (30.91%) makes the process slow. To overcome this, a biological pretreatment method was tried using two microbial cultures belonging to fungal genera known to be lignin decomposers, viz., *Trichoderma* and *Pleurotus*. By using *Trichoderma*, lignin content was reduced by 3.7%, and the maximum gas production was obtained in a shorter time (19 days) in comparison with the sample without any pretreatment (24 days). When *Pleurotus* was used for lignin degradation, the lignin content was reduced by 6.78%, and the maximum gas production was obtained in a much shorter time period (14 days) in comparison with the former two methods. The gas produced comprises 74 ppm of methane, which has fuel value. The sludge after digestion was tested, which indicated a marginal increase in NPK value and hence can be used as fertilizer. The results of the study appear to be quite promising in the transition towards green energy by providing scope for the process of biomethanation, with the conclusion that further research can transform coir pith into a good renewable energy resource.

INTRODUCTION

The coir industry constitutes an important aspect among traditional cottage industries in the southern coastal regions of India, where the economy and livelihood of people are largely dependent on coconut farming. These industries mainly use coconut husk as the basic raw material, from which the coir fiber is extracted (Muneeswaran & Kesavan 2022). Coir pith, an elastic cellular cork-like material forming the nonfibrous component of coconut husk, is a major agricultural waste product generated in large quantities during the extraction of coir fiber. Coir pith, thus generated, along with the process of coir retting of coconut husk, eventually results in pollution of land and water bodies to a great extent (Khadeeja et al. 2012). For every ton of fiber extracted, pith is produced to the extent of 2 tons (Narendar & Priya Dasan 2014). Coir pith left behind after processing coconut husk normally accumulates in large dumps outside the mills (Prakash et al. 2021). It is estimated that there is an accumulation of nearly 7.5 million tons of coir pith in the coconut farming states of our country (Priyadarshini et al. 2021).

Present forms of management or utilization, such as landfilling, hydroponics, manuring, etc., are not sufficient to consume the waste generated, and it continues to be a perennial problem for the nearby aquatic and terrestrial environments (Kunchikannan et al. 2007). This high quantum of production of coir pith in the defibring units faces difficulty in disposal and makes the land unfit for any other purpose or activity. When burned, it smolders, thereby emitting a large quantity of smoke for several days and causing air pollution. Other problems are the generation of leachate from the dumps in the rainy season and the fire hazard in the summer. The high lignin and cellulose content in the pith makes biodegradation difficult (Paramanandham & Ronald Ross 2015).

Further, it decomposes in the soil at a slow rate, as its pentosan-lignin ratio is less than 0.5, which is the minimum required for the slow decomposition of organic matter in the soil (Deivanai & Kasturi Bai 1995). Recently, the waste management of coir pith has become a serious social problem. A much longer matter of concern facing the world

today is the energy crisis due to the depletion of fossil fuels, which are not renewable.

Several studies show that coir pith has an energy value (Kunchikannan et al. 2007). One approach to tapping this vast energy is methane production by anaerobic digestion. Agro-industrial residues such as coconut coir pith, banana waste, tea waste, cassava waste, and palm oil mill waste are generally considered the best substrates for the Solid State Fermentation processes (Karthick et al. 2015). Furthermore, a high moisture content and profusion of organic matter, methane as an alternative energy resource, and further use of the digested residue as manure are the factors that favor the technology of anaerobic digestion of coir pith (Kunchikannan et al. 2007). Various chemical treatment methods have been reported for lignin degradation. But biological treatment is always preferred over chemical means, owing to its eco-friendly nature. Since the major portion of coir pith contains lignin, aerobic microbial pre-treatments can be an option, as lignin was shown to degrade more effectively under aerobic conditions (Makela et al. 2002). Recent research regarding the lignin-degrading white rot and brown rot fungi is offering intriguing possibilities with aerobic fungal treatment followed by anaerobic digestion (Gharsallah et al. 1999).

Trichoderma fungi are commonly found on wood material (Justyna & Teresa 2020). They are known for their ability to decompose not only cellulose but also the lignin component in native plant biomass due to the simultaneous secretion of oxidoreductive enzymes (Chakroun et al. 2010). *Pleurotus* ostreatus is a species of white-rot fungus that effectively degrades lignin (Qian et al. 2020). The present study hence uses two microbial cultures, viz., *Trichoderma*, a biodecomposing agent to increase the speed of decomposition, and *Pleurotus*, an excellent delignifying microorganism to increase lignin reduction. The pretreated coir pith was further studied for anaerobic digestion.

MATERIALS AND METHODS

The sample for the present study was taken according to the standard sampling and preservation method from the coir-manufacturing center at Murukumpuzha village in Trivandrum district, Kerala. The analytical procedures described in the Standard Methods for the Examination of Water and Wastewater (APHA 1989) were followed for the characterization study. Lignin and cellulose were estimated by the method of Goering and Van Soest. For pretreatment, *Trichoderma* and *Pleurotus*, the fungal cultures prepared on PDA (Potato Dextrose Agar) slants, were collected from Kerala Agricultural University, Vellayani, Trivandrum.

Fig. 1 shows the experimental setup of an anaerobic digester. For the present study, borosilicate glass bottles of one-liter capacity were used as digesters. Three outlets were made in the digester for gas collection, sample collection, and the addition of buffer and other chemicals. One outlet is connected to the water displacement column using a rubber tube. The reading in the column directly shows the amount of gas produced during anaerobic digestion. The whole setup is perfectly sealed to maintain a complete anaerobic condition.

Experimental Studies

Optimization of pH: For the experimental study, 100 g of coir pith samples were mixed with dilution water along with a seed of 5% concentration to initiate digestion and charged into a digester of one-liter capacity. A buffer (sodium bicarbonate) was added to maintain the pH. The digester was kept at various pH levels (5, 6, 7, 8, 9), and the optimum pH was found by observing the gas production. The total solids

Fig. 1: Experimental setup.

Fig. 2: Pretreated coir pith with *Trichoderma*.

Fig. 3: Pretreated coir pith with *Pleurotus*.

and volatile solids of the samples were studied at various time intervals.

Pretreatment of coir pith using *Trichoderma*: For the pretreatment process, 10 g of *Trichoderma* was applied uniformly over 500 g of coir pith. The process was repeated by adding the microbial culture alternately with the coir pith and keeping it for thirty days for the degradation of the lignin. Proper moisture content was maintained by sprinkling water periodically. Fig. 2 shows the treatment of coir pith with *Trichoderma*. Then, the above sample was fed into the anaerobic digester, and pH 6 was maintained. The variation in gas production was noted at various time intervals.

Pretreatment of coir pith using *Pleurotus*: For the preparation of PDA slants, 40 g of PDA was accurately weighed and dissolved in one liter of distilled water. The solution was shaken well and heated to dissolve the PDA. The solution is poured into test tubes and sterilized at 1.5 $kg.cm^{-2}$ gauge pressure for 20 min. The test tubes were then kept in a slanting position in aseptic conditions to allow the medium to cool and solidify. The slants were then properly labeled and stored. The microorganism strains are subcultured on the thus-prepared PDA slants. The sub-culturing environment is maintained under aseptic conditions. The microorganism-transferring loop is sterilized on a Bunsen burner flame and allowed to cool. The microorganism is taken from the master stock with the help of the loop and inoculated on the PDA slant in a zig-zag manner to maximize growth. It is incubated at 30°C for 2-3 days. After visual observation for satisfactory growth, the subcultures were stored at 5°C, for further culturing and experimentation.

The coir pith collected from the site was cleaned and dried. To the 500-g batch of coir pith, 300 mL of distilled water and 1000 mL of liquid nutrient media were added for the nourishment of the microorganisms (Fig. 3). The substrate is kept in a moist state by adding distilled water every alternate day and kept for fifteen days for the degradation of the lignin. Then, the sample was fed into the anaerobic digester, and pH 6 was maintained. The variation in gas production was noted at various time intervals.

Table 1: Quality of coir pith.

Parameters	Value	Parameters	Value
pH	6.45	Total Solids [$g.L^{-1}$]	25.46
Chlorides [$mg.L^{-1}$]	163.3	Volatile Solids [$g.L^{-1}$]	22.98
Magnesium [$mg.L^{-1}$]	0.48	Alkalinity [$mg.L^{-1}$]	550
Calcium [$mg.L^{-1}$]	1.6	Inorganic Carbon [ppm]	0.1461
Sulphates [$mg.L^{-1}$]	27	Total Carbon [ppm]	390
Conductivity [$\mu s.cm^{-1}$]	64.4	Total protein [ppm]	22.94
Hardness [$mg.L^{-1}$]	6	Lignin [%]	30.91
Cellulose [%]	25.82	Total nitrogen [ppm]	3.67
TOC [ppm]	389.8	Potassium [%]	0.78
Phosphorus [%]	0.01		

RESULTS AND DISCUSSION

The characterization study of a fresh coir pith sample is shown in Table 1. From the characterization study, it can be observed that coir pith is suitable for anaerobic digestion since it possesses an appreciable amount of Total Organic Carbon and total solids and does not possess any toxic substances.

The anaerobic digester was set up with various pH values, and the variation of the gas production is shown in Fig. 4. It can be inferred that coir pith without any treatment yielded 8 mL of gas at optimum pH 6 in 24 days.

Table 2: Percentage reductions of volatile solids & total solids at various pH.

Variation in pH	Total solids	Volatile solids
pH 5	21.46%	39.25%
pH 6	24.35%	41.53%
pH 7	22.05%	38.84%
pH 8	16.57%	31.70%
pH 9	14.08%	26.96%

Table 3: Comparison of fresh and digested samples at pH 6.

Parameters	Fresh sample	Digested sample
pH	6	6
Volatile solids [$g.L^{-1}$]	20.74	12.13
Total solids [$g.L^{-1}$]	25.01	18.92
TOC [ppm]	389.8	313.2
Inorganic Carbon [ppm]	0.1461	0.101
Total Carbon [ppm]	390	313.3
Lignin [%]	30.91	30.12

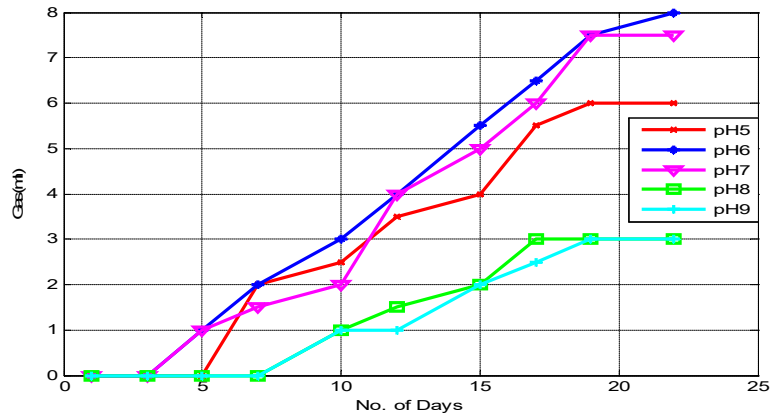

Fig. 4: Variation of gas production at various pH.

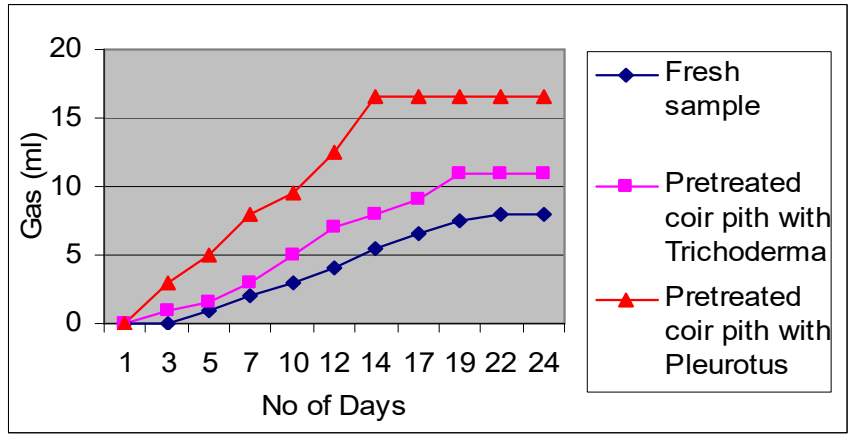

Fig. 5: Variation in gas production.

Since the maximum reduction of total solids and volatile solids was in the range of 6 to 7 (Table 2), the rest of the experiments were performed at pH 6. The characterization study for coir pith after digestion at pH 6 was done. The comparison between the fresh and digested samples of coir pith without any treatment at pH 6 is given in Table 3.

From Table 3, it can be observed that there is a gradual reduction of the parameters such as Total carbon and total solids, and also, there is yield of gas. The comparison of pretreated samples and digested samples of *Trichoderma* and *Pleurotus* and the variation in gas production are shown in Table 4. When *Trichoderma* was used, the lignin content was reduced by 3.7% after the pretreatment. There is a reduction of total solids (29.55%) and volatile solids (56.84%) during the digestion period. When *Pleurotus* was used as a delignifying agent, the lignin content was reduced

Table 4: Comparison of pretreated and digested samples using *Trichoderma* and *Pleurotus*.

Parameters	*Trichoderma*		*Pleurotus*	
	Pretreated sample	Digested sample	Pretreated sample	Digested sample
pH	6	6	6	6
Volatile solids [$g.L^{-1}$]	20.74	8.95	19.02	7.03
Total solids [$g.L^{-1}$]	23.34	16.44	22.88	14.92
TOC [ppm]	387.8	296.5	389.2	281.1
Inorganic Carbon [ppm]	0.1351	0.116	0.131	0.127
Total Carbon [ppm]	387.94	296.62	389.3	281.23
Lignin [%]	27.21	27.09	24.13	24.01

Table 5: Variation of methane content in the gas produced.

Parameters	Coir pith without pretreatment	Coir pith treated with *Trichoderma*	Coir pith treated with *Pleurotus*
Days for maximum gas production	24	17	14
Quantity of gas [mL]	8	11	16.5
Methane content [ppm]	26.9	59	74

Table 6: Characteristics of sludge after digestion.

Parameters	Coir pith without pretreatment	Coir pith treated with *Trichoderma*	Coir pith treated with *Pleurotus*
Nitrogen content [wt. %]	0.26	0.93	1.25
Phosphorus [%]	0.01	0.04	0.06
Potassium [%]	0.78	1.1	1.2
Lignin content [%]	30.91	27.09	24.01
Volatile matter [%]	43.1	44.2	43.29
Ash content [%]	25.95	24.42	26.77
Carbon content [%]	22.95	17	14.12
pH	5.67	6.2	6.28

by 6.78%, and 16.5 mL of gas was produced at an earlier time of 14 days when compared with the sample without any pretreatment (24 days). There is also a maximum reduction of total solids (34.79%) and volatile solids (63.04 %).

The gas produced was analyzed for the presence of methane using the Gas Chromatograph. The methane concentration was less than 1000 ppm, so the FID (Flame Ionization Detector) analyzer in the gas chromatograph was used for this analysis. For 2 mL of biogas, the results are shown in Table 5.

The variation in gas production of the anaerobic digesters is shown in Fig. 5. It is clear that the methane content was appreciably increased after the pretreatment of coir pith with *Pleurotus*. The quantitative and qualitative analysis of the sludge was conducted after digestion. The nitrogen content, lignin content, potassium, phosphorus, volatile matter, ash content, carbon content, and pH were studied for each digested sample, and the results are shown in Table 6.

The sludge after digestion indicates a marginal increase of 3.8%, 5%, and 0.53% in NPK value, which means it can be used as fertilizer.

CONCLUSIONS

From the experimental studies, it can be concluded that coir pith is suitable for anaerobic digestion since it possesses an appreciable amount of Total Organic Carbon, COD, total solids, and only trace amounts of calcium and magnesium. There is a considerable reduction of total solids (43.34%) and volatile solids (67.53%) during the digestion period of 24 days for the sample at pH 6 without any pretreatment of coir pith.

Pretreatment of coir pith with *Trichoderma* is found to be the effective reduction of total solids (50.52%) and volatile solids (70.32%) during the digestion period for the pretreated sample. Also, the maximum gas production was 11 mL in 19 days. The lignin content was reduced by 3.7% after the pretreatment. There is a reduction of total solids (29.55%) and volatile solids (56.84%) during the digestion period.

When *Pleurotus* was used as a delignifying agent, the lignin content was reduced by 6.78%, and 16.5 mL of gas was produced at an earlier time of 14 days when compared with the sample without any pretreatment (24 days). There is also a maximum reduction of total solids (34.79%) and volatile solids (63.04 %).

The gas produced was analyzed using a Gas chromatograph, and it was found that the methane content was 26.9 ppm, 59 ppm, and 74 ppm in three cases. The sludge after digestion indicates a marginal increase of 3.8%, 5%, and 0.53% in NPK value, which means it can be used as fertilizer. In the present work, batch digestion for a lab-scale model was made. The study of gas production with varying concentrations of coir pith, the effect of gas production with time of digestion, etc., is necessary to prepare guidelines for the actual design of a coir pith digester in the field.

REFERENCES

American Public Health Association (APHA) 1989. Standard Methods for the Examination of Water and Wastewater. Seventeenth edition. American Water Works Association, Washington DC.

Chakroun, H., Mechichi, T., Martinez, M.J., Dhouib, A. and Sayadi, S. 2010. Purification and characterization of a novel laccase from the ascomycete *Trichoderma atroviride*: application on bioremediation of phenolic compounds. Process Biochem., 45: 507-513.

Deivanai, K. and Kasturi Bai, R. 1995. Batch biomethanation of banana trash and coir pith. Bioresour. Technol., 52: 93-94.

Gharsallah, N., Labat, M., Aloui, F. and Sayadi, S. 1999. The effect of *Phanerochaete chrysosporium* pretreatment of olive mill wastewaters on anaerobic digestion. Resour. Conserv. Recycl., 27: 187-192.

Justyna, B. and Teresa, K.K. 2020. Modification of post-industrial lignin by fungal strains of the genus *Trichoderma* isolated from different composting stages. J. Environ. Manag., 266: 110573.

Karthick, R., Babu, M. and Arvind Bharani, R.S. 2015 Evaluation of lignocellulosic agro wastes for the enhanced production of extracellular cellulase and xylanase by *Trichoderma harzianum*. Nat. Environ. Pollut. Technol., 14: 47-52.

Khadeeja, B., Sreekumar, S. and Hiran Nazir, K. 2012. Ecological effects and occupational health hazards due to coir retting: A case study from the west coast of Kerala, India, Nat. environ. Pollut. Technol., 11: 585-590.

Kunchikannan, L.K.N.V., Mande, S.P., Kishore, V.V.N. and Jain, K.L. 2007. Coir pith: a potential agro residue for anaerobic digestion. Energy Sour. Part A Recov. Util. Environ. Effects, 29: 293-301.

Makela, M., Galkin, S., Hatakka, A. and Lundell, T. 2002. Production of organic acids and oxalate decarboxylase in lignin-degrading white rot fungi. Enzyme Microb. Technol., 30: 542- 549.

Muneeswaran, K. and Kesavan, N. 2022. Growth and development of the coir industry in India. Mukt Shabd J., 11: 695-707.

Narendar, R and Priya Dasan, K. 2014. Chemical treatments of coir pith: morphology, chemical composition, thermal and water retention behavior. Composites Part B: Engineering, 56: 770-779.

Paramanandham, J. and Ronald Ross, P. 2015. Lignin and cellulose content in coir waste on subject to sequential washing. J. Chem. Res., 1:10-13.

Prakash, V., Kavitha, J.R., Kamaleshwaran, R., Prabharan, P. and Alagendran, S. 2021. Effect of coir pith compost in agriculture. J. Med. Plants Stud., 9(4): 106-110.

Priyadarshini, V., Felixkala, T., Depaa, R.A.B., Hemamalinie, A., Francis Xavier, J., Surendra Babu, K. and Jeya Arthi, A. J. 2021. Experimental investigation on properties of coir pith and its influence as partial replacement of fine aggregate in concrete. Materials Today: Proceedings, 45(7): 6903-6906.

Qian, S., Xun, D. and Rui-Qing, S. 2020. Expression of *Pleurotus ostreatus* laccase gene in pichia pastoris and its degradation of corn stover lignin. Microorganisms, 8: 601.

ORCID DETAILS OF THE AUTHORS

Smitha Krishna Warrier: https://orcid.org/0009-0009-3559-7349

Nature Environment and Pollution Technology
An International Quarterly Scientific Journal

p-ISSN: 0972-6268
(Print copies up to 2016)
e-ISSN: 2395-3454

Vol. 23 | No. 1 | pp. 583-589 | 2024

Original Research Paper

https://doi.org/10.46488/NEPT.2024.v23i01.056

Open Access Journal

Determination of Mycotoxigenic Fungi and Total Aflatoxins in Stored Corn from Sites of Puebla and Tlaxcala, Mexico

K. Saez-Gomez*(***), R. Avila-Sosa(***), M. Huerta-Lara***(****), F. Avelino-Flores***(*****) and R. Munguia-Pérez*(***)†**

*Laboratorio de Micología del Centro de Investigaciones en Ciencias Microbiológicas, Instituto de Ciencias, Benemérita Universidad Autónoma de Puebla, Puebla, México

**Departamento de Bioquímica-Alimentos, Facultad de Ciencias Químicas, Benemérita Universidad Autónoma de Puebla, Puebla, México

***Posgrado en Ciencias Ambientales, Instituto de Ciencias, Benemérita Universidad Autónoma de Puebla, Puebla, Mexico

****Departamento de Desarrollo Sustentable, Instituto de Ciencias, Benemérita Universidad Autónoma de Puebla, Puebla, México

*****Centro de Investigaciones en Ciencias Microbiológicas, Instituto de Ciencias, Benemérita Universidad Autónoma de Puebla, Puebla, México

†Corresponding author: R. Munguia-Pérez; ricardo.munguia@correo.buap.mx

Nat. Env. & Poll. Tech.
Website: www.neptjournal.com

Received: 18-05-2023
Revised: 03-07-2023
Accepted: 05-07-2023

Key Words:
Mycotoxigenic fungi
Aspergillus flavus
Aflatoxins
Corn kernel

ABSTRACT

This paper aimed to evaluate the contamination with mycotoxigenic fungi and total aflatoxins in stored corn from different sites in Puebla and Tlaxcala, Mexico. Methodology. The study was conducted at two sites in Puebla (San Salvador El Seco and Junta Auxiliar La Resurrección) and two sites in Tlaxcala (Tlaltepango and Nativitas). A total of 80 samples of stored corn were collected. Identification of *Aspergillus flavus* was performed by microculture techniques and specific taxonomic keys (macromorphological and micromorphological). Then, samples of contaminated corn were selected, and aflatoxin production was confirmed using a direct solid-phase ELISA kit. A total of 25 *A. flavus* strains were identified. Other possible mycotoxin-producing fungi were *Penicillium* (n=52) and *Fusarium* (n=19). Regarding total aflatoxin contamination, all samples were contaminated within a range of 1.589 to 11.854 µg/kg, and the average concentration was 6.3 µg/kg corn. Implications. The detection of mycotoxigenic fungi in the samples tested and of aflatoxins in corn highlights the importance of monitoring these fungi. Since food safety is at risk, it shows the need for methods to control these fungi and their metabolites.

INTRODUCTION

Mycotoxins are toxic secondary metabolites that contaminate a variety of foods. Their consumption can be harmful to human and livestock health, as these metabolites can cause teratogenesis, immunosuppression, and cancer. These are substances produced mainly by strains of the genera *Penicillium, Fusarium,* and *Aspergillus*. The most studied mycotoxins are aflatoxins and the most toxic naturally produced mycotoxins. There are about 20 types of aflatoxins, with aflatoxin B1 being the most toxic and classified as carcinogenic by the International Agency for Research on Cancer (WHO & IARC 1993). Numerous studies have shown that aflatoxins can be carcinogenic, teratogenic, mutagenic, and hepatotoxic in both animals and humans (Díaz de León-Martínez et al. 2020).

Aflatoxins are produced mainly by *Aspergillus flavus*. This and other fungi colonize numerous cereals, including corn. Colonization and degradation of plant tissues occurs through enzymatic degradation of starch, proteins, and lipids (Lu et al. 2022). This occurs in response to stimuli and threats from the environment. It is known that most mycotoxins, including aflatoxins, can be taken up from the root in plants such as corn and then translocated to organs above the soil (Righetti et al. 2021). This colonization and production of mycotoxins is influenced by factors such as temperature, moisture, and nutrient content of corn grain. Therefore, grain storage conditions are critical to avoid this contamination by mycotoxic fungi and their metabolites. Corn is a crop of global importance and ranks third in the world, followed by wheat and rice, due to its high consumption (De Girolamo et al. 2016).

In Mexico, corn is a staple food and the main crop for domestic use, especially in rural areas. Climate change has created favorable conditions for the spread of fungi and their metabolites in places where this was not previously the case (Saez-Gomez et al. 2022). Contamination of these and other crops threatens food security. Therefore, monitoring is important to prevent the spread of these fungi and their metabolites. However, there is no uniform regulation worldwide for the permissible limits of these metabolites in cereals and their finished products. In Mexico, there is a National Standard (NOM-188-SSA1-2002) that establishes permissible limits for total aflatoxins (aflatoxin B1, aflatoxin B2, aflatoxin G1, and aflatoxin G2) in cereals for human and animal consumption. These limits state that the total content of aflatoxins in cereals must not exceed 20 µg/kg. If the concentration is between 21 and 300 µg/kg, the grain should be destined for animal feed. However, the European Union has more specific standards for aflatoxin B1, as 2 µg/kg-1 should not be exceeded in food for human consumption (Reinhold & Reinhardt 2011).

Techniques for monitoring aflatoxins in food include rigorous methods such as chromatographic techniques, e.g., thin-layer chromatography and HPLC. However, these methods are expensive and require extensive sample preparation. For this reason, the use of ELISA kits serves as a replacement technique because these tests are rapid, sensitive, specific, and less expensive (Tarannum et al. 2020). In a study conducted by Cabrera-Meraz et al. (2021), total aflatoxin contamination was quantified in samples of corn kernels, dough, and tortillas, with values ranging from 0.82 to 28.04, 0.66 to 14.36, and 0.63 to 12.04 $mg.kg^{-1}$, respectively, in 75% of the samples. Similarly, Jayaratne et al. (2020) reported aflatoxin B1 in corn kernels with concentrations of 60-70 ppb, while these concentrations in agricultural soils were 350-400 ppb. In another study by Rojas Jaimes et al. (2020), contamination by total aflatoxins was found in peanuts with a concentration of 149.7 ppb.

Monitoring of these metabolites is important from an economic point of view because of financial losses when crop yields decrease or because of the costs of prevention or decontamination. This work aimed to evaluate contamination by total aflatoxins (aflatoxin B1, aflatoxin B2, aflatoxin B3, and aflatoxin B4) in corn stored in the regions of Puebla and Tlaxcala, Mexico.

MATERIALS AND METHODS

Study Area and Sample Collection

The study was conducted at different sites: San Salvador El Seco (1909′50.50″N, 97037′48.50″W) and Junta Auxiliar La Resurrección (1906′50.30″N, 9808′10.50″W) in the State of Puebla (SSS and JAR, respectively). In Tlaltepango (1907′15.79″N, 9809′18.51″W) and Nativitas (19014′3.50″N, 98018′41.50″W) in Tlaxcala State (TLA or

Fig. 1: Test sites: Puebla (San Salvador El Seco and Junta Auxiliar la Resurrección) and Tlaxcala (Tlaltepango and Nativitas). Mapa Digital de México V6.3.0, 2023.

NAT). A total of 80 samples of corn were collected in January (n=40) and August (n=40) 2017. In the state of Puebla, 40 samples were collected from SSS as well as JAR, while in the state of Tlaxcala, 20 samples were collected from TLA and 20 samples from NAT (Fig. 1). Corn was collected from different storage locations (10 locations). In some locations, the corn was stored unpackaged, and only two locations used cloth bags (50 kg). Using a sterile plastic hand scoop. Approximately 100 g of samples were placed in Ziploc bags and transported to the laboratory, where they were stored at 4ºC until use.

Isolation and Phenotypic Identification of Presumptive Isolates of *A. flavus*

Samples were pounded in a mortar until a fine powder was obtained. From these samples, 1:10, 1:100, 1:1000, and 1:10,000 dilutions were prepared. Subsequently, 50 µL of the last two dilutions of each sample were inoculated into Sabouraud dextrose agar (SDA, Sigma-Aldrich, Mexico) and incubated at 28 °C for 7 days. Presumptive colonies of *Aspergillus* section *Flav*i were seeded in tubes containing SDA to obtain axenic cultures. Subsequently, the microculture technique was applied to perform macromorphological and micromorphological identification using specific taxonomic keys (Rippon & Castañeda 1992, Bonifaz 2015). The putative isolates of *A. flavus* and *A. parasiticus* were reseeded in an AFPA differential medium (*Aspergillus flavus parasiticus* agar, Sigma-Aldrich, Mexico). To confirm their identification by the production of orange-yellow pigment on the back of the colony.

Quantification of Total Aflatoxins

A direct competitive solid-phase ELISA kit (Astori S.N.C., Poncarale, Italy) was used to determine total aflatoxin contamination in corn samples. An extraction solution (70% methanol, Sigma-Aldrich, Mexico) was prepared from each sample. Once the sample was prepared, it was ground (Hamilton Beach Model 80335R, USA) until it had the particle size of fine instant coffee. Then, 1g of the sample was weighed, and 5 mL of the extraction solvent was added. The whole was mixed with stirring for about 2 min, the mixture was allowed to stand until it precipitated, and then it was filtered through Whatman #1 filter paper. The filtrate obtained was analyzed as mentioned below.

Analysis of the filtrate obtained from the sample: According to the sample analyzed, 200 µL of the aflatoxin-HRP conjugate was added to each dilution well, 100 µL of each standard and sample was added to the corresponding dilution well containing the conjugate, 100 µL of the contents of each dilution well was pipetted three times and transferred to a corresponding antibody-coated microtiter well, incubated at room temperature for 15 min, and then the contents of the microtiter wells were transferred to a waste cell. The microtiter wells were washed 5 times by filling each well with PBS-Tween wash buffer (Sigma-Aldrich, Mexico). Then, the remaining buffer was removed, 100 µL of substrate reagent was added to each microtiter well and incubated at room temperature for 5 min, followed by 100 µL of stop solution. Finally, the optical density (OD) of each microplate was read with a microplate reader (Accuris MR9600, USA) using a 450 nm filter. Concentrations were calculated by extrapolating the OD with the respective calibration curve generated from the following concentrations: 1.0, 2.5, 5.0, and 10.0 $\mu g.kg^{-1}$.

RESULTS AND DISCUSSION

The states of Puebla and Tlaxcala are located in the center of Mexico. Their climate is temperate and semi-humid. The average daily temperature is 25°C, but there is considerable seasonal variation. The rainy season lasts about 7 months, and humidity is very high during this period (Briones-Reyes et al. 2007). Corn is the most important agricultural product in both states. However, corn is also the most consumed product for humans. Considering the climatic conditions, with the prevailing hot and semi-humid conditions for considerable periods of time, there is a high probability of infestation with corn fungi during agricultural processes, grain storage, and processing (Domínguez-Hernández et al. 2022). In addition, Rodríguez-Ramírez et al. (2021) reported temperature and precipitation variability in this geographic zone during 2015-2017. They noted an increase in insect populations due to higher temperatures and an increase in fungi due to humidity.

Based on micromorphological and macromorphological characteristics (Fig. 2) and using specific taxonomic keys, *A. flavus* species were identified in native corn kernels stored outdoors at the four test sites. Colonies of *A. flavus* were apartment, greenish-yellowish, with white margins and spherical spores. In addition, strains positive for the morphological characteristics of *A. flavus* were seeded in the AFPA differential medium to be sure that they had been treated with this species since strains of this fungus produce a yellow-orange pigmentation on the back of the colony (Fig. 3). A total of 25 strains of *A. flavus* were isolated; Fig. 4 shows the number of isolates obtained at each test site. Similarly, strains of *Fusarium* and *Penicillium* were also identified. Fig. 5 shows that the greatest diversity of identified genera was obtained in JAR, followed by TLA, NAT, and SSS. However, only two genera were found in the latter: 3 isolates of *Penicillium* and 1 of *Fusarium*.

For the count of total aflatoxins in the 80 corn samples, a calibration curve was generated by linear regression with

Table 1: Concentration of total aflatoxins in stored corn collected from different sites in Puebla and Tlaxcala, Mexico.

Strains	Absorbance	Concentration[µg.kg^{-1}]	Strains	Absorbance	Concentration[µg.kg^{-1}]
2S-M5	0.765	5.637	2N-M4	0.645	8.239
2J-M5	0.985	3.516	2T-M2	0.495	6.215
2N-M5	0.86	4.721	1S-M9	0.705	*10.552
1T-M10	0.76	5.685	2J-M1	0.255	1.589
2T-M5	0.915	4.191	2N-M1	1.185	4.191
2S-M1	0.388	**9.27	1J-M6	0.915	8.769
2S-M4	0.975	3.613	2T-M1	0.44	5.203
2J-M4	0.423	8.933	1J-M10	0.81	**9.328
1N-M10	0.525	7.95	1N-M9	0.382	6.649
1T-M9	0.72	6.07	1J-M8	0.66	**9.637
2T-M4	0.408	**9.078	1T-M7	0.35	6.553
1S-M10	0.12	*11.854	1S-M8	0.67	8.384
2S-M3	0.935	3.998	1J-M9	0.48	6.89
2J-M3	1.09	2.504	1N-M8	0.635	7.227
2N-M3	0.975	3.613	1S-M7	0.6	**9.107
1N-M6	0.71	6.167	1T-M6	0.405	5.203
2T-M3	1.08	2.601	1S-M6	0.81	6.408
2S-M2	0.67	6.553	1J-M7	0.685	7.468
2N-M2	1.04	2.986	1N-M7	0.575	6.167
2J-M2	0.71	6.793	1T-M8	1.13	2.119

Total aflatoxin concentrations: * greater than 10 µg.kg^{-1} of maize; ** close to 10 µg.kg^{-1} of maize

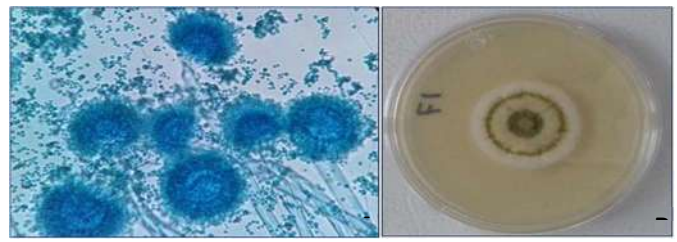

Fig. 2: Micromorphological (A) and macromorphological (B) characteristics of *Aspergillus flavus* isolated in stored corn collected from different sites in Puebla and Tlaxcala, Mexico.

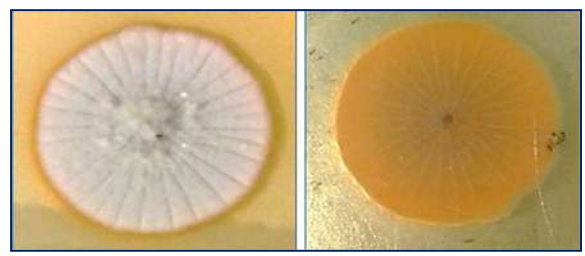

Fig. 3: Front and back of the *Aspergillus flavus* colony in AFPA differential medium isolated in stored corn collected from different sites in Puebla and Tlaxcala, Mexico.

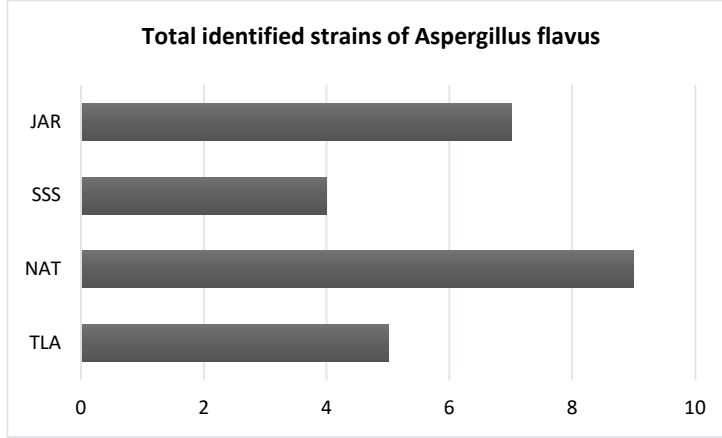

Fig. 4: Number of *Aspergillus flavus* isolated in stored corn collected from different sites in Puebla and Tlaxcala, Mexico.

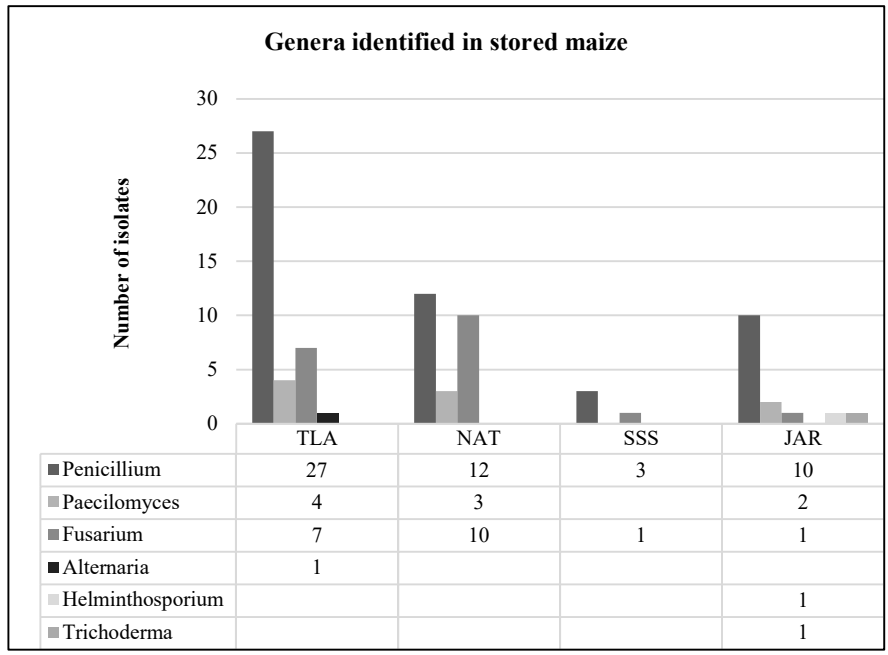

	TLA	NAT	SSS	JAR
Penicillium	27	12	3	10
Paecilomyces	4	3		2
Fusarium	7	10	1	1
Alternaria	1			
Helminthosporium				1
Trichoderma				1

Fig. 5: Genera identified in isolated stored corn collected from different sites in Puebla and Tlaxcala, Mexico.

the total aflatoxin standards at different concentrations. The results of the analysis of the corn samples are shown in Table 1. *A. flavus* is a potentially aflatoxigenic fungus. Inadequate storage conditions, controlling temperature and humidity, could be a critical factor in the formation of aflatoxins, toxic secondary metabolites commonly associated with liver cancer (Bbosa et al. 2013). The characterization of macro- and micromorphology is consistent with that of Seerat et al. (2022). In addition, fewer isolates of this aflatoxigenic species were obtained in SSS, possibly due to the temperate and semi-arid climate there. Although *Aspergillus* is a cosmopolitan fungus that occurs in different climates, according to Bonifaz (2015), the climate that favors its spread is a humid climate, which is also present in the other sampled sites. Based on these results, climate is a factor contributing to the spread of aflatoxigenic fungi and, in this study, to the production of *A. flavus*, the only aflatoxigenic species isolated in the sampled sites.

In addition, contamination with this fungus may begin during the field phase and increase during the storage phase. This is mainly due to poor grain storage practices, e.g., if the temperature is not controlled, if the contaminated grains are not removed, they may contaminate other grains, and if there are insect or mite populations, they may damage the

grains and make them more susceptible to contamination. These factors may have influenced the fact that the corn was contaminated with *A. flavus* because, at the sampling sites, the locations designated for corn storage were outdoors.

In a study by Seerat et al. (2022), contamination with *A. flavus* was also found in corn samples. 212 isolates were recovered from 80 analyzed corn seed samples. On the other hand, Wokorach et al. (2022) reported that *A. flavu*s was present in 63% of staple food samples. Similarly, Okoth et al. (2012) reported isolates of *A. flavu*s planted in AFPA with a yellow-orange coloration on the back of the colony. Contamination by this potentially aflatoxigenic fungus in these substrates (agricultural soils and corn) is an ongoing threat to human and animal health at the sites where sampling was conducted. This is because the crops are destined for consumption by the farmers' families or sold in the region. Therefore, the presence of these high aflatoxigenic species affects access to nutritious and culturally appropriate foods derived from these crops.

Other filamentous fungi identified and of economic importance were *Penicillium*, *Fusarium*, and *Alternaria*, some species of which are also potentially aflatoxigenic. Based on the number of strains found, we can assume that only the isolates of *Penicillium*, *Paecilomyces*, and *Fusarium* are important. In a study by Penagos-Tabares et al. (2022), the presence of *Penicillium roqueforti, Saccharomyces* spp., *Geotrichum candidum, Aspergillus fumigatus, Monascus ruber, Mucor circinelloides, Fusarium* spp., and *Paecilomyces niveus* was detected in corn silage. As you can see, the genera *Penicillium, Aspergillus,* and *Fusarium* are consistent with those reported in this study.

As for the quantification of total aflatoxins, contamination with total aflatoxins (AFB1, AFB2, AFB3, AFB4) was detected in all samples. The average concentration of aflatoxins in the samples tested was 6.3 $\mu g.kg^{-1}$ of maize. In 2 of these samples, the concentration was above 10 µg/kg, and in 5, it was close to this concentration. Although none of the samples exceeded the value of NOM -188-SSA1-2002, these concentrations are above the permissible values compared to the European standards. The fact that contamination with total aflatoxins was detected in all the samples tested (n=40) indicates that the storage conditions for this cereal are not optimal. Moreover, the presence of these metabolites in a cereal that is frequently consumed in the region where the sampling took place endangers the health of the inhabitants, as they are the main consumers.

It has also been shown that the ELISA technique contributes to the rapid identification of these metabolites. It is a cost-effective, sensitive, and reliable technique. Moreover, an analytical method with these characteristics is essential to identify agricultural products contaminated with these metabolites or other mycotoxins to prevent them from becoming final products and not being marketed.

Contamination by these metabolites in a cereal that is widely in our country, and especially in the sampled areas, poses a risk to human and animal health because of the effects these metabolites can cause since the sampled corn is marketed in the region. They also affect the nutritional and commercial value and threaten the family income of producers since agriculture is one of the main economic activities in the sampled areas.

In summary, this study shows that corn at sites in Puebla (SSS and JAR) and Tlaxcala (TLA and NAT) is susceptible to general aflatoxin contamination. *A. flavus*, a potentially aflatoxigenic strain, can also affect the quality of this grain and, at the same time, human and animal health. Therefore, it is important to adopt stricter regulations for total allowable aflatoxin levels in grains such as corn since they are so important for consumption. Finally, the ELISA technique for determining total aflatoxin content in corn is a simple, rapid, and practical technique. This can contribute to sustainable agriculture.

ACKNOWLEDGEMENTS

We appreciate the financial support for carrying out this work from the National Council of Science and Technology (CONACyT) and the Benemérita Universidad Autónoma de Puebla (Postgraduate in Environmental Sciences).

REFERENCES

Bbosa, G.S., Kitya, D., Lubega, A., Ogwal-Okeng, J., Anokbonggo, W.W. and Kyegombe, D.B. 2013. Review of the Biological and Health Effects of Aflatoxins on Body Organs and Body Systems. In Razzaghi-Abyaneh, M. (ed.) Aflatoxins-Recent Advances and Future Prospects. InTech, Lodon, UK, pp. 239-265.

Bonifaz, J. (ed.) 2015. Basic Medical Mycology. McGraw Hill, Mexico, p.725.

Briones-Reyes, D., Gómez-Martinez, L. and Cueva-Rolón, R. 2007. Zearalenone contamination in corn for human consumption in the state of Tlaxcala, Mexico. Food Chem., 100(2): 693-698.

Cabrera-Meraz, J., Maldonado, L., Bianchini, A. and Espinal, R. 2021. Incidence of aflatoxins and fumonisins in grain, masa, and maize tortillas in four municipalities in the department of Lempira, Honduras. Heliyon, 7(12): e08506.

De Girolamo, A., Lattanzio, V.M.T., Schena, R., Visconti, A. and Pascale, M. 2016. Effect of alkaline cooking of maize on the content of fumonisins B1 and B2 and their hydrolyzed forms. Food Chem., 192(2): 1083-1089.

Díaz De León-Martínez, L., Rodríguez-Aguilar, M., Wong-Arce, A., Díaz-Barriga, F., Bañuelos-Hernández, B., Rosales-Mendoza, S. and Flores-Ramírez, R. 2020. Evaluation of acute and chronic exposure to aflatoxin B1 in indigenous women of the Huasteca Potosina, Mexico. Env. Sci. Poll. Res., 27(5): 30583-30591.

Domínguez-Hernández, E., Gaytán-Martínez, M., Gutiérrez-Uribe, J.A.

and Domínguez-Hernández, M.E. 2022. The nutraceutical value of maize (*Zea mays* L.) landraces and the determinants of its variability: A review. J. Cereal Sci., 103: 103399.

Jayaratne, W.M.S.C., Abeyratne, A.H.M.A.K., De Zoysa, H.K.S., Dissanayake, D.M.R.B. N., Bamunuarachchige, T.C., Waisundara, V.Y. and Chang, S. 2020. Detection and quantification of Aflatoxin B1 in maize and maize-grown soils in the district of Anuradhapura, Sri Lanka. Heliyon, 6(10): e05319.

Lu, Y.N., Shan, Y., Huang, H., Zhu, L., Li, B., Wang, S. and Liu, F. 2022. Quantum dot microsphere-based immunochromatography test strips enabled sensitive and quantitative on-site detections for multiple mycotoxins in grains. Food Chem., 376(5), 131868.

Mexican Ministry of Health. 2002. Products and Services. Aflatoxin Control in Cereals for Human and Animal Consumption. Sanitary Specifications. SEGOB, Mexico

Okoth, S., Nyongesa, B., Ayugi, V., Kang'ethe, E., Korhonen, H. and Joutsjoki, V. 2012. The toxigenic potential of Aspergillus species occurring on maize kernels from two agroecological zones in Kenya. Toxins, 4(11): 991-1007.

Penagos-Tabares, F., Khiaosa-ard, R., Schmidt, M., Pacífico, C., Faas, J., Jenkins, T., Nagl, V., Sulyok, M., Labuda, R. and Zebeli, Q. 2022. Fungal species and mycotoxins in moldy spots of grass and maize silages in Austria. Mycotox. Res., 38(2): 117-136.

Reinhold, L. and Reinhardt, K. 2011. Mycotoxins in foods in Lower Saxony (Germany): results of official control analyses performed in 2009. Mycotox. Res, 27(1), 137-143.

Righetti, L., Bhandari, D.R., Rolli, E., Tortorella, S., Bruni, R., Dall'asta, C. and Spengler, B. 2021. Unveiling the spatial distribution of aflatoxin B1 and plant defense metabolites in maize using AP-SMALDI mass spectrometry imaging. Plant J., 106(1): 185-199.

Rippon, J. and Castañeda, L. (eds.) 1992. Medical Mycology: Pathogenic Fungi and Actinomycetes. McGraw-Hill, México, p.321.

Rodríguez-Ramírez, E.C., Williams-Linera, G., Díaz-Ávalos, C. and Luna-Vega, I. 2021. Masting effect on canopy greenness and climate response on seed production of *Fagus grandifolia* subsp. Mexicana across the Sierra Madre Oriental, Mexico. Clim. Change Ecol., 2: 10035.

Rojas Jaimes, J., Chacon-Cruzado, M., Diaz-Tello, A. and Castañeda-Pelaez, L. 2020. Quantification of carcinogenic aflatoxins in unprocessed foods and their implication for consumption in Lima, Peru. Nutr. Hosp., 38(1): 146-151.

Saez-Gomes, K.C., Castañeda-Roldán, E.I., Avila-Sosa, R. and Munguía-Pérez, R. 2022. Mycotoxins and Climate Change. In: Frías-De-León, M.G., Mendoza, C.B., Montes, M.D.R.R. and Escalante, E.D. (eds), The Impact of Climate Change on Fungal Diseases: Fungal Biology. Springer, Switzerland, pp. 239-256.

Seerat, W., Akram, A., Qureshi, R., Yaseen, G., Mukhtar, T. and Hanif, N.Q. 2022. Light and scanning electron microscopic characterization of aflatoxins producing *Aspergillus flavus* in the maize crop. Micro. Res. Tech., 85(8): 2894-2903.

Tarannum, N., Nipa, M.N., Das, S. and Parveen, S. 2020. Aflatoxin M1 detection by ELISA in raw and processed milk in Bangladesh. Tox. Rep., 7(5): 1339-1343.

Wokorach, G., Landschoot, S., Lakot, A., Karyeija, S.A., Audenaert, K., Echodu, R. and Haesaert, G. 2022. Characterization of Ugandan endemic Aspergillus species and identification of non-aflatoxigenic isolates for potential biocontrol of aflatoxins. Toxins, 14(5): 304-307.

World Health Organization and International Agency for Research on Cancer (WHO & IARC) 1993. Some naturally occurring substances: Food items and constituents, heterocyclic aromatic amines, and mycotoxins.

... Continued from inner front cover

- The text of the manuscript should run into Abstract, Introduction, Materials & Methods, Results, Discussion, Acknowledgement (if any) and References or other suitable headings in case of reviews and theoretically oriented papers. However, short communication can be submitted in running with Abstract and References. The references should be in full with the title of the paper.
- The figures should preferably be made on a computer with high resolution and should be capable of withstanding a reasonable reduction with the legends provided separately outside the figures. Photographs may be black and white or colour.
- Tables should be typed separately bearing a short title, preferably in vertical form. They should be of a size, which could easily be accommodated in the page of the Journal.
- References in the text should be cited by the authors' surname and year. In case of more than one reference of the same author in the same year, add suffix a,b,c,.... to the year. For example: (Thomas 1969, Mass 1973a, 1973b, Madony et al. 1990, Abasi & Soni 1991).

List of References

The references cited in the text should be arranged alphabetically by authors' surname in the following manner: (Note: The titles of the papers should be in running 'sentence case', while the titles of the books, reports, theses, journals, etc. should be in 'title case' with all words starting with CAPITAL letter.)

Dutta, A. and Chaudhury, M. 1991. Removal of arsenic from groundwater by lime softening with powdered coal additive. J. Water Supply Res. Techno. Aqua., 40(1) : 25-29.

Hammer, D.A. (ed.) 1989. Constructed Wetlands for Wastewater Treatment-Municipal, Industrial and Agricultural. Lewis Publishers Inc., pp. 831.

Haynes, R. J. 1986. Surface mining and wetland reclamation. In: Harper, J. and Plass, B. (eds.) New Horizons for Mined Land Reclamation. Proceedings of a National Meeting of the Ameri can Society for Surface Reclamation, Princeton, W.V.

Submission of Papers

- The paper can be submitted by e-mail as an attachment in a single WORD file at **contact@neptjournal.com**
- The paper can also be submitted online in a single WORD file through the online submission portal of journal's website: **www.neptjournal.com**

Attention

1. Any change in the authors' affiliation may please be notified at the earliest.
2. Please make all the correspondence by e-mail, and authors should always quote the manu script number.

Note: In order to speed up the publication, authors are requested to correct the galley proof immediately after receipt. The galley proof must be checked with utmost care, as publishers owe no responsibility for mistakes. The papers will be put on priority for publication only after receiving the processing and publication charges.

Nature Environment and Pollution Technology

(Abbreviation: Nat. Env. Poll. Tech.)

(An International Quarterly Scientific Journal)

Published by

Technoscience Publications

A-504, Bliss Avenue, Opp. SKP Campus

Balewadi, Pune-411 045, Maharashtra, India

In association with

Technoscience Knowledge Communications

Mira Road, Mumbai, India

For further details of the Journal, please visit the website. All the papers published on a particular subject/topic or by any particular author in the journal can be searched and accessed by typing a keyword or name of the author in the 'Search' option on the Home page of the website. All the papers containing that keyword or author will be shown on the home page from where they can be directly downloaded.

www.neptjournal.com

Published for Proprietor, Printer and Publisher: Mrs. T. P. Goel, A-504, Bliss Avenue, Balewadi, Pune, Maharashtra, India; Editors: Dr. P. K. Goel (Chief Editor) and Prof. K. P. Sharma